

NASA/TM—2012-217014



Beamed-Energy Propulsion (BEP) Study

*Patrick George and Raymond Beach
Glenn Research Center, Cleveland, Ohio*

Approved for Public Release, Distribution Unlimited

Notice for Copyrighted Information

This manuscript is a joint work of employees of the National Aeronautics and Space Administration and employees of Universities Space Research Association (USRA) under Contract No. 04550-013; NCSER NNC08BA08B with the National Aeronautics and Space Administration. The United States Government may prepare derivative works, publish or reproduce this manuscript, and allow others to do so. Any publisher accepting this manuscript for publication acknowledges that the United States Government retains a nonexclusive, irrevocable, worldwide license to prepare derivative works, publish or reproduce the published form of this manuscript, or allow others to do so, for United States Government purposes.

NASA STI Program . . . in Profile

Since its founding, NASA has been dedicated to the advancement of aeronautics and space science. The NASA Scientific and Technical Information (STI) program plays a key part in helping NASA maintain this important role.

The NASA STI Program operates under the auspices of the Agency Chief Information Officer. It collects, organizes, provides for archiving, and disseminates NASA's STI. The NASA STI program provides access to the NASA Aeronautics and Space Database and its public interface, the NASA Technical Reports Server, thus providing one of the largest collections of aeronautical and space science STI in the world. Results are published in both non-NASA channels and by NASA in the NASA STI Report Series, which includes the following report types:

- **TECHNICAL PUBLICATION.** Reports of completed research or a major significant phase of research that present the results of NASA programs and include extensive data or theoretical analysis. Includes compilations of significant scientific and technical data and information deemed to be of continuing reference value. NASA counterpart of peer-reviewed formal professional papers but has less stringent limitations on manuscript length and extent of graphic presentations.
- **TECHNICAL MEMORANDUM.** Scientific and technical findings that are preliminary or of specialized interest, e.g., quick release reports, working papers, and bibliographies that contain minimal annotation. Does not contain extensive analysis.
- **CONTRACTOR REPORT.** Scientific and technical findings by NASA-sponsored contractors and grantees.

- **CONFERENCE PUBLICATION.** Collected papers from scientific and technical conferences, symposia, seminars, or other meetings sponsored or cosponsored by NASA.
- **SPECIAL PUBLICATION.** Scientific, technical, or historical information from NASA programs, projects, and missions, often concerned with subjects having substantial public interest.
- **TECHNICAL TRANSLATION.** English-language translations of foreign scientific and technical material pertinent to NASA's mission.

Specialized services also include creating custom thesauri, building customized databases, organizing and publishing research results.

For more information about the NASA STI program, see the following:

- Access the NASA STI program home page at <http://www.sti.nasa.gov>
- E-mail your question via the Internet to help@sti.nasa.gov
- Fax your question to the NASA STI Help Desk at 443-757-5803
- Telephone the NASA STI Help Desk at 443-757-5802
- Write to:
NASA Center for AeroSpace Information (CASI)
7115 Standard Drive
Hanover, MD 21076-1320



Beamed-Energy Propulsion (BEP) Study

*Patrick George and Raymond Beach
Glenn Research Center, Cleveland, Ohio*

Approved for Public Release, Distribution Unlimited

Notice for Copyrighted Information

This manuscript is a joint work of employees of the National Aeronautics and Space Administration and employees of Universities Space Research Association (USRA) under Contract No. 04550-013; NCSER NNC08BA08B with the National Aeronautics and Space Administration. The United States Government may prepare derivative works, publish or reproduce this manuscript, and allow others to do so. Any publisher accepting this manuscript for publication acknowledges that the United States Government retains a nonexclusive, irrevocable, worldwide license to prepare derivative works, publish or reproduce the published form of this manuscript, or allow others to do so, for United States Government purposes.

National Aeronautics and
Space Administration

Glenn Research Center
Cleveland, Ohio 44135

This report is a formal draft or working paper, intended to solicit comments and ideas from a technical peer group.

Contents were reproduced from the best available copy as provided by the authors.

Trade names and trademarks are used in this report for identification only. Their usage does not constitute an official endorsement, either expressed or implied, by the National Aeronautics and Space Administration.

Level of Review: This material has been technically reviewed by technical management.

Available from

NASA Center for Aerospace Information
7115 Standard Drive
Hanover, MD 21076-1320

National Technical Information Service
5301 Shawnee Road
Alexandria, VA 22312

Available electronically at <http://www.sti.nasa.gov>

Contents

1.0	EXECUTIVE SUMMARY	1
2.0	STUDY SYNOPSIS	2
2.1	Study Background	2
2.1.1	Rationale	2
2.1.2	Previous Component Demonstrations	3
2.1.3	Study Scope	4
2.1.4	End Goals of Study	4
2.2	Study Approach	4
2.3	Study Findings	6
2.3.1	Launch DRMs	6
2.3.2	Space Design Reference Missions (DRMs)	19
2.4	Unexpected Findings	26
2.4.1	Spacecraft Remote Operation	26
2.4.2	Propulsion Engine	26
2.5	BEP Development Direction	27
2.6	Future Potential of BEP	30
3.0	STUDY REPORTS	31
3.1	Launch DRMs	31
3.1.1	Laser Optical Collaborative Modeling for Parametric Assessment of Space Systems (COMPASS) Report	32
3.1.2	Laser Optical Consultant Report—Design Reference Mission 1–A	112
3.1.3	Laser Optical Cost Analysis	188
3.1.4	Laser Thermal COMPASS Report	194
3.1.5	Laser Thermal Consultant Report—Design Reference Mission 1–B	228
3.1.6	Laser Thermal Cost	285
3.1.7	Millimeter-Wave Thermal Collaborative Modeling for Parametric Assessment of Space Systems (COMPASS) Report	291
3.1.8	Millimeter-Wave Thermal Consultant Report—Design Reference Mission 1–C	324
3.1.9	Millimeter-Wave Thermal Cost Estimates	370
3.2	Space Design Reference Missions	376
3.2.1	Low-Earth-Orbit to Geosynchronous-Earth-Orbit Collaborative Modeling for Parametric Assessment of Space Systems (COMPASS) Report	376
3.2.2	Low-Earth-Orbit to Geosynchronous-Earth-Orbit Consultant Reports—Design Reference Mission 2–A	433
3.2.3	Low-Earth-Orbit to Geosynchronous-Earth-Orbit Consultant Reports—Design Reference Mission 2–B	442
3.2.4	Low-Earth-Orbit to Geosynchronous-Earth-Orbit Cost	445
3.2.5	Deep Space Mission Design Lab (MDL) Report	447
3.2.6	Deep Space Consultant Report—Design Reference Mission 3	505
4.0	CONCLUDING REMARKS	515
	APPENDIX A.—ACRONYMS AND DEFINITIONS	517
	APPENDIX B.—CONSULTANT RESUMES	521
	APPENDIX C.—THRUST AUGMENTATION OF AN IN-SPACE PROPULSION SYSTEM	569
	APPENDIX D.—MICROWAVE ENERGY ISSUES	575
	APPENDIX E.—ABL EXPERIMENT	593
	APPENDIX F.—ENVIRONMENTAL CONSIDERATIONS FOR A GROUND-BASED BEP STATION	597
	APPENDIX G.—EFFECTS OF BEAMING ENERGY THROUGH THE ATMOSPHERE	619

G.9.2.1 Continuous Wave Source	642
G.9.2.2 Pulsed Source	644
APPENDIX H.—SUMMARY PRESENTATION.....	649

List of Tables

TABLE 2.1.—OTHER FOMS FOR THE DRMS.....	10
TABLE 2.2.—NONRECURRING AND RECURRING COSTS FOR LAUNCH VEHICLES	15
TABLE 2.3.—LAUNCH VEHICLE AND INFRASTRUCTURE COSTS ^A	18
TABLE 2.4.—LEO–GEO TUG CONOPS.....	21
TABLE 2.5.—RECURRING AND NONRECURRING COSTS FOR LEO–GEO DRM	22
TABLE 2.6.—RECURRING AND NONRECURRING COSTS FOR DEEP SPACE DRM.....	25
TABLE 3.1.—DRM 1—A SUMMARY OF REQUIREMENTS AND ASSUMPTIONS	117
TABLE 3.2.—MASS BREAKDOWN FOR 120-CM DRM 1—A SPACECRAFT	127
TABLE 3.3.—TRADE STUDY—DATA RATE AND COVERAGE VERSUS BEAM WIDTH TO <i>GATEWAY</i>	131
TABLE 3.4.—TRADE STUDY—DATA RATE AND COVERAGE VERSUS BEAM WIDTH TO <i>USER</i>	131
TABLE 3.5.—PEL FOR 120-CM LIGHTCRAFT LAUNCHER.....	132
TABLE 3.6.—THERMAL ANALYSIS ASSUMPTIONS—SPACECRAFT INSULATION.....	138
TABLE 3.7.—MEL FOR 120-CM LIGHTCRAFT LAUNCHER FOR SIX CUBESATS, DEPLOYED FROM DUAL P-POD ON ORBIT.....	142
TABLE 3.8.—MEL MASS BREAKDOWN FOR 35-CM VERSUS 120-CM BEPS LIGHTCRAFT	143
TABLE 3.9.—MEL BREAKDOWN FOR AFRL 35-CM NANOSAT LAUNCHER (REF. 5)	144
TABLE 3.10.—EXISTING SOLID STATE, DIODE-PUMPED LASERS	145
TABLE 3.11.—ISO 14644-1 CLEANROOM STANDARDS; (CLASS 1 IS PROPOSED FOR THE VAB)	155
TABLE 3.12.—SSDP LASER LAUNCH SYSTEM SPECIFICATIONS AND COST.....	163
TABLE 3.13.—LIFE-CYCLE COST MODEL FOR 35-CM LIGHTCRAFT LAUNCHED WITH 10-MW SOLID-STATE LASER (REF. 19)	165
TABLE 3.14.—MISSION ΔV SUMMARY FOR 1.2-M LTD (DRM 1—A) USING OTIS.....	171
TABLE 3.15.—MASS, ΔV , AND PROPELLANT SUMMARY FOR 1.2-M LTD.....	171
TABLE 3.16.—HX PARAMETERS FOR CURRENT (DRM–1B) DESIGN	231
TABLE 3.17.—ISSUES FOR LASER HX	232
TABLE 3.18.—PROPERTIES AND MASS BREAKDOWN OF CONCEPTUAL 100-MW HX LAUNCH VEHICLE AND DRM–1B LASER HX LAUNCH VEHICLE.....	236
TABLE 3.19.—DELTAS IN MASS FOR NON-DROP-TANK VERSION OF COMPASS DESIGN	238
TABLE 3.20.—CHARACTERISTICS OF CHEVROLET VOLT BATTERY PACK.....	249
TABLE 3.21.—LAUNCH VEHICLE COST PER KILOGRAM DRY MASS.....	261
TABLE 3.22.—CAPITAL COST FOR A NOMINAL 60-KW MAIN-LASER BEAM MODULE	266
TABLE 3.23.—CAPITAL COST FOR MAIN LASER SITE WITH 2500 BEAM MODULES	266
TABLE 3.24.—CAPITAL COST FOR A NOMINAL 200-KW BOOST-LASER BEAM MODULE.....	267
TABLE 3.25.—CAPITAL COST FOR BOOST LASER SITE WITH 1200 BEAM MODULES.....	267
TABLE 3.26.—CAPITAL COST FOR LAUNCH SITE.....	268
TABLE 3.27.—COST PER LAUNCH FOR 1000 LAUNCHES/YEAR, 80-KG PAYLOAD.....	269
TABLE 3.28.—TRL LEVELS AND BASIS FOR HX LAUNCH SYSTEMS	270
TABLE 3.29.—THE THREE DESIGN POINTS ASSOCIATED WITH DRM–1C.....	326

TABLE 3.30.—FIGURES OF MERIT FOR THE MICROWAVE THERMAL ROCKET VERSUS OTHER CONCEPTS FOR COMPARISON [RASCAL, RP1, ROCKET PROPELLANT 1.]	331
TABLE 3.31.—MARGINS OF OTHER CONCEPT STUDIES	332
TABLE 3.32.—TECHNOLOGY MARGINS PRIORITIZED BY GREATEST POTENTIAL IMPACT FIRST	333
TABLE 3.33.—PAYLOAD DESCRIPTION FOR EACH OF THE DESIGN POINTS ASSOCIATED WITH DRM-1C	336
TABLE 3.34.—BEAM FACILITY POINT DESIGNS	340
TABLE 3.35.—COMPARISON OF APERTURE PARAMETERS	342
TABLE 3.36.—CONOPS FOR ORBCOMM LAUNCH	344
TABLE 3.37.—ASSUMPTIONS USED IN THE BEAM FACILITY COST CALCULATION	345
TABLE 3.38.—ASSUMPTIONS USED IN THE BEAM FACILITY COST CALCULATION	347
TABLE 3.39.—KEY FACILITIES AND MILESTONES	351
TABLE 3.40.—PRELIMINARY EXPERIMENT ROSTER FOR THE GYROTRON BEAM FACILITY	354
TABLE 3.41.—WEATHER AT THE CONUS SITE EXAMPLES GIVEN IN FIGURE 3.131)	362
TABLE 3.42.—CONOPS FOR LEO-GEO LASER TRANSPORT	438
TABLE 3.43.—TECHNOLOGY READINESS	440
TABLE 3.44.—CONOPS FOR LEO-GEO LASER TRANSPORT 2-B	443
TABLE 3.45.—TECHNOLOGY READINESS FOR DRM 2-B	444
TABLE C.2.—AUGMENTED THRUSTER SYSTEM PERFORMANCE	571
TABLE C.3.—THRUSTER SYSTEM PARAMETERS	571
TABLE C.4.—MISSION PARAMETERS FOR AUGMENTED AND AUGMENTED THRUSTER SYSTEMS	573
TABLE D.1.—POWER BEAMING REQUIREMENTS, VARIABLES, AND ASSUMPTIONS	577
TABLE D.2.—REQUIRED TRANSMITTER EIRPS TO ACHIEVE A MINIMUM OF 30 MW/M ² AT THE MTR	579
TABLE D.3.—PHASED ARRAY ANTENNA ADVANTAGES AND DISADVANTAGES	579
TABLE D.4.—PHASED ARRAY ANTENNA INPUT PARAMETERS	589
TABLE F.1.—EXPOSURE LIMITS BY WAVELENGTH AND EXPOSURE TYPE (REPRODUCED FROM SOURCE 3)	601
TABLE G.1.—THRESHOLD POWER LEVELS BEYOND WHICH PROPAGATION EFFECTS OCCUR AT INFRARED AND MILLIMETER WAVELENGTHS FOR VARIOUS OUTPUT APERTURE RADII, R_{EFF}	623
TABLE G.2.—BEAM RADII AT TARGETS IN LOW EARTH ORBIT (LEO) AND GEOSYNCHRONOUS ORBIT (GEO) FOR VARIOUS OUTPUT APERTURE SIZES	627

List of Figures

FIGURE 2.1.—BEAMED THERMAL SYSTEM EFFICIENCY—LAUNCHING PAYLOADS AND SPACE PROPULSION. DDCU, DC-DC CONVERSION UNIT; PPU, POWER PROCESSING UNIT	5
FIGURE 2.2.—TWO SIZES OF LASER OPTICAL VEHICLES STUDIED	6
FIGURE 2.3.—FUNCTION OF EXTERNAL SURFACES IN AIR-BREATHING PROPULSION MODE	7
FIGURE 2.4.—LASER THERMAL VEHICLE. LASER THERMAL ROCKET CONFIGURATION SHOWING THE LASER RECEIVER HX MOUNTED ON ITS SIDE	8
FIGURE 2.5.—MILLIMETER-WAVE THERMAL DRM. MILLIMETER-WAVE THERMAL ROCKET CONFIGURATION SHOWING A CIRCUMFERENTIAL RECEIVER HX	9

FIGURE 2.6.—ORBCOMM SPACECRAFT. COURTESY OF ORBITAL SCIENCES CORPORATION; USED WITH PERMISSION.....	10
FIGURE 2.7.—PEGASUS XL.....	10
FIGURE 2.8.—LAUNCH VEHICLES COMPARED BY SIZE.....	10
FIGURE 2.9.—CONFIGURATION OF LASER OPTICAL GROUND FACILITIES.....	11
FIGURE 2.10.—CONCEPT FOR BEAM-COMBINING SYSTEM WITH CENTRAL ROTATING OUTPUT MIRROR.....	12
FIGURE 2.11.—TYPICAL LAUNCH CONCEPT OF OPERATIONS WITH L1 (BOOST) LASER ARRAY. MARKERS: (0) LAUNCH. (1) MAIN ARRAY “SEES” VEHICLE AND BEGINS TRACKING. (2) MAIN ARRAY TURNS ON; L1 ARRAY AT MAXIMUM FULL-POWER RANGE. (3) MAIN ARRAY AT FULL POWER; L1 ARRAY.....	12
FIGURE 2.12.—CONFIGURATION OF LASER THERMAL GROUND FACILITIES.....	13
FIGURE 2.13.—CONFIGURATION OF MILLIMETER-WAVE THERMAL GROUND FACILITIES.....	13
FIGURE 2.14.—MILLIMETER-WAVE THERMAL LAUNCH SYSTEM AND ASCENT TRAJECTORY.....	14
FIGURE 2.15.—LASER POWER LEVEL VERSUS COST. KARE TECHNICAL CONSULTING, USED WITH PERMISSION.....	16
FIGURE 2.16.—LASER OPTICAL ISSUES.....	17
FIGURE 2.17.—LEO–GEO TUG DIAGRAM. RCS, REACTION CONTROL SYSTEM.....	20
FIGURE 2.18.—LAUNCH ELEMENTS AND SEQUENCE.....	21
FIGURE 2.19.—STOWED DRM 3 PROPULSION MODULE IN FALCON 9 FAIRING.....	23
FIGURE 2.20.—SEQUENCE OF OPERATIONS FOR DRM 3: BEP-ENHANCED GALILEO MISSION.....	24
FIGURE 2.21.—BEP CONCEPT—INTEGRATED PROPULSION, POWER, COMMUNICATIONS, AND NAVIGATIONAL/ATTITUDE CONTROL ON THE SAME LASER BEAM (PV, PHOTOVOLTAICS; RCS, REACTION CONTROL SYSTEM).....	26
FIGURE 2.22.—BEP OPTICAL PLASMA ENGINE.....	27
FIGURE 2.23.—TIMELINE OF BEAMED-ENERGY DEVELOPMENT.....	27
FIGURE 2.24.—BEP DEVELOPMENT APPLICATIONS FROM LOW TO HIGH POWER.....	28
FIGURE 2.25.—DEMONSTRATIONS TO DEVELOP NEAR-TERM REMOTE POSITIONAL CONTROL TECHNOLOGY.....	28
FIGURE 2.26.—IN-SPACE FLIGHT DEMONSTRATION FROM THE INTERNATIONAL SPACE STATION TO FREE FLYER.....	29
FIGURE 2.27.—DEMONSTRATIONS TO DEVELOP NEAR-TERM OPTICAL PLASMA ENGINE TECHNOLOGY.....	30
FIGURE 3.1.—12-MW LASER LAUNCH FACILITY AT WSMR, NEW MEXICO (ARTIST CONCEPT BY P. RAWLINGS).....	112
FIGURE 3.2.—LIGHTCRAFT PLASMA ENGINE PULSING IN 1-BAR LABORATORY AIR (PHOTOGRAPHS BY J.E. SHRYNE, III). LEFT: 14.7-CM-DIAMETER #200 VEHICLE. RIGHT: 23-CM #100 VEHICLE.....	112
FIGURE 3.3.—ORBCOMM MESSAGING SATELLITE IN 800-KM CIRCULAR ORBIT (FROM REF. 4). COURTESY OF ORBITAL SCIENCES CORPORATION; USED WITH PERMISSION.....	113
FIGURE 3.4.—PROGRESSIVE TECHNOLOGY ROADMAP AND POSSIBLE DEVELOPMENT PROGRAM: GROUND AND FLIGHT DEMONSTRATIONS LEADING TO 35-CM NANOSAT LAUNCH SYSTEM.....	114
FIGURE 3.5.—FINAL LAUNCH CONFIGURATION OF 120-CM-DIAMETER DRM 1–A SPACECRAFT.....	115

FIGURE 3.6.—PRINCIPAL SPACECRAFT SYSTEMS. SA, SOLAR ARRAY; GN&C, GUIDANCE, NAVIGATION, AND CONTROL; C&DH, COMMAND AND DATA HANDLING; PMAD, POWER MANAGEMENT AND DISTRIBUTION; HE, HELIUM.	116
FIGURE 3.7.—SEMITRANSSPARENT VIEW OF 120-CM SPACECRAFT AND SATELLITE ELECTRONICS. IMU, INERTIAL MEASUREMENT UNIT.	119
FIGURE 3.8.—FUNCTION OF EXTERNAL SURFACES IN AIR-BREATHING PROPULSION MODE.	120
FIGURE 3.9.—PULSEJET ENGINE CYCLE BASED ON LSD WAVES. (DATA FOR 11- TO 14-CM LIGHTCRAFT ENGINE TESTS ON PULSED LASER VULNERABILITY TEST SYSTEM (PLVTS) LASER AT WSMR.)	120
FIGURE 3.10.—PROPELLANT INJECTOR SCHEMES FOR ROCKET PULSEJET MODE (REF. 16).	121
FIGURE 3.11.—CUTAWAY OF ENGINE “HOT SECTION,” SHOWING COOLING AND PROPELLANT INJECTOR SYSTEMS (REF. 16).	122
FIGURE 3.12.—SIDE AND TOP VIEWS OF SHROUD AND SUPPORT STRUTS, EXPLAINING COOLANT SCHEME (REF. 16).	122
FIGURE 3.13.—THRUST VECTORING, RCS, AND PROPELLANT INJECTOR DESIGN.	122
FIGURE 3.14.—LEFT: CENTERED VERSUS OFFSET BEAMS. RIGHT: THRUST IMPULSE, SIDE IMPULSE, AND PITCHING ANGULAR IMPULSE ARE FUNCTIONS OF LATERAL BEAM OFFSET DISTANCE (REFS. 13 TO 15).	123
FIGURE 3.15.—PERFORMANCE VARIATIONS IN AXIAL IMPULSE AND RESTORATIVE (I.E., BEAM-RIDING) IMPULSE VERSUS LATERAL OFFSET ARE ACTIVELY EXPLOITED IN THE AIM-POINT STRATEGY (REFS. 13 TO 15).	124
FIGURE 3.16.—AIM-POINT STRATEGY IN LAUNCHING A BEAM-RIDING LIGHTCRAFT (REFS. 13 TO 15).	124
FIGURE 3.17.—LIGHTCRAFT DRM 1—A CONFIGURATION—OBLIQUE, TOP, AND SIDE VIEWS.	125
FIGURE 3.18.—AVIONICS FUNCTIONALITY (120-CM LAUNCHER; I/O, INPUT/OUTPUT).	128
FIGURE 3.19.—COMMUNICATION OPERATIONS DIAGRAM.	129
FIGURE 3.20.—LAUNCH GATEWAY SITES.	130
FIGURE 3.21.—LEFT: FLEXIBLE PV ARRAY. RIGHT: POWER CIRCUIT SCHEMATIC.	132
FIGURE 3.22.—LIGHTCRAFT THERMAL SUBSYSTEMS. LEFT: DURING LAUNCH. RIGHT: ON-ORBIT.	135
FIGURE 3.23.—SURFACE MOUNT RADIATOR SIZING—THERMAL ANALYSIS.	137
FIGURE 3.24.—LEFT: SAMPLE COLD PLATE FOR ELECTRONICS COOLING. RIGHT: THERMAL ANALYSIS ASSUMPTIONS.	137
FIGURE 3.25.—MLI FOR SPACECRAFT ON-ORBIT.	138
FIGURE 3.26.—REFLECTANCE OF MULTILAYER DIELECTRIC FILM COATINGS VERSUS NORMALIZED FREQUENCY.	139
FIGURE 3.27.—RADIATION HEAT TRANSFER FROM ELECTRIC ARC IN 1-BAR ATMOSPHERE.	140
FIGURE 3.28.—DIFFUSE REFLECTING SURFACE FOR SCATTERING LASER LIGHT.	141
FIGURE 3.29.—ALTERNATIVE PAYLOAD FOR 120-CM SPACECRAFT—DUAL P-POD LAUNCHER.	142
FIGURE 3.30.—RELATIVE SCALE OF LIGHTCRAFT LAUNCHERS. LEFT: MICROSATELLITES. RIGHT: NANOSATELLITES.	143
FIGURE 3.31.—EXPONENTIAL GROWTH OF CONTINUOUS WORKING SSDP LASERS (REF. 20).	145
FIGURE 3.32.—LLNL’S 67-KW SSHCL (REF. 23).	146
FIGURE 3.33.—MERCURY HAPL AT LLNL (50- TO 100-J PULSES AT 10 HZ) (REF. 25).	146

FIGURE 3.34.—LEFT: IPG’S 10-KW SINGLE-MODE FIBER LASER WELDER. RIGHT: MASTER OSCILLATOR POWER AMPLIFIER (MOPA) SCHEMATIC (REF. 26). COPYRIGHT IPG PHOTONICS CORPORATION (OXFORD, MA) 10,000 W SINGLE MODE LASER; USED WITH PERMISSION.	147
FIGURE 3.35.—SCATTER PLOT OF SSDP LASER SPECIFICATIONS RELATIVE TO THE DESIRED BEAMLINER GOAL.	147
FIGURE 3.36.—11.5-MW RP SSDP LASER SYSTEM (24 BEAMLINES PER LEVEL, STACKED FOUR LEVELS DEEP FOR 96 TOTAL) (ARTIST CONCEPT BY P. RAWLINGS).	148
FIGURE 3.37.—WSMR FACILITY FOR HOUSING 12-MW LAUNCH LASER SYSTEM (ARTIST CONCEPT BY P. RAWLINGS).	148
FIGURE 3.38.—SCHEMATIC FOR SINGLE SSDP BEAMLINER DESIGNED FOR ORBIT DEBRIS MITIGATION (REFS. 28 AND 29).	149
FIGURE 3.39.—LEFT: DIODE BARS. RIGHT: HE GAS COOLING OF AMPLIFIER SLABLETS IN HAPL PROTOTYPE (REFS. 28 AND 29).	150
FIGURE 3.40.—HE GAS-COOLED AMPLIFIER SLABLETS AND OPTICAL SWITCHES IN HAPL PROTOTYPE (REF. 30).	150
FIGURE 3.41.—ALRU DESIGN FOR FLOWING-GAS HE COOLING (REF. 30).	151
FIGURE 3.42.—HIGH-POWER VCSEL DIODE TECHNOLOGY (REF. 31).	151
FIGURE 3.43.—ROTATING MIRROR BEAM COMBINING SYSTEM (ARTIST CONCEPT BY P. RAWLINGS). LEFT: PLANFORM VIEW. RIGHT: OBLIQUE VIEW.	152
FIGURE 3.44.—BEAM-COMBINING SYSTEM WITH CENTRAL ROTATING OUTPUT MIRROR (CENTER) AND TILT-TIP CORRECTION MIRRORS AND AO (RIGHT) (ARTIST CONCEPT BY P. RAWLINGS).	152
FIGURE 3.45.—ROTATING MIRROR BEAM-COMBINER UNIT STABILIZED BY VERTICAL 12- BY 12-M OPTICAL BENCH/WALL (ARTIST CONCEPT BY P. RAWLINGS).	152
FIGURE 3.46.—BEAM DELIVERY TUBE (LEFT), 3-M TELESCOPE (CENTER), AND RETRACTABLE LAUNCH RIG WITH 1-M 45° TURNING FLAT (RIGHT) (ARTIST CONCEPT BY P. RAWLINGS).	153
FIGURE 3.47.—SEMI-TRANSPARENT VIEW OF 3-M TELESCOPE AND DOME (ARTIST CONCEPT BY P. RAWLINGS).	153
FIGURE 3.48.—VIEW INSIDE BEAM DELIVERY TUNNEL, SHOWING RETRACTABLE 45° FLAT MIRROR THAT DIVERTS THE UNEXPANDED 25- BY 25-CM LASER BEAM VERTICALLY UPWARD INTO A 3-M-DIAMETER TELESCOPE (ARTIST CONCEPT BY P. RAWLINGS).	154
FIGURE 3.49.—AERIAL VIEW OF LASER HIGHBAY (LEFT), BEAM TUBE (CENTER), AND VAB WITH LAUNCH PAD (RIGHT) (ARTIST CONCEPT BY P. RAWLINGS).	156
FIGURE 3.50.—LAYOUT OF VAB (ARTIST CONCEPT BY P. RAWLINGS).	156
FIGURE 3.51.—ROBOTIC HANDLING OF 120-CM LIGHTCRAFT (318-KG WET MASS) (ARTIST CONCEPT BY P. RAWLINGS).	156
FIGURE 3.52.—POI-1000 SPIN BALANCE MACHINE (COURTESY OF SPACE ELECTRONICS, LLC; USED WITH PERMISSION), WITH SCALE 120-CM LIGHTCRAFT (REF. 32).	157
FIGURE 3.53.—ROBOT LOADS 120-CM LIGHTCRAFT ONTO MOBILE LAUNCHER RIG INSIDE VAB (ARTIST CONCEPT BY P. RAWLINGS).	157
FIGURE 3.54.—MOBILE LAUNCHER TRANSPORTS 120-CM LIGHTCRAFT OUT TO LAUNCH PAD AT END OF TRACK (ARTIST CONCEPT BY P. RAWLINGS).	158
FIGURE 3.55.—AERIAL VIEWS (ARTIST CONCEPT BY P. RAWLINGS). (A) LIGHTCRAFT ON LAUNCH PAD. (B) UNDER LASER BOOST.	158

FIGURE 3.56.—DAWN LAUNCH OF LIGHTCRAFT AT WHITE SANDS MISSILE RANGE, NEW MEXICO (BY L. MYRABO AND P. MOLONEY).....	159
FIGURE 3.57.—MISSION TIMELINE ALONG TRAJECTORY FOR DRM 1–A. LTD, LIGHTCRAFT TECHNOLOGY DEMONSTRATOR.....	160
FIGURE 3.58.—ON-ORBIT TIMELINE GIVES SPECIFICATIONS FOR DRM 1–A.....	161
FIGURE 3.59.—RP SOLID-STATE LASER COSTS VERSUS PULSE ENERGY (FROM REFS. 2 AND 33).....	162
FIGURE 3.60.—RP SOLID-STATE LASER COSTS VERSUS PRF (FROM REF. 2 AND 33).....	162
FIGURE 3.61.—LASER BEAM DIRECTOR COST VERSUS APERTURE DIAMETER (FROM REFS. 2 AND 33).....	163
FIGURE 3.62.—NASA (N) VERSUS COMMERCIAL (C) PRODUCTION COSTS FOR 35- CM LIGHTCRAFT.....	164
FIGURE 3.63.—LASER LAUNCH GEOMETRY FOR LIGHTCRAFT TRAJECTORY SIMULATIONS.....	166
FIGURE 3.64.—NET C_M VERSUS FLIGHT MACH NUMBER FOR LTD AIR-BREATHING MODE (REFS. 16 AND 17). (“BASELINE” 3-CM INLET GAP, 500-MW/CM ² AT FOCAL RING.).....	167
FIGURE 3.65.—THREE-DIMENSIONAL (3D) PLOT OF C_M VERSUS FLIGHT MACH NUMBER FOR LTD AIR-BREATHING MODE (REFS. 16 AND 17). (“BASELINE” 3-CM INLET GAP, 500-MW/CM ² AT FOCAL RING.).....	168
FIGURE 3.66.— E_p VERSUS FLIGHT MACH NUMBER FOR LTD AIR-BREATHING ENGINE MODE (REFS. 16 AND 17). (“BASELINE” 3-CM INLET GAP, 500-MW/CM ² AT FOCAL RING.).....	168
FIGURE 3.67.— PRF VERSUS FLIGHT MACH NUMBER FOR LTD AIR-BREATHING ENGINE MODE (REFS. 16 AND 17). (“BASELINE” 3-CM INLET GAP, 500-MW/CM ² AT FOCAL RING.).....	168
FIGURE 3.68.—AERODYNAMIC DRAG MODEL FOR LTD VEHICLE (REFS. 16 AND 17).....	169
FIGURE 3.69.—BURN PHASES, RANGES, AND ANGLES FROM THE SATELLITE ORBIT ANALYSIS PROGRAM (SOAP) SIMULATION FOR 1.2-M LTD (DRM 1–A).....	170
FIGURE 3.70.—OTIS SIMULATED LAUNCH TRAJECTORY FOR 1.2-M LTD (DRM 1–A). (A) ALTITUDE VERSUS TIME. (B) VELOCITY VERSUS TIME. (C) ALTITUDE VERSUS RANGE FROM LAUNCH PAD.....	170
FIGURE 3.71.—LASER POWER AND ENGINE THRUST VERSUS TIME FROM OTIS TRAJECTORY FOR 1.2-M LTD (DRM 1–A).....	171
FIGURE 3.72.—ALTITUDE VERSUS TIME FOR SIMULATED TRAJECTORIES OF 35-CM LCC (REF. 5).....	174
FIGURE 3.73.—CAPTURED 1.62-MM LASER POWER VERSUS SLANT RANGE FROM FOR 35-CM LIGHTCRAFT (REF. 5).....	175
FIGURE 3.74.—MACH NUMBER VERSUS TIME FOR 7-DOF SIMULATED TRAJECTORIES.....	176
FIGURE 3.75.—ALTITUDE VERSUS TIME FOR 7-DOF SIMULATED TRAJECTORIES.....	177
FIGURE 3.76.—VELOCITY VERSUS TIME FOR 7-DOF SIMULATED TRAJECTORIES.....	177
FIGURE 3.77.—BEAM POWER VERSUS TIME FOR 7-DOF SIMULATED TRAJECTORIES FOR 120-CM LTD CRAFT.....	177
FIGURE 3.78.—BEAM POWER VERSUS TIME FOR 7-DOF SIMULATED TRAJECTORIES FOR 35-CM CRAFT.....	178
FIGURE 3.79.—MACH NUMBER VERSUS ALTITUDE FOR 7-DOF SIMULATED TRAJECTORIES.....	178
FIGURE 3.80.—ZENITH ANGLE VERSUS TIME FOR 7-DOF SIMULATED TRAJECTORIES.....	178

FIGURE 3.81.—KEY ISSUES AFFECTING THE FEASIBILITY OF A LIGHTCRAFT VEHICLE AND A COMBINED-CYCLE ENGINE.....	180
FIGURE 3.82.—PROGRAM 1—LASER LAUNCH DEMONSTRATIONS TO 1 KM AT HELSTF USING 10-KW PLVTS CO ₂ LASER.....	182
FIGURE 3.83.—PROGRAM 2—SUBORBITAL LAUNCH DEMONSTRATIONS TO 10 TO 30 KM AT HELSTF USING THE 105-KW JHPSSL.....	182
FIGURE 3.84.—PROGRAM 3—SUBORBITAL LAUNCH DEMONSTRATIONS USING ALTB’S MULTIMEGAWATT COIL.....	183
FIGURE 3.85.—PROGRAM 4—ON-ORBIT LAUNCH DEMONSTRATIONS FROM THE ISS USING A SPACE-RATED VERSION OF THE HAPL 1- KW LASER.....	184
FIGURE 3.86.—TYPICAL LAUNCH CONCEPT OF OPERATIONS WITH L1 (BOOST) LASER ARRAY. MARKERS: (0) LAUNCH. (1) MAIN ARRAY “SEES” VEHICLE AND BEGINS TRACKING. (2) MAIN ARRAY TURNS ON; L1 ARRAY AT MAXIMUM FULL-POWER RANGE. (3) MAIN ARRAY AT FULL POWER; L1 ARRAY TURNS OFF. (4) VEHICLE PITCHES DOWN TO CIRCULARIZE ORBIT. (5) ORBIT INSERTION; MAIN LASER TURNS OFF. COPYRIGHT KARE TECHNICAL CONSULTING; USED WITH PERMISSION.....	228
FIGURE 3.87.—HX THRUSTER CONCEPT; LH ₂ , LIQUID HYDROGEN. COPYRIGHT KARE TECHNICAL CONSULTING; USED WITH PERMISSION.....	229
FIGURE 3.88.—CONVENTIONAL HX VERSUS LAMINAR-FLOW MICROCHANNEL HX. COPYRIGHT KARE TECHNICAL CONSULTING; USED WITH PERMISSION.....	230
FIGURE 3.89.—CONCEPTUAL DESIGN OF 100-MW HX LAUNCH VEHICLE. COPYRIGHT KARE TECHNICAL CONSULTING; USED WITH PERMISSION.....	235
FIGURE 3.90.—GROUND FACILITIES FOR LASER HX LAUNCH SYSTEM. MIDDLE IMAGE: COPYRIGHT LASERMOTIVE, LLC; USED WITH PERMISSION. RIGHT IMAGE: COPYRIGHT KARE TECHNICAL CONSULTING; USED WITH PERMISSION.....	240
FIGURE 3.91.—BLOCK DIAGRAM OF 60-KW BEAM MODULE. COPYRIGHT KARE TECHNICAL CONSULTING; USED WITH PERMISSION.....	242
FIGURE 3.92.—IPG YLS-10000-SM 10-KW SINGLE-MODE LASER. COPYRIGHT IPG PHOTONICS CORPORATION (OXFORD, MA) 10,000 W SINGLE MODE LASER; USED WITH PERMISSION.....	243
FIGURE 3.93.—ADAPTIVE OPTICS BEACON OFFSET VERSUS TIME FOR A TYPICAL LEO TRAJECTORY. THE NOTCH AT 420 S CATES A POINT IN THE TRAJECTORY WHERE THE VEHICLE PITCHES NOSE DOWN SLIGHTLY (~10°) TO CIRCULARIZE ITS ORBIT AND IMPROVE THE LASER HX VIEWING ANGLE.....	245
FIGURE 3.94.—BEAM MODULES IN THE FIELD. COPYRIGHT KARE TECHNICAL CONSULTING; USED WITH PERMISSION.....	247
FIGURE 3.95.—MODULAR DATA CENTER, AS ENVISIONED IN IEEE SPECTRUM (REF. 25). COPYRIGHT KARE TECHNICAL CONSULTING; USED WITH PERMISSION.....	247
FIGURE 3.96.—A 2000-MODULE ARRAY, WITH 40 BY 50 M SPACING, IS 2 × 1.6 KM, OR ABOUT THE SIZE OF A 18-HOLE GOLF COURSE. COPYRIGHT KARE TECHNICAL CONSULTING; USED WITH PERMISSION.....	248
FIGURE 3.97.—BOOST LASER BEAM MODULE CONCEPT.....	251
FIGURE 3.98.—ATMOSPHERIC TRANSMISSION VERSUS WAVELENGTH FOR A 20-KM HORIZONTAL PATH AT MIDLATITUDE DURING WINTER (MOLECULAR ABSORPTION/SCATTERING ONLY; NO PARTICULATES).....	253
FIGURE 3.99.—VARIABLE LAUNCH AZIMUTH AND DOGLEG TRAJECTORY OFFSET CAPABILITY WITH A SINGLE LAUNCH SITE AND LASER SITE.....	258
FIGURE 3.100.—LAWRENCE LIVERMORE NATIONAL LABORATORY LASER DIODE COST ESTIMATES.....	262

FIGURE 3.101.—HAITZ’S LAW FOR LIGHT-EMITTING DIODE (LED) PRICE AND PERFORMANCE VERSUS TIME.	263
FIGURE 3.102.—EXAMPLE OF SCALING ULTRAVIOLET LIGHT-EMITTING DIODE (LED) PRICES OVER 6 DECADES OF QUANTITY.	264
FIGURE 3.103.—ROADMAP FOR LAUNCH SYSTEM DEVELOPMENT AND DEPLOYMENT.	272
FIGURE 3.104.—POSSIBLE GROUND (BLUE) AND FLIGHT (GREEN) DEMONSTRATION PROGRAM FOR HX VEHICLE.	273
FIGURE 3.105.—LEFT: THE ADVENT OF GYROTRON TECHNOLOGY HAS RAISED THE POWER OUTPUT OF SOURCES IN THE KEY MILLIMETER-WAVELENGTH RANGE BY 3 ORDERS OF MAGNITUDE SINCE 1970. RIGHT: VGB-8125 GYROTRON MANUFACTURED IN PALO ALTO BY CPI INC. THIS TUBE PRODUCES A 2.5-MW BEAM AT 95 GHZ. (IMAGE COURTESY OF COMMUNICATIONS & POWER INDUSTRIES (CPI); USED WITH PERMISSION).	324
FIGURE 3.106—MICROWAVE THERMAL LAUNCH SYSTEM AND ASCENT TRAJECTORY ARISING FROM DRM-1C.	325
FIGURE 3.107.—PYROLYTIC GRAPHITE WAS FIRST PRODUCED IN THE LATE 1800S FOR LAMP FILAMENTS. LEFT: PYROLYTIC GRAPHITE SHEETING. RIGHT: THERMAL CONDUCTIVITY IN WATTS PER METERS KELVIN OF PYROLYTIC GRAPHITE SHEET VERSUS OTHER METALS (PANASONIC PGS DATA SHEET). COPYRIGHT ©2011 PANASONIC CORPORATION OF NORTH AMERICA; USED WITH PERMISSION.	327
FIGURE 3.108.—(A) PLAN AND SECTION VIEWS OF AN ANGLE-INTERLOCK ARCHITECTURE. IN THE LOOM, THE WARP YARNS ARE MOVED UP AND DOWN SELECTIVELY BY HARNESSSES, WHEREAS THE WEFT YARNS ARE INSERTED BETWEEN THEM BY A FLYING SHUTTLE OR RAPIER. THE SECTION VIEWS SHOW HOW THE LOOM MOTIONS CAUSE WARP YARNS TO PASS RIGHT THROUGH THE THICKNESS OF THE RESULTING FABRIC, TYING TOGETHER LAYERS OF WEFT YARNS. THUS, THE ANGLE-INTERLOCK ARCHITECTURE SUPPRESSES DELAMINATION. (B) SCHEMATIC OF AN ADAPTATION OF AN ANGLE-INTERLOCK ARCHITECTURE TO FORM AN INTEGRAL SET OF ROCKET NOZZLE TUBES. THE TUBE WALLS HAVE AN INTERNAL ARCHITECTURE SIMILAR TO THAT SHOWN IN PANEL (A), WITH THE TOPS AND BOTTOMS OF THE TUBES JOINED AT NEXUS REGIONS FORMED IN THE LOOM. (C) FORMED C-SIC COMPOSITE STRUCTURE, SHOWING INTEGRALLY WOVEN STRUTS FOR CONNECTING TO THE ROCKET BODY AND DETAILS OF THE HIGH-DENSITY MATRIX FORMED WITHIN THE TUBE WALLS (REF. 1).	328
FIGURE 3.109.—LEFT: CONFORMAL SECTIONS OF WOVEN H ₂ HX FOR ROCKET NOZZLE COOLING. RIGHT: LINEAR SECTION OF WOVEN HX UNDERGOING TESTING AT GLENN. THE TESTS ENTAILED CONNECTING THE COMPOSITE TUBES TO METAL MANIFOLDS FOR THE SUPPLY AND RETURN OF 300-TO 400-BAR H ₂ COOLANT. ONE SIDE OF THE PANEL WAS EXPOSED TO A HYDROGEN/OXYGEN COMBUSTION PLUME FROM A SMALL ROCKET COMBUSTION CHAMBER DELIVERING A FREE-STREAM TEMPERATURE APPROACHING 3,300 K. PANELS SURVIVED MULTIPLE CYCLES SIMULATING OPERATING CONDITIONS OF A BOOST ROCKET ENGINE (COLD-WALL HEAT FLUX OF 20 MW M ⁻²), WITH INDIVIDUAL CYCLES AS LONG AS 8 MIN AND CUMULATIVE TIMES OF 40 MIN.	329
FIGURE 3.110.—REACTION CONTROL SYSTEM (RCS) PODS.	329
FIGURE 3.111.—GRAPHITE ANNULAR AEROSPIKE/PLUG NOZZLE DEVELOPED AND TESTED BY CALSTATE LONG BEACH/GARVEY SPACECRAFT CORPORATION IN	

2003. COPYRIGHT GARVEY SPACECRAFT CORPORATION; USED WITH PERMISSION.	330
FIGURE 3.112.—LEFT: SCANNING ELECTRON MICROSCOPE (SEM) IMAGE (CROSS-SECTION) OF ZRO ₂ INTERFACE COATING ON CARBON FIBERS (WHITE RINGS AROUND EACH FIBER) SHOWING UNIFORMITY OF COVERAGE ACHIEVED BY THE ULTRAVIOLET CHEMICAL VAPOR DEPOSITION (UVCVD) TECHNIQUE (ULTRAMET.COM). RIGHT: SEM IMAGE SHOWING FIBER PULLOUT IN CERAMIC MATRIX COMPOSITE WITH ZRO ₂ INTERFACE COATING (ULTRAMET.COM).	334
FIGURE 3.113.—SATELLITE DATA INDICATING THE INTERNATIONAL LOCATIONS WHERE ATMOSPHERIC WATER VAPOR CONTENT IS LOWEST, AND THEREFORE MILLIMETER-WAVE PROPAGATION IS MOST EFFICIENT. COPYRIGHT EUROPEAN SPACE AGENCY (ESA); USED WITH PERMISSION.	337
FIGURE 3.114.—EXAMPLES OF CONUS SITES WITH LOW LOSSES DUE TO WATER VAPOR ABSORPTION. SUCH SITES ARE PREDOMINANTLY IN THE SOUTHWEST. FOR MT. EVANS AND PIKES PEAK, A MILLIMETER-WAVE BEAM VERTICALLY TRANSMITTED TO SPACE WOULD LOSE 5% TO 10% OF ITS ENERGY TO ATMOSPHERIC ABSORPTION AT 170 GHZ.	338
FIGURE 3.115.—BEAM FACILITY ARRANGEMENT ALONG AN ASCENT TRAJECTORY. THE RED LINE IS THE ASCENT TRAJECTORY. DURING INITIAL ASCENT, A BOOST BEAM FACILITY WITH A MAXIMUM RANGE OF 60 KM PROPELS THE VEHICLE, WHICH IS THEN HANDED OVER TO A LARGER SUSTAIN FACILITY WITH A 125-KM RANGE AND HIGHER POWER. PROGRAMMATICALLY, A SUBSCALE DEMONSTRATION BEAM FACILITY WOULD PROBABLY BECOME THE BOOST FACILITY, AND THE DECISION TO PROCEED ON THE SUSTAIN FACILITY WOULD BE BASED ON ITS SUCCESSFUL OPERATION. THE BLUE LINE IS AN ALTERNATE ASCENT TRAJECTORY CONSIDERED BY THE COMPASS TEAM. BECAUSE TWICE THE RANGE WOULD REQUIRE TWICE THE SOURCE OR TARGET DIAMETER, IT WAS NOT FURTHER CONSIDERED FOR THESE POINT DESIGNS.	339
FIGURE 3.116.—THREE GENERATIONS OF MILLIMETER-WAVE TELESCOPES. TOP: 1990S-ERA GBT (LEFT) AND SECONDARY (RIGHT). MIDDLE: 2000S-ERA ATACAMA PATHFINDER EXPERIMENT (APEX) AT LLANO CHAJNANTOR (COURTESY OF APEX; USED WITH PERMISSION). VIEWED HERE AT DUSK, THE PANELS AND RETROREFLECTORS OF ITS ACTIVE SURFACE ARE CLEARLY VISIBLE. THE TELESCOPE WAS MANUFACTURED BY VERTEX ANTENNENTECHNIK IN DUISBURG, GERMANY. BOTTOM: 2010S-ERA CORNELL-CALTECH ATACAMA TELESCOPE (CCAT) (COURTESY TMT OBSERVATORY CORPORATION; USED WITH PERMISSION).	341
FIGURE 3.117.—LEFT: 12-CM-DIAMETER FAST-STEERING MIRROR FOR HIGH-POWER LASER APPLICATIONS (IMAGE COURTESY OF ATA; USED WITH PERMISSION). A 30-CM-DIAMETER MODEL FEATURES >1-KHZ OPEN-LOOP BANDWIDTH, >300 RAD/S ² ANGULAR ACCELERATION, <0.2-μM SURFACE ACCURACY, AND ±8-MRAD MECHANICAL TRAVEL WITH <10-μRAD (2-ARCSEC) POINTING ACCURACY. RIGHT: YAL-1A ABL PROTOTYPE IN FLIGHT, 1.5-M TELESCOPE, MEGAWATT-CLASS 1.3-μM LASER WITH UNDISCLOSED RANGE.	342
FIGURE 3.118.—MILLIMETER-WAVE BEAM FACILITY OPTICAL ARRANGEMENT.	343
FIGURE 3.119.—TOP: BEAM FACILITY COST BASED ON ASSUMPTIONS IN TABLE 3.37. BOTTOM: EFFECT OF CHINES AND GREATER SPILLAGE.	346

FIGURE 3.120.—TRL, RISK, AND UNCERTAINTY SUMMARY FOR THE MICROWAVE THERMAL ROCKET. FSM, FAST STEERING MIRROR; FADIS, FAST DIRECTIONAL SWITCH; KKV, KINETIC KILL VEHICLE; CVD, CHEMICAL VAPOR DEPOSITION; PSI, PRESSURE SYSTEMS, INC.; AND TPS, THERMAL PROTECTION SYSTEM. 350

FIGURE 3.121.—MICROWAVE THERMAL LAUNCH ROADMAP. 351

FIGURE 3.122.—LABORATORY DEMONSTRATION OF MICROWAVE THERMAL HEAT-EXCHANGE PRINCIPLE IN A 2.45-GHZ RESONANT CAVITY (REF. 12). SINGLE MULLITE THERMOCOUPLE TUBE WITH H₂ PROPELLANT. D_H , 1.19 MM; LENGTH OF TUBE, L , 36.6 CM; INLET POWER, P_{INLET} , 1.1 BARS; INLET REYNOLDS NUMBER, Re_{INLET} , 280; AND PEAK WALL TEMPERATURE, T_{WALL} , (1800 ± 100) K. THE END OF THE TUBE WAS DIPPED IN BRINE TO MAKE THE HYDROGEN PLUME VISIBLE. 352

FIGURE 3.123.—LEFT: THE 10-KW TEST STAND USES A LARGE PARABOLIC MIRROR TO CONCENTRATE THE ENERGY FROM A 20-KW TUNGSTEN LIGHT BULB ONTO A CREDIT-CARD-SIZED HX (YELLOW BOX). RIGHT: ALUMINUM PROOF-OF-CONCEPT HX, SOON TO BE ATTEMPTED IN GRAPHITE. SUCH SMALL CHANNEL SIZES AND A CREDIT-CARD SIZE ARE NECESSARY AT THIS POWER LEVEL. 353

FIGURE 3.124.—SCENE FROM THE 2009 SPACE ELEVATOR GAMES, WITH PRIZE MONEY PROVIDED BY THE NASA CENTENNIAL CHALLENGES PROGRAM. THE CONTAINERIZED, MOBILE, AND FLEXIBLE CONOPS WAS A GREAT SUCCESS. 355

FIGURE 3.125.—GODDARD’S PROGRESS IN ROCKETS AND ALTITUDE FROM 1925 TO 1936 SUGGESTS THE SCALE, TIMEFRAME, NUMBER OF TRIALS AND SUCCESS RATE AT WHICH A MICROWAVE THERMAL ROCKET MIGHT BE EXPECTED TO DEVELOP. EACH DATA POINT IS A LAUNCH ATTEMPT; SOME MORE SUCCESSFUL THAN OTHERS. 356

FIGURE 3.126.—THERMAL IMAGE OF THE ABL (RIGHT) ENGAGING A DUMMY TARGET (LEFT) GRAPHICALLY DEMONSTRATES THAT A SHAKY, SLEWING PLATFORM CAN LOCK ONTO AND TRACK A DISTANT TARGET ASCENDING TO ORBIT. WHAT IF THE UNCOOPERATIVE DUMMY WERE REPLACED BY A COOPERATIVE THERMAL ROCKET? HEL, HIGH ENERGY LASER; 357

FIGURE 3.127.—A SINGLE BEAM FACILITY SIZED FOR A 130-KM RANGE COULD, IN PRINCIPLE, ILLUMINATE A ROCKET THROUGHOUT THE ENTIRE ASCENT TRAJECTORY. THE AREAS WITHIN THE BEAM FACILITY RANGE ARE SHADED PURPLE, AND THE BASELINE ASCENT TRAJECTORY IS THE RED (LOWER) LINE. A KEY UNKNOWN IS THE MINIMUM PRACTICAL ELEVATION ANGLE AT WHICH THE BEAM COULD ACQUIRE THE ROCKET ON LIFTOFF (ALT, ALTITUDE). 359

FIGURE 3.128.—COMPARISON OF TAYLOR THEORETICAL EQUATION WITH EXPERIMENTAL DATA (REF. 13). 360

FIGURE 3.129.—PRESSURE VERSUS RF BREAKDOWN FIELD STRENGTH AT 2.4 GHZ (REF. 14). SOLID SYMBOLS DENOTE BULK AIR, AND OPEN SYMBOLS DENOTE WITH SURFACE. 360

FIGURE 3.130.—RESULTS OF BREAKDOWN MEASUREMENTS WITH A HOT WIRE IN THE PRESENCE OF GAS FLOW (REF. 15). 361

FIGURE 3.131.—LAUNCH TIME VERSUS RANGE OF INTERSECTING SATELLITE. EACH COLOR REPRESENTS A SINGLE DAY OF LAUNCHES (I.E., THE 8 DAYS ARE OVERLAID). THE NORTH AMERICAN AEROSPACE DEFENSE COMMAND (NORAD) SATELLITE ID IS LISTED ALONG WITH THE INTERSECTION DURATION AND RANGE. 362

FIGURE 3.132.—LAUNCH TIME VERSUS INVERSE RANGE SQUARED ($1/R^2$) OF INTERSECTING SATELLITE. EACH COLOR REPRESENTS A SINGLE DAY OF LAUNCHES (I.E., THE 8 DAYS ARE OVERLAID).	363
FIGURE 3.133.—PROBABILITY OF AN INTERSECTION HAPPENING IN EACH HALF HOUR PERIOD, OVER THE 8 DAYS.	363
FIGURE 3.134.—HISTOGRAM OF CLEAR LAUNCH WINDOWS—PERIODS THAT HAVE NO INTERSECTIONS. OVER THE 8 DAYS THERE WERE 29 PERIODS WITH MORE THAN 1 HR OF CLEARANCE.	364
FIGURE 3.135.—HISTOGRAM SHOWING THE DISTRIBUTION OF INTERSECTION MAXIMUM INTENSITY, I_{MAX} , DURING THE 8 DAYS. NOTE THAT MOST DAYS HAVE I_{MAX} LESS THAN 100 W/M ² (I.E., 8% OF SOLAR CONSTANT).	364
FIGURE 3.136.—HISTOGRAM OF THE MAXIMUM ENERGY INCIDENT ON A SATELLITE PER SQUARE METER DURING AN INTERSECTION. THIS WAS CALCULATED USING $I_{MAX} \times$ INTERSECTION DURATION.	365
FIGURE 3.137.—LAUNCH TIME VERSUS RANGE OF INTERSECTING SATELLITE. EACH COLOR REPRESENTS A SINGLE DAY OF LAUNCHES (I.E., THE 8 DAYS ARE OVERLAID). THE NORAD SATELLITE ID IS LISTED ALONG WITH THE INTERSECTION DURATION AND RANGE.	365
FIGURE 3.138.—LAUNCH TIME VERSUS RANGE OF INTERSECTING SATELLITE. EACH COLOR REPRESENTS A SINGLE DAY OF LAUNCHES (I.E., THE 8 DAYS ARE OVERLAID). THE NORAD SATELLITE ID IS LISTED ALONG WITH INTERSECTION DURATION AND RANGE.	366
FIGURE 3.139.—PROBABILITY OF AN INTERSECTION HAPPENING IN EACH HALF-HOUR PERIOD, OVER THE 8 DAYS.	366
FIGURE 3.140.—HISTOGRAM OF CLEAR LAUNCH WINDOWS—PERIODS THAT HAVE NO INTERSECTIONS. OVER THE 8 DAYS, THERE WERE 41 PERIODS WITH MORE THAN 1 HR OF CLEARANCE.	367
FIGURE 3.141.—HISTOGRAM SHOWING THE DISTRIBUTION OF INTERSECTION MAXIMUM INTENSITY DURING THE 8 DAYS. NOTE THAT MOST HAVE I_{MAX} LESS THAN 200 W/M ² (I.E., 15% OF SOLAR CONSTANT).	367
FIGURE 3.142.—HISTOGRAM OF THE MAXIMUM ENERGY INCIDENT ON A SATELLITE PER SQUARE METER DURING AN INTERSECTION. THIS WAS CALCULATED USING $I_{MAX} \times T$, WHERE T IS THE INTERSECTION DURATION.	368
FIGURE 3.143.—CONCEPTUAL TUG AND PROPELLANT STAGE. RCS, REACTION CONTROL SYSTEM.	434
FIGURE 3.144.—CONCEPTUAL TUG, PROPELLANT STAGE, AND GEO SATELLITES.	434
FIGURE 3.145.—HALF-SYMMETRIC (HS) AXICON MIRROR ANNULAR RESONATOR FOR POSSIBLE DPAL EMITTER.	435
FIGURE 3.146.—STARFIRE OPTICAL RANGE (SOR).	436
FIGURE 3.147.—30-METER-TELESCOPE (TMT). COURTESY TMT OBSERVATORY CORPORATION; USED WITH PERMISSION.	437
FIGURE 3.148.—TUG RENDEZVOUS WITH PROPELLANT AND GEO SATELLITES.	437
FIGURE 3.149.—LEO–GEO LASER TRANSPORT ORBITAL TRANSFER.	438
FIGURE 3.150.—LEO–GEO LASER TRANSPORT STOWED FOR LAUNCH.	439
FIGURE 3.151.—PROPOSED TECHNOLOGY ROADMAP.	441
FIGURE 3.152.—GRAPHIC REPRESENTATION OF BEPS DRM 3 TRANSFER TRAJECTORY FROM EARTH ORBIT TO JUPITER DIRECT TRANSFER ORBIT SHOWING PATH OF BEP ACCELERATION.	505
FIGURE 3.153.—DRAWING OF STOWED DRM 3 PROPULSION MODULE IN FALCON 9 FAIRING.	506

FIGURE 3.154.—DRAWING OF THE DRM 2 ORBIT RAISING-TUG SHOWING THE MAJOR VEHICLE SYSTEMS. THE PRIMARY REFLECTOR IS NOT SHOWN FOR CLARITY.....	508
FIGURE 3.155.—DRAWING OF THE DRM 3 EXPENDABLE PROPULSION BOOSTER SHOWING THE MAJOR VEHICLE SYSTEMS.....	508
FIGURE 3.156.—SCHEMATIC OF LASER TRACKING AND GUIDANCE SYSTEM.....	510
FIGURE 3.157.—DRAWING OF CRITICAL LASER ELEVATION, FLIGHT PATH ANGLE AND REFLECTOR ANGLE AT BEGINNING AND END OF JUPITER TRANSFER TRAJECTORY INSERTION BURN.....	511
FIGURE 3.158.—SEQUENCE OF OPERATIONS FOR DRM 3: BEP-ENHANCED GALILEO MISSION.....	512
FIGURE 4.1.—BEP EVALUATION SUMMARY. LEO TO GEO, LOW EARTH ORBIT TO GEOSYNCHRONOUS EARTH ORBIT; TRL, TECHNOLOGY READINESS LEVEL; OCT, OFFICE OF THE CHIEF TECHNOLOGIST; BAA, BROAD AGENCY ANNOUNCEMENT.....	515
FIGURE D.1.—BASELINE POWER BEAMING CONFIGURATION AND MTR DETAILS.....	575
FIGURE D.2.—MTR ALTITUDE, RANGE, AND ELEVATION ANGLE WITH RESPECT TO THE TRANSMITTER.....	576
FIGURE D.3.—CLEAR SKY ATMOSPHERIC SPECIFIC ATTENUATION AT CHINA LAKE, CA AND THE LLANO DE CHAJNANTOR OBSERVATORY IN THE ATACAMA DESERT, CHILE.....	577
FIGURE D.4.—CLEAR SKY ATMOSPHERIC ATTENUATION AT CHINA LAKE AND ATACAMA.....	577
FIGURE D.5.—POWER DENSITIES AT THE MTR FROM POWER BEAMING TURN-ON TO TURN-OFF AT (A) 95 GHZ, (B) 140 GHZ, (C) 170 GHZ, AND (D) 220 GHZ.....	578
FIGURE D.6.—JPL’S 1993 UPLINK PHASED ARRAY DEMONSTRATION (REF. 2).....	580
FIGURE D.7.—UPLINK ARRAY PHASED LOCKED LOOP SCHEMATIC AND RECEIVE SIGNAL STRUCTURE (REF. 2).....	580
FIGURE F.1.—PROPOSED EUROPEAN SPACE AGENCY LASER LAUNCH FACILITY (REPRODUCED FROM SOURCE 1).....	597
FIGURE F.2.—EXISTING LAUNCH SITES AROUND THE WORLD.....	598
FIGURE F.3.—AVERAGE ANNUAL NUMBER OF CLOUD OBSCURATION DAYS ACROSS THE U.S. (REPRODUCED FROM 2).....	599
FIGURE F.4.—MEAN MAXIMUM DAILY PRECIPITATION ACROSS THE U.S. (REPRODUCED FROM 2).....	599
FIGURE F.5.—ANNUAL MEAN DAILY AVERAGE TEMPERATURE (REPRODUCED FROM 2).....	600
FIGURE F.6.—POTENTIAL BEP GROUND COMPLEX LOCATIONS.....	600
FIGURE F.7.—ILLUSTRATION OF SPECULAR REFLECTION (REPRODUCED FROM SOURCE 4).....	603
FIGURE F.8.—ILLUSTRATION OF DIFFUSE REFLECTION (REPRODUCED FROM SOURCE 4).....	603
FIGURE F.9.—DIFFUSE REFLECTION NOMINAL HAZARD ZONE.....	604
FIGURE F.10(A).—MPE COMPARED WITH 3 M BEP EXPOSURE AS A FUNCTION OF DISTANCE.....	606
FIGURE F.10(B).—MPE COMPARED WITH 1 M BEP EXPOSURE AS A FUNCTION OF DISTANCE.....	607
FIGURE F.11.—INITIAL SAFETY ZONE COMPARISON WITH CONVENTIONAL ESTABLISHED FACILITIES.....	609
FIGURE F.12.—GEOMETRIC SAFETY ZONE COMPARISON WITH CONVENTIONAL ESTABLISHED LAUNCH FACILITIES.....	610

FIGURE F.13.—PLOT OF LAUNCH TIME AGAINST RANGE OF INTERSECTING SATELLITE. EACH COLOR REPRESENTS A SINGLE DAY OF LAUNCHES (I.E., THE 8 DAYS ARE OVERLAID). THE NORAD SAT ID IS LISTED ALONG WITH INTERSECTION DURATION AND RANGE.	611
FIGURE F.14.—PLOT OF LAUNCH TIME AGAINST $1/R^2$ OF INTERSECTING SATELLITE. EACH COLOR REPRESENTS A SINGLE DAY OF LAUNCHES (I.E., THE 8 DAYS ARE OVERLAID).....	611
FIGURE F.15.—PROBABILITY OF AN INTERSECTION HAPPENING IN EACH HALF HOUR PERIOD, OVER THE 8 DAYS.....	612
FIGURE F.16.—HISTOGRAM OF CLEAR LAUNCH WINDOWS—PERIODS THAT HAVE NO INTERSECTIONS. OVER THE 8 DAYS THERE ARE 29 PERIODS WITH MORE THAN 1 HOUR OF CLEARANCE.	612
FIGURE F.17.—HISTOGRAM SHOWING THE DISTRIBUTION OF INTERSECTION MAXIMUM INTENSITY DURING THE 8 DAYS—NOTE THAT MOST HAVE I_{MAX} LESS THAN 100 W/M^2 (I.E., 8% OF SOLAR CONST.).....	613
FIGURE F.18.—HISTOGRAM OF THE MAX ENERGY INCIDENT ON A SATELLITE PER SQUARE METER DURING AN INTERSECTION—THIS IS CALCULATED USING $I_{MAX} \times T$ INTERSECTION DURATION.	613
FIGURE F.19.—PLOT OF LAUNCH TIME AGAINST RANGE OF INTERSECTING SATELLITE. EACH COLOR REPRESENTS A SINGLE DAY OF LAUNCHES (I.E., THE 8 DAYS ARE OVERLAID). THE NORAD SAT ID IS LISTED ALONG WITH INTERSECTION DURATION AND RANGE.	614
FIGURE F.20.—PLOT OF LAUNCH TIME AGAINST RANGE OF INTERSECTING SATELLITE. EACH COLOR REPRESENTS A SINGLE DAY OF LAUNCHES (I.E., THE 8 DAYS ARE OVERLAID). THE NORAD SAT ID IS LISTED ALONG WITH INTERSECTION DURATION AND RANGE.	614
FIGURE F.21.—PROBABILITY OF AN INTERSECTION HAPPENING IN EACH HALF HOUR PERIOD, OVER THE 8 DAYS.....	615
FIGURE F.22.—HISTOGRAM OF CLEAR LAUNCH WINDOWS—PERIODS THAT HAVE NO INTERSECTIONS. OVER THE 8 DAYS THERE ARE 41 PERIODS WITH MORE THAN 1 HOUR OF CLEARANCE.	615
FIGURE F.23.—HISTOGRAM SHOWING THE DISTRIBUTION OF INTERSECTION MAXIMUM INTENSITY DURING THE 8 DAYS—NOTE THAT MOST HAVE I_{MAX} LESS THAN 200 W/M^2 (I.E., 15% OF SOLAR CONST.).....	616
FIGURE F.24.—HISTOGRAM OF THE MAX ENERGY INCIDENT ON A SATELLITE PER SQUARE METER DURING AN INTERSECTION—THIS IS CALCULATED USING $I_{MAX} \times T$, WHERE T IS THE INTERSECTION DURATION.....	616
FIGURE F.25.—MIGRATORY BIRD PATTERNS (REPRODUCED FROM SOURCE 6).....	618

Beamed-Energy Propulsion (BEP) Study

Patrick George and Raymond Beach
National Aeronautics and Space Administration
Glenn Research Center
Cleveland, Ohio 44135

1.0 Executive Summary

The official scope of this study was (1) to review and analyze the state-of-art in beamed-energy propulsion (BEP) by identifying potential game-changing applications, (2) to formulate a roadmap of technology development, and (3) to identify key near-term technology demonstrations to rapidly advance elements of BEP technology to Technology Readiness Level (TRL) 6. The two major areas of interest were launching payloads and space propulsion. More generally, the study was requested and structured to address basic mission feasibility.

The attraction of BEP is the potential for high specific impulse (I_{sp}) while removing the power-generation mass. The rapid advancements in high-energy beamed-power systems and optics over the past 20 years warranted a fresh look at the technology. BEP could help meet the known needs of NASA and/or the Department of Defense (DOD), providing low-cost, rapid access to space for operationally responsive military systems, scientific payloads, and the commercialization of space.

For launching payloads, the study concluded that using BEP to propel vehicles into space is technically feasible if a commitment to develop new technologies and large investments can be made over long periods of time. Such a commitment would include specific technologies like multimegawatt power lasers and microwave sources as well as building new launch facility infrastructure. The costs of the infrastructure are high. From a commercial competitive standpoint, if an advantage of beamed energy for Earth-to-orbit (ETO) is to be found, it will rest with smaller, frequently launched payloads.

For space propulsion, the study concluded that using beamed energy to propel vehicles from low Earth orbit to geosynchronous Earth orbit (LEO–GEO) and into deep space is definitely feasible and showed distinct advantages and greater potential over current propulsion technologies. However, this conclusion also assumes that upfront infrastructure investments and commitments to critical technologies will be made over long periods of time. BEP energy source requirements are much less than for the launch applications. Lower propulsion costs with shorter transit times for LEO–GEO servicing missions and faster science missions to the outer planets are the major benefits. The chief issue, similar to that for payloads, is high infrastructure costs.

Since cost (nonrecurring and recurring) emerged as a critical element of this study for both launch and space missions, the following should be noted. The cost estimate method used in this study was the same as is used by the NASA Glenn Research Center on all of its spaceflight projects, and the expert personnel involved in such estimates were employed for this study. Launch facility requirements were obtained by working with the NASA Kennedy Space Center, which has extensive experience with launch facilities. Per specific direction received at the final outbrief to the study's sponsors, independent estimates for the laser portions of the infrastructure were gathered from knowledgeable DOD personnel; their estimates of cost were considerably higher than the NASA Glenn estimate, that is, the Glenn cost estimate was nearly an order of magnitude too low. On the other hand, outside expert consultants to the study have stated their belief that the Glenn estimates were somewhat too high; the study's authors and the expert cost estimators believe that the consultants' estimates fail to include several elements of the necessary infrastructure.

It was hoped that beamed-energy technology would be a “silver bullet” solution to low-cost access to space and less-expensive deep space missions, or that at least it would find a niche where the benefits could be great. The authors of this report would like to make it clear that there are factors, as with all

studies, that, if the ground rules of the study change or if costs for critical elements (e.g., lasers, ground facilities) come down significantly, it follows that the conclusions could change.

As can happen in detailed examinations of innovative approaches, the study uncovered two unanticipated areas that appear to have great potential and therefore are worthy of consideration for new investment, at least at the “detailed study” level. BEP could provide the key to combining propulsion, power, and communications systems for in-space applications, thus creating a new class of small spacecraft with minimal systems and reducing their complexity, cost, and mass. Beaming energy to a thermal optical plasma engine could provide a highly efficient technology for high-thrust and high- I_{sp} space propulsion. The specifics of these concepts are provided in the main body of the report.

Finally, the intention of this study was to work within the time and resources allotted to determine the feasibility of BEP. This involved achieving a single closed-design solution for each mission analyzed which is, in all probability, not the optimum solution. As such, proponents of the investigated concepts may not agree with the study’s findings and final design solutions, citing that better performance could be achieved with additional design effort. The authors do not disagree with that perspective. Nonetheless, the study management team was satisfied that the results were sufficient to meet the primary objective, which was to prove or disprove the feasibility of the concept and missions. It is also noted that at this time all possible future demonstrations of beamed energy and power transfer will be pursued solely by NASA.

2.0 Study Synopsis

The following subsections summarize the detailed reports from the design analysis team, consultant team, and cost team, which appear in full in Section 3.0.

2.1 Study Background

In June 2010, NASA and the Defense Advanced Research Projects Agency (DARPA) agreed to co-fund this study to determine the feasibility of using beamed energy for propulsion. The reason for the study stemmed from a joint interest in the technology, but without a definitive in-depth review clearly stating the case. NASA’s main area of interest is in-space applications, and DARPA’s is for launch to LEO, although each organization has at least some interest in both areas. The study concluded in January 2011, with the Summary Presentation containing the basic results given on April 14, 2011.

2.1.1 Rationale

Since the early conceptualization/realization of the laser in the late 1950s, one of its theoretical applications has been to utilize photonic energy for wireless power transmission and propulsion. By the early 1970s, BEP was envisioned as a launch system using conventional gas-dynamic expansion of laser-heated propellant to accelerate payloads up to a ton into orbit, with the hot gas using a de Laval nozzle to produce thrust. Another early concept was the use of laser energy that was subsequently converted into electric energy for propulsion. This type of power transmission has been constrained primarily by the electrical-to-photonic conversion efficiencies at the laser source and the ability for a photovoltaic receiver device to efficiently reconvert the beam back to electrical energy at high levels of irradiance. Other limitations are described later in this document.

Since the 1970s, the continual development of low-cost, compact, and efficient high-energy sources and supporting optics has enabled a limited number of directed energy demonstrations. For example, in the late 1980s, under the Strategic Defense Initiative Organization (SDIO)-sponsorship, Prof. Leik Myrabo developed a laser-propelled vehicle concept envisioned to propel a 120-kg sensor payload using a 100-MW-class laser. At that time, a goal of \$100/kg was set. By the late 1990s, ambitious estimates of \$1000/kg for a 1- to 10-kg lightsat were being reported. Myrabo’s concept used a reflector on the underside of the vehicle to increase the intensity of the beam and produce a region of extremely high temperature. The result was a pulsed-detonation concept that propels the vehicle. This concept was validated with the Air Force Research Laboratory’s (AFRL’s) 10-cm Lightcraft flight test demonstrations

at White Sands in the late 1990s. In 2000, these flight demonstrations reached 233 ft and lasted 12.7 s. Succeeding this work was a 9-year effort including a scaled-up X-25LR bench model demonstration, and the X-50LR program, in which propellant and vehicle fabrication techniques were advanced through a series of successful test flights of a 50-cm laser ramjet vehicle.

In 2003 NASA demonstrated a sustained flight of an indoor aircraft by providing 7 W of power to the electrical system through 24 triple-junction photovoltaic cells with a near-infrared laser.

A more recent system demonstration concentrated on utilizing optical directed energy as a solution to provide power to space elevators ascending a composite cable, with the eventual desire to carry payloads into space. This was and is the fundamental premise of today's Spaceward Foundation's Power Beaming (Climber) Competition. The competition's recent success, LaserMotive's competitive system, was able to achieve a successful power transfer of several hundred watts to the climber over a distance of 1 km, to accomplish a climbing rate of 2 m/s.

Microwave technology has been used to demonstrate wireless power transmission. In 1975, the joint Jet Propulsion Laboratory (JPL)/Raytheon program at the Goldstone complex was able to achieve ground-to-ground system conversion efficiencies up to 84 percent at 30 kW at a range of 1 mile. Since then, flight demonstrations such as the Stationary High Altitude Relay Platform (SHARP) in Canada and the Phased Array Model Airplane Experiment in Japan have successfully demonstrated the high-efficiency benefit of microwave-power-beaming utilizing rectennas. This work has extended into endo-atmospheric applications, such as the successful firing of an "Ion Breeze" engine from a 6-kV rectenna, and orbital concepts, such as a space-based microwave power station to provide a boost to lightcraft ascending from LEO-GEO.

2.1.2 Previous Component Demonstrations

At the component level, recent advancements in both diode laser technology and high-energy vertical multi-junction (VMJ) photovoltaic cells allowed for significantly higher power optical systems to be demonstrated, such as the AFRL's high-intensity laser-power beaming program, which has demonstrated up to 20-W/cm² output at the receiver and 44-percent optical-to-electrical conversion efficiencies for recharging electric aircraft. This performance was achieved with nonoptimized commercially available components. Multikilowatt systems may be assembled by fiber-combining several diode sources. At this point in time, the end-to-end system efficiencies are around 10 to 15 percent, with the primary limitations residing in the diode laser efficiency (30 percent typical). Future advances in laser technology—fueled by an emerging market demand for high-power, highly efficient sources—and a refinement in chemical composition and antireflective coatings in the photovoltaic cells will continue to improve overall system performance.

In 2007, the NASA Goddard Space Flight Center demonstrated creating, modulating, and detecting x rays for communication applications, and this has implications for both power beaming and propulsion. The ability for an x ray to penetrate through hypersonic plasmas and exhibit narrow beamwidths because of their short wavelengths makes this an attractive region in which to operate in a point-to-point directed energy system. The potential applications for x-ray-directed energy may be limited to the space environment, because of high ionospheric attenuation. The concepts for x-ray power have grown from driving nanorobots to large 1-TW sources with 1-km apertures propelling a craft to circumnavigate the universe. Although large controllable x-ray sources do not exist today, the growing need for this technology beyond biomedical imaging will facilitate its development into higher output energies, which may eventually be used for power transmission and propulsion.

The attraction of BEP is the potential for high- I_{sp} while removing the power-generation mass. The rapid advancements in high-energy beamed-power systems and optics over the past 20 years warrant a fresh look at the technology and potential game-changing applications. For example, BEP could help meet the following known needs of NASA or DOD, providing low-cost, rapid access to space for operationally responsive military systems, scientific payloads, and the commercialization of space through

- Launch to Earth orbit of small selected payloads
- Stationkeeping at very low Earth orbit (DOD use—reconnaissance; NASA use—Earth observing)

- LEO–GEO transportation system
- Deep space exploration

2.1.3 Study Scope

The study scope was to review and analyze the state-of-art in BEP and to identify potential game-changing applications, formulate a roadmap of technology development, and identify key near-term technology demonstrations to rapidly advance elements of BEP technology to TRL 6. The study includes the following specific areas:

- ETO and space-to-space BEP
- Thermal propulsion using beamed power
- Electric (plasma) propulsion using beamed power
- Synergies of integrated systems (i.e., beamed power and the propulsion implications)
- Candidate technologies and solutions to achieve the reference missions (drawn from the categories of the electromagnetic spectrum: microwave, optical, and x ray)
- Trades to evaluate not only the directed-energy trades but also the various energy-conversion mechanisms from the beam into thrust
- Concepts defined to a level that will allow effective comparison of performance and operation costs with those of conventional combustion-based, self-contained fuel/oxidizer systems

2.1.4 End Goals of Study

Initial goals were established and later refined at the mid-term review to provide a more precise focus of the study. The following list provides the combined DARPA/NASA direction.

- Via analysis, prove or disprove the feasibility of ETO via BEP, or at a minimum provide significant new insights into the limiting performance factors of BEP technology, quantify efficiency losses, and analyze atmospheric and environmental considerations
- Identify synergies of BEP, if any, with crew servicing at GEO, horizontal launch access to space, and deep space exploration
- Identify a list of proposed ground-based and space-flight demonstrations
- Develop rough order-of-magnitude (ROM) nonrecurring costs for vehicles and ground systems
- Develop ROM vehicle and ground facility costs for recurring launches
- Investigate and analyze the effects of thermal blooming on laser and millimeter-wave propagation through the atmosphere
- Emphasize concepts utilizing and extending from high-TRL commercial lasers like diode-pumped lasers; descope concepts that require low-TRL lasers
- The primary product of this study needs to be a determination of TRLs for near-term concepts of beamed-energy technology and rocket vehicle technology in BEP

2.2 Study Approach

The study incorporated the use of Design Reference Missions (DRMs) to determine BEP feasibility. Having specific missions on which to focus allowed preliminary design efforts to be conducted at a high level, although not with a complete systems analysis, with the intention of including all aspects of aerospace design practices, including applying standard design margins. The approach was successful in exposing major and minor issues and allowed exploring potential solutions to arrive at closed designs for feasibility evaluation.

The study team consisted primarily of external experts selected for their depth of knowledge in the following fields: advanced propulsion technology, high-power microwave and lasers, continuous- and

pulsed-laser satellite pointing and tracking, and aerospace mission design. Experts from industry, the U.S. Air Force, and academia were included. Resumes of team members are shown in Appendix B. The full team worked together to create a set of DRMs that covered a wide envelope of applications.

The intention of this study was to work within the time and resources allotted to determine the feasibility of BEP. This involved achieving a single closed-design solution for each DRM, which is, in all probability, is not the optimum solution. As such, proponents of the investigated concepts may not agree with the findings and the study final design solutions, citing that better performance could be achieved with additional design effort. However, the study management team was satisfied that the results were sufficient to prove the feasibility of the technology.

Existing mission integrated-design-analysis teams were utilized to speed the process of mission design. Glenn’s Collaborative Modeling for Parametric Assessment of Space Systems (COMPASS) team was assigned to the launch DRMs and the LEO–GEO DRM. Goddard’s Integrated Design Center Mission Design laboratory team was assigned to the deep space DRM. In both cases, the assignments were based on previous experience with the type of mission, team availability, and cost. Both are multidisciplinary collaborative engineering teams whose primary purpose is to perform integrated vehicle systems analyses. Through these analyses, the teams conduct and provide system designs based on trades studies.

In order to narrow the trade space for the launching payload (laser) and space propulsion (space DRMs), an initial comparison was made between electric and thermal engines to determine which offered the best efficiency. Our results indicated that thermal engines would be the better choice. The details are shown in Figure 2.1 and were based on technology previously demonstrated at system and component levels in projects like Integrated Solar Upper Stage (ISUS) and High Delta-V (HiDVE).

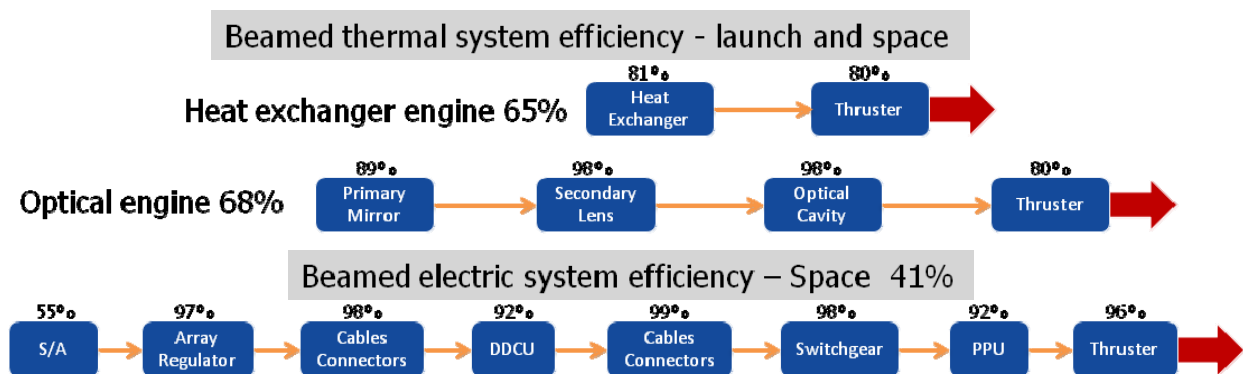


Figure 2.1.—Beamed thermal system efficiency—launching payloads and space propulsion. DDCU, DC–DC conversion unit; PPU, power processing unit.

The DRMs were selected and created during the first meeting with the consultants. The collaborative effort signified concurrence within the group that the technologies selected were indeed the major ones to consider and spanned the envelope of those available.

The cost estimates shown in this report represent the estimated “prime contractor” cost for each spacecraft based on Glenn’s COMPASS mission design team analysis. These estimates were generated at the subsystem and component levels using mostly mass-based, parametric relationships developed with historical cost data. Commercial costs also were estimated on selected DRMs as part of the trade space. These commercial estimates also were based on the COMPASS spacecraft design but were generated using PRICE System’s costing model. These estimates followed a methodology delineated by PRICE Systems for estimating commercial satellites with their software. A more detailed description and a list of cost assumptions for each of the various estimates are included in the individual reports. In addition, several lifecycle cost estimates were generated to evaluate the total cost of the technology over an assumed time horizon. The ground facilities necessary to beam energy proved to be the major cost driver in each case. The launch facility cost estimates are based mainly on data provided by the NASA Kennedy

Space Center and were adjusted to address each case. A detailed description of the lifecycle and facility costs is included with each DRM report.

2.3 Study Findings

This section brings together the information generated by the mission design teams, consultant teams, and cost teams in each of the major study areas.

2.3.1 Launch DRMs

Three launch concepts were selected for evaluation, each having unique characteristics that span the envelope of relevant current technologies. This was to ensure that the study touched potential areas offering opportunities to uncover promising technologies. The decision to limit the study to laser and microwave energy sources for launch was made by the management team during preliminary discussions with NASA experts at GRC and an extensive literature search. The energy from x-rays could be used for transmitting; however, the technology for developing high-power transmitters and receivers was considered to not be available for a long time in comparison to the other technologies.

2.3.1.1 DRM Envelope Selection and Definition

The first DRM created utilized laser optical technology. This technology was selected because it involved the options of a continuous or pulsed-laser source and the optical plasma engine utilizing air and water as propellants. Some of the related technology challenges (TRL 2 to 4) and resultant launch profiles are very tough to meet; however, the potential of very low vehicle mass made this concept a good candidate for investigation. The estimated payload range is 1 to 100 kg which, for example, could consist of six CubeSats plus support hardware totaling 40 kg. Ultimately, two vehicle sizes were studied. The first, a 120-cm-diameter unit, was based on previous studies. The second, a 35-cm-diameter unit, was studied to determine the characteristics and performance of a CubeSat-sized payload option (see Figure 2.2).

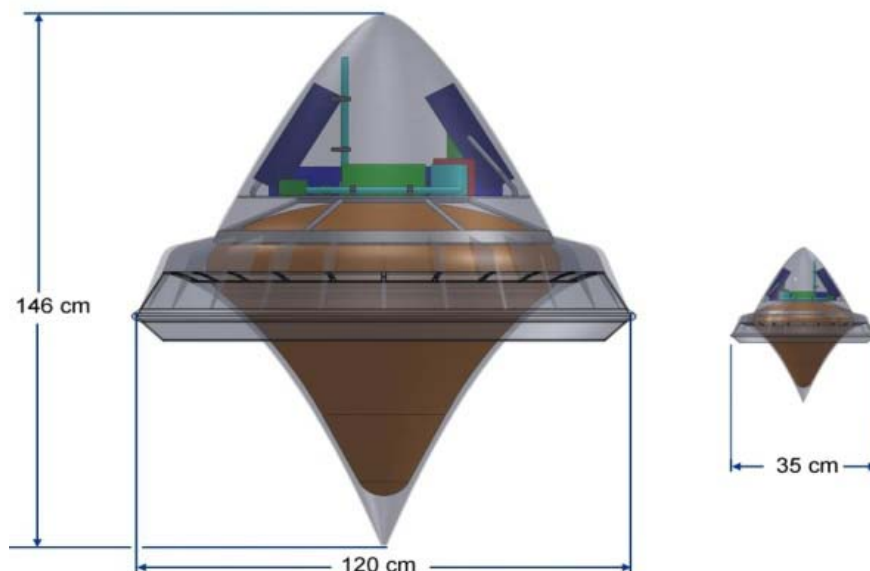


Figure 2.2.—Two sizes of laser optical vehicles studied.

The engine operates in air-breathing laser ramjet mode up to Mach 6 to 7 and an altitude of 35 km. Then it switches into rocket mode, whereupon H₂O is pressure fed to the 120-cm propellant injector ring for the remainder of the flight to LEO. As indicated in Figure 2.3, the entire vehicle aeroshell is designed to serve multiple structural- and propulsion-related functions. The axisymmetric nose/forebody serves as an external compression inlet in supersonic flight, precompressing air through a short annular slit into the engine “hot section.”

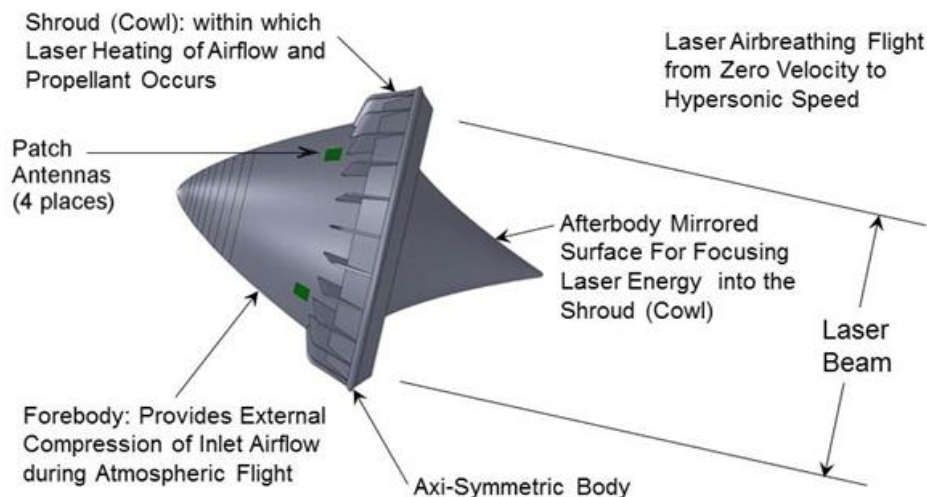


Figure 2.3.—Function of external surfaces in air-breathing propulsion mode.

A wealth of material exists on this technology because of the previous development and tests of Dr. Leik Myrabo, who was a part of the BEP study team. Dr. Myrabo was relied upon to provide details of the technology as it applied to this DRM. His previous analysis and tests on the lightcraft design provided the basis for use as a launch vehicle for 1- to 100-kg payloads. For this reason, this design was chosen as the first DRM and a good starting point for developing our missions. A full report is in Section 3.2.1 and covers two sizes of vehicles.

The second DRM was selected because it utilizes laser thermal technology. Dr. Jordin Kare agreed to be a consultant and team lead because of his years of experience and successful practical testing that used lasers to power a multitude of experiments. This application included a single-stage vehicle with a heat exchanger (HX) using liquid hydrogen (LH₂) and water powered by a continuous-wave (CW) laser. Payloads in the 10- to 100-kg range were estimated to be launched. A full report is shown in Section 3.2.2.1, Section 3.2.2.2, and Section 3.2.2.3.

The propulsion system operates by using a liquid propellant that is pressure-fed or pumped through an HX, which absorbs the laser energy and transfers it to the propellant, vaporizing it and heating it to high temperature. The hot propellant is exhausted from a conventional nozzle (Figure 2.4).

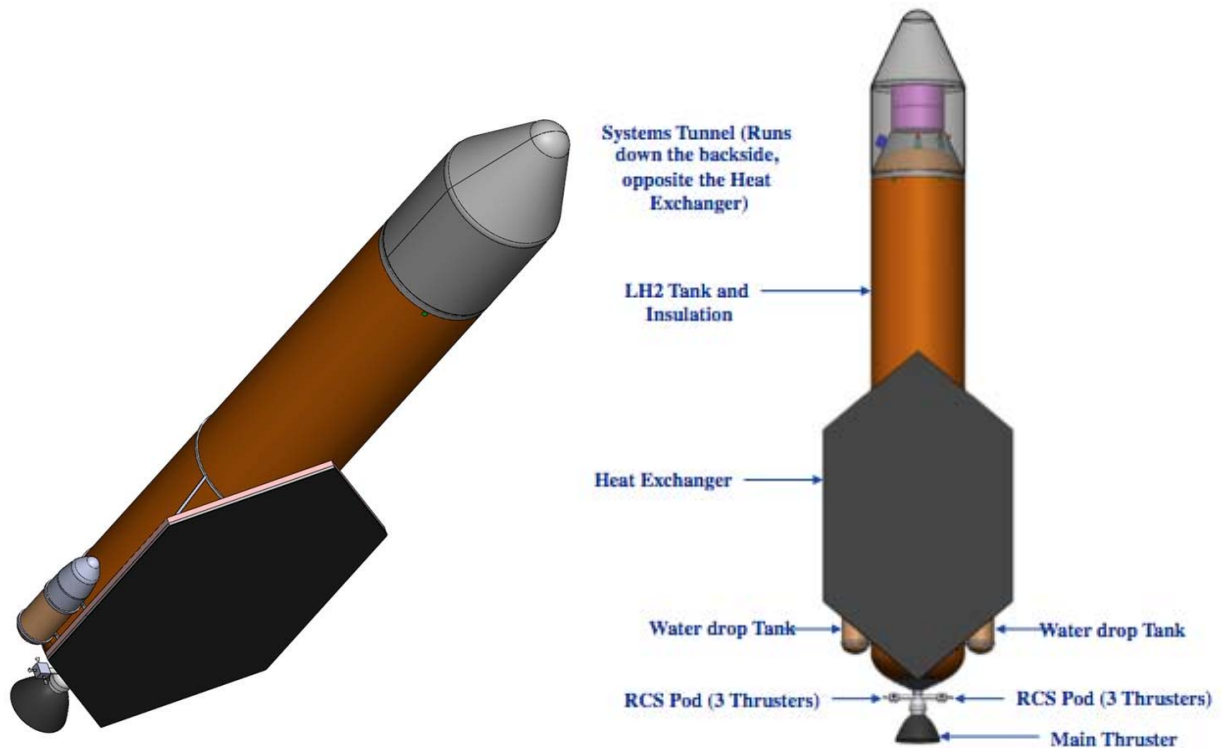


Figure 2.4.—Laser thermal vehicle. Laser thermal rocket configuration showing the laser receiver HX mounted on its side.

The third DRM featured a millimeter-wave source and an LH₂ thermal engine on a two-stage vehicle with a solid booster to enable orbit. The target payload range was 10 to 100 kg. Dr. Kevin Parkin headed this team because of his previous work on high-power transfer using millimeter waves and his recent work on building a 1-MW system for launching small payloads. A full report is shown in Section 3.2.3.1, Section 3.2.3.2, and Section 3.2.2.3. The operation of the propulsion system is similar to that of the laser thermal DRM, but the energy source is a millimeter wave and the HX material and configuration matches the source (Figure 2.5). Over the past 60 years, the time-average power output of high-power microwave sources in the key millimeter-wavelength range has increased by over 6 orders-of-magnitude, for the first time putting ETO launch within economic reach by using gyrotron technology. Today, a 1-MW gyrotron oscillator can be purchased for about \$2M. By combining the output of many such oscillators, the power and spot size needed to propel a vehicle to orbit are possible.

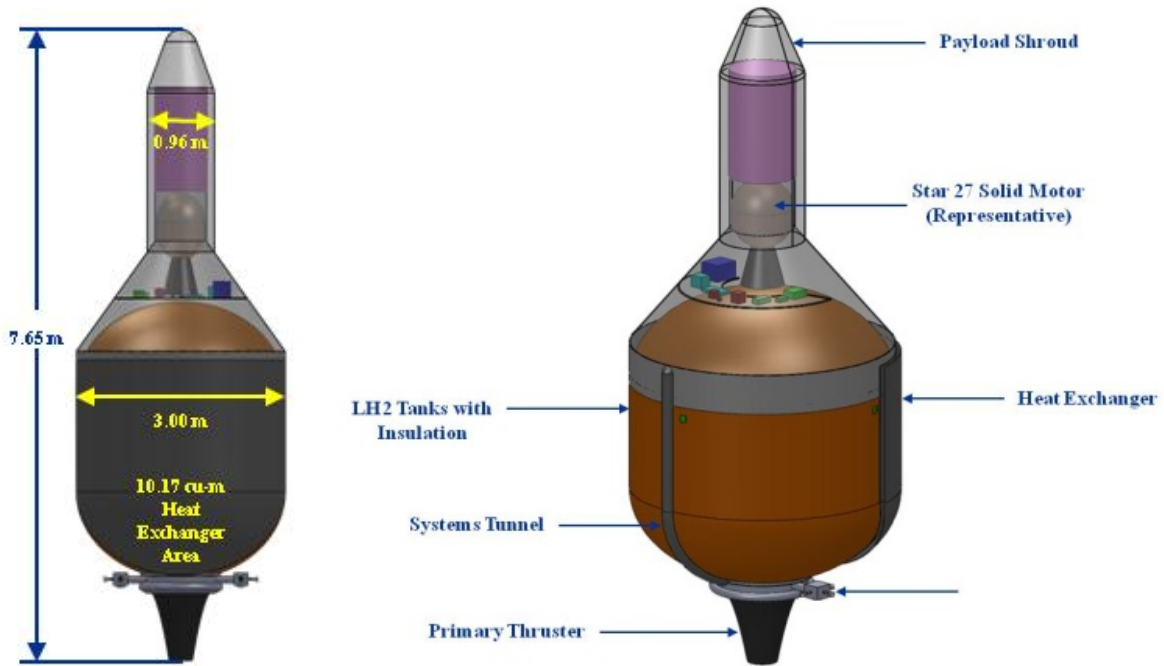


Figure 2.5.—Millimeter-wave thermal DRM. Millimeter-wave thermal rocket configuration showing a circumferential receiver HX.

Central to the microwave thermal rocket is a microwave-absorbent HX covering the underside of the vehicle. The refractory HX bypasses the specific enthalpy limits of conventional combustion, imparting 30 to 40 MJ/kg of H_2 propellant as opposed to 16 MJ/kg for conventional hydrogen peroxide (H_2/O_2) combustion. This higher specific energy halves the propellant flow rate needed to produce a given thrust and reduces the total propellant needed to put a given dry mass into orbit by a factor of 3.

The downside to an LH_2 thermal rocket is the relatively low density of hydrogen, making the tank and turbopump larger and heavier than for dense propellants. The larger tank adds to the drag losses of the vehicle, requiring extra propellant to compensate.

2.3.1.2 DRM Evaluation Method and Comparisons

Each DRM was designed by defining the necessary subsystems, conducting trades, examining various options to achieve a launch profile to the required orbit altitude, defining an operational procedure, and analyzing costs. The subsystems included thermal, power, communications and data handling (C&DH), navigation and control, structure, propulsion, mechanical systems, and vehicle configuration.

For a reference point of feasibility, the Pegasus XL/ORBCOMM (Figure 2.6) was selected as an existing launch/payload operation. It was the closest comparable system found, but is not directly applicable, so allowances must be made when making comparisons. The Pegasus XL (Figure 2.7) can carry a payload up to 420 kg, is air launched from 40,000 ft, and uses three stages to orbit. The ORBCOMM satellite has been optimized to fit eight units into the Pegasus XL available mass and volume limitations. Each satellite costs \$1.2M and has a mass of 40 kg.



Figure 2.6.—ORBCOMM spacecraft. Courtesy of Orbital Sciences Corporation; used with permission.

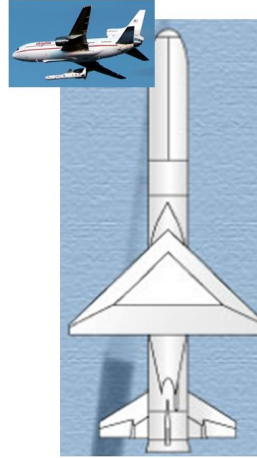


Figure 2.7.—Pegasus XL.

Figure 2.8 compares the sizes of the vehicles. It clearly shows that the laser optical vehicle is much smaller. Other figures of merit (FOMs) are shown in Table 2.1. All DRMs require two beaming sites to provide sufficient energy to the vehicle to achieve orbit altitude.

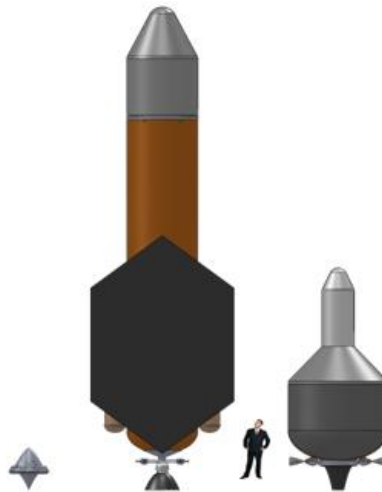


Figure 2.8.—Launch vehicles compared by size.

TABLE 2.1.—OTHER FOMS FOR THE DRMs

FOM	Laser Optical	Laser Thermal	Millimeter Wave Thermal
Payload mass	40kg	80kg	40kg
Wet mass	332kg	5415 kg	2153 kg
ISP	985 s	785 s	760 s
Thrust/mass	233	29	13
Max launch Power (output)	Laser 350 MW Cont./ 1 GW Pulsed	Laser 240 MW	Millimeter Wave 600 MW
Stage to orbit	1	1	2
Propellant	Air/H ₂ O	LH ₂ /H ₂ O	LH ₂ /Solid

2.3.1.3 Energy Source Facilities

All three missions utilize three facilities; a control center where the launch vehicle and payload are assembled and readied for launch; a “boost” beaming station for the primary source that takes the launch vehicle to high altitude; and a “main” beaming station that provides the energy to take the vehicle to orbit. Some variations exist among the missions because of their different technologies. The following subsections briefly outline their differences. For a detailed description, see Section 3.0 for the individual COMPASS reports and consultant reports.

2.3.1.3.1 Laser Optical Ground Facilities

The laser optical ground facilities for the 120-cm vehicle have a combined boost station/vehicle assembly building since the laser beam has to be placed under the vehicle. The boost laser consists of a continuous or a pulsed 140-MW (Figure 2.9) output laser constructed of up to 2900 (continuous or pulsed), 120-kW commercial-off-the-shelf (COTS) modules. Two options exist for the “main” laser: (1) a ground system of up to 7250 COTS lasers (20 kW each) or (2) a space-based relay station that utilizes the boost laser facility.

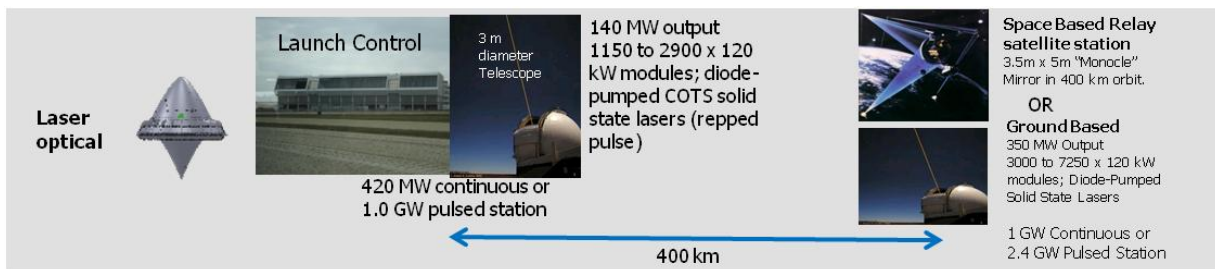


Figure 2.9.—Configuration of laser optical ground facilities.

Only one ground facility is required for the 35-cm craft with a CubeSat payload. The beam is redirected from a vertical arrangement for the boost phase to a tiltable mirror used for the main phase. The source requires only 96 beamlets (12 kW each) for total of ~12-MW of power output. Laser pulsing is in the kilohertz range for efficient air-breathing engine performance: for example, 96 beamlines at 60 Hz each = 5760 Hz, which falls in the viable range. Note that only with pulsed lasers can a “temporal” approach to beam-combining be realized, wherein all beamlines are fired sequentially like a “Gatling” gun onto a rotating mirror that efficiently shepherds pulses into a single 3-m telescope. With 60-Hz beamlines, the mirror must rotate at 3600 rpm (Figure 2.10). The ring-mirror diameter is set by the 96 adjacent turning flats positioned around the ring, each sized at 25 by 25 cm. These flat mirrors would be remotely adjusted with servodriven, three-axis mirror mounts to precisely target the on-axis rotating mirror.

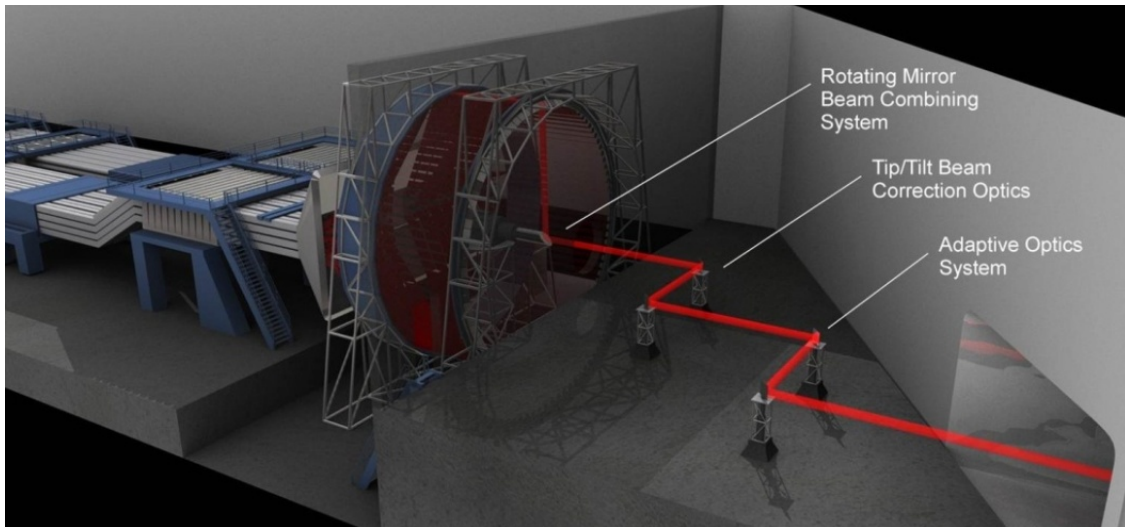


Figure 2.10.—Concept for beam-combining system with central rotating output mirror.

2.3.1.3.2 Laser Thermal Ground Facilities

The laser thermal boost station is located 20 km down range from the launch site to allow energy to be transmitted to the vehicle in the initial part of the ascent. The main station is located 400 km down range from the boost site, as shown in Figure 2.11.

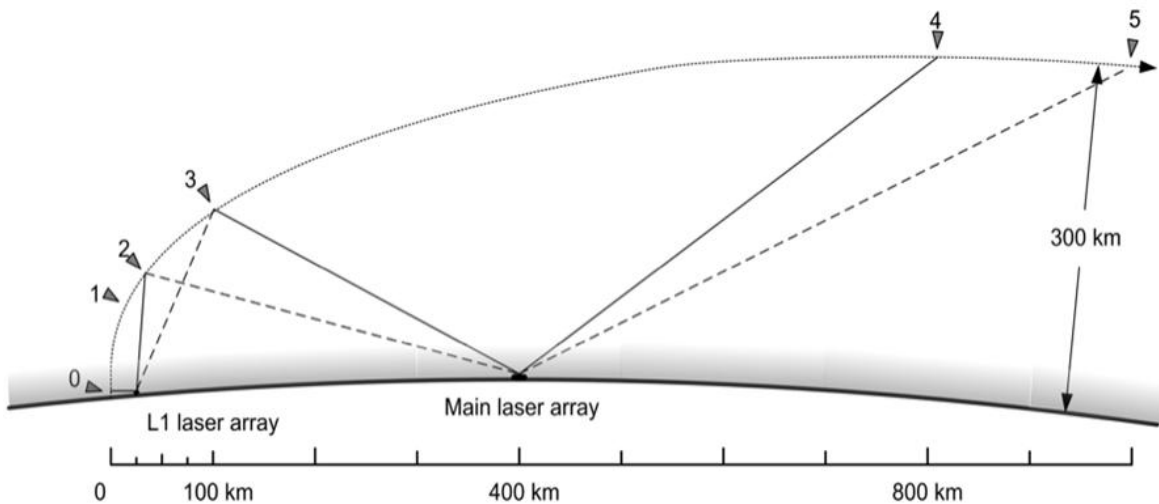


Figure 2.11.—Typical launch concept of operations with L1 (boost) laser array. Markers: (0) Launch. (1) Main array “sees” vehicle and begins tracking. (2) Main array turns on; L1 array at maximum full-power range. (3) Main array at full power; L1 array.

The vehicle launch site is where the vehicles actually leave the ground. The launch site will include at least one launch tower along with auxiliary equipment for handling vehicles, payloads, and propellant. The boost, or L1, laser site will provide laser power to the vehicle for its initial launch and climb from the launch site through the atmosphere, until the vehicle is high enough to receive power from the main laser.

Currently available laser sources have been selected to eliminate development of single high-powered lasers (Figure 2.12). However, the arrangement and control of the many low-powered laser modules is only at a concept stage, although this is seemingly fairly straightforward.

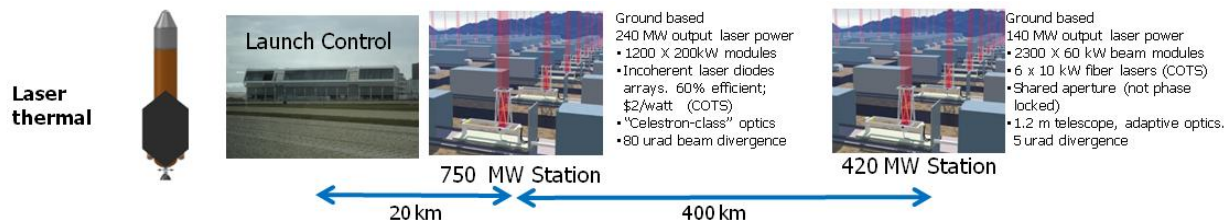


Figure 2.12.—Configuration of laser thermal ground facilities.

The boost laser site will have a layout generally similar to the main laser site, with hundreds to a few thousand modules installed over an area on the order of 1 km² (possibly less, if land area is limited). Each module will be largely independent, with its own power supplies, tracking, and so forth. The laser power and aperture area per module are not yet defined, but a plausible configuration might use 20-kW diode array assemblies, each with its own ~1-m mirror, mounted in groups of 10 on a common elevation mount. Because the boost laser needs to point at, or very close to, the horizon in one direction, but only slightly past the zenith in the opposite direction, the boost laser array should be built on a slope facing the launch site. The altitude of the boost laser array is somewhat less important than that of the main laser array (because when the vehicle is at maximum range for the boost laser, it is also near zenith and atmospheric effects are minimized). It may be desirable to put the boost laser array slightly below the launch-site altitude (if the intervening terrain is lower still) so that even at launch, the beam would never be aimed to intersect the Earth’s surface (i.e., it would always point at least slightly upward).

The main laser site is the heart of the launch system and consists of an array of beam modules— independent lasers with small beam directors and tracking systems—with a total output power (for the DRM baseline system) of ~140 MW. It is typically several hundred kilometers downrange (east) of the launch site, so that the vehicle trajectory passes over the main laser near the midpoint of its trajectory.

2.3.1.3.3 Millimeter-Wave Thermal Ground Facilities

The millimeter-wave thermal ascent trajectory consists of two segments: In the first (Figure 2.13), the vehicle is powered by a short-range “boost” beam facility, maintaining vertical ascent of the rocket at 40% throttle to minimize drag losses. The first segment transitions to the second at an altitude of 30 to 60 km. In this time, the “boost” beam facility hands the rocket over to the “main” or “sustain” beam facility as the rocket levels off and begins to accelerate horizontally at 100% throttle. The acceleration of 9g to 19g during this segment of the ascent raises the velocity from 1.5 to 8 km/s in only 60 s and enables the rocket to achieve orbital velocity within the 125-km range of the beam source (Figure 2.14). This minimizes the initial cost of the beam facility and could eventually be expanded to allow a gentler ascent trajectory suitable for human launch (Figure 2.13).

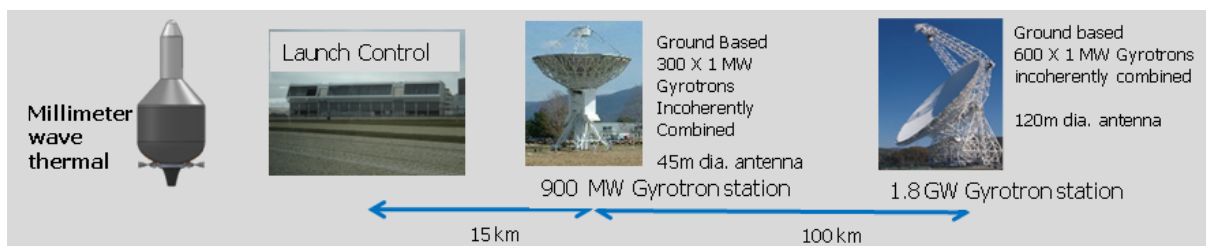


Figure 2.13.—Configuration of millimeter-wave thermal ground facilities.

Although the 1990s-era Green Bank Telescope aperture is about the right size for application to a millimeter-wave thermal rocket, it is the current era of closed-loop active surfaces that provide the necessary surface accuracy. Surface accuracies now exceed those needed for the microwave thermal rocket by nearly an order of magnitude, albeit for smaller apertures. The key question to answer in a beam facility conceptual design will be what combination of structural rigidity and active surfaces can correct for changing gravitational distortions and mechanical bending modes as the structure slews; sudden thermal deformations can be negated using heaters. If greater mechanical stiffness is required, there are Fresnel reflector and even holographic techniques that would be unsuitable for astronomical work but might be advantageous for beam direction, provided they turn out to be compatible with the spectral beam-combining approach used in the optical back end.

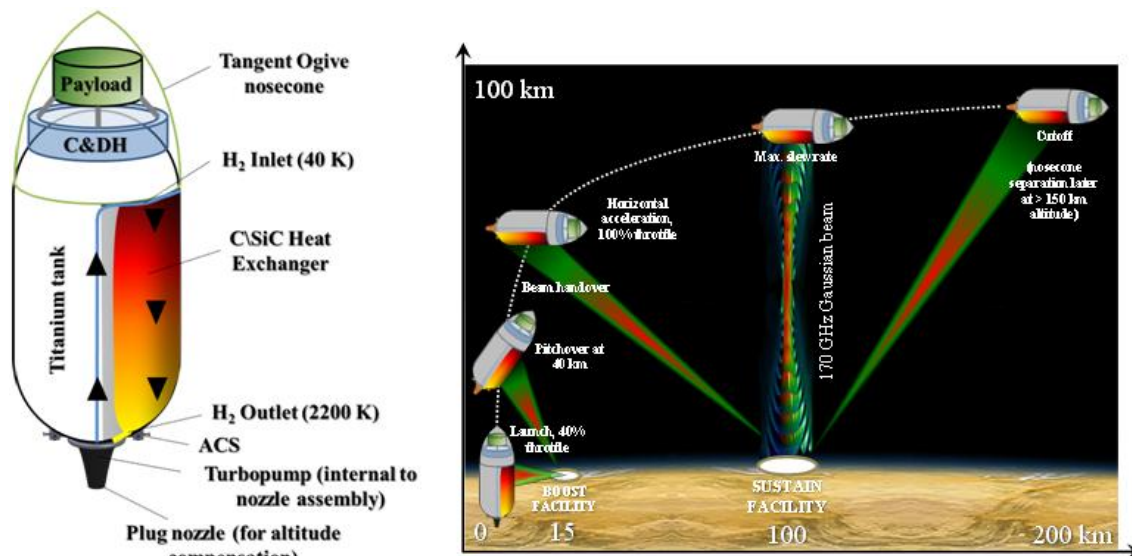


Figure 2.14.—Millimeter-wave thermal launch system and ascent trajectory.

2.3.1.4 Costs

Table 2.2 shows the nonrecurring and recurring costs for the launch vehicles. The costs were determined during the 2- to 3-week mission design process—a very intense exercise that made a fair set of assumptions. As a result, the cost estimates are at the top level but are sufficient to expose any major issues. A list of what is and is not included in the estimate is in the full reports in Section 3.2.1.3, Section 3.2.2.3, and Section 3.2.3.3. The most noteworthy assumption is that the estimates do not include the costs for technology development.

The nonrecurring costs are for design, development, testing, and engineering (DDT&E). The recurring cost is for the first unit produced using government-based cost models. Realizing that DDT&E government costs would be high in comparison to a commercial venture, we processed the estimates through a commercial model. As expected, the costs were lower and give some idea of what the differences could be between government and commercial approaches. A proportionate drop in cost was seen using both models after a number of vehicles were produced.

Table 2.2 shows the estimated ground facility nonrecurring and operating costs for each mission. The nonrecurring costs were based on a costing model used by Kennedy to estimate the construction of their facilities. The beaming-source costs were provided by the respective consultants using estimates based on current technologies. Ground operations costs were based on 360 launches per year. This number was chosen to represent the existence of a market for the launch capabilities so that an operations cost per launch could be determined.

TABLE 2.2.—NONRECURRING AND RECURRING COSTS FOR LAUNCH VEHICLES

Vehicle	Non-Recurring Cost (\$M)	Recurring Cost (First Unit) \$M	Commercial (First Unit) \$M
Laser Optical DRM 1-A	63	15	5
Laser Thermal Rocket DRM 1-B	126	35	13*
MM Wave Thermal Rocket DRM 1-C'	110	28	11*

Vehicle	Ground Facility Non-Recurring Cost (\$B)	Ground Operations Yearly Cost 360 Launches/yr(\$M)
Laser Optical DRM 1-A	5	240
Laser Thermal Rocket DRM 1-B	6.7	330
MM Wave Thermal Rocket DRM 1-C	5.7	285

2.3.1.4.1 Cost Variation

In order to obtain a sanity check on the cost estimates for the launch facilities, two efforts were undertaken. First, knowledgeable personnel from the Directed Energy Directorate at Kirtland Air Force Base in New Mexico, where the Starfire Optical Range (SOR) is based, were contacted to obtain information on the cost to build the facility. Data on the cost of the laser and the optics used for imaging and identification of space objects is limited. However, the authors were directed to two reports that contain estimates of megawatt-class laser systems. Both “New Concepts for Space-Based and Ground-Based Laser Weapons” and “A Preliminary Assessment of the Potential Cost and Cost-Effectiveness of Space Based Weapons” were used as a reference for facility costing. The cost estimates in the reports were determined to have low fidelity such as no factor for scaling or taking into consideration the cost reduction as the number of lasers increased. The facility estimates range from \$165/W to \$1070/W.

The second effort to get a better estimate on facility costs involved discussions with a major defense contractor with many years of expertise in building lasers. Although this input was voluntary, per study guidelines, it was felt to be more accurate than other sources. Their estimate, which was based on a description of the application and the energy required, was \$250/W.

This study’s facility cost estimate was \$28/W, which is a dramatic difference from both of the preceding estimates. The difference is explainable by the assumed cost of the laser source used in each case. This report optimistically took into account a number of what the authors believe to be realizable factors, such as the likely increases in laser power over the next 10 years as well as the associated cost reduction due to a gradually increasing commercial demand. This approach takes advantage of using hundreds of smaller powered lasers versus single large units, drastically reducing the nonrecurring costs and individual laser costs. Figure 2.15 shows an anticipated laser power level development versus cost.

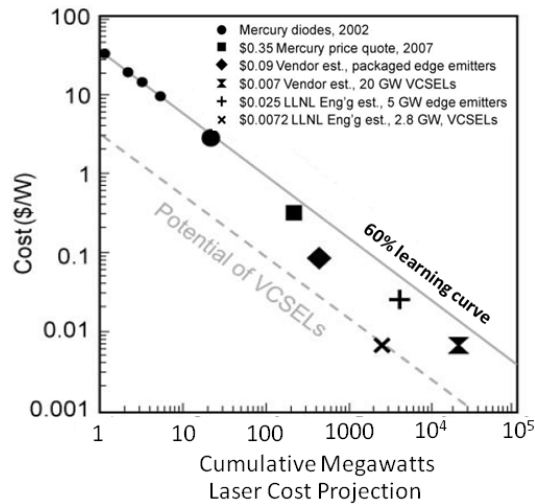


Figure 2.15.—Laser power level versus cost. Kare Technical Consulting, used with permission.

Using a large number of lasers creates the additional problem of combining a large number of beams, but this is taken to be an achievable engineering challenge via fiber optics rather than a technical barrier. Details of this methodology and the cost for a launch system can be found in the 2006 paper by Jordin Kare and Kevin Parkin, both consultants on this study, “A Comparison of Laser and Microwave Approach to CW Beamed Energy Launch.” They reported that a 100-MW laser system would cost \$24/W and that a 250-MW microwave system would cost \$22/W. Adding in the cost for land, buildings, and other infrastructure, the study cost of \$28/W falls in line.

The two referenced “external” estimates indicate that the study cost data could be off by at least a factor of 10 on the ground facility costs. If our assumptions are incorrect and the reference estimates are correct, take our laser costs (68% of total) and multiply them by 10. This yields \$207/W versus our original estimate of \$28/W. It is probable that the correct value lies somewhere between the two and that it would depend on the rate of higher power laser development and commercial demand. However, for the purposes of this study, whose goal was to prove feasibility, the conclusion that infrastructure costs would be too high to make this economically feasible at this time still holds. The higher costs from the other sources cited here would only exacerbate the problem and makes the conclusion stronger.

2.3.1.5 Risks and Issues

The following subsections discuss a set of risks and issues with the proposed launch methods. These are intended to express the challenge to be overcome for success.

2.3.1.5.1 Laser Optical

The main risk with the thermal system components pertains to the laser reflectors and the plasma degradation of the mirror and heat transfer during ascent (Figure 2.16).

Any damage or degradation to the mirrored surface experienced during launch can cause excessive local heating because of the intensity of the laser beam (approximately 3000 W/cm²). Debris impact, or erosion from the nearby plasma can potentially degrade the mirror reflectivity, which would cause catastrophic heating and loss of the vehicle. The very high reflectivity of the mirror (99.99%) must be maintained throughout the launch phase.

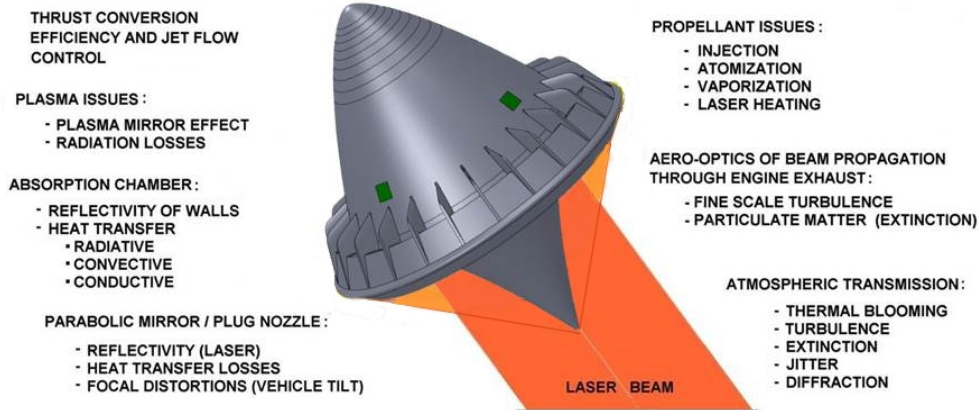


Figure 2.16.—Laser optical issues.

If the plasma gets within a few centimeters of the mirror surface, there could be excessive heating. The mirror surface is not as reflective in the frequency in which the plasma will be radiating. Therefore, it can absorb significant amounts of heat if the plasma moves too close to the mirror surface. Depending on the distance of the plasma from the wall, heating can range from 20 to 80 W/mm².

Laser light scattered off of the reflective shield can potentially be reflected back to Earth. This could be a health hazard to someone who inadvertently looks into the reflected beam. The power of the reflected beam that reaches the Earth's surface will depend on the curvature of the shield mirror's surface and the distance from the Earth. The higher the shield curvature, the greater the laser light dispersion and, therefore, the lower the intensity of the reflected beam. To reduce this risk, developers would need a diffuse reflecting surface. A mirrored surface that has conical reflecting surfaces etched onto it may be able to disperse the incoming laser perpendicular to the incoming beam, limiting the reflection back toward the surface.

2.3.1.5.2 Laser Thermal

The main risk with the thermal system concerns the operation and structural integrity of the HX, which is to achieve the required heat transfer capabilities, designers made the HX walls very thin. This thin-wall construction could cause significant structural problems because of the various loadings that the HX will experience. These include

- Aerodynamic loading during ascent
- Thermal stresses due to the large temperature variations encountered during the launch
- The temperature gradient experienced across the HX during operation
- The high internal pressure due to the heating and expanding hydrogen gas

The operational feasibility of the HX concerns the ability to transfer the required amount of laser energy to the hydrogen gas and the ability to construct the HX to provide the flow characteristics needed to achieve this heat transfer.

A simplifying assumption made during the analysis was that the dividing walls between the fluid passages of the HX were operating at the same temperature as the HX surface. This assumption is very optimistic. Under actual conditions, this inner wall will be at a temperature gradient less than that of the surface. Further, more detailed analysis should be performed to determine what the temperature gradient is and what effect it will have on the HX operation.

The HX design utilized a complex manifold that brought in the cool hydrogen gas and collected the hot hydrogen gas at spacing of 15 cm over the total area of the HX. This complex manifold arrangement and the subsequent heat losses associated with it need to be analyzed in much greater detail to assess the feasibility of the design.

2.3.1.5.3 Millimeter-Wave Thermal System

The main risks with the thermal system are similar to those described in Section 2.3.1.5.2. The operational feasibility of the HX concerns the ability to transfer the required amount of microwave energy to the hydrogen gas and the ability to construct the HX to provide the flow characteristics needed to achieve this heat transfer. Convective heat transfer coefficients of greater than 14,000 were required. These were calculated to be theoretically possible on the basis of the flow conditions. However, a more detailed analysis and experimental work would be required to determine if this level of heat transfer is truly possible.

2.3.1.6 Summary of Launch Mission Findings

The technical feasibility evaluation factors selected for all missions included a complete closed-design solution, a defined basis for technology and technology improvements, designs that include allowable margins for mass, engine performance, and thermal and structural subsystems. All three missions were able to achieve feasibility, although some particular tough challenges lie ahead for all because of high infrastructure costs (Table 2.3) and because some key technologies are at low TRLs, especially with the optical laser option.

TABLE 2.3.—LAUNCH VEHICLE AND INFRASTRUCTURE COSTS^a
[MM, millimeter.]

All Costs in FY11\$	Launch Vehicle				Beam Source Infrastructure					
	Type	Payload Mass	Gross Take Off Mass	Recurring Cost	Non-Recurring Cost (\$M)	Type	Input Power	Output Power	Non-Recurring Cost (\$B)	Operations Cost (\$M) 360 Launches /yr
Existing: Air Launched at 40,000 ft Pegasus XL	420 kg	Vehicle launch mass 23130 kg	\$22M	N/A	N/A	N/A	N/A	N/A	N/A	N/A
Optical Laser (6 cubeSat's or 1 integrated s/c)*	40kg	335kg	\$15M	\$63M	Laser	Two Sources 420MW & 1 GW	Two Sources 140 MW & 350 MW	\$5	\$240	
Thermal Laser	80 kg	5337 kg	\$35M	\$126M	Laser	Two Sources 750 & 420 MW	Two sources 240 & 140 MW	\$6.70	\$330	
Thermal MM Wave	40 kg	2153 kg	\$28M	\$110M	Millimeter Wave	Two Sources 900 MW & 1.8 GW	Two Sources 300 & 600 MW	\$5.70	\$285	

^aLaunch vehicle cost assumptions: (1) Prime contractor costs (no fee), (2) No technology development costs, (3) Protoflight development approach, and (4) Before reserves, insight/oversight, launch services.

A game-changing technology evaluation criteria defined by the NASA Office of the Chief Technologist (OCT) is “Technology that is innovative, unique and promises to enable revolutionary improvements to the efficiency and effectiveness of our country’s space capability.” The study interpreted this for launch missions as reusability, improved payload mass fraction, improved mission capability (like an increase in available operations time), and providing a new method for access to space. As can be seen in the comparison table (Table 2.3), the air-launched Pegasus XL/ORBCOMM combination is difficult to beat in most of the areas, such as the cost for getting payload to orbit. However, the launch missions

studied excel in the future capability to enable revolutionary access to space. Using high-powered lasers or millimeter waves to send payloads into orbit is definitely a new way of launching. This technology is in its early phase of development, and investments could lead to increases in performance and reduced costs. These benefits, with the added possibility for other uses of the beaming station like orbital debris removal, makes each of the technologies game-changing.

Although economic viability could be considered to be a game-changing factor, the study anticipated that it was so important that it was deemed to be worthy of its own category. Its evaluation factors were lower vehicle costs (\$/kg); lower launch facility operation costs like range safety, vehicle preparation and handling, and infrastructure costs. This area was the biggest challenge for all of the launch missions. Launch vehicle recurring costs in comparison with the selected point of reference Pegasus XL/ORBCOMM could be debated. The costs are in the same range, but this is not a good comparable mission because the designs have been optimized and the vehicles can launch to a variety of trajectories. Facility operations costs were based on a standardized proportion of the facility costs for a potential market for launching 360 flights per year, so determining the facility costs will play a large role in economic viability. Because there are common needs for all three missions—land needed for buildings, range safety, security, transportation accessibility, and electrical power lines—the major differencing factor was the beaming-source costs. However, the total costs for all missions were considered to be nonfeasible because of the extremely high infrastructure costs.

It was determined that all three missions have technical feasibility. Achieving game-changing viability would rely on large investments of funds to develop the technologies required. None of the missions were able to meet the economic requirements for feasibility. Therefore, the overall evaluation of this study was that utilizing beamed-energy for launching small payloads into orbit is not feasible.

2.3.2 Space Design Reference Missions (DRMs)

The mission analyses for the space DRMs were scheduled and configured to take advantage of the analysis and lessons learned from the launch DRMs. An ETO launch power requirement, estimated in previous studies at 1 MW/kg, was used as an early gauge to decide on the maximum satellite size to be addressed in this study. In addition to the power requirement, the potential atmospheric affects at high power levels led to the decision to limit the ETO launch to microsatellites or smaller CubeSats. Thus, the initial maximum power expected for the ETO application was estimated at 100 MW or less. To take full advantage of the launch facilities' potential for the space applications, the BEP team chose a LEO–GEO reusable tug as the first space DRM. This decision led to a synergistic relationship for a deep space DRM that would utilize the ground facilities, as well as the LEO–GEO tug design and analysis. The following subsections provide a synopsis of the space DRMs, with pointers and references to the mission designs and analyses.

2.3.2.1 LEO–GEO DRMs

2.3.2.1.1 Vehicle Description

The beamed-energy tug propulsion stage shown in Figure 2.17 is 5.78 m long and cylindrical, consisting of a 4.0- by 5.6-m elliptical primary reflector cantilevered off the side of the vehicle on a $\pm 60^\circ$ gimbal. Two degrees of freedom will be required to track the ground-based emitter, and either the entire vehicle will be rolled during a burn or another degree of freedom will be added to the gimbal (although a two-degree-of-freedom gimbal creates complications because the rotation does not occur about the focal point). The secondary reflector will be fixed. Both reflectors and shielding to protect the entire vehicle from the laser flux will be 97%-efficient, 0.9999 reflective carbon-fiber composite. A 1.5- by 3.3-m solar array will supply 560 W of nominal operating power, and a 2000-W-hr lithium-ion

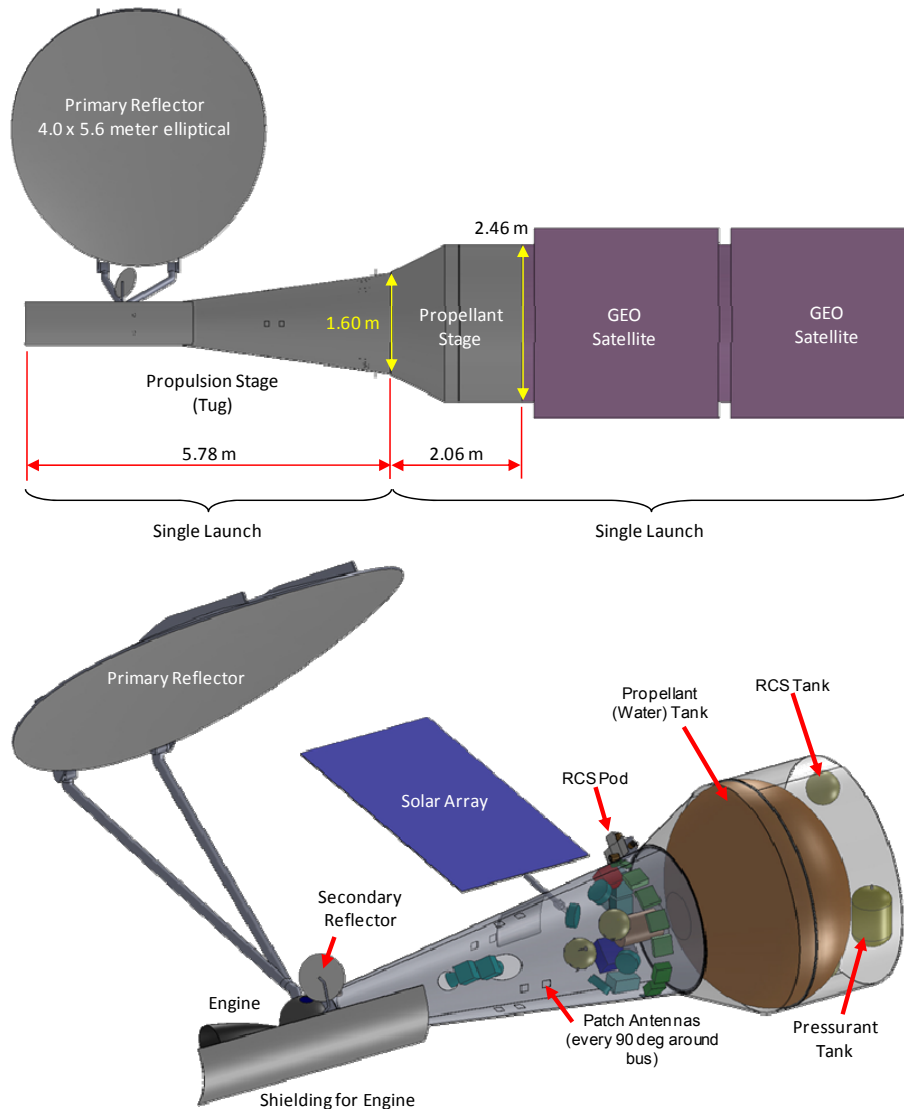


Figure 2.17.—LEO–GEO tug diagram. RCS, Reaction Control System.

(Li-ion) battery pack will supply an additional 1625 W during 5- to 15-min burns to run pumps, tracking, and so forth. The main engine will provide 5000 N of thrust with 50-psia pressure in a 30-cm spherical combustion chamber. The engine will use water heated to 6000 K to provide 813-s I_{sp} . The plasma ball will be electromagnetically suspended in the chamber, and the nozzle will be regeneratively cooled or film cooled. The beamed energy will pass through a 10-cm-diameter sapphire refractory window into the combustion chamber. The nozzle will have an area ratio of 50, will be regeneratively cooled, and will be gimballed for communications pointing on a screw or ball mechanical motor.

2.3.2.1.2 Concept of Operations (CONOPS)

A standard CONOPS involves the launch of two 1970-kg GEO satellites and 4895 kg of water propellant on a Falcon 9 Block 2 from Kwajalein into a 400-km circular orbit with an inclination of 9°. The tug will rendezvous with the stack of two GEO satellites and propellant and begin orbit-raising burns within 3 days of launch. Six 5- to 8-min burns are required to raise the initial orbit to a 3000-km, 9° inclination circular orbit. Three 15-min burns at 3000 km are required to raise apogee to GEO: one 15-min apogee burn is required to change planes to 0° inclination, and two more 15-min apogee burns are

required to circularize. The total transit time to GEO assuming burns every orbit is 32 hr, requiring 4.2 km/s Δv .

Following undocking from the GEO spacecraft, the tug returns to a 400-km, 9° inclination, using residual water propellant that was launched with the two GEO spacecraft, and is ready for the next transit in 24 hr (Figure 2.18). The tug itself is assumed to have been launched separately. The overall concept is summarized in Table 2.4.

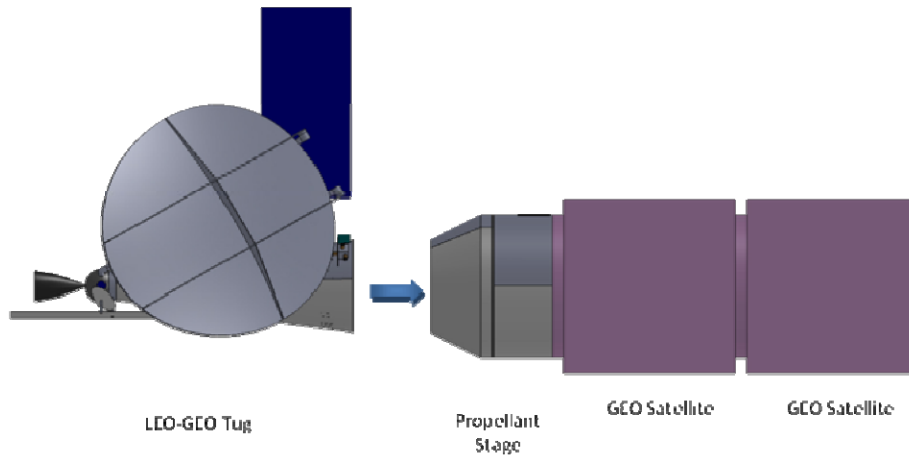


Figure 2.18.—Launch elements and sequence.

TABLE 2.4.—LEO–GEO TUG CONOPS

Test Step	Beaming	Receiving	Control / Operation
0			Launch of Tug on Falcon 9 from Kwaj
1			Launch of <i>two</i> 2000 kg GEO sats and 5000 kg propellant on Falcon 9 from Kwaj
1a			Rendezvous and docking with Tug
2–7	Perigee	Tug + 2 GEO Sats	400 km circular 9° inc to 3000 km circular 9° inc
8–10	Perigee	Tug + 2 GEO Sats	3000 km circular 9° inc to 3000 x 36000 km 9° inc
11	Apogee	Tug + 2 GEO Sats	3000 x 36000 km 9° inc to 0° inc
12–13	Apogee	Tug + 2 GEO Sats	3000 x 36000 km 0° inc to 36000 km circular 0° inc
14	Apogee and Perigee	Tug	Return to LEO

2.3.2.1.3 Ground Facilities

The DRM 2 mission as defined, requires two types of laser ground facilities, a 2- to 3-m-diameter-aperture Perigee Facility for burns for altitudes between 400 and 3000 km, and a much larger diameter Apogee Facility for burns for GEO. Both types of laser facilities will be required to deliver about 50 MW of laser energy to the spacecraft. On the basis of atmospheric losses, each of the ground facilities will need an 80-MW laser to deliver the required power to the tug. The apertures for these ground facilities will resemble large astronomical telescopes such as SOR and the proposed 30-Meter Telescope (TMT).

All of the facilities will have two main components, a Beam Generation system and a Beam Control system. In addition, each facility will require sufficient power and heat-dissipation capacity for the operation of the laser.

Perigee facilities.—Three Perigee Facilities spaced evenly around the globe on or near the equator should provide the best viewing opportunities to enable perigee burns on nearly every orbit. DRM 2–A uses the Kwajalein Atoll as the launch site, which is located at a latitude of 9°. The Perigee Facilities will require only 2-m apertures to compensate for beam diffraction, but the ability of the optical coatings to handle the 80-MW power levels may drive larger optics to lower the flux. The Perigee Facilities will most likely resemble the 3-m telescope at SOR at Kirtland Air Force Base (AFB) (see Figure 2.17) or the Advanced Electro-Optical System (AEOS) 3.67-m telescope on Maui. The near-equator locations of the Perigee Facilities implies that they could be ship based.

Apogee facility.—The Apogee Facility has more flexibility on location, but it will need to be at least 30 m in diameter to focus the spot on the spacecraft’s reflector at GEO. The facility could be located below a latitude of 45° and still provide good lasing opportunities for both the 3000-km altitude (and so could be used for perigee burns) and GEO. The TMT being constructed at Mauna Kea, Hawaii, is a good representation of a baseline Apogee Facility. The laser requires the same 80-MW power as the Perigee Facility and for practical reasons could be identical.

2.3.2.1.4 Costs

The costs associated with the LEO–GEO tug are shown in Table 2.5. These costs were determined based on a reuse of the tug for 10 round trip transfers from LEO, with fuel transported with the satellite payload for each mission. For comparison purposes recurring costs for a LEO–GEO transfer, using a centaur stage, were developed. Reuse of the tug for 10 transfers provides a cost saving of \$15M per launch, with further cost saving potential if additional reuse can be provided.

The nonrecurring costs are for DDT&E. The recurring cost is for the first unit produced, and uses a government based cost model for the estimate. Table 2.6 shows the estimated ground facility nonrecurring and operating costs for each mission. The non-recurring costs were based on a costing model used by the NASA Kennedy Space Center to estimate construction of their facilities. The beaming source costs were provided by the respective consultants using estimates based on current technologies. Ground operations costs were based on a dual use scenario for launch and space operations.

As an alternative to the ground-based infrastructure, a space-based system was analyzed and is shown in the second row of Table 2.5. For the space-based system a lower power level of 500 kW was analyzed, with the corresponding increase in costs and transfer time given in the table.

TABLE 2.5.—RECURRING AND NONRECURRING COSTS FOR LEO–GEO DRM

All Costs in FY11\$	Space Vehicle			Infrastructure						
	Recurring Cost	Non-Recurring Cost	Time from LEO to GEO	Launch Vehicle		Energy Source				
				Type	Cost (ROM) for 20 payloads	Input Power	Output Power	Non-recurring Cost (ROM)	Operations Cost (ROM)	
Comparable Disposable system 1 Transit One 2000kg satellite Chemical kick-motor	\$100M	N/A	7 Days including orbit insertion and checkout	Twenty Falcon 9 Rockets	\$1B	Chemical	N/A	N/A	N/A	N/A
Reusable Tug; Energy Source in Space 10 transits ----- Two 2000 kg satellites 4900kg Water Propellant	\$85M	\$237M	20 Days including orbit insertion and checkout	Eleven Falcon 9 rockets	\$550M	Laser	One In-Space 1.5 MW Station [ISS sized Station w/"FAST" arrays located in GEO]	Space Based 0.5 MW	\$5B*	\$250M*
Reusable Tug; Energy Source on Ground 10 transits ----- Two 2000 kg satellites 4900kg Water Propellant	\$85M	\$237M	8 Days including orbit insertion and checkout	Eleven Falcon 9 rockets	\$550M	Laser	One Ground Based 195 MW Stations [Max existing 105kW] [Best located at high altitude around equator]	Ground Based 78 MW	\$3B**	\$150M**

2.3.2.2 Deep Space Mission

Several possible applications of BEP were explored for deep space missions. The primary goal of this portion of the study was to find an application of BEP that would either enable a mission not otherwise achievable or measurably enhance myriad possible missions.

Early work on the direct propulsion of gossamer bodies such as the Forward-Landis Star Wisp microwave-propelled interstellar craft and the success of the Japanese Interplanetary Kite-craft Accelerated by Radiation Of the Sun (IKAROS) solar sail mission to Venus led to the consideration of laser-powered sails to propel payloads to the outer planets.

The concept finally adopted for DRM 3 was to show how BEP as used in DRM 2 for an orbit-raising tug could improve the performance of a planetary or deep space mission. The study was performed in collaboration with the Mission Design Laboratory at Goddard. The approach was to use the results of the Glenn's COMPASS team design for the orbit-raising tug with the minimal changes necessary to adapt the design to provide acceleration for the one-way trip to Jupiter: the object being to investigate performance enhancements possible with BEP. The Galileo mission to Jupiter (1989 to 2003) was chosen for the comparison.

2.3.2.1.5 Vehicle Description

The vehicle design for DRM 3 was adapted directly from the orbit-raising tug designed by Glenn's COMPASS design team for DRM 2. Like DRM 2, the payload and propulsion vehicles are launched separately and joined on orbit. However, whereas the orbit-raising tug was designed to be reusable, to deliver self-contained payloads to geostationary orbit, the propulsion vehicle in DRM 3 was designed to be an expendable booster. For the orbit-raising tug to be reusable under the DRM 2 CONOPS, the propellant would have to be replaced for each mission and be manifested as part of the satellite payload launch. In the DRM 3 configuration, the propulsion module includes the water propellant for the laser plasma engine for near-Earth orbit-raising and Jupiter Transfer Trajectory Insertion burns. The propulsion module is by far the heavier payload for the two Falcon-9-class launches used in DRM 3.

The Galileo payload analog for the study was updated from the original Galileo mission by replacing the original Radioisotope Thermoelectric Generators with Advanced Stirling Radioisotope Generators (ASRGs), otherwise all power, mass, and size specifications from the original Galileo vehicle were used to define the payload. Three of the four ASRGs needed to power the Galileo-like science payload will be launched with the propulsion module. Including these ASRGs with the propulsion module will eliminate the need for the solar panel used for power on the DRM 2 orbit-raising tug and will have the advantage of additional mass fraction being available on the payload launch vehicle, should it be needed.

The propulsion module will easily fit within the 5.2-m Falcon 9 fairing (see Figure 2.19). The stowed module will have an overall length of about 8 m.

The major components of the propulsion module follow: (1) the BEP system, consisting of the beam collecting and focusing optics, the thrust chamber and nozzle, and propellant

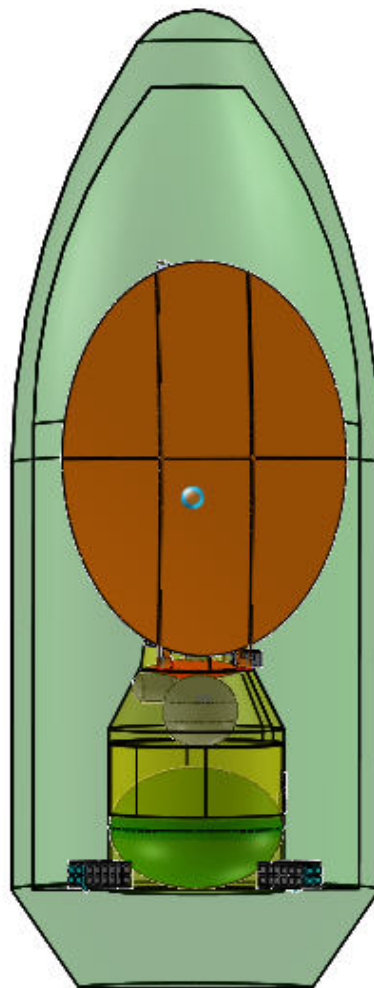


Figure 2.19.—Stowed DRM 3 propulsion module in Falcon 9 fairing.

storage and delivery; (2) the electrical energy system consisting of the ASRGs, a battery, and power management and distribution; (3) the attitude and control system consisting of reaction wheels for fine pointing, an autonomous docking system, and monopropellant thrusters with fuel for maneuvering; (4) the thermal management system; and (5) the communications system.

Electric power for the propulsion module will be provided by three ASRG units and a rechargeable Li-ion battery launched with the propulsion module. A fourth ASRG will be launched with the Galileo-like payload and added when the payload and propulsion modules are docked. The ASRGs (with beginning-of-life power of 143 W each) will be used for primary power for all functions except propulsion, when the 100-Ah Li-ion battery will provide supplemental power for the propellant pumps during laser engine operation. For a typical 10-min orbit-raising propulsion firing, the battery depth of discharge will be 8.3%; and for the Jupiter Transfer Trajectory Insertion firing of 100 min, the depth of discharge will be 83%. The power system will be a 28-V-battery-dominated bus, with separate 28-V buses on the payload and propulsion modules. The ASRGs will be retained by the payload during separation of the payload from the expended booster and used for power during the remainder of the mission.

2.3.2.1.6 CONOPS

Differences between the LEO–GEO tug (DRM 2–A) and the deep space mission led to design changes in the propulsion module design and spacecraft systems allocations (e.g., photovoltaic panel replaced by ASRGs, greater battery capacity, and water propellant launched as part of the propulsion module). The notional operational timeline (from launch) is shown in Figure 2.20.

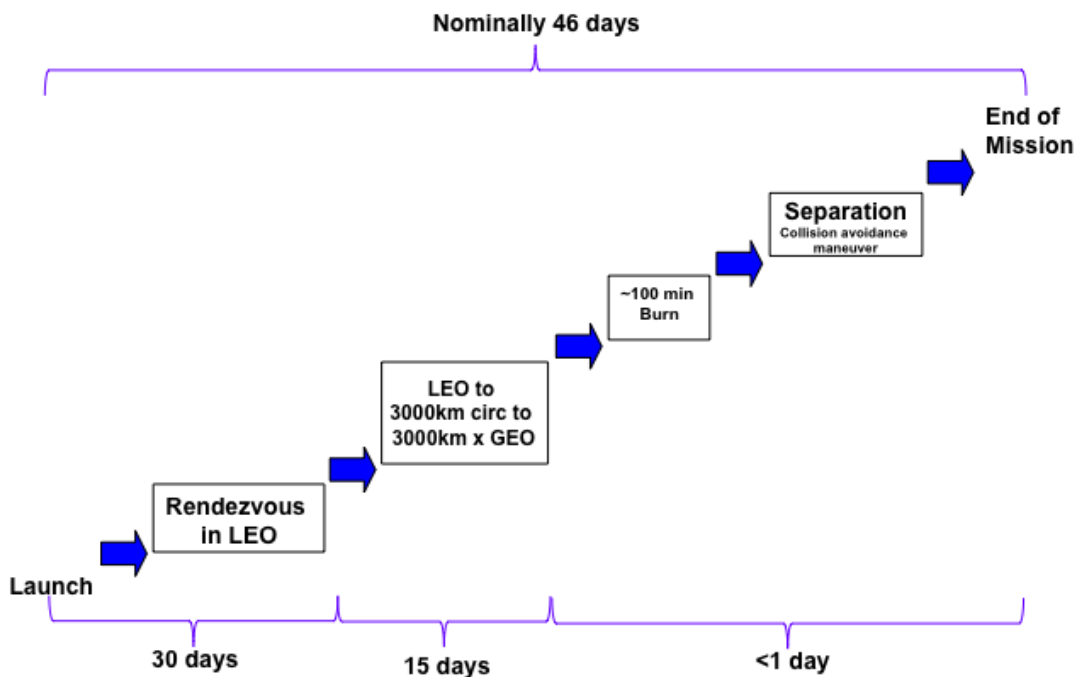


Figure 2.20.—Sequence of operations for DRM 3: BEP-enhanced Galileo mission.

The initial launch and orbit-raising sequence closely mirror that of DRM 2 and will employ two Falcon 9 launch vehicles (one for the propulsion module and one for the Galileo payload). The propulsion module and Galileo mission spacecraft will be launched separately from Kwajalein Atoll into an 800-km, 9° inclined circular LEO.

The propulsion module and Galileo mission spacecraft will be joined on orbit using Next Generation Advanced Video Guidance Sensors and automated rendezvous and docking hardware, firmware, and software. The time allocated for the launch, docking, and spacecraft diagnostics is 1 month.

Orbit-raising protocols from DRM 2 will be followed to first transfer the combined spacecraft from an 800-km, 9° inclined circular orbit to a 3000-km, 9° inclined circular orbit and then to a 3000- by 35,000-km, 9° inclined Jupiter Departure Orbit. The time allocated for the orbit change maneuvers is 15 days.

The final phase of near-Earth operation will be the 100-min laser-beam-powered Jupiter Transfer Trajectory Insertion acceleration from Jupiter Departure Orbit to Jupiter Transfer Orbit, followed by separation of the propulsion module from the Galileo mission craft with a collision avoidance maneuver.

Here, the BEP phase of the mission will end with the propulsion module flying away and the Galileo craft continuing to Jupiter, where it will use onboard hydrazine monopropellant to perform a Jupiter Orbit Insertion burn of 70 min and enter the highly elliptical Galileo Jupiter Orbit of 200,000 by 12,000,000 km with a 98-day period.

2.3.2.1.7 Cost

The design of the propulsion module and the CONOPS for DRM 3 were adapted with minimal changes from DRM 2, and cost estimates for the BEP-enhanced Galileo mission can be derived from DRM 2 estimates.

BEP can open new opportunities for deep space exploration and science missions. The cost and time to develop the 80-MW ground station will be the most significant obstacles to the realization of the potential of BEP for this deep space application.

2.3.2.2 Deep Space Costs

The costs associated with the deep space DRM are shown in Table 2.6. Since the deep space DRM utilizes the LEO–GEO tug, the costs are similar with addition of the advanced Stirling radioisotope generator needed for power operation at the outer planets. Also, the recurring cost of \$85M is based on the ten times reuse for the LEO–GEO tug.

As with the LEO–GEO DRM, an alternative to the use of a ground-based system was analyzed. The high power requirement for the deep space mission (50 MW) necessitates the need for a low-cost, high-power, long-life system. Both nuclear and solar options were considered for this application, but the costs based on the Jupiter Icy Moon Orbiter and the ISS were considered impractical for this alternative.

TABLE 2.6.—RECURRING AND NONRECURRING COSTS FOR DEEP SPACE DRM

Space Vehicle					Infrastructure				
All Costs in FY11\$	Recurring Cost Range	Non-Recurring Cost	Time from LEO to Jupiter	Time from LEO to Jupiter	Energy Source				
						Input Power	Output Power	Non-recurring Cost (ROM)	Operations Cost (ROM)
Comparable Chemical System	N/A	N/A	6 yrs	11 yrs**	Chemical	N/A	N/A	N/A	N/A
Deep Space Vehicle (Similar to the LEO to GEO Tug) Source in space	\$85M* +ASRG Cost	\$237M* +ASRG Cost	2.5 yrs	6.5 yrs	Laser	150 MW In-Space Power Source [100 ISS sized Stations w/"FAST" arrays located in GEO]	Space Based 50 MW	Too High***	
Deep Space Vehicle (Similar to the LEO to GEO Tug) Source on ground	\$85M* +ASRG Cost	\$237M* +ASRG Cost	2.5 yrs	6.5 yrs	Laser	One Ground Based 195 MW Station [Max existing 105kW] [Best located at high altitude around equator]	Ground Based 78 MW	\$3B^	\$150M^

2.4 Unexpected Findings

The following subsections describe two technologies that evolved out of discussions during the process of the study. They represent concepts that have high potential and should be considered for further investigation.

2.4.1 Spacecraft Remote Operation

The first concept is an integrated power, communications, propulsion, and navigation and attitude control system. This concept, shown schematically in Figure 2.21, could control the operation of a cooperating spacecraft. By utilizing the communications aspect of the power beam through optical

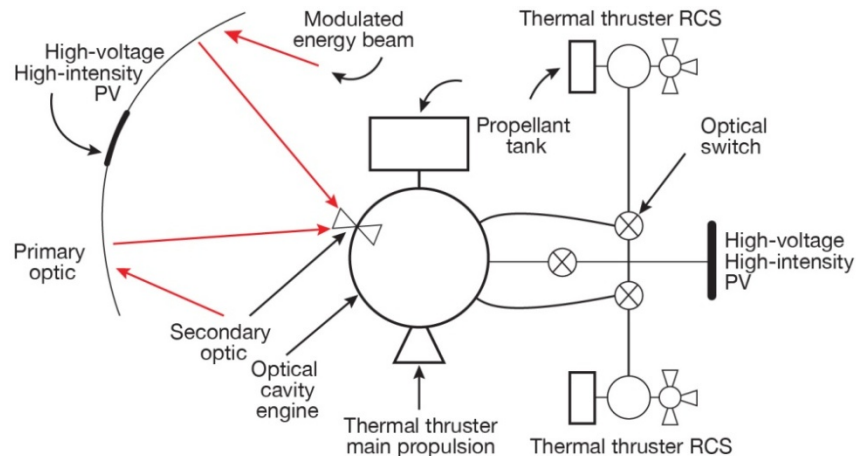


Figure 2.21.—BEP concept—integrated propulsion, power, communications, and navigational/attitude control on the same laser beam (PV, photovoltaics; RCS, reaction control system).

retrodirective beam control, it is possible to achieve a closed-loop control capability between the beamed source and the receiving spacecraft. Thus, the spacecraft's propulsion system could be controlled by the amount of energy transmitted. This, in combination with the communications link, could also be used to control the spacecraft's attitude, move it into close proximity, and berth it, if required, without having to have the dynamics of the two spacecraft physically coupled during the rendezvous and berthing operation. Navigation data could be transmitted on the laser beam, relieving the receiving craft of the need for that systems equipment.

If successfully developed, this technology could lead to a new class of spacecraft with enhanced operational capability, lower complexity, higher reliability, and lower mass.

2.4.2 Propulsion Engine

The second concept is not new but one that has an application with energy beaming to provide propulsion with both high thrust and high I_{sp} (concept shown in Figure 2.22). The optical plasma engine requires temperatures above 6000 K to heat propellant within a cavity, expanding the material that is creating the propulsive force. This system is able to utilize diverse new propellant types such as water and ammonia, thus eliminating toxic chemicals and associated safety issues both in space and on the ground. The environmentally friendly water propellant is potentially available on the Moon and Mars. The energy source can be solar, laser, or millimeter wave, making it flexible to match the technologies as they develop. Since this system is an optical-to-optical conversion, it naturally has high efficiency with the potential for the highest propulsion engine performance because the oxidizer/energy source is eliminated on the spacecraft.

Development work could begin on this concept with very little investment.

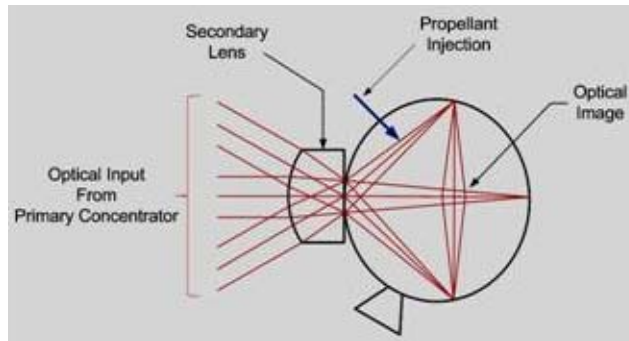


Figure 2.22.—BEP optical plasma engine.

2.5 BEP Development Direction

It is shown in Section 2.3 that the high infrastructure cost of ground- and space-based beamed-energy infrastructure makes BEP unfeasible at this time. But this does not mean that BEP should be dropped as a potential game-changing technology. There are near-term applications, as explained in Section 2.4, that have the potential for high investment return. The launch and in-space applications, deemed unfeasible now, should be pursued by attacking the key issue of high energy-source costs. However, the cost of developing megawatt energy sources should be borne by those in need of them at this time. NASA and DARPA should take on role of developing the key technologies that will be needed later to implement their specific applications. Figure 2.23 provides a proposed timeline of how the various applications of beamed energy should align to maximize the total overall investment.

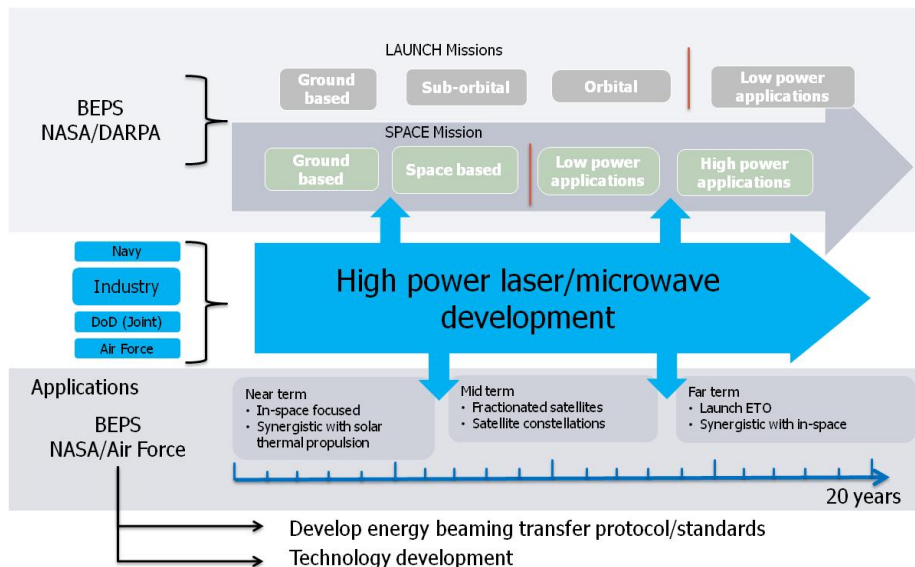


Figure 2.23.—Timeline of beamed-energy development.

Development of beamed-energy transmission protocols and standards (P&S), and along with the previously mentioned applications, is worth pursuing since these P&S and applications will provide the foundation and early applications on which to build the more complex and technologically challenging components of the program.

Development of P&S should be addressed initially to lay the groundwork and direction for BEP. The P&S should define the most appropriate organizations to baseline and maintain the regulations governing such areas as the characterization of transmitted and received beam quality. The scope could include describing the limitations on ground, aviation, and space applications along with equipment performance.

It is recommended that a set of low-cost ground development demonstrations related to the near-term applications should be funded to begin the development process. These demonstrations could be combined with industry and academia competitions similar to NASA’s Centennial Challenge. Other longer term developments could include laser and millimeter-wave beam-combining techniques to allow the use of numerous low-cost commercial energy sources, long-distance pointing and tracking techniques, and optical systems to direct high-power energy sources. Figure 2.24 shows how the gradual buildup of knowledge through testing at low flux and low power levels to high flux and high power levels could be infused into applications.

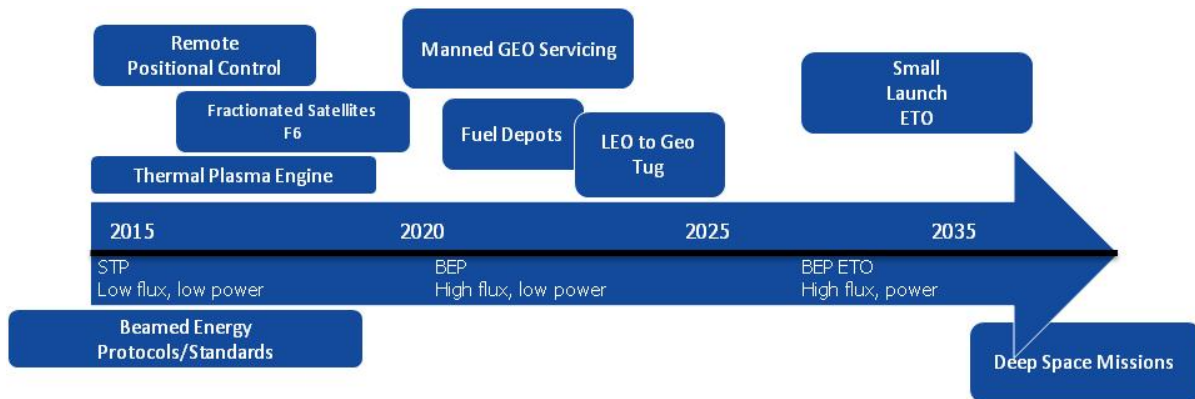


Figure 2.24.—BEP development applications from low to high power.

As reported in Section 2.4, the integration of power, propulsion, control/communications, and navigation is possible via a single laser beam to enable remote positional control. Near-term ground applications include unmanned aerial vehicles (UAVs) and low-flying aircraft. Space applications, such as solar electric propulsion and DARPA’s Exo-SPHERES, could utilize this technology. In the long term, these developments could enable lower cost access to space by minimizing the complexity of systems needed for smaller craft operations. Suggested development tests and demonstration are shown in Figure 2.25.

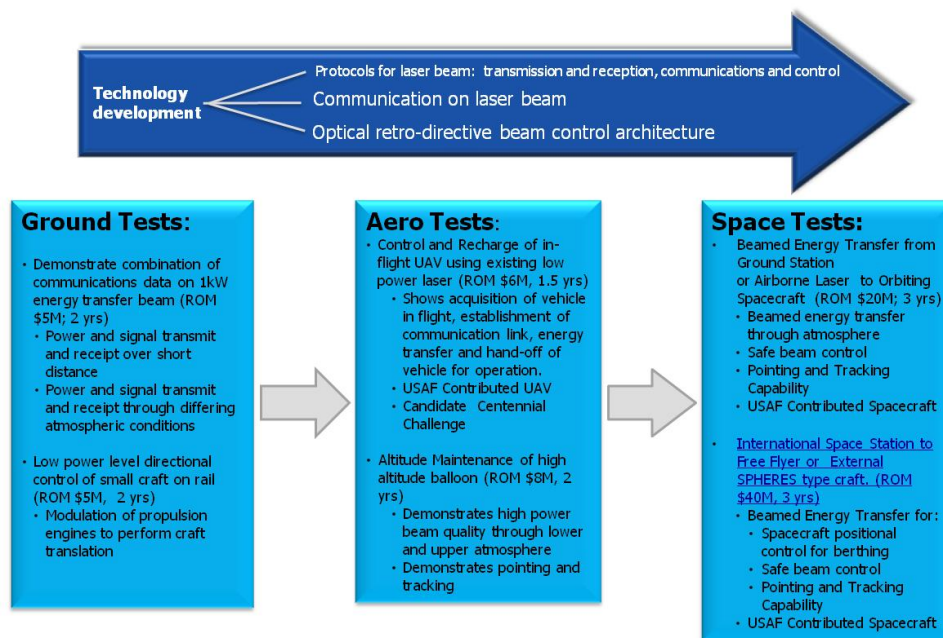


Figure 2.25.—Demonstrations to develop near-term remote positional control technology.

One of the key demonstrations that would provide a critical stepping stone for evolving wireless power beaming in space would be to place a laser on the International Space Station (ISS) and beam energy for propulsion to a free-flyer. The free-flyer would reposition by changing orbit as a result of the energy. Performing a test in the space environment would anchor the design models, confirm the environmental assumptions, and establish energy beaming as a new way of thinking about the design of future spacecraft (Figure 2.26). It could also demonstrate safe beaming control for space and terrestrial energy transfer, along with determining beam locator sensor efficiencies and accuracies in a controlled application. It would support growth and future applications for beaming energy in space to the Earth, to the Moon, and to other satellites for both propulsion and power.

To show the potential of BEP and beamed energy in general, Figure 2.26 describes a similar demonstration, also designated for the ISS, that was detailed in 2008 for another study.

National Aeronautics and Space Administration

DARPA

NASA

In-Space Flight Demonstration International Space Station to Free Flyer

Demonstration:

- Beamed Energy Transfer for:
 - Phase 1 Free-flyer Orbit Raising
 - Phase 2 Free-flyer positional control
- Spacecraft positional control
- Safe beam control
- Pointing and Tracking Capability

**Cost ROM: Ph. 1 \$40M
Ph. 2 TBD**

Significant Contributions:

- USAF supplied FalconSat free-flyer
- JAXA location on ISS
- Utilize existing flight qualified components
- Launch on Space X Falcon 9

Time: 3.5 / TBD years

Receiver Satellite (USAF)

- In orbit close to station – 200km
- 3-axis control to point receiver panel toward station during beaming passes
- Corner-cube enables retro-directive beam lock before power transfer
- 300 w usable power
- Command and control from AFIT and USAFA ground stations

Optimization study

- Beam aimed away from Earth's surface
- Number of cross orbit paths
- 10² km rel. dist provides many more beaming opportunities, less time per pass

Potential Partners:
NASA, DARPA, US Air Force, Japanese Space Agency

Energy Transfer

- 3 kW laser
- 30 sec. beam time
- 300 W usable energy
- Charge batteries
- Power thruster directly

ISS Payload

- JEM-EF location
- 3kW at 120Vdc
- Nadir or Zenith pointing

Final Report

www.nasa.gov

Figure 2.26.—In-space flight demonstration from the International Space Station to Free Flyer.

The other early technology development reported in Section 2.4 that would have a far-reaching effect in the development of BEP is the optical plasma engine. The most promising factor in this case is the potential of high systems efficiency in comparison to existing or near future propulsion technologies. As with most high-potential undeveloped technologies, the rewards could be great but come with the need for investment and major challenges. Maintaining control of the plasma ball within the chamber and away from the walls is considered to be the major hurdle to be proven. The work could begin by using solar energy as the source rather than laser energy and, therefore, is not dependent on the development of lasers. Some early work (10 or more years ago) has been performed in this area with a first prototype model. A low funding level could go a long way to determining the feasibility of this technology. Figure 2.27 lists a set of tests/demonstrations that could be performed, gradually building to a space test.

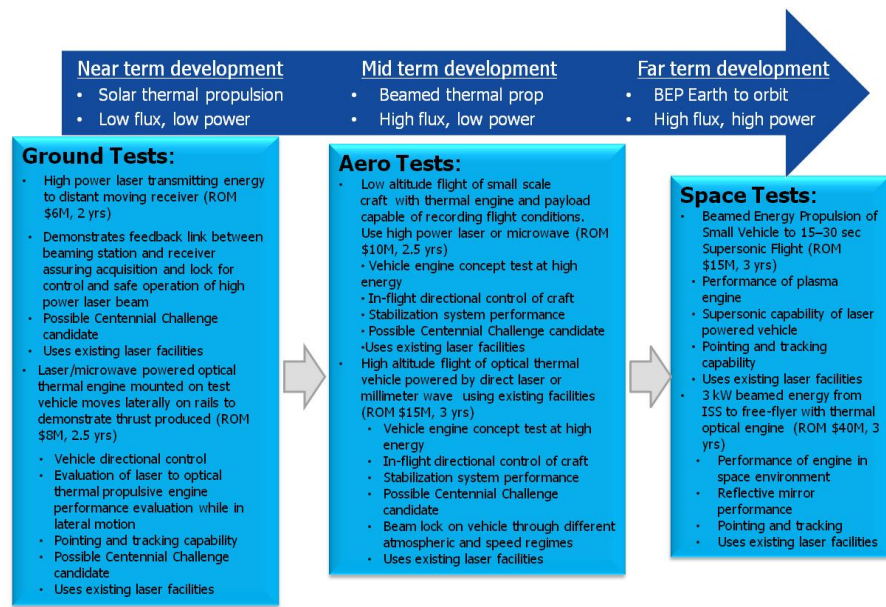


Figure 2.27.—Demonstrations to develop near-term optical plasma engine technology.

Development demonstrations for each of the DRMs appear in the specific consultant reports in Sections 3.1 and 3.2.

2.6 Future Potential of BEP

As mentioned in this report, and as shown in the investigations into the DRMs, BEP has the potential to realize low-cost access to space and the transportation of vehicles from LEO to GEO and deep space. If successfully developed, these applications alone would be game changing. It should be kept in mind that there are applications of beamed energy in general that also have game changing potential.

Beamed-energy technology, when developed and appropriately demonstrated, has the potential to significantly impact future NASA Exploration and Science Missions. The flexible path strategy for space exploration envisions a hybrid approach involving robots and men to explore the Moon and near-Earth asteroids. Early missions may not land men on the surface but would utilize robots controlled by astronauts on an orbiting spacecraft to explore the surface and return samples to the orbiting spacecraft. Expectations of water ice, located in craters or buried in crevices, will require power to be delivered to the robot to enable exploration of these areas. Beamed energy has the potential to deliver power and enable control of the mobile robot, thus providing a virtual wire allowing the astronauts the freedom to explore the surface from the orbiting spacecraft. Knowledge obtained from the remotely controlled robots will then be utilized to prepare for human operations on the surface.

Lunar studies have identified the potential for laser power beaming that utilizes orbital platforms to capture and convert solar energy for transmission to the surface. Lunar in situ resource utilization (ISRU) work, done in anticipation of water ice in the Shackleton crater, has demonstrated the value of beamed energy in processing ice to obtain hydrogen and oxygen. Thus, the power-beaming technology and assets developed and utilized during the early hybrid phase of exploration will form the basis for the infrastructure for future human campaigns.

The flexible-path strategy, by design, couples the Exploration and Science Missions. Thus, robotic technology developed for science missions could form the technology base for robots utilized in the controlled robot phase of crewed missions, or vice versa. The nature of beamed energy allows for the integration of power, propulsion, communications, and navigation/attitude control. This integrated capability could be utilized to enable satellite constellations for planet finder, other formation-flying missions, and future fractionated satellite applications. When properly scripted, the power-beaming

technology utilized for human-controlled robotic exploration of craters and crevices could be utilized for autonomous robotic science applications.

Development of BEP could provide the key to a new method of launch and in-space transportation as well as aid in exploration and science missions.

3.0 Study Reports

The approach to this study was to engage consultants, external to NASA, to obtain the widest possible viewpoints on launch and in-space beamed-energy propulsion (BEP). Their input was incorporated into the formulation of Design Reference Missions (DRMs) and then processed through NASA-based mission design teams to bring a sense of practicality to the actual vehicle configuration and mission operations utilizing NASA standard design practices. NASA Glenn Research Center project costing techniques and methods were used to apply a known basis of cost estimating for costing the missions. The complete set of reports from the mission design teams, the consultants, and the cost-estimating teams are included here without editing by the authors to provide the reader with original data. This approach was an attempt to ensure that the conclusions of the report were not biased and to provide the reader with information by which their own conclusions may be drawn.

3.1 Launch DRMs

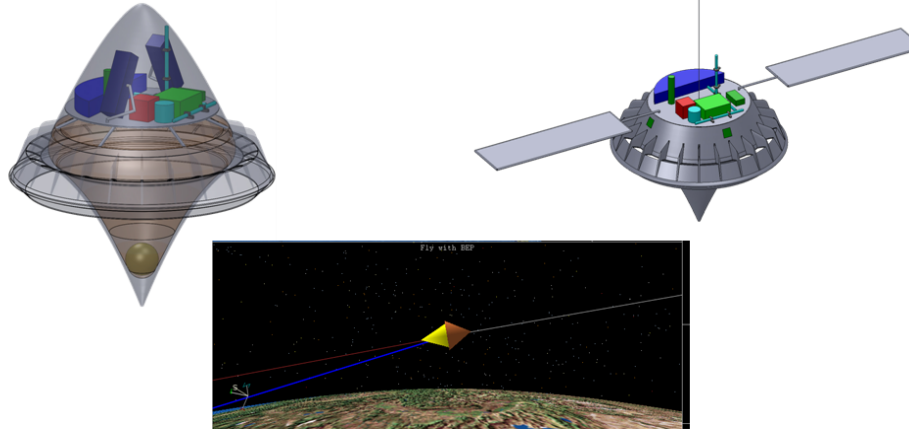
The rationale, description, and subsequent evaluation of each DRM are given in the following subsections. It is important to note that it was not the intention of this study to make a comparison and select a “best choice.” Each technology has distinct features and was evaluated to answer the feasibility question. Side-by-side evaluations were made only to point out the distinguishing characteristics of each technology. The details must be read for a full understanding of the potential and challenges of each technology.

Three specific DRMs were deemed necessary to determine feasibility for the launch case because of the wide range of technologies that have been applied to this specific area and the high level of development activity that has occurred over the last few years.

Each DRM was put through the same mission analysis process with the same team to maintain consistency between developments of the technology applications. This approach removed the relative effect of any bias within the team’s process.

3.1.1 Laser Optical Collaborative Modeling for Parametric Assessment of Space Systems (COMPASS) Report

Beamed Energy Propulsion (BEP) Launch Vehicle Conceptual Design DRM#1: Draft



COMPASS Team
12-10-10

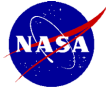
National Aeronautics and Space Administration



Team Roster



- COMPASS Lead - Steve Oleson
- Program Study Leads – Pat George, Ray Beach
- PI – Leik Myrabo
- Lead System Integration, MEL - Melissa McGuire, David Grantier
- CONOPS, system integration – Jeff Woytach
- Integration PEL, Mission Visualization - Michael Bur
- Mission –Dave Smith, Waldy Sjauw, Camille Moore
- GN&C –Mike Martini
- Propulsion - James Fittje, Geoff Landis
- Mechanical Systems - John Gyekenyesi, Tom Haag
- Thermal - Tony Colozza,
- Power - James Fincannon, Kristen Bury
- C&DH, Software- Glenn Williams
- Communications - Joe Warner
- Configuration - Tom Packard
- Cost - Jon Drexler
- Risk - Anita Tenteris

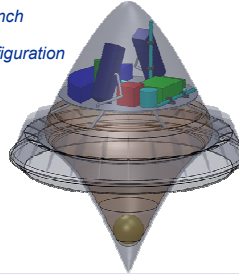


Lightcraft Summary

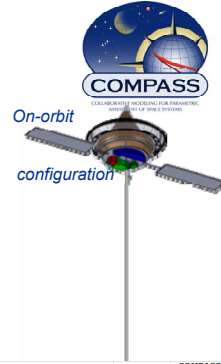
- **1.2 m top shaped launcher/spacecraft: no separate launch vehicle required**
- **Sample vehicle emulates ORBCOMM messaging spacecraft**
 - laser can be reused for orbit maintenance, repositioning & deorbit
- **Launched 30° elevation, requires two Laser stations (up to 350 MW) for complete launch**
- **Propulsion and thermal technologies still in TRL 2-4 range**
- **Propulsion:**
 - Parabolic mirror doubles as plug nozzle
 - Pulsed Laser focused onto ring where temps > 6000 ° K theoretically provide 1 Isp > 900 seconds
 - Laser power up to 350 MW required
 - Water propellant best for density, cooling, ground handling
- **Guidance, Navigation, Control**
 - Vehicle spun up to 120 rpm for stabilization at launch, differential water inlet injection for pitching
- **Some Launch power, C&DH, Comm systems reused for spacecraft functions**

Use of on S/C remaining launch vehicle reduces launch vehicle costs by more than half! (does not include differences in launch support, range, and laser facilities)

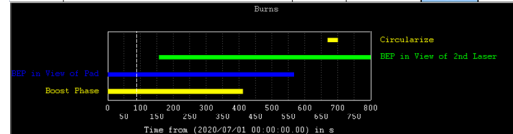
Launch configuration



On-orbit configuration



Spacecraft Master Equipment List Rack-up (Mass) - Lightcraft				COMPASS S/C Design	
WBS	Main Subsystem	Basic Mass (kg)	Growth (kg)	Estimated Total Mass (kg)	Aggregate Growth (%)
06	Lightcraft/Spacecraft	300.1	18	318	
06.1	Lightcraft Stage 1	300	18	318	
06.1.1	Payload	0	0	0	TBD
06.1.2	Attitude Determination and Control	4	0	5	7%
06.1.3	Avionics	11	3	13	30%
06.1.4	Communications and Tracking	4	1	5	22%
06.1.5	Electrical Power Subsystem	4	1	5	30%
06.1.6	Thermal Control (Non-Propellant)	15	0	15	0%
06.1.7	Propulsion (Hardware)	17	2	20	14%
06.1.8	Propellant	188		188	
06.1.9	Structures and Mechanisms	56	10	66	17%



www.nasa.gov 3



Further Work to Ensure Feasibility of This Design



- **Mission:**
 - Improved fidelity of trajectory design to include: beam pointing loss terms and off center beam pointing for steering (current trajectory is optimistic). Examination of optimal trajectories including a study of a vertical launch followed by an immediate pitch over to remove current 30 degree launch conditions and simplify the launch apparatus.
- **Propulsion/Vehicle Dynamics:**
 - Heat Leak, Injector options, Propellant selection, off-nominal performance (thrust vector/Isp/thrust as a function of off-pointing, angle of attack, as a function of off-center)
 - Atmospheric compensation of the laser (determine if beacon is required)
- **Thermal:**
 - Modeling of reflector and injector ring cooling (heating from laser, plasma (conductive, convection, radiation) in all modes), Pressure loss on cooling channels (pressure design)
 - Estimate Thermal damage of mirror reflectivity due to thermal cycling
 - Final velocity profile (with mach < 0.6 hold removed) was not evaluated for its impact on thermal and structures (max Q considerations)
- **GN&C:**
 - Final launch profile change to 30° elevation – pitch requirements not yet evaluated for this trajectory
 - Differential injection/thrust for pitching
 - Error margin analysis on the laser pointing/position on S/C body
 - Required spin-rate for adequate stability/Thermal control in various propulsion modes



Beamed Energy Propulsion: Laser Launcher



The COMPASS team has been tasked by DARPA/NASA to create an independent concept design for a Laser powered launch vehicle.

The COMPASS design will give the DARPA/NASA a point-of-reference to the feasibility of the concept and a what technologies and demonstrations need to be developed to support development of a laser launcher.



Schedule



- **This Week**
 - Today: Customer technical interchange
 - Friday: NO SESSION (develop MEL)

- **Next Week**
 - MTW (with customer), F
 - Monday: Kickoff, Mission Analysis, Begin laying out vehicle, define trades, Scratch PEL
 - Tuesday-Wednesday: CONOPs, Perform design
 - Friday: Review Trades, Assess MEL, Configuration

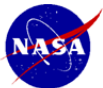
- **2nd Week**
 - MW: Complete Design
 - F: Draft Results Flip-thru



Starting Requirements



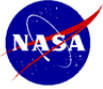
- **Must Deliver to LEO a Lightcraft that doubles as a spacecraft (compare to an ORBCOMM s/c)**
- **Will provide for comparable payload volume**
- **Will utilize Single stage to orbit**
 - Final Design requires on-board circularization stage
- **Will Utilize a ground based laser beam (~1MW for 1 kg payload to orbit)**
 - Tentatively 100-350MW
- **Will emphasize simplicity and low cost**



FOMs and Fault Tolerance



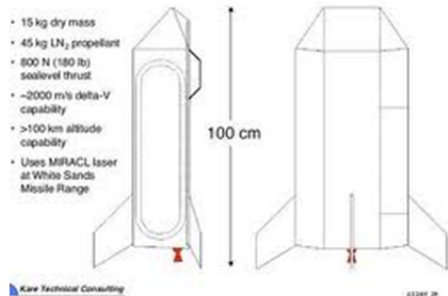
- **Mass: Single Stage to orbit, payload up to 100 kg**
- **Reliability: Single Fault Safe**
 - Satellite systems – compare to ORBCOMM
- **Cost:**
 - Cost for launch vehicle
- **Single fault for safety**
 - What kind of range safety is needed?
 - To be evaluated by separate effort under KSC
 - Currently vehicle does NOT carry any destruct systems
- **Fault tolerance for vehicle**
 - Single string – assume build/launch of another is affordable



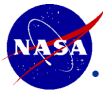
Past Designs



- Subscale (kW level) test to >200 ft
- High power (MW level) lasers under development
- Lightcraft spacecraft design 1990s



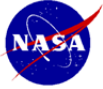
- 15 kg dry mass
- 45 kg LN₂ propellant
- 800 N (180 lb) sea-level thrust
- ~2000 m/s delta-V capability
- >100 km altitude capability
- Uses MIRACL laser at White Sands Missile Range



Lightcraft Reuse as a spacecraft



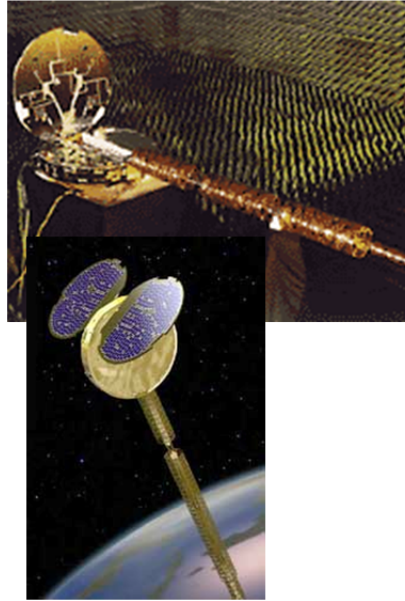
- **Constellations**
- **Self-assembled bigger spacecraft**
- **Communications**
 - Messaging
 - Cell
 - Internet
- **Reuse Laser engine**
 - Laser communications (in-space)
 - Optical imaging
 - Earth resource: multi-spectral, almost continuous imaging with 4000 S/C – new paradigm
 - Astronomy: customers want 6-15 m apertures (planet finders)
 - SETI search for alien laser communications
 - Repositioning, orbit maintenance, deorbit
- **LEO science spacecraft**
- **Quick way to demonstrate/qualify new technologies**
 - Electronics, solar cells, lubricants
- **Propellant for Depot**
- **Servicing spacecraft (viewing, deliver ORUs)**
- **Assist in deorbit of spacecraft**



Representative Payload



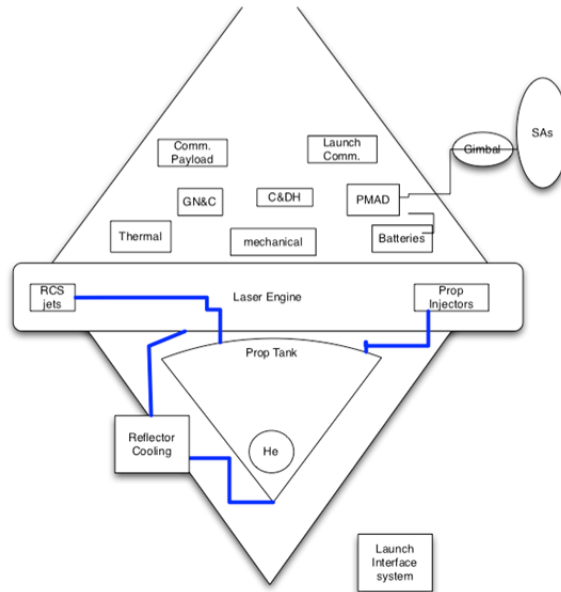
- **ORBCOMM**
- **Orbcomm is a commercial venture to provide global messaging services using a constellation of 26 low-Earth orbiting satellites.**
- **5 million messages**
- **26 satellite constellation**
 - 785 km circular (2 polar), 3 planes, 8 S/C per plane 45° inclined
- **Spacecraft (40 kg, \$1.2M each)**
 - 4 years life, 160W
 - VHF (138 MHz and 400 MHz): 57.6 kbps
 - Gravity gradient, mag torquers, cold gas N₂
 - 17 data processors, 7 antennas, 50,000 messages per hour



Bottom image courtesy of Orbital Sciences Corporation; used with permission.



Systems





Beamed Energy Propulsion PEL



Power Mode Title	Power Mode 1	Power Mode 2	Power Mode 3
	(W)	(W)	(W)
Launch	107	86	42
On-Orbit Operational			
On-Orbit Non-Operational			
Systems operating	All Except EPS/Thermal	All Except Thermal/Structures	AD&C/Avionics/Comm
Attitude Determination and Control	22	22	22
Avionics	36	36	13
Communications and Tracking	20	20	7
Electrical Power Subsystem	0	3	0
Thermal Control (Non-Propellant)	0	0	0
Propulsion (Hardware)	5	5	0
Structures and Mechanisms	24	0	0
Total (watts)	107	86	42
Power Requirement (Plus 30%)	139	112	54



Summary of Requirements/Assumptions



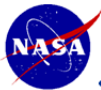
Requirements / Assumptions	Trades
Top-Level/ Science	<p>Lightsat shall perform both the launch and satellite functions. Representative satellite function to emulate ORCOMM. FOM: Cost per unit, payload mass, safety</p> <p>Separable payload (100 kg) vs integrated satellite, satellite functions</p>
System	<p>Single Fault Safe only, Otherwise zero fault tolerant. 4 year lifetime. Launch year open ended – current TRL assessment is an output.</p> <p>Mass Growth per AIAA 120-2006 (add growth to make system level 30%)</p>
Mission, Ops, GN&C	<p>Light engine attached to S/C performs launch from ground to sub-orbit, circularization with on-board chemical (circular, >=400km alt., 45 deg. inc (+/-0.2 deg.)) Desire reuse of light engine for repositioning, reboost, deorbit. High rotation rate for S/C stability</p> <p>Spin rate for stability (assumed 120 rpm) is this sufficient?</p>
Launch Vehicle	N/A
Propulsion	<p>Light Engine primary propulsion: performs Pulse detonation, laser ramjet, and laser rocket modes at appropriate altitudes. Water chosen as propellant due to better density, better cooling, easier handling on pad.</p> <p>Main propellant choice: H2 cleaner, H2O better density and cooling, On-board cold gas H2 for insertion, hydrazine for RCS, laser PD and rocket modes only</p>
Power	<p>Solar Arrays and secondary batteries</p> <p>Add primary batteries for launch needs</p>
C&DH Communications	<p>Pre-use flight computer to handle launch. Up-range telemetry communications. Equivalent Orbcomm messaging payload</p> <p>Computer type, data storage, data transfer rates, comm. Frequencies</p>
Thermal & Environment	<p>Remove laser and plasma heat from body by vaporizing propellant</p> <p>Propellant type for cooling: H2, H2O, HH3</p>
Mechanisms	<p>Inlet covers (open for ramjet mode, closed for other modes), Shroud ejection, solar array and tether deployment</p> <p>mechanisms, materials, power, ops,</p>
Structures	<p>High temp resistant inlet ring, 0.9999 reflective parabolic mirror/plug nozzle</p> <p>minimize mass</p>
Cost	<p>Assume light engine replaces launch vehicle, assume commercial spacecraft building cost models</p>
Risk	<p>Major Risks: temperature leaks from laser and plasma, fouling mirror, laser pointing thrust direction/angle of attack, high spin rate</p>



TRL Definitions



- SUMMARY
- **TRL 1** Basis principles observed and reported
- **TRL 2** Technology concept and/or application formulated
- **TRL 3** Analytical and experimental critical function
- **TRL 4** Component and/or breadboard validation in laboratory environment
- **TRL 5** Component and/or breadboard validation in relevant environment
- **TRL 6** System/Subsystem model or prototype demonstration in a relevant environment (ground or space)
- **TRL 7** System prototype in a space environment
- **TRL 8** Actual system completed and “flight qualified” through test and demonstration (ground or space)
- **TRL 9** Actual system “flight proven” through successful mission operations



TRL Levels (< TRL 6)



- **Propulsion & Flight Dynamics/Environments**
 - Laser Engine
 - PD mode: TRL 3
 - Ramjet: TRL 2
 - Rocket: TRL 4-5 (solid propellant), TRL 2 (liquid/gas)
 - Reflector: TRL 3
 - Injectors: TRL 4-5
 - RCS: TRL 4-5
 - Solid: TRL 5
- **Thermal: Mirror Coating TRL 2 in plasma environment (TRL ? in gas lasers, TRL >6 in astronomy applications. Mirror cooling TRL 3-4)**
- **GN&C: TRL 6**
- **C&DH: TRL 5**
- **Communications: TRL 3-4 (high temperature)**
- **Power**
 - Solar arrays TRL 4 (highly efficient packaging to fit in limited stowed volume)
 - Batteries TRL 4
- **Structures: TRL 4-6**

Configuration

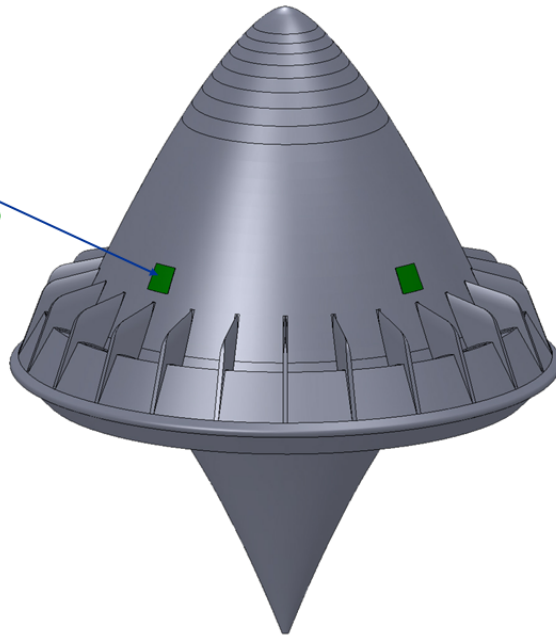
Tom Packard
COMPASS Team
10-08-10

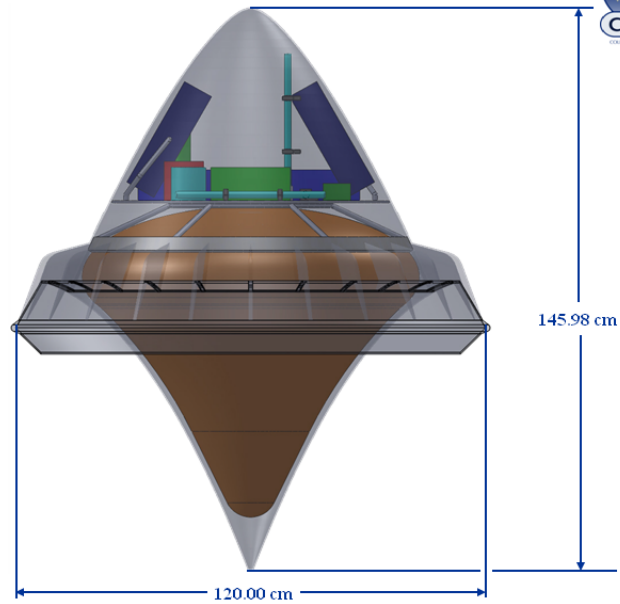
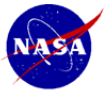
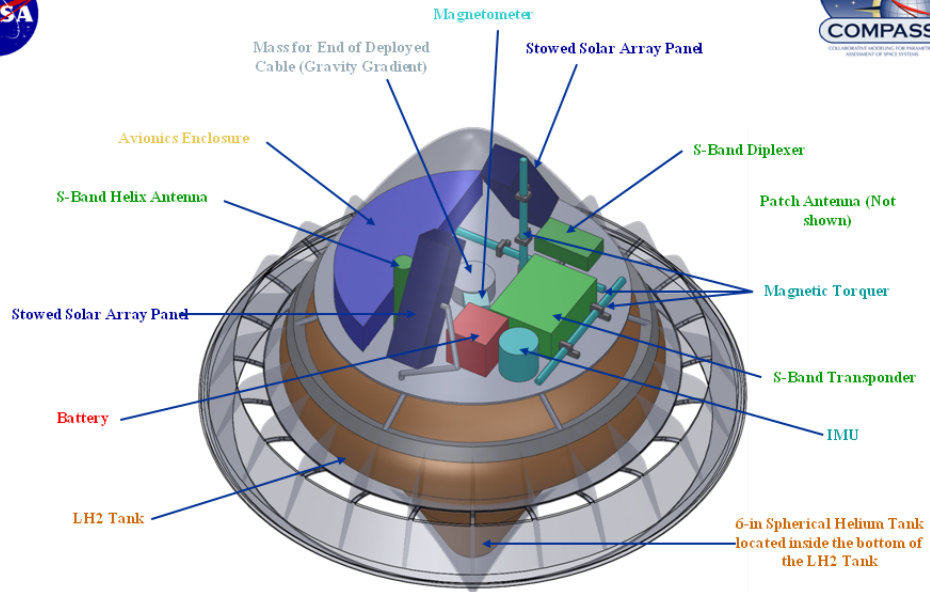
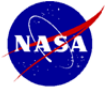
17

National Aeronautics and Space Administration

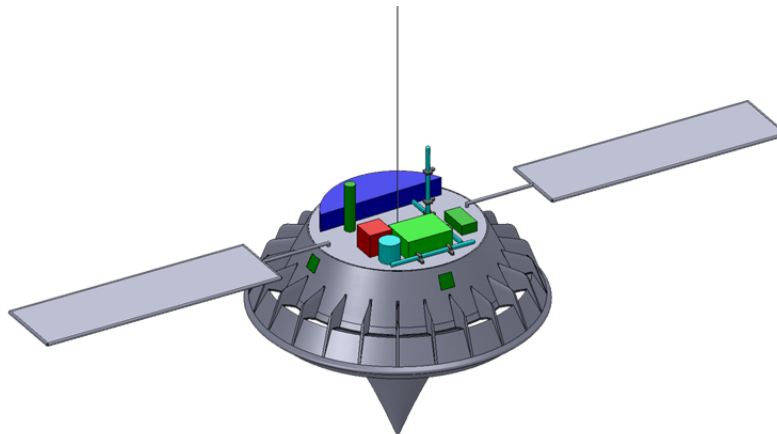
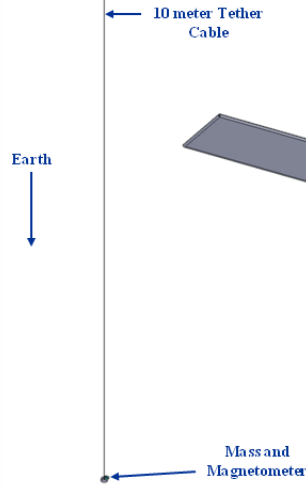
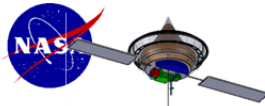


Patch Antenna for
pre-deployment
communications (4
Total, 90 deg apart)





o



Mission

David Smith, Camille Moore
COMPASS Team
10-08-10

23

National Aeronautics and Space Administration



BEP 1.2 m LTD: OTIS Simulation Details



Simulation overview: point-mass, 3DOF simulation with the overall objective to maximize payload mass for a minimum GLOM to 400 km sub-orbital target.

Launch from a 3km altitude launch with a 30° fixed flight path angle for 50 seconds.

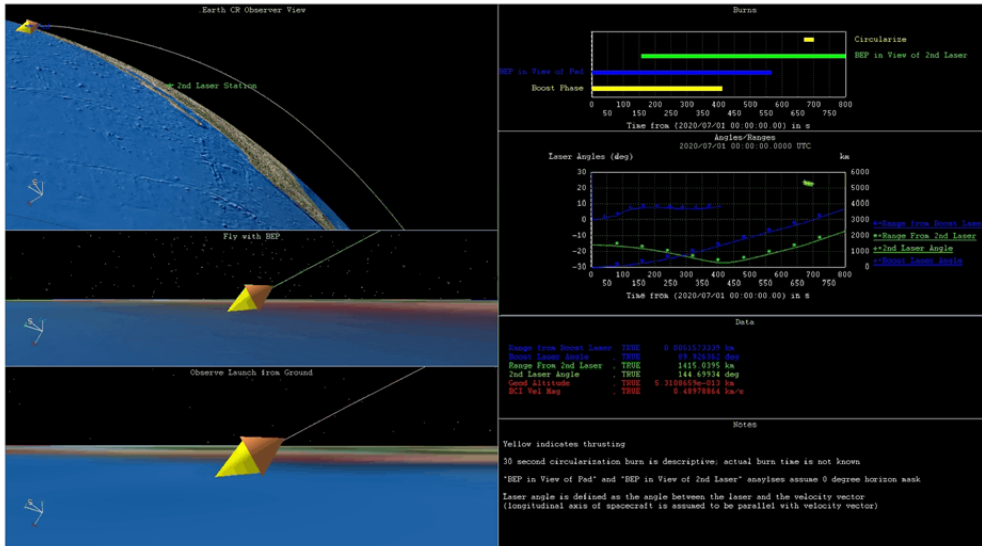
Climb to air-breather/rocket mode switch point (air-breather to rocket switch point optimally determined).

Climb with rocket mode to 400 km sub-orbital target

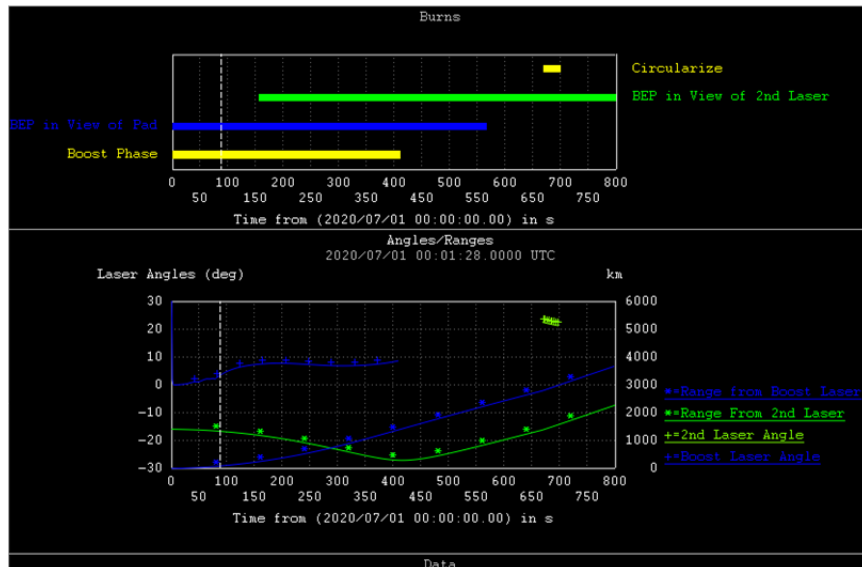
Coast to laser circularization into the final orbit



Trajectory Simulation Using SOAP (Movie)

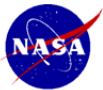
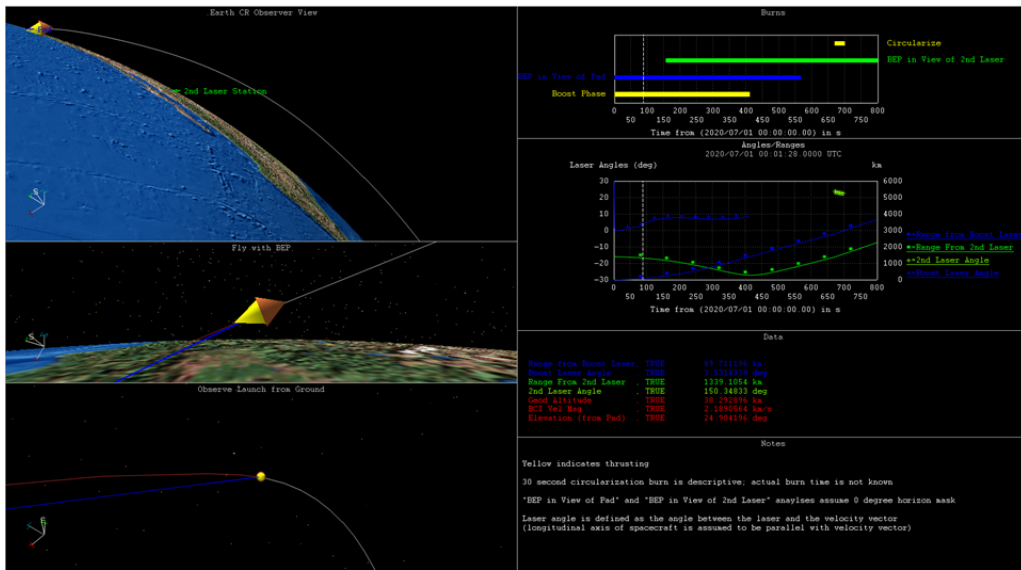


Phases and Angles from SOAP Simulation

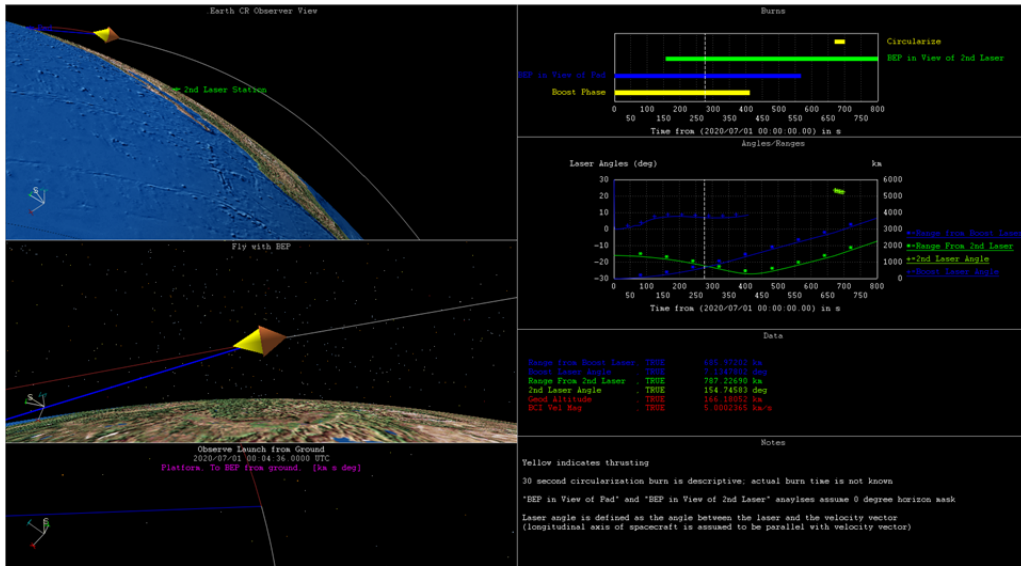




Early Boost Phase

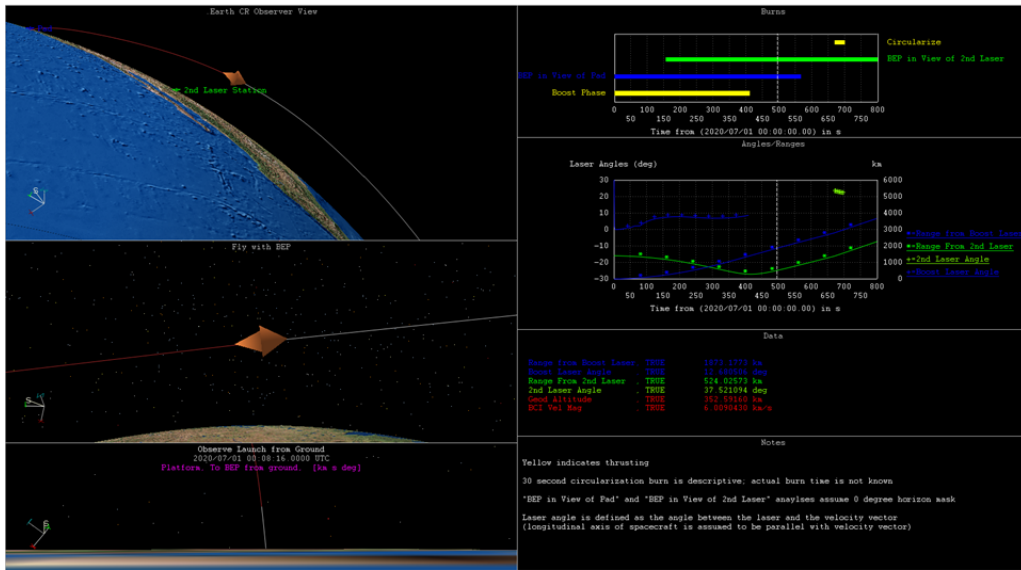


Boost Phase

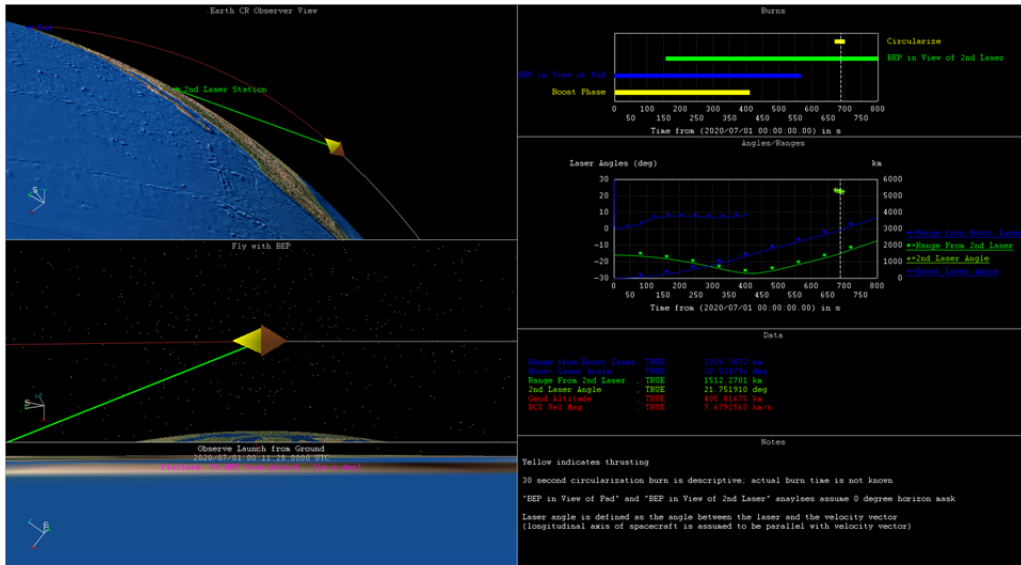


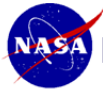


Coast



Circularization Burn





BEP 1.2 m LTD: OTIS Simulation Details



- **Air-breather mode assumptions and simulation details:**
 - Propulsion data consisting of mach and altitude table lookup of C_m (N/MW), EP (J) and PRF (Hz). (*Customer supplied*). Reference data for a 100MW laser. Simulation includes a throttle (to reduce thrust when/if necessary) and a scale factor (range 1 to 3.5) to simulate a more powerful laser (higher PRF) when required.
 - LTD burns surrounding air with an Infinite ISP (no mass flow).
 - Drag model from SDIO Final Tech Report (1989) (figure 11.2) with reference area of 0.7854 m^2 . (*Customer supplied*).
- **Rocket mode assumption and simulation details:**
 - Thrust as a function of laser power and atmospheric loss terms were modeled following formulation in “Laser Propulsion for ESA Mission, Final Report” (2004). (pgs. 82 and 85)
 - Reference laser = 100MW (scaled if necessary to be consistent, in power level, with the air-breather mode.)
 - LTD burns LH20 with an ISP of 950 sec.
 - Drag model from SDIO Final Tech Report (1989) (figure 11.2) with reference area of 0.7854 m^2 . (*Customer supplied*).
- **Key 3DOF (point mass) simplifying assumptions for entire trajectory (optimistic trajectory -- to include would require additional coordinate system in OTIS or full 6DOF simulation):**
 - No loss term for off angle laser pointing
 - No steering from off center beam targeting



BEP 1.2 m LTD: OTIS Summary



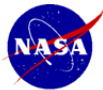
- OTIS optimal trajectory for specified flight profile to a 400 km sub-orbital target with final velocity of 5.5 km/s.
- Closed form calculation to circularize using a second laser source.
- Key trajectory parameters and timing of events summarized in con-ops portion of presentation
- Future work should include:
 - An investigation of different trajectories for optimality. The work should also include the implementation of a full propulsion model: at a minimum a complete propulsion table but preferably, direct formulations of propulsion as a function of received laser power.
 - Full assessment of the second laser station and location of the the vehicle pointing should full inclusion of a propulsion model fail to remove the necessity to perform circularization burn with the laser to capitalize on the high ISP associated with LH20 and the laser.
 - Secondary effects of off-center angle thrust terms and aim-pointing steering. These effects would require the addition of a coordinate system into OTIS, which may be out of scope of the study, or a full 6-DOF representation of the vehicle.



Requirements for Insertion into Circular 400 km orbit.



- OTIS trajectory ends in elliptical orbit, the following are the requirements necessary to circularize from the OTIS end point:
- Required delta-V to circularize: 1772 m/s
- Too far downrange (~1335 km) from laser/launch site to use launch laser directly.
 - Options to circularize.
 - On-board chemical: insufficient performance to achieve orbit
 - Orbital based laser or reflector: high cost and phasing problems
 - Another ground based laser site: high cost, non-optimal thrust pointing
- To the first order a second laser station is needed
 - Angle from the station to the vehicle needs to be assessed



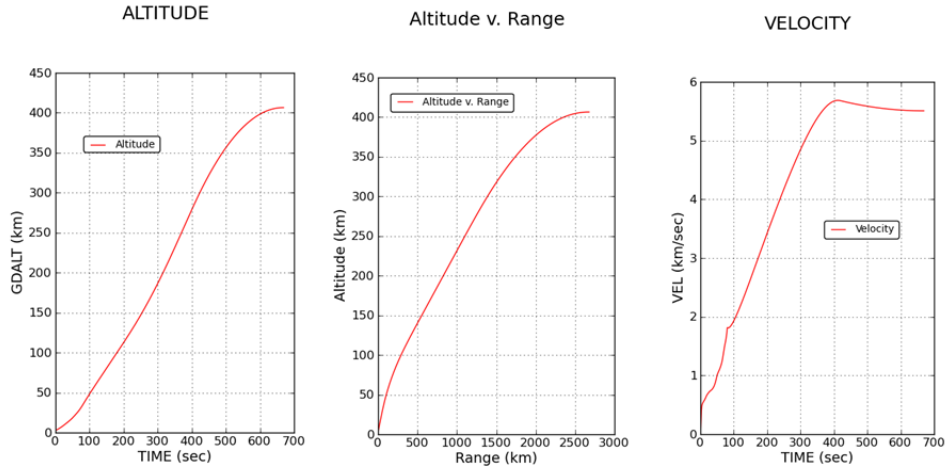
BEP 1.2 m LTD: Mass, ΔV and Propellant Summary



OTIS Mass, delta-V and Propellant Summary	
Gross Lift-off Mass (kg):	334.99
Nose cone mass (kg):	4.73
Total propellant (H₂O) consumed (kg):	171.20
Air-breather mode:	
mass at end of air-breather mode (kg)	334.99
propellant (air) consumed (kg)	NA
delta-V (m/s)	NA
Rocket Mode (propellant = H₂O)	
mass at end of rocket mode (pre circ) (kg)	192.20
mass at end of mode less nose cone (pre circ) (kg)	187.47
propellant (H ₂ O) consumed (kg)	137.86
delta-V (m/s)	4935.30
propellant (H ₂ O) to circularize (kg)**	33.34
final estimate mass to circular 400 km orbit (kg)**	159.15
delta-V to circularize (m/s)**	1771.90
** indicates estimates from closed form calculations	



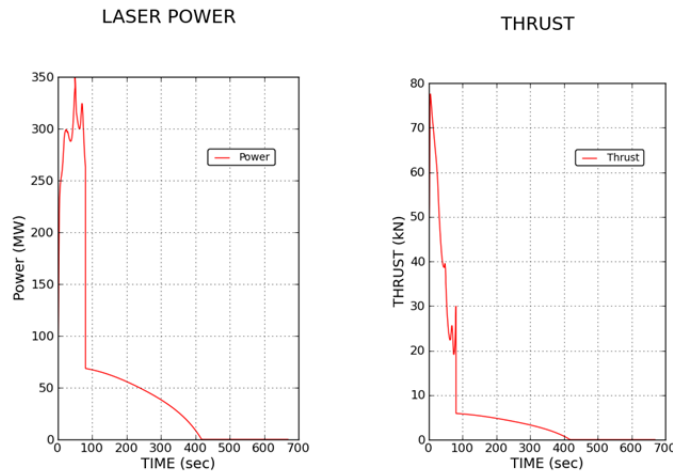
BEP 1.2 m LTD: Simulated Trajectory



Note: Does not include orbit circularization portion of trajectory



BEP 1.2 m LTD: Power and Thrust



Note: Does not include orbit circularization portion of trajectory



BEP Delta-V Summary



Mission DeltaV Summary					
Phase Number	Phase Name	DeltaV (m/s)	Isp (s)	Mass Drop (kg)	Propellant History (kg)
1	Vertical rise	***	***	***	173.1
2	Pitchover	4947	950	***	34.8
3	Deploy Nose Cone as Yo-Yo weights and then Jett	***	***	4.7	34.8
4	Orient For Insertion Burn	4.1	50	***	33.2
5	LEO Insertion	1779	950	***	0.0

CONOPS

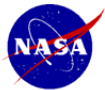
Jeff Woytach
 COMPASS Team
 10-08-10



CONOPS Assumptions



- **Launch site will be at an altitude ≥ 3 km**
- **Launch facilities will include:**
 - Vehicle processing facility
 - Vehicle/payload assembly in clean room environment
 - Vehicle balancing (static and dynamic) and mass properties determination
 - Cleaning before installation in transport container
 - Vehicle transport to the launch pad
 - Launch pad
 - Mount vehicle to launch stabilization system
 - Water loading and ground power
 - terminated before vehicle spin-up
 - Laser launch systems
- **Launch commit criteria will include:**
 - surface winds
 - winds aloft
 - clear skies over launch site and downrange trajectory
 - NORAD clearance (LEO spacecraft)
 - Local air traffic clearance



ISO 14644-1 Cleanroom Standards



Class	maximum particles/m ³						FED STD 209E equivalent
	$\geq 0.1 \mu\text{m}$	$\geq 0.2 \mu\text{m}$	$\geq 0.3 \mu\text{m}$	$\geq 0.5 \mu\text{m}$	$\geq 1 \mu\text{m}$	$\geq 5 \mu\text{m}$	
ISO 1	10	2					
ISO 2	100	24	10	4			
ISO 3	1,000	237	102	35	8		Class 1
ISO 4	10,000	2,370	1,020	352	83		Class 10
ISO 5	100,000	23,700	10,200	3,520	832	29	Class 100
ISO 6	1,000,000	237,000	102,000	35,200	8,320	293	Class 1000
ISO 7				352,000	83,200	2,930	Class 10,000
ISO 8				3,520,000	832,000	29,300	Class 100,000
ISO 9				35,200,000	8,320,000	293,000	Room air



POI Series Spin Balance Machine

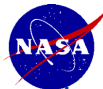


- Vertical two-plane spin balance machine measures all mass properties:
 - center of gravity (CG)
 - moment of inertia (MOI)
 - product of inertia (POI)
 - dynamic unbalance.

POI Series Spin Balance Machines - (export)								
MODEL	RECOMMENDED PAYLOAD RANGE (Kg)	RANGE OF SPIN SPEEDS (RPM)	MAX LOADING MOMENT (Kg-cm)	MAXIMUM CG HEIGHT (Kg @ mm)	MOI ACCURACY (% OF READING ± Kg-cm ²)	FULL SCALE DYNAMIC UNBALANCE (Kg-mm ² @ RPM)	MINIMUM ACHIEVABLE READOUT (Kg-mm ² @ RPM)	UNBALANCE REDUCTION RATIO (%)
POI 1000	5-450	30-300	5,760	350 @ 1300 @50RPM	0,1% + 2.2	5,6 @ 50 1,4 @ 100 0,35 @ 200 0,16 @ 300	148,3 @ 50 29,3 @ 100 7,3 @ 200 4,4 @ 300	95%

<http://www.space-electronics.com/Products/spin.php>

Image copyright Space Electronics LLC; used with permission.



Processing and Launch

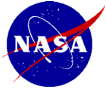


L - 10 days:

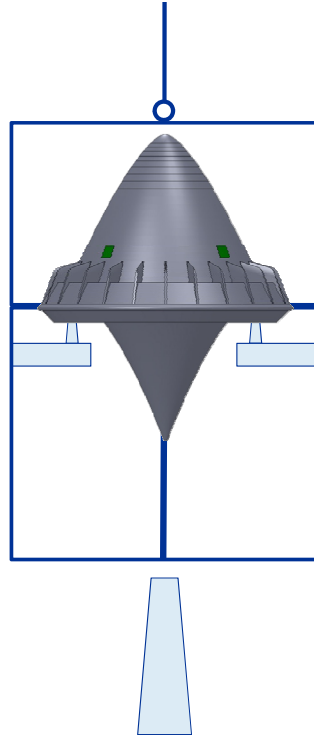
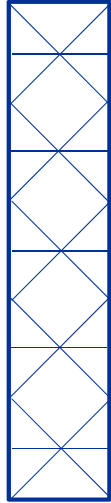
- The vehicle, including payload is assembled in a clean room
- The vehicle is placed on a spin balance machine and undergoes static and dynamic spin balancing, and mass properties (c.g., moments and cross products of inertia) are determined
- Any guidance updates to the vehicle's flight computer are done
- Vehicle is fueled with water propellant, cleaned and loaded into its transport container for roll-out to the launch pad.
 - the container supports the vehicle at its ring fins during transport to the pad
 - the container is open at the bottom
 - the container has horizontal and vertical split-line so that its top half can be removed to mount the vehicle to the pad, and so its bottom half can be opened for removal from around the vehicle

L – 2 hours:

- The vehicle in its transport container is rolled out to the launch pad
- A crane lifts the transport container and lowers it onto the pad spin bearing
 - viewing ports in transport container allow for visually aligning vehicle on pad
- Latches holding the transport container's top cover in place are released and the top cover is removed by the crane
- The pad service tower extends a balance arm with spin bearing, ground power umbilical and water fueling line. The power umbilical and fueling line are automatically mated when the spin cap is placed on the vehicle



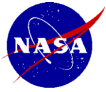
Service Tower



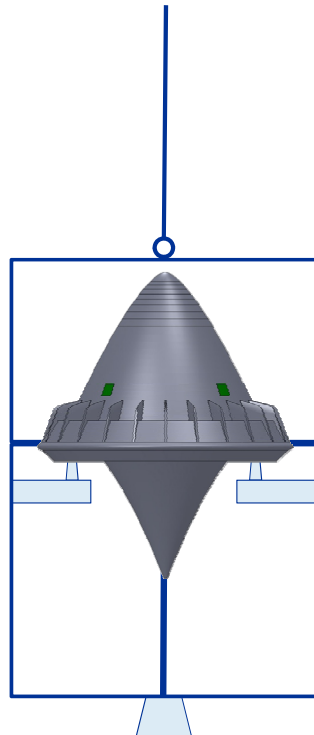
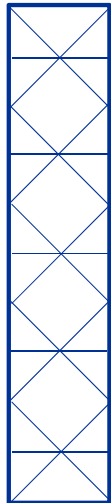
Transport Container

Pad Spin bearing

43



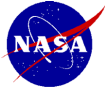
Service Tower



Transport Container

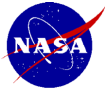
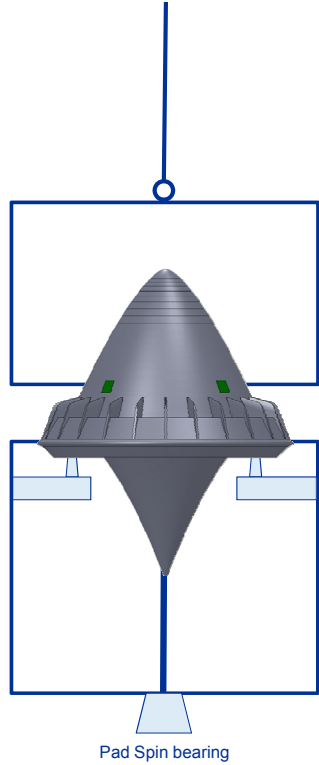
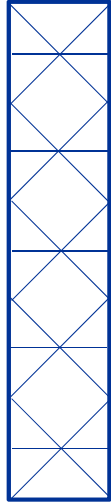
Pad Spin bearing

44



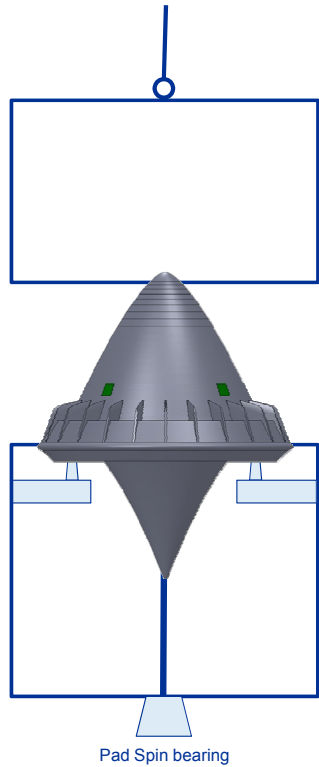
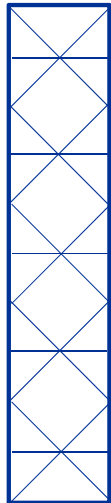
Transport Container

Service Tower



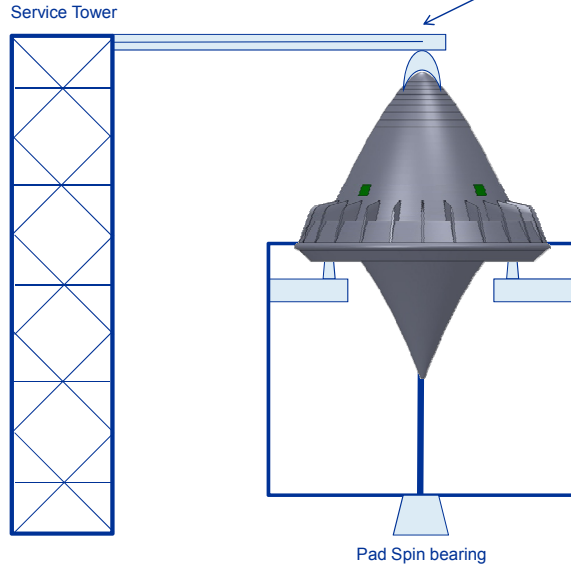
Transport Container

Service Tower

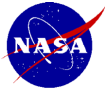




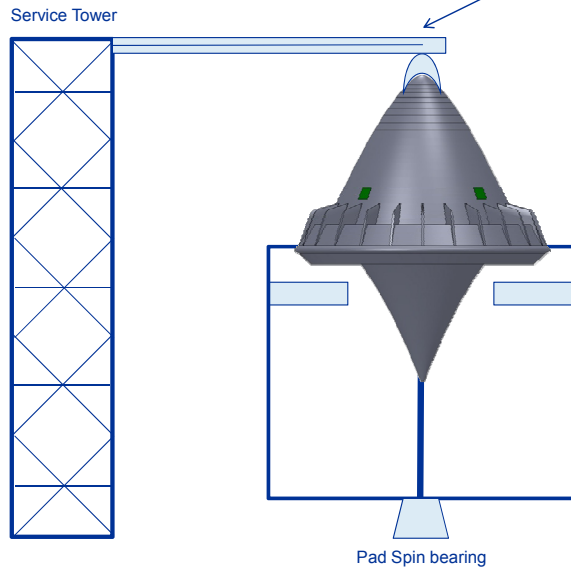
Balance arm with spin bearing, ground power umbilical



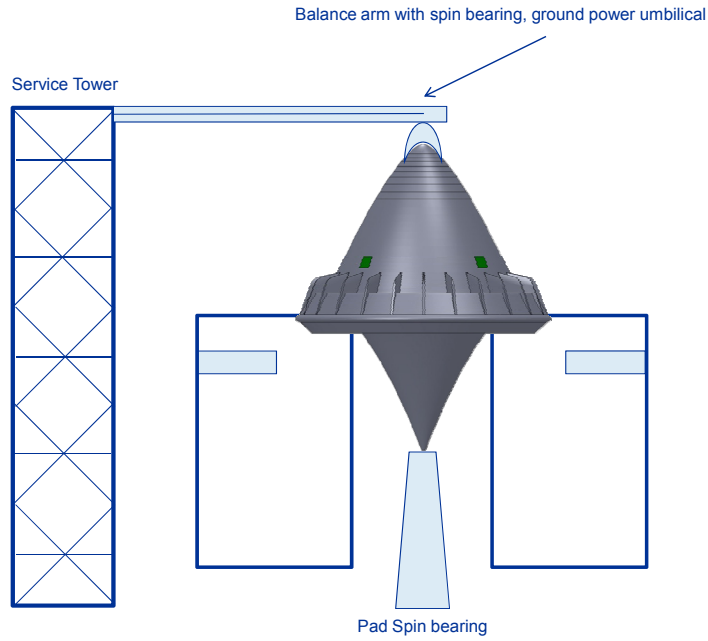
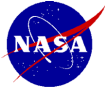
47



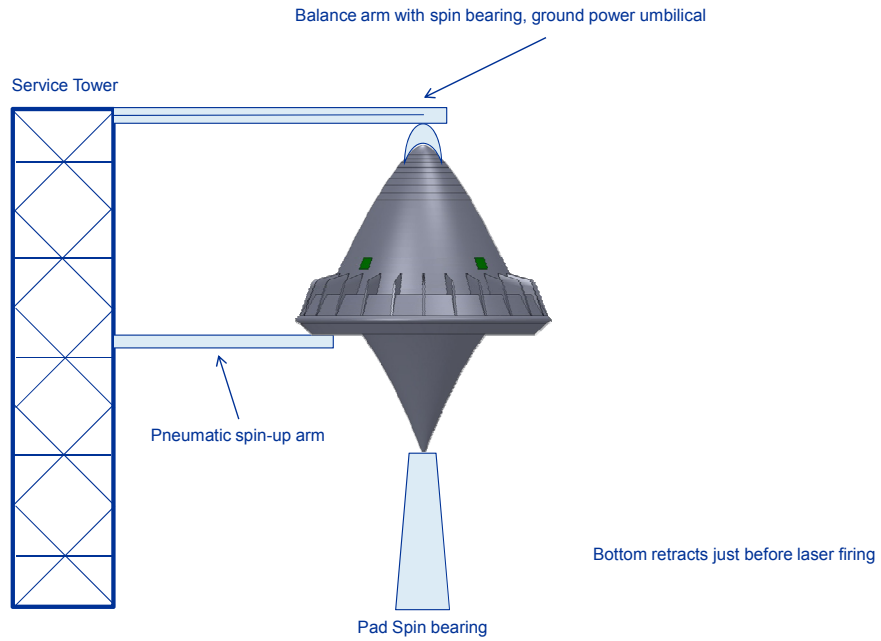
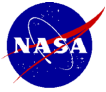
Balance arm with spin bearing, ground power umbilical



48



49



50



L - 4 hours:

- rawinsonde is launched to determine altitude wind profiles for launch

L - 3 hours:

- wind speed/direction data from rawinsonde is processed and "GO/NO_GO" for launch operations is issued

L - 2 hours:

- The vehicle is rolled out to the launch pad and prepared for launch

L - 1 hour:

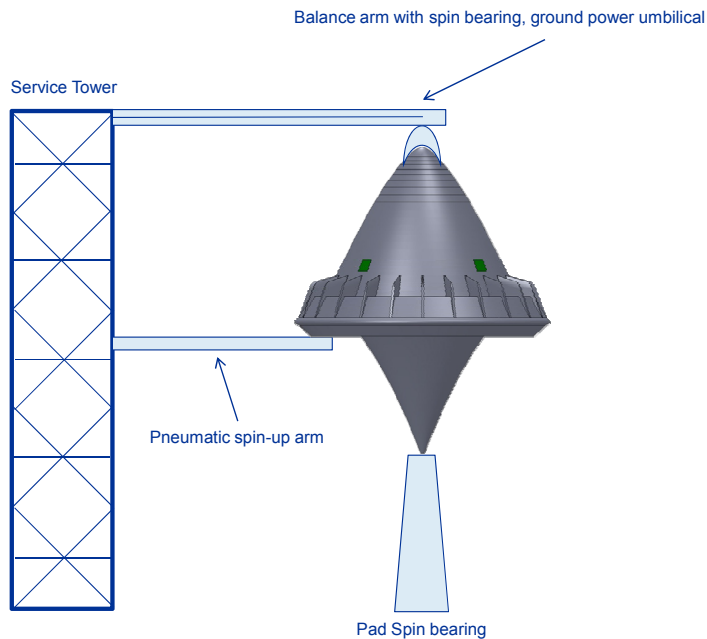
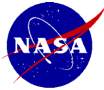
- final guidance update to the vehicle computer is performed
- Final launch clearance are obtained (weather, NORAD, air traffic)

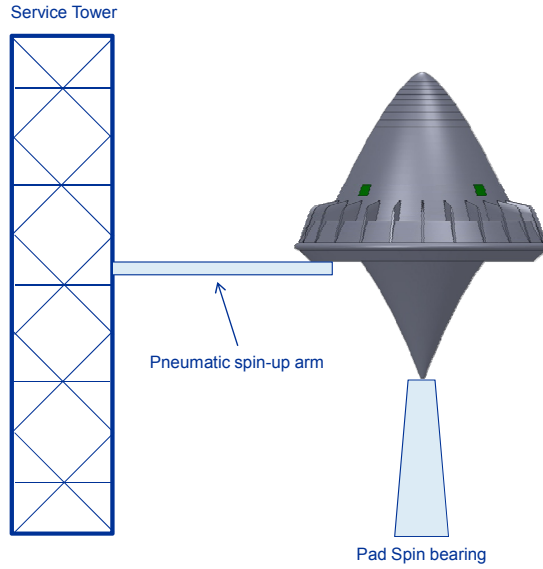
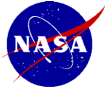
L - 10 minutes:

- vehicle fueling is complete and the fueling line is retracted
- the vehicle is transferred to internal power and the ground power umbilical is retracted
- the pneumatic system spins the vehicle to the 120 rpm launch rate
- the balance arm is retracted by the service tower
- the pneumatic arm is retracted by the service tower
- launch!!

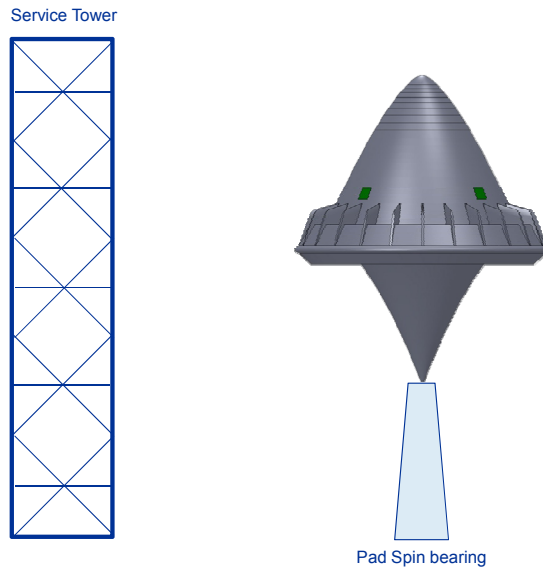
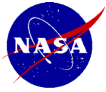
Pre-decisional. For NASA use only.

www.nasa.gov

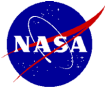




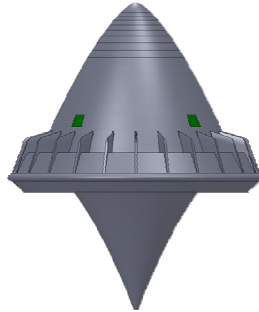
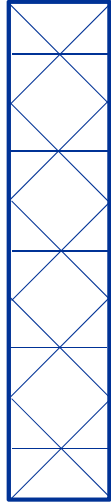
53



54

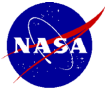


Service Tower

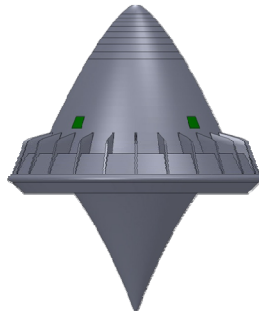
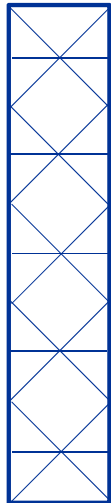


Pad Spin bearing

55



Service Tower



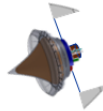
Pad Spin bearing

**T= 0 sec
At this point differential
thrusting to pitch over to the
30° elevation is required**

56



T=418 sec (alt= 295.8 km)
LTD no longer visible
from main laser, un-
powered coast begins.



Nosecone separates;
used as yo-yo weigh to despin
vehicle from 120 to 60 rpm

Reorient vehicle;
Laser insertion



T=660 sec
(down range = 1330 km) circ
burn
Begins using downrange
laser. Length of burn
estimated
Between 30 and 50 sec.
laser firing also de-spins
vehicle



T=80.4 (alt=35 km) (optimally determined) switch from air-breather to rocket
mode (H2O@950ISP) burn initiated.

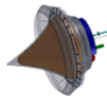


T=50 sec. (alt=18.5 km) 30 degree flight path angle (FPA) hold released and
climb to end of air-beather mode begins with free FPA.



T=0 sec
Altitude = 3 km
30 degree launch with in pure air-breather mode

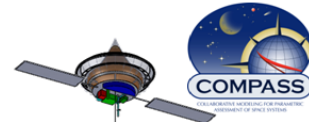
Mission timeline



Reorient Vehicle;
use magnetic torquers to
despin the vehicle



Deploy mass on 10m. tether
to begin gravity gradient
stabilization mode



Deploy solar arrays;
begin payload
activation and checkout

On-orbit Timeline

Systems

David Grantier, Melissa McGuire,
COMPASS Team
10-08-10

59

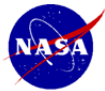
National Aeronautics and Space Administration



COMPASS Spacecraft Design Process



- Build Spacecraft MEL (Master Equipment List) in a WBS hierarchy by major subsystem down to a line item level appropriate to the level of design detail of the request
- Apply MGA from AIAA to each of the line items at the subsystem level
- Gather the total masses and calculate the total system growth % on the Basic dry mass
- Carry an additional system level (or program level) mass to reach a total of 30% mass book-kept on the dry Basic Mass



Mass Growth Allowance (MGA) Schedule



Taken from AIAA S-120-2006, *Standard Mass Properties Control for Space Systems*

- Basic Mass**
 - The current mass data based on an assessment of the most recent baseline design
 - NOTE 1 This design assessment includes the estimated, calculated, or measured (or actual) mass, and includes an estimate for undefined design details like cables, multi-layer insulation and adhesives.
 - NOTE 2 the mass growth allowances (MGA) and uncertainties are not included in the basic mass.
- Mass Growth Allowance (MGA)**
 - The predicted change to the basic mass of an item based on an assessment of the design maturity and fabrication status of the item, and an estimate of the in-scope design changes that may still occur
- Predicted Mass**
 - The basic mass plus the mass growth allowance

Code	Design maturity (basis for mass determination)	Electrical/electronic components			Percent MGA						
		0 to 5 kg	5 to 15 kg	>15 kg	Structure	Thermal control	Propulsion	Batteries	Wire harnesses	Mechanisms	Instrumentation
E	Estimated (preliminary sketches)	30	20	15	15	15	15	20	50	15	50
L	Layout (or major modification of existing hardware)	25	20	15	12	12	12	15	30	12	30
P	Pre-release drawings (or minor modification of existing hardware)	20	15	10	8	8	8	10	25	8	25
C	Released drawings (calculated values)	10	5	5	4	4	4	5	5	4	5
X	Existing hardware (actual mass from another program)	3	3	3	2	2	2	3	3	2	3
A	Actual mass (measured flight hardware)	0	0	0	0	0	0	0	0	0	0
FE	Customer furnished equipment	0	0	0	0	0	0	0	0	0	0

For the COMPASS process, the total percentage on dry mass is desired to be 30% total

*Predicted Mass = Basic Mass + Bottoms up MGA% * Basic Mass*

Therefore, Additional System level margin = 30% - Bottoms up MGA%



Top Level BEP Characteristics

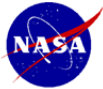


Bottoms up MGA growth is 14% of the Basic mass (also known as Current Best Estimate or CBE) (16 kg)

Desire 30% growth, carry additional 18 kg at system level (16% of basic mass)

Spacecraft Master Equipment List Rack-up (Mass) - Lightcraft					COMPASS S/C Design
WBS	Main Subsystems	Basic Mass (kg)	Growth (kg)	Estimated Total Mass (kg)	Aggregate Growth (%)
06	Lightcraft/Spacecraft	300.1	18	318	
06.1	Lightcraft Stage 1	300	18	318	
06.1.1	Payload	0	0	0	TBD
06.1.2	Attitude Determination and Control	4	0	5	7%
06.1.3	Avionics	11	3	15	30%
06.1.4	Communications and Tracking	4	1	5	22%
06.1.5	Electrical Power Subsystem	4	1	5	30%
06.1.6	Thermal Control (Non-Propellant)	15	0	15	0%
06.1.7	Propulsion (Hardware)	17	2	20	14%
06.1.8	Propellant	188		188	
06.1.9	Structures and Mechanisms	56	10	66	17%
Inert Mass Calculations					
Lightcraft Mass Calculations					
		Basic Mass (kg)	Growth (kg)	Total Mass (kg)	Aggregate Growth (%)
	Lightcraft Estimated Total Wet Mass	300	18	318	
	Lightcraft Estimated Total Dry Mass	112	18	130	16%
	Total Dry Mass with Desired System Level Growth	112	34	146	30%
	Additional Growth (carried at system level)		16		14%
	Total Useable Propellant	180		180	
	Total Trapped Propellants, Margin, pressurant	17		17	
	Total Inert Mass with Growth	129.9	34	163	
	Lightcraft Total Wet Mass with Growth	300		334	

- Inert mass is dry mass + trapped residuals + propellant margin + pressurant
- Dry mass on each segment is calculated as the total bottoms up dry mass with the MGA % applied + additional system mass so that the total growth on each stage is 30% of the basic mass
 - The dry basic mass of the BEP is 112 kg
 - The Total mass with the bottom's up growth is 129 kg
 - The inert mass of the BEP with 30% growth carried on the Basic masses is 163 kg
- Mission applies the ΔVs and the rocket equation to the appropriate total vehicle mass based on the mission event and what stages have been jettisoned
- Total inert mass with the 30% growth incorporated is: 334kg



BEP Inert Mass Calculations



Inert Mass Calculations				
	Basic Mass (kg)	Growth (kg)	Total Mass (kg)	Aggregate Growth (%)
Lightcraft Mass Calculations				
Lightcraft Estimated Total Wet Mass	300	18	318	
Lightcraft Estimated Total Dry Mass	112	18	130	16%
Total Dry Mass with Desired System Level Growth	112	34	146	30%
Additional Growth (carried at system level)		16		14%
Total Useable Propellant	180		180	
Total Trapped Propellants, Margin, pressurant	17		17	
Total Inert Mass with Growth	128.9	34	163	
Lightcraft Total Wet Mass with Growth	300		334	

- Inert mass is dry mass + trapped residuals + propellant margin + pressurant
- Dry mass on each segment is calculated as the total bottoms up dry mass with the MGA % applied + additional system mass so that the total growth on each stage is 30% of the basic mass

- The dry basic mass of the BEP is 112 kg
- The Total mass with the bottom's up growth is 129 kg
- The inert mass of the BEP with 30% growth carried on the Basic masses is 146 kg

- Mission applies the ΔV s and the rocket equation to the appropriate total vehicle mass based on the mission event and what stages have been jettisoned
- Total inert mass with the 30% growth incorporated is: 334 kg



BEP and Propellant Details



Mission DeltaV Summary					
Phase Number	Phase Name	DeltaV (m/s)	Isp (s)	Mass Drop (kg)	Propellant History (kg)
1	Vertical rise	***	***	***	173.1
2	Pitchover	4947	950	***	34.8
3	Deploy Nose Cone as Yo-Yo weights and then Jett	***	***	4.7	34.8
4	Orient For Insertion Burn	4.1	50	***	33.2
5	LEO Insertion	1779	950	***	0.0

WBS	Description	QTY	Unit Mass	Basic Mass	Growth	Growth	Total Mass
Number	Beamed Energy Propulsion (BEP)		(kg)	(kg)	(%)	(kg)	(kg)
06	Lightcraft/Spacecraft			300.37	5.9%	17.63	318.00
06.1	Lightcraft Stage 1			300.37	5.9%	17.63	318.00
06.1.8	Propellant (Chemical)			182.21	0.0%	0.00	182.21
06.1.8.a	Main Engine Propellant			180.51	0.0%	0.00	180.51
06.1.8.a.a	Fuel			180.25	0.0%	0.00	180.25
06.1.8.a.a.a	Fuel Usable	1	165.80	165.80	0.0%	0.00	165.80
06.1.8.a.a.b	Fuel Margin	1	8.29	8.29	0.0%	0.00	8.29
06.1.8.a.a.c	Fuel Residuals (Unused)	1	6.15	6.15	0.0%	0.00	6.15
06.1.8.a.b	Main Engine Pressurant	1	0.26	0.26	0.0%	0.00	0.26
06.1.8.b	Reaction Control System Propellant			1.71	0.0%	0.00	1.71
06.1.8.b.a	Fuel			0.00	0	0.00	0.00
06.1.8.b.b	RCS Propellant	1	1.71	1.71	0.0%	0.00	1.71



BEP MEL



When originally built, the BEP MEL was subdivided by subsystem discipline (Avionics, Communications, Power, etc), since the lightcraft itself doubles as the operational satellite, no additional payload is carried (so payload is shown as zero)

WBS	Description	QTY	Unit Mass	Basic Mass	Growth	Growth	Total Mass
Number	Beamed Energy Propulsion (BEP)		(kg)	(kg)	(%)	(kg)	(kg)
06	Lightcraft/Spacecraft			300.37	5.9%	17.63	318.00
06.1	Lightcraft Stage 1			300.37	5.9%	17.63	318.00
06.1.1	Payload			0.00	0	0.00	0.00
06.1.2	Attitude Determination and Control			4.48	7.2%	0.32	4.80
06.1.2.a	Guidance, Navigation, & Control			4.48	7.2%	0.32	4.80
06.1.3	Avionics			11.30	30.0%	3.39	14.69
06.1.3.a	Command & Data Handling			10.40	30.0%	3.12	13.52
06.1.3.b	Instrumentation & Wiring			0.90	30.0%	0.27	1.17
06.1.4	Communications and Tracking			3.85	21.9%	0.85	4.70
06.1.4.a	S-band Comm. System			3.85	21.9%	0.85	4.70
06.1.4.b	K-band Comm. System			0.00	0	0.00	0.00
06.1.4.c	LED communications System	0	0.00	0.00	0	0.00	0.00
06.1.4.d	Communications Instrumentation			0.00	0	0.00	0.00
06.1.5	Electrical Power Subsystem			3.62	30.0%	1.09	4.71
06.1.5.a	Battery System			0.70	30.0%	0.21	0.91
06.1.5.b	Power Management & Distribution			0.00	0	0.00	0.00
06.1.5.c	Power Cable and Harness Subsystem (C and HS)			0.00	0	0.00	0.00
06.1.5.d	Solar Array			2.92	30.0%	0.88	3.80
06.1.6	Thermal Control (Non-Propellant)			15.23	0.0%	0.00	15.23
06.1.6.a	Active Thermal Control			1.25	0.0%	0.00	1.25
06.1.6.b	Passive Thermal Control			6.06	0.0%	0.00	6.06
06.1.6.c	Semi-Passive Thermal Control			7.93	0.0%	0.00	7.93
06.1.7	Propulsion (Hardware)			17.34	13.8%	2.40	19.74
06.1.7.a	Main Propulsion System			0.00	0	0.00	0.00
06.1.7.b	Propellant Management			17.34	13.8%	2.40	19.74
06.1.8	Propellant (Chemical)			188.37	0.0%	0.00	188.37
06.1.8.a	Main Engine Propellant			186.61	0.0%	0.00	186.61
06.1.8.b	Reaction Control System Propellant			1.76	0.0%	0.00	1.76
06.1.9	Structures and Mechanisms			56.18	17.1%	9.59	65.77
06.1.9.a	Structures			46.26	18.0%	8.33	54.59
06.1.9.b	Mechanisms			9.92	12.7%	1.26	11.18

www.nasa.gov es



BEP: Avionics



WBS	Description	QTY	Unit Mass	Basic Mass	Growth	Growth	Total Mass
Number	Beamed Energy Propulsion (BEP)		(kg)	(kg)	(%)	(kg)	(kg)
06	Lightcraft/Spacecraft			300.37	5.9%	17.63	318.00
06.1	Lightcraft Stage 1			300.37	5.9%	17.63	318.00
06.1.3	Avionics			11.30	30.0%	3.39	14.69
06.1.3.a	Command & Data Handling			10.40	30.0%	3.12	13.52
06.1.3.a.a	FPGA-based IP for PowerPC	1	0.60	0.60	30.0%	0.18	0.78
06.1.3.a.b	Enclosure with power supply	1	3.30	3.30	30.0%	0.99	4.29
06.1.3.a.c	Ultra Stable Oscillator	0	0.00	0.00	30.0%	0.00	0.00
06.1.3.a.d	48 channel AD/DA/SDI card	1	0.90	0.90	30.0%	0.27	1.17
06.1.3.a.e	48 channel SDO card	1	0.50	0.50	30.0%	0.15	0.65
06.1.3.a.f	Gimbal Control Card	0	1.00	0.00	30.0%	0.00	0.00
06.1.3.a.g	Feed System Driver	0	1.00	0.00	30.0%	0.00	0.00
06.1.3.a.h	Thermocouple Ref. Card	1	1.00	1.00	30.0%	0.30	1.30
06.1.3.a.i	Camera Controller	1	0.50	0.50	30.0%	0.15	0.65
06.1.3.a.j	Charge control card	1	1.50	1.50	30.0%	0.45	1.95
06.1.3.a.k	load control card	1	1.50	1.50	30.0%	0.45	1.95
06.1.3.a.l	router	1	0.60	0.60	30.0%	0.18	0.78
06.1.3.a.m	Misc#4	0	0.00	0.00	0.0%	0.00	0.00
06.1.3.b	Instrumentation & Wiring			0.90	30.0%	0.27	1.17
06.1.3.b.a	Electrical Harnessing associated with the CDH system	1	0.90	0.90	30.0%	0.27	1.17

WBS	Description	QTY	Unit Mass	Basic Mass	Growth	Growth	Total Mass
Number	Beamed Energy Propulsion (BEP)		(kg)	(kg)	(%)	(kg)	(kg)
06	Lightcraft/Spacecraft			300.37	5.9%	17.63	318.00
06.1	Lightcraft Stage 1			300.37	5.9%	17.63	318.00



BEP: Communications



WBS	Description	QTY	Unit Mass	Basic Mass	Growt h	Growt h	Total Mass
Number	Beamed Energy Propulsion (BEP)		(kg)	(kg)	(%)	(kg)	(kg)
06	Lightcraft/Spacecraft			300.37	5.9%	17.63	318.00
06.1	Lightcraft Stage 1			300.37	5.9%	17.63	318.00
06.1.4	Communications and Tracking			3.85	21.9%	0.85	4.70
06.1.4.a	S-band Comm. System			3.85	21.9%	0.85	4.70
06.1.4.a.a	Transponder	1	1.20	1.20	15.0%	0.18	1.38
06.1.4.a.b	Diplexer	1	0.60	0.60	15.0%	0.09	0.69
06.1.4.a.c	Switchbox	1	0.50	0.50	30.0%	0.15	0.65
06.1.4.a.d	Cabling	1	0.70	0.70	30.0%	0.21	0.91
06.1.4.a.e	S-band Helix Antenna	1	0.27	0.27	30.0%	0.08	0.35
06.1.4.a.f	Misc#2	3	0.06	0.18	30.0%	0.05	0.23
06.1.4.a.g	Misc#3	1	0.40	0.40	20.0%	0.08	0.48
06.1.4.a.h	Misc#4	0	0.00	0.00	0.0%	0.00	0.00



BEP: Attitude Determination and Control



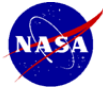
WBS	Description	QTY	Unit Mass	Basic Mass	Growt h	Growt h	Total Mass
Number	Beamed Energy Propulsion (BEP)		(kg)	(kg)	(%)	(kg)	(kg)
06	Lightcraft/Spacecraft			300.37	5.9%	17.63	318.00
06.1	Lightcraft Stage 1			300.37	5.9%	17.63	318.00
06.1.2	Attitude Determination and Control			4.48	7.2%	0.32	4.80
06.1.2.a	Guidance, Navigation, & Control			4.48	7.2%	0.32	4.80
06.1.2.a.a	Inertial Measurement Units	1	0.75	0.75	5.0%	0.04	0.79
06.1.2.a.b	Gyros	0	0.00	0.00	0.0%	0.00	0.00
06.1.2.a.c	GPS	4	0.25	1.00	5.0%	0.05	1.05
06.1.2.a.d	Magnetometers	1	0.23	0.23	5.0%	0.01	0.24
06.1.2.a.e	Mag torquers	3	0.50	1.50	5.0%	0.08	1.58
06.1.2.a.f	Yo Yo despin	0	0.00	0.00	0.0%	0.00	0.00
06.1.2.a.g	nutation dampers	1	1.00	1.00	15.0%	0.15	1.15



BEP: Propulsion Hardware



WBS	Description	QTY	Unit Mass	Basic Mass	Growt h	Growt h	Total Mass
Number	Beamed Energy Propulsion (BEP)		(kg)	(kg)	(%)	(kg)	(kg)
06	Lightcraft/Spacecraft			300.37	5.9%	17.63	318.00
06.1	Lightcraft Stage 1			300.37	5.9%	17.63	318.00
06.1.7	Propulsion (Hardware)			17.34	13.8%	2.40	19.74
06.1.7.a	Main Propulsion System			0.00	0	0.00	0.00
06.1.7.b	Propellant Management			17.34	13.8%	2.40	19.74
06.1.7.b.a	<i>Main Engine Propellant Management</i>			17.34	13.8%	2.40	19.74
06.1.7.b.a.a	Fuel Tanks	1	9.70	9.70	12.0%	1.16	10.86
06.1.7.b.a.b	Fuel Lines	1	0.50	0.50	12.0%	0.06	0.56
06.1.7.b.a.c	Pressurant Tanks	1	0.50	0.50	12.0%	0.06	0.56
06.1.7.b.a.d	Pressurant Lines	0	0.00	0.00	0.0%	0.00	0.00
06.1.7.b.a.e	Pressurization System - valves, lines	1	2.34	2.34	18.0%	0.42	2.76
06.1.7.b.a.f	Feed System - regulators, valves, etc	1	2.90	2.90	18.0%	0.52	3.42
06.1.7.b.a.g	Thrust Vectoring Valves	4	0.35	1.40	12.0%	0.17	1.57
06.1.7.b.a.h	Misc#2	0	0.00	0.00	0.0%	0.00	0.00
06.1.7.b.a.i	Misc#3	0	0.00	0.00	0.0%	0.00	0.00
06.1.7.b.a.j	Misc#4	0	0.00	0.00	0.0%	0.00	0.00



BEP: Propellant



WBS	Description	QTY	Unit Mass	Basic Mass	Growt h	Growt h	Total Mass
Number	Beamed Energy Propulsion (BEP)		(kg)	(kg)	(%)	(kg)	(kg)
06	Lightcraft/Spacecraft			300.37	5.9%	17.63	318.00
06.1	Lightcraft Stage 1			300.37	5.9%	17.63	318.00
06.1.8	Propellant (Chemical)			182.21	0.0%	0.00	182.21
06.1.8.a	Main Engine Propellant			180.51	0.0%	0.00	180.51
06.1.8.a.a	<i>Fuel</i>			180.25	0.0%	0.00	180.25
06.1.8.a.a.a	Fuel Usable	1	165.80	165.80	0.0%	0.00	165.80
06.1.8.a.a.b	Fuel Margin	1	8.29	8.29	0.0%	0.00	8.29
06.1.8.a.a.c	Fuel Residuals (Unused)	1	6.15	6.15	0.0%	0.00	6.15
06.1.8.a.b	<i>Main Engine Pressurant</i>	1	0.26	0.26	0.0%	0.00	0.26
06.1.8.b	Reaction Control System Propellant			1.71	0.0%	0.00	1.71
06.1.8.b.a	<i>Fuel</i>			0.00	0	0.00	0.00
06.1.8.b.b	<i>RCS Propellant</i>	1	1.71	1.71	0.0%	0.00	1.71



BEP: Structures



WBS	Description	QTY	Unit Mass	Basic Mass	Growt h	Growt h	Total Mass
Number	Beamed Energy Propulsion (BEP)		(kg)	(kg)	(%)	(kg)	(kg)
06	Lightcraft/Spacecraft			300.37	5.9%	17.63	318.00
06.1	Lightcraft Stage 1			300.37	5.9%	17.63	318.00
06.1.9	Structures and Mechanisms			56.18	17.1%	9.59	65.77
06.1.9.a	Structures			46.26	18.0%	8.33	54.59
06.1.9.a.a	<i>Primary Structures</i>			36.52	18.0%	6.57	43.09
06.1.9.a.a.a	Forebody	4	5.33	5.33	18.0%	0.96	6.29
06.1.9.a.a.b	Afterbody	3	8.09	8.09	18.0%	1.46	9.54
06.1.9.a.a.c	Thrust Structure	2	16.02	16.02	18.0%	2.88	18.90
06.1.9.a.a.d	Misc #1	1	0.50	0.50	18.0%	0.09	0.59
06.1.9.a.a.e	Misc #2	1	2.32	2.32	18.0%	0.42	2.74
06.1.9.a.a.f	Misc #3	1	2.67	2.67	18.0%	0.48	3.15
06.1.9.a.a.g	Misc #4	1	1.58	1.58	18.0%	0.28	1.86
06.1.9.a.a.h	Misc #5	0	0.00	0.00	0.0%	0.00	0.00
06.1.9.a.a.i	Misc #6	0	0.00	0.00	0.0%	0.00	0.00
06.1.9.a.a.j	Misc #7	0	0.00	0.00	0.0%	0.00	0.00
06.1.9.a.a.k	Misc #8	0	0.00	0.00	0.0%	0.00	0.00
06.1.9.a.b	<i>Secondary Structures</i>			9.75	18.0%	1.75	11.50
06.1.9.a.b.a	Support Structure	1	2.00	2.00	18.0%	0.36	2.36
06.1.9.a.b.b	Tank Supports and Bracketry	1	5.00	5.00	18.0%	0.90	5.90
06.1.9.a.b.c	cable, tether for motor casing	1	0.11	0.11	18.0%	0.02	0.13
06.1.9.a.b.d	cable, tether for shells	2	0.01	0.02	18.0%	0.00	0.02
06.1.9.a.b.e	boom, solar array	2	0.06	0.12	18.0%	0.02	0.14
06.1.9.a.b.f	casing mass	1	2.50	2.50	18.0%	0.45	2.95



BEP: Mechanisms



WBS	Description	QTY	Unit Mass	Basic Mass	Growt h	Growt h	Total Mass
Number	Beamed Energy Propulsion (BEP)		(kg)	(kg)	(%)	(kg)	(kg)
06	Lightcraft/Spacecraft			300.37	5.9%	17.63	318.00
06.1	Lightcraft Stage 1			300.37	5.9%	17.63	318.00
06.1.9	Structures and Mechanisms			56.18	17.1%	9.59	65.77
06.1.9.a	Structures			46.26	18.0%	8.33	54.59
06.1.9.b	Mechanisms			9.92	12.7%	1.26	11.18
06.1.9.b.a	<i>Power System Mechanisms</i>			0.00	0	0.00	0.00
06.1.9.b.b	<i>Misc Mechanisms</i>			3.98	13.07%	0.52	4.50
06.1.9.b.b.a	Air Inlet Shutters	24	0.05	1.49	18.00%	0.27	1.76
06.1.9.b.b.b	Gravity Gradient boom	1	0.50	0.50	18.00%	0.09	0.59
06.1.9.b.b.c	Boom motor	1	0.50	0.50	18.00%	0.09	0.59
06.1.9.b.b.d	Misc#1	24	0.05	1.09	0.00%	0.00	1.09
06.1.9.b.b.e	Misc#2	4	0.10	0.40	18.00%	0.07	0.47
06.1.9.b.c	<i>Communications Mechanisms</i>			0.50	18.00%	0.09	0.59
06.1.9.b.c.a	Antenna Drive Assemblies/Motors	1	0.50	0.50	18.00%	0.09	0.59
06.1.9.b.c.b	Misc#1	0	0.00	0.00	0.00%	0.00	0.00
06.1.9.b.d	<i>Thermal Mechanisms</i>			0.00	0	0.00	0.00
06.1.9.b.e	<i>Adaptors and Separation</i>			4.64	10.94%	0.51	5.14
06.1.9.b.e.a	Launch Adaptor	1	1.00	1.00	18.00%	0.18	1.18
06.1.9.b.e.b	Separation Mechanisms at xxx	1	1.82	1.82	18.00%	0.33	2.15
06.1.9.b.e.c	Separation Mechanisms at xxx	1	1.82	1.82	0.00%	0.00	1.82
06.1.9.b.e.d	Adaptor Mechanisms to xxx	0	0.00	0.00	0.00%	0.00	0.00
06.1.9.b.e.e	Adaptor Mechanisms to xxx	0	0.00	0.00	0.00%	0.00	0.00
06.1.9.b.e.f	Adaptor Mechanisms to xxx	0	0.00	0.00	0.00%	0.00	0.00
06.1.9.b.e.g	Misc #1	0	0.00	0.00	0.00%	0.00	0.00
06.1.9.b.f	<i>Installations</i>			0.80	18.00%	0.14	0.94
06.1.9.b.f.a	GN&C Installation	1	0.10	0.10	18.00%	0.02	0.12
06.1.9.b.f.b	C&DH Installation	1	0.10	0.10	18.00%	0.02	0.12
06.1.9.b.f.c	Communications and Tracking Installation	1	0.10	0.10	18.00%	0.02	0.12
06.1.9.b.f.d	GN&C Installation	1	0.10	0.10	18.00%	0.02	0.12
06.1.9.b.f.e	Electrical Power Installation	1	0.10	0.10	18.00%	0.02	0.12
06.1.9.b.f.f	Thermal Control Installation	1	0.10	0.10	18.00%	0.02	0.12
06.1.9.b.f.g	Propulsion Installation	1	0.10	0.10	18.00%	0.02	0.12
06.1.9.b.f.h	Payload Installation	1	0.10	0.10	18.00%	0.02	0.12



Top level MEL percentages



WBS	Description	QTY	Unit Mass	Basic Mass	Growth	Growth	Total Mass
Number	Beamed Energy Propulsion (BEP)		(kg)	(kg)	(%)	(kg)	(kg)
06	Lightcraft/Spacecraft			300.37	5.9%	17.63	318.00
06.1	Lightcraft Stage 1			300.37	5.9%	17.63	318.00
06.1.1	Payload			0.00	0	0.00	0.00
06.1.2	Attitude Determination and Control			4.48	7.2%	0.32	4.80
06.1.3	Avionics			11.30	30.0%	3.39	14.69
06.1.4	Communications and Tracking			3.85	21.9%	0.85	4.70
06.1.5	Electrical Power Subsystem			3.62	30.0%	1.09	4.71
06.1.6	Thermal Control (Non-Propellant)			15.23	0.0%	0.00	15.23
06.1.7	Propulsion (Hardware)			17.34	13.8%	2.40	19.74
06.1.8	Propellant (Chemical)			188.37	0.0%	0.00	188.37
06.1.9	Structures and Mechanisms			56.18	17.1%	9.59	65.77

Propulsion

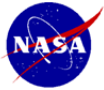
James Fittje
COMPASS Team
10-08-10



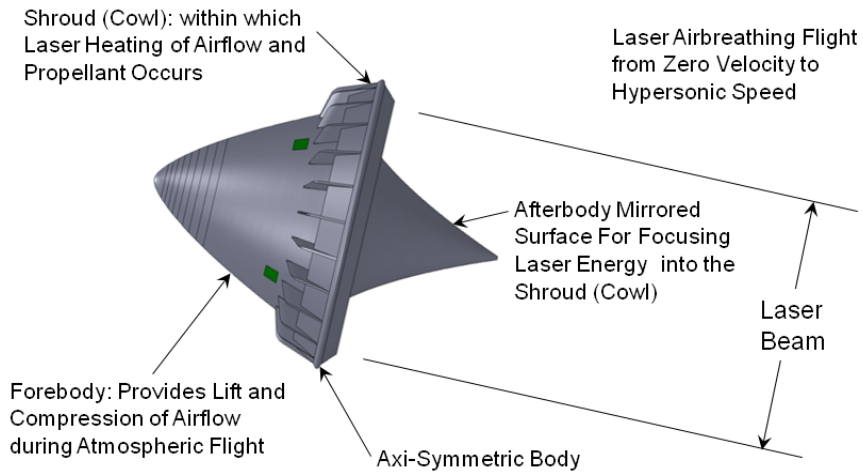
Beamed Energy Propulsion



- Provides Energy for Vehicle Propulsion via Ground Based Laser
- Parabolic Optical Surface Forms Aft Surface of Vehicle
- Propulsion System is Air Breathing Through Most of the Atmosphere
- Onboard Monopropellant is Used in Rocket Mode, but is Still Energized by the Ground Based Laser
- Propulsion is Provided via Rapid Pulsing of Laser Creating Successive High Pressure Blast Waves
- Propulsion System Generates Restorative Force Allowing the Vehicle to be a Beam Rider



Basic Light Craft Operation

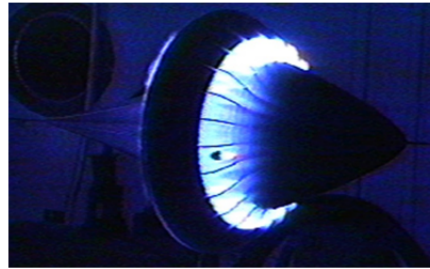




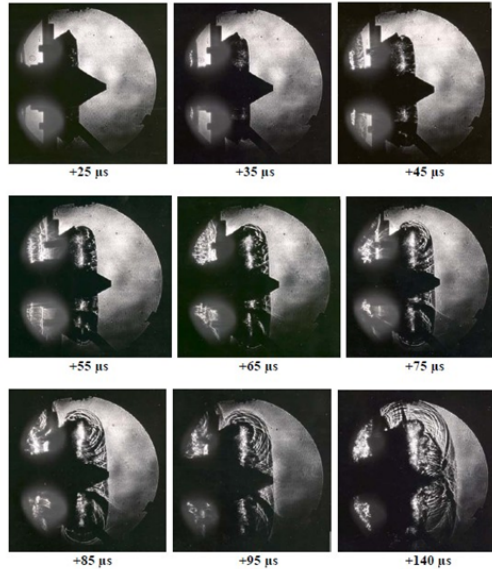
Beamed Energy Propulsion Cont.



- Laser Energy is Concentrated into Shroud Region
- Laser Heating of Propellant Causes
 - Ionization
 - Dissociation
 - Creation of Plasma Toroid Inside Shroud
 - High Pressure Pulse
- Continuous Propulsive Force is Created Rapidly Pulsing Laser



Time Lapse Schlieren of Lightcraft Flowfield





Requirements and Assumptions



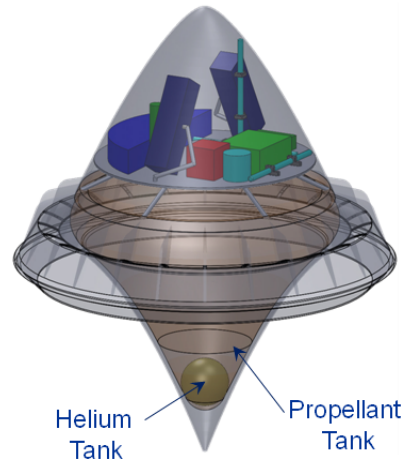
- **Requirements**
 - Zero Fault Tolerant System
 - Tanks Remain Internal to Vehicle
 - No Staging
 - Laser Based Air Breathing Mode to Gain Altitude and Velocity
 - Laser Based Rocket Mode to Build Up Velocity Using Onboard Propellant
- **Assumptions**
 - ISP of 950s with Water Monopropellant
 - Laser System Can Continuously Track and Beam Energy to Vehicle
 - Helium Pressurization
 - Regenerative and Film Cooling of Optic Surfaces



Propulsion Overview



- Central Optic Surface Forming Vehicle Aft Section
- Outer Shroud for Beam Focusing and Propellant Injection During Rocket Mode
- Pear Shaped Propellant Tank w/ Integral High Pressure Helium Sphere
- Water Monopropellant (Blow Down Design)
- Integral RCS and Main Propellant Storage

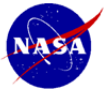




Propulsion Overview Cont.



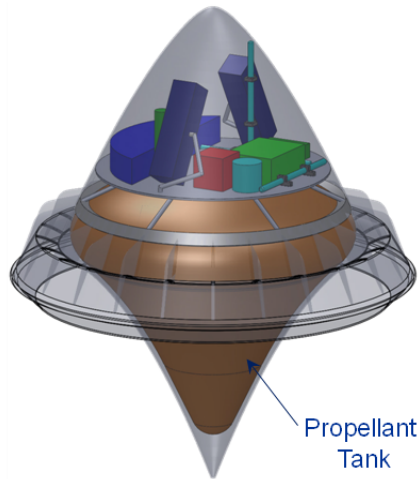
- **Acoustic Valving of Rocket Mode Fuel Injectors**
 - Tuned to Operate at Laser Pulse Frequency
 - Injector System Designed to Prevent Chug
- **Four Additional Equal Spaced Pulsed Injectors on Shroud**
 - Provide for Differential Propellant Injection in Torodial Beam Focus Area
 - Serve as RCS while on Orbit
 - Based on COTS High Speed RCS Valves
- **Propellant Provides Regenerative Cooling of Primary Optic Surface and Cowl Support Struts**
- **Film/Transpiration Cooling on Inner Cowl Surface**
- **Air Breathing Mode to ~Mach 5**
- **Rocket Mode from ~Mach 5+ to Orbit**



Propellant Tank



- **Titanium Alloy Propellant Tank**
 - Unique “Pear” Shape
 - Channel PMD Around Tank Periphery due to Centrifugal Forces on Propellant
 - Slosh Baffles
- **Integrated Ti-Alloy High Pressure Helium Tank**
- **Blown Down Operation**
- **Heat Leak into Tank Assists in Pressurization**

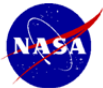
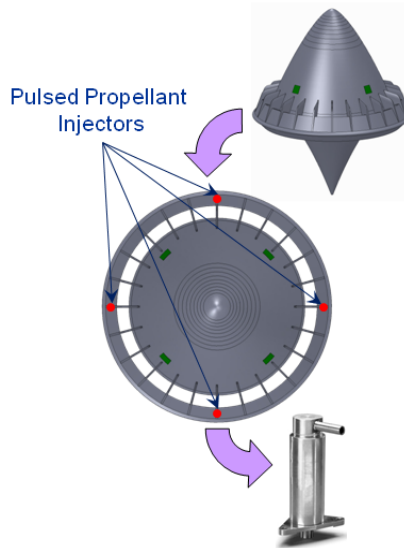




Thrust Vectoring and RCS



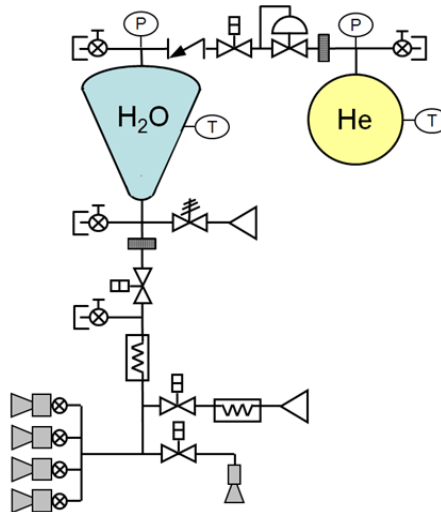
- Differential Propellant Injection via Four Equally Spaced Pulsed Injectors
- Injector Valves Based on COTS RCS Valves
- Can Be Used in All Flight Regimes
- Plumbed on Isolated Feed System Leg
- Vehicle Rotation Ensures All Injectors can Access Entire Focus Volume



Preliminary P&ID



- Blow-Down System
- Single Propellant Tank
- Single Helium Pressurant Tank
- Zero Fault Tolerant Feed System
- Propellant Actively Cools Vehicle Aftbody
- Three Branches
 - Differential Injectors/RCS (4)
 - Uniform Rocket Mode Injectors
 - Film Cooling Flow

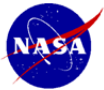




Risks



- **TRL 2 Time Averaged Specific Impulse Value**
- **Maintenance of Appropriate Beam Angle Relative to Vehicle Spin Axis**
- **Adequate Control Authority of Beam to Enable Vehicle Thrust Vectoring via Beam Angular Offset and Differential Propellant Injection**
- **Excessive Propellant Pressure Drop Along Cooling Channels Resulting in Inadequate Propellant Flow Rates**
- **Acoustic Valve Failure Resulting in Incorrect Propellant Injection Timing and/or Inadequate Propellant Flow Rates**
- **Inadequate Regenerative Cooling of Optic Surfaces and Exposed Hot Surfaces**



Risks, cont.



- **Failure of Any Component due to Zero Fault Tolerant Design**
- **Unknown Film Cooling Requirements for Exposed Hot surfaces**
- **Unproven Performance of Air Breathing Ramjet/Scramjet Mode**
- **Proper Inlet Door Operation in Air Breathing to Rocket Mode Transition**



Future Trades



- **Dense Non-Cryogenic Propellants**
 - Ammonia
 - Hydrazine
- **Moving Optic Focus from Annular Surface to Flow Field to Reduce Cooling Requirements**
- **Varying Number of Pulsed Propellant Injectors**
- **Pumped System vs. Helium Pressurized**

Guidance, Navigation, Control

Michael Martini
COMPASS Team
10-08-10



BEP GNC



- **Requirements**
 - Inject the Lightcraft into a 400 km circular orbit with a 28.5 degree inclination
- **Assumptions**
 - BEP Lightcraft has zero products of inertia
 - Pitch control on ascent
 - Provided by differential thrust while in sight of the laser
 - Provided by cold gas thrusting when not in sight of the laser
 - Needed for orienting the vehicle to the correct attitude for the 2nd laser burn (LEO insertion burn)
- **Navigation Design**
 - One LN-200s IMU
 - IMU is low mass (0.75 kg) with spaceflight proven design on Clementine, Deep Space I and the MER rovers
 - Gyros – 3 solid state fiber optic with a bias stability of 0.1 deg/hr
 - Accelerometers – 3 solid state silicon with a bias of 0.3 mg
 - One Ithaco IM-103 3-axis magnetometer to measure the strength and direction of Earth's magnetic field
 - 4 patch antennas used for GPS orbit and attitude determination

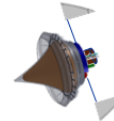
89



BEP GNC



- **Control**
 - Launch
 - Passive stability provided by spinning the vehicle at 120 rpm
 - The vehicle uses the inherent beamriding feature while in sight of the laser
 - Main pitchover maneuver is provided by differential thrusting
 - Prior to orbit insertion the nose cone separates and acts as yo-yo weights to despin the vehicle from 120 rpm to 60 rpm
 - Cold gas thrusting is used to pitch the vehicle to the correct attitude for the LEO insertion burn
 - On orbit
 - Three Ithaco TR10CFR magnetic torquers capable of providing up to a 15 Am² dipole moment
 - Magnetic torquers are used to despin the vehicle after injection into the circular orbit as well as for three axis control for on-orbit operations
 - Gravity gradient stabilization
 - After the vehicle has been beamriding on orbit a tether is deployed with a 2.6 kg mass attached
 - Nutation damper – used to provide additional energy dissipation for increased stability



Avionics

Glenn L. Williams
COMPASS Team
10-08-10

91

National Aeronautics and Space Administration



BEP Avionics Overview



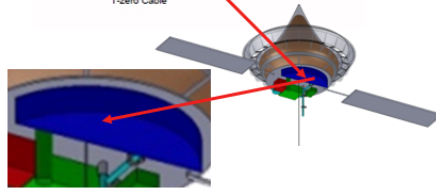
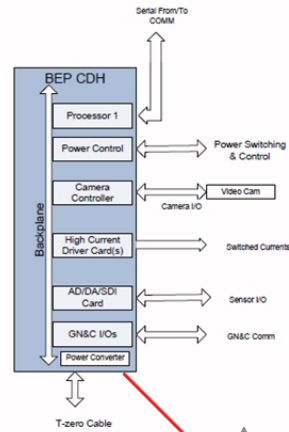
- **Design Requirements**
 - Avionics for systems command, control, and health management
 - Single string processor architecture
 - Low mass optimization required
 - Operational power modes vary according requirements, quiescent until needed
- **Assumptions**
 - 50 kRad avionics for stable operation for duration of mission
 - Cabling mass estimated with Monte Carlo simulation
 - Length
 - Mass
 - All Avionics TRL 5 needing only to fly, due to EEE and Class-S parts usage
- **Design Description**
 - Enclosure space allocation requires semi-circular package
 - Rad-tolerant FPGAs packaged with IP for processor capability,
 - **Embedded software kernels without major O/S overhead (optimized GN&C)**
 - Memory 5 GB with error correction
 - Power Supply stabilized with switching regulators, filter, and EMI shielding accept wide variations in supply voltage
 - Discretes and Power driver cards for general vehicle functions
 - Sensors/drivers I/O cards
 - Housekeeping data and H&S data to ground via comm channel at ~ TBD bps
 - High TRL EEE parts in custom card designs, -40° C ratings



BEP Avionics Functionality



- **General Avionics Processor**
 - PowerPC, chip, or Intellectual Property in an FPGA
 - Semi-Circular avionics card cage. Uses stacked custom boards in open frame design
 - Gimbals and TVC cards mass reduced, control any necessary positioning
 - (Solar array deployment and gimbaling on orbit)
 - (Comm antenna gimbaling TBR on orbit)
 - GNC navigation – data from IMUs used to derive and control TVC parameters (0.16 MIPS nom.)
 - Systems health and status reporting
 - Power managed for various power modes (power trimmed with specialized sentinel switching) and full on for launch
 - System management – includes control of valves, and heaters
 - TBD bps serial interface between CDH and comm channel
- **Software**
 - ROM SLOC estimate ~140 - 180k includes launch
- **Sensors/Drivers**
 - 24 valves, TBD igniters, pyros, RCS, pressure & temperature



BEP Avionics Risks



1. RAD 750 FX obsolescence likely, replace with FPGA
 - **VHDL Intellectual Property**
2. Particle Radiation Tolerance
 - **Shielding?**
 - **High-rad EEE parts**
 - **FPGAs exist with high rad tolerance**
3. Vibration Levels - need to tune structure and board layout for stiffness
 - **Add stiffening members to enclosure and printed circuit boards**
 - **Perform stress analyses**

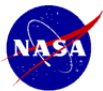


Communication Beam Power Propulsion



- **Introduction**

- The communication system will provide communication during launch and demonstrate a capability similar to that of OrbComm
- The system is a single string system
- To reduce the mass and size of the communication system S-band at NASA frequencies was chosen
 - Other frequency bands can be chosen and analyzed later
- The system will communicate from individual transmitters at 4.8 kbps or greater and from space gateways at 57.6 kbps or greater with a non-gimbaled antenna system.
- On transit to orbit the satellite will communicate to an airplane or balloon near the launch site and to communication systems on the ground as it approaches them in the trajectory



Communication Beam Power Propulsion



- **Introduction**

- There will be 3 patch antenna on the nose cone of the spacecraft to communicate with the airplane or balloon, and the Earth stations down range of the launch site.
- The antenna used for analysis when the spacecraft is in orbit was an helix antenna. Other antenna types like patch antennas should be considered in the future.
- The helix antenna will be inside the nose cone until the nose cone is jettison.
- The helix antenna will not be gimbaled and will be pointed along the axis of the spacecraft toward ground.
- There was a trade on the communication link budget versus the antenna gain and the coverage of the Earth.
- The largest helix antenna was used for the master equipment list to estimate the mass of the communication system.



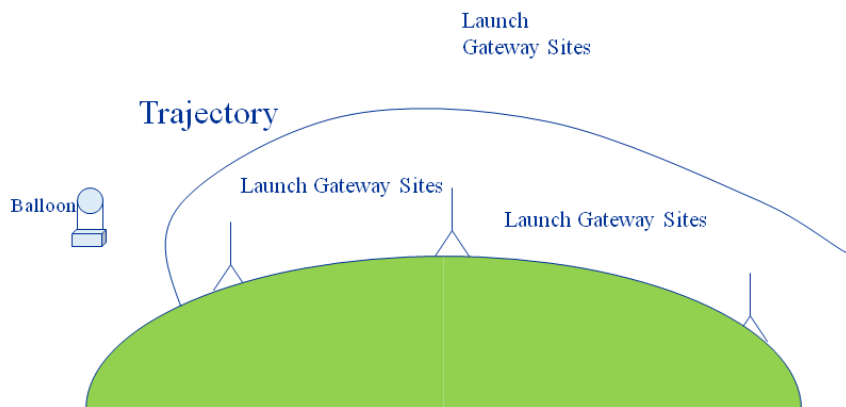
Communication Beam Power Propulsion



- **Trades performed**
 - Communication spot size versus antenna gain
 - Maximum communication range from user versus antenna gain
 - Data rate versus antenna gain
 - Different antenna gain for individual user versus gateway user
 - Data rate versus LNA noise temperature



Communication Beam Power Propulsion – Concept Liftoff





Communication Beam Power Propulsion – Concept Liftoff



- The satellite will communicate at S-band to the communication balloon at the site. As it sails into orbit one or two more down range communication terminals will be needed. The number will be determined by the trajectory and the antenna gain chosen.
- In orbit the satellite will communicate to the ground at S-band with an helix antenna



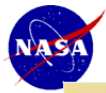
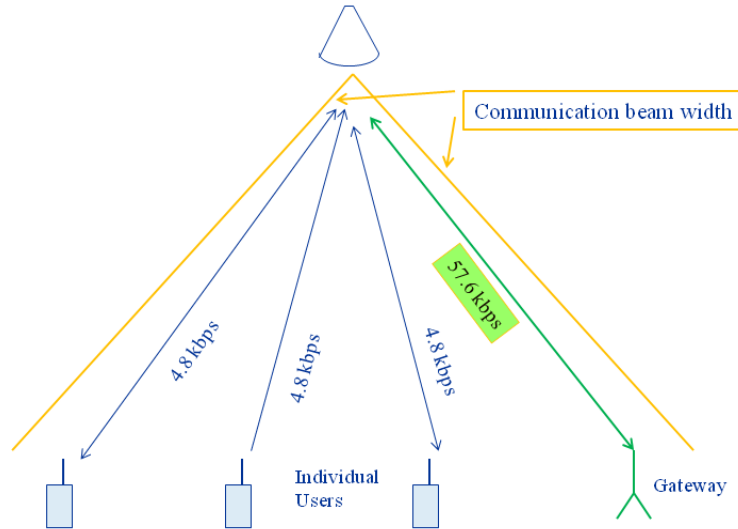
Communication Beam Power Propulsion – Operations



- The satellite will communicate to individual users and to gateway users. The satellite will relay the information between users and gateways. The satellite will use store-and-forward to help relay the information between sites.
- The gateway users will be connected to the internet.



Communication Beam Power Propulsion – Operations Diagram

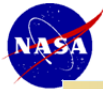


Communication Beam Power Propulsion – Trades



Fixed Conditions			
Frequency	2.2 GHz	Gateway antenna size	1 meter diameter
Satellite transmit power	1 watt	Sat Antenna diameter (cm)	4.13
User transmit power	.25 watts	User antenna gain	2 dBi

Trade Study data rate and coverage versus beam width to Gateway for use of a helix antenna on the spacecraft						
Beam Width (deg)	Antenna Gain (dBi)	Earth Coverage Diameter (km)	Maximum range (km)	Data rate (kbps)	Antenna Length (cm)	Antenna Mass (kg)
150	4.31	2985	3012	114	---	---
120	6.02	1386	1442	1000	3.25	.19
90	8.34	800	894	4600	5.52	.20
60	11.74	461	611	6000	12	.20
45	14.2	331	519	6000	21.1	.20
30	17.69	214	453	6000	47.06	.20



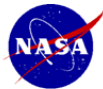
Communication Beam Power Propulsion – Trades



Fixed Conditions			
Frequency	2.2 GHz	Gateway antenna size	1 meter diameter
Satellite transmit power	1 watt	Sat Antenna diameter (cm)	4.13
User transmit power	.25/1/2 watts	User antenna gain	2 dBi

Trade Study data rate and coverage versus beam width to user for use of a helix antenna on the spacecraft						
Beam Width (deg)	Data Rate (kbps) versus user transmit power (watts)					
	3 db Margin			20 db Margin		
	.25 W	1 W	2 W	.25 W	1 W	2 W
150	.3	1.2	2.4	0.008	.032	.064
120	2.4	9.8	19.6	0.05	.2	.4
90	9.6	38.4	76.8	0.11	.44	.88
60	38.4	153.6	308	0.6	2.4	4.8
45	115.2	460	920	2.4	9.6	19.2
30	256	1024	2048	4.8	19.2	38.4

Acceptable communications



Communication Beam Power Propulsion – Trades



•From the previous table on the gateway to the satellite one can see that almost all the beam angles will meet the minimum data rate requirements from the satellite to the gateway station when the gateway station is using a 1 meter diameter dish. Only the largest beam angle is not achievable for the helix antenna design because the helix antenna will have less than 1 coil.

•For beam angles of less than 30 degrees the length of the helix antenna becomes too large for the spacecraft.

•For the low data rate users with the requirement of 4.8 kbps most of the beam angles of the antenna will work even for a transmit power of 0.25 watts if only 3 dB of margin is needed. But for many applications especially within cities a higher margin is required. The table shows the data rate for the two margins for 3 different user transmit power of 0.25 W, 1 W and 2 W. The boxes colored green fulfill the minimum requirement of the study.



Communication Beam Power Propulsion – Applications



- Communication applications of a constellation of beam power satellites.
 - Applications will range from Earth observing applications to mining to trucking and to any low data rate systems that is power sensitive.

- Example of Earth Observing Applications.
 - Monitor of sea temperatures, salinity, CO2 concentration, wind speed, wave actions, solar flux
 - Seismic activities in remote locations
 - Earth quakes
 - CO2 concentration
 - Temperature
 - Monitor of forest for fires
 - Where about of tagged animals
- Monitor of remote mining and oil pumping stations



Communication Beam Power Propulsion – Linkbudget



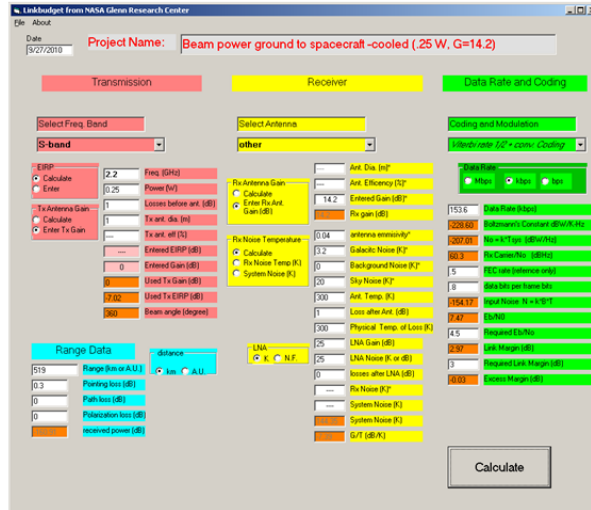
1/4 watt user transmit power to satellite with antenna gain of 8.3 dBi and 3 dB margin

The screenshot shows the 'Linkbudget from NASA Glenn Research Center' software interface. The 'Project Name' is 'Beam power ground to spacecraft-cooled (.25 W, G=8.3)'. The interface is divided into three main sections: Transmission (red), Receiver (yellow), and Data Rate and Coding (green).
 - **Transmission:** Select Freq. Band: S-band; ERP: 2.2 W; Tx Antenna Gain: 8.3 dBi; Beam angle: 30 degrees.
 - **Receiver:** Select Antenna: other; Rx Antenna Gain: 8.3 dBi; System Noise (K): 0.
 - **Data Rate and Coding:** Coding and Modulation: BPSK/16QAM; Data Rate (kbps): 14.4; Required EIRP: 207.61 dBm; Required Link Margin: 3 dB.
 A 'Calculate' button is located at the bottom right of the interface.



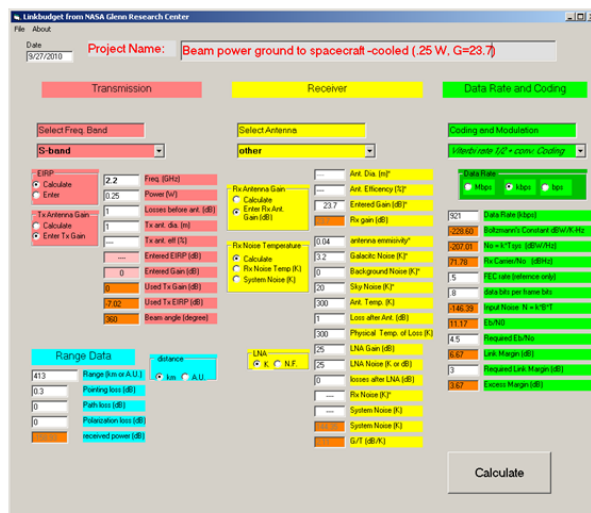
Communication Beam Power Propulsion – Linkbudget

1/4 watt user transmit power to satellite with antenna gain of 14.2 dBi and 3 dB margin



Communication Beam Power Propulsion – Linkbudget

1/4 watt user transmit power to satellite with antenna gain of 23.7 dBi and 3 dB margin

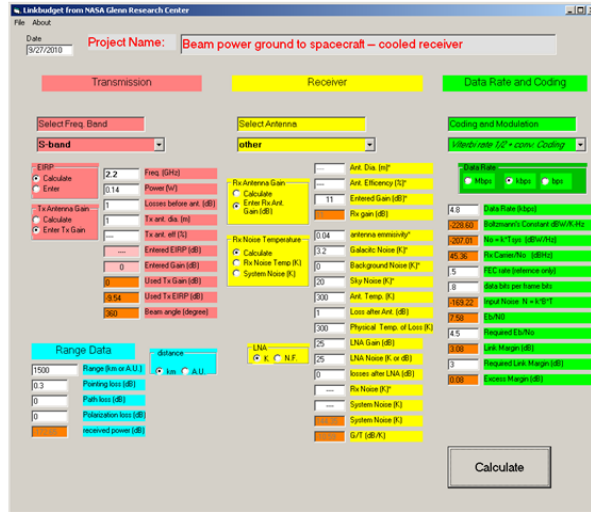




Communication Beam Power Propulsion – Linkbudget

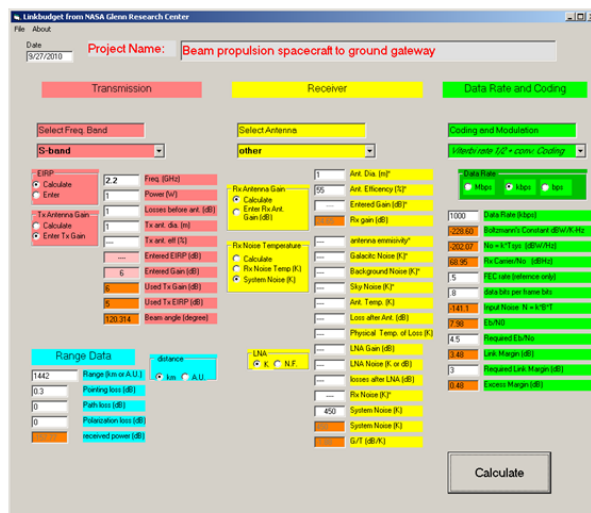


.14 watt user transmit power to satellite with antenna gain of 23.7 dBi and 3 dB margin
Notice the reduced power needs of the user when a cooled LNA is used on the spacecraft.
This will be important for many remote locations operations.



Communication Beam Power Propulsion – Linkbudget

1 watt Satellite transmit power to 1 m gateway antenna
satellite antenna gain of 6 dBi and 3 dB margin





Communication Beam Power Propulsion – Linkbudget

1watt Satellite transmit power to 1 m gateway antenna
satellite antenna gain of 8.34 dBi and 3 dB margin



Communication Beam Power Propulsion – Risk



- No unusual communication component risks
- There is concept of operations risks though
 - Airplane needed for communications at launch site
 - Flipping spacecraft over for communications with the ground

Power

James Fincannon, Kristen Bury
COMPASS Team
10-08-10

113

National Aeronautics and Space Administration



BEP Power Requirements/Assumptions



- **Requirements:**

- No redundancy, single string (i.e. no redundant battery cells, battery packs, solar array strings).
- Orbital user power (day and night)= 105W (includes 30% growth)
- Orbit=400 km (93 minute orbit period/36 minute eclipse) (No orbital altitude degradation, eclipse period is worst case)
- Life= 2 years

- **Assumptions**

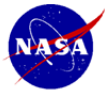
- To minimize the solar array area and mass, full Sun tracking is assumed.
- Two solar array wings (for full sun tracking to minimize the solar array area, with only one axis gimbal per array and yaw steering, each wing gimbal axis must be parallel, thus one or two are possible.)
- 10% of solar array power degraded over mission due to radiation, atomic oxygen, ultraviolet radiation, thermal cycling, contamination, orbital debris/micrometeorites
- Array thermal properties: Emissivity top=.85; Emissivity bottom=.8; Absorptivity top=.92; Absorptivity bottom=.6
- Triple Junction Solar Cell Efficiency
 - 28C (no degradations) = 36%
 - 70C (400km, no degradations)= 32%
 - 70C (400km, with degradations)= 29%
- 10% losses in power system (due to electronics/harness/connector efficiencies)
- Areal mass= 3.66 kg/m² (assuming 3 mil coverglass on each side of solar cell)
- Cell packing factor into solar array = .85
- Lithium batteries= 200 W-hr/kg, 50% depth of discharge (limited due to number of cycles)
- 28 Vdc



Beamed Energy Propulsion PEL



Power Mode Title	Power Mode 1	Power Mode 2	Power Mode 3
	(W)	(W)	(W)
Power Mode Title	Launch	On-Orbit Operational	On-Orbit Non-Operational
Systems operating	All Except EPS/Thermal	All Except Thermal/Structures	AD&C/Avionics/Comm
Attitude Determination and Control	22	22	22
Avionics	36	36	13
Communications and Tracking	20	20	7
Electrical Power Subsystem	0	3	0
Thermal Control (Non-Propellant)	0	0	0
Propulsion (Hardware)	5	5	0
Structures and Mechanisms	24	0	0
Total (watts)	107	86	42
Power Requirement (Plus 30%)	139	112	54

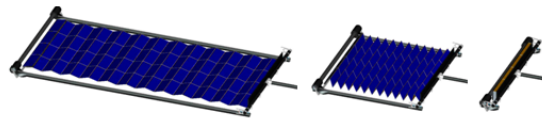


BEP Power Design

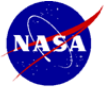


- **Design Description:**

- **2 solar arrays**
- Roll Out Solar Array (ROSA); Z-fold type
- Self deploying, highly compact stowed volume, much lighter than rigid panel solar arrays, thermally favorable for optimized efficiency, minimum parts/complexity.
- Area/wing= 0.3 m²
- Mass/wing= 1.5 kg (with 30% growth)



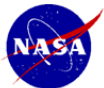
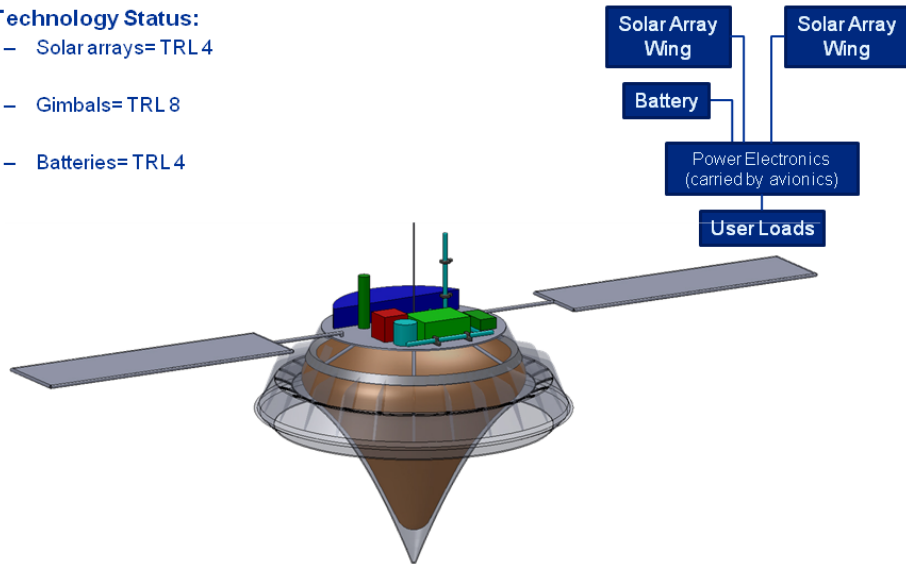
- **2 single axis gimbals**
- Standard, very light, low power gimbals.
- Mass/gimbal= 0.4 kg (with 30% growth)
- **1 lithium ion battery**
- Operation temperature= 10-35C
- Rated energy capacity= 150 W-hr
- Size= 31 cubic inches
- Mass= 0.91 kg (includes 30% growth)
- *Power electronics (solar array peak power regulator, power distribution, battery charge/discharge regulator), gimbal electronics and harness carried by avionics subsystem*



BEP Power Design



- **Technology Status:**
 - Solar arrays= TRL 4
 - Gimbals= TRL 8
 - Batteries= TRL 4



BEP Power Risks



- **Complex launch environment may impact the hardware/design.**
 - High spin acceleration combined with pulsed accelerations along vehicle launch direction/spin axis as well as high thermal loads from both the laser and aero-heating add a great deal of uncertainty to the power system design.
 - While stowed flexible arrays can be designed for high uniform load accelerations (20-50 g), it requires more analysis than a conceptual design to confirm, especially for a low-moderate TRL type array (not off the shelf).
 - Even batteries cannot be assumed immune from spin accelerations due to internal electrolytes that may require the battery package to have a specific orientation to function properly.
 - Thermal loads require more analysis. The present stowed solar array design was focused on being able to separate/partition the power system from this problem as much as possible, but the need for thermal blankets or isolation has not been quantified.
 - Consider reducing the spin rate, orientation of stowed solar arrays parallel with spin axis to minimize differential loading and structural analysis to determine required supports for stowed solar array during launch.

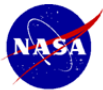


BEP Power Trades



- **Trades Performed:**

- Fixed vs Tracking Solar Arrays: Although fixed arrays could be assumed, this would increase the size of the solar array (50-100%) due to a decreased effective sun period and cosine losses while the energy storage mass would also increase due to an increased effective eclipse period. **Tracking arrays** were selected.
- Tracking Method of Solar Arrays: There are various ways to Sun track the solar arrays: 1) inertial flight (i.e. pointing the entire spacecraft at Sun), 2) two axis gimbals for each solar array or 3) **one axis gimbal for each solar array wing with yaw steering** (i.e. this gimbal tracks about the lengthwise axis of the solar array, the other axis is handled using yaw steering of the spacecraft). For small spacecraft, the yaw steering method is the most economical method for Sun tracking since inertial flight modes are somewhat costly as are too many gimbals.
- Energy storage type: The options for projected available technology for energy storage include 1) electrodynamic tether (extracts energy by passing through the Earth's magnetic field, but is likely heavier than other options, has a tether dynamics risk and causes orbit altitude reduction), 2) lithium sulfur battery (very high specific energy but presently has too few demonstrated charge/discharge cycles to meet LEO orbit life of >1 year and has a low operating depth of discharge to limit degradation, likely not ready by 2020), and 3) **lithium ion battery** (has extensive GEO and some LEO testing and the potential is high for LEO cycling rates at moderate depth of discharge). Although the lithium ion battery type assumed has a higher specific energy compared to SOA LEO lithium ion batteries, it is anticipated the technology will advance rapidly. If not, then a moderate mass penalty due to lower specific energy SOA lithium ion battery can be assumed.
- Power generation type: The options for projected power generation technologies include 1) Electrodynamic Tether (which can provide power during entire orbit, but which really requires some method of orbit raising which is likely not a minimum mass solution), 2) solar array painted/grown on outer structure (low efficiency (~10%), high development risk due to stress/vibrations/thermal, need conductive surface to keep solar cells cool to operate efficiently, but outer surface must be an insulator, unknown radiation/UVAO effects of solar cells, and low TRL, likely not ready by 2020), 3) Concentrator cells using BEP mirror pointing at Sun (low TRL, unknown degradation of reflective surface over time, requires high Sun pointing accuracy or larger area of solar cells, unknown integrated impacts of this on vehicle, requires significant radiator area to keep cells cool to have reasonable efficiency, and not melt, with likely some sort of pumped loop cooling, and requires much more analysis to determine if it can be practical)



BEP Power Trades



- **Trades Performed:**

- Power generation type (continued): 4) Thin film solar cells (low efficiency, thus too large of an area if deployed or used on limited surface area of vehicle, but it has a high TRL level), 5) Deployable rigid panel wings (high TRL, fairly heavy, 2-3 times more than flexible ones, hinges simple/reliable, but fitting into the limited volume vehicle "bay" a problem because the stowed volume is large, risk due to centripetal and launch pulse accelerations/vibrations and due to integration into non-optimal vehicle structure, if integrated into "nose" of rocket inner surface, due to other components, adequate surface area unlikely for power levels required, because articulation is required to minimize the solar array surface area, it is harder to articulate the heavier surfaces and extend them), 6) Inflatable wings (low TRL, needs significant development, could integrate various cell types into inflatable surface and could be rigidized by UV), 7) **Deployable flexible wings** (moderate TRL, ROSA or similar simple unrolling/unfolding types, no thick substrate/mass to attach cells to, highly compact during launch, very light, thermally favorable to keep solar cells at low operating temperature and at high efficiency, low mass, minimizes gimbal requirements)



BEP Power Recommendations/Work to be Done



- **General:**
 - Better factor into the design the range of orbit altitudes (i.e. what is the minimum operational altitude?)
 - Reduce payload compartment spin rate and increase payload volume.
 - Consider jettisoning the rocket stage of the spacecraft.
 - Batteries/solar arrays need spin testing for this unique acceleration/force launch environment.
 - Since this is a commercial vehicle and COMPASS does space-rated/government vehicle designs, we do not minimize cost by using lower quality solar cells, non-space rated batteries/cells or gimbals. This needs to be considered in some manner.
- **Solar arrays:**
 - Perform more thermal load/stress analysis on solar array and perform more detailed layout of the array
 - Obtain re-entry requirements to determine need for retraction or jettison of solar array.
 - Consider modified design of solar array deployment boom/articulation by increasing the length of the solar array and permitting the bottom quarter/third be unpopulated by solar cells (possibly by radiative surface) to simplify the deployment booms/mechanisms.
 - Consider using only one solar array wing. Requires stowed packaging and orbital dynamics analyses. Could help reduce complexity/part count, increase reliability (one wing deploy rather than two), reduce shadowing impacts. However, the balance of the spacecraft through the orbit is impacted.
 - Consider one gimbal for both solar arrays. They both rotate the same direction so some cost can be saved by connecting them to eliminate one gimbal.
- **Battery:**
 - Obtain and analyze time phased load profile for the launch phase (and re-entry phase, if applicable, since solar power is not available at this time) to better size the battery and determine nominal and peak current impacts.
 - Consider use of higher TRL, heavier battery (somewhat heavier) to reduce design risk.
 - Confirm thermal analysis of battery to assure will survive launch and orbit environment.

Thermal

Anthony Colozza
COMPASS Team
10-08-10

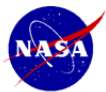


Thermal Subsystem - Description

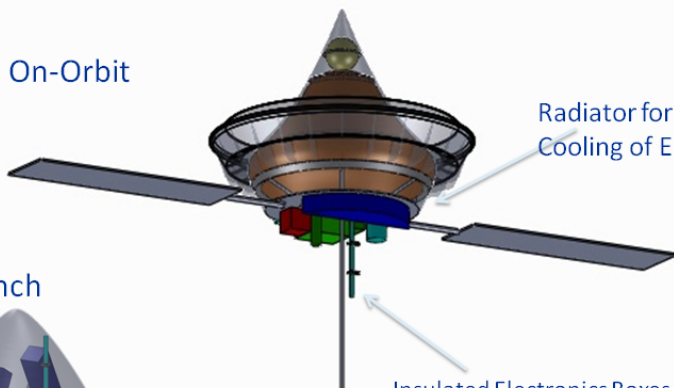


- **Thermal assumptions In orbit**
 - Heat dissipation for 100 W while in orbit.
 - Earth view factor of 0.5
 - Solar array view factor of 0.15
 - 30° sun angle
- **Thermal assumptions Ascent**
 - Mirror reflectivity 0.9999
 - Plasma is located sufficiently from the mirror surface to reduce the needed cooling to that available by the propellant flow.
- **The thermal subsystem components**
 - Cooling channels and pump for circulating water to cool the mirrored optic section and around the cowling where the plasma is formed.
 - Mirrored section will be also utilized as the radiator when in orbit.
 - Cold plates and heat pipes to transfer from the electronics to the radiator section.
 - Cooling passages and pump to cool mirror during ascent.
 - MLI will be used to insulate the electronics boxes.
- **Environmental models**
 - LEO environmental conditions were used to determine the heat transfer while in orbit.
- **Thermal System Mass: 15.23 kg**
- **Trades considered in analysis**
 - The high reflectivity of the mirror is critical to the operation of the vehicle. If the reflectivity degrades during launch there will not be sufficient fuel to cool the surface and complete the mission.
 - The placement of the plasma relative to the optic walls is critical to the operation of the vehicle. If the plasma is within a few centimeters of the wall excessive heating will occur and there will not be sufficient cooling available from the propellant to complete the mission.
- **Options to Reduce mass and recommendations:**
 - A more detailed analysis of the plasma thermal interaction with the vehicle has to be performed to accurately assess its impact.
 - Further analysis and experimentation should be performed to determine the amount of mirror degradation that will occur (if any) during launch and ascent.

123

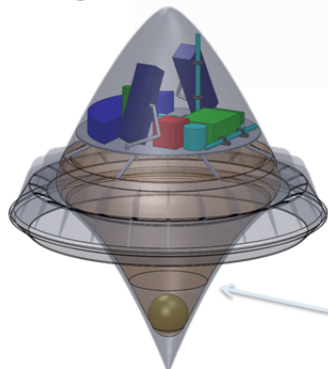


On-Orbit



Radiator for In-Space Cooling of Electronics

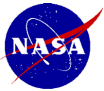
During Launch



Insulated Electronics Boxes with Cold Plates & Heat Pipes

During launch propellant will be pumped in tubes along the inside of the mirror laser reflector to cool it from both the laser and plasma.

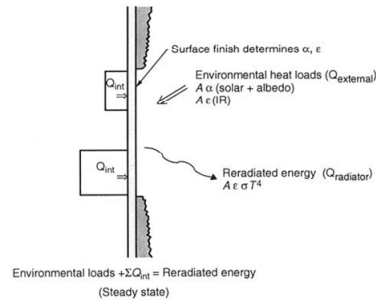
124



Thermal Analysis: Radiator Sizing

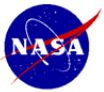


- A radiator panel was sized for use on the vehicle to reject the excess heat from the electronics once in orbit.
- A surface mount radiator was utilized.
- The radiator model was based on a first principles analysis of the area needed to reject the identified heat load to space. From the area a series of scaling equations were used to determine the mass of the radiator. Worst case thermal environment of LEO was used to size the radiator.
- No louvers were utilized
- Heat Pipes were used to conduct heat to the radiator surface.



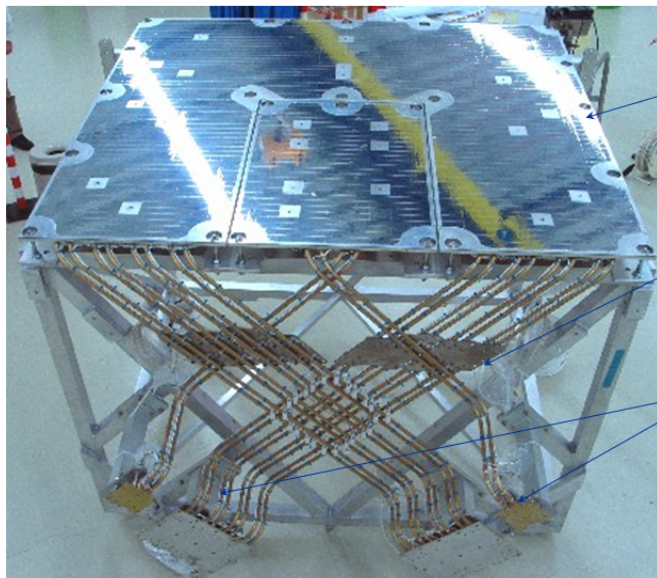
Variable	Value
Radiator Solar Absorptivity	0.14
Radiator Emissivity	0.84
Radiator Sun Angle	70°
Radiator Operating Temperature	320 K
Total Radiator Dissipation Power	90 W
View Factor to Earth	0.5
View Factor to the Solar Array	0.15

125



Spacecraft Radiator System Example

Cold plates are used to remove heat from the electronics. The heat is transferred to the radiator through a series of heat pipes connected to the cold plates and the radiator.



Radiator Panel

Heat Pipes
(transfer heat through phase change of an internal working fluid)

Cold Plates
(conductive aluminum plates)

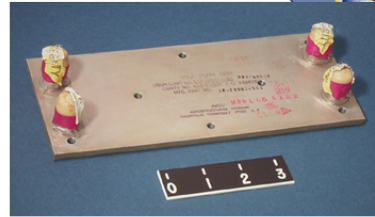
www.nasa.gov



Thermal Analysis: Electronics Cooling



- The electronics cooling is accomplished through the use of cold plates and heat pipes. The electronic components are mounted onto the cold plates which have integral heat pipes incorporated into them. The heat pipes remove heat from the cold plate and transport it to the radiator.
- The cold plates also have heaters integrated onto the and can be used to maintain the electronics at the desired temperature throughout the mission.



Example Cold Plate

Assumptions used

Variable	Value
Cooling Plate & Line Material	Aluminum
Cooling Plate & Line Material Density	2,770 kg/m ³
Number of Cooling Plates	4
Cooling Plate Length	0.1 m
Cooling Plate Width	0.1 m
Cooling Plate Thickness	5 mm
Heat Pipe Specific Mass	0.15 kg/m

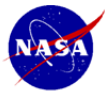


Heaters & Thermal Control



Flat plate heaters were used on the cold plates to provide heat to the electronics if necessary. Additional heaters were placed throughout the interior to provide adequate temperature control of the vehicle.

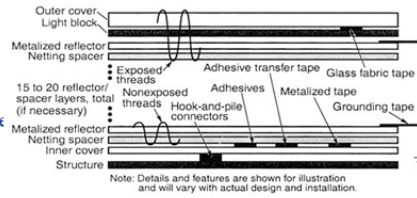
Thermal control is accomplished through the use of a network of thermocouples whose output is used to control the power to the various heaters. A data acquisition and control computer is used to operate the thermal system.



Thermal Analysis: Spacecraft Insulation



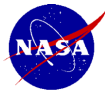
- Multi-Layer Insulation (MLI) was used to insulate the spacecraft for operation in orbit.
- MLI operates by limiting radiation heat transfer to and from the spacecraft. Each layer of the MLI has a low emissivity which limits radiation heat transfer between the layers.
- MLI is constructed of a number of layers of metalized material with a nonconductive spacer between the layers. The metalized material has a low absorptivity which resists radiative heat transfer between the layers.



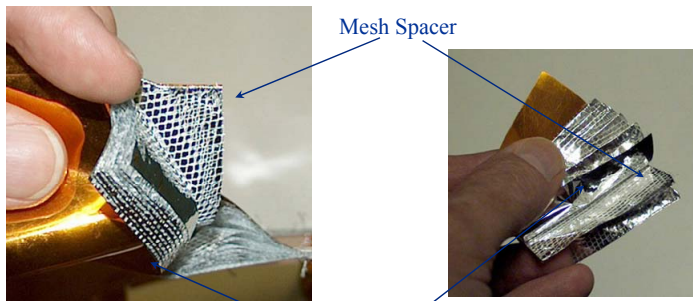
Assumptions used

Variable	Value
Tank Surface Emissivity (ϵ_t)	0.1
MLI Emissivity (ϵ_i)	0.07
MLI Material	Aluminum
MLI Material Density (ρ_i)	2,770 kg/m ³
Internal Tank Temperature (T_i)	300 K
MLI Layer Thickness (t_i)	0.025 mm
Number of Insulation Layers (n_i)	10
MLI Layer Spacing (d_i)	1.0 mm
Tank Immersion Heater Mass & Power Level	1.02 kg @ up to 1,000 W
Spacecraft Inner Wall Surface Emissivity	0.98
Spacecraft Outer Wall Surface Emissivity	0.93
Line Foam Insulation Conductivity	0.0027 W/m K
Line Foam Insulation Emissivity	0.07
Propellant Line Heater Specific Mass & Power	0.143 kg/m @ up to 39 W/m
Line Foam Insulation Density	56 kg/m ³

www.nasa.gov



MLI Blanket



Mesh Spacer

Individual Metalized Layers

MLI can be conformed to fit over various shapes. It can be held in place with Velcro or glue.



MLI covering the outside of a spacecraft





The main risk with the thermal system components pertains to the laser reflectors and the plasma degradation of the mirror and heat transfer during ascent.

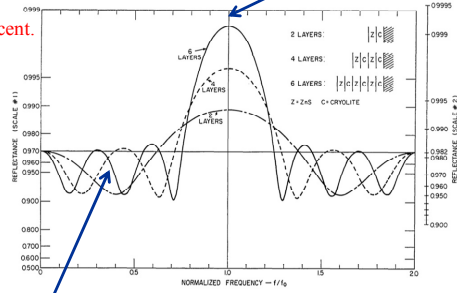
Risks

Laser Fr



Mirror Reflectivity

Any damage or degradation to the mirrored surface experienced during launch can cause excessive local heating due to the intensity of the laser beam (approximately 3000 W/cm²). Debris impact, or erosion from the near by plasma can potentially degrade the mirror reflectivity which would cause catastrophic heating and loss of the vehicle. The very high reflectivity of the mirror (99.99%) must be maintained throughout the launch phase.

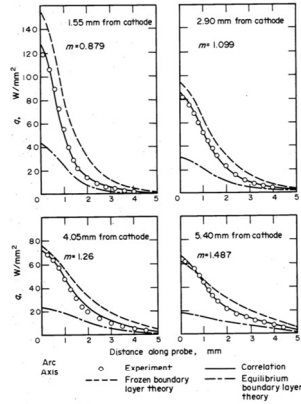


Plasma Frequency

Multi-index laser reflectivity

Plasma Heating

Localized heating due to the plasma. If the plasma gets within a few centimeters of the mirror surface there could be excessive heating. The mirror surface is not as reflective in the frequency the plasma will be radiating in. Therefore it can absorb significant amounts of heat if the plasma moves too close to the mirror surface. Depending on the distance of the plasma from the wall heating can be in the range of 20 to 80 W/mm².

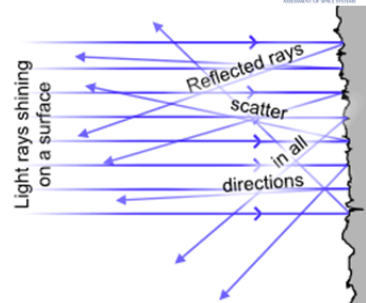


Risks Continued



Reflected Laser Light

Laser Light scattered off of the reflective shield can potentially be reflected back to earth. This could be a health hazard to someone who inadvertently looks into the reflected beam. The power of the reflected beam that reaches the Earth's surface will depend on the curvature of the shield mirror's surface and the distance from the Earth. The higher the shield curvature the greater the laser light dispersion and therefore the lower the intensity of the reflected beam. To reduce this risk a diffuse reflecting surface would be needed. A mirrored surface that has conical reflecting surfaces etched onto it may be able to disperse the incoming laser perpendicular to the incoming beam, limiting the reflection back toward the surface.



Mechanical

John Gyekenyesi
COMPASS Team
10-08-10

133

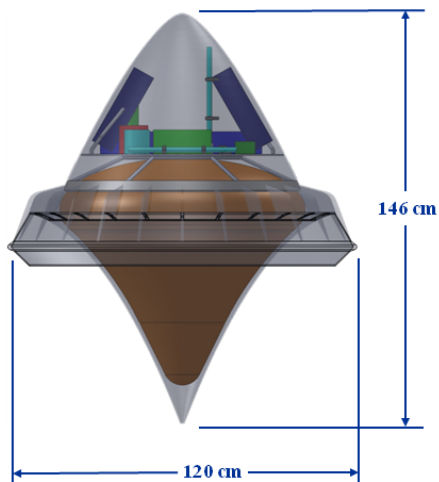
National Aeronautics and Space Administration



Structure Subsystem - Description

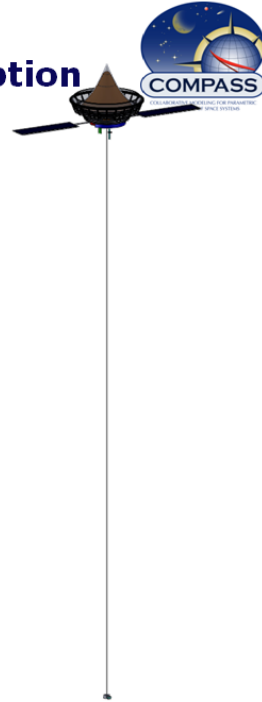


- **Structures and Mechanisms Design Requirements**
 - Contain necessary hardware for research instrumentation, avionics, communications, propulsion and power
 - Withstand applied mechanical and thermal loads from launching
 - Provide minimum deflections, sufficient stiffness, and vibration damping
 - Minimize weight

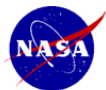




Structure Subsystem - Description



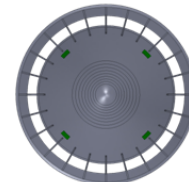
- **Structures assumptions**
 - Provides main structures backbone for BEP vehicle
 - Materials: graphite/polyimide, C/SiC, titanium, & aluminum
 - Shells with beam or stringer reinforcement
 - Bonded, welded and threaded fastener assembly
- **The structures subsystem**
 - Shells bearing all operational loads
 - Aluminum composite sandwich structure deck and beams for mounting hardware
 - Science probes, payload to support.
- **Main structure material and design choice:**
 - Coated carbon/SiC parabolic mirror afterbody
 - Minimum weight and high temperature capability are primary drivers
 - NASA Technology Readiness Level TRL4
 - Carbon/carbon nose cone
 - TRL6
 - Graphite/polyimide shell with aluminum flanges and stringers in primary structure
 - TRL6
 - Titanium shroud and flaps
 - TRL6
 - Aluminum flanges and stringers
- **Primary Structure mass:**
 - Forebody with carbon/carbon and graphite/polyimide with aluminum flanges and stringers
 - Afterbody of C/SiC
 - Thrust structure of titanium
- **Secondary Structure Mass:**
 - Aluminum composite sandwich structure instrumentation deck
 - Installations
- **Spacecraft adaptor and separation mechanism details**
 - Pyrotechnic bolts clamping at flanges of Forebody



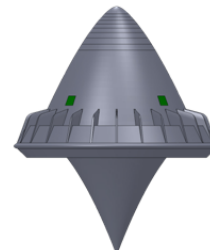
Structure Subsystem - Description



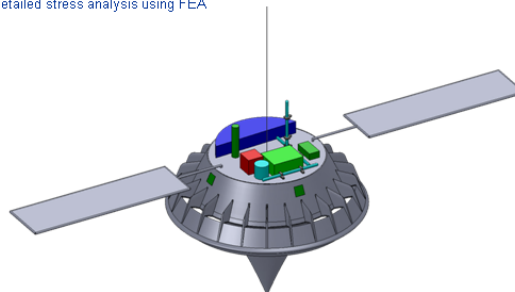
- **Design Highlights**
 - Advanced composites and titanium components
 - Flanges for joining sections and mounting internal hardware of aluminum
- **Analytical Methods**
 - Analytical methods with spreadsheet for stress analysis
 - Stresses
 - C/SiC mirror loaded to ~43 Mpa (including 1.5 safety factor)
 - Well below ~240 MPa failure stress of C/SiC
 - Supported on launch pad, mass ~300 kg at 1 G
- **Trades considered in analysis**
 - Initial components of aluminum
 - Final construction graphite/polyimide forebody sections
- **Options to Reduce mass and recommendations:**
 - Detailed stress analysis using FEA



Top view



Side view

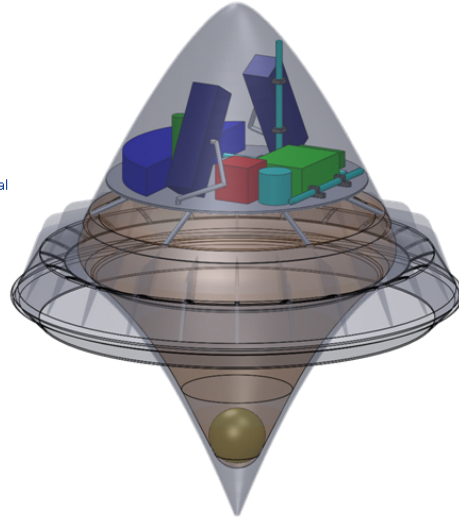




Mechanisms Subsystem - Description



- **Mechanisms assumptions**
 - Provides support for
 - Forebody shells and nose cone
 - Separate
 - Tethers for shell sections
 - Separation and tether
 - Shroud flaps
- **Mechanisms Mass:**
 - Pyrotechnic bolts and springs
 - Forebody shells and nose cone, 1.82 kg basic mass total
 - Forebody shells tethers, 0.4 kg each, qty. 2
 - Solid rocket motor, 1.82 kg basic mass total
 - Solid rocket motor casing tether, 0.11 kg
 - Shroud flaps linear actuators, 0.05 kg each, qty. 24



Cost

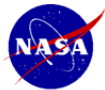
Jonathan Drexler,
COMPASS Team
12-11-10



COMPASS Cost Assumptions



- **DRAFT Cost Estimate based on COMPASS design**
- **All costs are in FY10\$M**
- **This estimate assumes the following:**
 - Proto-flight development approach
 - No ground spares included
 - Model assumes TRL Level 6
 - This estimate does not include any cost for technology development
 - Represents the most likely estimate based on cost-risk simulation results
 - Parametric estimate based on mostly mass based CERs from historical cost data
 - Planetary systems integration wraps
 - Software not included
- **Does not include:**
 - Contractor Fee (10-12% on top of the contractor estimates)
 - Any insight/oversight costs (for NASA-managed estimates)
 - Reserves (can be as high as 40-50%)
 - Ground System Cost (ie. Laser)
 - Launch Services Costs (ie. Special launch approval process)
 - Technology costs for components lower than TRL-6



BEPS Preliminary Parametric COMPASS Cost ROM

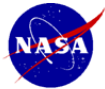


(Represents estimated Prime Contractor cost)

WBS	Description	DDT&E	Flight	Total
		Total	HW	
		BY \$M	BY \$M	BY \$M
06.1.1	Payload	0.0	0.0	0.0
06.1.2	Attitude Determination and Control	4.4	1.6	5.9
06.1.3	Avionics	3.8	1.7	5.5
06.1.4	Communications and Tracking	1.3	0.5	1.8
06.1.5	Electrical Power Subsystem	2.2	1.2	3.4
06.1.6	Thermal Control (Non-Propellant)	5.3	1.0	6.4
06.1.7	Propulsion (Hardware)	4.8	1.3	6.1
06.1.8	Propellant (Chemical)	0.0	0.0	0.0
06.1.9	Structures and Mechanisms	7.9	2.8	10.7
	Subtotal	29.5	10.2	39.7
	Systems Integration	25.0	3.7	28.6
	IACO	2.0	0.5	2.5
	STO	1.8	0.0	1.8
	GSE Hardware	3.7	0.0	3.7
	SE&I	8.6	2.5	11.1
	PM	5.8	0.8	6.5
	LOOS	3.1	0.0	3.1
	Spacecraft Total	54.5	13.9	68.4

- **NOTE:**
 - LOOS/GSE not in PRICE - \$6.8M

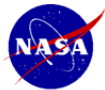
Costs in FY10\$M



Developing a Commercial Estimate



- Customer interested in estimating this spacecraft as a commercial venture
- Price Estimating Software (PRICE) published a white-paper that describes methodology for developing a commercial estimate
 - Based on actual costs from commercial venture
 - Step 1: Develop a space-rated estimate in Price
 - Step 2: Lower the complexity level across the board
- Began by modeling the COMPASS design in PRICE



Step 1: PRICE Estimate – NASA Managed



- Developed from the COMPASS MEL and previous assumptions
- Estimate Costs
 - DD: \$41.6M + \$5M (GSE/LOOS)
 - FH: \$11.8M
 - Total: \$58.4M

Note: Must add GSE/LOOS because it's not included in PRICE

Basic Estimate (Metric)			
Cost Summary	LM Totals	LM Production	LM Development
Spacecraft BEPS			
Mon November 22 2010 8:40 AM (PRICE Estimating Suite 2009 SR1)			
System Cost Summary			
Costs in (\$1000 Constant 2011)			
Program Cost	Development	Production	Total Cost
Engineering			
Draft	6674.4	987.1	7661.5
Design	21819.7	3975.4	25795.2
System	5036.9	-	5036.9
Proj. Mgmt.	3602.5	1044.2	4646.7
Data	1887.4	522.8	2410.1
SubTotal(ENQ)	39021.0	6529.5	45550.5
Manufacturing			
Production	-	4817.8	4817.8
Prototype	2135.8	-	2135.8
Tool Test Eq.	487.9	404.0	892.0
SubTotal(MFO)	2623.8	5221.8	7845.6
G & A / Com	0.0	0.0	0.0
Fee / Profit	0.0	0.0	0.0
Total Cost	41644.8	11751.3	53396.1
System Total	41644.8	11751.3	53396.1
Schedule Start	Nov 10 [36]	Feb 11 [48]	
First Item	Oct 13 [36]	Jan 15 [1]	
Finish	Oct 13 [36]	Feb 15 [49]	
System Weight	131.68	System WS	105.97
System Series MTBF Hrs	3040157	Unit Sys Cost	4817.79
System Quantity	0	Avg System Cost	11751.33



Step2: PRICE Commercial Estimate



- Changed Platform and Complexities (per reference)
- Estimate Costs
 - DD: \$27.0M +\$3.2 (GSE/LOOS)
 - FH: \$5.3M
 - Total: \$35.5M
- Government Hands Off!

Basic Estimate (Metric)			
Cost Summary	LM Totals	LM Production	LM Development
Spacecraft BEPS			
Mon November 22 2010 8:40 AM (PRICE Estimating Suite 2009 SR1)			
System Cost Summary Costs in (\$1000 Constant 2011)			
Program Cost	Development	Production	Total Cost
Engineering			
Draft	4171.3	348.2	4519.5
Design	13756.6	1316.5	15073.1
System	3590.0	-	3590.0
Proj. Mgmt.	2491.9	494.5	2986.4
Data	1328.2	182.1	1510.3
SubTotal(ENG)	25338.0	2341.4	27679.4
Manufacturing			
Production	-	2768.9	2768.9
Prototype	1272.6	-	1272.6
Tool Test Eq.	368.8	151.0	519.8
SubTotal(MFG)	1641.4	2919.9	4561.3
O & A/T Cost	0.0	0.0	0.0
Fee / Profit	0.0	0.0	0.0
Total Cost	26979.4	5261.3	32240.6
System Total	26979.4	5261.3	32240.6
Schedule Start	Nov 10 [35]	Jan 11 [49]	
First Item	Sep 13 [11]	Jan 15 [11]	
Finish	Sep 13 [35]	Feb 15 [50]	
System Weight	131.66	System WS	105.97
System Series MTBF Hrs	85.606	Unit Sys Cost	2768.89
System Quantity	0	Avg System Cost	5261.26



Summary Table



- Developed three estimates
- Parametric Commercial Estimate*:
 - Scaled the COMPASS NASA estimate according to the PRICE analysis
- Table Illustrates the range of estimates
 - Different methodologies

	Parametric	PRICE
NASA	DD: 54.5 FH :13.9 Tot: 68.4	DD: 46.6 FH: 11.8 Tot: 58.4
Commercial	DD: 35.3* FH: 6.2* Tot: 41.6*	DD: 30.2 FH: 5.3 Tot: 35.5



ORBCOMM



- Developed a parametric estimate based on historical equipment listing and masses
- Parametric Estimate Based on masses:

WBS	Description	DDT&E	Flight	Total
		Total	HW	
		BY \$M	BY \$M	BY \$M
06.1.1	Microstar	7.8	7.1	15.0
	Subtotal	7.8	7.1	15.0
	Systems Integration	7.9	2.7	10.6
	Spacecraft Total	15.7	9.8	25.6



Full Summary Comparison



Lightcraft Lightcraft

	Parametric	PRICE	ORBCOMM
NASA	DD: 54.5 FH :13.9 Tot: 68.4	DD: 46.6 FH: 11.8 Tot: 58.4	DD: 15.7 FH: 9.8 Tot: 25.6
Commercial	DD: 35.3* FH: 6.2* Tot: 41.6*	DD: 30.2 FH: 5.3 Tot: 35.5	DD: 10.2* FH: 4.4* Tot: 14.6*

- ORCOMM Cost:
 - \$10.7M in FY97\$M
 - \$16.0M in FY10\$M
 - Estimated split:
 - DD:10.5
 - FH: 5.5



Cost Comparison and Learning Curve



- **Learning Curve:**
 - Theoretical First Unit (TFU) - the flight hardware (FW) cost estimate
 - Learning Curve is based on how much “learning” can be assumed
 - Production Number (N) – assumed number of units
 - Resulting calculations:
 - Cumulative average cost of the N units
 - Nth unit cost – cost to produce the last unit

Learning Curve Calculator

TFU Cost (K)	6.2	5.3	4.4
Learning Curve (b)	0.85	0.85	0.85
Production Number (N)	30	30	30
Cumulative Average Cost for N units	2.79	2.39	1.98
Nth Unit Cost	2.15	1.83	1.52

All Costs in FY10\$M



Cost Comparisons to Orbcomm (FY2010\$)



- Orbcomm with integrated BEP propulsion Compared to Orbcomm
 - 30th unit: \$2.8M vs \$2.0M
 - Average Launch vehicle (8 ORCOMM per launcher) : \$0 vs ~\$3M
 - Launch Oversight, Range, Facilities, etc.: ?\$ vs \$9M
 - Need KSC to estimate these costs for Laser launch site and operations
- Excluding Launch Agency, Range, Facilities, lasers...
 - **Launch Vehicle cost savings ~ \$0.8M vs \$3M : Saves ~\$2M in launch vehicle costs for each Orbcomm**
 - **Launch vehicle costs more than halved**
 - **How does the other launch costs and laser facility costs impact this?**



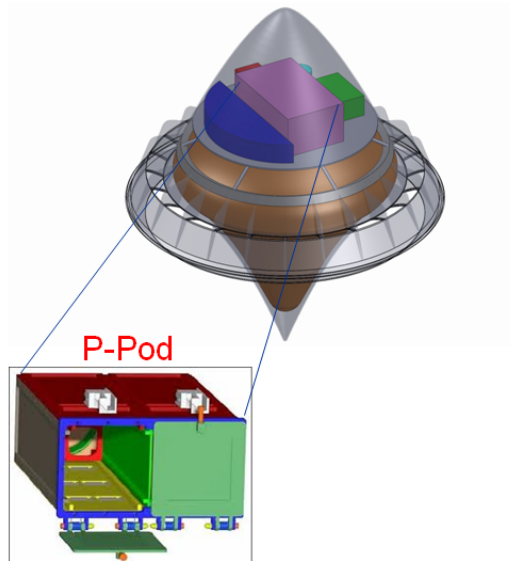
Appendix: Cubesat Launcher Option



Alternative Configuration: Cubesat Launcher



- Option to explore the use of the Lightsat concept to launch Cubesats
- Ground ruled
 - Keeping the same trajectory/power levels stations
 - Removed only the Orbcomm equivalent and satellite equipment – kept everything needed for launch and insertion
 - Added a dual pea-pod cube sat launcher – launches six (1 kg) cubesats once on-orbit
- P-Pod device seems to fit
 - Issues of high spin rate will require redesign of P-Pod and cubesats
- Launcher costs still at about \$2M ROM
 - Is it worth it to launch six \$30,000 cubesats?





Cubesat Launcher MEL



COMPASS study: BEP Lightcraft

Study Date 10/1/10

GLIDE container: BEP: Lightcraft_Case1		COMPASS S/C Design			
WBS	Main Subsystems	Basic Mass (kg)	Growth (kg)	Estimated Total Mass (kg)	Aggregate Growth (%)
06	Lightcraft/Spacecraft	296.3	17	313	
06.1	Lightcraft Stage 1	296	17	313	
06.1.1	Payload	0	0	0	TBD
06.1.2	Attitude Determination and Control	2	0	2	5%
06.1.3	Avionics	11	3	15	30%
06.1.4	Communications and Tracking	2	1	3	21%
06.1.5	Electrical Power Subsystem	0	0	0	30%
06.1.6	Thermal Control (Non-Propellant)	15	0	15	0%
06.1.7	Propulsion (Hardware)	17	2	20	14%
06.1.8	Propellant	188		188	
06.1.9	Structures and Mechanisms	59	10	70	18%
Estimated Spacecraft Dry Mass		108	17	125	16%
Estimated Spacecraft Wet Mass		296	17	313	
System Level Growth Calculations					Total Growth
Lightcraft Estimated Dry mass		108	17	125	16%
Dry Mass with Desired System Level Growth		108	32	140	30%
Additional Growth (carried at system level)			15		14%
Total Wet Mass with Growth		296	32	329	

- P-Pod Deployment device and Cubesats carried in structures.
- An additional 3 kg is unallocated but is held for designing the p-pod and cubesats to the high g spin rate.

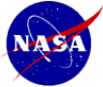
BEP- Beamed Energy Propulsion

GLIDE study setup details



Melissa McGuire - Lead System Integration Engineer

COMPASS
9-27-2010



BEP GLIDE study details



(1) StudyShare on Armor server

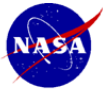
<https://armor.grc.nasa.gov/BEP>

- **Remember - this is your GLIDE 1.0 username/password.**
 - Note: I set this up as a new share, and chose a group to access it. If you cannot get to it, you are not in that group. Do not panic, and just send me an email. Let me know and I will add you.
- **If you need a GLIDE 1.0 account, go to <https://armor.grc.nasa.gov/>**
 - sign up for one and then email me telling me that you have done so. I don't always get an email letting me know.
 - I will activate it and let you in the group with access to the study above.
 - If you have forgotten your username/password, you can also reset it at the above link.

(2) MELs and the GLIDE 2.0 server and database

Architecture: **BEP**
Study containers: **TBD**

- **Remember - this is your GLIDE 2.0 username/password**
 - GLIDE 2.0 usernames are your x500 email address @nasa.gov
 - We will be running this using The GLIDE 2.0 application and server.
 - When you launch the GLIDE 2.0 client, make sure you are pointing to the following server:
glide.grc.nasa.gov
 - Note the removal of the "v" as in glidev.grc.nasa.gov



HERROV MELs details



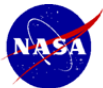
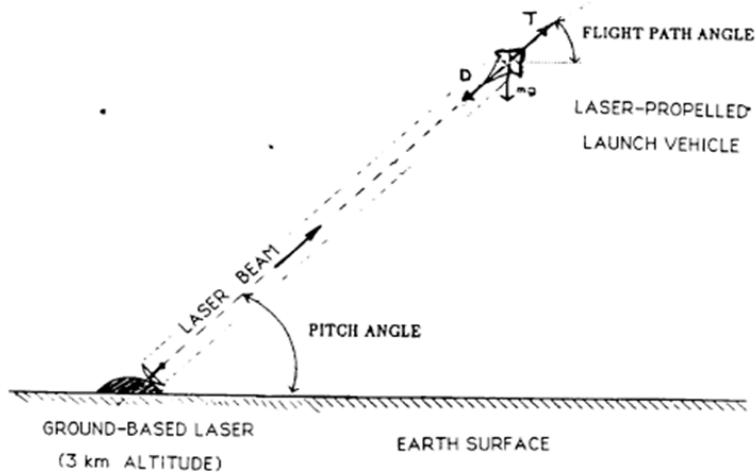
- **Draft MELs are available and can be found on the server in the following share location:**
 - <https://armor.grc.nasa.gov/BEP>
 - Note, the CAD and Cost MELs will be made once the items listing in the master MEL is finished with editing.

File name	Subsystem Title
BEP_subSys-avionics.xls	Avionics
BEP_subSys-comm.xls	Communications
BEP_subSys-gnc.xls	Guidance, Navigation and Control
BEP_subSys-prop.xls	Propulsion and Propellant
BEP_subSys-power.xls	Power
BEP_subSys-struct.xls	Structures and Mechanisms
BEP_subSys-sci.xls	Science
BEP_subSys-thermal.xls	Thermal
BEP_MasterMEL.xls	Master MEL
BEP_Master_PEL.xls	Master PEL

- **GLIDE 2.0 Study Container details**
 - Architecture: **BEP**
 - I have also created the two cases called **Lightcraft_Case1**, **TBD**



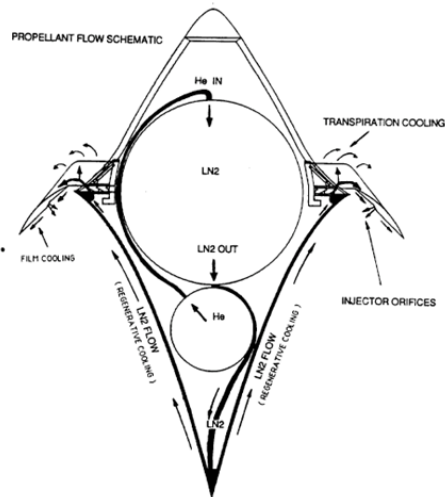
Trajectory

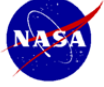


Past SDIO Design



Section	Mass(kg)
FOREBODY	
C-C Nosecap	1.0
Primary Structure	4.0
TPS(FRCI)	3.5
Internal Support Frame	10.0
AFTERBODY	
Parabolic Mirror (Faceplate)	15.0
Mirror Support Structure	8.0
Manifolds	2.0
THRUST STRUCTURE	
Shroud	15.0
Strut Support Structure (24)	15.0
Air Inlet Shutters	5.0
PROPELLANT MANAGEMENT SYSTEM	
LN2 Tank	8.0
He Tank	2.5
Insulation	1.0
Feed Lines/Regulators	5.5
SATELLITE SYSTEMS	
Mechanical Actuators	3.0
Electrical	5.0
Electronics	5.0
Attitude Control	2.5
GROWTH CONTINGENCY (10%)	12.0
VEHICLE TOTAL DRY MASS	180.0





Scout Example (1960-1994)



- **G&C in third Stage**
 - Provides attitude ref and the resultant control signals/forces for stabilization in YPR
 - Yaw and Roll maintained at launch reference, Pitch axis is programmed through a preselected angle corresponding to the desired vehicle zero-lift trajectory
 - Mini-integrating gyros detect angular deviation about programmed vehicle path and generate proportional error signals to controls to keep vehicle on programmed path
 - Contents: strapped-down gyro sensors, relay unit (power and ignition switching), intervalometer to provide precise scheduling of events during flight, programmer to provide torqing voltages to pitch gyro, electronic signal conditioner to convert gyro outputs to proper control signals, cycle inverter and batteries
- **Each stage had its own ACS system**
 - First stage has fins and exhaust vanes
 - 2nd&3rd stages on-off H₂O₂ motors (3rd stage ~2000 kg wet use 60 lbf pitch, 14 lbf roll, 2 lbf yaw thrusters), Pitch is probably highest since it must follow programmed angle
 - Fourth stage: Pointed by third stage, separated, spin stabilized by 4 rocket motors then ignited
- **Ignition System**
 - Dual squibs: completely dualized ignition system
 - Separate circuit, separate battery
 - Controlled by guidance program timer
 - Contents: battery packs, timer actuated control relays, safe-arm latching relays (heat shield), spin motors, separation bolts, motor ignitor circuits

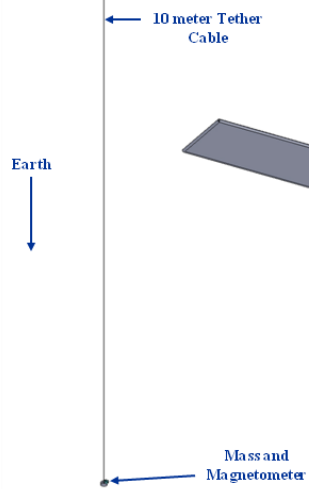
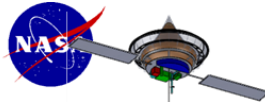


Other Scout Systems



- **Stage Separation: 3rd and 4th 'cold separation' of springs in a clamp retainer, released by explosive bolts**
- **Instrumentation/telecom:**
 - 21 channel IRIG PAM/FM/FM
 - Two channels commutated to allow 56 data signals of 10 samples per second
 - 2230.5 mhz transmitter (6 watts output power)
- **Radar Tracking system**
 - 500W rf , single pulse
- **Propulsion System**
 - Four solid rocket motors
 - H₂O₂ ACS systems on stages 2 and 3
- **Destruct system**

National Aeronautics and Space Administration



3.1.2 Laser Optical Consultant Report—Design Reference Mission 1–A

This section covers the design and feasibility of pulsed-laser-launching microsattellites (10 to 100 kg) and nanosatellites (1 to 10 kg) into low Earth orbit (LEO) (see Figure 3.1). Note, however, that picosatellites (0.1 to 1 kg) may be the nearest “target of opportunity” for emergent ~1-MW-class, pulsed, 1- μm solid-state diode-pumped (SSDP) laser technology. Provided herein are descriptions of the requisite lightcraft engine/vehicle/payload, ground-based laser (GBL) facility, concept of operations (CONOPS), costs, and overall feasibility assessment.

The Beamed Energy Propulsion Study (BEPS) examined the state-of-the-art (SOA) in BEP (both lightcraft and lasers) applicable to (1) identifying potential game-changing applications (e.g., CubeSats, fractionated satellites, and Responsive Space), (2) formulating a roadmap of technology development, and (3) pinpointing key near-term technology demonstrations to rapidly advance elements of BEP technology to Technology Readiness Level 6 (TRL 6). This section explores the application of existing lightcraft pulsed-plasma engines (Figure 3.2) that have seen 150 successful flights at White Sands Missile Range (WSMR, Refs. 1 and 2), and set the current 71-m world altitude record on October 2, 2000 (Ref. 3).

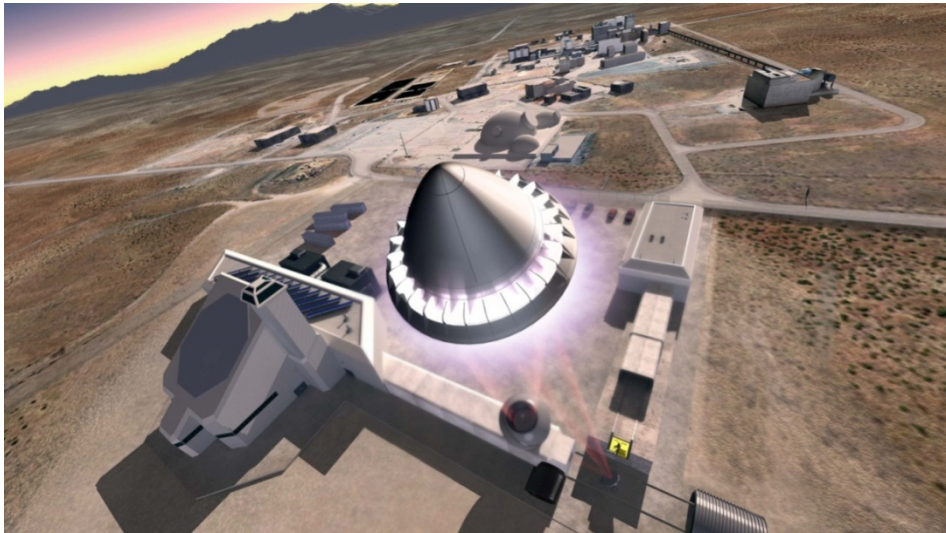


Figure 3.1.—12-MW laser launch facility at WSMR, New Mexico (artist concept by P. Rawlings).

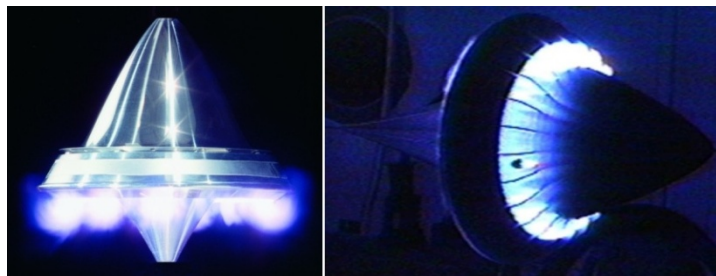


Figure 3.2.—Lightcraft plasma engine pulsing in 1-bar laboratory air (photographs by J.E. Shryne, III). Left: 14.7-cm-diameter #200 vehicle. Right: 23-cm #100 vehicle.

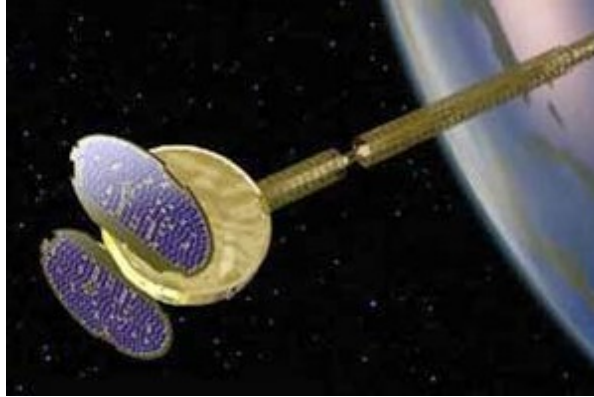


Figure 3.3.—ORBCOMM messaging satellite in 800-km circular orbit (from Ref. 4). Courtesy of Orbital Sciences Corporation; used with permission.

One key feature of lightcraft technology is its scalability which, in fact, helps to mitigate or manage technological and financial uncertainties. The specific DRMs considered in this section are for single-stage-to-orbit (SSTO) 120-cm lightcraft (DRM 1–A) and 35-cm lightcraft (DRM 1–A) powered by repped-pulse 1 μm SSDP lasers.

For the DRM 1–A mission (120-cm lightcraft launcher), the COMPASS team produced a detailed conceptual design configured as an ORBCOMM (Ref. 4) satellite replacement with full functionality (see Figure 3.3). These design results were then scaled down to shed insight into a 35-cm-diameter nanosat launcher, which was subsequently compared and contrasted with the Air Force Research Laboratory’s (AFRL’s) 2007 lightcraft concept (Ref. 5), including engine and vehicle design, mass breakdown, payload specifications, and boost performance.

3.1.2.1 Lightcraft Technology Development

The lightcraft development process is an interdisciplinary endeavor involving engine/optics/airframe integration, mostly through applying traditional engineering design practices. The process begins with first creating an efficient engine concept, engineered for maximum/optimum efficiency with a given photon source: that is, source specifications must closely match engine requirements (and vice versa) to avoid a performance-degrading “impedance mismatch.” Once a workable engine concept is demonstrated, it can be integrated into the whole lightcraft vehicle concept.

Both airbreathing and rocket engine options, as well as combined cycles that transition between these propulsion modes, have to be investigated. Each engine design will involve the construction of one or several prototypes, exploiting variations on a theme (i.e., on one or multiple design features). Initial rough prototype engines for laboratory testing can be heavy and employ heat-sink cooling (i.e., lots of thermal mass). Later, increasingly refined flight-weight engines will exploit more exotic high-temperature structural materials, refractory metal coatings, and so forth.

The most efficient and most cost-effective approach to lightcraft engine/vehicle development is to thoroughly exploit existing laser sources located at Government, Department of Defense (DOD), and industry laboratories, and some of these are already set up as *photon users facilities*. Such facilities can be used to quickly extend engine performance data bases, at reasonable cost.

The lightcraft concept has inherent scalability characteristics that can facilitate a progressive technology development roadmap (see Figure 3.4) that minimizes risks and upfront investment for the infrastructure. A principal measure of technological progress in this roadmap is the setting of increasingly higher altitude records (e.g., as was done by Goddard and Von Braun).

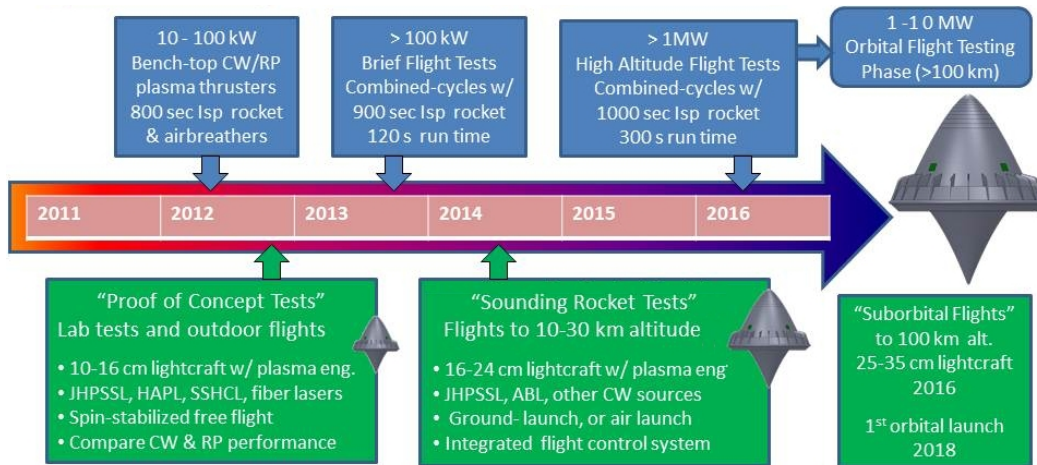


Figure 3.4.—Progressive technology roadmap and possible development program: ground and flight demonstrations leading to 35-cm nanosat launch system.

The development process will emphasize hardware creation (i.e., build, test, break, redesign, and retest), while judiciously exploiting available engineering design software to expedite the development cycle. (*Extensive testing on repetitive-pulsed (RP) plasma engines has established the proof of concept, but a similar endeavor is still needed for continuous-wave (CW) plasma engines.*) This approach enables rapid optimization, refinement, and evolution of any engine/vehicle geometry, especially in areas of aerodynamics, structural and heat-transfer analysis, flight dynamics and stability/control, and so forth. The essential development steps will be

- *Bench-top static tests:* Thrust stand and ballistic pendulum tests with pulsed and CW photon sources; beam-riding performance measurements with additive-increase multiplicative-decrease (AIMD) (Refs. 6 to 9)) apparatus
- *Wind tunnel spinning lightcraft tests:* Measuring aerodynamics of unpowered spinning lightcraft aeroshells in subsonic and/or transonic wind tunnels versus angle of attack and revolutions per minute (rpm) (Ref. 10)
- *Direct-connect engine tests:* Measuring laser propulsion performance in subsonic and transonic wind tunnels (blow-down and/or Ludwig tube) with two-dimensional lightcraft plasma engine geometries
- *Supersonic and hypersonic tests:* Measuring laser engine performance in blow-down and/or impulsive supersonic- and hypersonic shock tunnels with two- and three-dimensional engine and/or vehicle geometries; hypersonic tests at Mach 6 to 10 are ongoing in Brazil (Refs. 11 and 12)
- *Indoor vertical beam-riding tests:* Short 5- to 10-m free flights up to the lab ceiling with flight-weight lightcraft models (likely spin-stabilized, Ref. 2))
- *Outdoor vertical beam-riding tests:* Flights to altitudes of 10, 30, 100 m for proof of concept; no flight control system needed (Refs. 1 to 3)
- *Numerical flight dynamics studies:* Incorporate above engine performance data, vehicle aerodynamics data, trajectory data, and so forth into a comprehensive numerical simulation model for optimization and control systems studies (Refs. 13 to 15)
- *Flights to extreme altitudes:* Boosts to 1, 10, 30, and 100 km requiring full flight control systems; altitude records demonstrably track technology progress

At the present point in time, RP plasma engine development is substantially more mature than its CW counterpart and was, thus, the focus of the BEPS. However, CW plasma engines have great potential to

leverage the recent rapid evolution of high-power CW beam sources by extending into entirely new propulsion territory. In addition, the engineering development of such CW engines is expected to benefit from hard lessons learned in RP engine research and testing.

3.1.2.2 Description of 120-cm Vehicle

The BEPS objective was to create an independent concept design for a laser-powered launch vehicle utilizing the combined-cycle, pulsed detonation engine (PDE) in Figure 3.3 that was first postulated in References 16 and 17. The basic operating principles and performance parameters for that engine are well established and were characterized in early theoretical studies (Ref. 16 and 17), before hardware development campaigns (lab and outdoor free-flight tests) began at WSMR in 1996 (Refs. 1 and 3). Hence, the BEPS 120-cm spacecraft in Figure 3.5 was conceived as a point of reference for assessing the feasibility of the concept and for identifying what technologies and demonstrations needed to be carried forward to expedite development.

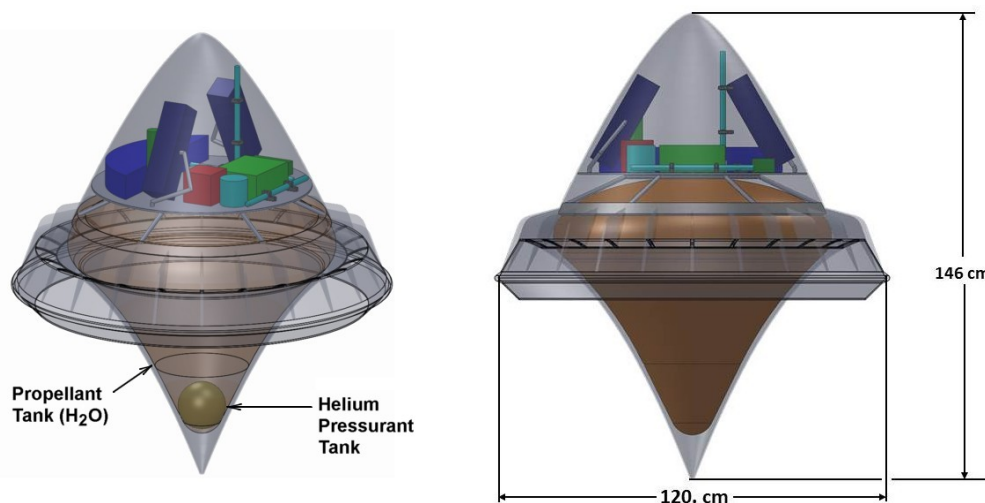


Figure 3.5.—Final launch configuration of 120-cm-diameter DRM 1-A spacecraft.

The toy-top-shaped, nonreusable spacecraft requires no separate launch vehicle: that is, the satellite and vehicle hardware are assumed to be inseparable, and in this 120-cm BEPS design option, both fly into orbit. (*An alternative option could be a separable satellite payload with an integral chemical kick rocket for orbit circularization. This was studied by the COMPASS team, but the launch trajectory “closed” on 180 km instead of the desired 400 km altitude.*)

The COMPASS team began this design and feasibility study by examining a wide variety of missions and applications for the reuse of a single-stage lightcraft: that is, the vehicles become spacecraft or satellites after attaining orbit:

- Satellite constellations
- Self-assembled bigger spacecraft
- Communications (messaging, cell, and Internet)
- Reuse of laser propulsive engine parts and/or functionality
 - Laser communications (in-space)
 - Optical imaging
 - Earth resource: multispectral, almost continuous imaging with 4000 spacecraft—new paradigm
 - Astronomy: customers want 6- to 15-m apertures (planet finders)
 - SETI Institute search for alien laser communications
 - Repositioning, orbit maintenance, and deorbit

- LEO science spacecraft
- Quick way to demonstrate and/or qualify new technologies (electronics, solar cells, and lubricants)
- Propellant for orbiting depots
- Servicing spacecraft (viewing and delivering orbital replacement units (ORUs); low-Earth-orbit to geosynchronous-Earth-orbit (LEO–GEO) shuttles)
- Assist in deorbit of spacecraft and/or orbital debris

After reviewing the options, the COMPASS team selected a spacecraft that emulates the ORBCOMM satellite (as mentioned previously), except that its 40-kg payload would be delivered to a 400-km circular orbit. This slightly less energetic launch trajectory may demand a slightly larger number of satellites in the constellation for the same coverage. ORBCOMM is a commercial venture that provides global messaging services (handling 50,000/hr), using a constellation of 26 LEO satellites in 785-km circular (two polar), three planes, eight spacecraft per plane, 45 ° inclined. Each spacecraft would weigh 40 kg, cost \$1.2M, and consume 160 W of power over its 4-year lifetime. Very-high-frequency (VHF) communication (138 and 400 MHz) will be at 57.6 kbps. There will be 17 data processors and 7 antennas. The satellite will be gravity-gradient stabilized, with magnetic torquers and cold gas nitrogen (N₂) Reaction Control System (RCS) thrusters.

3.1.2.3 Spacecraft Key Features

Figure 3.6 highlights the essential DRM 1–A spacecraft systems for which key features are itemized in the following list:

- The GBL laser could be reused for orbit maintenance and reposition of the spacecraft, and could finally *deorbit* when the satellite electronics fail or become obsolete—that is, using “*planned retirement*” rather than aggravating the orbital debris problem.

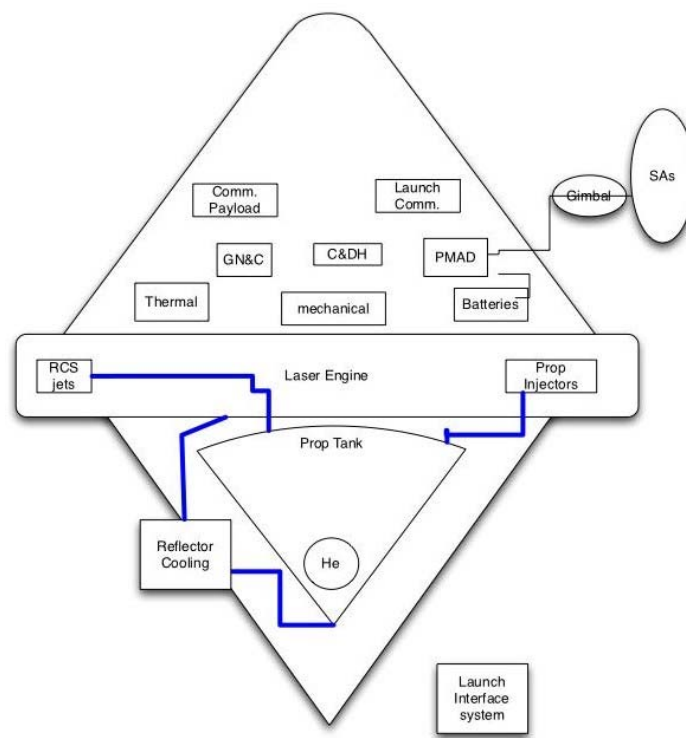


Figure 3.6.—Principal spacecraft systems. SA, solar array; GN&C, guidance, navigation, and control; C&DH, command and data handling; PMAD, power management and distribution; He, helium.

- The 120-cm COMPASS vehicle will be launched at a 30° elevation off the horizon and will require just one GBL station (350–MW maximum in air-breathing mode; 250 MW in rocket mode) at the launch point, and a laser relay mirror in LEO for orbit circulation;
- Combined-cycle pulsed-detonation propulsion system and thermal control technologies (which are still in the TRL 2 to 4 range) include
 - o A rear parabolic mirror will serve the double function of a focusing optic and a plug nozzle.
 - o Pulsed laser power will be concentrated into a 1.2-m-diameter annular ring, where working fluid temperatures may exceed 6000 K and theoretically will provide specific impulse I_{sp} in excess of 900 s.
 - o Water propellant is best for density, cooling, and ground handling, but liquid nitrogen (LN₂) and hydrogen peroxide (H₂O₂) are alternative options.
- Guidance, navigation, and control
 - o The vehicle is assumed to be spun at 120 rpm for stabilization during launch. Higher vehicle rotation may be required for desired stability levels in flight, but the payload bay could be despun to avoid acceleration constraints on payload.
 - o Differential water propellant injection into the laser focal ring (60-cm radius) will be used for pitch and yaw control of the vehicle under laser boost, in both air-breathing and rocket modes.
- Some launch power, C&DH, and communications systems will be reused for satellite functions once in orbit.
- Eliminating the separate (first-stage) launch vehicle should reduce the lightcraft costs by more than half. (*This does not include differences in launch support, range, and laser facilities.*)

3.1.2.4 Spacecraft Requirements and Assumptions

Table 3.1 summarizes the principal requirements and assumptions made by the COMPASS team in the DRM 1–A design and feasibility study, which considered various important tradeoffs.

TABLE 3.1.—DRM 1–A SUMMARY OF REQUIREMENTS AND ASSUMPTIONS

	Item	Requirements and assumptions
1	Top-level/science	Lightsat shall perform both the launch and satellite functions. Representative satellite function to emulate ORBCOMM. Figures of merit (FOM): Cost per n units, payload mass, and safety.
2	System	Single fault safe only; otherwise zero fault tolerant; 4-year lifetime; launch year open ended—current TRL assessment is an output. Mass growth per AIAA 120–2006 (additional growth to make system level 30%).
3	Mission, operations, and GN&C	Lightcraft engine attached to spacecraft performs launch from ground to suborbit, circularization with relay mirror satellite or onboard chemical (circular, ≥ 400 -km altitude, 45° inclined ($\pm 0.2^\circ$)). Desire reuse of lightcraft engine for repositioning, reboost, and deorbit; high rotation rate for spacecraft stability.
4	Launch vehicle	Not applicable (N/A) (integral SSTO vehicle reused as satellite/spacecraft in orbit)
5	Propulsion	Lightcraft engine primary propulsion: transitions through pulse detonation, laser ramjet, and laser rocket modes at appropriate altitudes. Water chosen as rocket propellant because of better density and cooling, and easier handling on pad.
6	Power	Solar photovoltaic (PV) arrays and secondary batteries
7	C&DH and communications	Preuse of flight computer to handle launch; uprange telemetry communications; equivalent ORBCOMM messaging payload
8	Thermal/environment	Remove laser and plasma heat from body by vaporizing propellant. (<i>Trades:</i> propellant type for cooling: N ₂ , water (H ₂ O), or ammonia (NH ₃)). Maintain high reflectivity (>0.9999) of rear parabolic optic during laser boost.
9	Mechanisms	Air-breathing inlet covers (open for laser ramjet mode, closed for rocket modes); nosecone ejection; solar PV array and tether deployment

TABLE 3.1.—DRM 1—A SUMMARY OF REQUIREMENTS AND ASSUMPTIONS

	Item	Requirements and assumptions
10	Structures	High-temperature-resistant inlet ring/annular shroud; maintain 0.9999 reflective parabolic mirror/plug nozzle under laser boost
11	Cost	Assume that lightcraft engine/vehicle replaces need for separate launch vehicle. Assume that commercial spacecraft building cost models are used.
12	Risks	Temperature leaks from laser and plasma; fouling mirror HX, laser pointing, thrust direction, and angle of attack, high spin rate

At the top-level, the major tradeoff was the choice for an *integrated vehicle/satellite* with shared satellite functions (selected for DRM 1–A with a LEO laser relay mirror for orbit circularization) versus a smaller *separable satellite payload* (favored for DRM 1–A' with an onboard chemical kick rocket to circularize orbit).

In Item 3, a vehicle rotation of 120 rpm was assumed, but higher spin rates may be required for adequate stability under laser boost. Under Item 5, two main propellants (H₂O and LN₂) were initially considered for the pulsed-detonation (PD) rocket mode, but H₂O was selected because of its 20% higher density and better cooling capacity. N₂ has better potential than H₂O for dual use on orbit in the RCS. Onboard RCS propellant trades were cold gas N₂ (favored) versus hydrazine. The trade in Item 6 was additional primary batteries for launch needs. In Item 7, the obvious trades were computer type, data storage, data transfer rates, and communication frequencies. Mechanism trades in Item 9 faced materials, power, and operations issues. Finally in Item 10, the overriding concern was for minimum structural mass to sustain expected thermomechanical loads. Microchannel water (H₂O) -cooled titanium and high-temperature ceramic matrix composites (carbon/silicon carbide (C/SiC) and SiC/SiC)) were both considered. The rear parabolic mirror/plug nozzle must maintain 0.9999 reflectivity under laser boost.

3.1.2.5 Satellite Function and On-Orbit Configuration

Figure 3.7 gives a semitransparent view of the satellite electronics packages required for the ORBCOMM-like messaging function. The COMPASS team’s objective was to conceptually design and assemble all essential electronics into the conical-shaped payload bay (i.e., nose volume) of the 120-cm lightcraft launcher—for example, the avionics, communications, PV/battery power system, gravity-gradient stabilization system, RCS, magnetometer, magnetic torquers, and inertial measurement unit—using components largely scaled from existing technology and commercially available units.

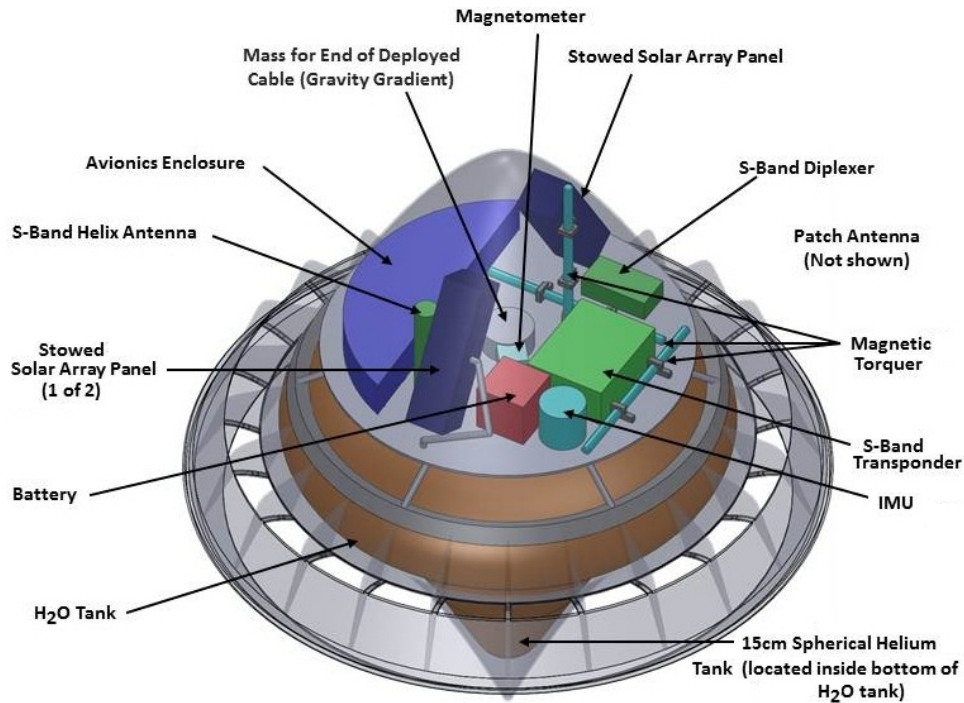


Figure 3.7.—Semitransparent view of 120-cm spacecraft and satellite electronics. IMU, inertial measurement unit.

A more integrated, compact, and mass-efficient spacecraft/satellite electronics package could be created for the 120-cm lightcraft by using an *integrated systems engineering approach*, rather than the “first-order” subsystem-by-subsystem aggregate, as the COMPASS team has spearheaded. With a critical eye toward small payload and microsatellite engineering practices, the lightcraft electronics package could be designed for minimum volume, mass, and power needs. For example, by tightly integrating separate electronics enclosures into larger boxes (rather than “piece-meal” assemblies), a significant reduction in mass budget can be obtained, which in turn will reduce costs through mass production. Engineers already experienced in microsatellite and launch systems engineering and design, coming from major microsatellite companies, would welcome this challenge and make quick work of this.

3.1.2.6 Combined-Cycle Propulsion System

This section provides a brief overview of the lightcraft’s combined-cycle propulsion system, for which the energy is provided via a GBL.

The engine operates in air-breathing laser ramjet mode up to Mach 6 to 7 and an altitude of 35 km and then switches into rocket mode (whereupon H₂O is pressure fed to the 120-cm propellant injector ring, with no need for a boost pump) for the remainder of the flight to LEO (Refs. 16 and 17). As indicated in Figure 3.8, the entire vehicle aeroshell is designed to serve multiple structural- and propulsion-related functions. The axisymmetric nose/forebody serves as an external compression inlet in supersonic flight (Ref. 18), precompressing air through a short annular slit into the engine “hot section.” (*Incidentally, the nose also supports four patch antennas—90° apart—for pre-deployment communications.*)

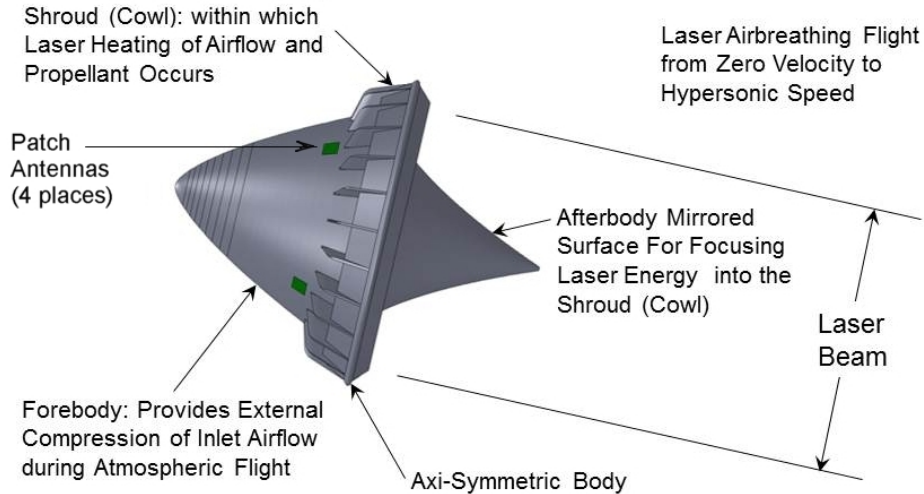


Figure 3.8.—Function of external surfaces in air-breathing propulsion mode.

The entire vehicle aft surface is a parabolic mirror that concentrates incident laser power into the annular shroud region to heat the engine working propellant, which is either (1) atmospheric air or (2) onboard liquid propellant (H_2O ; liquid nitrogen, LN_2 ; hydrogen peroxide, H_2O_2 , etc.). Laser heating of the working fluid causes ionization, dissociation, and the creation of a high-pressure, high-temperature plasma toroid inside the shroud and laser-supported detonation (LSD) waves generate pulse-periodic high-pressure blast waves (see Figure 3.9). Hence, a quasi-continuous propulsive force is produced by the rapidly pulsing laser. The rear parabolic optic also serves as a plug nozzle surface for the expanding blast waves to efficiently impart impulse. Flight control (pitch and yaw) in the air-breathing mode is achieved by differential injection of H_2O sacrificial coolant (very low flow rates).

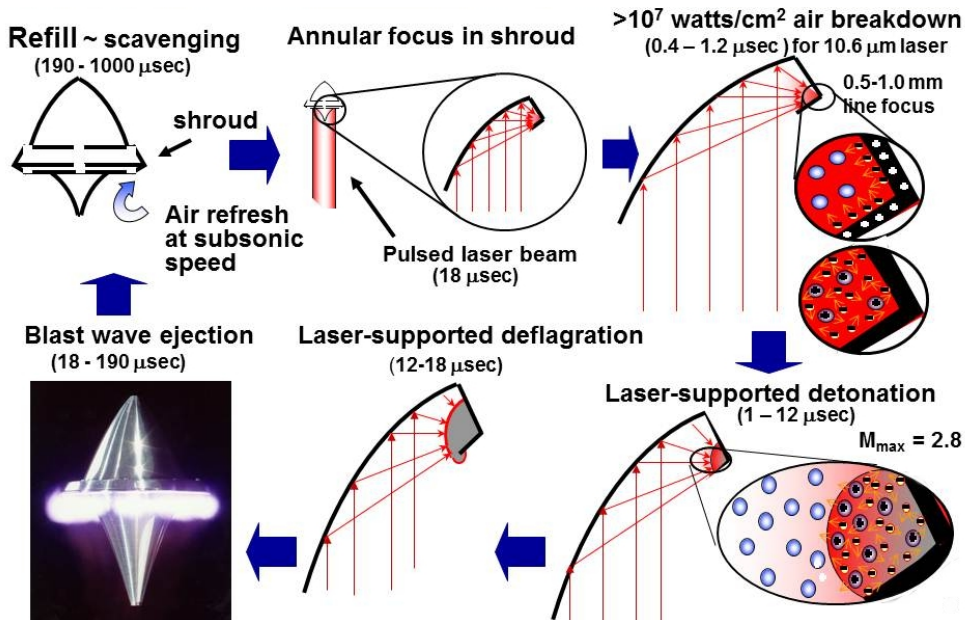


Figure 3.9.—Pulsejet engine cycle based on LSD waves. (Data for 11- to 14-cm lightcraft engine tests on Pulsed Laser Vulnerability Test System (PLVTS) laser at WSMR.)

The annular shroud functions to enclose the engine “hot section” (laser energy absorption chamber) and to inject onboard liquid monopropellant (H_2O) for subsequent laser heating in the rocket mode. Again, this monopropellant is still energized by the GBL, using repetitive LSD waves to process the propellant into a high-temperature plasma that generates successive high-pressure blast waves (Figure 3.9). The injectors (see Figure 3.10) employ self-acoustic valving to meter the propellant flow, tuned to operate at the laser pulse repetition frequency. This injector system is designed to prevent “chug.”

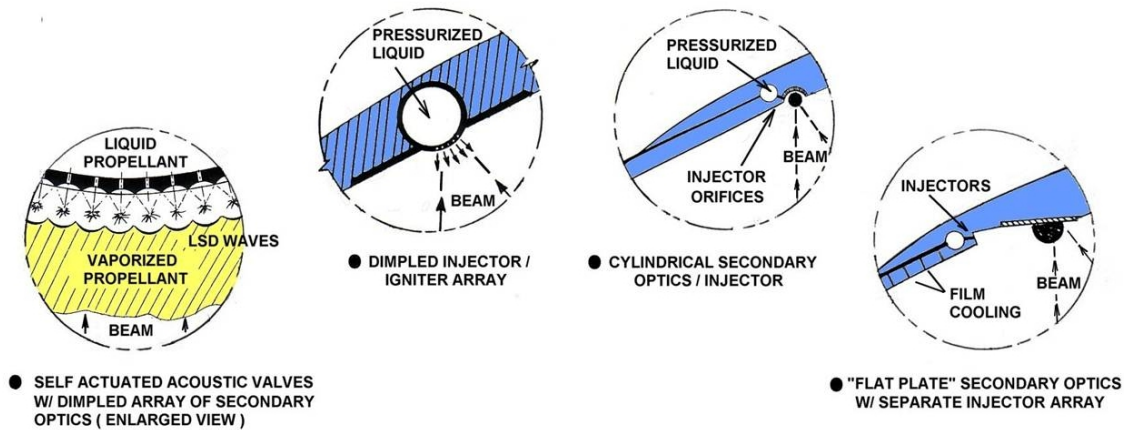


Figure 3.10.—Propellant injector schemes for rocket pulsejet mode (Ref. 16).

Note in Figure 3.5 and Figure 3.7 the inverted “Hershey’s kiss”-shaped (or pear-shaped) H_2O main propellant tank and its 15.2-cm-diameter helium pressurant tank that is bonded inside the bottom tip. The helium tank is constructed of titanium alloy and reinforces the lower tip of the main tank. The H_2O tank, also made from titanium, is bonded to the regeneratively cooled, 100-cm-diameter parabolic optic so that the resultant sandwich structure reinforces the mirror’s precise surface contour.

The propellant flow provides regenerative cooling of the primary optic surface and the 24 cowl support struts (titanium), as well as film/transpiration cooling on the inner cowl surface (and possibly, the cowl and strut leading edges), as shown in Figure 3.11 and Figure 3.12. An integral RCS and main propellant storage system employ four additional equal-spaced, pulsed injectors on the rotating shroud, specifically for the RCS function (see Figure 3.13). The pear-shaped titanium H_2O propellant tank with integral He spherical pressurant tank is a blow-down design—that is, pressure fed (no pump).

The preliminary propellant injection and distribution (PI&D) in Figure 3.13 (left diagram) reveals the essential elements for this blow-down system equipped with a single propellant tank and single He pressurant tank. The pear-shaped, titanium alloy propellant tank is equipped with slosh baffles and has a channel propellant management device (PMD) around the tank periphery because of centrifugal forces on the propellant. The heat leak into the main and He tanks aids in the pressurization of the blow-down system.

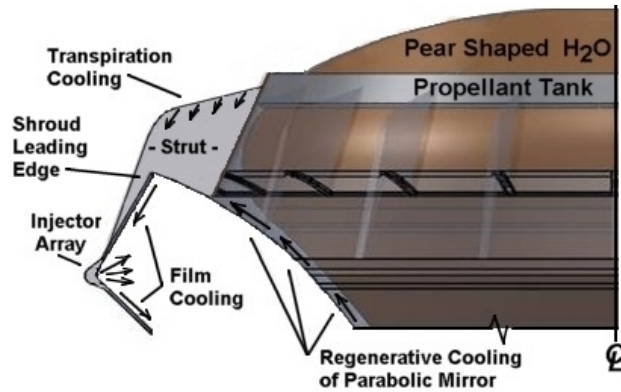


Figure 3.11.—Cutaway of engine “hot section,” showing cooling and propellant injector systems (Ref. 16).

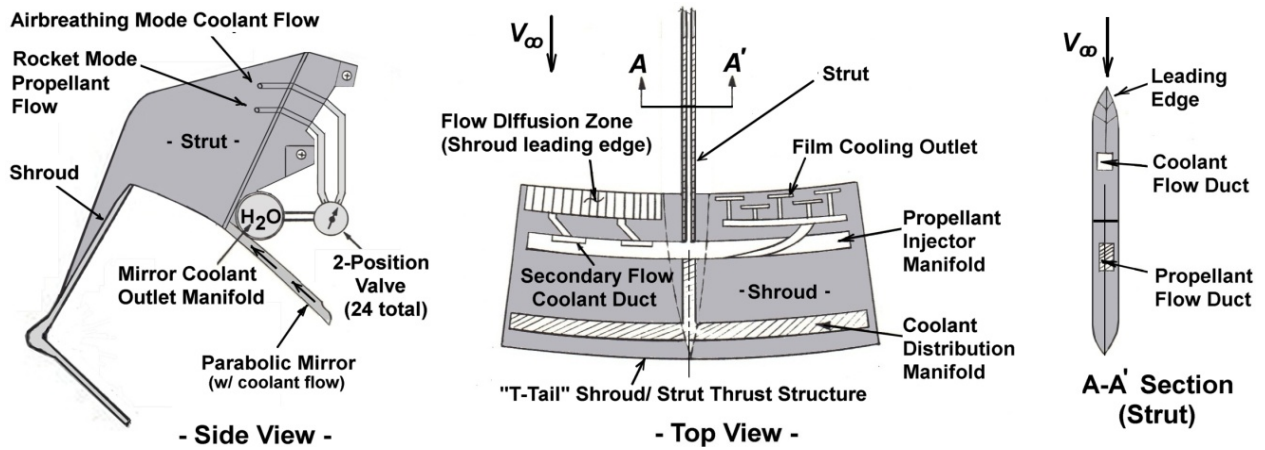


Figure 3.12.—Side and top views of shroud and support struts, explaining coolant scheme (Ref. 16).

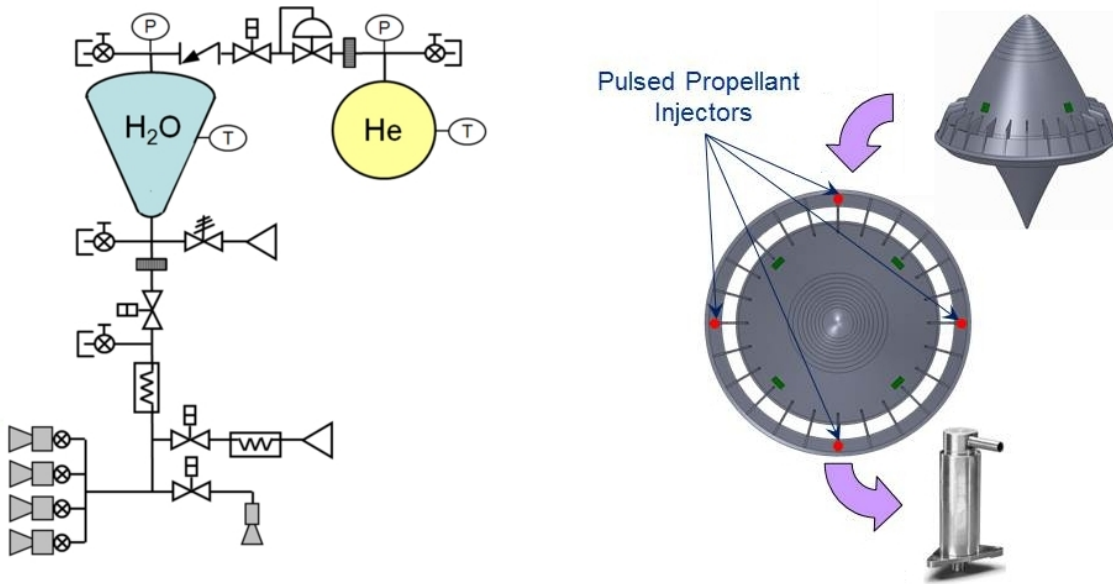


Figure 3.13.—Thrust vectoring, RCS, and propellant injector design.

This zero-fault-tolerant feed system has three branches: (1) differential injectors/RCS (four); (2) uniform rocket-mode injectors (evenly distributed around the 120-cm shroud); and (3) film/transpiration cooling flow. As mentioned earlier, the H₂O propellant flow also regeneratively cools the vehicle aftbody (parabolic mirror). The pulsed injectors provide vehicle attitude control through differential propellant injection into the toroidal beam focus area (i.e., the engine’s annular “*absorption chamber*” or “*hot section*”) during both air-breathing and rocket modes. Relying on commercial-off-the-shelf (COTS) high-speed RCS valves, the system would also provide on-orbit attitude control of the spacecraft.

3.1.2.6.1 Propulsion System Requirements and Assumptions

Briefly summarized, the principal requirements and assumptions for this DRM 1–A propulsion system are

- Requirements
 - o Zero-fault-tolerant system
 - o Tanks remain internal to vehicle
 - o No staging
 - o Laser-based air-breathing mode to gain altitude and velocity (Mach 6 to 7 and 35 km) to minimize the added ΔV of the rocket mode to reach orbit
 - o Laser-based rocket mode to build up velocity using onboard propellant
- Assumptions
 - o I_{sp} of 950 s with water monopropellant in rocket mode
 - o Laser system can continuously track and beam energy to engine/vehicle.
 - o He pressurization of main propellant tank (H₂O)
 - o Effective regenerative and film/transpiration cooling of optic and other surfaces

3.1.2.6.2 Beam-Riding Feature and Aim-Point Strategy

A unique and special feature of this lightcraft engine bears further elaboration; that is, *the propulsion system generates a lateral restorative force that allows the vehicle to be a beam rider in both atmospheric and vacuum space environments.* Figure 3.14 shows the impulsive forces and moments applied to a lightcraft engine when the laser beam is offset from the vehicle’s axis of symmetry.

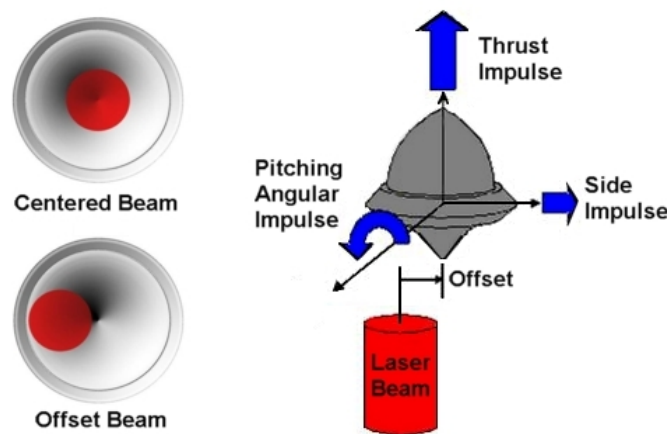


Figure 3.14.—Left: Centered versus offset beams. Right: Thrust impulse, side impulse, and pitching angular impulse are functions of lateral beam offset distance (Refs. 13 to 15).

Figure 3.15 explains how axial impulse and lateral impulse vary as a function of laser beam offset and angular offset from the engine’s longitudinal axis. (*This engine performance data has been extensively measured for a family of lightcraft engine geometries under stationary conditions in Refs. 6 to 8).*

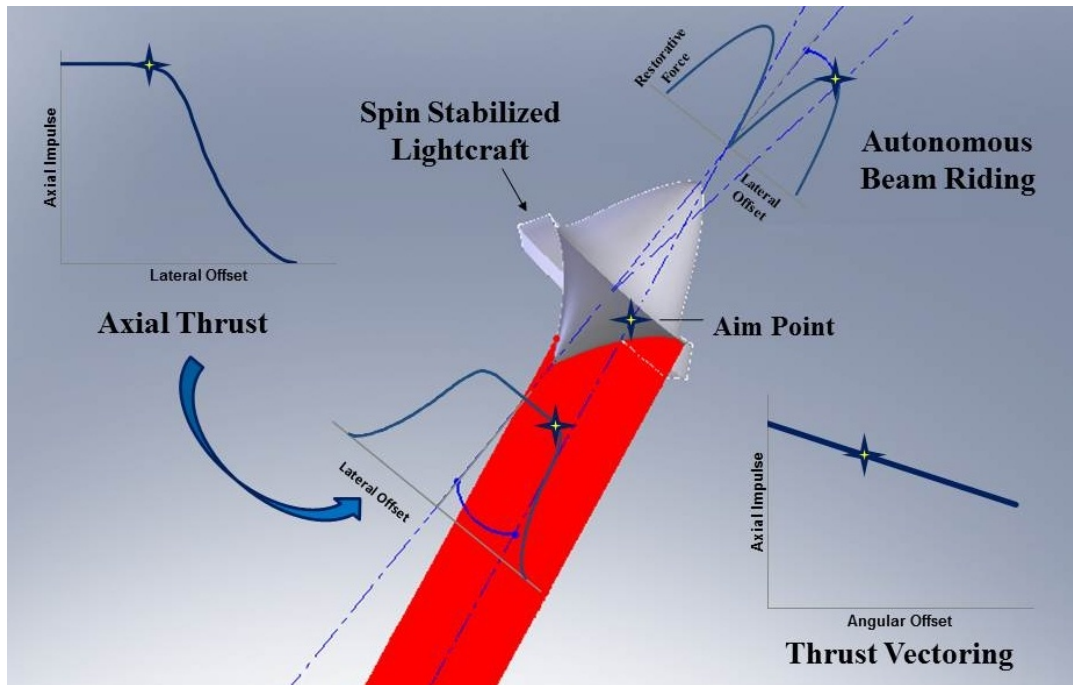


Figure 3.15.—Performance variations in axial impulse and restorative (i.e., beam-riding) impulse versus lateral offset are actively exploited in the aim-point strategy (Refs. 13 to 15).

The autonomous beam-riding feature significantly reduces the total RCS propellant load consumed in the laser boost phase, because only the vehicular pitch and yaw must be controlled. Furthermore, by directing the laser beam with a precise lateral offset on the lightcraft’s rear optic, the engine thrust may be vectored at will. By targeting a given “aim point,” the laser beam can effectively lead the vehicle (with a prescribed offset), coaxing it to fly along the desired boost trajectory.

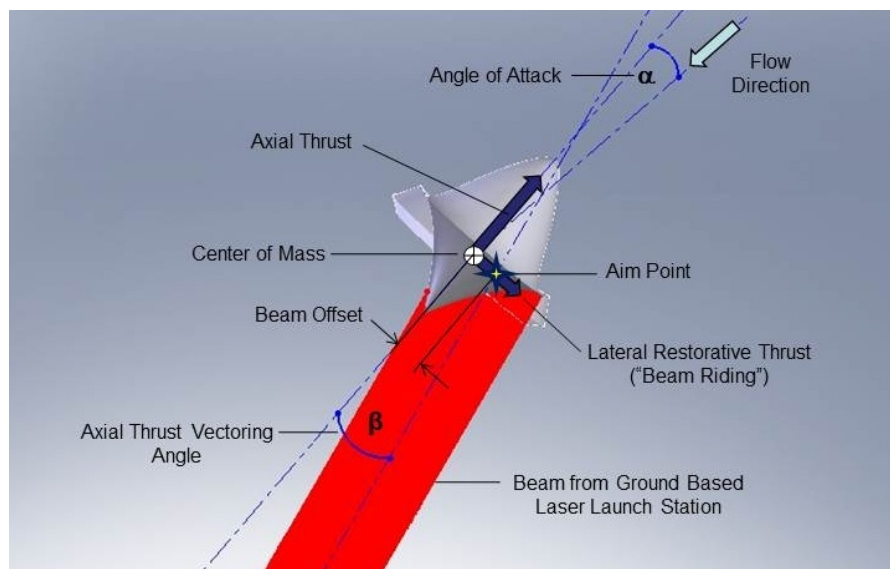


Figure 3.16.—Aim-point strategy in launching a beam-riding lightcraft (Refs. 13 to 15).

3.1.2.6.3 Propulsion System Risks

The following is an itemized list of propulsion system risks identified in the DRM 1–A study:

- Confirm that rocket-mode time-averaged I_{sp} value of 950 s can be achieved with H₂O propellant (estimated at TRL 2)
- Maintenance of appropriate beam angle and offset relative to vehicle spin axis
- Adequate control authority of beam to enable engine thrust vectoring via beam lateral (and angular) offset and differential propellant injection
- Excessive propellant pressure drop along cooling channels resulting in inadequate propellant flow rates
- Acoustic valve failure resulting in incorrect propellant injection timing and/or inadequate propellant flow rates
- Inadequate regenerative cooling of optic surfaces and exposed hot surfaces
- Unknown film cooling requirements for exposed hot surfaces
- Unproven performance of air-breathing ramjet/scramjet mode
- Proper air inlet annular door/gap closing operation in air-breathing to rocket mode transition
- Robust design: allow for margin in component design to support *zero fault tolerant* requirement

3.1.2.6.4 Recommended Future Trades

Future trades considered in the combined-cycle laser propulsion system design include (but not limited to):

- Dense noncryogenic propellants: for example, ammonia, hydrazine, and hydrogen peroxide
- Moving the rear optic focus from the inner shroud surface, into the flowfield (i.e., smaller focal radius than 60 cm) in order to reduce cooling requirements
- Varying the number and configuration of pulsed propellant injectors
- Pumped propellant system versus He pressurized (blow down)

3.1.2.7 Structures and Mechanisms Subsystems—Description

The high-level design requirements for structures and mechanisms are

- Contain the necessary hardware for research instrumentation, communications, avionics, propulsion, and power (see Figure 3.17)
- Withstand applied mechanical and thermal loads from launching
- Provide minimum deflections, sufficient stiffness, and vibration damping
- Minimize mass

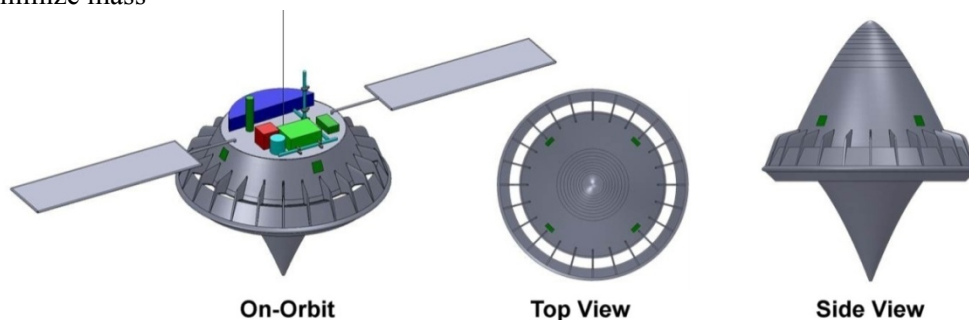


Figure 3.17.—Lightcraft DRM 1–A configuration—oblique, top, and side views.

The lightcraft structures assumptions are

- Provide main structures backbone for BEP vehicle
- Materials include graphite/polyimide, C/SiC or SiC/SiC, titanium, and aluminum
- Shells have beam and/or stringer reinforcement
- Fastener assembly is bonded, welded, and threaded

The mechanisms assumptions are

- Provide support for (1) forebody clam shells and nose cone, (2) separation and tether (for forebody shells), and (3) shroud air inlet flaps
- Mass of mechanisms for pyrotechnic bolts and springs—
 - o Forebody shells and nose cone, 1.82-kg basic mass total
 - o Forebody shells tethers, 0.4 kg each; quantity, 2
 - o Gravity gradient tether, 0.11 kg
- Mass of mechanisms for shroud air inlet gap/flaps linear actuators—0.05 kg each; quantity, 24 (i.e., one flap sandwiched between each pair of struts).

The structural design was ultimately to exploit advanced composites and titanium components, with flanges for joining sections and mounting internal hardware made from aluminum. The structure subsystems will employ shells to bear all operational loads. Aluminum composite sandwich structures will see application in deck and beams for mounting hardware (science probes, payload support, etc.).

The primary mass components of the structure will be (1) the forebody of carbon/carbon and graphite/polyimide with aluminum flanges and stringers, (2) the annular shroud thrust structure (with 24 support struts) of titanium, (3) the main propellant tank of titanium, and (4) the afterbody parabolic mirror of C/SiC. The carbon/carbon nose cone is at TRL 6, as is a graphite/polyimide shell forebody, with aluminum flanges and stringers in the primary structure. The annular shroud and inlet gap flaps will be of titanium alloy (TRL 6).

The secondary mass components of the structure will be (1) the aluminum composite sandwich structure instrumentation deck and installations, (2) the spacecraft adaptor and separation mechanism details, and (3) the pyrotechnic bolts that clamp the flanges of the two-part forebody. The favored design choice for the main structure material would ultimately be refractory metal-coated C/SiC, especially for the annular shroud and parabolic mirror afterbody. This choice would likely lead to the minimum mass and maximum high-temperature capability (i.e., the primary drivers); the NASA Technology Readiness Level of such ceramic matrix composites is at TRL 4. Analytical methods were applied for stress analysis scoping studies. For example, an advanced C/SiC mirror, supported on the launch pad with a point load of ~300 kg (at 1g) applied to the mirror's lower tip, must sustain ~43 MPa (including a 1.5 safety factor), which is well below the 240-MPa failure stress of C/SiC. In the early stages of development, the forebody sections could be made of aluminum, but final construction would likely use graphite/polyimide. Structural mass could be reduced (or margin increased) with a more detailed stress analysis using FEA.

Table 3.2 gives the mass breakdown for the 120-cm DRM 1–A spacecraft. The spacecraft dry mass will be 141 kg, so with 188 kg of H₂O propellant, the estimated total (wet) launch mass will be 318 kg (based on the Optimal Trajectories by Impact Simulation (OTIS)).

TABLE 3.2.—MASS BREAKDOWN FOR 120-cm DRM 1–A SPACECRAFT

DRM-1A Spacecraft: Master Equipment List Rackup (Mass)				COMPASS S/C Design
Main Subsystems	Basic Mass (kg)	Growth (kg)	Estimated Total Mass (kg)	Aggregate Growth (%)
Lightcraft/Spacecraft - 120 cm	300.1	18	318	
Lightcraft Stage 1	300	18	318	
Payload	0	0	0	TBD
Attitude Determination and Control	4	0	5	7%
Avionics	11	3	15	30%
Communications and Tracking	4	1	5	22%
Electrical Power Subsystem	4	1	5	30%
Thermal Control (Non-Propellant)	15	0	15	0%
Propulsion (Hardware)	17	2	20	14%
Propellant	188		188	
Structures and Mechanisms	56	10	66	17%

3.1.2.8 GN&C Overview

The objective of the GN&C system will be to facilitate lightcraft injection into a 400-km circular orbit with a 28.5° inclination. The pitch control on ascent was assumed to be provided by (1) differential thrust while in sight of the laser and (2) cold gas thrusting when not in sight of the laser (i.e., needed for orienting the vehicle to the correct attitude for the second laser burn (LEO insertion) using a relay mirror satellite). For this first-order analysis, the BEP lightcraft was assumed to have zero products of inertia.

The navigation electronics included the following:

- One LN–200S IMU
- An IMU with low mass (0.75 kg) and a design proven in space flight on Clementine, Deep Space I, and the Mars Exploration Rovers (MERs)
- Three solid-state fiber-optic gyros with a bias stability of 0.1°/hr
- Three solid-state silicon accelerometers with a bias of 0.3 mg
- One Ithaco IM–103 three-axis magnetometer to measure the strength and direction of Earth’s magnetic field
- Four patch antennas to be used for Global Positioning System (GPS) orbit and attitude determination

The control system electronics will manage both launch and on-orbit functions. The launch trajectory control system will encompass

- Passive stability will be provided by spinning the vehicle at 120 rpm.
- The vehicle will use the inherent beam-riding feature while in sight of the laser.
- The main pitchover maneuver will be provided by differential thrusting.
- Prior to orbit insertion, the nosecone will separate and act as yo-yo weights to despin the vehicle from 120 to 60 rpm.
- Cold gas thrusting will be used to pitch the vehicle to the correct attitude for the LEO insertion burn.

The on-orbit system will utilize

- *Three Ithaco TRI0CFR magnetic torquers* to provide up to a 15-Am² dipole moment magnetic torquers to despin the vehicle after injection into the circular orbit as well as to provide three-axis control for on-orbit operations
- *Gravity gradient stabilization* will be activated after the vehicle has been despun in orbit. A tether will be deployed with a 2.6-kg mass attached.
- *A nutation damper* will be used to provide additional energy dissipation for increased stability.

3.1.2.9 Avionics Overview

The avionics package design requirements follow: (1) avionics for systems command, control, and health management; (2) single-string processor architecture; (c) low-mass optimization; and (4) operational power modes that vary according to requirements, quiescent until needed. The space allocation for the avionics enclosure will specify a semicircular package (see Figure 3.18).

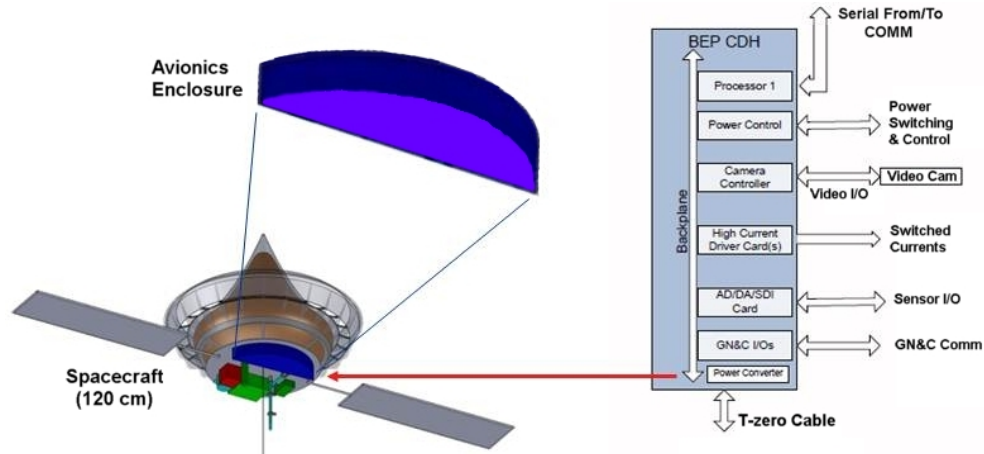


Figure 3.18.—Avionics functionality (120-cm launcher; I/O, input/output).

The principal assumptions include (1) 50-kRad avionics will be used for stable operation for the duration of the mission, (b) cabling mass will be estimated with a Monte Carlo simulation (mass and length), and (3) all avionics are at TRL 5—needing only to fly because of electrical, electronic, and electromechanical (EEE) and Class-S parts usage.

The following design features will be included in the avionics subsystem:

- Radiation-tolerant field-programmable gate arrays (FPGAs) packaged with Internet Protocol (IP) for processor capability, embedded software kernels without major operating system (O/S) overhead (optimized GN&C)
- Memory of 5 GB with error correction
- Power supply stabilized with switching regulators, filter, and electromagnetic interference (EMI) shielding to accept wide variations in supply voltage
- Discrete devices and power driver cards for general vehicle functions
- I/O cards for sensors and drivers
- Housekeeping data and health and safety (H&S) data to ground via a communication channel at ~ to be determined (TBD) bits per second
- High-TRL EEE parts in custom card designs, $-40\text{ }^{\circ}\text{C}$ ratings

The *general avionics processor* could be a Power Personal Computer (PC), chip, or intellectual property in an FPGA. The semicircular avionics card cage will use stacked custom boards in an open frame design. Other processor functionalities include

- Gimbals and thrust vector control (TVC) cards will be mass reduced and will control any necessary positioning (e.g., solar array deployment and gimbaling on orbit; communication antenna gimbaling to be resolved (TBR) on orbit).
- GN&C navigation—data from IMUs will be used to derive and control TVC parameters (0.16 MIPS nominally).
- Systems health and status reporting

- Power will be managed for various power modes (power trimmed with specialized sentinel switching) and will be full on for launch.
- System management will include control of valves and heaters.
- There will be a TBD bps serial interface between C&DH and the communications channel.

The sensors and drivers list includes 24 valves, TBD igniters, pyros, RCS, and pressure and temperature sensors. The software rough-order-of-magnitude (ROM) source lines of code (SLOC) estimate of ~140,000 to 180,000 includes launch.

Avionics risks include

- RAD 750 FX obsolescence likely, replace with FPGA (very-high-speed integrated circuits (VHSIC) hardware description language (VHDL) intellectual property)
- Particle radiation tolerance (shielding, high-radiation EEE parts; FPGAs exist with high radiation tolerance)
- Elevated vibration levels from the pulsejet engine during launch—may require “tuning” of the structure and board layout for stiffness

The geometry of stiffening members for enclosure and printed circuit boards will be determined through vibration analyses (experimental and numerical).

3.1.2.10 Communications—Description

The communications system will provide communication to the vehicle during launch and will demonstrate capabilities similar to that of ORBCOMM in space, using a single-string system. The S-band at NASA frequencies was chosen to reduce the mass and size of the communication system, but other frequency bands could be visited and analyzed later. The system will communicate from individual transmitters at 4.8 kbps or greater, and from space gateways at 57.6 kbps or greater with a nongimbaled antenna system (Figure 3.19).

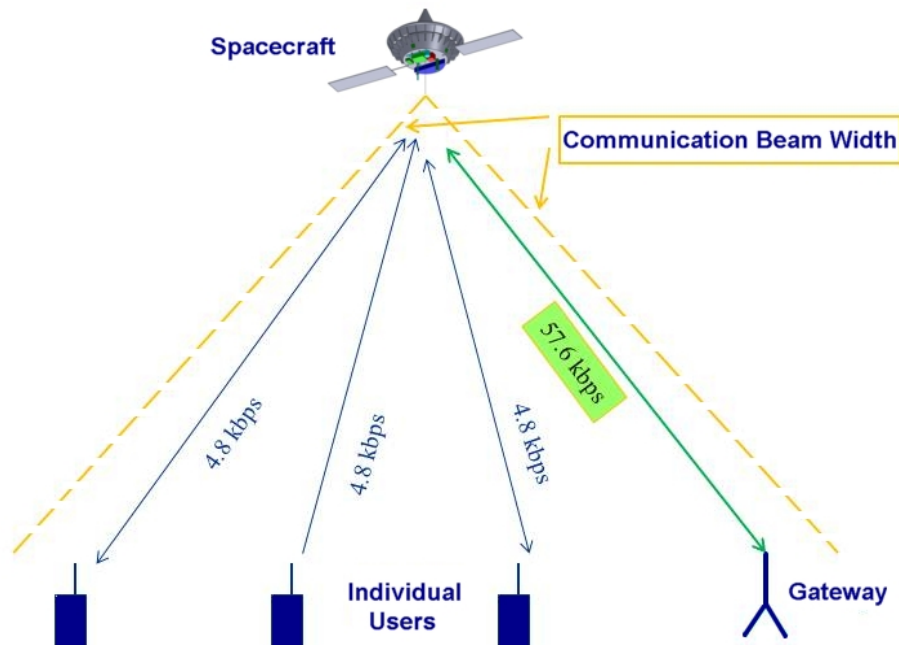


Figure 3.19.—Communication operations diagram.

At liftoff, the spacecraft will communicate initially to a balloon or airplane near the launch site before switching to down-range gateways on the ground as it overflies these terminals along the trajectory (see Figure 3.20). The number of gateways will be determined by the trajectory and antenna gain chosen. A four-patch antenna (see Figure 3.7 and Figure 3.16) on the spacecraft nose will enable S-band communications with the airplane or balloon, as well as Earth stations down range of the launch site. In orbit, the satellite will communicate to the ground with a helix antenna. Other types, like patch antennas, should be considered in the future. The helix antenna, which is entirely enclosed by the nosecone until it is jettisoned, will be pointed along the spacecraft axis toward the ground, and it will not be gimbaled. The satellite will communicate to individual users and to gateway users and will transfer the information between users and gateways. A *store-and-forward* function will facilitate the relay of information between sites. Gateway users will be connected to the Internet. The only identifiable risk is the need for flipping the spacecraft over for communications with the ground.

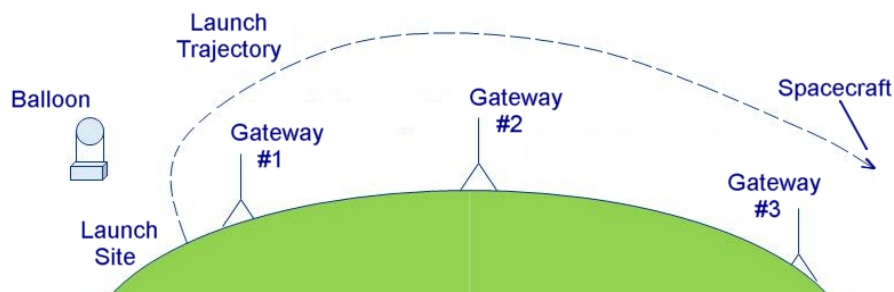


Figure 3.20.—Launch gateway sites.

A trade study was conducted on the communication link budget versus the antenna gain and Earth coverage. The largest feasible helix antenna was assumed in the master equipment list (MEL) for estimating communications system mass. The specific trades performed were

- Communication spot size versus antenna gain
- Maximum communication range from the user versus antenna gain
- Data rate versus antenna gain
- Different antenna gain for an individual user versus a gateway user
- Data rate versus low-noise amplifier (LNA) noise temperature

From Table 3.3 on the gateway to the satellite/spacecraft, one can see that almost all beam angles will meet minimum data rate requirements from the satellite to the gateway station, when the gateway station is using a 1-m-diameter dish. Only the largest beam angle is not achievable for the helix antenna design, because the antenna will have less than 1 coil. The helix antenna will become too long for the spacecraft for beam angles of less than 30°.

Table 3.4 displays data rates for two margins (3 and 20 dB) for three different user transmit powers: 0.25, 1, and 2 W. *The green boxes fulfill the minimum requirements of the study.* For low-data-rate users requiring 4.8 kbps, most antenna beam angles will work even with only 0.25 W of transmit power, if only 3 dB of margin is needed. However for many users, especially within cities, a higher margin will be required.

TABLE 3.3.—TRADE STUDY—DATA RATE AND COVERAGE VERSUS BEAM WIDTH TO *GATEWAY*

Communication—Trades: Fixed Conditions						
Frequency	2.2 GHz		Gateway antenna diam.	1 m		
Satellite transmit power	1 watt		Sat. antenna diam. (cm)	4.13		
User transmit power	0.25 watts		User antenna gain	2 dBi		
Trade Study data rate and coverage versus beam width to Gateway for use of a helix antenna on the spacecraft						
Beam Width (deg)	Antenna Gain (dBi)	Earth Coverage Diam. (km)	Maximum range (km)	Data rate (kbps)	Antenna Length (cm)	Antenna Mass (kg)
150	4.31	2985	3012	114	---	---
120	6.02	1386	1442	1000	3.25	0.19
90	8.34	800	894	4600	5.52	0.20
60	11.74	461	611	6000	12.0	0.20
45	14.2	331	519	6000	21.1	0.20
30	17.69	214	453	6000	47.06	0.20

Many communication applications exist for a constellation of laser-launched satellites, ranging from Earth-observing to mining, trucking, and just about any low-data-rate system that is power sensitive. Examples of Earth-observing applications include the monitoring of

- Sea (and land) temperatures, salinity, carbon dioxide (CO₂)/pollutant concentrations, wind speed, wave actions (height, frequency, etc.), and solar flux
- Seismic activities in remote locations (e.g., earthquakes)
- Vegetation coverage and assessments
- Forest fires
- Tagged-animal movements
- Data from remote mining, oil pumping stations, and so forth.

TABLE 3.4.—TRADE STUDY—DATA RATE AND COVERAGE VERSUS BEAM WIDTH TO *USER*

Communication—Trades: Fixed Conditions						
Frequency	2.2 GHz		Gateway antenna diam.	1 m		
Sat. transmit power	1 watt		Sat antenna diam.(cm)	4.13		
User transmit power	0.25/0.5 watts		User antenna gain	2 dBi		
Trade Study data rate and coverage versus beam width to user for use of a helix antenna on the spacecraft						
Beam Width (deg)	Data Rate (kbps) versus user transmit power (watts)					
	3 db Margin			20 db Margin		
	0.25 W	1 W	2 W	0.25 W	1 W	2 W
150	0.3	1.2	2.4	0.008	0.032	0.064
120	2.4	9.8	19.6	0.05	0.2	0.4
90	9.6	38.4	76.8	0.11	0.44	0.88
60	38.4	153.6	308	0.6	2.4	4.8
45	115.2	460	920	2.4	9.6	19.2
30	256	1024	2048	4.8	19.2	38.4
Acceptable communications						

3.1.2.11 Power System—PV Array and Battery Description

Itemized in the following subsections are the *requirements and assumptions* used in the design of the DRM 1–A spacecraft’s PV and battery power system (see Figure 3.21), followed by the *power system risks*. Table 3.5 shows the power equipment list (PEL) for the 120-cm spacecraft.

3.1.2.11.1 Power System Requirements

- No redundancy, single string (i.e., no redundant battery cells, battery packs, or solar array strings)
- Orbital user power (day and night) = 105 W (*includes 30% growth*)
- Orbit = 400 km (*93-min orbit period/36-min eclipse*); no orbital altitude degradation, eclipse period is worst case
- Life = 4 years

TABLE 3.5.—PEL FOR 120-cm LIGHTCRAFT LAUNCHER

PEL: 120 cm Lightcraft	Power Mode 1 (W)	Power Mode 2 (W)	Power Mode 3 (W)
<i>Power Mode Function</i>	<i>Launch</i>	<i>On-Orbit Operational</i>	<i>On-Orbit Non-Operational</i>
Systems operating	All Except EPS/Thermal	All Except Thermal/Structures	AD&C/Avionics/Comm
Attitude Determination and Control	22	22	22
Avionics	36	36	13
Communications and Tracking	20	20	7
Electrical Power Subsystem	0	3	0
Thermal Control (Non-Propellant)	0	0	0
Propulsion (Hardware)	5	5	0
Structures and Mechanisms	24	0	0
Total (watts)	107	86	42
Power Requirement (Plus 30%)	139	112	54

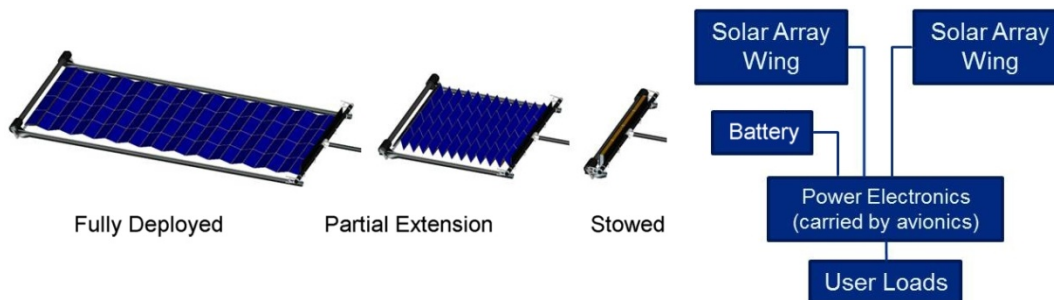


Figure 3.21.—Left: Flexible PV array. Right: Power circuit schematic.

3.1.2.11.2 Power System Assumptions

- Full Sun-tracking will be used to minimize the solar array area and mass.
- Two solar array wings will be used with only one axis gimbal per array and yaw steering (full Sun-tracking to minimize solar array area); each wing gimbal axis must be parallel, thus one or two will be possible.
- 10% of solar array power will be degraded over the mission because of radiation, atomic oxygen, ultraviolet radiation, thermal cycling, contamination, and orbital debris and micrometeorites.

- Array thermal properties: emissivity top = 0.85, emissivity bottom = 0.8, absorptivity top = 0.92, and absorptivity bottom = 0.6.
- Triple Junction Solar Cell efficiency: at 28C (no degradations) = 36%; 70C (400 km, no degradations) = 32%; 70C (400 km, with degradations) = 29%.
- 10% losses in power system (due to electronics, harness, and connector efficiencies).
- Areal mass = 3.66 kg/m² (if 3-mil coverglass assumed on each side of solar cell).
- Cell packing factor into solar array = 0.85.
- Lithium batteries = 200 W-hr/kg, 50% depth of discharge (limited because of number of cycles).
- 28 Vdc
- Technology status: solar arrays = TRL 4, gimbals = TRL 8, and batteries = TRL 4.

3.1.2.11.3 Power System Risks

- The complex launch environment (i.e., vibrations induced by the pulsed detonation engine) will impact the power system's hardware and design.
- High-spin acceleration combined with pulsed accelerations along the vehicle launch direction and spin axis, as well as high thermal loads from both the laser and aero-heating, will add uncertainty to the power system design.
- Although stowed flexible arrays can be designed for high uniform load accelerations (20g to 50g), this concept requires more analysis than a conceptual design to confirm, especially for a low to moderate TRL array (not off the shelf).
- Even lithium batteries cannot be assumed to be immune from spin accelerations due to internal electrolytes that may require the battery package to have a specific orientation to function properly.
- Thermal loads require more analysis. The present stowed solar array design was focused on being able to separate/partition the power system from this problem as much as possible, but the need for thermal blankets or isolation has not been quantified.
- Consider reducing the vehicle spin rate (or despin payload), orienting stowed solar arrays parallel with the spin axis to minimize differential loading, and structural analysis to determine required supports for the stowed solar array during launch.

3.1.2.11.4 Power System Trades

Fixed versus tracking solar arrays.—Although fixed arrays could be assumed, this would increase the size of the solar array (50% to 100%) because of a decreased effective Sun period and cosine losses; the energy storage mass would also increase because of an increased effective eclipse period. Therefore, tracking arrays were selected.

Tracking method of solar arrays.—There are various ways to Sun-track the solar arrays:

- (1) Inertial flight (i.e., pointing the entire spacecraft at the Sun)
- (2) Two-axis gimbals for each solar array
- (3) One-axis gimbal for each solar array wing with yaw steering (i.e., this gimbal tracks about the lengthwise axis of the solar array; the other axis is handled using yaw steering of the spacecraft)

For small spacecraft, yaw steering is the most economical method for Sun tracking since inertial flight modes are somewhat costly, as are too many gimbals.

Energy storage type.—The options for projected available technology for energy storage include

- (1) *Electrodynamic tether*: Extracts energy by passing through the Earth's magnetic field; it is likely heavier than other options, has a tether dynamics risk, and causes orbit altitude reduction
- (2) *Lithium sulfur battery*: Has very high specific energy but presently has too few demonstrated charge/discharge cycles to meet the LEO orbit life of >1 year; also has a low operating depth of discharge to limit degradation (likely not ready by 2020)

(3) *Lithium ion battery*: Has extensive GEO and some LEO testing and the potential is high for LEO cycling rates at a moderate depth of discharge

Although the lithium ion battery type assumed has a higher specific energy than for SOA LEO lithium ion batteries, it is anticipated that the technology will advance rapidly. If not, then a moderate mass penalty due to a lower specific energy SOA lithium ion battery can be assumed.

Power generation type.—The options for projected power generation technologies include

(1) *Electrodynamic tether*: Can provide power during the entire orbit but will really require some method of orbit-raising, which is likely not a minimum mass solution

(2) *Solar PV array painted or grown on the outer structure*: Low efficiency (~10%), high development risk because of stress, vibrations, and thermal problems; need conductive surface to keep solar cells cool to operate efficiently, but the outer surface must be an insulator; unknown radiation, ultraviolet light (UV), and atomic oxygen effects on solar cells; and low TRL—likely not ready by 2020

(3) *Concentrator PV cells using BEP mirror pointing at Sun*: Low TRL; unknown degradation of reflective surface over time; requires high Sun pointing accuracy or larger area of solar cells; unknown integrated impacts of this on the vehicle; requires significant radiator area to keep the cells cool to have reasonable efficiency and not melt, with likely some sort of pumped loop cooling; and requires much more analysis to determine if it can be practical

(4) *Thin-film solar cells*: Low efficiency, thus too large of an area if deployed or used on limited surface area of the vehicle, but they are at a high TRL

(5) *Deployable rigid panel wings*: High TRL, fairly heavy—2 to 3 times heavier than flexible panel wings; hinges are simple and reliable, but fitting into the limited volume vehicle “bay” may present a problem because the stowed volume is large; risk due to centripetal and launch pulse accelerations and vibrations and due to integration into nonoptimal vehicle structure; if integrated into the “nose” of the spacecraft inner surface because of other components, adequate surface area would be unlikely for the power levels required; and, because articulation is required to minimize the solar array surface area, it is harder to articulate the heavier surfaces and extend them)

(6) *Inflatable PV wings*: Low TRL, need significant development, could integrate various cell types into the inflatable surface, and could rigidize the wings by UV

(7) *Deployable flexible PV wings*: Moderate TRL, Roll-Out Solar Array (ROSA) or similar simple unrolling or unfolding types, no thick substrate or mass to attach cells to, highly compact during launch, very light, thermally favorable to keep solar cells at low operating temperature and at high efficiency, low mass, and minimizes gimbal requirements

3.1.2.11.5 Power System Recommendations and Work to be Done

General

- Factor the range of orbit altitudes (i.e., what is the minimum operational altitude?) into the design.
- Reduce payload compartment spin rate and increase payload volume—could despin the entire payload and/or nose components.
- Consider jettisoning the annular shroud of the spacecraft.
- Batteries/solar arrays need spin-testing for this unique acceleration/impulsive force launch environment.
- Since this is a commercial vehicle and COMPASS does space-rated/government vehicle designs, cost is *not* minimized by using lower quality solar cells, non-space-rated batteries or cells, or gimbals. This needs to be considered in some manner.

Solar Arrays

- Perform more thermal load and stress analysis on the solar array, and perform more detailed layout of the array.

- If lightcraft is reusable, obtain reentry requirements to determine the need for retraction or jettison of solar array.
- Consider a modified design of the solar array deployment boom and articulation by increasing the length of the solar array and permitting the bottom quarter or third to be unpopulated by solar cells (possibly by a radiative surface) to simplify the deployment booms and mechanisms.
- Consider using only one solar array wing. This will require stowed packaging and orbital dynamics analyses. It could help to reduce complexity and part count, increase reliability (one wing deploy rather than two), and reduce shadowing impacts. However, the balance of the spacecraft through the orbit would be impacted.
- Consider one gimbal for both solar arrays. They would both rotate in the same direction, so some cost could be saved by connecting them to eliminate one gimbal.

Battery

- Obtain and analyze the time-phased load profile for the launch phase (and reentry phase, if applicable, since solar power is not available at this time) to better size the battery and determine nominal and peak current impacts.
- Consider the use of a higher TRL, heavier battery (somewhat heavier) to reduce design risk.
- Confirm thermal analysis of the battery to ensure that it will survive the launch and orbit environment.

3.1.2.12 Thermal Subsystem—Description

Lightcraft thermal subsystems must address two entirely different flight environments: (1) during launch and (2) on-orbit (see Figure 3.22). The total thermal subsystem mass is estimated at 15.23 kg.

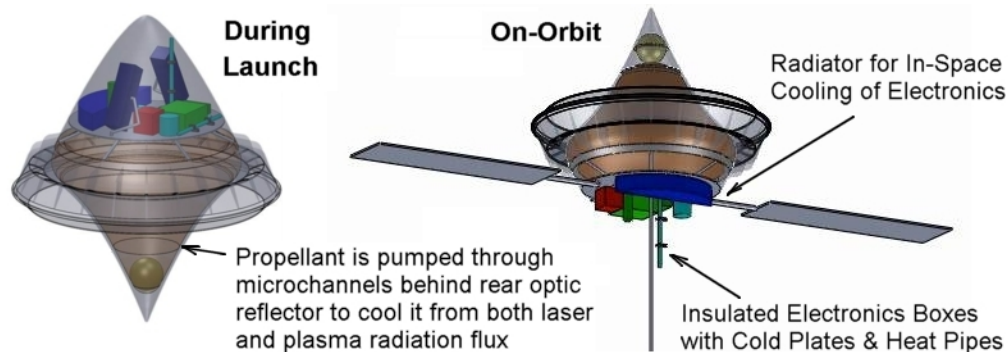


Figure 3.22.—Lightcraft thermal subsystems. Left: During launch. Right: On-orbit.

The *ascent thermal subsystem* will cool the aft parabolic mirror and the engine “hot section” parts (i.e., annular shroud and 24 support struts), largely through regenerative, film, and transpiration cooling. The principal assumptions are

- The plasma toroid (created by pulsed laser heating) will be located sufficiently far from the aft parabolic mirror and shroud lower surface such that the needed cooling will be reduced to that available by the propellant flow.
- The aft mirror reflectivity will be 0.9999 through the use of multilayer high-reflectivity coatings tuned for the laser wavelength (~1 mm).

The *on-orbit thermal subsystem* must cool the electronics payload, including avionics, communications, and GN&C components. The assumptions include

- Heat dissipation for 100 W while in orbit
- An Earth-view factor of 0.5
- A solar-array-view factor of 0.15
- A Sun angle of 30°

LEO environmental conditions were used to determine the heat transfer while in orbit.

The thermal subsystem components include the following:

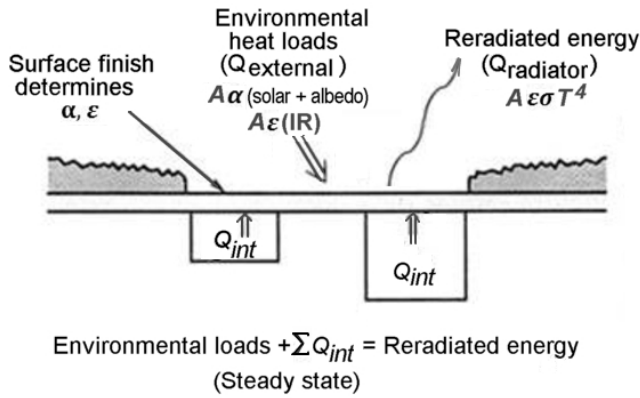
- Microchannel heat exchanger (HX) passages and pressure-fed H₂O to regeneratively cool the aft parabolic mirror and the shroud undersurface where the laser plasma is formed during ascent
- Additional transpiration and/or film cooling of the engine “hot section” parts as needed during ascent
- Cold plates and heat pipes to transfer heat from the electronics to the radiator section (Figure 3.22) in space
- Possible use of the aft parabolic mirror as a radiator when in orbit
- Multi-Layer Insulation (MLI) used to insulate the electronics boxes

3.1.2.12.1 Trades Considered in Thermal Analysis

- High reflectivity of the aft parabolic mirror will be critical to the successful operation of the engine/vehicle. If reflectivity degrades badly during launch, insufficient H₂O propellant flow will be available to cool this surface and complete the boost (could lead to catastrophic failure: i.e., loss of integrity of mirror reflectivity leads to increased thermal load on the mirror).
- Hence, placement of the high-temperature, pulsed plasma toroid at a safe distance from the optic (and shroud) walls is critical to engine functionality. If the plasma is positioned too close (i.e., within a few centimeters) to these walls, excessive heating will occur—potentially leading to structural failure (melting and disintegration). This could be resolved by varying engine design geometry.

3.1.2.12.2 Radiator Sizing

- A radiator panel (Figure 3.23) was sized to reject excess heat from the electronics packages once in orbit.
- A surface mount radiator was utilized.
- The radiator model was based on a first-principles analysis of the area needed to reject the identified heat load to space. The assumptions are given in Figure 3.23. From this radiator area, a series of scaling equations were used to determine radiator mass. The worst case thermal environment of LEO was used to size the radiator.
- No louvers were utilized.
- Heat pipes were used to conduct excess heat to the radiator surface.



Variable	Value
Radiator Solar Absorptivity	0.14
Radiator Emissivity	0.84
Radiator Sun Angle	70°
Radiator Operating Temperature	320 K
Total Radiator Dissipation Power	90 W
View Factor to Earth	0.5
View Factor to the Solar Array	0.15

Figure 3.23.—Surface mount radiator sizing—thermal analysis.

3.1.2.12.3 Cold Plates

- Electronics cooling will be accomplished by cold plates (see Figure 3.24) and heat pipes.
- Electronic components will be mounted onto cold plates that have integral heat pipes to transport excess heat to the radiator.
- Cold plates also will have heaters integrated onto them for maintaining electronics at desired temperatures throughout the mission.
- Flat plate heaters on these cold plates can provide heat to electronics if necessary. Additional heaters will be placed throughout the spacecraft interior to facilitate adequate temperature control of the vehicle.
- Thermal control will be accomplished through a network of thermocouples, whose data will be used to control the thermal power input to various heaters. A data acquisition and control computer will operate this thermal management system.

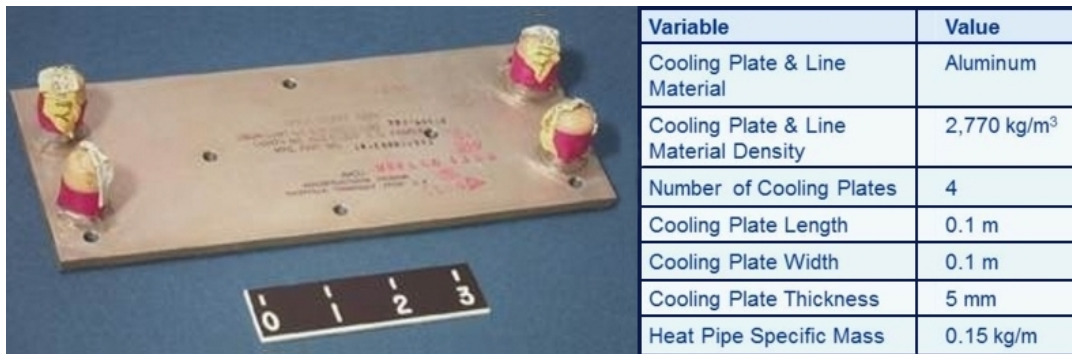


Figure 3.24.—Left: Sample cold plate for electronics cooling. Right: Thermal analysis assumptions.

3.1.2.12.4 Spacecraft Insulation

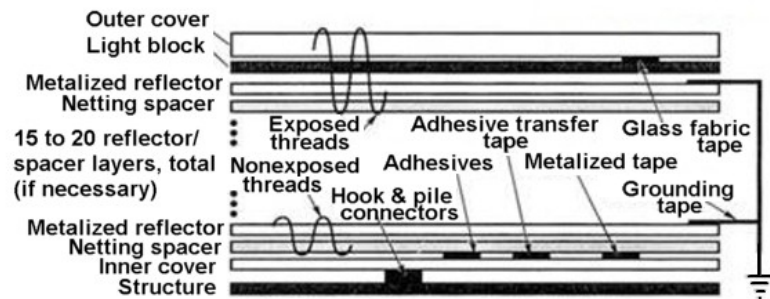
A first-order thermal analysis of the spacecraft insulation needs was carried out for which the principal assumptions are given in Table 3.6.

- MLI will insulate the spacecraft for operation in orbit.
- MLI provides its function by limiting radiation heat transfer to and from the spacecraft.
- MLI will be constructed of numerous layers of metalized material with a nonconductive spacer between the layers (see Figure 3.25).

- Each layer of insulating material will have a low emissivity, which will limit radiation heat transfer between the layers.
- The metalized material will have a low absorptivity, which will resist radiative heat transfer between the layers.

TABLE 3.6.—THERMAL ANALYSIS ASSUMPTIONS—SPACECRAFT INSULATION

<i>Variable</i>	<i>Value</i>
Tank Surface Emissivity (ϵ_t)	0.1
MLI Emissivity (ϵ_i)	0.07
MLI Material	Aluminum
MLI Material Density (ρ_i)	2,770 kg/m ³
Internal Tank Temperature (T_i)	300 K
MLI Layer Thickness (t_i)	0.025 mm
Number of Insulation Layers (n_i)	10
MLI Layer Spacing (d_i)	1.0 mm
Tank Immersion Heater Mass & Power Level	1.02 kg @ up to 1,000 W
Spacecraft Inner Wall Surface Emissivity	0.98
Spacecraft Outer Wall Surface Emissivity	0.93
Line Foam Insulation Conductivity	0.0027 W/m K
Line Foam Insulation Emissivity	0.07
Propellant Line Heater Specific Mass & Power	0.143 kg/m @ up to 39 W/m
Line Foam Insulation Density	56 kg/m ³



Note: Details and features are shown for illustration and will vary with actual design and installation

Figure 3.25.—MLI for spacecraft on-orbit.

3.1.2.12.5 Heaters and Thermal Control

Flat-plate heaters on the cold plates will provide heat to the electronics when necessary. Additional heaters will be placed throughout the spacecraft interior to facilitate adequate temperature control of the vehicle. Thermal management will be accomplished through a network of thermocouples whose data output will be used to control the power of the various heaters. A data acquisition and control computer will operate the thermal management system.

3.1.2.12.6 Thermal Risks

The main risk with the *ascent thermal subsystem* components pertains to the rear laser reflector, plasma degradation of that mirrored surface, and high potential heat transfer rates during ascent:

Mirror reflectivity.—Any damage or degradation to the mirrored surface experienced during launch could cause excessive local heating because of the intensity of the laser beam (approximately 3-kW/cm² incident). Debris impact or erosion from the nearby hot plasma could potentially degrade mirror reflectivity and cause catastrophic heating and loss of the vehicle. The very high reflectivity of the mirror

(99.99%—using multilayer coatings tuned to the laser wavelength) will have to be maintained throughout the launch phase. This is indeed possible with high multilayer dielectric film coatings today (see Figure 3.26).

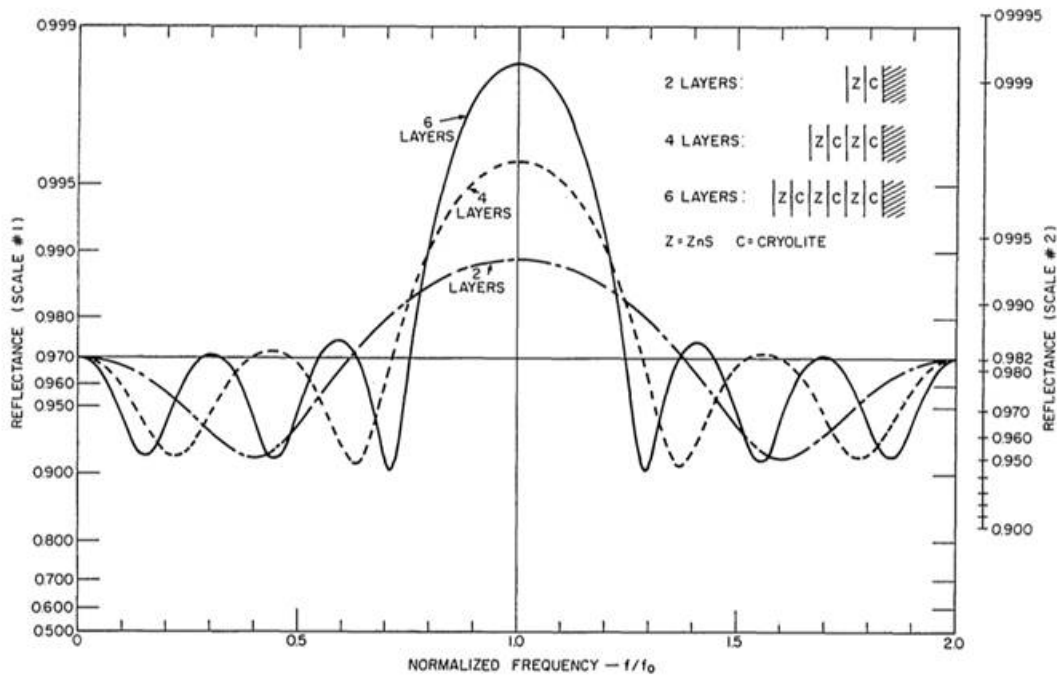


Figure 3.26.—Reflectance of multilayer dielectric film coatings versus normalized frequency.

Plasma heating.—Localized heating is due to the laser-created plasma “working fluid.” If this pulsed plasma is deliberately positioned within a few centimeters of the mirror surface, excessive heating of nearby walls will result. The mirrored surfaces cannot be highly reflective over the broad range of frequencies radiated by this hot plasma. Therefore, these walls will absorb significant amounts of heat if the plasma moves too close to the mirrored surface—likely in the range of 20 to 80W/mm² depending on the plasma distance (see Figure 3.27). *In comparison, the throat section of the Space Shuttle Main Engine (SSME) nozzle saw ~10 W/mm².* Such thermal loadings can be estimated from electric arcs (e.g., in 1-bar atmosphere), wherein plasma temperatures easily reach 30,000 K—quite typical of peak temperatures in pulsed laser propulsion.

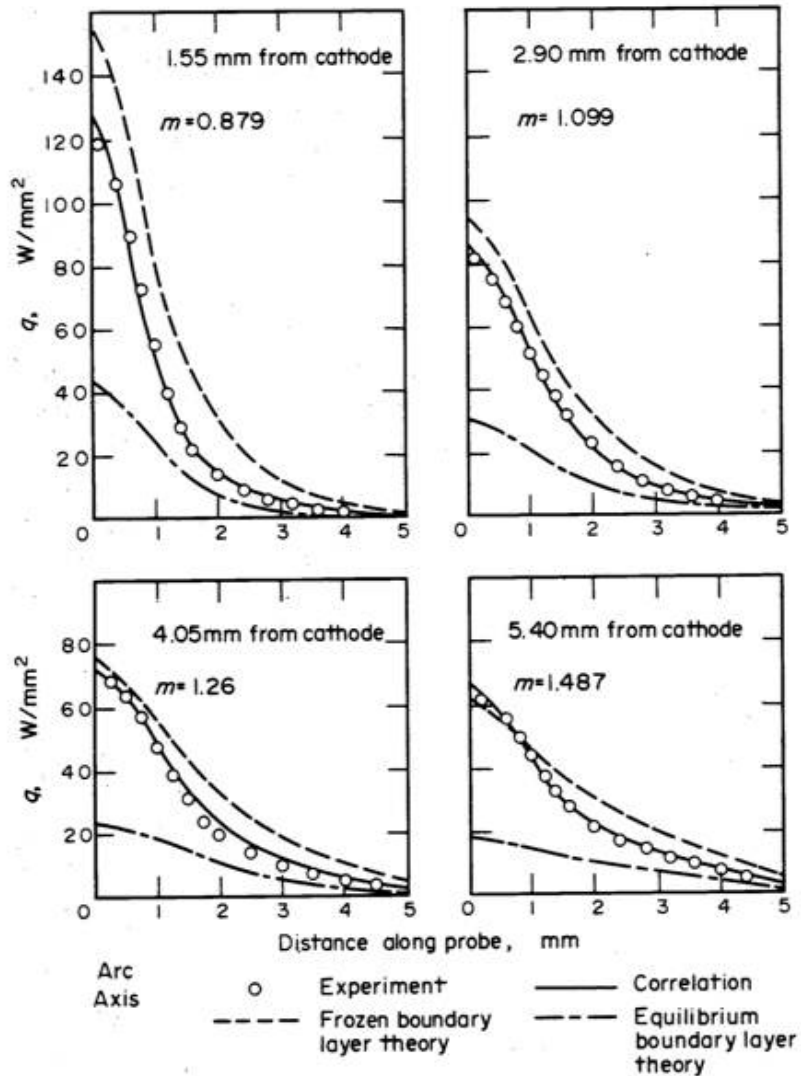


Figure 3.27.—Radiation heat transfer from electric arc in 1-bar atmosphere.

Reflected laser light.—Laser light scattered off of the annular shroud’s rear-facing (convex) surfaces and aft mirror (concave) surface will be reflected back to Earth. In essence, this could be a health hazard to someone inadvertently looking into the reflected beam, because $\sim 1\text{-}\mu\text{m}$ laser light is not eye-safe (i.e., the beam will propagate through the cornea and lens and onto the retina). The incident intensity in watts per centimeter squared of the reflected beam that reaches the Earth’s surface will depend on the curvature of the mirrored surface and the line-of-sight range to that spot on the Earth. And, of course, the smallest radius of mirror curvature yields the greatest dispersion and therefore lowest intensity of the reflected beam. For this reason, all external rear-facing lightcraft surfaces were designed as convex or concave optics to quickly dissipate reflected intensities to nonhazardous levels. In contrast, for planar surfaces, such as the flat sides of the 24 struts that support the annular shroud, another approach will have to be taken. Diffuse reflecting surfaces (Figure 3.28) will be applied to prevent planar reflections of incident laser light back toward the Earth. However, these struts would only be exposed to the incident laser power beam if the lightcraft were tumbling out of control, whereupon the beam would have normally been shut off anyway.

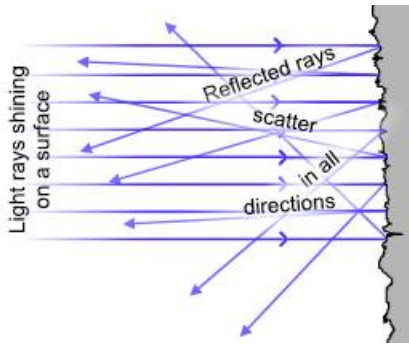


Figure 3.28.—Diffuse reflecting surface for scattering laser light.

3.1.2.12.7 Options and Recommendations (Thermal Subsystems)

- A more detailed analysis of plasma thermal interaction with the rear optics and other engine “hot section” components must be performed to accurately assess its impact and identify options for further reductions in thermal subsystem mass.
- Further analysis and experimentation should be performed to determine the amount of mirror degradation that will occur (if any) during launch and ascent.

3.1.2.12.8 CONOPS—Description

See section 3.1.2.18, CONOPS—Frequency of Launch and Repeat Time.

3.1.2.12.9 OTIS Trajectory Simulation—Description

See section 3.1.2.20, Launch Trajectory Simulations.

3.1.2.13 Multi-CubeSat Launcher Design for 120-cm Lightcraft

After completion of the ORBCOMM emulation study, the COMPASS team briefly explored the option to launch six CubeSats (~1 kg, 10 by 10 by 10 cm each) with the 120-cm lightcraft concept—see Figure 3.29. The basic ground rules were as follows:

- Retain the same launch trajectory, beam power levels, and infrastructure/stations.
- Remove only the ORBCOMM equivalent and satellite equipment, and keep everything needed for launch and insertion.
- Add a dual Poly-Pico Satellite Orbital Deployer (P-POD) CubeSat dispenser for deploying six CubeSats (1 kg) once on orbit (Figure 3.27).

The P-POD dispenser fits nicely in the conical payload bay, but the 120-rpm spin rate issue will likely dictate a redesign of the P-POD and CubeSats unless the payload section (spacecraft nose) is despun from the moment of launch. However, since the 120-cm launcher may still cost ~\$2M ROM, would it make economic sense to launch six \$30,000 CubeSats with it?

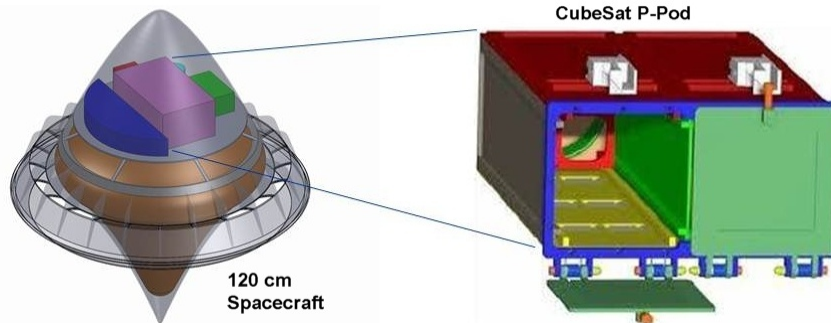


Figure 3.29.—Alternative payload for 120-cm spacecraft—dual P-POD launcher.

The MEL for this modified 120-cm CubeSat launcher is given in Table 3.7. The P-POD deployment device and CubeSat mass is carried (i.e., accounted for) in the structures and mechanisms allotment. An additional 3 kg is unallocated but is held for redesigning the P-POD and CubeSats to handle the high-g spin rate.

TABLE 3.7.—MEL FOR 120-cm LIGHTCRAFT LAUNCHER FOR SIX CUBESATS, DEPLOYED FROM DUAL P-POD ON ORBIT

Master Equipment List Rack-up (Mass) - Lightcraft Cubesat Launcher				COMPASS S/C Design
Main Subsystems	Basic Mass (kg)	Growth (kg)	Estimated Total Mass (kg)	Aggregate Growth (%)
Lightcraft/Spacecraft (120 cm)	296.3	17	313	
Lightcraft Stage 1	296	17	313	
Payload	0	0	0	TBD
Attitude Determination and Control	2	0	2	5%
Avionics	11	3	15	30%
Communications and Tracking	2	1	3	21%
Electrical Power Subsystem	0	0	0	30%
Thermal Control (Non-Propellant)	15	0	15	0%
Propulsion (Hardware)	17	2	20	14%
Propellant	188		188	
Structures and Mechanisms	59	10	70	18%
Estimated Spacecraft Dry Mass	108	17	125	16%
Estimated Spacecraft Wet Mass	296	17	313	
System Level Growth Calculations				Total Growth
Lightcraft Estimated Dry mass	108	17	125	16%
Dry Mass with Desired System Level Growth	108	32	140	30%
Additional Growth (carried at system level)		15		14%
Total Wet Mass with Growth	296	32	329	

However, considering the embryonic state of diode-pumped, solid-state lasers (e.g., now at the 100- to 120-kW level), it seems more prudent to first examine prospects for launching just a single CubeSat, with a much smaller and lighter launcher—for example, a 35-cm craft like that proposed in AFRL’s recent study (Refs. 5 and 19) invokes a 12-MW GBL. That far smaller launch infrastructure would be 20 to 30 times less powerful than what the 120-cm lightcraft requires (i.e., 250 to 350 MW). Clearly, a single nanosat launcher is the more prudent and attainable objective in the near term.

3.1.2.14 Description of 35-cm Vehicle

Figure 3.30 shows the relative scales of the 120-cm (i.e., DRM 1–A) and 35-cm lightcraft (designated DRM 1–A’) next to AFRL’s 35-cm nanosat launcher concept from References 5 and 19. The objective of launching 1.33-kg CubeSats (DRM 1–A’) with a 12-MW laser is consistent with the *progressive technology roadmap* (see sections 3.1.2.1 Lightcraft Technology Development and section 4.0 Summary and Conclusions), a growth strategy that may begin with 0.1- to 1-kg picosatellites (picosats)—the first *target of opportunity* for a ~1-MW laser. The natural progression would be to demonstrate boosting

increasingly larger payloads to ever higher altitudes over time: that is, starting with picosat (0.1- to 1-kg), then nanosat (1- to 10-kg), then microsat (10- to 100-kg) payloads.

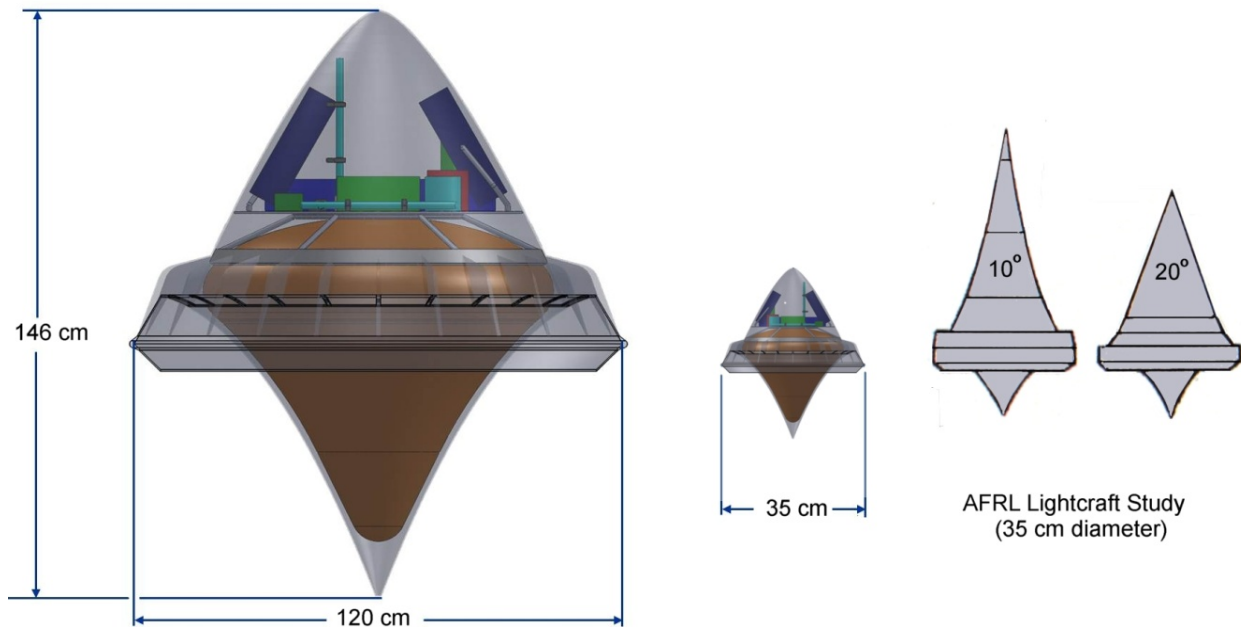


Figure 3.30.—Relative scale of lightcraft launchers. Left: Microsatellites. Right: Nanosatellites.

Table 3.8 compares the MEL component mass breakdown of the two BEPS lightcraft launchers. Note the assumed CubeSat payload of 1.33 kg. To the first order, lightcraft mass can be assumed to scale with the cube of its diameter, so the 35-cm craft will be ~40 times lighter. Table 3.9 gives the mass breakdown for AFRL's 35-cm lightcraft, designed for a 12-MW GBL and showing a liftoff mass of 8.0 kg.

TABLE 3.8.—MEL MASS BREAKDOWN FOR 35-cm VERSUS 120-cm BEPS LIGHTCRAFT

Spacecraft Master Equipment List Rack-up (Mass) - 35 cm*

Main Subsystems	120 cm Basic Mass (kg)	120 cm Vehicle Growth (kg)	Est. 35 cm Total Mass (kg)
Lightcraft/Spacecraft	300.1	18	8.02
Lightcraft Stage 1	300	18	8.0
Separable "CubeSat" Payload	0	0	1.33
Attitude Determination and Control	4	0	0.124
Avionics	11	3	0.372
Communications and Tracking	4	1	0.124
Electrical Power Subsystem	4	1	0.124
Thermal Control (Non-Propellant)	15	0	0.372
Cubesat Structure	0	0	0.110
Orbit Circ. Propulsion	17	2	0.496
Propellant (water) - Rocket Mode	188		4.66
Structures and Mechanisms	56	10	1.64

*NOTE: 35cm vehicle is scaled from 120 cm COMPASS results.

TABLE 3.9.—MEL BREAKDOWN FOR AFRL 35-CM
NANOSAT LAUNCHER (REF. 5)

• Laser Propulsion Propellant	4.00 kg
• Orbit Circularization Propulsion	0.46 kg
> Thruster (400 N)	0.408 kg
> Propellant (MMH/MON)	0.042 kg
> Propellant Tank	0.010 kg
• Airframe/Structure	~0.63 kg
> Nose Tip	0.025 kg
> Nose Cone	0.314 kg
> Shroud	0.208 kg
> Optics	0.079 kg
• Guidance/Control/Power	0.45 kg
• 30% Contingency	0.46 kg
• Payload	2.00 kg
Laser Vehicle Takeoff Weight	~8.00 kg

3.1.2.15 BEPS Versus AFRL Vehicle/Engine Comparison

- Both 35-cm lightcraft will use combined-cycle air-breathing rocket engines to minimize onboard liquid propellant mass (consumed in the rocket mode).
- The BEPS craft will have a 30° nose half angle versus AFRL’s more pointed 10° to 20°. Both vehicle forebodies will function as external compression air inlets.
- The BEPS craft will transition to rocket mode at Mach 6 to 7 and 30 km (Refs. 16 and 17), whereas the AFRL craft will transition at Mach ~9+ and 68 km.
- The AFRL air-breathing engine mode will transition from ramjet to scramjet mode beyond Mach 5 or 6 (in contrast, at this Mach number, the BEPS ramjet will switch into rocket mode).
- The AFRL craft will accelerate in scramjet mode to Mach ~9+ to reduce liquid propellant load down to ~4 kg (the BEPS craft has a larger propellant load of 4.66 kg).
- The physics of pulsed laser scramjet propulsion is presently under investigation in Brazil (Refs. 11 and 12). The Mach 6 to 10 impulsive flow will be produced by a hypersonic shock tunnel; twin gigawatt pulsed CO₂ lasers will be able to supply two sequential pulses to simulate high pulse repetition frequency (PRF) engine operation.
- Both 35-cm vehicles will invoke onboard chemical kick rockets for orbit circularization, without the need for a laser relay mirror in LEO.

3.1.2.16 Technical Challenges

- Can pulsed laser scramjets generate positive thrust in the Mach 6 to 10 range?
- AFRL’s concept has a larger internal nose volume and external surface area, indicating the potential for higher structural mass fractions and heat transfer loads in the hypersonic regime.
- Can the AFRL craft be spin-stabilized, for autonomous beam riding? Will its center of mass, aerodynamic center, and moment of inertia ratios allow stable flight, or will the AFRL vehicle design tumble?
- These technical issues should be investigated in the BEPS follow-on hardware/flight demonstration program for lightcraft technology.

3.1.2.17 Description of Ground Facility

Arguably, one viable technological approach to constructing a 12-MW repped-pulse SSDP laser can be described as follows. Table 3.10 lists specifications for existing SOA, high-power 1- μ m SSDP lasers, a technology that has experienced exponential growth (Figure 3.31) since 1995.

TABLE 3.10.—EXISTING SOLID STATE, DIODE-PUMPED LASERS

Solid State Laser	Manufacturer	Power (kW)	Pulse Energy (joules)	PRF (Hz)	Pulse Duration	Beam Quality (D.L.)	Wallplug Efficiency (%)	Run Time
JHPSSL (ARMY)	Northrup Grumman (NG)	105	N/A	CW	N/A	2-3x	19.2	minutes
HELLADS* (DARPA)	NG & Textron (competition)	150 (goal)	N/A	CW	N/A	>2x? (goal)	> 20%? (goal)	minutes (goal)
SSHCL	LLNL (prototype)	67	335	200	500 μs	2x	~10%?	5-10 s
ThinZag	Textron Systems (prototype)	60	N/A	CW	N/A	2-3x	>10%?	minutes
YLS-10000-SM	IPG Photonics (single-mode)	10	N/A	CW	N/A	< 1.3x	>23%	hours
YLS-50000-MM	IPG Photonics (multimode)	50	N/A	CW	N/A	33x	30%	hours
Mercury HAPL	LLNL (prototype)	1	55-100	10	5-20 ns	2-3x?	~10%?	hours
SILL (for ABL)	NG (classified)	1-4?	0.2-1.0?	5000	5-20 ns?	1.1-1.3x?	10-20%?	minutes

* High Energy Liquid Laser Area Defense System (HELLADS) research program.

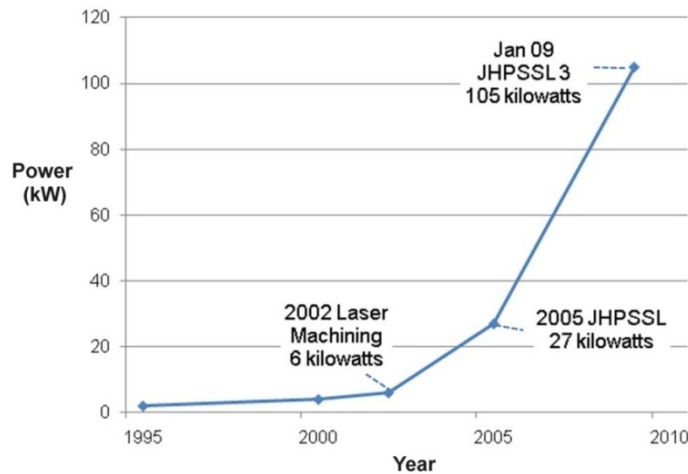


Figure 3.31.—Exponential growth of continuous working SSDP Lasers (Ref. 20).

For example, in January 2009, Northrop Grumman’s seven-chain Joint High Power Solid-State Laser (JHPSSL) CW laser demonstrated 105 kW with a beam quality better than 3 times the diffraction limit (D.L.), and wall-plug efficiency of 19.3%. Adding an eighth chain to JHPSSL would increase its output power to 120 kW (from Ref. 21).

Other strong contenders are Textron’s 60-kW Thin-Zag CW laser, and Lawrence Livermore National Laboratory’s (LLNL’s) 67-kW solid-state heat capacity laser (SSHCL), which is *repetitively pulsed* (335 J pulses at 200 Hz; 500-μs pulse duration)—see Figure 3.32. SSHCL, which has no active cooling system, emits 335 J/pulse at 200 Hz, with a 500-μs pulse duration; diode bar pumping is 900 μs at 872 nm.



Figure 3.32.—LLNL's 67-kW SSHCL (Ref. 23).

LLNL's 1-kW solid-state, diode-pumped Mercury High Average Power Laser (HAPL) (Figure 3.33) puts out 50- to 100-J pulses at 10 Hz, with a selectable duration of 5 to 20 ns. Finally, note that IPG Photonics manufactures extremely reliable, 10- to 50-kW fiber laser welders (Figure 3.34) that run continuously. Their 10-kW single-mode unit (YLS-10000-SM) has an outstanding 1.3 times D.L. beam quality and a wall-plug efficiency exceeding 23%. One must conclude that, yes indeed, high-average power, RP SSDP lasers are already here, but they are generally more expensive than their CW counterparts.

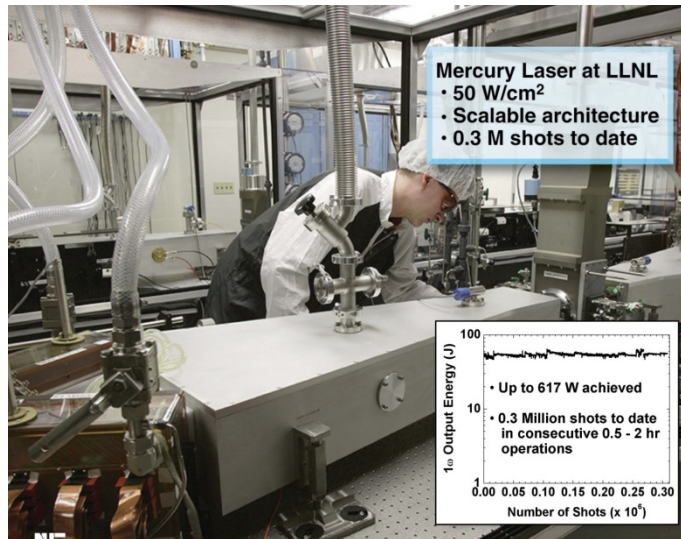


Figure 3.33.—Mercury HAPL at LLNL (50- to 100-J pulses at 10 Hz) (Ref. 25).

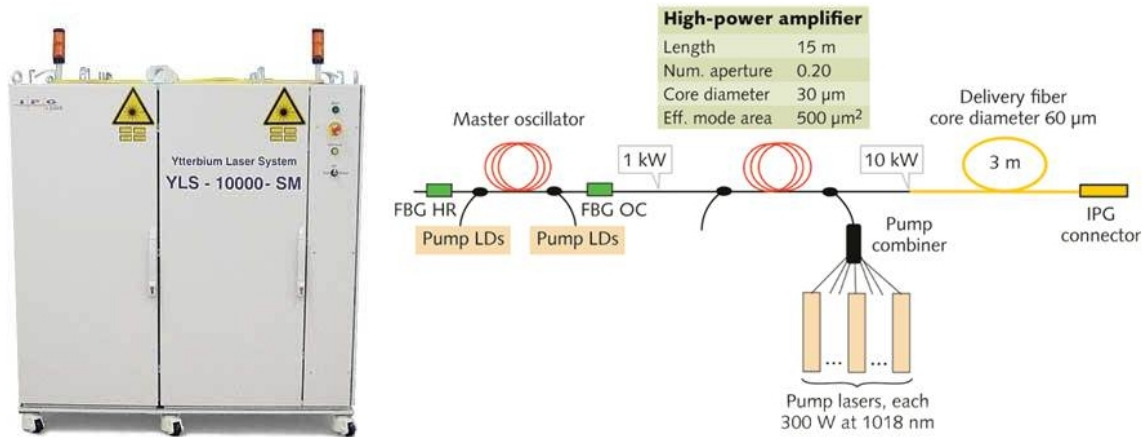


Figure 3.34.—Left: IPG’s 10-kW single-mode fiber laser welder. Right: Master Oscillator Power Amplifier (MOPA) schematic (Ref. 26). Copyright IPG Photonics Corporation (Oxford, MA) 10,000 W Single Mode Laser; used with permission.

Figure 3.35 is a scatter plot of existing SSDP laser specifications relative to the desired 120-kW “beamline” module for our 35-cm lightcraft launcher (i.e., a *short pulse* version of JHPPSL and/or SSHCL technology, e.g., 2 kJ at 60 Hz). Demonstrated short-pulse (50- to 100-ns) technology would be favored to minimize risk, development time, and cost.

Scaling up from the 10- by 10-cm output beam of SSHCL (at 335 J/pulse), our aperture must increase to 25 by 25 cm for emitting 2 kJ pulses. Note that the desired 60-Hz PRF is 6 times higher than HAPL, but only 30% of SSHCL’s 200 Hz. HAPL’s pulse duration of 5 to 20ns is 5 to 10 times too short for our specifications, and SSHCL’s 500-μs pulses are 500 to 1000 times too long. One is tempted to conclude that SSDP laser technology is now sufficiently mature to spawn a 120-kW short-pulse, 2 kJ at 60 Hz, beamline with 10% to 20% wall-plug efficiency, but no government or military agency has asked for it!

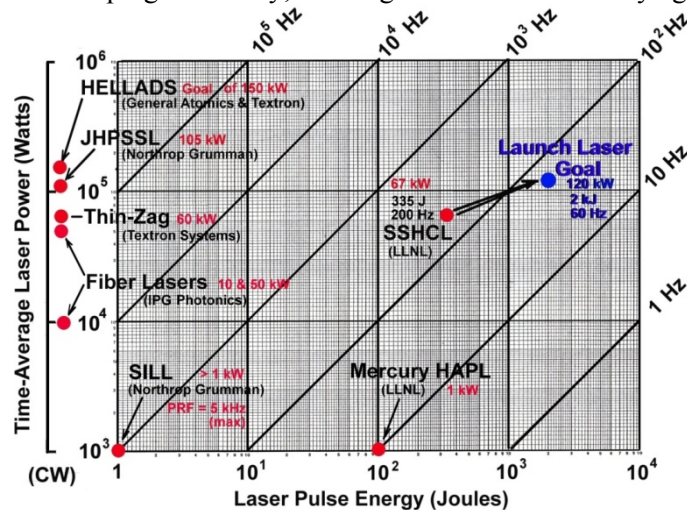


Figure 3.35.—Scatter plot of SSDP laser specifications relative to the desired beamline goal.

The 35-cm lightcraft requires laser PRF’s in the kilohertz range for efficient air-breathing engine performance: for example, 96 beamlines at 60 Hz/each = 5760 Hz, which falls in the viable range. Note that only with pulsed lasers can a “temporal” approach to beam-combining be realized, wherein all beamlines are fired sequentially like a “Gatling” gun onto a rotating mirror that efficiently shepherds pulses into a single 3-m telescope; with 60-Hz beamlines, the mirror must rotate at 3600 rpm.

Figure 3.36 shows an artist concept for a 12-MW repped-pulsed SSDP launch laser system designed to fit within a 60- by 12- by 12-m highbay, a positive-pressure cleanroom facility (Figure 3.37), to prevent contamination of exposed beam-combining and adaptive optics (AO). Although it could take many forms, the artist concept is laid out similar to one-half of the National Ignition Facility (NIF, LLNL, Livermore, CA): that is, 24 beamlines per level, stacked four levels deep.

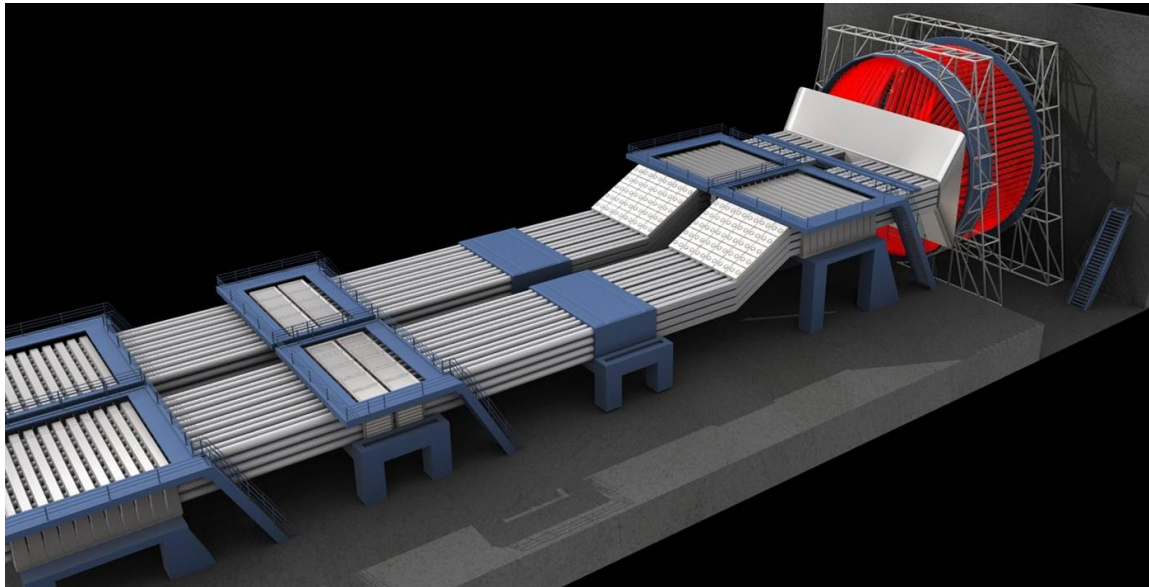


Figure 3.36.—11.5-MW RP SSDP laser system (24 beamlines per level, stacked four levels deep for 96 total) (artist concept by P. Rawlings).

Our launch laser beamline concept could resemble a recent LLNL design proposed for orbit debris removal (see Figure 3.38 from References 3 and 4). That 1- μm ground-based, RP SSDP laser design would have a 25- by 25- cm^2 output aperture emitting 8-kJ pulses of 5-ns duration at 15-Hz PRF for a time-average power of 120 kW.

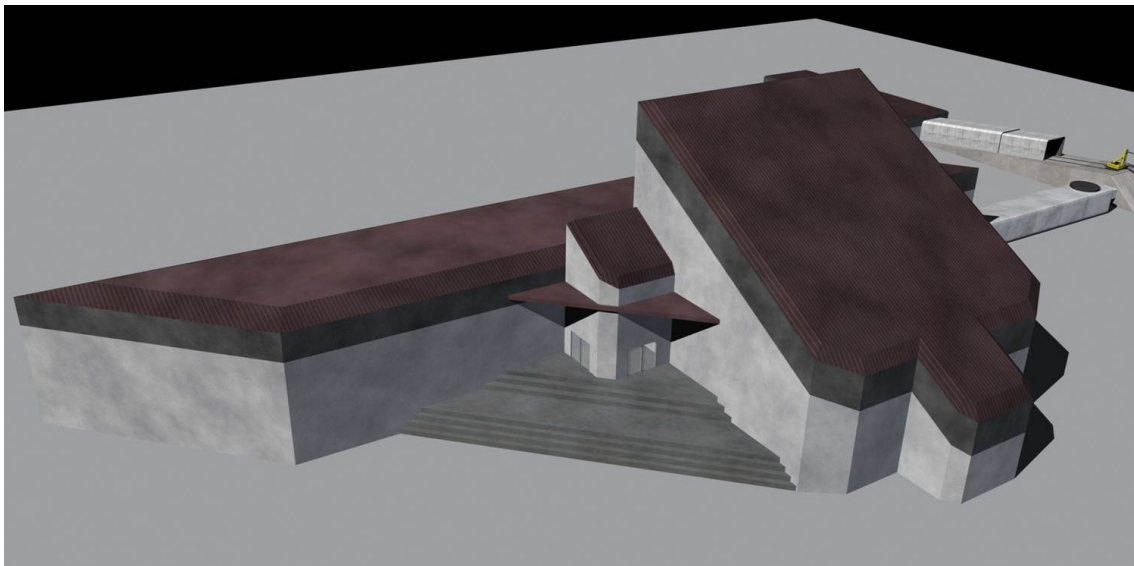


Figure 3.37.—WSMR facility for housing 12-MW launch laser system (artist concept by P. Rawlings).

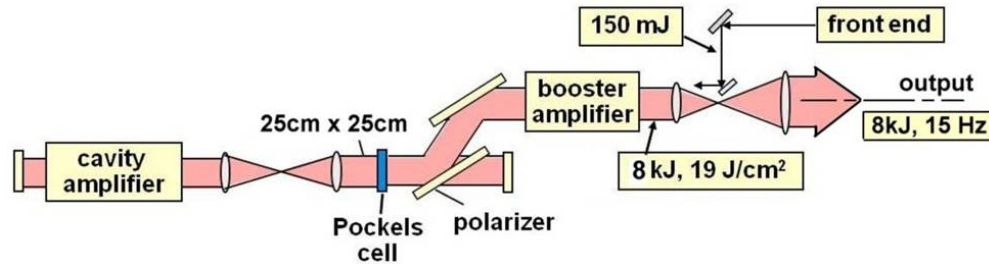


Figure 3.38.—Schematic for single SSDP beamline designed for orbit debris mitigation (Refs. 28 and 29).

Omitting the need for 3ω harmonic conversion parts would result in a simplified and lower cost beamline design. LLNL’s intent was to deorbit a representative ~ 10 -cm debris chunk of aluminum with a weight of 70 g and an orbital altitude of 500 km. If we assume a ~ 1 - μm beam, a range of 800 km, a target area of $\sim 100\text{ cm}^2$, a transmitter diameter of 3 m, a pulse duration of 5 ns, a pulse energy of 6 kJ, and a momentum coupling coefficient (CM) of 6 dynes/W, then about 240 pulses would be required to change the orbit of that debris chunk into an elliptical one with perigee of 100 km (for subsequent atmospheric entry). Therefore, a ΔV of 115 m/s would be needed (Refs. 28 and 29). A 12-MW pulsed laser would take only 0.167 s to accomplish this task. The cost of launch laser facilities for a 12-MW system could approach \$900M (in U.S. dollars, USD) for diode pumping. Fortunately, this nanosat launcher investment could potentially be shared for *dual use* in space debris removal, possibly with international collaboration. A multipurpose laser with a *selectable* pulse duration of 5 ns for orbit debris removal or of 50 to 100 ns for laser LEO launch propulsion, has been judged to be technically feasible. LLNL cost estimates for its RP, solid-state, 1- μm laser range from \$2500/J to \$5000/J (Ref. 29), depending on the choices for laser gain medium, amplifier pump source, and thermal management method. The latter cost is representative of *diode-pumped systems*, which would be required for high wall-plug efficiency and reliable RP operation.

Our 35-cm lightcraft engine will require a beamline with identical average power of 120 kW to that portrayed in Figure 3.44 but with 4 times smaller pulse energies, 4 times higher PRF, and a much longer pulse duration (e.g., 10 to 20 times longer). Hence, our desired launch laser specifications are

- Output wavelength = ~ 1000 nm (maybe 1053 or 1047 nm)
- Time-average power = $2\text{ kJ} \times 60\text{ Hz} \times 96\text{ beamlines}$ yields 11.52 MW
- PRF = $60 \times 96 = 5760$ Hz with rotating mirror beam combining
- Square output beam = 25 by 25 cm
- Laser output pulse duration = 50 to 100 ns (for good pulsejet engine efficiency)
- Diode pulse length = 900 μs ; pumping wavelength = 808, 872, or 900 nm
- Wall-plug efficiency = 10% or better

Fortunately, several kilowatt-level RP SSDP prototype lasers (with short pulses) are in the hardware stage today, including the SILL (Ref. 24) and Mercury HAPL (Refs. 25 and 29), as mentioned earlier. The intent here is to highlight examples of critical technology that will enable upgrades to $\sim 100+$ kW RP lasers in short order. Take for example, the Mercury HAPL at LLNL, which features the two novel elements in Figure 3.39 and Figure 3.40: (1) pulsed high-power pump diodes (in eight 100-kW, 900-nm arrays) and (2) high-speed He gas cooling of *amplifier slabs* (3 W/cm² average) and *optical switches*.

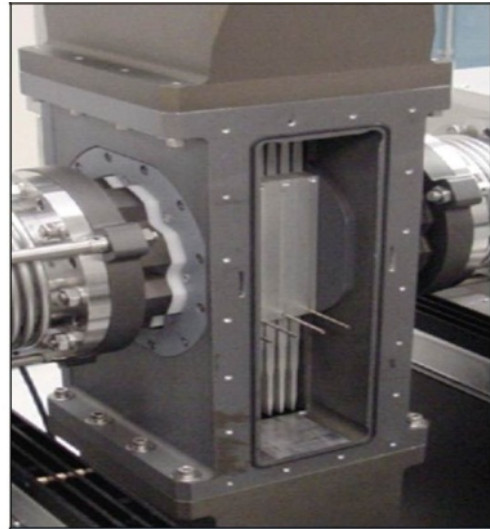
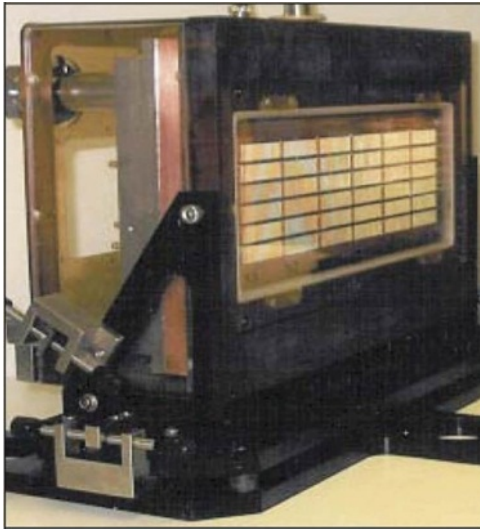
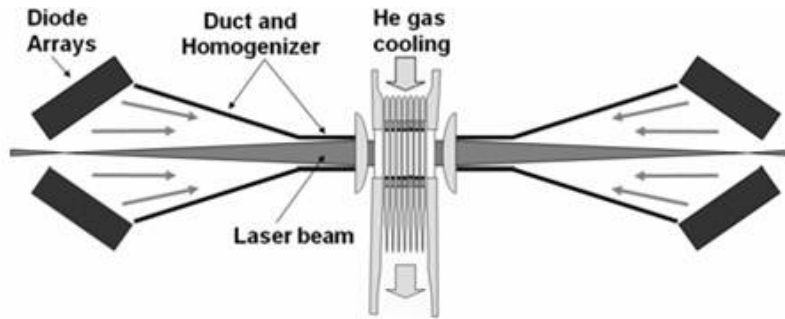


Figure 3.39.—Left: Diode bars. Right: He gas cooling of amplifier slabs in HAPL prototype (Refs. 28 and 29).

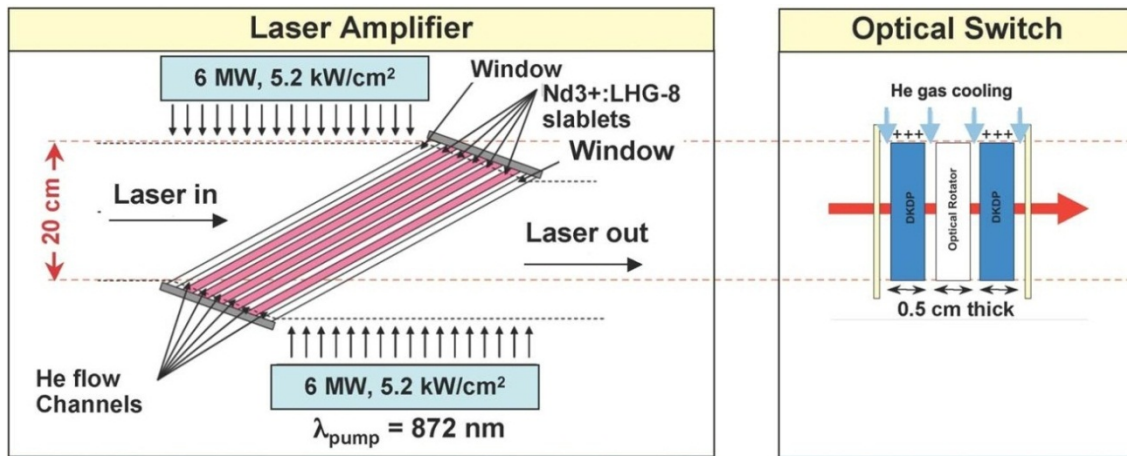


Figure 3.40.—He gas-cooled amplifier slabs and optical switches in HAPL prototype (Ref. 30).

Figure 3.41 shows the Amplifier Line Replaceable Unit (ALRU) concept proposed by LLNL for flowing-gas He cooling of four vertically stacked beamlines (e.g., the laser geometry in Figure 3.36). Another innovation with potential to cut diode pumping costs by more than threefold in the near future is high-power Vertical Cavity Surface-Emitting Laser (VCSEL) diode technology (Figure 3.42). VCSEL has already enabled reliable high-temperature operation for optical pumping, industrial, and medical applications (Ref. 31).

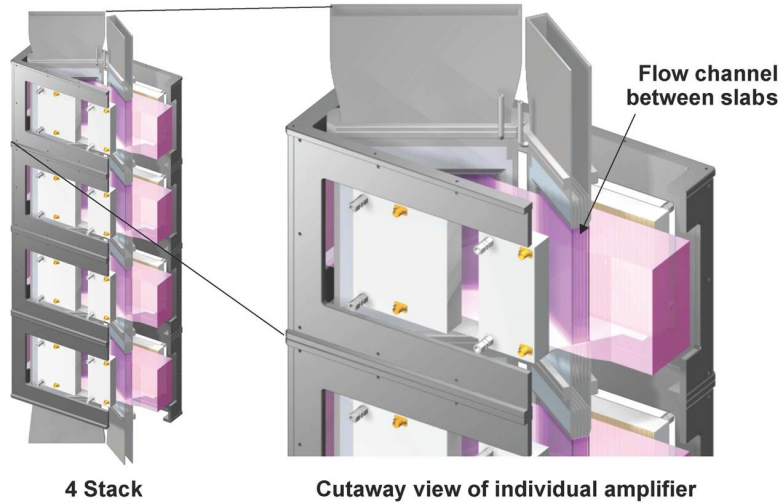


Figure 3.41.—ALRU design for flowing-gas He cooling (Ref. 30).

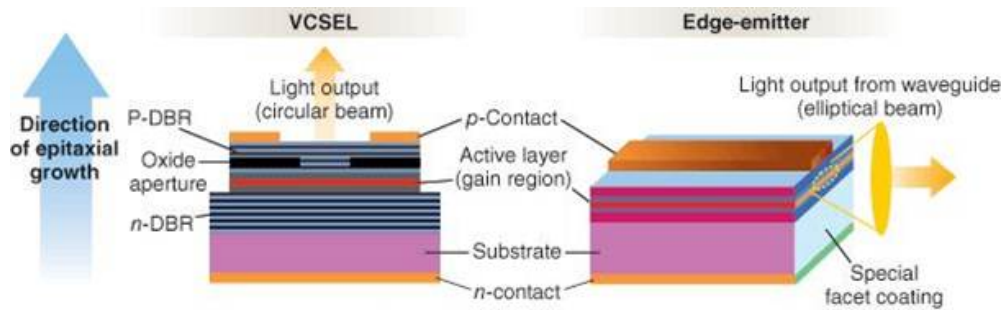


Figure 3.42.—High-power VCSEL diode technology (Ref. 31).

Figure 3.43 is the concept for a 96-element, 850-cm-diameter beam-combining system for the envisioned ~12-MW launch laser. The central mirror would rotate at 3600 rpm. The ring-mirror diameter would be set by the 96 adjacent turning flats positioned around the ring, each sized at 25 by 25 cm. These flat mirrors would be remotely adjusted with servodriven, three-axis mirror mounts to precisely target the on-axis rotating mirror. The 850-cm ring trusswork would be rigidly attached to a vertical 30-cm-thick, steel-bar-reinforced, poured 12- by 12-m concrete wall (see Figure 3.44 and Figure 3.45) that will serve as its optical bench. A similar 60- by 12-m reinforced-concrete optical bench would support and stabilize the 96 beamlines in Figure 3.36. The entire laser highbay will be temperature controlled to reduce thermal-induced movements of optical elements to negligible levels. Note in Figure 3.44 and Figure 3.45 that tip and tilt errors in the 25- by 25-cm “on-axis” output beam are removed by the first pair of turning flats, and the second pair serves as AO to counter atmospheric distortion effects (turbulence, thermal blooming, etc.), before the beam enters the 3-m telescope.

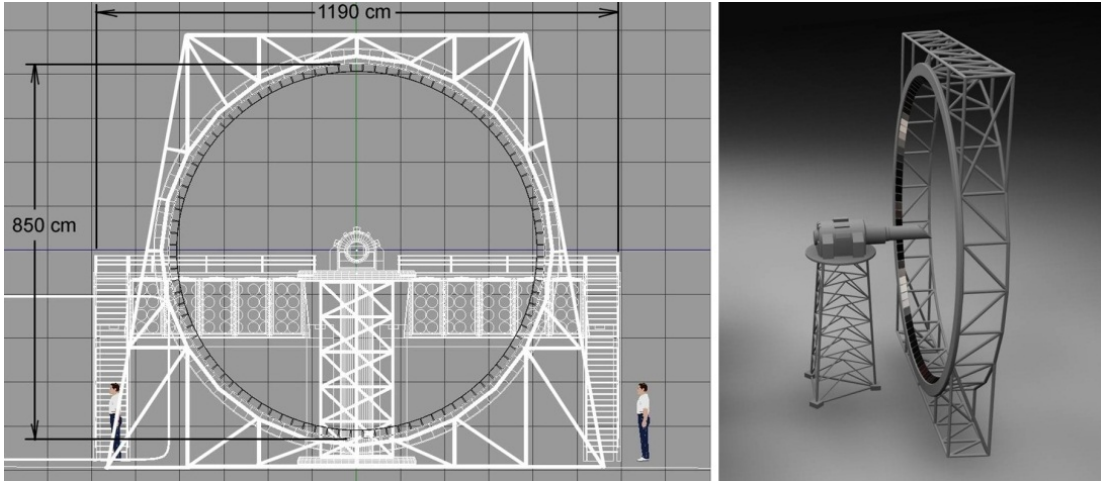


Figure 3.43.—Rotating mirror beam combining system (artist concept by P. Rawlings). Left: Planform view. Right: Oblique view.

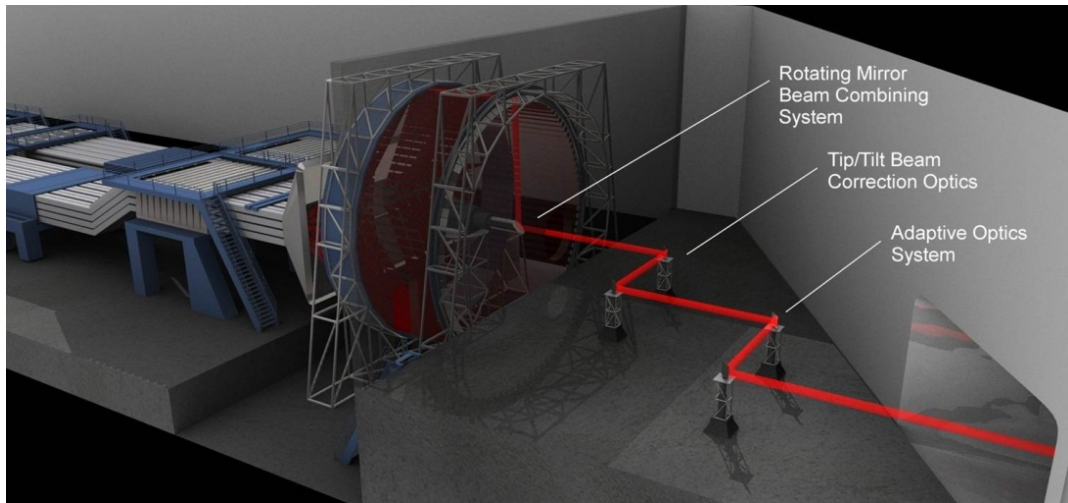


Figure 3.44.—Beam-combining system with central rotating output mirror (center) and tilt-tip correction mirrors and AO (right) (artist concept by P. Rawlings).

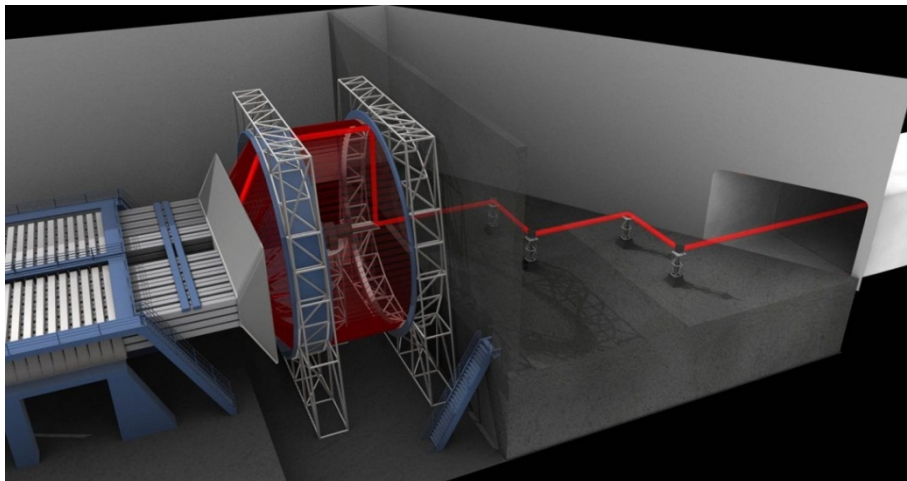


Figure 3.45.—Rotating mirror beam-combiner unit stabilized by vertical 12- by 12-m optical bench/wall (artist concept by P. Rawlings).

Note that in Figure 3.44 and Figure 3.45 the output laser beam will vacate the highbay toward the right, then enter a “light-tight” beam-tube (tunnel) stretching out to the launch pad. This 25- by 25-cm square beam will be able to be delivered selectively onto three different “targets”: (1) a large calorimeter to measure the total output beam power, (2) a 3-m telescope, or (3) a 1-m flat turning mirror, positioned at 45° just below the launch pad to direct the beam vertically onto the lightcraft’s rear parabolic optic.

Handoff of the unexpanded beam from the 1-m flat mirror to the 3-m telescope takes place when the lightcraft reaches an altitude of 1 km or more. Redirection (i.e., “handoff”) of this high power beam will be done by rapidly inserting (i.e., in 1/10 s or less) track-mounted mirror flats, which will be driven by linear actuators like that used in the 150-kW *Laser* Hardened Materials Evaluation Laboratory (*LHMEL*) II CO₂ laser at Wright Patterson Air Force Base, Ohio.

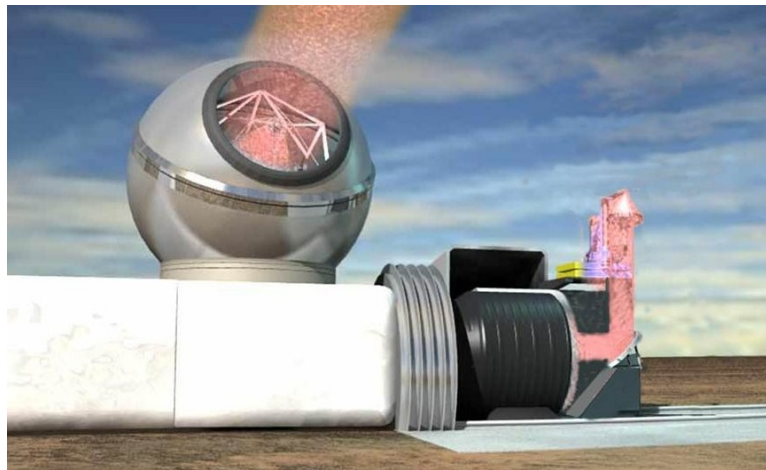


Figure 3.46.—Beam delivery tube (left), 3-m telescope (center), and retractable launch rig with 1-m 45° turning flat (right) (artist concept by P. Rawlings).

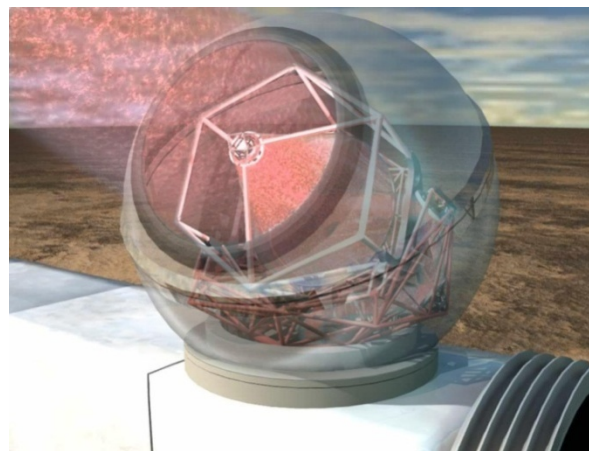


Figure 3.47—Semi-transparent view of 3-m telescope and dome (artist concept by P. Rawlings).

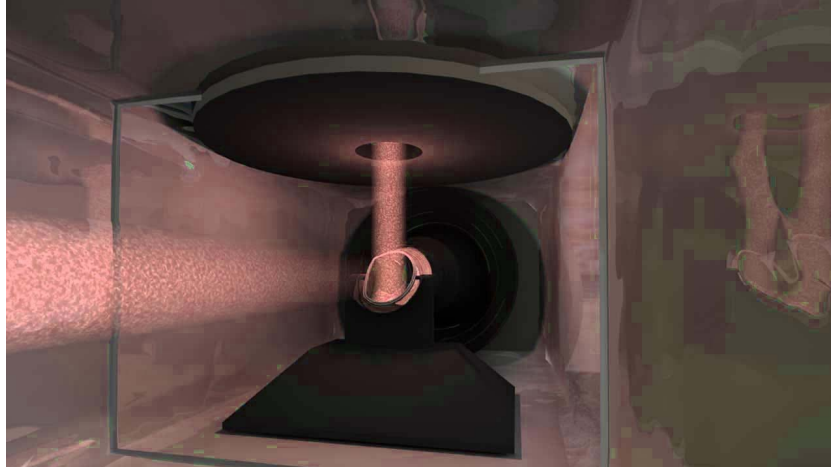


Figure 3.48.—View inside beam delivery tunnel, showing retractable 45° flat mirror that diverts the unexpanded 25- by 25-cm laser beam vertically upward into a 3-m-diameter telescope (artist concept by P. Rawlings).

3.1.2.18 CONOPS—Frequency of Launch and Repeat Time

This section provides (1) the *CONOPS Description* for both 120- and 35-cm lightcraft (with mission timelines), employing a LEO laser relay satellite or onboard chemical kick rocket options, respectively, and (2) the *Mission Description* resulting from the OTIS Trajectory Simulation, probably necessitating a laser relay satellite for the orbit circularization burn. The fully-mature commercial laser launch site will be built at an altitude ≥ 3 km (mountain top) to minimize atmospheric attenuation, although the prototype infrastructure is likely to be first deployed on the High Energy Laser Systems Test Facility (HELSTF) at WSMR. This laser launch facility will include the following

- Vehicle Assembly-processing Building (VAB)
 - o Vehicle and payload assembly in Class 1 (ISO3) clean room environment (see Table 11)
 - o Vehicle balancing (static and dynamic) and mass properties determination
 - o Cleaning before placement on launcher, active queue rack, or installation in storage container
 - o Robotic placement of vehicle on launch stabilization system
- Vehicle transport out to the launch pad
- Launcher pad functions
 - o Umbilical cord for ground power
 - o Propellant (water) loading
 - o Both terminated before vehicle spin-up
- Laser launch systems
 - o Laser facility building
 - o Electrical power supply including energy storage system (flywheels, SMES, etc.)
 - o Telescope/transmitter with AO

TABLE 3.11.—ISO 14644-1 CLEANROOM STANDARDS;
(CLASS 1 IS PROPOSED FOR THE VAB)

Class	Maximum Particles/m ³						FED STD 209E equivalent
	≥0.1 μm	≥0.2 μm	≥0.3 μm	≥0.5 μm	≥1 μm	≥5 μm	
ISO 1	10	2					
ISO 2	100	24	10	4			
ISO 3	1,000	237	102	35	8		Class 1
ISO 4	10,000	2,370	1,020	352	83		Class 10
ISO 5	100,000	23,700	10,200	3,520	832	29	Class 100
ISO 6	1,000,000	237,000	102,000	35,200	8,320	293	Class 1000
ISO 7				352,000	83,200	2,930	Class 10,000
ISO 8				3,520,000	832,000	29,300	Class 100,000
ISO 9				35,200,000	8,320,000	293,000	Room air

The Launch Commit criteria will include

- Surface winds survey
- Winds aloft survey
- Clear skies over launch site and downrange trajectory
- Launch clearance (LEO spacecraft)—from *Laser Beam Clearing House*.
- Local air traffic clearance

Figure 3.49 shows an aerial perspective of the VAB with its track-mounted launch pad; the 3-m telescope and dome (Figure 3.46 and Figure 3.47) are omitted for clarity. This mobile, rail-guided launch rig will transport the lightcraft out from the protective shed, through a dust curtain (to mitigate dust infiltration), and to the launch point. The VAB three-view drawing (Figure 3.50) highlights the use of robotic handling of lightcraft (see Figure 3.51) to facilitate (1) autonomous retrieval of the correct vehicle from the warehouse, (2) spin balancing (Figure 3.52) and measurement of three-axis moments of inertia (I_{XX} , I_{YY} , I_{ZZ})—e.g., POI-1000 from Space Electronics, LLC (Ref. 32), and I_{ZZ} , and (3) loading the vehicle onto the mobile launcher (Figure 3.53).

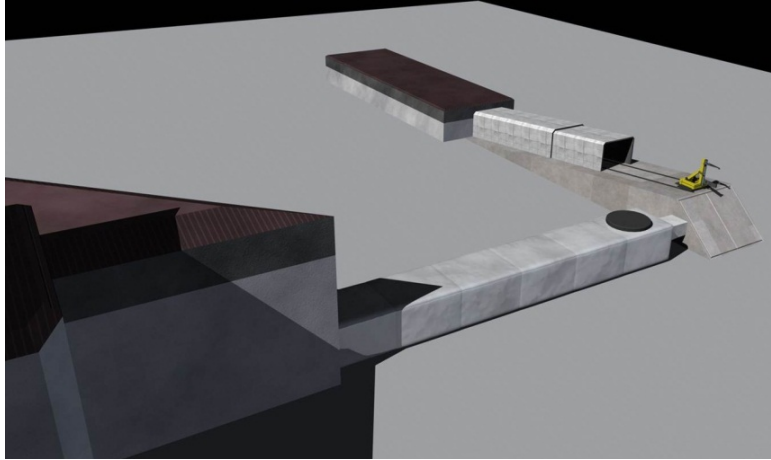


Figure 3.49.—Aerial view of laser highbay (left), beam tube (center), and VAB with launch pad (right) (artist concept by P. Rawlings).

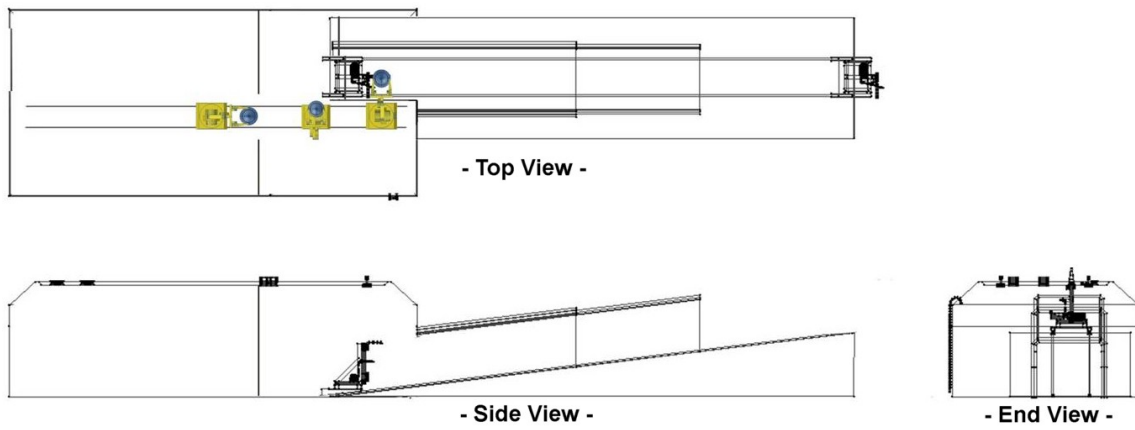


Figure 3.50.—Layout of VAB (artist concept by P. Rawlings).

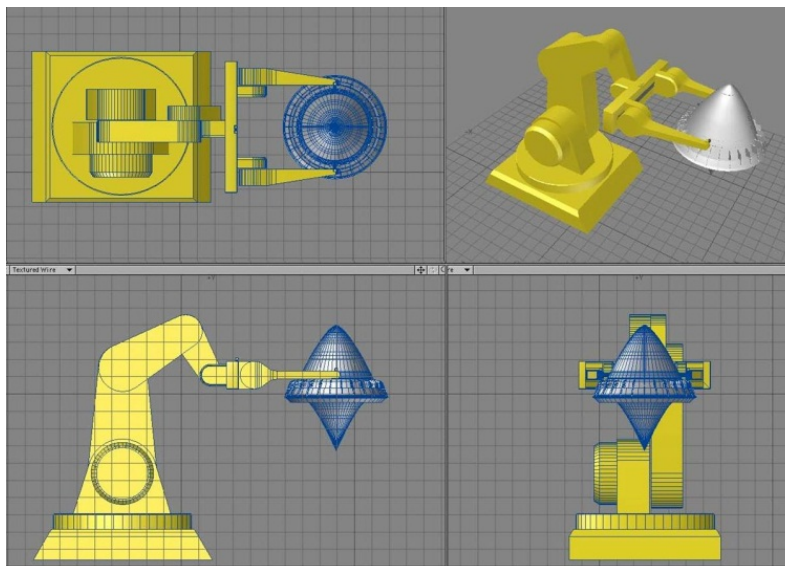


Figure 3.51.—Robotic handling of 120-cm lightcraft (318-kg wet mass) (artist concept by P. Rawlings).

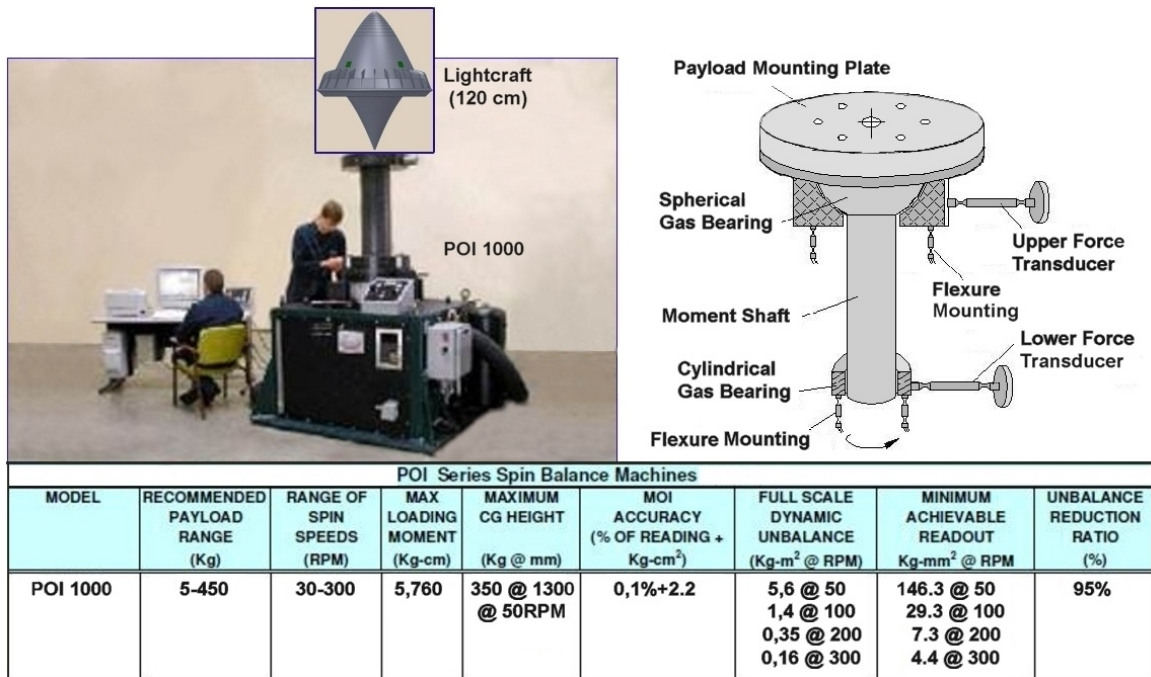


Figure 3.52.—POI-1000 spin balance machine (courtesy of Space Electronics, LLC; used with permission), with scale 120-cm lightcraft (Ref. 32).

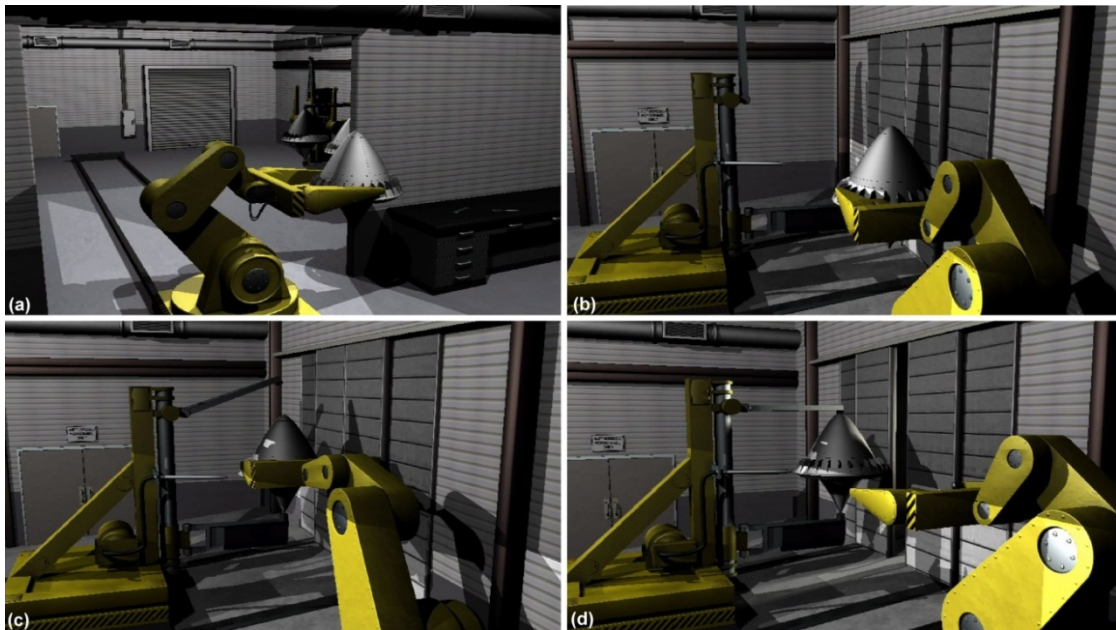


Figure 3.53.—Robot loads 120-cm lightcraft onto mobile launcher rig inside VAB (artist concept by P. Rawlings).

Accurate spin-balancing and measurement of vehicle inertial properties is essential. Such data will be required input for the flight simulation and control software that will ultimately dictate the launch trajectory and vehicle dynamics. With its all-up wet mass of 318 kg, *robotic handling* of the 120-cm lightcraft will be essential, but at 8 kg, the nearer-term 35-cm vehicle will be clearly light enough for

manual processing. (Dust covers on the 3-m beam expander and 45° turning flat below the launcher will be retracted just prior to beam delivery and liftoff.)

3.1.2.18.1 Processing and Launch

Launch minus 10 days (or perhaps only 1 day)

- The vehicle, including payload is assembled in a clean room.
- The vehicle is placed on a spin balance machine and undergoes static and dynamic spin balancing, and mass properties (center of mass (C.M.), moments, and cross products of inertia) are determined.
- Any guidance updates to the vehicle's flight computer are done.
- Vehicle is fueled with water propellant inside the VAB, cleaned, and robotically placed on the mobile launcher for roll-out to the launch pad.
 - The mobile launcher supports the lightcraft from a fixed lower stabilizing bar (bearing mates to rear optic tip) during transport to the pad.
 - The upper stabilizer arm, which is retractable, secures the lightcraft nose with another bearing (see Figure 3.54d and Figure 3.55a).

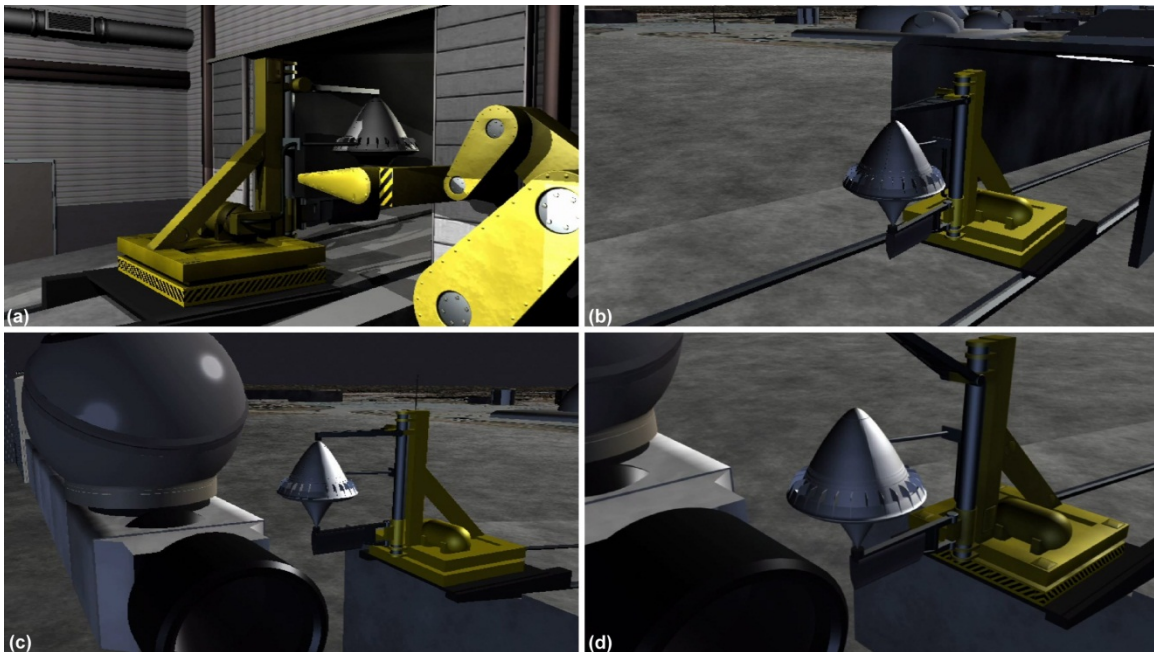


Figure 3.54.—Mobile launcher transports 120-cm lightcraft out to launch pad at end of track (artist concept by P. Rawlings).

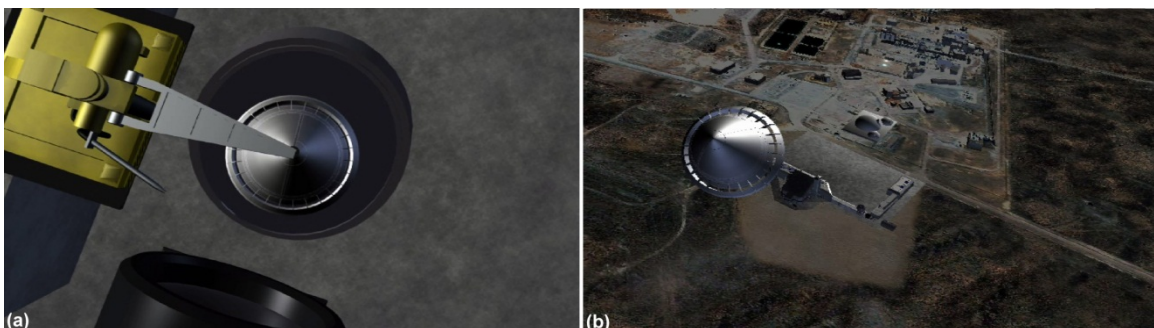


Figure 3.55.—Aerial views (artist concept by P. Rawlings). (a) Lightcraft on launch pad. (b) Under laser boost.

Launch minus 2 hr (or as little as ½ hr)

- The vehicle on its mobile launcher is rolled out to the launch pad.
- The upper balance arm has a spin bearing, ground power umbilical, and water fueling line. The power umbilical and fueling line are automatically mated when the spin cap is placed on the vehicle nose.
- After vehicle spin-up using compressed air jets impinging on the lightcraft rim, the upper stabilizer bar is lifted (Figure 3.54d), the laser is fired, and the vehicle lifts off.
- Once the vehicle clears the launcher ($T = \sim 1$ s), the launcher is retracted out of the beam so that the lower stabilizer is no longer illuminated (i.e., robbing power).

Figure 62 is an artist concept drawing of a lightcraft launch over the White Sands National Monument, showing a visible H₂O vapor trail and low power red tracking laser beam; the 1- μ m propulsive laser beam would of course not be visible with the naked eye.



Figure 3.56.—Dawn launch of lightcraft at White Sands Missile Range, New Mexico (by L. Myrabo and P. Moloney).

3.1.2.18.2 Mission Timeline

Figure 3.57 describes the *Mission Timeline* following liftoff. The COMPASS simulation assumes liftoff at a 30° flight path angle (FPA), from a 3-km mountain site. But in practice, the vehicle would launch vertically and then immediately pitch over to the desired FPA before climbing beyond 1 km above the pad. During this climbout, the 1-m launch mirror (flat) would simply be rotated from vertical through 60°. At $T = 50$ s (altitude = 18.5 km), the 30° FPA hold will be released and the FPA will begin to decline.

At 80.4 s and 35 km (optimally determined), the combined-cycle engine will switch from air-breathing mode into a laser-heated rocket mode with $I_{sp} = 950$ s using onboard H₂O propellant. At 418 s (altitude = 296 km), the lightcraft will begin an unpowered coast, since it will no longer be visible from the launch laser. Shortly thereafter, the lightcraft's nosecone will split in two halves and separate for use as a yo-yo to despin the vehicle from 120 to 60 rpm. The vehicle will then reorient for the circularization

burn, which will occur at $T = 660$ s (down range = 1330 km) using a 3.5-m laser relay mirror in 400-km circular orbit. The length of the laser-heated rocket burn is estimated to be between 30 and 50 s, and the firing will also despin the vehicle.

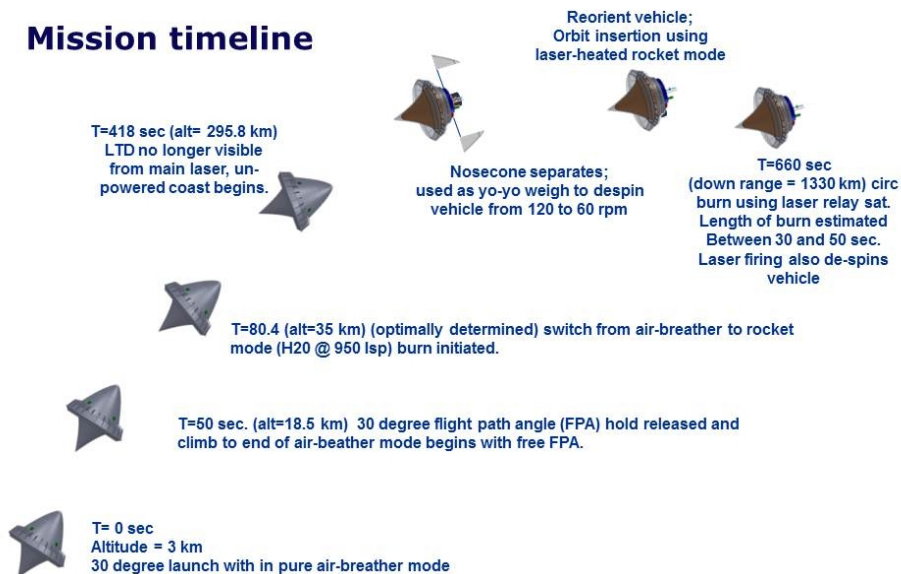


Figure 3.57.—Mission timeline along trajectory for DRM 1–A. LTD, Lightcraft Technology Demonstrator.

Note: the original COMPASS study imagined a second laser—placed downrange—for orbit circularization. However, a “dual-use” elliptical 3.5 by 5-m “Monocle” laser relay mirror in ~400 km orbit might be substantially less costly. A fully “commercial” laser launch system may require at least six such relay stations in LEO; that could also enable orbital debris mitigation.

3.1.2.18.3 On-Orbit Timeline

Figure 3.58 describes the *on-orbit timeline* for a microsatellite deployed in LEO. First, the vehicle is despun using magnetic torquers and then oriented vertically. Next a counter-mass is deployed on a 10-m-long tether to begin the gravity gradient stabilization mode. Finally, the solar photovoltaic arrays are deployed to begin activation and checkout of the payload.

3.1.2.19 Costs—Comments

The total cost of this advanced launch-on-demand system were derived from (1) the ground-based power-beaming infrastructure cost and service life plus (2) the lightcraft vehicle cost and (3) the launch rate. A representative payload cost estimate for 35-cm lightcraft (based on of the amortization/ payback costs, the laser station operating costs, etc.) is provided at the end of this section.

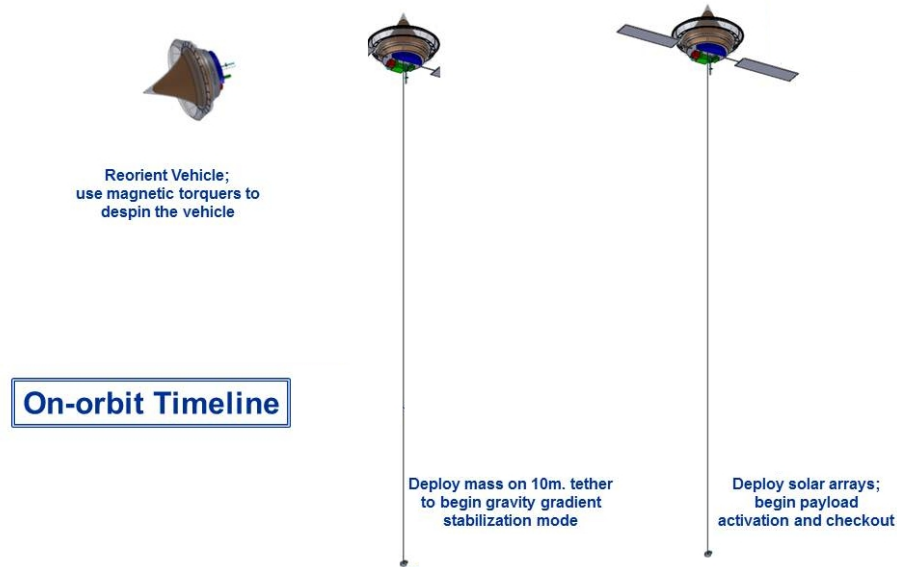


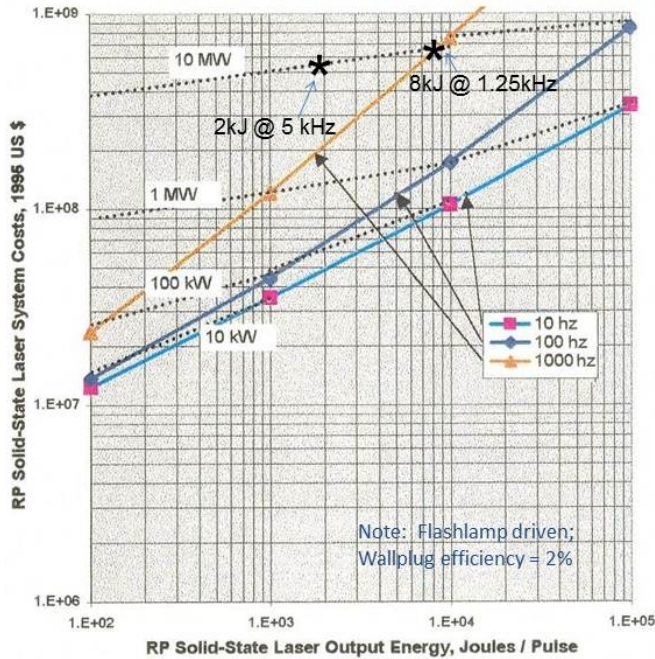
Figure 3.58.—On-orbit timeline gives specifications for DRM 1–A.

3.1.2.19.1 Laser Power-beaming Infrastructure Cost Estimate

At the present state of RP SSDP laser technology, the cost of laser launch infrastructure for nanosat and picosat payloads is the main cost driver—even more so with larger microsat launchers. However, SSDP laser and related photonic technologies are now rapidly evolving in a climate where innovation is predominantly driven by DOD, commercial, and industrial applications (e.g., laser welders, optical pumping, medical usages, etc.), and these markets have had little to do with BEP. The cost of such sources can be leveraged by mass production with attractive learning curves in the long run. Note that, for whatever reasons, CW sources clearly dominate the marketplace today.

The cost-scaling algorithms plotted in Figure 3.59 and Figure 3.61 were generated by J.P. Reilly of Northeast Science & Technology (Ref. 33), specifically for a recent feasibility study on the LTD. Sponsored by the AFRL and NASA (Ref. 2), the LTD Program’s technical objective was to launch a 35-cm lightcraft into LEO using a ~10-MW ground-based laser. Figure 3.59 shows the estimated cost for 0.01-, 0.1-, 1-, and 10-MW RP 1- μ m solid-state lasers as a function of output energy in joules/pulse. Note the asterisks placed at 2 kJ at 5-kHz PRF (launch mission) and 8 kJ at 1.25-kHz PRF (debris-removal mission)—both “point designs” on the 10-MW curve. Reilly’s costing applies to flashlamp-driven Nd-glass lasers with only 2% wallplug efficiency, whereas SSDP lasers demonstrate 10% to 20% today. Hence, for our pulsed SSDP laser system, the reduced cost of 5 to 10 times smaller electric power supplies will be offset by the increased cost of diode-bars (vs. the much cheaper flashlamp pumping technology).

Using the Consumer Price Index (CPI) inflation index to bring Reilly’s 1995 estimates up to 2010, we find the 2 kJ at 5-kHz laser would cost \$787M today, or \$79/W. For our 11.5-MW laser (2 kHz), the price would be \$904M for the 96 beam-lines running at 60 Hz each. Both Figure 3.59 and Figure 3.60 indicate that for a fixed time-average laser output power, cost falls with increasing pulse-repetition frequency (and lower output pulse energies).

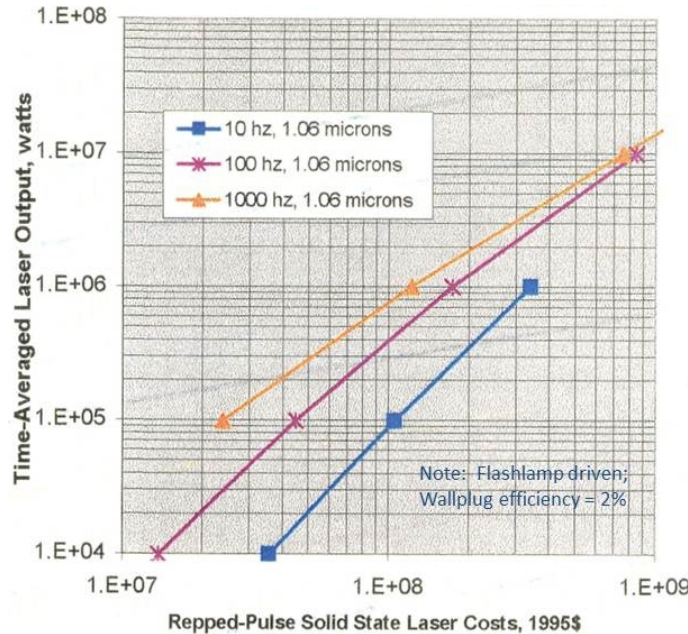


10 MW laser cost est:
 *8kJ @ 1.25kHz = \$650M (1995)
 → \$930M (FY2010) → \$93/watt
 or
 *2kJ @ 5 kHz = \$550M (1995)
 → \$787M (FY2010) → \$79/watt

11.5 MW laser cost est (2010):
 2 kJ @ 5.76 kHz = \$904 M
 [w/ 96 beam-lines; PRF=60 Hz each;
 cost of \$4710./joule, or \$79/watt]

Note: CPI Inflation Index
 1995 to 2010 → 1.43

Figure 3.59.—RP solid-state laser costs versus pulse energy (from Refs. 2 and 33).



For a fixed time-averaged laser output power, costs fall with increasing pulse repetition frequency.

[Wallplug efficiency of solid state diode-pumped (SSDP) pulsed lasers is 10-20%, vs. 2% for flashlamp pumping. So reduced cost of 5-10x smaller electric power supplies will be offset by increased cost of diode-bars over much cheaper flashlamps.

Note: CPI inflation index
 1995 to 2010 → 1.43

Figure 3.60.—RP solid-state laser costs versus PRF (from Ref. 2 and 33).

Table 3.12 summarizes the laser power-station infrastructure for a 35-cm nanosat and 17.5-cm picosat launchers. In the nanosat case, a ballpark cost figure for the 11.5-MW SSDP laser is \$904M in 2010 USD, and a 3-m telescope would add another \$17 to \$30M. Hence, the total infrastructure cost would be \$920M to \$934M. These cost algorithms, originally generated by J.P. Reilly of Northeast Science & Technology, were taken from Reference 2 and the CPI inflation index was used to adjust for 2010 USD to account for intervening years. Note that the laser price point for the 11.5-MW system comes to \$4710/J—nearly identical to LLNL’s \$5000/J estimate for RP SSDP lasers (Ref. 29).

TABLE 3.12.—SSDP LASER LAUNCH SYSTEM SPECIFICATIONS AND COST

Parameter	Nanosat launcher	Picosat launcher
Lightcraft diameter, m	0.35	0.175
Launch mass—wet, kg	8.0	1.0
Payload mass, kg	1.33	0.125
Laser power, MW	11.5	1.0
Laser wavelength, μm	~ 1.06	~ 1.06
Pulse energy, kJ	2.0	0.33
Repetition frequency, kHz	5.76	3.5
Telescope diameter, m	3	6
Telescope cost, ^a \$M	17 to 30	40 to 70
Laser cost, ^a \$M	904	110
Infrastructure cost, ^a \$M	921 to 934	150 to 180

^a2010 USD, based on cost algorithms from Reference 2.

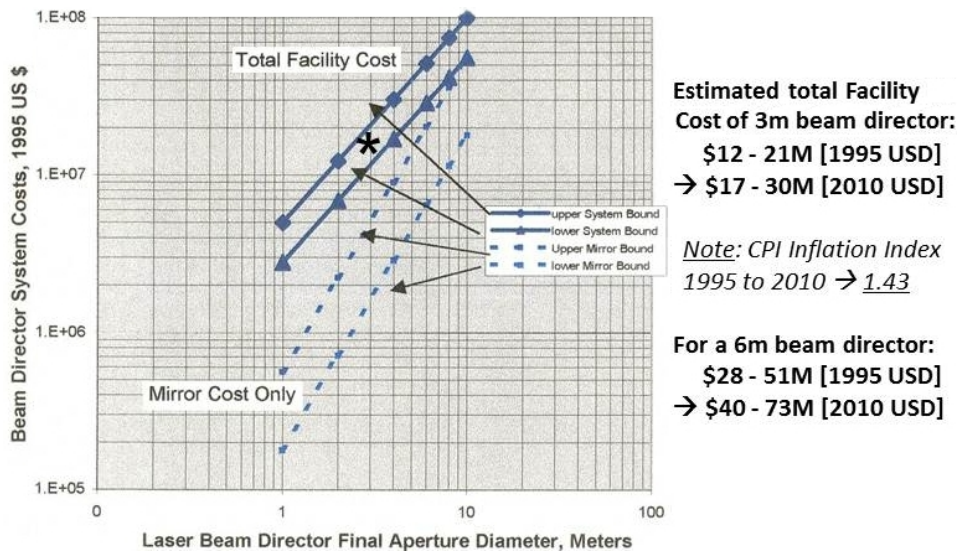


Figure 3.61.—Laser beam director cost versus aperture diameter (from Refs. 2 and 33).

Since lightcraft and plasma engine technology is eminently scalable, even a picosat-class (i.e., 100 to 1000 g) launcher could be viable. Imagine a 17.5-cm-diameter lightcraft with wet launch mass of 1 kg, designed for boosting 125 g of electronics payload to LEO. (Note that a 16.1-cm aluminum lightcraft model was flown on the 10-kW PLVTS pulsed CO₂ laser at WSMR on Feb. 6, 1998, in the air-breathing pulsejet mode with 54.4-g launch mass.) This mission would likely require a ~1-MW pulsed SSDP laser (e.g., 330 J/pulse at 3.5 kHz; ~\$110 M cost) with a 6-m telescope (about \$40M to \$73M in Figure 3.61)—for a total infrastructure investment of \$150 to \$180 M. Incidentally, this is roughly the size of NASA’s 6.5-m Next Generation Telescope (NGT), which will comprise 18 hexagonal-shaped mirror subassemblies.

But what cost reductions can we anticipate in the next 3 to 5 years of high-power laser development? J.T. Kare (Ref. 34) suggests that the lower efficiency and more difficult cooling of pulsed slab lasers versus fiber lasers probably puts the cost of a high-power RP system at 3 to 5 times the cost per watt of a CW system. Presently, the 10- to 50-kW single-mode and multimode fiber lasers from IPG Photonics run \$135/W and \$50/W to \$70/W, respectively. However, multimode fiber lasers could fall to \$35/W in 1-MW quantities within 3 years and could fall as low as \$20/W with 10- to 100-MW production rates within 5 years. (Note that the present kilowatt-level commercial fiber-laser systems include the power

supply, cooling, delivery fiber, control system, and packaging, and are actually overdesigned in terms of operating life—i.e., multiyear operation, 24/7.)

Furthermore, if LLNL’s suggestion in Reference 30 that high-power VCSEL arrays (Ref. 31) will become available for about one-third of the cost of edge-emitting laser diode arrays proves to be correct, then CW SSDP lasers could drop to \$10/W for systems of 100 MW or more, and pulsed SSDP lasers might become as low as \$35/W for systems of 10 MW or more. This would halve the price of our 11.5-MW laser for 35-cm nanosats to ~\$400M—and maybe cut a 1-MW picosat laser cost to just \$35M.

3.1.2.19.2 Lightcraft Vehicle Cost Estimate

Figure 3.62 gives the COMPASS team’s production cost estimates for 35-cm lightcraft (DRM 1–A) generated by two different routines that were applied to confirm differences between the curve sets. The differences reveal an opportunity (with learning curves) to reduce per unit cost by going from NASA (N) government to commercial (C) requirements and production methods.

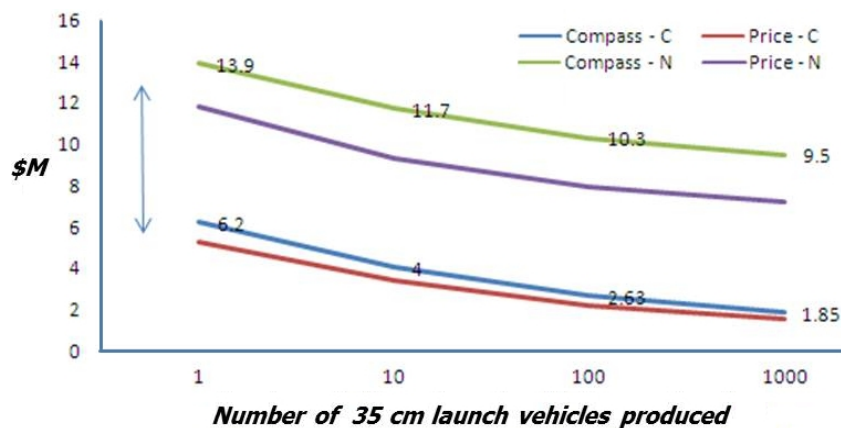


Figure 3.62.—NASA (N) versus commercial (C) production costs for 35-cm lightcraft.

However, this first-order lightcraft vehicle cost analysis (Figure 3.59) faces several unresolved issues that, taken altogether, may present an erroneous picture in the near term. One critical issue relates to the type of costing models presently in use by NASA, the Aerospace Corp, and others, which have been shown, repeatedly, to break down in the lower mass regime. These vehicle cost models perform well for systems of around 1000 kg and up. However, especially below 500 kg and critically below 200 kg, they break down completely and tend to show much higher than actual costs in comparison to space systems already deployed and in use. Such broad parametric models were applied for cost analyses of DRM 1–A and DRM 1–A’ vehicles by the COMPASS team—talented aerospace engineers who are not necessarily microsatellite and launcher specialists.

The *lifetime issues* present another problem. Although an ORBCOMM mission would have a multiyear lifetime, the launcher components would not. Similarly, the 30th unit would not have a full set of ground spares (e.g., no launch operator would build 60 launch systems when 30 will actually be launched). Operationally, there would be some optimum ratio of launches to spares when the five- to seven-launch milestone has past.

In addition, the COMPASS *learning curve analysis* may not have been on a level playing field. From the first unit to the 30th, the analysis assumed a 75% reduction in costs for conventional ORBCOMM satellites and only a 66.67% reduction in costs for the BEPS vehicle. This alone biases the outcome because a similar 75% reduction in costs would put BEPS several million dollars lower than the traditional ORBCOMM.

Furthermore, a meticulous *systems engineering approach* must be taken, rather than just a subsystem-by-subsystem “piece-meal” approach, with an eye toward small payload and microsatellite engineering practice in order to properly assess the costs. For example, by combining electronics enclosures into

larger boxes rather than subsystem by subsystem, a significant reduction in mass budget could be obtained, which in turn, would reduce overall costs.

These and other considerations must be taken into account to secure a true assessment of BEP launcher costs. To resolve this conundrum, analysts should solicit input from those engineers and designers presently working on microsatellite and launch systems (i.e., in major microsatellite companies). We can now build upon what the COMPASS team has started by enlisting help from personnel who already know this satellite and launch system design regime very well. Economic viability of revolutionary lightcraft launchers is *the* critical issue here, and to move forward without properly assessing vehicle costs seems ill advised.

3.1.2.19.3 AFRL’s Life Cycle Cost (LCC) Study for 35-cm Lightcraft Launcher

Table 12 from Reference 19 reveals some details on the AFRL *Life Cycle Cost (LCC) Summary* for a 35-cm lightcraft capable of delivering 2 kg of payload to 185-km circular orbit, using the 10-MW class SSDP ground-based laser.

Judging from the \$635M acquisition cost listed for the 10-MW laser, the table likely represents FY2000 USD since the laser would be \$550M (Figure 3.58) in FY1995 USD, and the CPI from 1995 to 2000 was ~ 1.13. Note that the 3-m telescope cost (\$12M to \$21M in 1995 USD) was not broken out separately under *DDT&E/Acquisition Costs*.

AFRL’s lightcraft launcher LCC model specifies a mission length of 10 years, with a laser service life equaling this term. The “*Average Cost per Flight*” listed in Table 3.13 (\$74,141), then, absorbs the aggregate of *DDT&E/Acquisition Costs* and *Operations Costs* over that period (i.e., \$743 M) into 10,000 launches, which might turn out to be conservative; a launch rate of 1000 per year represents only 20 per week or 3 per day, on average. Also stated in Reference 19: “*Laser acquisition and operation costs were assumed to be shared with another user, and all operations costs are reduced to ½ of those values estimated from historical data.*”

The AFRL study apparently assumes a single production run of 10,000 vehicles at the stated price of \$3760 per unit. For a vehicle burnout mass of 3.52 kg, this comes to just \$1062/kg which seems highly optimistic and not likely representative of the specialized 1.33- to 2-kg electronics payloads that must be tailored for each customer’s mission.

TABLE 3.13.—LIFE-CYCLE COST MODEL FOR 35-CM LIGHTCRAFT LAUNCHED WITH 10-MW SOLID-STATE LASER (REF. 19)

Lightcraft model cost summary	Share SSDP laser to cut ops costs by 50%	Percentage
Mission model length (yr)	10	
Launch rate per year	1,000	
Payload per launch (kg)	2.0	
Mission flight time (s)	221.52	
Total program cost (\$M)	741.41	
DDT&E/acquisition costs (\$M)	680.358	91.77
Operations costs (\$M)	61.053	8.23
Average cost per flight (\$)	74,141	
Average cost per kg (based on operations costs) (\$)	3,052	
DDT&E / acquisition costs (\$M)	680.358	
Laser lightcraft (LLC) development cost (\$M)	18.000	2.65
Laser lightcraft (LLC) acquisition (\$M)	37.596	5.53
10-MW ground-based laser acquisition (\$M)	624.762	91.83
Launch site facility costs (construction) (\$M)	5.000	0.73
Operations costs, annual (\$M)	6.105	
Laser annual operations cost (\$M)	3.750	61.42
Laser refurbishment, annual (\$M)	0.750	12.28
Laser consumables, annual (\$M)	-----	-----
Energy cost, annual (\$M)	0.101	1.65

TABLE 3.13.—LIFE-CYCLE COST MODEL FOR 35-CM LIGHTCRAFT
LAUNCHED WITH 10-MW SOLID-STATE LASER (REF. 19)

Lightcraft model cost summary	Share SSDP laser to cut ops costs by 50%	Percentage
Launch site facility cost, annual (\$M)	0.250	4.09
USAF ^a systems program office (SPO) cost, annual (\$M)	0.250	4.09
NORAD ^b coordination cost, annual (\$M)	0.500	8.19
FAA ^c coordination cost, annual (\$M)	0.250	4.09
Range (safety, tracking, telemetry), annual (\$M)	0.255	4.17

^aU.S. Air Force.

^bNorth American Aerospace Defense Command.

^cFederal Aviation Administration.

For the sake of argument, though, let us assume that the basic 35-cm lightcraft vehicle/engine technology is updated yearly in annual production runs of 1000 units at the same costs displayed in Table 3.12 (i.e., spacecraft development cost of \$18M plus acquisition cost of \$37.6M = \$55.6M total). Then, for a 1000-unit production run, each vehicle comes to \$55.6K—which is somewhat more in line with the infrastructure’s “Average Cost per Flight” in Table 12 of \$71K. Note that this is still 33 times less expensive than the COMPASS estimate of \$1.85M each, but the correct/realistic vehicle pricing may fall between them.

3.1.2.20 Launch Trajectory Simulations

3.1.2.20.1 Compass Team’s Simulation Details for 1.2-m LTD (DRM 1–A)

The laser launch geometry for lightcraft trajectory simulations is shown in Figure 3.63; the relay mirror satellite in LEO (e.g., 400-km altitude) is required under some conditions. Compass Team’s DRM 1–A simulation overview:

- (1) Point-mass is assumed for the vehicle
- (2) 3-DOF simulation using OTIS code, with overall objective to maximize payload mass for a minimum gross liftoff mass (GLOM) to a 400-km suborbital target
- (3) Launch from a 3-km altitude mountain-top laser station with a 30° fixed laser pitch angle and 30° vehicle flight path angle for 50 s
- (4) Climb out in air-breather/rocket mode until switch point into laser rocket mode (switch point optimally determined)
- (5) Climb in laser rocket mode to 400-km suborbital target
- (6) Coast until laser-heated circularization burn into final orbit

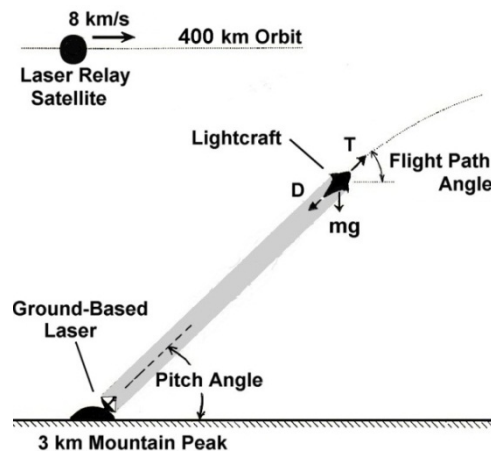


Figure 3.63.—Laser launch geometry for lightcraft trajectory simulations.

Air-breather mode assumptions and simulation details

- Air-breathing engine performance data consists of Mach and altitude table lookup of C_M (N/MW), E_P (J), and PRF (Hz)—from References 16 and 17 (see Figure 3.64 and Figure 3.68). Note in Figure 3.65 that C_M is modeled as a smoothly varying function of both altitude and Mach number. Data for 35-km altitude had to be estimated; unfortunately, the original code burned up in a fire.
- Reference data for a 100-MW-class pulsed laser. Simulation includes a throttle (to reduce thrust when or if necessary) and a scale factor (range 1 to 3.5) to simulate a more powerful laser (with higher PRF) when required.
- In the air-breathing mode, the LTD's pulsed laser-ramjet engine heats surrounding air with an infinite I_{sp} (no on-board mass flow is expended), and thrust is developed by momentum exchange with the atmosphere.
- The vehicle drag model in Figure 3.68 is taken from References 16 and 17 with a reference frontal area of 0.7854 m^2 —representing the 1-m-diameter vehicle forebody, which is modeled as a 30° half angle cone. The annular shroud's frontal area is accounted for within the engine model.

Rocket mode assumption and simulation details

- Thrust is a function of laser power ($PRF \times EP$). Thrust is then found by multiplying $C_M \times PRF \times EP$.
- Laser atmospheric propagation loss was modeled after a formulation in Reference 38 (pp. 82 and 85).
- Reference laser power is 100 MW, scaled as necessary to be consistent in power level with the air-breathing engine model's needs.
- Laser rocket mode “burns” LH20 with an I_{sp} of 950 s.
- Vehicle drag model is taken from References 16 and 17 for a reference frontal area of 0.7854 m^2 (see Figure 3.68).

Note that key 3-DOF (point mass) simplifying assumptions are used for entire trajectory (i.e., optimistic trajectory). More rigor would require additional coordinate system in OTIS and/or full 6-DOF simulation to circumvent the present code's limitations

- No loss term for off-angle laser pointing.
- No steering (restoring forces or moments) from off-centerline beam targeting upon the LTD engine.

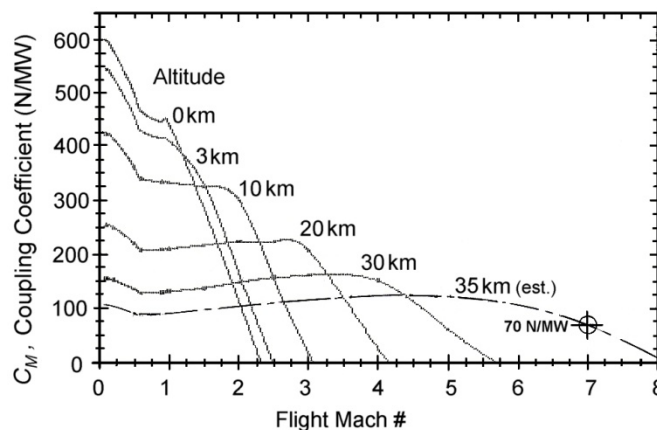


Figure 3.64.—Net C_M versus flight Mach number for LTD air-breathing mode (Refs. 16 and 17). (“Baseline” 3-cm inlet gap, 500-MW/cm^2 at focal ring.)

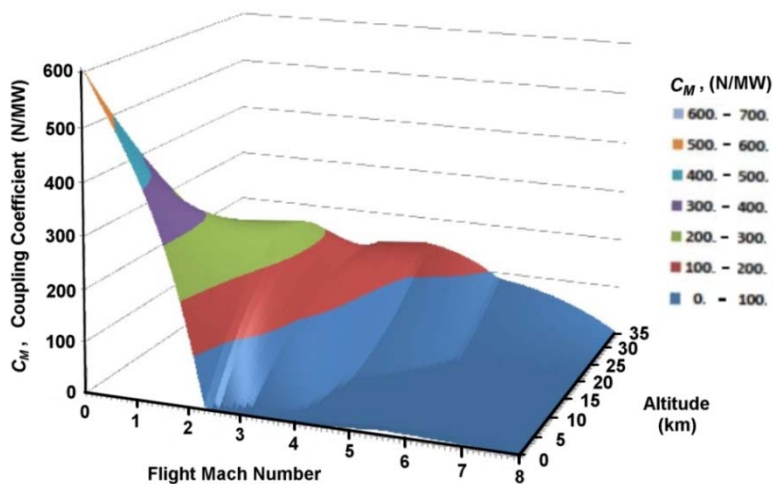


Figure 3.65.—Three-dimensional (3D) plot of C_M versus flight Mach number for LTD air-breathing mode (Refs. 16 and 17). (“Baseline” 3-cm inlet gap, 500-MW/cm² at focal ring.)

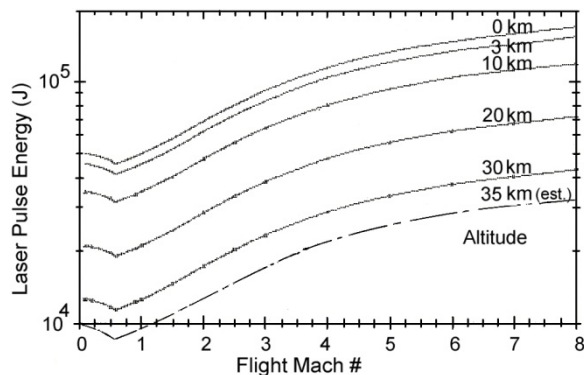


Figure 3.66.— E_P versus flight Mach number for LTD air-breathing engine mode (Refs. 16 and 17). (“Baseline” 3-cm inlet gap, 500-MW/cm² at focal ring.)

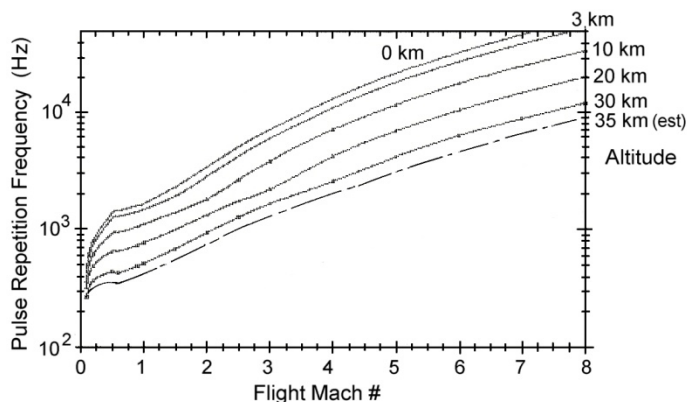


Figure 3.67.— PRF versus flight Mach number for LTD air-breathing engine mode (Refs. 16 and 17). (“Baseline” 3-cm inlet gap, 500-MW/cm² at focal ring.)

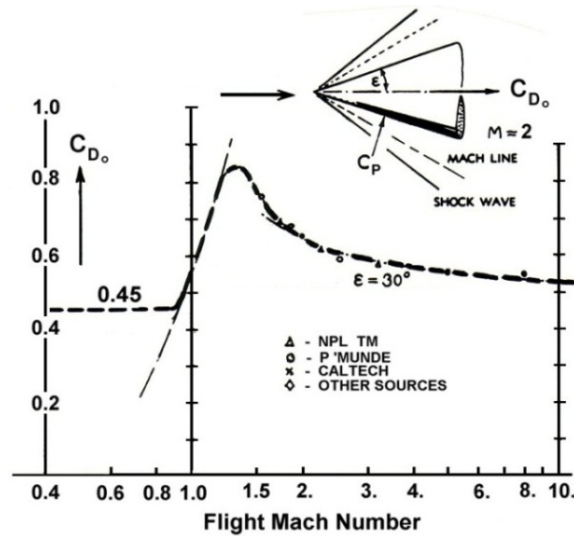


Figure 3.68.—Aerodynamic drag model for LTD vehicle (Refs. 16 and 17).

OTIS results summary (see Figure 3.69 to Figure 3.71, and Table 3.14 to Table 3.15)

- The OTIS optimal trajectory for a specified flight profile to a 400-km suborbital target with final velocity of 5.5 km/s is shown in Figure 3.69 to Figure 3.71.
- The closed-form rocket-mode calculation to circularize LTD orbit using a relay mirror satellite (or second laser source) is in the results summary in Table 3.14 and Table 3.15.
- Key trajectory parameters and timing of events are summarized in the CONOPS section.
- Future work should include
 - o An investigation of different trajectories for optimality. The work should also include the implementation of a full air-breathing propulsion model: at minimum, a complete propulsion table, but preferably direct formulations of propulsion performance as a function of altitude, Mach number, and required/received laser power.
 - o A full assessment of the relay mirror satellite (or second laser station) and location of the LTD vehicle pointing, should full inclusion of an air-breathing propulsion model fail to eliminate the necessity of performing the rocket-mode circularization burn with the laser (i.e., to capitalize on the high I_{sp} associated with laser-heated LH_2O propellant).
 - o Secondary effects of off-centerline angle thrust terms and aim-pointing steering (i.e., a more complete beam-riding engine model). These effects would require the addition of a coordinate system into OTIS or a full 6-DOF representation of the vehicle (outside the scope of the COMPASS/OTIS study).

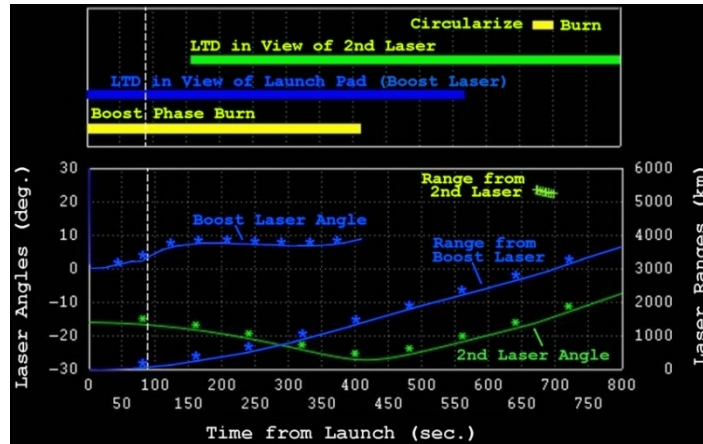


Figure 3.69.—Burn phases, ranges, and angles from the Satellite Orbit Analysis Program (SOAP) simulation for 1.2-m LTD (DRM 1–A).

Requirements for insertion into circular 400-km orbit:

- OTIS trajectory ends in elliptical orbit; the following are the requirements necessary to circularize from the OTIS end point (see Table 3.14 and Table 3.15)
 - o Required ΔV to circularize: 1772 m/s
 - o Too far downrange (~1335 km) from laser/launch site to use launch laser directly
- Options to circularize
 - o Onboard chemical “kick” rocket gives insufficient performance to achieve orbit unless electronics payload (with smaller rocket) is separated from vehicle
 - o Orbital-based reflector: unknown cost and phasing problems
 - o A second ground-based laser site: high cost, nonoptimal thrust pointing
- To first order, a 400-km relay mirror satellite (Figure 3.63) or second GBL station is needed
 - o Angle from the station’s power beam to the vehicle centerline axis needs to be assessed (Figure 3.69)
 - o For the laser rocket circularization “burn,” the angular offset of the vehicle centerline axis to the laser beam appears to be extreme for the GBL option, and this is probably best accommodated with a 400-km relay satellite.

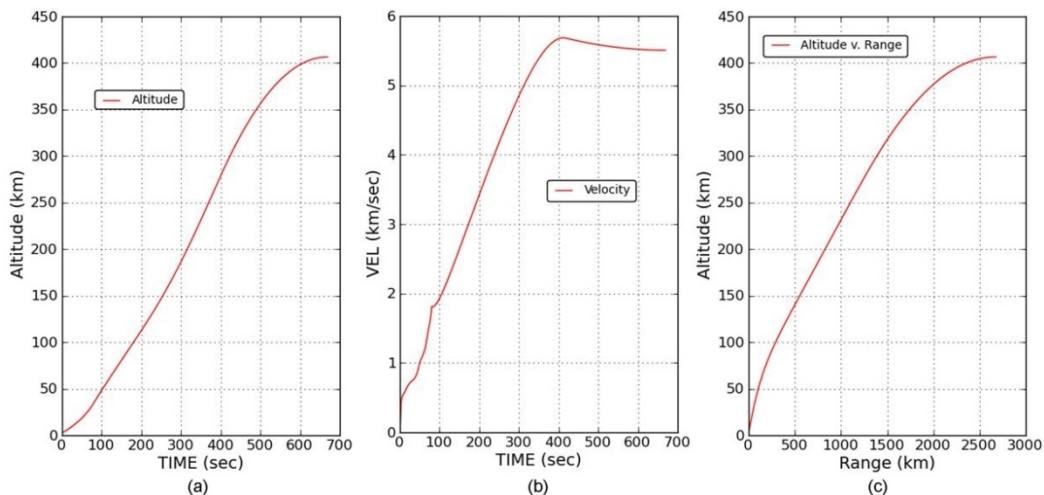


Figure 3.70.—OTIS simulated launch trajectory for 1.2-m LTD (DRM 1–A). (a) Altitude versus time. (b) Velocity versus time. (c) Altitude versus range from launch pad.

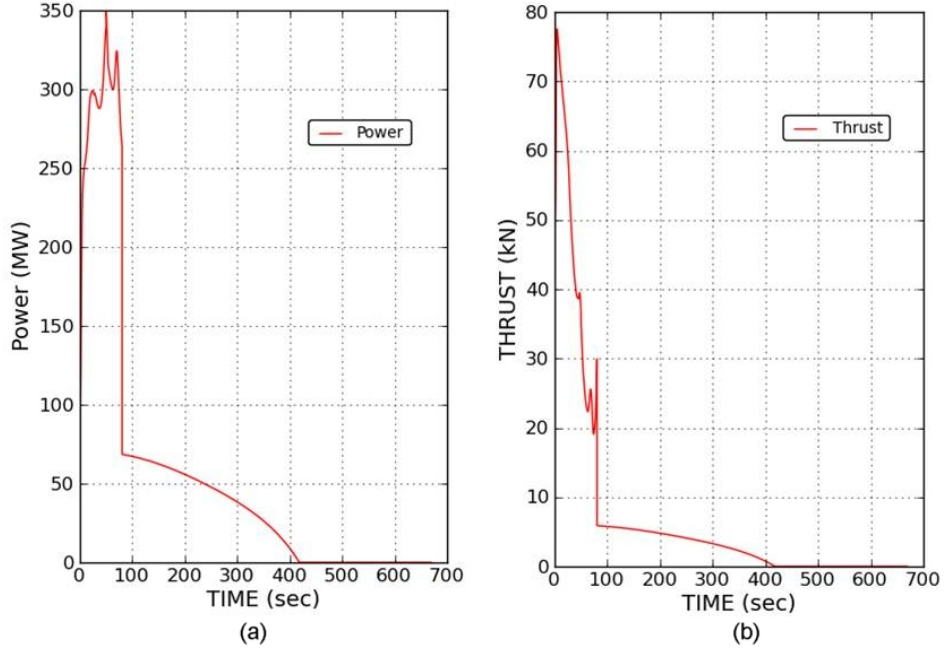


Figure 3.71.—Laser power and engine thrust versus time from OTIS trajectory for 1.2-m LTD (DRM 1–A).

TABLE 3.14.—MISSION ΔV SUMMARY FOR 1.2-M LTD (DRM 1–A) USING OTIS

Mission DeltaV Summary						
Phase Number	Phase Name	DeltaV (m/s)	Isp (s)	Mass Drop (kg)	Propellant History (kg)	
1	Vertical rise	***	***	***	173.1	
2	Pitchover	4947	950	***	34.8	
3	Deploy Nose Cone as Yo-Yo weights and then Jettison	***	***	4.7	34.8	
4	Orient For Insertion Burn	4.1	50	***	33.2	
5	LEO Insertion	1779	950	***	0.0	

TABLE 3.15.—MASS, ΔV , AND PROPELLANT SUMMARY FOR 1.2-M LTD

Variable	Value
Gross lift-off mass (kg)	334.99
Nose cone mass (kg)	4.73
Total propellant (H₂O) consumed (kg)	171.20
Air-breather mode	
Mass at end of air-breather mode (kg)	334.99
Propellant (air) consumed (kg)	N/A
ΔV (m/s)	N/A
Rocket mode (propellant = H₂O)	
Mass at end of rocket mode (pre circ) (kg)	192.20
Mass at end of mode less nose cone (pre circ) (kg)	187.47
Propellant (H ₂ O) consumed (kg)	137.86
ΔV (m/s)	4935.30
Propellant (H ₂ O) to circularize (kg) ^a	33.34
Final estimate mass to circular 400 km orbit (kg) ^a	159.15
ΔV to circularize (m/s) ^a	1771.90

^aIndicates that estimates are from closed form calculations.

3.1.2.20.2 AFRL 3-DOF Simulation Results for 35-cm Lightcraft

The laser launch geometry for AFRL’s 35-cm lightcraft launch simulation (Refs. 5 and 19) is as indicated in Figure 3.63, requiring no LEO relay mirror satellite for orbit circularization. The combined-cycle propulsion system encompasses two air-breathing modes (laser ramjet and laser scramjet) and a laser rocket mode.

OTIS simulation overview.—

- (1) Point-mass assumed for 35-cm vehicles (Figure 3.30) with a GLOM of 8 kg (Table 3.9)
- (2) 3-DOF simulation using the OTIS code, with overall objective to transport 2-kg payload mass into a 185-km circular orbit
- (3) Launch vertically from mountain-top laser power station, then pitch over to 30° fixed laser pitch angle and 30° vehicle flight path angle
- (4) Climb out in laser ramjet mode (air-breather) until the switch point into laser scramjet mode (switch point optimally determined)
- (5) Climb in laser scramjet mode (air-breather) until switch point into laser rocket mode (switch point optimally determined)
- (6) Climb in laser rocket mode to 185-km suborbital target
- (7) Coast until chemical “kick” circularization burn into final orbit

Air-breather mode assumptions and simulation details

- The air-breathing engine performance model used thrust coefficients and delivered I_{sp} (as a function of Mach number and altitude) from an Aerojet Techsystems fixed geometry scramjet.
- Reference data were for a 10-MW-class pulsed laser with optimum wavelengths of 1.06 and 1.62 μm . As with the COMPASS BEPS effort, the simulation likely includes a throttle to reduce thrust when or if necessary or a scale factor to model a more powerful laser when required.
- In air-breathing mode, the laser scramjet engine exploits the surrounding air for an infinite I_{sp} (no onboard mass flow expended), developing thrust by momentum exchange with the atmosphere.
- The 35-cm vehicle drag model is based on vehicle geometries in Figure 3.30. Transonic drag coefficients of 0.2167 and 0.45 are suggested for 10° and 20° conical forebodies (frontal area = 0.096 m^2)—for much higher fineness ratios than the LTD’s 30° half-angle cone with $C_D = 0.85$. Such 2 to 4 times lower drag coefficients were mandatory to extend the air-breathing envelope to the Mach 9 to 10 regime.

Rocket mode assumption and simulation details

- Thrust is a function of available laser power versus range collected by 30-cm-diameter lightcraft rear parabolic optic. Laser rocket performance (C_M, I_{sp}) was defined as a function of laser pulse-width (t_p) and pulse energy (E_p).
- Laser atmospheric propagation losses were modeled with code, include thermal blooming, atmospheric turbulence, and extinction (molecular and particulate absorption and scattering; telescope jitter was not mentioned in Refs. 5 and 19)
- Reference laser power is 10 MW, scaled versus range to account for atmospheric propagation losses.
- Laser rocket mode can “burn” 4 kg of propellant. Apparently I_{sp} varies from 100 s at beginning of firing 1000 s at end.
- Vehicle drag model is likely based on 10° and 20° half-angle cones.

The 3-DOF (point mass) simplifying assumptions are likely applied for the entire trajectory (i.e., optimistic trajectory). The OTIS-based trajectory simulation describes all laser beam and lightcraft kinematics and associated combined-cycle air-breathing/rocket propulsion performance. As with the COMPASS simulations, more precision would require an additional coordinate system in OTIS and/or a full 6-DOF simulation to eliminate the present code's limitations

- No loss term for off-angle laser pointing (i.e., incidence relative to centerline axis of rear optic)
- No steering (restoring forces or moments) from off-centerline beam targeting on the lightcraft engine
- No beam-riding engine/vehicle performance modeling

OTIS results summary

- The OTIS optimal trajectory for the specified flight profile to the 185-km suborbital target uses laser rocket mode burnout at 221 s into the final transfer orbit of 185 by 92.5 km, coast to 185 km, and a final injection burn with a chemical rocket (Figure 3.72 (a)).
- Near final trajectory plots in Figure 3.72 (b) to (e) are for an 8-kg GLOM vehicle with 3 kg expended of 4-kg total propellant allotment (see Table 3.9) for laser rocket burn. Logically, 1 kg more boosts altitude from 82 to 92.5 km.
- The OTIS trajectory ends in a 92.5- by 185-km elliptical orbit. This used a closed-form rocket-mode calculation to circularize the orbit at 1953 s with a very low thrust bipropellant rocket.
 - o Chemical “kick” rocket system mass = 0.46 kg; this exploits microelectromechanical systems (MEMS) technology
 - o Motor mass = 0.408 kg; bipropellant tank = 0.01 kg (19.2% mass penalty)
 - o Monomethyl hydrazine (MMH)/mixed oxides of nitrogen (MON) propellant mass = 0.042 kg to circularize orbit (Table 3.9)
- Key trajectory parameters and timing of events are
 - o Laser ramjet to scramjet transition near Mach 5 and 45 km at 105 s
 - o Laser scramjet mode ends at 2.6 km/s (Mach 9), 70 km, and 155 s
 - o Laser rocket burnout at >7.5 km/s, 92.5 km, 221 s
 - o Coast to 185-km altitude from 221 to 1953 s
 - o Very low thrust circularization burn of 25 s duration begins at 1953 s

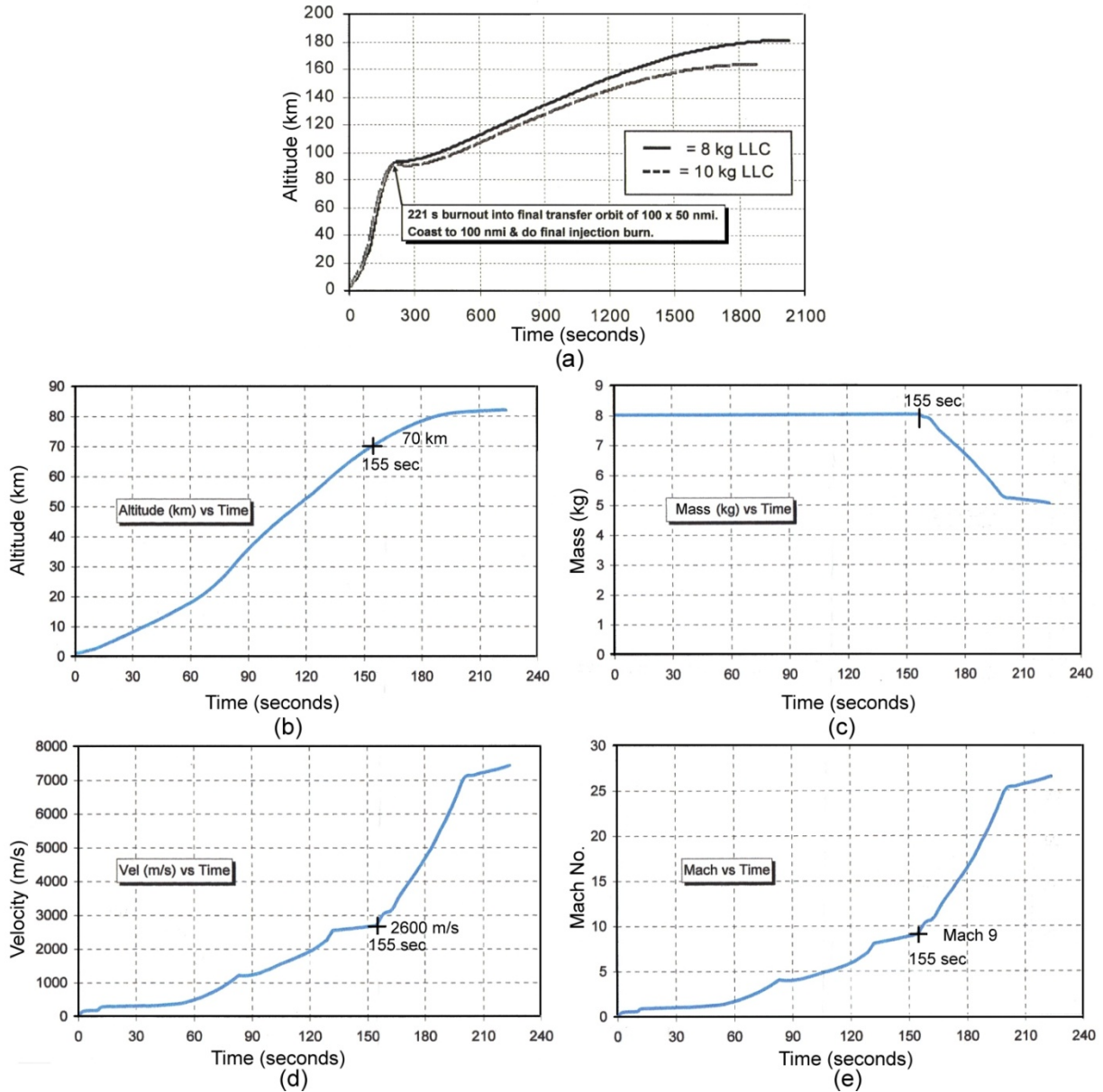


Figure 3.72.—Altitude versus time for simulated trajectories of 35-cm LCC (Ref. 5).

According to Reference 5, this chemical “kick” rocket would exploit “emerging MEMS technologies (being developed under the national Nanotechnology Initiative), to secure a 7 to 12 times mass advantage over existing small off-the-shelf chemical rockets”— for example, the *S-400* control motor, a 400-N (thrust) bipropellant rocket designed for MMH/MON and built by MBB, now called Astrium (an EADS company). It had an I_{sp} performance of 3000 N-s/kg and mass of ~ 2.8 kg—and hence the MEMS mass reduction objective of $2.8/0.408 = 6.9$.

Further Observations

- The OTIS trajectory optimizer indicates that it is best to launch a lightcraft at a very near vertical attitude and then rotate its flight path angle downward as it accelerates upward. Lifting off at 30° off-vertical (as suggested in Ref. 16 for the LTD), may be less than optimum.
- Lightcraft drag and light capture ratio (see Figure 3.73) are critical issues affecting mission performance. The LTD's higher drag coefficient reduces laser ramjet air-breathing performance in comparison with AFRL's 35 cm, lower C_D vehicles with 10° to 20° conical forebodies. However, the 1.2-m LTD's larger laser energy capture efficiency gives it greater laser rocket performance at high altitude and in space.
- Although the LTD reaches Mach 7 at 35 km with the laser ramjet mode, it is not likely to reach Mach 8 to 10 (in air-breathing mode) because of its fairly low forebody fineness ratio. However, the LTD's heavier payload configuration and higher laser power capture efficiency (in terms of vehicle mass/light capture area) reaching Mach 8 to 10 might not be so important to the mission.
- AFRL's 35-cm craft accelerates in laser scramjet mode to Mach ~9+ to reduce the liquid propellant load (for laser rocket mode) down to ~ 4 kg. With its laser ramjet engine, the BEPS 35-cm craft requires a larger propellant load of 4.66 kg.
- Candidate liquid propellants: Water or ammonia are likely more viable liquid propellants for the laser rocket mode than liquefied natural gas (LNG), whose low density could make tank volume and structural mass penalties excessive.

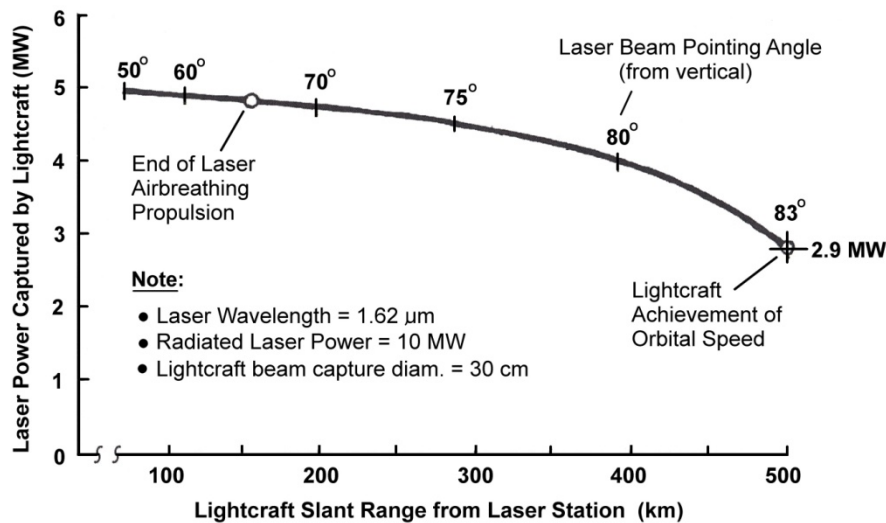


Figure 3.73.—Captured 1.62- μm laser power versus slant range from for 35-cm lightcraft (Ref. 5).

3.1.2.20.3 DOF Simulation Results for 35-cm and 120-cm Lightcraft

The study objectives were to (1) attempt to replicate the LEO launch trajectory performance for the 120-cm (focal-ring diameter) LTD vehicle (120-kg dry mass, plus 140 kg LN_2 and 2-kg He = 262 kg GLOM; described in Ref. 16), (2) simulate flights to LEO of a BEPS 35-cm, 8-kg GLOM lightcraft (see Figure 3.30, and see Table 3.8 for mass breakdown), and (3) investigate beam-riding potential (Figure 3.15 and Figure 3.16) of both lightcraft to orbital velocity. To enable such simulations, it was first necessary to upgrade the existing 7-DOF code (Refs. 13 to 15) with a suitable combined-cycle, air-breathing/rocket pulsejet engine model by incorporating the pulsed laser ramjet performance given in Figure 3.64 to Figure 3.67, along with a pulsed laser rocket mode with specified performance and propellant mass inventory, using the vehicle drag model shown in Figure 3.68. No previous 7-DOF code runs had modeled the pulsed laser ramjet mode.

3.1.2.20.3.1 7-DOF Study Tasks

The 7-DOF study tasks are (1) upgrade the existing 7-DOF operational code for simulating 120- and 35-cm lightcraft with combined-cycle engines in trajectories to orbit: for example, transitioning from air-breathing to rocket mode at about Mach 7 and 35 km (see Ref. 16); (2) perform flight dynamics and launch simulations with refined 7-DOF code, simulating trajectories to ~ 8 km/s; identify optimum pitch angle for launch and boost to orbital velocity; and (3) plot out associated output variables for comparison with the 120-cm BEPS vehicle trajectory (COMPASS team) and AFRL's 35-cm vehicle trajectory—both of which employed OTIS.

3.1.2.20.3.2 7-DOF Code Overview

The 7-DOF code utilized for this endeavor has been developed, validated, and calibrated against existing experimental lightcraft flight trajectory data to improve the understanding of beam-riding flight dynamics in order to accurately predict the flight performance of future lightcraft engine/vehicle designs (Refs. 13 to 15, 39, and 40). Both the axial thrust characteristics and beam-riding characteristics of the Type-200 lightcraft engine have been modeled and verified against extensive laboratory experimental data. The flight dynamics system model was originally a 6-DOF code, and was later extended to include a seventh DOF for a despun forebody—a feature not invoked in the present study.

3.1.2.20.3.3 7-DOF Simulation Results

Using the 7-DOF code, the flight dynamics, stability, and control of 35- and 120-cm diameter lightcraft were successfully modeled in autonomous beam riding under laser boost to extreme altitudes and orbital velocities. The interim results are presented in Figure 3.74 to Figure 3.80. The 35-cm craft used the same C_M and PRF schedules as the 120-cm craft (see Figure 3.64 and Figure 3.67), but the E_P schedule in Figure 3.66 was reduced by 11.75 times (E_P scales with engine cross-sectional area) to account for the smaller scale craft. As shown in Figure 3.74 to Figure 3.80, this goal was achieved by both 35- and 120-cm vehicles. Note that the Mach number “bumps” appearing in Figure 3.74 at 80 and 130 s (35 and 120 cm, respectively) are due to the atmospheric model, not actual changes in velocity—as verified in Figure 3.76.

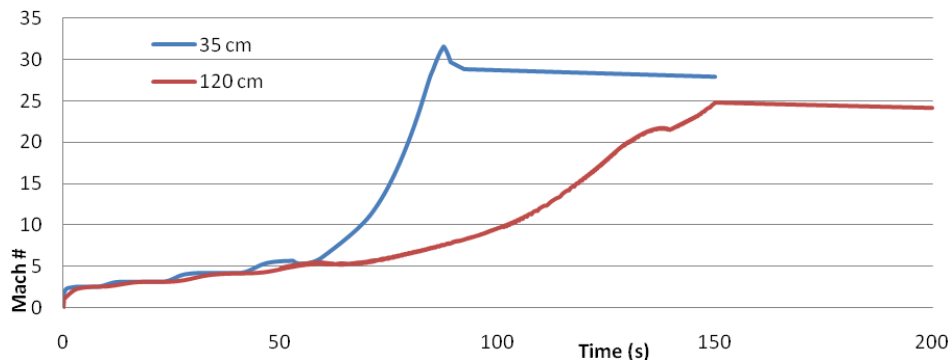


Figure 3.74.—Mach number versus time for 7-DOF simulated trajectories.

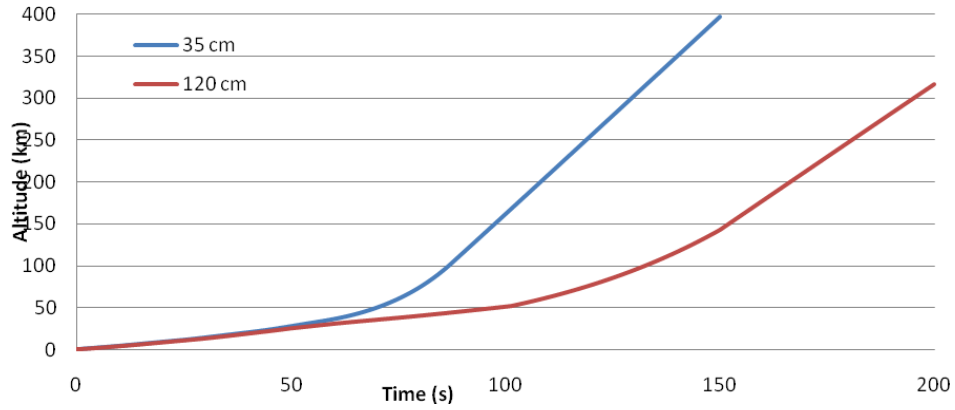


Figure 3.75.—Altitude versus time for 7-DOF simulated trajectories.

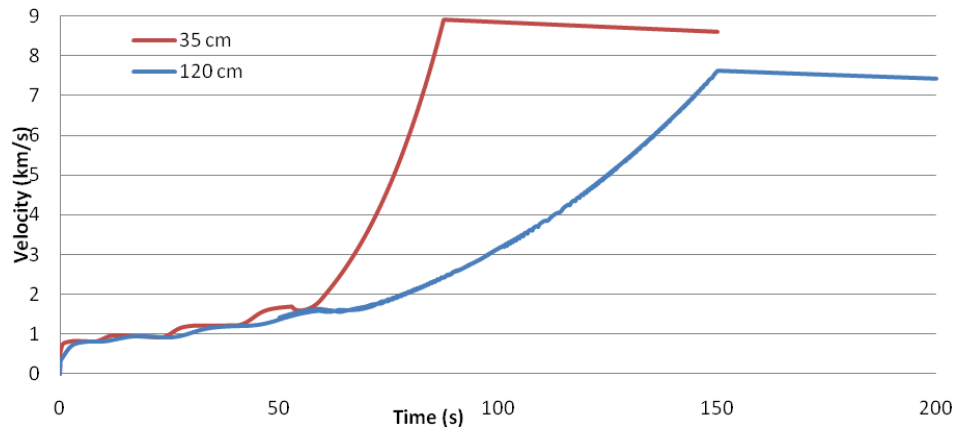


Figure 3.76.—Velocity versus time for 7-DOF simulated trajectories.

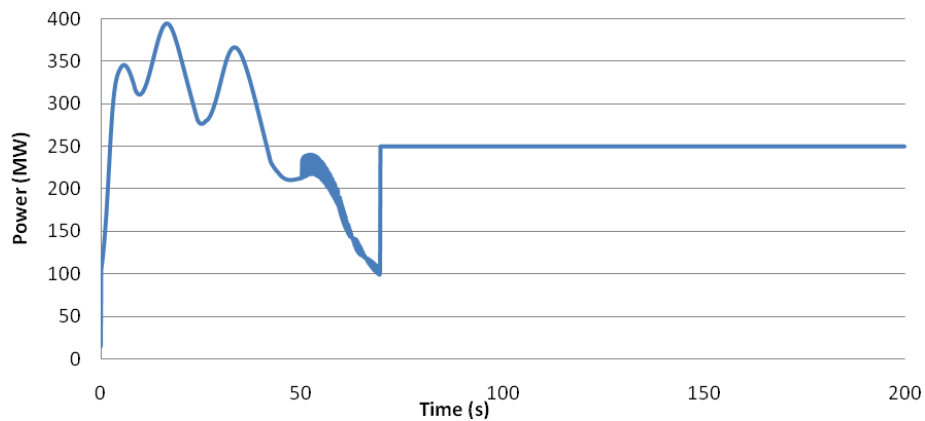


Figure 3.77.—Beam power versus time for 7-DOF simulated trajectories for 120-cm LTD craft.

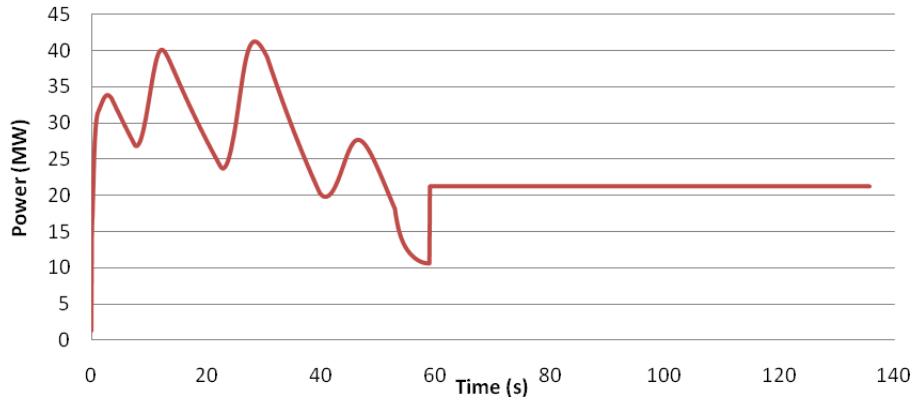


Figure 3.78.—Beam power versus time for 7-DOF simulated trajectories for 35-cm craft.

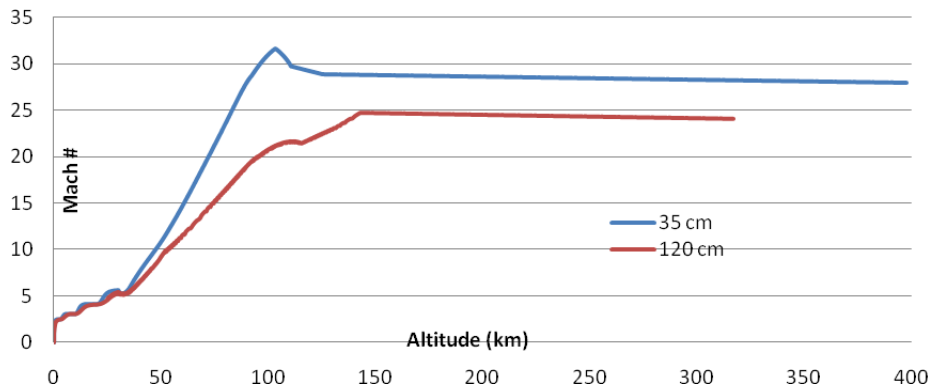


Figure 3.79.—Mach number versus altitude for 7-DOF simulated trajectories.

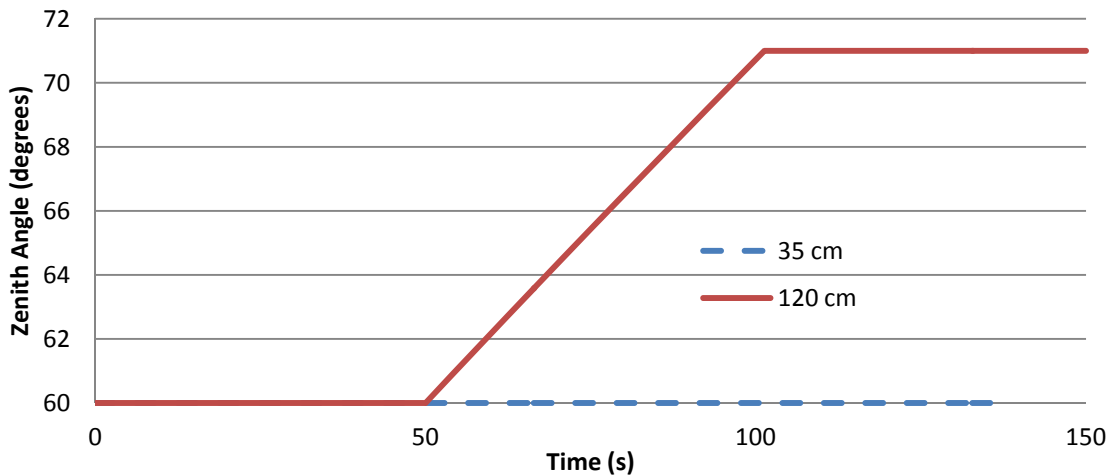


Figure 3.80.—Zenith angle versus time for 7-DOF simulated trajectories.

The 35-cm vehicle exhibited much larger accelerations and a shorter “burn” time in laser rocket mode than its 120-cm counterpart. The resultant laser rocket mode ΔV 's calculated from Equation (1) are nearly identical for both craft, but the propellant burn rates \dot{m} and total propellant masses from Equations (2) and (3), respectively, are different. The same propellant ablation rate (kg/J) is assumed to be constant for both engines (throughout the burn), whereas the beam power and, consequently, the burn rate (kg/s) scales roughly with the square of the engine diameter. The propellant mass scales with the tank volume or the cube of the craft diameter. Because of these scaling effects, the smaller craft's laser rocket propellant

“burns out” more quickly than that of the larger craft while providing roughly the same ΔV . Hence, the 35-cm craft sees larger accelerations over the burn duration, and the higher “burnout” velocity achieved benefits from smaller losses to atmospheric drag along the trajectory.

$$\Delta v = I_{sp} g_0 \ln \frac{m_0}{m_1} \quad (1)$$

$$\dot{m} = \text{Beam Power } (W) \times \text{Ablation Rate } (\text{kg/J}) \quad (2)$$

$$m_{\text{Propellant}} = \text{propellant density} \times \text{volume} \quad (3)$$

3.1.2.20.3.4 Summary and Future Work

A simple model for the air-breathing laser ramjet engine has been added to the 7-DOF code, giving C_M , PRF , and E_P as functions of altitude and Mach number. The resulting lightcraft “burnout” velocities and attainable altitudes are well within the targeted range, indicating that the launch concept is feasible under autonomous beam-riding flight. Further work is required to optimize such trajectories to reduce the required laser power and increase flight performance under boost.

3.1.2.20.4 Feasibility Assessment

The present feasibility study began with an “end-game” vision of a laser launcher for 130-kg payloads (DRM 1–A)—an *ideal final result* (IFR) requiring a monolithic, 100-MW-class infrastructure. Although this IFR was clearly useful in structuring technology roadmaps for lightcraft R&D and for assessing feasibility, the optimal laser launch concept likely resides at a smaller scale, and perhaps that decision must await the completion of subsequent trade-off studies. Hence, the strategy for a *progressive* technology roadmap has been presented herein, calling for a smaller 12-MW laser launcher for 1.33-kg CubeSat-class payloads (DRM 1–A’)—an initially more attainable system and closest “target of opportunity,” that is, 1- to 10-kg nanosats (and maybe even 0.1- to 1-kg picosats).

Barring a rapid evolution of free-electron lasers from the present 14-kW level into long-planned 100-kW and 1-MW devices (Refs. 35 to 37), the RP SSDP laser technology is our *source of choice* for lightcraft propulsion of nanosats and picosats to LEO in the near future—*simply because it enables the highest engine performance and most energetic spacecraft for the DRM 1–A mission*. However, because of the sizeable cost of GBL infrastructure, the feasibility/affordability of this launch system may hinge on its potential for *shared use* with another crucial role such as orbital debris mitigation, anti-satellite (ASAT), anti-missile, ballistic missile defense (BMD), or other use—a conclusion shared with AFRL’s nanosat launcher study (Refs. 5 and 19).

Moreover, note that the SSDP laser and other competitive source technologies are rapidly evolving, and innovation appears to be driven both by commercial and DOD weapons applications (e.g., laser welders, fusion plasma heaters, etc.). In addition, the cost of such photon sources can leverage mass production with attractive learning curves in the long term.

To ensure the feasibility of the spacecraft/lightcraft design, we recommend further work on the following fronts:

- **Propulsion/Vehicle Dynamics:** (1) Heat leaks, injector options, propellant selection, off-nominal performance (thrust vector/ I_{sp} /thrust as a function of off-pointing, angle of attack, and/or off-center beam displacement), and (2) atmospheric compensation for the laser power delivery (determine if beacon is required); see Figure 3.81 for key issues affecting engine performance and efficiency
- **Thermal:** (1) Modeling of reflector and injector-ring cooling (heating from laser, plasma—conductive, convection, and radiation—in all modes), in addition to pressure loss in cooling

channels (pressure design); (2) estimate thermal damage of mirror reflectivity due to thermal cycling; and (3) final velocity profile (with Mach < 0.6 “pop-up” hold removed) was not evaluated for its impact on thermal and structures (max-Q considerations)

- **Mission:** Improved fidelity of trajectory design to include (1) beam pointing loss terms and off-center beam pointing for steering (current trajectory is optimistic) and (2) examination of optimal trajectories including a study of a vertical launch followed by an immediate pitch-over to remove the current 30° launch conditions and to simplify the launch apparatus
- **GN&C:** (1) Final launch profile change to 30° elevation—pitch requirements not yet evaluated for this trajectory, (2) differential injection/thrust for pitching, (3) error margin analysis on the laser pointing/position on the spacecraft body, (4) required spin-rate for adequate stability, and (5) thermal control in various propulsion modes
- **Microelectronics:** A critical issue for 35-cm nanosat, and for the smaller picosat launchers is the microminiaturization of electronics packages (both size and mass).

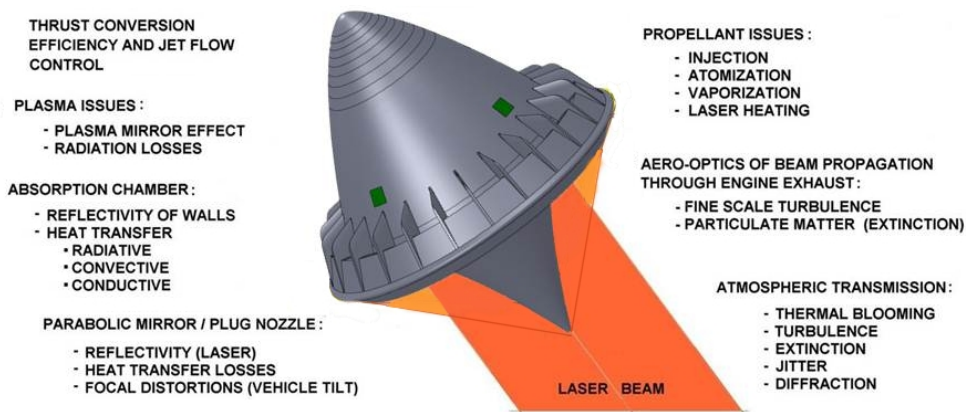


Figure 3.81.—Key issues affecting the feasibility of a lightcraft vehicle and a combined-cycle engine.

We must also maintain focus on (1) increasing design margins (e.g., materials and costs), (2) reliance on multiple technological choices for each element, and (3) flexible integration (e.g., Responsive Space goals). Again, the real game changer here is a very simple and *CHEAP* vehicle that relies on mass production to offset operational costs (associated with the laser launch facility), in addition to inherent fail-safe features, the use of environmentally friendly H₂O propellant, and so forth.

Succinctly stated, engineering research and development (R&D) is needed across the two main BEP subsystems: (1) the lightcraft engine/vehicle and (2) ground-based power-beaming infrastructure. These subsystems are intimately and inseparably linked, and as mentioned earlier, cost may likely be the major driver in the selection of ground-based power-beaming infrastructure (RP laser versus CW laser versus millimeter wave).

3.1.2.21 Ground and Flight Demonstrations

In the meantime, until such multimegawatt SSDP laser launch infrastructures become available and operational, the “go-forward” plan for advancing embryonic BEP technology in the next half-decade should include the following agenda, leading swiftly to high-visibility flight demonstrations to extreme altitudes:

- Develop a variety of lightcraft plasma engine/vehicle designs, at various scales, *by exploiting existing photon sources* (RP-lasers, CW-lasers, CW, and RP millimeter wave) and diverse engine modes (e.g., pulsejet, ramjet, scramjet, rocket, combined-cycle, etc.)

- Systematically assess, through joint experimental/theoretical/numerical studies, the relative merits and performance of CW versus RP plasma engines (laser vs. millimeter wave), *prior* to down-selecting a specific power-beaming infrastructure for initial deployment
- Continue to expand the BEP database by validating plasma engine models and vehicle flight simulation results; then define the feasible and optimal range of beam source functional requirements, margins, and tolerances
- Closely monitor the development of high-power CW and RP photon sources (laser and millimeter wave), and influence/encourage trends that enhance BEP capability

Furthermore, in a broader context, we must

- Create a progressive technology roadmap with a focus on managing risks, both technological and financial
- Design and prototype a modular launch infrastructure that can grow over time, starting with a small-scale system, then gradually expanding it as technology evolves and uncertainties are resolved
- Maintain focus on increased design margins (e.g., materials and costs), reliance on multiple technological choices for each element, and flexible integration (Responsive Space goals)
- Identify technology gaps and leverage the flexibility of the private sector—both small and large enterprises—specialized in addressing exacting technological challenges, within efficient and cost-effective working cultures

Figure 3.64 to Figure 3.67 lay out four *candidate* programs (each progressively more ambitious) for high-visibility flight demonstrations to extreme altitudes using existing photon sources with powers ranging from 10 kW upwards into the megawatt range. (*As mentioned earlier, an attractive feature of lightcraft technology is its scalability which, in fact, helps to mitigate or manage such technological and financial uncertainties.*)

The least expensive, Program 1 (see Figure 3.82), would exploit the Pulsed Laser Vulnerability Test System (PLVTS) 10-kW CO₂ pulsed laser presently operational at HELSTF (WSMR) to accomplish the following objectives: (1) demonstrate the “handoff maneuver” in flight, by passing the 10- by 10-cm PLVTS unexpanded beam off to a larger telescope (e.g., 25 to 30 cm or more), enabling higher flights beyond the current 71-m record; (2) establish the 1-km world altitude record with this new “hand-off” beam expander; and (3) exhibit controlled flight during “pitch-over” of the telescope wherein the vehicle must ride a nonvertical, slewing beam and accelerate horizontally for cross-range capability. The estimated cost is ~\$2.5M for 18 months.

Figure 3.83 gives the objectives for Program 2, which would utilize the Army’s JHPSSL 105-kW CW laser linked to the 70-cm diameter Tactical High Energy Laser (THEL) beam expander, already recoated for ~1.06 μm. The laser facility is being set up at HELSTF now that its new building has been completed. The \$6M, 2- to 3-yr program would require the development of a new CW plasma engine with autonomous beam-riding abilities, and an attitude control system for lightcraft flights to altitudes of 10 to 30 km. The program objectives include (1) accelerating the vehicle to transonic speeds while climbing vertically to an altitude of 10 km, (2) demonstrating a location communications link to the JHPSSL facility, (3) exhibiting successful attitude control, and (4) proving safe laser beam control, pointing, and tracking capability.

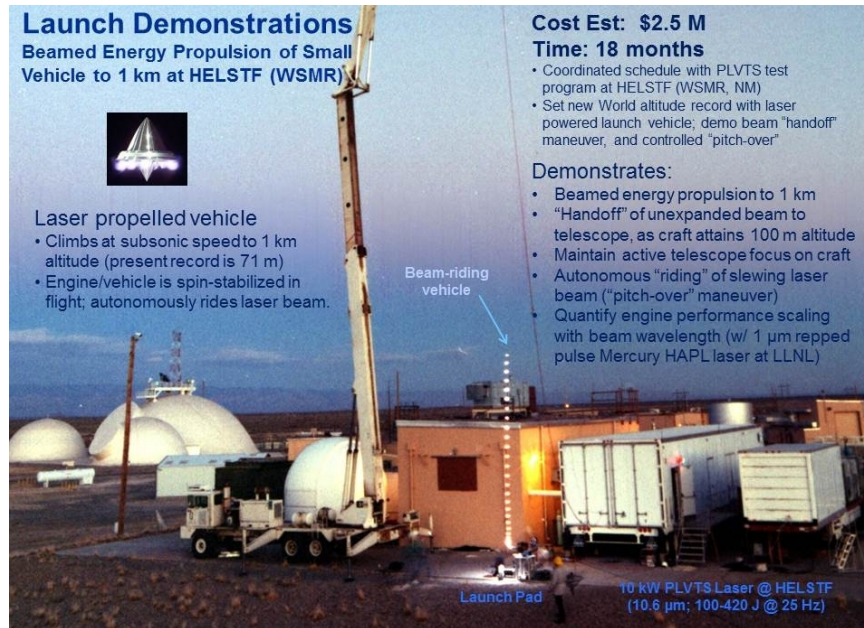


Figure 3.82.—Program 1—Laser launch demonstrations to 1 km at HELSTF using 10-kW PLVTS CO₂ laser.

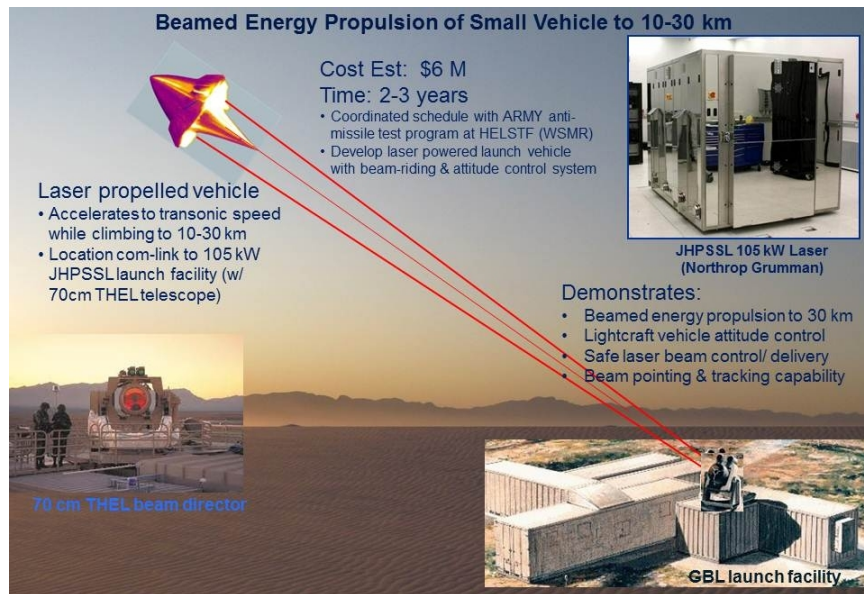


Figure 3.83.—Program 2—Suborbital launch demonstrations to 10 to 30 km at HELSTF using the 105-kW JHPSSL.

Program 3 in Figure 3.84 seeks several ambitious objectives using the multimegawatt chemical oxygen iodine laser (COIL) installed in the Airborne Laser Test Bed (ALTB), and boosting lightcraft with a new CW plasma engine (mentioned above). Several air-launched lightcraft vehicles would be fired in succession (two to six per sortie) by a fighter jet cruising at an altitude of 35 to 40 km in formation with the ALT B mothership. Each air-to-air missile would eject its lightcraft at a range suitable for direct engagement by COIL's 1.5-m telescope—aided by ultrabright light-emitting diodes (LEDs) and/or corner-cubes installed around the lightcraft's shroud.



Figure 3.84.—Program 3—Suborbital launch demonstrations using ALTB's multimewatt COIL.

The technical objectives would be to (1) exhibit beamed energy transfer through the upper atmosphere to a beam-riding lightcraft, (2) accelerate the vehicle through the transonic and into the supersonic regime, (3) validate safe ALTB beam control for 15-to 30-s lightcraft flights, and (4) prove ALTB pointing and tracking capability with beam-riding lightcraft. The estimated cost of \$12 M (2- to 3-yr duration) includes ~\$2.5 M for ALTB operations.

Program 4 in Figure 3.85, clearly the most expensive at \$50M to \$150M (3 to 4 yr), takes place on orbit, utilizing the ISS as the platform for a 1-kW laser based on the Mercury HAPL prototype at LLNL. This prototype RP, 1- μ m laser emits 55 to 100 J at a pulse repetition frequency of up to 100 Hz, and must be space-hardened for a high-vibration launch environment in order to fulfill its role as a multipurpose laser power-beaming station. The "wall-plug" efficiency should be in the 10% to 20% range.

The objectives would be to (1) establish a multipurpose 1-kW space-power-beaming infrastructure, (2) develop a laser-propelled orbit transfer vehicle around a simple laser solid ablative rocket engine, (3) launch repeatedly from a magazine loaded with numerous vehicles (6 to 12 or more), (4) explore fractionated spacecraft architectures, with maneuvering using BEP, and (5) impart a 100-m/s velocity change to deorbit vehicles. Lightcraft vehicles would be 10 to 12 cm in diameter with a mass of 25 to 50 g, with each spin stabilized prior to launch. Furthermore, the 1-kW power-beaming station might also demonstrate recharging of satellites (batteries) by illuminating their PV arrays, and enable experiments on long-range laser communications.

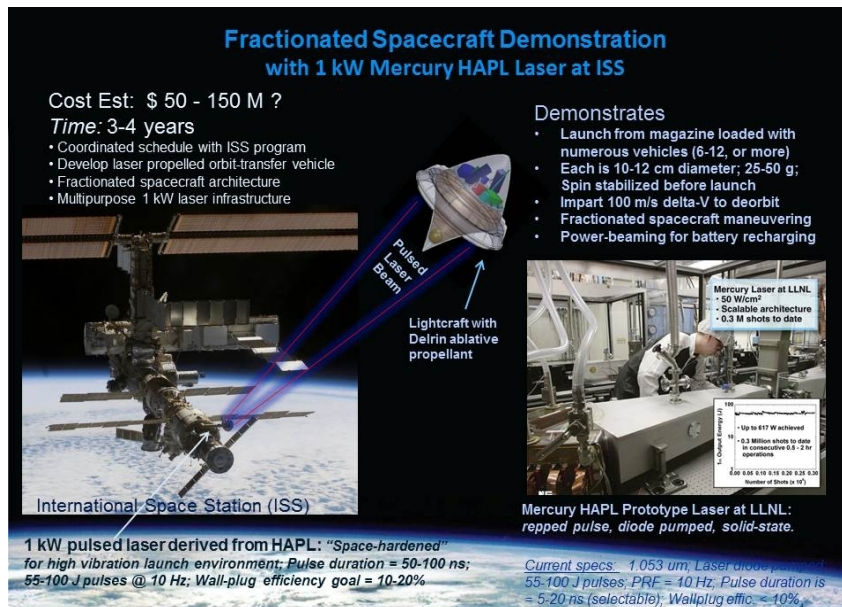


Figure 3.85.—Program 4—On-orbit launch demonstrations from the ISS using a space-rated version of the HAPL 1- kW laser.

As a final note, a high-visibility *BEP Launch Demonstration* program funded at the \$3M to \$10M level by a government or private entity would be exceptionally effective in promoting the development of low-cost space access. The program could be structured for record-breaking flights at extreme altitudes (e.g., 30 to 100 km) in a timeframe of 3 to 5 yr or less, using existing 10- to 100-kW photon sources. For example, organized as a \$10M BEP X Prize competition, it could easily attract a dozen or more entries from multinational participants, spawning a cornucopia of novel approaches. Once these demonstration flights have proven successful, then attracting private capital for the commercialization of BEP technology should be at hand. At this point, even raising \$75M to \$180M for launching nanosats into LEO should be feasible.

3.1.2.22 Responsive Space and Fractionated Architectures

It is common knowledge that today’s space launch industry is quite unresponsive to changes and uncertainties. Making progress in the *traditional* launch infrastructure—based on chemical rocket boosters—has relied on small optimizations and innovative business strategies, but it has finally “hit the wall.” A change in *Vision* is badly needed, and *responsive space architecture* appears to be the key. Its merit has already been demonstrated in industry segments. However, *flexible* space systems must rely on *fractionated architectures*, and the extreme rigidity of traditional chemical-fueled launch systems prevents progress in this direction.

Fundamental change will not be achieved *unless the same level of flexibility is extended to the launch apparatus*—which is exactly what BEP brings to the table. In addition, because of BEP’s ultra-energetic performance, it is uniquely able to embrace the subtleties of (1) increased design margins, (2) reliance on multiple technological choices for each element, and (3) flexible integration—that is, the *Responsive Space* goals.

Exploitation of BEP technology can achieve this vision by offering

- A *multipurpose laser power-beaming infrastructure* on the ground (where BEP is only one of its functions)
- A *scalable laser launch system* that responds rapidly to all sources of uncertainty, rather than adhering to rigid missions
- A *game-changer technology* that will create new markets and new opportunities unforeseen today

Note that *dramatically reduced launch costs* would in itself qualify as *game-changing*, but if the BEP launcher design could also support “*responsive and fractionated space architectures*,” the fusion may be unstoppable. Indeed, this “*scaled versatility*” will soon enable lightcraft to open a new paradigm for space access.

3.1.2.23 References for DRM 1–A

1. L.N. Myrabo, “Brief History of the Lightcraft Technology Demonstrator (LTD) Project,” in *1st International Symposium on Beamed Energy Propulsion, Huntsville, Alabama, November 2002*, edited by A.V. Pakhomov, AIP Conference Proceedings 664, American Institute of Physics, Melville, NY, 2003, pp. 49-59.
2. F.B. Mead, Jr., “Part 1 – The Lightcraft Technology Demonstration Program,” Final Report, AFRL-RZ-ED-TR-2007-0078, Nov. 2007.
3. L.N. Myrabo, “World Record Flights of Beam-Riding Rocket Lightcraft: Demonstration of ‘Disruptive’ Propulsion Technology,” AIAA Paper 2001-3798, *37th AIAA/ASME/SAE/ASEE Joint Propulsion Conference*, Salt Lake City, Utah, July 2001.
4. http://www.sncorp.com/news/press/snc_2008_snc_orbcomm.shtml
5. D. Froning, L. McKinney, F. Mead, W. Larson, and A. Pike, “Some Results of a Study of the effectiveness and cost of a laser-powered “lightcraft” vehicle system,” in *Proceedings of High-Power Laser Ablation (HPLA) 2004*, April 2004, pp. 25-30; see also: D. Froning, L. McKinney, F. Mead, W. Larson, and A. Pike, “Some Results of a Study of the effectiveness and cost of a laser-powered ‘lightcraft’ vehicle system,” Technical Report AFRL-PR-ED-TP-2004-094, AFRL/PRS, Edwards AFB, CA, 26 March 2004; see also: D. Froning, L. McKinney, F. Mead, W. Larson, and A. Pike, “Some Results of a Study of the effectiveness and cost of a laser-powered “lightcraft” vehicle system,” in *2nd International Symposium on Beamed Energy Propulsion*, edited by K. Komurasaki, AIP Conference Proceedings 702 American Institute of Physics, Melville, NY, 2003, pp. 242-250.
6. D.A. Kenoyer, I.I. Salvador, and L.N. Myrabo, “Axial Impulse Generation of lightcraft Engines with $\sim 1 \mu\text{s}$ Pulsed TEA CO₂ Laser,” in *7th International Symposium on Beamed Energy Propulsion*, edited by H.-A. Eckel and S. Scharring, AIP Conference Proceedings, American Institute of Physics, Melville, NY, 2011, pp. 98 - 108.
7. D.A. Kenoyer, I.I. Salvador, and L.N. Myrabo, “Beam-Riding Behavior of Lightcraft Engines with $\sim 1 \mu\text{s}$ Pulsed TEA CO₂ Laser,” in *7th International Symposium on Beamed Energy Propulsion*, edited by H.-A. Eckel and S. Scharring, AIP Conference Proceedings, American Institute of Physics, Melville, NY, 2011, pp. 109 - 121.
8. D.A. Kenoyer, I.I. Salvador, S.N. Notaro, and L.N. Myrabo, “Flow Visualization of Thrust-Vectoring Lightcraft Engines with $\sim 1\mu\text{s}$ Pulsed TEA CO₂ Laser,” in *7th International Symposium on Beamed Energy Propulsion*, edited by H.-A. Eckel and S. Scharring, AIP Conference Proceedings, American Institute of Physics, Melville, NY, 2011, pp. 122 - 130.
9. L.N. Myrabo, P.W. Lyons, R.A. Jones, S. Liu, and C. Manka, “Airbreathing Laser Propulsion Experiments with 1 μm Terawatt *Pharos III* Laser: Parts 1 & 2,” in *7th International Symposium on Beamed Energy Propulsion*, edited by H.-A. Eckel and S. Scharring, AIP Conference Proceedings, American Institute of Physics, Melville, NY, 2011, pp. 203-239.
10. D.A. Kenoyer, L.N. Myrabo, “Subsonic Aerodynamics of Spinning and Non-Spinning Type 200 Lightcraft: Progress Report,” in *6th International Symposium on Beamed Energy Propulsion*, edited by C. Phipps, K. Komurasaki, and J. Sinko, AIP Proceedings 1230, American Institute of Physics, Melville, NY, 2010, pp. 30-40.

11. I.I. Salvador, L.N. Myrabo, M.A.S. Minucci, A.C. de Oliveira, P.G.P. Toro, J.B. Channes Jr. and I.S. Rego, "2-D Airbreathing Lightcraft Engine Experiments in Quiescent Conditions," in *7th International Symposium on Beamed Energy Propulsion*, edited by H.-A. Eckel and S. Scharring, AIP Conference Proceedings, American Institute of Physics, Melville, NY, 2011, pp. 174 – 189. See also: I.S. Salvador, "Static and Hypersonic Experimental Analysis of Impulse Generation in AirBreathing Laser Thermal Propulsion," Ph.D. Thesis, Rensselaer Polytechnic Institute, Troy, NY, 2010.
12. I.I. Salvador, L.N. Myrabo, M.A.S. Minucci, A.C. de Oliveira, P.G.P. Toro, J.B. Channes Jr. and I.S. Rego, "2-D Airbreathing Lightcraft Engine Experiments in Hypersonic Flow Conditions," in *7th International Symposium on Beamed Energy Propulsion*, edited by H.-A. Eckel and S. Scharring, AIP Conference Proceedings, American Institute of Physics, Melville, NY, 2011, pp. 190 – 202. See also: I.S. Salvador, "Static and Hypersonic Experimental Analysis of Impulse Generation in AirBreathing Laser Thermal Propulsion," Ph.D. Thesis, Rensselaer Polytechnic Institute, Troy, NY, 2010.
13. C.G. Ballard, K.S. Anderson, and L.N. Myrabo, "Flight Dynamics and Simulation of Laser Propelled Lightcraft" *ASME Journal of Computational and Nonlinear Dynamics*, Vol. 4, Issue 4, Oct. 2009.
14. D.A. Kenoyer, K.S. Anderson, L.N. Myrabo, "Trajectory Simulations For Laser-Launched Microsatellites Using a 7-DOF Flight Dynamics Model," Paper 86664, *Proc. of IDETC/MSNDC7*, 2009.
15. D.A. Kenoyer, K.S. Anderson, and L.N. Myrabo, "Calibration and Validation of a 6-DOF Laser Propelled Lightcraft Flight Dynamics Model Upon Experimental Data, in *5th International Symposium on Beamed Energy Propulsion*, edited by A.V. Pakhomov, AIP Proceedings 997, American Institute of Physics, Melville, NY, 2008, pp. 325-337.
16. L.N. Myrabo (ed.), et.al., "Lightcraft Technology Demonstrator," Final Technical Report, *SDIO Laser Propulsion Program*, prepared under contract to Lawrence Livermore National Laboratory, No. 2073803, 1989.
17. Richard, J.C., and Myrabo, L.N., "Analysis of Laser-Generated Impulse in an Airbreathing Pulsed Detonation Engine - Parts 1 & 2," in *3rd International Symposium on Beamed Energy Propulsion*, edited by A.V. Pakhomov and L.N. Myrabo, AIP Conference Proceedings 766, American Institute of Physics, Melville, NY, 2005, pp. 265-278; see also: J.C. Richard, "Analysis of Pulsed Laser-Generated Impulse in an Advanced Airbreathing Thruster," PhD Thesis, Rensselaer Polytechnic Institute, Troy, NY, 1989.
18. T. Langener, L.N. Myrabo, and Z. Rusak, "Inlet Aerodynamics and Ram Drag of Laser Propelled Lightcraft Vehicles," in *6th International Symposium on Beamed Energy Propulsion*, edited by C. Phipps, K. Komurasaki, and J. Sinko, AIP Proceedings 1230, American Institute of Physics, Melville, NY, 2010, pp. 41-60.
19. E.W. Davis and F.B. Mead, Jr., "Review of Laser Lightcraft Propulsion System," in *5th International Symposium on Beamed Energy Propulsion*, edited by A.V. Pakhomov, AIP Proceedings 997, American Institute of Physics, Melville, NY, 2008, pp. 283-294.
20. A. Krepinevich, T. Ehrhard, and B. Watts, "Solid-State Laser Weapon Systems, Bridging the Gap—or Bridge Too Far?," Center for Strategic & Budgetary Assessments (CSBA), May 20, 2009.
21. S. Weinberger, "Defense Technology International: Solid-State Lasers; 100 Kilowatts or Bust; Rivals Vie To Develop Next Generation of Lasers," *Aviation Week & Space Technology*, 22 May 2006.
22. http://www.textrondefense.com/news/2010/02_18_10.html
23. B. Yamamoto, et.al., "Evolution of a solid state laser," SPIE 6551: 55205 (2007); see also: https://lasers.llnl.gov/programs/psa/directed_energy/sshcl.php
24. http://www.sflorg.com/technews/tn101206_02.html
25. A. Bayramian, et.al., "The Mercury project: A high average power, gas-cooled laser for inertial fusion energy development," *Fus. Sci and Tech.*, 52, pp. 383-387 (2007).

26. www.ipgphotonics.com; see also: <http://www.optoiq.com/index/photronics-technologies-applications/lfw-display/lfw-article-display/371319/articles/laser-focus-world/volume-45/issue-12/features/photonic-frontiers-fiber-lasers-fiber-lasers-ramp-up-the-power.html>
27. www.trassa.org.
28. A.M. Rubenchik, C.P.J. Barty, R.J. Beach, A.C. Erlandson, J.A. Caird, "Laser Systems for Orbit Debris Removal," LLNL PROC-423323, Lawrence Livermore National Laboratory, February 8, 2010; also given at the *High Power Laser Ablation '11 conf. (HPLA 2010)*, April 18-22, 2010.
29. C.P.J. Barty, J.A. Caird, A.E. Erlandson, R. Beach, A.M. Rubenchik, "High Energy Laser for Space Debris Removal," LLNL-TR-419114, Lawrence Livermore National Laboratory, October 31, 2009.
30. J.A. Caird, et.al., "Nd:glass laser design for laser ICF fission energy (LIFE)," *Fusion Science and Technology*, 56, 607 (2009); also, see ppt with same title presented by J.A. Caird to the American Nuclear Society 18th Meeting, 29 Sept. – 2 Oct. 2008.
31. <http://www.optoiq.com/index/photronics-technologies-applications/lfw-display/lfw-article-display/311588/articles/laser-focus-world/volume-43/issue-11/features/vcsels-powerful-vcsel-arrays-beat-the-heat.html>
32. <http://www.space-electronics.com/Literature/POISeriesMetric.pdf>; <http://www.space-electronics.com/Literature/POI%20Specs.PDF>
33. J.P. Reilly, "NASA Design Study on Laser Propulsion Concepts – Requirements and Options," Northeast Science and Technology, Inc., East Sandwich, MA, for Anteon Corporation, Dayton, OH, under Contract No. F33615-97-D-5403, dated 31 Dec. 1999, 62 pages.
34. J.T. Kare (personal communication), Kare Technical Consulting, Seattle, WA.
35. <http://www.engadget.com/2011/02/21/us-navys-free-electron-laser-breaks-another-record-takes-aim-a/>; and <http://www.geek.com/articles/geek-cetera/navys-record-breaking-laser-burns-through-20-feet-of-steel-per-second-20110221/>
36. S.E. Sampayan, et.al., "Performance Characteristics of an Induction Linac Magnetic Pulse Compression Modular at Multi-Kilohertz Pulse Repetition Frequencies," Lawrence Livermore National Laboratory, UCRL-JC-105442 Preprint, prepared for 1991 IEEE Particle Accelerator Conference 6-9 May 1991.
37. R. Whitney, D. Douglas, and G.Neil, "Airborne megawatt class free-electron laser for defense and security," Jefferson Lab, 12000 Jefferson Avenue, Newport News, VA USA 23606; whitney@jlab.org; phone 757.269.7536; www.jlab.org
38. D.P. Resendes, S. Mota, G. Sorasio, J.T. Mendonca, B. Sanders, and J. Encarnação, "Laser Propulsion for ESA Missions: Ground to Orbit Launch," Final Report, ESA CR 17048/03/NL/PA, Dec. 2004, pp. 82 and 85; see also: D.P. Resendes, S. Mota, J.T. Mendonca, B. Sanders, J. Encarnação, J. Gonzalez del Amo, and L.N. Myrabo, "Laser Propulsion for ESA Missions: Ground to Orbit Launch Project Overview - Part I," in 4th International Symposium on Beamed Energy Propulsion, edited by K Komurasaki, T. Yabe, S. Uchida, and A. Sasoh, AIP Conference Proceedings, American Institute of Physics, Melville, NY, 2006, pp. 576-587.
39. D.A. Kenoyer, "Validation and Calibration of a 6-DOF Laser Propelled Lightcraft Flight Dynamics Model vs. Experimental Data," M.S. Thesis, Rensselaer Polytechnic Institute, Troy, N.Y., Dec. 2007.
40. D.A. Kenoyer, "Combine Experimental and Numerical Investigations into Laser Propulsion Engineering Physics," Ph.D. dissertation, Rensselaer Polytechnic Institute, Troy, NY. June, 2010.

3.1.3 Laser Optical Cost Analysis

National Aeronautics and Space Administration



Beamed Energy Propulsion Facility ROM Cost Estimate

March 28, 2011

National Aeronautics and Space Administration



General BEPS Launch Facility Assumptions

- All cost are rough order of magnitude (ROM) estimates in FY11M\$.
- Estimates assume all facilities are built new on government land, no existing infrastructure is used. Available infrastructure will reduce costs.
- Costs do not include remediation of potential significant environmental impact issues that may be identified.
- Range estimates are presented to highlight the uncertainty associated with the lack of definition and supporting cost information available at this time.
- Range estimates for the launch site also includes the uncertainty associated with the selected location and the cost impact of materials that may be required to protect against environmental conditions.



General BEPS Launch Facility Assumptions

- Launch site ROM estimates are based on a NASA KSC launch site estimating approach. Microwave and laser sites use the same approach for 'like function' facilities which are scaled for expected differences in size or function.
- All sites include site design and testing and activation costs.
- Launch facility design is estimated at 12% of estimated total site costs less testing and activation.
- Launch facility testing and activation is estimated at 30% of the capital facilities cost.
- Microwave and laser site design is estimated at 8% of estimated total site costs less testing and activation.
- Microwave and laser site testing and activation is estimated at 15% of the capital facilities cost.



Operations Cost Assumptions

- All costs are estimated for one year of operation in FY11\$.
- Yearly operations cost assume 360 launches per year (one/day). Additional study is required to determine the feasible number of launches per year from a single launch pad. The number of launches per pad is affected by the CONOPS, pad turnaround time, launch facility maintenance, weather, and launch window requirements.
- Total estimated facility operations costs are assumed to be allocated to the beamed launch operations. Facility sharing can reduce costs.
- Facility equipment and maintenance is estimated at 5% of the total value of capital assets per year resulting in an estimated 70-80% of total operations costs.



Laser Optical Launch Site Assumptions

- **Launch Site facility requirements**
 - General – site work, roads
 - Support Facilities/Launch Pad – see details below
 - Site Infrastructure – water, fire, sewer, power, communications, HVAC, environmental control system
 - Ground support equipment
- **Key cost estimate assumptions**
 - New facility on government land in secluded area due to danger associated with beamed energy. Launch rate 1-4 vehicles a day, if CONOPS allows.
 - Launch pad includes all related hardware/services (scaled from microwave estimate). Rocket will be small, approximately 1.5 meters in length, and less than 500 kg total wet mass with payload.
 - Command center includes all related services.
 - Payload integration facility (assuming an integrated payload) can process/integrate up to four payloads per day (scaled from microwave estimate).
 - Water storage facility sized for ~6,000 kg with no on-site processing.
 - Rocket storage facility size for 8 rockets (scaled from microwave estimate).
 - Admin facility sized for launch site staffing needs (estimated at 100 people).
 - Security facilities/equipment includes fencing, cameras, etc.



Laser Optical Launch Site Assumptions

- **Launch site boost laser facility requirements**
 - Laser/Optics – diode lasers(140 MW), optics (Qty.1150, 120 kWe modules)
 - Power Storage/Distribution – energy storage, power supply, power distribution
- **Key cost estimate assumptions**
 - Diode Laser – Projected multi-MW price \$2/W (ref: J. Kare) used as low (ML +50%, high +100%)
 - Optics – Projected \$200K/module (ref: J. Kare) use as low (ML +25%, high +50%)
 - Energy Storage - \$50K/kWh estimated as most likely based on GRC experience with wind tunnels (low -40%, high +20%)



Laser Optical Main Laser Site Assumptions

- Main Laser Site facility requirements
 - General – site work, roads
 - Support Facilities – admin facility (50 people), command center (75% of launch site center), guard gate facility
 - Site Infrastructure – water, fire, sewer, power, communications, HVAC, environmental control system
 - Ground support equipment
 - Laser/Optics – diode lasers(350 MW), optics (Qty. 3000, 120 kWe modules)
 - Power Storage/Distribution – energy storage, power supply, power distribution
- Key cost estimate assumptions
 - Diode Laser – Projected multi-MW price \$2/W (ref: J. Kare) used as low (ML +50%, high +100%)
 - Optics – Projected \$200K/module (ref: J. Kare) use as low (ML +25%, high +50%)
 - Energy Storage - \$50K/kWh estimated as most likely based on GRC experience with wind tunnels (low -40%, high +20%)



Laser Optical Launch Facility Development ROM

Laser Optical Launch Facilities ROM (FY11\$M)
(Excludes FTE/WYE personnel and O&M costs)

	Launch Site Complex - ROM Subtotal (\$M)				Main Laser Site - ROM Subtotal (\$M)				Laser Optical Facilities - Total ROM (\$M)			
	Low	ML	High	Mean Est	Low	ML	High	Mean Est	Low	ML	High	Mean Est
Project Total ROM (\$M)	\$1,116.8	\$1,713.4	\$2,741.1	\$1,857.1	\$2,103.3	\$3,119.0	\$4,460.7	\$3,227.6	\$3,220.1	\$4,832.4	\$7,201.7	\$5,084.7
Design	\$95.1	\$145.9	\$233.3	\$158.1	\$137.1	\$203.2	\$290.7	\$210.3	\$232.2	\$349.1	\$524.0	\$368.4
Testing & Activation	\$228.9	\$351.7	\$563.7	\$381.5	\$253.0	\$375.2	\$536.0	\$388.1	\$481.9	\$726.9	\$1,099.8	\$769.5
Laser Optical Facilities ROM Subtotal	\$792.7	\$1,215.8	\$1,944.1	\$1,317.5	\$1,713.3	\$2,540.6	\$3,633.9	\$2,629.2	\$2,506.0	\$3,756.3	\$5,578.0	\$3,946.8
WBS Item												
Site Work	\$11.2	\$15.4	\$18.8	\$15.1	\$8.4	\$11.6	\$14.1	\$11.3	\$19.6	\$27.0	\$32.9	\$26.5
Roads	\$18.4	\$27.9	\$46.2	\$30.8	\$18.4	\$27.9	\$46.2	\$30.8	\$36.9	\$55.8	\$92.4	\$61.7
Support Facilities	\$22.0	\$45.7	\$95.7	\$54.5	\$7.1	\$14.9	\$36.1	\$19.4	\$29.2	\$60.6	\$131.7	\$79.8
Concrete Administration Facility	\$7.4	\$10.8	\$28.5	\$17.7	\$5.4	\$14.2	\$31.0	\$17.0	\$11.0	\$16.1	\$42.7	\$24.0
8 Rocket Storage Facility	\$2.8	\$3.8	\$6.1	\$4.4	\$0.0	\$0.0	\$0.0	\$0.0	\$2.8	\$3.8	\$6.1	\$4.4
Concrete Command Center	\$3.3	\$10.4	\$25.3	\$12.5	\$2.5	\$7.8	\$19.0	\$10.0	\$5.8	\$18.2	\$44.4	\$24.0
Payload Integration Facility	\$7.6	\$19.1	\$32.9	\$20.0	\$0.0	\$0.0	\$0.0	\$0.0	\$7.6	\$19.1	\$32.9	\$20.0
Guard Gate Facility	\$1.0	\$1.8	\$2.8	\$1.8	\$1.0	\$1.8	\$2.8	\$1.8	\$1.9	\$3.5	\$5.6	\$3.4
Pad Structure	\$6.6	\$9.8	\$12.2	\$9.5	\$0.0	\$0.0	\$0.0	\$0.0	\$6.6	\$9.8	\$12.2	\$9.5
Pad Structure	\$2.2	\$3.1	\$4.2	\$3.2	\$0.0	\$0.0	\$0.0	\$0.0	\$2.2	\$3.1	\$4.2	\$3.2
Emergency Egress System	\$0.0	\$0.0	\$0.0	\$0.0	\$0.0	\$0.0	\$0.0	\$0.0	\$0.0	\$0.0	\$0.0	\$0.0
Flame Trench	\$3.4	\$4.0	\$4.5	\$3.9	\$0.0	\$0.0	\$0.0	\$0.0	\$3.4	\$4.0	\$4.5	\$3.9
Lightning Protection Towers	\$1.1	\$2.7	\$3.5	\$2.4	\$0.0	\$0.0	\$0.0	\$0.0	\$1.1	\$2.7	\$3.5	\$2.4
Infrastructure	\$99.2	\$174.5	\$435.5	\$236.4	\$91.3	\$142.7	\$260.5	\$164.8	\$190.5	\$317.2	\$696.0	\$401.3
GSE	\$13.5	\$23.4	\$53.3	\$30.0	\$8.4	\$14.6	\$33.3	\$18.8	\$21.9	\$38.0	\$86.5	\$48.8
Laser/Optics Equipment	\$510.0	\$707.5	\$905.0	\$707.5	\$1,300.0	\$1,800.0	\$2,300.0	\$1,800.0	\$1,810.0	\$2,507.5	\$3,205.0	\$2,507.5
Power Storage/Processing Facilities	\$111.8	\$211.5	\$377.5	\$233.6	\$279.6	\$528.9	\$943.8	\$584.1	\$391.4	\$740.4	\$1,321.3	\$817.7



Laser Optical Launch Facility Operations ROM

Laser Optical Launch Facilities Operations ROM (FY11\$M/Year)
(Does not include vehicle/payload)

	Laser Optical Operations - Total ROM (\$M/Yr)			
	Low	ML	High	Mean Est
Laser Optical Operations Total ROM (\$M/Year)	\$152.2	\$228.1	\$331.7	\$237.3
Facility/Equipment Maintenance	\$122.5	\$183.7	\$272.6	\$192.9
Operations Personnel	\$22.5	\$30.0	\$37.5	\$30.0
Propellant/Energy/Consumables	\$7.2	\$14.4	\$21.6	\$14.4
Other	\$0.0	\$0.0	\$0.0	\$0.0
Launch Site Complex - ROM Subtotal (\$M/Year)	\$56.8	\$85.8	\$129.8	\$90.8
Facility/Equipment Maintenance	\$38.2	\$58.6	\$94.0	\$63.6
Operations Personnel	\$15.0	\$20.0	\$25.0	\$20.0
Propellant/Energy/Consumables	\$3.6	\$7.2	\$10.8	\$7.2
Other	\$0.0	\$0.0	\$0.0	\$0.0
Main Laser Site - ROM Subtotal (\$M/Year)	\$95.4	\$142.3	\$202.0	\$146.6
Facility/Equipment Maintenance	\$84.3	\$125.1	\$178.7	\$129.4
Operations Personnel	\$7.5	\$10.0	\$12.5	\$10.0
Propellant/Energy/Consumables	\$3.6	\$7.2	\$10.8	\$7.2
Other	\$0.0	\$0.0	\$0.0	\$0.0



Beamed Energy Propulsion Study Laser Optical Vehicle Cost Estimate as determined by the COMPASS Team

March 2011



COMPASS Cost Assumptions - Lightcraft

- DRAFT Cost Estimate based on COMPASS design
- All costs are in FY11\$M
- This estimate assumes the following:
 - Proto-flight development approach
 - No ground spares included
 - Model assumes TRL Level 6
 - This estimate does not include any cost for technology development
 - Represents the most likely estimate based on cost-risk simulation results
 - Flight heritage is assumed as Off-The-Shelf (OTS) for most components
 - Excluding new or advanced technology items
 - Parametric estimate based on mostly mass based CERs from historical cost data
 - Launch vehicle systems integration wraps
 - Software not included
- Does not include:
 - Contractor Fee (10-12% on top of the contractor estimates)
 - Any insight/oversight costs (for NASA-managed estimates)
 - Reserves (can be as high as 40-50%)
 - Ground System Cost (ie. Laser)
 - Launch Services Costs (ie. Special launch approval process)
 - Technology costs for components lower than TRL-6



Lightcraft Preliminary COMPASS Cost ROM

(Represents estimated Prime Contractor cost)

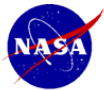
WBS	Description	DDT&E	Flight	Total
		Total	HW	
		BY \$M	BY \$M	BY \$M
06.1.1	Payload	0.0	0.0	0.0
06.1.2	Attitude Determination and Control	4.4	1.6	6.0
06.1.3	Avionics	3.8	1.7	5.5
06.1.4	Communications and Tracking	1.3	0.5	1.8
06.1.5	Electrical Power Subsystem	2.2	1.2	3.4
06.1.6	Thermal Control (Non-Propellant)	5.4	1.0	6.4
06.1.7	Propulsion (Hardware)	4.8	1.3	6.1
06.1.8	Propellant (Chemical)	0.0	0.0	0.0
06.1.9	Structures and Mechanisms	7.9	2.9	10.8
	Subtotal	29.7	10.3	40.1
	Systems Integration	33.1	4.4	37.5
	Spacecraft Total	62.8	14.8	77.6

Costs in FY11\$M

3.1.4 Laser Thermal COMPASS Report



National Aeronautics and Space Administration



Team Roster



- COMPASS Lead - Steve Oleson
- Program RFI Study Lead – John Dankanich
- Lead System Integration, MEL - Melissa McGuire, David Grantier
- CONOPS, system integration – Jeff Woytach
- Integration PEL , Mission Visualization - Michael Bur
- Mission –Laura Burke, Ian Dux, Dave Smith
- GN&C –Mike Martini
- Propulsion - James Fittje, Geoff Landis
- TVC – Robert Tornabene
- Mechanical Systems - John Gyekenyesi, Tom Haag
- Thermal - Tony Colozza,
- Power - James Fincannon, Kristen Bury
- C&DH, Software- Glenn Williams
- Communications - Joe Warner
- Configuration and Launch Vehicle Integration - Tom Packard
- Cost - Jon Drexler
- Risk - Anita Tenteris

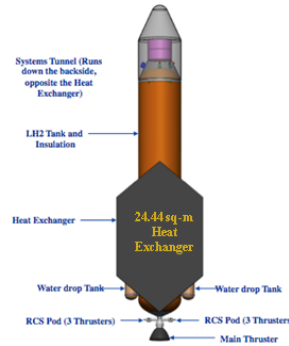
2



DRM 1B Launcher Summary



- Laser powered Expansion Deflection nozzle 'single stage to orbit' (with water propellant drop tanks)
- Launches 2 equivalent 40 kg ORBCOMM messaging spacecraft
- 17m tall launcher dominated by 2 m hydrogen tank
- Launched vertically, requires two laser stations (over 200 MW each) for launch
 - Laser stations consist of up to 2000, 60 kW per module (each has 6 separate 10 kW lasers with a common ~1.5 m telescope)
- Thermal heat exchanger technology TRL 2-3
- Propulsion and Thermal:
 - 20-60 kN ED nozzle, 2000° K hot hydrogen from heat exchanger 'wing'
 - Higher thrust provided by water injection to provide more thrust during first 100 seconds, water tanks dropped when empty
 - Up to 300 MW absorbed by hydrogen in heat exchanger provides 1sps up to 760 sec
 - Hot hydrogen for RCS
 - Highly Reflective (99.9999%) coatings on vehicle to avoid over heating of shroud, tank, etc.



Spacecraft Master Equipment List Rack-up (Mass) - BEP Thermal Laser				COMPASS S/C Design	
WBS	Main Subsystems	Basic Mass (kg)	Growth (kg)	Total Mass (kg)	Aggregate Growth (%)
06	Thermal Laser Launcher Case 3	5302.0	119.2	5421.2	
06.1	Payload	89.0	0.0	89.0	0%
06.2	Launch Vehicle	5222.0	119.2	5341.2	2%
06.2.1	Attitude Determination and Control	5.0	0.7	5.6	14%
06.2.2	Command and Data Handling	9.05	2.7	11.8	30%
06.2.3	Communications and Tracking	3.0	1.0	4.0	33%
06.2.4	Electrical Power Subsystem	8.3	3.7	12.0	44%
06.2.5	Thermal Control	92.9	13.9	106.8	15%
06.2.6	Propulsion	444.4	54.8	499.2	12%
06.2.7	Propellant	4446.2		4446.2	0%
06.2.8	Structures and Mechanisms	212.2	38.4	250.6	18%
	Estimated Launch Vehicle Dry Mass (no payload)	778	115	893	15%
System Level Growth Calculations					Total Growth
	Dry Mass Derived System Level Growth (no payload)	778	233	1011.0	13%
	Additional Growth (carried at system level)		118		15%
	Total Wet Mass with Growth (w payload)	5302	233	5535.0	
		Basic Mass (kg)	Growth (kg)	Total Mass (kg)	
		778	233	1011.0	13%
	Total Spacecraft Wet Mass (w/growth)	5534.7			
	Mass of Orignal Tanks, payload mass	162.9			
	Vehicle On Orbit Mass (incl residual/PPG, w P/L)	5371.8	kg		
	OTM total burn out mass	522.0	kg	1000	kg
	Additional mass				
		145.2	kg		

* NOTE: pressurant/residuals included as Dry Mass

3



TRL Definitions



- SUMMARY
- TRL 1 Basis principles observed and reported
- TRL 2 Technology concept and/or application formulated
- TRL 3 Analytical and experimental critical function
- TRL 4 Component and/or breadboard validation in laboratory environment
- TRL 5 Component and/or breadboard validation in relevant environment
- TRL 6 System/Subsystem model or prototype demonstration in a relevant environment (ground or space)
- TRL 7 System prototype in a space environment
- TRL 8 Actual system completed and "flight qualified" through test and demonstration (ground or space)
- TRL 9 Actual system "flight proven" through successful mission operations

4



TRL Levels (< TRL 6)



- **Propulsion & Flight Dynamics/Environments**
 - Hydrogen/H₂O Engine (50,000N class):
 - High Temperature components (2000° K): TRL 4
 - ED Nozzle: TRL 5
 - RCS: TRL 5-6
- **Thermal:**
 - Heat Exchanger: TRL 2-3
- **GN&C: TRL 6**
- **C&DH: TRL 6**
- **Communications: TRL 5-6 (thermal environment)**
- **Power**
 - Batteries TRL 3-4
- **Mechanical:**
 - Advanced, high temperature (C/C composites) TRL 3-4

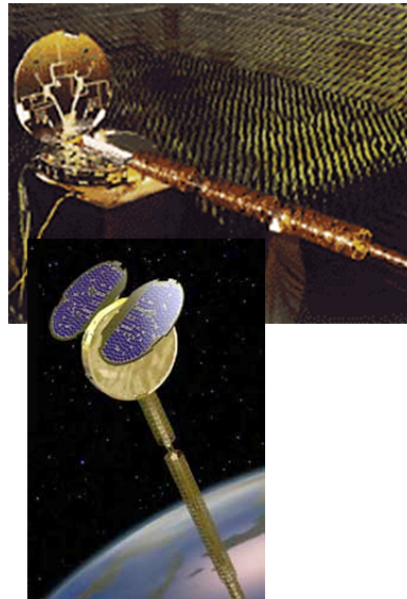
5



Proposed Representative Payload



- **ORBCOMM Class**
- **Orbcomm is a commercial venture to provide global messaging services using a constellation of 26 low-Earth orbiting satellites.**
- **Spacecraft (40 kg, \$1.2M each)**
 - 4 years life, 160W
 - VHF (138 MHz and 400 MHz): 57.6 kbps
 - Gravity gradient, mag torquers, cold gas N₂
 - 17 data processors, 7 antennas, 50,000 messages per hour
- **100 kg separated payload**



6



Beamed Energy Propulsion: Laser Launcher



The COMPASS team has been tasked by DARPA/NASA to create an independent concept design for a Laser powered launch vehicle.

The COMPASS design will give the DARPA/NASA a point-of-reference to the feasibility of the concept and a what technologies and demonstrations need to be developed to support development of a laser launcher.



Schedule



- **Next Week**
 - MTW (with customer), F
 - Monday: Kickoff, Mission Analysis, Begin laying out vehicle, define trades, Scratch PEL
 - Tuesday-Wednesday: CONOPs, Perform design
 - Friday: Review Trades, Assess MEL, Configuration

- **2nd Week**
 - MW: Complete Design
 - F: Draft Results Flip-thru

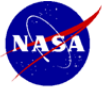


Starting Requirements



- **Must Deliver to LEO a 100 kg payload (400 km x 30° inclination)**
- **Will utilize Single stage to orbit**
- **Will Utilize a ground based laser beams (~1MW for 1 kg payload to orbit – at vehicle)**
- **Will emphasize simplicity and low cost**

9



FOMs



- **Mass: Single Stage to orbit, payload 80 kg (two orbcomm)**
- **Reliability: Single Fault Safe**
- **Cost:**
 - Launcher mass, volume, single stage to orbit
 - Cost for launch system

10



Fault Tolerance



- **Single fault for safety**
 - What kind of range safety is needed?
- **Fault tolerance for vehicle**
 - How valuable are payloads?
 - What systems should be fault tolerant?

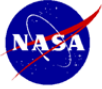
11



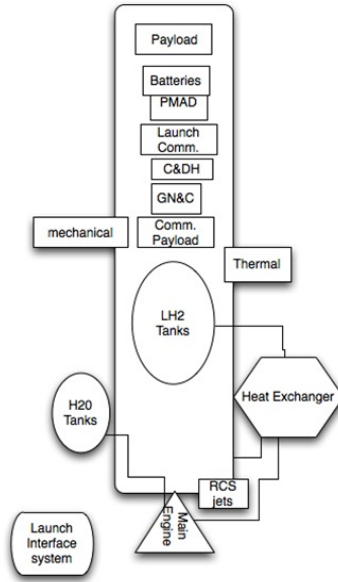
Summary of Requirements/Assumptions



Item	Requirements / Assumptions	Trades
Top-Level/ Science	Laser launcher shall place at 80kg into a 400 km orbit. FOM Cost per n units, payload mass, safety, single stage to orbit. First launch 2020.	Payload vs altitude, drop tanks for dense propellants
System	Single Fault Safe only. Otherwise zero fault tolerant. Launch lifetime. Shelf life of 2 years. Launch year open ended – current TRL assessment is an output. Laser density 5 MW/m ² Mass Growth per AIAA 120-2006 (add growth to make system level 30%)	
Mission, Ops, GN&C	Hydrogen/Nitrogen heated by laser heat exchanger, launch from ground to sub-orbit, circularization with laser (circular, >=400km alt., 30 deg. inc (+/-0.2 deg.) Y-P-R using high temp propellants. Beacon needs to be ~25 m out in front of vehicle to 'tune' laser to allow for a smaller heat exchanger / lower laser power	Gimballed main engine
Launch Vehicle	N/A	
Propulsion	2000 k heat exchanger primary propulsion; performs entire launch ΔV, same warm propellant for warm gas RCS	Main propellant choice: Hydrogen with H ₂ O or water for dense Isp phase. Option for atmospheric inlet for afterburner for thrust augmentation. Microthrusters on heat exchanger instead of a main engine. Pintle atm correcting engine
Power	Primary batteries	Thermal batteries, secondary
C&DH Communications	Pre-use flight computer to handle launch. Up-range telemetry communications.	Computer type, data storage, data transfer rates, comm. Frequencies
Thermal & Environment	Gather heat from laser to heat propellant for an expansion rocket.	Trade heat exchanger material / design. Safety issues with hitting active spacecraft
Mechanisms	Thruster Gimbal, separation systems	mechanisms, materials, power, ops,
Structures	aluminum	minimize mass,
Cost		
Risk	Major Risks: Laser heating on rest of vehicle	



Systems



13



Timeline

- Pad prep
- Jettison Thermal Cocoon (-5 sec)
- Launch (0 sec, 2 km): L1 laser only
- Drop Water tanks (x sec)
- Main laser in view (60 sec, 12 km): combined laser illumination
- Begin Beacon operation (80 sec, 25 km)
- Fairing Separation (100 sec)
- L1 laser off (180 sec, 100 km)
- Final insertion (400 sec, 400 km)
- Payload separation (500 sec)
- Launcher Deorbit maneuver (2500 sec?)

14



OTIS BEP-2 Mission Model



• Proposed vehicle is a SSTO vehicle

- first stage burns dense/light propellant (H₂/LH₂)
- second stage burns only LH₂ to deliver a fixed payload to a fixed 400 km circular orbit.
- OTIS switches from stage 1 to stage 2 at an optimally determined altitude for a given GLOM and propellant loads (supplied by the compass team).

• OTIS used to produce optimal trajectory for the microwave/heat exchanger stage of the vehicle (trajectory described below)

- Objective function: for a fixed initial mass, propellant loads and mixing ratio (compass team supplied) maximize mass to insertion of 400 km circular orbit.
- Trajectory (con-ops)
 - Vertical lift under power of the boost laser off to an optimal altitude.
 - Pitch over and burn to dense propellant cut-off (tank depletion).
 - H₂ tank jettison
 - LH₂ burn to 400 km circular orbit.

• Launch site near Vandenberg AFB, CA (fictional alt approx 2000 m). Boost ground station 20 km downrange and main station 400 km downrange

• Trajectory constraints:

- Power/thrust calculation constrains trajectory to stay in "view" and range of the laser stations while meeting flight objectives.



Power and Propulsion Details

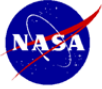


• Drag model

- Lift coefficient assumed to be 0.
- Drag coefficient calculated as prescribed by customer.
- Reference area for drag model is set to be 4 m² to account for main structure and H₂ tanks during ascent through atmosphere.
- It was beyond the scope of this simulation to fully account for drag and lift of heat exchanger and supporting structure. Any future work with this design should include a full examination of lift and drag and more representative models should be developed.

• Power/Propulsion model (key equations, constraints and assumptions)

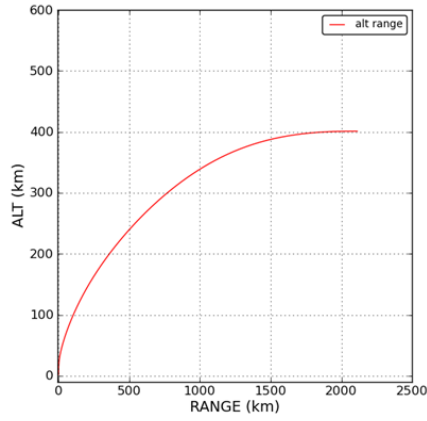
- Power received by the vehicle was modeled as a function of distance and orientation between the vehicle and the ground station(s). Power loss due to atmospheric losses and beam divergence were modeled in accordance to the customer's supplied equations.
- Received power was not allowed to exceed 220 MW (when the two ground stations combine power) in an attempt to minimize heating impact on the heat exchanger.
- The heat exchanger size of 25 m² was provided by the compass design team.
- Propulsion (thrust and ISP) were calculated as a function of received power and engine parameters. Isp was calculated as a function of altitude and differences between atmospheric and chamber pressures. (Chamber pressure was set to 25 atm).
- Nozzle efficiency was set to 95% (customer supplied) and a maximum vacuum ISP was determined as a function of nozzle expansion.



OTIS Results



ALT v. RANGE

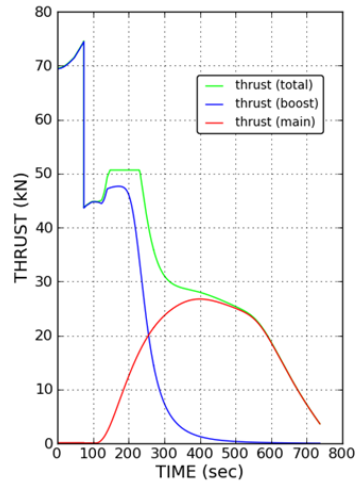
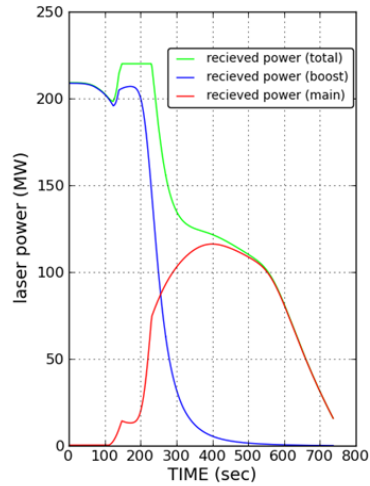


OTIS Results



received power

laser thrust

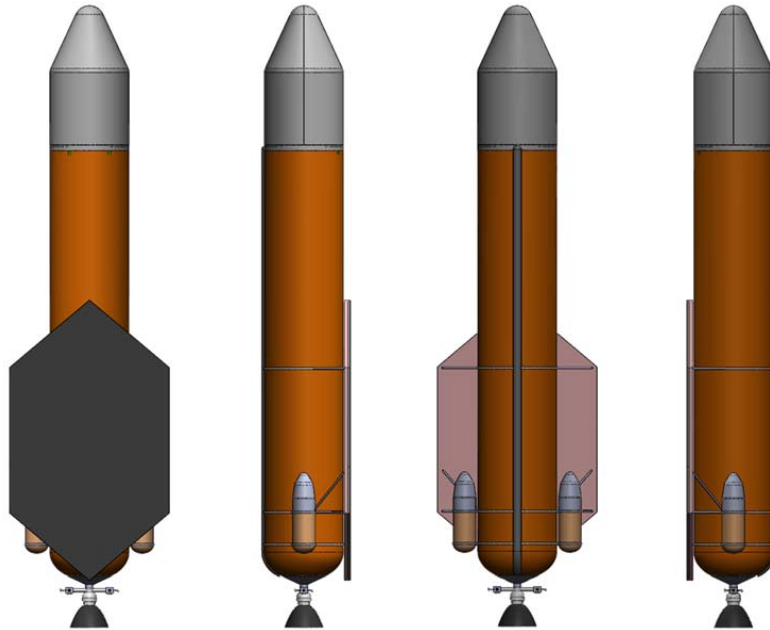


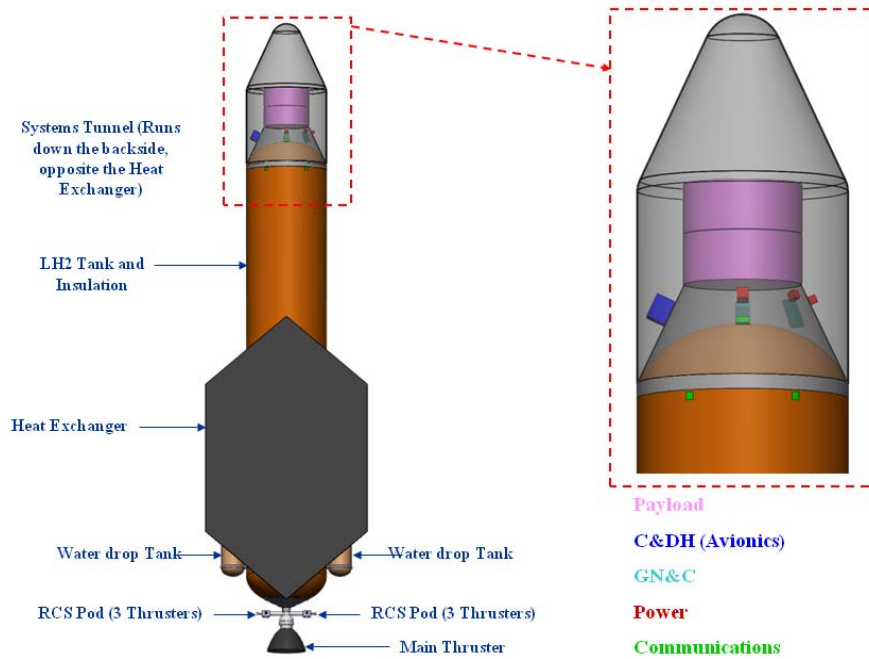
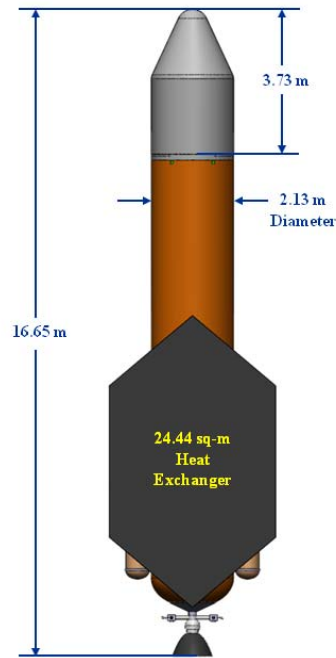


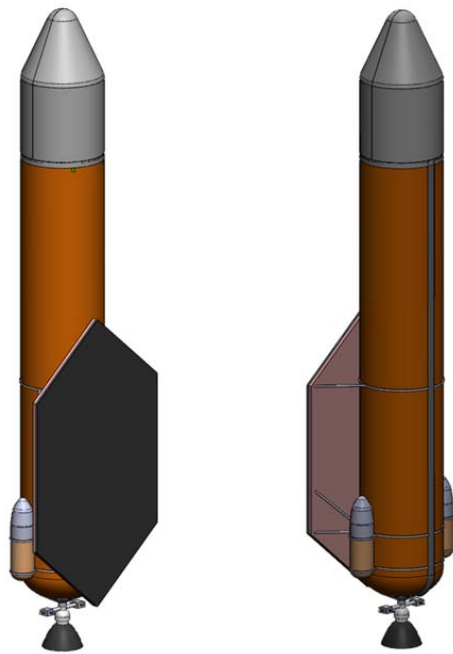
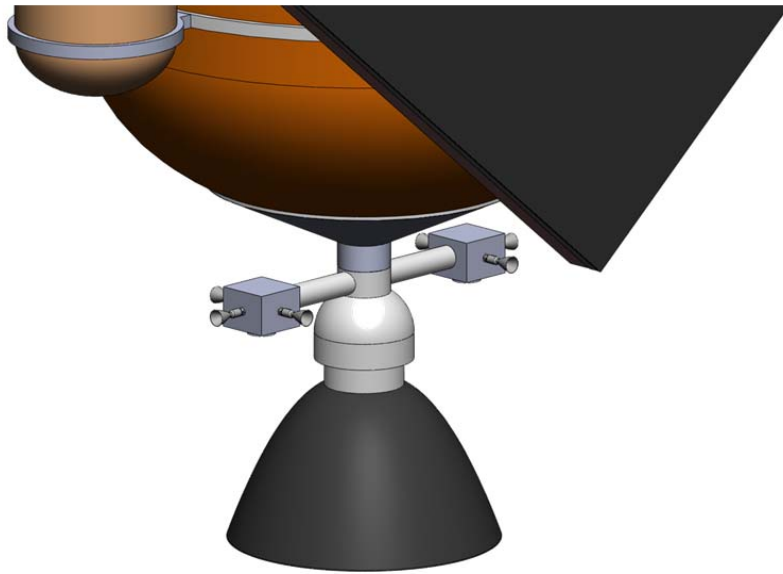
J. Kare Vehicle Mass and Delta-V Summary

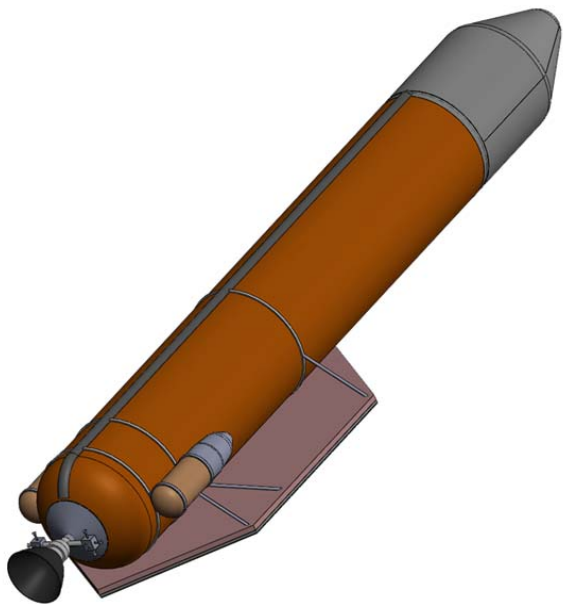
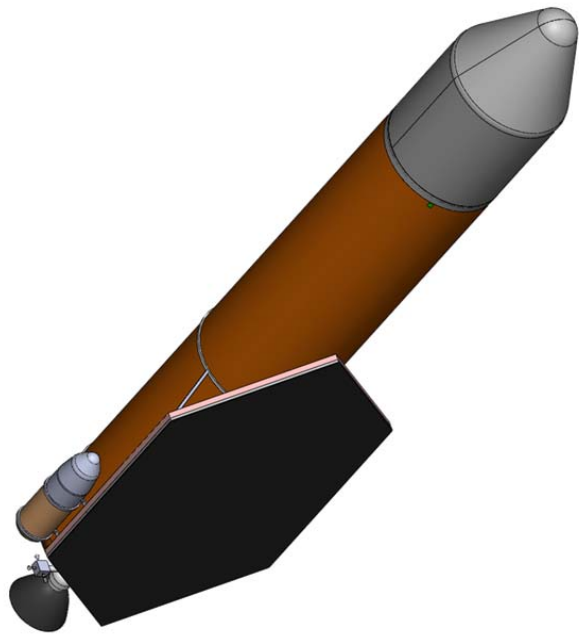


Mass and Delta-V Summary	
GLOM (kg)	5543
Stage 1 BO Mass (kg)	3970
Stage 1 H2O Consumed (kg)	1227
Stage 1 LH2 Consumed (kg)	346
Stage 1 delta-V (km/s)	1.131
Jettison Mass (kg)*	190
* (includes H2O tanks, struct, and RCS prop)	
Stage 2 BO Mass (kg) (optimal)	960
Stage 2 H2O Consumed (kg)	0
Stage 2 LH2 Consumed (kg)	2820
Stage 2 delta-V (km/s)	9.527
Total H2O (kg)	1227
Total LH2 (kg)	3166
Total delta-V (km/s)	10.658









Beamed Energy Propulsion (BEP) Thermal Laser Case 3: Preliminary System Summary

**Melissa L. McGuire,
Lead Systems Engineer
Design by COMPASS**

January 25, 2011

2

National Aeronautics and Space Administration

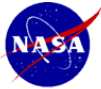


COMPASS Spacecraft Design Process



- Build Spacecraft MEL (Master Equipment List) in a WBS hierarchy by major subsystem down to a line item level appropriate to the level of design detail of the request
- Apply MGA from AIAA to each of the line items at the subsystem level
- Gather the total masses and calculate the total system growth % on the Basic dry mass
- Carry an additional system level (or program level) mass to reach a total of 30% mass book-kept on the dry Basic Mass

3



Mass Growth Allowance (MGA) Schedule

Taken from AIAA S-120-2006, *Standard Mass Properties Control for Space Systems*



- Basic Mass**
 - The current mass data based on an assessment of the most recent baseline design
 - NOTE 1 This design assessment includes the estimated, calculated, or measured (or actual) mass, and includes an estimate for undefined design details like cables, multi-layer insulation and adhesives.
 - NOTE 2 the mass growth allowances (MGA) and uncertainties are not included in the basic mass.
- Mass Growth Allowance (MGA)**
 - The predicted change to the basic mass of an item based on an assessment of the design maturity and fabrication status of the item, and an estimate of the in-scope design changes that may still occur
- Predicted Mass**
 - The basic mass plus the mass growth allowance

Code	Design maturity (basis for mass determination)	Electrical/electronic components			Percent MGA						
		0 to 5 kg	5 to 15 kg	>15 kg	Structure	Thermal control	Propulsion	Batteries	Wire harnesses	Mechanisms	Instrumentation
E	Estimated (preliminary sketches)	30	20	15	18	18	18	20	50	18	50
L	Layout (or major modification of existing hardware)	25	20	15	12	12	12	15	30	12	30
P	Prerelease drawings (or minor modification of existing hardware)	20	15	10	8	8	8	10	25	8	25
C	Released drawings (calculated values)	10	5	5	4	4	4	5	5	4	5
X	Existing hardware (actual mass from another program)	3	3	3	2	2	2	3	3	2	3
A	Actual mass (measured flight hardware)	0	0	0	0	0	0	0	0	0	0
FE	Customer furnished equipment	0	0	0	0	0	0	0	0	0	0

For the COMPASS process, the total percentage on dry mass is desired to be 30% total

$$\text{Predicted Mass} = \text{Basic Mass} + \text{Bottoms up MGA} \% \times \text{Basic Mass}$$

Therefore, Additional System level margin = 30% - Bottoms up MGA%

29



Top Level BEP 3 Characteristics



Spacecraft Master Equipment List Rack-up (Mass) - BEP Thermal Laser				COMPASS S/C Design	
WBS	Main Subsystems	Basic Mass (kg)	Growth (kg)	Total Mass (kg)	Aggregate Growth (%)
06	Thermal Laser Launcher Case 3	5302.0	115.2	5417.1	
06.1	Payload	80.0	0.0	80.0	0%
06.2	Launch Vehicle	5222.0	115.2	5337.1	2%
06.2.1	Attitude Determination and Control	5.0	0.7	5.6	14%
06.2.2	Command and Data Handling	9.05	2.7	11.8	30%
06.2.3	Communications and Tracking	3.0	1.0	4.0	32%
06.2.4	Electrical Power Subsystem	8.3	3.7	12.0	44%
06.2.5	Thermal Control	92.9	13.9	106.8	15%
06.2.6	Propulsion	444.4	54.8	499.2	12%
06.2.7	Propellant	4446.2		4446.2	0%
06.2.8	Structures and Mechanisms	213.2	38.4	251.6	18%
	Estimated Launch Vehicle Dry Mass (no payload)	776	115	891.0	15%
		5302	115	5417	
System Level Growth Calculations					Total Growth
	Dry Mass Desired System Level Growth (no payload)	776	233	1008.6	30%
	Additional Growth (carried at system level)		118		15%
	Total Wet Mass with Growth (w payload)	5302	233	5534.7	
		Basic Mass (kg)	Growth (kg)	Total Mass (kg)	
		776	233	5534.7	kg
	Total Spacecraft Wet Mass (w/growth)	5534.7			
	Mass of Dropped Tanks, jettisoned mass	169.9			
	Vehicle On Orbit Mass (incl residual/FPR, w P/L)	950.5		1000	kg
	OTIS total burn out mass	965.0			kg
	Additional margin	14.5			kg

- Inert mass is dry mass + trapped residuals + propellant margin + pressurant
- Dry mass on each segment is calculated as the total bottoms up dry mass with the MGA % applied + additional system mass so that the total growth on each stage is 30% of the basic mass
 - The dry basic mass of the BEP launcher without the payload is 776 kg
 - The Total dry mass with the bottom's up growth without the payload is 891 kg
 - The inert mass of the BEP launcher without the payload with 30% growth carried on the Basic masses is 1008 kg
- Mission applies the -Vs and the rocket equation to the appropriate total vehicle mass based on the mission event and what stages have been jettisoned
- Total inert mass (this includes the payload, trapped residuals) with the 30% growth incorporated is: 950 kg

30



BEP 3 – Top Level MEL (Master Equipment List)



WBS	Description	QTY	Unit Mass	Basic Mass	Growth	Growth	Total Mass
Number	BEP3 - Dec 2010 - Thermal Laser Case 3		(kg)	(kg)	(%)	(kg)	(kg)
06	Thermal Laser Launcher Case 3			5301.97	2.2%	115.16	5417.13
06.1	Payload			80.00	0.0%	0.00	80.00
06.1.1	Payload			80.00	0.0%	0.00	80.00
06.1.2	Additional Instruments			0.00	0	0.00	0.00
06.2	Launch Vehicle			5221.97	2.2%	115.16	5337.13
06.2.1	Attitude Determination and Control			4.95	14.0%	0.70	5.65
06.2.1.a	Guidance, Navigation, & Control			4.95	14.0%	0.70	5.65
06.2.2	Command and Data Handling			9.05	30.0%	2.72	11.77
06.2.2.a	Command & Data Handling			7.30	30.0%	2.19	9.49
06.2.2.b	Instrumentation & Wiring			1.75	30.0%	0.53	2.28
06.2.3	Communications and Tracking			3.00	31.7%	0.95	3.95
06.2.3.a	S Band			3.00	31.7%	0.95	3.95
06.2.3.b	Laser Beacon			0.00	0	0.00	0.00
06.2.3.c	Comm Avionics			0.00	0	0.00	0.00
06.2.3.d	Antennas			0.00	0	0.00	0.00
06.2.3.e	Communications Instrumentation			0.00	0	0.00	0.00
06.2.3.f	Misc#1			0.00	0	0.00	0.00
06.2.3.g	Misc#2			0.00	0	0.00	0.00
06.2.4	Electrical Power Subsystem			8.31	44.1%	3.66	11.97
06.2.4.a	Energy Storage			0.91	30.0%	0.27	1.18
06.2.4.b	Power Management & Distribution			1.56	30.0%	0.47	2.03
06.2.4.c	Power Cable and Harness			5.84	50.0%	2.92	8.76
06.2.4.d	Misc#1			0.00	0	0.00	0.00
06.2.4.e	Misc#2			0.00	0	0.00	0.00
06.2.5	Thermal Control			92.89	15.0%	13.93	106.82
06.2.5.a	Active Thermal Control			1.29	15.0%	0.19	1.48
06.2.5.b	Passive Thermal Control			17.72	15.0%	2.66	20.38
06.2.5.c	Heat Exchanger System			73.88	15.0%	11.08	84.96
06.2.6	Propulsion			444.38	12.3%	54.83	499.20
06.2.6.a	Propulsion Hardware			25.00	18.0%	4.50	29.50
06.2.6.b	Propellant Management			286.01	12.0%	34.32	320.33
06.2.6.c	Reaction Control System Hardware			12.36	12.0%	1.48	13.85
06.2.6.d	Misc#1			0.00	0	0.00	0.00
06.2.6.e	Drop Tank Assemblies			121.00	12.0%	14.52	135.52
06.2.6.f	Misc#2			0.00	0	0.00	0.00
06.2.6.g	Misc#3			0.00	0	0.00	0.00
06.2.6.h	Misc#4			0.00	0	0.00	0.00
06.2.7	Propellant			4446.15	0.0%	0.00	4446.15
06.2.7.a	RCS Propellant			21.09	0.0%	0.00	21.09
06.2.7.b	Propellant (Laser)			4425.07	0.0%	0.00	4425.07
06.2.7.c	Misc			0.00	0	0.00	0.00
06.2.7.d	RCS Pressurant	0	0.00	0.00	0.0%	0.00	0.00
06.2.8	Structures and Mechanisms			213.25	18.0%	38.38	251.63
06.2.8.a	Structures			180.35	18.0%	32.46	212.82
06.2.8.b	Mechanisms			32.89	18.0%	5.92	38.81

31



BEP 3 – Thermal Laser - Attitude Determination and Control MEL



WBS	Description	QTY	Unit Mass	Basic Mass	Growth	Growth	Total Mass
Number	BEP3 - Dec 2010 - Thermal Laser Case 3		(kg)	(kg)	(%)	(kg)	(kg)
06	Thermal Laser Launcher Case 3			5301.97	2.2%	115.16	5417.13
06.1	Payload			80.00	0.0%	0.00	80.00
06.2	Launch Vehicle			5221.97	2.2%	115.16	5337.13
06.2.1	Attitude Determination and Control			4.95	14.0%	0.70	5.65
06.2.1.a	Guidance, Navigation, & Control			4.95	14.0%	0.70	5.65
06.2.1.a.a	GPS	1	1.00	1.00	20.0%	0.20	1.20
06.2.1.a.b	IMU	1	2.95	2.95	10.0%	0.30	3.25
06.2.1.a.c	Beam Sensors	2	0.50	1.00	20.0%	0.20	1.20
06.2.1.a.d	Misc#1	0	0.00	0.00	0.0%	0.00	0.00

32



BEP 3 – Thermal Laser - Command and Data Handling (C&DH) MEL



WBS	Description	QTY	Unit Mass	Basic Mass	Growth	Growth	Total Mass
Number	BEP3 - Dec 2010 - Thermal Laser Case 3		(kg)	(kg)	(%)	(kg)	(kg)
06	Thermal Laser Launcher Case 3			5301.97	2.2%	115.16	5417.13
06.1	Payload			80.00	0.0%	0.00	80.00
06.2	Launch Vehicle			5221.97	2.2%	115.16	5337.13
06.2.1	Attitude Determination and Control			4.95	14.0%	0.70	5.65
06.2.2	Command and Data Handling			9.05	30.0%	2.72	11.77
06.2.2.a	Command & Data Handling			7.30	30.0%	2.19	9.49
06.2.2.a.a	FPGA-based IP e.g. PPC	1	0.60	0.60	30.0%	0.18	0.78
06.2.2.a.b	FPGA-based IP e.g. PPC	1	0.60	0.60	30.0%	0.18	0.78
06.2.2.a.c	Watchdog switcher	1	0.30	0.30	30.0%	0.09	0.39
06.2.2.a.d	Enclosure with power supply	1	1.20	1.20	30.0%	0.36	1.56
06.2.2.a.e	Command and Control Harness (data)	1	4.00	4.00	30.0%	1.20	5.20
06.2.2.a.f	Sensor & Discrete I/O card (DCIU)	1	0.60	0.60	30.0%	0.18	0.78
06.2.2.a.g	Misc #1	0	0.00	0.00	0.0%	0.00	0.00
06.2.2.a.h	Misc #2	0	0.00	0.00	0.0%	0.00	0.00
06.2.2.a.i	Misc #3	0	0.00	0.00	0.0%	0.00	0.00
06.2.2.a.j	Misc #4	0	0.00	0.00	0.0%	0.00	0.00
06.2.2.a.k	Misc #5	0	0.00	0.00	0.0%	0.00	0.00
06.2.2.a.l	Misc #6	0	0.00	0.00	0.0%	0.00	0.00
06.2.2.a.m	Misc #7	0	0.00	0.00	0.0%	0.00	0.00
06.2.2.b	Instrumentation & Wiring			1.75	30.0%	0.53	2.28
06.2.2.b.a	TVC Card	1	0.25	0.25	30.0%	0.08	0.33
06.2.2.b.b	Feed System Driver Card	1	0.25	0.25	30.0%	0.08	0.33
06.2.2.b.c	Ignition Card	0	0.00	0.00	30.0%	0.00	0.00
06.2.2.b.d	Separation System Card	1	0.25	0.25	30.0%	0.08	0.33
06.2.2.b.e	Thermocouple Ref. Card	1	1.00	1.00	30.0%	0.30	1.30

33



BEP 3 – Thermal Laser - Communications System MEL



WBS	Description	QTY	Unit Mass	Basic Mass	Growth	Growth	Total Mass
Number	BEP3 - Dec 2010 - Thermal Laser Case 3		(kg)	(kg)	(%)	(kg)	(kg)
06	Thermal Laser Launcher Case 3			5301.97	2.2%	115.16	5417.13
06.1	Payload			80.00	0.0%	0.00	80.00
06.2	Launch Vehicle			5221.97	2.2%	115.16	5337.13
06.2.1	Attitude Determination and Control			4.95	14.0%	0.70	5.65
06.2.2	Command and Data Handling			9.05	30.0%	2.72	11.77
06.2.3	Communications and Tracking			3.00	31.7%	0.95	3.95
06.2.3.a	S Band			3.00	31.7%	0.95	3.95
06.2.3.a.a	Transmitter/Receiver/BBP	1	2.00	2.00	30.0%	0.60	2.60
06.2.3.a.b	Power Amp	0	0.00	0.00	30.0%	0.00	0.00
06.2.3.a.c	Directional coupler	0	0.00	0.00	0.0%	0.00	0.00
06.2.3.a.d	CTN Diplexer	1	0.50	0.50	30.0%	0.15	0.65
06.2.3.a.e	S-Band Surge Protector	0	0.00	0.00	0.0%	0.00	0.00
06.2.3.a.f	LNA	0	0.00	0.00	0.0%	0.00	0.00
06.2.3.a.g	Patch Antenna	0	0.00	0.00	0.0%	0.00	0.00
06.2.3.a.h	Transmission Line(s), Cables	1	0.50	0.50	40.0%	0.20	0.70
06.2.3.a.i	Diplexer	0	0.00	0.00	0.0%	0.00	0.00
06.2.3.a.j	Coupler	0	0.00	0.00	0.0%	0.00	0.00

34



BEP 3 – Thermal Laser - Electrical Power Subsystem MEL



WBS	Description	QTY	Unit Mass	Basic Mass	Growth	Growth	Total Mass
Number	BEP3 - Dec 2010 - Thermal Laser Case 3		(kg)	(kg)	(%)	(kg)	(kg)
06	Thermal Laser Launcher Case 3			5301.97	2.2%	115.16	5417.13
06.1	Payload			80.00	0.0%	0.00	80.00
06.2	Launch Vehicle			5221.97	2.2%	115.16	5337.13
06.2.1	Attitude Determination and Control			4.95	14.0%	0.70	5.65
06.2.2	Command and Data Handling			9.05	30.0%	2.72	11.77
06.2.3	Communications and Tracking			3.00	31.7%	0.95	3.95
06.2.4	Electrical Power Subsystem			8.31	44.1%	3.66	11.97
06.2.4.a	Energy Storage			0.91	30.0%	0.27	1.18
06.2.4.a.a	Primary Battery	1	0.91	0.91	30.0%	0.27	1.18
06.2.4.a.b	Secondary Battery	0	0.00	0.00	0.0%	0.00	0.00
06.2.4.a.c	Thermal Battery	0	0.00	0.00	0.0%	0.00	0.00
06.2.4.a.d	Misc#1	0	0.00	0.00	0.0%	0.00	0.00
06.2.4.b	Power Management & Distribution			1.56	30.0%	0.47	2.03
06.2.4.b.a	Battery Regulator/Control	1	0.52	0.52	30.0%	0.16	0.68
06.2.4.b.b	Power distribution Unit	1	1.04	1.04	30.0%	0.31	1.35
06.2.4.b.c	Misc#1	0	0.00	0.00	0.0%	0.00	0.00
06.2.4.b.d	Misc#2	0	0.00	0.00	0.0%	0.00	0.00
06.2.4.b.e	Misc#3	0	0.00	0.00	0.0%	0.00	0.00
06.2.4.c	Power Cable and Harness			5.84	50.0%	2.92	8.76
06.2.4.c.a	Spacecraft Bus Harness	1	5.84	5.84	50.0%	2.92	8.76

35



BEP 3 – Thermal Laser - Thermal Control System MEL



WBS	Description	QTY	Unit Mass	Basic Mass	Growth	Growth	Total Mass
Number	BEP3 - Dec 2010 - Thermal Laser Case 3		(kg)	(kg)	(%)	(kg)	(kg)
06	Thermal Laser Launcher Case 3			5301.97	2.2%	115.16	5417.13
06.1	Payload			80.00	0.0%	0.00	80.00
06.2	Launch Vehicle			5221.97	2.2%	115.16	5337.13
06.2.5	Thermal Control			92.89	15.0%	13.93	106.82
06.2.5.a	Active Thermal Control			1.29	15.0%	0.19	1.48
06.2.5.a.a	Data Acquisition	1	1.00	1.00	15.0%	0.15	1.15
06.2.5.a.b	Thermocouples	29	0.01	0.29	15.0%	0.04	0.33
06.2.5.a.c	Misc#1	0	0.00	0.00	15.0%	0.00	0.00
06.2.5.a.d	Misc#2	0	0.00	0.00	15.0%	0.00	0.00
06.2.5.a.e	Misc#3	0	0.00	0.00	15.0%	0.00	0.00
06.2.5.a.f	Misc#4	0	0.00	0.00	0.0%	0.00	0.00
06.2.5.b	Passive Thermal Control			17.72	15.0%	2.66	20.38
06.2.5.b.a	Cold Plate	4	0.14	0.55	15.0%	0.08	0.64
06.2.5.b.b	Light Shield	1	16.65	16.65	15.0%	2.50	19.15
06.2.5.b.c	Misc#1	1	0.52	0.52	15.0%	0.08	0.59
06.2.5.b.d	Misc#2	0	0.00	0.00	15.0%	0.00	0.00
06.2.5.c	Heat Exchanger System			73.88	15.0%	11.08	84.96
06.2.5.c.a	Heat Exchanger	1	37.89	37.89	15.0%	5.68	43.57
06.2.5.c.b	Manifolds	1	35.99	35.99	15.0%	5.40	41.39

36



BEP 3 – Thermal Laser - Propulsion Hardware MEL



WBS	Description	QTY	Unit Mass	Basic Mass	Growth	Growth	Total Mass
Number	BEP3 - Dec 2010 - Thermal Laser Case 3		(kg)	(kg)	(%)	(kg)	(kg)
06	Thermal Laser Launcher Case 3			5301.97	2.2%	115.16	5417.13
06.1	Payload			80.00	0.0%	0.00	80.00
06.2	Launch Vehicle			5221.97	2.2%	115.16	5337.13
06.2.6	Propulsion			444.38	12.3%	54.83	499.20
06.2.6.a	Propulsion Hardware			25.00	18.0%	4.50	29.50
06.2.6.a.a	Primary Thrusters	1	25.00	25.00	18.0%	4.50	29.50
06.2.6.a.b	MISC	0	0.00	0.00	0.0%	0.00	0.00
06.2.6.a.c	Propulsion Structure			0.00	0	0.00	0.00
06.2.6.a.d	Misc#1			0.00	0	0.00	0.00
06.2.6.b	Propellant Management			286.01	12.0%	34.32	320.33
06.2.6.b.a	Primary Fuel Tank(s)	1	238.79	238.79	12.0%	28.65	267.44
06.2.6.b.b	Dense Fuel Tank	0	0.00	0.00	0.0%	0.00	0.00
06.2.6.b.c	Primary H2 Feed System	1	16.22	16.22	12.0%	1.95	18.17
06.2.6.b.d	Primary Dense Feed System	1	6.00	6.00	12.0%	0.72	6.72
06.2.6.b.e	TPA	1	25.00	25.00	12.0%	3.00	28.00
06.2.6.b.f	Start-up System	0	0.00	0.00	0.0%	0.00	0.00
06.2.6.b.g	Misc#1	0	0.00	0.00	0.0%	0.00	0.00
06.2.6.b.h	Misc#2	0	0.00	0.00	0.0%	0.00	0.00
06.2.6.b.i	Misc#3	0	0.00	0.00	0.0%	0.00	0.00
06.2.6.b.j	Misc#4	0	0.00	0.00	0.0%	0.00	0.00
06.2.6.c	Reaction Control System Hardware			12.36	12.0%	1.48	13.85
06.2.6.c.a	RCS Tank Subassembly	0	0.00	0.00	12.0%	0.00	0.00
06.2.6.c.b	RCS Propellant Management Subassembly	1	2.36	2.36	12.0%	0.28	2.65
06.2.6.c.c	RCS Thruster Subassembly	2	5.00	10.00	12.0%	1.20	11.20
06.2.6.c.d	Misc#1	0	0.00	0.00	0.0%	0.00	0.00
06.2.6.c.e	Misc#2	0	0.00	0.00	0.0%	0.00	0.00
06.2.6.d	Misc#1			0.00	0	0.00	0.00
06.2.6.e	Drop Tank Assemblies			121.00	12.0%	14.52	135.52
06.2.6.e.a	Drop Tank	2	52.00	104.00	12.0%	12.48	116.48
06.2.6.e.b	Pressurant Tank	0	0.00	0.00	12.0%	0.00	0.00
06.2.6.e.c	Pressurant Feed System	2	3.00	6.00	12.0%	0.72	6.72
06.2.6.e.d	Propellant Feed System	2	5.50	11.00	12.0%	1.32	12.32
06.2.6.e.e	Pressurant	0	0.00	0.00	0.0%	0.00	0.00
06.2.6.e.f	Residuals	2	0.00	0.00	0.0%	0.00	0.00

37



BEP 3 – Thermal Laser – Propellant MEL



WBS	Description	QTY	Unit Mass	Basic Mass	Growth	Growth	Total Mass
Number	BEP3 - Dec 2010 - Thermal Laser Case 3		(kg)	(kg)	(%)	(kg)	(kg)
06	Thermal Laser Launcher Case 3			5301.97	2.2%	115.16	5417.13
06.1	Payload			80.00	0.0%	0.00	80.00
06.2	Launch Vehicle			5221.97	2.2%	115.16	5337.13
06.2.6	Propulsion			444.38	12.3%	54.83	499.20
06.2.7	Propellant			4446.15	0.0%	0.00	4446.15
06.2.7.a	RCS Propellant			21.09	0.0%	0.00	21.09
06.2.7.a.a	RCS Propellant Used	1	20.88	20.88	0.0%	0.00	20.88
06.2.7.a.b	RCS Propellant Residuals (Unused)	1	0.21	0.21	0.0%	0.00	0.21
06.2.7.a.c	RCS Propellant Performance Margin (Unused)	1	0.00	0.00	0.0%	0.00	0.00
06.2.7.b	Propellant (Laser)			4425.07	0.0%	0.00	4425.07
06.2.7.b.a	Main Engine Propellant			4425.07	0.0%	0.00	4425.07
06.2.7.b.a	Hydrogen			3198.13	0.0%	0.00	3198.13
06.2.7.b.a	Fuel Usable	1	3166.46	3166.46	0.0%	0.00	3166.46
06.2.7.b.a	Fuel Margin	1	0.00	0.00	0.0%	0.00	0.00
06.2.7.b.a	Fuel Residuals (Unused)	1	31.66	31.66	0.0%	0.00	31.66
06.2.7.b.a	Dense Propellant			1226.94	0.0%	0.00	1226.94
06.2.7.b.a	Dense Propellant Usable	1	1226.94	1226.94	0.0%	0.00	1226.94
06.2.7.b.a	Dense Propellant Margin	1	0.00	0.00	0.0%	0.00	0.00
06.2.7.b.a	Dense Propellant Residuals (Unused)	1	0.00	0.00	0.0%	0.00	0.00
06.2.7.b.b	Pressurant	0	0.00	0.00	0.0%	0.00	0.00

38



BEP 3 – Thermal Laser - Structures and Mechanisms MEL



WBS	Description	QTY	Unit Mass	Basic Mass	Growth	Growth	Total Mass
Number	BEP3 - Dec 2010 - Thermal Laser Case 3		(kg)	(kg)	(%)	(kg)	(kg)
06	Thermal Laser Launcher Case 3			5301.97	2.2%	115.16	5417.13
06.1	Payload			80.00	0.0%	0.00	80.00
06.2	Launch Vehicle			5221.97	2.2%	115.16	5337.13
06.2.8	Structures and Mechanisms			213.25	18.0%	38.38	251.63
06.2.8.a	Structures			180.35	18.0%	32.46	212.82
06.2.8.a.a	Primary Structures			21.54	18.0%	3.89	25.42
06.2.8.a.a.a	AP Structure	1	9.59	9.59	18.0%	1.73	11.31
06.2.8.a.a.a.a	Forward Structure	0	4.00	0.00	18.0%	0.00	0.00
06.2.8.a.a.a.a.a	Inter-Tank Structure	0	0.00	0.00	18.0%	0.00	0.00
06.2.8.a.a.a.a.a.a	Shroud (nose)	1	11.96	11.96	18.0%	2.15	14.11
06.2.8.a.a.a.a.a.a.a	Misc#1	0	0.00	0.00	18.0%	0.00	0.00
06.2.8.a.a.a.a.a.a.a.a	Secondary Structures			158.81	18.0%	28.59	187.39
06.2.8.a.a.a.a.a.a.a.a.a	Heat Exchanger Structure	1	87.02	87.02	18.0%	15.66	102.68
06.2.8.a.a.a.a.a.a.a.a.a.a	Tank Mounting Hdw/H2 Propellant	1	18.18	18.18	18.0%	3.27	21.45
06.2.8.a.a.a.a.a.a.a.a.a.a.a	Tank Mounting Hdw/Dense Propellant	0	3.51	0.00	18.0%	0.00	0.00
06.2.8.a.a.a.a.a.a.a.a.a.a.a.a	Systems Tunnel	1	0.60	0.60	18.0%	0.11	0.71
06.2.8.a.a.a.a.a.a.a.a.a.a.a.a.a	Fairings (Hv Protection, etc.)	0	0.00	0.00	18.0%	0.00	0.00
06.2.8.a.a.a.a.a.a.a.a.a.a.a.a.a.a	Payload Adapter	1	3.43	3.43	18.0%	0.62	4.05
06.2.8.a.a.a.a.a.a.a.a.a.a.a.a.a.a.a	Drop Tank Attachment structure	2	13.35	26.71	18.0%	4.81	31.51
06.2.8.a.a.a.a.a.a.a.a.a.a.a.a.a.a.a.a	Drop Tank Attachment Structure, Vehicle	1	22.87	22.87	18.0%	4.12	26.99
06.2.8.a.a.a.a.a.a.a.a.a.a.a.a.a.a.a.a.a	Misc#3	0	0.00	0.00	0.0%	0.00	0.00
06.2.8.a.a.a.a.a.a.a.a.a.a.a.a.a.a.a.a.a.a	Misc#4	0	0.00	0.00	0.0%	0.00	0.00
06.2.8.b	Mechanisms			32.89	18.0%	5.92	38.81
06.2.8.b.a	Shroud Separation Mechanism			1.64	18.0%	0.29	1.93
06.2.8.b.a.a	Shroud Separation Mechanism	6	0.27	1.64	18.0%	0.29	1.93
06.2.8.b.a.a.a	Misc #1	0	0.00	0.00	0.0%	0.00	0.00
06.2.8.b.a.a.a.a	Payload Deployment Mechanism			0.82	18.0%	0.15	0.97
06.2.8.b.a.a.a.a.a	Payload Deployment Mechanism	3	0.27	0.82	18.0%	0.15	0.97
06.2.8.b.a.a.a.a.a.a	Misc#1	0	0.00	0.00	0.0%	0.00	0.00
06.2.8.b.a.a.a.a.a.a.a	Misc#2	0	0.00	0.00	0.0%	0.00	0.00
06.2.8.b.c	Communications Mechanisms			0.00	0	0.00	0.00
06.2.8.b.c.a	Tank Separation Mechanisms			2.27	18.0%	0.41	2.68
06.2.8.b.c.a.a	Tank Separation Mechanisms	2	1.14	2.27	18.0%	0.41	2.68
06.2.8.b.c.a.a.a	Misc#2	0	0.00	0.00	0.0%	0.00	0.00
06.2.8.b.c.a.a.a.a	Misc#1			0.00	0	0.00	0.00
06.2.8.b.c.a.a.a.a.a	Misc#2			0.00	0	0.00	0.00
06.2.8.b.d	Installations			28.16	18.0%	5.07	33.23
06.2.8.b.d.a	Science Payload Installation	1	3.20	3.20	18.0%	0.58	3.78
06.2.8.b.d.a.a	C&DH Installation	1	0.36	0.36	18.0%	0.07	0.43
06.2.8.b.d.a.a.a	Communications and Tracking Installation	1	0.12	0.12	18.0%	0.02	0.14
06.2.8.b.d.a.a.a.a	GNSS Installation	1	0.20	0.20	18.0%	0.04	0.23
06.2.8.b.d.a.a.a.a.a	Electrical Power Installation	1	0.33	0.33	18.0%	0.06	0.39
06.2.8.b.d.a.a.a.a.a.a	Thermal Control Installation	1	3.72	3.72	18.0%	0.67	4.38
06.2.8.b.d.a.a.a.a.a.a.a	Propulsion Installation	1	20.24	20.24	18.0%	3.64	23.88
06.2.8.b.d.a.a.a.a.a.a.a.a	Misc #1	0	0.00	0.00	0.0%	0.00	0.00

39



BEP Avionics Overview



- **Design Requirements**
 - Avionics for systems command, control, and health management
 - Single fault tolerant processor architecture
 - Low mass optimization required for BEP
 - Operational power modes vary according requirements, BEP quiescent until needed
- **Assumptions**
 - Cabling mass estimated with Monte Carlo simulation
- **Design Description**
 - Enclosure assumes 6U-160 cPCI form factor cards
 - FPGAs packaged with IP for processor capability,
 - Fail over to backup processor if one faults out or has SEU (reboot attempted)
 - Embedded software kernels without major O/S overhead
 - Memory 2 GB with EDAC
 - Power Supply using DC-DC converters, filter, and EMI shielding accept wide variations in supply voltage
 - Discretes and Power switching card for general vehicle functions
 - Sensor I/O card
 - RS422 interfaces between stages - 2 Mbps RS422 Manchester coded
 - Housekeeping data and H&S data to ground via comm at 4.8 kbps

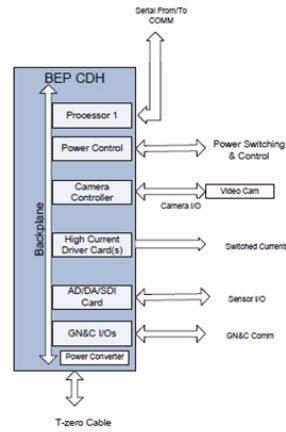
40



BEP Avionics Functionality



- **General Avionics Processors**
 - Power PC Intellectual Property in rad-hard FPGA
 - Avionics cPCI card cage. BEP uses stacked custom cards in closed box design
 - BEP navigation – data from IMUs
 - Systems health and status reporting
 - Card Power managed for various power modes (power trimmed with specialized sentinel switching)
 - System management – includes control of valves, heaters, PMAD
 - System fault detection fail over must respond quickly during BEP Transport launch
 - Dual 2 Mbps bps serial interfaces between stages and comm channels at 4.8 kbps.
 - ROM SLOC estimate ~80k. Includes auto sequenced BEP launch.
- **Sensors/Drivers**
 - TBD valves, TBD pumps, TBD pressure & temperature



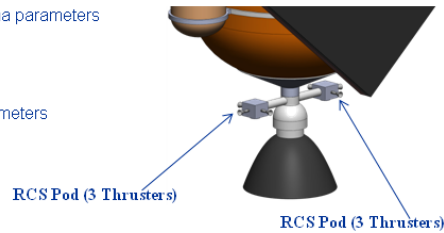
41



BEP DRM 1B – GNC



- **Requirements**
 - Single fault safe
 - Maintain vehicle attitude so the heat exchanger is incident to the laser
- **Design**
 - 1 Honeywell HG9900 IMU
 - Mass of 2.95 kg
 - Honeywell GG1320AN Digital Laser Gyros 1-sigma parameters
 - Bias stability < 0.0035 deg/hr
 - Angle Random Walk < 0.002 deg/rt*hr
 - Scale Factor < 5.0 ppm,
 - Honeywell QA2000 Accelerometers 1-sigma parameters
 - Bias < 25 µg
 - Scale Factor < 100 ppm
 - 1 Surrey SGR1020 GPS Receiver
 - Mass of 1.0 kg
 - Includes 4 antennas
 - Aid in state estimation, including attitude determination
 - 2 Beam Sensors
 - Provides knowledge of the direction of the laser
 - Control is provided by 6 RCS thrusters located below the heat exchanger
 - 2 pods of 3 provide pitch, yaw and roll control
 - Guidance
 - Open loop pitch profile uploaded before launch



42



BEP DRM 1B – GNC



- **Future Work / Recommendations**
 - Analyze aerodynamic stability
 - The heat exchanger may require additional aerodynamic design of the vehicle
 - Due to time constraints, this was not analyzed
 - Analyze controllability using RCS thrusters
 - Common thrust level of 100 lbf for all thrusters was calculated for a adequate control authority to counter act disturbance torques
 - Design may require different thrust levels for different axes
 - Conduct Monte Carlo analysis
 - Assess orbit injection accuracy
 - Assess footprint dispersions of drop tanks
- **Risks**
 - Possible loss of control due to RCS thrusters getting hit by the laser

43



BEP DRM 1B – Mission Delta-V



Phase Name	Pre-Burn Mass kg	Avg. Delta-V m/s	Avg. Isp s	Dense Prop kg	Light Prop kg	RCS Prop kg	Total Prop kg	Mass Drop kg	Post Burn Mass kg
Phase 1 Burn	5535.7	1120.0	345.3	1226.9	346.1	0.0	1573.0	0.0	3962.7
Drop Tank & Structure	3962.7	***	***	***	***	***	***	169.9	3792.8
Disturbance Torques	3792.8	15.6	300.0	0.0	0.0	20.1	20.1	0.0	3772.7
Phase 2 Burn	3772.7	9571.0	708.9	0.0	2820.4	0.0	2820.4	0.0	952.3
Separate	952.3	2.0	250.0	0.0	0.0	0.8	0.8	871.5	80.0
Total	***	10708.6	***	1226.9	3166.5	20.9	4414.3	***	***

44

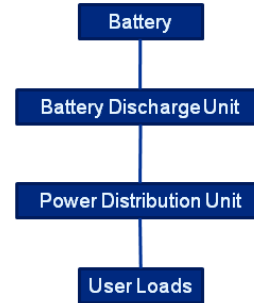


BEP DRM 1B Power System

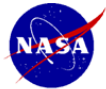


- **Requirements:**
 - No redundancy, single string (i.e. no redundant battery cells, harnessing)
 - User power = 189 W (includes 30% growth)
 - Life = 41.7 minutes
 - Energy capacity required = 131 W-hr

- **Assumptions**
 - 28 Vdc
 - Advanced Primary Lithium battery = 200 W-hr/kg, 400 W-hr/L, 80% depth of discharge (DOD)
 - Battery discharge unit (BDU) efficiency loss = 5%
 - BDU specific power = 366 W/kg
 - Power distribution unit (PDU) loss = 5%
 - PDU specific power = 182 W/kg



45



BEP DRM 1B Power System



- **Design Description**
 - 1 advanced primary Lithium battery
 - Provides 182 W-hr (this is the energy capacity necessary to overcome the losses due to DOD, BDU and PDU in efficiencies, and still provide the spacecraft with 131 W-hr)
 - Size = 7.68 x 7.68 x 7.68 cm
 - Mass = 0.91 kg
 - TRL 3
 - 1 battery discharge unit
 - Size = 8.58 x 8.58 x 8.58 cm
 - Mass = 0.52 kg
 - TRL 6
 - 1 power distribution unit
 - Size = 11.7 x 11.7 x 11.7 cm
 - Mass = 1.04 kg
 - TRL 6
 - 1 power harness
 - 5.84 kg (based on spacecraft dry mass)
 - TRL 6

Description	QTY	Unit	Basic	Growth	Growth	Total Mass
		Mass	Mass	(%)	(kg)	(kg)
		(kg)	(kg)			
Electrical Power Subsystem			8.31	44.1%	3.66	11.97
Energy Storage			0.91	30.0%	0.27	1.18
Primary Battery	1	0.91	0.91	30.0%	0.27	1.18
Power Management & Distribution			1.56	30.0%	0.47	2.03
Battery Regulator/Control	1	0.52	0.52	30.0%	0.16	0.68
Power distribution Unit	1	1.04	1.04	30.0%	0.31	1.35
Power Cable and Harness			5.84	50.0%	2.92	8.76
Spacecraft Bus Harness	1	5.84	5.84	50.0%	2.92	8.76

46



BEP DRM 1B Power System Trades



- **Battery technology**
 - For this study, both thermal and primary batteries were considered. Thermal batteries can tolerate high current draws, but have a lower specific energy (~75 Whr/kg) than primary batteries and therefore are more massive. Additionally, thermal batteries generate significant amounts of heat that must be radiated away from the spacecraft, which adds complexity and mass to the thermal subsystem. Therefore, primary batteries were chosen for this mission application. Secondary lithium batteries have higher current capabilities than primary lithium batteries so could also be used. For this study, only projected/advanced batteries/properties were considered, so it is moot which type is assumed.
- **Battery sizing strategy**
 - Batteries can either be sized to provide a specified energy or a specified current at a given voltage level. To size the batteries for a specific current and voltage, data from an existing battery is required. For this mission, a SAFT primary lithium sulfur dioxide cell (LO 26 SHX) had been chosen. The spacecraft loads require at most 7 A at 28 V. To meet these requirements, 22 of the SAFT cells were required, which resulted in a battery mass of 2.43 kg. To reduce the power system mass, it was decided to size the batteries based solely on the energy requirement which would rely on projected/new space rated cells suitable for this specific mission application. Since the specific properties (current versus voltage) for these projected cells are not known, limitations of current discharge cannot be included into the sizing.

47



BEP DRM 1B Power System Risks



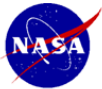
- **0 fault tolerance for all power system components – failure in one of the components will likely result in loss of mission. A detailed design of the battery (cell bypass due to failure) was not done due to the unknown properties of the projected cells. It is possible that the battery could be designed to accommodate a loss of a cell and operate at higher DOD and not lose the mission.**

48



Thermal

49

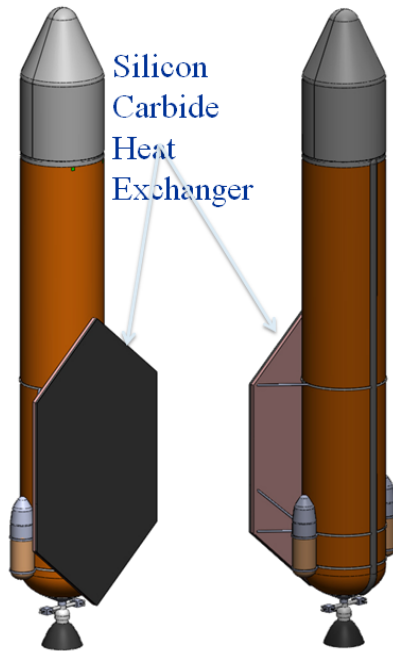


Thermal Subsystem - Description

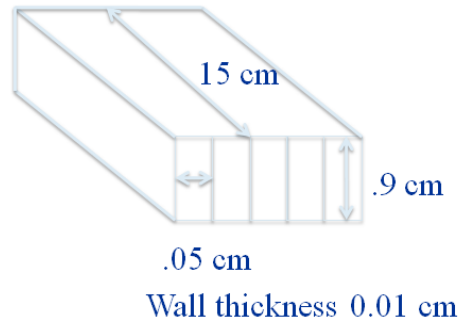


- **Thermal Components and Assumptions Summary**
 - Main heat exchanger is used to absorb laser radiation and heat hydrogen gas. Heat exchanger is constructed of channels through which the hydrogen gas flows. The main heat transfer is conduction through the walls to laminar flow of the hydrogen gas.
 - Desired exit temperature of the hydrogen gas is at 2000 K
 - Maximum wall temperature of the heat exchanger is 3000 K
 - Heat exchanger is constructed of silicon carbide.
 - Emissivity of the outer heat exchanger is 0.3
 - Operating scheme: liquid hydrogen is pumped to the heat exchanger, vaporized and heated to the desired temperature. It then flows to the engine and is expanded to produce thrust. Some initial flow is bled off to be utilized in the reaction control system.
 - A thin layer, 1 cm, of foam insulation is used on the tank wall to reduce boil off of the liquid hydrogen.
 - 10 cm of insulation is used behind the heat exchanger to minimize heat transfer to the propellant tank.
- **Environmental models**
 - An energy balance is performed between the incoming laser radiation and the heat losses of the system to determine the heat exchanger size and hydrogen temperature.
 - Heat losses from the system include: Heat transfer to the hydrogen gas, convection to the atmosphere, radiation to the atmosphere and vaporization of the liquid hydrogen.
- **Thermal System Mass: 92.89 kg**
- **Options to Reduce mass and recommendations:**
 - A more detailed analysis of the heat exchanger including gradients along its surface should be performed.
 - A more detailed analysis of the heat loss mechanisms should be performed to provide a high fidelity estimate of the heat exchanger performance.
 - The structural integrity of the heat exchanger should be evaluated.

Heat Exchanger Sizing



- The heat exchanger utilized laminar flow rectangular channels through which the hydrogen gas would flow through and be heated.
- The heating mechanism is through conduction from the heat exchanger wall.
- A manifold on the back side of the heat exchanger brings in the cold hydrogen and removes the hot hydrogen gas. Since the segments are only 15 cm in length this manifold will need to be incorporated along the complete backside of the heat exchanger



National Aeronautics and Space Administration

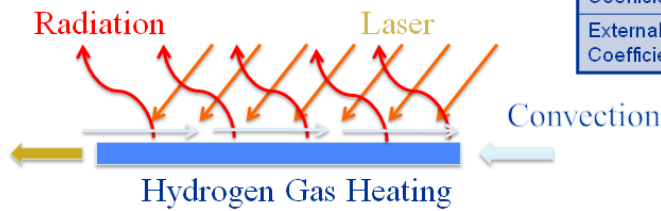


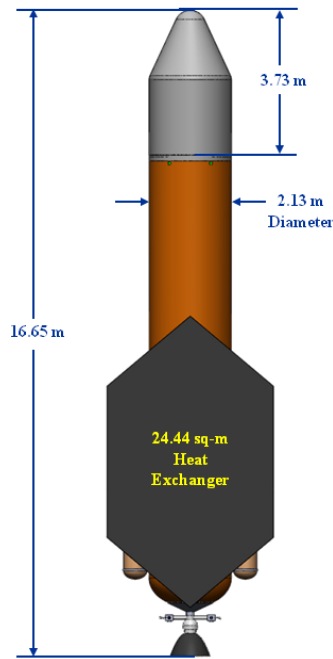
Heat Exchanger Energy Balance



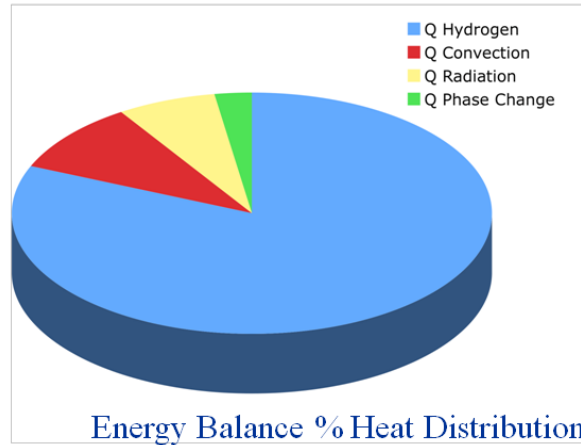
- Based on the incoming power from the laser an energy balance on the heat exchanger was set up to determine its operating temperature.
- The heat exchanger model was based on a first principles analysis of the incoming laser power to the heat transfer to the flowing hydrogen gas and heat losses through radiation and convection to the atmosphere. From the area a series of scaling equations were used to determine the mass of the radiator, flow rate of hydrogen and hydrogen exit temperature.

Variable	Value
Heat Exchanger Emissivity	0.3
Hydrogen Inlet Temp	20 K
Hydrogen Inlet Pressure	50 bar
Silicon Carbide Conductivity	120 W/mK
Incoming Laser Power	220 MW
Hydrogen Flow Rate	11.7 kg/s
Internal Convective Coefficient	6845 W/m ² K
External Convective Coefficient	414 W/m ² K





Power Component for Total Energy Balance	Value
Incoming Laser Power	220 MW
Heat Transfer to Hydrogen	179.1 MW
Heat Lost due to External Convection	20.7 MW
Heat Lost due to Radiation from the Heat Exchanger	14.4 MW
Heat Needed to Boil the Liquid Hydrogen	5.8 MW



National Aeronautics and Space Administration



Risks



The main risk with the thermal system deals with the operation and integrity of the heat exchanger.

Structural Integrity

The structural integrity of the heat exchanger is a major risk of the system. To achieve the required heat transfer capabilities the heat exchanger walls were very thin. This thin wall construction can cause significant structural problems due to the various loadings that the heat exchanger will experience. These include:

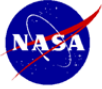
- Aerodynamic loading during ascent
- Thermal stresses due to the large temperature variations encountered during the launch
- The temperature gradient experienced across the heat exchanger during operation
- The high internal pressure due to the heating and expanding hydrogen gas.

Heat Exchanger Operational Feasibility

The operational feasibility of the heat exchanger concerns the ability to transfer the required amount of laser energy to the hydrogen gas and the ability to construct the heat exchanger to provide the flow characteristics needed to achieve this heat transfer.

A simplifying assumption made during the analysis was that the dividing walls between the fluid passages of the heat exchanger was operating at the same temperature as the heat exchanger surface. This assumption is very optimistic. Under actual conditions this inner wall will be at a temperature gradient less than that of the surface. Further more detailed analysis should be performed to determine what the temperature gradient is and what effect it has on the heat exchanger operation.

The heat exchanger design utilized a complex manifold that brought in the cool hydrogen gas and collected the hot hydrogen gas at spacing of 15 cm over the total area of the heat exchanger. This complex manifold arrangement and the subsequent heat losses associated with it need to be analyzed in much greater detail to assess its feasibility.



Propulsion

55



Requirements and Assumptions

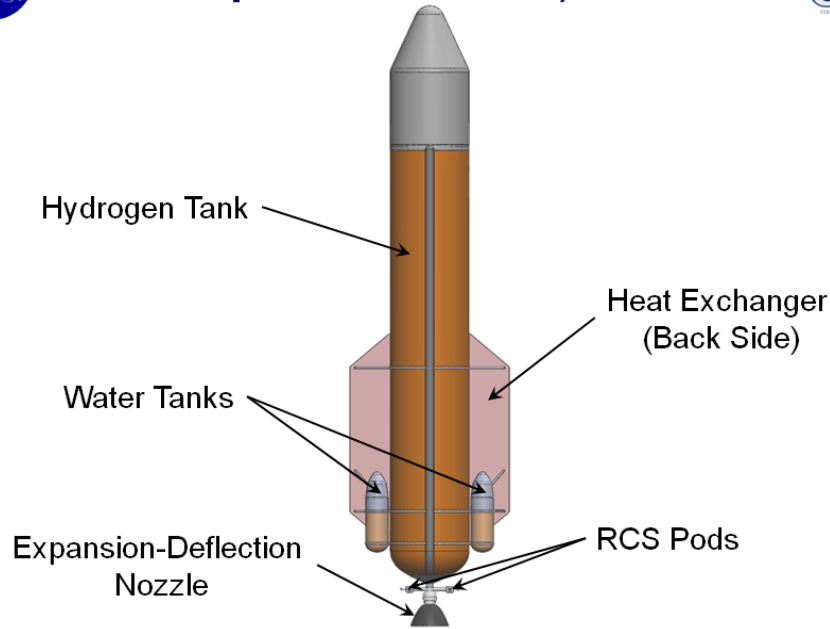


- **Requirements**
 - Zero Fault Tolerant System
 - Laser Energy Beamed from Ground Station(s) Provides Thermal Energy for Propulsion System
 - Monopropellant Main Propulsion System
 - No Chemical Combustion for Primary Propulsion
- **Assumptions**
 - Expansion-Deflection Nozzle for Primary Propulsion
 - Throat Sized for Take Off Thrust and Mass Flow Requirements
 - Requires Lower Chamber Pressure During Rest of Ascent
 - Expander Cycle Based System
 - Dense Propellant Utilized During Take-Off Only
 - Laser System Can Continuously Track and Beam Energy to Vehicle Heat Exchanger
 - Adequate Thermal Performance from Primary Heat Exchanger
 - RCS to Provide Attitude Control

56



Propulsion Overview, Cont.



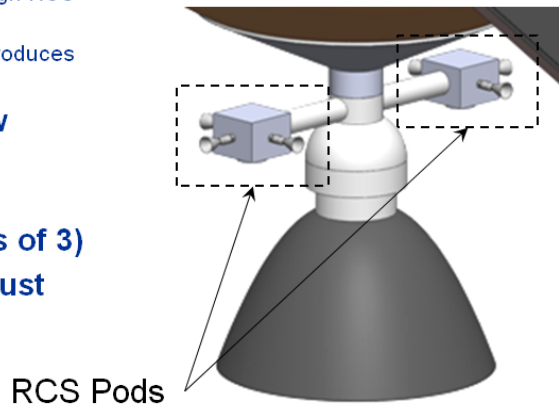
58



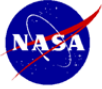
RCS



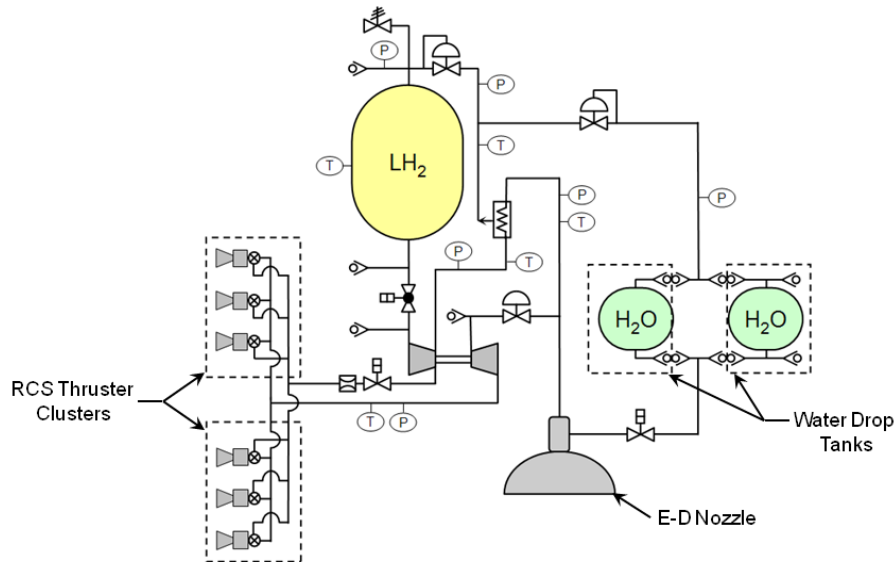
- **RCS Propellant Derived from Turbine Exhaust Flow**
 - Continuous Flow Through RCS System
 - Differential Throttling Produces Resultant Force
- **Some Cooling Flow Required for Valve Actuators**
- **6 Thrusters (2 Pods of 3)**
- **Nominal 100lbf Thrust**



59



Preliminary P&ID



Risks



- Maintenance of Appropriate Beam Angle Relative to Vehicle Heat Exchanger
- Excessive Heating of Heat Exchanger Walls
- Potential Material Temperature Limitation Issues
- Hot Hydrogen Rapidly Corroding the Carbon-Carbon Components
- Water Injector Operability and Adequate Flow Mixing
- Inadequate RCS Control Authority with Turbine Exhaust Flow
- Cooling of RCS Actuators
- Tank Over-Pressurization Due to Excessive Heat Leak
- Adverse Thermal Interactions with Aft Vehicle Structure and Hydrogen Tank



Future Trades



- **Different Dense Propellants**
 - Ammonia
 - Methane
 - Liquid Nitrogen
- **Traditional RCS System (Hydrazine, etc.)**
- **Different Take-Off Assist Methods**
 - Solid Boosters
 - Air Launch
- **Utilizing Tank Heat Leak to Pressurize Tank**
- **Gimbal on Main Nozzle to Reduce RCS**
- **Aerospike Nozzle**

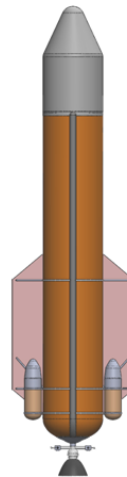
62



Structure Subsystem - Description



- **Structures and Mechanisms Design Requirements**
 - Contain necessary hardware for research instrumentation, avionics, communications, propulsion and power
 - Withstand applied mechanical and thermal loads from launching and operation
 - Provide minimum deflections, sufficient stiffness, and vibration damping
 - Minimize weight



DRM 1B Launch Vehicle

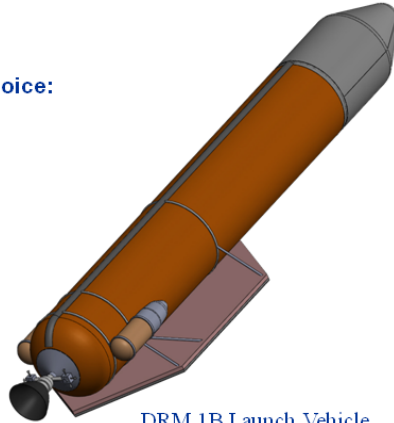
63



Structure Subsystem - Description



- **Structures assumptions**
 - Provides main structures backbone for BEP vehicle
 - Materials: aluminum, graphite/epoxy, c/c
 - Shells with flanges
 - Bonded, welded and threaded fastener assembly
- **The structures subsystem**
 - Shells or thrust tube bearing all operational loads
 - Science probes, payload to support
 - Load bearing, structurally integrated LH2 tank
- **Main structure material and design choice:**
 - Graphite/epoxy shells with aluminum flanges
 - TRL6
- **Primary Structure mass:**
 - Graphite/epoxy shells with aluminum flanges
- **Secondary Structure Mass:**
 - Aluminum, graphite/epoxy, c/c construction
 - Installations
- **Separation mechanisms**
 - Shroud separation, pyrotechnic fasteners & springs
 - Payload deployment, pyrotechnic fasteners & springs
 - Tank separation, pyrotechnic fasteners & springs



DRM 1B Launch Vehicle

64



Structure Subsystem - Description



- **Design Highlights**
 - g/epoxy, c/c, Aluminum components
 - Flanges for joining sections and mounting internal hardware of aluminum
 - c/c w/environmental barrier coating (EBC) support for heat exchanger, 2000+ ° C
- **Analytical Methods**
 - Analytical methods with spreadsheet for stress analysis
 - Stresses
 - Shroud – aerodynamic load 6 kN
 - 3.1 kPa
 - Propellant tank check for buckling (Roark's Formulas for Stress & Strain)
 - 171 MPa w/0.8 mm wall thickness providing positive margin with 46 MPa max. operating load
 - Payload adapter
 - 5.6 MPa $\ll \sigma_y$ including 1.5 s.f.
 - Mass for installations
 - 4% of mass of installed hardware
 - Science Payload
 - C&DH
 - Communications & Tracking
 - GN&C
 - Electrical Power
 - Thermal Control
 - Propulsion
- **Trades considered in analysis**
 - c/epoxy replaced aluminum for necessary weight reduction
 - c/c implemented due to high temperature of supported hardware
- **Options to Reduce mass and recommendations:**
 - Detailed stress analysis using FEA

65

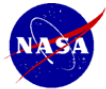


Mechanisms Subsystem - Description



- **Mechanisms assumptions**
 - Provide separation functions for shroud, payload, and tanks
- **Mechanisms Mass:**
 - 1.64 kg mass for shroud
 - 0.82 kg for payload
 - 2.27 kg total for tanks
- **Trades considered in analysis**
 - None at this time

66



Cost Assumptions



- **DRAFT Cost Estimate based on COMPASS design**
- **All costs are in FY11\$M**
- **Estimates represent prime contractor cost plus fee (10%)**
- **This estimate assumes the following:**
 - Proto-flight development approach
 - Full set of ground spares included
 - Model assumes TRL Level 6
 - This estimate does not include any cost for technology development
 - Represents the mean estimate based on cost-risk simulation results
 - Parametric estimate based on mostly mass based CERs from historical cost data
 - Planetary systems integration wraps
 - Software not included
- **Does not include:**
 - Any insight/oversight costs (by a NASA lead center)
 - Reserves (can be as high as 40-50%)
 - Ground System Cost (ie. Laser)
 - Launch Services Costs (ie. Special launch approval process)
 - Technology costs for components lower than TRL-6

67



BEPS Preliminary Cost ROM

(Represents estimated Prime Contractor cost)



WBS	Description	DDT&E Total BY \$M	Flight HW BY \$M	DD&FH Total BY \$M
06.1.1	Payload	0.0	0.0	0.0
06.2.1	Attitude Determination and Control	2.6	2.4	4.9
06.2.2	Command and Data Handling	4.3	2.6	6.9
06.2.3	Communications and Tracking	1.1	0.8	1.8
06.2.4	Electrical Power Subsystem	1.0	1.1	2.1
06.2.5	Thermal Control	22.7	4.2	26.9
06.2.6	Propulsion	14.0	6.2	20.2
06.2.7	Propellant	0.0	0.0	0.0
06.2.8	Structures and Mechanisms	15.2	7.6	22.8
	Subtotal	60.9	24.8	85.7
	Systems Integration	46.5	8.0	54.5
	Spacecraft Total	107.4	32.8	140.2

All Costs in FY11\$M

3.1.5 Laser Thermal Consultant Report—Design Reference Mission 1–B

Design Reference Mission 1–B (DRM 1–B) is based on the laser-heated heat exchanger (HX) vehicle originally proposed by Kare (Ref. 1) and since elaborated on (Refs. 2 and 3). The beam source is an array of “beam modules”—small, independent lasers and associated beam directors, not mutually coherent—that individually track the vehicle (Ref. 4). This approach allows the laser array to be developed at the single-module scale for minimal cost. Current off-the-shelf industrial laser technology is sufficient to build a launch system, but more advanced lasers can be incorporated as they become available.

The nominal reference mission was to launch 100-kg payloads (independent satellites or consumables such as tanks of propellant) to circular orbit (nominally 34° inclined, 300- to 400-km altitude), with a capacity of 1000 launches per year. The overall concept of operations (CONOPS) is shown in Figure 3.86.

3.1.5.1 Description of Vehicle

3.1.5.1.1 Overview

The general propulsion concept is shown in Figure 3.86. An inert liquid propellant is pressure-fed or pumped through an HX, which absorbs the laser energy and transfers it to the propellant, vaporizing it and heating it to high temperature. The hot propellant is exhausted from a more-or-less conventional nozzle.

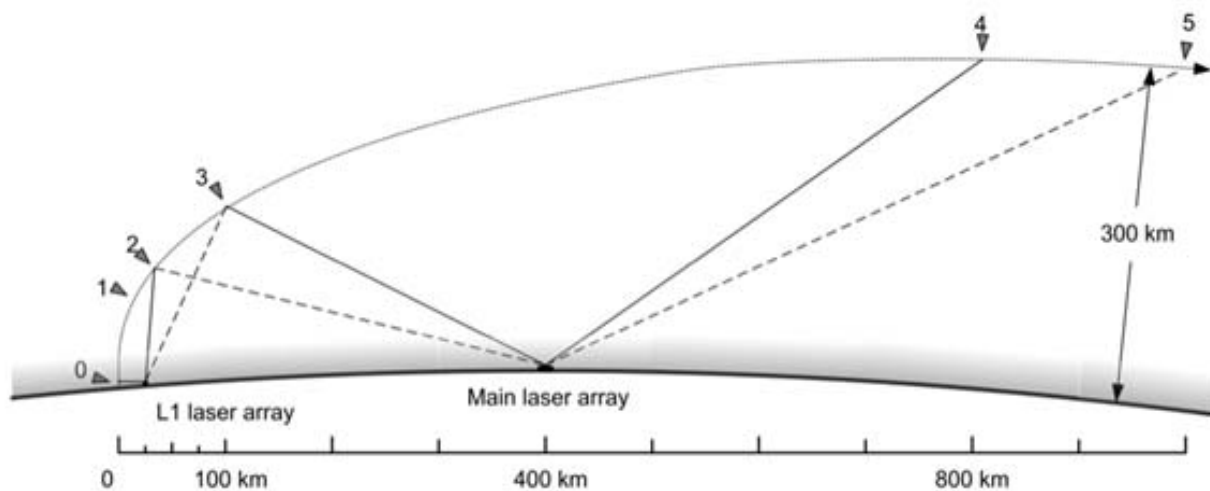


Figure 3.86.—Typical launch concept of operations with L1 (boost) laser array. Markers: (0) Launch. (1) Main array “sees” vehicle and begins tracking. (2) Main array turns on; L1 array at maximum full-power range. (3) Main array at full power; L1 array turns off. (4) Vehicle pitches down to circularize orbit. (5) Orbit insertion; main laser turns off. Copyright Kare Technical Consulting; used with permission.

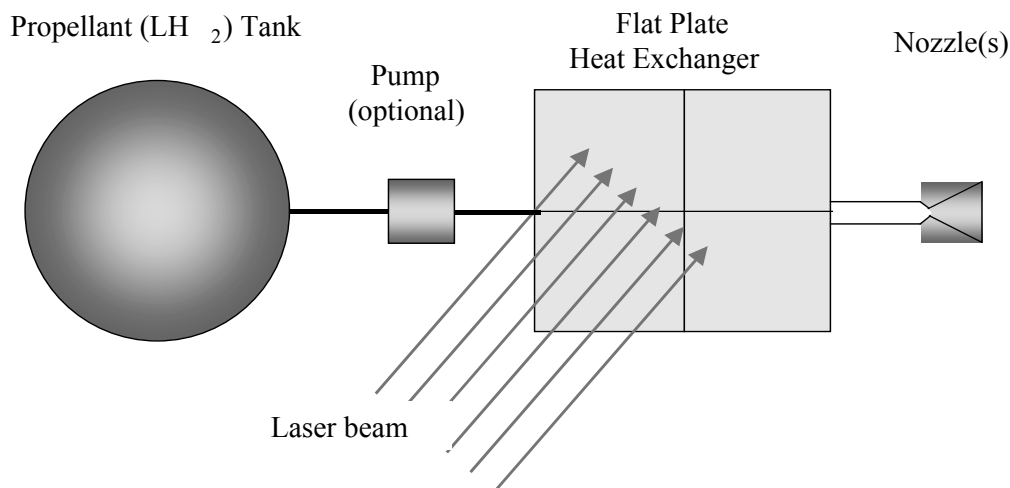


Figure 3.87.—HX thruster concept; LH₂, liquid hydrogen. Copyright Kare Technical Consulting; used with permission.

Relative to other beamed-energy propulsion (BEP) approaches, notably pulsed-detonation thrusters, the HX thruster has several important advantages:

High efficiency.—Exhaust kinetic power/laser power up to ~90%

Wide beam-acceptance angle.

Thrust direction independent of receiver orientation.—Receiver can be oriented as needed to satisfy drag or beam-angle constraints

Large receiver area.—Allows comparatively high beam divergence and small apertures

No onboard focusing optics or windows.

Easy to design/develop.—Remainder of propulsion system is essentially conventional

Works with any laser.—Ground or suborbital flight testing can use any available laser or low-cost “bare” diode arrays

Testable with non-laser heat sources.—Ground testing can use resistive or combustion heating

However, the HX thruster does have two major (and related) disadvantages: It has an upper limit on the propellant temperature, set by the material properties of the HX, and it requires hydrogen propellant to achieve high (>500 s) specific impulse I_{sp} .

One feature of the HX thruster not shown in Figure 3.87 is that the propellant composition, and thus the exhaust velocity and I_{sp} can be varied in flight. In particular, a denser propellant such as water or liquid nitrogen can be used instead of, or in addition to, liquid hydrogen for the early, low-velocity part of the launch trajectory. Increasing the mean molecular weight of the propellant (and the mass flow), while keeping the HX temperature constant, yields increased thrust for a given laser power.

3.1.5.1.2 HX

3.1.5.1.2.5 DRM vehicle HX baseline

The baseline HX design approach is a laminar flow microchannel HX, based on the original work of Tuckerman (Ref. 5). This type of HX has heat transfer characteristics that are nearly independent of the gas flow velocity, and thus, it can be designed for low flow velocity with many parallel channels, as shown in Figure 3.88. This gives a very low pressure drop in the HX, which is enabling, or at least highly

desirable, for a pressure-fed system but is less critical if a propellant pump is used. It also keeps the gas flow far from sonic velocity.

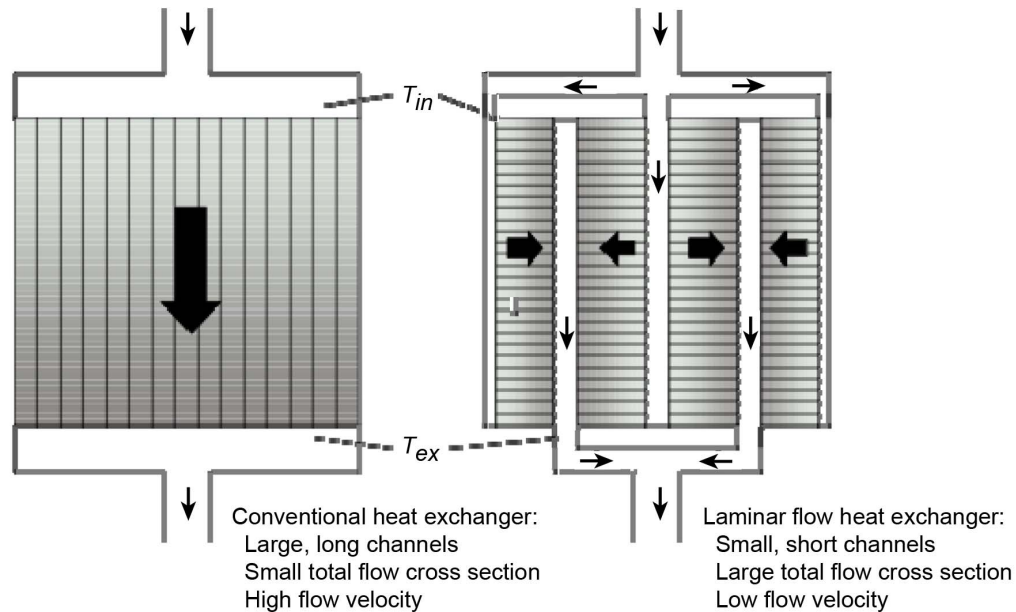


Figure 3.88.—Conventional HX versus laminar-flow microchannel HX. Copyright Kare Technical Consulting; used with permission.

The microchannel HX inherently uses a short channel length (typically 0.1 to 0.5 m) which allows a large HX to be fabricated and tested in smaller segments (panels). A large HX also can be shaped to match the expected beam profile (e.g., approximating a circle, with panels near the edge having longer channels to match the lower flux).

The microchannel HX has very low surface-to-gas thermal resistance because of the large thermal contact area (7 times the frontal area) and, thus, a very low surface-to-gas temperature drop. Analytical design calculations for the microchannel HX are given in (Ref. 6). Disadvantages of the microchannel HX include very small channel dimensions (nominally 0.2 by 1.2 mm) and relatively complex manifolds to interconnect panels.

The microchannel HX was originally conceived of as being made of metal (nickel, Ni), with panels fabricated and joined by electroforming (Ref. 7), but Ni melts at 1726 K, limiting the maximum exit temperature to <1500 K. Higher temperature metals are very dense, and generally expensive and difficult to fabricate, but may be used for test articles or for supports, fasteners, coatings, and so forth.

The current baseline HX material is silicon carbide (SiC), possibly with carbon fiber reinforcement (C-SiC). The SiC structure temperature required for 2000 K gas temperature is 2200 to 2300 K, well below the SiC vacuum melting point of ~2850 K.

The current HX parameters, as used in the DRM–B design, are given in Table 3.16.

TABLE 3.16.—HX PARAMETERS FOR CURRENT (DRM–1B) DESIGN

Size	4 by 6 m (approx.); 24 m ²	Elongated to reduce drag and improve stiffness; foreshortened to ~1:1 aspect ratio when beam is 50° off normal
Type	Laminar flow microchannel	See discussion
Material	SiC or C/SiC	Low-temperature manifolds/structure may be metallic or composite; high- temperature structure TBD
Design flux	9 MW/m ²	Absorbed flux, area average. Incident laser flux may be up to ~10% higher to allow for reflection and reradiation
Inlet pressure	5 MPa	
Pressure drop	<1 MPa	
Design flow	7 kg/s	H ₂
Exit gas temperature	2000 K	
Maximum surface temperature	2300 K	Mean surface-gas ΔT needs to be modeled; a simple approximation gives ~300 K for 10-MW/m ² absorbed flux.
Panel size	TBD	Cross-channel width of SiC panels may be limited by fabrication process or thermal stresses
Channel length	40 cm	COMPASS ^a design used 15 cm because of a calculation error related to inlet flow velocity
Channel cross section	200 by 1200 μm	
Channel spacing	400 μm	
Areal density	2.9 kg/m ²	HX only, for a 100- μm front and 200- μm back facesheet (average)

^aCollaborative Modeling for Parametric Assessment of Space Systems.

In the current conceptual design, the HX would be fabricated as SiC channel sections that would be attached to high-temperature outlet manifolds to form panels, nominally 80 cm wide by the full HX length. These panels would be assembled onto the HX support structure and attached to the low-temperature inlet manifolds. The individual panel outlets would be attached to a common ceramic or metallic outlet duct leading to the nozzle assembly.

3.1.5.1.2.6 HX Options

The major alternative would be a conventional turbulent-flow HX, consisting of parallel thin-walled tubes, typically ~5 mm in diameter and 2 to 3 m long, as used in the microwave-powered vehicle design (Ref. 8). A turbulent-flow HX has higher pressure drop, requiring more pump power, and higher surface temperature, but lower manifold complexity. Further study, and probably fabrication and testing of prototypes of both kinds of HX, are needed to make a final selection.

The baseline HX is a single stage. This design requires that the hydrogen propellant be above critical pressure (so there will be no two-phase flow) and may require some tapering of the channels to maintain stable flow and prevent channel-to-channel flow instabilities. In addition, it is potentially fragile and may be expensive to fabricate.

An alternative that should be considered is a two- or even three-stage HX, using the microchannel SiC HX only for the high-temperature stage. The low-temperature stage(s) could afford a much larger surface-to-gas thermal resistance, allowing a broader design space, including turbulent-flow designs. The low-temperature stage(s) could also use a wider range of materials, including metals, for lower cost or easier fabrication. Operating the SiC stage over a more limited temperature range would also decrease thermal stresses and potential flow instabilities.

The current leading material alternative to SiC is pyrolytic graphite, which has an even higher limiting temperature and better thermal conductivity, but it may require greater protection from air at high temperatures, or be eroded by hot hydrogen. Other ceramics and metals capable of higher temperatures than with SiC seem to be either too expensive or too easily oxidized (or both) to be good candidates, but further research is needed.

3.1.5.1.2.7 HX Fabrication

The best way to fabricate SiC microchannel HXs is not known, but possibilities include

- Fabricating graphite structures and converting them to SiC by reaction with liquid Si
- Molding “green” SiC blanks of fins and one face sheet, and firing, with either prefiring or postfiring bonding of the other face sheet and manifolds
- Preassembling fins and using vapor deposition to create one or both thin face sheets (similar to electrodeposition of metal face sheets.)

Note that components other than the HX itself, especially the hot-gas manifolds, do not require high thermal conductivity, and can be comparatively thick (limited by mass budgets). In general, they will also be at least slightly cooler than the gas temperature because of conductive and/or radiative cooling.

3.1.5.1.2.8 Laser HX Issues

The HX is the lowest Technology Readiness Level (TRL) aspect of the HX laser launch system. Some of the issues that have been raised for laser HXs are discussed in Table 3.17.

TABLE 3.17.—ISSUES FOR LASER HX

Issue	Description	Potential solution/mitigation
Absorption/ reflection loss	<p>Some laser light will reflect from the HX surface, wasting energy. (Reflected light is also a potential hazard; see Section 3.3.5.3—Issues and Resolutions)</p> <p>Reflection is assumed to be negligible in the baseline system design, since good-quality black surfaces are ~98% absorbing.</p>	<ul style="list-style-type: none"> • Add carbon to the SiC surface layer to make it more absorbing. • Deposit mechanically thin (<10 μm) but optically thick absorbing layers on the HX surface. Note that, to the author’s knowledge, a highly absorbing surface that remains intact up to the full SiC temperature limits has not been demonstrated. • Structure the surface to be optically absorbing. Nanostructured black surfaces generated by ultrashort laser pulse irradiation have been demonstrated on refractory metals (Ref. 9). Narrow V-grooves parallel to the vehicle axis can act as cavity light traps. • Compensate for reflection loss by increasing laser power.
Reradiation	<p>The hot HX surfaces will radiate energy, which is both a loss and a potential thermal problem for other vehicle components.</p> <p>At 2200 K, the black-body radiation flux is ~1.3 MW/m². For a linear temperature gradient (i.e., equal area for each temperature level) the mean radiated flux is 1/5 of the peak, or 0.26 MW/m².</p> <p>This is 6.5 MW for a 25-m² HX, which is an acceptable loss for 100- to 200-MW incident power. However, at lower power levels (near end-of-trajectory), the temperature gradient may be nonlinear, because the reradiation at the extreme hot end will approach the incident flux.</p>	<ul style="list-style-type: none"> • Make HX surfaces not intended to absorb the laser shiny or white, reducing emittance and thus radiated flux by 10 to 100 times. • Cover surfaces not facing the laser with opaque insulation to lower the radiated flux. • Minimize the surface-to-gas temperature drop by optimizing the HX design, for example, increasing the rib cross section and reducing the channel width for the highest-temperature part of the HX. Since emitted flux is proportional to T^4, even a slight reduction in surface temperature will significantly reduce reradiation. • Raise the laser flux on the HX, and reduce the HX area. Reduce the laser spot size or use reflective surfaces to keep the collecting area constant. • Use a surface or coating that absorbs efficiently (and thus has high emissivity) at the laser wavelength but has low emissivity at other wavelengths. The peak reradiation wavelength is unfortunately in the near-infrared (~1.5 μm), close to the laser wavelength, so achieving a large emissivity ratio may be impractical. (In this respect, the COMPASS design is optimistic because it assumes an emissivity of 0.3 for the face of the HX, instead of ~1.0. However, the COMPASS estimate of reradiation is pessimistic by an even larger factor because it assumes that the entire HX surface is at the maximum temperature).

Issue	Description	Potential solution/mitigation
Convective loss	<p>In the atmosphere, some heat will be lost to the air passing over the HX.</p> <p>The COMPASS group estimated convective loss at 20.7 MW, although their assumptions concerning surface temperature distribution and flow conditions are not given.</p>	<ul style="list-style-type: none"> • Raise the boost laser maximum power. Since this is a surface loss, no change in HX design is required; the boost laser power can be adjusted to maintain constant absorbed power. • Maintain laminar flow over the HX (as over an airplane wing) to maximize boundary layer thickness • Insulate or enclose non-laser-absorbing surfaces (back of HX, manifolds) • Configure the HX surface (e.g. with grooves or flow fences) to create stagnant or low-velocity flow over at least part of the absorbing face.
Oxidation	<p>In air, SiC begins to oxidize well below its vacuum melting temperature. The usual working temperature given for SiC in air is 1600 to 1650 °C (1873 to 1923 K), but at least one manufacturer offers SiC with a maximum service temperature in air of 1900 °C (Ref. 10). However in a high-velocity airstream, the thin facesheet may fail quickly.</p>	<ul style="list-style-type: none"> • Flow or transpire an inert or reducing gas (nitrogen or hydrogen) over the HX face—possibly by deliberately making the HX facesheet slightly porous—to maintain a low oxygen concentration in the boundary layer. • Run the HX at lower temperature while in the atmosphere, by increasing the propellant flow or reducing the laser power, and either operating at lower I_{sp} or generating more heat by combustion. • Use available multilayer coatings (HfC/SiC) to withstand oxidation for short periods at ~2400 K (Ref. 11).
Stress and creep	<p>SiC does not melt until 2850 K, but it loses mechanical strength and begins to creep (plastically deform slowly under load) at lower temperatures. Both creep and stress failure can be caused by stress concentrations, hot spots, or weak points such as bond lines.</p> <p>The microchannel HX design is comparatively resistant to creep or pressure failure despite its thin structure because the unsupported span of material in the facesheets is very short (~200 μm).</p>	<ul style="list-style-type: none"> • Make the HX channels with rounded corners or oval cross sections to reduce stress concentration, if the fabrication technique allows. • Add reinforcing material such as carbon fibers to the SiC matrix. • Reduce the number of hot seams by operating at higher gas pressure and flow velocity, allowing longer channels and fewer panel joints. • Eliminate hot spots on the HX face by applying reflective material (or removing absorber) wherever cooling is inadequate. This can be done in fabrication for known hotspots (such as along manifolds) or in testing (e.g., if there are blocked channels).
Thermal stress	<p>Thermal gradients on the order of 1000 K/cm normal to the surface and 100 K/cm along the channels will create large thermal stresses, potentially fracturing SiC. Surface-normal gradients will stress the front faceplate in compression and the back face in tension. Along-channel gradients will stress the cold edge of each HX panel in tension, in the direction perpendicular to the gas flow.</p>	<ul style="list-style-type: none"> • Put gaps in the ribs, or use a “diamond post” structure instead of continuous ribs, to relieve stress accumulation. • Incorporate expansion features into the back facesheet, or allow the entire HX to bow slightly to relieve front-to-back gradient stress. • Add tensile strength members or inclusions (e.g., carbon fiber) along the cold edge of the HX. • Limit the maximum width (in the perpendicular-to-flow direction) of individual heat-exchanger panels, and incorporate compliance in the input manifold-to-panel junctions, or “expansion joints” in the input manifolds.

Issue	Description	Potential solution/mitigation
Thermal shock and over/underheating	Sudden variations in propellant flow or laser intensity may cause large changes in exit temperature on millisecond timescales. Variations in the laser beam profile (either fast, because of atmospheric effects, or slow, as a function of range) will change the relative flux on different parts of the HX.	<ul style="list-style-type: none"> • Limit gross thermal shock by controlling the ramping of the laser power and propellant flow at startup and shutdown. • Tailor the beam shape at shorter ranges (using pointing offsets between individual beam modules) to approximately match the beam profile at long range. • Sense the HX exit temperature at multiple points and adjust propellant flow via local valves. • Use a piston pump or pressure-fed system, rather than a turbopump, to allow fast changes in total propellant flow. • Use a two-stage HX that mixes the propellant between stages to smooth out heating variations from the first stage.

Overall, the microchannel SiC HX will be challenging to develop and represents the largest technical risk for the HX launch system. Conversely, there are many options for optimizing the design that have not yet been explored even minimally: varying channel cross sections, surface coatings, curved or textured surfaces, integrated structures and manifolds, and other options.

3.1.5.1.3 DRM Vehicle Design

The starting point was the conceptual design shown in Figure 3.89. (See COMPASS report for the DRM-1B end-point design).

LH2 tank*	129.4
Dense propellant tank*	43.8
Heat Exchanger	50.0
HX hardware & manifolds	25.0
Nozzle ass'y	15.8
Avionics	4.0
Plumbing and wiring	13.6
Structure@10%	28.1
Nominal vehicle mass	309.6
+Margin @30%	92.9
Vehicle mass with margin	402.5
+Payload mass	102.5
Final mass to orbit	505
Mass to orbit	505
+Dense Propellant	1750
+LH2	995
Initial (liftoff) mass	3250
Propellant mass fraction	84.5%
Dry vehicle mass fraction	12.4%
Payload mass fraction	3.2%
Payload/total dry mass	20.3%

*Including residual propellant and pressurant

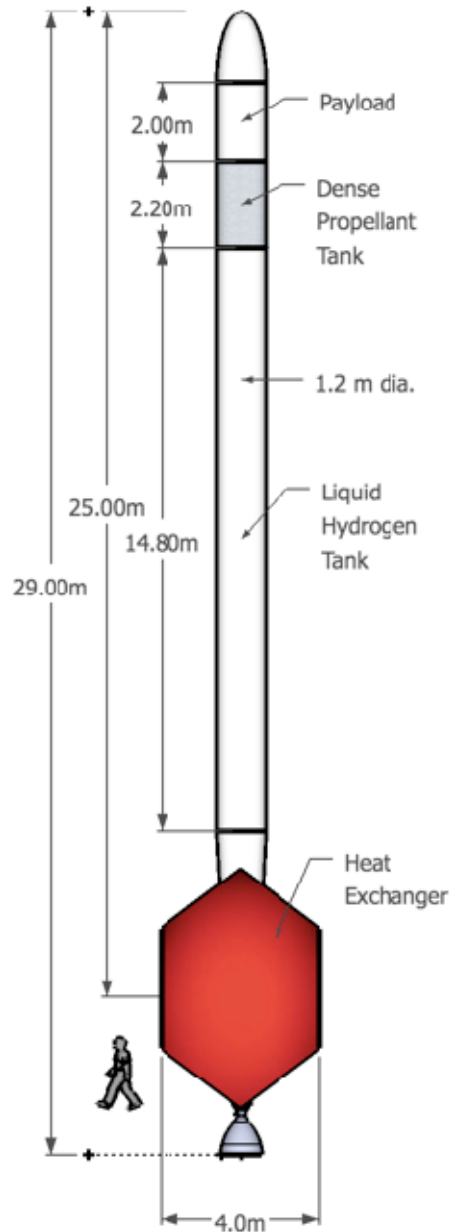


Figure 3.89.—Conceptual design of 100-MW HX launch vehicle.
Copyright Kare Technical Consulting; used with permission.

The overall dimensions of this design were driven by the desire to enable full adaptive optics (AO) correction for atmospheric turbulence using only a beacon on the vehicle, which forces the vehicle to be ~30 m long so the beacon can be far enough ahead of the HX (~25 m; see Section 3.1.5.2.2—Main Laser Site). The HX itself was sized conservatively, to minimize laser-pointing requirements (and to allow the system to work without AO, should they prove difficult to implement) and to minimize HX flux.

Also, the vehicle was designed with the assumption of particular values of tank mass fraction (13% for hydrogen and 2% for liquid nitrogen, LN₂) and structural mass fraction (10% of other dry mass) and the assumption of pressure-fed propellants (to avoid the cost of a turbopump) at a tank pressure of 250 psi. With these values, and the assumption that the maximum beam power is approximately constant (i.e., the boost laser power is equal to the main laser power), the design optimizes with a fairly high proportion of the propellant as dense propellant, to give high thrust for liftoff.

For the COMPASS team analysis, one change was made “going in”:

- Piston-pumped propellant feed, with 600-psi “chamber” (nozzle entrance) pressure. This was enabled by the demonstration of an LH₂ piston pump at roughly the correct scale by Xcor, allowing both a higher TRL and a basis for a mass estimate for the piston pump

In preliminary discussions, the long-thin “pencil” hydrogen tank was deemed to have several problems: high tank mass that was due to minimum-gauge issues and the need to prevent buckling (particularly when supporting ~2000 kg of dense propellant), high insulation mass that was due to the high surface-to-volume ratio, and the risk of vibrational resonances and bending instabilities. A shorter tank with a nominal diameter of 2 m was assumed, which was based on a rough compromise between structural efficiency and drag.

Initial estimates of the mass of a fixed tower/long shroud or a deployable boom to provide a point-ahead beacon were relatively high, so for the purposes of this modeling effort, we assumed that we would not consider beacon location as a design requirement.

The vehicle design as analyzed by NASA Glenn Research Center’s COMPASS team is discussed in Section 3.1.4. Key features of this design are given in Table 3.18:

TABLE 3.18.—PROPERTIES AND MASS BREAKDOWN OF CONCEPTUAL 100-MW HX LAUNCH VEHICLE AND DRM-1B LASER HX LAUNCH VEHICLE

	Concept	COMPASS DRM-1B
Design insertion altitude, km	300	400
Boost laser power, ^a MW	100	220
Main laser power, ^a MW	100	120
GLOW, ^b kg	3250	5543
LH ₂ propellant, kg	995	3166
Dense propellant, kg	1750 (LN ₂)	1227 (H ₂ O)
Dense propellant tank	Internal	External drop tank
Propellant feed system	Pressure fed	LH ₂ : Piston pump H ₂ O: Pressure fed
Tank pressure, MPa	1.6	0.35
“Chamber” pressure, MPa	1.0	4.0
HX area, m ²	25	24
HX channel length, cm	10	40
HX exit temperature, K	1700	2000
Maximum HX power, MW	100	220
Peak HX flux, MW/m ²	5	10
Estimated HX mass/area, ^c including manifold and structure, kg/m ²	~3	~8

^aNominal maximum power absorbed at vehicle; actual laser output power would be higher.

^bGross liftoff weight

^cBefore margins.

3.1.5.1.3.9 Collaborative Modeling for Parametric Assessment of Space Systems (COMPASS) Design Evolution

The COMPASS design was consistent with the author's earlier estimates in many respects. The Optimal Trajectories by Implicit Simulation (OTIS) trajectory model eventually obtained results very close to those predicted using the custom LAUNCH code (a nonoptimizing code) written by the author. The propellant tank mass fractions from the COMPASS analysis were generally lighter than the earlier estimates (albeit with a 50-psi tank pressure rather than 250 psi). Several components and subsystems were heavier in the COMPASS design than in the initial design because of the use of heritage components and design rules or simply because of a more detailed analysis, but the increased masses were generally manageable. Most of the difficulty in closing the COMPASS design came from the unexpected (by this author) high structural masses, particularly in supporting and attaching the HX.

An early (and possibly premature) decision was made to attempt to close the design without using dense propellants. When only hydrogen propellant was used, the initial vehicle mass was limited by the available thrust, and for constant laser power, the vehicle generally runs out of propellant well before it reaches the limits of the laser range, thus making inefficient use of the laser power. Increasing the boost laser power helps and is relatively inexpensive in terms of the ground system capital cost. However, even with a 200-MW boost laser, the design would not close for a true single-stage all-hydrogen vehicle.

One option that did allow the design to close was the use of a vertical catapult or small "strap-on" chemical booster rockets. If the vehicle is given a brief boost in addition to the laser-powered thrust so that it reaches 150 to 250 m/s, it can have a GLOW that is 30% to 50% higher than if it needs to accelerate from rest.

A catapult is a plausible solution as long as its cost is small compared with the rest of the system capital cost. The boost laser can acquire the vehicle, and the laser thruster can be running before the catapult fires, so no "in-flight engine start" is required. A subsonic catapult able to supply ~100-kN force for a few seconds is well within the state of the art (SOA) (comparable to an aircraft carrier catapult). However, a short vertical catapult (e.g., 200 m) necessarily applies substantial acceleration to the loaded vehicle, potentially increasing the vehicle structural mass considerably. A long vertical catapult (300+ m) would be an unprecedented structure, although large antenna towers are routinely built to heights >500 m.

Solid booster rockets were suggested, but although they are a plausible solution for tests, they would tend to defeat both the cost and range-safety advantages of a beamed-energy launch system.

The final design returns to the use of dense propellants to provide increased thrust, but with a much smaller ratio of dense propellant to hydrogen than in the earlier design, roughly 1:3 versus 1.75:1. Because of the time constraints of the study, the design uses the simplest possible form of dense propellant injection: pressure-fed injection after the HX (so that the HX does not need to handle varying propellant properties). The pressure-fed tanks and pressurizing system are too heavy to take to orbit, so they are configured as drop tanks.

3.1.5.1.3.10 Drop Tanks Are Not Required

The final COMPASS design can be made to close without drop tanks with only slight changes. The dense propellant tank is small (~1.2 m³) and, if the propellant is pump-fed, very light (<20 kg). If we allow 28 kg for the tank, added plumbing and hardware, and extra pump mass (32 kg including system-level margin) and assume that the 27 kg allocated for structure to support the drop tanks is enough to support fixed tanks, we can maintain the same gross liftoff mass (GLOW) and flight profile, up to the point where the tanks were dropped, while carrying substantially extra hydrogen. By slightly increasing the main laser power (by 154 kg /2820 kg, ~5.5%) this extra hydrogen can be burned without lengthening the trajectory but giving substantially greater final mass injected into orbit. A self-consistent set of mass deltas (relative to the COMPASS final design) at various points in the trajectory, assuming fixed GLOW, are given in Table 3.19.

TABLE 3.19.—DELTAS IN MASS FOR NON-DROP-TANK VERSION OF COMPASS DESIGN

Change	Mass delta, kg		
	Liftoff	Tank drop	Burnout
Remove drop tank assemblies	-194	--	--
Add integral tanks	+32	+32	+32
Add extra LH ₂ (including 1% residual)	+156	+156	+2
Increase LH ₂ tank size	+16	+16	+16
1% allowance for residual dense propellant + pressurant	--	+12	+12
Decrease payload as needed to make design change self-consistent	-10	-10	-10
Net vehicle mass change	0	+206	+52
Change in mass to orbit (mass ratio of 3.94 from tank drop)			+52

The mass deltas in Table 3.19 are estimates because there was no opportunity to rerun the COMPASS mass model or trajectory calculation. However, it is clear that a true single-stage vehicle, with no drop tanks or other dropped mass, will close even with the COMPASS mass margins, with a small decrease in payload.

3.1.5.1.3.11 Potential Future Design Directions

Optimized design.—Many aspects of the DRM-1B design are arbitrary, artifacts of earlier design choices, or chosen for ease of modeling, and are likely far from optimum. For example, the flat HX could be replaced by a sectioned or curved HX, allowing at least part of the HX to be supported directly by the tank wall, as in the DRM-1C design, and reducing the off-center aerodynamic loads on the vehicle. The shroud is considerably oversized, even for the large assumed payload volume, and could be replaced with a more tapered shroud with lower mass and drag.

SOA electronics.—The largely heritage electronics design has a total mass for guidance and control, telemetry, attitude determination, and electrical power of ~37 kg. This is clearly excessive for a vehicle with a total dry mass of <1000 kg. A new design, developed specifically for production runs of thousands of units, would certainly be lighter, possibly by 20 kg or more. It is worth noting that highly sophisticated, space-qualified avionics packages weighing well under 10 kg were developed for the Strategic Defense Initiative Organization (SDIO) Brilliant Pebbles program over a decade ago. Some options for weight (and cost) reduction follow:

- Microelectromechanical systems (MEMS) inertial sensors and gyroscopes, similar to those used in small unmanned aerial vehicles (UAVs)—The vehicle can also use optical beam sensing and differential Global Positioning System (GPS) to supply attitude data, and ground optical tracking data for guidance.
- Lithium polymer or lithium-iron-phosphorus (LiFePo) batteries—Neither long-term storage (low self-discharge) nor large total energy capacity are required.
- Single-board construction—A card cage is unnecessary.
- Wireless or serial-bus interconnects
- Separate batteries and controllers for the fore (payload) and aft (propulsion) bays, with wireless or optical-fiber connection between them; no multimeter electrical cable runs

Thrust vectoring.—The expansion-deflection (E-D) nozzle is ideally suited for thrust vectoring by fluid injection, either before or after the radial throat. Injecting dense propellant differentially around the nozzle would potentially give much more attitude control authority at low altitude, where it is most needed, and reduce the size and propellant usage of the attitude control system (ACS) thrusters, which would provide only roll control for most of the mission.

Dropped mass.—The DRM design assumes that, to minimize operational range-safety issues, no hardware at all is dropped from the vehicle other than, possibly, the dense propellant tanks, which would fall very close to the launch site. If the safety and operational impacts are acceptable, the vehicle could follow the common launch vehicle practice of dropping at least part of the payload shroud and any other hardware (such as tank insulation and parts of the HX structural support) needed only for prelaunch or for flight through the atmosphere.

More radical options include

Enhanced propellant cycles.—The DRM design feeds only hydrogen through the HX, thus requiring both hydrogen flow at all times and a small amount of combustion heating to maintain the propellant temperature when dense propellant is injected downstream of the HX. The HX may be able to accommodate both hydrogen and dense propellant (e.g., nitrogen, ideally with a fully variable mixture ratio). In that case, the vehicle could carry no oxidizing propellant at all and could turn the hydrogen flow down or completely off for at least the first few seconds of launch. An all-inert launch would protect both the launch site and the vehicle from any risk of a hydrogen-air fire or detonation.

Alternatively, the oxidizer content of the dense propellant could be increased to provide more energy from combustion. This would reduce the power and cost of the boost laser array. In the limit, the vehicle would be primarily a chemical rocket for the first part of its trajectory. A low level of laser power could still be used to heat some or all of the hydrogen flow and power the propellant pump. This would ensure ignition and fast burning of the oxidizer and would also allow the system to fail safe by cutting off propellant flow if the laser beam was lost or turned off.

Deployed reflectors.—Once above the atmosphere the vehicle could deploy lightweight reflectors to increase the effective beam-collecting area. These would typically be flat metal-foil reflectors, similar to the reflectors used on low-concentration solar panels. The HX area could be reduced or the useful laser range increased; either would increase payload or allow scaling to lower laser power. This is particularly beneficial for scaling the system to lower power and smaller vehicle size because the HX area and thus the mass of the HX and its support structure are set in part by the minimum practical laser spot size.

Ducted rocket.—The temptation to use the atmosphere as “free” oxidizer and reaction mass is always present in designing launch vehicles. For the laser HX rocket it is particularly strong given that its exhaust is hot hydrogen, which will immediately burn in air. The COMPASS team considered a ducted rocket or rocket-assisted ramjet configuration, operating over a wide Mach range. This gave very promising estimated performance, but required a variable inlet and a potentially complex air-exhaust mixing arrangement. The COMPASS group lacked the time and expertise to complete a credible design.

A high-performance air-breathing design, which can operate usefully from subsonic speeds and low altitudes up to, for example, Mach 5+ and 30+ km altitude, would require a major design effort and would add substantially to the cost and risk of development. An alternative that would be consistent with the general approach of minimizing vehicle complexity would be a fixed-inlet duct operating over a relatively narrow velocity range and discarded at an altitude of 30 to 40 km.

Air-breathing modes should certainly be considered in future vehicle design studies. We note, however, that, despite decades of proposals and research and development (R&D) efforts, only a handful of test engines of any kind have actually flown above roughly Mach 3, and no chemical-fuel launch vehicles (and very few missiles) have used air-assisted stages, suggesting that it is very difficult to actually build an air-breathing “accelerator” (as opposed to a constant-speed-and-altitude “cruiser”) that outperforms a pure rocket thruster. It is usually easier and cheaper to simply carry more rocket propellant.

Reusable vehicle.—We made no effort in this study to design the vehicle for intact reentry and reuse, but it is almost certainly possible to make a reusable version. The empty vehicle has low areal density, and a large part of its hot surface on reentry would be the already-refractory HX. Intact reentry would require some additional thermal protection, but possibly very little, plus adding a design constraint for stable reentry aerodynamics. The vehicle would need additional propellant for fully controlled reentry, as

well as a landing mechanism—possibly wings for horizontal landing, but more likely a parachute/airbag or similar system, given the vehicle’s low empty weight and low terminal velocity.

3.1.5.2 Description of Ground Facility

3.1.5.2.1 Overview

The overall ground system for DRM-1B consists of three facilities, as shown in Figure 3.90:

- The vehicle launch site is where the vehicles actually leave the ground. The launch site includes at least one launch tower or rail (which may be a vertical catapult), along with auxiliary equipment for handling vehicles, payloads, and propellant.
- The boost, or L1, laser site provides laser power to the vehicle for its initial launch and climb from the launch site through the atmosphere, until the vehicle is high enough to receive power from the main laser.
- The main laser site is the heart of the launch system, and consists of an array of beam modules— independent lasers with small beam directors and tracking systems—with a total output power (for the DRM baseline system) of ~120 MW. It is typically several hundred kilometers downrange (east) of the launch site, so that the vehicle trajectory passes over the main laser near the midpoint of its trajectory.

Details of these facilities are discussed in the following subsections in the order of cost, which is the reverse of the preceding sequence.

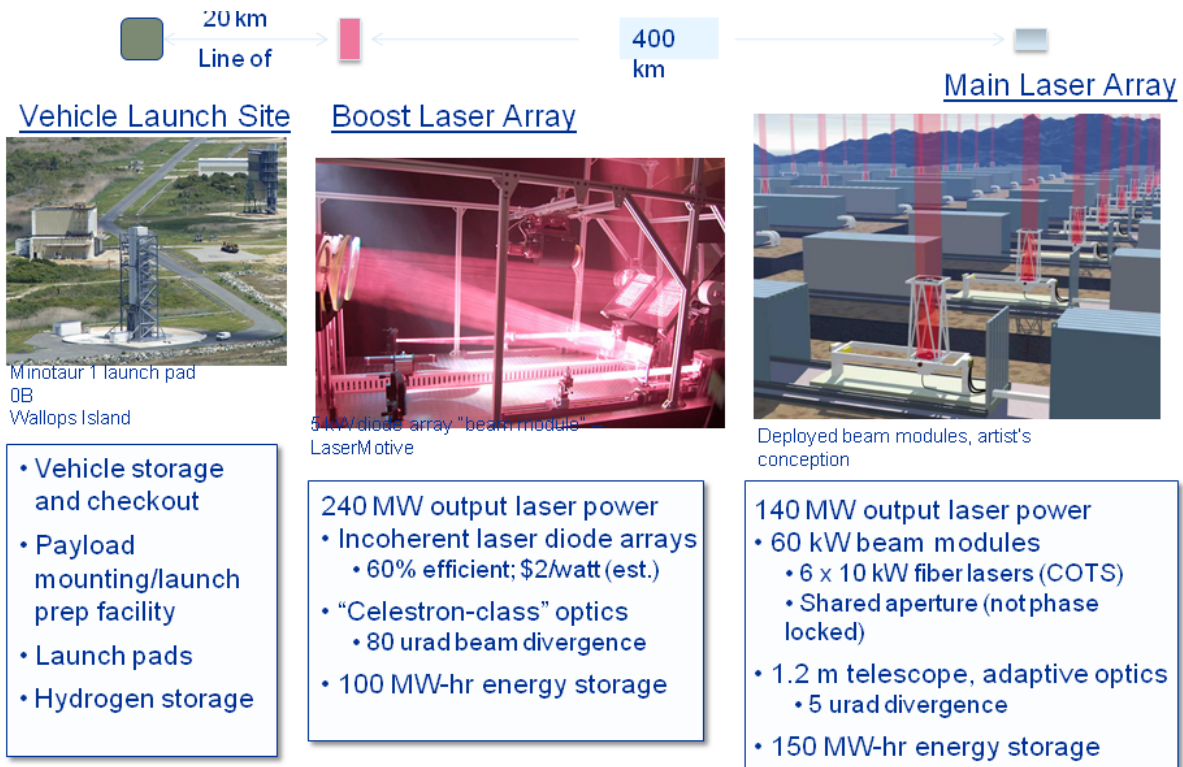


Figure 3.90.—Ground facilities for laser HX launch system. Middle image: copyright LaserMotive, LLC; used with permission. Right image: copyright Kare Technical Consulting; used with permission.

3.1.5.2.2 Main Laser Site

3.1.5.2.2.1 Beam Module Concept

The overwhelming problem with laser-beamed-energy launch has generally been seen as the need for a very large laser. An approximate rule of thumb is that it takes at least 1 MW of average laser power per kilogram of payload launched to low Earth orbit (LEO),¹ so that even few-kilogram payloads require multiple megawatts of power.

There is no requirement, however, that the laser energy come from a single coherent source. Many laser applications, including most directed energy weapon concepts, do require, or at least strongly prefer, a coherent source, since they are attempting to deliver as high a flux (power/area) as possible, or to deliver energy using as physically small an optical aperture as possible. In directed energy applications, pointing and tracking systems are often very expensive, since they need to track uncooperative targets, often at very high angular rates and under difficult conditions (e.g., from an airborne platform).

For laser launch, however, there is no inherent limit on the number of separate lasers and optical apertures used, as long as each individual laser and beam director can deliver its power efficiently, and the optics and tracking hardware do not dominate the system cost.²

There are multiple advantages to using many small lasers versus a single large laser:

- Lower development cost and risk
- Lower production costs through volume production and competitive production
- Higher system reliability and availability (using a small number of “spare” lasers)
- Continuous power expansion and incorporation of new technology
- Reduced propagation issues: no thermal blooming

3.1.5.2.2.2 DRM System Beam Module Design

The conceptual beam module design is sketched in Figure 3.91. The major components follow:

- Lasers: six by 10-kW single-mode fiber lasers
- Beam projector (telescope and mount)
- Tracking subsystem, including tip-tilt mirror
- AO subsystem, including Rayleigh beacon (laser guidestar) if needed
- Power supply, including local energy storage

¹ This “rule” was originally derived following the first SDIO/Defense Advanced Research Projects Agency (DARPA) Laser Propulsion Workshop. It arises from the dual constraints of thrust/weight >1 at liftoff, and horizon distances at LEO altitudes, both of which, in a simple model, limit the time for horizontal acceleration to a few hundred seconds, and thus the total energy delivered to a few hundred megajoules per megawatt of source power. If 100% of that energy ended up as payload kinetic energy (~32 MJ/kg for 8 km/s orbital velocity), we could put 10 to 20 kg/MW in orbit, but various inefficiencies reduce the actual useful payload by a factor of at least 10 for every propulsion scheme and vehicle design proposed to date.

² There is a surprisingly common misconception that multiple lasers must be phase-locked together to deliver laser power efficiently. This is generally based on misinterpreting the fact that phase-locking increases the **flux** delivered by an array of lasers; the peak flux possible using a coherent array of N lasers is N^2 times the peak flux from a single laser, versus N times for an incoherent array. However, the total power delivered is the same in both cases; the coherent array simply delivers the power into a smaller area.

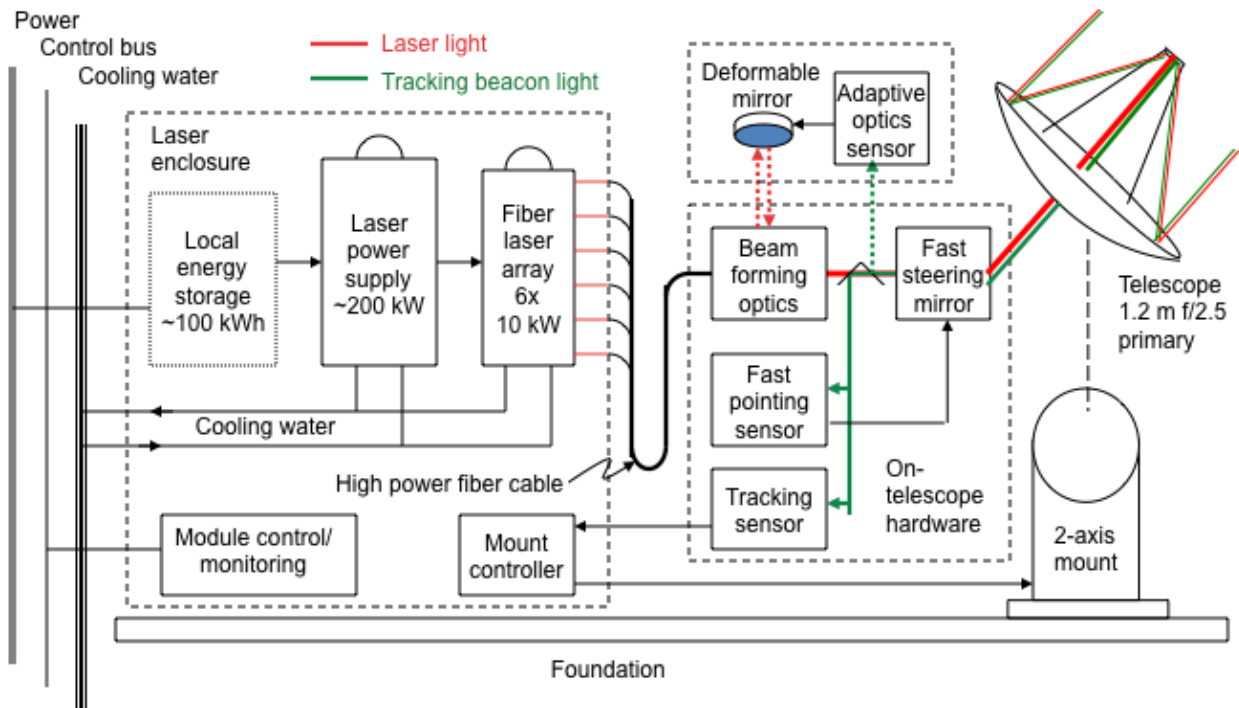


Figure 3.91.—Block diagram of 60-kW beam module. Copyright Kare Technical Consulting; used with permission.

The overall design is virtually identical to the beam module concept described in (Refs. 2 and 4), except for the use of full AO, and a slightly larger mirror to take advantage of the improved beam quality possible with AO.

As in the original design, the lasers are assumed to be completely independent, with each laser having its own “slice” of the telescope (i.e., the telescope acts as six separate off-axis telescopes). *This is by no means required* and other telescope and mount configurations are possible, including

- (1) Completely independent telescope (35 to 50 cm) and mount for each laser
- (2) Independent telescopes, but with some number of telescopes sharing part or all of a mount

Independent on-axis telescopes would be more compact (shorter focal length) and probably less expensive than a large telescope, but they would have a lower transmission efficiency (typically by a few percent) because of the secondary mirror and its support. Independent off-axis telescopes would in the past have cost much more than a single larger telescope, but with developments in optical fabrication including diamond turning, magnetorheological polishing, and deterministic polishing, plus automated measurement, assembly, and alignment techniques, the cost may be similar or lower.

The choice of a single 10-kW laser is based on the availability of such a laser as a commercial product, announced in July 2009 by IPG (Ref. 12) shown in Figure 3.92. Note that these are single-mode lasers with nearly diffraction-limited beam quality ($M^2 < 1.3$). IPG fiber lasers are built expressly for extremely high reliability, long-life operation in industrial production environments, and in particular use telecommunications-grade single laser diodes (with an operating life >100 000 hr) to pump the fiber. The beam is delivered over a single high-power optical fiber that could be directly connected to the beam director or adaptive optics system. They are therefore, uniquely, a TRL 8 beam source for laser launch, requiring (to the author’s knowledge) no modifications for use in a launch facility.



Figure 3.92.—IPG YLS–10000–SM 10-kW single-mode laser. Copyright IPG Photonics Corporation (Oxford, MA) 10,000 W Single Mode Laser; used with permission.

That said, the unmodified IPG 10-kW fiber laser is unlikely to be either the best or the least expensive laser for a launch system. It is an unusual design in that the actual 10-kW fiber is pumped by a set of lower-power fiber lasers rather than directly by diode lasers. This makes it more expensive and somewhat less efficient than IPG’s lower power fiber lasers (23% vs. >30% wall-plug efficiency).

The main alternatives to the IPG 10 kW laser follow:

Lower power (1- to 3-kW) single-mode fiber lasers.—These are available from IPG and potentially from other laser manufacturers (Refs. 13 and 14). Some form of beam combining, either coherent or, incoherent (i.e., wavelength combining), would be desirable to raise the unit beam power and thus keep the total area and cost of optics manageable, although even at 3 kW/beam it is unlikely that optics would dominate the main laser array cost. Incoherent combining of several continuous-wave (CW) fiber lasers using volume Bragg gratings has been demonstrated at power levels of a few hundred watts per beam (apparently limited by the available lasers) (Ref. 15), so this approach is at least at TRL 4.

Thin-disk lasers.—These are manufactured by TRUMPF (which holds fundamental patents on the design) in power levels up to 16 kW, also for industrial cutting and welding. These are sold as multimode lasers, with nominal beam quality of 8 mm-mrad (about 4 × diffraction limited) (Ref. 16), but Boeing has licensed the technology and has demonstrated weapons-quality beams (Ref. 17). Prices for TRUMPF’s welding lasers are comparable to or slightly higher than equivalent-power, equivalent-beam-quality fiber lasers from IPG because the two companies are direct competitors in this market.

“Conventional” solid-state lasers.—Joint High Power Solid-State Laser (JHPSSL) has demonstrated 100-kW beams with high beam quality (exact value unknown, but almost certainly adequate for a launch system) and has run (cumulatively) for >6 hr (Ref. 18). Northrop Grumman announced the FireStrike 15-kW Diode-Pumped Solid-State Laser (DPSSL) module as an orderable product in 2008 (Ref. 19). Textron Systems has also demonstrated 15 kW from its ThinZag diode-pumped ceramic slab laser, and other solid state lasers are under development (Ref. 20). This approach is thus at TRL 6, but costs and true operating lifetimes are unknown.

Diode pumped alkali lasers (Refs. 21 to 23).—These have been demonstrated only at 100-W power levels, but which are comparatively easy to scale to higher power. There is a reasonable chance that >10 kW will be demonstrated in 2011, which would raise this approach to TRL 4 or higher.

The “holy grail” would be a low-cost means of phase-locking large arrays of laser diodes at low cost, or, alternatively, of making high-power narrow-linewidth laser diodes that can be incoherently wavelength-combined to radiances of >10¹⁴ W/m-sr. There are tantalizing suggestions that one or both of these may be possible with external-cavity diode arrays, either edge-emitting or vertical-cavity, but so far these options remain at best at TRL 3.

The overall system design is nearly independent of the choice of laser,³ and development and testing of beam modules can be done at the level of a single module, so it is not necessary to choose a winner in laser technology now. Indeed, new laser technology can be incorporated into beam modules at any point, even after the launch array is built and operating, if it provides significant benefits.

Pointing and tracking.—The pointing and tracking subsystems in each beam module independently track the vehicle beacon through the launch. If the tracking subsystem for a particular laser does not have a positive signal from the beacon, it will shut the laser down for safety.

The detailed design and operation of the tracking subsystem is beyond the scope of this report, but it is well within the current SOA. A typical system would use an imaging camera (charge-coupled device, CCD, or complementary metal-oxide-semiconductor, CMOS), viewing either through the main telescope or through a separate “finder scope,” to acquire the vehicle beacon, and a higher-bandwidth quadrant detector, viewing through the telescope and tip-tilt mirror, to keep the line of sight centered on the beacon. This detector can take advantage of modulation of the beacon light (typically at 0.1 to 1 MHz) to suppress interference from both background light and reflected laser light that leaks through filtering.

A tip-tilt mirror is required to compensate for large-scale atmospheric turbulence, but it can also compensate for pointing errors and vibration of the telescope mount. (It is an open design question whether or not multiple beams sharing a telescope aperture should share a common tip-tilt mirror. Using separate mirrors and tracking sensors costs more, but it provides slightly better atmospheric correction if full adaptive optics are not used, and it reduces the adaptive optics dynamic range if they are.)

Adaptive optics.—The 100-MW baseline laser launch system in prior work was deliberately sized to avoid any need for adaptive optics beyond simple tip-tilt-focus correction because full adaptive optics were assumed to be too expensive for a \$1M-class beam module. However, progress in micro-optical devices, plus the predictable march of Moore’s Law in computing capacity, has driven the price of adaptive optics far below \$1M. For example, at this writing, Thorlabs, Inc., is offering a complete 140-element adaptive mirror with wavefront sensor and control electronics for roughly \$23,000. Although this system uses a MEMS mirror with limited power-handling capability, it has enough sensor resolution and enough actuators (140) to correct a beam up to ~54 cm across (assuming that $N = (d/r_0)^2$ for aperture diameter d and Fried parameter $r_0 = 4.5$ cm at a 60° zenith angle).

A detailed reanalysis of the beam divergence and beam module optics remains to be done, but if we assume that atmospheric turbulence is largely corrected, a 54-cm aperture (combined with appropriate improvements in jitter and pointing errors) will reduce the expected beam divergence (1/e² half-angle) from 8 to ~4 urad.

This improvement would allow the laser range to be increased, the HX dimensions to be decreased, or both. Increasing the laser range would increase the maximum trajectory length and, therefore, the energy delivered to the vehicle. This would increase the payload size for a given laser power. This would require revising several aspects of the system design (e.g., the orbit insertion altitude would have to be higher to keep the vehicle from going over the laser’s horizon).

Decreasing the HX area without changing the beam power would reduce the mass of the HX and (perhaps crucially) that of its support structure, but it would require the HX to accept higher flux.

Alternatively, the entire vehicle could be scaled to lower mass (including smaller payload) and lower power, reducing the cost of an initial launch system. Decreasing the beam divergence by a factor f would allow a reduction in HX area and mass by factor of 2 (f^2) (assuming constant HX thickness). Not all vehicle components would scale linearly with HX mass, nor would, for example, drag losses, so reducing the beam divergence to 4 urad would not allow scaling a 100-MW system with a 100-kg unit payload to a 25 MW/25 kg system, but preliminary modeling suggests that a 25-MW system would still have positive net payload.

³There would be differences in module design, safety requirements, and other parameters for different wavelengths, but all the proposed lasers are in the same general spectral range (0.7 to 1.1 μm), so the differences among them would be small.

Note that individual beam modules operate well below the power and beam diameter thresholds where significant thermal blooming occurs. If we assume that intermodule spacing would be reasonable, beam modules would not need to correct for thermal blooming.

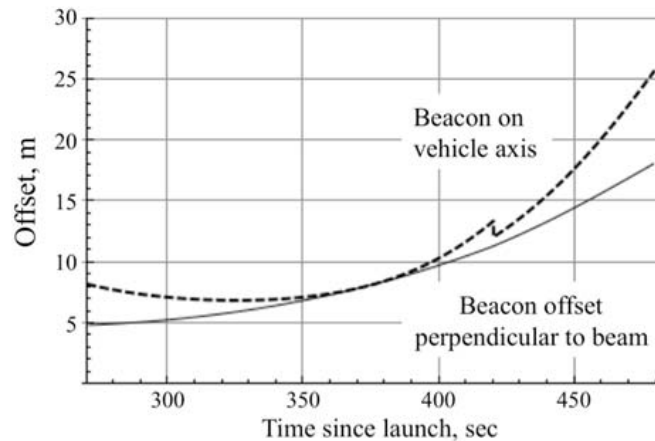


Figure 3.93.—Adaptive optics beacon offset versus time for a typical LEO trajectory. The notch at 420 s cates a point in the trajectory where the vehicle pitches nose down slightly ($\sim 10^\circ$) to circularize its orbit and improve the laser HX viewing angle.

Adaptive optics beacon requirement.—If full adaptive optics are used, a beacon located ahead of the HX by the point-ahead distance $d_{pa} = 2vR/c$ along the velocity vector is required, so that the downward-going beacon light samples the same part of the atmosphere as the outgoing power beam passes through. (Here v is the vehicle velocity, R the range to the laser, and c the speed of light; $2R/c$ is the round-trip time for a light signal from beacon to laser and back.) Note that if the vehicle has a nonzero angle of attack (i.e., velocity vector is not parallel to the vehicle axis) the physical offset between the beacon and HX may be different from the pointahead distance.

A plot of the beacon offset as a function of time for the last 200 s of a typical launch trajectory is shown in Figure 3.93. The offset initially declines, even though the vehicle is accelerating, because it is getting closer to the laser (which is 400-km downrange from the launch site); once the vehicle passes over the laser, the offset increases rapidly. The maximum offset of 25 m is typical for launches to LEO.

As noted in Section 3.1.5.1.3—DRM Vehicle Design, a vehicle long enough to support a beacon with a 25-m offset may be far from optimum structurally at the 100-MW scale. Further design work is needed to determine whether there is a practical solution using a fixed or deployable spike or boom on the nose of the vehicle. Note that the variation in beacon offset also means that either the beacon would have to be moveable or (more likely) that there would be beacon emitters (diode lasers or optical fiber tips) at several points.

An alternative to having a long vehicle with multiple onboard beacons is to equip each beam module with a laser-generated beacon. Rayleigh beacons (e.g., Ref. 24) require moderate beacon laser power (a few watts time-average) and provide good performance over the aperture diameters of interest. They can be operated in a pulsed mode with gated detectors, with adjacent modules using different pulse timeslots to minimize mutual interference. This approach would raise the capital cost of the system (although probably only by on the order of 1%) but would minimize the vehicle complexity and cost. An onboard optical beacon would still be needed for coarse tracking and tip-tilt beam steering, but a single beacon at any convenient point on the vehicle would be sufficient. Rayleigh beacons for this class of aperture are at least TRL 6, having been implemented on various ground-based telescopes and on the Airborne Laser (ABL).

The structure and scale length of atmospheric turbulence varies with time and location. Analytical modeling, simulations, and possibly onsite testing will be needed to predict the actual beam profiles to be expected for a particular launch site and a particular beacon configuration. The operational impact of a given degradation in beam quality also depends on the HX size and shape and the trajectory flown. We believe it is likely that an operational system *will not require* Rayleigh beacons for each beam module (i.e., a vehicle-mounted beacon will be sufficient even if it is not optimally placed) but that Rayleigh beacons may provide more than enough improvement in system performance to be worth their cost.

3.1.5.2.2.3 Main Laser Site Design

An artist's conception of a beam module array is shown in Figure 3.94. This particular version has the beam module packaged in two standard 40-ft cargo containers, with the lasers in one container and the beam director and associated optics in the other (with a roll-away roof and walls); the two would be connected by optical fiber cables.

Using standard containers would allow the modules to be easily trucked from a factory to the site and returned to the factory for repairs if needed. The modules could be emplaced on simple concrete pads and connected to cooling water and power. This general configuration has been proposed for large data centers, as illustrated in Figure 3.95. A large data center would have roughly the same number of containers and much greater power and cooling requirements than the DRM launch system array, differing mainly in that server containers could be placed closer together, since they have no field-of-view requirements. Google and others have built such modular data centers, although generally on a smaller scale, and cargo-container server modules are available from Sun, IBM, and other manufacturers. It would, of course, be possible to install beam modules in more conventional buildings if cargo containers were too small or otherwise unsuitable.

Figure 3.96 shows the scale of a 2000-module array, using modules on regular ~40- by 50-m centers. Many other configurations are possible, including regular or irregular patterns with closer or wider spacing, as long as the spacing is sufficient to keep one module from blocking another's beam—typically <10 m—and to allow access for installation and maintenance. (Some spacing is also needed to avoid collective thermal-blooming effects.) If land area were at a premium (e.g., on a mountaintop) a 2000-module array could fit into ~200 000 m², or 1/5 km²—slightly over 40 acres.

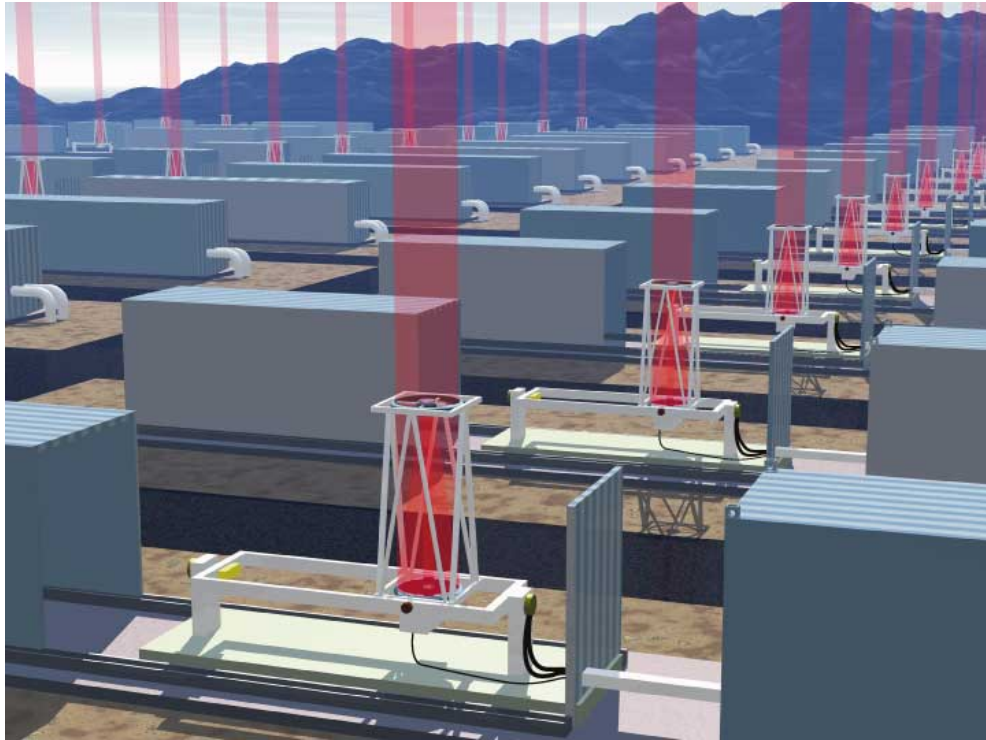


Figure 3.94.—Beam modules in the field. Copyright Kare Technical Consulting; used with permission.

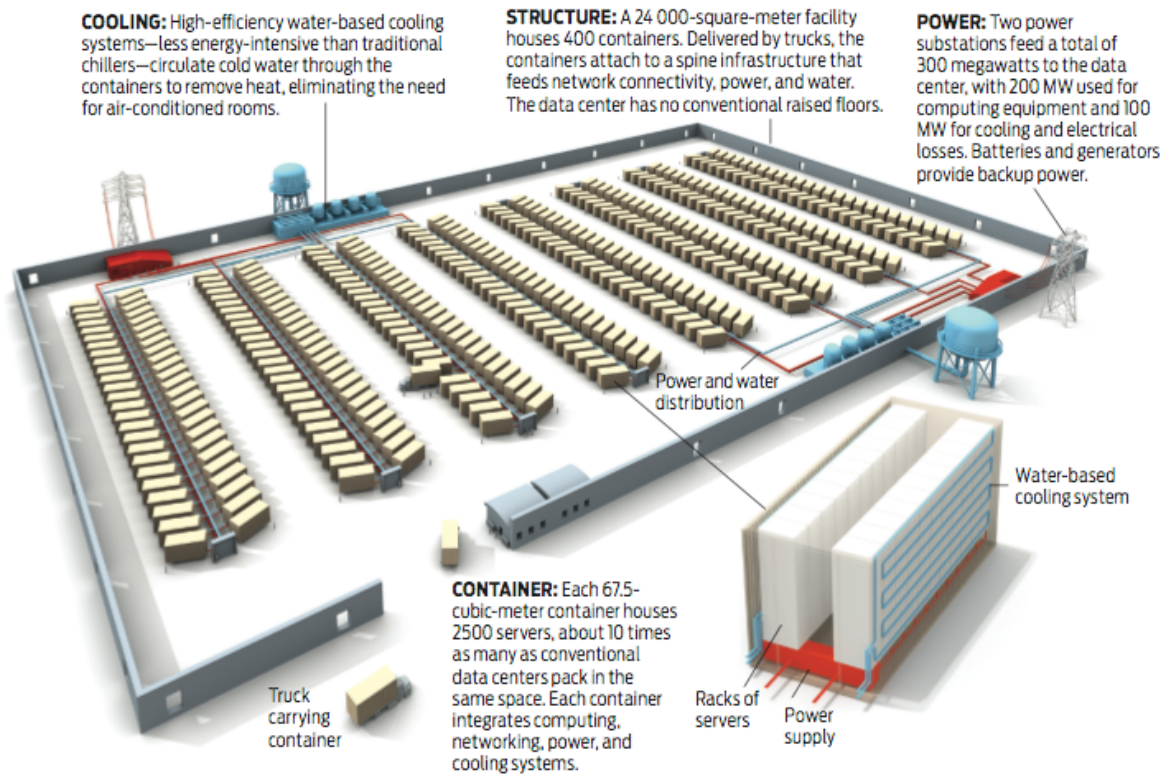


Figure 3.95.—Modular data center, as envisioned in IEEE Spectrum (Ref. 25). Copyright Kare Technical Consulting; used with permission.

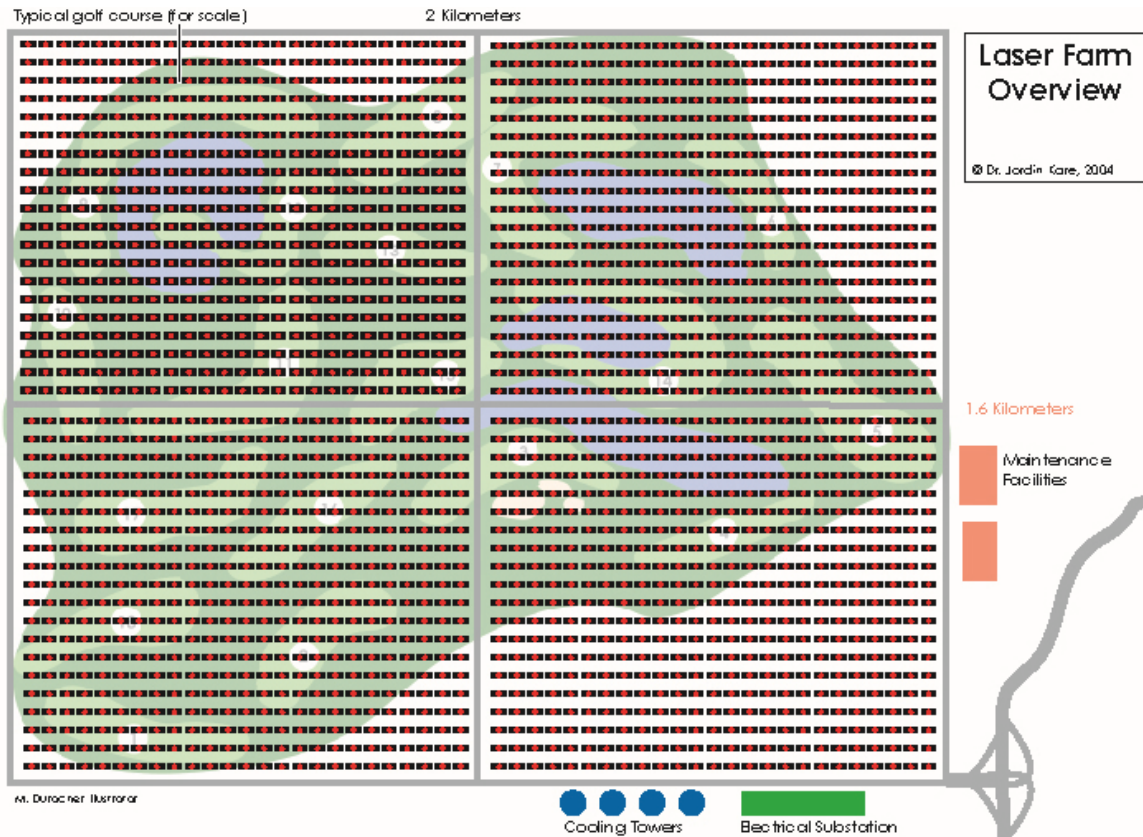


Figure 3.96.—A 2000-module array, with 40 by 50 m spacing, is 2 × 1.6 km, or about the size of a 18-hole golf course. Copyright Kare Technical Consulting; used with permission.

Power and cooling.—If we assume a wall-plug efficiency of 30% (present efficiency of IPG single-mode fiber lasers) and a total main-site laser output power of 140 MW (corresponding to 120 MW at the vehicle as it passes over the site)⁴, the main laser array would need 470-MW input electric power for ~400 s. Some additional power would be needed for electronics, pumps, telescope mounts, and so forth.; we estimate this at 20 kW per beam module, or about 10% of the power needed by the lasers. As discussed by Kare and Parkin (Ref. 26), a heavily used system could simply install 520 MW of gas-turbine generators, identical to those used for utility peaking power, at a cost of about \$0.60 to \$0.80/W.

For the DRM launch rate of 1000/year (a few launches per day) it will probably be less expensive to use a lower-power generator, or a grid connection, plus an energy-storage buffer. Any of several types of batteries are capable of storing the necessary energy (~210 GJ or ~60 MWh per launch) and providing the required power for a fraction of the capital cost of generators. However, most existing battery technologies do not have sufficient cycle life to be economical.

The availability of all-electric cars is encouraging, as they necessarily have battery packs designed for high cycle life. For example, the Chevrolet Volt battery pack characteristics from (Ref. 27) are given in Table 3.20.

⁴ This is the approximate power requirement for the COMPASS DRM vehicle design. Significantly lower power (100 to 150 MW at the vehicle) may be sufficient with an optimized design.

TABLE 3.20.—CHARACTERISTICS OF CHEVROLET VOLT BATTERY PACK

Energy storage	10.4 kWh (usable)
Power output	111 kW peak
Estimated usable power for 400 s	80 kW
Estimated cycle life (based on 8 year warranty, 1 cycle/day)	3000
Estimated cost today	\$7500
Estimated cost in 5 to 10 yr	\$4000

Nissan Leaf batteries are similar, with slightly higher cost estimated (<\$750/kWh total capacity, about \$18000 for 24 kWh (Ref. 28), presumably with similar power output.

At 80 kW per pack, three packs, costing (at \$4000 each) \$12,000 total, would be needed to power a single beam module for one launch, or roughly 6500 packs costing \$26 million to supply 520 MW (\$0.05/W). For operational flexibility, the launch system would probably have sufficient storage to allow at least two or three launches in quick succession, representing a capital cost of \$52 to \$78 million. With two launches worth of storage and 1000 launches/year, batteries would need to be replaced after 6 years (500 cycles/yr on each battery). With three launches worth of storage, the battery life would be 9 years, or very close to the nominal 10-yr system life.

Note that electric car batteries are probably not the optimum energy storage solution, but they do represent the SOA in mass-produced high-discharge-rate batteries, they are TRL 8 (in volume production) and they happen to fit the cycle-life requirements for the DRM (if we assume that the claimed cycle lives are achieved in practice) and the power requirements of nominal beam modules. Other high-cycle-life batteries being developed for stationary applications (sodium sulfide, NaS; vanadium redox, etc.) or energy storage devices such as flywheels may be cheaper or more reliable, especially in another 10 years. For launch rates less than 100 per year, older battery technologies (lead-acid; nickel metal hydride, NiMH; or nickel cadmium, NiCd, if cadmium is acceptably recycled) would probably be less expensive, even with life of ~300 cycles. For launch rates higher than roughly 3000 per year, or bursts of >10 launches, gas turbine generators would be competitive.

Using batteries at each beam module (or perhaps a battery system for each small group of modules) would reduce power distribution costs within the launch array, and might reduce power supply cost by providing direct direct-current (DC) input to the laser drivers at an appropriate voltage.

If we allow 8 hr to deliver energy for one launch, with 80% efficiency in battery charging, the input power needed would be only 75 MWh/8 to ~9.4 MW. Continuous housekeeping power of a few kilowatts per beam module would add another 5 to 10 MW, so the primary power source—generators or grid connection—for the main laser site should be rated at 20 MW or more.

Cooling.—For the DRM launch rate, cooling to a thermal sump (water tank or pool) during launches is convenient and cost effective. The total energy dumped would be $(470 - 140 + 50) \text{ MW} \times 400 \text{ s} = 152 \text{ GJ}$. A water volume of approximately $10\,000 \text{ m}^3$ (four Olympic swimming pools) would be heated by $3.6 \text{ }^\circ\text{C}$ by one launch. (A single 60-kW beam module, dissipating $160 \text{ kW} \times 400 \text{ s} = 64 \text{ MJ}$, would require 3.5 m^3 of water, or about 900 gal (3407 liters), for a similar temperature rise). Depending on the local climate and water supply, the thermal sump temperature could be maintained by an evaporative cooling tower or a system of chillers removing 500 GJ of heat per day or ~6 MW continuously. Housekeeping cooling—removing constant heat loads and solar heat—may be substantially more.

3.1.5.2.3 Boost Laser Site

The boost, or L1, laser site is a separate laser array located relatively close to the vehicle launch site, nominally 20-km downrange, with line of sight to the vehicle launch stand(s). The primary purpose of having a boost laser is to supply power to the vehicle until it is high enough to be in view of the main laser array at a reasonable elevation. Because the HX vehicle has a side-mounted HX, it is difficult to get a workable trajectory if the main laser is close enough to the launch site to see the vehicle on the ground: the vehicle quickly becomes tail-on to the beam. (It is possible to design a HX-based vehicle that will work in this geometry, using, e.g., a pivoting HX or deployed reflector), but the resulting system is still less efficient than one with the main laser farther downrange.)

A nonlaser “first stage” (in quotes because this option also includes non-rocket stages such as carrier aircraft or catapults) could be used to get the vehicle off the ground and up to a reasonable altitude, and this may be the preferred option for some testing, but it inherently makes the vehicle and operations concepts more complex. Also, many first-stage options, including air-dropping the vehicle from a carrier aircraft, cannot provide enough altitude to allow placing the main laser optimally far downrange.)

If the cost per watt of the boost laser and main laser were similar, using a boost laser would nearly double the overall system capital cost, and would probably not be justified except for a very high-volume launch system. However, the boost laser needs a range of only 50 to 100 km and can, thus, have ~10 times higher divergence and ~100 times lower brightness than the main laser. This makes lower-cost laser options usable.

If the boost laser is substantially cheaper per watt than the main laser array, then the overall system design could be optimized by making the boost laser somewhat more powerful (typically 1.5 to 2 times) than the main laser array. This would provide extra power for liftoff and flight through the atmosphere, allowing the vehicle to be sized to use the full capacity of the main laser without being limited by liftoff weight or wasting propellant during a low initial acceleration. Similarly (although less significantly) if the boost laser is more efficient than the main laser, using it for a large fraction of the powered flight duration (even though only a small part of the trajectory length) would reduce the overall launch-system electric power consumption.

3.1.5.2.3.4 Boost Laser Technology

The preferred technology for the boost laser is direct diode arrays. These are threefold to tenfold less expensive than fiber lasers and substantially more efficient. The actual diodes are routinely 60% efficient (DC to light) today, and efficiencies of over 70% have been demonstrated (Refs. 29 and 30).

The source radiance \mathcal{R} (power/[area(solid angle)], in $\text{W}/\text{m}^2\text{-sr}$), which is a conserved quantity through optical systems, determines the total transmitter aperture area needed to deliver a specified combination of intensity and range. (Note that, for fixed radiance, the aperture area is independent of the source power.)

Over the last few years, the radiance of laser diode array sources has increased significantly. As of 2008, a typical 808-nm diode stack with two-axis microlenses to collimate the individual diodes could produce a radiance of 6 to $8 \times 10^{10} \text{ W}/\text{m}^2\text{-sr}$ ($\sim 500 \text{ W}/\text{cm}^2$ with a divergence of $\sim 20 \times 4 \text{ mrad}$). Using polarization combining and optical interleaving would raise this by a factor between 3 and 4, to ~ 2 to $3 \times 10^{11} \text{ W}/\text{m}^2\text{-sr}$ (Ref. 31). This is slightly too low to be practical for the DRM system boost laser: to deliver $10 \text{ MW}/\text{m}^2$ at 50 km (which would actually be about $8 \text{ MW}/\text{m}^2$ at the vehicle, allowing for atmospheric absorption and scattering) would require $\sim 100\,000 \text{ m}^2$ of optical aperture.

However, diode arrays themselves are improving in power and beam quality, so the raw array radiance available, particularly at a slightly longer wavelength (980 to 1060 nm) is about a factor of 2 higher (and likely to increase). Demonstrated techniques exist for improving the optical collimation of the laser output, notably individual corrective micro-optics (Ref. 32), which can reduce the fast-axis divergence by several fold, essentially to the diffraction limit. Finally, dichroic combining of several (three to four) diode laser beams at kilowatt levels is done routinely, for example, by TRUMPF in their TruDiode industrial laser systems (Ref. 33). We thus assume that high-power diode sources at $\sim 4 \times 10^{12} \text{ W}/\text{m}^2\text{-sr}$ are at TRL 6, although this is slightly beyond what is currently sold commercially.

With a source radiance of $4 \times 10^{12} \text{ W}/\text{m}^2\text{-sr}$, the nominal DRM system boost laser array would require a total optical aperture of 6250 m^2 —roughly 3 times the area for the baseline main laser array, but the required optical quality and pointing accuracy are very low, literally worse than modern hobby-grade telescopes from Celestron and similar sources. Pointing accuracy of several arcseconds (20 to 30 μrad) is sufficient, and no adaptive optics are required except possibly tip-tilt steering. Such optics cost in the range of $\$10,000/\text{m}^2$ to $\$30,000/\text{m}^2$, with the high end being conventional optics and the low end being alternatives such as replica optics, plate-glass honeycomb primaries (Ref. 34), or transmissive diffractive optics “printed” on thin glass substrates (Ref. 35).

If the expected optics cost or diode-array performance is not achieved, there are multiple alternatives. Wavelength-stabilized high-power diode arrays have been demonstrated for alkali-vapor pumping (Ref. 36) and would allow much higher numbers of diode arrays to be combined with dichroics, diffraction gratings, or volume Bragg gratings. Single-mode high-power diodes are available with higher radiance (but also higher cost) than standard multimode arrays. Either of these would allow reducing the optics area by factors of 5 to 20.

Finally, the worst-case fallback for high TRL would be to use multimode fiber, slab, or thin-disk lasers, which are currently available at power levels >10 kW and radiances of $>10^{13}$ W/m²-sr (e.g., the TRUMPF TruDisk 16002 laser is 16 kW with a beam parameter product of 8 mm-mrad; radiance $\mathcal{R} = P/(\pi^2 BPP^2) = 2.5 \times 10^{13}$ W/m²-sr) with higher radiance versions in development. This would make the boost array only 1.5 to 2 times cheaper than the main laser array, but very compact.

3.1.5.2.3.5 Boost Laser Site Design

The boost laser site will have a layout generally similar to the main laser site, with hundreds to a few thousand modules installed over on the order of 1 km² (possibly less, if land area is limited). Each module will be largely independent, with its own power supplies, tracking, and other capabilities. The laser power and aperture area per module are not yet defined, but a plausible configuration might use 20-kW diode array assemblies, each with its own ~1-m mirror. The arrays would be mounted in groups of 10 on a common elevation mount as sketched in Figure 3.97. Such a 200-kW beam module would, like the main laser array beam module, fit conveniently into two standard cargo container-sized packages, one for the actual laser/telescope system and one for power supplies and control electronics.

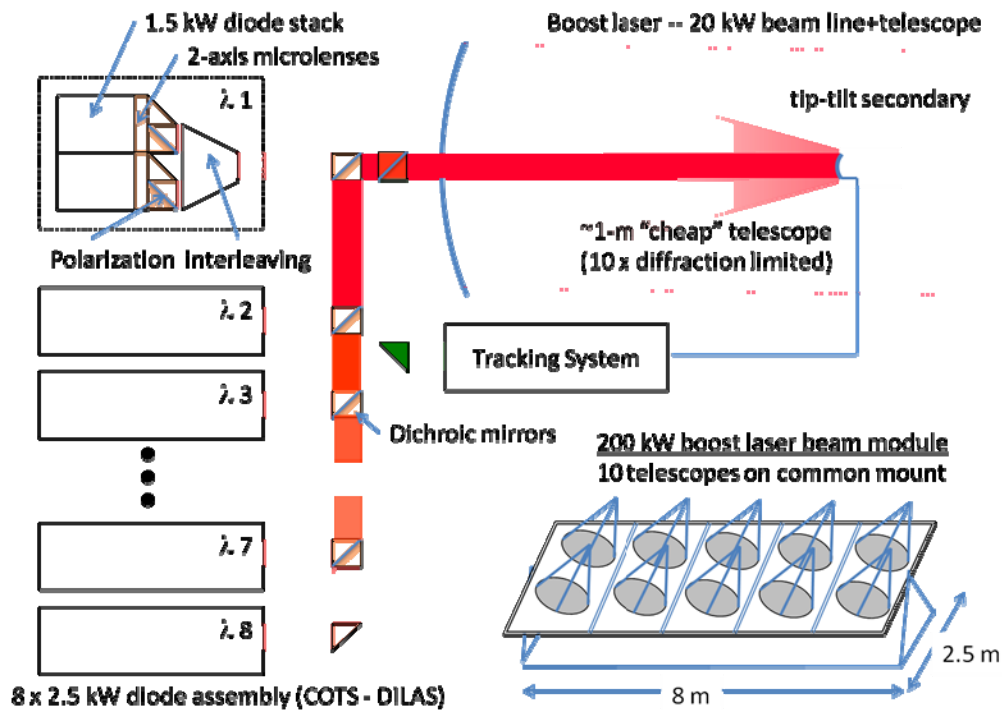


Figure 3.97.—Boost laser beam module concept.

Because the boost laser needs to point at, or very close to, the horizon in one direction, but only slightly past the zenith in the opposite direction, the boost laser array should be built on a slope facing the launch site. The altitude of the boost laser array is somewhat less important than that of the main laser array (because when the vehicle is at maximum range for the boost laser, it is also near zenith and atmospheric effects are minimized). It might be desirable to put the boost laser array slightly below the

launch-site altitude (if it is assumed that the intervening terrain is lower still) so that even at launch, the beam would never be aimed to intersect the Earth's surface (i.e., it would always point at least slightly upward).

A 250-MW, 60% efficient boost laser array (delivering 220 MW to the vehicle) will require either a ~420-MW prime power source (generators or grid connection) or, as with the main laser array, a distributed energy storage system and a much smaller prime power source.

3.1.5.2.4 Launch Site

The launch site provides facilities for

- Storing vehicles before launch
- Attaching payloads to vehicles (if they are not delivered with the vehicles)
- Moving vehicles to one or more launch pads
- Loading propellants and otherwise preparing for launch
- Maintaining the vehicle ready for launch
- Performing any prelaunch checks
- Safely handling the vehicle exhaust

The launch site will be similar in scale to existing small-vehicle launch sites such as Pad 0B at Wallops Island (which was built to launch the Minotaur I, a solid fuel vehicle roughly the same size as the HX vehicle, but much heavier), except that the HX launch site may be inland, and will have at least two, preferably three or four launch stands, so that multiple vehicles can be prepped and launched in quick succession.

The launch stands may have small-scale versions of chemical rocket facilities, such as “flame” trenches to conduct hot exhaust away from the vehicle and, if hydrogen propellant is used at liftoff, to safely burn off the hydrogen exhaust.

3.1.5.2.5 Location Constraints for Ground Facilities

3.1.5.2.5.6 Site positions

As noted previously, the launch system will require at least three sites: the launch site, the boost laser site, and the main laser site. Nominally, these would be on a straight line along the vehicle ground track, with the two laser sites at 20 and 400 km downrange from the launch site. In practice, the actual locations would be fairly flexible.

The boost laser site will be constrained in distance to the launch site: propagation losses over a horizontal path and the need for line-of-sight to the launcher will limit the maximum range, and the angle-of-view to the ascending vehicle will limit the minimum range. The boost laser could, however, be far off the trajectory ground track, by at least 45°, and possibly more; the vehicle could roll to present the HX to the boost laser initially and then to the main laser.

The main laser downrange distance will need to be optimized for a specific set of laser properties and vehicle trajectory, but in general should be as far downrange as possible without causing a large loss of power early in the trajectory; 400 km is probably shorter than the optimum distance. Changes of 50 or even 100 km, however, would have only modest effect on the overall system performance. Similarly, the main laser could be offset from the trajectory ground track by 50 km with very small effect. Indeed, as discussed later, the trajectory will be shifted to vary the inclination of the final orbit, so the main laser site could be anywhere in a zone of at least 100 by 100 km, and probably larger.

3.1.5.2.5.7 Altitude

Altitude is not a direct constraint for any of the laser launch facilities, and an all-sea-level launch system (including a ship-based launch system) is feasible. Some laser wavelengths in the ranges of

interest are significantly absorbed by water vapor, so high-altitude laser sites may have slightly wider ranges of usable wavelengths, but windows exist for both direct-diode and fiber laser wavelengths. Figure 3.98 shows the absorption versus wavelength over a 20-km horizontal path at sea level and at 3 km. (millimeter-wave or far-infrared (10.6 μm) sources are much more strongly affected by water vapor in the lower atmosphere, so those beam sources must be at high altitude.) Note that the propagation model used for the COMPASS trajectory modeling was a simple geometric model and did not model the effects of water vapor.

Placing the launch site at high altitude would slightly reduce air drag, gravity loss, and the impact of ambient pressure on thrust, but those are minor effects for altitudes below several kilometers. Very high elevation sites (both laser and vehicle launch) may have greater availability because they are above low-altitude cloud layers and precipitation.

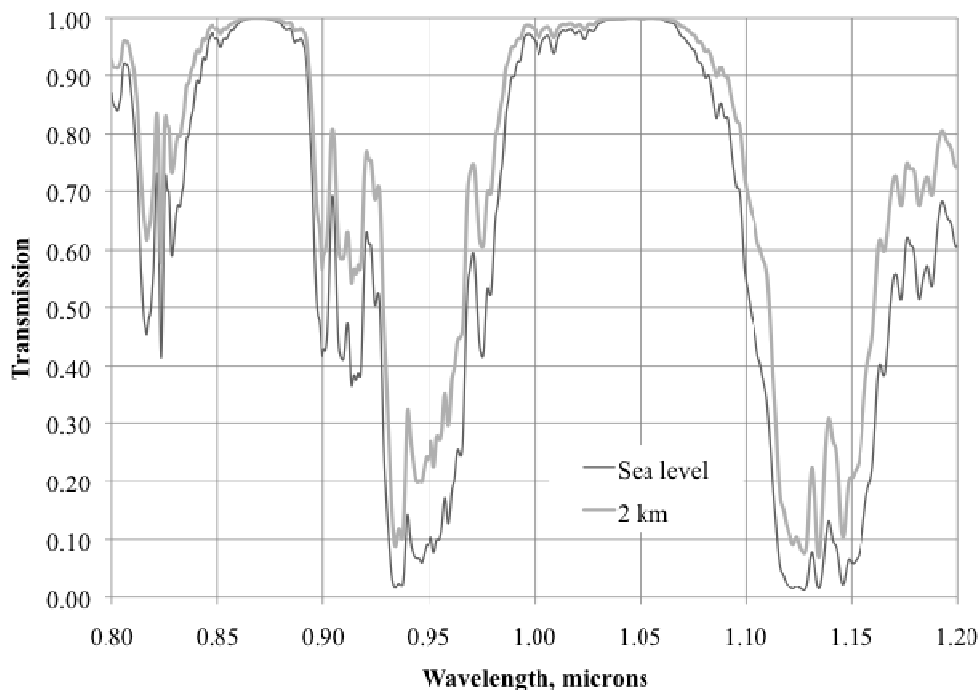


Figure 3.98.—Atmospheric transmission versus wavelength for a 20-km horizontal path at midlatitude during winter (molecular absorption/scattering only; no particulates).

3.1.5.2.5.8 Line of Sight

The boost laser array requires a line of sight to the launch site, and does not need to track the vehicle more than slightly past zenith, which implies that the optimum site for the boost array may be on a slope facing the launch site. The main laser requires visibility to 10° to 20° above the geometric horizon along the trajectory axis, which may rule out some sites adjacent to high ridges.

3.1.5.2.5.9 Particulates and Turbulence

Particulates will affect scattering losses and also will vary with location and season. The largest effect will be on the boost-laser to launch-site path, which is roughly parallel to the ground; the boost laser may have a slightly shorter wavelength than the main laser (0.8 to 1.0 μm versus 1.03 to 1.07 μm), which will make it more sensitive to scattering because scattering losses generally vary with λ^{-4} . For example, a standard value for particulate scattering loss between an altitude of 0 and 1 km is 0.06 km^{-1} at 860 nm and 0.045 km^{-1} at 1060 nm (Ref. 37). It may be necessary for the boost laser, the launch pad, or both to be elevated at least somewhat above the intervening terrain. High scattering losses may rule out some

otherwise appealing sites. More generally, scattering should be evaluated at prospective sites and factored into the overall system cost. This study assumed scattering losses of 10% (0.9 transmission) at zenith, which is good but not exceptional for high-altitude sites. Poor sites may have zenith losses as large as 50%, which would more than double laser power requirements.

Adaptive optics requirements for the main laser modules will depend on the levels of atmospheric turbulence, known in astronomy as the “seeing,” at and above the laser site. Seeing can vary considerably depending on local wind patterns and on season and time of day. Thus, there is some advantage to choosing a site with better-than-average seeing. If further analysis of adaptive optics requirements shows that the system can operate without Rayleigh beacons, or even without adaptive optics entirely, for some specified turbulence parameter r_0 , then there may be a significant advantage to finding a site that has low turbulence (large r_0) most or all of the time.

Near-ground turbulence due to thermal gradients can severely degrade seeing and make horizontal beam paths within a few meters of the ground unusable even over distances as short as a few hundred meters, so some minimal elevation (on the order of 10 m) of the launch stand and/or the boost laser will probably be needed if they are on flat ground.

3.1.5.2.5.10 Access, Infrastructure, and Resources

All sites will require road access for construction equipment (graders, concrete mixers, etc.) and heavy trucks delivering beam modules and other equipment. Traffic to the laser sites will be minimal during normal operation: primarily fuel (if delivered by truck) and beam modules or other equipment leaving the site for maintenance or being replaced.

The launch site will need large-truck access during normal operation for vehicle delivery, unless vehicle fabrication is done onsite, simply because each vehicle will fill a standard trailer. The launch site should also have, or have access to, a runway and facilities able to handle at least medium cargo aircraft, for air delivery of vehicles and payloads. (Air delivery would also accommodate future larger vehicles or vehicle components difficult to deliver by truck.) Rail and ship access will not be required.

Both laser sites will require either low- to medium-voltage transmission lines (e.g. 26 or 138 kV) if they do not derive power from onsite generators. (If they do not use energy storage on-site, a higher-voltage transmission line would be needed to deliver ~500 MW). Total energy use will be low enough (at ~1000 launches/year) that truck delivery of generator fuel would be acceptable if generators are used, although a pipeline would be preferable. The launch site will not have substantial power or fuel requirements unless hydrogen is generated on-site.

All sites will require a water supply, for cooling at the laser site and for noise and fire suppression at the launch site. The quantities needed are small by industrial standards—on the order of 1000 m³/day—but water supply may be an issue for desert or mountaintop sites.

3.1.5.3 CONOPS—Frequency of Launch and Repeat time

3.1.5.3.1 CONOPS

3.1.5.3.1.11 Prelaunch

Vehicles will be delivered from one or more manufacturing facilities to the launch site, either complete (preferred) or broken down for ease of transport with final assembly onsite. HXs or complete vehicles would typically be given a final integrated test on a static test stand or on a launch stand (with hold-downs), using the boost laser array for power. Note that the HX vehicle will be able to be fully tested on the pad, with the exception of one-shot (pyro or similar) mechanisms for releasing drop tanks or shrouds.

Most launches will be scheduled weeks or months in advance, allowing vehicle deliveries to be prescheduled—for example, for a few days before launch (which, at several launches per day, would still imply 10 or more vehicles onsite at a time). One or more vehicles (and possibly even some payloads) may

be stored onsite, however, to allow for short-notice (possibly <24-hr notice) launches or to replace vehicles that fail onsite testing. Launches would be scheduled within a given day based on

- Orbit requirements—Rendezvous with objects in orbit or injection into specific orbital planes will involve launch windows of a few minutes, usually twice per day.
- Priority/time criticality—Some launches may need to be timed to fixed external events (eclipses) or unpredictable short-duration events (solar flares, military missions, etc.).
- Predicted weather—Non-time-critical launches would presumably always have multiple launch dates in case of weather outages.
- Safety or operational restrictions—Although the launch system will generally not damage satellites exposed to the beam, such exposures are obviously undesirable, and coordination with other space activities will be needed.

Many details of the prelaunch operations are still undetermined: for example, whether vehicles are moved to the launch stands upright or horizontally, and whether payloads are loaded before or after vehicles are moved to a launch stand. Given the expected launch rate (up to several vehicles per day), vehicles would typically move to a launch stand less than a day before launch and would be unloaded and moved back to a storage/preparation area if a launch was aborted because of weather or technical problems.

Dense propellant could be loaded any time prior to launch. Liquid hydrogen would typically be loaded shortly (<1 hr) before launch to minimize boiloff. A swing-away jacket or housing would cover most of the vehicle, except the HX itself and the nozzle to provide additional insulation for the hydrogen tank. During and after hydrogen loading, the jacket would have dry gas flowed through it to prevent ice formation on the tank. (Depending on the tank insulation and coating, this may need to be hydrogen or helium to prevent cryopumping nitrogen or oxygen through the tank's own insulation.)

Safety and weather monitors would give the final approval for launch.

3.1.5.3.1.12 Launch

The general CONOPS for a launch is shown in Figure 3.86. A nominal timeline follows:

***T* – 30 s.**—The boost laser modules aim at the vehicle on the launch stand and begin tracking. Low-pressure hydrogen gas flows through the pump and HX inlet manifold to cool them to operating temperature.

***T* – 10 s.**—The boost laser array turns on at low power (~1% to 10% power), preheating the HX, and a small amount of hydrogen flows to bring the hot propulsion components up to temperature and provide an initial hot gas supply for the piston pump or turbopump. This will also provide an opportunity to check the pointing of the boost laser array.

***T* – 2 s.**—The boost laser turns on at full power, and hydrogen is pumped through the HX.

Liftoff.—Dense propellant flow is turned on, and the vehicle lifts off and accelerates vertically at ~0.5g acceleration (5 m/s^2)

***T* + 40 s.**—The vehicle reaches ~Mach 0.9. Dense propellant flow is turned off temporarily to reduce thrust and keep the vehicle subsonic. This reduces the peak dynamic pressure and avoids wasting propellant on air drag. (Dynamic pressure limits were not included in the COMPASS team's OTIS trajectory calculations, so this throttling was not performed, and the rest of the timeline is somewhat compressed).

***T* + 80 s.**—The vehicle reaches an altitude of ~20 km; dense propellant flow turns back on, and vehicle goes supersonic. The vehicle is now high enough for the main laser array to acquire the vehicle beacon and begin tracking, although atmospheric absorption and turbulence effects are still too high for efficient power transmission. Depending on various trades (power cost, laser life, and atmospheric properties) the main laser may switch on now or wait until the vehicle is higher.

If drop tanks are used, they would be dropped into a disposal zone close to the launch site. The DRM vehicle as defined by the COMPASS team will use two drop tanks released at $T \sim 75 \text{ s}$, while still

accelerating nearly straight up, which would put their nominal impact point very close to the launch site. A small sideways or downrange velocity increment would ensure that they fall a safe distance from the actual launch facility. It may be better to use the dense propellant somewhat more slowly, both for dynamic pressure control and to optimize the trajectory. In this case, the tanks could be released later and fall farther from the launch site, although still landing in a small disposal area. The tanks will be small and, when empty, lightweight: under 70 kg in the COMPASS design, which for simplicity uses a pressure feed system built into the tanks. (Their mass would be even less if they were low-pressure tanks feeding propellant to a pump.) The residual propellant will be nontoxic and minimally hazardous. We thus expect that the tanks can safely free fall into the disposal area, without needing any recovery system, but this will need to be considered in future range safety analyses if drop tanks are used.

T + 100 to 400 s.—The vehicle flies a conventional trajectory, approximating a gravity turn, although the turn starts at somewhat higher altitude than typical for conventional rockets, giving a “lofted” trajectory and keeping the vehicle positioned and oriented so that the boost laser has a reasonable incidence angle on the HX. Power comes mainly from the boost laser array until roughly $T + 200$ s and an altitude of 100 km. After that, both lasers provide power (with the main laser power adjusted to keep the total below the HX’s operating limits) until, somewhere between 300 and 400 s after launch, the boost laser beam has diverged far enough that it is not delivering significant power, and the boost array shuts off.

The lofted trajectory will serve two functions:

(1) It will keep the vehicle well above the horizon, as seen from the main laser site, out to the effective range of the laser array. Although some power can be delivered until the vehicle actually goes below the laser horizon, scattering losses and beamspread due to turbulence (or due to reaching the correction limits of practical adaptive optics) increase rapidly as the vehicle gets close to the horizon.

(2) It will allow the vehicle to release its payload directly into a stable orbit without a separate circularization burn. For the DRM system, the target orbit was a 400-km circular orbit, but payloads can reasonably be injected directly into essentially any circular or mildly elliptical orbit that has apogee > 300 km or perigee < 500 km and an accessible inclination (see Section 3.3.3.3—Accessible Orbits). This will eliminate the cost and complexity of keeping the vehicle stable and powered for a half-orbit, or equipping the payload with propulsion and attitude control for the circularization burn. In many cases, the circularization burn is the only maneuver required by a satellite, so injecting directly into the final orbit eliminates an entire propulsion subsystem.

Even if the payload cannot be injected directly into its final orbit, a stable initial orbit with a reasonable lifetime allows the payload to begin operations—for example, deploy solar panels or initialize attitude control systems—before maneuvering, and to use low-thrust propulsion (solar- or beam-powered) to reach its final orbit, if desired; this is generally not feasible without a circularization burn if the initial perigee is below ~ 200 km.

T + 400 to 600 s.—The vehicle accelerates horizontally, powered by the main laser, until it reaches nearly its orbital injection altitude.

T + 600 to 720 s.—The vehicle pitches increasingly nose-down, typically to between 10° and 30° below horizontal at burnout. This again serves two purposes:

(1) The lofted trajectory tends to give the vehicle some excess upward velocity, on the order of 100 m/s, which must be cancelled to bring the trajectory tangential to the final orbit. The nose-down maneuver provides a small downward component to the final part of the acceleration, with minimal impact on the total launch ΔV .

(2) The downward pitch increases the angle between the vehicle axis and the laser beam, increasing the projected area of the HX and thus the collected power.

T + 720 s.—Orbit insertion and main laser shutdown—The main laser beam modules begin to slew telescopes back toward launch site.

T + 900 s.—The vehicle opens its shroud (if it has not already been jettisoned) and releases the payload. The vehicle then aims its nozzle forward and vents residual hydrogen through the propulsion system, both to lower its orbit and to ensure that it will not rupture the propellant tank. It may further

rotate to a stable high-drag orientation to minimize the time before its orbit decays and it reenters. Alternatively, the vehicle can stay in orbit with the payload attached. For example, this might be preferred for a short-duration mission that could save cost by using the vehicle's electronics and attitude control system.

3.1.5.3.1.13 Reentry

Because the empty vehicle has a very low areal density (low beta), it will not necessarily burn up on reentry, and there may be a debris hazard if it reenters over land. If necessary, vehicles can be configured with enough residual propellant and power to control the approximate time and general area of reentry. If the vehicle is oriented with the HX toward Earth (or even better, toward the Sun), it can be kept at ~ 300 K or higher, so that residual hydrogen gas can deliver impulse at an I_{sp} of ~ 300 s. Alternatively, a small laser array—even a single beam module—can raise the HX temperature for low-thrust maneuvers that are regularly done over a fixed location.

3.1.5.3.2 Launch Rate

As noted previously, the launch facility would have at least two launch stands, preferably more, so that multiple vehicles could be prepared for launch at once (and also so that a problem with one vehicle or launch stand would not shut down operations).

The minimum time between launches would then be limited by the time needed to complete the first launch and move the laser array optics back to their starting positions. The boost laser array will typically operate for ~ 400 s, and could certainly reset in < 100 s. The main laser array will operate from (nominally) $T + 80$ s for start of tracking through $T + 720$ s. If it can slew back to the starting position in < 80 s, the next vehicle could launch at $T + 720$ s (and be acquired by the main laser array at $T + 800$ s), corresponding to 12 min between launches, sustainable as long as there is sufficient power and cooling for the lasers.

If the launch rate was critical (e.g., for launching multiple vehicles to a single orbital plane), the main laser array could begin tracking later and could cut off slightly earlier, since it would deliver relatively little power at the extremes of the trajectory. It may also be designed for faster slewing. Time between launches might thus be reduced to 10 min or less, with slightly reduced payload.

If the system is not designed for continuous rapid launch, then once a launch or burst of launches is complete, there would need to be a delay to recharge the energy storage system and cool down the thermal sink, as well as to move new vehicles onto the launch stands. For example, with energy storage and heat sink capacity for two launches, and an 8-hr recharge time, a system could maintain a rate of one launch every 4 hr, or a pair of launches 10 min apart once every 8 hr, until either personnel or launch-ready vehicles and payloads were exhausted.

3.1.5.3.3 Accessible Orbit

As shown in Figure 3.99, a single launch site and main laser array define a preferred launch azimuth by their relative positions, but small deviations from the preferred azimuth do not have much effect on the system performance. A $\pm 15^\circ$ deviation reduces the acceleration path by only 2%. Larger deviations will incur progressively larger performance penalties as the effective acceleration path gets shorter, but a single continental-U.S. launch site could easily access orbits from $\sim 30^\circ$ inclined (straight eastward launch from 30° latitude) to at least 60° inclined.

The accessible azimuth range might also be limited by range safety concerns, at least until the expected low probability and modest impact of launch failures was demonstrated and accepted. Launch trajectories with impact-point paths that cross major population centers might never be permitted. Similarly, impact-point paths that cross other countries or their territorial waters will require appropriate international agreements.

Individual cities or smaller hazard zones could be avoided by allowing small doglegs in the trajectory, as also shown in Figure 3.101. If done while the vehicle horizontal velocity was low, these doglegs would

cost very little ΔV , although a full analysis is needed to see how much deflection is feasible. Doglegs would also allow two or more vehicles to launch to the same inclined orbital plane in a single launch window, and allow azimuth-offset trajectories to pass closer to the laser array, potentially making up for the extra ΔV needed.

The main laser array will be the most expensive part of the launch system, so if a wider range of azimuths is needed, it may be possible to build two or more launch sites and boost laser sites that share a single main laser site (e.g., one west of the main array for equatorial launches and one north or south for polar launches). This does require the main laser array beam modules to point over a wide range of angles, which may raise the cost of the telescope mounts and the land area needed for the array (so that lines of sight are not blocked by neighboring beam modules).

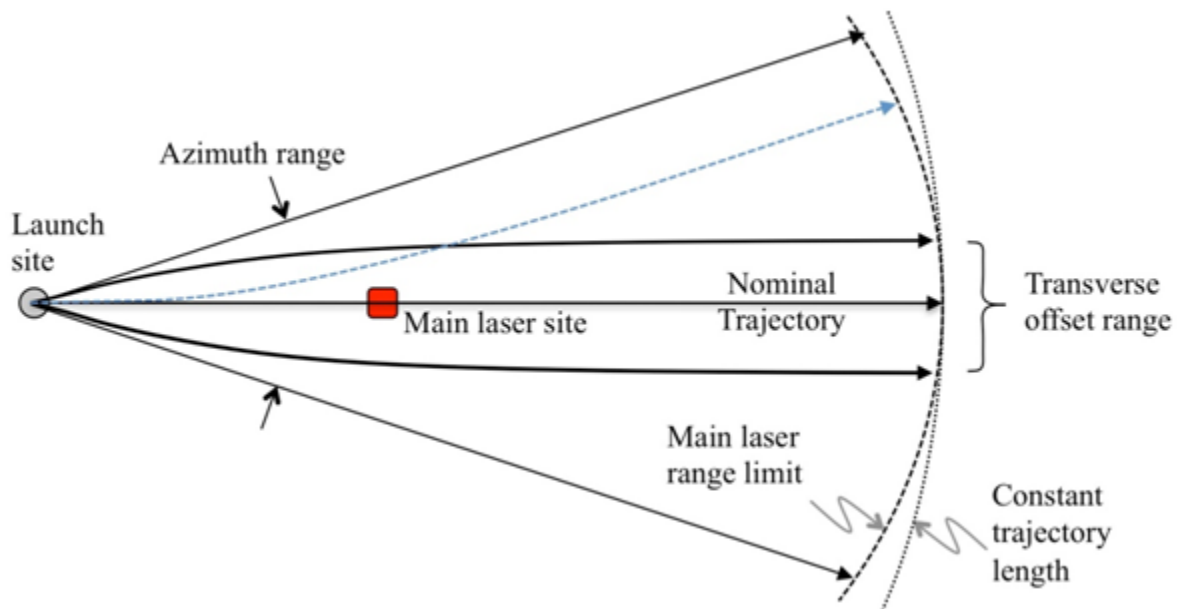


Figure 3.99.—Variable launch azimuth and dogleg trajectory offset capability with a single launch site and laser site.

The COMPASS DRM analysis considered only eastward launches, and there will be some reduction in payload for polar or retrograde launches. However, because of the high I_{sp} of the propulsion system, the effect will be small in comparison to the effect on a single- or even two-stage chemical rocket.

A partly or wholly sea-based launch system would allow launches to (almost) any azimuth, as well as having advantages for range safety, minimum orbit inclination, and so on. A partially sea-based system would put the vehicle launcher and boost laser array on ships, with the main laser array on land (possibly an island). Sea-based laser launch is not ruled out by atmospheric transmission (although some laser wavelengths would experience higher losses) or by any other fundamental issues we know of. However, the operating and maintenance costs would be substantially higher than for a land-based system. Similarly, an air-dropped vehicle using chemical strap-ons to climb into view of the main laser array could be launched from any point, and thus to any azimuth allowed by safety limits and array pointing capability.

3.1.5.3.3.14 Geosynchronous Transfer and Upper Stage Capability

The DRM vehicle does not have sufficient single-stage delta-V for direct injection of payloads into geosynchronous transfer orbit (GTO), but adding a solid- or liquid-fuel upper stage (using roughly 50% of the normal payload mass) would allow launching small payloads to GTO. Because the laser launch mass scales rapidly with final velocity (roughly as v_f^3) using such a small upper stage can also allow

launching significantly (~2 times) heavier individual payloads to LEO, although presumably at higher marginal launch cost per kilogram. This is similar to chemical single-stage-to-orbit (SSTO) designs, which can deliver much larger payloads to LEO if operated as “nearly SSTO” suborbital vehicles carrying payloads with attached kick stages.

3.1.5.3.4 Availability

Any ground-based laser (GBL) (or millimeter-wave) beam source will be blocked by any visible cloud, and may even be unacceptably attenuated by subvisible clouds. Laser sources may also have problems with unusually turbulent air or high ground-level winds. Selected sites in the southwest United States can have acceptable conditions for laser launch nearly continuously for large parts of the year, and on average for 70% to 80% of the year. For applications where operations can be limited during some parts of the year, or where individual launches can accept delays of up to several days, a single well-chosen launch site/boost laser array and a single main laser site can probably provide acceptable availability.

A second launch site and boost laser array (sharing a single main laser array) will slightly increase availability if the two launch sites are some distance apart, since one may be clear when the other is blocked, but unless the two launch sites serve different orbits (e.g., polar vs. low inclination), the weather at two sites is likely to be correlated.

Substantially higher probability of access is possible if two (or more) complete launch systems are built, far enough apart to have relatively uncorrelated local weather. In this case, the chances of both being unavailable at any given time can be as low as ~10%, with the chance of an extended (e.g., >24 hr) outage being even lower. A very-high-availability launch system (e.g., for military use) would thus require at least two fully independent launch systems, and possibly three or more. A multisite system might have each site optimized for one type of launch (most obviously polar vs. low inclination) with “backup” capability for other types of launches: for example, using chemical boosters rather than a boost laser array. The backup capability would be used only for time-critical launches when the corresponding primary site was down because of weather or other problems. An alternative for high availability would be a ship-based launch system, which could move to clear areas (typically equatorial) and move out of the paths of storms.

Finally, it is possible that, at the power levels of interest, a suitable laser array could actually clear at least light cloud cover. Unfortunately, the main and boost laser array wavelengths will be chosen to minimize water absorption, so they could not do their own cloud clearing. Most cloud-clearing experiments have used 10.6- μm carbon dioxide (CO_2) lasers, but other wavelengths may work.

The modular laser array will allow very close to 100% availability with respect to hardware failures, by providing a modest number of “spare” modules (and associated energy storage and cooling capacity). Redundant prime power (e.g., grid tie plus local generators) would eliminate downtime due to power failures. With appropriate design (e.g., duplicate control facilities) a laser launch system could be essentially immune to single-point failure or physical damage, including (nonnuclear) attack.

3.1.5.4 Costs

3.1.5.4.1 Vehicle

3.1.5.4.1.15 General Comments on the Cost of HX Vehicles

“If you do the same things you’ve always done, you’ll get the same results you’ve always gotten”
-- Jeff Greason, CEO, XCOR Aerospace

In theory, a chemical rocket able to launch payloads to Earth orbit should be simple and cheap to build. In practice, many attempts to build “cheap” launch vehicles have either failed (OTRAG, Beal,

Rotary Rocket, Kistler, etc.) or have succeeded in building launchers only modestly cheaper than previous ones, at a higher than originally projected cost (Orbital Sciences and SpaceX).

If expendable HX vehicles are built with the same programmatic approaches as past launch vehicles, they will be expensive, although marginally less so (by perhaps a factor of 2) than existing small expendables. They do have the advantage of being single-stage (or nearly so) versus at-least-two stage chemical rockets. However, single-stage expendable chemical rockets are feasible, and many have been proposed. HX vehicles are simple, but there have been many designs for equally simple chemical rockets, including solid (no valves), hybrid (one valve per stage), and pressure-fed liquid (two valves per stage) rockets. HX vehicles have better mass ratios than chemical launch vehicles—higher dry mass/gross liftoff weight (GLOW) than single-stage launchers and higher payload mass/dry mass than two-stage launchers—but not overwhelmingly so. They will still require advanced materials and lightweight construction.

The true advantage of HX vehicles is that they can be built like other industrial products, not like aerospace vehicles. They would be built in sufficient quantities to support assembly-line and mass-production techniques wholly unfeasible for production rates of a few per year, and also in quantities that would support development and production by two or more competing suppliers. Production quantities are sufficient, and testing costs low enough, to support development and flight testing of new components and subsystems rather than depending on heritage hardware wherever possible.

HX vehicles can be fully integrated and then tested on the ground before flight (unlike multistage vehicles and solid rockets). Components and subsystems can be certified and then built to print, as with most aircraft parts. They should not require extensive—and expensive—testing of each individual component and subsystem for each vehicle. Indeed, since launch failures will pose only modest financial risk (given the small vehicle size and ease of relaunching payloads) and no risk of loss of life, the certification and component tracking needed should be substantially less than for commercial or military aircraft.

Cars cost ~\$20/kg. Exotic, handbuilt cars, built in smaller numbers than we propose for HX launch vehicles, cost \$200/kg to \$500/kg. Light piston aircraft, which *do* kill people when they fail, cost ~\$500/kg.⁵ Tomahawk Block IV cruise missiles have a dry weight (less fuel and explosive) of roughly 800 kg; the 2004 Block IV production contract was for 2200 missiles at a unit cost of \$730,000. Since the unit cost presumably includes somewhat more than the actual missile (at a minimum, its solid booster) the specific cost is less than \$900/kg (Ref. 39).

The author of this section is not in a position to do a detailed vehicle cost estimate for this report. The cost of the HX in particular is very difficult to estimate, since neither the final design nor the fabrication approach is known. However, unless the HX vehicle has some specific component (such as the HX) that is *extremely* costly, the production cost at quantities on the order of 1000/yr should fall in this range: \$1000/kg worst case and \$500/kg nominal, with \$200/kg a reasonable goal. The corresponding complete vehicle cost would be nominally \$530 K (dry mass of 1060 kg, including drop tanks, at \$500/kg), with a worst case of \$1060 K and a goal (with no drop tanks and a slightly more optimistic vehicle dry mass of 800 kg) of \$160 K.

3.1.5.4.1.16 COMPASS Cost Estimate Versus Past Launch Vehicles

The COMPASS cost estimate of ~\$12 million per vehicle for the DRM-1B vehicle is extremely high, and inconsistent with all prior launch vehicle experience, both government and commercial. This appears to be an artifact of using spacecraft costing rules.

A very quick analysis of a few existing expendable launch vehicles is given in Table 3.21. (Much better and more extensive data are available, but locating, compiling, and analyzing it was outside this author's scope of work.) The general trend is evident even from this limited data set: launch vehicles tend

⁵For example, the Cessna 400 (Corvalis TT) composite aircraft, which was introduced in 2004—empty weight of 1134 kg, list price of \$644,500 (Ref. 38).

to cost \$3000/kg to \$6000/kg dry mass, with vehicles developed primarily for commercial launches on the low end of the range. (Ariane 5 is unusually low because ~80% of its dry mass is solid booster casings). The Falcon 1E and Delta IV Heavy differ by a factor of almost 30 in dry mass, but they have similar cost per kilogram. All of these vehicles were built in quantities of 10s, although generally with considerable variation so that any given configuration might launch only a few times. Note that this is the launch price, not the actual cost of manufacture, and it includes the vehicle provider’s development cost amortization and profit.

At the Falcon 1E cost of \$3250/kg, the DRM-1B vehicle (non-drop-tank configuration, dry mass of 920 kg) would cost \$3.0 million each. If we assume that this is for 20 vehicles, scaling to ~3000 vehicles (3 years of 1000/yr) would imply 7 doublings of production, and, with a 0.85 learning curve, a marginal vehicle cost of $\$3.0 \text{ million} \times 0.85^7 = \0.96 million , roughly \$1050/kg.

We thus estimate that the COMPASS cost estimate is about tenfold too high, even in comparison to existing launch vehicle production techniques and procedures. With all respect to the efforts of the COMPASS team in developing a cost estimate under difficult time and resource constraints, ***this author must recommend that the COMPASS cost estimates be considered to be invalid.***

(As a check on the preceding cost estimate, we note that the Space-X Falcon 1E is a two-stage launch vehicle with each stage comparable to the laser-HX vehicle in complexity. A firm launch price of \$9.1M was quoted in 2008, so the vehicle itself presumably cost significantly less. It is difficult to understand how the HX vehicle could cost *more* than the Falcon 1E even in small quantities, unless the HX itself is exorbitantly expensive.)

TABLE 3.21.—LAUNCH VEHICLE COST PER KILOGRAM DRY MASS

Launch vehicle	Dry mass	Cost, ^a \$M	Cost per mass, ^a \$/kg
Falcon 1E	3419	11.1	3252
Pegasus XL	3705	18.1	4891
Ariane 4L	32015	131	4092
Ariane 5G	97000	236	2431
Delta IV heavy	85770	302	3524
Saturn V	181965	1110	6100

^a2011 dollars.

3.1.5.4.2 Ground System Capital Cost

3.1.5.4.2.17 Laser Costs and Cost Trends

Diode lasers.—The ground system costs will almost certainly be dominated by the cost of the lasers themselves. Projecting laser costs is difficult because there is relatively little published data on high-power laser prices, and the total market for high-power lasers is small (compared to, e.g., computer systems) and highly diverse.

For semiconductor diode lasers, prices for small quantities of packaged high-power multimode diodes or diode bars have been roughly stable for the past decade at ~\$10/W (then-year dollars, so decreasing slowly in constant dollars), but the performance of the devices has improved considerably; in particular, the lifetime of diode bar stacks has more than doubled, from <10 000 to >20 000 hr. There does not seem to be any reason for this to be a limit, however. Figure 3.100 shows the decline in laser diode bar prices with quantity estimated by Lawrence Livermore National Laboratory (LLNL, Ref. 40) in connection with inertial confinement fusion laser designs. These would be very similar to the diode lasers needed for either direct use (boost laser) or pumping fiber or other solid-state lasers for a launch system, except for operating pulsed (which allows somewhat higher peak power per diode).

A launch system boost laser array would require ~2×10⁶ diode bars at 100 W/bar; this is similar to the LLNL Mercury laser project, for which LLNL was quoted \$0.35/W several years ago. Even if we assume

a factor of 3 for diode power and packaging differences for CW versus pulsed lasers, this would put the cost of the boost laser array diodes at $\sim \$1/W$, with no further progress in diode laser technology.

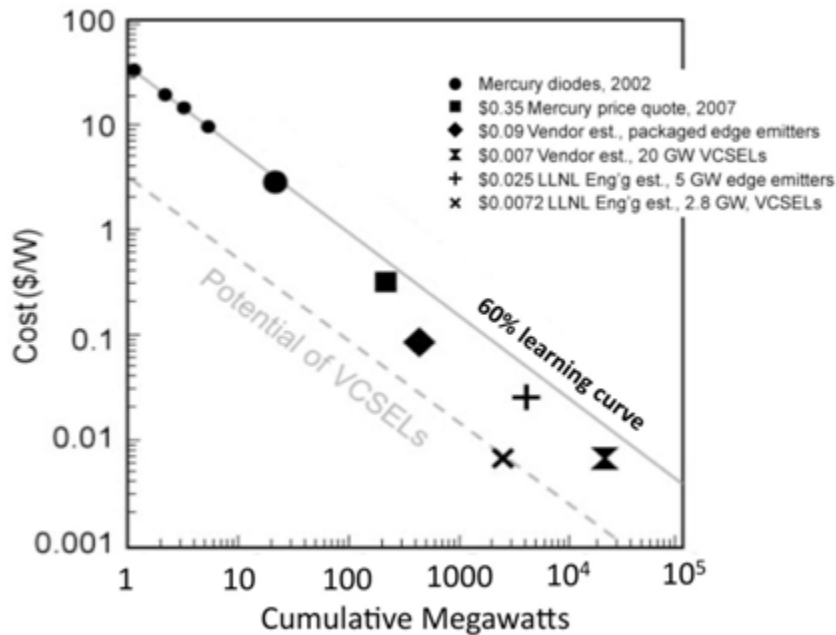


Figure 3.100.—Lawrence Livermore National Laboratory Laser diode cost estimates.

Although we were unable to find good price-versus-time data for laser diode bars, Figure 3.101 (Ref. 41) shows data for a reasonably good proxy: red light-emitting diodes (LEDs). This plot illustrates Haitz’s Law, analogous to Moore’s Law, which states that LED price per lumen falls 10 times per decade ($\sim 20\%$ per year), whereas the performance, in lumens per device, increases 20 times per decade. This has been driven in part by the adoption of LEDs for mass-market applications requiring high power, such as traffic signals and automobile taillights, but also by steady improvements in fabrication and packaging technology. If we assume that there will be comparable improvements in high-power diodes (i.e., a resumption of the “normal” development curve, possibly stimulated by the prospect of a substantial new market) the 2021 price would be $\sim \$1/W$.

As a worst-case estimate on a simple quantity-discount basis, if the “price break” for laser diode bars is 20% for each factor of 10 in quantity, the current price for ~ 2 million bars would be about 40% of the small-quantity (100-bar) price, or $\$4/W$.

An unusual example of price variation with quantity for SOA photonic devices is available online: Sensor Electronic Technology publishes a price list for their ultraviolet (240- to 366-nm) LEDs for quantities from 1 to 10 through 1 000 000 units (Ref. 42). Figure 3.102 shows prices for two typical devices (255 and 345 nm) in two packages (flat window and ball lens). Note that in all cases, there is a sharp break in the slope of price versus quantity at a few thousand units. For flat-window devices (where the packaging cost is low) the ratio between the 100-unit and million-unit price is roughly 20:1. Although we would not expect that large a ratio for commodity laser diodes or diode bars, it would be quite appropriate for current low-production devices such as single-mode or frequency-locked high-power diodes, or unusual wavelengths. For ball-lens packaging, the cost of the lens and alignment drops much more slowly with quantity, from a $\sim \$30/unit$ premium over a flat window for small quantities to $\$5/unit$ to $\$8/unit$ for a million units. This is consistent with an overall drop in price where packaging is a dominant cost of a factor of 4 to 6 over 6 decades, or about 25% to 30% per decade, but with most of the drop at higher quantities.

We, therefore, have four projections: $\sim \$1/W$, $\sim \$1/W$, $\sim \$2/W$ (if packaging dominates), and a worst case of $\sim \$4/W$. There would be an additional amount for wavelength- and polarization-combining optics (currently $\sim \$1/W$ for small quantities. This also would presumably drop by \sim fourfold for million-unit quantities). For system cost estimates, we assumed $\$2/W$ for fiber pumps and $\$1.50/W$ for boost laser diode arrays.

(With current assembly techniques, fiber-coupled laser diodes and diode arrays are substantially more expensive than “free-space” diodes, in the range of $\$25/W$ to $\$50/W$ retail. This contributes to the cost of fiber laser designs using fiber-coupled pump diodes (IPG and others). Fiber-coupled laser diodes also have somewhat lower radiance than free-space diodes. The baseline boost-laser beam module concept thus does not use fiber coupling but mounts the diodes directly on the telescopes.)

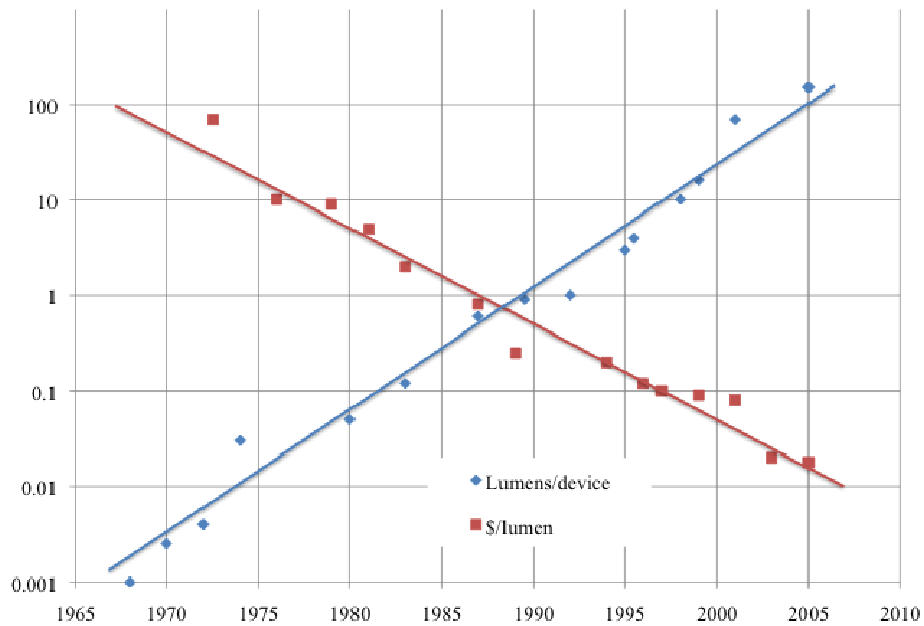


Figure 3.101.—Haitz’s Law for light-emitting diode (LED) price and performance versus time.

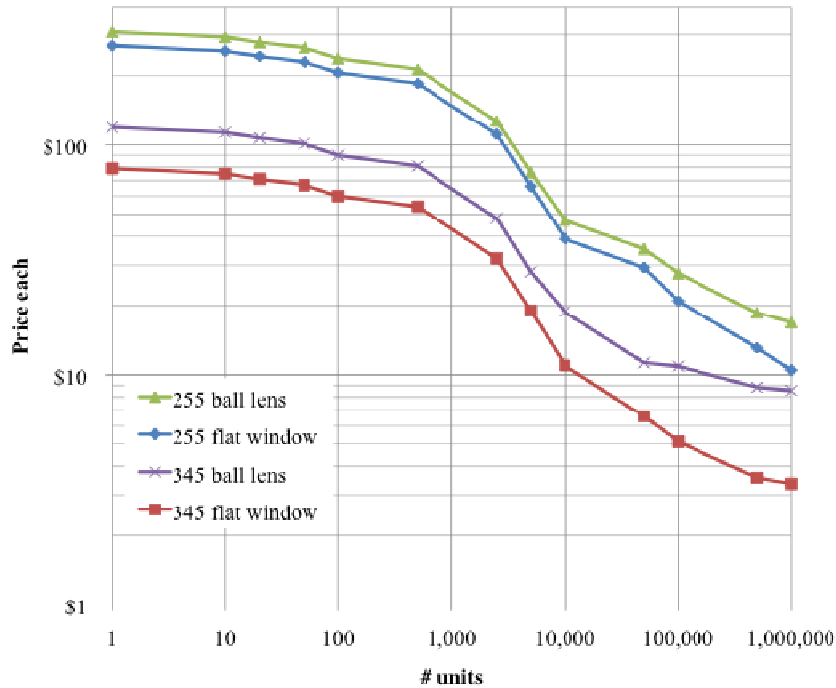


Figure 3.102.—Example of scaling ultraviolet light-emitting diode (LED) prices over 6 decades of quantity.

Fiber lasers.—Data on fiber lasers are even more limited than on high-power diodes. Current costs for high-power (>1-kW) multimode fiber lasers, which are manufactured in small quantities, are estimated at \$40/W to \$50/W (Ref. 43). Discussions with IPG suggest moderately higher real prices for their large systems, ~\$75/W, but with projected prices of \$35/W for a large order circa 2013.

Single-mode fiber lasers (and indeed all types of single-mode lasers) are somewhat more expensive than comparable multimode lasers. The IPG YLS-10000-SM 10-kW fiber laser, although it is proof of technology readiness, is a relatively high-cost design and not a good cost data point. One source estimates a cost of \$1000/W for the prototype (Ref. 43). We do not have a good reference for kilowatt-class single-mode fiber lasers but have recently been quoted \$135/W for a smaller (100-W) fiber laser for 100 units (i.e., 10 kW). We take the current cost for single-mode lasers as between 1.5 and 2 times the cost of multimode (within the power ranges where both are available).

Fiber lasers have generally scaled in price with the price of their pump lasers, with multimode fiber lasers costing ~3 times the pump laser cost. However, the production volume for high-power fiber lasers is very low, ~\$500M/year for all fiber lasers (Ref. 44), or ~5 MW of laser power, only a fraction of which is for kilowatt-class lasers. Kare and Parkin (Ref. 26) estimated \$10.50 for fiber lasers in the 150-MW quantity, assuming \$100/W for a single 10-kW laser (versus actual 2005 prices of \$200/W to 500/W) and an 85% learning curve. This is consistent with extrapolated pump diode pricing (\$2/W × 3 for single mode and × 5 for multimode).

Fiber laser prices appear to have dropped at least threefold to fourfold in 6 years (since 2005), which is consistent with a tenfold/10 year drop similar to Haitz’s law for LEDs. This would give a price of ~\$10/W to \$15/W for single-mode lasers in small quantities by 2021. Alternatively, a ~40-times increase in total production, from ~5 to ~200 MW, would give a sevenfold price drop for a 70% learning curve or a fifteenfold drop for the 60% learning curve estimated by LLNL for laser diodes.

We therefore still project a price for single-mode fiber lasers of \$10/W for quantities from ~150 to 200 MW, circa 2021, with the caveat that this could easily be in error by a factor of 2 in either direction.

A comment on lasers versus millimeter-wave sources.—The author of this section believes that lasers are cost competitive with millimeter-wave gyrotrons on a system basis, even though a naïve look at current prices (\$1 million buys a 1-MW gyrotron tube, or a 10-kW fiber laser) would suggest that lasers have an insurmountable price disadvantage. There are many reasons for this. Partly, this 100:1 ratio is not a valid comparison:

- The preceding comparison is between a bare tube and a complete industrial laser system (the correspondingly complete millimeter-wave system would cost between \$2 and \$4 million for 1 MW).
- The microwave system has a much shorter range, and therefore requires several times more power per unit mass to orbit. With equivalent assumptions about vehicle design and component masses, the higher power/vehicle mass ratio means that the millimeter-wave vehicle will also have a smaller payload (or require even higher power). The alternative of scaling the microwave system aperture to give laser-system-equivalent range appears to be more expensive and technically challenging.
- However, there are also issues relating to cost and technology projections:
- Lasers for a launch system would be built in much larger quantities (>10 000 units) than gyrotron systems (a few × 100 units), so the learning-curve discount will be much greater;
- High-power fiber lasers are a very new technology (developed circa 2001) and have multiple competing technologies (disk lasers, diode pumped alkali vapor lasers, and grating-combined wavelength-stabilized diode arrays). The cost/performance ratio is thus likely to improve much faster than for gyrotrons.
- Kilowatt-class lasers have a substantial industrial market and make use of technologies (optical fibers and laser diodes) that have very large markets and large R&D communities. Megawatt-class gyrotrons currently have a single specialized market (heating fusion plasmas) and use technologies from a specialized field (high-power microwave tubes).
- Laser costs are still dominated by the cost of the laser hardware itself and are far from being limited by mature supporting technologies (power supplies, connectors, and structural supports). millimeter-wave gyrotrons are already approaching that limit and thus are less likely to see substantial system-level cost reductions.

Some of these aspects have not yet been researched and were not within the scope of this study, but they should be addressed (e.g., through analysis of development funding and cost histories for these and comparable past technologies) before any decisions on source technology are made.

3.1.5.4.2.18 Main Laser Array Cost

A rough capital cost estimate for the main laser site is given in Table 3.22 and Table 3.23. Table 3.22 gives the cost of a single beam module, and Table 3.23 gives the overall site cost, assuming 2500 beam modules; 2500 beam modules would give 150 MW of laser output power, allowing for 20% total losses between the laser output and the maximum vehicle absorbed power.

TABLE 3.22.—CAPITAL COST FOR A NOMINAL
60-KW MAIN-LASER BEAM MODULE

Component	Cost, \$K	Basis
Single-mode fiber lasers	600	6 × 10 kW at \$10/W
Telescopes	120	6 × 40 cm at \$20K
Telescope mount	60	
Pointing and tracking	20	
Adaptive optics	90	6 × 15K ^a
AO beacon	20	1 × 30K
Assembly, transport, and installation	80	
TOTAL	\$990 K	

^aThorlabs AO system (\$24K) × 2 for a high-power mirror
× 0.32 for an 85% learning curve.

TABLE 3.23.—CAPITAL COST FOR MAIN LASER SITE WITH 2500 BEAM MODULES

Element		Cost, \$M	Basis
Beam modules	Number	2475	2500 at \$0.99M each
Telescopes, etc.	1500		
Lasers	500		
AO and beacon	275		
Assemble, test, and integrate (A T & I)	200		
Prime power and cooling		20	20 MW at \$1/W
Energy storage		80	Three launches at ~\$26M ^a
Control and safety systems		40	
Land and infrastructure		80	800 acres at \$100K/acre
Planning, permitting, etc.		100	
TOTAL		\$2795 M	

^aSee Section 3.1.5.2.2—Main Laser Site Design

Note that this estimate is for the lowest likely beam module power (60 kW). Several cost elements (land, site preparation, and optics and tracking) are roughly proportional to the number of beam modules, so higher module power would somewhat reduce costs.

3.1.5.4.2.19 Boost Laser Array Cost

An approximate capital cost for the boost laser site is given in Table 3.24 (beam modules) and Table 3.25(overall site), with the assumption of 1200 beam modules at 200 kW each. This would give 240 MW of laser output power.

TABLE 3.24.—CAPITAL COST FOR A NOMINAL 200-KW BOOST-LASER BEAM MODULE

Component	Cost, \$K	Basis
Laser diode arrays	300	200 kW at \$1.50/W
Power supplies	70	350 kW at \$0.20/W
Beam-shaping micro-optics	30	200 kW at \$0.15/W
Telescopes ^a	200	10 m ² at \$20 K/m ²
Telescope mount	50	
Pointing and tracking	20	
Adaptive optics, AO beacon	N/A ^b	
Assembly, transport, and installation	80	
TOTAL	\$750 K	

^aPlate-glass honeycomb or similar low-cost optics.

^bNot applicable.

TABLE 3.25.—CAPITAL COST FOR BOOST LASER SITE WITH 1200 BEAM MODULES

Element	Number	Cost, \$M	Basis
Beam modules		900	1200 at \$0.75M each
Lasers, etc.	480		
Telescopes, etc.	324		
A, T, & I	96		
Prime power and cooling		16	20 MW at \$0.80/W ^a
Energy storage		72	Three launches at \$24M ^a
Control and safety systems		40	
Land and infrastructure		80	400 acres at \$100K/acre
Planning, permitting, etc.		100	
TOTAL		\$1208 M	

^aSmaller cooling load and slightly lower total energy than main laser array because of higher efficiency of laser diodes versus fiber lasers.

The boost laser array cost is somewhat less dominated by the cost of the lasers themselves, and is thus more sensitive to other costs, especially optics.

3.1.5.4.2.20 Launch Site Cost

A token cost breakdown for the launch site is given in Table 3.26. The launch site can be a comparatively modest facility because of the small scale of the vehicles. The vehicles are roughly the same size as existing small launch vehicles (e.g., Minotaur or Pegasus) but much lower in both dry and wet mass. A new launch pad and gantry for Minotaur I was built at Wallops Island for approximately \$10 million. We take this as a typical cost for each of four launch stands. However, except for the cooling jacket and hydrogen plumbing, the launch stands will be very simple.

TABLE 3.26.—CAPITAL COST FOR LAUNCH SITE

Element	Cost, \$M	Basis
Launch stands	40	Four stands at \$10 M each
Launch control and range safety	80	
Static test stand	20	Launch stand and test equipment 12 bays at \$2.5M each ^a
Vehicle preparation facility	30	
Hydrogen storage and handling	10	
Land and infrastructure	40	
TOTAL	\$220 M	

^a~500 m² per bay, \$5000/m²

The largest single cost is assumed to be the launch control facility, including actual launch control and communications as well as safety systems (perimeter sensors and radar), optical and radar vehicle tracking, prelaunch vehicle monitoring, and vehicle test controls. The number given (for the laser sites as well as the launch site) is very much an order-of-magnitude estimate, but we note that the intent is to keep the total crew involved in a launch to a small number, on the order of 10, with most of the capital cost being in sensors and automation.

Other launch site infrastructure will depend on how much vehicle assembly and launch preparation is done onsite. Ideally, vehicles will be delivered from the vehicle plant, by truck or aircraft, essentially launch-ready except for installing the payload and closing the shroud. In keeping with the overall theme of high-volume “production-line” operation, there will be few or no high-cost facilities such as cleanrooms and very limited onsite storage for payloads or vehicles beyond those being actively prepped for launch.

We assume liquid hydrogen is delivered by truck (roughly one truckload per launch) at a cost of ~\$0.30/kg (Ref. 44) so there will be no onsite hydrogen production or bulk storage. If storage is needed, a 300 000-kg capacity tank (~100 launches) would be ~\$10 million.

The launch facility cost may be higher if road or (especially) runway construction is required.

3.1.5.4.2.21 Cost of Other Ground Facilities

We are not including the vehicle manufacturing facilities in the ground facilities; vehicles are presumed to be purchased from one or more vendors.

One possible large cost is for a full-scale test facility for HX propulsion. If a dedicated full-scale test facility is deemed to be necessary, however, we assume that an existing engine test facility could be used in conjunction with a short-range laser-diode beam source. “Cheap” low-brightness laser diodes and small optics would be sufficient for this, and we estimate the full cost at ~\$400 million for a 200-MW source. However, we would strongly recommend using the boost laser array and launch facility for full-scale testing. This would require only building a suitable thrust test stand with the ability to burn off ~10 kg/s of hydrogen exhaust safely. We allocate ~\$20 million for this within the launch site.

3.1.5.4.2.22 Total Capital Cost and Cost Scaling

The estimate in Table 3.22 to Table 3.26 gives a total system capital cost of approximately \$4.2 billion. This is somewhat higher than the prior estimate by Kare and Parkin (Ref. 26) of \$2.85 billion. The increase is due mainly to three factors:

(1) *Incorporating the boost laser site, which, at \$1.2 billion, is nearly 30% of the total cost:* This cost is particularly high because of the very high power level—220 MW—used for the COMPASS design effort. We expect that an 80- to 100-kg payload will in fact require no more than ~150 MW of boost laser power, reducing this cost to \$800 million or less. Note that \$1.2 billion, amortized over 10 000 launches, is \$120,000 per launch. If the per-launch cost of using, for example, solid booster rockets for vertical ascent to 100 km is substantially less than this. The DRM system would be more economical without the boost laser.

(2) *Including many system-level costs not covered in the earlier estimate:* These include land and infrastructure, launch site, control and safety systems, plus allowance for assembly, transport, and installation of beam modules. (Kare and Parkin included only the actual lasers and optics, plus power and cooling.) These costs total over \$500 million (excluding the costs relating to the boost laser). They are extremely rough estimates and should be considered largely as placeholders for more detailed studies. However, they serve to give an idea of the potential costs.

(3) *Including adaptive optics and Rayleigh beacons in the beam modules:* This adds ~\$250 million, mostly for the adaptive optics themselves. This would be lower if the power per beam were higher than 10 kW.

Offsetting these costs are a slightly lower laser cost estimate (\$10 vs. \$10.50) and lower power and cooling costs (\$100 million vs. \$240 million) because of the low launch rate assumed for the DRM system.

3.1.5.4.3 Operating Costs and Cost Per Launch

The operating and maintenance costs for large laser arrays is not well known. We have seen estimates ranging from 2% to 20% of capital costs per year (the high end being the entire operating budget for research facilities such as national laboratories). We assume an intermediate value of 5% of capital cost for operation and maintenance (O&M) for both laser sites and the launch site, or approximately \$200 million/year. (Note that this does not include depreciation or cost of capital.) Much of this would be for routine maintenance of mechanical and electronic hardware, and periodic cleaning of exposed optics. On the basis of industrial and telecommunications experience, fiber lasers themselves are extremely reliable, with essentially no maintenance needed over the launch system lifetime.

Marginal launch costs are dominated by the vehicle cost, which we assume (per the discussion in Section 3.1.5.4.1—Vehicle) will be on the order of \$1 million or less, possibly as low as \$200,000. If we assume a lifetime of >10 000 hr for both diode and fiber lasers, a launch rate of 1000/yr will use only ~1% of the laser life per year, so the lasers will not need to be replaced over the life of the launch facility. At much higher launch rates, laser replacement costs could become significant.

Power costs will be essentially negligible. A launch will require roughly $400 \text{ MW} \times 0.2 \text{ hr} = 80 \text{ MW-hr}$. Even at \$0.10/kWh, this would be only \$8000.

Propellant costs will be similarly small. Even at a conservative cost for liquid hydrogen of \$5/kg, the cost per launch would be \$15,830 for the COMPASS design, plus a negligible cost for water/hydrogen peroxide or liquid nitrogen.

Actual vehicle preparation and launch operations are expected to take on the order of 1 to 2 person-months (e.g., a four-person team per vehicle, working for 1 to 2 weeks) for checkout and payload attachment, plus <1 day of a ten-person launch operations team. At \$10K/person-month, this would be \$10,000 to \$20,000.

Thus, if the system capital cost is treated as a sunk cost, but including O&M costs and marginal launch costs, the nominal cost per launch is given in Table 3.27.

TABLE 3.27.—COST PER LAUNCH FOR 1000 LAUNCHES/YEAR, 80-KG PAYLOAD

Type of cost	Cost per launch, \$K	Cost per kg, \$
Vehicle	200 to 1000	2500 to 12,500
O&M ^a at 5% of capital cost	200	2500
Marginal operations cost	20	250
Propellant	20	250
Power	8	100
TOTAL	448 to 1248	5600 to 15,600

^aOperations and maintenance.

The costs are driven by vehicle cost and O&M cost. Both can be lowered directly, by lowering the vehicle manufacturing cost and the launch system O&M cost. Both can also be lowered substantially by assuming a higher launch rate. For example, at 10 000 launches per year, the vehicle cost would be about 60% as much (for an 85% learning curve), and although the total O&M cost might be higher, the cost per launch would be much less. A cost per launch of \$88,000, plus a vehicle cost between \$120,000 and 600,000, would be a reasonable goal, making the total cost per launch between \$208,000 and \$688,000 (\$1540/kg to \$8600/kg). Even lower launch costs would be attainable with true mass production of vehicles at significantly lower unit cost or with the development of reusable vehicles.

3.1.5.5 Feasibility Assessment

3.1.5.5.1 Roadmaps and Technology Readiness Levels

3.1.5.5.1.23 Technology Readiness Levels (TRLs)

TRLs are, by their nature, somewhat subjective, particularly for intermediate levels. We caution against directly comparing TRL levels as estimated by different authors, even within this report. Table 3.28 gives a breakdown of the nominal TRLs for various aspects of the launch system.

TABLE 3.28.—TRL LEVELS AND BASIS FOR HX LAUNCH SYSTEMS

Key technology	Current TRL	Rationale and proof of estimation	Time to reach TRL 6
HX	2 to 3	Theory understood, but new operating regime requires testing and engineering for flight	18 months for megawatt class 3 to 4 years for full scale
Piston pump	4	XCOR: Bench test with LH ₂ , flight operations with LOX/RP ^a	24 months
Expansion-deflection nozzle	5	E-D nozzles flown with other propellants; new design for LH ₂	18 months for megawatt class 3 to 4 years for full scale
Other vehicle components	4 to 8	Per COMPASS study; lowest TRLs are refractory materials and “advanced” batteries (LiPO)	N/A for suborbital tests 2 to 4 years for full scale hardware
Fiber laser	8 / 6	60-kW module: TRL 8—10-kW IPG laser 200- to 500-kW module: TRL 6—IPG laser + Bragg grating combining or JHPSSL	N/A
Diode array (boost laser)	6	Commercial multi-kilowatt, multi-wavelength diode sources (e.g., TRUMPF Tru-Diode)	N/A
Optics/tracking	6	COTS ^b telescopes/pointing systems (1-m aperture) ABL exceeds all requirements (at high cost)	N/A for technology, but 18 to 24 months for “low-cost” hardware demonstration
Adaptive optics/guidestar	5	ABL and Starfire Optical Range (SOR) exceed all requirements for single aperture; need to validate multi-aperture system and COTS hardware	18 months for low-power tests 3 to 4 years for high-power multi-aperture

^aLiquid oxygen/rocket propellant.

^bCommercial off the shelf.

Vehicle.—The laminar-flow HX itself is at TRL 2 to 3. To our knowledge, no other device has been demonstrated with a similar combination of thermal, gas flow, and optical properties, which would imply TRL 2. However, somewhat similar structures have been made in a variety of materials, including test laminar-flow HXs in nickel (Ref. 7) and various porous or small-channel ceramic structures for biochemical applications. The basic laminar-flow heat transfer technique is well established for liquid, gas, and two-phase flow (see, e.g., Ref. 45), and the other physical and engineering phenomena involved (optical absorption, reradiation, thermal conduction in solid SiC, and thermal failure modes of SiC) are generally well understood. The major technological issues are discussed in Section 3.3.1.2.4 (HX issues).

Fortunately, as discussed in the following section, it is straightforward to test the HX design and (assuming the tests are successful) reach at least TRL 4.

Turbulent-flow HXs are more common and have been built in a wide range of high-temperature materials and tested with high thermal fluxes applied to one surface (albeit usually via hot gas, rather than laser flux), so a turbulent-flow version of the laser HX can be classed as at least TRL 3 and possibly TRL 4 or higher. (See Ref. 46 for an example.)

Other than the HX, the vehicle can be built using standard aerospace materials and technologies, with varying amounts of development of actual components and subsystems. Reuse of existing flight-proven hardware (TRL 8 to 9) may be possible for some subsystems, but it would not in general be appropriate, given the differences between the laser launch system and past launch systems and spacecraft, and given that the development and testing of optimized hardware can be amortized over, by launch vehicle standards, a very large number of units. For example, existing space-qualified electronics could be used for control and data handling, attitude determination, and so forth., but with a penalty of as much as 30 kg in mass and \$1M or more in cost per launch in comparison to a new design. Similarly, even though an existing TRL 9 small turbopump might be adapted to the HX vehicle, a piston pump, currently at TRL 4, would almost certainly be much less expensive over hundreds to thousands of launches and would offer performance characteristics better matched to the HX propulsion system.

Laser arrays.—The reference example for the main laser is the IPG YLS-10000-SM, a 10-kW, single mode ($M^2 < 1.2$) fiber laser operating at 1070 nm. This is a commercial product and would be usable as is in a launch system. Provided the beam modules have environmental control (heating/air conditioning) comparable to that in heavy manufacturing plants (e.g., steel fabricators and automobile assembly plants), the lasers would be operational in the expected environment⁶ and would thus be at TRL 8. However, the current IPG laser is almost certainly not the best choice for a launch system. Even if we assume the use of only current (2011) laser technology, wavelength-combining of several 1- to 3-kW lasers would probably give lower cost and higher efficiency. However, because such wavelength-combined systems are not in production or regular use, they are only at TRL 6.

In reality, a fundamental advantage of the modular laser array is that the actual lasers are quite small and have an almost perfectly “clean” interface to the rest of the system: alternating-current (AC) or DC power and cooling water as input, and photons within a specified wavelength range as output. The technology freeze date for the lasers could, thus, be quite late, essentially as of the start of volume production of lasers. Indeed, new laser technology could be introduced during production. Given the rate of advance of laser technology (and the fact that it is being driven by industrial and military applications), it is very likely that the actual laser systems that would be used in a launcher to be deployed in, say, 2022, are currently at TRL 4 or lower.

This is even more true for direct-diode arrays as used in the DRM system for the boost laser. High-power arrays and wavelength-combining and beam-shaping optics which *could* be used for a launch system are in production and commercial use (TRL 8), but better arrays and optics are in development (one example is given in Ref. 47) and will almost certainly be at TRL 8 well before a launch system would be built.

⁶ IPG announced in 2009 that it has delivered 5-kW lasers using the same design to an industrial customer. They have not identified the customer or announced actual delivery of any 10-kW lasers.

3.1.5.5.1.24 Development Roadmap

Figure 3.103 shows a roadmap for the development and construction of a DRM-capable launch facility.

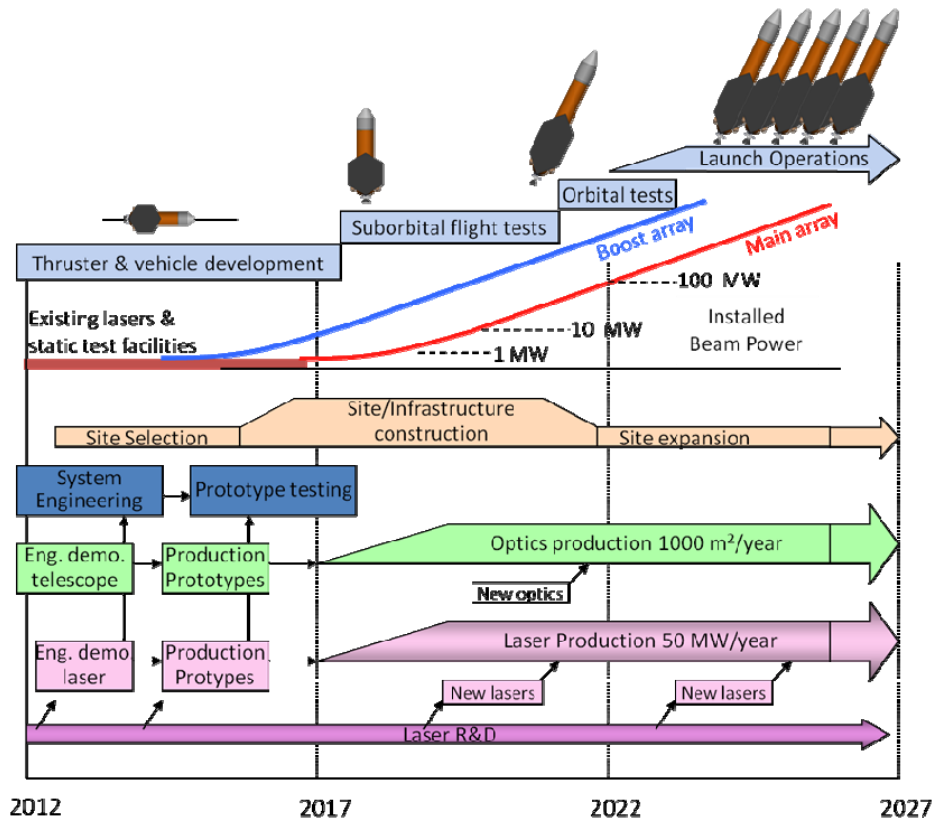


Figure 3.103.—Roadmap for launch system development and deployment.

A basic advantage of the modular laser/HX launch system is that nearly all aspects of the system can be developed and demonstrated at much less than the final vehicle scale and with less-expensive substitutes for the missing system elements.

3.1.5.5.2 Ground and Flight Demonstrations

There are several possible demonstration paths and options for the laser/HX system, depending on which aspects are regarded as most critical or highest risk. Figure 3.104 shows one possible set of ground and flight demonstrations for the HX vehicle.

We have not given costs and schedules because the costs will depend heavily on how the tests and demonstrations are defined, and particularly on what types of beam sources are used, versus what may be available, either from unrelated programs or from separate development activities within an overall beamed-energy-propulsion (BEP) program. For example, it may be decided to build a multi-megawatt diode laser or millimeter-wave source as a user facility, rather than as a single-purpose installation for this program.

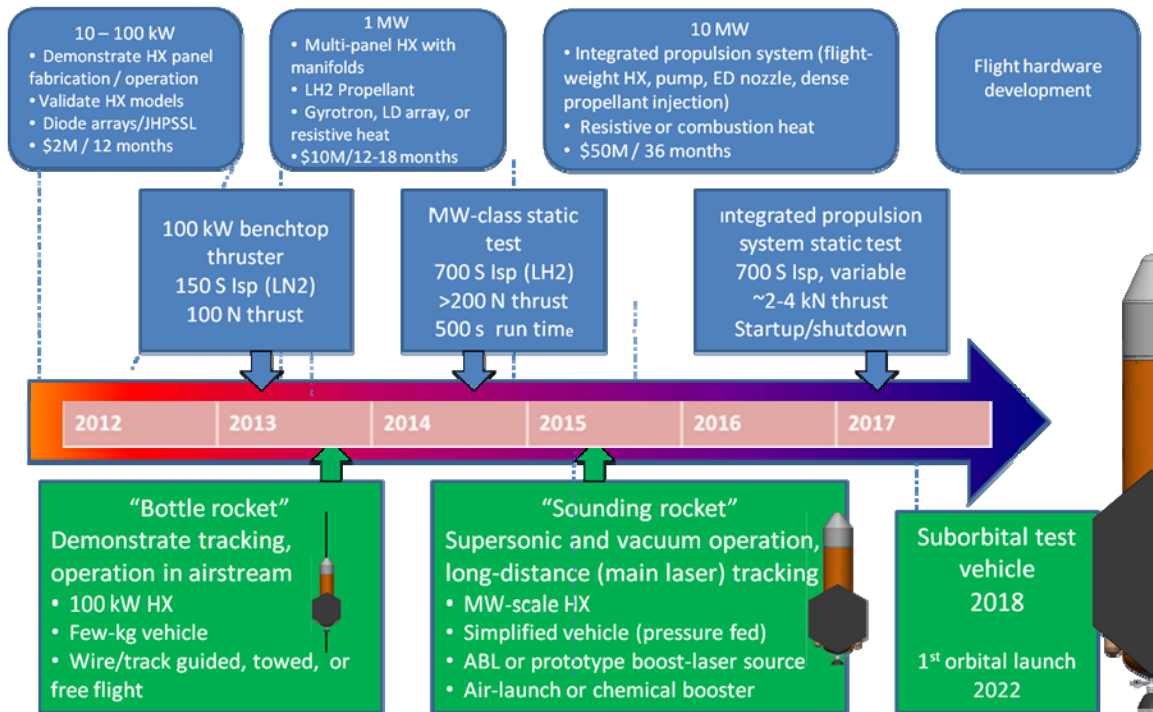


Figure 3.104.—Possible ground (blue) and flight (green) demonstration program for HX vehicle.

3.1.5.5.2.25 Static Demonstrations of Propulsion System

To the extent that the highest technical risk is associated with the HX, two possible milestone demonstrations are as follows:

100-kW HX/benchtop thruster

Objective: Demonstrate basic subscale HX thruster

Facilities: JHPSSL (100 kW) or ~100-kW diode array facility, wind tunnel, or blowdown air tank

Test unit: ~200-cm² SiC HX (2 × 100-cm² panels + manifolds) with low-expansion nozzle

Success criterion: Stable operation with nitrogen gas flow at flight conditions (nominally 2000 K gas temperature, ~5 g/s gas flow) for >100 s, including ~10-s operation with air flow (simulating thermal and surface-erosion conditions during ascent)

Megawatt HX/LH₂ thruster

Objective: Demonstrate subscale flight-performance HX thruster

Facilities: 200- to 1000-kW laser diode array, wind tunnel, or blowdown air tank; hydrogen handling

Test unit: ~200- to 1000-cm² SiC HX with low-expansion nozzle

Success criterion: Stable operation with hydrogen gas flow at flight conditions (nominally 2000 K gas temperature, ~5 g/s gas flow) for >500 s, including ~60-s operation with air flow (simulating thermal and surface-erosion conditions during ascent)

This demonstration might alternatively use the proposed Ames 1-MW gyrotron source, which would allow demonstration of a larger (>1000-cm²) HX segment, but this would require demonstration of a microwave absorber layer that would adequately reproduce the thermal effects of laser absorption without changing the HX thermomechanical properties. This might be a thin layer of resistive material. The microwave experiment would not test surface erosion and could be done in air or vacuum.

Full-scale propulsion system

Objective: Demonstrate full sounding-rocket-scale propulsion system (directly scalable to launch vehicle)

Facilities: Multi-megawatt heat source; vacuum chamber (>2 m diameter), engine test facility sized for 10,000-lbf thrusters

Test unit: Integrated propulsion system (LH₂ tank, pump, HX, and nozzle)

Success criterion: Startup, stable operation, and shutdown of HX, nozzle, and propellant flow system

This demonstration would require a large heat source (at least several megawatts), which could be a laser diode array or microwave tube array if a suitable array were available, but would more likely be either a high-temperature resistive heater array or tungsten-filament radiator. An alternative would be to use a combustion heater (essentially a rocket combustor) with the exhaust flowing either directly over the HX face or through a second HX (probably a simpler turbulent-flow design) coupled to the test HX face-to-face.

3.1.5.5.2.26 Vehicle Flight Demonstrations

Bottle rocket

Objective: Demonstrate integrated propulsion system and beam-source tracking of accelerating vehicle

Facilities: JHPSSL or 100-kW class diode array with steering mirror and tracking system; sled track or suspended cable at 2- to 5-km range

Test unit: 100-kW-scale propulsion system using water or LN₂ propellant, including tank, nozzle, and propulsion controls, and vehicle beacon (typical dry mass, 10 kg)

Success criterion: Track and accelerate bottle rocket continuously over available track length

Sounding rocket

Objective: Demonstrate integrated propulsion system and beam-source tracking of accelerating vehicle

Facilities: ABL or megawatt-class main laser (fiber, etc.) subarray; test range (e.g., WSMR)

Test unit: Megawatt-scale propulsion system using pressure-fed water or LN₂ propellant—including tank, nozzle, and propulsion controls—integrated into a partially or fully guided stage, either air-dropped or launched to an altitude of several kilometers by a small solid booster

Success criterion: Track and accelerate HX rocket stage over 10+ km and 30+ s; demonstrate acquisition and self-guidance including roll control; may demonstrate supersonic flight

This would be the near-term option for demonstration using ABL. The solid booster stage would be used (in preference to ground launch or air drop) to provide a plume for initial ABL acquisition and tracking. Because of the small size (0.1 to 1 m²) of a megawatt-class HX, this demonstration probably would require a high-quality beam source such as ABL or a small number of main-array beam modules (e.g., 20 × 60-kW modules). A boost array module would only be able to focus on the HX up to a range of ~10 km. (A section of the boost array could, of course, be used for preliminary tests, including ground launches of the sounding rocket stage.)

Suborbital launch

Objective: Demonstrate near-full-scale vehicle launch, transatmospheric flight, and acceleration

Facilities: 10- to 100-MW boost laser subarray deployed at either a test range or the eventual launch range

Test unit: Subscale “heavy” vehicle (10% to 50% of DRM vehicle gross liftoff mass, but built using off-the-shelf tanks and other hardware, a la DC-X); carries propellant (LH₂ and dense propellant)

for 100- to 200-s flight time, including at least some high- I_{sp} operation with straight LH₂ propellant; vehicle may be recoverable/reusable
Success criterion: Vehicle flight to TBD altitude and velocity, typically powered flight to 50 km altitude/1 km/s.

This would be a series of tests for validation of the vehicle design before a commitment was made to produce full-scale vehicles. It would also provide full validation of the boost array design and could validate operation of at least parts of the main array; that is, even if the siting of the tests and the state of completion of the main array did not allow using the main array modules for significant propulsion, it would at least be possible to test the vehicle acquisition and tracking and the laser pointing and beam properties of main-array beam modules.

To the extent that suborbital launches would approximate the conditions of an orbital launch (except for total burn duration), these launches could also flight-test avionics and other hardware for the full-sized vehicle.

On-orbit propulsive test

Objective: Demonstrate main laser array tracking and beam quality at high power/long range and full angular rates; validate vehicle design and operation at burnout and orbit insertion

Facilities: ~10-MW main laser subarray, deployed at a test range or (preferably) at the main laser site

Test unit: Subscale “light” vehicle (dry mass 10% to 20% of the DRM vehicle dry mass) configured to fit on top of a small conventional launch vehicle; carries a small hydrogen tank (e.g., 20% to 50% of wet mass is LH₂); HX vehicle is launched into LEO by the conventional stage and is powered by the laser array as it passes over the array; post-acceleration path may be a stable orbit or may reenter

Success criterion: Achieve planned delta-V

This demonstration could be done at a lower power level, possibly even using ABL, if a low-cost launch opportunity were available. However, to validate the beam module and HX vehicle design and operation, the demonstration probably needs to be done at fairly high power, using actual beam module prototypes.

An alternative to maneuvering a spacecraft already in a stable orbit would be to launch a laser-HX “upper stage” on a suborbital trajectory and boost it into orbit. However, this would be higher risk (only one chance to perform the maneuver) and would require either launching a conventional rocket on a trajectory over land or installing a sizeable laser array temporarily on an island or other site where it could see an appropriate portion of the trajectory of a suborbital launch from an existing launch range.

3.1.5.5.2.27 Beam module and Laser Array Demonstrations

Finally, there are also several possible milestone demonstrations that would involve only the beam modules, including tracking test targets (conventional rockets or satellites), delivering power from a single module to an instrumented test target, and demonstrating simultaneous operation of multiple modules at various total power levels. These are not addressed in any detail here, but should be considered in developing a full demonstration roadmap.

3.1.5.5.3 Issues and Resolutions

3.1.5.5.3.28 Atmospheric Transmission

The beam module array has no significant issues with thermal blooming because of the relatively low power in a single beam. Thermal blooming close to the vehicle, where individual beams overlap, may be a minor issue at launch, when the vehicle velocity is small. This may set a lower limit on the overall area of the boost laser array.

As noted earlier, at the wavelengths of interest, there is very little absorption for beam paths originating at an altitude of 2 km or higher. For lower altitudes, some wavelengths (notably 900 to 980 nm for the boost laser, and 1.06 to 1.1 μm for the main laser) have significant absorption because of water vapor, but laser wavelengths can be chosen such that absorption remains small. Scattering will be the dominant loss mechanism and will depend on the aerosol properties at the laser sites.

3.1.5.5.3.29 Environmental Issues

There are no known environmental issues associated with the vehicle exhaust, which will be mostly water or nitrogen (dense propellant) plus a small amount of hydrogen in the atmosphere. The HX surface or the burning of the hydrogen in air may be hot enough to generate some oxides of nitrogen. There are no chlorides or other long-lived ozone-depleting species in the exhaust.

To our current knowledge, the vehicle will not use substantial amounts of toxic or hazardous materials, and the total mass of structural material in reentering vehicles will be small (<1000 tons/year for the reference system). Silicon carbide is a widely used industrial abrasive, and carbon composites are also widely used. However, a review of possible hazards from scattered or vaporized vehicle structure will be needed when the vehicle and HX compositions are known.

High launch rates of small vehicles could cause a significant additional orbital debris hazard if vehicles do not reenter quickly, but that is primarily an engineering and operations issue. Orbital debris concerns may force the inclusion of some type of backup reentry mechanism such as the Terminator Tether (Ref. 48).

High-power laser beams of the type and power used for the HX launch system have no direct effect on the atmosphere or environment; they do not cause chemical reactions or heat the atmosphere enough to affect weather. The one potential environmental hazard from the laser arrays is injury to birds, which may suffer eye damage or minor burns if they fly directly through a beam (the beam intensity is generally too low to cause severe burns except close to the vehicle). Individual laser beams can be switched off by safety systems if birds enter the beam path, without affecting launch operations, but large flocks flying around or above the laser arrays might cause unacceptable power loss. (They would also tend to decrease the optical quality of the output apertures). This is unlikely if the arrays are at high altitude, but the impact on threatened and endangered birds will need to be analyzed and perhaps tested with prototype arrays. Measures similar to those used at airports can be used to keep birds away from the launch site and the laser arrays.

Finally, vehicles lifting off will be point noise sources, with much lower total power than chemical launch vehicles but more frequent operation. This may be an issue in the selection of launch sites, or impose some limits on, for example, hours of operation, although both people and wildlife around active launch facilities appear to become accustomed to the noise; the vertical ascent will limit vehicle noise to the immediate vicinity of the launch site.

3.1.5.5.3.30 Laser Safety

Laser safety hazards are generally characterized as being due to the direct beam, specular reflections, or diffuse reflections.

In general, the direct and specular-reflection hazards from the modular laser array are much lower than the hazards from a single beam of similar total power because, except for a small region close to the vehicle, the individual module beams do not overlap. Thus, direct and specular hazard estimates can be based on the power of a single module (60 to 200 kW) rather than the full array.

Direct viewing.—We assume that the space directly between the laser arrays and the vehicle will always be controlled, so that there is minimal risk of anyone or anything actually being hit by a direct beam. For the boost laser, this implies a controlled ground area directly under the beam wherever the beam is within a few meters of the ground, and a controlled airspace covering the area between the boost array and the launch site. For the main array, which never points below $\sim 15^\circ$ from the horizon (and could have mechanical hard stops at that angle), the controlled airspace is nominally a cone or inverted pyramid

extending upward from the array site. For example, at an 18-km (60,000-ft) altitude, the controlled region would have a major axis (along the launch trajectory) of roughly 140 km. The cross-track width of the controlled region would depend on the range of launch azimuths used, but it would generally be much smaller: a few kilometers at the “uprange” end and 10 km at the “downrange” end. A radar system would detect aircraft within this controlled space and, if necessary, delay or abort launches.

In addition, individual beam modules or subsections of the laser array would have “boresight” radars that track with the laser beam. These could detect aircraft (or birds) flying into the beam and shut down the beam. Since only a single module or a small section of the source would be shut down, this would not interfere even with a launch in progress.

The relatively few satellites orbiting below the trajectory altitude would be at risk of intercepting the main laser beam, but a combination of schedule coordination and boresight radar detection would make the chance of actually hitting a satellite extremely small. In the worst case, a satellite encountering a single module beam would be exposed to $<10 \text{ kW/m}^2$ (e.g., a 50-kW beam with a Gaussian full width of 5 m) for on the order of 1 ms, so the energy deposited on the satellite would be small ($<10 \text{ J/m}^2$ or 1 mJ/cm^2) and thus extremely unlikely to cause physical or thermal damage. The only significant hazard would be to optical instruments that might focus the laser energy. (Detection of optical reflection of a beam from a satellite would be possible, but the speed-of-light delay in reaction would generally be longer than the satellite would be in the beam).

Beyond the vehicle, there would be a direct-beam hazard due to “spillover” from the main beam or to individual beam modules that suffer pointing errors. (Loss of contact with the vehicle beacon, due to vehicle failure or gross pointing error, would immediately shut down a beam module in ~ 1 ms, so pointing a beam more than a few meters away from a vehicle would require multiple failures). This would be the primary concern for ground and aircraft hazards for the boost laser array.

We assume that the boost array and launch site would be located such that spillover energy at and immediately after liftoff would either not hit the ground at all (launch site altitude $>$ laser altitude), would be stopped by nearby terrain (such as a mountain “behind” the vehicle launch site), or would be directed at an unpopulated and reasonably controllable area, such as the ocean. The maximum range of concern would be ~ 200 km, since the distance to the horizon for a boost laser at 2 km above sea level is at most ~ 225 km, but in practice a typical boost-laser beam (10 kW, 100 μrad divergence) would be eye-safe for a 0.1-s exposure more than ~ 100 km from the laser, although not necessarily safe for observers with binoculars or telescopes. (One additional option would be to choose a wavelength range for the boost laser that has significant water-vapor absorption, so that a 20-km path at an altitude of 1 to 2 km would have acceptable attenuation (10% to 30%) but that, at lower altitudes and longer ranges, the beam would rapidly attenuate in most atmospheric conditions.)

For aircraft, there is a severe hazard for the first ~ 50 km beyond the launch site, and this would need to be restricted airspace during launches, although the restricted zone could be very narrow in both time (5 min per launch) and space (<1 km wide). Beyond 100 km, the combination of beam flux and exposure time would be eye-safe, and airplane pilots and passengers are generally not using (or able to use) large magnifying optics. At intermediate ranges, there is a marginal hazard (a worst-case exposure <5 times the ANSI/IEC maximum permitted exposure) and restricting air space may or may not be necessary. Note that in no case is there a risk of physical damage to aircraft that are more than a few kilometers beyond the launch vehicle.

(The ground level and aircraft hazards could be further reduced by using longer-wavelength lasers for the boost laser, for example, 1.55 μm , but currently the cost and performance of both diode arrays and fiber lasers at this wavelength are several times worse than near 1 μm . Alternatively, if laser diode prices drop sufficiently, a “preboost” laser array located at the vehicle launch site (within 1 to 2 km) could supply part or all of the power for the first few kilometers of the trajectory. The preboost lasers would need minimal optics and would have highly divergent beams, so they would be eye-safe a few kilometers beyond the vehicle, and the boost laser array would then never operate at high power below $\sim 15^\circ$ above

the horizon, so their beams would go above commercial flight altitudes only 40 to 60 km beyond the launch site.)

Spillover beams from the boost laser array would present minimal hazard to satellites, since the beams would be below 10 mW/cm^2 at the lowest satellite altitudes ($\sim 20\text{-m}$ beam diameter at 400 km, assuming $50\text{-}\mu\text{rad}$ divergence, with individual beam powers of $\sim 20 \text{ kW}$). However, coordination of satellite passes very close to the boost laser site would be desirable.

The largest hazard to satellites would be spillover or stray beams from the main laser site. These may have fluxes over 1000 W/m^2 (100 mW/cm^2) out to an altitude $>1000 \text{ km}$. It is also possible (although unlikely) that the beams could accidentally match the velocity of a satellite in orbit closely enough to stretch the exposure time considerably, possibly to as much as 1 s, or several seconds of intermittent exposure as the satellite passed through the array of beams. This would still be unlikely to cause thermal damage, but it could conceivably damage solar panels or related electronics, or sensors not aimed directly at the beam source. The cross section of the array of beams would also be fairly large, comparable to the dimensions of the array on the ground.

The hazard to LEO satellites will thus probably require coordination with satellite tracking agencies (currently done via the Laser ClearingHouse) and some constraints on launch windows. In addition, it may be desirable, and eventually necessary, to use a boresight radar system sufficiently powerful to detect satellites out to a range of $>1000 \text{ km}$ and to interrupt the laser beam if a satellite is detected approaching the beam. (For most satellites, the interruption would be a fraction of a second and would not cause a launch failure.)

Specular reflections.—Specular reflections from the vehicle are generally a small hazard, because the vehicle will be designed to have no flat, polished surfaces. Small reflective surfaces, such as might be caused by minor damage in vehicle processing, would reflect power from different beam modules in slightly different directions, so the flux reaching any one observer more than a few 10s of meters from the vehicle⁷ would be from one beam module.

The specular beam intensity ϕ_{refl} from an ideal reflective spot of area A at range R is

$$\phi_{\text{refl}} = \frac{\phi_{\text{in}} A^2}{\lambda^2 R^2}$$

where the incident flux ϕ_{in} is

$$\phi_{\text{in}} = \frac{4 P_{\text{beam}}}{\pi d_{\text{beam}}^2}$$

that is, the beam module power divided by the beam area at the vehicle.

For the main array, the worst case corresponds to the vehicle being directly over the laser: roughly $P_{\text{beam}} = 60 \text{ kW}$ and $d_{\text{beam}} \sim 1 \text{ m}$ (at a range of $\sim 200 \text{ km}$), so $\phi_{\text{in}} \sim 76 \text{ kW/m}^2$. $R = 200 \text{ km}$ and $\lambda = 1.06 \mu\text{m}$, so $\phi_{\text{refl}} \sim 1.7 \times 10^6 \text{ A}^2 \text{ W/m}^2$. For $A \sim 1 \text{ cm}^2$, $\phi_{\text{refl}} \sim 17 \text{ mW/m}^2$ or $1.7 \mu\text{W/cm}^2$, which is several orders of magnitude below the maximum permissible continuous exposure of 5 mW/cm^2 . Even an observer using a sizeable telescope would be unable to exceed the allowed eye exposure.

For the boost laser array, the potential hazards are somewhat greater. Depending on how the boost array is aimed and focused, ϕ_{in} will typically be between 10 and 100 kW/m^2 , but R could be much shorter,

⁷Or a few kilometers from the vehicle for the main laser array. However, since the vehicle only sees the main laser array when it is well above 50-km altitude, main-laser reflections are not a significant hazard.

and λ might be as short as 0.85 μm . If we assume that $\phi_{\text{in}} = 30 \text{ kW/m}^2$ and a 1- cm^2 reflector at 1.0 μm , $\phi_{\text{refl}} \sim 3 \times 10^8 R^{-2} \text{ W/m}^2$.

This falls below the naked-eye maximum permissible exposure (MPE) of $\sim 4 \text{ mW/cm}^2$ (40 W/m^2) at a range of approximately 2.7 km. This is a reasonable distance over which to exclude unprotected observers. However, observers using binoculars or telescopes may exceed the MPE at distances roughly 5 to 20 times larger (assuming 50-mm binoculars or a 200-mm telescope with ~ 3 milliradians of apparent blurring due to chromatic aberration between the visible and near-infrared). Excluding all binocular users from a 13-km radius would be difficult. Excluding all telescope users from a 50+ km radius may be unfeasible.

Fortunately, the actual hazard is almost certainly much lower. Real surfaces generally do not reflect beams even as narrow as a diffraction-limited 1- cm^2 mirror (Ref. 49), nor are they 100% efficient reflectors. Conversely, however, the extended array source means that the reflected beam flux is nearly constant for a wide range of reflected beam widths once the reflected beams from different sources begin to overlap. This area-average intensity is lower than the single-beam reflected intensity by roughly the fill-factor of the array source, that is, a factor on the order of several hundred for the nominal main laser array ($\sim 1\text{-m}$ apertures on $\sim 40\text{-m}$ centers) but possibly a factor of 10 or less for the boost laser array (2- by 5-m aperture for a single module, with modules spaced, for example, 2.5 by 40 m, as seen from the launch site.) If we assume that this reduces the peak beam flux by a factor of 10, the safe radii for binoculars/telescopes become 4 and ~ 16 km, respectively.

If a given observer sees reflections for less than 10 s, the allowable exposure is higher, increasing as $(10 \text{ s}/t)^{0.25}$. Once the vehicle is off the launch stand, typical exposure times are likely to be 0.1 s or less as the vehicle attitude changes. This would increase the MPE by \sim threefold, and reduce the minimum safe range by a factor of ~ 1.7 . For the vehicle on the stand, reflections might be stable for several seconds before the vehicle actually begins moving, but the hazard zone could be limited to a narrow “pie slice” toward the laser array by putting suitable barriers around the launch stand or launch site.

Finally, the MPE levels are conservative, and exposure levels up to 5 times higher generally require only a suitable warning notice. So whereas a telescope-safe distance may be 10 to 16 km from the launch site, an occasional observer who gets within as little as 4 to 5 km (or 7 to 8 km in certain specific directions) would still be both actually safe and within reasonable regulatory limits.

We reiterate, however, that the above safe distances are based on 1- cm^2 specular reflective areas, and a safety inspection able to detect reflective spots larger than this will be needed. Ideally, this would be an automated scan performed on the launch stand shortly before launch.

Diffuse reflections.—Diffuse reflections obviously present a less concentrated hazard than specular reflections, but because the total laser power is so high, the hazard can be significant. Again, there is no hazard from the main laser array because all observers are distant (unless a vehicle passes very close to a watching astronaut).

For the boost laser array, an analysis similar to the above analysis for specular reflections was done. We assumed approximately Lambertian scattering (even distribution of light in all directions) and a scattered flux of 1 MW/m^2 , corresponding to 10% scattering from the HX itself or complete scattering of the fringes of the beam (e.g., from the fuel tank). In this case, the exposure dropped below the MPE for naked-eye viewing at ~ 100 m from the vehicle. The scaling for aided viewing was similar, except that the probable chromatic error of binoculars or telescope eyepieces outside of the visible range did not reduce the hazard. The safe range became ~ 700 m for 50-mm binoculars and ~ 3 km for a 20-cm telescope.

However, it is difficult to ensure that scattering will be uniform, especially from the HX. There may also be “hot spots” in illumination or scattering. A conservative assumption, pending more detailed analysis, is that the keep-out zone should be at least 1 km for all observers, >3.5 km for users of binoculars or cameras with through-the-lens viewing, and >15 km for telescopes in directions where there might be peaks in the scattered intensity, primarily toward the laser site. This is consistent with the specular-reflection safety ranges.

3.1.5.5.3.31 Range Safety

The present study only minimally addressed range safety other than laser safety, and the differences between range safety requirements for HX laser launch in comparison to chemical launchers. We note briefly the following points, and recommend that range safety be considered in more detail in a future study:

- The combination of simple single-stage vehicles, extensive “type certification” testing, the ability to ground-fire complete vehicles, and a distributed laser array with reserve capacity will provide extremely high overall reliability.
- The laser launch vehicle will have minimal stored energy onboard. It, therefore, will not be able to generate significant explosive force on the pad or in flight provided the oxidizer component of any dense propellant is kept low. (The hydrogen propellant could readily burn in air, but it would be very difficult to mix with air and ignite in such a way as to produce a large detonation.)
- The vehicle will not generate significant thrust in the absence of the laser beam, so uncontrolled flight is essentially impossible. Turning off the laser arrays will provide reliable thrust termination.
- The total vehicle mass will be small in comparison to any prior launch vehicle and most suborbital rockets, including the V-2. The worst-case ground impact or explosion will be comparable to the crash of a small airplane.
- The combination of high launch rates and low unit launch cost will enable extensive ground and suborbital testing, plus orbital-launch testing with various deliberate failures, allowing much more complete demonstration of reliability *and of possible failure modes* and their effects than is possible with any other launch system.

3.1.5.5.3.32 Launch System Availability

See Section 3.1.5.3.4—Availability.

3.1.5.5.3.33 Power Source

As noted in Section 3.1.5.2.2—Main Laser Site Design, there are several options for powering the launch system using off-the-shelf technology, without imposing unprecedented loads on the national electrical grid or requiring special approvals and exceptional lead times (as would be needed, for example, for a new nuclear power plant or a major transmission line.) The worst-case option is a pair of dedicated gas-turbine power plants (at main and boost array sites) able to supply the entire launch system load. If grid power were used, it would be with some type of energy storage system able to spread the load in time to match available off-peak generating capacity, combined with a medium-voltage (<100-kV) transmission line from the nearest generating plant or grid tie point.

3.1.5.5.3.34 Co-use of Laser/HX Thruster Concept and Launch System

Co-use of Airborne Laser and future laser weapon systems.—The ABL is certainly compatible with an HX propulsion system and could potentially be used for development and demonstration as described above. The ABL is probably not capable of powering a full launch to orbit, even of a token payload, because of power, range, and run-time limitations.

Since HX propulsion will work with essentially any laser, it is possible to consider it as a way to extend the capabilities of the ABL or any future high-average-power laser with laser-powered projectiles, either for R&D purposes (discussed later) or as an additional weapon capability. For velocities up to roughly 5 km/s, a laser-powered missile could use water or, for example, LN₂ propellant, yielding a completely “wooden round” hypersonic missile with no fire or explosion hazard and (especially if “fueled” in the field) very low weight.

Conversely, any laser weapon system with megawatt-class or higher average power is a potential beam source for testing HX laser propulsion systems and vehicles.

The largest commonality between laser weapon systems and HX launch, however, is that individual technologies, including, for example, optics manufacturing or pointing and tracking, developed for either one may be applicable to the other. This commonality may be enhanced if development programs have at least some connection. For example, a laser weapon program may have comparatively short run-time requirements but may select a laser technology that can operate for longer times if the program management is aware of the potential application to laser launch.

Co-use of horizontal takeoff.—Horizontal takeoff appears to be a poor choice for purely laser-powered vehicles using GBL, because both line-of-sight geometry and atmospheric absorption and scattering limit the useful laser range to a few 10s of kilometers for vehicles in the sensible atmosphere (below 30 km). An HX-heated turbojet aircraft engine could provide fuelless (and pollutionless) propulsion up to perhaps Mach 2, but conventional hydrocarbon engines are already very good in this regime. At higher velocities, a subsonic-flow HX is a poor choice for heating air,⁸ and preheating fuel, while desirable, can generally be done using engine waste heat or energy from aerodynamic heating.

However, HX propulsion could potentially be used in connection with horizontal takeoff vehicles in at least two configurations:

- A two-stage launcher, using a horizontal-takeoff suborbital vehicle with conventional chemical engines (jet or combined cycle) as a first stage, and a laser HX vehicle—expendable or reusable—as an upper stage
- A single-stage reusable vehicle using chemical propulsion in the atmosphere but switching to a laser HX rocket mode for out-of-atmosphere acceleration and orbit insertion

The two-stage configuration is distinguished from an air-launched single-stage vehicle by the assumption of a first-stage vehicle with significantly higher altitude and velocity capability than existing aircraft. The two-stage configuration would make sense if the carrier aircraft could be built and operated at lower cost than a boost laser array (or possibly several boost arrays, if the first stage vehicle enabled launching to different azimuths, or if multiple launch systems were built). This is certainly possible; there are several active efforts to build reusable suborbital horizontal takeoff and landing (HTHL) vehicles that can carry several people or ton-scale payloads to 100+ km altitude at a price on the order of \$1K/kg (Ref. 50).

3.1.5.5.3.35 Other Applications of an HX Launch System or Technology

Suborbital launch and space tourism.—Laser launch could deliver much larger payloads on suborbital trajectories than to orbit. For example, the boost laser array proposed for the DRM launch system could lift ~2.5 tons (vehicle plus payload) to 150 km (thrust cutoff at 100 km and 1 km/s) with ~4 min of zero-gravity trajectory before reentry. The combination of very high reliability, demonstrated safety, low environmental impact, and low acceleration, plus extremely high launch rate and low per-launch cost with a reusable vehicle, would make this mode of operation ideal for suborbital space tourism as well as scientific and industrial activities.

A unique capability would be to launch large numbers of “reentry sondes” that could be targeted to reenter at specific locations over a wide area, sampling the atmosphere in all three spatial dimensions and in time over an extended period. Sondes could be launched in groups on a relatively large reusable suborbital vehicle or, with a subscale version of the main laser array (so as to allow focusing on sub-meter-sized HXs at 50 to 100 km), as expendable vehicles with ~ 100-kg GLOM.

Intercontinental parcel delivery.—Fast parcel delivery by an unmanned rocket has been proposed many times, and although problematic for various practical reasons (how do you clear customs?), it remains a possible application of low-cost, high-volume launches. An HX laser launch system would potentially be able to deliver (nonmilitary) payloads anywhere in the world within <1 hr. Laser launch

⁸More exotic approaches such as plasma-coupled laser scramjets might be of interest, but these are well beyond the scope of this study.

would be handicapped, however, by weather availability, which is not readily solved in this case by having multiple sites because the extra time to carry packages between launch sites would defeat much of the benefit.

Military applications.—Orbital launch systems would also be able to launch payloads onto suborbital trajectories or to launch orbital payloads with reentry capability. The payloads could include explosive warheads or kinetic energy impactors.

A laser launch system is very well suited to such a nonnuclear strike: It has a low cost per launch, has a high sustained launch rate (although not as high as some cannon-type launchers), and has sufficient flexibility in trajectories to reach most areas of the planet. A laser launch is very easily distinguished from an intercontinental ballistic missile (ICBM) launch or any other military activity. A laser array would also be robust against many kinds of attack. The main limitation of laser launch is that it could be disabled by weather, so having strike capability at all times would require multiple launch sites.

A launch system could be demilitarized for intercontinental strike either by limiting its range of trajectories (e.g., by building the beam director mounts with limited range) or by providing some type of international control, as well as by not developing or testing weaponlike payloads.

A laser launch system would be an efficient launcher of small orbit-resident antisatellite or antimissile weapons or decoys. This was the original basis for SDIO support of laser propulsion research in the late 1980s: as a launcher for Brilliant Pebbles interceptors and decoys (Ref. 51). A launch system could also launch direct-ascent antisatellite weapons to LEO or to geosynchronous transfer orbit.

A laser array with even a fraction of the power of a launch array would be able to promptly destroy LEO satellites passing within its field of view, provided that the array was designed and equipped to track noncooperative targets. As a large fixed system, however, a launch laser array would be both inefficient and conspicuous as an antisatellite laser.

A full launch-scale laser or laser array capable of delivering >10 MW/m² at a range of >400 km could also deliver >1 kW/m² at 40,000 km: that is, GEO. This could potentially allow an array to temporarily blind or permanently disable (by overheating) satellites in GEO. Again, a launch system would not be particularly efficient for this purpose in comparison to a purpose-built antisatellite laser, but it would provide some military capability unless it was explicitly designed to be incapable of striking GEO (e.g., by limiting pointing southward)

Further discussion of military applications is beyond the scope of this report.

Beam module/laser array technology.—Finally, beam modules as such, and more generally beam module technologies for low-cost laser power, pointing and tracking, and adaptive optics, may be relevant to nonpropulsive power beaming. Some possible applications include delivering power to satellites in eclipse or for peak power needs, annealing satellite photovoltaic panels, and powering high-altitude airships or “eternal” UAVs.

3.1.5.6 References for Laser Thermal Consultant Report—DRM 1–B

1. Kare, J.T., “Laser Powered Heat Exchanger Rocket for Ground-to-Orbit Launch,” *J. Propulsion and Power* 11(3), 535-543 (1995).
2. Kare, J.T., *Modular Laser Launch Architecture: Analysis and Beam Module Design*, Final Report, Phase I, University Space Research Association subcontract 07605-003-015, NASA Institute for Advanced Concepts, Atlanta, GA, May 2004
3. Kare, J.T., “Near-Term Laser Launch Capability: The Heat Exchanger Thruster,” *Proceedings, 1st Internat. Symposium on Beamed Energy Propulsion*, ed. by A. V. Pakhomov, AIP Conf. Proc. 664, 442 (2003), DOI:10.1063/1.1582132
4. Kare, J.T., “Development Program for the Heat Exchanger Thruster and HX Laser Launch System,” *Proceedings, 2nd Internat. Symposium on Beamed Energy Propulsion*, ed. by K. Komurasaki, AIP Conf. Proc. 702, 251 (2004), DOI:10.1063/1.1721005

5. Tuckerman, D. B., "Heat-Transfer Microstructures for Integrated Circuits," UCRL-53515, LLNL 1984.
6. Kare, J., High Performance Heat Exchanger for Laser Propulsion, AIAA 2005-5176, 36th AIAA Plasmadynamics and Lasers Conference, Toronto, Ontario, Canada, 2005.
7. Steffani, C., "Electroforming Thin Channel Heat Exchangers," in Proceedings of the Electroforming Symposium, SURFIN 91, Amer. Electroplaters and Surface Finishing Society (1991).
8. Parkin, K.L.G., DiDomenico, L.D., and Culick, F.E.C., "The Microwave Thermal Thruster Concept," Proceedings, 2nd Internat. Symposium on Beamed Energy Propulsion, ed. by K. Komurasaki, Vol. 702, AIP, Melville, New York, 2004, pp. 418-429.
9. A. Y. Vorobyev and C. Guo, Femtosecond laser blackening of platinum, *J. Appl. Phys.* 104, 053516 (2008)
10. <http://www.hexoloy.com/data-sheets/silicon-carbide-products/pdf/sic-capabilities.pdf>
11. http://www.ultramet.com/ceramic_protective_coatings.html
12. <http://optics.org/article/39511> 17 June 2009. (Accessed 3 May 2011) Also http://www.ipgphotonics.com/Collateral/Documents/EnglishUS/Summer_Newsletter_IPG_2009.pdf
13. http://www.nufern.com/specsheets/NukW_flyer.pdf> accessed May 31, 2011.
14. C. H. Liu et al., *Electronics Lett.* 40, 1471-1472, 2004. See also A. Galvanuska, "KW-Power Fiber Lasers with Single Transverse Mode Output," 22 Sep 2005, http://www.nufern.com/~whitepaper_detail.php/30, accessed May 31, 2011.
15. A. Sevian et al., "Efficient Power Scaling Of Laser Radiation By Spectral Beam Combining," *Optics Letters* 33, 384 (Feb 15, 2008).
16. D. Havrilla and R. Brockmann, "Latest advance in high power disk lasers," in *Solid State Lasers XIX: Technology and Devices*, Proc. SPIE 7578, 75780C, 2010. DOI: 10.1117/12.843204
17. "Boeing Fires New Thin-Disk Laser, Achieving Solid-State Laser Milestone" http://www.boeing.com/news/releases/2008/q2/080603a_nr.html accessed May 20, 2011.
18. "Northrop's 100kW Laser Weapon Runs For Six Hours," <http://optics.org/news/1/7/13> (09 Dec. 2010).
19. "Northrop Grumman Announces the FIRESTRIKE(tm) Laser, World's First Weaponized Solid-State Laser for U.S. Military Services" <http://www.globalsecurity.org/military/library/news/2008/11/mil-081113-northrop-grumman01.htm> accessed May 20, 2011. Also <http://en.wikipedia.org/wiki/FIRESTRIKE>
20. Warwick, G., "Solid-State Laser Programs Advance," *Aviation Week and Space Technology*, Jan 11, 2009.
21. R. Page, R. Beach, V. Kanz, and W. Krupke, "Multimode-diode-pumped gas (alkali-vapor) laser," *Opt. Lett.* 31, 353-355 (2006).
22. W. F. Krupke, DPALs: An Overview, Proc. SPIE 7005, 700521 (2008), doi:10.1117/12.782466
23. J. Zweiback, A. Komashko and W. F. Krupke, "Alkali-vapor lasers", Proc. SPIE 7581, 75810G (2010); doi:10.1117/12.843594
24. J. A. Georges et al., "Design and testing of a dynamic refocus system for Rayleigh laser beacons" in *Adaptive Optical System Technologies II*, Proc. SPIE 4839, pp. 473-483, 2003. DOI: 10.1117/12.459354

25. <http://spectrum.ieee.org/tech-talk/semiconductors/devices/what-will-the-data-center-of-the-future-look-like> accessed 6/27/2011.
26. Kare, J. T., and Parkin, K. L. G., A Comparison of Laser and Microwave Approaches to CW Beamed Energy Launch, AIP Conf. Proc. 830, 388 (2006), DOI:10.1063/1.2203282
27. http://en.wikipedia.org/wiki/Chevrolet_Volt#Battery or <http://gm-volt.com/2010/03/09/>
28. Ramsey, M., "Nissan Says Leaf Electric Will Be Profitable With U.S. Plant," Wall Street Journal, Autos, 13 May 2010.
29. P. Crump, W. Dong, M. Grimshaw, J. Wang, S. Peterson, D. Wise, M. DeFranza, S. Elim, S. Zang, M. Bougher, J. Peterson, S. Das, J. Bell, J. Farmer, M. DeVito, R. Martinsen, "100-W+ Diode Laser Bars Show >71% Power Conversion from 790-nm to 1000-nm and Have Clear Route to > 85%", Proc. SPIE 6456, paper 645660M, 2007
30. H. Li, I. Chyr, D. Brown, X. Jin, F. Reinhardt, T. Towe, T. Nguyen, R. Srinivasan, M. Berube, R. Miller, K. Kuppuswamy, Y. Hu, T. Crum, T. Truchan, J. Harrison "Ongoing Development of High-Efficiency and High-Reliability Laser Diodes at Spectra-Physics", Proc. of SPIE 6456-9, San Jose, California, 2007. doi: 10.1117/12.701714
31. Pandey, R., "High Power, High Brightness, Multi-purpose, Laser-head Module," presentation, AHPSL 2008, San Diego, Oct 2008.
http://www.dilas.com/gdresources/downloads/whitepapers/DILAS_AHPSL_Oct08.pdf
32. N. Trela, H. Baker, J. Wendland, and D. Hall, "Dual-axis beam correction for an array of single-mode diode laser emitters using a laser-written custom phase-plate," Opt. Express 17, 23576-23581 (2009).
33. D. Havrilla, M. Holzer, R. Brockmann, S. Strohmaier. "Dramatic Advances in Direct Diode Lasers," in High-Power Diode Laser Technology and Applications VIII, M. S. Zediker, ed., Proc. SPIE 7583, 2010. doi: 10.1117/12.843207
34. See <http://hubbleoptics.com>
35. Hyde, R. A. and Dixit, S., "Large-aperture Diffractive Optics for Space-Based Lasers," UCRL JC-139446, Lawrence Livermore National Laboratory, 2000.
36. J. Zweiback and B. Krupke, "Rubidium and potassium alkali lasers", Proc. SPIE 7196, 71960E (2009); doi:10.1117/12.807850
37. McClatchey, R. F., "Optical Properties of the Atmosphere, 3rd Edition" AFCRL-72-0497, 1972.
38. https://secure.wikimedia.org/wikipedia/en/wiki/Cessna_400 accessed 7/8/2011.
39. <http://www.globalsecurity.org/military/systems/munitions/bgm-109-inv.htm> accessed 7/8/2011.
40. Caird, J., et al., Nd:Glass Laser Design For Laser ICF Fission Energy (LIFE), Fusion Science and Technology 56, 607-617 (2009). Available at <https://e-reports-ext.llnl.gov/pdf/367075.pdf>
41. Haitz, R., and Tsao, J. Y., "Solid-state lighting: 'The case' 10 years after and future prospects," physica status solidi (a) 208, 1, pp. 17-29 (2011). DOI: 10.1002/pssa.201026349.
42. <http://www.s-et.com/datasheet/PriceList.pdf> accessed 6/26/2011.
43. Harder, C., "Power Laser Trends," 7/2/2009, p. 13.
<http://www.charder.ch/libraries.files/PowerLaserTrends.pdf> accessed 7/8/2011
44. Amos, W. A., Costs of Storing and Transporting Hydrogen, NREL/TP-570-25106, November, 1998. <http://www1.eere.energy.gov/hydrogenandfuelcells/pdfs/25106.pdf>

45. Heat Transfer and Fluid Flow in Minichannels and Microchannels, S. Kandlikar et al., Elsevier Science (October 2, 2005).
46. D. B. Marshall and B. N. Cox Integral Textile Ceramic Structures Annu. Rev. Mater. Res. 2008. 38:425–43.
47. R. K. Huang, “Ultra-high-brightness Kilowatt-class Fiber-coupled Diode Lasers” SPIE Newsroom, 16 May 2011. DOI: 10.1117/2.1201104.003648.
<http://spie.org/x48054.xml?ArticleID=x48054> accessed 7/21/2011
48. <http://www.tethers.com/TT.html> accessed 7/21/2011.
49. E. Early, G. Megaloudis, P. Kennedy, and R. J. Thomas, “Methodology for Reflected Laser Beam Hazard Analyses” Journal of Directed Energy 3. 4, Summer 2010.
50. http://en.wikipedia.org/wiki/Sub-orbital_spaceflight#Future_of_manned_sub-orbital_spaceflight accessed 7/21/2011.
51. Kare, J. T., “Laser Launch -- The Second Wave,” in Beamed Energy Propulsion, Proc. 1st Internat. Symp. on Beamed Energy Propulsion, A. V. Pakhomov, Ed., AIP 664 22 (2003).

3.1.6 Laser Thermal Cost

National Aeronautics and Space Administration



Beamed Energy Propulsion Facility ROM Cost Estimate

March 28, 2011



General BEPS Launch Facility Assumptions

- All cost are rough order of magnitude (ROM) estimates in FY11M\$.
- Estimates assume all facilities are built new on government land, no existing infrastructure is used. Available infrastructure will reduce costs.
- Costs do not include remediation of potential significant environmental impact issues that may be identified.
- Range estimates are presented to highlight the uncertainty associated with the lack of definition and supporting cost information available at this time.
- Range estimates for the launch site also includes the uncertainty associated with the selected location and the cost impact of materials that may be required to protect against environmental conditions.



General BEPS Launch Facility Assumptions

- Launch site ROM estimates are based on a NASA KSC launch site estimating approach. Microwave and laser sites use the same approach for 'like function' facilities which are scaled for expected differences in size or function.
- All sites include site design and testing and activation costs.
- Launch facility design is estimated at 12% of estimated total site costs less testing and activation.
- Launch facility testing and activation is estimated at 30% of the capital facilities cost.
- Microwave and laser site design is estimated at 8% of estimated total site costs less testing and activation.
- Microwave and laser site testing and activation is estimated at 15% of the capital facilities cost.



Operations Cost Assumptions

- All costs are estimated for one year of operation in FY11\$.
- Yearly operations cost assume 360 launches per year (one/day). Additional study is required to determine the feasible number of launches per year from a single launch pad. The number of launches per pad is affected by the CONOPS, pad turnaround time, launch facility maintenance, weather, and launch window requirements.
- Total estimated facility operations costs are assumed to be allocated to the beamed launch operations. Facility sharing can reduce costs.
- Facility equipment and maintenance is estimated at 5% of the total value of capital assets per year resulting in an estimated 70-80% of total operations costs.



Laser Thermal Rocket Launch Site Assumptions

- Launch Site facility requirements
 - General – site work, roads
 - Support Facilities/Launch Pad – see details below
 - Site Infrastructure – water, fire, sewer, power, communications, HVAC, environmental control system
 - Ground support equipment
- Key cost estimate assumptions
 - New facility on government land in secluded area due to danger associated with beamed energy. Launch rate 1-4 vehicles a day, if CONOPS allows.
 - Launch pad includes all related hardware/services (scaled from microwave estimate). Rocket will be approximately 29 meters in length and less than 5,000 kg total wet mass with payload.
 - Command center includes all related services.
 - Payload integration facility (small payloads <320 kg) can process/integrate up to four payloads per day (scaled from microwave estimate).
 - Hydrogen storage facility sized for ~30,000 kg with no on-site production.
 - Rocket storage facility size for 8 rockets (scaled from microwave estimate).
 - Admin facility sized for launch site staffing needs (estimated at 100 people).
 - Security facilities/equipment includes fencing, cameras, etc.



Laser Thermal Rocket Boost Laser Site Assumptions

- Boost Laser Site facility requirements
 - General – site work, roads
 - Support Facilities – admin facility (50 people), command center (75% of launch site center), guard gate facility
 - Site Infrastructure – water, fire, sewer, power, communications, HVAC, environmental control system
 - Ground support equipment
 - Laser/Optics– diode lasers(240 MW), optics (Qty.1200, 200 kWe modules)
 - Power Storage/Distribution – energy storage, power supply, power distribution
- Key cost estimate assumptions
 - Diode Laser – Projected multi-MW price \$2/W (ref: J. Kare) used as low (ML +50%, high +100%)
 - Optics – Projected \$200K/module (ref: J. Kare) use as low (ML +25%, high +50%)
 - Energy Storage - \$50K/kWh estimated as most likely based on GRC experience with wind tunnels (low -40%, high +20%)



Laser Thermal Rocket Main Laser Site Assumptions

- Main Laser Site facility requirements
 - General – site work, roads
 - Support Facilities – admin facility (50 people), command center (75% of launch site center), guard gate facility
 - Site Infrastructure – water, fire, sewer, power, communications, HVAC, environmental control system
 - Ground support equipment
 - Laser/Optics– fiber lasers(140 MW), optics (Qty.2300, 60 kWe modules)
 - Power Storage/Distribution – energy storage, power supply, power distribution
- Key cost estimate assumptions
 - Fiber Laser – Projected multi-MW price \$10/W (ref: J. Kare) used as low (ML +50%, high +100%)
 - Optics – Projected \$200K/module (ref: J. Kare) use as low (ML +25%, high +50%)
 - Energy Storage - \$50K/kWh estimated as most likely based on GRC experience with wind tunnels (low -40%, high +20%)



Laser Thermal Rocket Launch Facility Development ROM

Laser Thermal Rocket Launch Facilities ROM (FY11\$M)
(Excludes FTE/WYE personnel and O&M costs)

	Launch Site Complex - ROM Subtotal (\$M)				Boost Laser Site - ROM Subtotal (\$M)				Main Laser Site - ROM Subtotal (\$M)				Laser Thermal Rocket Facilities - Total ROM (\$M)			
	Low	ML	High	Mean Est	Low	ML	High	Mean Est	Low	ML	High	Mean Est	Low	ML	High	Mean Est
Project Total ROM (\$M)	\$279.0	\$460.0	\$1,395.0	\$609.0	\$1,290.0	\$1,962.0	\$2,987.0	\$2,029.0	\$2,413.0	\$3,851.0	\$5,298.0	\$3,261.0	\$4,272.0	\$6,444.0	\$9,566.0	\$6,761.0
Design	\$32.8	\$50.2	\$119.6	\$69.2	\$81.5	\$127.4	\$188.4	\$133.1	\$170.3	\$250.9	\$344.2	\$255.1	\$286.6	\$431.5	\$602.2	\$457.4
Testing & Activation	\$73.1	\$120.1	\$279.5	\$159.2	\$152.0	\$232.9	\$344.1	\$243.2	\$315.2	\$464.5	\$636.4	\$472.0	\$540.8	\$822.5	\$1,260.0	\$874.4
Laser Thermal Rocket Facilities ROM Subtotal	\$279.2	\$460.3	\$996.5	\$576.7	\$1,044.1	\$1,921.1	\$2,354.6	\$1,663.6	\$2,128.2	\$3,136.0	\$4,902.0	\$3,189.0	\$3,445.4	\$5,188.4	\$7,664.1	\$5,429.9
W&S Item																
Site Work	\$11.2	\$15.4	\$18.8	\$15.1	\$8.4	\$11.6	\$14.1	\$11.3	\$8.4	\$11.6	\$14.1	\$11.3	\$27.9	\$38.6	\$47.0	\$37.8
Roads	\$18.4	\$27.9	\$46.2	\$30.8	\$18.4	\$27.9	\$46.2	\$30.8	\$18.4	\$27.9	\$46.2	\$30.8	\$55.3	\$83.7	\$138.6	\$92.5
Support Facilities	\$37.6	\$79.9	\$154.2	\$90.6	\$7.1	\$14.9	\$36.1	\$19.4	\$7.1	\$14.9	\$36.1	\$19.4	\$51.9	\$109.8	\$226.9	\$129.9
Concrete Administration Facility	\$7.4	\$10.8	\$28.5	\$13.7	\$5.4	\$14.2	\$31.7	\$17.7	\$5.4	\$14.2	\$31.7	\$17.7	\$14.7	\$21.5	\$57.0	\$31.0
8 Rocket Storage Facility	\$7.0	\$9.4	\$15.3	\$10.9	\$0.0	\$0.0	\$0.0	\$0.0	\$0.0	\$0.0	\$0.0	\$0.0	\$7.0	\$9.4	\$15.3	\$10.9
Concrete Command Center	\$3.3	\$10.4	\$25.3	\$12.5	\$2.5	\$7.8	\$19.0	\$10.0	\$2.5	\$7.8	\$19.0	\$10.0	\$8.3	\$26.0	\$63.4	\$33.3
Payload Integration Facility	\$19.0	\$47.6	\$82.3	\$50.0	\$0.0	\$0.0	\$0.0	\$0.0	\$0.0	\$0.0	\$0.0	\$0.0	\$19.0	\$47.6	\$82.3	\$50.0
Guard Gate Facility	\$1.0	\$1.8	\$2.8	\$1.8	\$1.0	\$1.8	\$2.8	\$1.8	\$1.0	\$1.8	\$2.8	\$1.8	\$2.9	\$5.3	\$8.4	\$5.3
Pad Structure	\$16.4	\$24.4	\$30.4	\$23.7	\$0.0	\$0.0	\$0.0	\$0.0	\$0.0	\$0.0	\$0.0	\$0.0	\$16.4	\$24.4	\$30.4	\$23.7
Pad Structure	\$5.4	\$7.8	\$10.5	\$7.9	\$0.0	\$0.0	\$0.0	\$0.0	\$0.0	\$0.0	\$0.0	\$0.0	\$5.4	\$7.8	\$10.5	\$7.9
Emergency Egress System	\$0.0	\$0.0	\$0.0	\$0.0	\$0.0	\$0.0	\$0.0	\$0.0	\$0.0	\$0.0	\$0.0	\$0.0	\$0.0	\$0.0	\$0.0	\$0.0
Flame Trench	\$8.4	\$10.0	\$11.1	\$9.8	\$0.0	\$0.0	\$0.0	\$0.0	\$0.0	\$0.0	\$0.0	\$0.0	\$8.4	\$10.0	\$11.1	\$9.8
Lightning Protection Towers	\$2.6	\$6.6	\$8.8	\$6.0	\$0.0	\$0.0	\$0.0	\$0.0	\$0.0	\$0.0	\$0.0	\$0.0	\$2.6	\$6.6	\$8.8	\$6.0
Infrastructure	\$155.9	\$254.1	\$613.9	\$341.3	\$91.3	\$142.7	\$260.5	\$164.8	\$91.3	\$142.7	\$260.5	\$164.8	\$338.6	\$539.5	\$1,134.9	\$671.0
GSE	\$33.6	\$58.5	\$133.1	\$75.1	\$8.4	\$14.6	\$33.3	\$18.8	\$8.4	\$14.6	\$33.3	\$18.8	\$50.4	\$87.8	\$199.7	\$112.6
Laser/Optics Equipment	\$0.0	\$0.0	\$0.0	\$0.0	\$720.0	\$1,020.0	\$1,320.0	\$1,020.0	\$1,800.0	\$2,075.0	\$3,000.0	\$2,075.0	\$2,300.0	\$3,095.0	\$4,810.0	\$3,095.0
Power Storage/Processing Facilities	\$0.0	\$0.0	\$0.0	\$0.0	\$190.4	\$360.4	\$644.5	\$398.4	\$134.5	\$249.3	\$422.8	\$268.9	\$324.8	\$609.7	\$1,067.3	\$667.3



Laser Thermal Rocket Launch Facility Operations ROM

Laser Thermal Rocket Facilities Operations ROM (FY11\$M/Year)

(Does not include launch vehicle)

	Laser Thermal Rocket Operations - Total ROM (\$M/Yr)			
	Low	ML	High	Mean Est
Laser Operations Total ROM (\$M/Year)	\$208.9	\$314.9	\$455.8	\$326.5
Facility/Equipment Maintenance	\$168.1	\$253.3	\$373.4	\$264.9
Operations Personnel	\$30.0	\$40.0	\$50.0	\$40.0
Propellant/Energy/Consumables	\$10.8	\$21.6	\$32.4	\$21.6
Other	\$0.0	\$0.0	\$0.0	\$0.0
Launch Site Complex - ROM Subtotal (\$M/Year)	\$30.8	\$48.0	\$82.4	\$53.7
Facility/Equipment Maintenance	\$12.2	\$20.8	\$46.6	\$26.5
Operations Personnel	\$15.0	\$20.0	\$25.0	\$20.0
Propellant/Energy/Consumables	\$3.6	\$7.2	\$10.8	\$7.2
Other	\$0.0	\$0.0	\$0.0	\$0.0
Boost Laser Site - ROM Subtotal (\$M/Year)	\$62.0	\$94.8	\$138.0	\$98.3
Facility/Equipment Maintenance	\$50.9	\$77.6	\$114.7	\$81.1
Operations Personnel	\$7.5	\$10.0	\$12.5	\$10.0
Propellant/Energy/Consumables	\$3.6	\$7.2	\$10.8	\$7.2
Other	\$0.0	\$0.0	\$0.0	\$0.0
Main Laser Site - ROM Subtotal (\$M/Year)	\$116.2	\$172.0	\$235.4	\$174.5
Facility/Equipment Maintenance	\$105.1	\$154.8	\$212.1	\$157.3
Operations Personnel	\$7.5	\$10.0	\$12.5	\$10.0
Propellant/Energy/Consumables	\$3.6	\$7.2	\$10.8	\$7.2
Other	\$0.0	\$0.0	\$0.0	\$0.0



Beamed Energy Propulsion Study Laser Thermal Vehicle Cost Estimate as determined by the COMPASS Team

March 2011



Cost Assumptions

- DRAFT Cost Estimate based on COMPASS design
- All costs are in FY11\$M
- Estimates represent prime contractor cost plus fee (10%)
- This estimate assumes the following:
 - Proto-flight development approach
 - Full set of ground spares included
 - Model assumes TRL Level 6
 - This estimate does not include any cost for technology development
 - Represents the mean estimate based on cost-risk simulation results
 - Parametric estimate based on mostly mass based CERs from historical cost data
 - Planetary systems integration wraps
 - Software not included
- Does not include:
 - Any insight/oversight costs (by a NASA lead center)
 - Reserves (can be as high as 40-50%)
 - Ground System Cost (ie. Laser)
 - Launch Services Costs (ie. Special launch approval process)
 - Technology costs for components lower than TRL-6



BEPS Preliminary Cost ROM

(Represents estimated Prime Contractor cost)

WBS	Description	DDT&E Total BY \$M	Flight HW BY \$M	DD&FH Total BY \$M
06.1.1	Payload	0.0	0.0	0.0
06.2.1	Attitude Determination and Control	2.6	2.4	4.9
06.2.2	Command and Data Handling	4.3	2.6	6.9
06.2.3	Communications and Tracking	1.1	0.8	1.8
06.2.4	Electrical Power Subsystem	1.0	1.1	2.1
06.2.5	Thermal Control	22.7	4.2	26.9
06.2.6	Propulsion	14.0	6.2	20.2
06.2.7	Propellant	0.0	0.0	0.0
06.2.8	Structures and Mechanisms	15.2	7.6	22.8
	Subtotal	60.9	24.8	85.7
	Systems Integration	46.5	8.0	54.5
	Spacecraft Total	107.4	32.8	140.2

All Costs in FY11\$M

3.1.7 Millimeter-Wave Thermal Collaborative Modeling for Parametric Assessment of Space Systems (COMPASS) Report





Team Roster



- COMPASS Lead - Steve Oleson
- Program Study Leads – Ray Beach, Patrick George
- Lead System Integration, MEL - Melissa McGuire, David Grantier
- CONOPS, Integration PEL , Mission Visualization - Michael Bur
- Mission –Dave Smith
- GN&C –Mike Martini
- Propulsion - James Fittje, Geoff Landis
- Mechanical Systems - John Gyekenyesi
- Thermal - Tony Colozza
- Power - James Fincannon, Kristen Bury
- C&DH, Software- Glenn Williams
- Communications - Joe Warner
- Configuration and Launch Vehicle Integration - Tom Packard
- Cost - Jon Drexler
- Risk - Anita Tenteris

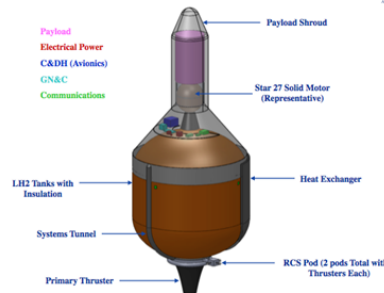
2



Microwave Launcher Summary



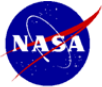
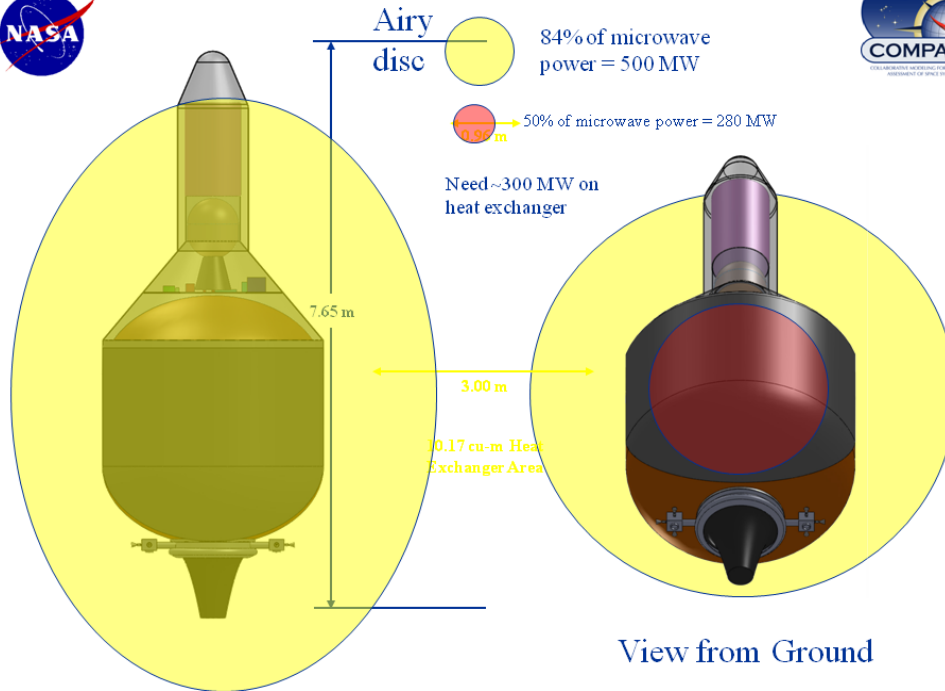
- 170 GHz Microwave powered plug nozzle first stage, Star 27 second stage
- Launches 1 equivalent 40 kg ORBCOMM messaging spacecraft
- 7.5 m launcher dominated by 3 m hydrogen tank that doubles to secure the heat exchangers
- Launched vertically, requires two 170 GHz microwave stations (up to 600 MW) for complete launch
 - Sustainer station ~600 MW emitted, 100 m diameter cassagrain
- Thermal heat exchanger technology still in TRL 2-3 range
- Propulsion and Thermal:
 - 60 kN plug nozzle, 2200° K hot hydrogen from heat exchanger supported by tank
 - Up to 300 MW absorbed by hydrogen in heat exchanger provides lpsps up to 760 sec
 - Hot hydrogen for RCS
 - Highly Reflective (99.9999%) coatings on vehicle to avoid over heating of shroud, tank, etc.



Cost bottom line: ~\$11M Launcher only Recurring Cost

Spacecraft Master Equipment List Rack-up (Mass) - BEP Thermal Laser				COMPASS S/C Design	
WBS	Main Subsystems	Basic Mass (kg)	Growth (kg)	Wet Mass (kg)	Aggregate Growth (%)
08	Microwave Launcher Case 2	2013.9	88.7	2082.6	4.4%
08.1	Payload	45.0	0.0	45.0	0%
08.2	Launch Vehicle	1967.9	88.7	2056.6	1%
08.2.1	Attitude Determination and Control	9.0	0.0	9.0	0%
08.2.2	Command and Data Handling	10.0	0.0	10.0	0%
08.2.3	Communications and Tracking	4.0	0.0	4.0	0%
08.2.4	Electrical Power Subsystem	7.0	0.0	7.0	0%
08.2.5	Thermal Control	100.0	10.0	110.0	10%
08.2.6	Propulsion	312.0	21.7	333.7	7%
08.2.7	Propellant	1490.0	0.0	1490.0	0%
08.2.8	Structures and Mechanisms	95.0	17.4	112.4	14%
	Estimated Launch Vehicle Dry Mass (no payload)	485	82	567	13%
		2212	89	2301	4%
System Level Growth Calculations					
	Dry Mass (excl. System Level Growth) (no payload)	485	82	567	13%
	Additional Growth (excl. payload)	212	140	352	73%
	Wet Mass (incl. Growth) (no payload)	697	222	919	32%
		Basic Mass (kg)	Growth (kg)	Total Mass (kg)	
	485	222	707		
	Total Structure Wet Mass (no growth)	312.0	0.0	312.0	
	Mass of Structure Tanks (no growth)	0.0	0.0	0.0	
	Vehicle On Orbit Mass (incl. residual) PPE, w/PPE	882.0	0.0	882.0	
	Vehicle On Orbit Mass (incl. residual) PPE, w/PPE	874.0	0.0	874.0	
	OTIS total burn out mass	820.0	0.0	820.0	
	Additional Margin	58.0	0.0	58.0	
	* NOTE: structure residual includes dry mass				

3



TRL Definitions

- SUMMARY
- **TRL 1** Basis principles observed and reported
- **TRL 2** Technology concept and/or application formulated
- **TRL 3** Analytical and experimental critical function
- **TRL 4** Component and/or breadboard validation in laboratory environment
- **TRL 5** Component and/or breadboard validation in relevant environment
- **TRL 6** System/Subsystem model or prototype demonstration in a relevant environment (ground or space)
- **TRL 7** System prototype in a space environment
- **TRL 8** Actual system completed and "flight qualified" through test and demonstration (ground or space)
- **TRL 9** Actual system "flight proven" through successful mission operations



TRL Levels (< TRL 6) Update



- **Propulsion & Flight Dynamics/Environments**
 - Hydrogen Engine (100,000N class):
 - High Temperature components (2200° K): TRL 4
 - Plug Nozzle: TRL 5
 - RCS: TRL 5-6
- **Thermal:**
 - Heat Exchanger: TRL 2-3
- **GN&C: TRL 6**
- **C&DH: EMI Shielding TRL 6**
- **Communications: TRL 5-6 (EMI/thermal environment)**
- **Power**
 - Batteries TRL 5-6
- **Mechanical:**
 - Advanced, high temperature (C/C composites) TRL 3-4

6



BEP4 Scratch PEL



Scratch PEL BEP 4		Power Mode 1
		(W)
Power Mode Title		Launch
Systems operating		All Except Structures
Time (days)		
	GN&C	15
	Propulsion System (hardware)	50
	Electrical Power	20
	Command and Data Handling	34
	Communications and Tracking	22
	Thermal and Environmental Control	10
	Structures & Mechanical Systems	0
	total	151

Plus 30% 196

7



Ground to Launch Vehicle Link Budget



	Individual efficiency			Wallplug to Jet cumulative			Gyrotron to Jet cumulative		
	Low	Med	High	Low	Med	High	Low	Med	High
Power supply	85%	92%	98%	85%	92%	98%			
Gyrotron	45%	54%	62%	38%	49%	61%			
Dish feed system	75%	86%	97%	29%	42%	59%	75%	86%	97%
Surface accuracy	95%	98%	100%	27%	41%	59%	71%	84%	97%
Diffraction	76%	86%	95%	21%	35%	56%	54%	72%	92%
Atmospheric transmission	75%	86%	97%	16%	30%	54%	41%	62%	89%
Absorption into propellant	80%	89%	98%	12%	27%	53%	32%	55%	88%

- Roughly Half of ground station power absorbed into propellant

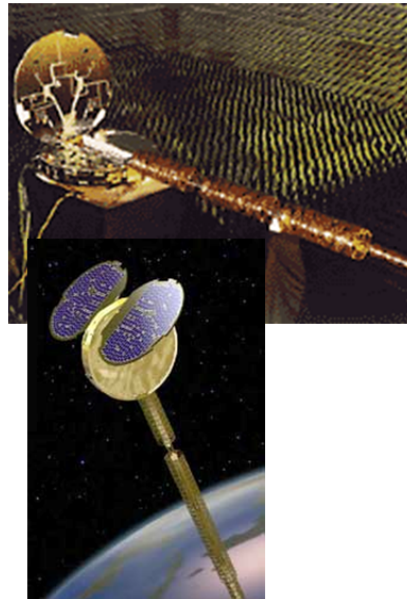
8



Proposed Representative Payload



- ORBCOMM Class
- Orbcomm is a commercial venture to provide global messaging services using a constellation of 26 low-Earth orbiting satellites.
- Spacecraft (40 kg, \$1.2M each)
 - 4 years life, 160W
 - VHF (138 MHz and 400 MHz): 57.6 kbps
 - Gravity gradient, mag torquers, cold gas N2
 - 17 data processors, 7 antennas, 50,000 messages per hour
- 40 kg separated payload



9

Bottom image: courtesy of Orbital Sciences Corporation; used with permission.



Beamed Energy Propulsion: Laser Launcher



The COMPASS team has been tasked by DARPA/NASA to create an independent concept design for a Laser powered launch vehicle.

The COMPASS design will give the DARPA/NASA a point-of-reference to the feasibility of the concept and a what technologies and demonstrations need to be developed to support development of a laser launcher.



Schedule



- **This Week**
 - MTW (with customer), F
 - Monday: Kickoff, Mission Analysis, Begin laying out vehicle, define trades, Scratch PEL
 - Tuesday-Wednesday: CONOPs, Perform design
 - Tuesday 9:30-11:30 am splinters
 - Wed 9:30-11:30 am splinters
 - » Microwave/atmospheric interaction attenuation
 - » Microwave Station strawman design
 - Friday: Review Trades, Assess MEL, Configuration
- **2nd Week**
 - MW: Complete Design
 - F: Draft Results Flip-thru



Starting Requirements



- **Must Deliver to LEO a payload to suborbit (100 km x 400 km x 30° inclination)**
- **Payload will circularize itself for a useful mass of 40 kg**
- **Will Utilize two ground based microwave beams (~2.5 MW for 1 kg to orbit – at vehicle)**
- **Will emphasize simplicity and low cost**

12



FOMs



- **Mass: Two payloads at 40 kg each**
- **Reliability: Single Fault Safe**
- **Cost:**
 - Launcher mass, volume
 - Cost for launch system

13



Fault Tolerance



- **Single fault for safety**
 - What kind of range safety is needed?
- **Fault tolerance for vehicle**
 - How valuable are payloads?
 - What systems should be fault tolerant?

14



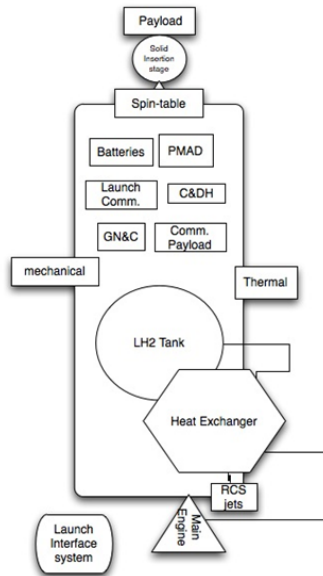
Summary of Requirements/Assumptions



	Requirements / Assumptions	Trades
Top-Level/ Science	Laser launcher shall place at least 40 kg into a 100x400 km orbit. FOM Cost per n units, payload mass, safety. First launch 2020.	Payload vs altitude
System	Single Fault Safe only. Otherwise zero fault tolerant. Launch lifetime. Shelf life of 2 years. Launch year open ended – current TRL assessment is an output. Laser density 5 MW/m ² Mass Growth per AIAA 120-2006 (add growth to make system level 30%)	
Mission, Ops, GN&C	Hydrogen heated by laser heat exchanger, launch from ground to sub-orbit, circularization with on-board system (circular, 100x400km alt., 30 deg. inc (+/-0.2 deg.) Y-P-R using high temp propellants.	Gimballed main engine, Beacon required?
Launch Vehicle	N/A	
Propulsion	2200 k heat exchanger primary propulsion: performs entire launch ΔV, same warm propellant for warm gas RCS	Main propellant choice: Hydrogen. exchanger instead of a main engine. Pintle atm correcting engine
Power	Primary batteries	Thermal batteries, secondary
C&DH Communications	Pre-use flight computer to handle launch. Up-range telemetry communications.	Computer type, data storage, data transfer rates, comm. Frequencies
Thermal & Environment	Gather heat from laser to heat propellant for an expansion rocket.	Trade heat exchanger material / design. Safety issues with hitting active spacecraft
Mechanisms	Thruster Gimbal, separation systems	mechanisms, materials, power, ops,
Structures	aluminum	minimize mass using composites
Cost		
Risk	Major Risks: microwave EM on avionics and payload and heating on rest of vehicle, down range aircraft and spacecraft (up to 200 km), wildlife	



Systems



16

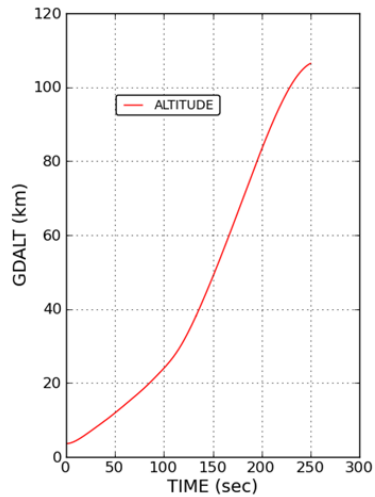


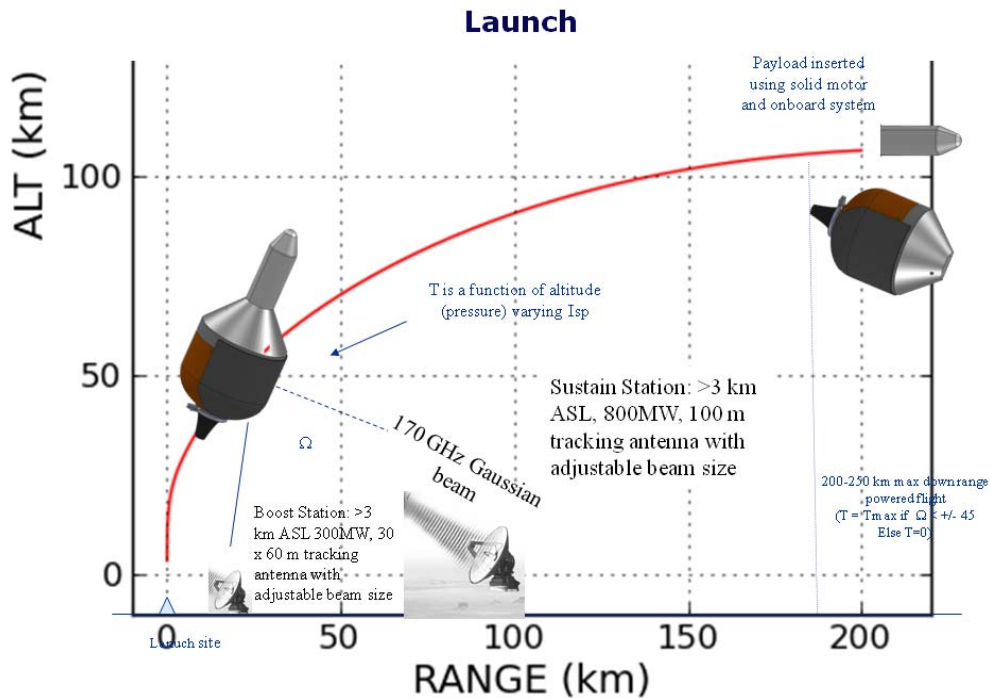
Timeline (draft)



- Pad prep
- Thermal Cocoon separation (-2 sec)
- Launch (0 sec, 3.5 km): Boost microwave only
- Sustainer microwave in view (? sec, ? km): combined microwave illumination
- Boost microwave off (? sec, 100 km)
- Fairing Separation (250 sec)
- Payload spin-up (252 sec)
- Payload Release (254 sec)
- Solid ignition (260 sec)
- Solid burnout (290 sec)
- Solid separation (300 sec)
- Payload Despin (330 sec)
- Final insertion (? Sec), 400 km circular

ALTITUDE





OTIS BEP-4 Mission Model (case 2)

- **Proposed vehicle is a TSTO vehicle (MW first stage with a two-burn upper stage)**

- first stage is a microwave/heat exchanger single propellant (LH2) (simulated with OTIS)
- second stage with delivers payload to 100 x 400 km circular orbit. (closed form calculations).
- Final circularization completed by on-board chemical system (400 x 400 km)

- **OTIS used to produce optimal trajectory for the microwave/heat exchanger stage of the vehicle (trajectory described below)**

- Objective function: for a fixed initial mass (compass team supplied) maximize mass (less estimated solid mass) to burn out at the end of MW stage. Subtracting solid mass "penalizes" OTIS for growing 2nd stage and optimally determines 1st stage cut-off.
- Trajectory (con-ops)
 - Vertical lift off to an optimal altitude to begin gravity turn
 - Gravity turn (angle of attack = 0) to an optimal altitude to begin climb to "orbit"
 - Climb with optimal control angles (as determined by optimizer) elliptical orbit (HA=100, HP=?)
 - Closed form calculation to perform transfer to 100 x 400 km using a solid
 - On-board system circularizes to 400 km circular (closed form)

- **Launch site near China Lake, CA (alt approx 3500 m). Boost ground station 20 km downrange and main station 100 km downrange**

- **Trajectory constraints:**

- +/- 45 deg angle between incident vehicle and "beam"
- Insertion w/in 200-250 km downrange of launch site.

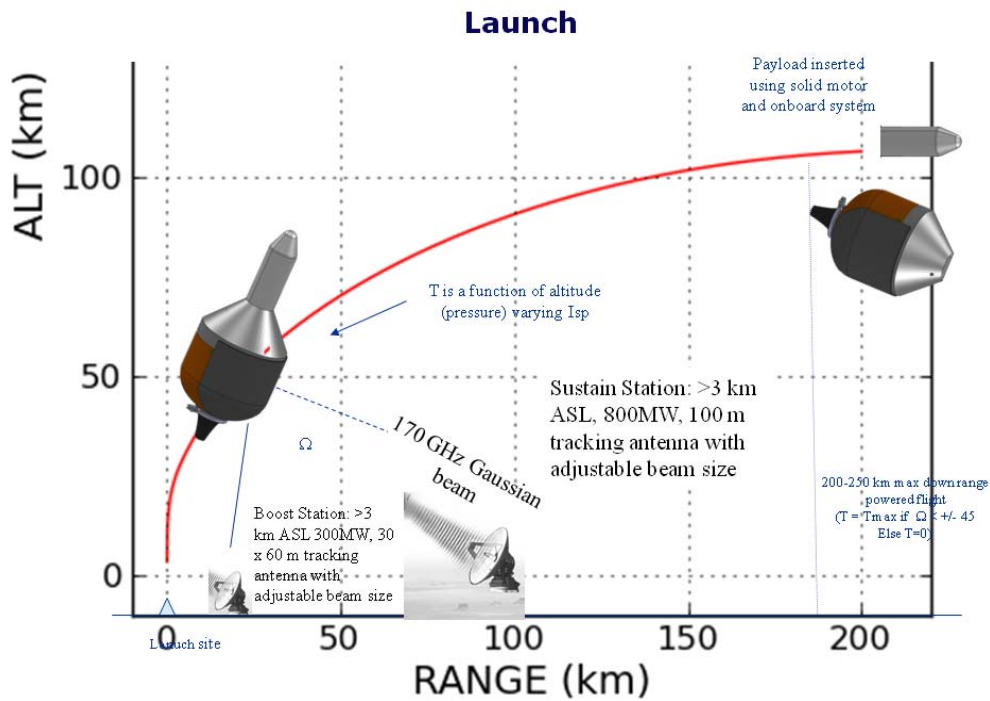
Power and Propulsion Details (case 2)

• Drag model

- Aeroshell model as prescribed in Parkin. Drag coefficient (C_d) calculated as a function of Mach.
- Drag calculated as function of C_d and cross-sectional area ('Afrontal') as determined by COMPASS design session.
 - Cross sectional area of 7.2 m^2 used for all phases.

• Power/Propulsion model (key equations, constraints and assumptions)

- Power transmission from the ground station to the vehicle (including atmospheric loss terms, etc. ...) **ARE NOT** directly modeled.
- Instead, T_{max} (and \dot{m}_{max}) will be calculated per the equations supplied by Parkin. Full thrust is assumed available (with no losses) as long as the following "constraints" are met:
 - The vehicle is w/in 200-250 km (downrange distance, optimally determined) of the launch site.
 - $\Omega < \pm 45$ degrees
- \dot{m}_{max} of 10 kg/s applied to limit heat exchanger mass.
- Optimal throttle from OTIS between 40 and 100% was applied to T_{max} .
- I_{spvac} 800 s (customer supplied). I_{sp} as a function of in-situ atmospheric and chamber pressure ($P_{\text{cham}} = 50 \text{ atm}$).

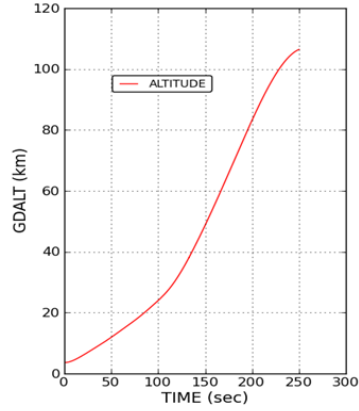




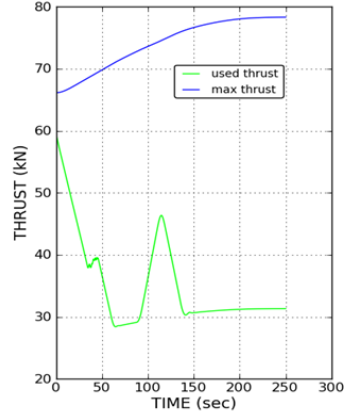
OTIS results (case 2)



ALTITUDE



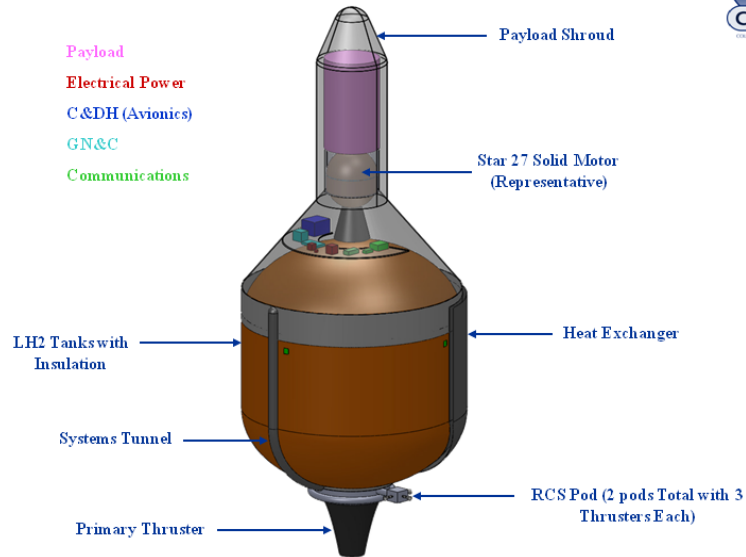
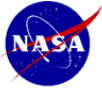
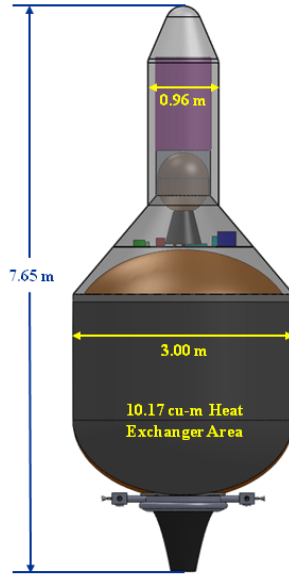
Thrust

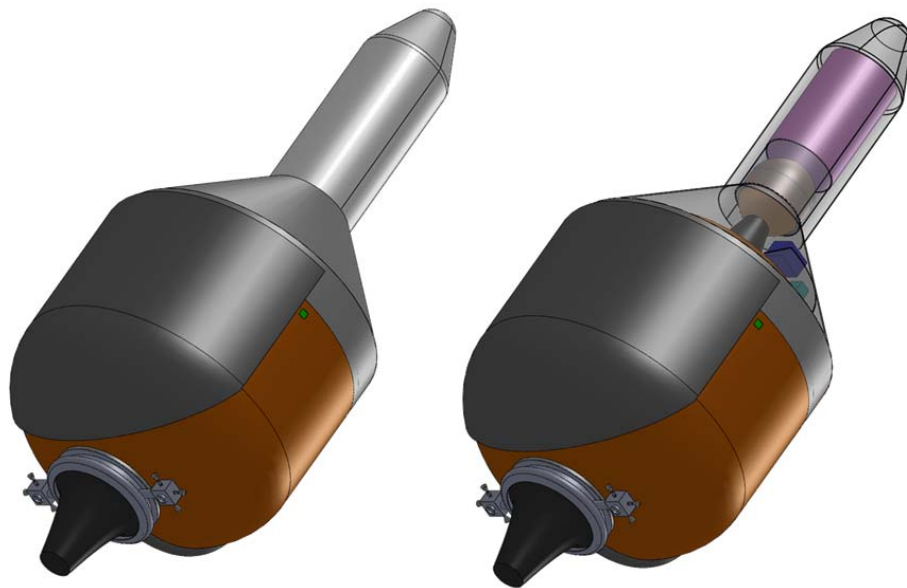


Mass and Delta-V Summary (case 2)

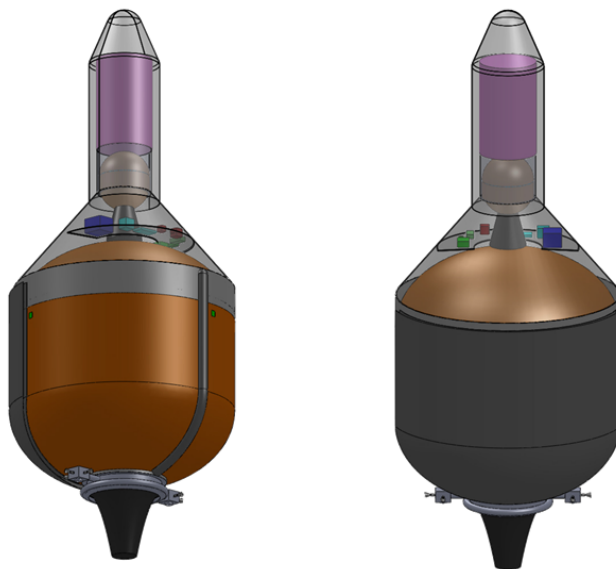


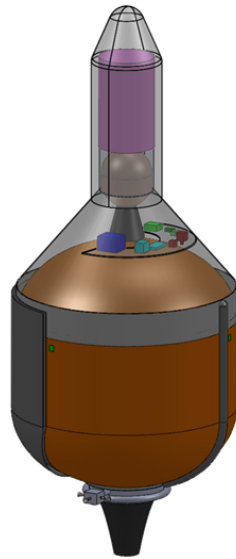
MWV Mass and Delta-V Summary	
case 2	
GLOM (kg)	2156
Stage 1 BO Mass (kg)	954
Stage 1 LH2 Consumed (kg)	1201
Stage 1 delta-V (km/s)	6.05
Stage 2 delta-V (km/s)	3.986
Stage 2 claculated mass of solid (kg)	197
Circ delta-V (km/s)	0.087





National Aeronautics and Space Administration





CONOPS Philosophy

- Reusable SSTO takes you to 100 km, drops payload off
- Rest is payload's problem
 - Obviously, this is not the way payloads are currently delivered
 - This rocket is not intended to deliver current payloads
 - The new payloads are intended to develop alongside the new launch approach (innovator's dilemma)
 - The incentive to develop for a rougher ride is
 - Much lower cost
 - Routine availability (i.e. take next week's launch if payload not ready this week)
 - Single payload—don't have to show that your payload will not break others
 - Higher risk tolerance

Beamed Energy Propulsion (BEP) Microwave Case 2: Preliminary System Summary

**Melissa L. McGuire,
Lead Systems Engineer
Design by COMPASS**

February 8, 2011

30

National Aeronautics and Space Administration



COMPASS Spacecraft Design Process



- Build Spacecraft MEL (Master Equipment List) in a WBS hierarchy by major subsystem down to a line item level appropriate to the level of design detail of the request
- Apply MGA from AIAA to each of the line items at the subsystem level
- Gather the total masses and calculate the total system growth % on the Basic dry mass
- Carry an additional system level (or program level) mass to reach a total of 30% mass book-kept on the dry Basic Mass

31



Mass Growth Allowance (MGA) Schedule



Taken from AIAA S-120-2006, *Standard Mass Properties Control for Space Systems*

- Basic Mass**
 - The current mass data based on an assessment of the most recent baseline design
 - NOTE 1 This design assessment includes the estimated, calculated, or measured (or actual) mass, and includes an estimate for undefined design details like cables, multi-layer insulation and adhesives.
 - NOTE 2 the mass growth allowances (MGA) and uncertainties are not included in the basic mass.
- Mass Growth Allowance (MGA)**
 - The predicted change to the basic mass of an item based on an assessment of the design maturity and fabrication status of the item, and an estimate of the in-scope design changes that may still occur
- Predicted Mass**
 - The basic mass plus the mass growth allowance

Code	Design maturity (basis for mass determination)	Electrical/electronic components			Percent MGA						
		0 to 5 kg	5 to 15 kg	>15 kg	Structure	Thermal control	Propulsion	Batteries	Wire harnesses	Mechanisms	Instrumentation
E	Estimated (preliminary sketches)	30	20	15	18	18	18	20	50	18	50
L	Layout (or major modification of existing hardware)	25	20	15	12	12	12	15	30	12	30
P	Prerelease drawings (or minor modification of existing hardware)	20	15	10	8	8	8	10	25	8	25
C	Released drawings (calculated values)	10	5	5	4	4	4	5	5	4	5
X	Existing hardware (actual mass from another program)	3	3	3	2	2	2	3	3	2	3
A	Actual mass (measured flight hardware)	0	0	0	0	0	0	0	0	0	0
FE	Customer furnished equipment	0	0	0	0	0	0	0	0	0	0

For the COMPASS process, the total percentage on dry mass is desired to be 30% total

$$\text{Predicted Mass} = \text{Basic Mass} + \text{Bottoms up MGA} \% \times \text{Basic Mass}$$

Therefore, Additional System level margin = 30% - Bottoms up MGA%

32



Top Level BEP 4 Characteristics



Spacecraft Master Equipment List Rack-up (Mass) - BEP Thermal Laser				COMPASS S/C Design	
WBS	Main Subsystems	Basic Mass (kg)	Growth (kg)	Total Mass (kg)	Aggregate Growth (%)
06	Microwave Launcher Case 2	2012.5	68.7	2081.2	
06.1	Payload	45.0	0.0	45.0	0%
06.2	Launch Vehicle	1967.5	68.7	2036.2	3%
06.2.1	Attitude Determination and Control	9.4	1.4	10.8	15%
06.2.2	Command and Data Handling	10.8	3.1	13.9	29%
06.2.3	Communications and Tracking	4.6	0.9	5.5	19%
06.2.4	Electrical Power Subsystem	9.8	4.1	13.9	42%
06.2.5	Thermal Control	100.3	15.1	115.4	15%
06.2.6	Propulsion	235.9	26.7	262.6	11%
06.2.7	Propellant	1499.9		1499.9	0%
06.2.8	Structures and Mechanisms	96.8	17.4	114.2	18%
	Estimated Launch Vehicle Dry Mass (no payload)	468	69	536.3	15%
		2012	69	2081	
System Level Growth Calculations					
	Dry Mass Desired System Level Growth (no payload)	468	140	607.9	30%
	Additional Growth (carried at system level)		72		15%
	Total Wet Mass with Growth (w/payload)	2012	140	2152.7	
		Basic Mass (kg)	Growth (kg)	Total Mass (kg)	
		468	140	2152.7	kg
	Total Spacecraft Wet Mass (w/growth)	2152.7			
	Mass of Dropped Tanks, jettisoned mass	0.0			
	Vehicle On Orbit Mass (incl residual/FPR, w P/L)	665.7	kg	1000	kg
	Vehicle On Orbit Mass (incl residual/FPR, w P/L w/solid)	875.4	kg		
	OTIS total burn out mass	922.0	kg		
	Additional margin	46.6	kg		
	* NOTE: pressurants/residuals included as Dry Mass				

- Inert mass is dry mass + trapped residuals + propellant margin + pressurant
- Dry mass on each segment is calculated as the total bottoms up dry mass with the MGA % applied + additional system mass so that the total growth on each stage is 30% of the basic mass
 - The dry basic mass of the BEP launcher without the payload is 468 kg
 - The Total dry mass with the bottom's up growth without the payload is 536 kg
 - The inert mass of the BEP launcher without the payload with 30% growth carried on the Basic mass is 608 kg
- Mission applies the -Vs and the rocket equation to the appropriate total vehicle mass based on the mission event and what stages have been jettisoned
- Total inert mass (this includes the payload, trapped residuals) with the 30% growth incorporated is: 665.7 kg

33

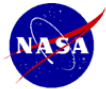


BEP Microwave Case 2 – Top Level MEL (Master Equipment List)



WBS	Description	QTY	Unit Mass	Basic Mass	Growth	Growth	Total Mass
Number	BEP4 - Jan 2011 - Microwave Case 2		(kg)	(kg)	(%)	(kg)	(kg)
06	Microwave Launcher Case 2			2012.47	3.4%	68.74	2081.20
06.1	Payload			45.00	0.0%	0.00	45.00
06.1.1	Payload			45.00	0.0%	0.00	45.00
06.1.2	Additional Instruments			0.00	0	0.00	0.00
06.2	Launch Vehicle			1967.47	3.9%	68.74	2036.20
06.2.1	Attitude Determination and Control			9.40	15.3%	1.44	10.84
06.2.1.a	Guidance, Navigation, & Control			9.40	15.3%	1.44	10.84
06.2.2	Command and Data Handling			10.80	28.6%	3.09	13.89
06.2.2.a	Command & Data Handling			9.05	28.3%	2.57	11.62
06.2.2.b	Instrumentation & Wiring			1.75	30.0%	0.53	2.28
06.2.3	Communications and Tracking			4.61	19.4%	0.90	5.51
06.2.3.a	S Band			4.61	19.4%	0.90	5.51
06.2.4	Electrical Power Subsystem			9.83	41.9%	4.12	13.95
06.2.4.a	Energy Storage			2.43	30.0%	0.73	3.16
06.2.4.b	Power Management & Distribution			1.56	30.0%	0.47	2.03
06.2.4.c	Power Cable and Harness			5.84	50.0%	2.92	8.76
06.2.4.d	Misc#1			0.00	0	0.00	0.00
06.2.4.e	Misc#2			0.00	0	0.00	0.00
06.2.5	Thermal Control			100.34	15.0%	15.05	115.39
06.2.5.a	Active Thermal Control			3.65	15.0%	0.55	4.20
06.2.5.b	Passive Thermal Control			13.37	15.0%	2.01	15.37
06.2.5.c	Heat Exchanger System			83.32	15.0%	12.50	95.82
06.2.6	Propulsion			235.86	11.3%	26.73	262.58
06.2.6.a	Propulsion Hardware			26.70	18.0%	4.81	31.51
06.2.6.b	Propellant Management			173.45	10.8%	18.90	192.35
06.2.6.c	Reaction Control System Hardware			10.00	15.0%	1.50	11.50
06.2.6.d	Solid Rocket for Orbit Insertion			25.70	9.9%	1.53	27.23
06.2.6.e	Misc			0.00	0	0.00	0.00
06.2.6.f	Misc#3			0.00	0	0.00	0.00
06.2.6.g	Misc#4			0.00	0	0.00	0.00
06.2.7	Propellant			1499.87	0.0%	0.00	1499.87
06.2.7.a	RCS Propellant			67.68	0.0%	0.00	67.68
06.2.7.b	Propellant (Microwave)			1222.50	0.0%	0.00	1222.50
06.2.7.c	Solid Rocket for Orbit Insertion			209.69	0.0%	0.00	209.69
06.2.7.d	RCS Pressurant	0	0.00	0.00	0.0%	0.00	0.00
06.2.8	Structures and Mechanisms			96.76	18.0%	17.42	114.18
06.2.8.a	Structures			77.52	18.0%	13.95	91.48
06.2.8.b	Mechanisms			19.23	18.0%	3.46	22.70

34



Microwave Case 2 – Payload MEL



WBS	Description	QTY	Unit Mass	Basic Mass	Growth	Growth	Total Mass
Number	BEP4 - Jan 2011 - Microwave Case 2		(kg)	(kg)	(%)	(kg)	(kg)
06	Microwave Launcher Case 2			2012.47	3.4%	68.74	2081.20
06.1	Payload			45.00	0.0%	0.00	45.00
06.1.1	Payload			45.00	0.0%	0.00	45.00
06.1.1.a	Payload	1	45.00	45.00	0.0%	0.00	45.00
06.1.1.b	Misc#1	0	0.00	0.00	0.0%	0.00	0.00
06.1.1.c	Misc#2	0	0.00	0.00	0.0%	0.00	0.00
06.1.1.d	Misc#3	0	0.00	0.00	0.0%	0.00	0.00

35

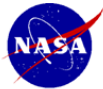


Microwave Case 2 – Attitude Determination and Control MEL



WBS	Description	QTY	Unit Mass	Basic Mass	Growth	Growth	Total Mass
Number	BEP4 - Jan 2011 - Microwave Case 2		(kg)	(kg)	(%)	(kg)	(kg)
06	Microwave Launcher Case 2			2012.47	3.4%	68.74	2081.20
06.1	Payload			45.00	0.0%	0.00	45.00
06.1.1	Payload			45.00	0.0%	0.00	45.00
06.1.2	Additional Instruments			0.00	0	0.00	0.00
06.2	Launch Vehicle			1967.47	3.5%	68.74	2036.20
06.2.1	Attitude Determination and Control			9.40	15.3%	1.44	10.84
06.2.1.a	Guidance, Navigation, & Control			9.40	15.3%	1.44	10.84
06.2.1.a.a	GPS	1	1.00	1.00	20.0%	0.20	1.20
06.2.1.a.b	IMU	1	2.95	2.95	5.0%	0.15	3.10
06.2.1.a.c	Beam Sensors	2	0.50	1.00	20.0%	0.20	1.20
06.2.1.a.d	Spin Table	1	4.45	4.45	20.0%	0.89	5.34

36



Microwave Case 2 – Command and Data Handling MEL



WBS	Description	QTY	Unit Mass	Basic Mass	Growth	Growth	Total Mass
Number	BEP4 - Jan 2011 - Microwave Case 2		(kg)	(kg)	(%)	(kg)	(kg)
06	Microwave Launcher Case 2			2012.47	3.4%	68.74	2081.20
06.1	Payload			45.00	0.0%	0.00	45.00
06.1.1	Payload			45.00	0.0%	0.00	45.00
06.1.2	Additional Instruments			0.00	0	0.00	0.00
06.2	Launch Vehicle			1967.47	3.5%	68.74	2036.20
06.2.2	Command and Data Handling			10.80	28.6%	3.09	13.89
06.2.2.a	Command & Data Handling			9.05	28.3%	2.57	11.62
06.2.2.a.a	FPGA-based IP e.g. PPC	1	0.60	0.60	30.0%	0.18	0.78
06.2.2.a.b	FPGA-based IP e.g. PPC	1	0.60	0.60	30.0%	0.18	0.78
06.2.2.a.c	Watchdog switcher	1	0.30	0.30	30.0%	0.09	0.39
06.2.2.a.d	Enclosure with power supply	1	1.20	1.20	30.0%	0.36	1.56
06.2.2.a.e	Command and Control Harness (data)	1	5.25	5.25	30.0%	1.58	6.83
06.2.2.a.f	Sensor & Discrete VO card (DCIU)	1	0.60	0.60	30.0%	0.18	0.78
06.2.2.a.g	EMI shielding	1	0.50	0.50	0.0%	0.00	0.50
06.2.2.a.h	Misc #2	0	0.00	0.00	0.0%	0.00	0.00
06.2.2.a.i	Misc #3	0	0.00	0.00	0.0%	0.00	0.00
06.2.2.a.j	Misc #4	0	0.00	0.00	0.0%	0.00	0.00
06.2.2.a.k	Misc #5	0	0.00	0.00	0.0%	0.00	0.00
06.2.2.a.l	Misc #6	0	0.00	0.00	0.0%	0.00	0.00
06.2.2.a.m	Misc #7	0	0.00	0.00	0.0%	0.00	0.00
06.2.2.b	Instrumentation & Wiring			1.75	30.0%	0.53	2.28
06.2.2.b.a	TVC Card	1	0.25	0.25	30.0%	0.08	0.33
06.2.2.b.b	Feed System Driver Card	1	0.25	0.25	30.0%	0.08	0.33
06.2.2.b.c	Ignition Card	0	0.00	0.00	30.0%	0.00	0.00
06.2.2.b.d	Separation System Card	1	0.25	0.25	30.0%	0.08	0.33
06.2.2.b.e	Thermocouple Ref. Card	1	1.00	1.00	30.0%	0.30	1.30

37



Microwave Case 2 – Communications MEL



WBS	Description	QTY	Unit Mass	Basic Mass	Growth	Growth	Total Mass
Number	BEP4 - Jan 2011 - Microwave Case 2		(kg)	(kg)	(%)	(kg)	(kg)
06	Microwave Launcher Case 2			2012.47	3.4%	68.74	2081.20
06.1	Payload			45.00	0.0%	0.00	45.00
06.1.1	Payload			45.00	0.0%	0.00	45.00
06.1.2	Additional Instruments			0.00	0	0.00	0.00
06.2	Launch Vehicle			1967.47	3.5%	68.74	2036.20
06.2.3	Communications and Tracking			4.61	19.4%	0.90	5.51
06.2.3.a	S Band			4.61	19.4%	0.90	5.51
06.2.3.a.a	Transceiver RS422	1	2.27	2.27	15.0%	0.34	2.61
06.2.3.a.b	Power Amp	0	0.00	0.00	30.0%	0.00	0.00
06.2.3.a.c	Directional coupler	0	0.00	0.00	0.0%	0.00	0.00
06.2.3.a.d	CTN Diplexer	1	0.60	0.60	14.0%	0.08	0.68
06.2.3.a.e	S-Band Surge Protector	0	0.00	0.00	0.0%	0.00	0.00
06.2.3.a.f	LNA	0	0.00	0.00	0.0%	0.00	0.00
06.2.3.a.g	Patch Antenna	3	0.08	0.24	30.0%	0.07	0.31
06.2.3.a.h	Transmission Line(s), Cables	1	1.00	1.00	30.0%	0.30	1.30
06.2.3.a.i	Diplexer	0	0.00	0.00	0.0%	0.00	0.00
06.2.3.a.j	Combiner/Switcher Box	1	0.50	0.50	20.0%	0.10	0.60

38



Microwave Case 2 – Electrical Power System MEL



WBS	Description	QTY	Unit Mass	Basic Mass	Growth	Growth	Total Mass
Number	BEP4 - Jan 2011 - Microwave Case 2		(kg)	(kg)	(%)	(kg)	(kg)
06	Microwave Launcher Case 2			2012.47	3.4%	68.74	2081.20
06.1	Payload			45.00	0.0%	0.00	45.00
06.1.1	Payload			45.00	0.0%	0.00	45.00
06.1.2	Additional Instruments			0.00	0	0.00	0.00
06.2	Launch Vehicle			1967.47	3.5%	68.74	2036.20
06.2.4	Electrical Power Subsystem			9.83	41.9%	4.12	13.95
06.2.4.a	Energy Storage			2.43	30.0%	0.73	3.16
06.2.4.a.a	Primary Battery	1	2.43	2.43	30.0%	0.73	3.16
06.2.4.a.b	Secondary Battery	0	0.00	0.00	0.0%	0.00	0.00
06.2.4.a.c	Thermal Battery	0	0.00	0.00	0.0%	0.00	0.00
06.2.4.a.d	Misc#1	0	0.00	0.00	0.0%	0.00	0.00
06.2.4.b	Power Management & Distribution			1.56	30.0%	0.47	2.03
06.2.4.b.a	Battery Regulator/Control	1	0.52	0.52	30.0%	0.16	0.68
06.2.4.b.b	Power distribution Unit	1	1.04	1.04	30.0%	0.31	1.35
06.2.4.b.c	Misc#1	0	0.00	0.00	0.0%	0.00	0.00
06.2.4.b.d	Misc#2	0	0.00	0.00	0.0%	0.00	0.00
06.2.4.b.e	Misc#3	0	0.00	0.00	0.0%	0.00	0.00
06.2.4.c	Power Cable and Harness			5.84	50.0%	2.92	8.76
06.2.4.c.a	Spacecraft Bus Harness	1	5.84	5.84	50.0%	2.92	8.76
06.2.4.c.b	Misc#1	0	0.00	0.00	50.0%	0.00	0.00

39

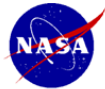


Microwave Case 2 – Thermal Control MEL



WBS Number	Description	QTY	Unit Mass (kg)	Basic Mass (kg)	Growth (%)	Growth (kg)	Total Mass (kg)
06	Microwave Launcher Case 2			2012.47	3.4%	68.74	2081.20
06.1	Payload			45.00	0.0%	0.00	45.00
06.1.1	Payload			45.00	0.0%	0.00	45.00
06.1.2	Additional Instruments			0.00	0	0.00	0.00
06.2	Launch Vehicle			1967.47	3.5%	68.74	2036.20
06.2.5	Thermal Control			100.34	15.0%	15.05	115.39
06.2.5.a	Active Thermal Control			3.65	15.0%	0.55	4.20
06.2.5.a.a	Data Acquisition	1	1.00	1.00	15.0%	0.15	1.15
06.2.5.a.b	Thermocouples	265	0.01	2.65	15.0%	0.40	3.05
06.2.5.a.c	Misc#1	0	0.00	0.00	15.0%	0.00	0.00
06.2.5.a.d	Misc#2	0	0.00	0.00	15.0%	0.00	0.00
06.2.5.a.e	Misc#3	0	0.00	0.00	15.0%	0.00	0.00
06.2.5.a.f	Misc#4	0	0.00	0.00	0.0%	0.00	0.00
06.2.5.b	Passive Thermal Control			13.37	15.0%	2.01	15.37
06.2.5.b.a	Cold Plate	4	0.14	0.55	15.0%	0.08	0.64
06.2.5.b.b	Shield	1	11.27	11.27	15.0%	1.69	12.96
06.2.5.b.c	Thermal Paint	1	1.55	1.55	15.0%	0.23	1.78
06.2.5.b.d	Misc#2	0	0.00	0.00	15.0%	0.00	0.00
06.2.5.b.e	Misc#3	0	0.00	0.00	15.0%	0.00	0.00
06.2.5.c	Heat Exchanger System			83.32	15.0%	12.50	95.82
06.2.5.c.a	Heat Exchanger	1	40.26	40.26	15.0%	6.04	46.30
06.2.5.c.b	Manifolds	1	2.81	2.81	15.0%	0.42	3.23
06.2.5.c.c	Heat Exchanger Insulation	1	0.00	0.00	15.0%	0.00	0.00
06.2.5.c.d	Secondary Heat Exchanger	1	40.26	40.26	15.0%	6.04	46.30

40



Microwave Case 2 – Propulsion Hardware MEL



WBS Number	Description	QTY	Unit Mass (kg)	Basic Mass (kg)	Growth (%)	Growth (kg)	Total Mass (kg)
06	Microwave Launcher Case 2			2012.47	3.4%	68.74	2081.20
06.1	Payload			45.00	0.0%	0.00	45.00
06.1.1	Payload			45.00	0.0%	0.00	45.00
06.1.2	Additional Instruments			0.00	0	0.00	0.00
06.2	Launch Vehicle			1967.47	3.5%	68.74	2036.20
06.2.6	Propulsion			235.86	11.3%	26.73	262.58
06.2.6.a	Propulsion Hardware			26.70	18.0%	4.81	31.51
06.2.6.a.a	Primary Thrusters	1	26.70	26.70	18.0%	4.81	31.51
06.2.6.a.b	MISC	0	0.00	0.00	0.0%	0.00	0.00
06.2.6.a.c	Propulsion Structure			0.00	0	0.00	0.00
06.2.6.a.d	Misc#1			0.00	0	0.00	0.00
06.2.6.b	Propellant Management			173.45	10.8%	18.90	192.35
06.2.6.b.a	Primary Fuel Tank(s)	1	103.71	103.71	10.0%	10.37	114.08
06.2.6.b.b	Misc	0	0.00	0.00	0.0%	0.00	0.00
06.2.6.b.c	Primary H2 Feed System	1	38.70	38.70	10.0%	3.87	42.57
06.2.6.b.d	Misc	0	0.00	0.00	0.0%	0.00	0.00
06.2.6.b.e	TPA	1	31.04	31.04	15.0%	4.66	35.70
06.2.6.b.f	Secondary HX TPA	0	0.00	0.00	0.0%	0.00	0.00
06.2.6.b.g	Misc#1	0	0.00	0.00	0.0%	0.00	0.00
06.2.6.b.h	Misc#2	0	0.00	0.00	0.0%	0.00	0.00
06.2.6.b.i	Misc#3	0	0.00	0.00	0.0%	0.00	0.00
06.2.6.b.j	Misc#4	0	0.00	0.00	0.0%	0.00	0.00
06.2.6.c	Reaction Control System Hardware			10.00	15.0%	1.50	11.50
06.2.6.c.a	RCS Tank Subassembly	0	0.00	0.00	0.0%	0.00	0.00
06.2.6.c.b	RCS Propellant Management Subassembly	0	0.00	0.00	0.0%	0.00	0.00
06.2.6.c.c	RCS Thruster Subassembly	2	5.00	10.00	15.0%	1.50	11.50
06.2.6.c.d	Misc#1	0	0.00	0.00	0.0%	0.00	0.00
06.2.6.c.e	Misc#2	0	0.00	0.00	0.0%	0.00	0.00
06.2.6.d	Solid Rocket for Orbit Insertion			25.70	5.9%	1.53	27.23
06.2.6.d.a	Solid Rocket			25.70	5.9%	1.53	27.23
06.2.6.d.a.a	Solid Casing for Payload Insertion	1	23.30	23.30	5.0%	1.16	24.46
06.2.6.d.a.b	Thrust Structure/Adapter	1	2.41	2.41	15.0%	0.36	2.77
06.2.6.d.a.c	Misc#2	0	0.00	0.00	0.0%	0.00	0.00

41



Microwave Case 2 – Propellant MEL



WBS	Description	QTY	Unit Mass	Basic Mass	Growth	Growth	Total Mass
Number	BEP4 - Jan 2011 - Microwave Case 2		(kg)	(kg)	(%)	(kg)	(kg)
06	Microwave Launcher Case 2			2012.47	3.4%	68.74	2081.20
06.1	Payload			45.00	0.0%	0.00	45.00
06.1.1	Payload			45.00	0.0%	0.00	45.00
06.1.2	Additional Instruments			0.00	0	0.00	0.00
06.2	Launch Vehicle			1967.47	3.6%	68.74	2036.20
06.2.7	Propellant			1499.87	0.0%	0.00	1499.87
06.2.7.a	RCS Propellant			67.68	0.0%	0.00	67.68
06.2.7.a.a	RCS Propellant Used	1	60.92	60.92	0.0%	0.00	60.92
06.2.7.a.b	RCS Propellant Residuals (Unused)	1	0.67	0.67	0.0%	0.00	0.67
06.2.7.a.c	RCS Propellant Performance Margin (Unused)	1	6.09	6.09	0.0%	0.00	6.09
06.2.7.b	Propellant (Microwave)			1222.50	0.0%	0.00	1222.50
06.2.7.b.a	Main Engine Propellant			1222.50	0.0%	0.00	1222.50
06.2.7.b.a.a	Hydrogen			1222.50	0.0%	0.00	1222.50
06.2.7.b.a.a.a	Fuel Usable	1	1210.39	1210.39	0.0%	0.00	1210.39
06.2.7.b.a.a.b	Fuel Margin	1	0.00	0.00	0.0%	0.00	0.00
06.2.7.b.a.a.c	Fuel Residuals (Unused)	1	12.10	12.10	0.0%	0.00	12.10
06.2.7.b.a.b	Misc Propellant			0.00	0	0.00	0.00
06.2.7.b.a.b.a	Misc Propellant Usable	0	0.00	0.00	0.0%	0.00	0.00
06.2.7.b.a.b.b	Misc Propellant Margin	0	0.00	0.00	0.0%	0.00	0.00
06.2.7.b.a.b.c	Misc Propellant Residuals (Unused)	0	0.02	0.00	0.0%	0.00	0.00
06.2.7.b.b	Pressurant	0	0.00	0.00	0.0%	0.00	0.00
06.2.7.c	Solid Rocket for Orbit Insertion			209.69	0.0%	0.00	209.69
06.2.7.c.a	Solid Fuel for Payload Insertion	1	209.69	209.69	0.0%	0.00	209.69
06.2.7.c.b	Misc#2	0	0.00	0.00	0.0%	0.00	0.00
06.2.7.d	RCS Pressurant	0	0.00	0.00	0.0%	0.00	0.00

42



Microwave Case 2 – Structures and Mechanisms MEL



WBS	Description	QTY	Unit Mass	Basic Mass	Growth	Growth	Total Mass
Number	BEP4 - Jan 2011 - Microwave Case 2		(kg)	(kg)	(%)	(kg)	(kg)
06	Microwave Launcher Case 2			2012.47	3.4%	68.74	2081.20
06.1	Payload			45.00	0.0%	0.00	45.00
06.1.1	Payload			45.00	0.0%	0.00	45.00
06.1.2	Additional Instruments			0.00	0	0.00	0.00
06.2	Launch Vehicle			1967.47	3.6%	68.74	2036.20
06.2.8	Structures and Mechanisms			96.76	18.0%	17.42	114.18
06.2.8.a	Structures			77.52	18.0%	13.95	91.48
06.2.8.a.a	Primary Structures			44.40	18.0%	7.89	52.29
06.2.8.a.a.a	Aft Structure	1	19.07	19.07	18.0%	3.43	22.50
06.2.8.a.a.b	Forward Structure	1	14.84	14.84	18.0%	2.67	17.51
06.2.8.a.a.c	Inter-Tank Structure	0	0.00	0.00	18.0%	0.00	0.00
06.2.8.a.a.d	Shroud (nose)	1	10.50	10.50	18.0%	1.89	12.39
06.2.8.a.a.e	Misc#1	0	0.00	0.00	18.0%	0.00	0.00
06.2.8.a.b	Secondary Structures			33.12	18.0%	3.96	37.09
06.2.8.a.b.a	Heat Exchanger Structure	1	0.20	0.20	18.0%	0.04	0.24
06.2.8.a.b.b	Tank Mounting Hold-Down Propellant	1	18.18	18.18	18.0%	3.27	21.45
06.2.8.a.b.c	Tank Mounting Hold-Dense Propellant	0	0.00	0.00	18.0%	0.00	0.00
06.2.8.a.b.d	Systems Tuning	1	1.54	1.54	18.0%	0.28	1.82
06.2.8.a.b.e	Ramp-Up (no Protection, etc.)	0	0.00	0.00	18.0%	0.00	0.00
06.2.8.a.b.f	Payload Adapter	1	13.20	13.20	18.0%	2.38	15.58
06.2.8.b	Mechanisms			19.23	18.0%	3.46	22.70
06.2.8.b.a	Shroud Separation Mechanism			1.84	18.0%	0.29	1.93
06.2.8.b.a.a	Shroud Separation Mechanism	6	0.27	1.64	18.0%	0.29	1.93
06.2.8.b.a.b	Misc#1	0	0.00	0.00	0.0%	0.00	0.00
06.2.8.b.b	Payload Deployment Mechanism			0.82	18.0%	0.15	0.97
06.2.8.b.b.a	Payload Deployment Mechanism	3	0.27	0.82	18.0%	0.15	0.97
06.2.8.b.b.b	Misc#1	0	0.00	0.00	0.0%	0.00	0.00
06.2.8.b.b.c	Misc#2	0	0.00	0.00	0.0%	0.00	0.00
06.2.8.b.c	Communications Mechanisms			0.00	0	0.00	0.00
06.2.8.b.c.a	Tank Separation Mechanisms			0.00	0	0.00	0.00
06.2.8.b.c.b	Misc#1			0.00	0	0.00	0.00
06.2.8.b.c.c	Misc#2			0.00	0	0.00	0.00
06.2.8.b.d	Installations			16.78	18.0%	3.02	19.80
06.2.8.b.d.a	Science Payload Installation	1	1.80	1.80	18.0%	0.32	2.12
06.2.8.b.d.b	Cache Installation	1	0.43	0.43	18.0%	0.08	0.51
06.2.8.b.d.c	Communications and Tracking Installation	1	0.18	0.18	18.0%	0.03	0.21
06.2.8.b.d.d	GN&C Installation	1	0.38	0.38	18.0%	0.07	0.44
06.2.8.b.d.e	Electrical Power Installation	1	0.30	0.30	18.0%	0.05	0.35
06.2.8.b.d.f	Thermal Control Installation	1	4.01	4.01	18.0%	0.72	4.74
06.2.8.b.d.g	Propulsion Installation	1	9.67	9.67	18.0%	1.74	11.42
06.2.8.b.d.h	Misc#1	0	0.00	0.00	0.0%	0.00	0.00

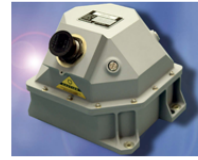
43



BEP DRM 1C – GNC



- **Requirements**
 - Maintain vehicle attitude so the heat exchanger is incident to the microwave beam
- **Design**
 - Honeywell HG9900 IMU
 - Mass = 2.95 kg
 - Honeywell GG1320AN Digital Laser Gyros 1-sigma parameters
 - Bias stability < 0.0035 deg/hr
 - Angle Random Walk < 0.002 deg/rt³hr
 - Scale Factor < 5.0 ppm,
 - Honeywell QA2000 Accelerometers 1-sigma parameters
 - Bias < 25 µg
 - Scale Factor < 100 ppm
 - Beam Sensors
 - Provides knowledge of the direction of the microwave beam
 - GPS Receivers
 - Aid in state estimation, including attitude determination
 - Spin Table
 - Provides gyroscopic stiffness to the 2nd stage for attitude control during the solid rocket burn



HG9900 IMU



HG9900 IMU

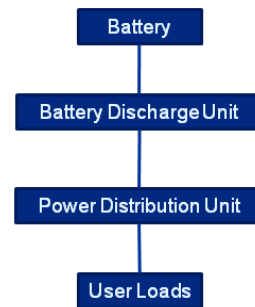
44



BEP DRM 1C Power System



- **Requirements:**
 - No redundancy, single string (i.e. no redundant battery cells, harnessing)
 - User power = 196 W (includes 30% growth)
 - Life = 4.2 minutes
 - User energy capacity required = 13.7 W-hr
- **Assumptions**
 - 28 Vdc
 - Primary Lithium battery based on present SAFT cells (LO 26 SHX, 4 Amp peak continuous current cells, 2.6 V nominal cell voltage, 238 W-hr/kg, 375 W-hr/L, 80% allowable depth of discharge); battery level = ~169 W-hr/kg
 - Battery discharge unit (BDU) efficiency loss = 5%
 - BDU specific power = 366 W/kg
 - Power distribution unit (PDU) loss = 5%
 - PDU specific power = 182 W/kg



45



BEP DRM 1C Power System



- **Design Description**

- **1 SOA primary Lithium battery**
 - Results in 11 cell strings and two strings (to meet current needs)
 - Battery oversized for energy... sized is based on current requirements/cell current limits
 - Size = 16 cm x 16 cm x 16 cm
 - Basic Mass = 2.4 kg
 - TRL 5
- **1 battery discharge unit**
 - Size = 9 cm x 9 cm x 9 cm
 - Basic Mass = 0.52 kg
 - TRL 6
- **1 power distribution unit**
 - Size = 12 cm x 12 cm x 12 cm
 - Basic Mass = 1.04 kg
 - TRL 6
- **1 power harness**
 - Basic Mass = 5.84 kg
 - TRL 6

46



BEP DRM 1C Power System Trades



- **Battery technology**

- For this study, both thermal and primary batteries were considered. Thermal batteries can tolerate high current draws, but have a lower specific energy (~75 W-hr/kg) than primary batteries and therefore are more massive. Additionally, thermal batteries generate significant amounts of heat that must be radiated away from the spacecraft, which adds complexity and mass to the thermal subsystem. Therefore, primary batteries were chosen for this mission application. Secondary lithium batteries have higher current capabilities than primary lithium batteries and could potentially result in some mass savings (requires more mass for a battery charge unit though).

47



BEP DRM 1C Power System Risks



- **0 fault tolerance for all power system components – failure in one of the components will likely result in loss of mission. Loss of a battery string will likely reduce the available current. It is possible that a high short term current draw of the remaining string can still provide the required power (pulses up to 15 A can be handled, however, the duration is critical). The cell vendor can resolve the durations and possible enhancement of the cell current capabilities.**

45



BEP4 Avionics Overview



- **Design Requirements**
 - Avionics for systems command, control, and health management separate for Transport and P/P
 - Single fault tolerant processor architecture
 - Low mass optimization required for BEP
 - Operational power modes vary according requirements, BEP quiescent until needed
- **Assumptions**
 - 50 kRad avionics for stable operation for duration of mission
 - Cabling mass estimated with Monte Carlo simulation
- **Design Description**
 - Transport enclosure assumes 6U-160 cPCI form factor cards
 - Rad-tolerant FPGAs packaged with IP for processor capability,
 - **Fail over to backup processor if one faults out or has SEU (reboot attempted)**
 - **Embedded software kernels without major O/S overhead**
 - Memory 5 GB with EDAC
 - Power Supply using DC-DC converters, filter, and EMI shielding accept wide variations in supply voltage
 - Discretes and Power switching card for general vehicle functions
 - Sensor I/O card
 - RS422 interfaces between stages - 2 Mbps RS422 Manchester coded
 - Housekeeping data and H&S data to ground via comm at 4.8 kbps

46

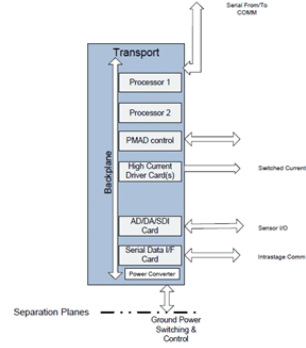


BEP4 Avionics Functionality

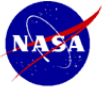


- **General Avionics Processors**
 - Power PC Intellectual Property in FPGA
 - avionics cPCI card cage. BEP uses stacked custom cards in closed box design
 - BEP navigation – data from IMUs
 - Systems health and status reporting
 - Card Power managed for various power modes (power trimmed with specialized sentinel switching)
 - System management – includes control of valves, heaters, PMAD
 - System fault detection fail over must respond quickly during BEP Transport launch
 - Dual 2 Mbps bps serial interfaces between Transport and P/P stage, and comm channels at 4.8 kbps.
 - ROM SLOC estimate ~100k. Includes auto sequenced BEP launch.

- **Sensors/Drivers**
 - n valves, n pumps, n pressure & temperature



50



Propulsion

51



Requirements and Assumptions



- **Requirements**
 - Zero Fault Tolerant System
 - Microwave Energy Beamed from Ground Station(s) Provides Thermal Energy for Propulsion System
 - Monopropellant Main Propulsion System
 - No Chemical Combustion for Primary Propulsion
- **Assumptions**
 - Expander Cycle Based System
 - Microwave System Can Continuously Track and Beam Energy to Vehicle Heat Exchanger
 - Adequate Thermal Performance from Primary Heat Exchanger
 - RCS to Provide Attitude Control

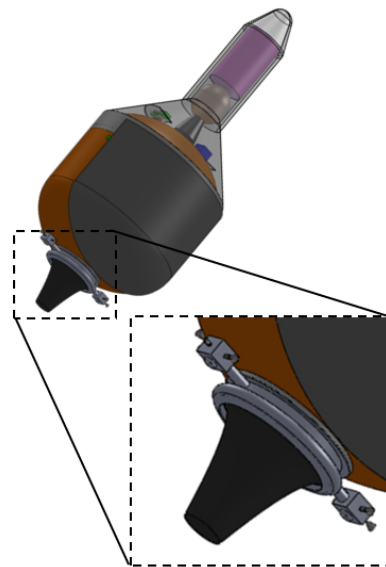
2



Propulsion Overview



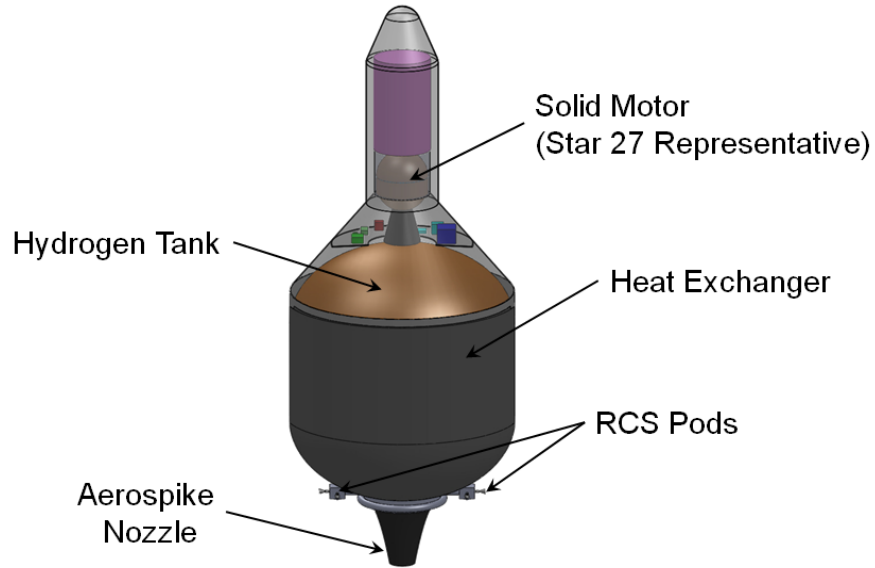
- **Single Main Heat Exchanger**
- **Single Aerospike Nozzle**
- **RCS Mounted on Engine Structure**
- **Autogenous Tank Pressurization**
- **Zero Fault Tolerant Feed System**
- **Two Stage Centrifugal Pump w/ Turbine**
- **Extensive use of Carbon-Carbon Composite Components**
- **Turbo-Pump Assembly Located Inside Aerospike Cavity**



3



Propulsion Overview, Cont.



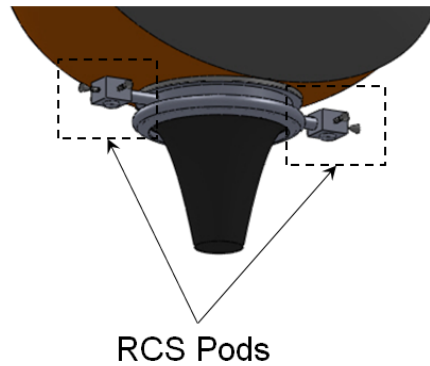
54



RCS



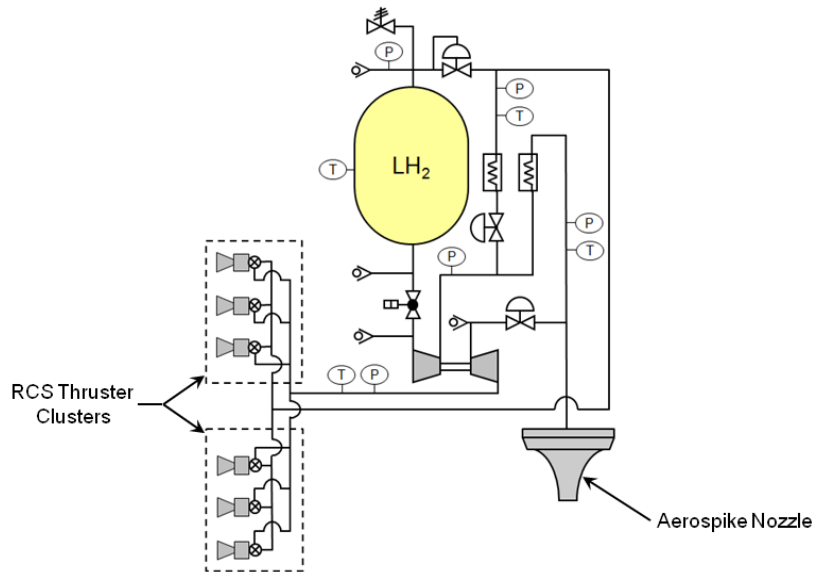
- **RCS Propellant Derived from Turbine Exhaust Flow**
 - Continuous Flow Through RCS System
 - Differential Throttling Produces Resultant Force
- **Some Cooling Flow Required for Valve Actuators**
- **6 Thrusters (2 Pods of 3)**
- **Nominal 100lbf Thrust**



55



Preliminary P&ID



Risks



- Maintenance of Appropriate Beam Angle Relative to Vehicle Heat Exchanger
- Excessive Heating of Heat Exchanger Walls
- Potential Material Temperature Limitation Issues
- Hot Hydrogen Rapidly Corroding the Carbon-Carbon Components
- Inadequate RCS Control Authority with Turbine Exhaust Flow
- Cooling of RCS Actuators
- Tank Over-Pressurization Due to Excessive Heat Leak
- Adverse Thermal Interactions with Aft Vehicle Structure and Hydrogen Tank

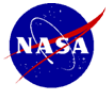


Future Trades



- **Different Dense Propellants**
 - Ammonia
 - Methane
 - Liquid Nitrogen
- **Traditional RCS System (Hydrazine, etc.)**
- **Utilizing Tank Heat Leak to Pressurize Tank**
- **Differential Propellant Injection on Aerospike Nozzle to Reduce RCS Requirement**

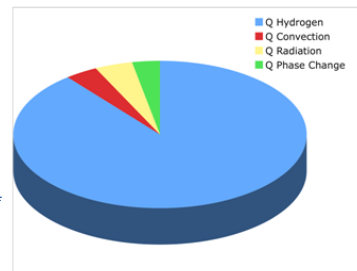
58



Thermal Subsystem - Description



- **Thermal Components and Assumptions**
 - Main heat exchanger is used to absorb microwave radiation and heat hydrogen gas. Heat exchanger is constructed of tubes. The main heat transfer is conduction through the walls to turbulent flow of the hydrogen gas.
 - Secondary heat exchanger is used as a thermal barrier between the main heat exchanger and the vehicle. Heat exchanger is constructed of tubes. Hydrogen gas is bled off of the main stream to maintain the wall temperature at 300 K.
 - Desired exit temperature of the hydrogen gas is at 2200 K
 - Maximum wall temperature of the heat exchanger is 3000 K
 - Outer Heat exchanger is constructed of carbon-carbon composite with a silicon carbide outer layer.
 - Inner heat exchanger is made of carbon with a aluminum reflective surface.
 - Emissivity of the outer heat exchanger is 0.3
 - Emissivity of the inner heat exchanger is 0.07
 - Operating scheme: liquid hydrogen is pumped to the heat exchanger, vaporized and heated to the desired temperature. It then flows to the engine and is expanded to produce thrust. Some initial flow is bled off to the inner heat exchanger to keep the spacecraft wall cool and to be utilized in the reaction control system.
 - A thin layer, 1 cm, of foam insulation is used on the tank wall to reduce boil off of the liquid hydrogen.
 - Reflector shield for other exposed portions of stage needs to be 99.9999 reflective in microwave frequency to avoid excessive heating
- **Environmental models**
 - An energy balance is performed between the incoming microwave radiation and the heat losses of the system to determine the heat exchanger size and hydrogen temperature.
 - Heat losses from the system include: Heat transfer to the hydrogen gas, convection to the atmosphere, radiation to the atmosphere and inner heat exchanger, vaporization of the liquid hydrogen.
- **Options to Reduce mass and recommendations:**
 - A more detailed analysis of the heat exchanger including gradients along its surface should be performed.
 - A more detailed analysis of the heat loss mechanisms should be performed to provide a high fidelity estimate of the heat exchanger performance.
 - The structural integrity of the heat exchanger should be evaluated.

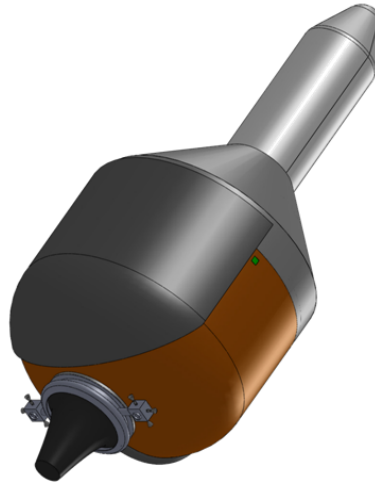




Structure Subsystem - Description



- **Structures and Mechanisms Design Requirements**
 - Contain necessary hardware for research instrumentation, avionics, communications, propulsion and power
 - Withstand applied mechanical and thermal loads from launching and operation
 - Provide minimum deflections, sufficient stiffness, and vibration damping
 - Minimize weight



DRM 1C Launch Vehicle

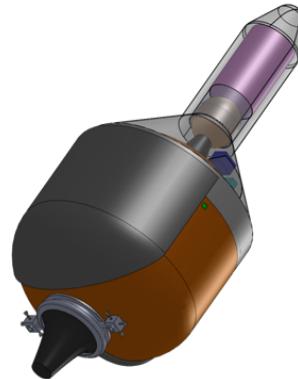
60



Structure Subsystem - Description



- **Structures assumptions**
 - Provides main structures backbone for BEP vehicle
 - Materials: aluminum, graphite/epoxy, c/c
 - Shells with flanges
 - Bonded, welded and threaded fastener assembly
- **The structures subsystem**
 - Shells or thrust tube bearing all operational loads
 - Science probes, payload to support
 - Load bearing, structurally integrated tank
- **Main structure material and design choice:**
 - Graphite/epoxy shells with aluminum flanges
 - TRL6
- **Primary Structure mass:**
 - Graphite/epoxy shells with aluminum flanges
- **Secondary Structure Mass:**
 - Aluminum, graphite/epoxy, c/c construction
 - Installations
- **Separation mechanisms**
 - Shroud separation, pyrotechnic fasteners & springs
 - Payload deployment, pyrotechnic fasteners & springs
 - Upper stage, pyrotechnic fasteners & springs



DRM 1C Launch Vehicle

61



Structure Subsystem - Description



- **Design Highlights**
 - g/epoxy, c/c, Aluminum components
 - Flanges for joining sections and mounting internal hardware of aluminum
 - c/c w/environmental barrier coating (EBC) support for heat exchanger
- **Analytical Methods**
 - Analytical methods with spreadsheet for stress analysis
 - Stresses
 - Shroud – aerodynamic load 6 kN
 - 2 kPa
 - Propellant tank check for buckling (Roark's Formulas for Stress & Strain)
 - 192 MPa w/0.8 mm wall thickness providing positive margin with 59 MPa max. operating load
 - Payload adapter
 - 10 MPa $\ll \sigma_u$ including 1.5 s.f.
 - Mass for installation
 - 4% of mass of installed hardware
 - Science Payload
 - C&DH
 - Communications & Tracking
 - GN&C
 - Electrical Power
 - Thermal Control
 - Propulsion
- **Trades considered in analysis**
 - c/epoxy replaced aluminum for necessary weight reduction
 - c/c implemented due to high temperature of supported hardware
- **Options to Reduce mass and recommendations:**
 - Detailed stress analysis using FEA

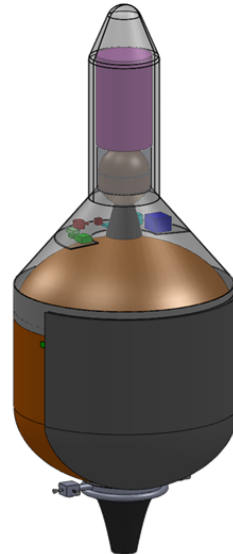
62



Mechanisms Subsystem - Description



- **Mechanisms assumptions**
 - Provide separation functions for shroud, payload, and upper stage
- **Mechanisms Mass:**
 - 1.82 kg mass for shroud
 - 2.36 kg for payload
 - 1.82 kg total for upper stage
- **Trades considered in analysis**
 - None at this time



63



Cost Assumptions



- **DRAFT Cost Estimate based on COMPASS design**
- **All costs are in FY11\$M**
- **Estimates represent prime contractor cost before fee**
- **This estimate assumes the following:**
 - Proto-flight development approach
 - No ground spares are included
 - Model assumes TRL Level 6
 - This estimate does not include any cost for technology development
 - Represents the mean estimate based on cost-risk simulation results
 - Parametric estimate based on mostly mass-based CERs from historical cost data
 - Launch vehicle systems integration wraps
 - Software not included
- **Does not include:**
 - Any insight/oversight costs (by a NASA lead center)
 - Reserves (can be as high as 40-50%)
 - Ground System Cost (ie. Microwave Station, Launch Pad, Booster Station, etc...)
 - Launch Services Costs (ie. Special launch approval process)
 - Technology costs for components lower than TRL-6

64



Microwave Launcher Preliminary Cost ROM

(Represents estimated Prime Contractor cost)



WBS	Description	DDT&E Total BY \$M	Flight HW BY \$M	DD&FH Total BY \$M
06.1	Payload	0.0	0.0	0.0
06.2.1	Attitude Determination and Control	6.4	4.8	11.2
06.2.2	Command and Data Handling	4.7	2.7	7.4
06.2.3	Communications and Tracking	1.8	1.3	3.0
06.2.4	Electrical Power Subsystem	1.7	1.2	2.9
06.2.5	Thermal Control	12.6	2.3	14.8
06.2.6	Propulsion	14.6	2.5	17.1
06.2.7	Propellant	0.0	0.0	0.0
06.2.8	Structures and Mechanisms	11.0	5.6	16.6
	Subtotal	52.7	20.3	73.0
	Systems Integration	57.0	8.1	65.2
	Spacecraft Total	109.7	28.4	138.1

All Costs in FY11\$M

65

3.1.8 Millimeter-Wave Thermal Consultant Report—Design Reference Mission 1–C

Over the past 60 years, the time-average power output of high-power microwave sources in the key millimeter-wavelength range has increased by over 6 orders of magnitude, for the first time putting Earth-to-orbit launch within economic reach using gyrotron technology. Today, a 1-MW gyrotron oscillator can be purchased for about \$2M. By combining the output of many such oscillators, the power and spot size needed to propel a vehicle to orbit are possible.

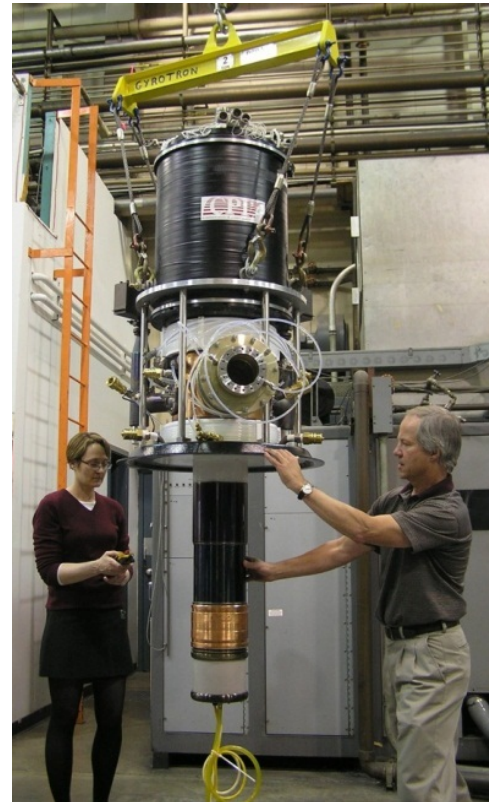
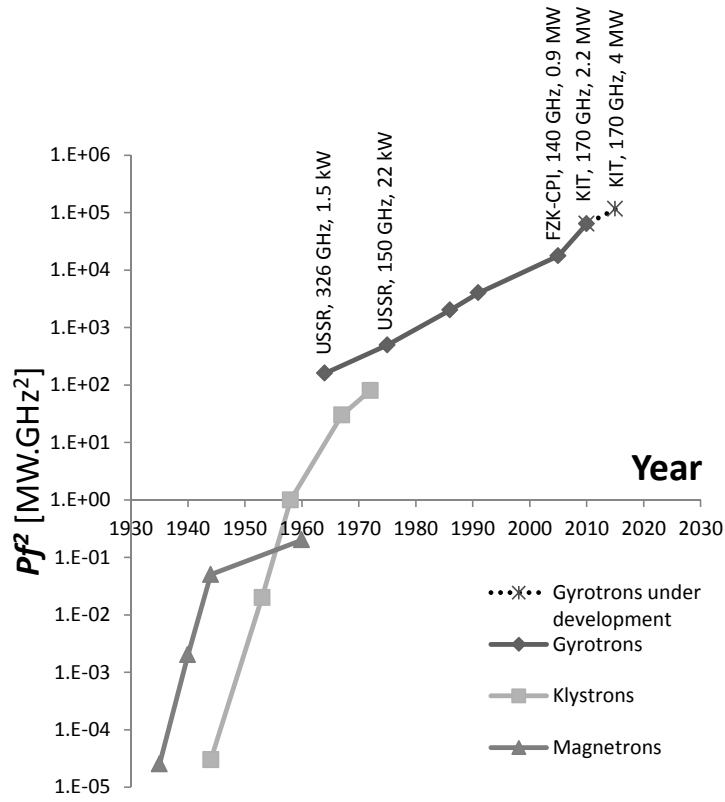


Figure 3.105.—Left: The advent of gyrotron technology has raised the power output of sources in the key millimeter-wavelength range by 3 orders of magnitude since 1970. Right: VGB–8125 gyrotron manufactured in Palo Alto by CPI Inc. This tube produces a 2.5-MW beam at 95 GHz. (Image courtesy of Communications & Power Industries (CPI); used with permission).

Central to the microwave thermal rocket is a microwave-absorbent heat exchanger (HX) covering the underside of the vehicle. The refractory HX bypasses the specific enthalpy limits of conventional combustion, imparting 30- to 40-MJ per kilogram of H₂ propellant as opposed to 16 MJ/kg for conventional hydrogen peroxide (H₂/O₂) combustion. This higher specific energy will halve the propellant flow rate needed to produce a given thrust and reduce the total propellant needed to put a given dry mass into orbit by a factor of 3 (because there is a compound effect as described by the rocket equation). Separate liquid hydrogen (LH₂) and liquid oxygen (LOX) tanks will be replaced by a single LH₂ tank—likewise for the turbopumps and adjoining pipes. There will be no intertank structure, injector, or combustion chamber.

The downside to an LH₂ thermal rocket is the relatively low density of hydrogen, which will make the tank and turbopump larger and heavier than for dense propellants. The larger tank will add to the drag losses of the vehicle, requiring extra propellant to compensate. From a systems point of view, the key question is whether or not the benefits of higher specific energy and fewer components will be negated by the extra weight indirectly incurred by the low density of LH₂.

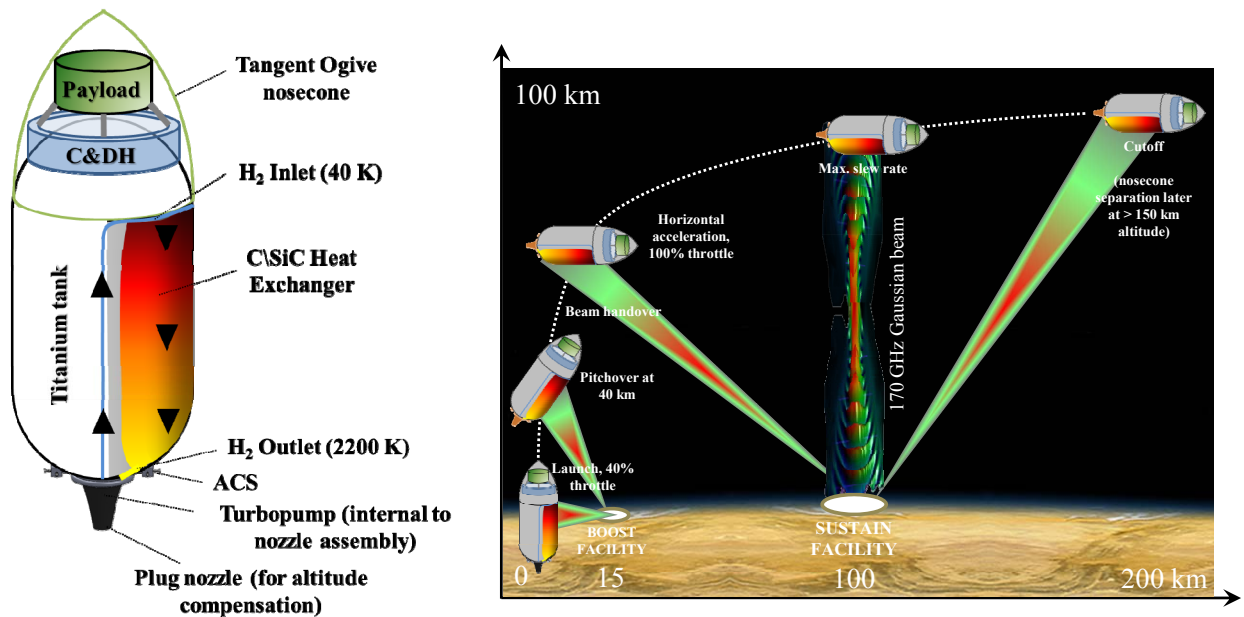


Figure 3.106—Microwave thermal launch system and ascent trajectory arising from DRM-1C.

3.1.8.1 Description of Vehicle

For the 2-week Design Reference Mission 1-C (DRM-1C) study, a single-stage-to-orbit (SSTO) baseline design point was provided by Dr. Parkin, along with detail on the technologies by which various aspects of the design could be achieved. Independently, the Collaborative Modeling for Parametric Assessment of Space Systems (COMPASS) team chose how to vary that design and made alternative technical choices to close the mass budget. In particular, COMPASS required that the mass budget close with at least a mass growth allowance (MGA) and dry mass margin (DMM) totaling about 30% of the rocket dry mass. As a result, they were inevitably driven to a larger scale SSTO than the baseline and also tried a two-stage-to-orbit (TSTO) configuration. Mass budgets converged in both of those cases. In the 2 weeks available, they did not try a solid rocket first-stage TSTO or a LOX/LH₂ SSTO comparison design computed under the same methodology.

TABLE 3.29.—THE THREE DESIGN POINTS ASSOCIATED WITH DRM-1C

		Parkin baseline (expendable SSTO)	COMPASS SSTO design point	COMPASS TSTO design point
Stage 1	Type	LH ₂ thermal	LH ₂ thermal	LH ₂ thermal
	Initial mass (kg)	2,500	4,734	2,156
	Final mass (kg)	580	1,084	954
	Payload (kg)	45	45	240
	ΔV (m/s)	10,378	10,471	6,050
	Final orbit (km)	(optimal perigee) by 400	100 by 400	100 by (optimal apogee)
	HX Power (MW)	450	850	300
Stage 2	Type	-----	-----	Star 27
	Initial mass (kg)	-----	-----	240
	Final mass (kg)	-----	-----	60
	Payload (kg)	-----	-----	40
	ΔV (m/s)	-----	-----	3,986
	Final orbit (km)	-----	-----	100 by 400 km

3.1.8.2 Baseline Components and Technologies

In flowpath order,

Tank and structures.—The tank will be a 3-m-diameter titanium tank of traditional construction. The length will be 6 m for the baseline and will be varied to accommodate changes in wet mass. The structural factor of safety is 1.25, and the baseline tank pressure is 3 bars. The structural approach is to transmit loads into this pressure-stabilized tank with the minimum of intervening structure, analogous to attaching weights to a balloon.

Turbopump.—A single-stage LH₂ turbopump with 117-bars discharge pressure will be used.

Low-flux HX.—This will be a low-temperature low-flux backing layer that “mops up” stray heat that cannot be reflected. In essence, it will shield the LH₂ tank from heat loads emanating from the primary HX and stray beam flux. The backing layer will be maintained at an average temperature of 300 K via cryogenic hydrogen (H₂) microtubes running in parallel about a centimeter apart. The distance between the microtubes will be maximized by maximizing the reflectance and thermal conductivity of the backing layer. Hence, it was originally envisaged to be aluminum foil. The effective thermal conductivity could be increased by sticking a layer of commercially available pyrolytic graphite sheeting to the underside. Silver foil could be substituted for aluminum to increase the reflectance in areas of particularly high flux—for example, under the hot end of the HX.

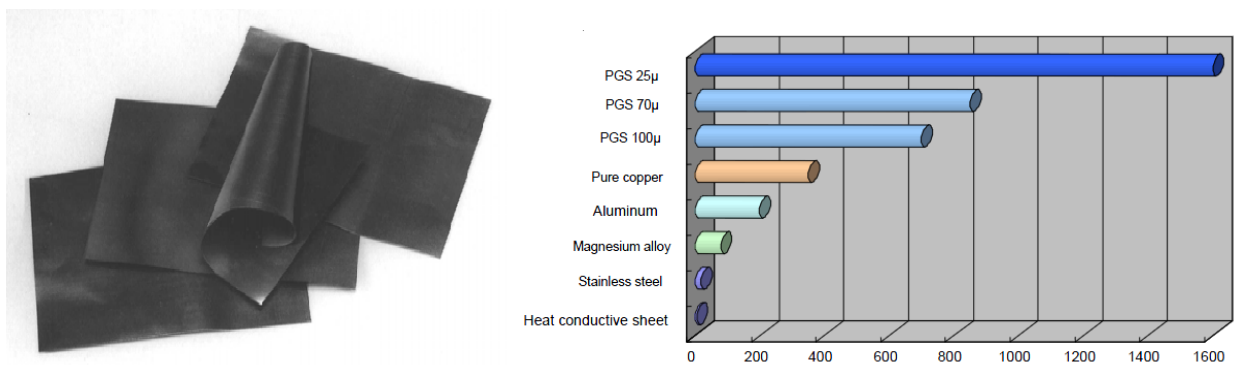


Figure 3.107.—Pyrolytic graphite was first produced in the late 1800s for lamp filaments. Left: Pyrolytic graphite sheeting. Right: Thermal conductivity in watts per meters kelvin of pyrolytic graphite sheet versus other metals (Panasonic PGS data sheet). Copyright ©2011 Panasonic Corporation of North America; used with permission.

High-flux HX.—The high-temperature high-flux HX will sit at the focus of the incoming millimeter-wave beam and will be conformal with the tank. For the baseline, it was based on a prototype woven composite developed by Teledyne and tested at the NASA Glenn Research Center (Ref. 1). As shown in the Figure 3.108, the prototype was woven from carbon fiber and infiltrated with silicon carbide. The wall thickness is 0.7 mm and channel diameter is about 1.2 cm. The inside channel roughness is about 40 μm .

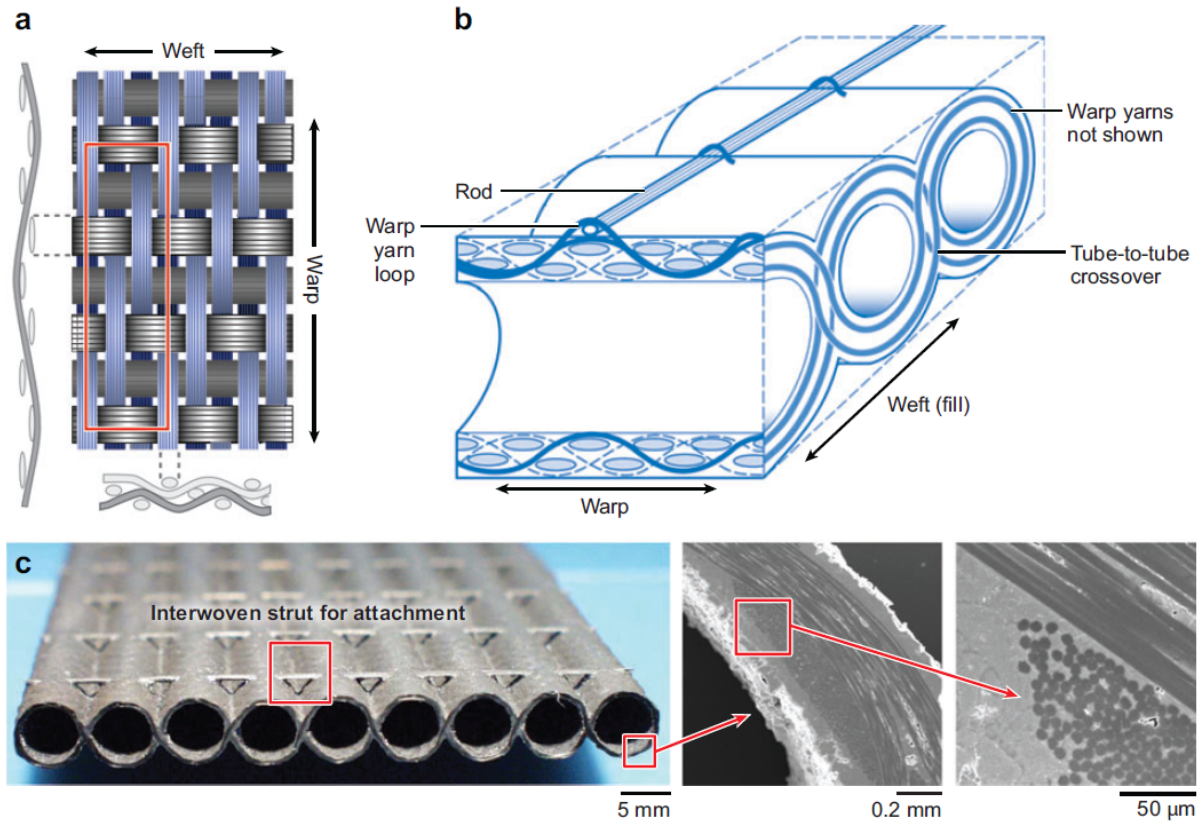


Figure 3.108.—(a) Plan and section views of an angle-interlock architecture. In the loom, the warp yarns are moved up and down selectively by harnesses, whereas the weft yarns are inserted between them by a flying shuttle or rapier. The section views show how the loom motions cause warp yarns to pass right through the thickness of the resulting fabric, tying together layers of weft yarns. Thus, the angle-interlock architecture suppresses delamination. (b) Schematic of an adaptation of an angle-interlock architecture to form an integral set of rocket nozzle tubes. The tube walls have an internal architecture similar to that shown in panel (a), with the tops and bottoms of the tubes joined at nexus regions formed in the loom. (c) Formed C-SiC composite structure, showing integrally woven struts for connecting to the rocket body and details of the high-density matrix formed within the tube walls (Ref. 1).



Figure 3.109.—Left: Conformal sections of woven H₂ HX for rocket nozzle cooling. Right: Linear section of woven HX undergoing testing at Glenn. The tests entailed connecting the composite tubes to metal manifolds for the supply and return of 300-to 400-bar H₂ coolant. One side of the panel was exposed to a hydrogen/oxygen combustion plume from a small rocket combustion chamber delivering a free-stream temperature approaching 3,300 K. Panels survived multiple cycles simulating operating conditions of a boost rocket engine (cold-wall heat flux of 20 MW m⁻²), with individual cycles as long as 8 min and cumulative times of 40 min.

Attitude Control System (ACS).—Attitude control will be achieved in a similar way to conventional “cold” gas attitude control system, except that the propellant gas will be either warm H₂ discharge from the turbopump or hot H₂ bled from the HX outlet. The ACS subsystem controls will roll such that the HX will not rotate out of view of the beam, and it will provide a pitch-over maneuver that will transition the rocket from vertical atmospheric ascent to horizontal acceleration once atmospheric drag becomes low enough to do so.

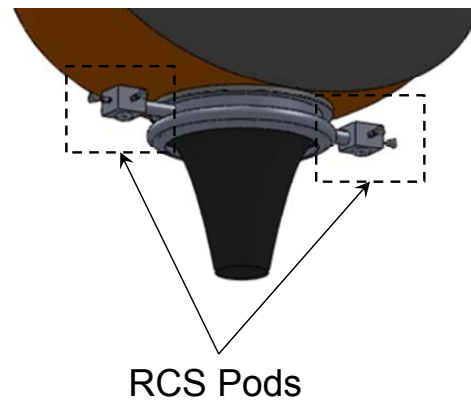


Figure 3.110.—Reaction control system (RCS) pods.

Nozzle.—The baseline nozzle was a conventional bell nozzle. Owing to the low specific impulse during atmospheric operation, it became clear that some form of altitude-compensating nozzle was needed for the SSTO concept. Options were dual-bell, expansion-deflection, and plug nozzle. Based on experimental data suggesting superior performance (Ref. 2) and the recent testing of graphite plug nozzles by Garvey (Figure 3.111), it was decided to use a carbon-composite plug nozzle. It should be noted that the stagnation temperature of the propellant as it travels through the nozzle is less than or equal to the peak achieved at the exit of the HX. Ergo, any uncooled materials scheme used for the HX should also be usable for the nozzle; no cooling will be necessary.

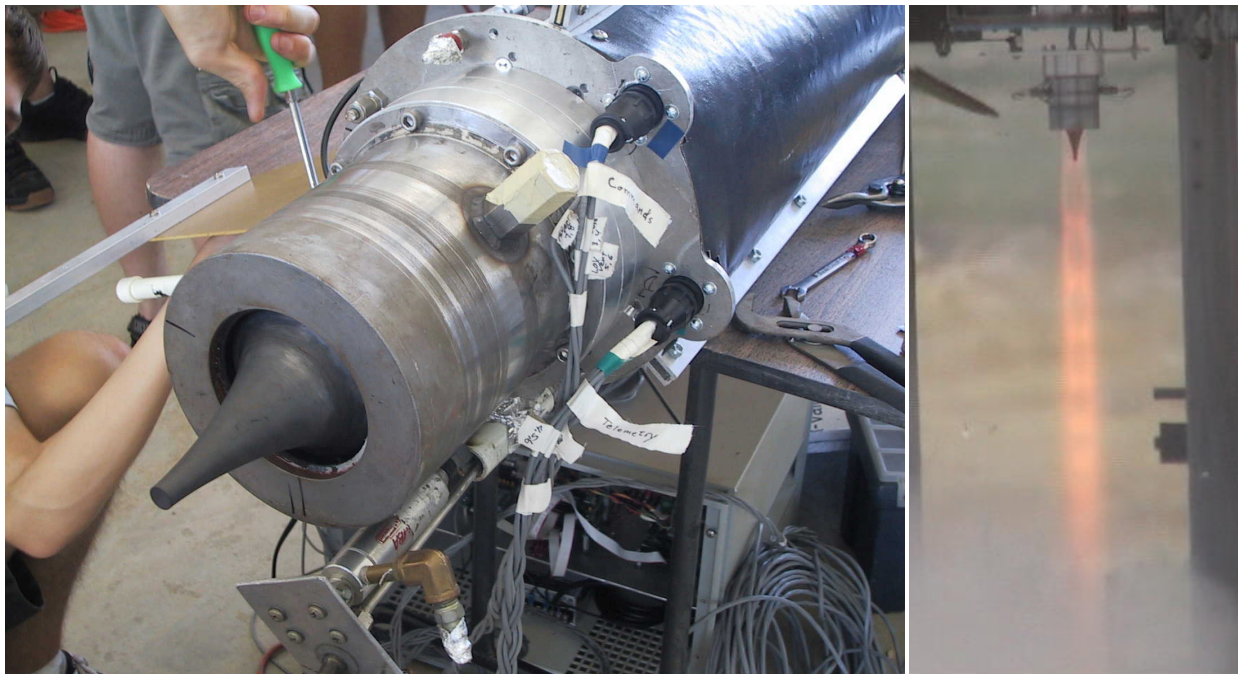


Figure 3.111.—Graphite annular aerospike/plug nozzle developed and tested by Calstate Long Beach/Garvey Spacecraft Corporation in 2003. Copyright Garvey Spacecraft Corporation; used with permission.

Command and data handling (C&DH).—For the baseline design, the command and data handling subsystem is envisaged to be located in the nosecone under the payload. Recent demonstrations of cell phone technology in the context of satellite and rocket applications have highlighted that the C&DH subsystem could potentially be built for very low mass, power, and cost. This is not to say that a cell phone would actually be used, more that the aerospace industry standard hardware is costly and cumbersome compared to what it could be. To facilitate fair comparisons, the baseline C&DH subsystem was sized according to COMPASS usual practices. Following techniques used for electromagnetic isolation in the Department of Defense (DOD) Transient Electromagnetic Pulse Emanations Standard (TEMPEST) shielded-enclosure handbook, the team used filters to remove any 170-GHz beam energy that might couple into antenna wires prior to entering the C&DH enclosure.

Nosecone and payload.—A tangent Ogive nosecone was baselined for two reasons. First, it has lower drag and better represents the aerodynamics of this design than the X-33 drag model originally used by Parkin. Second, the drag model was represented by simple closed-form equations (Ref. 3).

The payload will be enclosed by the nosecone, which will also act as a Faraday cage, protecting electronics from stray beam energy. Millimeter-wave radiation at 170 GHz is qualitatively similar to far infrared in that it is line-of-sight and does not wrap around obstacles in the way that radio waves do. The skin depth in aluminum is 0.2 μm , meaning that the millimeter waves are completely stopped by even ordinary kitchen foil. The only way for 170-GHz radiation to leak into the payload enclosure is via unshielded wires (as already discussed) and via edges/seams that do not make proper electrical contact with their opposing surface. If the amount of leakage via seams proved to be a problem, the seams could be electrically sealed using conductive gaskets or paste.

3.1.8.3 Figures of Merit and Margins

The figures of merit for DRM-1C are closely related to the choice of design margins. Keeping design margins builds underperformance into the rocket design in order to guarantee a given payload with a certain statistical confidence. This confidence can be traded with performance and ultimately reflects the risk tolerance of the customer. The COMPASS team's ~30% margin on dry mass was based on the AIAA S-120-2006 industry standard for an authorization to proceed (ATP) situation and was supported by a subsequent study examining historical mass growth (Ref. 4). Under these guidelines, 30% and above represents a green light, 19% to 30% a yellow light, and 0% to 19% a red light.

The decision to proceed on a conventional multistage rocket after a 2- to 5-month conceptual design study is not the same as the decision to proceed on an SSTO thermal rocket after a 2-week feasibility assessment. Despite this, the microwave thermal rocket will perform well when held to a conventional standard.

TABLE 3.30.—FIGURES OF MERIT FOR THE MICROWAVE THERMAL ROCKET VERSUS OTHER CONCEPTS FOR COMPARISON
[RASCAL, RP1, rocket propellant 1.]

	Parkin baseline	COMPASS SSTO	COMPASS TSTO	RASCAL baseline	LOX/LH ₂ SSTO	LOX/RP1 SSTO	Pegasus	Scout G
Stages	1	1	2	3	1	1	4	4
Type (E = expendable, R = reusable)	E	E	E	R 1 st	R	R	E	E
Growth allowance on dry mass excluding payload (%)	--	31.5 15 0	33.4 15	15	30 15 0	30 15 0	--	--
Wet mass (tons)	2.5	4.7	2.2	7.2 ^a	1,065	1,693	19 ^a	21
LEO payload (kg)	40	40 189 338	40 63	68	-18,658 ^b 680 ^b 21,825 ^b	-635 ^b 9000 ^b 18,644 ^b	375	210
Payload fraction (%)	1.8	1.0 4.0 7.1	2.0 2.9	0.9 ^a	0.6 ^b 2.3 ^b	0.5 ^b 1.1 ^b	2 ^a	1
Structural mass/payload	13	23 4.7 2.2	18.4 8.79	15.1 ^a	15.1 ^b 4.6 ^b	7.1 ^b 3.5 ^b	6.4 ^a	12.7

^aNot counting airbreathing first stage.

^bPayload mass adjusted from original to provide given margin.

Numbers generated by the COMPASS team are shown in **green**. The COMPASS SSTO point design is similar to the RASCAL point design (not counting the airbreathing first stage) in wet mass (4.7 vs. 7.2 tons), payload (40 vs. 68 kg), payload fraction (1.0% vs. 0.9%), and the cost-related metric of structure to payload mass ratio (23 vs. 15.1). It has the clear advantage of one stage versus three for RASCAL. A single stage simplifies range constraints and eliminates the cost, complexity and risk associated with staging.

However, that comparison is not an equal one. Table 3.31 shows the margins typically used for concepts that the microwave thermal rocket would be compared to. For example, the RASCAL baseline point design carries a 15% dry mass growth allowance, whereas the COMPASS point designs are encumbered by more than a 30% dry mass growth allowance. For an “apples-to-apples” comparison, the values shown in **blue** were adjusted such that additional margin beyond 15% was counted as payload. With this adjustment, the COMPASS SSTO design clearly outperforms RASCAL, having quadruple the payload fraction (4.0% vs. 0.9%) and one-third the ratio of the structural mass to the payload (4.7 vs. 15.1).

TABLE 3.31.—MARGINS OF OTHER CONCEPT STUDIES

	Total margin used on dry mass excluding payload (%)	Study type	Reference
RASCAL bBaseline	15	Reusable 1 st stage	5
RASCAL GT	10		
NASA Access to Space Study (includes SSTO designs)	10	SSTO	6

Because the growth allowance methodology masks the underlying performance of the microwave thermal approach, the values shown in **red** are adjusted such that all margin *is* payload. This corresponds to a totally risk averse “build it and see if we get a positive payload mass” approach. Under this methodology, the payload fraction is predicted to be 7.1%. This is greater than the Saturn V U.S. record payload fraction of 4% to low Earth orbit (LEO), lighter than the Saturn V liftoff mass by 640 times, and does so using only a single stage instead of three.

3.1.8.4 Technology Margins

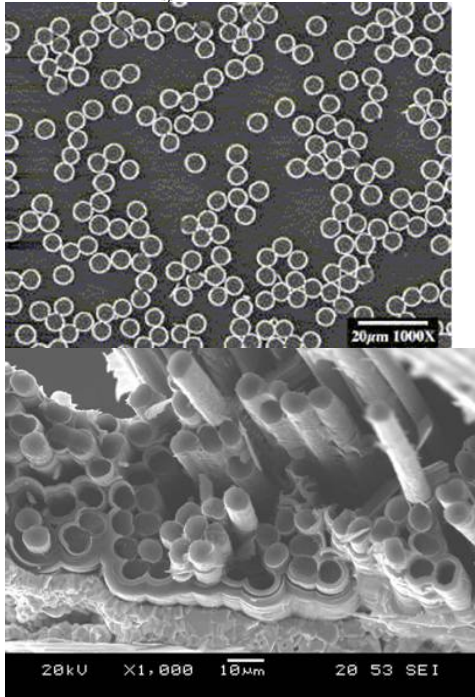
Even greater performance will be possible if the impact of various technological options not considered in the feasibility studies are taken into account. Technology margins are margins that would be realized as increases in mass margin if changes in the technologies used were made. The technology margins for the microwave thermal rocket are currently greater than for a conventional rocket at this stage of a decision to proceed for three reasons: First, microwave thermal rockets are an almost conceptually unexplored approach, and the technology options and performance limits are not well understood or quantified; second, the COMPASS conceptual design activity was a 2-week activity, as opposed to the 2- to 5-month activity typical of missile conceptual designs (Ref. 3); third, some higher performance approaches were not taken in order to keep the design closer to a documented “real-world” component with demonstrated performance in the desired range. This was the case for the choice of tank material, HX fabrication methodology, and non-subcooled propellant.

For the compass SSTO point design in Table 3.30, each 10% gain in dry mass margin in Table 3.32 can be used in any of the following ways:

- Kept as increased margin (increased confidence in final payload mass)
- Increased structural mass for reduced fabrication costs
- Increased payload by about 100 kg (2% increased payload fraction)
- Reduced wet mass by roughly 10% (375 kg) and corresponding decrease in beam power and scale
- A combination of the above

TABLE 3.32.—TECHNOLOGY MARGINS PRIORITIZED BY GREATEST POTENTIAL IMPACT FIRST

Element	DMM ⁸ gain (%)	From	To	Description of potential gain
Propellant	<30	LH ₂	NH ₃ , N ₂ H ₄ or CH ₄	A rocket-equation-based scaling analysis conducted by Parkin suggests that some dense propellants could provide up to 30% greater dry mass margin than LH ₂ for missions at ~10.5-km/s ΔV . The full 30% is for propellants that are heated to 3000 K (i.e., the effect is larger as the HXs are able to operate hotter). In addition, hydrazine (N ₂ H ₄) adds mission flexibility as a monopropellant in its own right and methane (CH ₄) and other nontoxic noncryogenic hydrocarbons probably can be heated by a molecular mechanism in the bulk propellant itself to achieve temperatures exceeding 3000 K at the expense of fouling concerns and wall materials to investigate. Ammonia (NH ₃) will provide the greatest performance of the three for a given temperature. Lithium hydride (LiH) and ammonium fluoborate (NH ₄ BH ₄) have the best performance of the “exotic” propellant possibilities but this class of propellants is unlisted because they are assumed to be too toxic or uneconomical.
Airbreathing first stage	20			Preliminary investigation by Parkin finds that changing the initial altitude of the rocket from 2 to 20 km increases the rocket mass at cutoff by about 20%. Other advantages to an airbreathing first stage are (1) no boost beam facility is needed (only sustain), (2) it is easier to achieve a range of orbital inclinations, (3) oxidation of the HX coating is reduced, (4) a conventional nozzle may suffice instead of a plug nozzle, and (5) it should be possible to run the 3 Meter Target Microwave Thermal Rocket (MTR) at 100% throttle for its full trajectory, so no throttle-down maneuver is needed.
Propellant	15	Not subcooled	Subcooled	For LH ₂ , subcooling from 20 to 14 K densifies the tank mixture into slush with about 20% higher density than conventional LH ₂ . Paradoxically, it may reduce the insulation needed on the tank because during ascent, more heat leakage is needed into the tank to melt the solid phase and maintain tank pressurization. This effective 20% margin on propellant translates to about a 15% additional margin on dry mass.

HX coating	~15	SiC	ZrO ₂	<p>Zirconia (ZrO₂) is already used as an oxidation resistant coating in rocket nozzles. For example, the Scout missile uses a flame-sprayed zirconia coating to protect its ZTA graphite nozzle (Ref. 7). At refractory temperatures, zirconia has similar millimeter-wave absorption properties (resistivity) to silicon carbide, but it potentially increases the HX peak temperature from >2250 to >2700 K. Continuous-use temperature for fused stabilized ZrO₂ coating is quoted as 2670 K with good resistance to thermal cycling. We plan to investigate zirconia coatings in the current 10-kW and future 1-MW static test series. If borne out by experiment, it would raise the I_{sp} from 800 to 900 s, in turn increasing the dry mass margin by about 15%.</p>  <p>Figure 3.112.—Left: Scanning electron microscope (SEM) image (cross-section) of ZrO₂ interface coating on carbon fibers (white rings around each fiber) showing uniformity of coverage achieved by the ultraviolet chemical vapor deposition (UVCVD) technique (Ultramet.com). Right: SEM image showing fiber pullout in ceramic matrix composite with ZrO₂ interface coating (Ultramet.com).</p>
Structures	<15	Unoptimized	Optimized	<p>Excluding the tank, the next major structural masses for the COMPASS design were incurred by the thrust structure and pipes at the aft end of the vehicle. HX supports and nosecone masses were secondary to this. In particular the aft structure was heavier than budgeted for in the baseline and there was not the time or documentation available to determine why. A thoughtful and detailed design could result in up to a 15% saving in overall rocket dry mass.</p>
Ascent trajectory	<10	Nonoptimal	Optimized	<p>The ascent trajectories obtained by COMPASS were optimized using the OTIS software, saving >400 m/s relative to the quasi-optimized trajectories computed by Parkin. However, the trajectories obtained display behavior suggesting that constraints given to the optimizer caused it to erroneously use a lower fraction of available throttle, resulting in an oversized propulsion system (or equivalently a longer downrange distance than needed). There was not time to reconcile the trajectories obtained from OTIS with physical reasoning about what the optimizer should be doing at any given stage of ascent. Consequently, it is possible that the accelerations required of the propulsion system could be reduced by a few g's and/or more saved on the ΔV's, with the Parkin baseline being the worst case in this regard. Despite this, trajectory improvements are unlikely to contribute more than 10% to the dry mass margin. But they will make a large difference to turbomachinery throttling requirements and beam facility cost.</p>
Tank material	9	Ti	Graphite-epoxy (Gr-Ep)	<p>Titanium (Ti) tank was chosen because Gr-Ep was at less than minimum gauge for a 700-kg wet-mass rocket. Depending on assumptions including what the minimum gauge actually is (0.76 mm is indicated in some literature), Gr-Ep could be used for designs of 10 tons wet mass and greater. In this case and excluding insulation, it would be about 5 times lighter than the equivalent Ti tank, adding about 9% to the dry mass margin.</p>

HX fabrication	<8	Woven textile	CVD / other	The 0.7-mm channel thickness is an order of magnitude greater than needed to contain the channel pressure of ~100 bars (i.e., it could be more than 10 times thinner if fabricated by other means, such a chemical vapor deposition (CVD) or perhaps lithography or micromachining). The design space here is large. In the theoretical limit that HX mass were reduced to zero, then at most the dry mass margin would be increased by 8%.
Enhanced heat transfer surfaces	~7	Smooth/rough circular channels	Heat-transfer-enhancing "tricks"	Enhanced Heat Transfer is an entire field of techniques used to reduce the temperature difference between the bulk flow and channel wall, usually at the expense of greater pressure drop across the HX. At the hot end of the HX, enhanced heat transfer techniques have not been factored into the conceptual design but will certainly be combined with thinned tube walls and "high k" fibers to reduce the temperature differential to < 200 K and at best within 50 K of the absorbing material thermal limit. A resulting 200-K increase in propellant temperature increases I_{sp} by about 5% and the dry mass margin by about 7%. In addition, the flow regime can adjusted to optimize the tradeoff between heat transfer performance and pressure drop. This has unquantified performance advantages felt via the increased nozzle chamber pressure and/or decreased turbopump pressure requirements.
HX temperature throttling	<6	Constant peak T	Variable peak T	The HX would be operated at reduced temperatures (T ; e.g., 2250 K) in low atmospheric conditions to minimize oxidation erosion of the absorbing layer, increasing toward the melting/decomposition temperature of the layer orbital altitudes. For example with zirconia, the melting point is 3000 K, corresponding to a vacuum I_{sp} of at most 950 s. The extra 50 s of I_{sp} averaged over the ~8 km/s of acceleration occurring in near vacuum corresponds to at most a 6% increase in dry mass margin above that gained by using zirconia in the first place. Nevertheless, it is a gain that will be realized in the natural course of thruster evolution.
Tank insulation	<3	SOFI	State of the art (SOA) or no insulation	Spray-on foam insulation (SOFI) may be easy to apply, but in principle, it would be outperformed by aerogel or fiberglass insulation. Preliminary thermal balances suggest that no insulation at all is required during ascent, with insulation only needed on the pad to prevent ice buildup. There are schemes by which ice buildup may be prevented on a bare or lightly insulated tank: for example, by external heating. Also, recent progress in superhydrophobic coatings (Ref. 8) could significantly reduce ice buildup and increase the amount that falls off at launch. Finally, a helium balloon/tent could surround the launch vehicle on the pad and could be rapidly retracted just prior to launch. There is a liftoff acceleration of >3g, as opposed to a more conventional 1.2g, so the initial ice weight might have a comparatively small effect on overall performance. Since a lightweight externally heated SOFI scheme was accepted by COMPASS for use in the study, the most that remains to be saved is about 3% of dry mass.
HX wall thickness	2	0.7 mm	0.5 mm	This decreases HX mass by 25% (rocket dry mass by about 2%) and temperature drop across channel wall by 30% at the expense of slightly higher porosity. The 0.5-mm figure is a lower limit given in Jan. 2011 by Teledyne, makers of the 0.7-mm-thickness channel.
Tank structural safety factor	1.5	1.25	1.1	This is a traditional fallback, at the expense of trickier tank fabrication. This would decrease tank weight by about 10%, but because the tank itself is very light, it would only increase overall rocket dry mass margin by about 1.5%.
Pyrometry	<1.5	Conventional	Woven thermocouple	COMPASS budget mass for >100 thermocouples and associated wire, primarily for the HX. Teledyne advises that tiny thermocouple strands can be woven into the HX.
Pyrometry	<1.5	Thermocouples	Remote optical	If the HX was tracked optically using a telescope that tracks with the beam facility, then imaging optical pyrometry could be used to follow the thermal performance of the HX. Such a system will be used in static testing and it is envisaged that this will be adapted to short-range, and then long-range, flight. This will save most mass and data associated with onboard thermal diagnostics.

Turbopump	<1.5	100 bars	160 bars	Previous experience with microwave thermal rocket system analyses indicates that performance is maximized when the maximum pressure rise for a single turbopump stage is used. Humble indicates that this limit is 160 bars, although this figure may be out of date. A lower pressure was used for the study baseline because it corresponded to an existing point design published for a nuclear thermal rocket LH ₂ turbopump. As it turns out, the COMPASS team member who sized the turbomachinery was a coauthor of that paper. Because full flowpath iterations were not really possible in the time allowed, the original pressure assumption was not varied.
Aerodynamics ^{CS}	<1.5			Worst-case boattail drag was assumed. The aerodynamics has not been optimized. For example, neither the impact of the nose fineness ratio nor of the fins (to increase HX area) has been investigated. Also, the addition of a nose aerospike similar to that used on Trident missiles will reduce supersonic drag.
Nozzle	<1.5			The optimal truncation length for the plug nozzle is not currently known. This also relates to boattail drag.

^aDifferential Mass Margin.

3.1.8.5 Payload

The payload for all cases was defined to be a 40 kg ORBCOMM-like satellite delivered to a 400- by 400-km orbit.

Because the microwave thermal ascent trajectory does not lend itself to achieving fully circular trajectories, the payload itself provides a small delta V to circularize the orbit. If, like ORBCOMM, the payload has no primary propulsion system, a Star 5A solid rocket weighing 4.6 kg could be added to provide the necessary impulse over a 30-s burn.

TABLE 3.33.—PAYLOAD DESCRIPTION FOR EACH OF THE DESIGN POINTS ASSOCIATED WITH DRM-1C

		Parkin baseline (expendable SSTO) (optional) Star 5A*1 or 2	COMPASS SSTO design point (optional) Star 5A	COMPASS TSTO design point Star 5A
Payload	Type			
	Initial mass (kg)	45 or 50	45	45
	Final mass (kg)	43 or 46	43	43
	Payload (kg)	40	40	40
	ΔV (m/s)	100-300	87	87
	Init. orbit (km)	(optimal apogee) by 400 km	100 by 400 km	100 by 400 km
	Final orbit (km)	400 by 400 km	400 by 400 km	400 by 400 km

In the baseline design, the circularization ΔV is between 100 and 300 m/s, as opposed to 87 m/s because the perigee of the initial orbit is left unconstrained. Though lower payload ΔV appears to be more desirable, subsequent analysis by Parkin suggests that it is less optimal for the rocket because an apogee of ~ -200 km naturally arises by optimizing a gravity turn followed by horizontal acceleration at full throttle. Consequently, the difference in optimizer constraints caused COMPASS's ascent trajectory solutions deviate far from the desired behavior of Parkin's solution, and they are not optimal with respect to maximizing payload mass.

3.1.8.6 Description of Ground Facility

The advent of submillimeter-wavelength astronomy has highlighted the existence of locations with particularly low atmospheric water content, opening up new microwave transmission windows from 35 to 300 GHz and sometimes beyond. The atmospheric scale height of water vapor is only 1 to 2 km, allowing mountain ranges to create “rain-shadow” regions with comparatively good millimeter-wave propagation. As seen in Figure 3.113, the Himalayas hold back the water vapor, making Tibet an ideal location for China. The Alps are suitable for Europe, and the Andes suitable for South America, with the Chilean Atacama desert particularly prolific for submillimeter-wave astronomy. This resolution is insufficient to see particular mountains in Ecuador and Kenya that have both good propagation conditions and are close to the equator; these mountains are visible in the larger dataset. Also not easily visible are the islands of Hawaii, which are known to have excellent propagation characteristics.

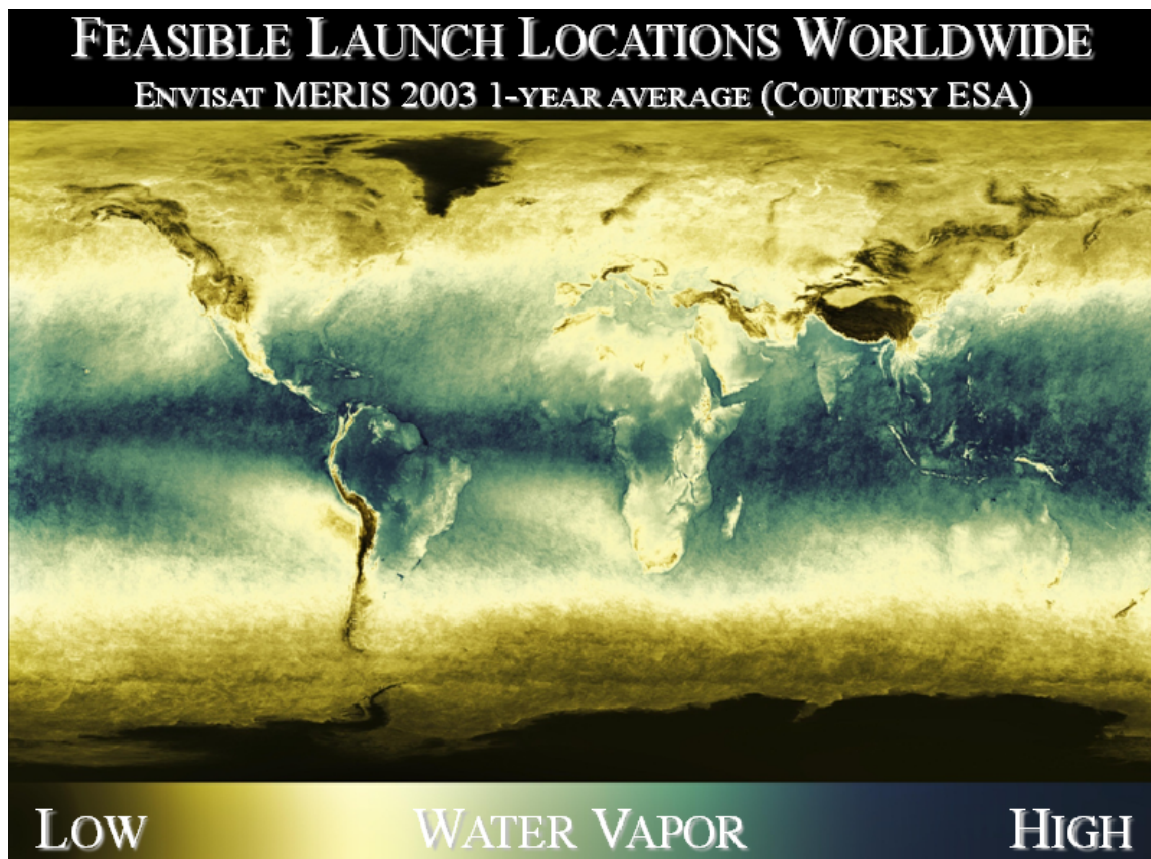


Figure 3.113.—Satellite data indicating the international locations where atmospheric water vapor content is lowest, and therefore millimeter-wave propagation is most efficient. Copyright European Space Agency (ESA); used with permission.

For the continental United States (CONUS), Figure 3.113 clearly shows that the mountainous southwest of the country is better suited than the southeast, with Florida being essentially underwater as far as millimeter-wave propagation is concerned. Zooming in to the southwest, Figure 3.114 shows that the Sierra mountains east of California's Central Valley provide some of the best propagation opportunities. Ongoing site surveys and millimeter-wavelength projects, such as the Combined Array for Research in Millimeter-wave Astronomy (CARMA) in eastern California, are revealing many suitable locations for a beam facility on the U.S. mainland. Because the southwest is relatively sparsely populated and contains large regions of government land, there are several ways in which a 200+ km-long ascent trajectory might be constructed. For polar orbits, Alaska appears to provide many of the best sites.

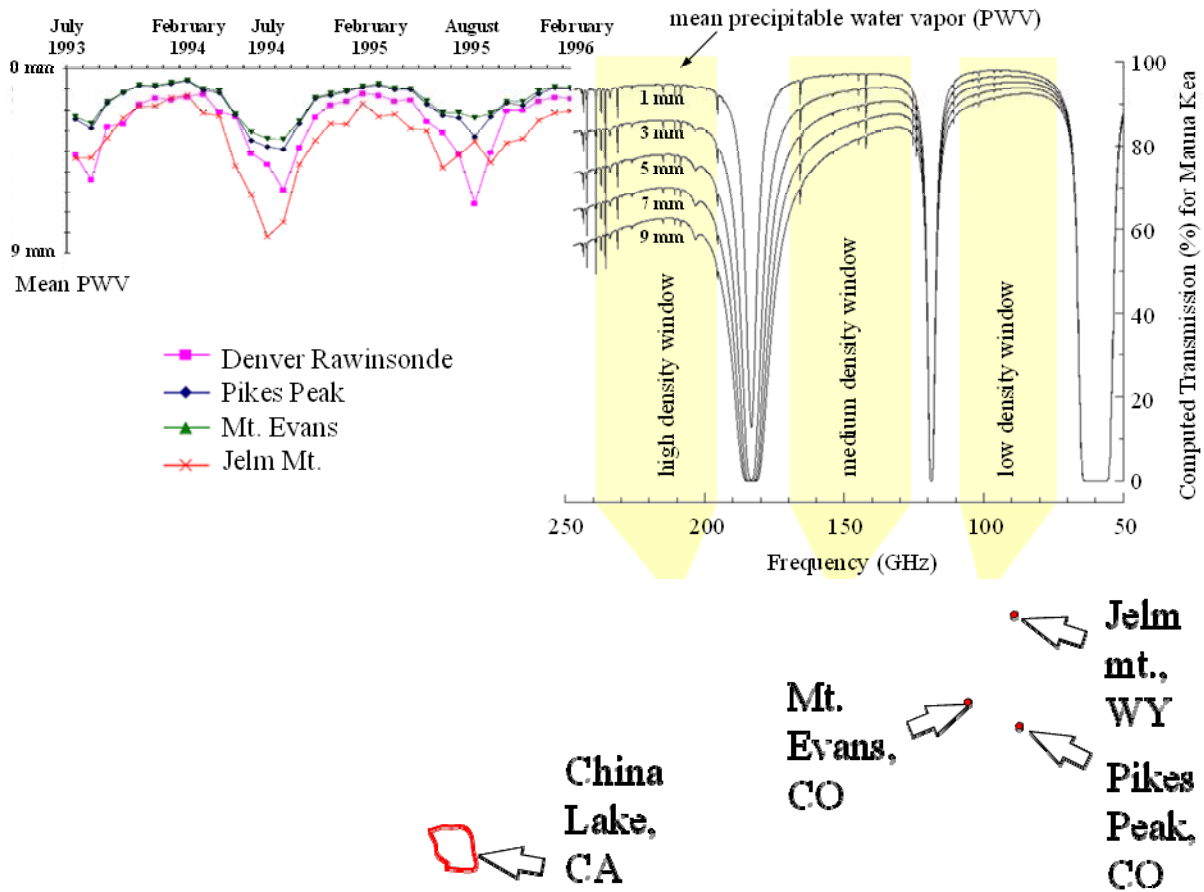


Figure 3.114.—Examples of CONUS sites with low losses due to water vapor absorption. Such sites are predominantly in the southwest. For Mt. Evans and Pikes Peak, a millimeter-wave beam vertically transmitted to space would lose 5% to 10% of its energy to atmospheric absorption at 170 GHz.

The ascent trajectory in this DRM consists of two segments: In the first, at the bottom left of Figure 3.115, the vehicle is powered by a short-range “boost” beam facility, maintaining vertical ascent of the rocket at 40% throttle to minimize drag losses. The first segment transitions to the second at an altitude of 30 to 60 km. In this time, the boost beam facility hands the rocket over to the “sustain” beam facility as rocket levels off and begins to accelerate horizontally at 100% throttle. The acceleration of 9g to 19g during this segment of the ascent raises the velocity from 1.5 to 8 km/s in only 60 s and enables the rocket to achieve orbital velocity within 125 km range of the beam source. This was to minimize the initial cost of the beam facility and could eventually be expanded to allow a gentler ascent trajectory suitable for human launch.

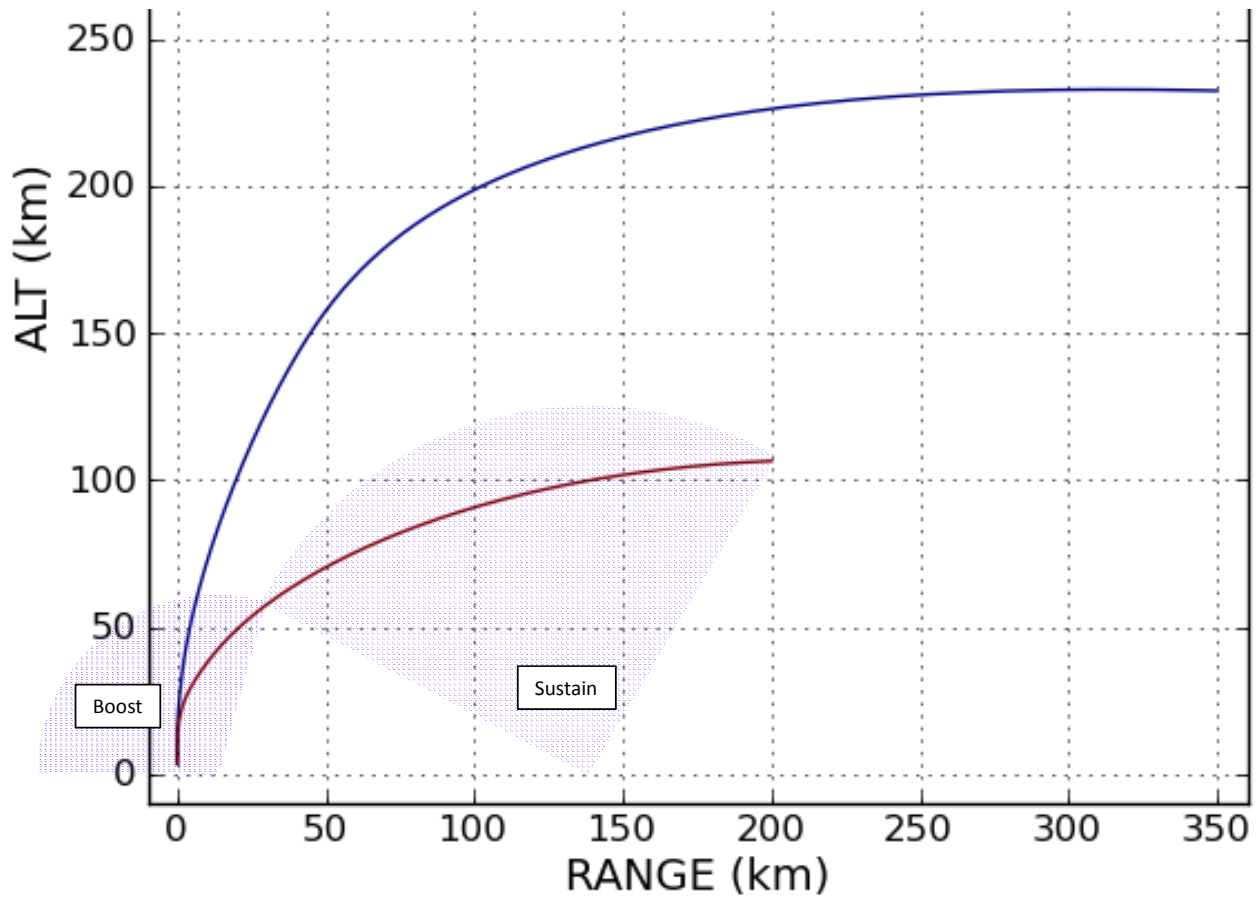


Figure 3.115.—Beam facility arrangement along an ascent trajectory. The red line is the ascent trajectory. During initial ascent, a boost beam facility with a maximum range of 60 km propels the vehicle, which is then handed over to a larger sustain facility with a 125-km range and higher power. Programmatically, a subscale demonstration beam facility would probably become the boost facility, and the decision to proceed on the sustain facility would be based on its successful operation. The blue line is an alternate ascent trajectory considered by the COMPASS team. Because twice the range would require twice the source or target diameter, it was not further considered for these point designs.

The size and power of the boost and sustain beam facilities for each of the design points is given in Table 3.34. Tsiolkovsky originally predicted that a microwave beam facility would need to be 12 km across, but owing to the shorter wavelength and high acceleration ascent trajectory, the beam facilities of DRM 1–C will be closer to 100 m in diameter, comparable in size to existing millimeter-wave telescopes.

TABLE 3.34.—BEAM FACILITY POINT DESIGNS

		Parkin baseline (expendable SSTO)	COMPASS SSTO	COMPASS TSTO
Boost	Primary diameter (m)	58	58	58
	Maximum range (km)	60	60	60
	Output power (MW)	350	665	300
	Downrange distance (km)	15	15	40
	Beam spillage (%)	20	20	20
Sustain	Primary diameter (m)	122	122	122
	Maximum range (km)	125	125	125
	Output power (MW)	870	1,650	800
	Downrange distance (km)	140	140	40
	Beam spillage (%)	20	20	20

Although the 1990s-era Green Bank Telescope (GBT) aperture is about the right size for application to a microwave thermal rocket, it is the current era of closed-loop active surfaces that provide the necessary surface accuracy. In fact, surface accuracies now exceed those needed for the microwave thermal rocket by nearly an order of magnitude, albeit for smaller apertures. The key question to answer in a beam facility conceptual design will be what combination of structural rigidity and active surfaces can correct for changing gravitational distortions and mechanical bending modes as the structure slews; sudden thermal deformations could be negated using heaters. If greater mechanical stiffness is required, there are Fresnel reflector and even holographic techniques that would be unsuitable for astronomical work but may be advantageous for beam direction, provided they turn out to be compatible with the spectral-beam-combining approach used in the optical back end.

Active surfaces aside, the beam facility could provide pointing on three different temporal and angular scales to track a target HX through its ascent trajectory. The first scale is provided by the primary mirror, with low angular acceleration and slew rate but a range of motion from -40° to $+40^\circ$. The second scale of pointing would be provided by moving the secondary mirror relative to the primary, and the third and finest scale of pointing could be provided in the feed system for each gyrotron beam by means of a fast-steering mirror, such as that pictured on the left of Figure 3.117. Mirrors of this kind are used to stabilize sections of the optical train in the ABL shown on the right of the figure and, in principle, could be adapted to perform fine pointing of quasi-optical gyrotron beams prior to their transformation through the secondary and primary mirrors.

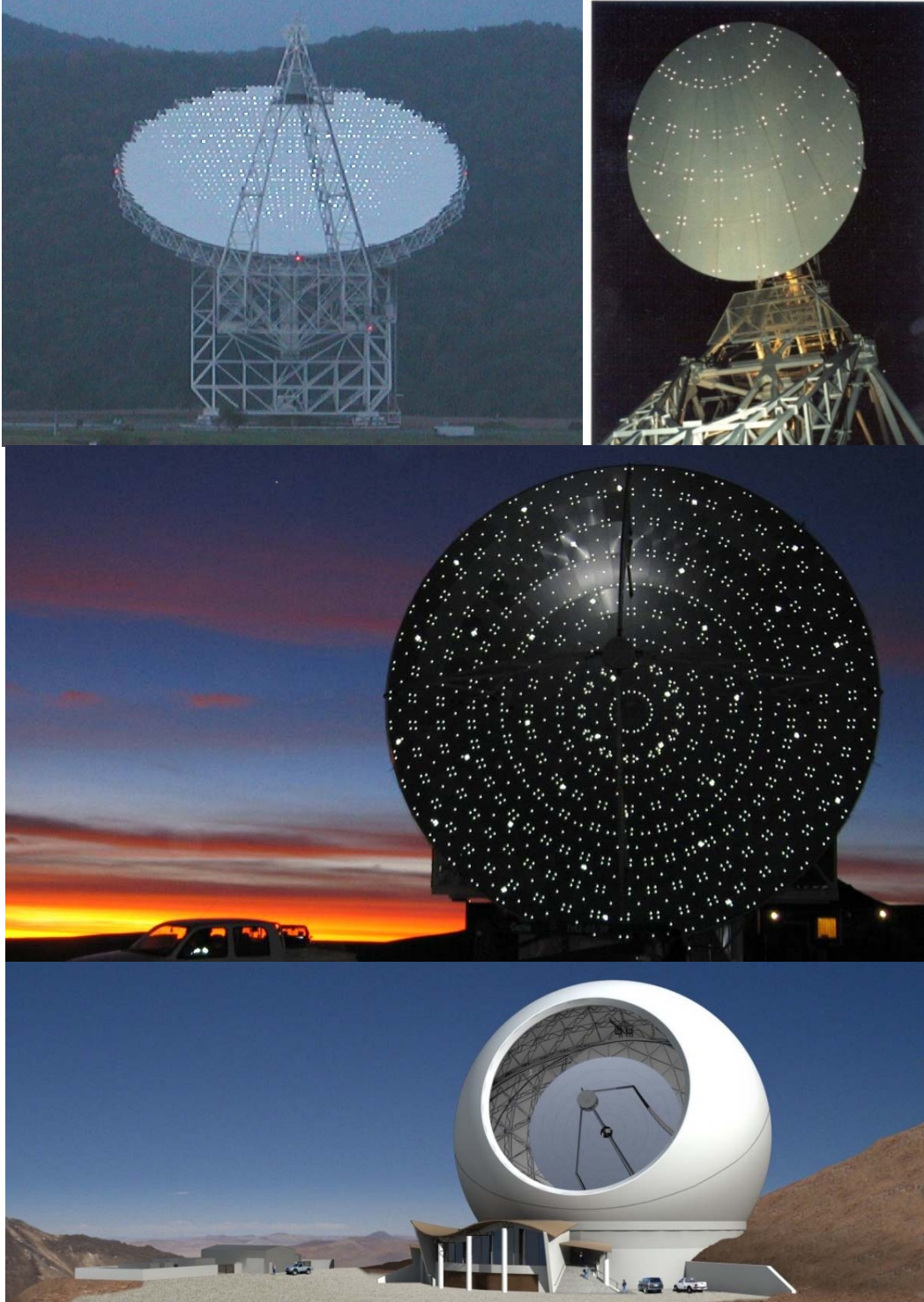


Figure 3.116.—Three generations of millimeter-wave telescopes. Top: 1990s-era GBT (left) and secondary (right). Middle: 2000s-era Atacama Pathfinder Experiment (APEX) at Llano Chajnantor (courtesy of APEX; used with permission). Viewed here at dusk, the panels and retroreflectors of its active surface are clearly visible. The telescope was manufactured by VERTEX Antennentechnik in Duisburg, Germany. Bottom: 2010s-era Cornell-Caltech Atacama Telescope (CCAT) (Courtesy TMT Observatory Corporation; used with permission).

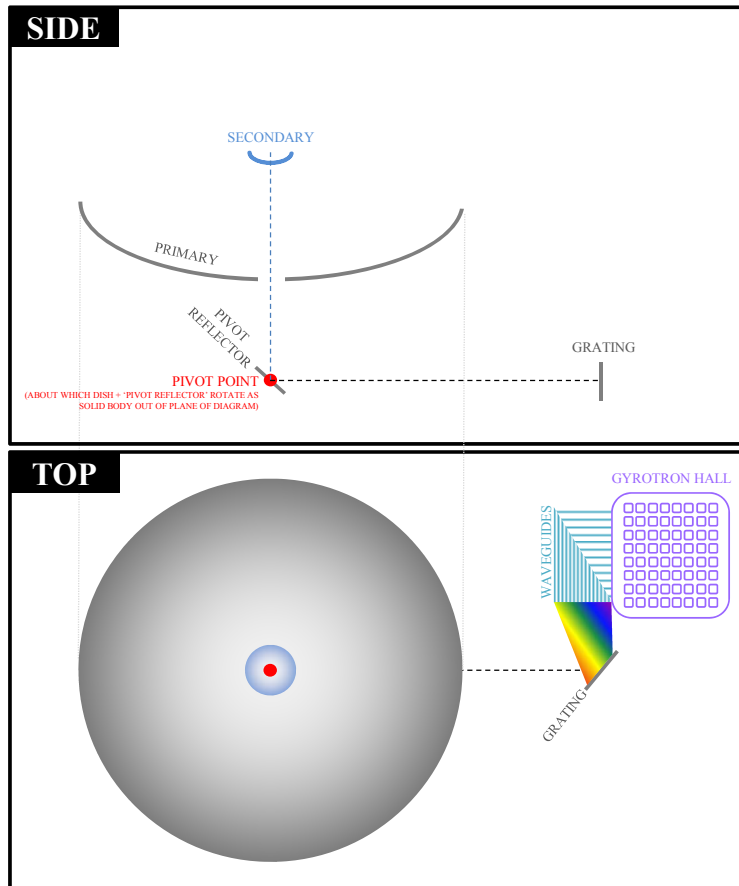
TABLE 3.35.—COMPARISON OF APERTURE PARAMETERS

	GBT	Atacama Large Millimeter Array (ALMA)	CCAT	MTR at 120 km
Optical Arrangement	Parabolic off-axis reflector	Cassegrain quasi-random array	Cassegrain	Cassegrain
Diameter of primary (m)	100 by 110	12 by 12 and 7 by 7	25 by 25	120 by 120
FWHM beamwidth (arcsec)	5.3 at 140 GHz			5.2 at 170 GHz
Pointing accuracy (arcsec)	2.7 (open loop)	2	2-0.5 (blind)	1 (closed loop)
RMS ^a surface accuracy (μm)	450 (passive) 390 (open loop) 68 (intra-panel)	17.2 measured by near-field radiometric holography (Ref. 9)	<12.5 (closed loop)	88 (closed loop)
Minimum elevation angle (deg)	5		5	40
Maximum slew rate (deg/s)	0.3 (elevation)		0.2 to 1	4
Cost	FY1990 \$97M (~\$12 K/m ²)	FY2010 \$1.3Bn (~\$7.5 K/m ²)	FY2020 \$110M	FY2010 <\$1Bn
Construction time	11 years (1990–2001)	2003–2011	6 year	< 10 year

^aRoot mean square.



Figure 3.117.—Left: 12-cm-diameter fast-steering mirror for high-power laser applications (image courtesy of ATA; used with permission). A 30-cm-diameter model features >1-kHz open-loop bandwidth, >300 rad/s² angular acceleration, <0.2-μm surface accuracy, and ±8-mrad mechanical travel with <10-μrad (2-arcsec) pointing accuracy. Right: YAL-1A ABL prototype in flight, 1.5-m telescope, megawatt-class 1.3-μm laser with undisclosed range .



Sequence:

1. Each beam begins in a gyrotron
2. Emitted into evacuated corrugated waveguide (65W/m measured loss at 1 MW) and propagates to vicinity of grating
3. Each beam 'launched' into free-space Gaussian beam and exits waveguide via window
 1. (option of adding fast steering mirror at this stage)
4. Each beam of slightly different frequency hits grating at slightly different angle
5. Grating combines 'rainbow' into single Gaussian beam (grating can theoretically combine up to 2500 sub-beams; will actually need O(100))
6. Beam hits pivot reflector (pivots as primary slews so gyrotrons don't have to rotate with the dish)
 1. Option of adding adaptive optics here
7. Beam hits secondary
 1. Option of adding adaptive optics here
8. Beam hits primary
9. Beam hits target heat exchanger (not shown)

In general:

- Ohmic loss from each reflection is 0.1% for Al.
- Grating loss expected to be 1-5% (2-beam loss of a simple millimeter wave grating has been measured at <0.5%, n-beam loss experiments and analysis planned)
- To provide for various orbital inclinations, the entire arrangement including dish gyrotron hall will be built on a platform that can be rotated. This platform will be mounted on circular rails to hold and distribute the weight and provide power
- Depending on detailed analysis, the primary and/or secondary may be collapsed down to flat fresnel reflectors

Figure 3.118.—Millimeter-wave beam facility optical arrangement.

For the most part, the frequencies needed for microwave thermal launch are readily generated using gyrotron or gyrokystron microwave sources. Gyrotron development has been spurred by its application to electron cyclotron heating systems in fusion reactors, and in particular the goal of a 4-MW continuous-wave (CW) gyrotron oscillator at 170 GHz for the ITER fusion reactor. The advent of edge-cooled diamond windows in the late 1990s marked a significant advance in these high-power CW systems, and in March 2005 the commercially available 140-GHz CPI VGT-8141 gyrotron demonstrated 30-min pulses of nearly 0.9-MW output power. This continues a trend that has seen time-average power output of millimeter-wave sources increase by *6 orders of magnitude* over the past 60 years.

Prospects for the long term are focused on increasing the CW power output of coaxial gyrotrons together with greater reliability. Present design efforts for "super-power" tubes aim to achieve 4- to 5-MW CW output power at frequencies of 95, 130, 140, and 170 GHz. Diamond windows become a limiting factor at such high power levels, and future generations of devices are expected to use multiple diamond output windows.

From a practical perspective, the present commercially available gyrotrons cost \$2M/MW to \$3M/MW and have a lead time of 2 years, depending on how much of the supporting equipment (e.g., power supply, optics, and cooling) is included. In low-production quantities (1 to 10 units), the costs mentioned earlier in this section include the gyrotron oscillator itself, a diamond output window (~\$100K), a superconducting magnet system (~\$500K), and a power supply (~\$300K).

A key parameter affecting the ultimate payload price of microwave thermal launch is gyrotron service life and maintenance overheads. Although the present generation of gyrotrons is commercially available, they are still undergoing refinement for high reliability. In this regard, the experiences of General Atomics with three different gyrotrons for fusion work give some indication of the present state of affairs:

Of the three development gyrotrons, two repairable failures are described by Lohr et al. (Ref. 10). The first was a filament short that occurred after 5000 hr of operation, and the second was a braze failure causing a loss of vacuum. In both cases, the gyrotrons were repaired for about 10% of their original cost.

Aside from these early problems, there is little fundamental difference between gyrotrons and other high-power vacuum devices such as klystrons as far as reliability and lifetime are concerned, and a mean time between failures of 30,000 hr is a reasonable expectation as the products mature. Lifetimes of only a few thousand hours were anticipated during the proposal to construct the Stanford Linear Accelerator; however, actual experience led to a mean time between failures now exceeding 50,000 hr.

3.1.8.7 Concept of Operations (CONOPS)—Frequency of Launch and Repeat Time

There was insufficient time to investigate the operational and economic questions surrounding a microwave thermal launch system, in particular the flight rates needed. From an economic point of view, a CONOPS resembling airport operations with frequent routine operations is clearly better than a traditional spaceport with infrequent, one-off “spectacular” operations. ORBCOMM was chosen as the type of payload for which a large number of routine launches may be needed. The launch sequence for an expendable microwave thermal launch of an ORBCOMM is given in Table 3.36.

TABLE 3.36.—CONOPS FOR ORBCOMM LAUNCH

Time	Event
<i>T</i> – 1 day	50-kg payload is integrated into rocket on pad
<i>T</i> – 30 min	Rocket is enclosed in helium-filled tent and LH ₂ tank is filled
<i>T</i> – 5 s	Tent and umbilicals are retracted
<i>T</i> + 100 s	Rocket reaches 40-km altitude, transitions from boost to sustain beam facility, vertical ascent to horizontal acceleration, and throttles up from 40% to 100%
<i>T</i> + 200 s	Rocket cuts off into –360- by +400-km transit orbit
<i>T</i> + 10 min	Nosecone separated and payload ejected
<i>T</i> + 45 min	Payload circularization burn to 400 by 400 km (230 m/s, < 10 kg solid rocket)

3.1.8.8 Costs—Comments

It is elasticity of demand that provides the incentive for launch prices to go down. If reducing the price of launch from \$10,000/kg to \$5,000/kg does not at least double demand, then there is no incentive to do it, and indeed this has not happened in 40 years.

\$10,000/kg is a metastable price level, with 1990s-era economic analyses predicting \$600/kg to be the next stable price level because it corresponds to a predicted spike in demand and flight rate. Of course, \$600/kg could only be attained if the cost price was less. This is not the case for conventional rockets, the cheapest foreign examples of which probably cost in the region of \$2000/kg to make. Not even the economies of scale achieved in Minuteman production achieved \$600/kg, and these quantities of production are unlikely to be reached again.

If the economic barrier to space access is ever to be broken, it will most likely be by the first concept to achieve reusability, enabled by the first technology that achieves the highest margins at the smallest scale. According to the results of DRM 1–C and specifically Table 3.30, microwave thermal rockets are a candidate.

The logical first step is an expendable small satellite launcher, which corresponds to a scale and power level that minimizes initial beam facility cost. There is yet some uncertainty about where this minimum lies and how low it goes, but it is certainly less than the cost of developing a heavy launcher.

Currently, small launchers cost substantially more per unit mass than their larger counterparts. If improvements in vehicle technical performance can be translated into improvements in cost performance, this should have the greatest impact the soonest for small satellites.

In reading the cost estimates associated with the DRM 1–C vehicle and beam facility, it is important to consider what the same estimation methodology applied to a conventional alternative might be, and whether the cost estimation methodology is likely to capture the efficiencies of a microwave thermal launch approach versus a conventional alternative.

3.1.8.8.1 Beam Facility Costs

If a 1-MW gyrotron and its power supply costs \$1M plus an equal amount in lifetime maintenance and lasts for 20,000 hr of operation, then its average cost is 10 cents/kWh. In October 2010, year-to-date average U.S. retail prices of electricity were 9.91 cents/kWh.

In other words, the cost of converting electricity to a millimeter-wave beam is comparable with the cost of the electricity itself. Rolled into the electricity price is the cost of the generator, step-up transformer, transmission line, step-down transformer and the personnel to maintain it. The gyrotron and its power supply are of similar complexity.

The GBT is about the size needed for the microwave thermal beam facility. Its fiscal year 2007 (FY2007) operating budget was \$10.4M, which included 109 full-time equivalents (FTEs).

3.1.8.8.2 Minimum Beam Facility Cost

It is possible to estimate the size of a rocket that minimizes beam facility cost. This minimum cost occurs at a balance between two opposing expenses: one that gets smaller as the rocket gets larger, and one that gets larger as the rocket gets larger.

The first expense is optics. The smaller the rocket to aim at, the larger and more expensive the dish needed on the ground. In fact, the relationship is inversely proportional: If the HX diameter is doubled (e.g., from 3 to 6 m), then the ground dish diameter is halved (e.g., from 120 to 60 m). The second expense is millimeter-wave power. The larger the rocket, though easier to aim at, the more power needed to propel it.

When the cost of the aperture area equals the cost of the millimeter-wave power, the beam facility cost is minimized. On the basis of the assumptions in Table 3.37 and if it is assumed that the HX size is equal to the tank size, the beam facility cost for DRM 1–C can be estimated versus vehicle wet mass (Figure 3.119, top).

TABLE 3.37.—ASSUMPTIONS USED IN THE BEAM FACILITY COST CALCULATION

Energy loss assumptions	
Gaussian beam spillage	20%
Atmospheric absorption	10%
Dish scattering/absorption	10%
HX reflection/reradiation	20%
Geometric assumptions	
Beam wavelength	1.76 mm (170 GHz) ($\lambda/20 = 88 \mu\text{m}$)
(HX length)/(tank length)	1
(HX width)/(tank width)	1
Tank length to diameter (L/D) ratio	1 (elliptical end caps)
Tank ullage	10%
Tank propellant density	68.9 kg/m ³ (LH ₂ , 22 K)
Maximum beam tilt angle	60° along-track, 10° cross-track
Maximum target range	125 km (at cutoff)
Other assumptions	
Trajectory average specific impulse I_{sp}	724 s (LH ₂)
Vacuum specific impulse	800 s (LH ₂)
ΔV	10,378 m/s
Peak acceleration	19g (just before cutoff)

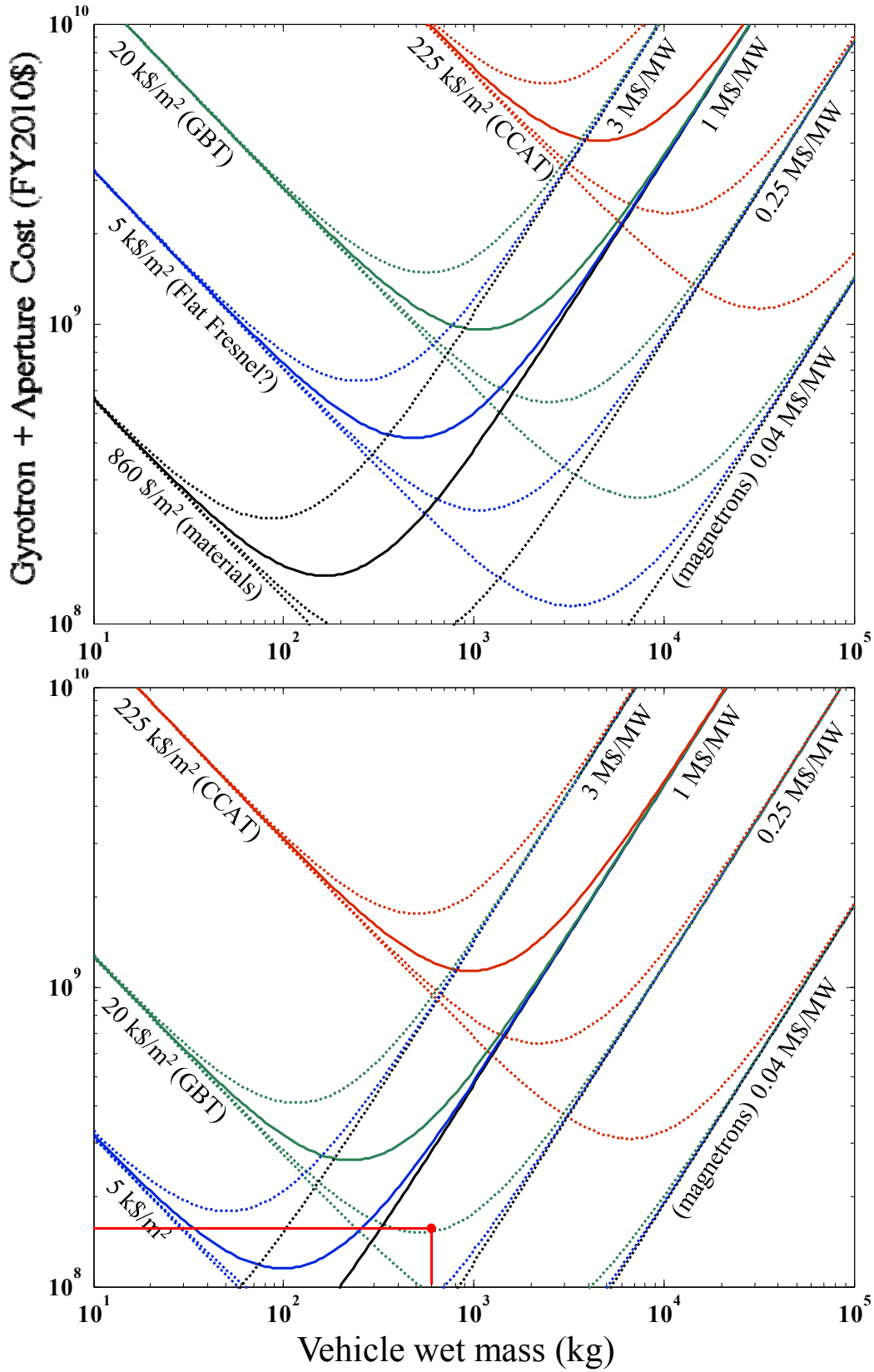


Figure 3.119.—Top: Beam facility cost based on assumptions in Table 3.37. Bottom: Effect of chine and greater spillage.

The minimum beam facility cost is found by choosing an aperture cost (\$/m²) on the top and a gyrotron cost (\$/MW) on the bottom Figure 3.119, and following the line that connects them until a minimum is found. This minimum corresponds to a given wet mass and beam facility cost. The choices of gyrotron and aperture cost are taken from Table 3.38.

The worst-case gyrotron cost is taken to be the current cost, and the best is super-power tubes combined with the effect of increased production. The lower bound on aperture cost is the materials cost, and GBT is the closest analogy for a 100 meter-class dish. The relation between technology factors and overall dish cost is not yet well understood. If a duplicate of the GBT were built today, it might be significantly cheaper because it is no longer cutting edge and could make use of carbon composites, but water cooling of the panels would increase cost as might upgrading the active surface to 80- μ m accuracy. It is not yet known whether the higher CCAT areal cost is due to its increased surface accuracy relative to GBT or because it is a single small dish and there is fixed overhead independent of size. The ALMA areal cost, which averages over fifty-four 12-m dishes and twelve 7-m dishes, suggests that economy of scale more than surface accuracy that drives these areal costs.

TABLE 3.38.—ASSUMPTIONS USED IN THE BEAM FACILITY COST CALCULATION

Gyrotron cost	FY2010 \$/MW
Current commercial off-the-shelf cost for ITER and others (Ref. 11)	3
Assumed cost of 2- to 4-MW super-power tubes circa 2014 to 2020	1
Cost of 100th gyrotron; initial 1M\$/MW with 85% learning curve	0.25
Assumed lower limit to vacuum tube approach: Retail magnetron cost	0.04
Aperture cost	FY2010 \$/m ²
CCAT (2012, 25-m, 8- μ m closed-loop active surface)	225
Millimeter-wave telescope rule of thumb	40
GBT (1990, 100- by 110-m, 390- μ m open-loop active surface)	20
ALMA (2010, many 12- by 12-m and 7- by 7-m, 17.2- μ m active surface)	7.5
Fresnel reflector flat primary (feasibility analysis needed)	5
25- μ m surface accuracy (ground) Al 6060 T6 panels	0.86
Unground Al 6060 T6 panels	0.28

As an example that corresponds to the 2500-kg baseline design, choosing the blue GBT aperture line at the top of Figure 3.119 combined with a \$1M/MW estimate for gyrotron bulk cost gives a beam facility cost of \$1.2Bn. This corresponds to 880 MW of millimeter-waves transmitted from a 128-m aperture to a 2.8-m target.

Pushing the envelope further, the bottom of Figure 3.119 shows how a more exotic vehicle might substantially decrease the minimum beam facility cost and the wet mass at which that occurs. The curves are generated using the assumptions of Table 3.38 except for a tank L/D of 6, (HX width)/(tank width) of 3, and beam spillage of 40%. This corresponds to a longer, thinner tank attached to a high-pressure rigid HX that is triple the width of the tank. If we assume a GBT-class aperture cost and a decade of gyrotron power increases and cost reductions, the beam facility minimum cost drops to \$150M for a vehicle of only 600-kg wet mass, corresponding to 280 MW of millimeter-waves transmitted from a 64-m dish onto a 4.4-m target. A rocket at this scale would probably require an HX areal density better than that of the woven composite example baselined for DRM 1–C. This example suggests that over time, better exploration of the design tradespace combined with evolutionary technology improvements in gyrotrons, millimeter-wave telescopes and HX will correspondingly reduce the initial cost and scale at which a microwave thermal launch system can be reduced to practice.

3.1.8.9 Feasibility Assessment

The following is a list of issues which need to be addressed

1. What are the attenuation effects of high flux levels (MW/m^2) at the frequencies of interest on the atmosphere?
2. What would be the expected availability and transmittance of the BEP ground terminal at a given frequency, given aerosol and precipitation conditions at a proposed ground site?
3. How large of a keep-away zone must be maintained around and beyond an ascending craft to accommodate reflection, refraction and scattering components of the beam exceeding substantial irradiances, and what level is to be considered substantial? Considerations should be given to maximum permissible exposure for humans, and damage thresholds for ground, airborne and space-based assets within proximity of the BEP activity.
4. For a ground based terminal operations, how much grid power over what duration is required? To meet these requirements, what would the generation, storage and conversion system look like?
5. How would a micro/mm-wave BEP system work within the spectrum constructs of the NTIA/FCC?
6. Does it make sense to collocate beamed energy propulsion and power technologies on the craft, for each phase of a proposed mission?
7. Would there be a benefit to developing a hybrid aperture to handle multiple BEP frequencies depending upon range to target, atmospheric conditions, etc.?
8. Can retro-directive control be utilized to aid in the beam pointing, acquisition and tracking of the craft?
9. What is the most practical way of performing high power beam combination using COTS technology for the frequencies of interest? What are the potential near term accomplishments that could influence this capability?
10. What are the cost/benefit tradeoffs in considering multiple BEP transmission locations, both at the ground range and at an intermediate relay point in space?
11. Could deployable array technologies be implemented to decrease the weight of a BEP aperture, and increase the allowable size that can be launched?

3.1.8.10 Roadmaps and Technology Readiness Levels

Part of the task in developing a technology roadmap has been to produce a way to best represent the technology readiness for DRM 1–C. It is particularly important to identify feasibility issues and to communicate the level of technical risk in each choice, so *comprehensive* technology profiles are important.

In the TRL summary that follows Figure 3.120), the system elements of DRM 1–C are laid out by work breakdown structure (WBS). Alternate possibilities are denoted using A, B, C notations, where A is baseline and B, C, and so forth are fallback technologies ordered by preference, usually with lower performance than the baseline by some metric. To make the baseline plan clearer, the fallback options are grayed out.

For many of the WBS elements, it was necessary to revert their TRLs back to TRL 3 even on highly developed technologies like mirrors simply because they will be operating in a high-power microwave environment. Since the TRL alone would incorrectly give the impression nobody has built a millimeter-wave telescope before (for example), the format of the sheet has been modified to represent the degree to which analogy plays a role.

Analogy is important because the process of choosing a technological path usually involves finding the closest analogy to the unit wanted and assessing what has to be changed in order to fit the new purpose. That change can be quantitative in nature, such as scaling-up a power supply to higher power. Or it can be qualitative in nature, such as changing the surface accuracy of a large dish from 5000 to 5 μm , requiring a qualitatively different approach. It matters if a close analogy to the propellant tank has flown to LEO. So, an extra dimension has been added to the TRL summary by introducing a three-symbol system:

- x A unit fulfilling the application criteria *exactly* has passed this milestone.
- o A unit substantially analogous to the exact unit has passed this milestone.
- ? Unclear at this time

Also, there are “Quantitative” and “Qualitative” analogy fields to indicate what kind of analogy is being used. In general, the sheet is laid out so that gaps in key milestones are obvious and suggest a definite and traditional course of action, such as a detailed conceptual design, lab prototype effort, sub-scale demonstration, further survey of the literature and so forth. As technologies become ready for application to the microwave thermal rocket, the “bleeding edge” red blocks should disappear roughly from left to right.

MICROWAVE THERMAL ROCKET TECHNOLOGY RISK AND UNCERTAINTY SUMMARY		Theory			Practise			Relevant environment				Diff. from analogy		Qual'd for exact purpose	Formal TRL	Notes		
		Concept formulated	Proof-of-principle	Performance est'd.	Comprehensive models	Proof-of-principle	Breadboard	Subsystem proto.	System proto.	Ground ops	Relevant environment						Qualitative	Quantitative
											<1 km	1 - 60 km	> 60 km (suborbital)					
1	Beam Facility																	
1.1A	Power supply: Pulse via flywheels	x	o	o	o	o	o	o	o	?	-	-	-	-	?	x	3	60 kV to be demonstrated
1.1B	Power supply: Pulse via NiCd cell array	x	x	x	o	o	o	o	o	o	-	-	-	-	-	x	3	Active denial uses more expensive Li-ion cells
1.1C	Power supply: Grid via solid state regulator	x	x	x	x	x	x	x	x	x	-	-	-	-	-	x	3	In use by CPI and others
1.2A	mm-wave sources: Gyrotron oscillator	x	x	x	x	x	x	x	x	o	-	-	-	-	-	-	6	
1.2B	mm-wave sources: Gyrokystron amplifier	x	x	x	x	x	x	x	x	o	-	-	-	-	-	-	3	
1.3A	Power combining: Spectral via diffractive element(s)	x	x	x	o	o	o	o	o	o	-	-	-	-	?	x	2	Analogy insufficient for 100 beam combiner
1.3B	Power combining: Phase-locked oscillators	x	o	o	o	o	o	o	o	o	-	-	-	-	x	x	3	
1.3C	Power combining: Master oscillator power amplifier (MOPA)	x	o	o	o	o	o	o	o	o	-	-	-	-	x	x	3	Haystack RADAR
1.4A	Optical front end: Single large cassegrain telescope	x	x	x	o	o	o	o	o	o	-	-	-	-	x	x	3	GBT/ALMA/CCAT
1.4A.1	Secondary optic: Al hyperbolic reflector	x	o	o	o	o	o	o	o	o	-	-	-	-	x	x	3	GBT/ALMA/CCAT
1.4A.2A	Primary optic: Al Fresnel reflector	x	o	o	o	o	o	o	o	o	-	-	-	-	x	x	3	
1.4A.2B	Primary optic: Al hyperbolic reflector	x	o	o	o	o	o	o	o	o	-	-	-	-	x	x	3	GBT/ALMA/CCAT
1.4A.3	Wavefront control: Segmented active surface (closed-loop)	x	o	o	o	?	?	?	?	?	-	-	-	-	x	x	3	CCAT
1.4A.4	Coarse beam steering: Mechanical	x	o	o	o	o	o	o	o	o	-	-	-	-	?	x	3	GBT/ALMA/CCAT
1.4A.5A	Fine beam steering: Mechanical, fast steering mirror(s)	x	o	o	o	o	o	o	o	o	o	o	o	o	?	?	3	FSMs used on ABL at 1.3 microns
1.4A.5B	Fine beam steering: Spectral / diffractive	x	o	o	?	?	?	?	?	?	-	-	-	-	?	x	3	Analogy is FADIS
1.4B	Optical front end: Multiple small cassegrain telescope	x	x	x	o	o	o	o	o	o	-	-	-	-	x	x	3	Analogy is ALMA. Fed by phase-locked or split
1.4B.1	Secondary optic: Al hyperbolic reflector	x	o	o	o	o	o	o	o	o	-	-	-	-	?	?	3	GBT/ALMA/CCAT
1.4B.2	Primary optic: Al hyperbolic reflector	x	o	o	o	o	o	o	o	o	-	-	-	-	?	?	3	GBT/ALMA/CCAT
1.4B.3	Wavefront control: Segmented active surface (open-loop)	x	o	o	o	o	o	o	o	o	-	-	-	-	?	x	3	Analogy is GBT/ALMA
1.4B.4	Coarse beam steering: Mechanical	x	o	o	o	o	o	o	o	o	-	-	-	-	?	x	3	GBT/ALMA/CCAT
1.4B.5A	Fine beam steering: Mechanical phase shifters	x	o	o	?	?	?	?	?	?	-	-	-	-	?	x	3	Was used in the past according to B.Bridges
1.4B.5B	Fine beam steering: Mechanical fast steering mirrors	x	o	o	o	o	o	o	o	o	o	o	o	o	?	?	3	FSMs used on ABL at 1.3 microns
1.5A	Pointing knowledge: Coherent doppler transponding	x	o	o	o	o	o	o	o	o	o	o	o	o	x	x	3	
1.5B	Pointing knowledge: Closed-loop IR optical tracking	x	o	o	o	o	o	o	o	o	o	o	o	o	?	x	3	KKV
1.5C	Pointing knowledge: Retrodirective beam control	x	o	o	o	o	o	o	o	o	o	o	o	o	?	x	3	1990's JPL experiment at Goldstone
2	Vehicle																	
2.1	Tank: Ti	x	x	x	?	?	?	?	?	?	?	?	?	?	?	x	3	PSI Ti Tanks
2.2A	Heat exchanger: Textile C/SiC	x	o	o	o	o	o	o	o	?	?	?	?	?	x	x	3	Teledyne prototypes
2.2B	Heat exchanger: Extruded/Sintered/CVD SiC segments	x	x	x	o	?	?	?	?	?	?	?	?	?	?	x	3	Reaction Engines SiC HX
2.3A	Nozzle: Uncooled C/SiC	x	o	o	o	o	o	o	o	?	?	?	?	?	x	x	3	
2.3B	Nozzle: Regeneratively-cooled C/SiC	x	o	?	?	?	?	?	?	?	?	?	?	?	x	x	3	
2.4A	Pressurization: Turbopump, autogeneous	x	x	x	o	o	o	o	o	o	o	o	o	o	x	x	3	
2.4B	Pressurization: Blowdown, autogeneous	x	x	o	o	o	o	o	o	?	?	?	?	?	?	x	3	
2.5A	Avionics: Cell phone-derived	x	o	o	o	o	o	o	o	o	o	o	o	o	x	x	2	PhoneSAT
2.5B	Avionics: Conventional	x	o	o	o	o	o	o	o	o	o	o	o	o	x	x	3	
2.6A	Attitude control: LH2 warm/cold gas	x	o	o	o	o	o	o	o	?	?	?	?	?	?	x	2	
2.6B	Attitude control: Gas generator	x	o	o	o	o	o	o	o	o	o	o	o	o	x	x	3	
2.7A	Aeroshell: Expendable	x	?	?	?	?	?	?	?	?	?	?	?	?	x	x	3	Anything else that needs to be added
2.7B	Aeroshell: Reusable	x	o	o	o	o	o	o	o	o	o	o	o	o	x	x	3	Analogies are shuttle, X33, X34, X37
2.7B.1A	TPS: Woven load-bearing C/SiC shell	x	o	?	?	?	?	?	?	?	?	?	?	?	x	x	3	
2.7B.1B	TPS: Carbon foam panels	x	o	o	o	o	o	o	o	?	?	?	?	?	?	?	3	Ultramet C foam panel tested at GRC
2.7B.1C	TPS: Conventional best-practise	x	o	o	o	o	o	o	o	o	o	o	o	o	?	x	3	
2.7B.2	TPS: Integrated cryo-insulation	x	o	o	?	o	?	?	?	?	?	?	?	?	?	x	3	Listed as TRL 2 in SOA review paper 2001. See also
2.7B.3A	Vehicle recovery: Landing gear	x	o	o	o	o	o	o	o	o	o	o	o	o	x	x	3	
2.7B.3B	Vehicle recovery: Parachute	x	o	o	o	o	o	o	o	o	o	o	o	o	x	x	3	
2.7B.3C	Vehicle recovery: Precision thruster docking above ground	x	o	o	o	o	o	o	o	o	-	-	-	-	?	x	3	Analogy is Pixel
2.8	Payload storage and release mechanism: TBD	?	?	?	?	?	?	?	?	?	?	?	?	?	?	?		

Figure 3.120.—TRL, risk, and uncertainty summary for the microwave thermal rocket. FSM, fast steering mirror; FADIS, Fast Directional Switch; KKV, kinetic kill vehicle; CVD, chemical vapor deposition; PSI, Pressure Systems, Inc.; and TPS, thermal protection system.

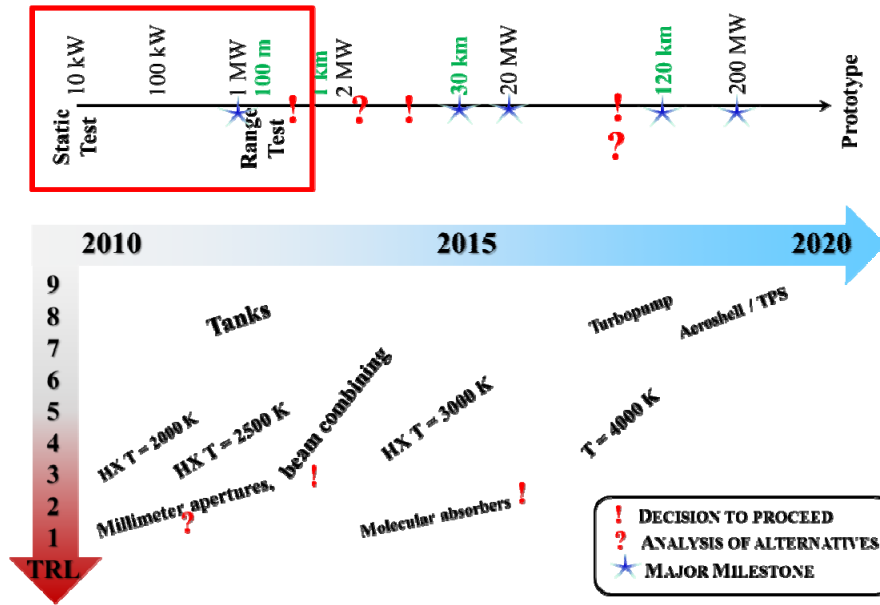


Figure 3.121.—Microwave thermal launch roadmap.

3.1.8.11 Ground and Flight Demonstrations

To date, the development approach has been a series of tests progressing to higher power levels and greater realism. The primary objective of these tests is to identify and retire risks as early as possible in the program, and the corresponding milestones are given in the sections that follow. The secondary objective is use high-profile milestones amenable to media coverage to attract, involve, train and motivate a cadre of talented engineers and institutions needed to implement the full-scale microwave thermal launch system. Such milestones are listed in Table 3.39. Prestige and momentum are the keys.

TABLE 3.39.—KEY FACILITIES AND MILESTONES

Years	Power level	Type	Goals and milestones
2005 to 2007	200 W	Static	<ul style="list-style-type: none"> Microwave thermal principle demonstrated for first time. Nuclear-thermal class wall temperature of ~2000 K demonstrated with H₂ in single channel.
2010 to 2012	20 kW	Static	<ul style="list-style-type: none"> First operation of credit-card-size multichannel microwave thermal thruster Beat game-changing peak wall temperature of 2250 K, held for at least 3 min
2012+	1.2 MW	Static/free flight	<ul style="list-style-type: none"> Year 1: Beat Myrabo’s beamed-energy altitude record of 71 meters (set in year 2000) Year 2+: Grand Challenge to beat Goddard’s curve (and each other) using beamed-energy rockets
2014+	2 MW	Static/free flight	<ul style="list-style-type: none"> Year 1: “Breakthrough” in combining power of gyrotrons into single beam Year 2: Green light given for 20-MW facility.
2015+	Megawatt class	Exoatmopheric free flight using ABL	<ul style="list-style-type: none"> Year 1: ABL locks onto target; target generates thrust. Year 2+: ABL-propelled beamed-energy rocket reaches edge of space (e.g., 30-, 50-, or 100-km apogees). Picosatellite placed in orbit?
2016+	20 MW	Static/free flight	<ul style="list-style-type: none"> Year 1: 20-MW beam power achieved; exceeds most powerful laser ever constructed. Year 2: Beam propels largest rocket yet from California to Nevada; delivers bowl of petunias and airmail.
2019+	200 MW	Static/free flight	<ul style="list-style-type: none"> Year 1: 200-MW milestone achieved. Year 2+: Air-launched prototype achieves orbit for first time.

It is quite likely that the game-changing peak wall temperature of 2250 K will be achieved by 2012, so the rough-order-of-magnitude (ROM) cost for this first important milestone is at most \$250K. Beating Myrabo's altitude record entails constructing the beam facility, developing the steerable optics, and developing a small-scale pressure-fed test vehicle. Only the gyrotron portion of the 1-MW beam facility has been funded, and it lacks a power supply, container integration, cooling, steering optics and most important, all engineering personnel with expertise in these areas and a project manager. Therefore, the ROM cost for this milestone is estimated to be more than \$1M and less than \$10M. The necessary elements are already fairly well-defined and uncoupled, so they could be shared into parallel tasks starting in summer 2011 and integrated back into a final record attempt by early 2013 if no major obstacles are encountered.

3.1.8.11.1 200-W Static Test Stand

An initial test stand was built at Caltech by Parkin in 2005 and used to demonstrate the basic operating principle of microwave thermal propulsion for the first time. Numerical methods were developed to simulate the arrangement and predictions were shown to be consistent with measurements. If the hottest part of the tube seen in Figure 3.122 were attached to a nozzle, the vacuum specific impulse I_{sp} would be about 700 s.

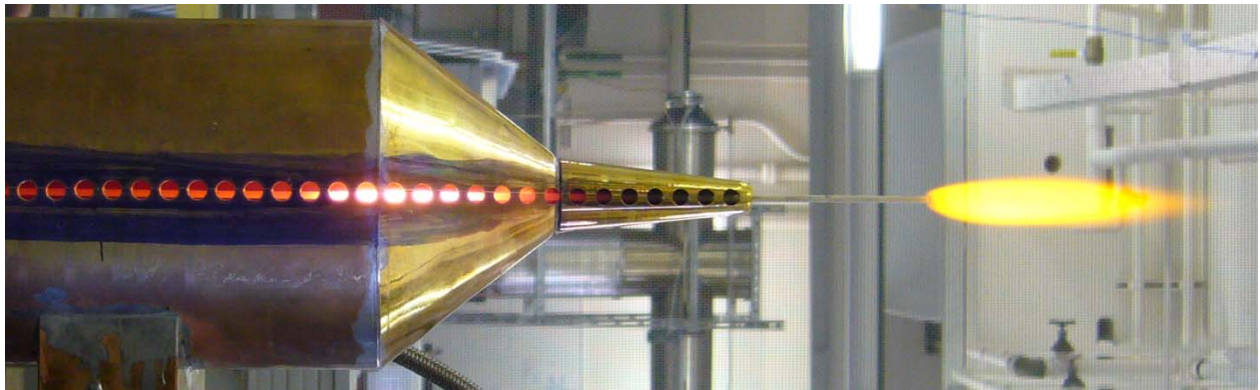


Figure 3.122.—Laboratory demonstration of microwave thermal heat-exchange principle in a 2.45-GHz resonant cavity (Ref. 12). Single mullite thermocouple tube with H_2 propellant. D_h , 1.19 mm; length of tube, L , 36.6 cm; inlet power, P_{inlet} , 1.1 bars; inlet Reynolds number, Re_{inlet} , 280; and peak wall temperature, T_{wall} , (1800 ± 100) K. The end of the tube was dipped in brine to make the hydrogen plume visible.

3.1.8.11.2 10-kW Static Test Stand

The next evolutionary step has been to increase the power level from 200 W to 10 kW, move from a resonant cavity to a free-space power-beaming geometry, move from a single channel to multichannel HX, and add a simple nozzle. Owing to various administrative constraints at Carnegie Mellon and the NASA Ames Research Center (ARC), it was necessary to substitute a floodlight for a microwave source and helium for the hydrogen propellant. As part of his graduate research at Stanford, David Murakami has used the test stand to bring the microchannel aluminum HX shown on the right of Figure 3.123 up to its melting point. In the next few months, he will remake the HX from graphite and run to refractory wall temperatures. In particular, this arrangement will be used to explore the temperature limits and oxidation rates of SiC and ZrO_2 coatings. A similar specification of facility is under construction at Caltech by Escape Dynamics Inc (<http://www.escapedynamics.com>). It is expected to feature magnetrons instead of a floodlight.

The most successful HX approaches from these test stands will be carried forward and tested using the next generation of test stand.

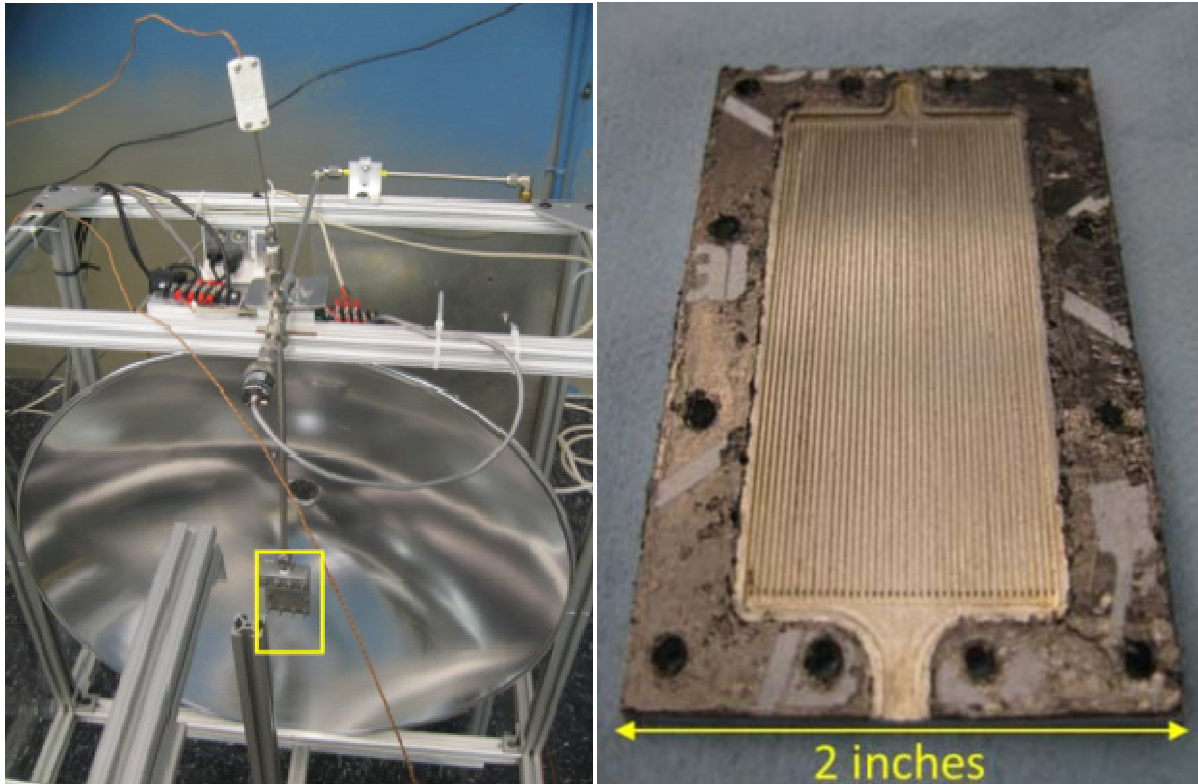


Figure 3.123.—Left: The 10-kW test stand uses a large parabolic mirror to concentrate the energy from a 20-kW tungsten light bulb onto a credit-card-sized HX (yellow box). Right: Aluminum proof-of-concept HX, soon to be attempted in graphite. Such small channel sizes and a credit-card size are necessary at this power level.

3.1.8.11.3 1.2-MW Portable Static/Free-Flight Test Facility

Many of the most important technical uncertainties surrounding a microwave thermal launch system can be addressed using a gyrotron beam facility. Most questions that have been raised in the course of DRM 1–C and others that were raised beforehand have been translated into a corresponding experiment in Table 3.40, which is the preliminary experiment roster for the gyrotron beam facility. The outcome of most of these experiments is believed to be known, nevertheless they affirm important assumptions and need to be demonstrated.

ARC has procured a \$2M gyrotron for this facility, and it is due to arrive in April 2012. The gyrotron facility CONOPS is based on Figure 3.124, a scene from the 2009 Space Elevator Games in which Jordin Kare and Lasermotive won \$900K for propelling a laser-powered vehicle up a helicopter-suspended ribbon. In observing the proceedings, it was most striking that every subsystem involved was containerized and mobile, from the test control van to the beam source and power supply.

The “organizational template” for this beam facility is that of a wind tunnel: a facility provided by the government for academic and industrial users to visit. It has been too expensive for any one team of developers to buy and maintain, yet it is needed by all for progress to be made. This is a type of public-private partnership with a clear interface and a proven track record.

TABLE 3.40.—PRELIMINARY EXPERIMENT ROSTER FOR THE GYROTRON BEAM FACILITY

Experiment name	Test type	Description
Dirt	Static	Effect of dirt on optics. Measure absorption coefficient as function of time. Determines cleaning interval to prevent unacceptable absorption loss/temperature buildup.
Coherent doppler	Static	Investigate operation of coherent Doppler transponder in a high-particle medium (HPM) environment. Measure downrange position and determine methods to mitigate interference, should it arise.
Bandwidth	Static	Measure actual bandwidth of gyrotron and compare with theory to determine whether theory is adequate to predict bandwidth of 170-GHz models. Will be needed for spectral beam combining design.
Propagate	Dynamic	Measure atmospheric scintillation and absorption properties if relevant studies similar to Etcheverry do not exist
Striate	Dynamic	Investigate ionospheric effects such as striation on beam using reflection for orbital test spheres. Only do this if studies in relevant regime do not exist.
Fresnel strip	Static	Investigate design of Fresnel reflector primary and/or secondary by assembling a 0.5-m-wide cross section on the ground and measuring optical characteristics in one dimension.
Active panel	Static	Investigate various active panel concepts at full-scale and power loading for final aperture.
HX ^a	Static	1-MW HX tests—measure peak wall temperature with imaging pyrometer, mass flow rate, thrust, and material reflectance versus temperature versus angle using ellipsometer
HX vehicle ^a	Dynamic	Dynamic tests of 1-MW vehicle, beginning with one-dimensional ribbon-guided leading up to unconstrained ascent to < 150 m. Longer distances may be attempted with larger and faster optics
Surface breakdown	Static/dynamic	Define stability boundary of surface breakdown
Thermal blooming	Static/dynamic	Analog of intensity
Tracking	Dynamic	Verify the tracking accuracy of a large aperture slewed to a fast-moving target.
HX	Static	Measure the temperature of the HX with multiple low-power beams incident on its surface. Also measure any intermodulation products produced at the transmitter or the HX.

Given that ARC is located in the heart of Silicon Valley and can only support static tests, the containerized CONOPS enables the whole facility to be periodically relocated to support free-space tests at China Lake Naval Air Weapons Station (NAWS) and other locations as needed. Preliminary discussions with China Lake have affirmed that short-range testing is relatively straightforward and can be accomplished with the gyrotron(s) operated under delegated National Telecommunications and Information Administration (NTIA) authority. Sky-facing beams would be scheduled via the laser clearing house at Vandenberg, as has been the procedure for ABL, the Space Elevator Games, and so forth. A preliminary visit to the Bircham Mesa site formerly considered for the 1995 SELENE power beaming project revealed the presence of Indian petroglyphs in that area. For this reason and others, Junction Ranch is a more likely initial test location within the China Lake NAWS base.

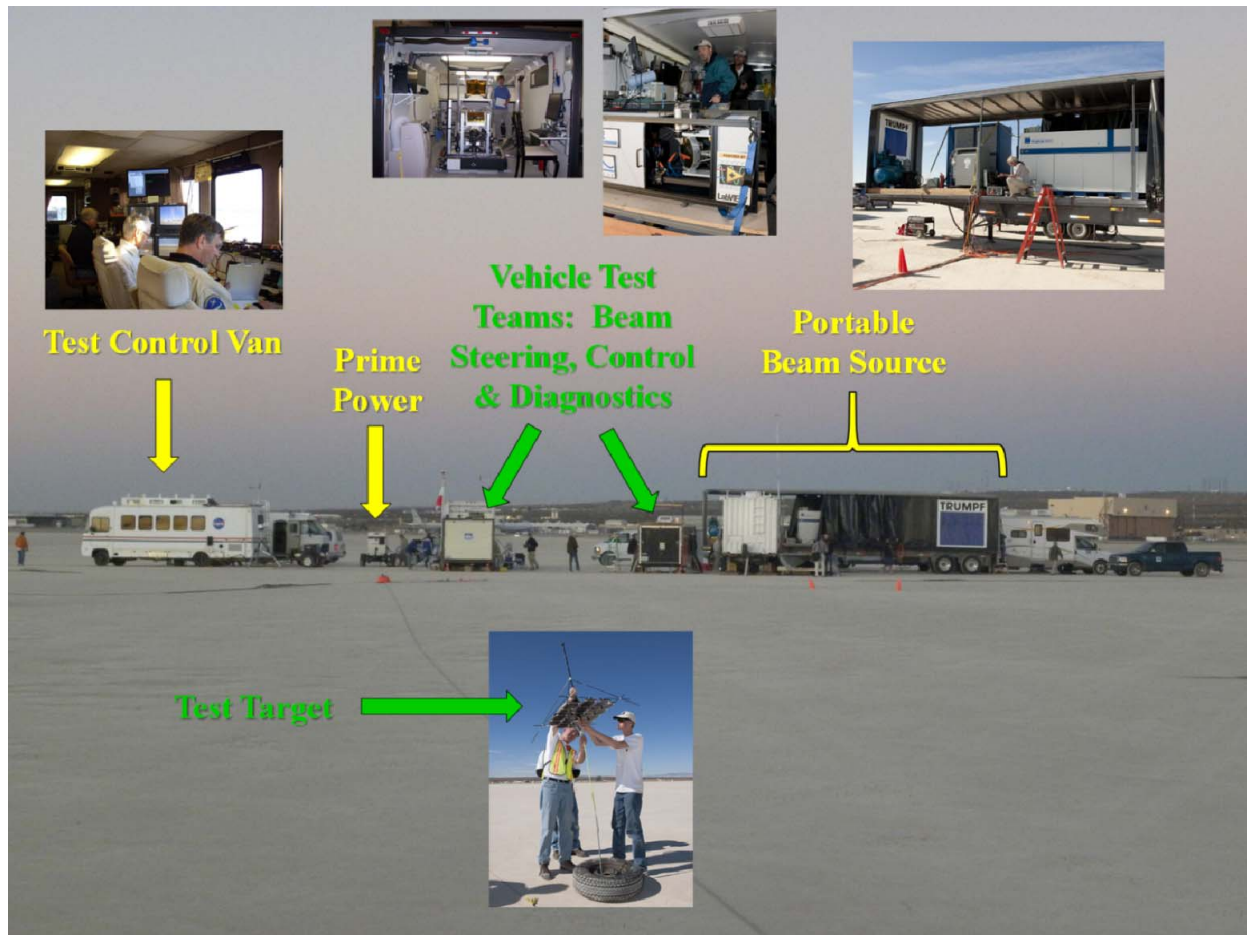


Figure 3.124.—Scene from the 2009 Space Elevator Games, with prize money provided by the NASA Centennial Challenges program. The containerized, mobile, and flexible CONOPS was a great success.

A grand-challenge competition is possible using the 1-MW beam facility. At this power level, the rocket sizes and attainable altitude are comparable with those of Goddard’s early flights. A competition could leverage the prestige associated with being a rocket pioneer, this time for beamed-energy rockets. Figure 3.125 shows the altitude attained by Goddard’s test launches from 1925 to 1936, with two record-breaking launches in particular defining a rate of progress to beat. The timer might be started by the first team to beat Myrabo’s record of 71 m, set over a decade ago. Thereafter, teams would compete against Goddard’s rate of progress and each other.

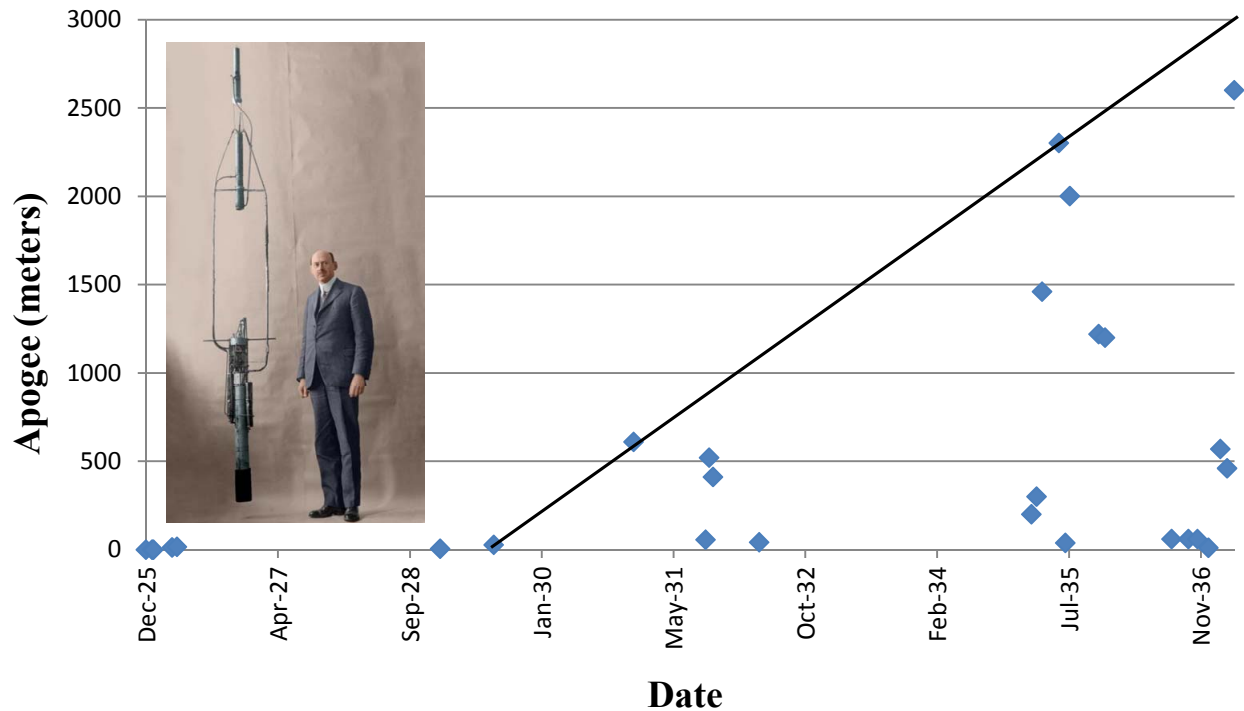


Figure 3.125.—Goddard’s progress in rockets and altitude from 1925 to 1936 suggests the scale, timeframe, number of trials and success rate at which a microwave thermal rocket might be expected to develop. Each data point is a launch attempt; some more successful than others.

From the perspective of achieving an operational microwave thermal launch system, there are several benefits to a prize-based approach at this stage of development. First, it attracts and trains the workforce subsequently needed to implement a full-scale microwave thermal launch system. Second, it enables a more thorough exploration of the heat-exchanger/vehicle tradespace prior to vehicle scale-up. Third, it allows all the concepts to be measured to the same standard at roughly the same time. Fourth, if it is judged by outsiders to be a definitive stepping-stone, it is likely to bring in outside investment equivalent to about 10 times the prize purse. And fifth, the spirit of competition could be a powerful accelerator of the development roadmap presented here.

3.1.8.11.4 2-MW Portable Static/Free-Flight Test Facility

This facility is an evolution of the 1.2-MW facility to include a second gyrotron of nearly the same frequency combined with the first into a single beam via a diffraction grating. If increased power for short-range testing is of limited interest at this stage, it might be possible to accomplish the objectives of this stage by combining with one or more gyrotrons from an external facility such as at General Atomics in San Diego.

3.1.8.11.5 MW-class Exoatmospheric Free Flight Test Capability (ABL)

After the 2-MW beam facility demonstrates beam combining, but before the decision to proceed with a 20-MW facility, it will be advantageous to use ABL to retire various risks associated with transatmospheric operation.

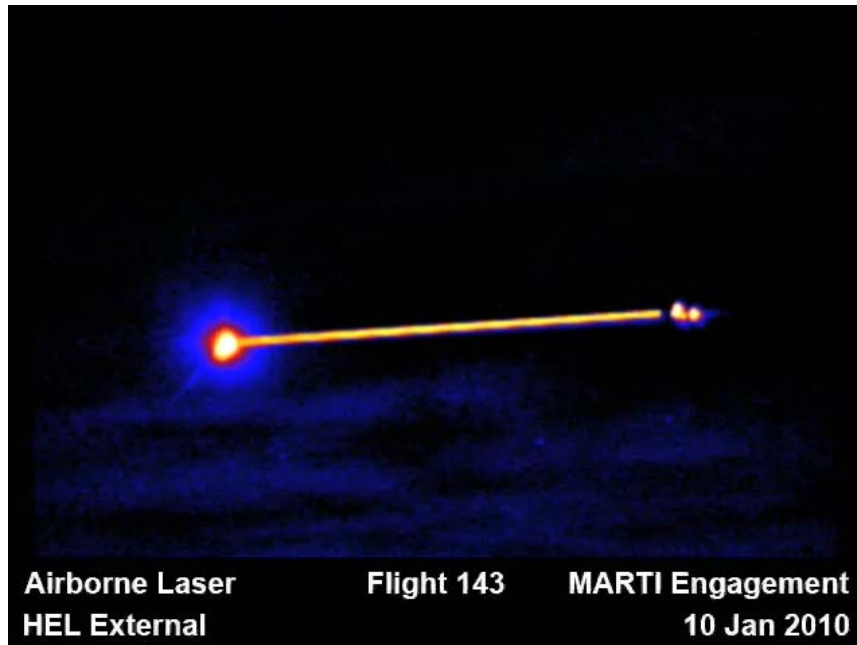


Figure 3.126.—Thermal image of the ABL (right) engaging a dummy target (left) graphically demonstrates that a shaky, slewing platform can lock onto and track a distant target ascending to orbit. What if the uncooperative dummy were replaced by a cooperative thermal rocket? HEL, High Energy Laser; .

In particular, ABL could be used in combination with a small-scale demonstrator vehicle to validate HX performance at altitudes of about 10 to 100 km. Depending on the particular power, spot size, and tracking accuracy of ABL, it may be possible to reach “space” (100 km) or even to place a picosatellite in orbit at this relatively early stage of the program.

3.1.8.11.6 20-MW Static/Free-Flight Test Facility

The purpose of the 20-MW facility will be to provide a subscale facility that is qualitatively similar to the large-scale facility in every way, such that the only problems anticipated in scale-up are those of resizing components according to established design rules. In addition to enabling sub-orbital hops, completion and successful operation of a beam facility at this scale will signal readiness for scale-up to a full-scale prototype.

3.1.8.11.7 200-MW Static/Free-Flight Test Facility

Construction of the full-scale prototype facility should be executed by a larger and more “operational” style team according to design rules established by earlier research-style teams. This facility will be at a dish diameter and power level sufficient to acquire an air-launched microwave thermal rocket and propel it from an altitude of about 20 km through to LEO.

Because the dish size will be slightly larger than needed for a higher power vehicle, the remaining step to transition from a prototype vehicle with small payload to a larger vehicle should mainly be to add more gyrotrons to the optical back end. It should not entail a new dish.

3.1.8.12 Issues and Resolutions

Minimum gauges.—Scaling a rocket down to these small sizes correspondingly decreases the thickness of the HX walls and Gr-Ep LH₂ tank walls to the point where the minimum gauges (minimum fabrication thicknesses) are reached. For the HX, the extra HX mass due to thicker-than-necessary walls was accepted. For the tank, the baseline material was changed from Gr-Ep to Ti, making the tank

relatively heavy but cheaper to make, and giving it considerable room to become smaller without reaching minimum gauge.

Thermal blooming.—In verifying propagation characteristics of the millimeter-wave beams, Manning found that thermal-blooming effects were not negligible as previously assumed for the size and power level of beams considered in this study. The calculations show that corrections will probably need to be made for the beam bending into the wind (which can be corrected by a tracker) and, possibly a few orders of aberration. This will add some extra complexity to one of the mirrors in the optical back-end.

Nozzle.—For the HX pressures under consideration, the conventional nozzle was found to have unacceptably low I_{sp} at low altitudes. This was resolved by replacing it with a plug nozzle.

Heat transfer.—The COMPASS study predicted temperature differences between the HX channel wall and bulk flow of up to 800 K based on the relatively poor heat transfer of smooth-walled tubes. Though only briefly mentioned in the COMPASS report, this number may generate concern, so it is addressed here: The thermal engineer did not have time to take into account surface roughness, which considerably improves heat transfer by disrupting the laminar sublayer surrounding the turbulent core flow, essentially destroying a layer of insulation. For example, Parkin predicts that the 40- μm surface roughness of the Teledyne woven channels reduces the temperature difference between inner channel wall and flow to less than 100 K in the regime of interest. Various additional mitigations could be used including narrowing the channels, patterning the channel surface to rotate the flow, periodically weaving “high-k” carbon fibers across the flow channel to conduct heat from the surface directly into the core flow, refractory foam / porous flow heat exchange for the final 200 K of heating, and various other mitigations. Data from the heat exchange experiments at 200 W was very carefully compared to theory. A similar process will soon be underway at 10 kW, and static tests at 1, 20, and 200 MW will afford many opportunities to make sure that a minimal temperature drop between the channel wall and bulk flow is realized.

Birds and lost aircraft.—The vicinity of the beam will be monitored by radar, if something was about to enter the beam, the beam could momentarily dodge the obstacle and power could be reduced or be turned off if needed. If a bird flew toward the center of the beam near the ground and did not turn around as the intensity increased, it would eventually experience about 20 suns equivalent of heating and presumably die quickly of effects related to that. It is something that we would want to avoid as much as birds hitting cars, turbines, windmills, and so forth. Thankfully, the beam facilities will be located at dry, high-altitude sites where birds tend not to live, and data quantifying the probability of birds interrupting a launch is relatively easy to gather. Migrating birds can achieve remarkable altitudes, so for planning purposes, we would consult maps of North American flyways—the seasonal migration routes taken by particular species.

Horizontal and low-angle propagation.—The atmospheric scale height of atmospheric water vapor (distance over which the concentration of water vapor decreases by a factor of e) is about 1.5 km because water is a relatively heavy molecule. This means that most of the beam absorption that occurs does so close to the ground. For this reason, horizontal propagation over more than a few kilometers from a boost beam facility only looks attractive for high optical quality sites such as Atacama, and not from China Lake, California. One potential mitigation is to reduce the frequency of the boost facility, reducing horizontal attenuation but increasing the boost dish diameter. Another option is to use just a single sustain beam facility (Figure 3.127) in combination with an airbreathing first stage (or solid rocket, or N_2H_4 propellant dual mode approach). The key question in sizing the first stage cutoff altitude is the angle at which propagation of the beam becomes erratic (adversely steered by water vapor gradients) or attenuation reduces the beam energy to less than 30%. This issue needs further analysis prior to an airbreathing first-stage study.

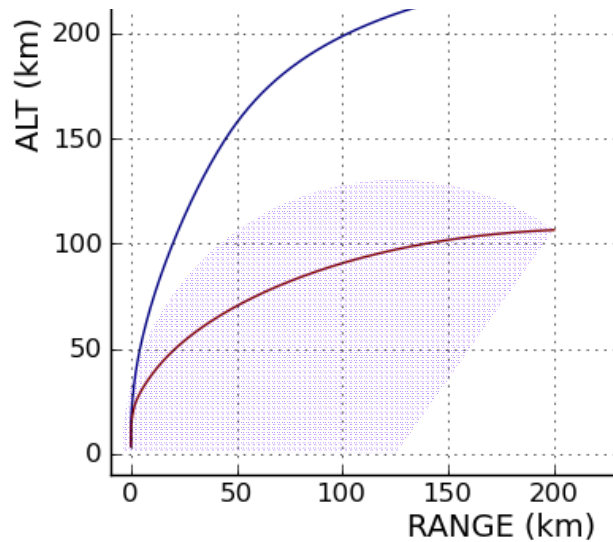


Figure 3.127.—A single beam facility sized for a 130-km range could, in principle, illuminate a rocket throughout the entire ascent trajectory. The areas within the beam facility range are shaded purple, and the baseline ascent trajectory is the red (lower) line. A key unknown is the minimum practical elevation angle at which the beam could acquire the rocket on liftoff (ALT, altitude).

Primary aperture size, slew rate, and surface accuracy. In short, the beam facility primary aperture needs to be about the size of the GBT, at a surface accuracy better than GBT but worse than ALMA, and at a slew rate about 4 times the maximum of CCAT. High slew rates are not needed for astronomical dishes. Because the GBT active surface already corrects for gravitational sag as the dish slews, it is reasonable to expect that at low slew rates the more modern active surface control approach of ALMA, if applied to a larger dish, could still maintain the same surface accuracy across it. If any factor prevents the realization of high surface accuracy across a large dish, it will most likely be the transient response of the dish structure to the high slew rate. If the transient response cannot be fully compensated using the existing active surface, additional mitigations could be passive or active. Passive mitigations include a more rigid structure, more extensive use of carbon fiber composites, and collapsing the dish down into a flat Fresnel reflector, which would probably reduce cost also. Active mitigations include a second level of larger displacement actuators behind the dish surface to correct for bulk motion. There may also be lessons to be learned from the ABL optical stabilization system. Ideally, a beam facility conceptual design will be needed that involves the engineers who designed the GBT, ALMA, and/or CCAT telescope structure and active surfaces.

Millimeter-wave electrical breakdown. Electrical breakdown due to high power radiofrequency (RF) fields (i.e., a gigawatt millimeter wave) is possible if the electric field strength exceeds the breakdown strength of the surrounding media. Air breakdown with pressures in range of 760×10^{-6} torr have been studied and are fairly understood. The most widely accepted formula that combines the effects of pressure and frequency is the W.C. Taylor work (Ref. 12). This was experimentally confirmed by several researchers and was found to be quite accurate over a large parameter space. Figure 3.128 shows experimental data from Massachusetts Institute of Technology's 110-GHz gyrotron oscillator experimental facility.

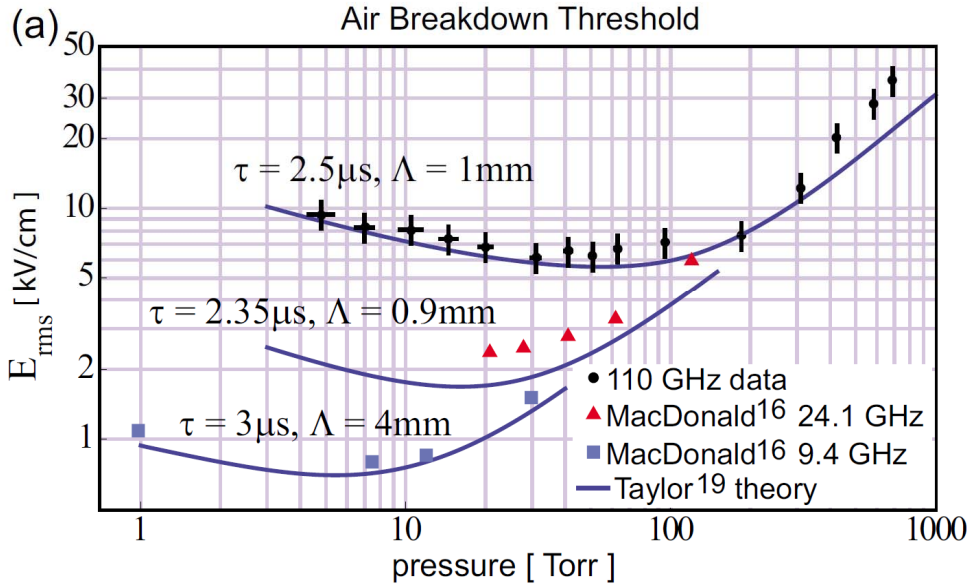


Figure 3.128.—Comparison of Taylor theoretical equation with experimental data (Ref. 13).

Extrapolating both the theoretical and experimental data, results in a minimum RF breakdown strength for bulk air of 2.5 to 3 MW/m² at 70 torr and 170 GHz. This extrapolation is for bulk air only and does not account for surface flashover effects, field enhancements (surfaces and structures), high-temperature surfaces (>2500 °C), or aerosols (dust, etc). Each of these adds additional complexity to the breakdown problem. Although the effect of each of these additional parameters has been studied, extrapolating the data to frequency and power levels required for this program is difficult.

The secondary parameter most studied for its effect on RF breakdown is surface flashover. Many studies have been performed on surface flashover in the 2- to 140-GHz range, but few, if any, have been published in the 170-GHz range. The main effect seen in the lower frequency range has been a flattening of the breakdown curve in the low-pressure regime (i.e., breakdown remains at the Paschen minimum even as the pressure is reduced from 10s of torrs to 10⁻⁶ torr). Some studies also suggest a possible reduction of the overall breakdown strength at a surface by a factor of 2, but it is not clear from this research whether the reduction is due to unique surface physics or simply to field enhancement effects. Figure 3.129 shows experimental data illustrating this phenomenon. In any event, the dominant role of surface flashover is in the low-pressure regime, on the left-hand side of the curve. In the high pressure regime (right-hand side of the curve), the role of surface flashover seems to be at the minimum and is most likely due to surface defects and roughness causing localized field enhancements.

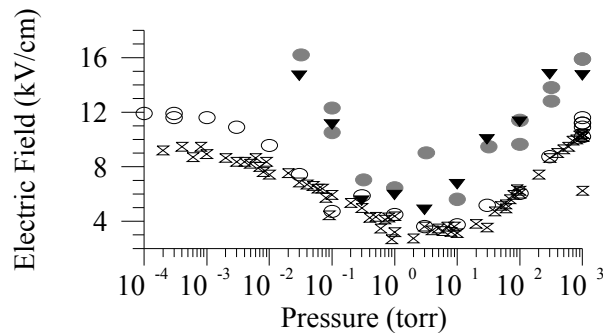


Figure 3.129.—Pressure versus RF breakdown field strength at 2.4 GHz (Ref. 14). Solid symbols denote bulk air, and open symbols denote with surface.

Much less data are available in the 170-GHz range of the effects of aerosols and/or dust on electrical breakdown strength. This topic has been well studied and documented in the optical range, but no data has been published in the millimeter-wave regime. From a theoretical perspective and extrapolating optical data and trends, the effect of dust on electrical breakdown was predicted to be of minimal impact until the particle size approaches a significant fraction of a wavelength. At smaller sizes, the localized electric field (on the surface of the individual particle) remains unperturbed and relatively small. Extrapolation and physical arguments are less certain and more complex for aerosols, where possible chemical reactions and polar molecules are likely to be found. In this environment, wavelength-dependent effects can be seen in single molecules. Although studies at optical wavelengths have shown the effects of aerosols to be of secondary concern, some testing laboratory will be required at 170 GHz to determine safe operating conditions with a high confidence level.

The effect of high-temperature surfaces on millimeter-wave breakdown is the least studied and least understood. Only a single reference (Ref. 15, M. Golden et al.) has been identified that contains some experimental data at microwave frequencies. The experimental data in this paper was limited to the effects on breakdown of a hot wire at 1200 °C in a 5-GHz cavity (Figure 3.130). Combining the observed decrease in breakdown strength with other papers and later theory indicates that the primary effect was due to variations in gas density near the hot surface. Electron emission is also thought to play a role, but additional data will be required to quantify what role this emission will play and in what regime it will be the most significant.

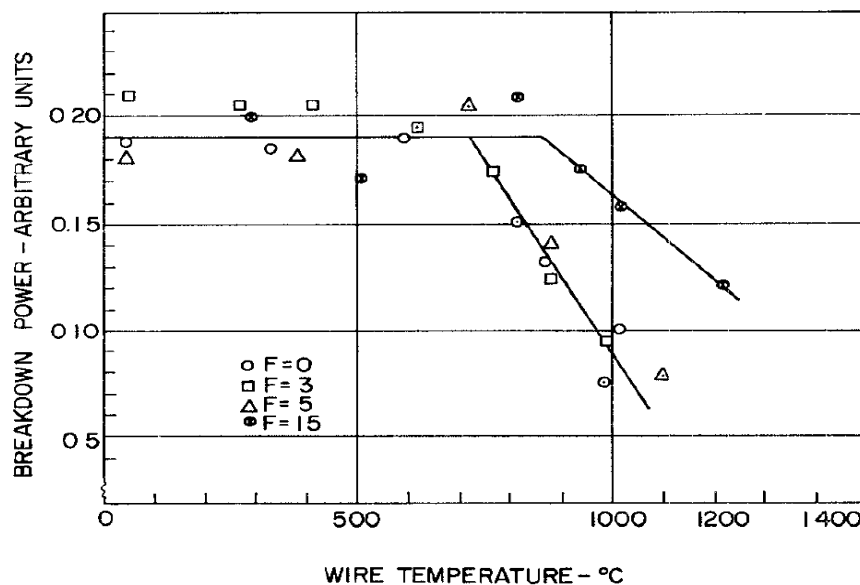


Figure 3.130.—Results of breakdown measurements with a hot wire in the presence of gas flow (Ref. 15).

3.1.8.13 Launch Window Analysis

Launch opportunities are constrained by the weather and the potential for beam conjunction with a LEO satellite. The weather at potential beam facility sites has been relatively well studied by astronomical site surveys. Table 3.41 shows that weather at the CONUS site examples given in Figure 3.131 is sufficiently good, with more than 50% probability of suitable weather at any given time.

TABLE 3.41.—WEATHER AT THE CONUS SITE EXAMPLES GIVEN IN FIGURE 3.131)
 [Only nighttime data were published because the data were taken for an astronomical site survey.]

	% of night with clear sky	% of night with transitional sky
Pikes Peak, CO	64	11
Mt. Evans, CO	54	15
Jelm Mountain, WY	32	18

A beam-satellite conjunction analysis was very kindly carried out by Dr. James Mason at ARC. His results, listed shortly, show that space is big—you could launch continuously and only once or twice a day would you hit a satellite with more than 0.1 suns of illumination intensity. Even then, it would last for only about 0.2 s because of the large relative velocities between the beam and satellite. In reality, those conjunctions would be predicted and avoided.

3.1.8.14 Conjunction Analysis Results for Equatorial Launch

Launch into 36° inclination from China Lake. Launches were simulated every 4 min for 8 days. Each intersection between the microwave beam and background satellites was recorded. On average, there were 5.25 intersections per day, each for 0.2 s.

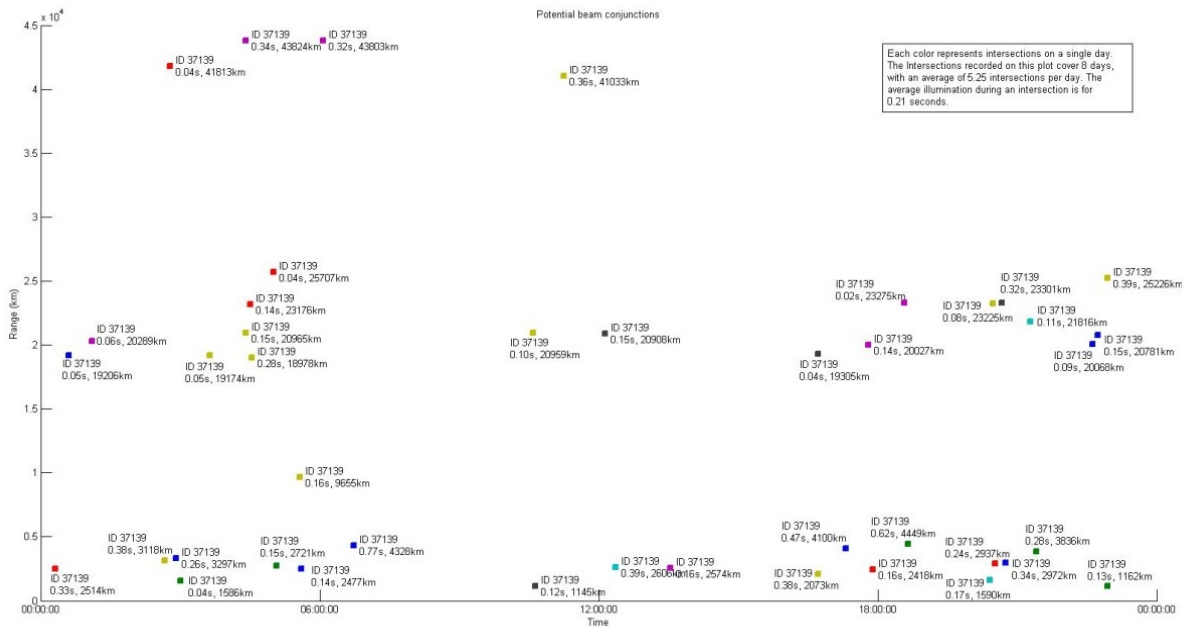


Figure 3.131.—Launch time versus range of intersecting satellite. Each color represents a single day of launches (i.e., the 8 days are overlaid). The North American Aerospace Defense Command (NORAD) satellite ID is listed along with the intersection duration and range.

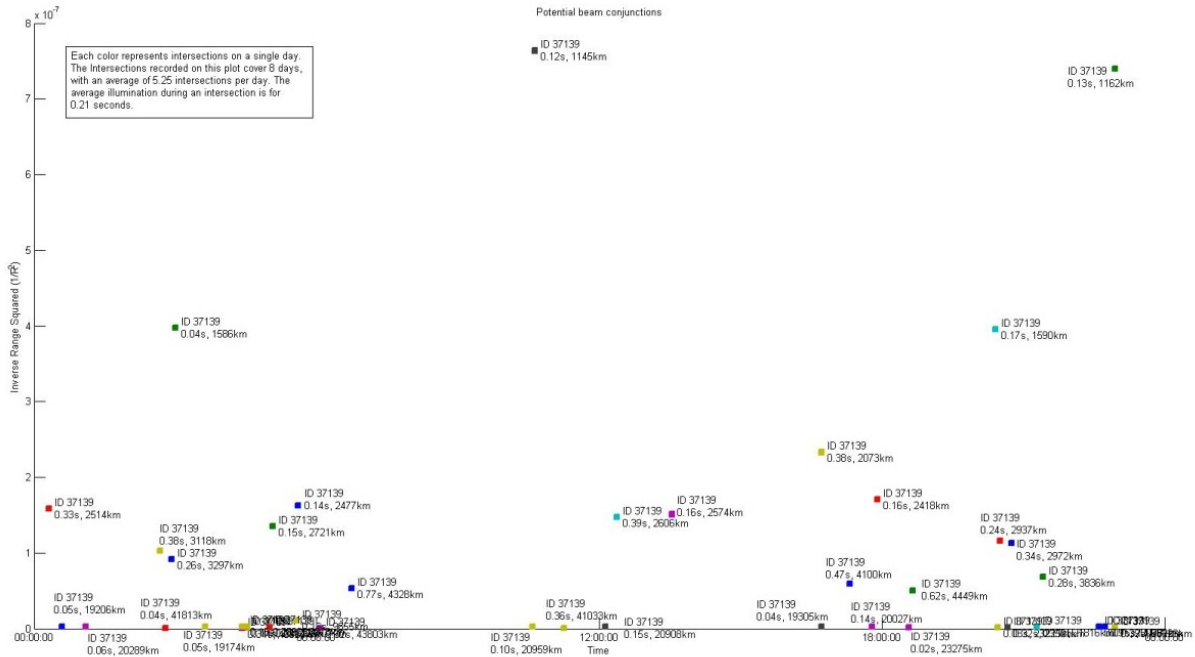


Figure 3.132.—Launch time versus inverse range squared ($1/R^2$) of intersecting satellite. Each color represents a single day of launches (i.e., the 8 days are overlaid).

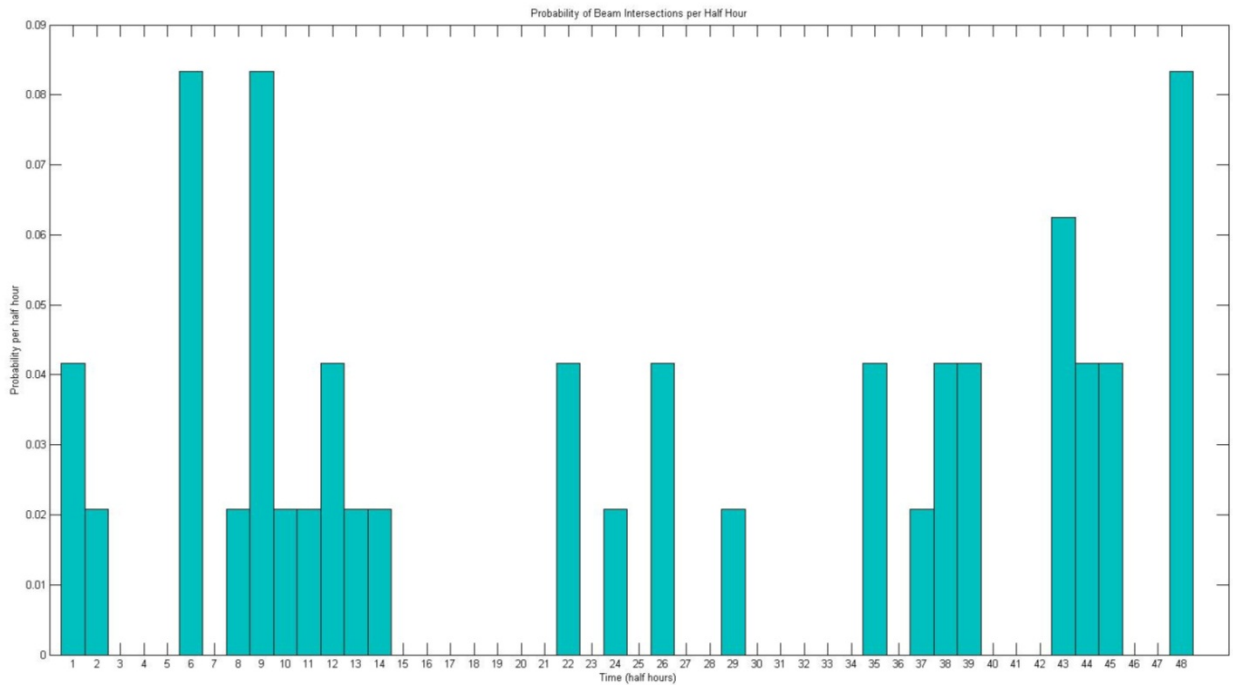


Figure 3.133.—Probability of an intersection happening in each half hour period, over the 8 days.

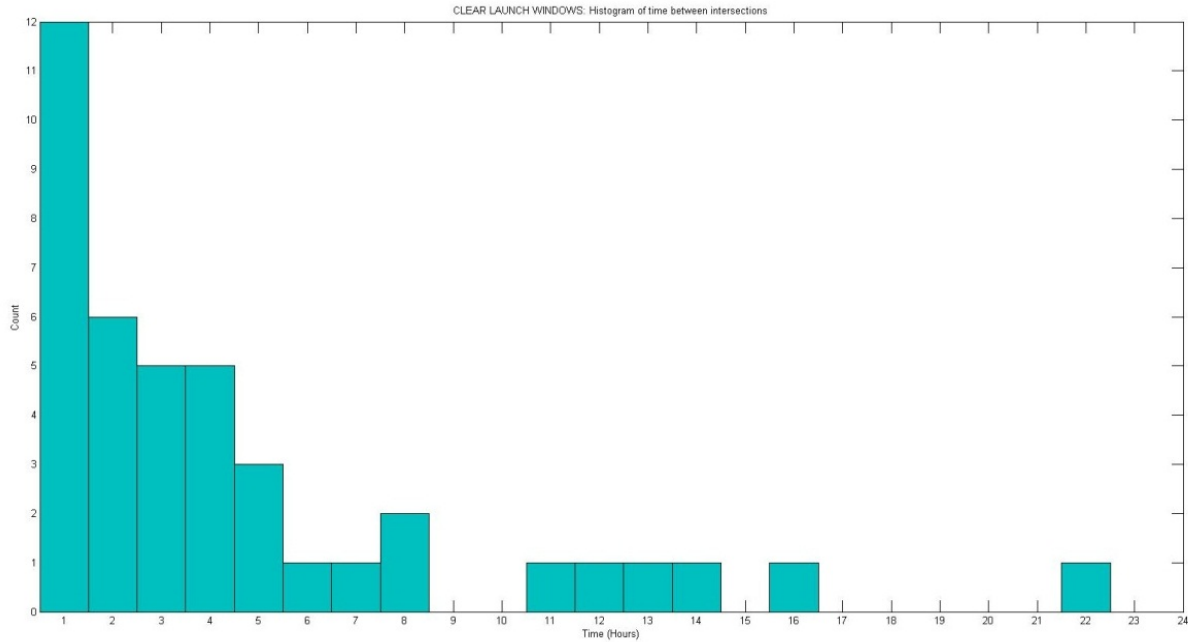


Figure 3.134.—Histogram of clear launch windows—periods that have no intersections. Over the 8 days there were 29 periods with more than 1 hr of clearance.

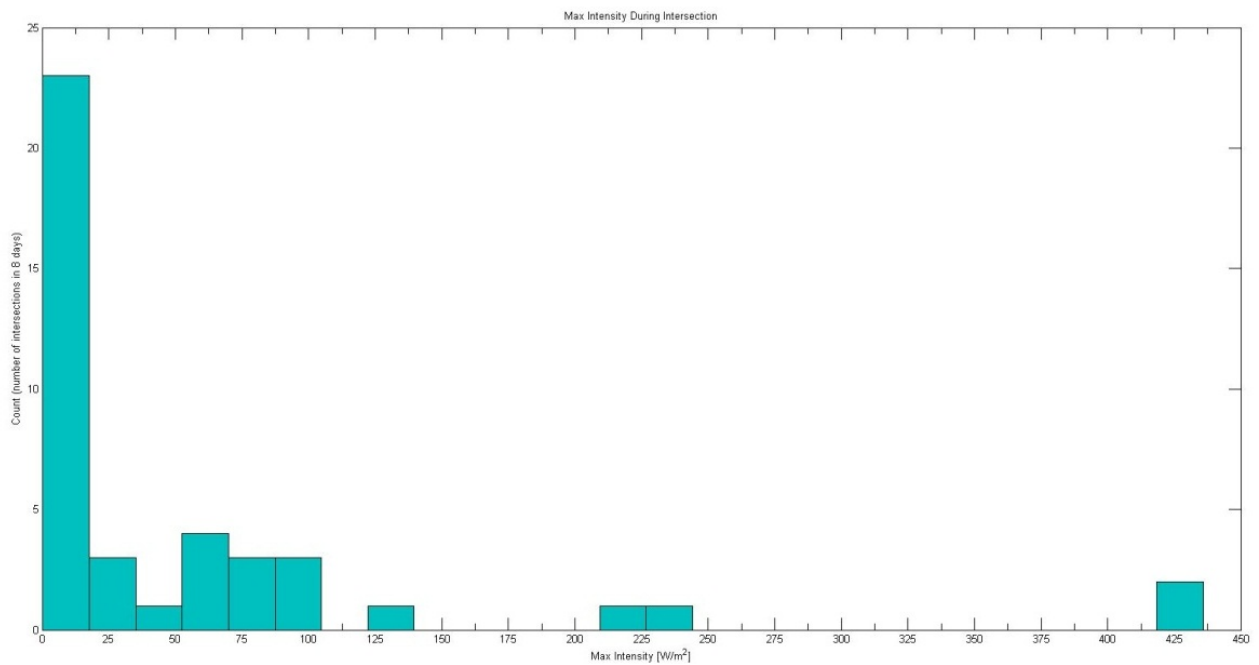


Figure 3.135.—Histogram showing the distribution of intersection maximum intensity, I_{max} , during the 8 days. Note that most days have I_{max} less than 100 W/m^2 (i.e., 8% of solar constant).

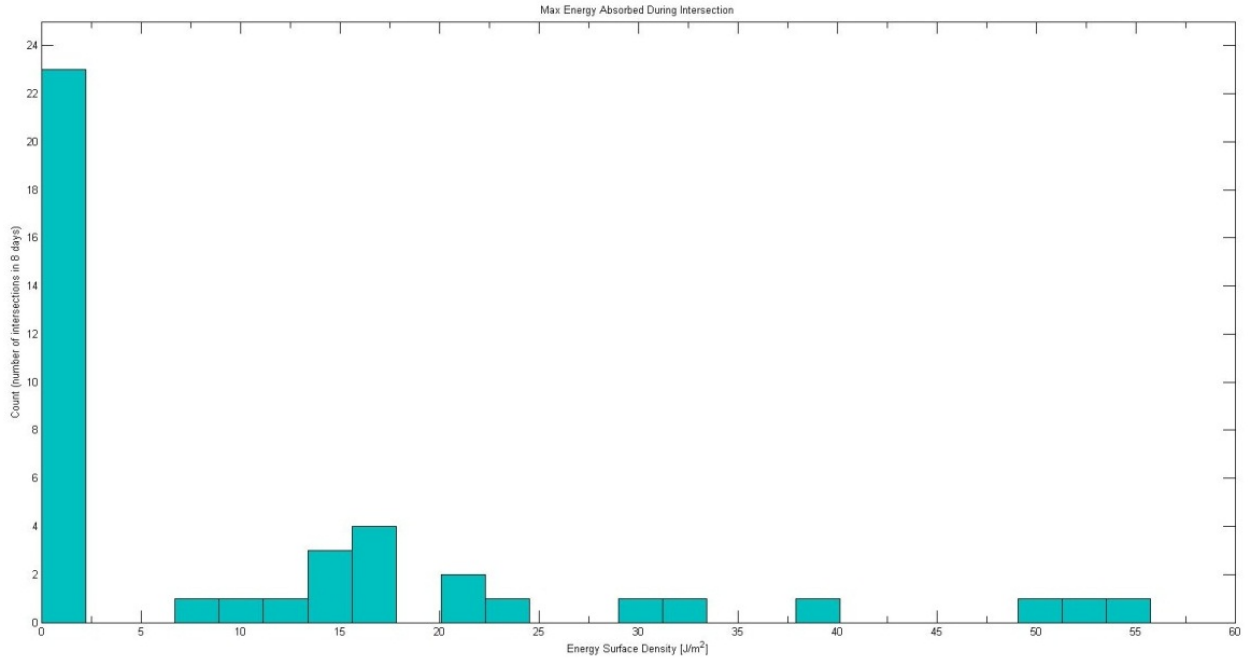


Figure 3.136.—Histogram of the maximum energy incident on a satellite per square meter during an intersection. This was calculated using $I_{\max} \times$ intersection duration.

3.1.8.15 Conjunction Analysis Results for Sun Synchronous Orbit

Direct launch was into a 98° Sun-synchronous inclination from China Lake. Launches were simulated every 4 min for 8 days. Each intersection between the microwave beam and background satellites was recorded. On average, there were 12.75 intersections per day, each for 0.03 s.

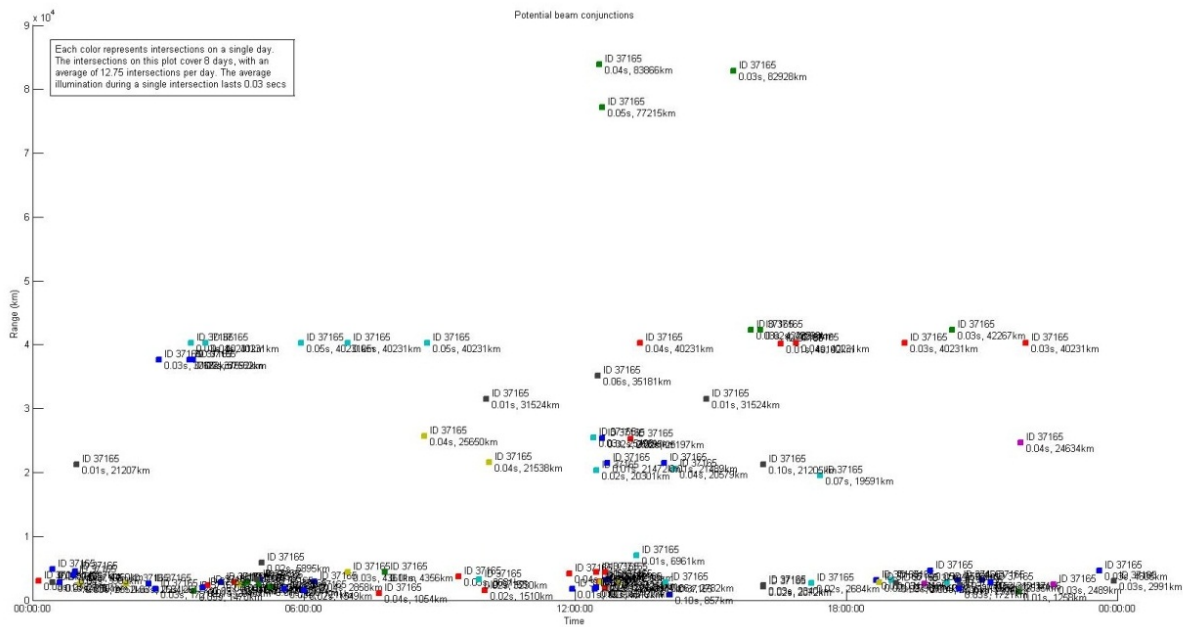


Figure 3.137.—Launch time versus range of intersecting satellite. Each color represents a single day of launches (i.e., the 8 days are overlaid). The NORAD satellite ID is listed along with the intersection duration and range.

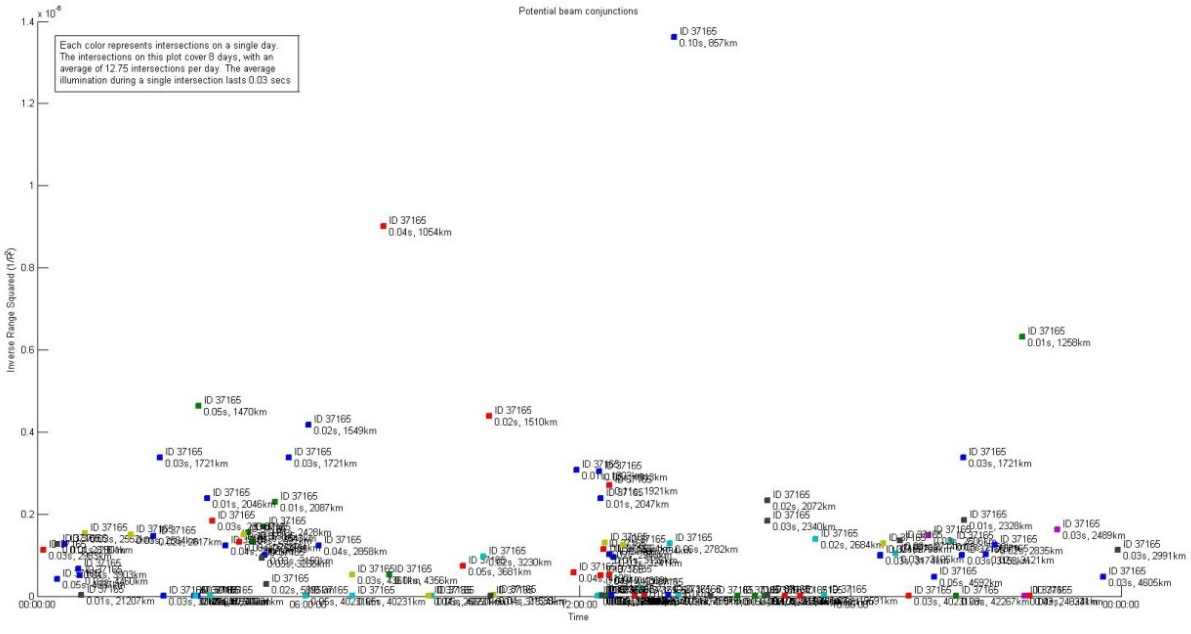


Figure 3.138.—Launch time versus range of intersecting satellite. Each color represents a single day of launches (i.e., the 8 days are overlaid). The NORAD satellite ID is listed along with intersection duration and range.

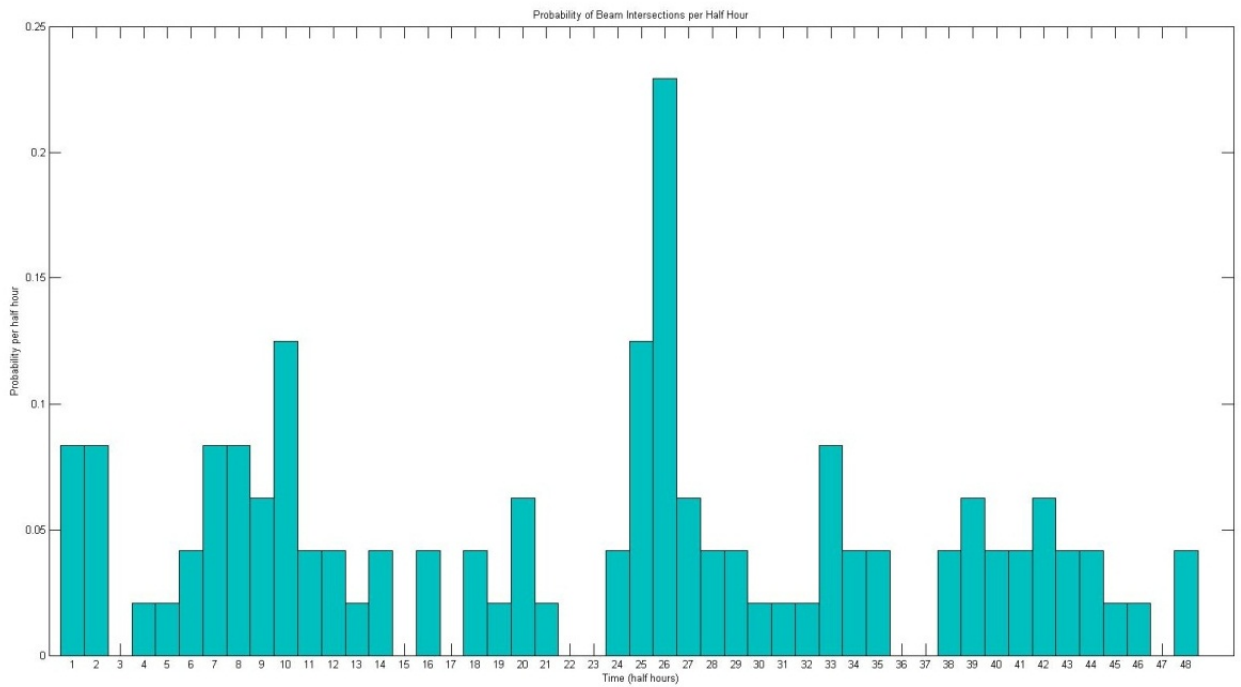


Figure 3.139.—Probability of an intersection happening in each half-hour period, over the 8 days.

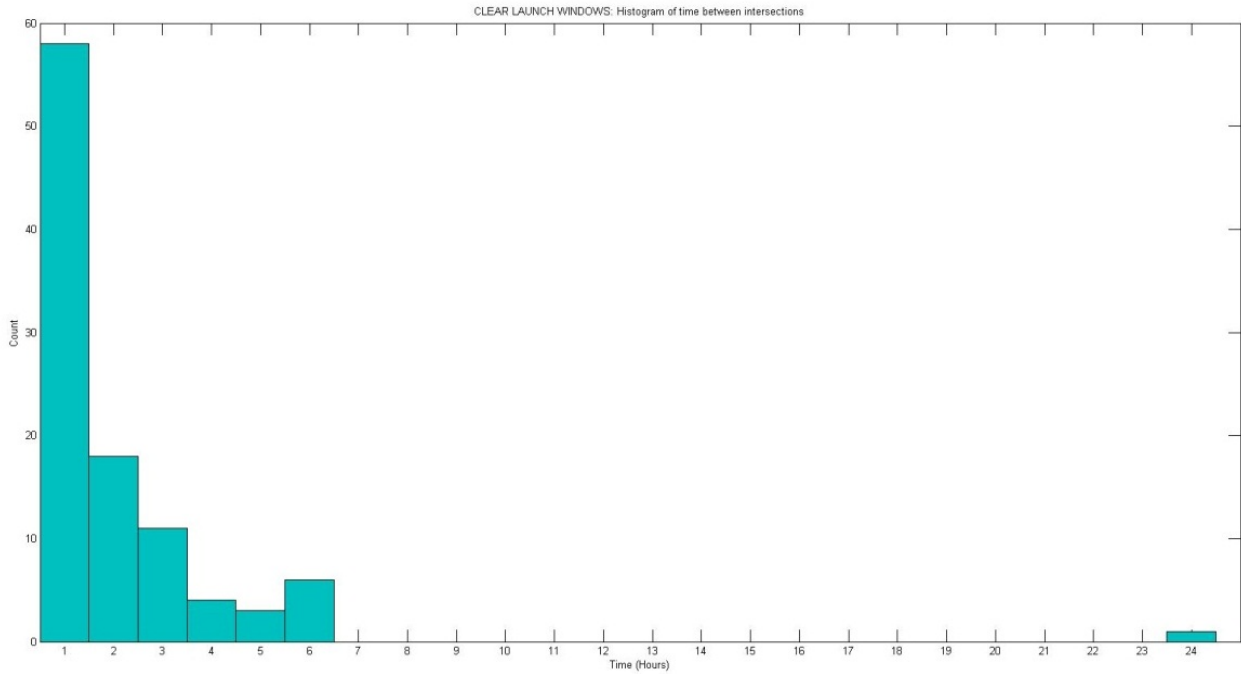


Figure 3.140.—Histogram of clear launch windows—periods that have no intersections. Over the 8 days, there were 41 periods with more than 1 hr of clearance.

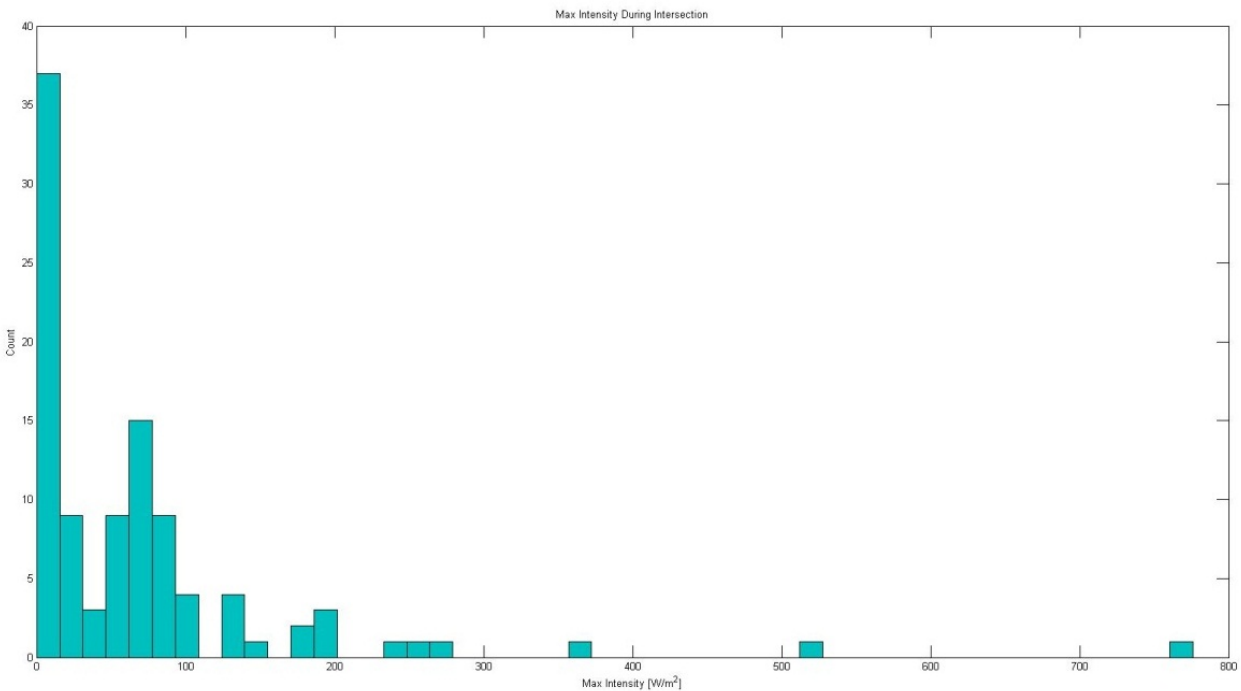


Figure 3.141.—Histogram showing the distribution of intersection maximum intensity during the 8 days. Note that most have I_{\max} less than 200 W/m² (i.e., 15% of solar constant).

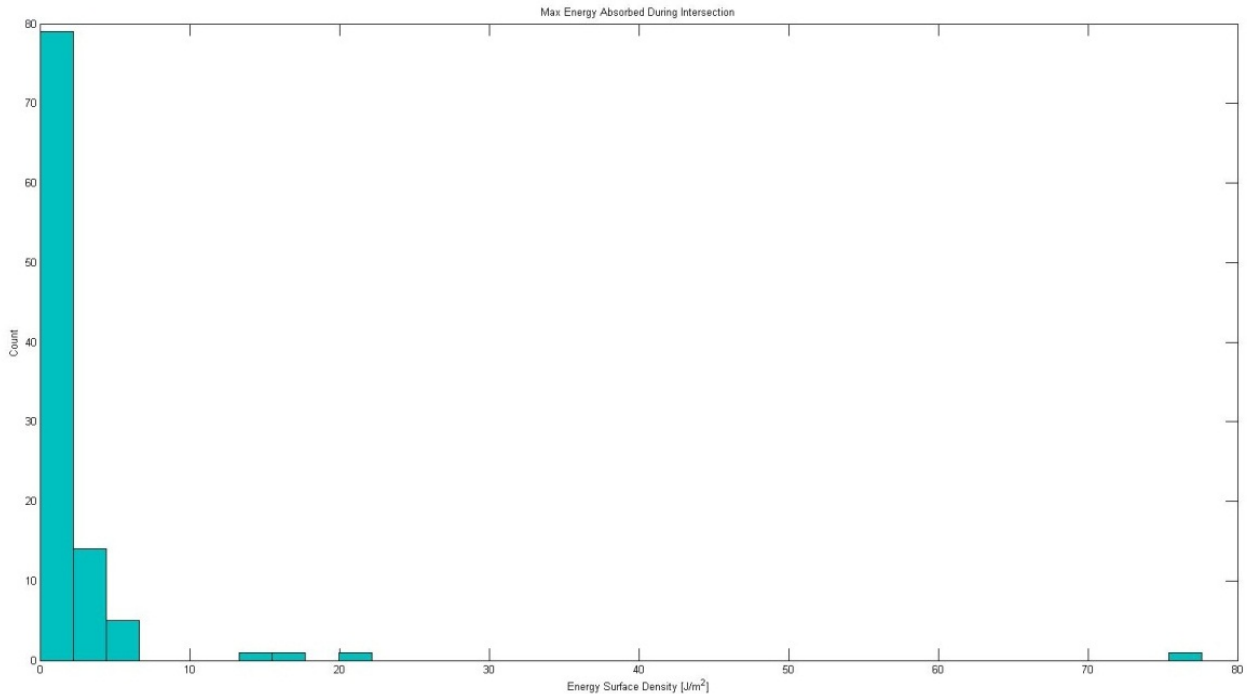


Figure 3.142.—Histogram of the maximum energy incident on a satellite per square meter during an intersection. This was calculated using $I_{max} \times t$, where t is the intersection duration.

3.1.8.16 Beam-Combining Analysis

There are several ways of combining the power output of millimeter-wave sources, including

- Master Oscillator Power Amplifier (MOPA) beam combining
- Phase-locked oscillators
- Temporal beam combining
- Spectral beam combining

The first and second approaches require the millimeter-wave sources to have a systematic phase relationship between them (mutual coherence). For MOPA, this is achieved by a single oscillator producing a wave that is amplified by a large number of amplifiers. This approach is not as financially attractive as combining the output of a large number of oscillators because amplifiers are more expensive per watt of output.

The high cost of amplifiers would make phase-locking oscillators together look more attractive. The phase locking of two oscillators is achieved by leaking some of the signal from oscillator A into oscillator B and vice versa, with the exact conditions described by Adler’s relation. Unfortunately, gyrotron oscillators are highly overmoded structures of many wavelengths across resonating far from their fundamental frequency, so this type of phase locking would require fundamental research to accomplish in a reliable way.

Temporal beam combining is best suited to sources that are optimized for pulsed operation. Since the available gyrotrons are CW, it was not considered here or elsewhere.

Spectral beam combining is the reverse of splitting white light into a rainbow using a prism or diffraction grating. This technique is commonly used in the telecommunications industry. A reflective metal grating is used to combine the gaussian beams from a large number of gyrotron oscillators of slightly different frequencies and incident angles into a single gaussian output beam (which can subsequently be directed to the rocket via a telescope). The physics of diffraction gratings has been well understood for over 200 hundred years.

The maximum number of gyrotron beams that can be combined this way is equal to the spectrometer resolution R , which is a function of their frequency f and bandwidth Δf . For ~170-GHz step-tunable gyrotrons with a bandwidth of 70 MHz, this means that

$$R \equiv \frac{\lambda}{\delta\lambda} \cong \frac{\delta f}{f} = \frac{70 \text{ MHz}}{170 \text{ GHz}} = 2428 \text{ gyrotrons}$$

This number would be reduced by practical considerations and unusable bands in the atmospheric absorption peaks. Nevertheless, a 20-GHz band from 150 to 170 GHz (Figure 3.114—Figure 3.131) could in principle support 285 gyrotrons, each with its own 70 MHz of bandwidth. For 4-MW gyrotron oscillators, that corresponds to more than 1 GW of power in total. If more power is needed, lower and higher wavelengths and/or additional dishes could be used, depending on which option minimized cost. One of the difficulties with diffraction gratings at optical wavelengths has been fabricating the fine grooves, which are spaced approximately a wavelength apart, and achieving high efficiency. At 170 GHz, the grooves could be made by an end mill and are 1.8 mm apart. For combining ~2500 gyrotron beams, 3092 grooves total would be needed, making the grating length about 5.7 m. The grating would not need to be a single piece and could be milled in sections and then mounted to a water-cooled backing plane. Because it is possible to achieve high tolerances and reflectance, the beam-combining losses are expected to be only 1 to 2 percent of the incident energy. Belousov et al. (Ref. 16) measure less than 1% energy loss in combining a 70- and 79-GHz beam. This kind of performance should be demonstrated with many simultaneous frequencies. Earlier it was suggested that this could be demonstrated at low power using IMPact ionization Avalanche Transit-Time (IMPATT) diodes.

3.1.8.17 References for Millimeter-Wave Thermal Consultant Report for DRM 1–C

1. Marshall; and Cox: Integral Textile Ceramic Structures, 2008.
2. Wasko, Robert A.: Performance of Annular Plug and Expansion-Deflection Nozzles Including External Flow Effects at Transonic Mach Numbers. NASA TN–D–4462, 1968.
3. Fleeman: Tactical Missile Design, 2001.
4. Thompson: 2009.
5. Young; and Olds: Responsive Access Small Cargo Affordable Launch (RASCAL) Independent Performance Evaluation, AIAA 2005–3241, 2005.
6. Access to Space Study. Summary Report, Office of Space Systems Development, NASA Headquarters, Washington D.C., 1994.
7. National Research Council: High-Temperature Oxidation-Resistant Coatings, 1970.
8. U.S. PTO patent application 2008/0286473, 2008.
9. Mangum: 2007.
10. Lohr, et al.: Operating Experience on Six 110 GHz, 1MW Gyrotrons for ECH Applications, 2008.
11. Kare, J.T.; and Parkin, K.L.G.: Comparison of Laser and Microwave Approaches to CW Beamed Energy Launch, Beamed Energy Propulsion. AIP Conference Proceedings 830, K. Komurasaki, ed., Melville, NY, 2006, p. 388.
12. Parkin, K.L.G.: The Microwave Thermal Thruster and Its Application to the Launch Problem. Ph.D. thesis, June, 2006.
13. Temkin, Richard: W-Band Breakdown Research. Kick-Off Meeting Counter High Power Microwaves, Albuquerque, NM, 2010.
14. Hemmert, David, et al.: High-Power Microwave Window Breakdown Under Vacuum and Atmospheric Conditions. Proc. SPIE 4031, vol. 90, 2000.
15. Gilden, M.; and Pergola, J.: Microwave Breakdown Near a Hot Surface. PTGTT National Symposium Digest, 1963, pp. 39–44. Belousov, V.I.; Denisov, G.G.; and Peskov, N. N. Yu: Quasi-Optical Multiplexer Based on Reflecting Diffraction Grating, Int. J. Infrared Millimeter Waves, vol. 12, no. 9, 1991.

3.1.9 Millimeter-Wave Thermal Cost Estimates

National Aeronautics and Space Administration



Beamed Energy Propulsion Facility ROM Cost Estimate

March 28, 2011

National Aeronautics and Space Administration



General BEPS Launch Facility Assumptions

- Launch site ROM estimates are based on a NASA KSC launch site estimating approach. Microwave and laser sites use the same approach for 'like function' facilities which are scaled for expected differences in size or function.
- All sites include site design and testing and activation costs.
- Launch facility design is estimated at 12% of estimated total site costs less testing and activation.
- Launch facility testing and activation is estimated at 30% of the capital facilities cost.
- Microwave and laser site design is estimated at 8% of estimated total site costs less testing and activation.
- Microwave and laser site testing and activation is estimated at 15% of the capital facilities cost.



General BEPS Launch Facility Assumptions

- All cost are rough order of magnitude (ROM) estimates in FY11M\$.
- Estimates assume all facilities are built new on government land, no existing infrastructure is used. Available infrastructure will reduce costs.
- Costs do not include remediation of potential significant environmental impact issues that may be identified.
- Range estimates are presented to highlight the uncertainty associated with the lack of definition and supporting cost information available at this time.
- Range estimates for the launch site also includes the uncertainty associated with the selected location and the cost impact of materials that may be required to protect against environmental conditions.



Operations Cost Assumptions

- All costs are estimated for one year of operation in FY11\$.
- Yearly operations cost assume 360 launches per year (one/day). Additional study is required to determine the feasible number of launches per year from a single launch pad. The number of launches per pad is affected by the CONOPS, pad turnaround time, launch facility maintenance, weather, and launch window requirements.
- Total estimated facility operations costs are assumed to be allocated to the beamed launch operations. Facility sharing can reduce costs.
- Facility equipment and maintenance is estimated at 5% of the total value of capital assets per year resulting in an estimated 70-80% of total operations costs.



Microwave Launch Site Assumptions

- **Launch Site facility requirements**
 - General – site work, roads
 - Support Facilities/Launch Pad – see details below
 - Site Infrastructure – water, fire, sewer, power, communications, HVAC, environmental control system
 - Ground support equipment
- **Key cost estimate assumptions**
 - New facility on government land in secluded area due to danger associated with beamed energy. Launch rate 1-4 vehicles a day, if CONOPS allows.
 - Launch pad includes all related hardware/services. Rocket will be small, approximately 9 meters in length, and less than 3,000 kg total wet mass with payload.
 - Command center includes all related services.
 - Payload integration facility (small payloads <200 kg) can process/integrate up to four payloads per day.
 - Hydrogen storage facility sized for ~30,000 kg with no on-site production.
 - Rocket storage facility size for 8 rockets.
 - Admin facility sized for launch site staffing needs (estimated at 100 people).
 - Security facilities/equipment includes fencing, cameras, etc.



Microwave Booster Station Assumptions

- **Microwave Booster Station facility requirements**
 - General – site work, roads
 - Support Facilities – admin facility (50 people), command center (75% of launch site center), guard gate facility
 - Site Infrastructure – water, fire, sewer, power, communications, HVAC, environmental control system
 - Ground support equipment
 - Beam Generation/Pointing – gyrotron field (300 MW + 10% reserve), antenna system (45m), beam combiner
 - Power Storage/Distribution – energy storage, power supply, power distribution
- **Key cost estimate assumptions**
 - Gyrotron/Power Supply cost – Current market \$2M per 1 MW based on NASA ARC information used as high, projected market information \$2M per 4 MW used as low, most likely estimated as \$2M per 2 MW
 - Energy Storage - \$50K/kWh estimated as most likely based on GRC experience with wind tunnels (low -40%, high +20%)
 - Antenna System - \$50K/m² (Ref: J. Kare, \$40K/m² escalated) used as low (ML +50%, high +100%)



Microwave Sustaining Station Assumptions

- Microwave Sustaining Station facility requirements
 - General – site work, roads
 - Support Facilities – admin facility (50 people), command center (75% of launch site center), guard gate facility
 - Site Infrastructure – water, fire, sewer, power, communications, HVAC, environmental control system
 - Ground support equipment
 - Beam Generation/Pointing – gyrotron field (600 MW + 10% reserve), antenna system (120m), beam combiner
 - Power Storage/Distribution – energy storage, power supply, power distribution
- Key cost estimate assumptions
 - Gyrotron/Power Supply cost – Current market \$2M per 1 MW based on NASA ARC information used as high, projected market information \$2M per 4 MW used as low, most likely estimated as \$2M per 2 MW
 - Energy Storage - \$50K/kWh estimated as most likely based on GRC experience with wind tunnels (low -40%, high +20%)
 - Antenna System - \$50K/m² (Ref: J. Kare, \$40K/m² escalated) used as low (ML +50%, high +100%)



Microwave Launch Facility Development ROM

Microwave Beamed Energy Launch Facilities ROM (FY115M)
(Excludes FTE/WVE personnel and O&M costs)

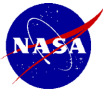
	Launch Site Complex - ROM Subtotal (\$M)				Booster Station Site - ROM Subtotal (\$M)				Sustaining Station Site - ROM Subtotal (\$M)				Microwave Launch Facilities - Total ROM (\$M)			
	Low	ML	High	Mean Est.	Low	ML	High	Mean Est.	Low	ML	High	Mean Est.	Low	ML	High	Mean Est.
Project Total ROM (\$M)	\$324.5	\$553.9	\$1,224.4	\$701.0	\$851.4	\$1,446.7	\$2,605.7	\$1,634.6	\$1,781.0	\$3,088.3	\$5,316.4	\$3,395.2	\$2,956.5	\$5,088.0	\$9,146.5	\$5,730.8
Design	\$28.2	\$47.9	\$105.1	\$60.4	\$55.6	\$94.5	\$170.1	\$106.7	\$116.1	\$201.2	\$346.4	\$221.2	\$199.9	\$343.6	\$621.6	\$388.4
Testing & Activation	\$61.6	\$106.8	\$243.3	\$137.2	\$100.3	\$171.2	\$379.8	\$193.8	\$213.7	\$371.4	\$640.4	\$408.5	\$375.5	\$649.4	\$1,193.5	\$739.5
Microwave Launch Facilities ROM Subtotal	\$294.8	\$399.2	\$876.0	\$503.3	\$695.5	\$1,181.0	\$2,125.8	\$1,324.1	\$1,451.2	\$2,515.6	\$4,329.6	\$2,765.5	\$2,381.5	\$4,095.0	\$7,331.4	\$4,602.9
WBS Item																
Site Work	\$11.2	\$15.4	\$18.8	\$15.1	\$8.4	\$11.6	\$14.1	\$11.3	\$8.4	\$11.6	\$14.1	\$11.3	\$27.9	\$38.6	\$47.0	\$37.8
Roads	\$18.4	\$27.9	\$46.2	\$30.8	\$18.4	\$27.9	\$46.2	\$30.8	\$18.4	\$27.9	\$46.2	\$30.8	\$55.3	\$83.7	\$138.6	\$92.5
Support Facilities	\$32.4	\$68.5	\$134.7	\$78.5	\$7.1	\$14.9	\$36.1	\$19.4	\$7.1	\$14.9	\$36.1	\$19.4	\$46.7	\$98.4	\$206.8	\$117.5
Concrete Administration Facility	\$7.4	\$10.8	\$28.5	\$13.7	\$3.7	\$5.4	\$14.2	\$7.7	\$3.7	\$5.4	\$14.2	\$7.7	\$14.7	\$21.5	\$57.0	\$29.2
8 Rocket Storage Facility	\$5.6	\$7.5	\$12.2	\$9.0	\$0.0	\$0.0	\$0.0	\$0.0	\$0.0	\$0.0	\$0.0	\$0.0	\$5.6	\$7.5	\$12.2	\$9.0
Concrete Command Center	\$3.3	\$10.4	\$25.3	\$12.5	\$2.5	\$7.8	\$19.0	\$9.0	\$2.5	\$7.8	\$19.0	\$9.0	\$8.3	\$26.0	\$63.4	\$31.3
Payload Integration Facility	\$15.2	\$38.1	\$65.8	\$40.0	\$0.0	\$0.0	\$0.0	\$0.0	\$0.0	\$0.0	\$0.0	\$0.0	\$15.2	\$38.1	\$65.8	\$40.0
Guard Gate Facility	\$1.0	\$1.8	\$2.8	\$1.0	\$1.0	\$2.8	\$1.0	\$1.0	\$1.0	\$2.8	\$1.0	\$1.0	\$2.8	\$1.0	\$2.8	\$1.0
Pad Structure	\$13.1	\$19.5	\$24.3	\$19.0	\$0.0	\$0.0	\$0.0	\$0.0	\$0.0	\$0.0	\$0.0	\$0.0	\$13.1	\$19.5	\$24.3	\$19.0
Pad Structure	\$4.3	\$6.2	\$8.4	\$6.3	\$0.0	\$0.0	\$0.0	\$0.0	\$0.0	\$0.0	\$0.0	\$0.0	\$4.3	\$6.2	\$8.4	\$6.3
Emergency Egress System	\$0.0	\$0.0	\$0.0	\$0.0	\$0.0	\$0.0	\$0.0	\$0.0	\$0.0	\$0.0	\$0.0	\$0.0	\$0.0	\$0.0	\$0.0	\$0.0
Flame Trench	\$6.7	\$8.0	\$8.8	\$7.8	\$0.0	\$0.0	\$0.0	\$0.0	\$0.0	\$0.0	\$0.0	\$0.0	\$6.7	\$8.0	\$8.8	\$7.8
Lightning Protection Towers	\$2.1	\$5.3	\$7.0	\$4.8	\$0.0	\$0.0	\$0.0	\$0.0	\$0.0	\$0.0	\$0.0	\$0.0	\$2.1	\$5.3	\$7.0	\$4.8
Infrastructure	\$132.8	\$221.1	\$545.5	\$299.8	\$88.5	\$138.3	\$254.2	\$160.3	\$88.5	\$138.3	\$254.2	\$160.3	\$309.7	\$497.7	\$1,063.8	\$620.4
OSF	\$26.9	\$46.8	\$106.5	\$60.1	\$6.7	\$11.7	\$26.6	\$15.0	\$6.7	\$11.7	\$26.6	\$15.0	\$40.4	\$70.2	\$159.8	\$90.1
Beam Generation/Pointing Equipment	\$0.0	\$0.0	\$0.0	\$0.0	\$388.5	\$593.1	\$1,023.5	\$661.7	\$926.5	\$1,544.2	\$2,502.1	\$1,657.4	\$1,295.0	\$2,337.2	\$3,525.5	\$2,318.8
Power Storage/Processing Facilities	\$0.0	\$0.0	\$0.0	\$0.0	\$197.8	\$383.5	\$725.2	\$435.5	\$395.5	\$767.0	\$1,450.4	\$871.0	\$593.3	\$1,150.6	\$2,175.7	\$1,306.3



Microwave Launch Facility Operations ROM

Microwave Launch Facilities Operations ROM (FY11\$M/Year)
(Does not include launch vehicle)

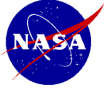
	Microwave Launch Operations - Total ROM (\$M/Yr)			
	Low	ML	High	Mean Est
Microwave Operations Total ROM (\$M/Year)	\$155.7	\$260.3	\$439.7	\$285.2
Facility/Equipment Maintenance	\$114.9	\$198.7	\$357.3	\$223.6
Operations Personnel	\$30.0	\$40.0	\$50.0	\$40.0
Propellant/Energy/Consumables	\$10.8	\$21.6	\$32.4	\$21.6
Other	\$0.0	\$0.0	\$0.0	\$0.0
Launch Site Complex - ROM Subtotal (\$M/Year)	\$28.9	\$45.0	\$76.4	\$50.1
Facility/Equipment Maintenance	\$10.3	\$17.8	\$40.6	\$22.9
Operations Personnel	\$15.0	\$20.0	\$25.0	\$20.0
Propellant/Energy/Consumables	\$3.6	\$7.2	\$10.8	\$7.2
Other	\$0.0	\$0.0	\$0.0	\$0.0
Booster Station Site - ROM Subtotal (\$M/Year)	\$44.5	\$74.3	\$126.6	\$81.8
Facility/Equipment Maintenance	\$33.4	\$57.1	\$103.3	\$64.6
Operations Personnel	\$7.5	\$10.0	\$12.5	\$10.0
Propellant/Energy/Consumables	\$3.6	\$7.2	\$10.8	\$7.2
Other	\$0.0	\$0.0	\$0.0	\$0.0
Sustaining Station Site - ROM Subtotal (\$M/Year)	\$82.3	\$141.0	\$236.8	\$153.4
Facility/Equipment Maintenance	\$71.2	\$123.8	\$213.5	\$136.2
Operations Personnel	\$7.5	\$10.0	\$12.5	\$10.0
Propellant/Energy/Consumables	\$3.6	\$7.2	\$10.8	\$7.2
Other	\$0.0	\$0.0	\$0.0	\$0.0



Cost Assumptions



- **DRAFT Cost Estimate based on COMPASS design**
- **All costs are in FY11\$M**
- **Estimates represent prime contractor cost before fee**
- **This estimate assumes the following:**
 - Proto-flight development approach
 - No ground spares are included
 - Model assumes TRL Level 6
 - This estimate does not include any cost for technology development
 - Represents the mean estimate based on cost-risk simulation results
 - Parametric estimate based on mostly mass-based CERs from historical cost data
 - Launch vehicle systems integration wraps
 - Software not included
- **Does not include:**
 - Any insight/oversight costs (by a NASA lead center)
 - Reserves (can be as high as 40-50%)
 - Ground System Cost (ie. Microwave Station, Launch Pad, Booster Station, etc...)
 - Launch Services Costs (ie. Special launch approval process)
 - Technology costs for components lower than TRL-6



Microwave Launcher Preliminary Cost ROM

(Represents estimated Prime Contractor cost)

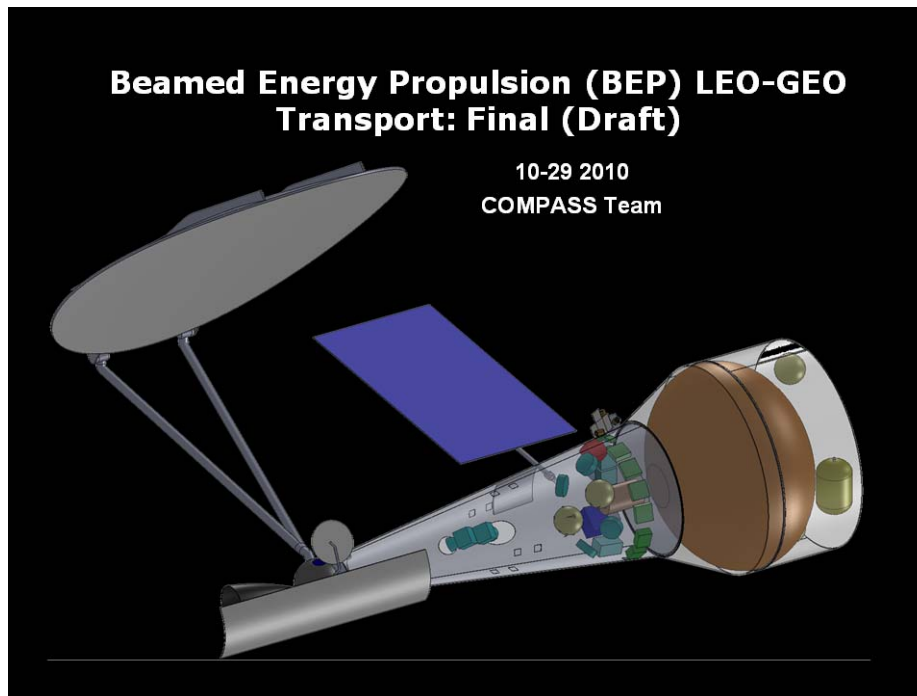


WBS	Description	DDT&E Total BY \$M	Flight HW BY \$M	DD&FH Total BY \$M
06.1	Payload	0.0	0.0	0.0
06.2.1	Attitude Determination and Control	6.4	4.8	11.2
06.2.2	Command and Data Handling	4.7	2.7	7.4
06.2.3	Communications and Tracking	1.8	1.3	3.0
06.2.4	Electrical Power Subsystem	1.7	1.2	2.9
06.2.5	Thermal Control	12.6	2.3	14.8
06.2.6	Propulsion	14.6	2.5	17.1
06.2.7	Propellant	0.0	0.0	0.0
06.2.8	Structures and Mechanisms	11.0	5.6	16.6
	Subtotal	52.7	20.3	73.0
	Systems Integration	57.0	8.1	65.2
	Spacecraft Total	109.7	28.4	138.1

All Costs in FY11\$M

3.2 Space Design Reference Missions

3.2.1 Low-Earth-Orbit to Geosynchronous-Earth-Orbit Collaborative Modeling for Parametric Assessment of Space Systems (COMPASS) Report



National Aeronautics and Space Administration



Team Roster



- Program Study Lead – Ray Beach, Pat George
- Study PI – Jon Black (AFIT)
- COMPASS Lead - Steve Oleson
- Lead System Integration, MEL, PEL - Melissa McGuire, David Grantier
- CONOPS, system integration – Jeff Woytach
- Mission – Laura Burke, Camille Moore
- Mission Visualization - Carl Sandifer
- GN&C – Mike Martini
- Laser Propulsion - James Fittje, Tony Colozza, Geoff Landis, Tom Haag
- Laser Atmospheric Propagation – Robert Manning
- Propulsion – James Fittje
- Mechanical Systems - John Gyekenyesi, Tom Haag
- Thermal - Tony Colozza
- Power - James Fincannon, Kristen Bury
- C&DH, Software- Glenn Williams
- Communications - Joe Warner
- Configuration and Launch Vehicle Integration - Tom Packard
- Cost - Jon Drexler
- Risk - Anita Tenteris

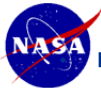


Beamed Energy Propulsion: Laser Launcher



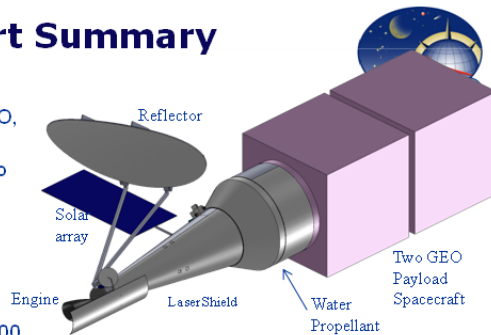
The COMPASS team has been tasked by DARPA/NASA to create an independent concept design for a Laser powered LEO-GEO re-useable transport. Determine size, number, placement of laser stations.

The COMPASS design will give the DARPA/NASA a point-of-reference to the feasibility of the concept and a what technologies and demonstrations need to be developed to support development of a re-useable laser tug.



Laser Transport Summary

- Reusable Laser powered Transport**
 - Can deliver two 1900 kg GEO birds to GEO, <10 day delivery
 - Propellant and Two GEO birds launched to 400 km, 9th LEO by Falcon 9
- Docking capability**
 - Assume payload and propellant a free-floating target (self shielding)
- Laser System**
 - Engine (6000° K, 5000 N), 810 s water (900 sec LH2 alternative)
 - Reflector ~3 x 5 M
- Other propulsion**
 - Adv. Monoprop for ACS/docking
- Power**
 - Solar array /batteries
- GN&C**
 - Perigee/Apogee burns—laser tangential to ground—5-15 minute burns— only point during burns— otherwise inertial pointing
- Comm/C&DH**
 - Stage housekeeping and control
- Thermal:** Highly Reflective shields for Transport stage, Propellant tank and payloads



Equipment List Rack-up (Mass) - BEP Inspace			COMPASS S/C Design
Main Subsystems	Basic Mass (kg)	Growth (kg)	Total Mass (kg)
BEP LEO GEO Inspace	9566	100	9666
Transport Stage	457	59	516
Attitude Determination and Control	53	6	59
Command and Data Handling	34	9	43
Communications and Tracking	7	2	9
Electrical Power Subsystem	20	6	26
Thermal Control (Non-Propellant)	116	14	130
Propulsion (Hardware)	144	12	156
Propellant (Chemical)	21		21
Structures and Mechanisms	63	11	73



Starting Requirements



- **Deliver to Two ~2300 kg spacecraft to GEO**
 - Equivalent payload for Two SOA Falcon 9 (Block 2)
- **Re-useable Laser Transport**
- **Outbound Trip Times <10 days**
- **Will Utilize ground based laser stations**
 - (~1MW for each 100N of Laser Engine)
- **Will emphasize simplicity and low cost**
- **Payload and Propellant launched on Falcon 9 - @ two per launch**
 - Allows launch cost savings

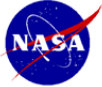


FOMs



- **Mass: Mass to GEO (>2000 kg)**
- **Trip Time: ~ 10 days**
- **Reliability: Gov't**
- **Cost: Halve Earth to GEO delivery costs**

- **Fault tolerance for vehicle**
 - Re-useable
 - Single Fault Tolerant



Past Designs



- Laser Electric Propulsion Studies (early 90's)
- Solar Thermal upper stage studies
- SLICK



Technology Options



- Laser Electric Propulsion
 - Specially laser tuned solar arrays (>50% efficient)
 - Direct drive to Hall thrusters (1500-2500 sec Isp, ~50% efficient)
 - Xenon propellant (dense, stored supercritical, ~\$1000/kg)
- Laser Thermal Propulsion
 - Laser reflector/concentrator to focus Laser beam
 - Laser thermal engine: Beam focused to center point in chamber, plasma ball
 - Allows very high temperatures (>10,000° - 15000° K?) TBR
 - Isps ~800-900 sec TBR
 - LH2: ~2000° K, 900 sec
 - H2O: >6,000° K TBR, 800 sec



Mission Options



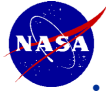
- **Impulsive Thrust**
 - Lower ΔV (~4.2 km/s) (less propellant)
 - Shorter but higher Laser bursts (~5mins)
 - Lots of coast times
 - High engine thrust level
 - ~5000N for 10 days to GEO
 - Laser power ~50 MW?
- **Continuous Thrust**
 - Higher ΔV (~6 km/s) (more propellant)
 - Continuous Illumination (Multiple laser stations)
 - Lower engine thrust level
 - ~50N for 10 days to GEO
 - Laser power ~500 kW?



Possible All Chemical Missions for Performance/Cost Comparison



- **Atlas 551**
 - ~3300 kg to GEO (S/C does apogee burn with on-board Bipropellant system (~328 sec Isp)
 - Atlas 551 costs: ~\$160M (FY2010)?
- **Sea launch**
 - 3000 kg? to Geostationary Orbit
 - Sea launch Costs: \$75-95M (FY2008)
- **Falcon 9**
 - 2500 kg To Geostationary Orbit
 - Falcon Launch Costs: ~\$50M (FY2010)
- **Comparison**
 - Falcon 9 launches two GEO birds plus propellant
 - Transport launched by Falcon 9 or 1?
- **Laser Station Costs:**
 - Assume Station exists – just use recurring costs for our use



Baseline for Comparison

- **SOA Geostationary Delivery**
 - Falcon 9 launched from Kwajalein, 9° inclination
 - Single ~2375 kg (not including Biprop Apogee system) payload S/C
 - Falcon 9 upper stage takes S/C to GTO, onboard biprop system performs final delivery to GEO
- **Laser Propelled Transport**
 - Falcon 9 launched from Kwajalein to 400 km circular (for better ground laser visibility)
 - Two ~1970 kg (less than SOA) GEO Payload S/C plus single water tank
 - Separate launch (dry) Transport vehicle
 - Falcon 9
 - Used 10 times
 - Transport (dry) should be ~ 600 kg (with margin)
- **Objective: reduced launch costs approaching 50%...**

1600kg MMH/NTO prop load. Results are 4 propellant tanks ~0.9m dia, two GN2 pressurant tanks (the 0.42m by 0.67m tank by ATK is basically an exact fit), and a SFT feed system. Total Mass: 146kg
 Total Inert: 133kg
 Total Dry: 96kg

Item	Mass (kg)
Q/D valves	2
Filter/Lines	6
Regulators	2
Valves	6
HP Valves	1.5
N2 Mass	37
Ox Mass	1000
Fuel Mass	605
N2 Tank	20
Ox Tank	26
Fuel Tank	26
Engine	6

11



Summary of Requirements/Assumptions

Item	Requirements / Assumptions	Trades
Top-Level/ Science	Re-usable LEO to GEO laser transport system consisting of a Laser transport (no propellant tank) and a propellant tank section launched with the GEO payload. Falcon 9 launches the Laser transport (1) and the propellant tank section and GEO payloads (2). Transport reused 10 times. LEO to GEO time < 1 week. FOM. Cost launch (transport used 10 times), GEO spacecraft mass (Two of them)	Geo payload spacecraft mass and number, return payload?
System	Single fault tolerant. 2 year lifetime. Launch year open ended – current TRL assessment is an output. Mass Growth per AIAA 120-2006 (add growth to make system level 30%)	
Mission, Ops, GN&C	Payload and propellant section launched first on falcon 9 from Kwajalein to 9° inclination, 800 km circular. Transport launched next by falcon 9 to Kwajalein to 9° incl. 800 km circular. 3 day rendezvous with payload. 5-15 minute (max based on view-ability) 5000 IJ burns at perigees or apogees to recircularize to 3000 km (to improve viewability) then perigee and apogee burns to GEO. Deploy GEO spacecraft – return to 800 km for next payload (30 days).	Intermediate circular orbit to improve view-ability. Starting orbit, inclination.
Launch Vehicle	N/A	
Propulsion	Laser Steam Engine primary propulsion; performs Perigee and apogee raises. 5000 IJ engine (assumes 5000° K plasma ball in chamber) regeneratively cooled.	Main propellant choice: H2O better density and cooling, Hydrogen for higher Isp. On-board hydrazine for ACS, docking.
Power	Solar Arrays and secondary batteries to run transport only (payloads self-sufficient). Main loads: 1000 W water pump for laser engine	Add primary batteries for launch needs
C&DH Communications	Pre-use flight computer to handle launch. Up-range telemetry communications.	Computer type, data storage, data transfer rates, comm. Frequencies
Thermal & Environment	Remove laser and plasma heat from body by vaporizing propellant	Propellant type for cooling: H2O, NH3
Mechanisms	Reflector deployment, pointing (120° arc). Solar array deployment and nozzle gimbal.	mechanisms, materials, power, ops,
Structures	0.9999 reflective parabolic, 4x5 m parabolic mirror. Secondary reflector. Laser engine. Focuses on laser engine.	minimize mass,
Cost	Utilize MEL and iterate with subsystems for new DDT&E	
Risk	Major Risks: temperature leaks from laser and plasma, fouling mirror, laser pointing/thrust direction/angle of attack	



TRL Definitions



- SUMMARY
- **TRL 1** Basis principles observed and reported
- **TRL 2** Technology concept and/or application formulated
- **TRL 3** Analytical and experimental critical function
- **TRL 4** Component and/or breadboard validation in laboratory environment
- **TRL 5** Component and/or breadboard validation in relevant environment
- **TRL 6** System/Subsystem model or prototype demonstration in a relevant environment (ground or space)
- **TRL 7** System prototype in a space environment
- **TRL 8** Actual system completed and “flight qualified” through test and demonstration (ground or space)
- **TRL 9** Actual system “flight proven” through successful mission operations



TRL Levels (< TRL 6)



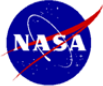
- **Laser Ground Station:**
 - Laser: TRL 4
 - Beam Director (30 m Mirror): TRL 3, (2 m Mirror): TRL 5-6
 - Atmospheric Compensation: TRL 4-5
- **Transport:**
 - Propulsion & Flight Dynamics/Environments
 - **Laser Engine**
 - Chamber: TRL 2
 - Reflectors: TRL 4-5
 - Environmental: laser shield TRL 4
 - GN&C: TRL 5 (visualization system)
 - C&DH: TRL 6
 - Communications: TRL 6
 - Power
 - Solar arrays TRL 4
 - Batteries TRL 4
 - Structures: TRL 4-6

CONOPS

Carl Sandifer
 COMPASS Team
 10-29-10

15

National Aeronautics and Space Administration



Architecture



- **Laser Stations**
 - On the ground (atmospheric losses added to complexities)
 - Laser Transmitter diameter inversely proportional to receiver diameter
 - $R(\text{receiver}) = 0.61 d \lambda / r(\text{transmitter})$
 - 4 m diameter laser requires 20 m diameter receiver
 - Larger (JWST sized 6.5 m diameter) allow for a 12 m receiver
 - Equivalent Solar reflector to get 0.5 MW of power would be roughly 22 m diameter
 - Continuous might benefit from just going solar....

distance km	35786.00	500.00	35786.00	500.00	35786.00	500.00
wavelength (m)	1E-06	0.000001	0.000001	0.000001	0.000001	0.000001
Transmitter R (m)	1	1	2	2	3.25	3.25
Receiver R(m)	21.83	0.31	10.91	0.15	6.72	0.09

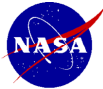
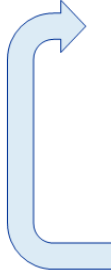
- **Laser Station size/#/placement part of challenge**
 - Impulsive requires 50 MW laser power (reasonable only from surface)
 - Continuous requires 500 kW but may require receivers similar in size to solar receiver for same thrust – what is laser buying you?



CONOPS



- **Transport**
 - Transport launched (Falcon 9? From Kwajalein)
 - To 800 km circular (3 day rendezvous)
 - Deploy solar array and reflector
 - Maneuver to Payload/Propellant stack
 - Dock with payload/propellant (transport is the active S/C)
 - Outbound Perigee Campaign
 - Outbound Apogee Campaign
 - Separate Payload in GEO
 - Return Apogee Campaign
 - Return Perigee Campaign
 - Hold in LEO until next payload ready (up to a month)
 - Jettison empty tanks
- **Payload/Propellant**
 - Transport launched (Falcon 9? From Kwajalein)
 - To 800 km circular
 - Gravity gradient wait for Transport
 - Dock with payload/propellant (Payload is the passive S/C)
 - Deployed in GEO by transport



400km: Communication Times to Equatorial Ground Stations



Report Data View: Equational View Durations: 400km
2011/12/08 05:50:37.5000 UTC

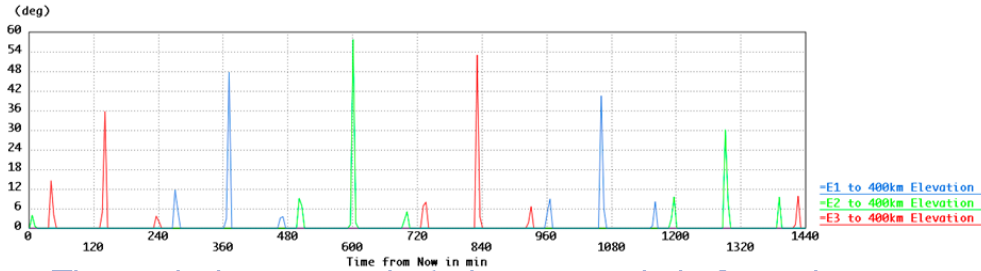
SOAP Report Data Output for BEP v3.orb
Relative to: 2011/12/08 05:50:37.5000 UTC
Number of Time Samples 3153600 Sample Rate: 0.166667 min

	MIN	MAX	AVE	SEDEV	95.0	90.0	50.0
E1 Elevation Above 30 deg							
REVISIT TIME	295.1392	1478.9566	767.2361	230.5013	1478.9034	788.4575	688.8911
RESPONSE TIME	0.0000	1478.9566	416.9369	298.4481	1068.2864	702.3487	382.5911
ACCESS INTERVAL	0.0901	2.9473	2.3134	0.6602			
DAILY VISIBILITY	0.8917	8.5834	4.3225	1.7379			
ACCESSES PER DAY	1.0000	3.0000	1.8767	0.4666			
E2 Elevation Above 30 deg							
REVISIT TIME	64.7838	1478.9595	767.2352	233.7515	1478.9033	788.4723	688.8863
RESPONSE TIME	0.0000	1478.9595	417.9150	299.5837	1074.6035	709.2521	383.1043
ACCESS INTERVAL	0.1768	2.9473	2.3143	0.6586			
DAILY VISIBILITY	0.0000	8.5914	4.3242	1.7729			
ACCESSES PER DAY	0.0000	3.0000	1.8712	0.4937			
E3 Elevation Above 30 deg							
REVISIT TIME	492.9507	1478.9583	768.3617	231.9657	1478.9025	788.4448	688.8887
RESPONSE TIME	0.0000	1478.9583	417.8865	299.5370	1074.6041	709.2507	383.0245
ACCESS INTERVAL	0.1242	2.9473	2.3162	0.6554			
DAILY VISIBILITY	0.3554	8.5915	4.3214	1.7472			
ACCESSES PER DAY	1.0000	3.0000	1.8658	0.4576			

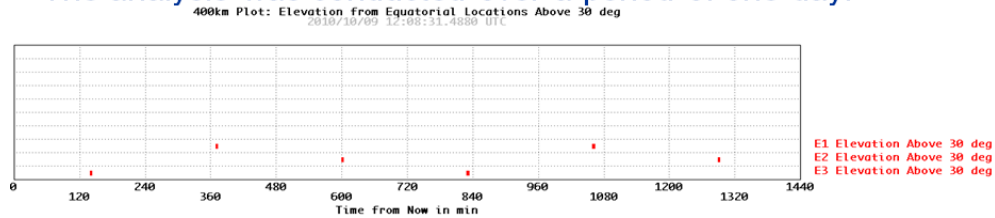
- The analysis was conducted over a 1 year period.
- On average, the spacecraft is visible from each ground site ~2.3 minutes per pass.



Sample Elevation Analysis: Ground Stations to Spacecraft at 400km



- The analysis was conducted over a period of one day.



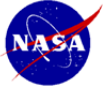
- This plot shows opportunities when the elevation to the spacecraft is above 30 degrees.



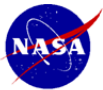
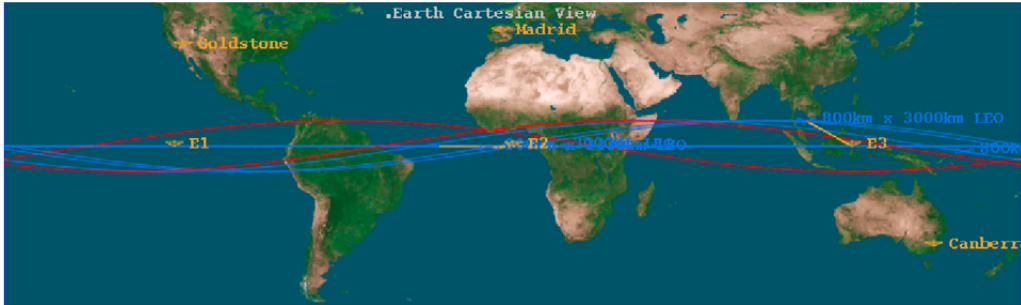
Impulsive Laser Engine Options



- 5000 N
- Propellant
 - H₂O
 - LH₂ backup
 - Di-borene?, Plastics?, NH₃, Li
- Engine Options
 - Plasma Ball: Reflection Chamber, CW plasma engine
 - Potential for very high temperatures (~15,000° K) TRL1-2
 - Is a Magnetic mirror required?
 - Isps ~800-900s for dense propellants (H₂O)
 - Isp ~1300s for light propellants (LH₂, Li)
 - Film cooling of nozzle
 - Direct Thermal
 - Lower temperatures (2000° K), Higher TRL
 - Isps ~400s (TBR) for dense propellants
 - Isps 800-900 s for light propellants
- Reflector Options
 - Diffractive Concentrator (can be a flat reflector)



Strawman Laser Sites



Laser Receiver



- Will have to track ($\pm 60^\circ$) to ground (or thrust losses)
 - Gimbals and offset to allow swing
- Pointing accuracy: $\pm 1/2^\circ$
- Options
 - Cassegrain
 - Offset Cassegrain
- Placed to protect payload as much as possible
 - Vehicle still may need shielding
- Will need primary and secondary optics
 - Will need to be cool
- Engine has a third optic (refractive tertiary): optional
- Lifetime Issues
 - MMOD degradation of mirror- major issue!
 - Atomic oxygen degradation?
 - Will Radiation belt degrade reflectivity?

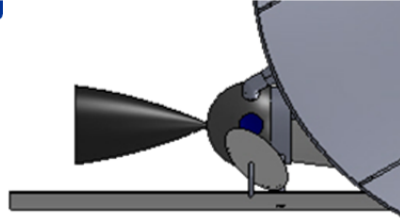




Laser Engine



- H₂O (steam propellant)
- 5000N, @ 5000K, 730s
- Thrust Chamber: 50 psi, 30 cm spherical, Regen cooled, film cooling?
- Refractory window: sapphire?, 10 cm diameter
- Nozzle: area ratio 50, Regen Cooled
- Gimbaled nozzle for COM pointing
 - Screw/Ball mechanical motor



Laser Energies



- A 5000 N engine will need
 - ~ 50 MW at the S/C
 - ~80 MW ground laser (output)
 - ~200 MW of power from the grid

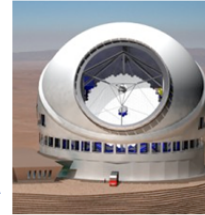
Engine Isp	900	s
Thrust Level	5000	N
Engine Eff	0.5	
Power into Engine	44	MW
Receiver eff	0.9	Losses, absorp
Power up to S/C	49	MW
Atmospheric Eff	0.7	Losses, absorp
Transmitted laser from surface	70	MW
Transmitter Efficiency	0.9	
Ground laser power (output)	78	MW
Laser Efficiency	0.4	
Ground laser power (input from 'grid')	195	MW



Laser Stations



- Two types of Stations seem to be needed
 - Perigee station
 - ~800 km distance from surface to S/C
 - Transmitter size can be small
 - Needs to be at launch latitude or less
 - If launch at 28.5° each station only sees S/C twice a day
 - Equatorial launch and equatorial stations would have better viewing
 - Nuclear powered ships (Virginia Class Cruisers –two 150 MWth Reactors, Aircraft Carrier)
 - Apogee stations
 - Large distances (~40000 km)
 - Transmitter needs to be large (30 m diameter – TMT planned for Mauna Kea) to minimize reflector
 - Viewing should be sufficient from 45° latitude or less, (high mountains – above clouds ideal)



	Perigee laser	Apogee Laser	Small	SOA Telescope
distance km	900.00	40000.00	40000.00	40000.00
wavelength (m)	0.000001	0.000001	0.000001	0.000001
Transmitter D (m)	0.75	30	2	10
Receiver D(m)	2.93	3.25	48.80	9.76



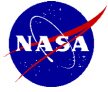
Launchers



- Falcon 9, Block 2
- Estimated Performance from Kwaj. (9° inclination)
 - 400 km circular: 10,200 kg
 - 800 km circular: 9280 kg
 - GTO: 4682 kg



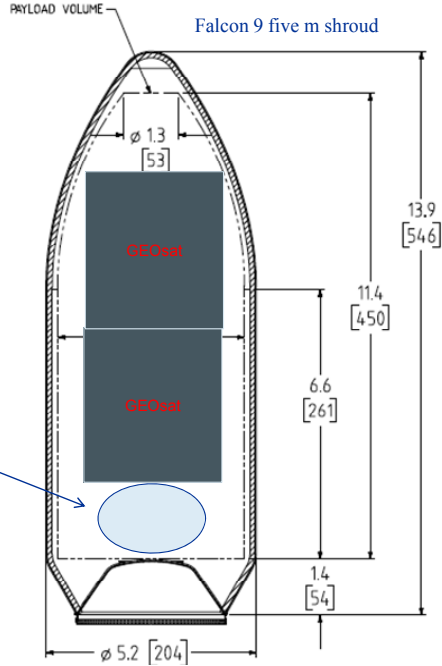
Image: courtesy of Space Exploration Technologies Corporation (SpaceX); used with permission.



Propellant Selection



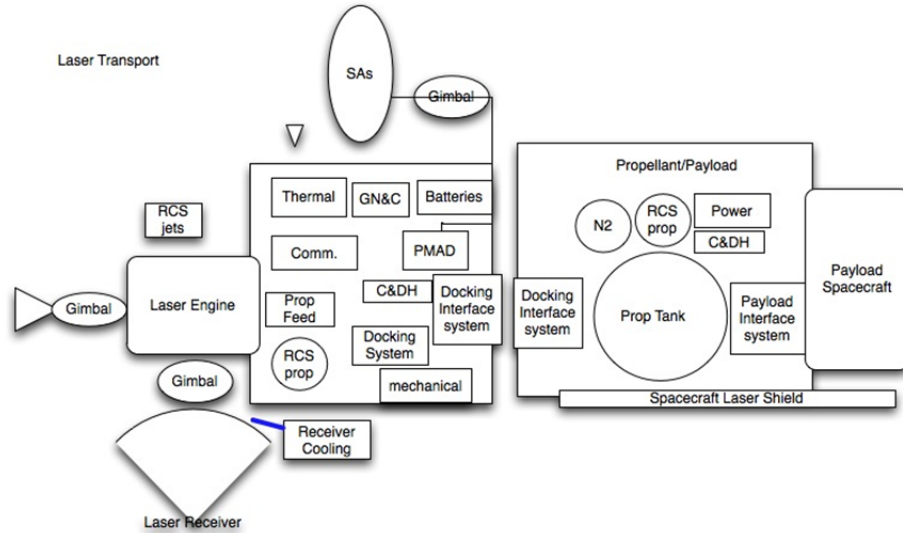
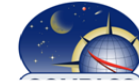
- **Water (or other dense propellant- Ar?) leave more room for payload**
 - But 800 seconds with H₂O is TRL 1-2
- **LH₂ propellants much less dense (~68 kg/m³) but 900 seconds performance (TRL-4?)**
 - From Impulsive case
 - 5000 kg LH₂ would take up about half of volume
 - 5000 kg of Water should fit



27



Laser Transport Systems



28

Configuration

Tom Packard
COMPASS Team
10-29-10

29

National Aeronautics and Space Administration



Architectural Components



- **Transport**
 - Engine, Reflector, docking system, power system
 - Launched by falcon 9
- **Payload Spacecraft and Transport Propellants**
 - Launched on separate Falcon 9

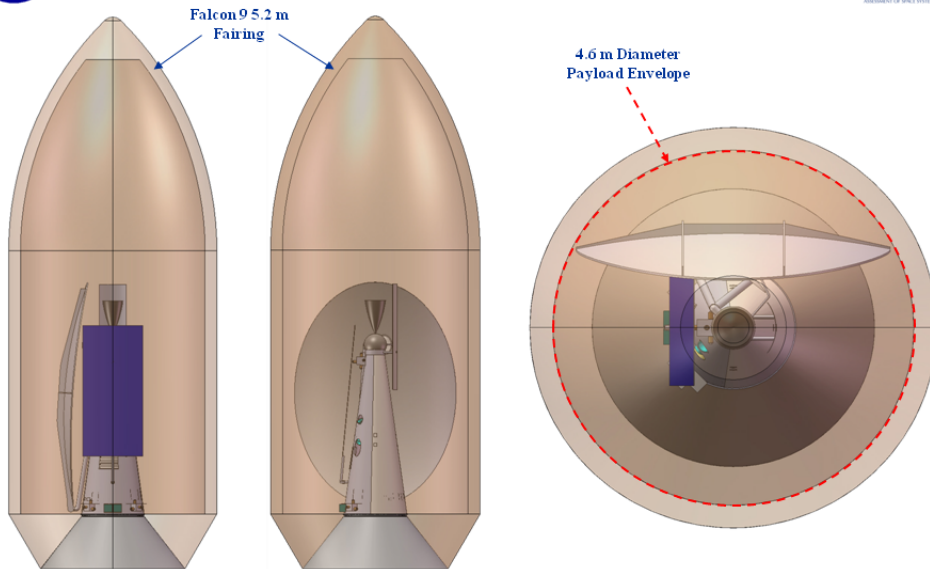
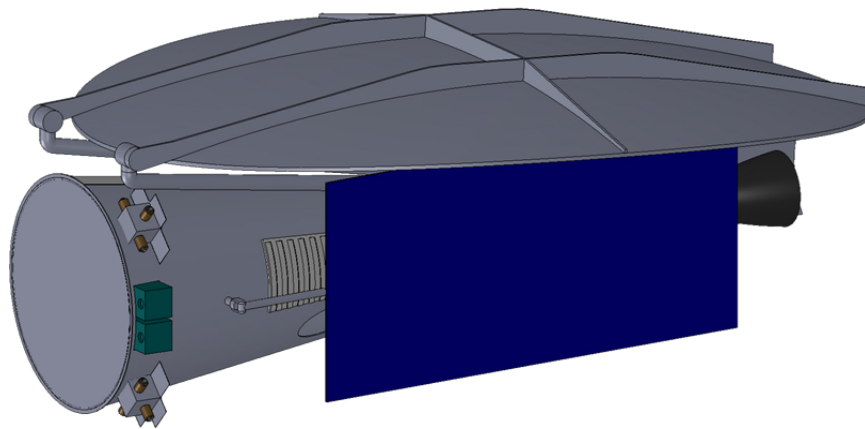
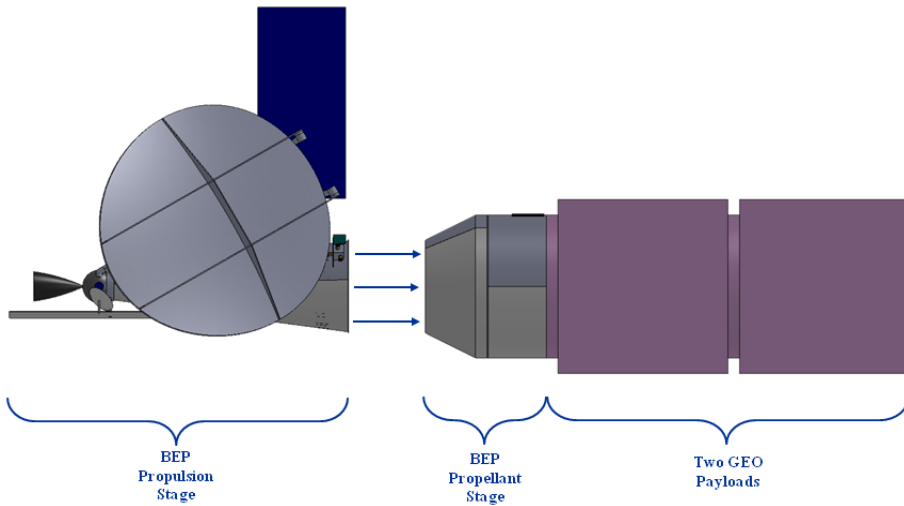
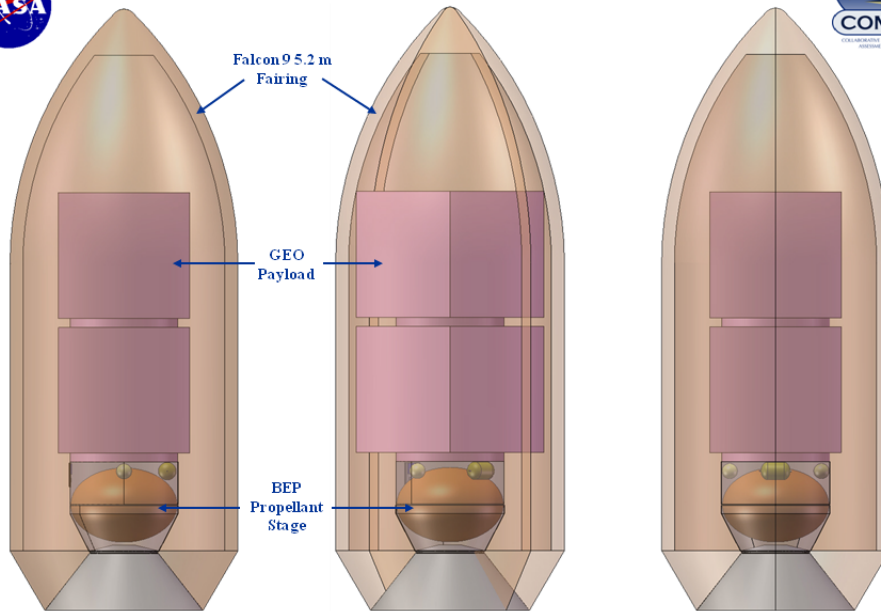
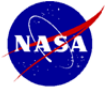
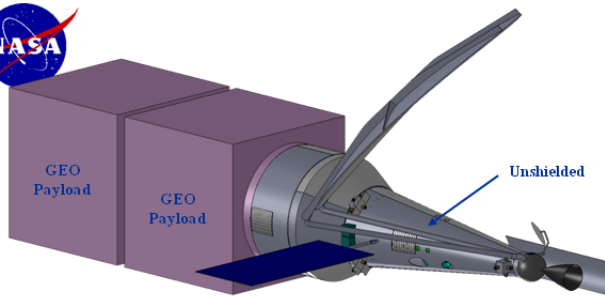
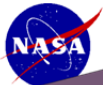


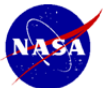
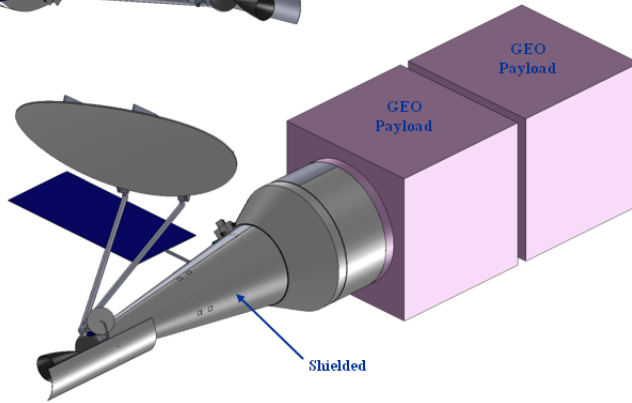
Figure 1. Falcon 9 5.2 m Fairing and 4.6 m Diameter Payload Envelope





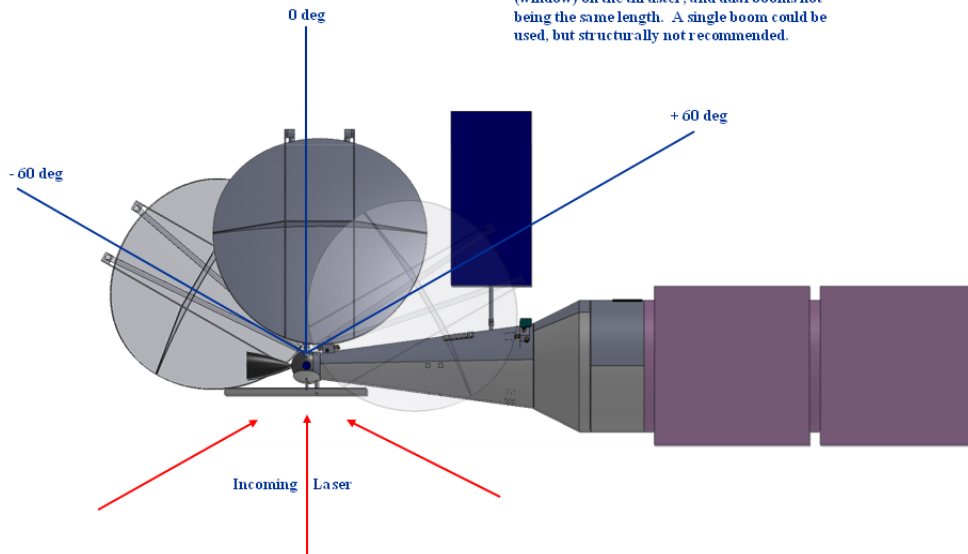


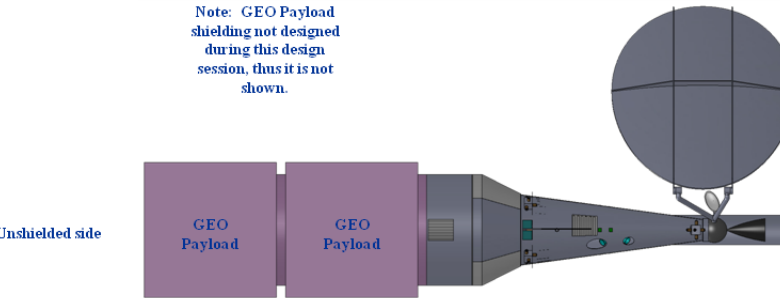
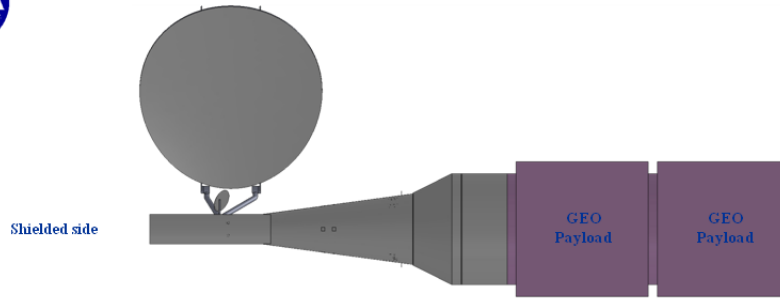
Note: GEO Payload shielding not designed during this design session, thus it is not shown.



Required Range Of Motion for the Mirror

Note: The need for a 2-axis gimbal on the mirror needs to be examined further due to the axis of rotation not being aligned with the laser inlet (window) on the thruster, and dual booms not being the same length. A single boom could be used, but structurally not recommended.

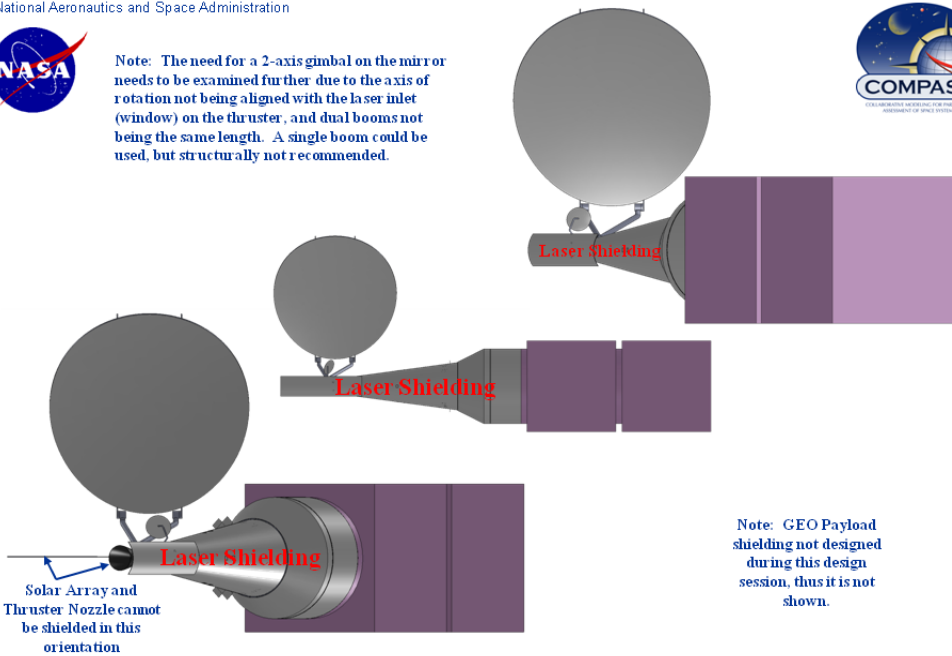




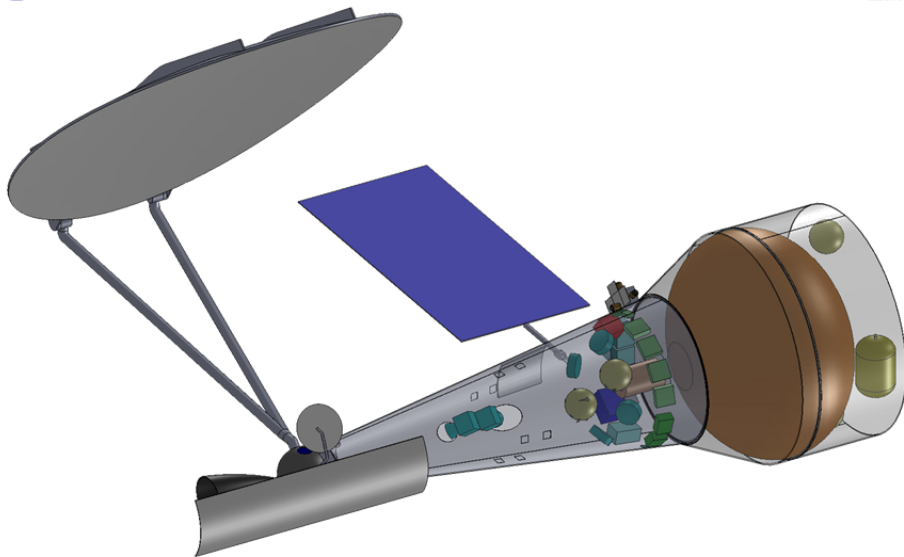
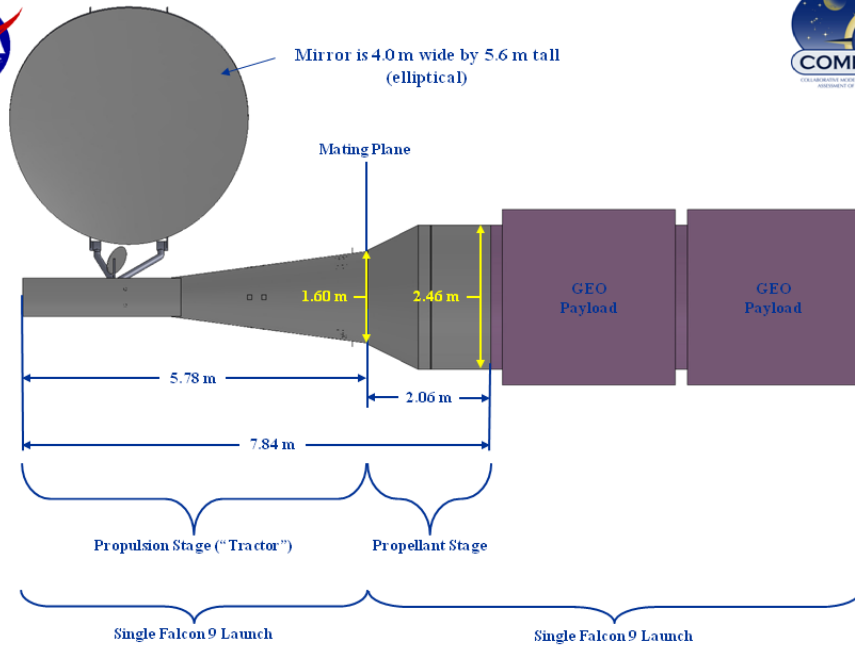
Note: GEO Payload shielding not designed during this design session, thus it is not shown.

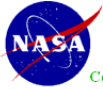


Note: The need for a 2-axis gimbal on the mirror needs to be examined further due to the axis of rotation not being aligned with the laser inlet (window) on the thruster, and dual booms not being the same length. A single boom could be used, but structurally not recommended.



Note: GEO Payload shielding not designed during this design session, thus it is not shown.





Communications Electronics

Battery

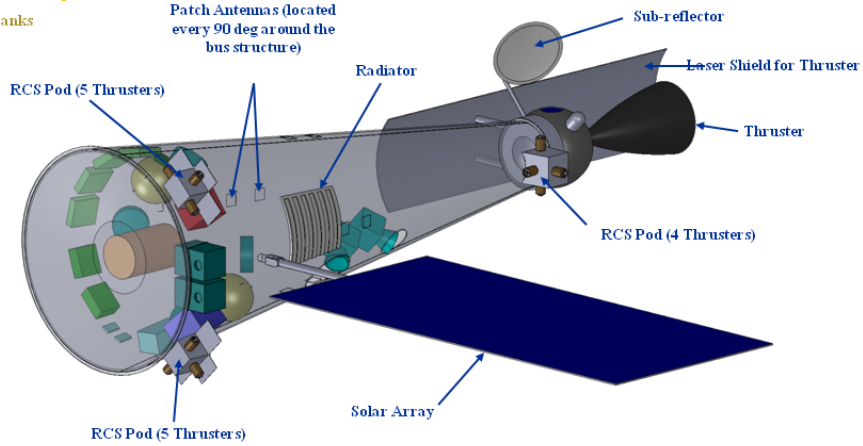
GN&C

Avionics Enclosure

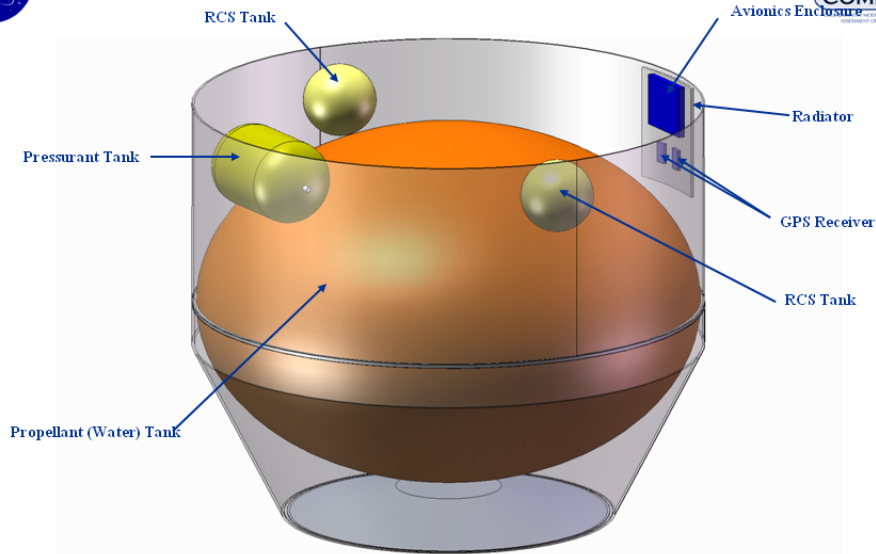
Propellant Pump

RCS Tanks

Propulsion Stage



Propellant Stage

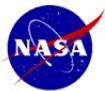


Systems

David Grantier, Melissa McGuire,
COMPASS Team
10-29-10

43

National Aeronautics and Space Administration



COMPASS Spacecraft Design Process



- **Build Spacecraft MEL (Master Equipment List) in a WBS hierarchy by major subsystem down to a line item level appropriate to the level of design detail of the request**
- **Apply MGA from AIAA to each of the line items at the subsystem level**
- **Gather the total masses and calculate the total system growth % on the Basic dry mass**
- **Carry an additional system level (or program level) mass to reach a total of 30% mass book-kept on the dry Basic Mass**



Mass Growth Allowance (MGA) Schedule

Taken from AIAA S-120-2006, *Standard Mass Properties Control for Space Systems*



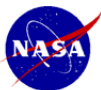
- Basic Mass**
 - The current mass data based on an assessment of the most recent baseline design
 - NOTE 1 This design assessment includes the estimated, calculated, or measured (or actual) mass, and includes an estimate for undefined design details like cables, multi-layer insulation and adhesives.
 - NOTE 2 the mass growth allowances (MGA) and uncertainties are not included in the basic mass.
- Mass Growth Allowance (MGA)**
 - The predicted change to the basic mass of an item based on an assessment of the design maturity and fabrication status of the item, and an estimate of the in-scope design changes that may still occur
- Predicted Mass**
 - The basic mass plus the mass growth allowance

Code	Design maturity (basis for mass determination)	Electrical/electronic components			Percent MGA						
		0 to 5 kg	5 to 15 kg	>15 kg	Structure	Thermal control	Propulsion	Batteries	Wire harnesses	Mechanisms	Instrumentation
E	Estimated (preliminary sketches)	30	20	15	15	15	15	20	50	15	50
L	Layout (or major modification of existing hardware)	25	20	15	12	12	12	15	30	12	30
P	Pre-release drawings (or minor modification of existing hardware)	20	15	10	8	8	8	10	25	8	25
C	Released drawings (calculated values)	10	5	5	4	4	4	5	5	4	5
X	Existing hardware (actual mass from another program)	3	3	3	2	2	2	3	3	2	3
A	Actual mass (measured flight hardware)	0	0	0	0	0	0	0	0	0	0
FE	Customer furnished equipment	0	0	0	0	0	0	0	0	0	0

For the COMPASS process, the total percentage on dry mass is desired to be 30% total

*Predicted Mass = Basic Mass + Bottoms up MGA% * Basic Mass*

Therefore, Additional System level margin = 30% - Bottoms up MGA%



Top Level BEP LEO GEO Characteristics Transport Stage



- Bottoms up MGA growth on the Transport Stage is 14% of the Basic mass (also known as Current Best Estimate or CBE) (59 kg)
- Desire 30% growth, carry additional 72 kg at Transport Stage system level (16% of basic mass)

Master Equipment List Rack-up (Mass) - BEP Inspace				COMPASS S/C Design	
WBS	Main Subsystems	Basic Mass (kg)	Growth (kg)	Total Mass (kg)	Aggregate Growth (%)
06	BEP LEO GEO Inspace	9566	100	9666	
06.1	Transport Stage	457	59	516	
06.1.1	Attitude Determination and Control	53	6	59	11%
06.1.2	Command and Data Handling	34	9	43	28%
06.1.3	Communications and Tracking	7	2	9	25%
06.1.4	Electrical Power Subsystem	20	6	26	30%
06.1.5	Thermal Control (Non-Propellant)	116	14	130	12%
06.1.6	Propulsion (Hardware)	144	12	156	8%
06.1.7	Propellant (Chemical)	21		21	
06.1.8	Structures and Mechanisms	63	11	73	17%

Inert Mass Calculations				
	Basic Mass (kg)	Growth (kg)	Total Mass (kg)	Aggregate Growth (%)
Transport Stage Mass Calculations				
Transport Stage Total Wet Mass	457	59	516	
Transport Stage total Dry Mass	437	59	496	14%
Dry Mass Desired System Level Growth	437	131	568	30%
Additional Growth (carried at system level)		72		16%
Total Usable Propellant	19		19	
Total Trapped Propellants, Margin, pressurant	1		1	
Total Inert Mass with Growth	438	131	569	
Transport Stage Total Wet Mass with Growth	457		588	

- Inert mass is dry mass + trapped residuals + propellant margin + pressurant
- Dry mass on each segment is calculated as the total bottoms up dry mass with the MGA% applied + additional system mass so that the total growth on each stage is 30% of the basic mass
 - The dry basic mass of the Transport Stage is 437 kg
 - The Total mass of the Transport Stage with the bottom's up growth is 496 kg
 - The inert mass of the Transport Stage with 30% growth carried on the Basic masses is 568 kg
- Mission applies the -Vs and the rocket equation to the appropriate total vehicle mass based on the mission event
- Total inert mass with the 30% growth incorporated is: 588 kg



Top Level BEP LEO GEO Characteristics Payload/Propellant Stage



- Bottoms up MGA growth on the Transport Stage is 15% of the Basic mass (also known as Current Best Estimate or CBE) (41 kg)
- Desire 30% growth, carry additional 41 kg at Transport Stage system level (15% of basic mass)

Master Equipment List Rack-up (Mass) - BEP Inspace

WBS	Main Subsystems	Basic Mass (kg)	Growth (kg)	COMPASS S/C Design	
				Total Mass (kg)	Aggregate Growth (%)
06	BEP LEO GEO Inspace	9566	100	9666	
06.2	Payload/Propellant Stage	9109	41	9149	
06.2.1	Payload Spacecraft	3940	0	3940	0%
06.2.2	Propellant	4895	0	4895	0%
06.2.3	Command and Data Handling	4	1	5	29%
06.2.4	Communications and Tracking	0	0	0	TBD
06.2.5	Electrical Power Subsystem	0	0	0	TBD
06.2.6	Thermal Control	67	10	77	15%
06.2.7	Propulsion Hardware	121	15	136	12%
06.2.8	Structures and Mechanisms	81	15	96	18%

Inert Mass Calculations

	Basic Mass (kg)	Growth (kg)	Total Mass (kg)	Aggregate Growth (%)
Payload/Propellant Stage Mass Calculations				
Payload/Propellant Stage Total Wet Mass	9109	41	9149	
Propellant Stage total Dry Mass (no P/L)	273	41	314	15%
Dry Mass Desired System Level Growth	273	82	355	30%
Additional Growth (earned at system level)		41		15%
Total Inert Mass with Growth	273	82	355	
Payload/Propellant Stage Total Wet Mass with Growth	273		355	

- Inert mass is dry mass + trapped residuals + propellant margin + pressurant
- Dry mass on each segment is calculated as the total bottoms up dry mass with the MGA % applied + additional system mass so that the total growth on each stage is 30% of the basic mass
 - The dry basic mass of the Payload/Propellant Stage is 273 kg
 - The Total dry mass of the Payload/Propellant Stage with the bottom's up growth is 314 kg
 - The inert mass of the Payload/Propellant Stage with 30% growth carried on the Basic masses is 355 kg
- Mission applies the $-V_s$ and the rocket equation to the appropriate total vehicle mass based on the mission event
- Total inert mass with the 30% growth incorporated is: 355 kg



BEP LEO GEO and Propellant Details



- Total ΔV for mission: ~4240 m/s (each leg)

MAV TEST0 Mission Details

Value	units
288.2	kg
Stage 1	
171.6	
	m/s
	m/s
	m/s
Stage 2	
35.0	kg
1482.9	m/s
44.5	m/s
1527.4	m/s
206.6	kg

NEED UPDATED MISSION DATA!

Spacecraft Totals

BEP LEO GEO Inspace Totals		
Transport Stage Wet mass	588	kg
Transport Stage Dry mass	568	kg
Transport Stage Inert mass	569	kg
Payload/Propellant Stage Wet mass	9149	kg
Payload/Propellant Stage Dry mass	314	kg
Payload/Propellant Stage Inert mass	355	kg
BEP LEO GEO Inspace Wet mass	9738	kg
BEP LEO GEO Inspace Dry mass	882	kg
BEP LEO GEO Inspace Inert mass	924	kg



BEP LEO GEO MEL Transport Stage



- When originally built, the BEP LEO GEO MEL was subdivided by subsystem discipline (Avionics, Communications, Power, etc)
- The BEP LEO GEO MEL was intended to be launched as two discrete segments that are to be integrated in LEO.

WBS	Description	QTY	Unit Mass	Basic Mass	Growth	Growth	Total Mass
Number	BEP LEO GEO Inspace - October 2010		(kg)	(kg)	(%)	(kg)	(kg)
06	BEP LEO GEO Inspace			9576.91	1.1%	103.06	9679.97
06.1	Transport Stage			468.37	11.3%	62.33	530.70
06.1.1	Attitude Determination and Control			53.02	10.6%	5.65	58.67
06.1.1.a	Guidance, Navigation, & Control			53.02	10.6%	5.65	58.67
06.1.2	Command and Data Handling			33.93	27.7%	9.40	43.33
06.1.2.a	Command & Data Handling			33.93	27.7%	9.40	43.33
06.1.2.b	Instrumentation & Wiring			0.00	0	0.00	0.00
06.1.3	Communications and Tracking			6.94	24.8%	1.72	8.66
06.1.3.a	S Band Communications System			6.94	24.8%	1.72	8.66
06.1.3.b	Misc 1			0.00	0	0.00	0.00
06.1.3.c	Misc 2			0.00	0	0.00	0.00
06.1.4	Electrical Power Subsystem			31.00	30.0%	9.30	40.30
06.1.4.a	Solar Array Power System			19.00	30.0%	5.70	24.70
06.1.4.b	n/a 1			0.00	0	0.00	0.00
06.1.4.c	n/a 2			0.00	0	0.00	0.00
06.1.4.d	Battery System			12.00	30.0%	3.60	15.60
06.1.4.e	Misc#1			0.00	0	0.00	0.00
06.1.5	Thermal Control (Non-Propellant)			115.92	12.1%	14.05	129.97
06.1.5.a	Active Thermal Control			2.65	0.0%	0.00	2.65
06.1.5.b	Passive Thermal Control			19.61	0.0%	0.00	19.61
06.1.5.c	Mirror System			93.66	15.0%	14.05	107.71
06.1.6	Propulsion (Hardware)			143.97	8.1%	11.70	155.68
06.1.6.a	Primary Propulsion System Hardware			69.24	14.0%	9.70	78.94
06.1.6.b	Propellant Management (Chemical)			74.73	2.7%	2.00	76.74
06.1.7	Propellant (Chemical)			20.62	0.0%	0.00	20.62
06.1.7.a	Main Engine Propellant			0.00	0	0.00	0.00
06.1.7.b	RCS Propellant			20.62	0.0%	0.00	20.62
06.1.8	Structures and Mechanisms			62.97	16.7%	10.51	73.48
06.1.8.a	Structures			61.61	17.1%	10.51	72.13
06.1.8.b	Mechanisms			1.36	0.0%	0.00	1.36



Scratch PEL



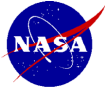
	Power Mode 1	Power Mode 2	Power Mode 3	Power Mode 4
	(W)	(W)	(W)	(W)
Power Mode Title	Launch	LEO Integration	BEP Cruise w/Thrust	BEP Cruise No Thrust
Systems operating	All Except EPS/ Thermal	All Except Thermal/ Structures	AD&C/ Avionics/ Comm	AD&C/ Avionics/ Comm
Attitude Determination and Control	22	60	60	22
Avionics	36	40	40	13
Communications and Tracking	20	20	20	7
Electrical Power Subsystem	0	20	20	0
Thermal Control (Non-Propellant)	0	5	5	0
Propulsion (Hardware)	5	60	60	0
Structures and Mechanisms	24	30	30	0
Total (watts)	107	235	235	42
Power Requirement (Plus 30%)	139.1	305.5	305.5	54.6

Mission

Laura Burke, Mike Martini, Carl Sandifer, Camille Moore
 COMPASS Team
 10-29-10

51

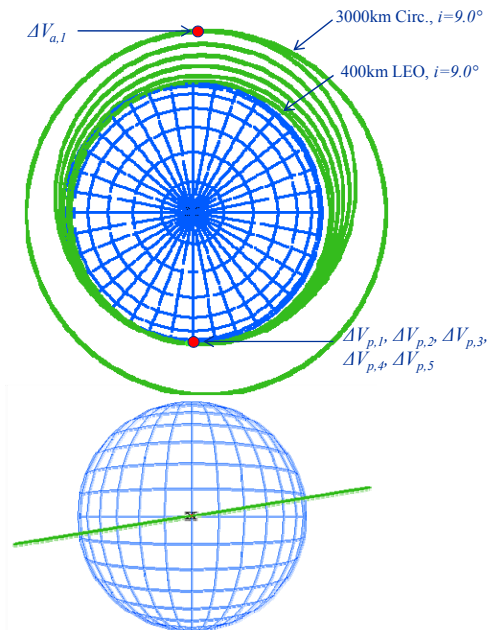
National Aeronautics and Space Administration

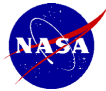


Copernicus: 400km LEO to 3000km Circ Mission



400km LEO to 3000km		
Apogee Raise Burns		
	ΔV	$inclination_{final}$
$\Delta V_{p,1}$	87.06 m/s	9.0°
$\Delta V_{p,2}$	123.56 m/s	9.0°
$\Delta V_{p,3}$	125.64 m/s	9.0°
$\Delta V_{p,4}$	127.78 m/s	9.0°
$\Delta V_{p,5}$	129.99 m/s	9.0°
Perigee Raise Burns		
$\Delta V_{a,1}$	546.83 m/s	9.0°
Total ΔV	1140.86 m/s	
3000km to GEO		
Apogee Raise Burns		
	ΔV	$inclination_{final}$
$\Delta V_{p,1}$	266.42 m/s	9.0°
$\Delta V_{p,2}$	736.40 m/s	9.0°
$\Delta V_{p,3}$	816.76 m/s	9.0°
Perigee Raise/Inc. Change Burns		
$\Delta V_{a,1}$	315.02 m/s	5.88°
$\Delta V_{a,2}$	959.81 m/s	0.0°
Total ΔV	3094.41 m/s	
Mission ΔV	4235.27 m/s	

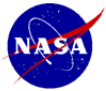
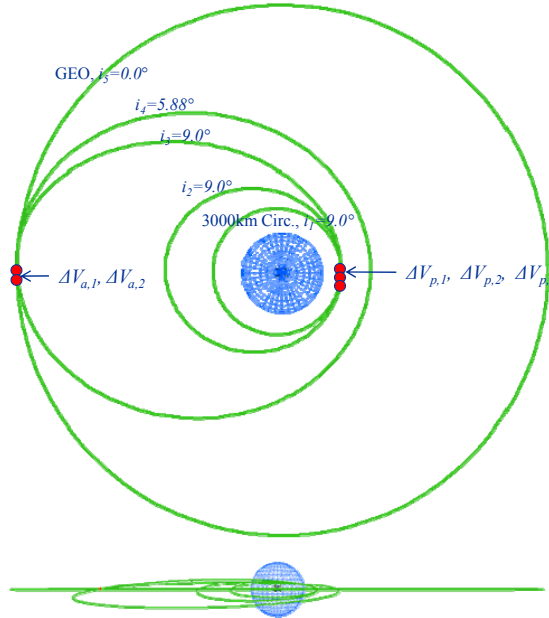




Copernicus: 3000km Circ to GEO Mission



800km LEO to 3000km		
Apogee Raise Burns		
	ΔV	$inclination_{final}$
$\Delta V_{p,1}$	154.63 m/s	9.0°
$\Delta V_{p,2}$	325.04 m/s	9.0°
Perigee Raise Burns		
$\Delta V_{a,1}$	447.86 m/s	9.0°
Total ΔV	927.53 m/s	
3000km to GEO		
Apogee Raise Burns		
	ΔV	$inclination_{final}$
$\Delta V_{p,1}$	266.42 m/s	9.0°
$\Delta V_{p,2}$	736.40 m/s	9.0°
$\Delta V_{p,3}$	816.76 m/s	9.0°
Perigee Raise/Inc. Change Burns		
$\Delta V_{a,1}$	315.02 m/s	5.88°
$\Delta V_{a,2}$	959.81 m/s	0.0°
Total ΔV	3094.41 m/s	
Mission ΔV	4021.94 m/s	



Sample Impulsive Mission: 400km to 3000km, 3000km to GEO



```
>> results=LEO_to_GEO_v2(3000,1500,763.92,5290.32,2,15,400,9,3000,9)
```

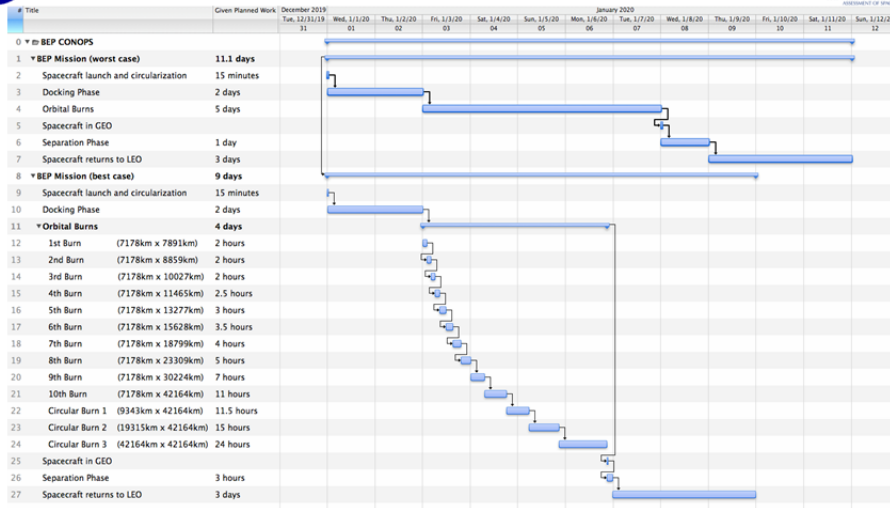
	PREBURN ORBIT				POSTBURN ORBIT						
PHASE	M0 (kg)	RP1 (km)	RA1 (km)	DV (m/s)	RP2 (km)	RA2 (km)	T (hr)	INC (dg)	dWt (dg)	dtDW (s)	MET (hr)
CIRC BURN1	4841.24	6778.14	9378.14	547.576	9378.14	9378.14	2.511	9.00	3.212	0.00	7.9415
BURN5	4925.98	6778.14	8709.18	129.997	6778.14	9378.14	2.007	9.00	2.245	4.42	6.9379
BURN4	5010.72	6778.14	8112.66	127.780	6778.14	8709.18	1.884	9.00	2.903	9.58	5.0542
BURN3	5095.46	6778.14	7577.55	125.637	6778.14	8112.66	1.776	9.00	2.245	10.37	3.2782
BURN2	5180.20	6778.14	7094.92	123.564	6778.14	7577.55	1.681	9.00	1.543	11.22	1.5971
BURN1	5240.75	6778.14	6778.14	87.057	6778.14	7094.92	1.597	9.00	0.796	12.14	0.0000
LEO ORBIT	5240.75	6778.14	6778.14	0.000	6778.14	6778.14	1.543	9.00	0.000	0.00	0.0000


```
>> results=LEO_to_GEO_v2(3000,1500,763.92,5290.32,15,15,3000,9,35786,0)
```

	PREBURN ORBIT				POSTBURN ORBIT						
PHASE	M0 (kg)	RP1 (km)	RA1 (km)	DV (m/s)	RP2 (km)	RA2 (km)	T (hr)	INC (dg)	dWt (dg)	dtDW (s)	MET (hr)
CIRC BURN2	5135.56	12588.41	42164.14	989.711	42164.14	42164.14	23.934	0.00	0.825	0.00	25.6821
CIRC BURN1	5295.80	9378.14	42164.14	230.185	12588.41	42164.14	12.522	0.00	0.698	3.98	13.1602
INC BURN1	5505.60	9378.14	42164.14	291.046	9378.14	42164.14	11.437	0.00	0.698	0.00	13.1602
BURN3	6141.15	9378.14	18646.01	818.430	9378.14	42164.14	11.437	9.00	0.698	1.60	7.4417
BURN2	6776.71	9378.14	11063.22	737.759	9378.14	18646.01	4.585	9.00	0.617	5.35	2.8565
BURN1	7019.21	9378.14	9378.14	263.393	9378.14	11063.22	2.856	9.00	0.371	8.96	0.0000
LEO ORBIT	7019.21	9378.14	9378.14	0.000	9378.14	9378.14	2.511	9.00	0.000	0.00	0.0000



BEP CONOPS (Will be updated ASAP)



- It is possible for the BEP mission to be achieved within 9 days.



BEP LEO To GEO Delta-V Summary



Mission DeltaV Summary			
Phase Number	Phase Name	Main DV (m/s)	RCS DV (m/s)
1	Loiter	-	10.0
2	Rendezvous	-	54.0
3	400 km LEO to 3000km	1145.6	1.0
4	3000 km to GEO	3094.4	1.0
5	GEO to 3000 km	3094.4	1.0
6	3000 km to 400 km LEO	1145.6	1.0
7	Separate	-	0.5
8	Loiter	-	10.0
9	Rendezvous	-	54.0
Total		8480.0	132.5

C&DH

Glenn Williams
COMPASS Team
10-29-10

57

National Aeronautics and Space Administration



BEP Avionics Overview



- **Design Requirements**
 - Avionics for systems command, control, and health management separate for Transport and P/P
 - Single fault tolerant processor architecture
 - Low mass optimization required for BEP
 - Operational power modes vary according requirements, BEP quiescent until needed
- **Assumptions**
 - 50 kRad avionics for stable operation for duration of mission
 - Cabling mass estimated with Monte Carlo simulation
- **Design Description**
 - Transport assumes 6U-160 cPCI form factor cards
 - Rad-tolerant FPGAs packaged with IP for processor capability,
 - **Fail over to backup processor if one faults out or has SEU (reboot attempted)**
 - **Embedded software kernels without major O/S overhead**
 - Memory 5 GB with EDAC
 - Power Supply using DC-DC converters, filter, and EMI shielding accept wide variations in supply voltage
 - Discrete and Power switching card for general vehicle functions
 - Sensor I/O card
 - RS422 interfaces between stages - 2 Mbps RS422 Manchester coded
 - Housekeeping data and H&S data to ground via comm at 4.5 kbps

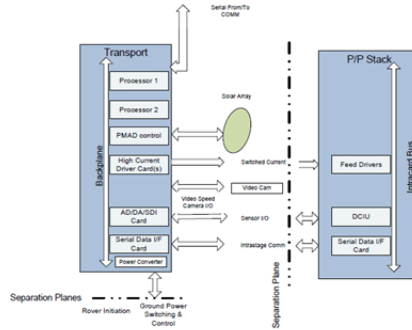


BEP Avionics Functionality



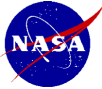
- **General Avionics Processors**

- PowerPC Intellectual Property in rad-hard FPGA
- Transport avionics cPCI card cage.
- Gimbals and TVC cards mass reduced, control any necessary positioning
- Solar array deployment and gimbaling in Lander
- Comm antenna gimbaling only in Lander
- BEP navigation – data from IMUs
- Systems health and status reporting
- Card Power managed for various power modes (potrimmed with specialized sentinel switching)
- System management – includes control of valves, heaters, PMAD
- System fault detection fail over must respond quick during BEP Transport operations
- Dual 38400 bps serial interfaces between stages ar comm channels
- ROM SLOC estimate ~100k. Includes autosequenced BEP operations.



GN&C

Mike Martini
COMPASS Team
10-29-10

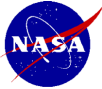


BEP GNC



- **Requirements**
 - Deliver spacecraft to GEO in less than 10 days
 - Point the reflector with 0.5 degrees of accuracy
 - Rendezvous and dock with the propellant stage in a LEO circular orbit
 - Single fault tolerant
- **Assumptions**
 - BEP Lightcraft has zero products of inertia
- **Navigation Design**
 - Eight Sun sensors for course attitude determination
 - One Northrop Grumman internally redundant SIRU
 - Fault tolerant, redundant HRGs, accelerometers and electronics
 - Spaceflight heritage – Deep Impact, MESSENGER, Cassini, NEAR and others
 - Two Selex-Galileo Avionica Autonomous Star Trackers (A-STR)
 - Includes processing electronics and data/command interfaces
 - Spaceflight heritage – MESSENGER, STEREO, MRO, SDO
 - Up to 10 tracked stars
 - Bias error < 10 arcsec, 3 sigma
 - Two Surrey Satellite Technology GPS receivers

61



BEP GNC



- **Control**
 - Four Teldix RSI 12-75/60 reaction wheels for fine pointing accuracy and momentum storage
 - Thirteen 5 lbf (22.2 N) RCS thrusters for momentum management, rendezvous with propellant stage and proximity operations during docking
 - 2 pods of 4
 - 1 pod of 5
- **Automated Rendezvous and Docking**
 - 2 Next Generation Advanced Video Guidance Sensors (NGAVGS) for Automated Rendezvous and Docking (AR&D)
 - Derivative of the AVGS used on Orbital Express
 - Two sets of laser diodes which operate at nominal wavelengths of 806 and 845 nm and a mirror through which the lasers fire
 - Camera that images the return from the lasers
 - hardware, software, and firmware that process the returned images into relative position and attitude data
 - Designed to interact with retro-reflectors placed on the target spacecraft target retro-reflectors are arranged in a pattern known to the AVGS software
 - Data is output from the sensor and fed to the spacecraft Guidance and Navigation System
 - Breadboard version of the NGAVGS was built at MSFC

62

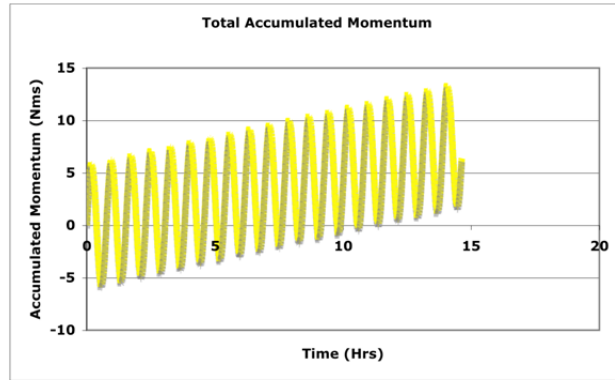


Momentum Storage for 400 km Circular Orbit



Assumptions:

- Inertially Pointed
 - Gravity gradient torque is cyclic
 - Solar torque is constant
- Moments of Inertia
 - $I_{xx} = 8125 \text{ kg}^{\text{m}}^2$
 - $I_{yy} = 1250 \text{ kg}^{\text{m}}^2$
 - $I_{zz} = 1250 \text{ kg}^{\text{m}}^2$
- CP-CG offset is 1 m
 - results in a solar torque of $1.5 \times 10^{-4} \text{ Nm}$
- Dump momentum wheels at 75% capacity $\sim 9 \text{ Nms}$



- Reaction wheels saturate in ~ 8 hours before wheel saturation

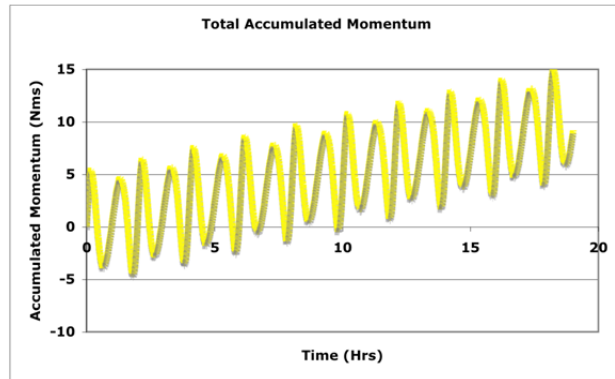


Momentum Storage for 400 km x 3000 km Orbit



Assumptions:

- Inertially Pointed
 - Gravity gradient torque is cyclic
 - Solar torque is constant
- Moments of Inertia
 - $I_{xx} = 8125 \text{ kg}^{\text{m}}^2$
 - $I_{yy} = 1250 \text{ kg}^{\text{m}}^2$
 - $I_{zz} = 1250 \text{ kg}^{\text{m}}^2$
- CP-CG offset is 1 m
 - results in a solar torque of $1.5 \times 10^{-4} \text{ Nm}$
- Dump momentum wheels at 75% capacity $\sim 9 \text{ Nms}$



- Reaction wheels saturate in ~ 10 hours before wheel saturation

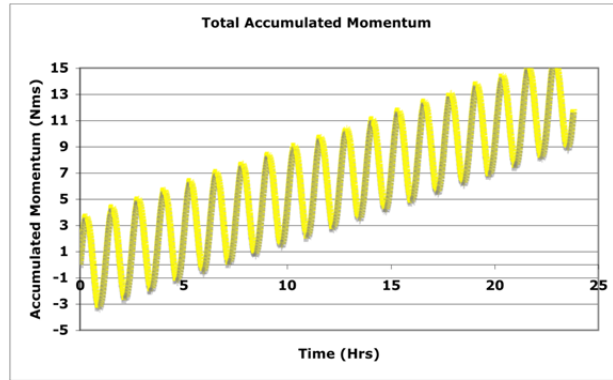


Momentum Storage for 3000 km Circular Orbit



Assumptions:

- Inertially Pointed
 - Gravity gradient torque is cyclic
 - Solar torque is constant
- Moments of Inertia
 - $I_{xx} = 8125 \text{ kg}^{\text{m}}^2$
 - $I_{yy} = 1250 \text{ kg}^{\text{m}}^2$
 - $I_{zz} = 1250 \text{ kg}^{\text{m}}^2$
- CP-CG offset is 1 m
 - results in a solar torque of $1.5 \text{ e-}4 \text{ Nm}$
- Dump momentum wheels at 75% capacity $\sim 9 \text{ Nms}$



• Reaction wheels saturate in ~ 11 hours before wheel saturation

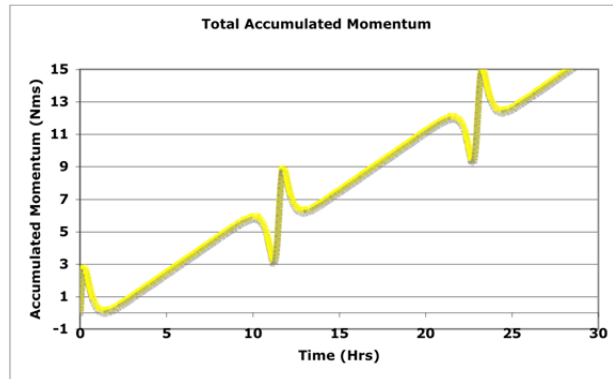


Momentum Storage For 3000 km x GEO Orbit



Assumptions:

- Inertially Pointed
 - Gravity gradient torque is cyclic
 - Solar torque is constant
- Moments of Inertia
 - $I_{xx} = 8125 \text{ kg}^{\text{m}}^2$
 - $I_{yy} = 1250 \text{ kg}^{\text{m}}^2$
 - $I_{zz} = 1250 \text{ kg}^{\text{m}}^2$
- CP-CG offset is 1 m
 - results in a solar torque of $1.5 \text{ e-}4 \text{ Nm}$
- Dump momentum wheels at 75% capacity $\sim 9 \text{ Nms}$



• Reaction wheels saturate in ~ 12 hours before wheel saturation

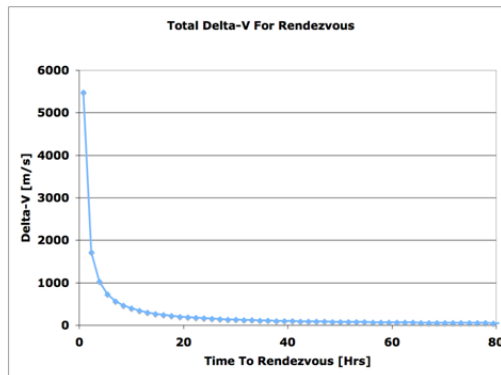


Delta-V For Rendezvous

Assuming:

The two vehicles share the same initial orbit and differ by 180 degrees of true anomaly

Initial Orbit = 400 km circular



Time to Rendezvous [Days]	Delta-V [m/s]	Prop. Used* [kg]
1	164.9	43.4
2	81.1	21.8
3	54.0	14.8
4	40.9	11.1

• A 3 day rendezvous was chosen

* Assuming an initial mass of 590 kg and Isp of 220 s

Communications

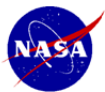
Joe Warner
COMPASS Team
10-29-10



Communications for Beam Propulsion Spacecraft LEO to GEO and back Introduction



- **Concept of operations**
 - The spacecraft will be in low Earth orbit and ferry another spacecraft to GEO
 - The spacecraft will return to LEO by itself or with another satellite
 - The spacecraft will use beam propulsion to change orbits
- **Communication concept**
 - When the laser beam is on the spacecraft will communicate to TDRS at a data rate of 4.8 kbps maximum
 - When the laser beam is off the spacecraft will communicate to on of Earth's 34 meter diameter dishes at data rates up to 3 Mbps
 - There is no need for navigation to use two-way coherent navigation
 - The system will be redundant
 - Lifetime of the spacecraft 5 years or less
 - No software defined radio on the spacecraft



Communications for Beam Propulsion Spacecraft LEO to GEO and back Communication system



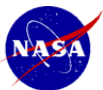
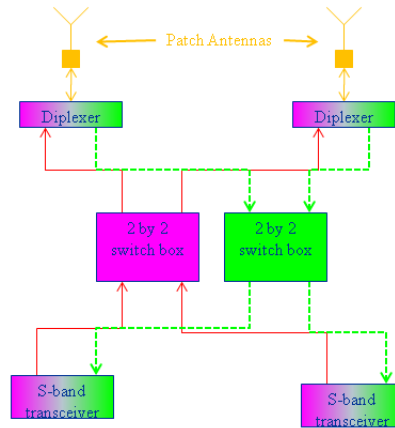
- **Communication System**
 - The communication system will be single fault tolerant
 - The components will be off the shelf
 - The transmit power will be 8 Watts
 - The maximum range is 73,000 km
 - The antennas will be patch antennas to form a donut shaped beam pattern
 - Communicate at S-band to TDRSS and to the ground
 - 26 Watts of total DC power will be needed
 - 21 Watts transmit
 - 5 Watts receive
 - Coding Viterbi rate $\frac{1}{2}$ with Reed-Solomon
 - BER 10^{-8}
 - $E_b/N_0 > 4.5$ dB



Communications for Beam Propulsion Spacecraft LEO to GEO and back Communication system



- **Communication System Diagram**

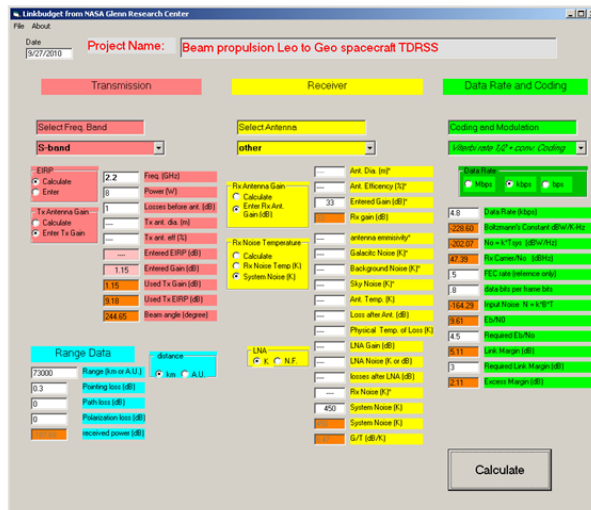


Communications for Beam Propulsion Spacecraft LEO to GEO and back Communication system



- **Communication System Linkbudget**

- At maximum distance the spacecraft will be away from a TDRS satellite
- Data rate 4.8 kbps



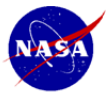
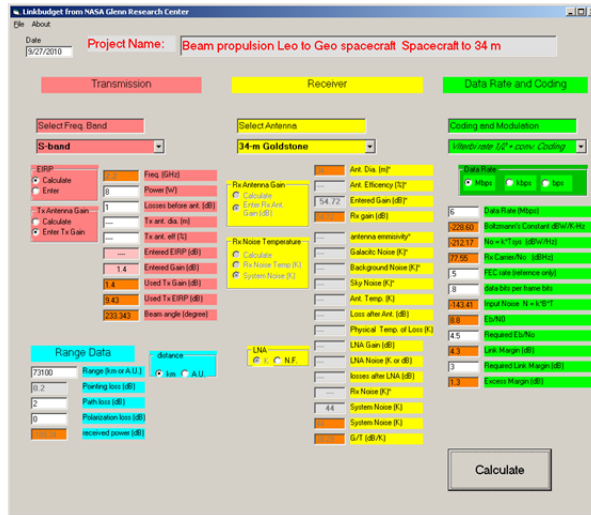


Communications for Beam Propulsion Spacecraft LEO to GEO and back Communication system



- **Communication System Linkbudget From GEO to Earth**

- At maximum distance the spacecraft will be away from an Earth station
- Data rate 3 Mbps

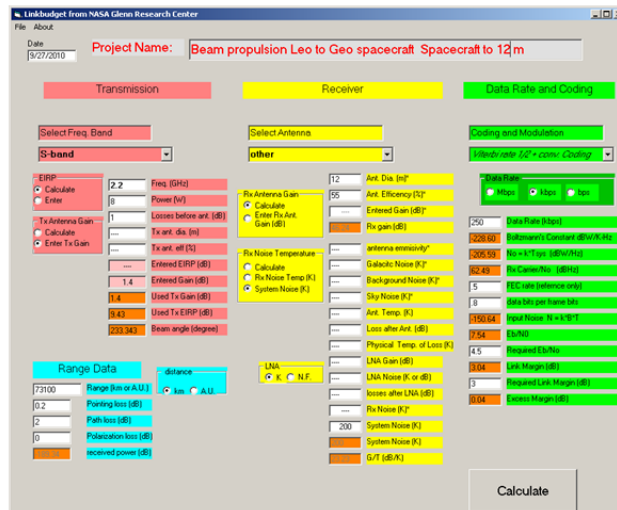


Communications for Beam Propulsion Spacecraft LEO to GEO and back Communication system



- **Communication System Linkbudget From GEO to Earth 12 meter**

- At maximum distance the spacecraft will be away from an Earth station
- Data rate 250 kbps





Communications for Beam Propulsion Spacecraft LEO to GEO and back Communication system



- **Risks beyond standard risks**
 - The main risk is the impingement of the laser beam on the patch antennas.
 - With a beam power of 300 MW over a 10 square meter area the power intensity on the patch antenna is 3000 W/cm².
 - Even using a mirror coating on the patch antenna that is 99.9% reflective still gives 3 W/cm² to be absorbed by the film
- **Level of risk is severe**
 - Loss of mission is high
 - Probability of occurrence is high
- **Mitigation of the risk**
 - On the patch antennas use the same dielectric / metal coating that is used on rest of the space craft
 - Change the shape of the antennas to compensate for the decrease gain.
 - Use lower power laser beams to align high power laser before firing.
- **Technology development and testing**
 - Develop the high reflective film to be used on the patch antenna
 - Measure is microwave properties
 - Design the patch antennas with the reflective film
 - Measure the patch antennas microwave properties
 - Measure the patch antennas performance in the laser beam
 - Adjust the transmit power levels for the gain of the patch antennas

Power

James Fincannon, Kristen Bury
COMPASS Team
10-29-10



BEP LEO GEO Power Requirements/Assumptions



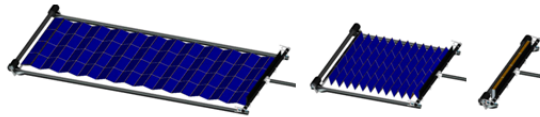
- **Requirements:**
 - One fault tolerant battery pack, solar array strings, gimbal motor/gearbox
 - Nominal orbital user power (day and night)= 529W (includes 30% growth)
 - Extra power needed during laser firing for pumps = 1625 W (includes 30% growth) for 10 minutes
 - LEO Orbit=800 km (102 minute orbit period/35 minute eclipse)
 - GEO Orbit= 67 minutes of umbra+ 4 minutes of penumbra=71 minutes
 - Intermediate orbits based on 24 hr from LEO to GEO using 10 orbits (no missed firing periods) and 9 deg in inclination for LEO phase and 3000 km intermediate orbit
 - Life= 2 years (10 cycles from LEO to GEO to LEO)
- **Assumptions**
 - To minimize the solar array area and mass, full two axis gimbal Sun tracking is assumed.
 - Worst case LEO battery sizing includes 1 minutes solar array off-pointing (1 minute to move behind spacecraft)+ 5 minute laser firing+ 1 minute solar array re-tracking immediately prior to eclipse period
 - Worst case LEO battery sizing includes extra energy to power pump.
 - Worst case GEO battery sizing assumes not laser firing near eclipse
 - Using SPENVIS, radiation degradation over mission profile using 12 mil coverglass= 15%
 - Other solar array degradation over mission due to atomic oxygen, ultraviolet radiation, thermal cycling, contamination, orbital debris/micrometeorites= 12%
 - Triple Junction Solar Cell Efficiency :Beginning of life (no degradations) = 32%,End of life (with degradations)= 24%
 - 13% losses in power system (due to electronics/harness/connector efficiencies)
 - Areal mass= 3.25 kg/m² (assuming 12 mil coverglass on each side of solar cell)
 - Cell packing factor into solar array = .86
 - Lithium batteries= 200 W-hr/kg, 33% depth of discharge (limited due to redundancy requirement and high LEO cycling)
 - 28 Vdc



BEP LEO GEO Power Design



- **Design Description:**
 - **1 solar arrays**
 - Roll Out Solar Array (ROSA); Z-fold type
 - Self deploying, highly compact stowed volume, much lighter than rigid panel solar arrays (reduces gimbal requirements), minimum parts/complexity, should be minimum cost in quantity
 - Area/wing= 5 m²
 - Size= 1.5 m by 3.3 m
 - Stowed volume= 1.5 m by .14 m by .14 m
 - Mass/wing= 20.8 kg (includes 30% growth)
 - **1 two axis gimbal**
 - Standard, low power gimbals with redundant motor/gears
 - Mass/gimbal= 3.9 kg (includes 30% growth)
 - **1 lithium ion battery pack**
 - SOA lithium batteries have testing experience at low to moderate depth of discharge for LEO use; the advanced ones (200 W-hr/kg) should have accumulated adequate LEO testing by the TRL cutoff date.
 - Rated energy capacity= 2000 W-hr
 - Size= 8 inches by 8 inches by 8 inches
 - Mass= 15.6 kg (includes 30% growth)
 - *Power electronics (solar array peak power regulator, power distribution, battery charge/discharge regulator), gimbal electronics and harness carried by avionics subsystem*



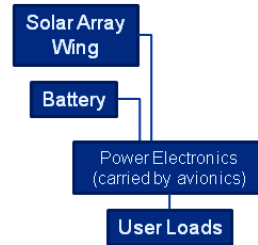


BEP LEO GEO Power Design



- **Technology Status:**

- Solar array= TRL 4
- Gimbal= TRL 8
- Batteries= TRL 4



WBS Number	Description	QTY	Unit Mass (kg)	Basic Mass (kg)	Growth (%)	Growth (kg)	Total Mass (kg)
	BEP LEO GEO Inspace			31.00	30.0%	9.30	40.30
06	BEP LEO GEO Inspace			31.00	30.0%	9.30	40.30
06.1	Transport Stage			31.00	30.0%	9.30	40.30
06.1.4	Electrical Power Subsystem			31.00	30.0%	9.30	40.30
06.1.4.a	Solar Array Power System			19.00	30.0%	5.70	24.70
06.1.4.a.a	Solar Array	1	16.00	16.00	30.0%	4.80	20.80
06.1.4.a.b	Solar Array gimbal	1	3.00	3.00	30.0%	0.90	3.90
06.1.4.d	Battery System			12.00	30.0%	3.60	15.60
06.1.4.d.b	Battery Assembly-Secondary	1	12.00	12.00	30.0%	3.60	15.60



BEP LEO GEO Power Risks/Trades

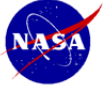


- **Risk**

- Unknown laser firing frequency: Due to likely desired avoidance of orbiting objects and the uncertainty of the orbital elements (frequency of passing through NORAD radar fences), and due to the large swaths of azimuth and elevation the laser must pass for the LEO altitude firings, it may not be possible to fire within the desired 24 hour LEO to GEO period (orbits missed and thus must be added, regardless of how many stations). This will increase the amount of radiation flux and result in the need for larger solar arrays (size and/or mass due to coverglass thickness increase).

- **Trades:**

- Fixed vs Tracking Solar Arrays: Body mounted arrays increase the size of the solar array (50-100%) due to a decreased effective sun period and cosine losses while the energy storage mass would also increase due to an increased effective eclipse period. **Tracking arrays** were selected.
- Tracking Method of Solar Arrays: To Sun-track the solar arrays, you can use: 1) inertial flight (i.e. pointing the entire spacecraft at Sun), 2) two axis gimbals for each solar array or 3) one axis gimbal for each solar array wing with yaw steering. For this large spacecraft, the yaw steering method may not be practical, so **two axis gimbals** were selected with some TBD favorable spacecraft attitude tracking.
- Radiation Amelioration: To handle the radiation degradation, one can either increase the size of the solar arrays and use a thin coverglass or have a smaller solar array with heavy thick coverglass or some optimum in between. An analysis using SPENVIS data for the orbits provided showed that **12 mil coverglass** (rather than the original 3 mil) was an optimum mass solution. This will change depending on the precise design of the solar array and transfer orbits/durations and number of missions.



BEP LEO GEO Power Recommendations/Work to be Done



- **Must include more realistic durations during radiation belt passages (due to missing laser firings for whatever reason)**
- **Assess shadowing impact and attitude/tracking method on solar arrays.**
- **Use improved PEL to assess sizing needs better.**
- **Consider use of higher TRL, heavier battery (SOA lithium) and solar array (SOA rigid panel solar array) to reduce design risk.**

Propulsion

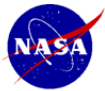
**James Fittje
COMPASS Team
10-29-10**



Beamed Energy Propulsion



- Provides Energy for Vehicle Main Propulsion via Ground Based Laser
- Parabolic Optical Surfaces Concentrate Laser Energy into Engine Thrust Chamber
- Sapphire Window Allows Passage of Concentrated Laser Energy into Thrust Chamber
- Propulsion is Provided via Laser Heating of Water Monopropellant into Plasma
- Engine Thrust Chamber Shaped to Focus Radiant Energy onto Propellant at Center of Thrust Chamber
- Thrust Chamber and Nozzle Regeneratively Cooled to AR=50



Requirements and Assumptions



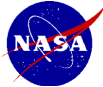
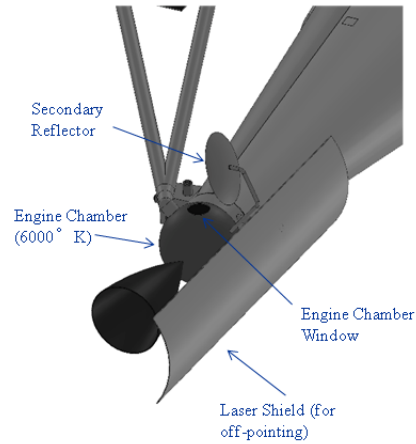
- **Requirements**
 - Single Fault Tolerant System
 - Transport Stage to Dock with Propellant Tank Stage which Carries Propellant for Entire Mission
 - Laser Based Rocket Engine to Provide Main Propulsion
 - Additional Propulsion System to Return Transport and Tank Stage to LEO
 - RCS to Provide Attitude Control
- **Assumptions**
 - ISP of 813 with Water Monopropellant
 - Chamber Conditions of 6000K and 50Psia
 - 1/3 Equilibrium Flow, 2/3 Frozen Flow
 - 98.5% Efficient Nozzle (AR=500)
 - 30MW of Beamed Power Reach Thrust Chamber
 - Laser System Can Adequately Continuously Track and Beam Energy to Vehicle
 - Regenerative and Film Cooling of Thrust Chamber Surfaces



Propulsion Overview



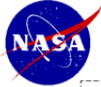
- **Two Reflectors to Concentrate the Beam**
- **Single Main Engine w/ Gimbaled Nozzle**
- **RCS on Transport Stage**
- **RCS Refueled by Propellant on Transport Stage**
- **Propellants Carried to LEO on Tank Stage**
- **Water Pumps on Transport Stage to Feed Main Engine**
- **Main Engine both Regeneratively and Film Cooled**
- **Single Fault Tolerant Feed Systems**



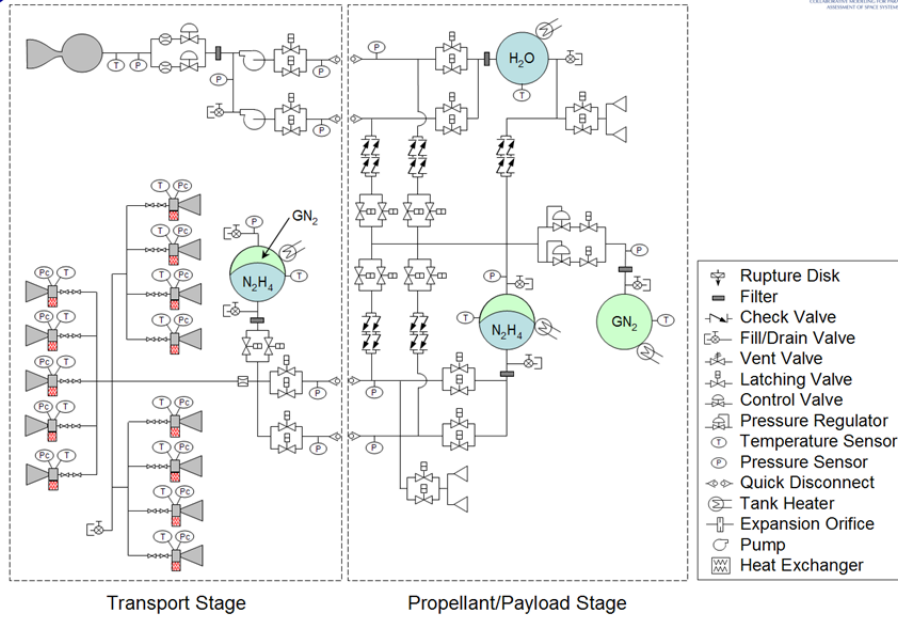
RCS



- **COTS Membrane Tank on Both Transport and Tank Stages**
- **Gaseous Nitrogen Pressurant**
- **13 Aerojet MR-50S Thrusters**
 - 228s ISP
 - 5lbf Thrust
- **Located in 3 Locations**
 - 2 Pods of 4
 - 1 Pod of 5
- **Unique Placement Required to Avoid Possible Exposure to Beam**



Preliminary P&ID



BEP LEO GEO Payload/Propellant Stage: Propellant



WBS	Description	QTY	Unit Mass	Basic Mass	Growth	Growth	Total Mass
Number			(kg)	(kg)	(%)	(kg)	(kg)
06	BEP LEO GEO Inspace - October 2010			9576.91	1.1%	103.06	9679.97
06.1	Transport Stage			468.37	13.3%	62.33	530.70
06.2	Payload/Propellant Stage			9108.54	0.4%	40.73	9149.27
06.2.2	Propellant			4895.50	0.0%	0.00	4895.50
06.2.2.a	Propellant			4895.50	0.0%	0.00	4895.50
06.2.2.a.a	Main Propellant	1	4814.53	4814.53	0.0%	0.00	4814.526752
06.2.2.a.b	Propellant Stage RCS Propellant	1	31.26	31.26	0.0%	0.00	31.26429623
06.2.2.a.c	Main Propellant Residuals	1	48.15	48.15	0.0%	0.00	48.14526752
06.2.2.a.d	RCS Residuals	1	1.56	1.56	0.0%	0.00	1.563214811
06.2.2.a.e	Misc#5	0	0.00	0.00	0.0%	0.00	0
06.2.2.a.f	Misc#6	0	0.00	0.00	0.0%	0.00	0
06.2.2.a.g	Misc#7	0	0.00	0.00	0.0%	0.00	0
06.2.2.a.h	Misc#8	0	0.00	0.00	0.0%	0.00	0
06.2.2.a.i	Misc#9	0	0.00	0.00	0.0%	0.00	0
06.2.2.a.j	Misc#10	0	0.00	0.00	0.0%	0.00	0
06.2.2.b	Misc#1			0.00	0	0.00	0



BEP LEO GEO Payload/Propellant Stage: Propulsion (Hardware)



WBS	Description	QTY	Unit Mass	Basic Mass	Growth	Growth	Total Mass
Number	BEP LEO GEO Inspace - October 2010		(kg)	(kg)	(%)	(kg)	(kg)
06	BEP LEO GEO Inspace			9576.91	1.1%	103.06	9679.97
06.1	Transport Stage			468.37	13.3%	62.33	530.70
06.2	Payload/Propellant Stage			9108.54	0.4%	40.73	9149.27
06.2.7	Propulsion Hardware			120.92	12.3%	14.93	135.85
06.2.7.a	Misc#1			0.00	0	0.00	0.00
06.2.7.b	Propulsion Hardware			120.92	12.3%	14.93	135.85
06.2.7.b.a	Main Propellant Feed System	1	4.15	4.15	12.0%	0.50	4.65
06.2.7.b.b	RCS Propellant Feed System	1	3.75	3.75	8.0%	0.30	4.05
06.2.7.b.c	Main Propellant Tank	1	67.66	67.66	18.0%	12.18	79.84030846
06.2.7.b.d	RCS Propellant Tank	2	7.71	15.43	2.0%	0.31	15.74
06.2.7.b.e	Pressurant Tank	1	9.98	9.98	2.0%	0.20	10.1814882
06.2.7.b.f	Main Docking H/W	2	2.00	4.00	18.0%	0.72	4.72
06.2.7.b.g	RCS Docking H/W	2	2.00	4.00	18.0%	0.72	4.72
06.2.7.b.h	Trapped Pressurant GN2	1	11.95	11.95	0.0%	0.00	11.95



Risks



- Maintenance of Appropriate Beam Angle Relative to Vehicle Reflectors
- Excessive Heating of Thrust Chamber Walls
- Inability of Reflectors and Thrust Chamber to Achieve Adequate Plasma Temperatures and Flow Rates
- Inadequate Regenerative Cooling Exposed Hot Surfaces
- Unobtainable Specific Impulse Value
- Failure to Successfully Dock with Payload Stage



Future Trades



- **Different Main Propellants**
 - Ammonia
 - Methane
 - Hydrazine
 - Hydrogen
- **Possible Integration of RCS and Main Propellant if New Main Propellant is Chosen**
- **Storing Some Main Propellant on Transport Stage Allowing Main Engine to Assist with Orbital Maneuvers in LEO**

Thermal

Tony Colozza
COMPASS Team
10-29-10



Thermal Subsystem - Overview



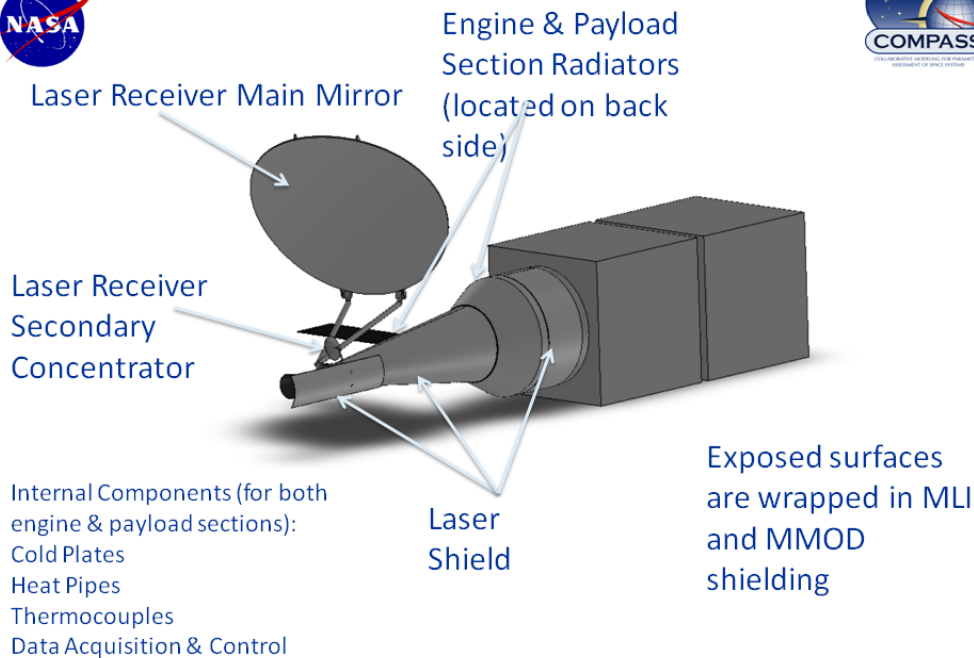
- Thermal assumptions In orbit**
- Heat dissipation of 90 w each for both the engine and payload sections
 - Earth view factor of 0.5
 - Solar array view factor of 0.15
 - 30° sun angle
- Thermal assumptions Laser Receiver**
- A off-set parabolic surface will be used to receive the laser beam and concentrate it into the engine plasma chamber.
 - Mirror reflectivity 0.9999
 - Back side of the mirror can be used to radiate excess heat to space.
 - The mirror consists of a single reflective surface with a secondary concentrator, structure, drive motors, shield and launch structure
 - Laser mirror shields are placed on the bottom half of the vehicle (both engine and payload sections), in the direction facing the laser to reflect any inadvertent laser impact from hitting the vehicle.
- The thermal subsystem components**
- MMOD Shielding
 - Cold plates and heat pipes to transfer from the electronics to the radiator section.
 - Heaters, sensors, data acquisition and controller
 - MLI is used to insulate the outside of the vehicle.
 - Heaters, sensors, data acquisition and controller
 - MLI is used to insulate the outside of the vehicle.
- Environmental models**
- LEO environmental conditions were used to determine the heat transfer while in orbit.
- Thermal System Mass: 182.66 kg**
- Trades considered in analysis**
- 2 mirror shapes were considered, a standard parabolic Cassigrainan arrangement and an off-set parabola.
 - Mirror arrangement to shield the vehicle and the use of additional mirrored laser shields.
- Options to Reduce mass and recommendations:**
- The mirror surface (for both the laser receiver and shielding) is vulnerable to micro meteor impacts. These impacts can cause a failure of the mirror if its surface reflectivity is reduced. Mitigation approaches should be investigated to minimize this impact.
 - Further analysis and experimentation should be performed to determine the amount of mirror degradation that will occur (if any) during operation.

BEP LEO GEO Inspace		182.66
Transport Stage		115.92
Thermal Control (Non-Propellant)		115.92
Active Thermal Control		2.65
Heaters	10	0.10
Thermal Control/Heaters Circuit	2	0.20
Data Acquisition	1	1.00
Thermocouples	20	0.18
Misc#1	0	0.00
Misc#2	0	0.00
Passive Thermal Control		19.61
Heat Sinks	4	0.14
Heat Pipes	4	0.30
Radiators	1	2.02
MLI (Multi Layer Insulation)	1	4.20
Temperature sensors	0	0.00
Louvers	0	0.00
Thermal Coatings/Paint	1	0.10
Micro Meteor shielding	1	8.21
Laser Shield (mirror)	1	3.33
Misc#1	0	0.00
Misc#3	0	0.00
Misc#4	0	0.00
Misc#5	0	0.00
Misc#6	0	0.00
Mirror System		93.66
Mirror, Primary	1	25.99
Structure, Mirrors	1	14.85
Drive Motor (airbrak), Primary Mirror	1	18.28
Misc_1	1	0.00
Walk-off shield	1	2.17
Misc_2	1	0.00
Instrumentation	1	7.12
Mirror Launch Support System	1	24.75
Payload/Propellant Stage		66.74
Thermal Control		66.74
Active Thermal Control		3.34
Heaters	10	0.10
Thermal Control/Heaters Circuit	2	0.20
Data Acquisition	1	1.00
Thermocouples	14	0.04
Misc#1	0	0.00
Misc#2	0	0.00
Misc#3	0	0.00
Passive Thermal Control		26.76
Heat Sinks	4	0.14
Heat Pipes	4	0.12
Radiators	1	2.02
MLI (Multi Layer Insulation)	1	33.37
Temperature sensors	0	0.00
Thermal Coatings/Paint	1	0.33
Misc#1	0	0.00
Misc#2	0	0.00
Misc#3	0	0.00
Misc#	1	62.64
Payload Laser Shield	1	26.64

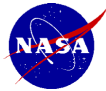
93



Thermal System Components & Layout



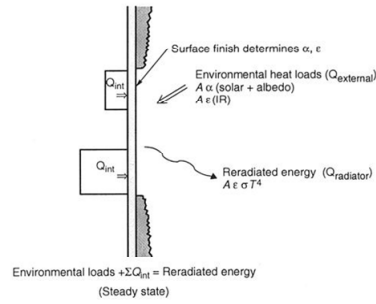
94



Thermal Analysis: Radiator Sizing

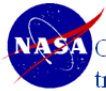


- 2 Radiator panels were sized for use on the vehicle. One for the engine section and one for the payload section.
- A surface mount radiator was used for both locations.
- The radiator model was based on a first principles analysis of the area needed to reject the identified heat load to space. From the area a series of scaling equations were used to determine the mass of the radiator. Worst case thermal environment of LEO was used to size the radiator.
- No louvers were utilized
- Heat Pipes were used to conducted heat to the radiator surface.



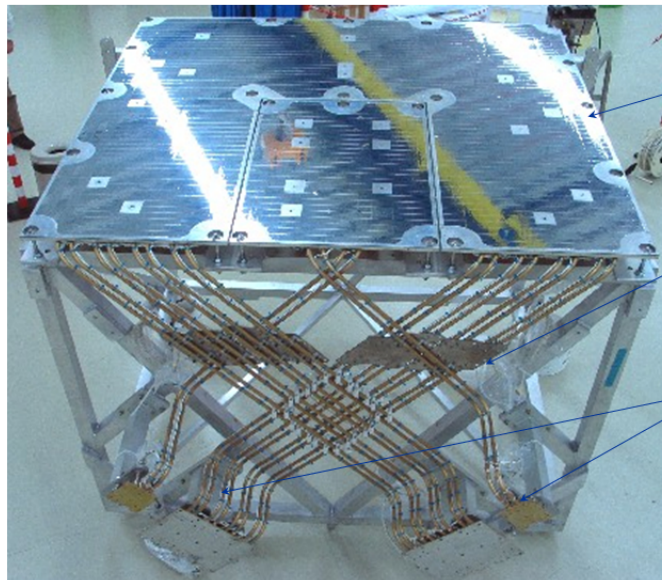
Variable	Value
Radiator Solar Absorptivity	0.14
Radiator Emissivity	0.84
Radiator Sun Angle	70°
Radiator Operating Temperature	320 K
Total Radiator Dissipation Power	90 W
View Factor to Earth	0.5
View Factor to the Solar Array	0.15

95



Spacecraft Radiator System Example

Cold plates are used to remove heat from the electronics. The heat is transferred to the radiator through a series of heat pipes connected to the cold plates and the radiator.



Radiator Panel

Heat Pipes (transfer heat through phase change of an internal working fluid)

Cold Plates (conductive aluminum plates)

www.nasa.gov

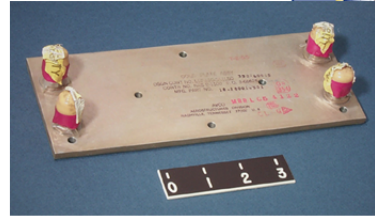


Thermal Analysis: Electronics Cooling



•The electronics cooling is accomplished through the use of cold plates and heat pipes. The electronic components are mounted onto the cold plates which have integral heat pipes incorporated into them. The heat pipes remove heat from the cold plate and transport it to the radiator.

•The cold plates also have heaters integrated onto them and can be used to maintain the electronics at the desired temperature throughout the mission.



Example Cold Plate

Assumptions used

Variable	Value
Cooling Plate & Line Material	Aluminum
Cooling Plate & Line Material Density	2,770 kg/m ³
Number of Cooling Plates	4 Engine Section & 4 Payload Section
Cooling Plate Length	0.1 m
Cooling Plate Width	0.1 m
Cooling Plate Thickness	5 mm
Heat Pipe Specific Mass	0.15 kg/m

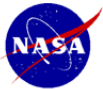


Heaters & Thermal Control



Strip heaters, were used to provide heat to the propellant lines and other components within the spacecraft. Immersion heaters, were used to provide heat to the propellant tanks. Flat plate heaters were used on the cold plates to provide heat to the electronics if necessary.

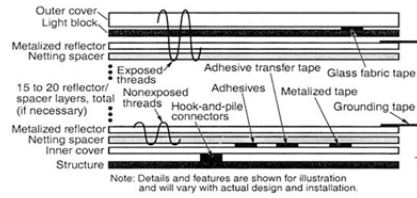
Thermal control is accomplished through the use of a network of thermocouples whose output is used to control the power to the various heaters. A data acquisition and control computer is used to operate the thermal system.



Thermal Analysis: Spacecraft Insulation



- Multi-Layer Insulation (MLI) was used to insulate the spacecraft, both the engine and payload sections.
- MLI operates by limiting radiation heat transfer to and from the spacecraft. Each layer of the MLI has a low emissivity which limits radiation heat transfer between the layers.
- MLI is constructed of a number of layers of metalized material with a nonconductive spacer between the layers. The metalized material has a low absorptivity which resists radiative heat transfer between the layers.



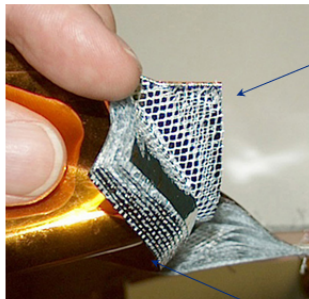
Assumptions used

Variable	Value
Tank Surface Emissivity (ϵ_r)	0.1
MLI Emissivity (ϵ_i)	0.07
MLI Material	Aluminum
MLI Material Density (ρ_i)	2,770 kg/m ³
Internal Tank Temperature (T_i)	300 K
MLI Layer Thickness (t_i)	0.025 mm
Number of Insulation Layers (n_i)	10
MLI Layer Spacing (d_i)	1.0 mm
Tank Immersion Heater Mass & Power Level	1.02 kg @ up to 1,000 W
Spacecraft Inner Wall Surface Emissivity	0.98
Spacecraft Outer Wall Surface Emissivity	0.93
Line Foam Insulation Conductivity	0.0027 W/m K
Line Foam Insulation Emissivity	0.07
Propellant Line Heater Specific Mass & Power	0.143 kg/m @ up to 39 W/m
Line Foam Insulation Density	56 kg/m ³

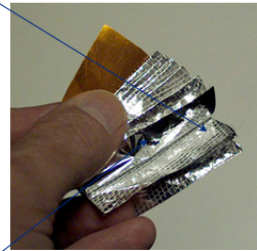
www.nasa.gov



MLI Blanket



Mesh Spacer



Individual Metalized Layers

MLI can be conformed to fit over various shapes. It can be held in place with Velcro or glue.



MLI covering the outside of a spacecraft

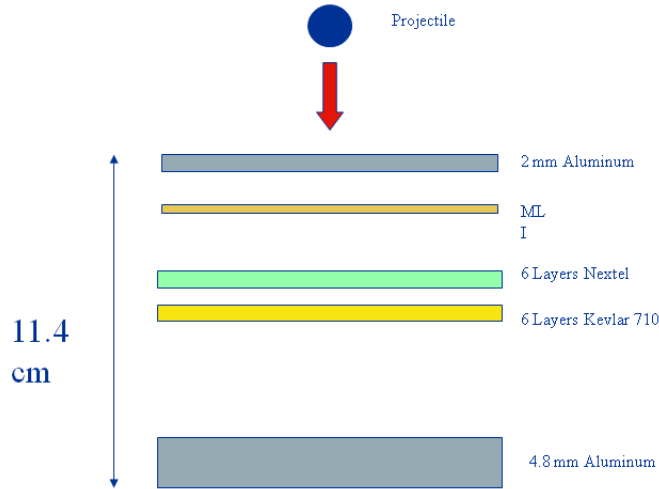




US Module MMOD Shielding Configuration on the International Space Station

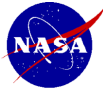


Micro-Meteor and Orbital Debris (MMOD) shielding was placed on the deep space facing side of the engine and payload portions of the spacecraft. This shielding minimizes the effect of impacts to the vehicle by shattering the particle and absorbing its kinetic energy.



Reference: TP-2003-210788, "Meteoroid/Debris Shielding"

Laser Reflector and Concentrator

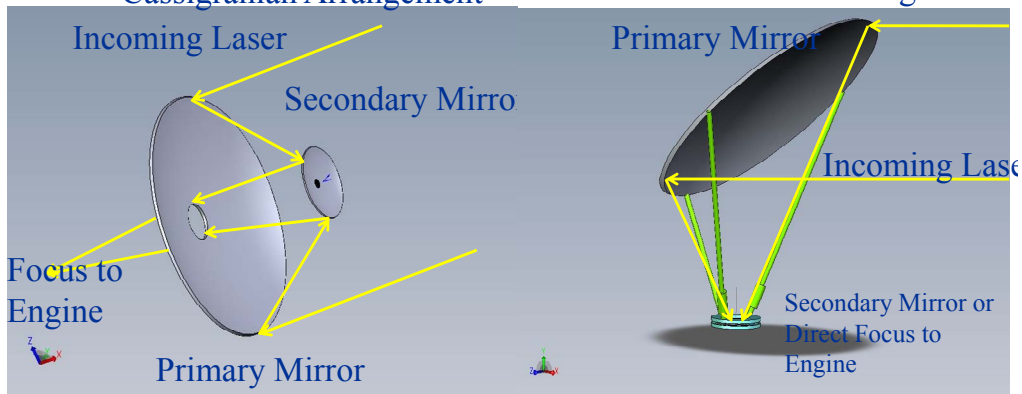


- The laser reflector is used to collect the incoming laser radiation and direct and concentrate it into the plasma engine.
- Two types of laser reflectors were considered:
 - A parabolic Cassigranian configuration
 - A off-set parabolic configuration.
- Both utilize a secondary reflector to further concentrate and direct the laser into the plasma engine.

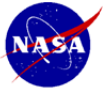


Cassigranian Arrangement

Off-Set Parabola Arrangement



•The Off-set Parabola was selected due to the entrance angle limitations of the laser into the plasma engine. The cassigranian design required entrance angles of up to 60°, this was beyond the capabilities of the refractive optics on the plasma engine.

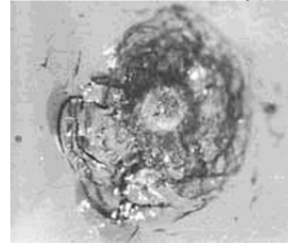


Risks



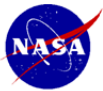
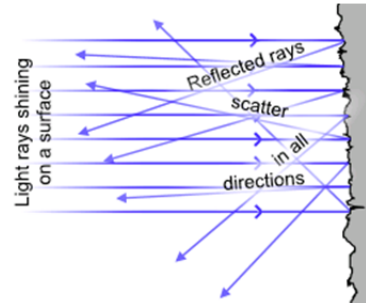
The main risk with the thermal system components pertains to the laser reflectors and shielding.

Any damage to the mirrored surface of these components can cause excessive local heating due to the intensity of the laser beam (approximately 312 W/cm²). Micro meteor or other debris can pose a mission risk if they impact the mirror surfaces.



Mercury Spacecraft Micrometer Impact on Window

Laser Light scattered off of the reflective shield can potentially be reflected back to earth. This could be a health hazard to someone who inadvertently looks into the reflected beam. The power of the reflected beam that reaches the Earth's surface will depend on the curvature of the shield mirror's surface and the distance from the Earth. The higher the shield curvature the greater the laser light dispersion and therefore the lower the intensity of the reflected beam. To reduce this risk a diffuse reflecting surface would be needed. A mirrored surface that has conical reflecting surfaces etched onto it may be able to disperse the incoming laser perpendicular to the incoming beam, limiting the reflection back toward the surface.



BEP LEO GEO Payload/Propellant Stage: Thermal Control



WBS	Description	QTY	Unit Mass	Basic Mass	Growth	Growth	Total Mass
Number	BEP LEO GEO Inspace - October 2010		(kg)	(kg)	(%)	(kg)	(kg)
06	BEP LEO GEO Inspace			9576.91	1.1%	103.06	9679.97
06.1	Transport Stage			468.37	13.3%	62.33	530.70
06.2	Payload/Propellant Stage			9108.54	0.4%	40.73	9149.27
06.2.6	Thermal Control			66.74	15.0%	10.01	76.75
06.2.6.a	Active Thermal Control			3.34	15.0%	0.50	3.84
06.2.6.a.a	Heaters	10	0.10	1.00	15.0%	0.15	1.15
06.2.6.a.b	Thermal Control/Heaters Circuit	2	0.20	0.40	15.0%	0.06	0.46
06.2.6.a.c	Data Acquisition	1	1.00	1.00	15.0%	0.15	1.15
06.2.6.a.d	Thermocouples	94	0.01	0.94	15.0%	0.14	1.081
06.2.6.a.e	Misc#1	0	0.00	0.00	15.0%	0.00	0
06.2.6.a.f	Misc#2	0	0.00	0.00	15.0%	0.00	0
06.2.6.a.g	Misc#3	0	0.00	0.00	15.0%	0.00	0
06.2.6.b	Passive Thermal Control			36.76	15.0%	5.51	42.27
06.2.6.b.a	Heat Sinks	4	0.14	0.55	15.0%	0.08	0.64
06.2.6.b.b	Heat Pipes	4	0.12	0.48	15.0%	0.07	0.55
06.2.6.b.c	Radiators	1	2.02	2.02	15.0%	0.30	2.32
06.2.6.b.d	MLI (Multi Layer Insulation)	1	33.37	33.37	15.0%	5.01	38.38
06.2.6.b.e	Temperature sensors	0	0.00	0.00	15.0%	0.00	0.00
06.2.6.b.f	Thermal Coatings/Paint	1	0.33	0.33	15.0%	0.05	0.38
06.2.6.b.g	Misc#1	0	0.00	0.00	15.0%	0.00	0.00
06.2.6.b.h	Misc#2	0	0.00	0.00	15.0%	0.00	0.00
06.2.6.b.i	Misc#3	0	0.00	0.00	15.0%	0.00	0.00
06.2.6.c	Misc			26.64	15.0%	4.00	30.64
06.2.6.c.a	Payload Laser Shield	1	26.64	26.64	15.0%	4.00	30.64

Mechanical

John Gyekenyesi
COMPASS Team
10-29-10

105

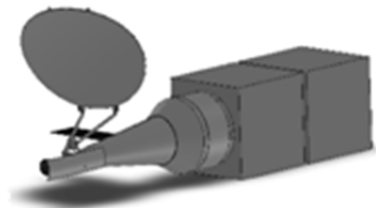
National Aeronautics and Space Administration



Structure Subsystem - Description



- **Structures and Mechanisms Design Requirements**
 - Contain necessary hardware for research instrumentation, avionics, communications, propulsion and power
 - Withstand applied mechanical and thermal loads from launching and operation
 - Provide minimum deflections, sufficient stiffness, and vibration damping
 - Minimize weight



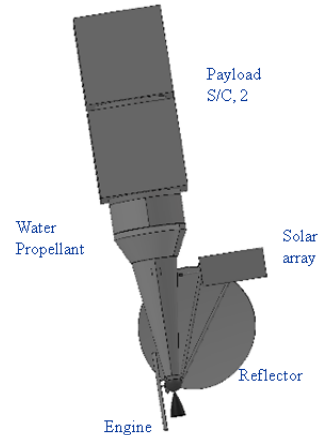
Transport stage docked with
Propellant/Payload stage



Structure Subsystem - Description



- **Structures assumptions**
 - Provides main structures backbone for BEP vehicle
 - Materials: aluminum
 - Shells with flanges
 - Bonded, welded and threaded fastener assembly
- **The structures subsystem**
 - Shells or thrust tube bearing all operational loads
 - Science probes, payload to support.
- **Main structure material and design choice:**
 - All aluminum construction
 - TRL6
- **Primary Structure mass:**
 - All aluminum construction
- **Secondary Structure Mass:**
 - All aluminum construction
 - Installations
- **Spacecraft adaptor and separation/docking mechanism details**
 - Mechanical system mounts propulsion stage to launch vehicle and payload vehicle



Transport stage docked with Propellant/Payload stage



Structure Subsystem - Description



- **Design Highlights**
 - Aluminum components
 - Flanges for joining sections and mounting internal hardware of aluminum
- **Analytical Methods**
 - Analytical methods with spreadsheet for stress analysis
 - Stresses
 - Transport stage frustum
 - 25 MPa $< \sigma_y$ including 1.4 s.f., from 6 G launch vehicle axial loading
 - Propellant/Payload stage thrust tube
 - 23 MPa $< \sigma_y$ including 1.4 s.f., from 6 G launch vehicle axial loading
 - Propellant tank check
 - 114 MPa < 131 MPa limit for C/epoxy, with 49 kN load, 6 G, and 200 kPa
- **Trades considered in analysis**
 - None at this time
- **Options to Reduce mass and recommendations:**
 - Polymer matrix composites
 - Detailed stress analysis using FEA



Mechanisms Subsystem - Description



- **Mechanisms assumptions**
 - Provides docking and separation functions for transport stage with launch vehicle and payload stage
- **Mechanisms Mass:**
 - 3.2 kg mass
- **Trades considered in analysis**
 - None at this time



BEP LEO GEO Payload/Propellant Stage: Structures and Mechanisms



WBS	Description	QTY	Unit Mass	Basic Mass	Growth	Growth	Total Mass
Number	BEP LEO GEO Inspace - October 2010		(kg)	(kg)	(%)	(kg)	(kg)
06	BEP LEO GEO Inspace			9576.91	1.1%	103.06	9679.97
06.1	Transport Stage			468.37	13.3%	62.33	530.70
06.2	Payload/Propellant Stage			9108.54	0.4%	40.73	9149.27
06.2.8	Structures and Mechanisms			81.44	18.0%	14.66	96.10
06.2.8.a	Structures			81.44	18.0%	14.66	96.10
06.2.8.a.a	<i>Primary Structures</i>			76.28	18.0%	13.73	90.01
06.2.8.a.a.a	Main Bus Structure	1	76.28	76.28	18.0%	13.73	90.01
06.2.8.a.a.b	Misc#1	0	0.00	0.00	0.0%	0.00	0
06.2.8.a.a.c	Misc#2	0	0.00	0.00	0.0%	0.00	0
06.2.8.a.a.d	Misc#3	0	0.00	0.00	0.0%	0.00	0
06.2.8.a.a.e	Misc#4	0	0.00	0.00	0.0%	0.00	0
06.2.8.a.a.f	Misc#5	0	0.00	0.00	0.0%	0.00	0
06.2.8.a.a.g	Misc#6	0	0.00	0.00	0.0%	0.00	0
06.2.8.a.a.h	Misc#7	0	0.00	0.00	0.0%	0.00	0
06.2.8.a.b	<i>Secondary Structures</i>			5.16	18.0%	0.93	6.09
06.2.8.a.b.a	Balance Mass	0	0.00	0.00	0.0%	0.00	0
06.2.8.a.b.b	Support structure	1	1.76	1.76	18.0%	0.32	2.0768
06.2.8.a.b.c	Docking I/F System	1	1.44	1.44	18.0%	0.26	1.6992
06.2.8.a.b.d	Payload I/F System	1	1.96	1.96	18.0%	0.35	2.3128

Cost

John Drexler
COMPASS Team
10-29-10

iii

National Aeronautics and Space Administration



Cost Assumptions



- **DRAFT Cost Estimate based on COMPASS design**
- **All costs are in FY11\$M**
- **Estimates represent prime contractor cost plus fee (10%)**
- **This estimate assumes the following:**
 - Development approach: proto-flight
 - No ground spares included
 - Flight heritage is assumed as Off-The-Shelf (OTS) for most components
 - Model assumes TRL Level 6
 - This estimate does not include any cost for technology development
 - Represents the most likely estimate based on cost-risk simulation results
 - Parametric estimate based on mostly mass based CERs
 - Planetary systems integration wraps
 - Software not included
- **Does not include:**
 - Any insight/oversight costs (by NASA lead center)
 - Project Reserves
 - Mission Operations Costs
 - Ground Data Systems
 - Ground Laser System Costs



LEO-GEO Laser Tug Preliminary Cost ROM

(Represents Prime Contractor cost)



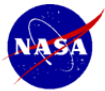
WBS	Description	DDT&E	Flight	Total
		Total BY \$M	HW BY \$M	
06.1	Transport Stage	111.9	56.3	168.2
06.1.1	Attitude Determination and Control	18.7	15.1	33.8
06.1.2	Command and Data Handling	7.0	5.5	12.5
06.1.3	Communications and Tracking	2.6	2.9	5.6
06.1.4	Electrical Power Subsystem	3.9	1.4	5.2
06.1.5	Thermal Control (Non-Propellant)	35.4	15.4	50.8 *
06.1.6	Propulsion (Hardware)	37.7	13.1	50.9
06.1.7	Propellant (Chemical)	0.0	0.0	0.0
06.1.8	Structures and Mechanisms	6.6	2.9	9.4
06.2	Payload/Propellant Stage	28.0	10.0	38.0
06.2.1	Payload Spacecraft	0.0	0.0	0.0
06.2.2	Propellant	0.0	0.0	0.0
06.2.3	Command and Data Handling	3.1	2.4	5.5
06.2.4	Communications and Tracking	0.0	0.0	0.0
06.2.5	Electrical Power Subsystem	0.0	0.0	0.0
06.2.6	Thermal Control	10.2	1.6	11.8 *
06.2.7	Propulsion	8.1	2.8	10.9
06.2.8	Structures and Mechanisms	6.6	3.3	9.9
Subtotal before Systems Integration		140.0	66.3	206.2
Systems Integration		97.4	18.9	116.3
Spacecraft Total		237.4	85.2	322.6
Prime Contractor Fee (Assumed 10%)		23.7	8.5	32.3
Spacecraft Total with Fee		261.1	93.7	354.8

Half of cost from docking system

Primarily laser reflectors and shielding

All Costs in FY11 \$M

* Moved cost of the Payload Mirror to the Transport Stage per direction



Cost Advantage of a Laser Transport (Preliminary)



- SOA Delivery Costs to deploy 20 GEO Spacecraft (Example)
 - Ten Falcon 9 : ~\$1000 M (@\$50M each)
 - Ten On-board apogee insertion system: ~\$100M (@ \$5M each)
 - Operations (Ten):
 - LEO restart of Upper stage, Perigee burn, separation and disposal ?
 - Apogee insertion burn with on-board system ?
- Laser Transport Costs to deploy 20 GEO Spacecraft (Example)
 - Eleven Falcon 9: \$550 M (10 for GEO birds, one for re-useable laser transport)
 - One laser Transport ~\$78M
 - Five Propellant Stage Systems ~\$100M
 - Operations:
 - Rendezvous of Transport and Payloads (10 times)
 - ~15 Laser burns in LEO and GEO to delivery payload (10 times)
 - ~5 laser burns to return transport to LEO (10 times)
- Cost Delta (excluding operations delta and cost of laser stations)
 - SOA (\$1100M) – Laser Transportation (\$728M) = ~\$372 M (~33% savings – without Laser and ops cost difference): Saves ~\$20 M / GEO Delivery
- How to increase savings?
 - Need to reuse transport more times (to offset the AR&D costs)
 - Reduce cost of propellant stage

3.2.2 Low-Earth-Orbit to Geosynchronous-Earth-Orbit Consultant Reports—Design Reference Mission 2–A

The Design Reference Mission 2–A (DRM 2–A) low-Earth-orbit to geosynchronous-Earth-orbit (LEO–GEO) *beamed-energy transport* tug will cut GEO lost costs in *half*. This savings will be enabled by the elimination of the Centaur upper stage and circularization engine required in current GEO launches. Instead, two 2000-kg GEO satellites will be launched into LEO on a single launch vehicle, rendezvous with the tug, and be transported to their circular GEO orbits in 32 hr. The tug will then return to LEO for another transport. In this manner, two GEO satellites could be placed into their orbits on a single launch.

3.2.2.1 Description of Vehicle

The DRM 2–A LEO–GEO tug was designed around a 5000-N thermal plasma engine. At 6000 K and a chamber pressure of 50 psia, the engine achieves a specific impulse I_{sp} of 813 s with a steam (H₂O) monopropellant. Forty-four megawatts of beamed power must reach the thrust chamber to achieve the required 6000 K temperature. To realize this energy level, power will be beamed from the ground and focused into the thrust chamber through primary and secondary reflectors and a large sapphire window. The primary reflector will actively track the laser emitters. Figure 3.143 shows a concept drawing of the tug and propellant stage.

The beamed-energy tug propulsion stage shown in Figure 3.144 is 5.78 m long and cylindrical, consisting of a 4.0- by 5.6-m elliptical primary reflector cantilevered off the side of the vehicle on a $\pm 60^\circ$ gimbal. Two degrees of freedom will be required to track the ground-based emitter, and either the entire vehicle will be rolled during a burn or another degree of freedom will be added to the gimbal (although a two-degree-of-freedom gimbal creates complications because the rotation does not occur about the focal point). The secondary reflector will be fixed. Both reflectors and shielding to protect the entire vehicle from the laser flux will be 97% efficient, 0.9999 reflective carbon fiber composite. A 1.5- by 3.3-m solar array will supply 560 W of nominal operating power, and a 2000-W-hr lithium-ion battery pack will supply an additional 1625 W during 5- to 15-min burns to run pumps, tracking, and so forth. The main engine will provide 5000 N of thrust with 50-psia pressure in a 30-cm spherical combustion chamber. The engine will use water heated to 6000 K to provide 813-s I_{sp} . The plasma ball will be electromagnetically suspended in the chamber, and the nozzle will be regeneratively cooled or film cooled. The beamed energy will pass through a 10-cm-diameter sapphire refractory window into the combustion chamber. The nozzle will have an area ratio of 50, will be regeneratively cooled, and will be gimbaled which will allow for orientation for communication pointing on a screw or ball mechanical motor.

The thermal plasma engine was selected because of the potential to provide sufficient thrust to perform the LEO–GEO transfer in a short time at a high enough I_{sp} to reduce fuel mass to enable the launch of two GEO satellites per launch.

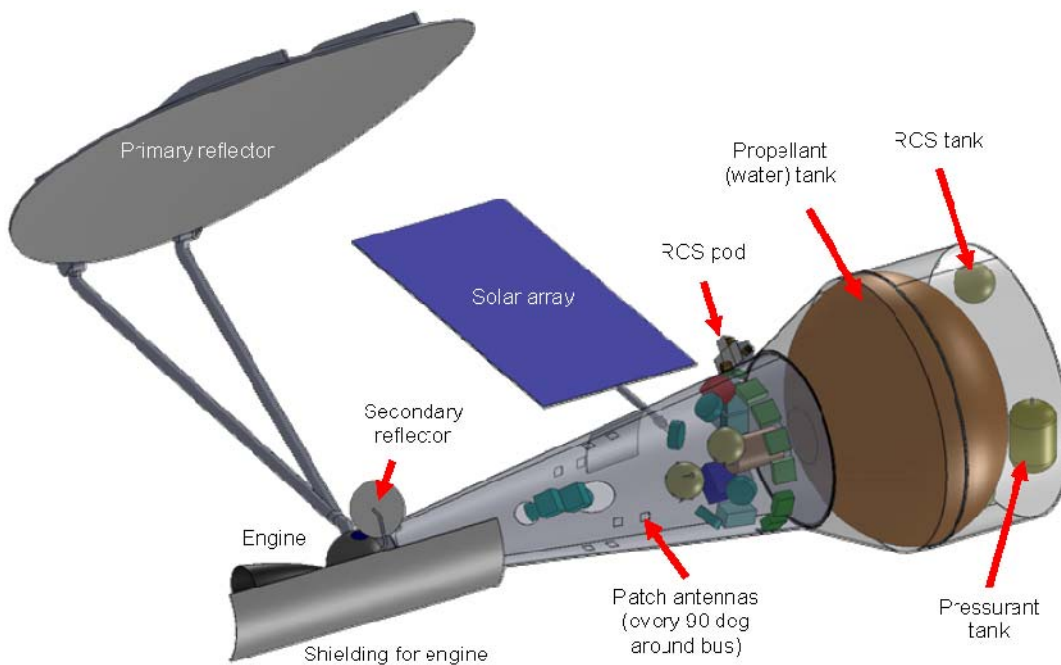


Figure 3.143.—Conceptual tug and propellant stage. RCS, Reaction Control System.

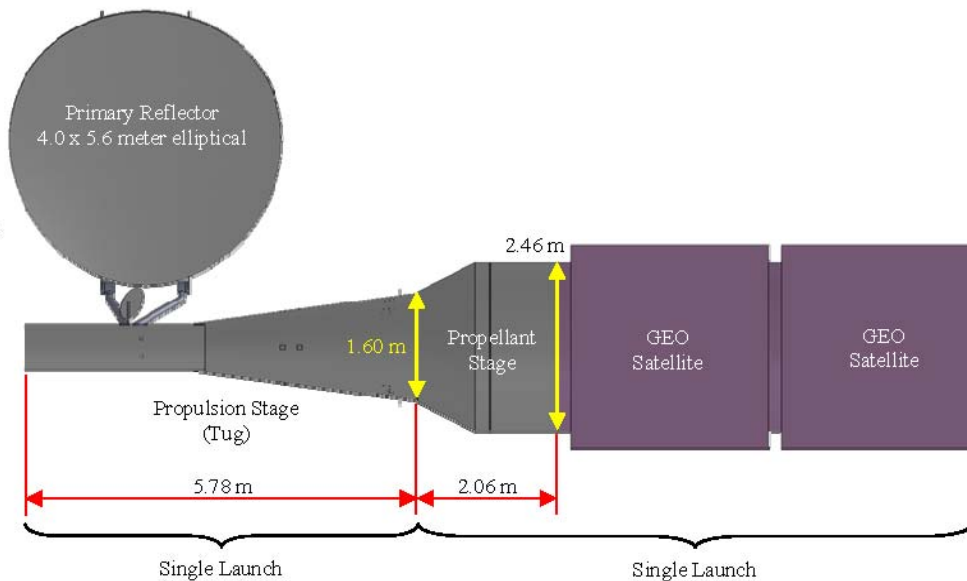


Figure 3.144.—Conceptual tug, propellant stage, and GEO satellites.

3.2.2.2 Description of Ground Facility

The DRM 2 mission as defined requires two types of laser ground facilities, a 2- to 3-m-diameter aperture Perigee Facility for burns for altitudes between 400 and 3000 km and a much larger diameter Apogee Facility for burns at GEO. Both types of laser facilities will be required to deliver about 50 MW of laser energy to the spacecraft. On the basis of atmospheric losses, each of the ground facilities will need an 80MW laser to deliver the required power to the tug. The apertures for these ground facilities will resemble large astronomical telescopes such as the Starfire Optical Range (SOR) and the proposed 30-Meter Telescope (TMT).

All of the facilities will have two main components, a Beam Generation system and a Beam Control System. In addition, each facility will require sufficient power and heat dissipation capacity for the operation of the laser.

3.2.2.2.1 Beam Generation

The Beam Generation system will create the photons at the power levels needed for beamed-energy propulsion (BEP). The laser could be solid state, chemical, or electrical, but the wavelength must be optimized for transmission through the atmosphere. The 80-MW laser required by this DRM is a technological challenge in that currently the chemical oxygen iodine laser (COIL) on the Airborne Laser Test Bed (ALTB) is the only megawatt-class laser currently in use. Solid state and electrically driven lasers are rated at about 100 kW.

The Solid State Laser's (SSL's) current efficiency of power output to all power consumed (wall-plug efficiency) is about 8% to 10%. There are significant variations to the above numbers (IPG claims ~25% wall-plug efficiency), but none of those devices offer a path to the power goal as coherent light.

Chemical lasers such as COIL offer a less risky path for the power goal, but these devices require pressure recovery systems that would eliminate any possibility of transportability at that power level. Also, the environmental opposition to the chemicals involved would pose a high political price for any program. COIL has shown that its power is directly scalable by adding additional laser modules in series. The research has also shown that COIL's performance could be dramatically improved with modified laser fuels and an improved singlet oxygen generator. The COIL runs at a very low internal pressure and requires the use of large vacuum reservoirs. It is feasible that enough laser modules could be linked together to generate the needed 80 MW. At this power (flux) level, the critical technologies would be the vacuum management, the optics, and the ability to maintain the integrity of the coatings.

An electrically driven 80-MW laser will require about 200 MW of electrical wall-plug power to operate. Laser run times are projected to be 5 to 15 min, and this power could be provided from batteries or flywheel energy storage systems instead of being drawn directly from the grid. Less developed than SSL, Diode-Pumped Alkali Laser (DPAL) gain generators use rubidium or cesium gas as the lasing species with narrow-band diode lasers for the pump. Their efficiency will be similar to SSL since both suffer from the poor efficiency of the diode laser pumps estimated today at about 50% (reported higher efficiencies usually ignore the losses due to poor spectral matching with the stimulated species). To date, no electric laser has been able to show direct scalability to 80 MW. At this power level, the laser would be 2 orders of magnitude larger than any current state-of-the-art electrically driven laser. Current research on DPALs shows promise and scalability at a basic physics level, but current efforts have not been able to demonstrate the potential in the lab. If the efficiency of SSLs and DPALs were improved in terms of total efficiency and wall-plug efficiency, the DPALs would be the better choice because of the thermal effects of the SSL medium.

A high risk for DPALs is the design of a resonator that can produce 80 MW of DPAL power. The highest power generated to date is in the hundreds of watts. The high gain per centimeter of the DPAL gain medium requires innovative designs similar to the efforts proposed for chemical devices in the 1980s. A possible strawman device would use a short-length annular gain cell with half-symmetric axicon mirrors to compact the annular resonator, such as the one shown in Figure 3.145.

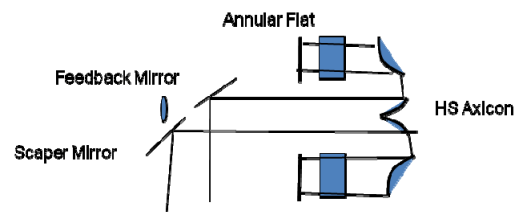


Figure 3.145.—Half-symmetric (HS) axicon mirror annular resonator for possible DPAL emitter.

DPAL resonators have been predicted with power densities of 40 kW/cm². Therefore, achieving the required 80 MW leads to an annular ring on the order of 1.5 m in diameter with a length (longitudinal axis) of 5 to 8 cm and a radial cross section of 5 cm. Packaging of the diode pumps and gas flow for cooling would clearly be an engineering challenge.

Obvious challenges for the laser source and beam path include improvement in wall-plug efficiency 10% to 50% (dominated by pump diodes), improvement in the reliability of very low absorption (VLA) coatings to handle power densities without thermal distortion, and improvements in beam path conditioning to avoid thermal blooming in the code path.

3.2.2.2.2 Beam Control

The Beam Control system will resemble the optics of a large telescope and will provide the acquisition, tracking, and pointing required to beam the energy to the orbiting spacecraft. It also will have the safety systems required to shut down the laser in the event of an optical coating failure, beam misalignment, or a predictive avoidance issue. In addition, the Beam Control system will use adaptive optics such as those at the Starfire Optical Range (Figure 3.146) for atmospheric compensation and fast steering mirrors for fine beam alignment and jitter control. It may also be possible to use radiant intensity at the target, known as gradient descent optimization (GDO) wave-front control for the atmospheric compensation measurement.

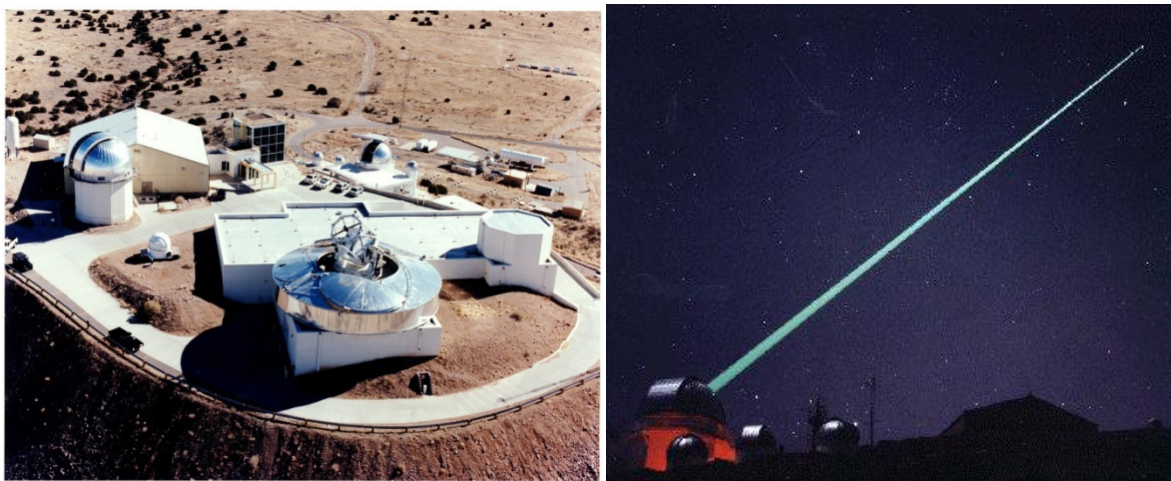


Figure 3.146.—Starfire optical range (SOR).

3.2.2.2.3 Perigee Facilities

Three Perigee Facilities spaced evenly around the globe on or near the equator should provide the best viewing opportunities to enable perigee burns on nearly every orbit. DRM 2–A uses the Kwajalein Atoll as the launch site, which is located at a latitude of 9°. The Perigee Facilities will require only 2-m apertures to compensate for beam diffraction, but the ability of the optical coatings to handle the 80-MW power levels may drive larger optics to lower the flux. The Perigee Facilities will most likely resemble the 3-m telescope at SOR at Kirtland Air Force Base (see Figure 3.143) or the Advanced Electro-Optical System (AEOS) 3.67-m telescope on Maui. The near equator locations of the Perigee Facilities implies they could be ship based. Lasers based on ships similar to the now-decommissioned Virginia-class cruisers with two 150-MW reactors or a nuclear-powered aircraft carrier would provide sufficient power and mobility to maximize the burn duration for each orbit of the tug. If some or all of the Perigee Facilities are ship based, the lasers may require additional power to compensate for the additional water content in the air due to the marine environment.

3.2.2.2.4 Apogee Facility

There will be more flexibility on the location, but the Apogee Facility will need to be at least 30 m in diameter to focus the spot on the spacecraft's reflector at GEO. The facility could be located below a latitude of 45° and still provide good lasing opportunities at both the 3000-km altitude (and so could be used for perigee burns) and GEO. The TMT (Figure 3.147) being constructed at Mauna Kea, Hawaii, is a good representation of a baseline Apogee Facility. The laser requires the same 80-MW power as the Perigee Facility and for practical reasons could be identical.

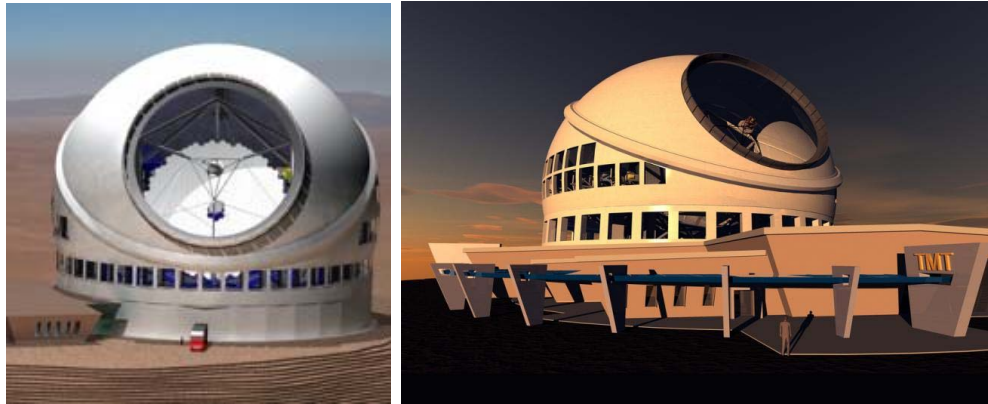


Figure 3.147.—30-Meter-Telescope (TMT). Courtesy TMT Observatory Corporation; used with permission.

3.2.2.3 CONOPS—Frequency of Launch and Repeat Time

The LEO–GEO tug described here will *halve* the number of launches required to place satellites in GEO (Figure 3.148). A standard CONOPS will involve the launch of two 1970-kg GEO satellites and 4895 kg of water propellant on a Falcon 9 Block 2 from Kwajalein into a 400-km circular orbit with an inclination of 9°. The tug will rendezvous with the stack of two GEO satellites and propellant and begin orbit-raising burns within 3 days of launch. Six 5- to 8-min burns will be required to raise the initial orbit to a 3000-km, 9°-inclined circular orbit. Three 15-min burns at 3000 km will be required to raise the apogee to GEO, one 15-min apogee burn will be required to change planes to a 0° inclination, and two more 15-min apogee burns will be required to circularize. The total transit time to GEO, if we assume that there are burns every orbit, will be 32 hr, requiring 4.2 km/s Δv .

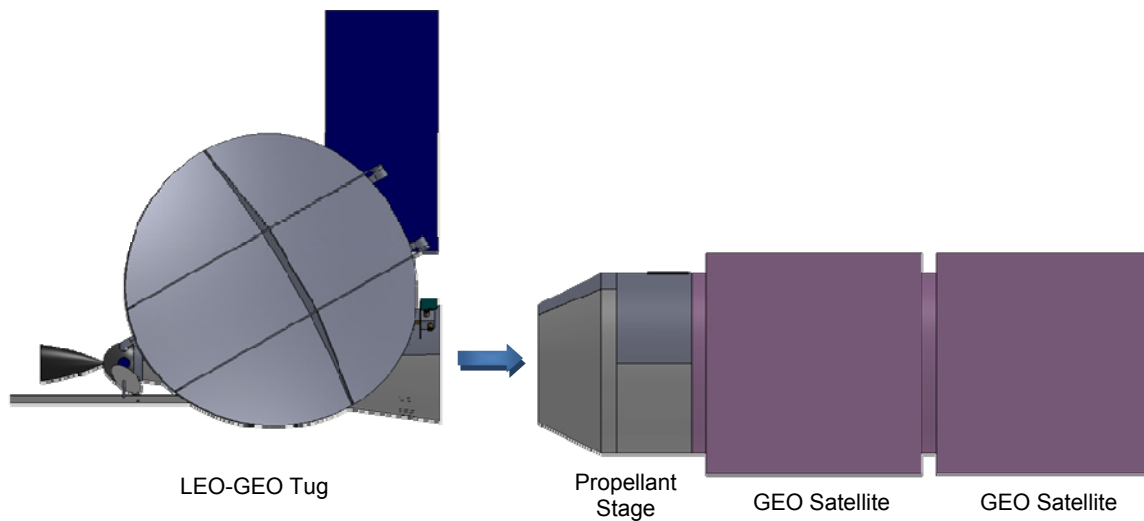


Figure 3.148.—Tug rendezvous with propellant and GEO satellites.

Following undocking from the GEO spacecraft, the tug will return to a 400-km, 9° inclined orbit, using residual water propellant that was launched with the two GEO spacecraft, and will be ready for the next transit in 24 hr. We assume that the tug itself will have been launched separately. The overall concept is summarized in Table 3.29, and orbital diagrams are shown in Figure 3.149. Figure 3.150 shows the tug stowed for launch.

TABLE 3.42.—CONOPS FOR LEO–GEO LASER TRANSPORT

Test step	Beaming	Receiving	Control and operation
0			Launch of tug on Falcon 9 from Kwajalein Atoll
1			Launch of <i>two</i> 2000-kg GEO satellites and 5000-kg propellant on Falcon 9 from Kwajalein Atoll
1a			Rendezvous and docking with tug
2 to 7	Perigee	Tug + two GEO satellites	400-km circular orbit with 9° inclination to 3000-km circular orbit with 9° inclination
8 to 10	Perigee	Tug + two GEO satellites	3000-km circular orbit with 9° inclination to 3000- by 36,000-km orbit with 9° inclination
11	Apogee	Tug + two GEO satellites	3000- by 36,000-km orbit with 9° inclination to 0° inclination
12 to 13	Apogee	Tug + two GEO satellites	3000- by 36000-km orbit with 0° inclination to 36,000-km circular orbit with 0° inclination
14	Apogee and perigee	Tug	Return to LEO

Other operational scenarios include the tug rendezvousing with existing GEO spacecraft for either servicing or return to LEO.

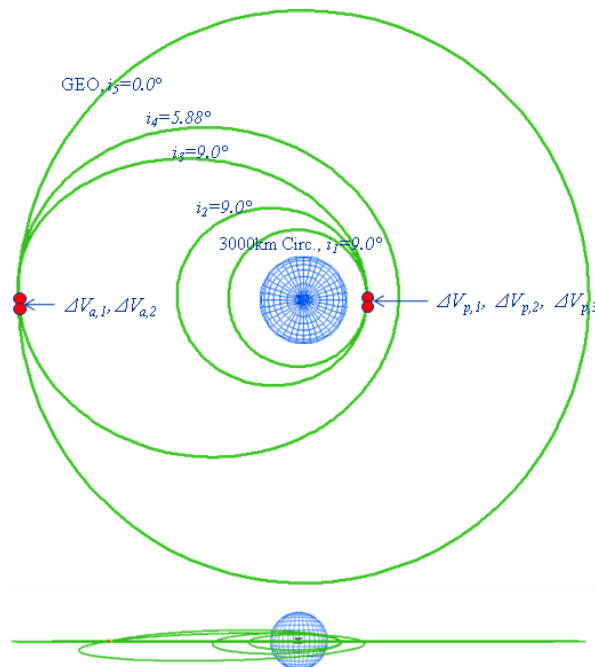


Figure 3.149.—LEO–GEO Laser Transport Orbital Transfer.

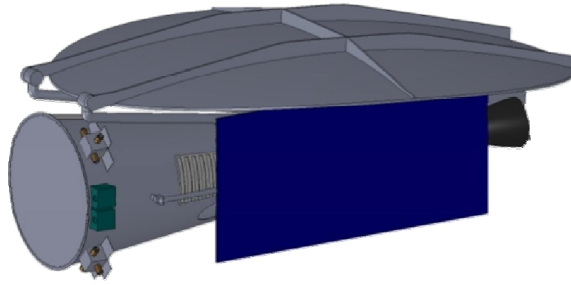


Figure 3.150.—LEO–GEO laser transport stowed for launch.

3.2.2.4 Costs—Comments

3.2.2.4.1 Recurring Costs

The DRM 2–A LEO–GEO beamed-energy transport tug will cut recurring GEO lost costs in *half*. This savings will be enabled by the elimination of the Centaur upper stage and circularization engine on the satellite required in current GEO launches. Instead, two 2000-kg GEO satellites could be launched into LEO on a single Falcon 9, rendezvous with the tug, and be transported to their circular GEO orbits in 32 hr. The tug would then return to LEO for another transport. In this manner, two GEO satellites could be placed into their orbits on a single Falcon 9 launch.

Additional recurring costs would include the negligible liquid water fuel cost and the cost to operate the laser. For the purposes of this project, a usage cost of 0.12 \$/kW-hr can be assumed. Although this cost is not negligible, it is less than 10% of the launch cost.

Therefore, with the combination of (1) the reduction in cost versus current launch vehicles of the Falcon 9 and (2) the ability to stack two satellites on a single launch, recurring costs of GEO launch will be cut in *half*.

3.2.2.4.2 Nonrecurring Costs

The Mauna Kea TMT provides a good parametric comparison to the laser ground facilities required for the DRM 2 mission. The cost estimate for building a Giant Segmented Mirror Telescope such as the TMT is \$1.1 to \$1.4B. The TMT is scheduled for completion in 2018. The ABL, which is currently the only megawatt-class laser in use, cost about \$5B to develop and build. The ABL laser and beam control systems have been estimated to cost about \$1B each. The High Energy Laser Joint Technology Office estimates that it currently costs about \$1000/W for a solid-state laser. If we assume that there will be significant reductions in cost in the coming decades, it will likely cost about \$10B to build the required 80-MW laser. Because of the limited usage time of the lasers (maximum 30-min burn), substantial cost-sharing could be realized with other applications.

Moore’s law of doubling results in about 10 steps to get to 80 MW from the current 100-kW electric lasers. If laser power doubles occurs every 3 years, ground lasers should be available around 2038.

3.2.2.5 Feasibility Assessment

The following is a list of issues which need to be addressed

1. What are the attenuation effects of high flux levels (MW/m^2) at the frequencies of interest on the atmosphere?
2. What would be the expected availability and transmittance of the BEP ground terminal at a given frequency, given aerosol and precipitation conditions at a proposed ground site?
3. How large of a keep-away zone must be maintained around and beyond an ascending craft to accommodate reflection, refraction and scattering components of the beam exceeding substantial irradiances, and what level is to be considered substantial? Considerations should be given to

maximum permissible exposure for humans, and damage thresholds for ground, airborne and space-based assets within proximity of the BEP activity.

4. For a ground based terminal operations, how much grid power over what duration is required? To meet these requirements, what would the generation, storage and conversion system look like?
5. How would a micro/mm-wave BEP system work within the spectrum constructs of the NTIA/FCC?
6. Does it make sense to collocate beamed energy propulsion and power technologies on the craft, for each phase of a proposed mission?
7. Would there be a benefit to developing a hybrid aperture to handle multiple BEP frequencies depending upon range to target, atmospheric conditions, etc.?
8. Can retro-directive control be utilized to aid in the beam pointing, acquisition and tracking of the craft?
9. What is the most practical way of performing high power beam combination using COTS technology for the frequencies of interest? What are the potential near term accomplishments that could influence this capability?
10. What are the cost/benefit tradeoffs in considering multiple BEP transmission locations, both at the ground range and at an intermediate relay point in space?
11. Could deployable array technologies be implemented to decrease the weight of a BEP aperture, and increase the allowable size that can be launched?
12. What are some near term demonstrations that may be accomplished to establish a maturity level for critical technologies, and support the overall feasibility of the BEP concept?

3.2.2.5.1 Roadmaps and Technology Readiness Levels

The five technology drivers for DRM 2 are the 80-MW laser, high-flux optical coatings, the beam director, the 5000-N laser plasma engine, and the reflective surfaces for the laser mirrors. Table 3.43 summarizes the current Technology Readiness Levels (TRLs) and time required to reach TRL 6.

TABLE 3.43.—TECHNOLOGY READINESS

Key technology	Current TRL	Rational and proof of estimation	Time to reach TRL 6
Laser 80 MW	2	Approximately 100 kW is the largest electric laser available.	2038
High-flux optical coatings	2	Current optics accommodate current laser power.	2038
Beam director (30-m mirror)	3	The TMT is scheduled to be complete in 2018.	2018
Thermal laser engine chamber	2	Some solar plasma work has been accomplished but not at this energy level or thrust.	2025
Laser engine reflectors	3	The secondary reflector is very-high-energy-loaded optic, beam control, and thermal control critical.	2025

3.2.2.5.2 Ground and Flight Demonstrations

One possible path to developing the 5000-N, 50-MW laser plasma engine is the series of ground demonstrations and tests summarized in Figure 3.151. The first step will be to use the solar thermal plasma chamber to measure temperatures and thermal loads in the plasma chamber. This small-scale thermal plasma engine testing will test the ability to create and maintain a plasma ball and could take place at the Satellite Propulsion Complex at Edwards Air Force Base. These tests will require an engine test section and a high-energy laser. The primary objectives will be to create and control the plasma ball and to measure engine thrust and I_{sp} . This testing should be able to be completed for approximately \$5M.

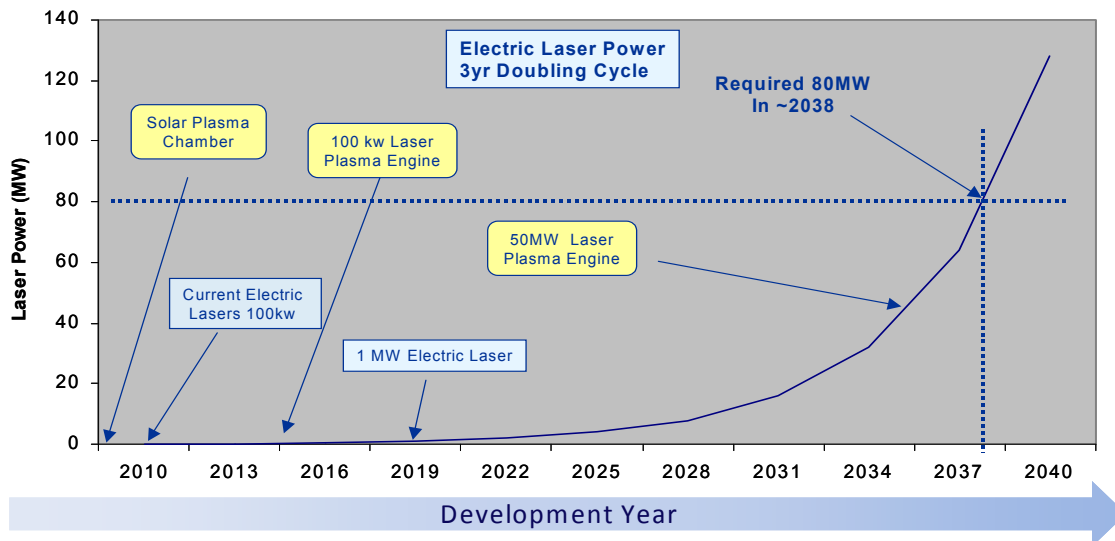


Figure 3.151.—Proposed technology roadmap.

The second step will be to build and test the performance of a full-scale engine at the 100-kW laser level. This engine would be a small-scale version the final 50-MW engine, and it would use current 100-kW lasers as the power source. Whereas the first chamber only created the plasma and measured its temperature, the second one will be a complete engine. It will need a propellant feed system and an expansion nozzle to measure the thrust. This engine should be used to fully understand the issues of plasma containment, propellant feed, and thrust control. It should also be space qualified. These tests will again use the Satellite Propulsion Complex at Edwards Air Force Base, and should be completed for approximately \$30M.

The first flight test should demonstrate the thermal plasma engine in space. It will require a high-energy laser-beaming facility capable of beaming to LEO, such as SOR. The space-qualified engine will be integrated onto an Expendable Evolved Launch Vehicle (EELV) Secondary Payload Adapter (ESPA)-class satellite to demonstrate engine performance in space and perform impulsive orbit-raising maneuvers. Because the performance of the engine is scalable with the input power, a full-power 80-MW facility will not be required. A power-beaming facility on the order of 0.5 to 1.0 MW will prove the technology. This flight test could be completed for \$50M.

When the full-power laser does become available, another ground demonstration should be run with a fully functioning version of the required flight engine. In the 2035 time frame, lasers may able to provide 50 MW of power, and this engine should be ready take advantage of those new lasers. It will take a few more years before the lasers are at the 80 MW of power needed to actually demonstrate the engine in space.

The development of an 80-MW laser and its optical systems will also be a challenge. There is a fair amount of high-power laser work going on within the Department of Defense (DOD), and hopefully, this work will progress to the power levels required for this mission.

3.2.2.5.3 Issues and Resolutions

The development of the laser plasma engine and the 80-MW laser are the two key technology issues that must be addressed. The technology roadmap described earlier provides a possible resolution. There will also be geopolitical issues with the construction of multiple 80-MW laser ground stations because other nations will consider the ground facilities to counter-space weapons. One path to resolve this political issue would be to build the ground facilities as a multiuse international effort for spacecraft

propulsion, debris removal, and possibly planetary defense. The other path will be to openly state that the ground stations are part of our national defense infrastructure but will be used primarily for on-orbit operations.

The U.S. Strategic Command Satellite Clearing House is responsible for determining when U.S. lasers can be fired into space so as not to cause damage to satellites. There may be a scheduling issue dictating when the laser can be fired, especially for the GEO burns. This issue could be resolved for the most part during mission planning, with contingencies for missed burns.

3.2.2.6 Bimodal Operation

If the ground facilities are designed for dual use, there will be the advantage of cost sharing between the DOD, NASA, and possibly even international partners. There will be very little difference between a ground-based laser used for propulsion and one used for national defense. Both the national defense and debris removal modes will require the ability to find and track uncooperative targets. If the DOD pursues the dual-use model, they may also invest in a space-based relay system. A space-based relay system would allow other missions, such as missile defense, in addition to debris removal and space propulsion.

3.2.3 Low-Earth-Orbit to Geosynchronous-Earth-Orbit Consultant Reports—Design Reference Mission 2–B

Design Reference Mission 2–B (DRM 2–B) is a mid-term capability based on DRM 2–A that replaces the multiple 80-MW ground-based beam emitters with a single 1-MW emitter if ground-based (or a 0.5-MW emitter if space-based). The design of the tug is identical to DRM 2–A. The modifications to the DRM 2–A mission are the concept of operations (CONOPS) of the power transfer, the orbital transfer burns, and the amount of water propellant required for a single transfer. In this manner, two GEO satellites could be placed into their orbits on a single launch in approximately 20 days.

3.2.3.1 Description of Vehicle

The low-Earth-orbit to geosynchronous-Earth-orbit (LEO–GEO) tug would be identical to that discussed in Section 3.2.2.1.

3.2.3.2 Description of Ground Facility

Two options are available for providing an in-space emitter capability: a 0.5-MW in-space GEO laser emitter and a 1.0-MW ground-based emitter and a GEO relay mirror. In the first option, 0.5 MW would be received at the tug (versus 50 MW in DRM 2–A) to power the 50-N laser plasma engine (versus 5000 N in DRM 2–A). For the laser to emit 0.5 MW, if we assume a 30% laser efficiency, 1.667 MW of input power will be required; 4065 m² of solar array area will be required to generate that much power if we assume that the triple-junction cells used will be 30% efficient. In addition, 4600 m² of radiator area will be required to dissipate the excess heat from the laser. For full power to be realized at a range of 81,000 km, a 57-m-diameter emitting aperture will be required. These requirements to realize a 0.5-MW GEO-based emitter do not represent midterm capability, and so a ground-based emitter with a GEO relay mirror also was considered.

The most significant technology challenge of the DRM 2–A mission, which would likely require more than a decade of technology development to achieve, is the 80-MW ground facility. A more near-term 1-MW emitter would have approximately the same configuration as the 80-MW apogee facility described in Section 3.2.2.2.4, including a 10-m-diameter aperture to maintain beam quality at GEO. A single-relay 7-m-diameter James Webb Space Telescope-type mirror at GEO would then steer the beam from the ground to the tug, providing continuous power.

The tug would be in view of the relay mirror for approximately 85% of its orbit; however, because of spot size growth, it would receive the full 0.5 MW of power for less than half of its orbit. This reduction in power will correspond to a reduction in thrust from 50 N, resulting in a longer transfer time—on the order of 20 days.

3.2.3.3 CONOPS—Frequency of Launch and Repeat Time

The change from 50-MW of power provided to the tug for multiple impulsive burns in DRM 2–A enabling a 32-hr transit time from LEO to GEO to 0.5 MW of continuous power for DRM 2–B will necessitate a longer transfer time. If we assume that the engine is identical engine to that of DRM 2–A, the 2 orders of magnitude reduction in received power will correspond to a 2 order-of-magnitude reduction in thrust (from 5000 to 50 N). This linear scaling would be achieved by maintaining the 6000-K plasma ball temperature by decreasing the propellant flow rate and thereby maintaining the 810-s specific impulse I_{sp} . A 50-N engine does not provide enough thrust for a Hohmann transfer on this size of a vehicle; therefore, a continuous-thrust spiral transfer will be used. Changing from the Hohmann to the spiral transfer will require an additional 1.8 km/s Δv (approx 6.0 vs. 4.2) and, therefore, will require approximately 6400 kg of water propellant instead of 4895 kg to transfer two 1970-kg GEO satellites and return to LEO. The total transfer time will also be greater—approximately 20 days instead of 32 hr. This CONOPS is summarized in Table 3.44.

TABLE 3.44.—CONOPS FOR LEO–GEO LASER TRANSPORT 2–B

Test step	Beaming	Receiving	Control and operation
0			Launch of tug and 8000-kg propellant on Falcon 9 from Kwajalein Atoll
1			Launch of <i>two</i> 2000-kg GEO satellites and 5000-kg propellant on Falcon 9 from Kwajalein Atoll
1a			Rendezvous and docking with tug
2	0.5-MW laser continuous	Tug + two GEO satellites	Spiral transfer from LEO to GEO in 20 days
3	0.5-MW laser continuous	Tug	Return to LEO

Note that the spiral transfer will require 6400 kg of propellant, exceeding the capacity of the Falcon 9 launch vehicle by 1400 kg. Additional propellant will be launched with the tug, enabling five transfers (10 satellites delivered to GEO). For additional transfers, it is assumed that the required propellant will be supplied by other launches or a depot.

3.2.3.4 Costs—Comments

3.2.3.4.1 Recurring Costs

The DRM 2–B LEO–GEO beamed-energy transport tug will cut recurring GEO lost costs in *half*. This savings will be enabled, as in DRM 2–A, by the elimination of the Centaur upper stage and the circularization engine on the satellite required in current GEO launches. Instead, two 2000-kg GEO satellites could be launched into LEO on a single Falcon 9, rendezvous with the tug, and be transported to their circular GEO orbits in 20 days. The tug would then return to LEO for another transport. In this manner, two GEO satellites could be placed into their orbits on a single Falcon 9 launch.

Additional recurring costs would include the negligible liquid water fuel cost and the cost to operate the laser. For the purposes of this project, a usage cost of 0.12 \$/kW-hr can be assumed. Although this cost is not negligible, it is less than 10% of the launch cost.

Therefore, with the combination of the reduction in cost versus current launch vehicles of the Falcon 9, and the ability to stack two satellites on a single launch, recurring costs of GEO launch will be cut in *half*.

3.2.3.4.2 Nonrecurring Costs

In the first power transfer option, a 0.5-MW emitter will be placed in GEO. On the basis of the DRM 2–A sizing of solar arrays and radiators, 8300 kg in solar arrays would be required if we assume an efficiency of 200 W/kg (ISS arrays are 32 W/kg efficient) and 20,000 kg in radiators would be required if we assume that they would have twice the mass of the solar arrays. This option will also require the

in-space construction of a 57-m-diameter aperture. The largest GEO transfer capacity currently available is on a Delta IV heavy launch vehicle at 5000 kg. If we assume a bulk purchase of 10 launches costing \$200M each (Delta IVs are currently estimated at \$1B each), \$2B would be incurred. The launches break down as follows: two launches for the solar arrays, four launches for the radiators, and four launches for the assembled or inflated aperture. The cost for the hardware itself is estimated at \$10B.

The second power transfer option involved a 1-MW ground-based emitter and a GEO relay mirror. The 10-m-diameter ground-based aperture and 1-MW emitter are estimated to cost \$500M. If we assume that the GEO relay mirror is a copy of the James Webb Space Telescope, it would have an estimated cost of \$500M. Therefore \$1B in nonrecurring total infrastructure is estimated. The nonrecurring tug launch on a Falcon 9 is assumed to cost \$30M.

3.2.3.5 Feasibility Assessment

The GEO relay mirror option is feasible in the mid-term, requiring approximately 10 years for initial operational capability.

3.2.3.5.1 Roadmaps and Technology Readiness Levels

The five technology drivers for DRM 2-B are the 1-MW laser, the GEO relay mirror, the beam director, the 50-N laser plasma engine, and reflective surfaces for the laser mirrors. The current Technology Readiness Levels (TRLs) and time required to reach TRL 6 are summarized in Table 3.45.

TABLE 3.45.—TECHNOLOGY READINESS FOR DRM 2-B

Key technology	Current TRL	Rational or proof of estimation	Time to reach TRL 6
1-MW laser	2	100-kW lasers are approximately the largest electric lasers available.	2015
GEO relay mirror	4	The James Webb Space Telescope 6.5-m-diameter mirror is scheduled for launch in 2014.	2018
Beam director (10-m mirror)	6	30-m Telescope (TMT) is scheduled to be complete in 2018.	2018
Thermal laser engine chamber	2	Some solar plasma work has been accomplished, but not at this energy level or thrust.	2018
Laser engine reflectors	3	The secondary reflector is very-high-energy-loaded optic, beam control, and thermal control critical.	2018

3.2.3.5.2 Ground and Flight Demonstrations

Ground and flight demonstrations will be substantially similar to those discussed in Section 3.2.2.5.2 scaled to the 50-N laser plasma engine and 1.0-MW ground-based emitter.

3.2.4 Low-Earth-Orbit to Geosynchronous-Earth-Orbit Cost

LEO to GEO Beam Source Infrastructure Cost

- Explanation – no actual analysis performed. Estimates only, based on other programs. See below

Executive summary of study findings:
LEO to GEO mission

All Costs in FY11\$	Space Vehicle			Infrastructure						
	Recurring Cost	Non-Recurring Cost	Time from LEO to GEO	Launch Vehicle		Energy Source				
				Type	Cost (\$0M) for 20 payloads	Input Power	Output Power	Non-recurring Cost (\$0M)	Operations Cost (\$0M)	
Comparable Disposable system: 1 Transit One 2000kg satellite Chemical kick motor	\$100M	N/A	7 Days including orbit insertion and checkout	Twenty Falcon 9 Rockets	\$18	Chemical	N/A	N/A	N/A	N/A
Reusable Top: Energy Source in Space 10 Months Two 2000 kg satellites 4900kg Water Propellant	\$85M	\$237M	20 Days including orbit insertion and checkout	Eleven Falcon 9 rockets	\$550M	Laser	One In-Space 1.5 MW Station (SS Albed Station w/ FAST array located in GEO)	Space Based 6.5 MW	\$5B*	\$250M*
Reusable Top: Energy Source on Ground 10 Months Two 2000 kg satellites 4900kg Water Propellant	\$85M	\$237M	8 Days including orbit insertion and checkout	Eleven Falcon 9 rockets	\$550M	Laser	One Ground Based 150 MW Stations (Max existing 100MW) (Best located at high latitude around equator)	Ground Based 78 MW	\$3B**	\$150M**

Notes:

- †** Do not consider the effects of launch rates for this study.
- ‡** Do not consider the operation of non-recurring, vehicle and ground system costs.
- §** Double RCH non-recurring costs for vehicles and ground systems (see 3.2.1.10).
- ¶** Double RCH vehicle and ground facility costs for reusable scenarios.

Space vehicle cost assumptions:

- Prime contractor costs (no fees)
- No technology development costs
- Protoflight development approach
- Before reserves, insight/oversight, launch services

* Extrapolation based on mission analysis of high efficiency space power systems project performed by COMPASS, 300xv1.8.1.8

** Based on Launch mission COMPASS analysis

National Aeronautics and Space Administration



Cost Assumptions



- **DRAFT Cost Estimate based on COMPASS design**
- **All costs are in FY11\$M**
- **Estimates represent prime contractor cost plus fee (10%)**
- **This estimate assumes the following:**
 - Development approach: proto-flight
 - No ground spares included
 - Flight heritage is assumed as Off-The-Shelf (OTS) for most components
 - Model assumes TRL Level 6
 - This estimate does not include any cost for technology development
 - Represents the most likely estimate based on cost-risk simulation results
 - Parametric estimate based on mostly mass based CERs
 - Planetary systems integration wraps
 - Software not included
- **Does not include:**
 - Any insight/oversight costs (by NASA lead center)
 - Project Reserves
 - Mission Operations Costs
 - Ground Data Systems
 - Ground Laser System Costs



LEO-GEO Laser Tug Preliminary Cost ROM

(Represents Prime Contractor cost)



WBS	Description	DDT&E	Flight	Total
		BY \$M	HW BY \$M	
06.1	Transport Stage	111.9	56.3	168.2
06.1.1	Attitude Determination and Control	18.7	15.1	33.8
06.1.2	Command and Data Handling	7.0	5.5	12.5
06.1.3	Communications and Tracking	2.6	2.9	5.6
06.1.4	Electrical Power Subsystem	3.9	1.4	5.2
06.1.5	Thermal Control (Non-Propellant)	35.4	15.4	50.8 *
06.1.6	Propulsion (Hardware)	37.7	13.1	50.9
06.1.7	Propellant (Chemical)	0.0	0.0	0.0
06.1.8	Structures and Mechanisms	6.6	2.9	9.4
06.2	Payload/Propellant Stage	28.0	10.0	38.0
06.2.1	Payload Spacecraft	0.0	0.0	0.0
06.2.2	Propellant	0.0	0.0	0.0
06.2.3	Command and Data Handling	3.1	2.4	5.5
06.2.4	Communications and Tracking	0.0	0.0	0.0
06.2.5	Electrical Power Subsystem	0.0	0.0	0.0
06.2.6	Thermal Control	10.2	1.6	11.8 *
06.2.7	Propulsion	8.1	2.8	10.9
06.2.8	Structures and Mechanisms	6.6	3.3	9.9
Subtotal before Systems Integration		140.0	66.3	206.2
Systems Integration		97.4	18.9	116.3
Spacecraft Total		237.4	85.2	322.6
Prime Contractor Fee (Assumed 10%)		23.7	8.5	32.3
Spacecraft Total with Fee		261.1	93.7	354.8

Half of cost from docking system

Primarily laser reflectors and shielding

All Costs in FY11\$M

* Moved cost of the Payload Mirror to the Transport Stage per direction



Cost Advantage of a Laser Transport (Preliminary)



- SOA Delivery Costs to deploy 20 GEO Spacecraft (Example)
 - Ten Falcon 9 : ~\$1000 M (@\$50M each)
 - Ten On-board apogee insertion system: ~\$100M (@ \$5M each)
 - Operations (Ten):
 - LEO restart of Upper stage, Perigee burn, separation and disposal ?
 - Apogee insertion burn with on-board system ?
- Laser Transport Costs to deploy 20 GEO Spacecraft (Example)
 - Eleven Falcon 9: \$550 M (10 for GEO birds, one for re-useable laser transport)
 - One laser Transport ~\$78M
 - Five Propellant Stage Systems ~\$100M
 - Operations:
 - Rendezvous of Transport and Payloads (10 times)
 - ~15 Laser burns in LEO and GEO to delivery payload (10 times)
 - ~5 laser burns to return transport to LEO (10 times)
- Cost Delta (excluding operations delta and cost of laser stations)
 - SOA (\$1100M) – Laser Transportation (\$728M) = ~\$372 M (~33% savings – without Laser and ops cost difference): Saves ~\$20 M / GEO Delivery
- How to increase savings?
 - Need to reuse transport more times (to offset the AR&D costs)
 - Reduce cost of propellant stage

3.2.5 Deep Space Mission Design Lab (MDL) Report



Integrated Design Center / Mission Design Laboratory

Beamed Energy Propulsion System DRM-3

TEAM LEAD
John Oberright

11/29-12/3



BEPS DRM3

Mission Design Laboratory

• Objectives

- Study the application of the Beamed Energy Propulsion System from DRM-2 to execute a planetary or deep space mission
- Identify BEPS possible improvements, system understanding and possible risks

• Approach:

- Minimize changes from Compass DRM 2 study
- Consider only necessary core subsystems
- Focus on potential issues with BEPS technology
 - Beam pointing control
 - Energy management
 - Reflector surface maintenance
- Attempt Galileo Mission



• DRM-3 Mission Phases

- Launch 1 (0 days)
- Launch 2 (+ 10 days)
- Complete R&D (+20 days)
- Establish 3000 x GTO (35,000) km Jupiter depart orbit (+30 days)
- (At this point, except for launch manifest, we depart from the DRM-2)
- Departure burn (+45 days)
- Cruise to Jupiter and execute Galileo mission



BEPS DRM3

- **Flight Dynamics (Mission Design)**
- **Mission Operations**
- **Mechanical Design**
- **Propulsion**
- **Thermal**
- **Controls**
- **Power**
- **Communications**
- **Debris assessment**
- **Systems Summary**
- **Major findings**



Summary

Mission Design Laboratory

- Basic system identified for DRM 2 can also be used to accomplish DRM 3 (execute Galileo mission)
 - 2 launches from Kwajalein to 800 km circular (equipment manifest different from DRM-2)
 - Rendezvous and dock followed by using BEPS to achieve 3000km by 35000km orbit (this is identical to DRM 2 GTO)
- Use BEPS to provide ~7 km/sec for Jupiter departure burn - Cruise is ~ 2-1/2 years
- Galileo basic hardware and fuel load will duplicate original mission including Jupiter orbit insertion
- Power is upgraded to use ASRGs rather than RTGs and used to power both launch payloads
- Suggested technology demonstration flights to support BEPS development
- Conclusion: BEPS should enable a robust suite of missions for planetary and deep space targets.



Integrated Design Center / Mission Design Laboratory

Attitude Control

Eric Stoneking

29 Nov – 3 Dec 2010



Scope of this Study

Mission Design Laboratory

- **GRC-Compass ACS design for DRM-2 works well for DRM-3 as well**
 - Flight profiles and environments are very similar
- **ACS functions for AR&D and loiter are straightforward**
 - Star tracker and IMU provide primary attitude knowledge
 - Reaction wheels and thrusters provide control actuation, momentum unloading
 - ReInav sensor supports AR&D
- **We adopt the DRM-2 ACS design as-is**
- **This study focuses on guidance and control of the ground-S/C laser beam link**



Guidance and Control of Power Beam

Mission Design Laboratory

- **Architecture and Components**
- **Laser Link Acquisition and Maintenance**
- **Flight Path Angle and Reflector Range of Motion**
- **Tracking Rate Requirements**
- **Pointing Accuracy Requirements**
- **Handling Time of Flight Lag**
- **Anomaly Detection and Response**



Architecture and Components

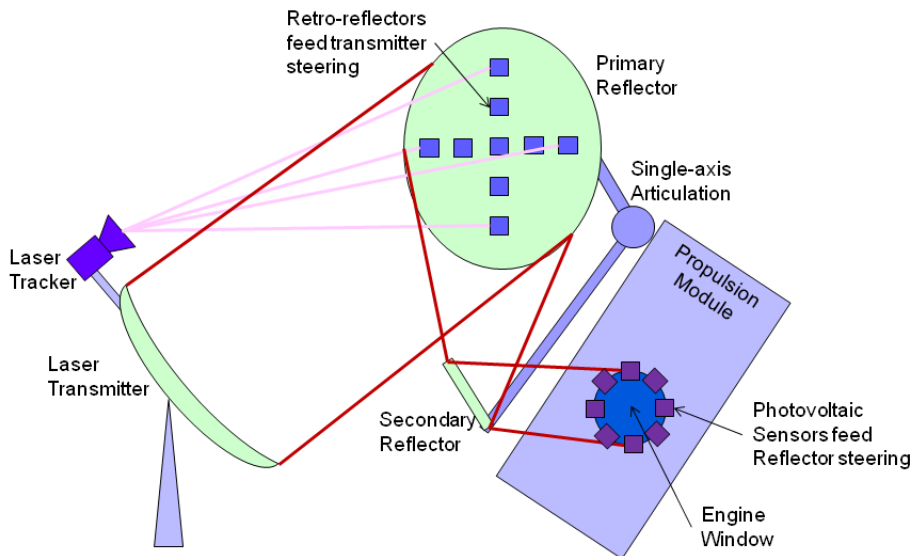
Mission Design Laboratory

- **Low-power (Guidance) laser beam shares optical path with high-power (Power) beam**
 - Lasers may be defocused
- **Ground-based laser transmitter**
 - 30-m aperture
 - Steered in azimuth and elevation
- **Reflector (primary and secondary) steers beam into engine window**
 - Primary reflector ~4-m aperture
 - One-axis articulation
 - Spacecraft roll provides second pointing degree of freedom
- **Retro-reflectors on primary reflector provide return signal to ground station**
 - Possibly also photovoltaic cells with active comm (see below)
- **Laser-sensitive tracking sensor mounted on ground transmitter**
- **Photo-voltaic cells on rim of engine window provide feedback for reflector steering**
 - Edge-illuminated Ge-based photovoltaic cells are candidates
 - Small, cheap, can sense guidance beam, and can withstand power beam



Architecture Schematic

Mission Design Laboratory





Laser Link Acquisition and Maintenance

Mission Design Laboratory

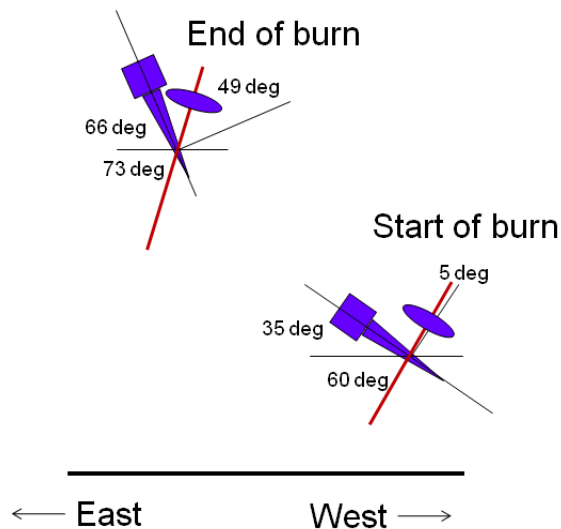
- **Guidance beam is used to search for spacecraft**
 - Power beam is OFF
 - Guidance beam is defocused to cover large region
 - GPS-based position knowledge easily good to ~100 m
- **When retro-reflectors are detected, guidance beam is progressively focused until beam is captured on primary reflector**
 - Transmitter-to-tracker pointing calibration is a natural by-product
- **Spacecraft roll attitude and reflector steering are adjusted until guidance beam is captured on engine window**
- **When guidance beam is centered on engine window, power beam may be switched ON**
- **Ground transmitter steering uses retro-reflector return signal to keep power beam centered on primary reflector**
- **Spacecraft uses photovoltaic sensor signals to feed attitude control, active steering of reflector**



Flight Path Angle and Reflector Range of Motion

Mission Design Laboratory

- **Rising elevation angle and flight path angle combine favorably to keep reflector hinge angle in range**
- **At beginning of burn:**
 - Elevation: 60 deg
 - Flight Path Angle: 35 deg
 - Reflector Angle: 5 deg
- **At end of burn:**
 - Elevation: 73 deg
 - Flight Path Angle: 66 deg
 - Reflector Angle: 49 deg

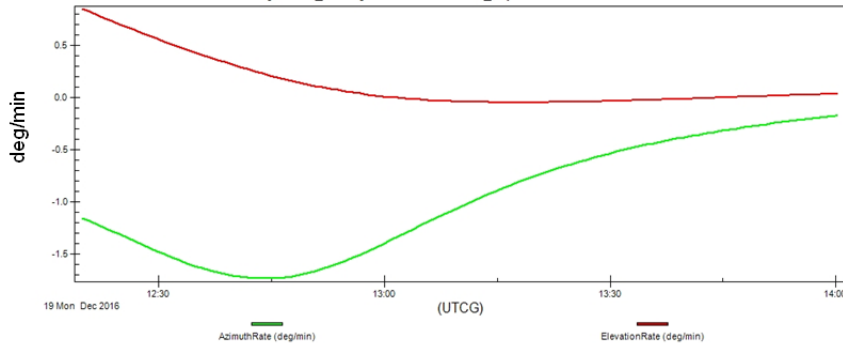




Tracking Rate Requirements

Mission Design Laboratory

Facility-Laser_Facility-To-Satellite-BEPS_Jupiter - 02 Dec 2010 11:00:25



- Laser transmitter must be able to smoothly track spacecraft over range of zero to 1.7 deg/min



Pointing Accuracy Requirements

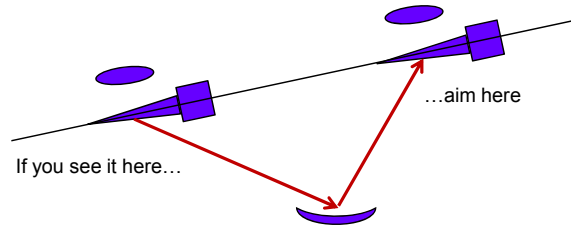
Mission Design Laboratory

- Range varies from 11900 km at start of burn to 44200 km at end of burn
- At max range, 1 m subtends 4.6 milli-arcsec
- Laser tracker must be able to resolve this angle to see retro-reflector pattern
- Laser transmitter must be able to steer with this accuracy to put beam on reflector



Handling Time of Flight Lag

Mission Design Laboratory



- **At start of burn:**
 - Range = 11900 km
 - Round-trip light time of flight = 0.08 sec
 - Tracking rate = 0.025 deg/sec
 - Pointing direction must “lead” observed position by 7 arcsec
- **At end of burn:**
 - Range = 44200 km
 - Round-trip light time of flight = 0.3 sec
 - Tracking rate = 0.005 deg/sec
 - Pointing direction must “lead” observed position by 5 arcsec



Anomaly Detection and Response

Mission Design Laboratory





Anomaly Detection and Response

Mission Design Laboratory

- Many spacecraft components may be sensitive to extended illumination by power beam
- Some components (star tracker optics?) may also be sensitive to guidance beam
- Laser steering and cutoff is likely to be much, much faster than reflector steering and spacecraft attitude control
- If power beam loses lock on primary reflector:
 - Laser tracker (on ground) detects loss of lock
 - Ground station commands shutdown of power beam
 - Ground station defocuses guidance beam, restarts acquisition sequence
- If power beam loses lock on engine window:
 - Photovoltaic cells detect loss of lock
 - Alert sent via RF comm to ground
 - Ground station defocuses guidance beam, restarts acquisition sequence



Challenges and Future Work

Mission Design Laboratory

- **Challenges**
 - Pointing accuracy driven by 5-m spot at 44000 km range
 - Tracking with a 30-m aperture requires muscle and finesse
 - Time-of-flight pointing offset is many times spot size
- **Demonstrate ground transmitter tracking using existing space assets**
 - Low-power demonstrations using existing Moon-based reflectors would enable comparison with other laser tracking systems
 - Tracking a reflector on a GTO-bound spacecraft would provide representative geometry, tracking rates



Beam Energy Propulsion Study (BEPS)-DRM 3

Communications

Ronald Vento

Blake Lorenz

29 Nov- 3 DEC, 2010



Topics

- Driving Requirements and Assumptions
- Selected Configuration and Rationale
- Functional Configuration
- Component Power/Mass Summary
- Signal Margin Summary
- Comments and Risks
- Backup



Driving Requirements & Assumptions

Mission Design Laboratory

- **Launch: Later than 2015**
- **Deliver a Galileo type spacecraft into a inter-planetary orbit using beamed energy propulsion**
- **Transport engine launched and will rendezvous with the Galileo package in orbit**
- **Rendezvous and docking may require TDRS communication**
- **Data rate as best available at 100,000 km**
- **Communication necessary with Galileo (This requires addition of two more complete transponder systems)**
- **Galileo and the propulsion package will have protection from the uplinked high power Laser**
- **Galileo HGA will not deploy until the Laser is no longer used**
- **Use the Compass study parameters, with any changes noted**
- **Communicate with the ground (NEN) and TDRSS when necessary**



Selected Configuration & Rationale

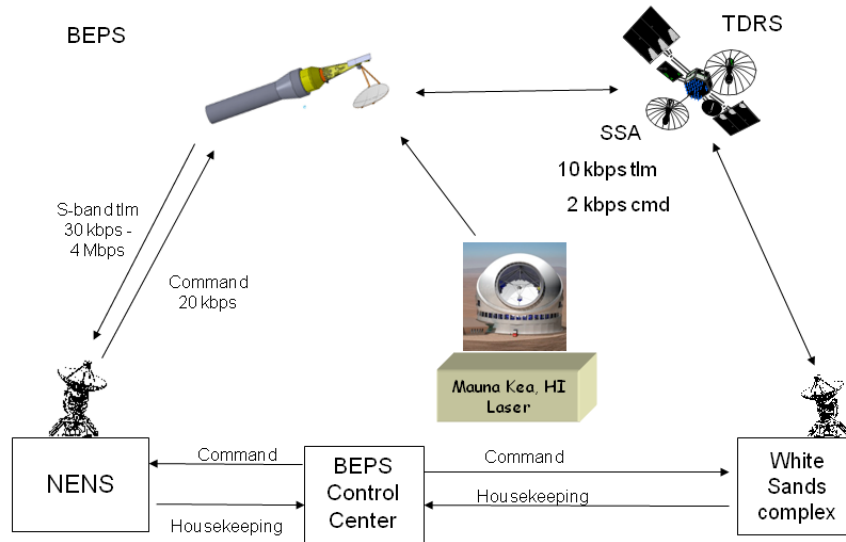
Mission Design Laboratory

- **Use dual S-Band Transceivers for ground communications**
 - Receivers on continuously
 - Transmit data at 30 kbps at 100,000 km (assumed maximum range)
 - Receive command data at 2 kbps to 200 kbps
 - LDPC rate 7/8 encoding used
 - Signal margins are baselined on a 11 meter ground antenna
 - 8 watts RF
- **Use dual S-Band Transceivers for Galileo communications**
 - Receivers on continuously when docking
 - Transmit data at 50 kbps at 50 km
 - Receive data up to 200 kbps
 - Frequency selection must be reversed from nominal
 - Signal margins are baselined on omni antennas on Galileo
 - Transceivers should receive and transmit LDPC
 - 1 watt RF
- **Two sets of Dual omnis**
 - -3 dBi for 90% spherical coverage
 - +3 dBi toward ground when nadir pointing
 - Omnis must be constructed to withstand $1000\text{w}/\text{cm}^2$
 - GSFC thinks omnis can be constructed to withstand $300\text{w}/\text{cm}^2$ without protection
 - With thin RF transparent reflective coverings with 90% reflectivity, there should be no problems (GRC indicates reflective material of 99.9%)
 - Omnis will be special order, not off the shelf



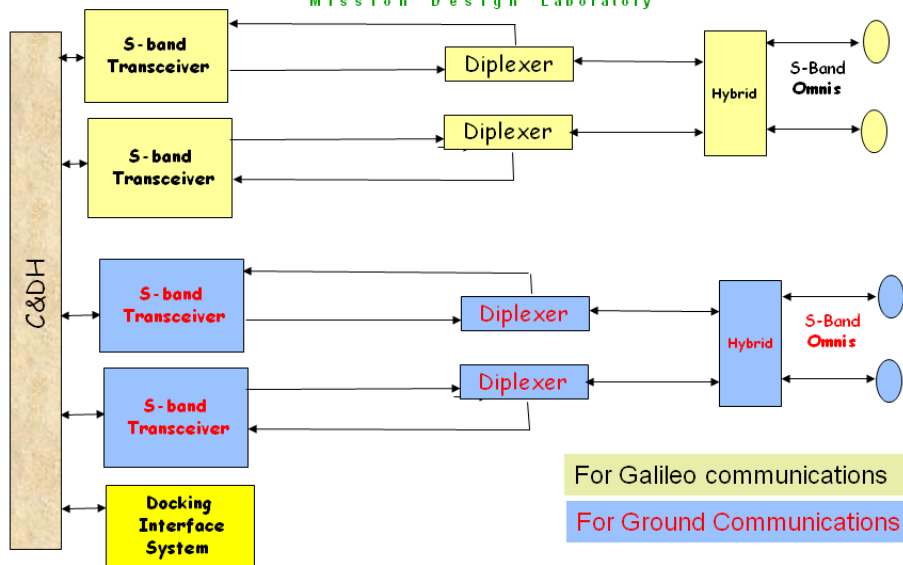
Selected Configuration

Mission Design Laboratory



Functional Block Diagram Propulsion Module

Mission Design Laboratory





Power/Mass Summary

Mission Design Laboratory

GRC BEPS Component	Power Receive (Watts)	Power Transmit (Watts)	Mass (Kg)
S-band Omnis (4)			2.0
S-band Transceiver Earth comm (2)	10	21	6.0
Diplexer (4)			1.0
Hybrid (2)			0.4
S-band Transceiver Galileo comm (2)	10	5	6.0
Miscellaneous			1.0
Totals	20	26	16.4
Notes: When not docking, the Galileo transceivers need not be on. For either system, only one transmitter would be on when needed.			



Signal Margins

Mission Design Laboratory

BEP Module	Link	Margin (dB)	Comments
S-Band telemetry to ground	30 kbps	3.2	Omni to 11 meter 100,000 km
S-band telemetry to ground	4 Mbps	22.1	Omni to 11 meter 1000 km
S-band to Galileo	50 kbps	0.8	Omni to Omni 50 Km range
S-band uplink from ground	20 kbps	12.9	11 meter to omni 100,000 km
TDRSS Return Link	10 kbps	0.1	Omni to TDRSS
TDRSS Forward Link	2 kbps	2.0	TDRSS to Omni
Note: Applicable Near Earth Network (NEN) station include Hawaii 13-m USN, Wallops 11-m, Santiago `12/7-m or 9-m, Dongara, Aus.13-m USN.			



Comments and Risks

Mission Design Laboratory

- If Galileo has only one set of S-band receivers, communications with the propulsion module and the ground cannot be simultaneous unless transmitting data needed at both receive locations.
- Transponders should be used if ranging data is required
- Laser power on the omni antennas and connecting co-ax cable is critical. GSFC antenna personal expect that antennas can be built to withstand 300 w/cm^2 . The COMPASS studies indicate levels of up to 3000 w/cm^2 , but have reflective material that can reduce this by 99.9%. If material capable of reflecting 90% and is RF transparent there should be no problem. If the reflective coating reduces the signal, the data rate could be reduced to compensate.
 - Choice of antennas may be dependent on the antenna materials properties. The use of a cross dipole type of antenna may be preferable.
- For 800 km, $\theta = 9$ degrees, the main ground station support would be from Hawaii (NEN), with additional support from Hartebeestock, South Africa (NEN) and Dongara, Australia (NEN). TDRS can provide low data rate support.



Integrated Design Center / Mission Design Laboratory

Beam Energy Propulsion Study (BEPS)-DRM 3

Electrical Power Systems

Bob G. Beaman

29 Nov- 3 Dec 2010



Driving Requirements

Mission Design Laboratory

Orbit: A Jupiter mission, since we will be far from the Sun and solar array power is greatly diminished, we are using ASRG's and no Solar Arrays:

Propulsion Module:

Battery: GRC COMPASS Team design of 29 Oct 2010 had a 1000 watt water pump. Typical operations to be under 10 Min. (requiring a 20 ah secondary battery) however the final insertion burn to be 100 minutes (requiring a larger secondary battery or an additional Primary battery. Trade in back up charts recommends a larger, 100 ah secondary battery.)

Galileo II Spacecraft:

Is a combination of the ASRG Ring and the Payload Module, assumed to be a power of 384.61 watts (500 watts with 30% contingency) .



EPS Assumptions

Mission Design Laboratory

Contingency: Electrical Power Contingency 30% for both Instruments and Spacecraft according to the GSFC Golden Rules.

Operational Margin: At EOL 36%, with 4 ASRG's at end of thrust for the Propulsion module. At EOL 5.5% margin in the Galileo II Spacecraft.

Bus Loads: Propulsion Module bus loads were provided from the MDL team except for two bus loads for mechanical and C&DH, were the GRC COMPASS Team design of 29 Oct 2010 power numbers were retained.

Spacecraft Modes: Day, Power requirement for the spacecraft bus.
Night, Power requirement for the use of the water propulsion system.
Launch, power, Space craft power required from initial launch to solar array deployment and spacecraft becoming power positive.
Check Out power: Match performance characteristic in orbit. Adjust for any calibration or anomalies differences.
Propulsion Mode: Water Prop mode, 1000w pump on.
Safe Hold and/or Survival:
Communications:
Peak:



Derived Requirements

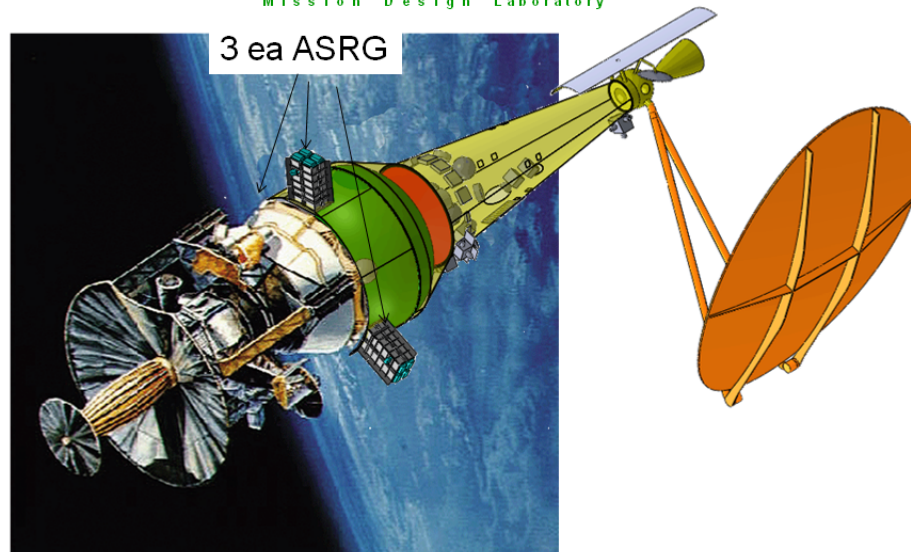
Mission Design Laboratory

- ASRG:** Sized for 3 ASRG's on the Propulsion Module and one on the Payload Module, giving a total of 4 ASRG's for the joined together with the Payload Module to become the Galileo II Spacecraft. The ASRG's stay with the Galileo II Spacecraft after the remainder of the Propulsion Module is separated and discarded.
- Each ASRG beginning of life electrical power is 143 watts each.
- Mounted so cold end provides heat to the water tank.
- Life, 10 year degradation of 8% assumed, power available at 130 watts each.
- Battery:** 100ah Lilon rechargeable battery in the Propulsion Module. Typical Propulsion 10 min firing battery DOD is 8.31%. For the one time Jupiter insertion of about 100 minutes the battery DOD goes to 83%.
- PSE:** Stand alone Power System Electronics. Heritage 28vDC battery dominated bus. To perform battery charging and output switch regulations. One PSE on the Propulsion Module and one on Payload Module that becomes the Galileo II Spacecraft.
- Load Analysis:** See chart page 8.
- Harness:** The Harness is a scale up from the power needed between the ASRG's, PSE and battery. Harness for the Payload Module/Galileo II spacecraft is not provided in this study.



Jupiter Ejection Spacecraft Configuration

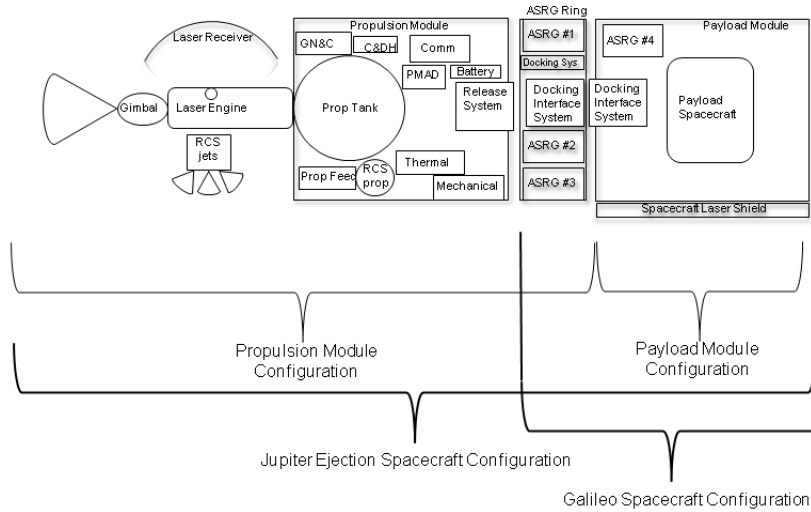
Mission Design Laboratory





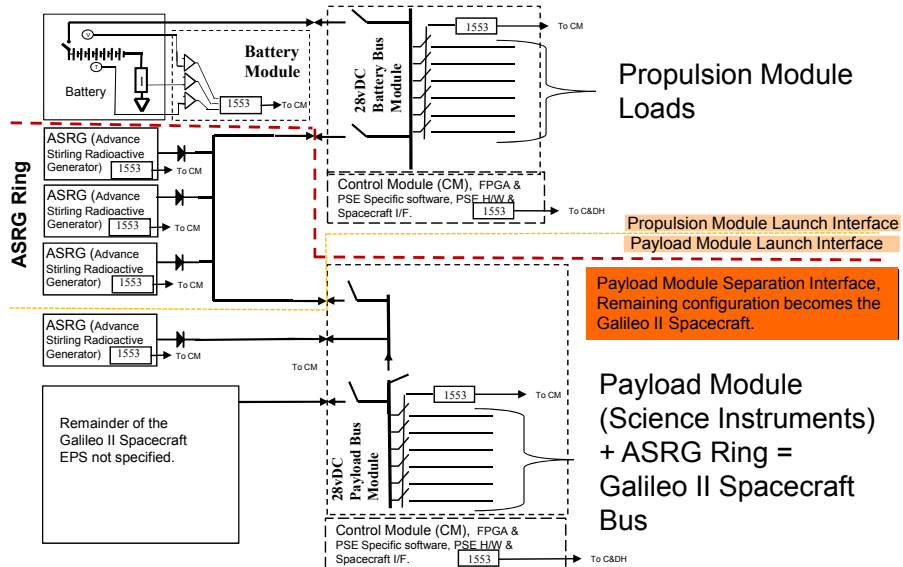
Spacecraft Configuration Diagram

Mission Design Laboratory



EPS Block Diagram

Mission Design Laboratory





Propulsion Module Load Analysis

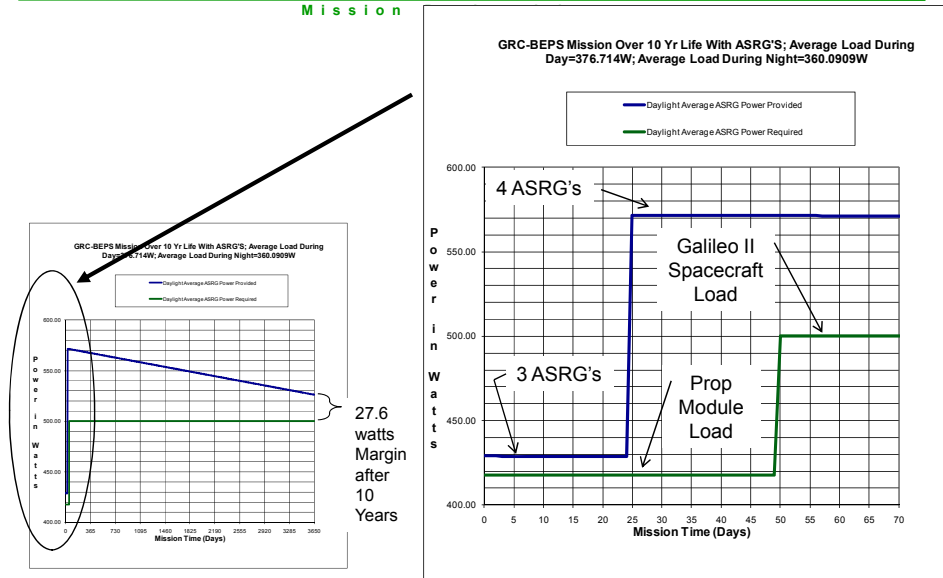
Mission Design Laboratory

GRC-BEPS		10.0 Mission Life in Years		Launch Power	Day Avg. Power Watts	Night Avg. Power Watts	Satbrhd Peak Power in Watts	Comm Downlink	Check Out	Laser Prop Mode	
EPS Load Item Description											
Total Power				37.1	376.7	368.1	315.6	629.7	424.8	362.3	1888.8
Ins Global Contingency 30											
Instruments with Contingency				8.8	8.8	8.8	8	8.8	8.8	8.8	1388.8
Water Pump 1000 watts				0.0	0.0	0.0	0.0	0.0	0.0	0	1000.0
Contingency 30				0.0	0.0	0.0	0.0	0.0	0.0	0.0	300.0
Spacecraft Loads with Contingency				37.1	376.7	368.1	315.6	629.7	424.8	362.3	588.8
Spcl Global Contingency 30											
PSE	MAP like (95.4% eff)	83.17		1.4	15.5	13.8	11.8	28.2	16.8	14.0	81.0
	Contingency 30			0.4	4.6	4.2	3.5	7.9	5.0	4.2	24.3
Electrical - Harness Losses	BGB			0.1	1.3	1.2	1.0	2.2	1.4	1.2	6.7
	Contingency 30			0.0	0.4	0.3	0.3	0.7	0.4	0.3	2.0
Command & Data Handling	Compass Study			8.0	40.0	40.0	8.0	80.0	60.0	8.0	40.0
	Contingency 30			2.4	12.0	12.0	2.4	18.0	18.0	2.4	12.0
Structures and Mechanisms	Compass Study			0.0	0.0	0.0	0.0	0.0	0.0	0.0	30.0
	Contingency 30			0.0	0.0	0.0	0.0	0.0	0.0	0.0	9.0
Attitude Control	Eric S			0.0	110.0	110.0	110.0	110.0	110.0	110.0	110.0
	Contingency 30			0.0	33.0	33.0	33.0	33.0	33.0	33.0	33.0
Thermal	Kim B.			9.0	90.0	90.0	90.0	90.0	90.0	90.0	90.0
	Contingency 30			2.7	27.0	27.0	27.0	27.0	27.0	27.0	27.0
Propulsion	Phillip K.			10.0	2.0	2.0	2.0	150.0	2.0	10.0	2.0
	Contingency 30			3.0	0.6	0.6	0.6	45.0	0.6	3.0	0.6
Data Systems	Ron V. & Blake L.			0.0	31.0	20.0	20.0	48.0	48.0	48.0	31.0
	Contingency 30			0.0	9.3	6.0	6.0	13.8	13.8	13.8	9.3



Electrical Power Curve

Mission





Propulsion Module EPS Material

Mission Design Laboratory

GRC-BEPS							Area M ² or	Total
				Dimensions (M)			Vol M ³	Mass(Kg)
ASRG's			0.725	0.29	0.41	3	0.09	60.60
Lith Ion, Battery 100 A 83.4% DOD			0.23	0.26	0.20	1	0.01	29.91
PSE			0.22	0.28	0.38	1	0.02	13.55
Available								
Harness spacecraft & solar array						1		13.53
							Total Materials	117.6

Conclusions and Recommendations:

- Develop a Load Profile for key time periods when only 3 ASRG's are available, during orbit adjustments and during Jupiter orbit insertion when the battery is being discharged.
- Recalculate everything.
- Look at combining the PSE with the C&DH to produce a Avionics Box.



Integrated Design Center / Mission Design Laboratory

Flight Dynamics
Frank Vaughn

29 Nov – 03 Dec 2010



Requirements and Assumptions

Mission Design Laboratory

- Use BEPS to transfer from GTO-like orbit to Jupiter
- Payload is Galileo-like and carries propellant for Jupiter orbit capture
- Laser site located in Hawaii
 - Burns limited to when spacecraft is within 30° of ground site zenith
 - Full thrust capability available up to 2X geosynchronous altitude



Requirements and Assumptions

Mission Design Laboratory

- Initial Orbit
 - 3000 x GEO orbit from GRC study
 - Epoch: 19 Dec 2016 00:00:00.0000 UTCG
 - Semi-major Axis: 25772 km
 - Eccentricity: 0.6361
 - Inclination: 9°
 - RAAN: 45°
 - AOP: 314°
 - TA: 0°
- BEPS Spacecraft Parameters
 - Initial Mass: 6800 kg
 - Payload Total Mass Plus BEPS Dry Mass: 3100 kg
 - BEPS Propellant: 3700 kg
 - Thrust: 5300 N
 - I_{sp} : 900 s
- “Galileo” Spacecraft Parameters
 - Initial Mass: 2223 kg
 - Dry Mass: 1300 kg
 - Propellant Mass: 923 kg
 - Thrust: 440 N
 - I_{sp} : 315 s
- Jupiter Orbit Insertion (JOI)
 - 600 kg propellant allocated (per Galileo)



Jupiter Transfer Trajectory Design

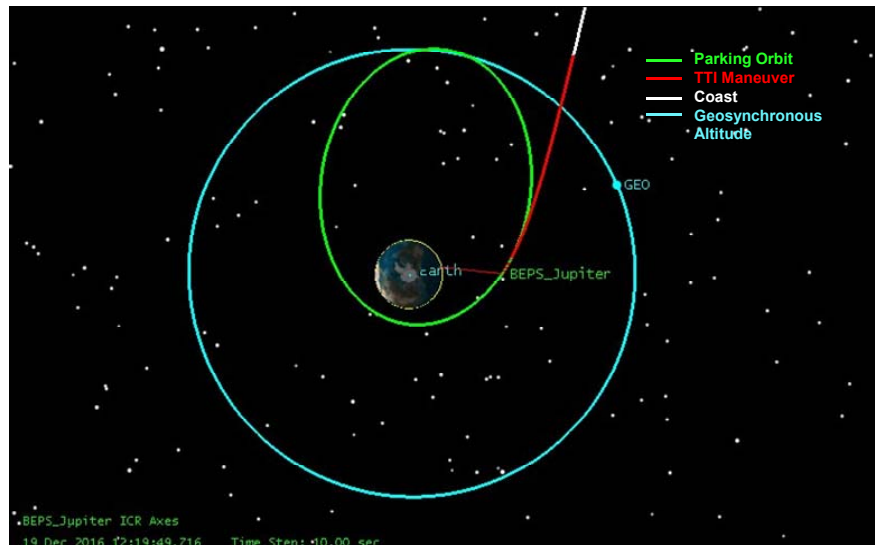
Mission Design Laboratory

- **Jupiter Transfer Trajectory Insertion (TTI) Burn**
 - Epoch: 19 Dec 2016 12:19:49.716 UT CG
 - Duration: 100.4 minutes
 - Departure C3: $80 \text{ km}^2/\text{s}^2$, V_{∞} : 8.9 km/s
 - ΔV : 6.7 km/s
 - Propellant Used: 3716 kg
 - Altitude range over burn: 11327 km – 43919 km
 - Flight Path Angle range over burn: 35.64° – 66.43° deg
 - Post-Burn Mass: 3183 kg
 - BEPS Dry Mass Plus BEPS Payload: 3100 kg
 - Residual BEPS Propellant: 83 kg
- **BEPS Propulsion Stage Dropped**
 - Spacecraft mass on Jupiter transfer trajectory : 2223 kg
 - Dry Mass: 1300 kg
 - Propellant Mass: 923 kg
- **Jupiter Transfer Orbit**
 - Transfer time is approximately 2.5 years
 - No accounting for trim maneuvers
- **Jupiter Orbit Insertion (JOI) Burn**
 - 600 kg propellant allocated (per Galileo)
 - Epoch: 31 May 2019 06:59:56.224 UT CG
 - Duration: 70.2 minutes
 - Arrival C3: $33.8 \text{ km}^2/\text{s}^2$, V_{∞} : 5.8 km/s
 - ΔV : 971.8 m/s
 - Capture Orbit: 200,000 km x 12,000,000 km -- Period: 98 days



Transfer Trajectory Insertion (TTI) Ignition

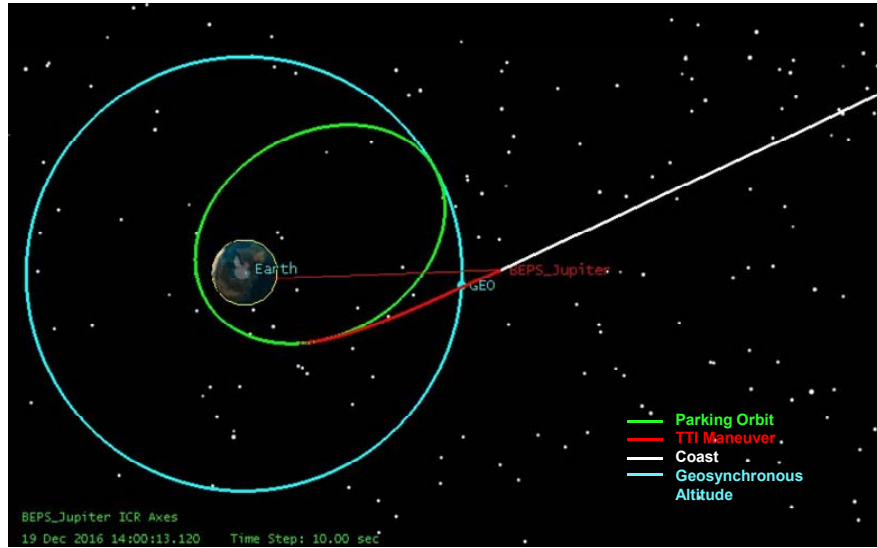
Mission Design Laboratory





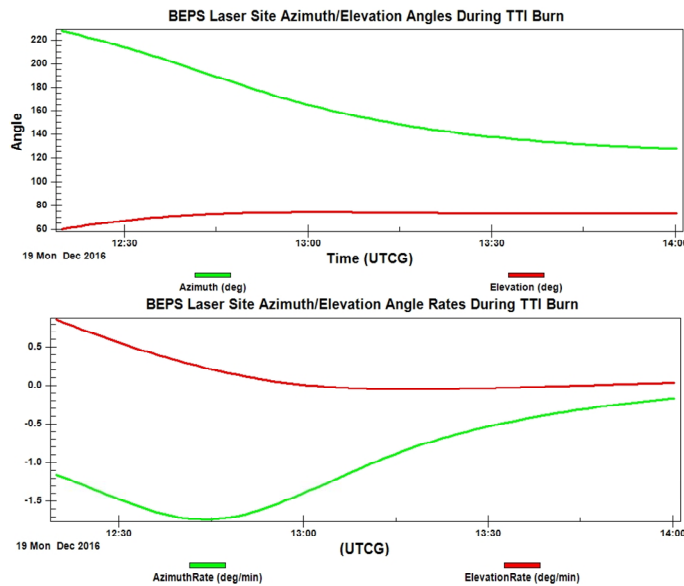
Transfer Trajectory Insertion (TTI) Burnout

Mission Design Laboratory



Laser Site Angles/Rates During TTI Burn

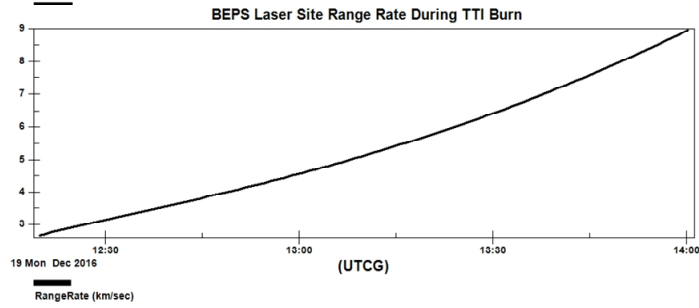
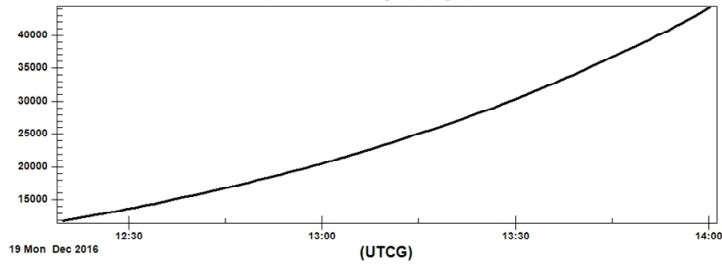
Mission Design Laboratory





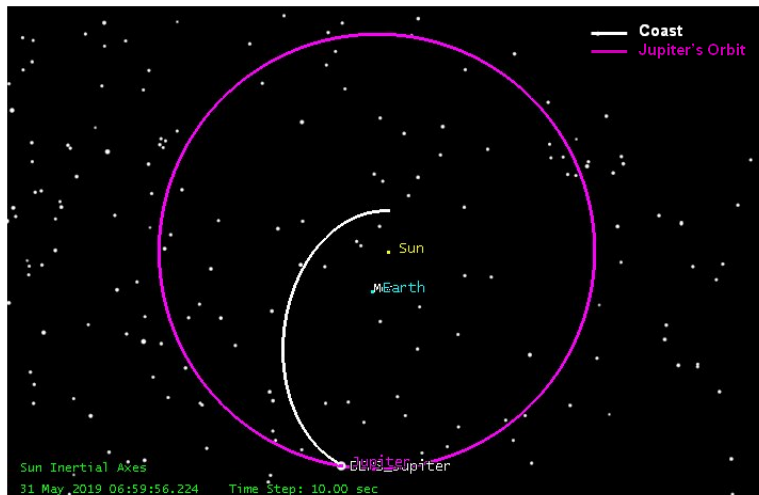
Laser Site Range/Range Rate During TTI Burn

Mission Design Laboratory
BEPS Laser Site Range During TTI Burn



Jupiter Transfer Trajectory

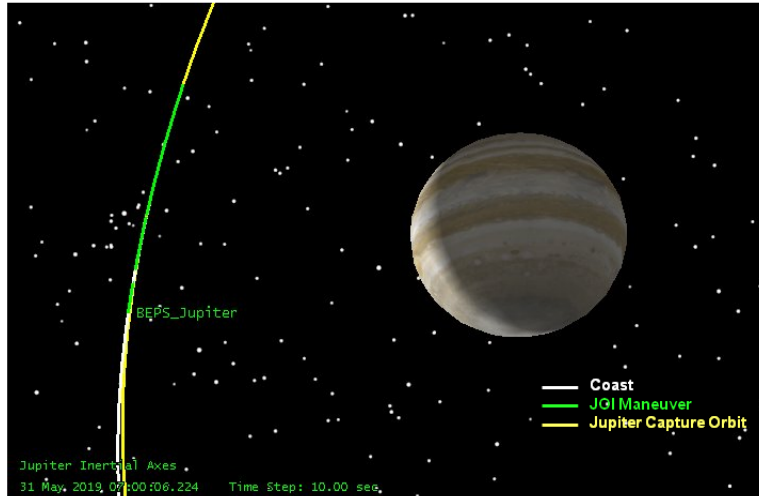
Mission Design Laboratory





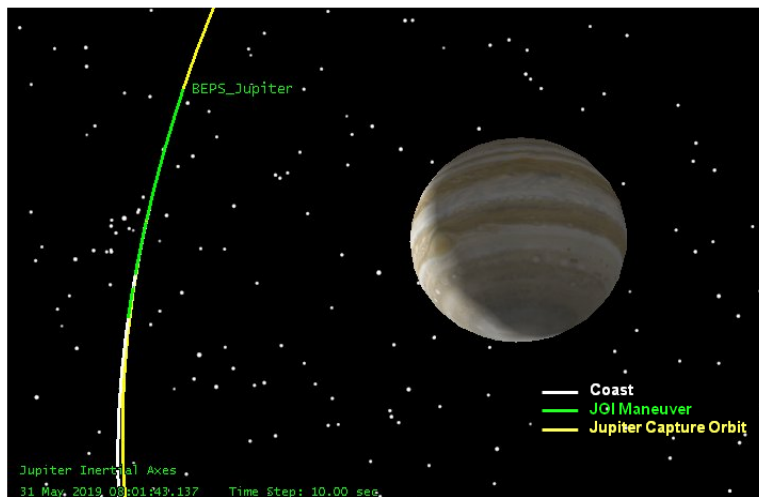
Jupiter Orbit Insertion (JOI) Ignition

Mission Design Laboratory



Jupiter Orbit Insertion (JOI) Burnout

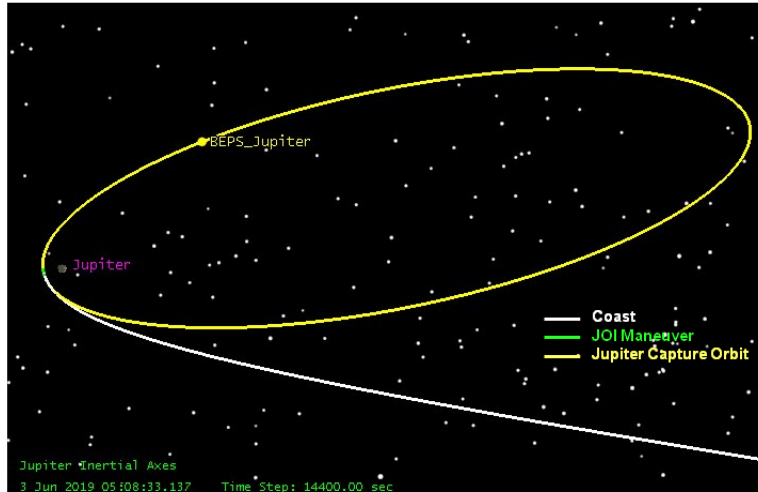
Mission Design Laboratory





Jupiter Capture Orbit

Mission Design Laboratory



Summary

Mission Design Laboratory

- A viable, point-solution trajectory to Jupiter was found that satisfies the given BEPS propulsion system constraints on the departure maneuver
- Launch opportunities will be spaced approximately 399 days apart (Earth-Jupiter synodic period), but the launch energy requirement will vary with each opportunity
- Future work should consider launch window planning for each launch opportunity
 - It is unclear at this time how sensitive the required Earth departure geometry is to the initial orbit elements
 - Nodal and apsidal rotation will eventually drive the “ideal” departure orbit out of alignment
 - Proper phasing with the laser site is an additional complication that requires further study
- With the “Galileo” payload removed, the 900 kg dry mass of the BEPS can be accelerated to a C3 of approximately $420 \text{ km}^2/\text{s}^2$ relative to the Sun.
 - Crosses the orbit of Pluto (44 AU) in approximately 10 years
 - By comparison, New Horizons (478 kg) will reach Pluto after a 9-year flight



Mechanical

Sara Riall

David Peters



November 29-December 03, 2010

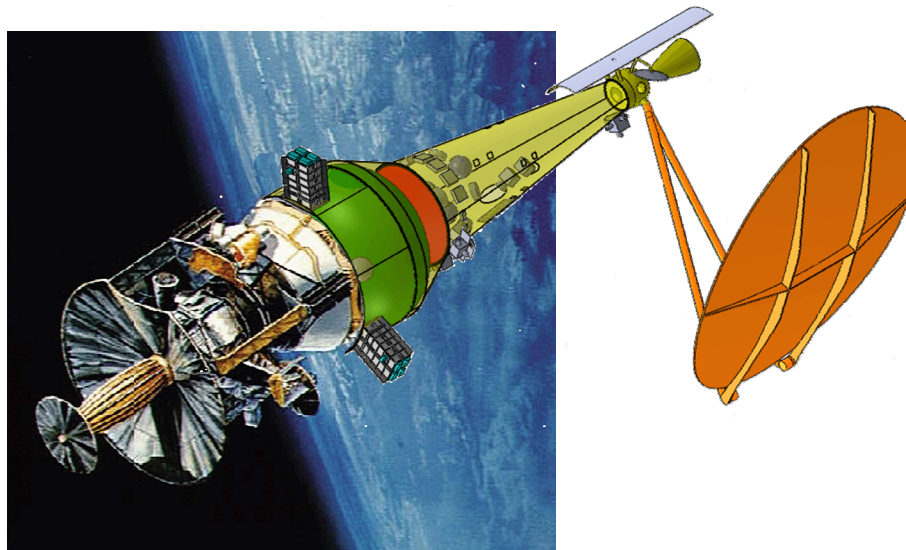
"I believe there is no philosophical high-road in science, with epistemological signposts. No, we are in a jungle and find our way by trial and error, building our road behind us as we proceed. "

Max Born (1882-1970) German Physicist. Nobel Prize, 1954.



Galileo & BEPS

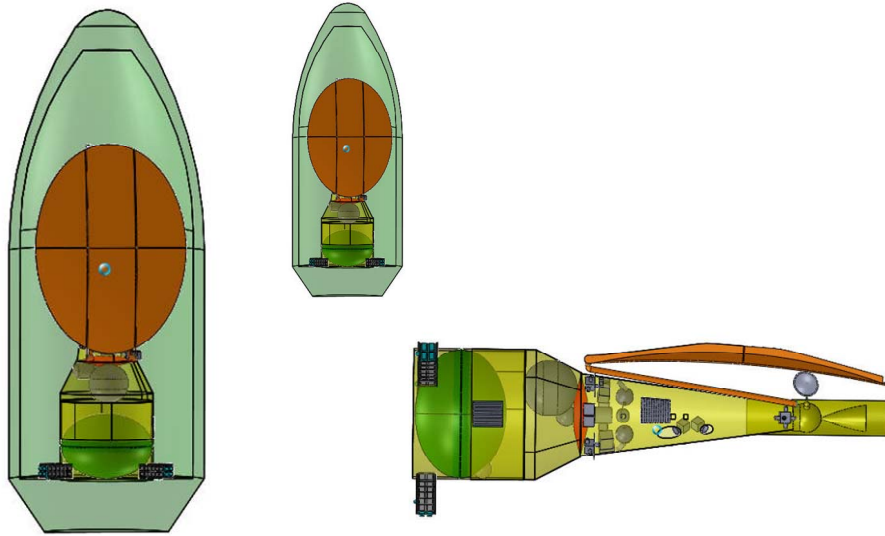
Mission Design Laboratory





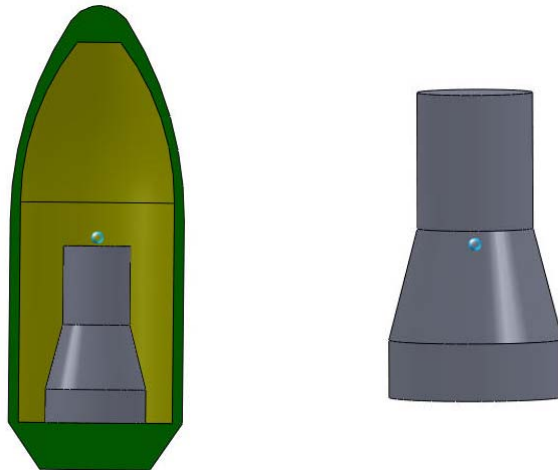
Launch Configuration of the Propulsion and Propellant Stage

Mission Design Laboratory



Launch Configuration of Galileo Payload

Mission Design Laboratory

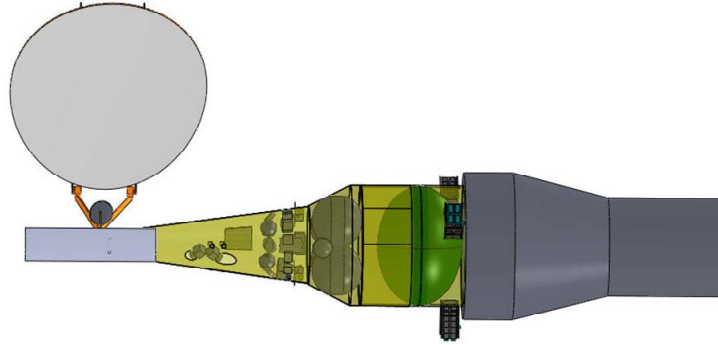


Note: Dimensions correspond closely with Galileo



Deployed Configuration

Mission Design Laboratory



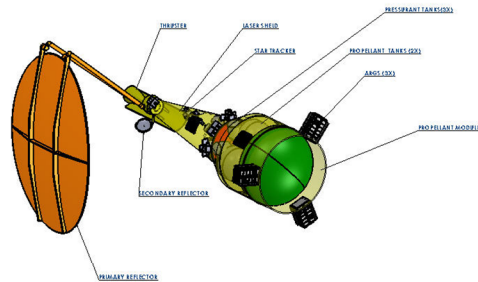
Note: Dimensions correspond closely with Galileo



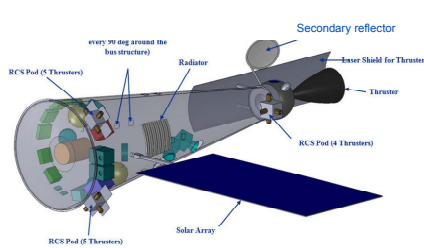
Propulsion Stage Deltas From DRM-2

Mission Design Laboratory

- 1) Added Propellant Stage in Launch Configuration
- 2) Removed Solar Array
- 3) Moved docking to Propellant stage



Current Layout



Original Layout

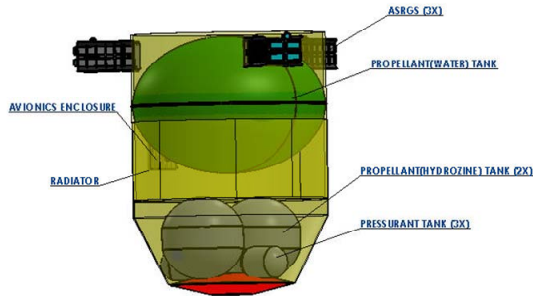
Note Main Reflector in DRM-2 version removed for simplicity



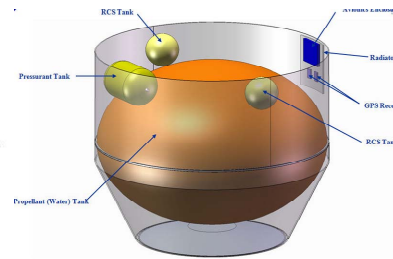
Propellant stage deltas

Mission Design Laboratory

- 1) Moved from Payload to Propulsion for Launch
- 2) Added 3 ASRGs
- 3) Added Separation ring to Tank/Structure
- 4) Expanded Tank Section to 3.3 m



Current Layout



Original Layout



Mass Rack-up

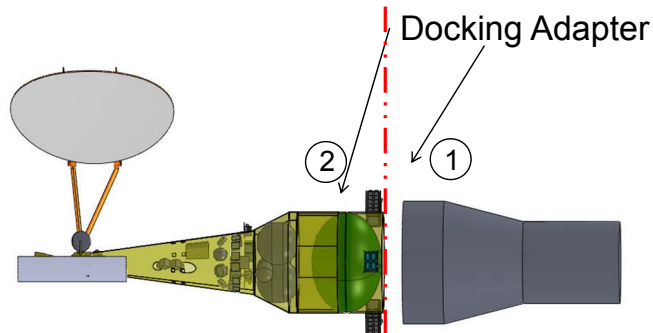
Mission Design Laboratory

1. Structures and mechanisms Propellant stage (COMPASS)	81.44
2. Structures and mechanisms Propulsion Stage (COMPASS)	62.97
3. Structure mass increase to support 3 ASRG's (MDL)	13.45
4. Addition of separation system (MDL)	<u>22.32</u>
	180.18



Docking and Separation Ring

Mission Design Laboratory



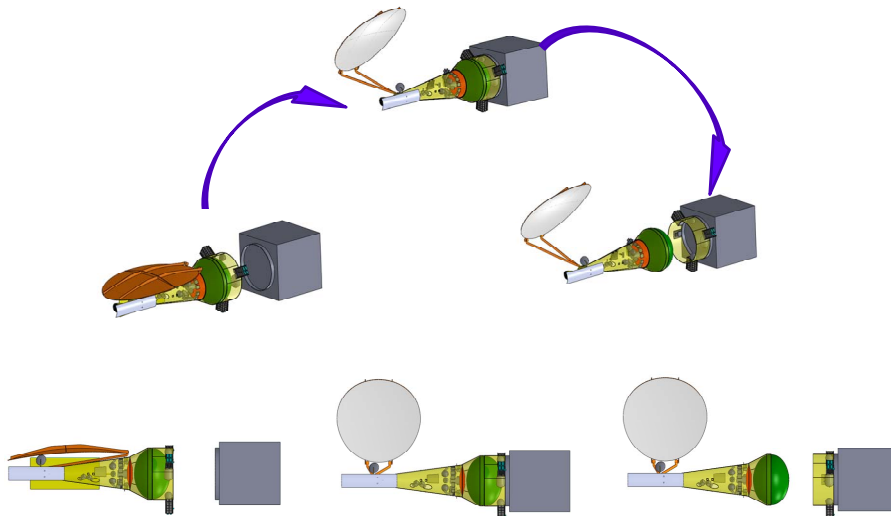
Note:

- 1) The Docking Adapter was moved from the Propulsion Stage/Propellant Stage interface to the Propellant/Payload interface.
- 2) A separation system was added to the propellant stage to separate the assembly after the trajectory burn. This interface allows the fuel tank to be jettisoned with the propulsion stage while permitting the ASRG's to stay with the payload.



Mission Timeline

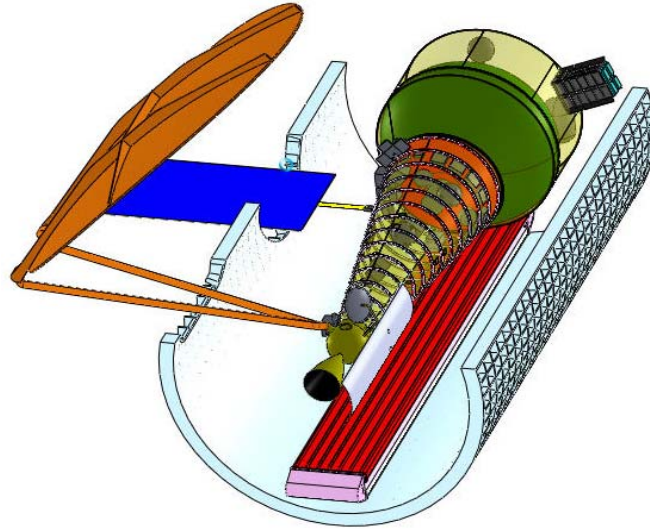
Mission Design Laboratory





OVERVIEW

Mission Design Laboratory



Integrated Design Center / Mission Design Laboratory

Mission Design Laboratory

Beamed Energy Propulsion System (BEPS)

Mission Operations

Deborah Knapp

November 29 – December 3, 2010



Topics

Mission Design Laboratory

- **Study Activities**
- **Customer Requirements**
- **Concept of Operations**
- **Overall Lifecycle**
- **Operations Timeline**
- **Design Requirements & Assumptions**
- **Ground System Functional Architecture**
- **Technology Required**
- **Risk/Issues/Concerns**
- **Additional Trades**



Study Activities

Mission Design Laboratory

- **Provide the BEPS customer with an Operations Concept**
- **Provide the BEPS customer with basic Ground System Architecture diagram**
- **Mission Operations costs are not required**



Customer Requirements

Mission Design Laboratory

- **Spacecraft data rates:**
 - NENS
 - 20 kbps command
 - 30 kbps, 4 Mbps telemetry downlink
 - TDRSS
 - 2 kbps command
 - 10 kbps telemetry downlink



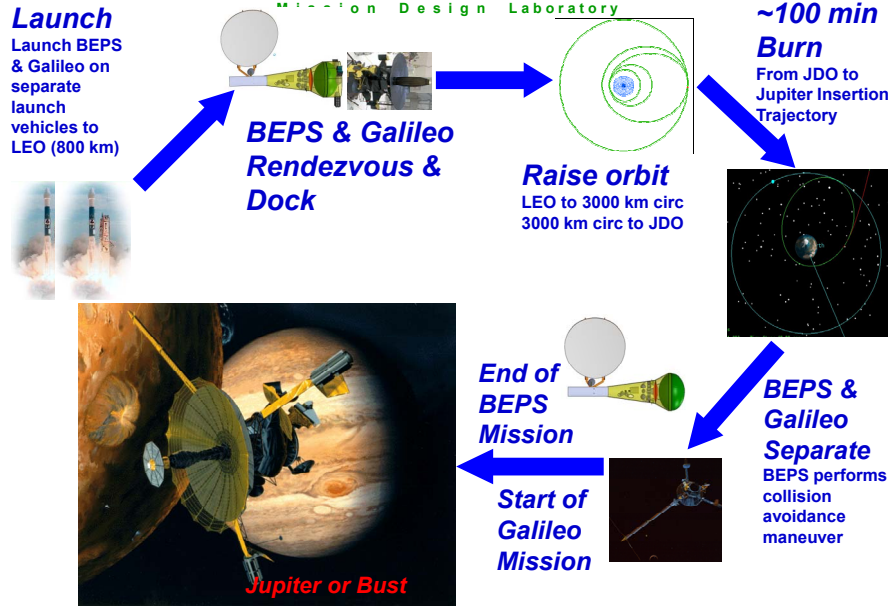
Concept of Operations

Mission Design Laboratory

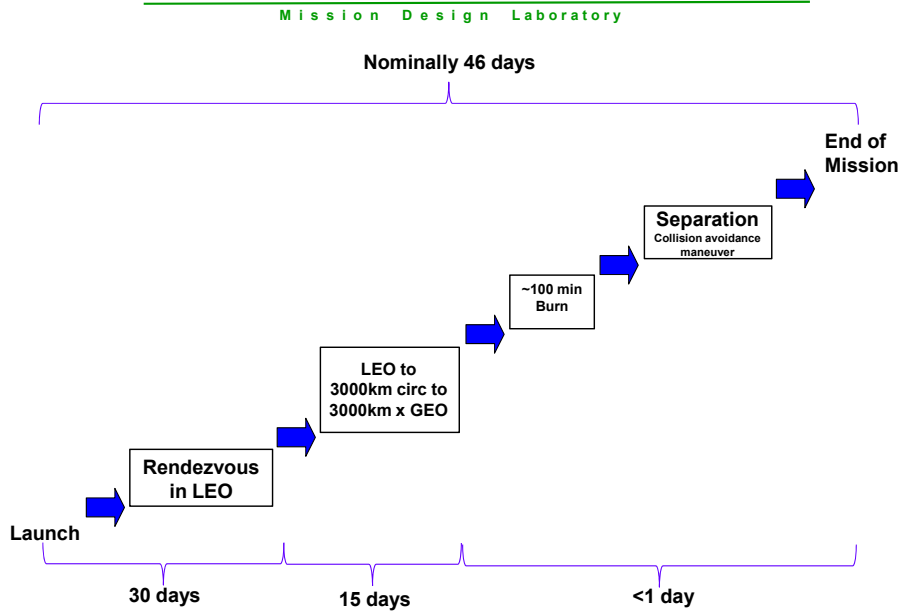
- **Launch BEPS & Galileo on separate launch vehicles into LEO**
- **BEPS & Galileo rendezvous in LEO (800 km circ)**
- **Transfer from LEO to 3000 km circular orbit**
- **Transfer from 3000 km circular orbit to 3000 x 35000 km orbit (Jupiter Departure Orbit (JDO))**
- **~100 min burn to transfer from JDO to Jupiter Intercept Trajectory**
- **BEPS & Galileo separate**
 - BEPS performs collision avoidance maneuver
- **BEPS Mission Ends and BEPS flies away**
- **Galileo mission continues to Jupiter**



Overall Lifecycle



Operations Timeline





Design Requirements & Assumptions

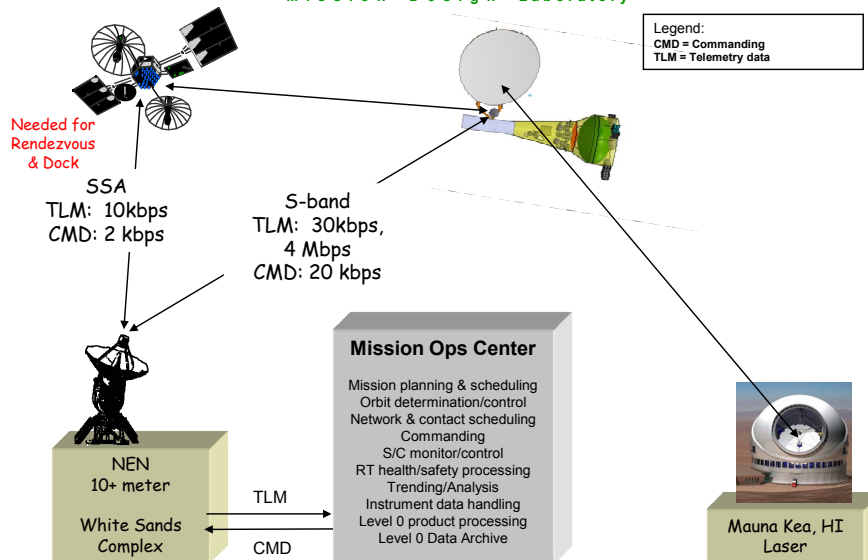
Mission Design Laboratory

- **Mission Operation Control (MOC):**
 - Provides “standard” set of functional components to support Mission Operations (e.g., S/C commanding, mission planning/scheduling, and RT TLM monitoring, HK trending and analysis).
 - Provides level zero processing (LZP)
 - Level 0 Products: Time-ordered, quality annotated data sets produced for each contact
- **Space-Ground contacts**
 - Near Earth Network (NEN) stations for telemetry & command
 - 10 meters or greater
 - Tracking and Data Relay Satellite System (TDRSS) for telemetry & command during rendezvous and docking
 - Laser at Mauna Kea, HI for laser burns
- **Space-Space contacts**
 - BEPS will communicate with the Galileo during rendezvous and docking with an omni antenna at Galileo data rates/frequencies
- **Spacecraft data rates:**
 - NENS
 - 20 kbps command
 - 30 kbps, 4 Mbps telemetry downlink
 - TDRSS
 - 2 kbps command
 - 10 kbps telemetry downlink
- **Data Latency Requirements:**
 - Real time for laser burn
- **Data Recovery:**
 - Assume 98% recovery requirement (end-to-end)
- **Orbit Determination via FDF**



Ground System Functional Architecture

Mission Design Laboratory





Technology Required

Mission Design Laboratory

- **Use COTS/GOTS-based MOC as basis for MOC implementation**
 - Software packages are available to satisfy MOC required functionality:
 - ITOS, ASIST, EPOCH 2000, ALTAIR are commercially available today and provide required functionality for Spacecraft Command/Control and Level Zero (LZ) Processing.
 - Low data volume so no special/new technology required
 - Most required technologies have been at least demonstrated; many in currently operational systems.
- **Technology Complexity: Low**
- **Technology Readiness Level: 9**



Risk/Issues/Concerns

Mission Design Laboratory

- **Risks**
 - Burn shutdown early
- **Issues**
 - none
- **Concerns**
 - none



Additional Trades

Mission Design Laboratory

- Co-locate BEPS MOC with either Galileo MOC or at Laser site



Integrated Design Center / Mission Design Laboratory

Beamed Energy Propulsion System (BEPS)

Orbital Debris and End of Mission Plans
Ivonne Rodriguez

November 29 – December 3, 2010



Assessment of Damage to Primary Mirror Due to Small Particle Collision During Earth Orbit Phase

Mission Design Laboratory

- In general terms, hypervelocity impact with small particles in orbit is not a significant problem in spacecraft design because the analysis is usually focused on structure penetration and subsequent damage to internal components. However, BEPS Primary Mirror (PM) represents a special case where the concern is not the total penetration of the component (which has extremely low probability of occurring) but how the integrity of the surface is affected by particles as small as a few microns in diameter.
- Because of the high-energy beams that will be focused on the PM as the spacecraft departs from Earth orbit, it is important to assess the extent of the damage that the PM optical surface might receive from hypervelocity impacts with micrometeoroids and orbital debris (MMOD) since the first insertion in LEO to the departure maneuver from GEO.
- The number of impacts is proportional to the surface area and the time. The results of the analysis will be presented in number of impacts to the PM per day on each orbit or transit orbit, for easy reference and adaptability to different scenarios.



Analysis Assumptions

Mission Design Laboratory

- Because of the complex distribution of the orbital debris flux, in particular at LEO, random orientation of the PM will be assumed.
- Although impacts inside already existing craters can occur, it is assumed that each particle strikes directly into the PM's surface, not into a crater.
- Although hypervelocity impacts frequently produce ejecta, possible secondary damage due to ejecta is not included in the analysis.
- Collision with objects ≥ 10 cm is considered catastrophic for the spacecraft. For that reason, only objects ≤ 10 cm will be included in the analysis.
- The PM is made of Aluminum, with general dimensions 4 m x 5.6 m x 26.6 mm.
- Average density of orbital debris = 2.8 g/cm^3
- Density of micrometeoroids: 2.0 g/cm^3 for particles of 10^{-6} g or less; 1.0 g/cm^3 for particles between 10^{-6} g and 0.01 g; 0.5 g/cm^3 for particles over 0.01 g (per NASA TM-4527).



Number of Impacts to the PM Optical Surface

Mission Design Laboratory

- The number of impacts to the PM optical surface is obtained from:

$$h = F \times A \times T$$
 where: **h** = number of impacts
F = particle flux (meteoroid or orbital debris), in impacts\m²\year.
A = cross-sectional area of the surface of interest, in m²
T = time, in years
- F** is obtained from environment models.
 - Orbital debris models:
 - ORDEM 2000 (Orbital Debris Environment Model)
 - Still the most widely used OD model, although it predates the FY-1C ASAT and Iridium-Cosmos collisions; tends to underestimate the current OD population.
 - Major limitation: Model is limited to the LEO region (<= 2000 km)
 - ORDEM 2008 Beta
 - Not released for official use yet. Expected to be released as ORDEM 2010.
 - Covers up to GEO (35,786 km).
 - Micrometeoroid models:
 - Grün model
 - Still used for near-Earth assessment of the micrometeoroid population. Simple and fast for quick computations.
 - MEM 1c (Meteoroid Engineering Model, version 1c)
 - Latest NASA micrometeoroid environment model.
 - Requires detailed ephemeris inputs.
 - Longer running time.

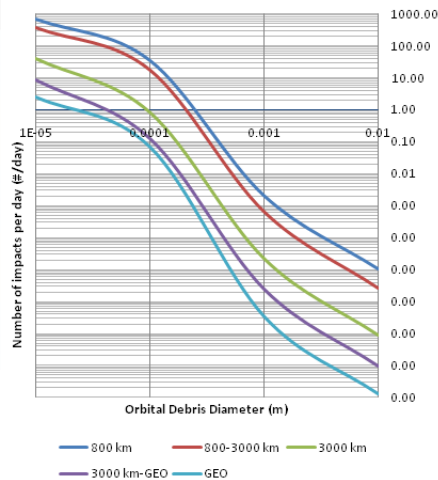


Orbital Debris Impacts on PM at the Different Altitudes, per Day

Mission Design Laboratory

Orbit	Particle range	Flux in range (#/m ² /yr)	Flux per day (#/m ² /day)	Impacts in 1 day	Total impacts per day
800 km	10 microns-99.9 microns	1.43E+04	3.91E+01	687.67	
	100 microns - 0.99 mm	7.33E+02	2.01E+00	35.33	
	1 mm - 0.99 cm	4.40E-02	1.20E-04	2.12E-03	
800-3000	1 cm - 9.99 cm	2.26E-04	6.19E-07	1.09E-05	723.0
	10 microns-99.9 microns	7.45E+03	2.04E+01	358.85	
	100 microns - 0.99 mm	3.55E+02	9.73E-01	17.11	
3000 km	1 mm - 0.99 cm	1.31E-02	3.60E-05	6.34E-04	
	1 cm - 9.99 cm	5.34E-05	1.46E-07	2.57E-06	376.0
	10 microns-99.9 microns	7.98E+02	2.19E+00	38.47	
3000 km-GEO	100 microns - 0.99 mm	1.69E+01	4.63E-02	0.81	
	1 mm - 0.99 cm	4.69E-04	1.29E-06	2.26E-05	
	1 cm - 9.99 cm	1.92E-06	5.26E-09	9.25E-08	39.3
GEO	10 microns-99.9 microns	1.78E+02	4.89E-01	8.60	
	100 microns - 0.99 mm	2.61E+00	7.15E-03	0.13	
	1 mm - 0.99 cm	5.06E-05	1.39E-07	2.44E-06	
GEO	1 cm - 9.99 cm	1.95E-07	5.34E-10	9.40E-09	8.7
	10 microns-99.9 microns	5.24E+01	1.43E-01	2.52	
	100 microns - 0.99 mm	1.44E+00	3.95E-03	0.07	
GEO	1 mm - 0.99 cm	6.98E-06	1.91E-08	3.37E-07	
	1 cm - 9.99 cm	2.60E-08	7.12E-11	1.25E-09	2.6

Orbital Debris Flux per Day for Different Orbits



- Calculations based on 17.6 m² total PM area.
- See Backup Slides for complete table.



Orbital Debris Impacts Are Expected to Be from Particles of < 1mm in Size

Mission Design Laboratory

Orbit	Particle range	Impacts in 1 day	Total impacts per day	Percent of impacts per day
800 km	10 microns-99.9 microns	687.67	723.0	95.11%
	100 microns - 0.99 mm	35.33		4.89%
	1 mm - 0.99 cm	2.12E-03		0.0003%
	1 cm - 9.99 cm	1.09E-05		0.000002%
800-3000	10 microns-99.9 microns	358.85	376.0	95.45%
	100 microns - 0.99 mm	17.11		4.55%
	1 mm - 0.99 cm	6.34E-04		0.0002%
	1 cm - 9.99 cm	2.57E-06		0.000001%
3000 km	10 microns-99.9 microns	38.47	39.3	97.926380%
	100 microns - 0.99 mm	0.81		2.073562%
	1 mm - 0.99 cm	2.26E-05		0.00006%
	1 cm - 9.99 cm	9.25E-08		0.0000002%
3000 km-GEO	10 microns-99.9 microns	8.60	8.7	98.56%
	100 microns - 0.99 mm	0.13		1.44%
	1 mm - 0.99 cm	2.44E-06		0.00003%
	1 cm - 9.99 cm	9.40E-09		0.0000001%
GEO	10 microns-99.9 microns	2.52	2.6	97.32%
	100 microns - 0.99 mm	0.07		2.68%
	1 mm - 0.99 cm	3.37E-07		0.00001%
	1 cm - 9.99 cm	1.25E-09		0.00000005%

• Note from the table in the previous slide that the artificial objects actually striking the surface are micron-size particles. Objects of millimeter-size and more have low probability of reaching the PM in the short time that BEPS will be in Earth orbit.



Micrometeoroid Environment

Mission Design Laboratory

- For this initial assessment, the Grün model of the Micrometeoroid Environment at 1 AU will be used.
 - The model assumes an omnidirectional particle flux in Earth’s vicinity; the flux is a function of the micrometeoroid mass.
 - Shielding and focusing effects due to Earth are taken into consideration.
 - Limited to particles < 10 g.
 - The model might underestimate the number of impacts, but even in that case the effect of micrometeoroids is expected to be low compared to that of orbital debris.

Altitude (km)	Particle Range	Particle Diameter (cm)	Particle Density (g/cm ³)	Mass (g)	Flux (#/m ² /year)	Shielding Factor	Focusing Factor	Adjusted Flux (#/m ² /yr)	Adjusted Flux per day (#/m ² /day)	Impacts in one day
800	10 microns-99.9 microns	0.005	2	1.3E-07	7.82E+00	0.7279	1.90248	10.82767	2.97E-02	5.22E-01
800	100 microns - 0.99 mm	0.05	1	6.5E-05	1.72E-02	0.7279	1.90248	0.023772	6.51E-05	1.15E-03
800	1 mm - 0.99 cm	0.5	0.5	0.03272	6.50E-06	0.7279	1.90248	9.01E-06	2.47E-08	4.34E-07
800	1 cm - 9.99 cm	5	0.5	32.7249				Out of range		
3000	10 microns-99.9 microns	0.005	2	1.3E-07	7.82E+00	0.86498	1.69077	11.43497	3.13E-02	5.51E-01
3000	100 microns - 0.99 mm	0.05	1	6.5E-05	1.72E-02	0.86498	1.69077	0.025105	6.88E-05	1.21E-03
3000	1 mm - 0.99 cm	0.5	0.5	0.03272	6.50E-06	0.86498	1.69077	9.51E-06	2.61E-08	4.58E-07
3000	1 cm - 9.99 cm	5	0.5	32.7249				Out of range		
35786	10 microns-99.9 microns	0.005	2	1.3E-07	7.82E+00	0.99409	1.15364	8.966848	2.46E-02	4.32E-01
35786	100 microns - 0.99 mm	0.05	1	6.5E-05	1.72E-02	0.99409	1.15364	0.019686	5.39E-05	9.49E-04
35786	1 mm - 0.99 cm	0.5	0.5	0.03272	6.50E-06	0.99409	1.15364	7.46E-06	2.04E-08	3.59E-07
35786	1 cm - 9.99 cm	5	0.5	32.7249				Out of range		

Reference: *Natural Orbital Environment Guidelines for Use in Aerospace Vehicle Development*, NASA TM-4527, pages 7-1 to 7-4



Crater Formation

Mission Design Laboratory

- The diameter of an impact crater on a semi-infinite single wall of monolithic material is characterized by:

$$d_c = 0.8 d_p^{1.056} \rho_p^{0.519} \rho_t^0 v^{0.667} (\cos(\alpha_p))^{0.667}$$

where:

d_c = crater diameter, in cm

d_p = particle diameter, in cm

ρ_p = particle density, in g/cm³

ρ_t = target density, in g/cm³

v = particle velocity, in km/s

α_p = particle impact angle with respect to surface normal

(From Klinrad, "Space Debris: Models and Risk Analysis", pp 206-207, using ESA coefficients for ductile materials).



Crater Size Results

Mission Design Laboratory

	Particle range	Average Particle Diameter (cm)	Target Density (g/cm ³)	Particle Density (g/cm ³)	Average Particle Velocity (km/s)	Crater Diameter (cm)	Crater to Particle Ratio
Orbital Debris	10 micron - 99.9 micron	0.003042	2.71	2.8	7	0.01098	3.61
	100 micron - 0.99 mm	0.0184	2.71	2.8	7	0.07349	3.99
	1 mm - 9.9 mm	0.1816	2.71	2.8	7	0.82450	4.54
	1 cm - 9.9 cm	2.144	2.71	2.8	7	11.17730	5.21
Micrometeoroids	10 micron - 99.9 micron	0.005	2.71	2.0	20	0.03139	6.28
	100 micron - 0.99 mm	0.05	2.71	1.0	20	0.24920	4.98
	1 mm - 9.9 mm	0.5	2.71	0.5	20	1.97843	3.96
	1 cm - 9.9 cm	N/A	N/A	N/A	N/A	N/A	N/A

- All ranges are evaluated for reference only; this does not imply that all sizes will be found in the PM.
- Micrometeoroids in the 1cm range are beyond the scope of the Grun model and thus are not included here.



Example: 45 Days on Earth Orbit

Mission Design Laboratory

Orbit	Particle Range	Time in orbit (days)	OD Impacts in 1 day	MM Impacts in 1 day	Total impacts
800 km	10 microns-99.9 microns	30	687.67	0.522	20645.65
	100 microns - 0.99 mm	30	35.33	0.001	1059.88
	1 mm - 0.99 cm	30	2.12E-03	4.34E-07	6.36E-02
	1 cm - 9.99 cm	30	1.09E-05	N/A	3.27E-04
800-3000	10 microns-99.9 microns	1	358.85		358.85
	100 microns - 0.99 mm	1	17.11		17.11
	1 mm - 0.99 cm	1	6.34E-04		6.34E-04
	1 cm - 9.99 cm	1	2.57E-06		2.57E-06
3000 km	10 microns-99.9 microns	12	38.47	5.51E-01	468.23
	100 microns - 0.99 mm	12	0.81	1.21E-03	9.79
	1 mm - 0.99 cm	12	2.26E-05	4.58E-07	2.77E-04
	1 cm - 9.99 cm	12	9.25E-08	N/A	1.11E-06
3000 km-GEO	10 microns-99.9 microns	1	8.60		8.60
	100 microns - 0.99 mm	1	0.13		0.13
	1 mm - 0.99 cm	1	2.44E-06		2.44E-06
	1 cm - 9.99 cm	1	9.40E-09		9.40E-09
GEO	10 microns-99.9 microns	1	2.52	0.432	2.96
	100 microns - 0.99 mm	1	0.07	9.49E-04	0.07
	1 mm - 0.99 cm	1	3.37E-07	3.59E-07	6.96E-07
	1 cm - 9.99 cm	1	1.25E-09	N/A	1.25E-09

Average Particle Diameter in range	# Impacts	Crater Diameter (m)	Crater Area (m2)	Total Damaged Area (m2)
3.04E-05	21484.28	1.10E-04	9.47E-09	2.03E-04
0.0184	1086.98	7.35E-04	4.24E-07	4.61E-04



Conclusions

Mission Design Laboratory

- **The damage to the PM comes primarily from the micron-size orbital debris particles.**
 - The short time spent in at the different altitudes favors the low probability of being impacted by objects of larger size.
 - The damage due to micrometeoroids while in Earth's vicinity is negligible compared to damage due to orbital debris environment.
- **More extensive analysis of MMOD damage is recommended. For more detailed analyses, contact:**
 - Eric Christiansen, Hypervelocity Impact expert at JSC, (Eric.L.Christiansen@nasa.gov)
 - Meteoroid Environment Office (MEO) at MSFC (Bill Cooke, william.i.cooke@nasa.gov).
- **Recommended to perform hypervelocity tests on surfaces with similar finishes than the PM to further study the damage and the effect on thermal absorption.**



Beam Energy Propulsion Study (BEPS)-DRM 3

Systems Engineering
Mark Baugh, Seymour Kant, John Panek

Nov 29-Dec 3, 2010

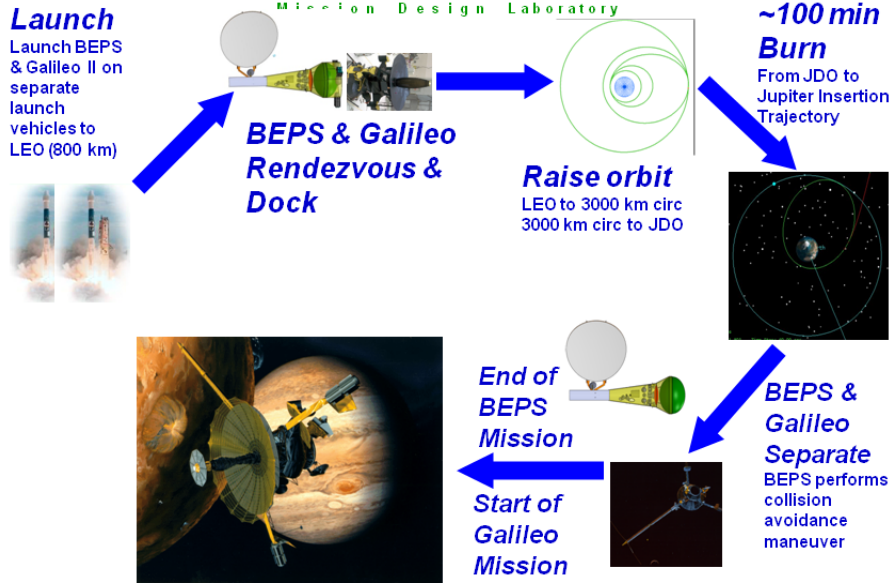


Mission Requirements

- **Modify the DRM-2 transport and propellant stages for interplanetary trajectory using the BEPS system**
 - C3 > 80
 - Galileo-class payload
 - 5300N thruster, Isp = 900 sec
- **50 MW optical power available at S/C**
 - 99.99% reflective primary and secondary mirrors
- **Initial Launches to 800 km altitude on Falcon 9 Block 2 vehicles**
 - 9° inclination, lift capability = 9280 kg
- **Estimate orbital debris and micrometeorite flux in all orbits prior to cruise**

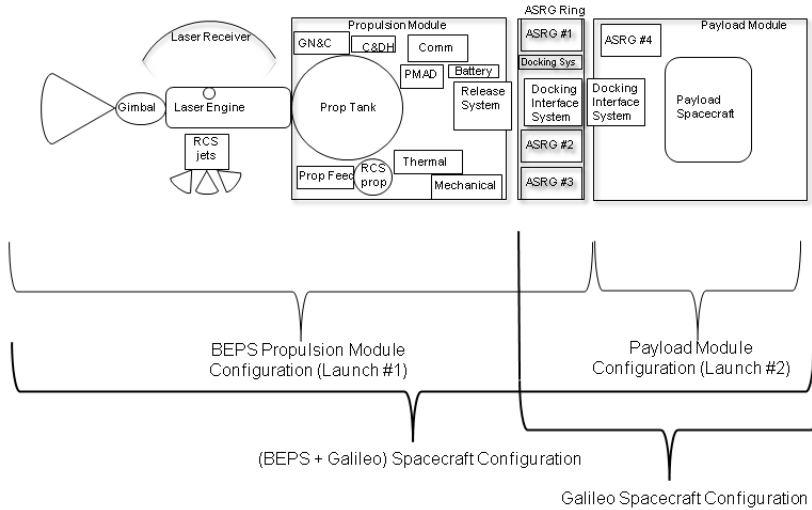


Mission Overview



Spacecraft Configuration Diagram

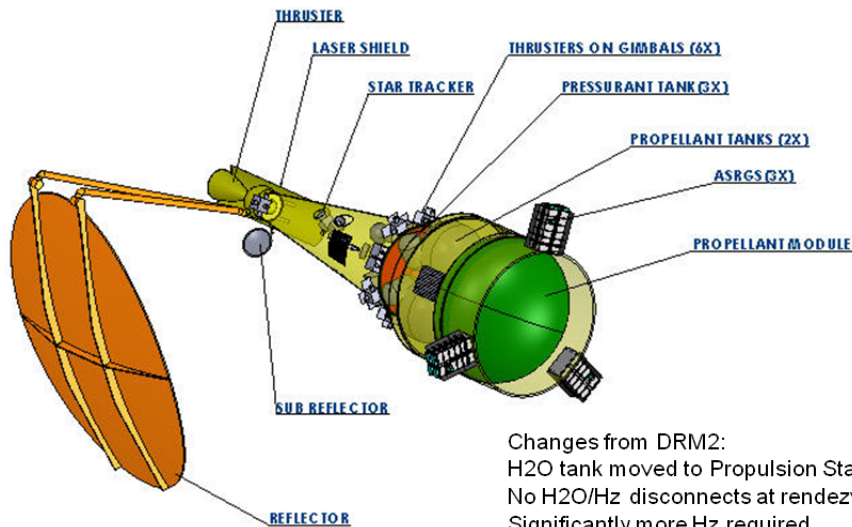
Mission Design Laboratory





Propulsion Stage Overview

Mission Design Laboratory



Changes from DRM2:
H₂O tank moved to Propulsion Stage
No H₂O/Hz disconnects at rendezvous I/F
Significantly more Hz required
ASRGs instead of Solar Array



Payload Stage Overview

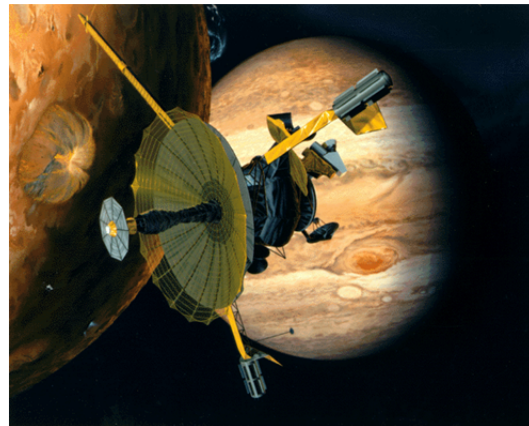
Mission Design Laboratory

Galileo-like Payload with Modifications:
Original Galileo mass = 2223 kg (118kg instruments, 925 kg propellant)

Remove RTGs (2), Replace with ASRGs (4); same power generation, approximately same total mass

3 ASRGs launched on Propulsion stage (61 kg); xferred to Payload stage for cruise to Jupiter

Power Requirement 500 W at Jupiter, <140 W during launch/rendezvous





Prop Module S/C Bus Design Summary

Mission Design Laboratory

- Mechanical – DRM-2 Propulsion stage with addition of water propellant tank
- Thermal – DRM-2 baseline, MLI, heaters, thermostatically controlled, additional pocketing on back of primary mirror
- Comm – 4 S-band omnis, transceivers
- EPS – 3 x ASRG, 100 Amp hour Li-Ion battery
- ACS – DRM-2 baseline
- Propulsion – BEPS, Chemical Monoprop Hz, 6 articulated 5lbf thrusters on Canfield joints
- Avionics – DRM-2 baseline



BEPS-DRM3 Mass Rackup

Mission Design Laboratory

BEPS-PROPULSION STAGE			
	CBE	SS Cont.	MEV
Mechanical	180 kg	15%	207 kg
Attitude Control	53 kg	18%	63 kg
Thermal+Mirror	232 kg	18%	274 kg
Propulsion	150 kg	18%	177 kg
Power (3ASRG+EPS)	116 kg	18%	137 kg
Avionics	34 kg	25%	43 kg
Communications	16 kg	18%	19 kg
Bus Total	781 kg	18%	919 kg

S/C Dry Mass			
	CBE	Cont.	Allocation
Payload Total	0 kg	0%	0 kg
S/C Bus Total	781 kg	18%	919 kg
S/C Dry Mass	781 kg		919 kg
Hydrazine	662 kg	0%	662 kg
Water	6560 kg	0%	6560 kg
He	6 kg	0%	6 kg
S/C Wet Mass			8147 kg
Sep Sys (LV portion)	48 kg	10%	53 kg
Launch Mass			8200 kg

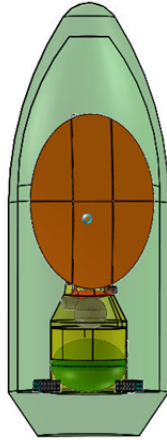
LAUNCH VEHICLE EVALUATION	
Falcon 9 Capability for 800 km/9 degree inclination	9280 kg
Throw Mass Margin	1080 kg
Throw Mass Margin %	13%

BEPS-PAYLOAD STAGE			
	CBE	Cont.	Allocation
Galileo II (1 ASRG)	2223.0 kg	0%	2223.0 kg
S/C Wet Mass			2223 kg
Sep Sys	25 kg	10%	28 kg
Launch Mass			2251 kg
LAUNCH VEHICLE EVALUATION			
Falcon 9 Capability for 800 km/9 degree inclination			9280 kg
Throw Mass Margin			7030 kg
Throw Mass Margin %			312%

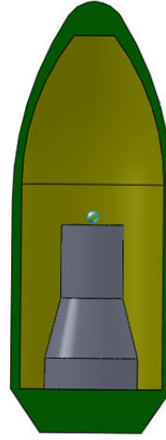


Launch Configurations

Mission Design Laboratory



Propulsion Stage



Payload Stage

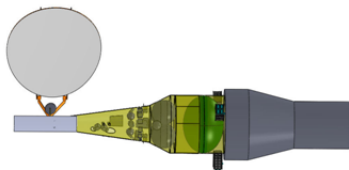


Deployed Configurations

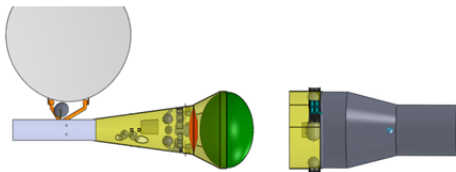
Mission Design Laboratory



Docking



Orbit Raise



Cruise



MEV Electrical Loads

Mission Design Laboratory

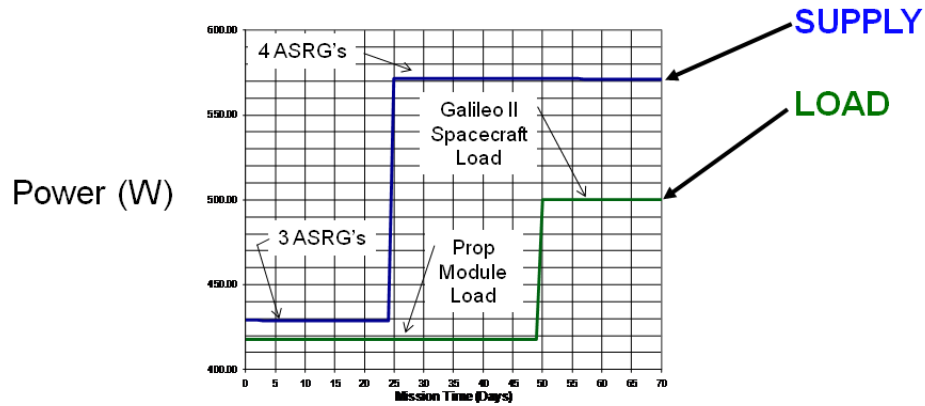
EPSMODE>>>	Launch	Checkout	Science Ops In Sun	Science Ops in Eclipse	Comm Downlink	Safehold	Laser Propulsion
Total Power (Watts)	30	293	306	290	354	245	1808
Instruments	0	0	0	0	0	0	1300
Spacecraft	30	293	306	290	354	245	508

Includes contingency of 30%
 These modes size battery/ASRG design
 Peak power mode (not shown) sizes harness



Electrical Power Curve

Mission Design Laboratory





Delta V Budget

Mission Design Laboratory

Delta V Budget (m/s)	BEPS	Chem
launch vehicle dispersion correction		29
rendezvous and docking		71
orbiter and collision avoidance		44
800 x 800 km to 3000 x 3000 km	928	
3000 x 3000 km to 3000 x GEO	1819	
3000 x GEO orbit to C3 = 80	6740	
Total:	9487	144

(Propulsion module only)



Orbital Debris Risk to Primary Mirror

Mission Design Laboratory

Average Particle Diameter in range	# Impacts	Crater Diameter (m)	Crater Area (m ²)	Total Damaged Area (m ²)
3.04E-05	21487.81	1.10E-04	9.47E-09	2.03E-04
0.0184	1096.15	7.35E-04	4.24E-07	4.65E-04



Technical Issues/Trades/Future Work

Mission Design Laboratory

- **Split water propellant into 2 tanks: 1 for 800km – 3000xGEO burn, 1 for 3000xGEO to C3=80 burn, and put second tank on second S/C (3600kg)**
 - Balances launch masses between the two vehicles – would increase first vehicle margin above 13%
 - Water I/F from DRM2 would be needed
 - If Payload S/C mass reduces by ~50% a single LV can do the job
 - Payload mass can increase significantly on second LV
- **Remove gimbal from BEP engine, use ACS articulated thrusters**
- **Assess thermal impact of primary mirror degradation from OD**
- **Don't lase other spacecraft:**
 - Conjunction Assessment and Risk Analysis Team at GSFC (Laurie Newman)
 - Similar to STK ground station coverage analysis with narrow beam
 - Existing laser ranging facilities and vehicles in the launch phase have similar issues
- **Revise flight dynamics calculations based on specific launch dates and windows**
- **Revise target to Kuiper Belt**
 - Travel time to Kuiper Belt ~10 years with minimal payload

BEPS-PROPULSION STAGE			
Payload			
	CBE	Cont.	Allocation
None	0.0 kg	0%	0.0 kg
Payload Total	0.00 kg	0%	0.0 kg
Bus			
	CBE	SS Cont.	MEV
Mechanical	180 kg	15%	207 kg
Attitude Control	53 kg	18%	63 kg
Thermal+Mirror	232 kg	18%	274 kg
Propulsion	150 kg	18%	177 kg
Power (3ASRG+EPS)	116 kg	18%	137 kg
Avionics	34 kg	25%	43 kg
Communications	16 kg	18%	19 kg
Bus Total	781 kg	18%	919 kg
S/C Dry Mass			
	CBE	Cont.	Allocation
Payload Total	0 kg	0%	0 kg
S/C Bus Total	781 kg	18%	919 kg
S/C Dry Mass	781 kg		919 kg
Hydrazine	662 kg	0%	662 kg
Water	6560 kg	0%	6560 kg
He	6 kg	0%	6 kg
S/C Wet Mass			8147 kg
Sep Sys (LV portion)	48 kg	10%	53 kg
PAF accounted for in	0 kg	0%	0 kg
Launch Mass			8200 kg
LAUNCH VEHICLE EVALUATION			
Falcon 9 Capability for 800 km/9 degree inclination			9280 kg
Throw Mass Margin			1080 kg
Throw Mass Margin %			13%

BEPS-PAYLOAD STAGE			
Payload			
	CBE	Cont.	Allocation
Galileo II (1 ASRG)	2223.0 kg	0%	2223.0 kg
Payload Total	2223.00 kg	0%	2223.0 kg
Bus			
	CBE	SS Cont.	MEV
Mechanical	0 kg	18%	0 kg
Attitude Control	0 kg	18%	0 kg
Thermal	0 kg	18%	0 kg
Propulsion	0 kg	18%	0 kg
Power incl harness	0 kg	18%	0 kg
Avionics	0 kg	18%	0 kg
Communications	0 kg	18%	0 kg
Bus Total	0 kg	#DIV/0!	0 kg
S/C Dry Mass			
	CBE	Cont.	Allocation
Payload Total	2223 kg	0%	2223 kg
S/C Bus Total	0 kg	0%	0 kg
S/C Dry Mass	2223 kg		2223 kg
Hydrazine		0%	0 kg
Water	0 kg	0%	0 kg
He		0%	0 kg
S/C Wet Mass			2223 kg
Sep Sys	25 kg	10%	28 kg
PAF accounted for in	0 kg	0%	0 kg
Launch Mass			2251 kg
LAUNCH VEHICLE EVALUATION			
Falcon 9 Capability for 800 km/9 degree inclination			9280 kg
Throw Mass Margin			7030 kg
Throw Mass Margin %			312%

Delta V Budget (m/s)	BEPS	Chem
launch vehicle dispersion correction		29
rendezvous and docking		71
loiter and collision avoidance		44
800 x 800 km to 3000 x 3000 km	928	
3000 x 3000 km to 3000 x GEO	1819	
3000 x GEO orbit to C3 = 80	6740	
Total	9487	144



Integrated Design Center / Mission Design Laboratory

Beamed Energy Propulsion System (BEPS)

Thermal System

Kimberly Brown

November 29 – December 3, 2010



Mission Requirements

Mission Design Laboratory

- **Design the system to do a Jupiter Departure Burn**
- **Maintain Mission Temperature Requirements**
 - Chemical Propulsion 10 to 40°C
 - Water Tank 10 to 40°C
 - Battery Li-Ion 10 to 30°C
 - ASRGs operate at 650°C at hot-end internally and cold-end at 90°C
 - Omni Antennas
 - Operational -40°C to +70°C
 - Electronics (avionics, comm system)
 - -10 to 40°C operational
 - -20 to 50°C survival
- **Handle Waste Heat of Laser Engine Burns using DRM-2 baseline design**
 - Primary Mirror
 - Secondary Mirror
 - Chamber



BEPS Thermal Components

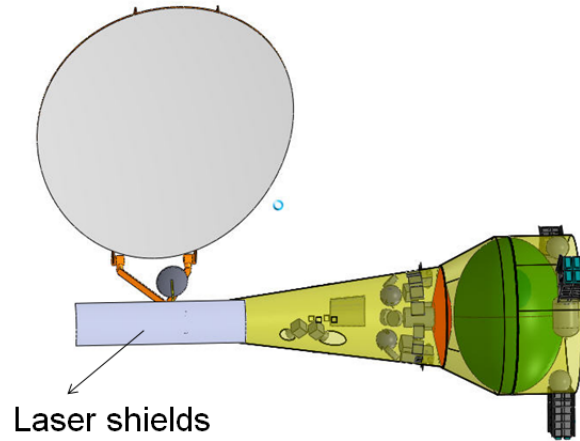
Mission Design Laboratory

- **MMOD (Micro-Meteor and Orbital Debris) Shielding (budgeted in thermal hardware)**
- **Cold plates and heat pipes to transfer from the electronics to the radiator section.**
- **Heaters, sensors**
- **Thermal Coatings/Paints**
- **MLI**
- **Primary Mirror Reflector**
 - Mirror reflectivity 0.9999 (specular + diffuse)
 - Back side of mirror pocketed to radiate excess heat to space
 - Parabolic surface
 - Laser mirror shields for protection of laser engine burns
- **Secondary Mirror Reflector**
 - Mirror reflectivity 0.9999 (specular + diffuse)
 - Back side of mirror coated to radiate excess heat to space
 - Parabolic surface
 - Laser mirror shields for protection of laser engine burns



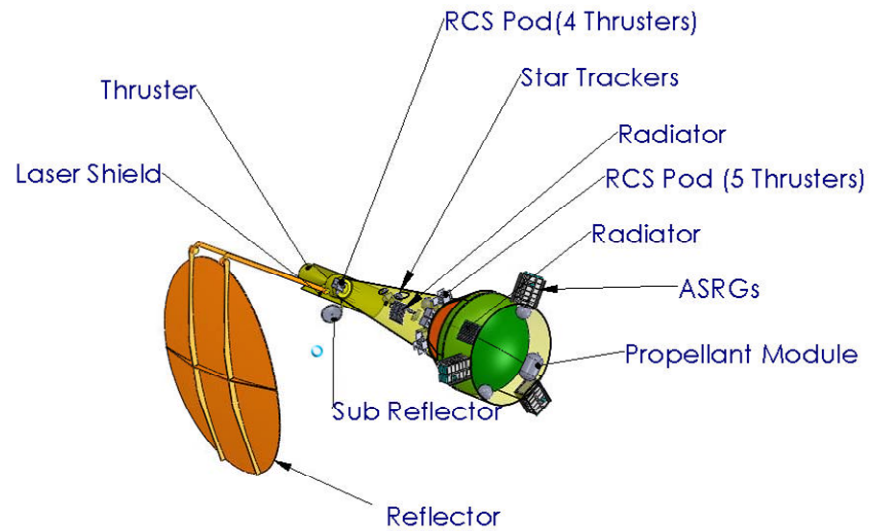
Mission Deployed Configuration

Mission Design Laboratory



Component Layout

Mission Design Laboratory





Waste Heat of BEPS

Mission Design Laboratory

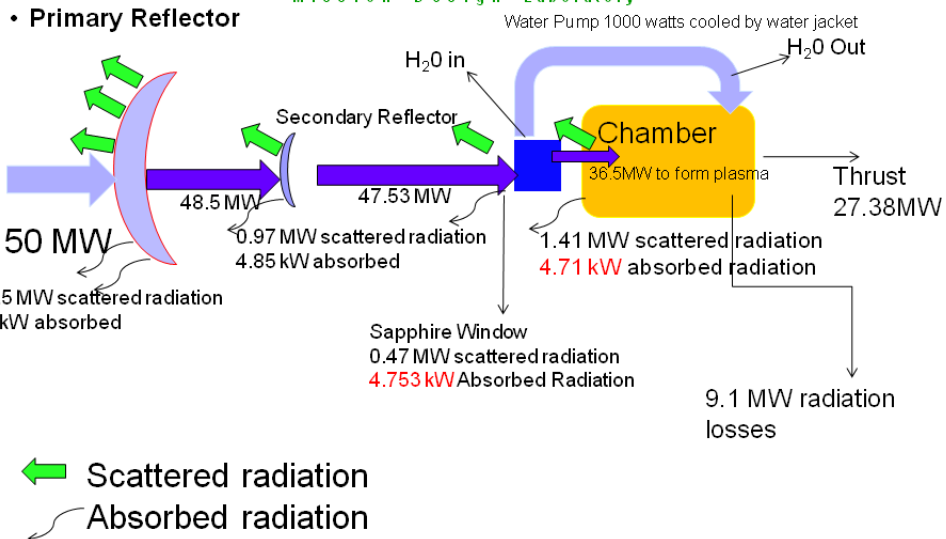
Laser power distribution		
Laser power nominally arriving at craft	50	MW
Primary mirror 97% efficient, .9999 reflective		
Scattered radiation MW	1.5	
Absorbed radiation kW	5	
Laser energy to secondary mirror	48.5	
Secondary mirror 98% efficient, .9999 reflective		
Scattered radiation MW	0.97	
Absorbed radiation kW	4.85	
Laser energy to window	47.53	
Sapphire window 99% efficient, .9999 transmissive		
scattered or reflected, MW	0.4753	
Absorbed radiation kW	4.753	
Laser energy into chamber	47.0547	
Chamber walls 97% efficient, .9999 reflective		
scattered or reflected, MW	1.411641	
absorbed radiation, kW	4.70547	
Chamber efficiency 80% (20% radiation losses out window and nozzle)		
Laser radiation losses	9.12767071	
Power available to form plasma, MW	36.5106828	
Plasma absorption efficiency 75% (25% losses into chemical reaction, ionization, etc)		
plasma inefficiency losses	9.12767071	
Power available for propulsive thrust, M	27.3830121	
Overall laser propulsion efficiency	54.7660242	

Total 20 kWatts



Heat Flow Map for BEPS

Mission Design Laboratory





Chamber Waste Heat

Mission Design Laboratory

- Water tank used to transfer sapphire window and chamber walls waste heat
- Water (water tank) heated to vapor (chamber walls)
- Consideration of Using the Water tank to handle all waste heats
 - Water Heat of vaporization**
 - 2260 J/g
 - Flow rate of engine 0.6 kg/sec
 - Waste heat the system can handle is 1.356 MegaWatts
 - Our system has ~20,000 Watts
 - Consider chamber transferring all the loads with water system



Mirror Reflectors

Mission Design Laboratory

- **Temperature of Mirror Reflector**
 - 5 kW absorbed
 - with assumed area of 23 m² pocketed radiator surface
 - 526°C operating temperature
- **Temperature of Secondary reflector**
 - 0.5 m diameter (non-pocketed area)
 - absorbed 4.85 kW operates at 918°C
 - Pocketed radiator will reduce temperature if area increased



ASRGs

Mission Design Laboratory

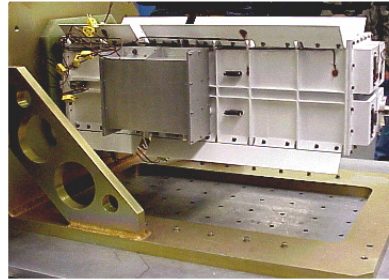
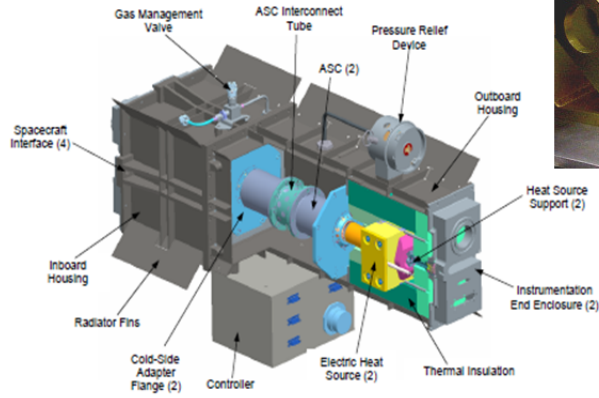
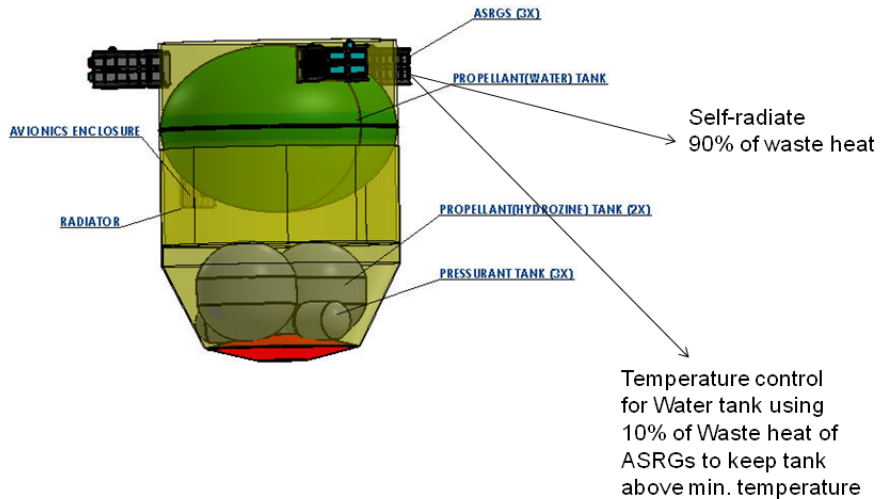


Figure 1.—Engineering ASRG longitudinal section view.



Propulsion Module

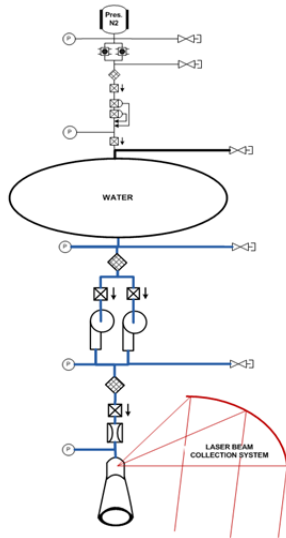
Mission Design Laboratory



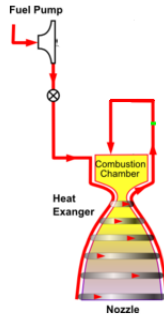


Beamed Energy Propulsion System

Mission Design Laboratory



- 10% of waste heat of ASRGs
- Used to control water

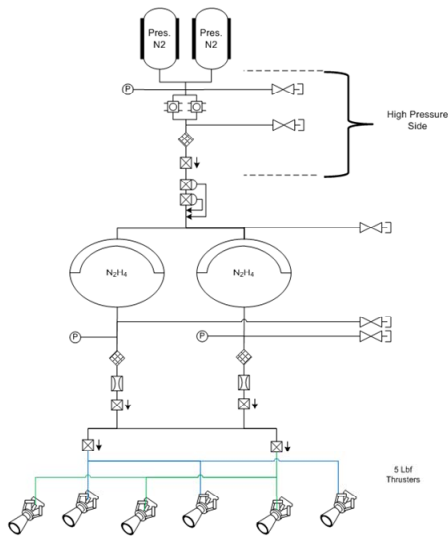


Regenerative cooling of chamber and nozzle by routing water through heat exchangers



Chemical Propulsion

Mission Design Laboratory



- heater control system
- MLI fuel tanks internal
- MLI module (external)
- MLI thrusters
- lines controlled and MLI
- Estimated heater power
 - 20 watts per tank (2)
 - 5 Watts per thrusters (6)
 - 20 Watts lines
 - Total 90 Watts



Mass Budget for Thermal

Mission Design Laboratory

Payload/Propellant Stage	
Active Thermal Control	3.34
Passive Thermal Control	36.76
Payload Laser Shield	26.64
	66.74
Thermal Control (Non-Propellant)	
Active thermal Control	2.65
Passive thermal control	19.61
Mirror System	93.66
Additional pocketed back side of Primary reflector	50.00*
Total	232.66

* Modification to DRM-2 baseline design



Risks (of Compass Report)

Mission Design Laboratory

- The main risk with the thermal system components pertains to the laser reflectors and shielding.
- Micro meteor or other debris can pose a mission risk if they impact the mirror surfaces. Any damage to the mirrored surface if these components can cause excessive local heating due to intensity of the laser beam.
- Laser light scattered off of the reflector shield can potentially be reflected back to earth. To reduce this risk a diffuse reflecting surface would be needed.

3.2.6 Deep Space Consultant Report—Design Reference Mission 3

Several possible applications of beamed-energy propulsion (BEP) were explored for deep space missions. The primary goal of this portion of the study was to find an application of BEP that would either enable a mission not otherwise achievable or measurably enhance myriad possible missions.

Early work on the direct propulsion of gossamer bodies such as the Forward-Landis StarWisp microwave-propelled interstellar craft and the success of the Japanese Interplanetary Kite-craft Accelerated by Radiation Of the Sun (IKAROS) solar sail mission to Venus led to the consideration of laser-powered sails to propel payloads to the outer planets.

The concept finally adopted for Design Reference Mission 3 (DRM 3) was to show how BEP as used in DRM 2 for an orbit-raising tug could improve the performance of a planetary or deep space mission. The study was performed in collaboration with the Mission Design Laboratory at the NASA Goddard Space Flight Center. The approach was to use the results of NASA Glenn Research Center's Compass team design for the orbit-raising tug with the minimal changes necessary to adapt the design to provide acceleration for the one-way trip to Jupiter; the object being to investigate performance enhancements possible with BEP. The Galileo Mission to Jupiter (1989 to 2003) was chosen for the comparison.

Galileo was launched from STS-34 Atlantis in October 1989 on a trajectory to Jupiter that included three planetary gravity well boosts (Venus-Earth-Earth) and took just over 6 years to reach its target. It was thought that BEP might provide for a direct Earth-to-Jupiter transit instead of the time-consuming triple-gravity-well boost trajectory necessitated by the use of a traditional chemical rocket upper stage as employed by the Galileo Mission.

The Galileo payload requirements (size, mass, electric power, and thermal management) were taken to be those of the payload for the comparison mission. The mission vehicle will be a compound of two modules, a modified Galileo payload and the propulsion module derived from the orbit-raising tug of DRM 2. The simulated Galileo payload and the propulsion module will be launched on separate Falcon 9 class launch vehicles and joined in an on-orbit docking maneuver as in DRM 2. The combined payload/booster will be put into a 3000-km by geosynchronous Earth orbit (GEO) and finally boosted into a direct Jupiter Transfer Orbit with an approximately 100-min BEP burn as shown in Figure 3.152.

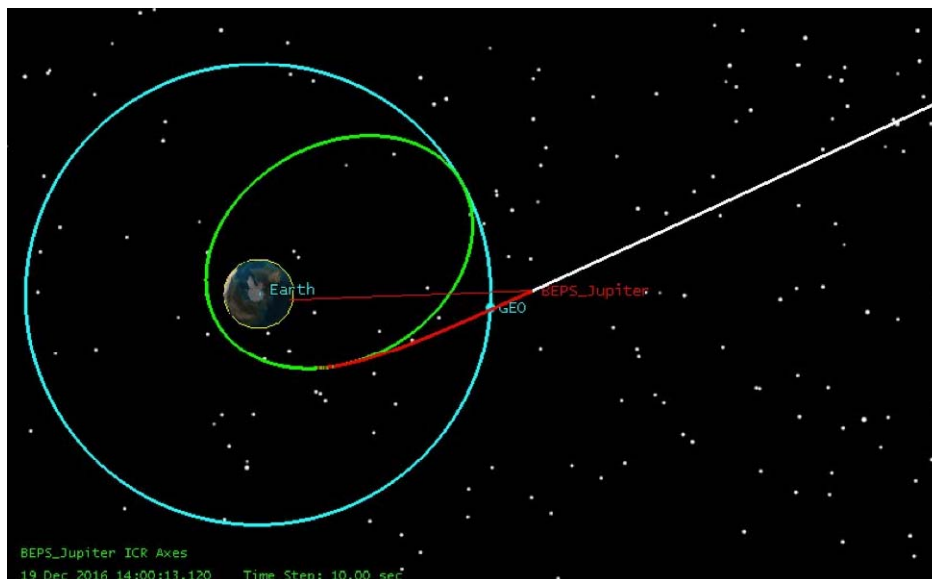


Figure 3.152.—Graphic representation of BEPS DRM 3 transfer trajectory from Earth orbit to Jupiter Direct Transfer Orbit showing path of BEP acceleration.

With BEP, it will be possible to gain enough velocity to arrive at Jupiter via a direct transfer orbit in about 2.5 years instead of the more than 6 years required for the original Galileo mission. An additional

benefit of the BEP-enhanced mission is that the launch opportunities for flights using similar direct transfer orbits will occur approximately every 400 days.

3.2.6.1 Description of Vehicle

The vehicle design for DRM 3 was adapted directly from the orbit-raising tug designed by Glenn's COMPASS design team for DRM 2. Like DRM 2, the payload and propulsion vehicles are launched separately and joined on orbit. However, whereas the orbit-raising tug was designed to be reusable, to deliver self-contained payloads to geostationary orbit, the propulsion vehicle in DRM 3 is designed to be an expendable booster. For the orbit-raising tug to be reusable under the DRM 2 concept of operations (CONOPS), the propellant would have to be replaced for each mission and be manifested as part of the satellite payload launch. In the DRM-3 configuration, the propulsion module includes the water propellant for the laser plasma engine for near-Earth orbit-raising and Jupiter Transfer Trajectory Insertion burns. The propulsion module is by far the heavier payload for the two Falcon-9-class launches used in DRM 3.

The Galileo payload analog for the study was updated from the original Galileo mission by replacing the original Radioisotope Thermoelectric Generators with Advanced Stirling Radioisotope Generators (ASRGs). Otherwise, all power, mass, and size specifications from the original Galileo vehicle were used to define the payload. Three of the four ASRGs needed to power the Galileo-like science payload will be launched with the propulsion module. Including these ASRGs with the propulsion module will eliminate the need for the solar panel used for power on the DRM 2 orbit-raising tug and will have the advantage of additional mass fraction being available on the payload launch vehicle, should it be needed.

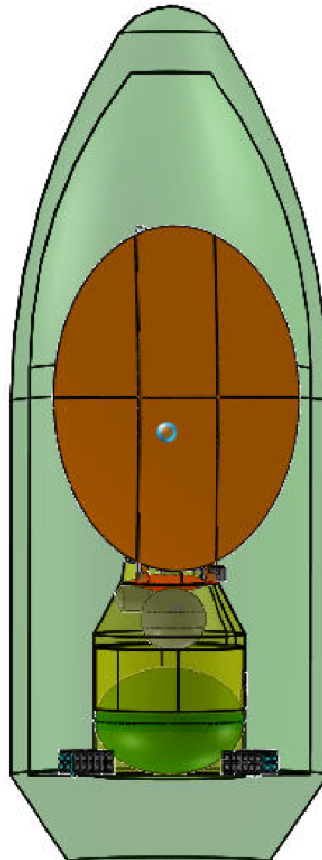


Figure 3.153.—Drawing of stowed DRM 3 propulsion module in Falcon 9 fairing.

The propulsion module will easily fit within the 5.2-m Falcon 9 fairing (See Figure 3.153). The stowed module will have an overall length of about 8 m.

The major components of the propulsion module follow: (1) the BEP system, consisting of the beam collecting and focusing optics, the thrust chamber and nozzle, and propellant storage and delivery; (2) the electrical energy system consisting of the ASRGs, a battery, and power management and distribution; (3) the attitude and control system consisting of reaction wheels for fine pointing, an autonomous docking system, and monopropellant thrusters with fuel for maneuvering; (4) the thermal management system; and (5) the communications system.

The optical components for the BEP system are essentially the same as for the orbit-raising tug for DRM 2 and will consist of a highly reflective, 97%-efficient 4- by 6-m elliptical primary collecting mirror that is mounted on an arm and gimbal that will enable it to track the laser beam and focus it onto a 98%-efficient, 0.5-m-diameter secondary turning mirror that will direct the beam through a 99%-efficient, 10-cm sapphire window into the thrust chamber. The reflectivity of the mirrors and the transmissivity of the sapphire window to the micron laser beam were taken to be 0.9999.

The laser engine will be a 30-cm spherical chamber operating at 50 psi with regenerative cooling of the chamber wall by the propellant. The chamber wall will be 97% efficient with 0.9999 reflectivity. The design efficiency of the chamber will be 80%, with 20% radiation losses out of the window and nozzle. The plasma absorption efficiency will be 75% (with losses in chemical reactions, ionization, etc.), resulting in an overall laser propulsion efficiency of greater than 50%. The nozzle will be regeneratively cooled with an area ratio of 50.

Propellant tanks will be provided on the propulsion module for the laser engine water propellant, the hydrazine monopropellant for the maneuvering thrusters and for pressurization gas. The payload module will carry its own hydrazine and pressurization tanks for maneuvering and for the Jupiter orbit insertion engine.

Electric power for the propulsion module will be provided by three ASRG units and a rechargeable lithium-ion (Li-Ion) battery that will be launched with the propulsion module. A fourth ASRG will be launched with the Galileo-like payload and added when the payload and propulsion modules are docked. The ASRGs (with beginning-of-life power of 143 W each) will be used for primary power for all functions except propulsion, when the 100-Ah Li-Ion battery will provide supplemental power for the propellant pumps during laser engine operation. For a typical 10-min orbit-raising propulsion firing, the battery depth of discharge will be 8.3%; and for the Jupiter Transfer Trajectory Insertion firing of 100 min, the depth of discharge will be 83%. The power system will be a 28-V-battery-dominated bus, with separate 28-V buses on the payload and propulsion modules. The ASRGs will be retained by the payload during separation of the payload from the expended booster and be used for power during the remainder of the mission.

The attitude control system will include autonomous rendezvous and docking capability. Reaction wheels will be used for attitude control and fine pointing of both the propulsion and payload modules. Hydrazine monopropellant systems will be provided on the propulsion and payload modules to provide maneuvering thrust and thrust to unload the reaction wheels. The hydrazine system on the payload also provides the propellant for decelerating the payload for Jupiter orbit insertion.

The propulsion module thermal management system has both passive and active elements. Cooling of the water propellant pump and the walls and window of the laser engine chamber and the nozzle will be accomplished by pumping the water propellant through tubes attached to the outer wall of the chamber and nozzle prior to injecting the water into the laser engine chamber. Thermal energy from the cool side of the ASRG will be used to maintain fluid temperatures in the propellant tanks. Electronic and battery temperature will be maintained through passive cooling. The approximately 5 kW of energy absorbed by each of the laser mirrors will be radiated from the backside of the mirror.

The communications system will be S-Band microwave, with direct communication to Earth through the Near Earth Network, with the Tracking and Data Relay Satellite System (TDRSS) available for backup.

The major physical changes between the DRM 2 orbit-raising tug and the DRM 3 booster are shown in Figure 3.154 (the orbit-raising tug) and Figure 3.155 (the booster). The most obvious difference is that

the solar panel has been removed and replaced with ASRGs to provide power, initially for the propulsion module, then for the combined payload and propulsion module, and finally, after separation, for the science payload on its path to Jupiter and its mission in the plane's environs. In addition, the 100-min Jupiter Transfer Trajectory Insertion burn increases the stored-energy requirement for the propulsion module and a larger capacity (100-Ah) battery is substituted for the DRM 2 design. A second difference is that the propellant for orbit raising and the Jupiter transit acceleration will be launched as part of the propulsion module rather than with the payload, as is the case with the reusable orbit-raising tug. The third major difference is the change of the separation point when the propulsion module and payload are separated at the conclusion of propulsion activity (achieving geostationary orbit for DRM 2 and Jupiter Transfer Orbit for DRM 3). For the DRM 3 Galileo analog mission, the separation ring will be added such that the propellant tanks are jettisoned with the propulsion unit and the ASRGs continue on to Jupiter as part of the Galileo spacecraft bus for the science mission.

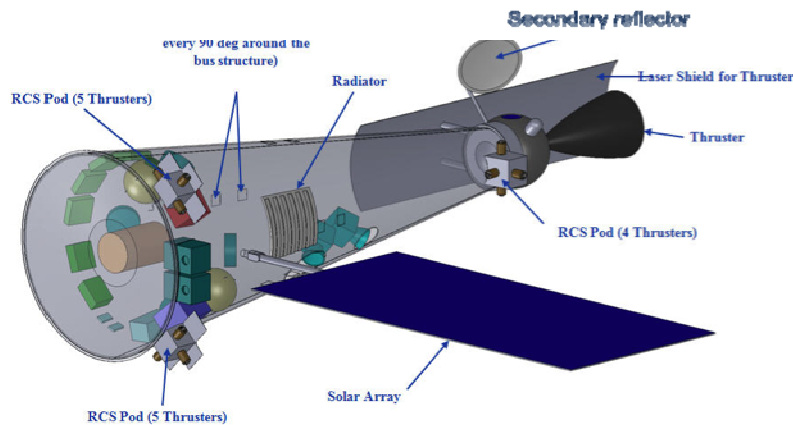


Figure 3.154.—Drawing of the DRM 2 orbit raising-tug showing the major vehicle systems. The primary reflector is not shown for clarity.

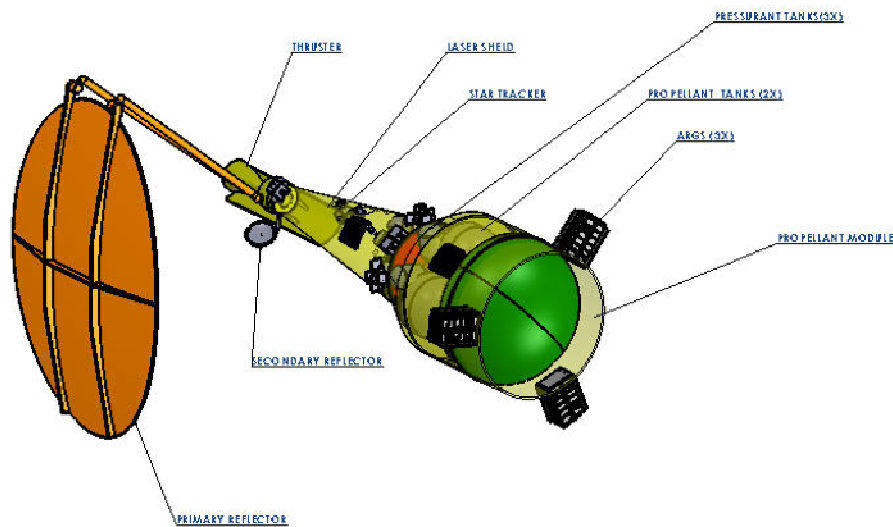


Figure 3.155.—Drawing of the DRM 3 expendable propulsion booster showing the major vehicle systems.

A minor difference between the DRM 2 orbit-raising tug and the DRM 3 expendable propulsion module is that the chemical monopropellant thruster pods will be replaced with six single-nozzle, articulated thrusters mounted on Canfield joints.

One feature that was added during the DRM 3 study and that should be applied to the DRM 2 orbit-raising tug is an enhanced method for the guidance and control of the ground-to-spacecraft laser beam link. Retroreflectors will be strategically positioned on the face of the primary collecting mirror, and photovoltaic sensors will be placed around the sapphire window into the laser engine chamber (see Figure 3.156). More complete descriptions of the laser system design and operation are given in the next two sections.

Because the payload and propulsion module will be launched separately and joined on orbit, there are necessary system redundancies, among which are attitude control, communications, and power management for the electric systems. A topic for future investigation would be whether or not installing a water propellant tank on the mission payload vehicle and moving a portion of the water propellant to the mission payload launch would result in a sufficient mass fraction margin gain for the propulsion module launch or enough increased mission capability to offset any added spacecraft design complexity. In this scheme, the propellant on the propulsion module would be used for orbit raising from LEO to the Jupiter Departure Orbit, and the propellant on the Galileo mission spacecraft used for the 100-min Jupiter Transfer Trajectory Insertion burn.

3.2.6.2 Description of Beaming Station

The laser-beaming stations are the same as defined and described for the orbit-raising tug in DRM 2. An 80-MW laser will be required to provide approximately 50 MW at the spacecraft. Two laser director systems will be used for power transmission to the spacecraft, depending on the spacecraft altitude. For orbit raising from the initial 800-km rendezvous circular orbit achieved through the Falcon 9 launch to the 3000-km circular intermediate orbit and the 3000-km by GEO Jupiter Departure Orbit, perigee burns (and 3000-km circularization apogee burns) will be accomplished with a small-aperture laser beam director that is 0.75 m in diameter. This laser aperture located on the Earth will provide a laser spot size of slightly less than 3 m in diameter at 800 km and about 3.2 m in diameter at 3000 km.

The 100-min Jupiter Transfer Trajectory Insertion burn from the Jupiter Departure Orbit to the Jupiter Direct Transfer Orbit (see Figure 3.156) will require the 30-m-diameter laser beam director to keep the beam spot within the area of the 4- by 6-m elliptical spacecraft primary collecting mirror.

Operation of the laser propulsion system will require a sophisticated interactive laser guidance and control system to maintain the ground-to-spacecraft link. The system will have to be able to acquire and maintain the high-power laser beam for spacecraft propulsion over a large flight path angle and reflector range of motion, with widely varying tracking rate requirements and varying laser time of flight lag, with a high degree of pointing accuracy. In addition it will have to account for anomaly detection and response.

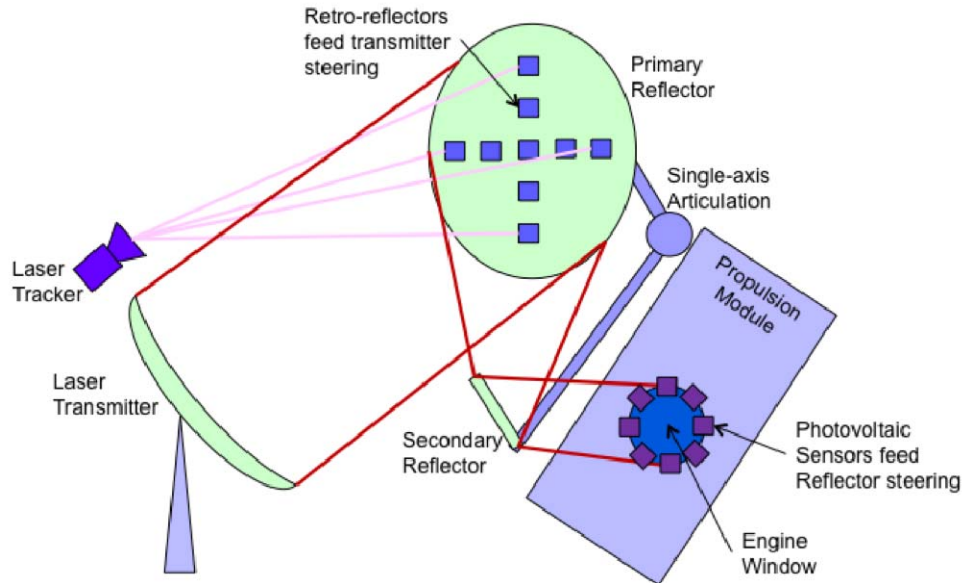


Figure 3.156.—Schematic of laser tracking and guidance system.

The components of the system as shown in Figure 3.156 include a laser tracker on the ground station, retroreflectors located on the spacecraft primary collecting mirror, and photovoltaic sensors around the sapphire window of the laser plasma engine. The ground-based portion of the system includes the 30-m-aperture transmitter (which will be able to be steered in azimuth and elevation and will be located on Mauna Kea in Hawaii to be above as much atmosphere and cloud cover as possible), a low-power laser guidance beam, the main propulsion beam, and a laser-sensitive beam-tracking system. Components on the satellite, which will collect and focus the beam into the laser plasma engine, include a primary collector and secondary reflector to direct the laser beam into the laser plasma chamber. The primary collecting reflector will have a 4-m aperture with a retroreflector pattern on the surface to provide a return signal to the laser-tracking sensor mounted on the ground transmitter. This return signal will affirm acquisition of the laser guide beam by the spacecraft. A secondary sensor set will consist of germanium photovoltaic cells arrayed around the rim of the plasma chamber window to provide fine control for reflector steering. The cells will be sensitive enough to detect the low-power guidance beam and will be sufficiently robust to withstand the full-power propulsion beam.

Laser link acquisition will be accomplished with the power beam off. The Global Positioning System will be used to provide position knowledge within 100 m. The guidance beam will be defocused to cover a large region. When the retroreflectors are detected, the guidance beam will be progressively focused until the beam is captured on the primary collecting reflector. Spacecraft roll attitude and reflector steering will be adjusted until the guidance beam is centered on the plasma engine chamber window, as determined by the photovoltaic sensor ring surrounding the window. When the guidance beam is centered on the engine window, the power beam may be switched on. The ground transmitter tracking and steering system will use the retroreflector return signal to keep the power beam centered on the primary collecting reflector and the spacecraft will use the photovoltaic sensor ring information for control of the spacecraft attitude and for reflector steering.

Any anomaly in the operation of the high-power laser will have to be detected and corrected instantaneously to prevent potential thermal damage to the spacecraft and sensitive instruments or optical damage to especially sensitive components, such as star trackers. Because laser steering and especially laser cutoff could occur more rapidly than reflector steering and spacecraft attitude control, fail-safe will be with the ground laser. If the power beam loses lock on the primary reflector as detected by loss of lock by the ground laser tracker, the ground station will command shutdown of the power beam and then

initiate reacquisition of the satellite with the defocused guidance beam. If the power beam loses lock on the engine chamber window as detected by the photovoltaic cells around the window, an alert will be sent by microwave communication to the ground, after which the ground station will command shutdown of the power beam and then initiate reacquisition of the satellite with the defocused guidance beam.

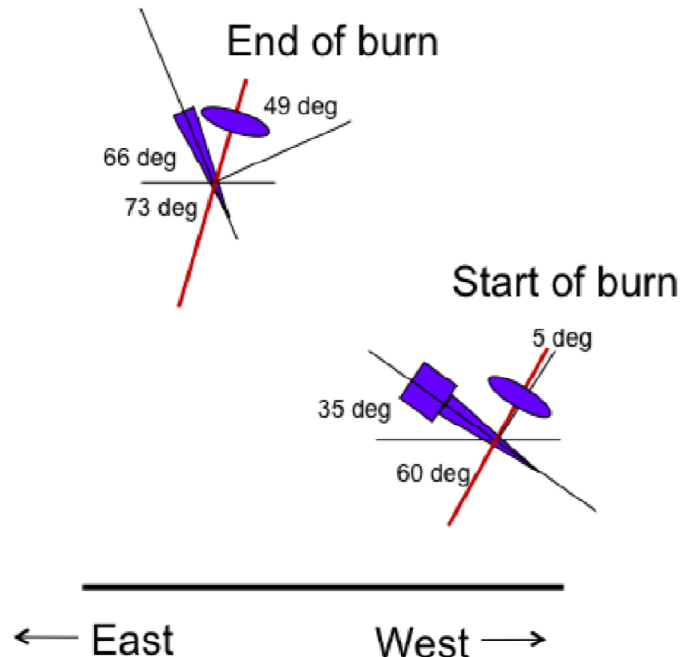


Figure 3.157.—Drawing of critical laser elevation, flight path angle and reflector angle at beginning and end of Jupiter Transfer Trajectory Insertion burn.

The elevation of the laser beam above the horizon is shown in Figure 3.157 along with the flight angle path and relative reflector angle for the start and finish of the 100-min Jupiter Transfer Trajectory Insertion burn, showing the reflector mirror angle travel to be well within the design swing of 60° from normal.

For the Jupiter Transfer Trajectory Insertion burn, the laser transmitter must be capable of smoothly tracking the spacecraft at a rate that varies from essentially 0°/min to 1.7°/min. In addition, at the end of the Jupiter Transition Trajectory Insertion burn, the range to the spacecraft will be 44,200 km, the laser tracker will have to resolve an angle of 4.6 milliarcsec (the angle subtended by 1 m) to see the retroreflector pattern, and the transmitter will have to steer to an equal accuracy to keep the beam on the reflector. To compensate for the round-trip time of flight of light, the beam will have to “lead” the spacecraft by varying amounts along the acceleration trajectory. At the start of the Jupiter Transfer Trajectory Insertion burn, with a range of 11,900 km, the round-trip time of flight for light will be 0.08 s. The laser tracking rate will be 0.025°/s, and the beam will have to “lead” the spacecraft’s observed position by 7 arcsec. At the end of the Jupiter Transfer Trajectory Insertion burn, the range will be 44,200 km and the round-trip time of flight for light will be 0.3 s. The laser tracking rate will be 0.005°/s, and the beam will have to “lead” the spacecraft’s observed position by 5 arcsec.

3.2.6.3 CONOPS—Frequency of Launch and Repeat Time

Differences between the two missions that lead to design changes in the propulsion module design and spacecraft systems allocations (e.g., photovoltaic panel replaced by ASRGs, greater battery capacity,

and water propellant launched as part of the propulsion module) have been dealt with in a previous section. The notional operational timeline (from launch) is shown as Figure 3.158.

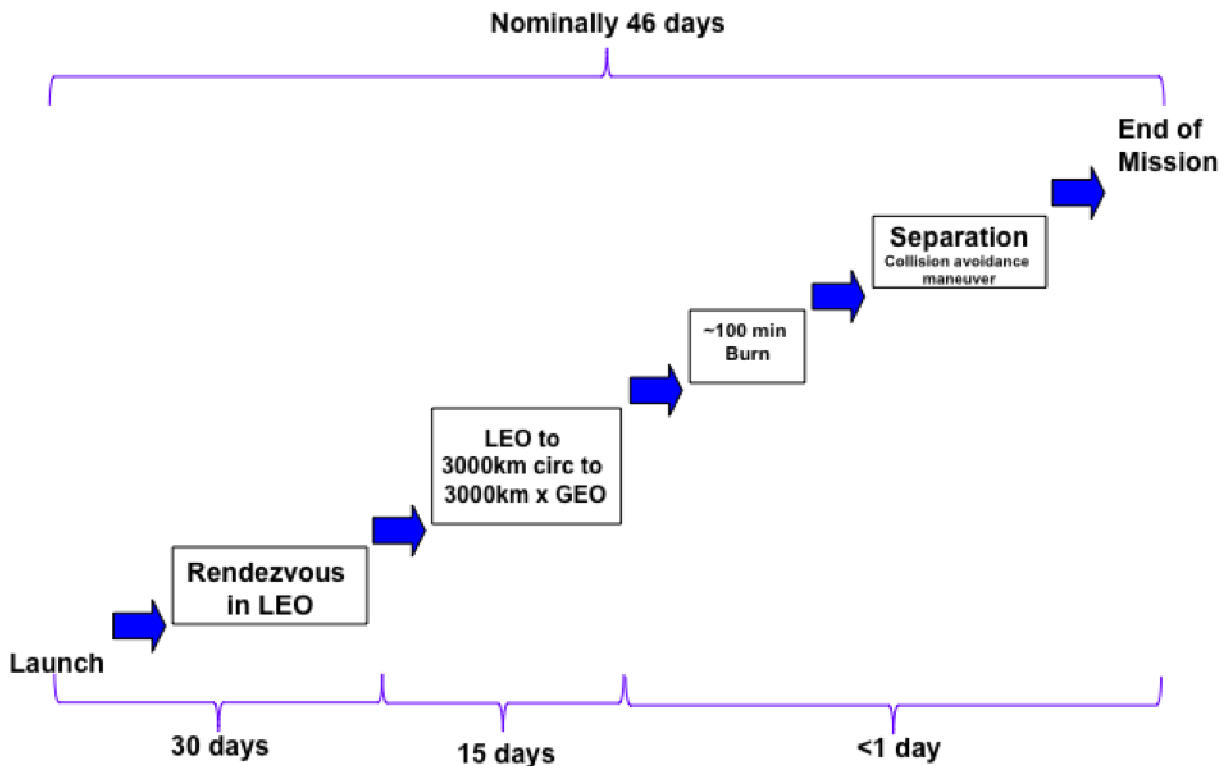


Figure 3.158.—Sequence of operations for DRM 3: BEP-enhanced Galileo mission.

The initial launch and orbit-raising sequence closely mirror that of DRM 2 and will employ two Falcon 9 launch vehicles (one for the propulsion module and one for the Galileo payload). The propulsion module and Galileo mission spacecraft will be launched separately from Kwajalein Atoll into an 800-km, 9°-inclined circular low Earth orbit (LEO).

The propulsion module and Galileo mission spacecraft will be joined on orbit using Next Generation Advanced Video Guidance Sensors and automated rendezvous and docking hardware, firmware, and software. The time allocated for the launch, docking, and spacecraft diagnostics is 1 month.

Orbit-raising protocols from DRM 2 will be followed to first transfer the combined spacecraft from an 800-km, 9°-inclined circular orbit to a 3000-km, 9°-inclined circular orbit and then to a 3000- by 35,000-km, 9°-inclined Jupiter Departure Orbit. The time allocated for the orbit change maneuvers is 15 days.

The final phase of near-Earth operation will be the 100-min laser-beam-powered Jupiter Transfer Trajectory Insertion acceleration from Jupiter Departure Orbit to Jupiter Transfer Orbit, followed by separation of the propulsion module from the Galileo mission craft with a collision avoidance maneuver.

Here, the BEP phase of the mission will end with the propulsion module flying away and the Galileo craft continuing to Jupiter, where it will use onboard hydrazine monopropellant to perform a Jupiter Orbit Insertion burn of 70 min and enter the highly elliptical Galileo Jupiter Orbit of 200,000- by 12,000,000-km with a 98-day period.

Because BEP provides the possibility of a direct Jupiter transfer trajectory, flight opportunities will not be limited by a requirement that inner solar system planets be positioned for gravity-well-flyby acceleration assists. Thus, flight opportunities will recur almost yearly with the 399-day Earth-Jupiter synodic period; however, flight energy requirements will vary with each opportunity.

3.2.6.4 Costs—Comments

The design of the propulsion module and the CONOPS for DRM 3 were adapted with minimal changes from DRM 2, and cost estimates for the BEP-enhanced Galileo mission can be derived from DRM 2 estimates.

BEP can open new opportunities for deep space exploration and science missions. The cost and time to develop the 80-MW ground station will be the most significant obstacles to the realization of the potential of beamed-power propulsion to this deep space application.

3.2.6.5 Feasibility Assessment

The following is a list of issues which need to be addressed

1. What are the attenuation effects of high flux levels (MW/m^2) at the frequencies of interest on the atmosphere?
2. What would be the expected availability and transmittance of the BEP ground terminal at a given frequency, given aerosol and precipitation conditions at a proposed ground site?
3. How large of a keep-away zone must be maintained around and beyond an ascending craft to accommodate reflection, refraction and scattering components of the beam exceeding substantial irradiances, and what level is to be considered substantial? Considerations should be given to maximum permissible exposure for humans, and damage thresholds for ground, airborne and space-based assets within proximity of the BEP activity.
4. For a ground based terminal operations, how much grid power over what duration is required? To meet these requirements, what would the generation, storage and conversion system look like?
5. How would a micro/mm-wave BEP system work within the spectrum constructs of the NTIA/FCC?
6. Does it make sense to collocate beamed energy propulsion and power technologies on the craft, for each phase of a proposed mission?
7. Would there be a benefit to developing a hybrid aperture to handle multiple BEP frequencies depending upon range to target, atmospheric conditions, etc.?
8. Can retro-directive control be utilized to aid in the beam pointing, acquisition and tracking of the craft?
9. What is the most practical way of performing high power beam combination using COTS technology for the frequencies of interest? What are the potential near term accomplishments that could influence this capability?
10. What are the cost/benefit tradeoffs in considering multiple BEP transmission locations, both at the ground range and at an intermediate relay point in space?
11. Could deployable array technologies be implemented to decrease the weight of a BEP aperture, and increase the allowable size that can be launched?
12. What are some near term demonstrations that may be accomplished to establish a maturity level for critical technologies, and support the overall feasibility of the BEP concept?

3.2.6.6 Roadmaps and Technology Readiness Levels

See DRM 2 LEO–GEO, Section 3.2.3.5.1.

3.2.6.7 Ground and Flight Demonstrations

See DRM 2 LEO–GEO, Section 3.2.3.5.2.

3.2.6.8 Issues and Resolutions

The baseline design for thermal management for the high-power laser system mirrors and sapphire lens is passive, with the back surface of each mirror providing its own radiative cooling and the sapphire lens being cooled by contact with the plasma chamber. For the short-duration beamed-energy thrusts

during orbit raising, the design should be adequate. However, for the 100-min Transfer Transition Insertion burn, the high operating temperature (918 °C) calculated for the secondary (0.5-m diameter) mirror could present a material problem. Pocketing the radiator surface to increase area would reduce the operating temperature. Alternatively, the water loop could be extended to the mirror or a heat pipe could be used as a bridge from the secondary mirror to the water loop. If additional cooling was required for the center of the sapphire lens, the lens could be segmented with thin cooling channels.

The development of high-power, efficient, continuous-wave (CW) lasers capable of satisfying the requirements for DRM 2 or DRM 3 is beyond the scope of NASA funding and will undoubtedly require many years. A nearer term alternative to the 80-MW ground-based laser-power-beaming station for DRM 2 and DRM 3 also was examined. The two potential solutions are an approximately 1.5-MW laser-power-beaming station on the ground capable of delivering 1 MW to a redirecting mirror in geostationary orbit or a 1-MW laser-power-beaming station in space in geostationary orbit.

The laser plasma thruster was assumed to be capable of linear operation over a range from 500 kW to greater than 50 MW. Thus, with a 1-MW beam originating at geostationary orbit (either from an orbiting power-beaming station or from a reflector in geostationary orbit fed from the ground), approximately 100 N of thrust could be generated from the engine. This would be adequate for a spiral orbit raising from LEO to geostationary orbit for DRM 2, although it will require more propellant than would be needed with the higher power 80-MW system.

For the critical Jupiter Transition Trajectory Insertion burn, calculations show that it would require more than 1.5 million km to achieve the velocity change of 6.7 km/s required for a direct Jupiter Transfer Orbit. At this range, if we assume a 30-m beaming aperture or reflector and a coherent beam, the laser beam spot will be greater than 100 m.

4.0 Concluding Remarks

This study took an in-depth look at the feasibility of beamed-energy propulsion (BEP) and concluded that although the technology is definitively game-changing and technically achievable given the appropriate development resources, the infrastructure costs would be extremely high, making it comparably unattractive at this time (Figure 4.1).

	Technically Feasible	Game Changing	Economically Viable
Feasibility Ranking	<ul style="list-style-type: none"> • Closed design solution – trajectory, beam power, thrust/weight, mass etc. • For low TRL - defined basis for technology and technology improvements • Allowable margins – mass, engine performance, thermal, structural 	<ul style="list-style-type: none"> • Reusability • Payload mass fraction • Improved mission capability – increase operations time, etc. • Reduced Transfer Time (2X) • “...Technology that is innovative, unique and promises to enable revolutionary improvements to the efficiency and effectiveness of our country’s space capability.” [OCT BAA] 	<ul style="list-style-type: none"> • Lower vehicle costs (\$/kg) • Lower launch facility operation costs – range safety, vehicle prep/handling • Infrastructure costs
YES Green – All			
YES/NO Yellow - >50%			
NO Red - <50%			
LEO to GEO	YES Low TRL’s	YES/NO, but might be combined with other applications	NO, high cost of beaming stations
Deep Space	YES Low TRL’s	YES, with investments	NO, high cost of beaming stations
Launch	YES Low TRL’s	YES, with investments	NO, high cost of beaming stations

Figure 4.1.—BEP evaluation summary. LEO to GEO, low Earth orbit to geosynchronous Earth orbit; TRL, Technology Readiness Level; OCT, Office of the Chief Technologist; BAA, Broad Agency Announcement.

Of course, it was hoped that beamed-energy technology would provide the “silver bullet” solution to low-cost access to space and enable less-expensive deep space missions, or that it would at least find a niche where the benefits would be great. The authors of this report would like to make it clear that, as with all studies, if the ground rules change, it follows that the conclusions will change. The approach used to determine costs was the method used by the NASA Glenn Research Center. This report recognized that vehicle costs for a commercial venture would be lower than for a government endeavor. A bottoms-up commercial cost approach could deliver a much lower cost not only for the facilities but also for the vehicles. A similar process to what is currently happening to the International Space Station (ISS) cargo/tourism launch vehicles could also be applied to the small payload area.

At the end of the study, it became apparent that the costs to create any new launch or space propulsion facility would range in the billions of dollars. Likewise, the costs to replace the NASA Kennedy Space Center would surely be in the same range. So it should not have come as a surprise to find high infrastructure costs for such a capability. Historically, any change to the current way business is done has involved a high initial investment. The enticement for the investment has been the potential of a valuable market. The definition of this possible market was outside of the scope of this study. But the findings indicate that the technology could be effectively used for the launch of payloads in the range of 1 to 10 kg, or “CubeSats” or “nanosats” as they are known. Investigations should be conducted on the market for small payloads.

During this study, two applications of BEP technology were revealed. They should be pursued since they could prove to be very beneficial to both DARPA and NASA. The path forward for BEP could start with a small, low-cost ground demonstration that would show the key components of the technology, achieving the next readiness level. However, it is the conclusion of the authors that sufficient equipment is currently available to enable an in-space experiment. The jump to this level would have a major impact on the spacecraft design community and would open up other possibilities.

Appendix A.—Acronyms and Definitions

ABL	Airborne Laser
ACS	attitude control system
AEOS	Advanced Electro-Optical System
AFB	Kirtland Air Force Base
AFRL	Air Force Research Laboratory
AIMD	additive increase/multiplicative decrease
ALRU	Amplifier Line Replaceable Unit
AO	adaptive optic
ASRG	Advanced Stirling Radioisotope Generators
BEPS	Beamed-Energy Propulsion Study
C	carbon
C&DH	command and data handling
CCD	charge-coupled device
CMOS	complementary metal-oxide-semiconductor
CO ₂	carbon dioxide
COMPASS	COllaborative Modeling for Parametric Assessment of Space Systems
CONOPS	concepts of operation
COTS	commercial off the shelf
CubeSat	miniature satellite that is usually a 10-cm cube
CVD	chemical vapor deposition
CW	continuous wave
DARPA	Defense Advanced Research Projects Agency
DC	direct-current
DDT&E	design, development, testing and engineering
DOD	Department of Defense
DPSSL	Diode-Pumped Solid-State Laser
DRM	Design Reference Mission
E–D	expansion-deflection
EEE	electrical, electronic, and electromechanical
EMI	electromagnetic interference
EPS	electrical power system
ESA	European Space Agency
ETO	Earth-to-orbit
FADIS	Fast Directional Switch
FOM	figures of merit
FPA	flight path angle
FPGA	field-programmable gate array
FSM	fast steering mirror
GBL	ground-based laser
GEO	geosynchronous orbit
GLOM	gross liftoff mass
GLOW	gross liftoff weight

GNC	guidance, navigation, and control
GPS	Global Positioning System
H&S	health and safety? DRM-1A
HiDVE	High Delta-V
H ₂ O ₂	hydrogen peroxide
He	helium
HX	heat exchanger
IFR	ideal final result
I/O	input/output
IMU	inertial measurement unit
IP	Internet Protocol
ISUS	Integrated Solar Upper Stage
JHPSSL	Joint High Power Solid-State Laser
KKV	Kinetic Kill Vehicle
LLNL	Lawrence Livermore National Laboratory
LED	light-emitting diodes
LEO	low Earth orbit
JPL	Jet Propulsion Laboratory
LLC	Laser lightcraft
LTD	Lightcraft Technology Demonstrator
LH ₂	liquid hydrogen
LiFePo	lithium-iron-polonium
LLNL	Lawrence Livermore National Laboratory
LN ₂	liquid nitrogen
LSD	laser-supported detonation
MDL	Mission Design Lab
MEL	Master Equipment List
MEMS	microelectromechanical systems
MLI	multilayer insulation
MOPA	Master Oscillator Power Amplifier
N ₂	nitrogen
NaS	sodium sulfide
NiCd	nickel cadmium
NiMH	nickel metal hydride
O&M	operation and maintenance
OCT	Office of the Chief Technologist
O/S	operating system
ORU	orbital replacement unit
OTIS	Optimal Trajectories by Impact Simulation
OTIS	Optimal Trajectories by Implicit Simulation
P&S	protocols and standards
PD	pulse detonation
PDE	pulsed detonation engine
PEL	power equipment list

PI&D	propellant injection and distribution
PLVTS	Pulsed Laser Vulnerability Test System
PMAD	power management and distribution
PMD	propellant management device
P-POD	Poly-Pico Satellite Orbital Deployer
PRF	pulse repetition frequency
PSI	Pressure Systems, Inc.
PV	photovoltaics
R&D	research and development
RCS	reaction control system
ROM	rough order of magnitude
ROSA	Roll-Out Solar Array
S/C	spacecraft
SABLE	Scaled Atmospheric Blooming Experiments
SA	solar array
SOR	Starfire Optical Range
SDIO	Strategic Defense Initiative Organization
SHARP	Stationary High Altitude Relay Platform
SiC	silicon carbide
SLOC	source lines of code
SOA	state of the art
SSDP	solid-state, diode-pumped
SSME	Space Shuttle Main Engine
SSTO	single stage to orbit
SPO	systems program office
TBD	to be determined
TBR	to be resolved
TDRSS	Tracking and Data Relay Satellite System
TEA laser	transversely excited atmospheric-pressure laser
TMT	30-Meter Telescope
TPS	thermal protection system
TRL	Technology Readiness Level
TVC	thrust vector control
UAV	unmanned aerial vehicles
UV	ultraviolet
VAB	Vehicle Assembly-processing Building
Δv	velocity
VHDL	very-high-speed integrated circuits (VHSIC) hardware description language
VHF	very high frequency
VMJ	vertical multi-junction
WSMR	White Sands Missile Range

Appendix B.—Consultant Resumes

Jonathan T. Black

Assistant Professor of Aeronautics and Astronautics
Air Force Institute of Technology, AFIT/ENY
2950 Hobson Way, Bldg. 640
Wright-Patterson AFB, Ohio 45433
jonathan.black@afit.edu 937-255-3636, Ext. 4578 Fax: 937-656-7053

Education

Ph.D. in Mechanical Engineering, University of Kentucky, December 2006
Support: University of Kentucky Dissertation Year Fellowship, NASA Graduate Student Researchers Program, Department of Mechanical Engineering

M.S. in Mechanical and Aerospace Engineering, George Washington University, August 2003
Support: Joint Institute for Advancement of Flight Sciences Graduate Research Scholar Assistantship

B.S. in Industrial Engineering, with Honors, International Minor in French Studies, University of Illinois at Urbana-Champaign, May 2001

Professional History

Air Force Institute of Technology, Dayton, Ohio

Jan. 2007 – present, Assistant Professor, Department of Aeronautics and Astronautics

University of Kentucky, Lexington, Kentucky

Jul. – Dec. 2006, University of Kentucky Dissertation Year Fellow, Dynamic Structures and Controls Laboratory, Department of Mechanical Engineering

Jul. 2004 – Jun. 2006, NASA Graduate Student Researchers Program Fellow, Dynamic Structures and Controls Laboratory, Department of Mechanical Engineering

Aug. 2003 – Jun. 2004, Graduate Research Assistant, Dynamic Structures and Controls Laboratory, Department of Mechanical Engineering

Air Force Research Laboratory, Albuquerque, New Mexico

Summer 2004 and 2005, Space Scholars Program, Space Vehicles Directorate, Kirtland Air Force Base

NASA Langley Research Center, Hampton, Virginia

Aug. 2001 – Jul. 2003, Graduate Research Scholar Assistant, Joint Institute for Advancement of Flight Sciences, Structural Dynamics Branch

Licenses, Registrations, and/or Certifications

- Member of the American Institute of Aeronautics and Astronautics (AIAA)
- Member of the Society of Experimental Mechanics (SEM)
- Member of the American Society of Mechanical Engineers (ASME)
- Engineer in training, State of Kentucky, no. 12668

Awards and Honors

- AFOSR Young Investigator Research Program Grant, 2007, 1 of 29 awardees nationally of 215 applicants, first ever AFIT recipient
- AIAA Associate Fellow, 2010
- Southwestern Ohio Council for Higher Education, Faculty Excellence in Teaching Award, 2010
- National Society of Black Engineers Aerospace Systems Conference Best Paper Award (co-author), 2010

- AIAA National Career Enhancement Award, First Place, Very Large Category, 2008
 - University of Kentucky Dissertation Year Fellowship, 2006/2007, 1 of 12 awardees university-wide
 - AIAA Foundation Willy Z. Sadeh Award in Space Sciences and Space Engineering, 2004/2005
 - Department of the Air Force, Special Act or Service Citation, 08/2004 and 08/2005
 - NASA Graduate Student Researchers Program Fellowship, 2004/2005, 2005/2006
 - Kentucky Graduate Scholarship, 2003-2006
 - AIAA Region I Student Paper Competition, Graduate Division, 2nd Place, 2003
- (1) Swenson, E.D., Wiesel, W., Black, J.T., Cobb, R.G., "Space Vehicle Research," Air Force Research Laboratory Space Vehicles Directorate, AFRL/RV – AFIT/ENY Memorandum of Agreement, FY12-FY17 \$1,250,000 (25%), awarded but not yet received.
 - (2) Black, J.T., "Beamed Energy Propulsion Study: LEO – GEO Tug," DARPA/NASA Joint Phase I Study (\$2,000,000 total study), FY11, \$70,000 (100%)
 - (3) Black, J.T., "Characterizing MAV Wings In Flight," AFOSR AFRL/AFIT MOA Small Grant Program, FY11 – FY13 \$135,000 (100%), awarded and first year funding received.
 - (4) Black, J.T., "Risk and Reward Metric for Space Systems," Air Force Research Laboratory Space Vehicles Directorate, FY11-FY12 \$130,000 (100%), awarded and first year funding received.
 - (5) Black, J.T., "OhioSAT CubeSat Senior Design Project Workshop," Ohio Space Grant Consortium, NASA Education Program, FY11 \$55,000 (100%).
 - (6) Black, J.T., Cobb, R.G., Swenson, E.D., "Novel Multifunctional Imaging Chromotomographic Spectrometer Flight Experiment (CTEx)," AS&T Outreach Program, FY10 – FY12 \$200,000 (34%).
 - (7) Cobb, R.G., Black, J.T., Raquet, J., "Dynamic Two-Way Time Transfer Flight Experiment," AS&T Outreach Program, FY11 – FY12 \$110,000 (45%).
 - (8) Black, J.T., Swenson, E.D., "Space Hardware Qualification Course," AFIT Distance Learning Tuition Re-imbursement, FY11 \$45,000 (50%)
 - (9) Swenson, E.D., Lawrence, T., Black, J.T., "Dynamic Responsive Orbital Networking Experimental Satellite (DRONES) Engineering Model Research," Air Force Space Command Space and Missiles Center, FY11 \$15,000 (10%)
 - (10) Swenson, E.D., Lawrence, T., Black, J.T., "FalconSat-7 Engineering Model Research," US Air Force Academy, FY11 \$10,000 (10%)
 - (11) Cobb, R.G., Black, J.T., and Swenson, E.D., "Space Telescope Control System," Air University Base Procured Investment Equipment Grant, FY11 \$295,000 (33%)
 - (12) Black, J.T., "3D Video Camera Measurement System," AFIT End-of-Year Supplemental Funding, FY10 \$177,000 (100%)
 - (13) Black, J.T., "Hybrid Laser/Video 3D Non-Contact Motion Capture and Analysis," AFOSR Young Investigator Research Program, FY09 – FY11 \$360,000 (100%)
 - (14) Cobb, R.G., Black, J.T., Collins, P., "Colony I CubeSat," AS&T University Outreach, FY10 – FY11 \$250,000 (50%)
 - (15) Cobb, R.G., Black, J.T., Raquet, J., "Dynamic Two-Way Time Transfer Flight Experiment," SAF/FMB, FY10 – FY11 \$110,000 (45%)
 - (16) Reeder, M.F., Cobb, R.G., Black, J., "Design and Testing of Flapping-Wing Micro Air Vehicles," Air Force Research Laboratory Air Vehicles Directorate (AFRL/RB), FY09 – FY11 \$155,000 (33%)
 - (17) Black, J.T., "Experimental Fin Tips for Reusable Launch Vehicles (ExFiT)," Air Force Research Laboratory Air Vehicles Directorate (AFRL/RB), FY09 – FY10 \$31,600 (100%)
 - (18) Black, J.T., "Experimental Fin Tips for Reusable Launch Vehicles (ExFiT)," Department of Defense Space Test Program (STP), Space Experiments Review Board (SERB), FY10 \$10,000 (100%)

- (19) Simmons, R., Black, J.T., “Experimental Fin Tips for Reusable Launch Vehicles (ExFiT),” AFIT Faculty Research Council, FY10 \$25,000 (50%)
- (20) Hartsfield, C., Black, J.T., “CubeSat Education and Flight Program,” AFIT Faculty Research Council, FY10 \$30,000 (50%)
- (21) Black, J.T., “Dynamic Surface Mapping of Lightweight Aerospace Structures in Motion,” Ohio Space Grant Consortium, FY09 \$30,000 (100%)
- (22) Petersen, G., Black, J.T., “Semi-Autonomous Lead Vehicle for Convoy Operations,” Air Force Research Laboratory Center for Rapid Product Development, FY09 \$100,000 (15%)
- (23) Cobb, R.G., Swenson, E.D., Black, J.T., “Attitude Path Planning for Responsive Spacecraft,” Air Force Research Laboratory Space Vehicles Directorate (AFRL/RV), FY09 \$35,000 (25%)
- (24) Black, J.T., Cobb, R.G., “Space Imaging Power Laboratory,” Air University Base Procured Investment Equipment Grant, FY09 \$256,000 (100%)
- (25) Black, J.T., “Multifunctional Chromotomography Imager,” AFIT Faculty Research Council, FY09 \$30,000 (100%)
- (26) Swenson, E.D., Black, J.T., Cobb, R.G., “Experimental Validation of Spacecraft Integration and Test Requirements for ORS Satellites,” Operationally Responsive Space Office, FY09 \$18,000 (25%)
- (27) Black, J.T., “Dynamic In-Flight Test and Measurement System,” AFIT End-of-Year Supplemental Funding, FY08 \$189,000 (100%)
- (28) Black, J.T., Swenson, E.D., “Satellite Model Refinement Using High-Density Experimental Data,” AFIT Faculty Research Council, FY08 \$25,000 (100%)
- (29) Black, J.T., “3D Non-Contact Surface Motion Capture and Analysis Video System,” AFIT New Faculty Seed Funding Award, FY07 \$30,000 (100%)

Student Grants

- (1) Simmons, J., Dayton Area Graduate Studies Institute (DAGSI) Fellowship, FY08 – FY11 \$105,000
- (2) Black, J.T., Ohio Space Grant Consortium (OSGC) CRADA for Summer Intern, FY08 \$6,000, FY09 \$6,500 and FY10 \$7,000

Space Experiments

- (1) Black, J.T., Cobb, R.G., Swenson, E.D., Hartsfield, C., and M. Hawks, “Space-Based Chromotomography Experiment (CTEx),” DoD Space Experiments Review Board (SERB), collaborative flight experiment with AFIT Engineering Physics department, 2013 scheduled launch.
- (2) Black, J.T. and R.G. Cobb, “AFITSAT I – Carbon Nanotube Field Emission Array Experiment,” Colony I Cubesat, collaborative flight experiment with AFIT Electrical Engineering department, 2012 scheduled launch.
- (3) Cobb, R.G. and J.T. Black, “AFITSAT II – Precision Timing and Ranging Experiment,” Colony II Cubesat, collaborative flight experiment with AFIT Electrical Engineering department, 2013 scheduled launch.
- (4) Black, J.T., “Experimental Fin Tips for Reusable Launch Vehicles (ExFiT),” Department of Defense Space Test Program (STP), Space Experiments Review Board (SERB), May 2010 flight.
- (5) Cobb, R.G., Black, J.T., and E.D. Swenson, “Rigidizable Inflatable Get-Away-Special Experiment (RIGEX),” Department of Defense Space Test Program (STP), Space Experiments Review Board (SERB), STS-123, Space Shuttle *Endeavour*, Mar. 2008 flight.

Personnel Supported on Grants or Contracts

- (1) Stoval, A., ENV PhD Student, FY11 – FY12
- (2) Blandino, J., ENY Visiting Faculty, FY10
- (3) Allen, C., ENY Research Associate, AD-21, FY08 – FY11
- (4) Jennings, A., ENY Research Associate, AD-21, FY11
- (5) Kaczmarek, J., ENY Research Associate, GS-5, FY10 – FY11
- (6) Simmons, J., DAGSI PhD Student, FY08 – FY11

- (7) Magree, D., DAGSI / SOCHE MS Student, FY09 – FY10
- (8) Jennings, A., SOCHE PhD Student, FY08 – FY10
- (9) Stein, E., SOCHE Research Associate, FY11 – FY12
- (10) Lomonno, C., SOCHE Research Associate, FY11
- (11) Briggs, G., SOCHE Research Associate, FY11
- (12) Alerding, J., SOCHE Summer Intern, FY11
- (13) Benson, M., SOCHE Summer Intern, FY11
- (14) Buhrman, N., SOCHE Summer Intern, FY11
- (15) Pace, T., ENY Summer Intern, FY10
- (16) Trinh, A., ENY Summer Intern, FY10
- (17) Rippl, M., ENY Summer Intern, FY09 – FY11
- (18) Jameson, M., ENY Summer Intern, FY09
- (19) Rodgers, D., ENY Summer Intern, FY09
- (20) Pollock, S., ENY Summer Intern, FY09
- (21) Simpkins, J., ENY Summer Intern, FY08
- (22) Sollars, R., ENY Summer Intern, FY08

Publications

Key:

- * Student advised by J. Black
- # Students advised by others
- ^A AFIT non-faculty researchers
- ^F Other AFIT faculty
- ^E External collaborators

Archival Journal Articles

- (1) Magree, D.*^A, Black, J.T., Jennings, A.A, Briggs, G.*^A, and C. Allen^A, “Pan-Tilt-Zoom Hybrid Camera System for Dynamic Tracking and Measurement,” *AIAA Journal*, accepted for publication, Dec. 2010.
- (2) Swenson, E.D.^F, and J.T. Black, “Measuring and Modeling 3D Mode Shapes of FalconSAT-5 Structural Engineering Model,” *Journal of Experimental Mechanics*, Vol. 51, No. 6, Jul. 2011, pp.933-945, DOI: 10.1007/s11340-010-9421-8.
- (3) Black, J.T., Cobb, R.C. F, Swenson, E.D. F, and B.J. Cooper*, “Rigidizable Inflatable Get-Away-Special Experiment Space Flight Data Analysis, *Journal of Spacecraft and Rockets*, Vol. 48, No. 3, May – June 2011, pp. 447-487, DOI: 10.2514/1.50939.
- (4) Jennings, A.A, Black, J., Allen, C.A, Simpkins, J. A, Sollars, R. A, “Vibrometer Steering System for Dynamic In-flight Tracking and Measurement,” *Journal of Experimental Mechanics*, Vol. 51, No. 1, Jan. 2011, pp. 71-84, DOI: 10.1007/s11340-010-9337-3. (for P&T consideration)
- (5) Cobb, R.G. F, Black, J.T., and E.D. Swenson^F, “Design and Flight Qualification of the Rigidizable Inflatable Get-Away-Special Experiment,” *Journal of Spacecraft and Rockets*, Vol. 47, No. 4, Jul. – Aug. 2010, pp. 659-669, DOI: 10.2514/1.48636.
- (6) Black, J.T., Pitcher, N.A. #, Reeder, M.F. F, and R.C. Maple^F, “Videogrammetry Dynamics Measurements of a Lightweight Flexible Wing in a Wind Tunnel,” *Journal of Aircraft*, Vol. 47, No. 1, Jan. – Feb. 2010, pp. 172-180, DOI: 10.2514/1.44545. (for P&T consideration)
- (7) Black, J.T., Leifer, J.E, and S.W. Smith^E, “Global Static Testing and Model Validation of Stiffened Thin-Film Polyimide Panels,” *Journal of Spacecraft and Rockets*, Vol. 45, No. 6, Nov. – Dec. 2008, pp. 1319-1324, DOI: 10.2514/1.37131.
- (8) Black, J.T., Smith, S.W. E, Leifer, J. E, and L.J. Bradford^E, “Local Testing and Reduced Model Validation of Thermal-Formed Thin-Film Polyimide Panels,” *Mechanical Systems and Signal Processing*, Vol. 22, Iss. 6, Aug. 2008, pp. 1412–1426, DOI:10.1016/j.ymsp.2007.11.010.

- (9) Black, J.T., Smith, S.W. E, Leifer, J. E, and L.J. BradfordE, “Measuring and Modeling the Dynamics of Stiffened Thin-Film Polyimide Panels,” *Journal of Guidance, Control, and Dynamics*, Vol. 31, No. 3, May – Jun. 2008, pp. 490-500, DOI: 10.2514/1.32236.
- (10) Leifer, J. E, Black, J.T., Smith, S.W. E, Ma, N. E, and J.K. LumpE, “Measurement of In-Plane Motion of Thin-Film Structures Using Videogrammetry,” *Journal of Spacecraft and Rockets*, Vol. 44, No. 6, Nov. – Dec. 2007, pp. 1317-1325, DOI: 10.2514/1.25566.
- (11) Black, J.T., Leifer, J. E, DeMoss, J.A. E, and E.N. WalkerE, “Experimental and Numerical Correlation of Gravity Sag in Solar-Sail-Quality Membranes,” *Journal of Spacecraft and Rockets*, Vol. 44, No. 3, May – Jun. 2007, pp. 522-527, DOI: 10.2514/1.20958.
- (12) Pappa, R.S. E, Black, J.T., Blandino, J.R. E, Jones, T.W. E, Danehy, P.M. E, and A.A. DorringtonE, “Dot-Projection Photogrammetry and Videogrammetry of Gossamer Space Structures,” *Journal of Spacecraft and Rockets*, Vol. 40, No. 6, Nov. – Dec. 2003, pp. 858-867.

Archival Journal Articles Submitted

- (1) Jennings, A.A, Black, J.T., Magree, D.*, Briggs, G. *, and C. AllenA, “Accuracy of Photogrammetry Texture-Based Surface Reconstruction on Curved Surfaces,” *AIAA Journal*, submitted Oct. 2010.

Refereed Conference Proceedings on Abstract Review

- (1) Niederhauser, J.D., and J.T. Black, “Characterization and Analysis for Flying COTS Electronics On-Orbit,” 25th AIAA Utah State University Conference on Small Satellites, Logan, UT, Aug. 2011, Paper SSC11-XII-3.
- (2) Debes, J., Howard, N., Harrington, R., Cobb, R., and J. Black, “Rapid Build and Space Qualification of CubeSats,” 25th AIAA Utah State University Conference on Small Satellites, Logan, UT, Aug. 2011, Paper SSC11-VII-7.
- (3) Ross, J.T., Risbeck, M.R., Simmons, R.J., Lofthouse, A.J., and J.T. Black, “Experimental Fin Tips For Reusable Launch Vehicles (ExFiT) Flight Data Validation,” 52nd AIAA/ASME/ASCE/AHS/ASC Conference on Structures, Structural Dynamics and Materials, Denver, CO, Apr. 2011, AIAA Paper 2011-2162
- (4) Grigsby, D.A. and J.T. Black, “Satellite Capabilities Mapping – Utilizing Small Satellites,” 24th AIAA Utah State University Conference on Small Satellites, Logan, UT, Aug. 2010, Paper SSC10-VII-1.
- (5) Book, T.A., Starr, W.J., Morse, A.J., Miller, S.D., Black, J.T., Swenson, E.D., Cobb, R.G., and C.R. Hartsfield, “A Design Overview of a Space-Based Chromotomographic Hyperspectral Imaging Experiment,” 24th AIAA Utah State University Conference on Small Satellites, Logan, UT, Aug. 2010, Paper SSC10-I-1.
- (6) Starr, W.J., Book, T.A., Morse, A.J., Miller, S.D., Swenson, E.D., Cobb, R.G., and J.T. Black, “Target Acquisition/Tracking for the Space-Based Chromotomographic Hyperspectral Imaging Experiment,” AIAA/AAS Astrodynamics Specialist Conference, Toronto, Canada, Aug. 2010, AIAA Paper 2010-7655.
- (7) Yates, J.M., Spanbauer, B.W., and J.T. Black, “Geostationary Orbit Development and Evaluation for Space Situational Awareness (GODESSA),” AIAA/AAS Astrodynamics Specialist Conference, Toronto, Canada, Aug. 2010, AIAA Paper 2010-7528.
- (8) Bellows, C.T., Keller, N.M., and J.T. Black, “Mission Feasibility Study for Space Based Wireless Power Transfer,” AIAA/AAS Astrodynamics Specialist Conference, Toronto, Canada, Aug. 2010, AIAA Paper 2010-7522.
- (9) O'Dell, D.C., Bostick, R., Hawks, M.R., Swenson, E.D., Black, J.T., Cobb, R.G., and G.P. Perram, “Chromotomographic Imager Field Demonstration Results,” 7th SPIE Airborne Intelligence, Surveillance, Reconnaissance (ISR) Systems and Applications Conference, Apr. 2010, Proc. SPIE, Vol. 7668, 766804 (2010), doi:10.1117/12.849702.

- (10) Swenson, E., Black, J., and R. Cobb, "Correcting the Effects of Orthogonalized Measured Modes When Tuning Finite Element Models," 51st AIAA/ASME/ASCE/AHS/ASC Conference on Structures, Structural Dynamics and Materials, Orlando, FL, Apr. 2010, AIAA Paper 2010-2546.
- (11) Jennings, A., Black, J., Magree, D., Briggs, G., Allen, C., and M. Jameson, "Effect of Camera Setup on Photogrammetry Texture-Based Surface Reconstruction," 51st AIAA/ASME/ASCE/AHS/ASC Conference on Structures, Structural Dynamics and Materials, Orlando, FL, Apr. 2010, AIAA Paper 2010-2749.
- (12) Magree, D., Briggs, G., Allen, C., Jennings, A., Pollock A., and J. Black, "Pan Tilt Zoom Camera System for Dynamic In-Flight Tracking and Measurement," 51st AIAA/ASME/ASCE/AHS/ASC Conference on Structures, Structural Dynamics and Materials, Orlando, FL, Apr. 2010, AIAA Paper 2010-2804.
- (13) Swenson, P., Thomas, G., Cobb, R., and J. Black, "Experiment Deployment Testing of a One Meter Reflector From a CubeSat," 51st AIAA/ASME/ASCE/AHS/ASC Conference on Structures, Structural Dynamics and Materials, Orlando, FL, Apr. 2010, AIAA Paper 2010-2906.
- (14) Thomas, G., Swenson, P., Cobb, R., Swenson, E., and J. Black, "Prototype Development and Dynamic Characterization of Deployable CubeSat Booms," 51st AIAA/ASME/ASCE/AHS/ASC Conference on Structures, Structural Dynamics and Materials, Orlando, FL, Apr. 2010, AIAA Paper 2010-2907.
- (15) Miller, S., Book, T., Morse, A., Swenson, E., Cobb, R., and J. Black, "Structural Design and Analysis of a Novel Space-Based Chromotomographic Spectrometer," 51st AIAA/ASME/ASCE/AHS/ASC Conference on Structures, Structural Dynamics and Materials, Orlando, FL, Apr. 2010, AIAA Paper 2010-2935.
- (16) Trottier, M., Baghal, L., Swenson, E., Black, J., and C. Finley, "Accurate Dynamic Response Predictions of Various Plug-and-Play SAT I Configurations," 51st AIAA/ASME/ASCE/AHS/ASC Conference on Structures, Structural Dynamics and Materials, Orlando, FL, Apr. 2010, AIAA Paper 2010-2958.
- (17) Jameson, M., Rogers, D., Allen, C., Blandino, J., Jennings, A., Magree, D., Pollock, S., and Black, J., "Motion Capture and Photogrammetry System Hybridization for Dynamic In-Flight Tracking and Measurement", 1st National Society of Black Engineers Aerospace Systems Conference, Feb. 2010, Conference Best Paper.
- (18) McFarland, D., Swenson, E., Black, J., Cobb, R., and Fosbury, A., "Near Real-Time Closed-Loop Optimal Control Feedback for Spacecraft Attitude Maneuvers," AIAA Modeling and Simulation Technologies Conference, Chicago, IL, Aug. 2009, AIAA Paper 2009-5814.
- (19) Doupe, C.C., Swenson, E.D., George, L.E., and Black, J.T., "Finite Element Model Tuning with Varying Experimental Data Density," AIAA Modeling and Simulation Technologies Conference, Chicago, IL, Aug. 2009, AIAA Paper 2009-6038.
- (20) Kahraman, M.O., Swenson, E.D., and J.T. Black, "A Constraint Based Approach for Building Operationally Responsive Space Satellites," 4th International Conference on Recent Advances in Space Technologies, June 2009.
- (21) Cooper, B., Cobb, R., and J. Black, "Rigidizable Inflatable Get-Away-Special Experiment Post Flight Analysis," 50th AIAA/ASME/ASCE/AHS/ASC Conference on Structures, Structural Dynamics and Materials, Palm Springs, CA, May 2009, AIAA Paper 2009-2157.
- (22) Doupe, C., Swenson, E., George, L., and J. Black, "Finite Element Model Tuning with 3D Mode Shapes from FalconSAT- 5," 50th AIAA/ASME/ASCE/AHS/ASC Conference on Structures, Structural Dynamics and Materials, Palm Springs, CA, May 2009, AIAA Paper 2009-2636.
- (23) Owens, J., Cobb, R., and Black, J., "Design and Flight Qualification of the Rigidizable Inflatable Get Away Special Experiment" 50th AIAA/ASME/ASCE/AHS/ASC Conference on Structures, Structural Dynamics and Materials, Palm Springs, CA, May 2009, AIAA Paper 2009-2155.

- (24) Pitcher, N.A., Black, J.T., Reeder, M.F., and R.C. Maple, "Videogrammetry Measurements of a Mini-UAV Wing in a Wind Tunnel," 50th AIAA/ASME/ASCE/AHS/ASC Conference on Structures, Structural Dynamics and Materials, Palm Springs, CA, May 2009, AIAA Paper 2009-2416.
- (25) Simpkins, J., Sollars, R., Allen, C., Jennings, A., and J.T. Black, "Dynamic Calibration and Performance of a Laser Steering System for Dynamic In-Flight Tracking and Measurement," 50th AIAA/ASME/ASCE/AHS/ASC Conference on Structures, Structural Dynamics and Materials, Palm Springs, CA, May 2009, AIAA Paper 2009-2159.
- (26) Quarles, W., Blandino, J., and J. Black, "Development of a Laser Positioning System for On-Orbit Characterization of Deployable Booms," 50th AIAA/ASME/ASCE/AHS/ASC Conference on Structures, Structural Dynamics and Materials, Palm Springs, CA, May 2009, AIAA Paper 2009-2176.
- (27) Simpkins, J., Sollars, R., Jennings, A., Allen, C., and J. Black, "Calibration and Performance of Laser Steering System for Dynamic In-Flight Tracking and Measurement," SPIE Smart Structures, Materials, and Non-Destructive Evaluation Conference, San Diego, CA, Mar 2009, SPIE Paper 7292-131.
- (28) Simmons, J., Deleon, A., Black, J., and E. Swenson, "Aeroelastic Analysis and Optimization of FalconLaunch Sounding Rocket Fin," 47th AIAA Aerospace Sciences Meeting, Orlando, FL, Jan. 2009, AIAA Paper 2009-515.
- (29) Black, J.T., Swenson, E.D., and L. George, "Extracting 3D Mode Shapes of FalconSAT-5 Structural Engineering Model," 49th AIAA/ASME/ASCE/AHS/ASC Conference on Structures, Structural Dynamics and Materials, Schaumburg, IL, Apr. 2008, AIAA Paper 2008-1851.
- (30) Black, J., Leifer, J., and S.W. Smith, "Global Static Testing and Model Validation of Thermal-Formed Thin Film Polyimide Panels," 49th AIAA/ASME/ASCE/AHS/ASC Conference on Structures, Structural Dynamics and Materials, 8th Gossamer Spacecraft Forum, Schaumburg, IL, Apr. 2008, AIAA Paper 2008-2137.
- (31) Black, J., Leifer, J., and S.W. Smith, "Global Static Testing and Model Validation of Thermal-Formed Thin Film Polyimide Panel-Arrays," 49th AIAA/ASME/ASCE/AHS/ASC Conference on Structures, Structural Dynamics and Materials, 8th Gossamer Spacecraft Forum, Schaumburg, IL, Apr. 2008, AIAA Paper 2008-2215.
- (32) Black, J., Smith, S.W., Leifer, J., and L. Bradford, "Experimental Characterization and Modeling of Global Behavior of Semi-Rigid Thin Film Polyimide Panels," 48th AIAA/ASME/ASCE/AHS/ASC Conference on Structures, Structural Dynamics and Materials, 8th Gossamer Spacecraft Forum, Waikiki, HI, Apr. 2007, AIAA Paper 2007-1833.
- (33) Black, J.T., Smith, S.W., and J. Leifer, "Reduced Model Validation of Thermal-Formed Polyimide Panels," 25th International Modal Analysis Conference, Model Validation Methods Special Session, Orlando, FL, Feb. 2007.
- (34) Black, J.T., Whetzal, J.A., deBlonk, B.J., and J.J. Massarello, "Deployment Repeatability of Testing of Composite Tape Springs for Space Optics Applications," 47th AIAA/ASME/ASCE/AHS/ASC Conference on Structures, Structural Dynamics and Materials, 7th Gossamer Spacecraft Forum, Newport, RI, May 2006, AIAA Paper 2006-1905.
- (35) Leifer, J., Smith, S.W., Black, J.T., Ma, N., and J.K. Lumpp, "Measurement of In-Plane Motion of Thin-Film Structures Using Videogrammetry," 47th AIAA/ASME/ASCE/AHS/ASC Conference on Structures, Structural Dynamics and Materials, 7th Gossamer Spacecraft Forum, Newport, RI, May 2006, AIAA Paper 2006-1805.
- (36) Black, J.T., Smith, S.W., and J. Leifer, "Investigating Semi-Rigid Kapton Panels for use in Space Telescopes," 56th International Astronautical Congress, Fukuoka, Japan, Oct. 2005, IAC-05-C2.1.B.05.
- (37) Campbell, J.E., Black, J.T., and S.W. Smith, "Toward Field Videogrammetry of Rivulets on Bridge Stay Cables," EURODYNE, 6th European Conference on Structural Dynamics, Paris, France, Sep. 2005.

- (38) Black, J.T., deBlonk, B.J., Patrick, B., and S. Chodimella, "A Composite Support Structure for a Membrane Mirror," 46th AIAA/ASME/ASCE/AHS/ASC Conference on Structures, Structural Dynamics and Materials, 6th Gossamer Spacecraft Forum, Austin, TX, Apr. 2005, AIAA Paper 2005-2195.
- (39) Smith, S.W., Song, H., Baker, J., Black, J.T., and D. Muheim, "Flexible Models for Solar Sail Control," 46th AIAA/ASME/ASCE/AHS/ASC Conference on Structures, Structural Dynamics and Materials, 6th Gossamer Spacecraft Forum, Austin, TX, Apr. 2005, AIAA Paper 2005-1801.
- (40) Campbell, J.E., Reichenbach, P.E., Black, J.T., and S.W. Smith, "Photogrammetric Characterization of Laboratory Rivulets for Cable Stayed Bridges," 23rd International Modal Analysis Conference, Orlando, FL, Feb. 2005.
- (41) Black, J.T. and R.S. Pappa, "Photogrammetry and Videogrammetry Methods for Solar Sails and Other Gossamer Space Structures," 45th AIAA/ASME/ASCE/AHS/ASC Conference on Structures, Structural Dynamics and Materials, 5th Gossamer Spacecraft Forum, Palm Springs, CA, Apr. 2004, AIAA Paper 2004-1662.
- (42) Black, J.T., Leifer, J., DeMoss, J.A., Walker, E.N., and W.K. Belvin, "Experimental and Numerical Correlation of Gravity Sag in Solar Sail Quality Membranes," 45th AIAA/ASME/ASCE/AHS/ASC Conference on Structures, Structural Dynamics and Materials, 5th Gossamer Spacecraft Forum, Palm Springs, CA, Apr. 2004, AIAA Paper 2004-1579.
- (43) Blandino, J.R., Sterling, J., Baginski, F., Steadman, E., Black, J.T., and R.S. Pappa, "Optical Strain Measurement of an Inflated Cylinder with Application to Scientific Balloons," 45th AIAA/ASME/ASCE/AHS/ASC Conference on Structures, Structural Dynamics and Materials, 5th Gossamer Spacecraft Forum, Palm Springs, CA, Apr. 2004, AIAA Paper 2004-1500.
- (44) Pappa, R.S., Black, J.T., and J.R. Blandino, "Photogrammetric Measurement of Gossamer Spacecraft Membrane Wrinkling," Society for Experimental Mechanics Annual Conference, Charlotte, NC, Jun. 2003.
- (45) Leifer, J., Black, J.T., Belvin, K.W., and V. Behun, "Evaluation of Shear Compliant Borders for Wrinkle Reduction in Thin Film Membrane Structures," 44th AIAA/ASME/ASCE/AHS/ASC Structures, Structural Dynamics and Materials Conference, 4th Gossamer Spacecraft Forum, Norfolk, VA, Apr. 2003, AIAA Paper 2003-1984.
- (46) Blandino, J.R., Pappa, R.S., and J.T. Black, "Modal Identification of Membrane Structures with Videogrammetry and Laser Vibrometry," 44th AIAA/ASME/ASCE/AHS/ASC Structures, Structural Dynamics and Materials Conference, 4th Gossamer Spacecraft Forum, Norfolk, VA, Apr. 2003, AIAA Paper 2003-1745.
- (47) Johnston, J.D., Blandino, J.R., Black, J.T., and R.S. Pappa, "Structural Analysis and Testing of a 1/20th Scale NGST Sunshield Membrane Layer," 44th AIAA/ASME/ASCE/AHS/ASC Structures, Structural Dynamics and Materials Conference, 4th Gossamer Spacecraft Forum, Norfolk, VA, Apr. 2003, AIAA Paper 2003-1742.
- (48) Black, J.T., "Photogrammetry and Videogrammetry Methods for Solar Sails and Other Gossamer Structures," AIAA Region I Student Conference, College Park, MD, Apr. 2003.
- (49) Black, J.T. and R.S. Pappa, "Videogrammetry Using Projected Circular Targets: Proof-of-Concept Test," 21st International Modal Analysis Conference, Orlando, FL, Feb. 2003.
- (50) Pappa, R.S., Black, J.T., Blandino, J.R., Jones, T.W., Danehy, P.M., and A.A. Dorrington, "Dot Projection Photogrammetry and Videogrammetry of Gossamer Space Structures," 21st International Modal Analysis Conference, Orlando, FL, Feb. 2003.
- (51) Pappa, R.S., Jones, T.W., Black, J.T., Walford, A., Robson, S. and M. Shortis, "Photogrammetry Methodology Development for Gossamer Spacecraft Structures," 43rd AIAA/ASME/ASCE/AHS/ASC Structures, Structural Dynamics, and Materials Conference, 3rd Gossamer Spacecraft Forum, Denver, CO, Apr. 2002, AIAA Paper 2002-1375.

NASA Technical Memoranda

- (1) Black, J.T., "Photogrammetry and Videogrammetry Methods Development for Solar Sail Structures," Masters Thesis, Joint Institute for Advancement of Flight Sciences, NASA Langley Research Center, Sep. 2003, NASA/CR-2003-212678.
- (2) Black, J.T. and R.S. Pappa, "Videogrammetry Using Projected Circular Targets: Proof-of-Concept Test," Feb. 2003, NASA/TM-2003-212148.
- (3) Pappa, R.S., Black, J.T., Blandino, J.R., Jones, T.W., Danehy, P.M., and A.A. Dorrington, "Dot Projection Photogrammetry and Videogrammetry of Gossamer Space Structures," Feb. 2003, NASA/TM-2003-212146.
- (4) Pappa, R.S., Jones, T.W., Black, J.T., Walford, A., Robson, S., and M.R. Shortis, "Photogrammetry Methodology Development for Gossamer Spacecraft Structures," Jun. 2003, NASA/TM-2002-211739.

Other

- (1) Anderson, J., Duple, C., Black, J., and E. Swenson, "Reach for the Sky: Small Satellite Finite Element Model Optimization Using Laser Vibrometry," Polytec InFocus, Iss. 01, 2011, pp. 11-13.
- (2) PhotoModeler Inc., PhotoModeler Video - Industrial Example, online at http://www.photomodeler.com/applications/scientific_engineering/pmv_muav.htm
- (3) Black, J.T., "New Ultra-lightweight Stiff Panels for Space Apertures," PhD Dissertation, Department of Mechanical Engineering, University of Kentucky, Dec. 2006, online at <http://lib.uky.edu/ETD/ukymeen2006d00532/BlackDis.pdf>
- (4) Black, J.T., "Photogrammetry and Videogrammetry Methods Development for Solar Sail Structures," Masters Thesis, Joint Institute for Advancement of Flight Sciences, NASA Langley Research Center, George Washington University, Gelman Library Special Collections, Stacks, Call Number: AS36.G3 2003, Sep. 2003.
- (5) Pappa, R.S., Jones, T.W., Black, J.T., Walford, A., Robson, S., and M.R. Shortis, "Photogrammetry Methodology Development for Gossamer Spacecraft Structures," Sound and Vibration, Aug. 2002, pp. 12-21.

Presentations

- (1) Black, J.T., "(YIP08) Hybrid Laser/Video 3D Non-contact Motion Capture and Analysis," Air Force Office of Scientific Research Structural Mechanics and Non-Destructive Evaluation Program Review, Destin, FL, Aug. 2010.
- (2) Black, J.T., "Freely Deploying Structures Analysis," AFOSR Workshop on Improved Precision for Space Structures, May 2010.
- (3) Black, J.T., and R.F. Beach, "Space Research and Education in Ohio," Ohio State University Department of Aeronautics Graduate Symposium, Nov. 2009, Invited Presentation.
- (4) Black, J.T., "Dynamic In-Flight Test and Measurement," US-Korean Conference on Science, Technology, and Entrepreneurship, July 2009, Invited Presentation
- (5) Jennings, A., Allen, C., and J.T. Black, "Calibration and Development of Laser Steering for In-Flight Noncontact Measurements," 34th AIAA Dayton-Cincinnati Aerospace Science Symposium, Dayton, OH, Mar. 2009.
- (6) Allen, C., Jennings, A., and J.T. Black, "Dynamic In-Flight Tracking and Measurement Labs: An Overview," 34th AIAA Dayton-Cincinnati Aerospace Science Symposium, Dayton, OH, Mar. 2009.
- (7) Cooper, B., Black, J., and R. Cobb, "Post Space Flight Analysis of the Rigidizable Inflatable Get-Away-Special Experiment," 34th AIAA Dayton-Cincinnati Aerospace Science Symposium, Dayton, OH, Mar. 2009.
- (8) Sheirich, P. and J. Black, "An Engineering Trade Space Analysis for a Space Based Hyperspectral Chromotomographic Scanner," 34th AIAA Dayton-Cincinnati Aerospace Science Symposium, Dayton, OH, Mar. 2009.

- (9) Doupe, C., Swenson, E., and J. Black, "FalconSAT 5 Finite Element Model Tuning Based on Laser Vibrometry," 34th AIAA Dayton-Cincinnati Aerospace Science Symposium, Dayton, OH, Mar. 2009.
- (10) Black, J.T. and R.F. Beach, "In-Space Laser Power Beaming Demonstration," invited presentation at the US Air Force Academy's FalconSAT-6 Symposium, Feb. 2009.
- (11) Cooper, B., Black, J., and R. Cobb, "Inflatable/Rigidizable Space Structures," 4th ASME Dayton Engineering Sciences Symposium, Dayton, OH, Oct. 2008.
- (12) Black, J.T., "Space Research and Education at AFIT," invited presentation at Sandia National Laboratories, Apr. 2008
- (13) Welty, N.F., Rohe, W.C., Roach, N.R., Black, J.T., and J. Walter, "Systems Engineering Approach to Development of a Research Testbed for Spacecraft Dynamics," 33rd AIAA Dayton-Cincinnati Aerospace Sciences Symposium, Dayton, OH, Mar. 2008.
- (14) Black, J.T., Smith, S.W., and J. Leifer, "New Ultra-lightweight Stiff Panels for Space Apertures," 32nd AIAA Dayton-Cincinnati Aerospace Science Symposium, Dayton, OH, Mar. 2007.
- (15) Black, J.T., "New Ultra-lightweight Stiff Panels for Space Apertures," Presentation to NASA Sponsors, NASA Langley Research Center, Hampton, VA, Nov. 2006.
- (16) Black, J.T., Smith, S.W., and J. Leifer, "Static Compression Testing and Modeling of Semi-Rigid Panels for Orbital Apertures," 31st Dayton-Cincinnati Aerospace Science Symposium, Dayton, OH, Mar. 2006.
- (17) Black, J.T., "New Gossamer Structures for use in Future Space Telescopes," University of North Dakota, Department of Space Studies, Space Studies Colloquium, 28 Nov. 2005.
- (18) Black, J.T., "56th International Astronautical Congress," University of North Dakota, Department of Space Studies, Brown Bag Lunch Seminar, 29 Nov. 2005.
- (19) Black, J.T., "New Gossamer Structures for use in Future Space Telescopes," Air Force Research Laboratory, Space Vehicles Directorate, Summer Seminar Series, 08 Jul. 2005.
- (20) Black, J.T., and W.K. Belvin, "Ultra-lightweight and Inflatable Space Structures," Air Force Research Laboratory, Space Vehicles Directorate, Summer Seminar Series, 15 Jul. 2004.
- (21) Black, J.T., and W.K. Belvin, "Ultra-lightweight and Inflatable Space Structures," University of Kentucky, Department of Mechanical Engineering, AIAA Seminar, 16 Feb. 2004.
- (22) Black, J.T., "Photogrammetry and Videogrammetry: The Second Generation," NASA Langley Research Center, Structural Dynamics Branch, Technical Interchange Meeting, 15 Oct. 2002.
- (23) Black, J.T. and R.S. Pappa, "Photogrammetry and Solar Sails," NASA Langley Research Center, Structural Dynamics Branch, Technical Interchange Meeting, 19 Mar. 2002.

**Service
Institute**

- Space Systems Certificate Program, Chair, Department of Aeronautics and Astronautics, Air Force Institute of Technology, 2008–present
- Executive Committee Member of the Ohio Space Grant Consortium representing the Air Force Institute of Technology, 2007–present
- AFIT Faculty Council Secretary, 2009–2010
- AIAA Faculty Advisor, Air Force Institute of Technology, 2007–present
- DoD Joint Space Academic Working Group (JSAG) member, 2008–present
- AFIT Inter-departmental Space Working Group (ISWG) member, 2008–present
- Faculty Search Committee, Chair, Department of Aeronautics and Astronautics, Air Force Institute of Technology, 2009, 2010
- Dean's Reader, Callaway, D., ENY Dissertation, 2011
- Dean's Reader, Hyde, M., ENG Dissertation, 2010

- Dayton Area Graduate Studies Institute (DAGSI) Application Evaluator, AFIT/ENY, Jan. 2008, Jan. 2009
- Best Thesis Award Committee, Department of Aeronautics and Astronautics, Air Force Institute of Technology, Mar. 2007, Mar. 2008

Professional

- 36th AIAA Dayton-Cincinnati Aerospace Sciences Symposium (DCASS) General Chair, Mar. 2012
- 53rd AIAA/ASME/ASCE/AHS/ASC Conference on Structures, Structural Dynamics and Materials, Structural Dynamics Technical Chair, Apr. 2012
- 35th AIAA Dayton-Cincinnati Aerospace Sciences Symposium (DCASS) Technical Chair, Mar. 2011
- 52nd AIAA/ASME/ASCE/AHS/ASC Conference on Structures, Structural Dynamics and Materials, Structural Dynamics co-Technical Chair, Apr. 2011
- AIAA Structural Dynamics Technical Committee, 2008–present
- AIAA Gossamer Spacecraft Program Committee, 2008–present
- AIAA Faculty Advisor, Air Force Institute of Technology, 2007–present
- AIAA Dayton-Cincinnati Section Treasurer, 2008–2010
- AIAA Journal Reviewer
- AIAA Journal of Aircraft Reviewer
- AIAA Journal of Spacecraft and Rockets Reviewer
- Shock and Vibration Reviewer
- International Micro Air Vehicle Journal Reviewer
- Acta Astronautica Reviewer
- Special Session Organizer, 10th Gossamer Spacecraft Forum, 50th AIAA/ASME/ASCE/AHS/ASC Conference on Structures, Structural Dynamics and Materials, Palm Springs, CA, May 2009
- Session co-chair at AIAA/ASME/ASCE/AHS/ASC Conference on Structures, Structural Dynamics and Materials, 2009, 2010
- Session co-chair at Gossamer Spacecraft Forum, AIAA/ASME/ASCE/AHS/ASC Conference on Structures, Structural Dynamics and Materials, 2005, 2007–2010
- 33rd AIAA Dayton-Cincinnati Aerospace Sciences Symposium (DCASS) Keynote and Invited Sessions Chair, Mar. 2008
- AIAA Gossamer Spacecraft Program Committee, special project on the history of gossamer programs, 2006
- Dayton Area Graduate Studies Institute (DAGSI) Graduate Fellowship Application Evaluator, 2008, 2009, 2010
- Abstract Reviewer, AIAA/ASME/ASCE/AHS/ASC Conference on Structures, Structural Dynamics and Materials, 2003 – 2011
- AIAA Langley Student Branch Executive Board, Hampton, VA, 2002–2003

James Claude Dickens, Ph.D., P.E.

Vice Director of the Center for Pulsed Power and Power Electronics
Professor of Electrical and Computer Engineering
Licensed Professional Engineer State of Texas, no. 88713
Texas Tech University, Lubbock, Texas 79409
james.dickens@ttu.edu 806-742-3533 Fax: 806-742-1245

8401 County Road 6940
Lubbock, Texas 79407

Cell: 806-790-9876
TTU: 806-742-1254

Education

Ph.D. in Electrical Engineering, Texas Tech University, 1995
M.S. in Electrical Engineering, Texas Tech University, 1993
B.S. in Electrical Engineering, Texas Tech University, 1991

Teaching areas: Electronics, Circuits, Pulsed Power, Electrical Power Distribution Systems, Power Electronics, Optics and Optical Systems, Failure Analysis, Fields, Microwave and RF Circuits, Communications and Communication Circuits, and Electric Space Propulsion.

Research areas: Pulsed Power, Pulsed RF Sources and Applications, Pulsed Lasers, Fiber Laser and applications, Electrical Failure Forensics, Grounding and Shielding, Power Electronics, High Efficiency DC/DC Converters, Explosive Pulsed Power, High Power Microwaves, Arc and Plasma Diagnostics, and Electric Space Propulsion.

Short courses taught: Grounding and Shielding, Power Electronics, Personnel Safety, Power Distribution Systems, Pulse Generators, High Voltage Generators, Compact Pulsed Power, Compact DC/DC Technology, High Power Microwaves, and Electrical and Optical Diagnostics.

Professional History

Texas Tech University

Charles Bates Thornton Professor, Electrical and Computer Engineering, Sept. 2009
Professor, Electrical & Computer Engineering, Sept. 2008
Associate Professor, Electrical & Computer Engineering, Sept. 2001–Aug. 2008
Assistant Professor, Electrical & Computer Engineering, Jan. 1999–Aug. 2001
Research Assistant Professor, Electrical & Computer Engineering, May 1996–Dec. 1998

Consulting

Multiple Expert Witness Cases (discovery, depositions, reports and testimony)
Primex Aerospace
FMV Swedish Defense Department
Federal Aviation Administration (FAA)
High Tech Consultants
BAE Systems
L3 Communications
Lockheed Martin
Boeing Corporation
White Sands Missile Range
NASA

Awards, Professional Societies, and Services

- Technical Program Chair for the 2008 IEEE Power Modulator Conference in Las Vegas, NV
- Guest editor of IEEE Transactions on Plasma Science Special Issue on Pulsed Power

- Lecturer at High Power Microwave Workshop at FOI in Grindsjön, Sweden, Aug. 2005.
- Presented an invited talk at Kumamoto University's International Forum on Pulsed Power Science. All expenses were paid by the host institution.
- 2005 Chancellor's Excellence in Research Award from Texas Tech University.
- Vice-Chairman of 2003 IEEE International Pulsed Power Conference.
- Civilian Research Defense Foundation (CRDF) Chairman of Physics panel 2003
- Civilian Research Defense Foundation (CRDF) International onsite reviewer 2000–present.
- CRDF Physics Review Panel 1999–present.
- AIAA Electric Propulsion Technical Committee Secretary 2000–2002.
- Session Organizer at 2002 International Conference of Plasma Science.
- Session Organizer at the 2002 Power Modulator Symposium.
- AIAA Electric Propulsion Technical Committee 1999–present.
- Organizer and lecturer at workshop on Pulsed Power Technology, Bechtel, 2001.
- Organizer at workshop on Pulsed Power Technology, China Lake.
- Workshop on Pulsed Power Technology workshop at Texas Tech University.
- Pulsed Power Science and Technology Committee 1999–present.
- Session Organizer at 2000 International Conference of Plasma Science.
- Japanese Society for the Promotion of Science (JSPS) Fellow 1996
- American Institute of Aeronautics and Astronautics (AIAA), 1993–present.
- Institute of Electrical and Electronics Engineers (IEEE), 1990–present.

Grants and Contracts

TTU ORS Report \$ 13,169,836 total award credited to individual PI. (1/20/11)

- Dr. Dickens has the highest funded research in the COE over the past decade.
- Dr. Dickens has been P.I / Co-P.I. on three highly competitive MURI grants.
- Dr. Dickens is P.I. on a highly competitive Navy IED basic research grant. (>400 original submissions 8 awarded)
- Dr. Dickens has been P.I. on five highly competitive DURIP equipment grants.

Direction of Graduate Students (all students wrote Thesis or Dissertation)

Student	Degree	Function	Grad date
Braxton Bragg	Ph.D.	Chair	Active
Billy Sullivan	Ph.D.	Chair	Active
Cameron Hettler	Ph.D.	Chair	Active
Jonathan Parson	Ph.D.	Chair	Active
John Walter	Ph.D.	Chair	Active
Shad Holt	Ph.D.	Chair	Active
Braxton Bragg	M.S.E.E.	Chair	2010
Colt James	Ph.D.	Chair	2010
Cameron Hettler	M.S.E.E..	Chair	2009
William Sullivan	M.S.E.E.	Chair	2009
Jonathan Parson	M.S.E.E.	Chair	2008
Yeong-Jer Chen	Ph.D.	Chair	2008
Thomas Holt	Ph.D.	Committee member	2008
David Belt	Ph.D.	Co-Chair	2008
Ryan Karhi	M.S.E.E.	Committee member	2007
Colt James	M.S.E.E.	Chair	2007
Brent McHale	Ph.D.	Committee member	2006

Student	Degree	Function	Grad date
Mic Cevallos	Ph.D.	Chair	2006
Shad Holt	M.S.E.E.	Chair	2006
Juan Carlos	Ph.D.	Committee member	2004
Michael Hoffman	M.S.E.E.	Chair	2003
Heath Keene	M.S.E.E.	Chair	2003
David J. Hemmert	Ph.D.	Committee member	2003
Johnathan Blackwell	M.S.E.E.	Chair	2002
Michael Cevallos	M.S.E.E.	Chair	2002
Roberto Izquierdo	M.S.E.E.	Chair	2001
Juan Carlos	M.S.E.E.	Chair	2001
Zhan Mei	M.S.E.E.	Chair	2001
Efren Brito	M.S.E.E.	Chair	2001
John Walter	M.S.E.E.	Chair	2000
Michael Cevallos	M.S.E.E.	Chair	2000
Guruprakash	M.S.E.E.	Committee member	2000
Radhakrishna			
Naveen Anumalla	M.S.E.E.	Committee member	1999

Publications

Journals

- (1) "Window Breakdown Caused by High Power Microwaves," IEEE Trans. Plasma Science, HPM Issue, 26 296 (1998) (with A. Neuber, M. Kristiansen, D. Hemmert, H. Krompholz, and L.L. Hatfield).
- (2) "High Voltage Subnanosecond Breakdown," IEEE Transactions on Plasma Science, Special Issue on High Power Microwave Generation, 26 874 (1998) (with J. Mankowski and M. Kristiansen).
- (3) "Imaging of High-Power Microwave-Induced Surface Flashover," IEEE Transactions on Plasma Science Special Issue "Images in Plasma Science", 27 138 (1999) (with A. Neuber, D. Hemmert, M. Kristiansen, H. Krompholz, and L.L. Hatfield).
- (4) "High Power Microwave Generation by a Coaxial Virtual Cathode Oscillator," IEEE Transactions on Plasma Science, 27 1538 (1999) (with W. Jiang, K. Woolverton, and M. Kristiansen).
- (5) "Efficiency Enhancement of Coaxial Virtual Cathode Oscillator," 27 1543 (1999) IEEE Transactions on Plasma Science, (with W. Jiang and M. Kristiansen).
- (6) "Pulsed Power Generation Using Ferromagnetic Circuits," IEEE Transactions on Plasma Science, Vol. 28, 2000. (with S.I. Shkuratov, M. Kristiansen, L.L. Hatfield, and R. Martin).
- (7) "High-Current and High-Voltage Pulsed Testing of Resistors," IEEE Transactions on Plasma Science, Volume: 28 , Issue: 5 , Oct. 2000 Pages:1607 - 1614 , (with S.I. Shkuratov, M. Kristiansen, L.L. Hatfield, and E. Horrocks).
- (8) "Optical Diagnostics on Helical Flux Compression Generators," IEEE Transactions on Plasma Science, Special Issue on Pulsed Power Science and Technology, Vol. 28, 1445-1450, 2000. (with A. Neuber, M. Kristiansen, and H. Krompholz).
- (9) "High Voltage Subnanosecond Corona Inception," IEEE Transactions on Plasma Science, Special Issue on Pulsed Power Science and Technology, Vol. 28, 2000. (with J. Mankowski and M. Kristiansen).
- (10) "Microwave Magnetic Field Effects on High Power Microwave Window Breakdown," IEEE Transactions on Plasma Science, Special Issue on High Power Microwaves, Vol. 28, 472-477, 2000. (with D. Hemmert, A. Neuber, M. Kristiansen, H. Krompholz, and L.L. Hatfield).

- (11) "Electrical Behavior of a Simple Helical Flux Compression Generator for Code Benchmarking," IEEE Transactions on Plasma Science, Volume: 29 , Issue: 4 , Aug. 2001, Pages:573 - 581 , (with A. Neuber, M. Kristiansen, J.B. Cornette, K. Jamison, R. Parinson, M. Giesselmann, P. Worsey, J. Baird, and M. Schmidt).
- (12) "Subnanosecond Corona Inception in an Ultra Wideband Environment," IEEE Transactions on Plasma Science, Volume: 30 , Issue: 3 , June 2002 Pages:1211 - 1214, (with John Mankowski M. Kristiansen, J. Lehr, W. Prather, and J. Gaudet).
- (13) "Compact Explosive-Driven Generator of Primary Power Based on a Longitudinal Shock Wave Demagnetization of Hard Ferri- and Ferromagnetics", IEEE Transactions on Plasma Science, Volume: 30, Issue: 5, Oct. 2002 Pages:1681 - 1691, (with S.I. Shkuratov, M. Kristiansen, and J.C. Hernandez).
- (14) "Current Mode of Pulsed Power Generation in Moving Magnet Systems", IEEE Transactions on Plasma Science, Volume: 30 , Issue: 5 , Oct. 2002 Pages:1674 - 1680, (with S.I. Shkuratov, M. Kristiansen, and J.C. Hernandez).
- (15) "Rapid decontamination of large surface areas," IEEE Transactions on Plasma Science, Volume: 28 , Issue: 1 , Feb. 2000, Pages:173 - 179. (with Farrar, L.C.; Haack, D.P.; McGrath, S.E.; O'Hair, E.A.; Fralick, J.A).
- (16) "Shock Wave Demagnetization of BaFe₁₂O₁₉ Hard Ferrimagnetics", Journal of Applied Physics 91 (2002) 3007-3009 (with S.I. Shkuratov, E.F. Talantsev and M. Kristiansen).
- (17) "Transverse Shock Wave Demagnetization of Nd₂Fe₁₄B High-Energy Hard Ferromagnetics, Journal of Applied Physics 92 (2002) 159-162 (with S.I. Shkuratov, E.F. Talantsev, and M. Kristiansen).
- (18) "Ultracompact Explosive-Driven High-Current Source of Primary Power Based on Shock Wave Demagnetization of Nd₂Fe₁₄B Hard Ferromagnetics", Review of Scientific Instruments, 73 (2002) 2738-2742 (with S.I. Shkuratov, E.F. Talantsev, and M. Kristiansen).
- (19) "The Conductivity of a Longitudinal-Shock-Wave-Compressed Nd₂Fe₁₄B Hard Ferromagnetics, Modern Physics Letters B, 16, No. 12 (2002) 1-11 (with E.F. Talantsev, S.I. Shkuratov, and M. Kristiansen).
- (20) "Theoretical Treatment of Explosive Driven Ferroelectric Generators", IEEE Transactions on Plasma Science, Volume: 30 , Issue: 5 , Oct. 2002 Pages:1665 - 1673, (with S.I. Shkuratov, Ya. Tkach, E.F. Talantsev, M. Kristiansen, L.L. Altgilbers, and P.T. Tracy).
- (21) "Single Shot, Repetitive and Life-Time High-Voltage Testing of Capacitors", IEEE Transactions on Plasma Science, Volume: 30 , Issue: 5 , Oct. 2002 Pages:1943 - 1949, (with S.I. Shkuratov, E.F. Talantsev, L.L. Hatfield, and M. Kristiansen).
- (22) "Studies on a Helical Magnetic Flux Compression Generator," SAE Transactions, Journal of Aerospace, vol. 109, pp. 865-869, 2000 (This Transactions volume was published in 2001 and "...contains the best 135 technical papers of all those presented in 2000.") (with A. Neuber, M. Kristiansen, M. Giesselmann, B. Freeman, D. Dorsey, P. Worsey, J. Baird, and M. Schmidt).
- (23) "Longitudinal Shock Wave Demagnetization of High Energy Nd₂Fe₁₄B Ferromagnetics," Appl. Phys. Lett. 82, 1248 (2003) (with S.I. Shkuratov, E.F. Talantsev, and M. Kristiansen).
- (24) "Thermodynamic State of The Magnetic Flux Compression Generator Volume," IEEE Trans. on Plasma Science, vol. 30, 1659-1664 (2002). (with A. Neuber, T. Holt, and M. Kristiansen).
- (25) "Helical MFCG For Driving A High Inductance Load," accepted for publication in the Special Edition of the Journal of EM Phenomenon on FCGs (Oct. 2003) (with Andreas A. Neuber, Juan-Carlos Hernández, Magne Kristiansen).
- (26) "Quantification of Ohmic and Intrinsic Flux Losses in Helical Flux Compression Generators," IEEE Transactions on Plasma Science, vol. 32, pp. 1902-1908 (2004) (with Juan-Carlos Hernandez, Andreas A. Neuber and Magne Kristiansen).
- (27) "DC Flashover of a Dielectric Surface in Atmospheric Conditions," IEEE Transactions on Plasma Science, vol. 32, pp. 1828-1834 (2004) (with John T. Krile, Andreas A. Neuber, and Hermann G. Krompholz).

- (28) “Magnetic Flux Compression Generators,” Proceeding of the IEEE, vol. 92 number 7, 1205-1215 July 2004. (with Andreas A. Neuber).
- (29) “Microwave Frequency Determination Mechanisms in A Coaxial Vircator,” IEEE Transactions on Plasma Science, vol. 32, pp. 1799-1804 (2004) (with X. Chen, J. Mankowski, L. Hatfield, E. Choi, and M. Kristiansen).
- (30) “A Bench Top Railgun With Distributed Energy Sources,” Mankowski, J.; Dickens, J.; Giesselmann, M.; McDaniel, B.; McHale, B.; Kristiansen, M., Magnetics, IEEE Transactions on Plasma Science, Volume 43, Issue 1, Part 2, Jan. 2007 Page(s):167 – 169.
- (31) “Interface Breakdown During High-Power Microwave Transmission,” Neuber, A. A.; Edmiston, G. F.; Krile, J. T.; Krompholz, H.; Dickens, J. C.; Kristiansen, M., Magnetics, IEEE Transactions on Plasma Science, Volume 43, Issue 1, Part 2, Jan. 2007 Page(s):496 – 500.
- (32) “High-Power Microwave Surface Flashover of a Gas–Dielectric Interface at 90–760 torr,” Edmiston, G.; Krile, J.; Neuber, A.; Dickens, J.; Krompholz, H., IEEE Transactions on Plasma Science, Volume 34, Issue 5, Part 1, Oct. 2006 Page(s):1782 – 1788.
- (33) “The Impact of Field Enhancements and Charge Injection on the Pulsed Breakdown Strength of Water,” Wetz, D.A.; Mankowski, J.J.; Dickens, J.C.; Kristiansen, M., IEEE Transactions on Plasma Science, Volume 34, Issue 5, Part 1, Oct. 2006 Page(s):1670 – 1679.
- (34) “Conduction and breakdown mechanisms in transformer oil,” Butcher, M.; Neuber, A.A.; Cevallos, M.D.; Dickens, J.C.; Krompholz, H., IEEE Transactions on Plasma Science, Volume 34, Issue 2, Part 3, April 2006 Page(s):467 – 475.
- (35) “A bench top railgun with distributed energy sources” Mankowski, J; Dickens, J; Giesselmann, M, et al., IEEE TRANSACTIONS ON MAGNETICS Volume: 43 Issue: 1 Special Issue: SI Pages: 167-169 Part: 2 Published: JAN 2007.
- (36) “Interface breakdown during high-power microwave transmission”, Neuber, AA; Edmiston, GF; Krile, JT, James Dickens, IEEE TRANSACTIONS ON MAGNETICS Volume: 43 Issue: 1 Special Issue: SI Pages: 496-500 Part: 2 Published: JAN 2007.
- (37) “Contributing factors to window flashover under pulsed high power microwave excitation at high altitude”, Edmiston, G; Neuber, A; McQuage, James Dickens, IEEE TRANSACTIONS ON DIELECTRICS AND ELECTRICAL INSULATION Volume: 14 Pages: 783-789 Published: 2007.
- (38) Low-Jitter Triggered Spark Gap With High-Pressure Gas Mixtures Yeong-Jer Chen; Mankowski, J.J.; Dickens, J.C.; Walter, J.; Kristiansen, M.; IEEE Transactions on Plasma Science, Volume 36, Issue 5, Part 3, Oct. 2008 Page(s):2546 - 2553 Digital Object Identifier 10.1109/TPS.2008.2004366.
- (39) Compact Electroexplosive Fuses for Explosively Driven Pulsed Power McCauley, D.R.; Belt, D.W.; Mankowski, J.J.; Dickens, J.C.; Neuber, A.A.; Kristiansen, M.; IEEE Transactions on Plasma Science Volume 36, Issue 5, Part 3, Oct. 2008 Page(s):2691 - 2699 Digital Object Identifier 10.1109/TPS.2008.2004230.
- (40) Utilization of a Nonexplosive Test Bed for Flux-Compression-Generator Electroexplosive Opening Switches Belt, D.W.; Mankowski, J.J.; Neuber, A.A.; Dickens, J.C.; Kristiansen, M.; IEEE Transactions on Plasma Science, Volume 36, Issue 5, Part 3, Oct. 2008 Page(s):2684 - 2690 Digital Object Identifier 10.1109/TPS.2008.2001889.
- (41) Secondary Arc Formation Within a Distributed Energy Railgun Karhi, R.W.; Mankowski, J.J.; Dickens, J.C.; Kristiansen, M.; Wetz, D.A.; IEEE Transactions on Plasma Science, Volume 36, Issue 5, Part 3, Oct. 2008 Page(s):2738 – 2746 Digital Object Identifier 10.1109/TPS.2008.2004228.
- (42) Imaging of the Explosive Emission Cathode Plasma in a Vircator High-Power Microwave Source Walter, J.; Mankowski, J.; Dickens, J.; IEEE Transactions on Plasma Science Volume 36, Issue 4, Part 1, Aug. 2008 Page(s):1388 - 1389 Digital Object Identifier 10.1109/TPS.2008.924489.

- (43) Optimization of a low jitter, 50 kV, 100 Hz triggered spark gap with high pressure gas mixtures, Chen, Y.; Dickens, J.; Mankowski, J.; Kristiansen, M.; IEEE Transactions on Dielectrics and Electrical Insulation, Volume 16, Issue 4, August 2009 Page(s):971 – 978 Digital Object Identifier 10.1109/TDEI.2009.5211842.
- (44) Optimization of an FCG-Based High-Power Microwave System Using Nonexplosive Pulsed Power, Davis, C. B.; Neuber, A. A.; Young, A.; Walter, J.; Dickens, J. C.; Kristiansen, M.; Plasma Science, IEEE transactions on Volume 37, Issue 12, Part 2, Dec. 2009 Page(s):2321 - 2327 Digital Object Identifier 10.1109/TPS.2009.2033602.
- (45) Recent Advances in Explosive Pulsed Power, L.L. Algilbers, A.H. Stults, J. Dickens, et. al., Journal of Directed Energy, Vol. 3, No. 2, Spring 2009, pg 149.
- (46) High electric field packaging of silicon carbide photoconductive switches Hettler, C.; James, C.; Dickens, J.; Pulsed Power Conference, 2009. PPC '09. IEEE June 28 2009-July 2 2009 Page(s):631-634 Digital Object Identifier 10.1109/PPC.2009.5386380.
- (47) VUV Emission and Streamer Formation in Pulsed Dielectric Surface Flashover at Atmospheric Pressure, Rogers, T.G.; Neuber, A.A.; Frank, K.; Laity, G.R.; Dickens, J.C.; IEEE Transactions on Plasma Science, Volume: 38 , Issue: 10 , Part: 1 Digital Object Identifier: 10.1109/TPS.2010.2059714 Publication Year: 2010 , Page(s): 2764 – 2770.
- (48) Design and Evaluation of a Compact Silicon Carbide Photoconductive Semiconductor Switch, James, C.; Hettler, C.; Dickens, J.; IEEE Transactions on Electron Devices, Volume: 58 , Issue: 2 Digital Object Identifier: 10.1109/TED.2010.2089689 Publication Year: 2011 , Page(s): 508 – 511.
- (49) Pulsed magnetic field excitation sensitivity of match-type electric blasting caps, Parson J., Dickens J., Walter J., et al., REVIEW OF SCIENTIFIC INSTRUMENTS Volume: 81 Issue: 10 Article Number: 105115 OCT 2010.

Book Chapters

- (1) Explosively Driven Pulsed Power, Helical Magnetic Flux Compression Generators”, A. Neuber Edtr., Springer Berlin Heidelberg New York, ISBN 3-540-26051-X, 2005.

Conference Proceedings and Presentations

- (1) “Insulator and Electrode Mass Erosion and Surface Voltage Holdoff Recovery for a Transient, High Current Surface Discharges,” Proceedings of the 6th EML Conference, April 1991 (with T. G. Engel and M. Kristiansen).
- (2) “Electrode Performance of a Three Electrode Triggered High Energy Spark Gap Switch,” Proceedings of the 9th IEEE International Pulsed Power Conference, Albuquerque, NM, June 21-23, pp 471-474 (with T. Engel and M. Kristiansen).
- (3) “Characterization of a Novel Single-Gap Transformer Coupled L-C Generator,” Proceedings of the 20th IEEE Power Modulator Symposium, Myrtle Beach, SC, June 23-25, 1992, p. 293 (with T. Engel and M. Kristiansen).
- (4) “Communications Impact of Hall Plasma Thrusters,” AIAA-95-2929, 31st AIAA Joint Propulsion Conference. San Diego CA, July 10-12, 1995, 95-2929 (with J. Mankowski, E. O’Hair, and M. Kristiansen).
- (5) “Instrumentation and Data Acquisition of the Hall Thruster,” AIAA-95-2930, 31st AIAA Joint Propulsion Conference. San Diego CA, July 10-12, 1995, 95-2929 (with J. Mankowski, E. O’Hair, and M. Kristiansen).
- (6) “Plume Model of Hall Effect Plasma Thrusters with Temporal Consideration,” XXIV International Electric Propulsion Conference, Moscow, Russia, September 19-23, 1995 (with E. O’Hair, and M. Kristiansen).
- (7) “Compact Modulator Using Inductive Energy Storage and a Solid State Opening Switch,” Proceedings of the 22nd International Power Modulator Symposium, Boca Raton, Florida, June 1996 (with J. Bridges and M. Kristiansen).

- (8) "Breakdown at Window Interfaces Caused by High-Power Microwave Fields," Intense Microwave Pulses IV, SPIE Proceedings, Volume 2843, Denver, Colorado, August 1996 (with J. Elliott, L.L. Hatfield, M. Kristiansen, and H. Krompholz).
- (9) "Window and Cavity Breakdown Caused by High Power Microwaves," Presented at the 24th IEEE International Conference on Plasma Science, San Diego, CA, May 1997 (with A. Neuber, D. Hemmert, H. Krompholz, L.L. Hatfield and M. Kristiansen).
- (10) "High Voltage Subnanosecond Dielectric Breakdown," Proceedings of the International Workshop on High Power Microwave Generation and Pulse Shortening, Edinburgh, Scotland, June 1997 (with J. Mankowski and M. Kristiansen).
- (11) "Breakdown at Window Interfaces Caused by High-Power Microwave Fields," Proceedings of the International Workshop on High Power Microwave Generation and Pulse Shortening, Edinburgh, Scotland, June 1997 (with A. Neuber, D. Hemmert, L.L. Hatfield, M. Kristiansen, and H. Krompholz).
- (12) "Evaluation of a Russian SOS Diode for Use in a Compact Modulator System," Proceedings of the 11th IEEE International Pulsed Power Conference, Baltimore, Maryland, June 29 - July 02, 1997 (with M. Kristiansen, M. Giesselmann and J.G. Kim).
- (13) "Window and Cavity Breakdown Caused by High-Power Microwave Fields," Proceedings of the 11th IEEE International Pulsed Power Conference, Baltimore, Maryland, June 29 - July 02, 1997 (with A. Neuber, D. Hemmert, L.L. Hatfield, M. Kristiansen, and H. Krompholz).
- (14) "Streamer Discharges by Pulsed Power on a Spiral Transmission Line," Proceedings of the 11th IEEE International Pulsed Power Conference, Baltimore, Maryland, June 29 - July 02, 1997 (with H. Akiyama, T. Sueda, S. Tsukamoto, Y. Nishihashi, S. Katsuki, M. Hagler and N. Inoue).
- (15) "A Subnanosecond High Voltage Pulser for the Investigation of Dielectric Breakdown," Proceedings of the 11th IEEE International Pulsed Power Conference, Baltimore, Maryland, June 29 - July 02, 1997 (with J. Mankowski and M. Kristiansen).
- (16) "Development of Improved Triggered Vacuum Switches," Submitted to International Workshop on Electromagnetic Launchers, Edinburgh, Scotland, 1998 (with T. Warren, M. Kristiansen, et.al.).
- (17) "High-Power Microwave Generation by Coaxial Vircator," Proc. 12th IEEE International Pulsed Power Conference, Monterey, CA, June 27-30, 1999 (with W. Jiang, K. Woolverton, M. Kristiansen).
- (18) "Energy Efficiency Analysis of an Inductive Storage System," Proc. 12th IEEE International Pulsed Power Conference, Monterey, CA, June 27-30, 1999 (with J.G. Kim, J. Zhang, M. Giesselmann, M. Kristiansen, and J. Mankowski).
- (19) "The Design of a Compact Pulse Transformer," Proc. 12th IEEE International Pulsed Power Conference, Monterey, CA, June 27-30, 1999 (with J. Zhang, M. Kristiansen, M. Giesselmann, J. Mankowski, D. Castro, and D. Garcia).
- (20) "Pulsed Power Conditioning with a Transformer for an Inductive Energy Storage System," Proc. 12th IEEE International Pulsed Power Conference, Monterey, CA, June 27-30, 1999 (with J. Zhang, M. Giesselmann, M. Kristiansen, J. Mankowski, D. Castro, and D. Garcia).
- (21) "Pulsed Power Generation Using Ferromagnetic Circuits," Proc. 12th IEEE International Pulsed Power Conference, Monterey, CA, June 27-30, 1999 (with S.I. Shkuratov, M. Kristiansen, L.L. Hatfield, and R. Martin).
- (22) "Pulsed, High Energy Testing of Resistors," Proc. 12th IEEE International Pulsed Power Conference, Monterey, CA, June 27-30, 1999 (with S.I. Shkuratov, M. Kristiansen, L.L. Hatfield, and E. Horrocks).
- (23) High Voltage Subnanosecond Corona Inception," Proc. 12th IEEE International Pulsed Power Conference, Monterey, CA, June 27-30, 1999 (with J. Mankowski, M. Kristiansen, J. Lehr, W. Prather, and J. Gaudet).
- (24) Optical Diagnostics on Helical Flux Compression Generators," Proc. 12th IEEE International Pulsed Power Conference, Monterey, CA, June 27-30, 1999 (with A. Neuber, M. Kristiansen and H. Krompholz).

- (25) "Simulation, Design and Test of a MOV Pulse Shaping Device for High Power Microwave Generators," Proc. 12th IEEE International Pulsed Power Conference, Monterey, CA, June 27-30, 1999 (with M. Giesselmann, M. Kristiansen, and E. Kristiansen).
- (26) "High Power Microwave Window Breakdown Under Vacuum and Atmospheric Conditions", SPIE's International Symposium on AeroSense, (Intense Microwave Pulsed VII", 24-28, April 2000, Orlando, FL (with D. Hemmert, A. Neuber, M. Kristiansen, H. Krompholz, L.L. Hatfield).
- (27) "Fundamental Studies of a Helical Magnetic Flux Compression Generator," 13th International Conference on High-Power Particle Beams, Nagaoka, Japan, June 25-30, 2000. (with M. Kristiansen and A. Neuber).
- (28) "Energy Balance of Shock Wave Ferromagnetic Generators," Proceedings of 12th Symposium on High Current Electronics, Tomsk, Russia, Sept. 24-29, 2000 (with S.I. Shkuratov and M. Kristiansen).
- (29) "Dielectric/Gas Interface Breakdown Caused by High Power Microwaves," 13th International Conference on High-Power Particle Beams, June 2000, Nagaoka, Japan (with D. Hemmert, A. Neuber, H. Krompholz, M. Kristiansen and L.L. Hatfield). (Invited).
- (30) "Helical Flux Compression Generator for Basic Research," Proc. 12th Symposium on High Current Electronics, Tomsk, Russia, Sept. 24-29, 2000 (with A. Neuber, M. Kristiansen, M. Giesselman, B. Freeman, P. Worsley, and H. Krompholz).
- (31) "3-D PIC Simulation of a Coaxial Vircator," 13th International Conference on High-Power Particle Beams, June 2000, Nagaoka, Japan (with W. Jiang (Nagaoka University of Technology), and M. Kristiansen).
- (32) "High-Power Microwave Generation by a Coaxial Vircator," 13th International Conference on High-Power Particle Beams, June 2000, Nagaoka, Japan (with W. Jiang (Nagaoka University of Technology), and M. Kristiansen).
- (33) "Pulsed Power Systems", Encyclopedia of Physical Science and Technology, Third Edition edited by Robert A. Meyers, Vol. 13 (2001), Academic Press, Inc., San Diego, CA (with M. Kristiansen).
- (34) "A Completely Explosive Pulsed Power Mini-System", Submitted for publication in the Review of Scientific Instruments, 2002, RSI MS # A02449 (with E.F. Talantsev, S.I. Shkura-tov, and M. Kristiansen).
- (35) "Autonomous Ultra-Compact Explosive-Driven High-Voltage Generator Based on a Trans-verse Shock Wave Demagnetization of Nd₂Fe₁₄B Hard Ferromagnetics", Submitted for publication in the Review of Scientific Instruments, 2002, RSI MS # A02200 (with S.I. Shkura-tov, E.F. Talantsev, and M. Kristiansen).
- (36) "Pre-Breakdown Current Behavior In Dc Volume Breakdown In Transformer Oil," Proceedings of the 14th IEEE Pulsed Power Conference, Dallas, TX, June 15-18, 2003, p. 289-292. (with M. Butcher, A. Neuber, and H. Krompholz).
- (37) "Optical Diagnostics Of Liquid Nitrogen Volume Pre-Breakdown Events," Proceedings of the 14th IEEE Pulsed Power Conference, Dallas, TX, June 15-18, 2003, p. 1029-1032. (with M. Butcher, A. Neuber, and H. Krompholz).
- (38) "Pulsed And Self Electrical Breakdown In Biodegradable Oil," Proceedings of the 14th IEEE Pulsed Power Conference, Dallas, TX, June 15-18, 2003, p. 1036-1039. (with M. Cevallos, A. Neuber, M. Haustein, and H. Krompholz).
- (39) "Physical Efficiency Limits Of Inch-Sized Helical MFCG's," Proceedings of the 14th IEEE Pulsed Power Conference, Dallas, TX, June 15-18, 2003, p. 413-416. (with A. Neuber, T. Holt, J. Hernandez, and M. Kristiansen).
- (40) "Small Sized MFCG For Driving A High Impedance Load," Proceedings of the 14th IEEE Pulsed Power Conference, Dallas, TX, June 15-18, 2003, p. 1065-1068. (J. Hernandez, A. Neuber and M. Kristiansen).
- (41) "Ferromagnetic and Ferroelectric Materials as Seed Sources for Magnetic Flux Compressors," Proceedings of the 14th IEEE Pulsed Power Conference, Dallas, TX, June 15-18, 2003, 1069-1072. (with N. Schoeneberg, J. Walter, A. Neuber, and M. Kristiansen).

- (42) “Design Criteria For Prevention Of Armature “Turn-Skipping” In Helical Magnetic Flux Compression Generators,” Proceedings of the 14th IEEE Pulsed Power Conference, Dallas, TX, June 15-18, 2003, p. 1077-1080. (with J. Rasty, X. Lee, A. Neuber, and M. Kristiansen).
- (43) “Conductivity Measurements Of Explosively Shocked Aluminum And OFHC Copper Used For Armature Material In A Magnetic Flux Compression Generator,” Proceedings of the 14th IEEE Pulsed Power Conference, Dallas, TX, June 15-18, 2003, p. 1073-1076. (with D. Hemmert, J. J. Mankowski, A. Neuber, J. Rasty, and M. Kristiansen).
- (44) “Surface Flashover Across Ceramic Disks In Vacuum At Cryogenic Temperatures,” Proceedings of the 14th IEEE Pulsed Power Conference, Dallas, TX, June 15-18, 2003, p. 305-308. (with H. Keene, A. Neuber, and H. Krompholz).
- (45) Physics Of Dielectric Surface Flashover At Atmospheric Pressure,” Proceedings of the 14th IEEE Pulsed Power Conference, Dallas, TX, June 15-18, 2003, p. 285-283. (with J. Krile, A. Neuber, J. Dickens, and H. Krompholz).
- (46) “Nanosecond Laser-Triggered Microwave Switch,” Proceedings of the 14th IEEE Pulsed Power Conference, Dallas, TX, June 15-18, 2003, p. 309-312. (with M. McQuage and A. Neuber).
- (47) “Short Pulse Electric Field Sterilization of Liquid Media,” Proceedings of the 14th IEEE Pulsed Power Conference, Dallas, TX, June 15-18, 2003, p. 1124-1127. (with D. Wetz, K. Truman, J.J. Mankowski, and A. Neuber).
- (48) “Electrical Breakdown in Transformer Oil,” Joint Fall Meeting of the Texas Sections of the APS and AAPT and Zone 13 Society of Physics Students, Lubbock, TX, Oct 2003 (abstract only published) (with M. Cevallos, A. Neuber, and H. Krompholz).
- (49) G. Edmiston, A. Neuber, H. Krompholz, J. Dickens, J. Krile, "High Power Microwave Surface Flashover of a Gas-Dielectric Interface at 90 to 760 Torr," Proceedings of the 15th Int. IEEE Pulsed Power Conference, Monterey, CA, June 13-17, 2005.
- (50) J. Krile, A. Neuber, J. Dickens, H. Krompholz, G. Edmiston, “Similarities of Dielectric Surface Flashover at Atmospheric Conditions for Pulsed Unipolar and RF Excitation,” Proceedings of the 15th Int. IEEE Pulsed Power Conference, Monterey, CA, June 13-17, 2005.
- (51) H. Krompholz, L.L. Hatfield, A. Neuber, D. Hemmert, K. Kohl, J. Chaparro, “Subnanosecond Breakdown in Argon at High Overvoltages,” Proceedings of the 15th Int. IEEE Pulsed Power Conference, Monterey, CA, June 13-17, 2005.
- (52) J. Qian, R.P. Joshi, J.F. Kolb, K.H. Schoenbach, J. Dickens, A. Neuber, M. Butcher, M. Cevallos, H. Krompholz, E. Schamiloglu, J. Gaudet, “Simulation Studies of Liquid Water Breakdown by a Sub-Microsecond Pulse,” Proceedings of the 15th Int. IEEE Pulsed Power Conference, Monterey, CA, June 13-17, 2005.
- (53) H. Veselka, A. Neuber, J. Dickens, “Shock Induced Conductivity for High Power Switching,” Proceedings of the 15th IEEE Pulsed Power Conference, Monterey, CA, June 13-17, 2005.
- (54) M. Butcher, M. Cevallos, A. Neuber, H. Krompholz, J. Dickens, “Investigation of Charge Conduction and Self-Breakdown in Transformer Oil,” Proceedings of the 15th Int. IEEE Pulsed Power Conference, Monterey, CA, June 13-17, 2005.
- (55) A.A. Neuber, Y.J. Chen, J.C. Dickens, M. Kristiansen, “A Compact, Repetitive, 500 kV, 500 J, Marx Generator,” Proceedings of the 15th Int. IEEE Pulsed Power Conference, Monterey, CA, June 13-17, 2005.
- (56) Y.J. Chen, J.J. Mankowski, A. Neuber, J.C. Dickens, “A Low-Cost Metallic Cathode for a Vircator HPM Source,” to be published in Proceedings of the 15th Int. IEEE Pulsed Power Conference, Monterey, CA, June 13-17, 2005.
- (57) D. Belt, J. Dickens, J. Mankowski, A. Neuber, “Multistage Helical Flux Compression Generator Non-Explosive Test Bed,” Proceedings of the 15th Int. IEEE Pulsed Power Conference, Monterey, CA, June 13-17, 2005.
- (58) M.D. Cevallos, M.D. Butcher, J.C. Dickens, A.A. Neuber, H.G. Krompholz, “Bubble Dynamics and Channel Formation for Cathode Initiated Discharges in Transformer Oil,” Proceedings of the 15th Int. IEEE Pulsed Power Conference, Monterey, CA, June 13-17, 2005.

- (59) M.D. Cevallos, M.D. Butcher, J.C. Dickens, A.A. Neuber, H.G. Krompholz, "Composite Shadowgraphy and Luminosity Images of Self Breakdown Discharge Channels in Transformer Oil," Proceedings of the 15th Int. IEEE Pulsed Power Conference, Monterey, CA, June 13-17, 2005.
- (60) A. Neuber, J. Krile, G. Edmiston, H. Krompholz, J. Dickens, "Limits of High Power Microwave Transmission due to Interface Breakdown," presented (oral) at 2005 Tri-Service VED Workshop, 12-16 September 2005.
- (61) A. Neuber, G. Edmiston, J. Krile, K. Morales, J. Dickens, H. Krompholz, "High Power Microwave Breakdown Limits of Dielectric/Gas Interfaces," 2005 International COE Forum on Pulsed Power Science will be held on November 13 – 14 at Kumamoto, Japan. (invited).
- (62) A. Neuber, J. Krile, G. Edmiston, H. Krompholz, J. Dickens, M. Kristiansen, "Interface Breakdown During High Power Microwave Transmission," 13th EML Symposium, May 22-25, 2006, Berlin, Germany.
- (63) Lynn, C.; Neuber, A.; Dickens, J, "Opening Switch Utilizing Shock Wave Induced Conduction in PMMA and PVC," Pulsed Power Plasma Science Conference, 2007. PPPS 2007. IEEE June 17 2007-April 22 2007 Page(s):556 - 556 Digital Object Identifier 10.1109/PPPS.2007.4345862.
- (64) Karhi, Ryan W.; Mankowski, John J.; Dickens, James C, "A Synchronous Free-Running Arc Distributed Energy Railgun," Pulsed Power Plasma Science Conference, 2007. PPPS 2007. IEEE June 17 2007-April 22 2007 Page(s):1016 - 1016 Digital Object Identifier 10.1109/PPPS.2007.4346322.
- (65) Chen, Hao; Jiang, Chunqi; Kuthi, Andras; Gundersen, Martin A.; Dickens, James, "Small Back-Lighted Thyratrons," Pulsed Power Plasma Science Conference, 2007. PPPS 2007. IEEE June 17 2007-April 22 2007 Page(s):430 - 430 Digital Object Identifier 10.1109/PPPS.2007.4345736.
- (66) James, Colt; Dickens, James C.; Holt, Shad, "Evaluation of Switch Jitter on a High Pressure Coaxial Spark Gap," Pulsed Power Plasma Science Conference, 2007. PPPS 2007. IEEE June 17 2007-April 22 2007 Page(s):429 - 429 Digital Object Identifier 10.1109/PPPS.2007.4345735.
- (67) McCauley, D.; Belt, D.; Mankowski, J.; Dickens, J.; Neuber, A.; Kristiansen, M, "Electro-Explosive Fuse Optimization for Helical Flux Compression Generator using a Non-Explosive Test Bed," Pulsed Power Plasma Science Conference, 2007. PPPS 2007. IEEE June 17 2007-April 22 2007 Page(s):656 - 656 Digital Object Identifier 10.1109/PPPS.2007.4345962 .
- (68) Belt, D.; Walter, J.; Mankowski, J.; Dickens, J,"Modeling of a Single Element Pulsed Ring-Down Antenna for Implementation in a Phased Array System," Pulsed Power Plasma Science Conference, 2007. PPPS 2007. IEEE June 17 2007-April 22 2007 Page(s):816 - 816 Digital Object Identifier 10.1109/PPPS.2007.4346122.
- (69) Walter, J.; Dickens, J.; Mankowski, J.; Kristiansen, M,"Theoretical Pulsed Ring Down Antenna Array Performance" Pulsed Power Plasma Science Conference, 2007. PPPS 2007. IEEE June 17 2007-April 22 2007 Page(s):482 - 482 Digital Object Identifier 10.1109/PPPS.2007.4345788.
- (70) Chen, Yeong-Jer; Mankowski, John J.; Walter, John W.; Dickens, James C "Jitter and Recovery Rate of a Triggered Spark Gap with High Pressure Gas Mixtures," Pulsed Power Plasma Science Conference, 2007. PPPS 2007. IEEE June 17 2007-April 22 2007 Page(s):255 - 255 Digital Object Identifier 10.1109/PPPS.2007.4345561.
- (71) Walter, J.; Dickens, J.; Kristiansen, M,"Electrical and Optical Measurements of Explosively Driven Plasma Jets," Pulsed Power Plasma Science Conference, 2007. PPPS 2007. IEEE June 17 2007-April 22 2007 Page(s):723 - 723 Digital Object Identifier 10.1109/PPPS.2007.4346029.
- (72) Holt, Shad L.; Krile, John T.; Hemmert, David J.; Hackenberger, Wesley S.; Alberta, Edward F.; Walter, John W.; Dickens, James C.; Altgilbers, Larry L.; Stults, Allen H "Testing of New Ferroelectric Elements Custom Engineered for Explosively Driven Ferroelectric Generator Applications," Pulsed Power Plasma Science Conference, 2007. PPPS 2007. IEEE June 17 2007-April 22 2007 Page(s):722 - 722 Digital Object Identifier 10.1109/PPPS.2007.4346028.
- (73) Krile, John T.; Holt, Shad L.; Hemmert, David J.; Walter, John W.; Dickens, James C.; Altgilbers, Larry L.; Stults, Allen H "Development of an Ultra-Compact Explosively Driven Magnetic Flux

- Compression Generator System,” Pulsed Power Plasma Science Conference, 2007. PPS 2007. IEEE June 17 2007-April 22 2007 Page(s):721 - 721 Digital Object Identifier 10.1109/PPPS.2007.4346027.
- (74) Veselka, H.; Neuber, A.; Dickens, J “Pressure Induced Conductivity for High Power Switching,” Power Modulator Symposium, 2006. Conference Record of the 2006 Twenty-Seventh International 14-18 May 2006 Page(s):219 - 219 Digital Object Identifier 10.1109/MODSYM.2006.365221.
- (75) Opening Switch Utilizing Stress Induced Conduction in Polymethylmethacrylate Lynn, C.; Krile, J.; Neuber, A.; Dickens, J.; IEEE International Power Modulators and High Voltage Conference, Proceedings of the 2008 27-31 May 2008 Page(s):483 - 486 Digital Object Identifier 10.1109/IPMC.2008.4743696.
- (76) A 50 kV, 100 Hz Low Jitter Triggered Spark Gap with High Pressure Gas Mixtures Chen, Yeong-Jer; Mankowski, John J.; Dickens, James C.; Walter, John; Kristiansen, Magne; IEEE International Power Modulators and High Voltage Conference, Proceedings of the 2008 27-31 May 2008 Page(s):197 - 200 Digital Object Identifier 10.1109/IPMC.2008.4743614.
- (77) Energy Deposition and Electromagnetic Compatibility Assessment of Electroexplosive Devices Parson, J.; Dickens, J.; Walter, J.; Neuber, A.; IEEE International Power Modulators and High Voltage Conference, Proceedings of the 2008 27-31 May 2008 Page(s):439 - 442 Digital Object Identifier 10.1109/IPMC.2008.4743684.
- (78) Analysis of Mesoband Single Element Pulsed Ring-Down Antennas for Implementation in Phased Array Systems Belt, D.; Mankowski, J.; Walter, J.; Dickens, J.; Kristiansen, M.; IEEE International Power Modulators and High Voltage Conference, Proceedings of the 2008 27-31 May 2008 Page(s):152 - 155 Digital Object Identifier 0.1109/IPMC.2008.4743602.
- (79) A Compact, Self-Contained High Power Microwave Source Based on a Reflex-Triode Vircator and Explosively Driven Pulsed Power Young, A.; Holt, T.; Elsayed, M.; Walter, J.; Dickens, J.; Neuber, A.; Kristiansen, M.; Altgilbers, L.L.; Stults, A.H.; IEEE International Power Modulators and High Voltage Conference, Proceedings of the 2008 27-31 May 2008 Page(s):147 - 150 Digital Object Identifier 10.1109/IPMC.2008.4743600.
- (80) Window Flashover Initiation under Pulsed Microwave Excitation Krile, J.; Edmiston, G.; Dickens, J.; Krompholz, H.; Neuber, A.; IEEE International Power Modulators and High Voltage Conference, Proceedings of the 2008 27-31 May 2008 Page(s):560 - 563 Digital Object Identifier 10.1109/IPMC.2008.4743719.
- (81) Scaling and Improvement of Compact Explosively-Driven Ferroelectric Generators Bolyard, D.; Neuber, A.; Krile, J.; Walter, J.; Dickens, J.; Kristiansen, M.; IEEE International Power Modulators and High Voltage Conference, Proceedings of the 2008 27-31 May 2008 Page(s):49 - 52 Digital Object Identifier 10.1109/IPMC.2008.47.
- (82) Shock Wave Simulation of Ferrite-Filled Coaxial Nonlinear Transmission Lines Sullivan, W.; Dickens, J.; Kristiansen, M.; IEEE International Power Modulators and High Voltage Conference, Proceedings of the 2008 27-31 May 2008 Page(s):517 - 520 Digital Object Identifier 10.1109/IPMC.2008.4743706.
- (83) High-Current Compact FCG Seed Source Implementing Solid State Switching Elsayed, M.; Holt, T.; Young, A.; Neuber, A.; Dickens, J.; Kristiansen, M.; Altgilbers, L.L.; Stults, A.H.; IEEE International Power Modulators and High Voltage Conference, Proceedings of the 2008 27-31 May 2008 Page(s):25 - 28 Digital Object Identifier 10.1109/IPMC.2008.4743567.
- (84) Compact Silicon Carbide Switch For High Voltage Operation James, C.; Hettler, C.; Dickens, J.; Neuber, A.; IEEE International Power Modulators and High Voltage Conference, Proceedings of the 2008 27-31 May 2008 Page(s):17 - 20 Digital Object Identifier 10.1109/IPMC.2008.4743565.
- (85) Jitter and recovery rate of a 50 kV, 100 Hz triggered spark gap with high pressure gas mixtures Yeong-Jer Chen; Mankowski, J.J.; Walter, J.W.; Dickens, J.C.; Plasma Science, 2008. ICOPS 2008. IEEE 35th International Conference on 15-19 June 2008 Page(s):1 - 1 Digital Object Identifier 10.1109/PLASMA.2008.4590809.

- (86) Jitter and recovery rate of a triggered spark gap with high pressure gas mixtures Chen, Yeong-Jer; Dickens, J.; Walter, J.; Kristiansen, M.; Pulsed Power Conference, 2009. PPC '09. IEEE June 28 2009-July 2 2009 Page(s):244 - 249 Digital Object Identifier 10.1109/PPC.2009.5386309.
- (87) High electric field packaging of silicon carbide photoconductive switches Hettler, C.; James, C.; Dickens, J.; Pulsed Power Conference, 2009. PPC '09. IEEE June 28 2009-July 2 2009 Page(s):631 - 634 Digital Object Identifier 10.1109/PPC.2009.5386380.
- (88) High voltage photoconductive switches using semi-insulating, vanadium doped 6H-SiC, James, C.; Hettler, C.; Dickens, J.; Pulsed Power Conference, 2009. PPC '09. IEEE June 28 2009-July 2 2009 Page(s):283 - 286 Digital Object Identifier 10.1109/PPC.2009.5386303.
- (89) Stand-alone, FCG-driven High Power Microwave system Young, A.; Neuber, A.; Elsayed, M.; Walter, J.; Dickens, J.; Kristiansen, M.; Altgilbers, L.L.; Pulsed Power Conference, 2009. PPC '09. IEEE. June 28 2009-July 2 2009 Page(s):292 - 296 Digital Object Identifier 10.1109/PPC.2009.5386301.
- (90) VUV emission from dielectric surface flashover at atmospheric pressure Rogers, G.; Neuber, A.; Laity, G.; Dickens, J.; Frank, K.; Schramm, T.; Pulsed Power Conference, 2009. PPC '09. IEEE June 28 2009-July 2 2009 Page(s):855 - 859 Digital Object Identifier 10.1109/PPC.2009.5386373.
- (91) Electrical conduction in select polymers under shock loading Lynn, C.; Neuber, A.; Krile, J.; Dickens, J.; Kristiansen, M.; Pulsed Power Conference, 2009. PPC '09. IEEE June 28 2009-July 2 2009 Page(s):171 - 174 Digital Object Identifier 10.1109/PPC.2009.5386199.
- (92) Performance of a compact triode vircator and Marx generator system Walter, J.; Dickens, J.; Kristiansen, M.; Pulsed Power Conference, 2009. PPC '09. IEEE June 28 2009-July 2 2009 Page(s):133 - 137 Digital Object Identifier 10.1109/PPC.2009.5386184.
- (93) Energy deposition assessment and electromagnetic evaluation of electroexplosive devices in a pulsed power environment Parson, J.; Dickens, J.; Walter, J.; Neuber, A.; Pulsed Power Conference, 2009. PPC '09. IEEE June 28 2009-July 2 2009 Page(s):892 - 896 Digital Object Identifier 10.1109/PPC.2009.5386262.
- (94) A compact 5kV battery-capacitor seed source with rapid capacitor charger Holt, S. L.; Dickens, J. C.; McKinney, J. L.; Kristiansen, M.; Pulsed Power Conference, 2009. PPC '09. IEEE June 28 2009-July 2 2009 Page(s):897 - 901 Digital Object Identifier 10.1109/PPC.2009.5386260.
- (95) Optimizing power conditioning components for a Flux Compression Generator using a non-explosive testing system Davis, C.; Neuber, A.; Young, A.; Walter, J.; Dickens, J.; Kristiansen, M.; Pulsed Power Conference, 2009. PPC '09. IEEE June 28 2009-July 2 2009 Page(s):951 - 955 Digital Object Identifier 10.1109/PPC.2009.5386110.
- (96) Prediction of compact explosively-driven ferroelectric generator performance Bolyard, D.; Neuber, A.; Krile, J.; Dickens, J.; Kristiansen, M.; Pulsed Power Conference, 2009. PPC '09. IEEE June 28 2009-July 2 2009 Page(s):167 - 170 Digital Object Identifier 10.1109/PPC.2009.5386196.
- (97) Low jitter triggered spark gap with high pressure gas mixtures and Kr85 Yeong-Jer Chen; Dickens, J.C.; Walter, J.W.; Kristiansen, M.; Plasma Science - Abstracts, 2009. ICOPS 2009. IEEE International Conference on 1-5 June 2009 Page(s):1 - 1 Digital Object Identifier 10.1109/PLASMA.2009.5227620.
- (98) Vacuum ultraviolet spectroscopy of dielectric surface flashover at atmospheric pressure Laity, G.; Frank, K.; Rogers, G.; Kristiansen, M.; Dickens, J.; Neuber, A.; Schramm, T.; Plasma Science - Abstracts, 2009. ICOPS 2009. IEEE International Conference on 1-5 June 2009 Page(s):1 - 1 Digital Object Identifier 10.1109/PLASMA.2009.5227565.
- (99) Spectral analysis of vacuum ultraviolet emission from pulsed atmospheric discharges, Laity, G.; Neuber, A.; Rogers, G.; Frank, K.; Hatfield, L.; Dickens, J.; Plasma Science, 2010 Abstracts IEEE International Conference on Digital Object Identifier: 10.1109/PLASMA.2010.5534416 Publication Year: 2010 , Page(s): 1 IEEE Conferences.

Laurence Andrew Dobrot

Executive Profile

Over 25 years of successful leadership, program management and systems engineering excellence with a reputation for building teams and getting the job done. Experienced Air Force leader with assignments in both the aircraft and space fields.

Highlights of Qualifications

Security Clearance: Top Secret/SCI (2007)	Systems Engineering
Certified Defense Program Manager (Lvl 3)	Risk Analysis
Team Building and Leadership	Budget and Cost Control
Personnel Development	Resource Management
Strategic Planning	Public Speaking
Systems Planning, Research, Development and Engineering (SPRDE Lvl 3)	

Professional History

Leadership/Team Work

- Deputy Program Director for the \$5B Airborne Laser weapon system, part of the Missile Defense Agency
 - Commanded a 200-person team of military, government civilians, support contractors and the 1,000-member prime contracting team that delivered the largest and most complex airborne laser weapon system in the world.
 - The Airborne Laser demonstrated lethal capability in shooting down threat representative ballistic missiles.
 - Managed all elements of cost, schedule and system performance.
 - Briefed members of Congress, Senior Defense Staff and Combatant Commanders on program plan and progress.
- Led a 100-member Military Space Plane Integrated Concept Team for Air Force Space Command.
 - Worked closely with NASA and the Air Force Research Labs to define missions, requirements, concepts, funding and technologies for the Air Force's reusable space architecture.
 - The Air Force recently launched an X-37B Orbital Test Vehicle, which is a direct result of the team's development work.
- Air Force's Protection Functional Capabilities Boards working group lead.
 - Managed the Protection portfolio and guided the requirement documents through the Joint Capabilities Integration System process on their way to the Joint Requirements Oversight Council.

Program Management

- Managed the Engineering/Manufacturing Development contract for the Stage I rocket motor and flight termination system of the Small Inter-Continental Ballistic Missile.
 - Directed the 40-person team that managed the cost, schedule and technical performance.
- Developed and administered the Air Force's critical infrastructure program.
 - Authored the Air Force policy for identification and management of critical infrastructure. Represented the Air Force at national level Homeland Defense forums and guided Department of Defense senior staff in the development of policy.
- Oversaw the entire military education program for the Afghan Ministry of Defense and the Afghan National Army while stationed in Afghanistan.
 - Created from the ground up, a native language computer training center for the Afghan Ministry of Defense, tapped into the local underemployed youth to teach.

Systems Engineering

- Mechanical/structural engineer responsible for all aspects of design, repair, modification and support of both mechanical and structural systems for the C-5 fleet.
 - Designed and installed repairs for C-5 main frame forgings cracked and damaged during Desert Storm, and instituted them into a standard Engineer's Repair Manual for the C-5 fleet.
- Chief investigating engineer on a Titan-IVB and three C-5 aircraft Class A mishaps.
 - Determined most the probable cause for each event and engineered solutions to ensure these accidents would not reoccur.
- Designed and coordinated the organic modification of a T-43 navigational trainer into the European Team travel aircraft, at less than 10% of contractor's proposed costs.
- Defined and documented requirements for the Evolved Expendable Launch Vehicle.
 - Clearly communicated and documented the needs of the customer in a language that the developers and manufacturers could build and test to.
 - Built and staffed requirement documents that were approved by the Joint Requirements Oversight Council.

Problem Solving

- Masterminded a strategic plan that transitioned three major programs, 850 personnel and closed down a 40 year organization.
- Designed a set of modifications that eliminated fire propagation between the engines and pylons on the C-5 aircraft.

Education and Training

- Master of Science in Systems Management, University of Southern California
- Master of Strategic Studies, Army War College
- Master of Arts in National Security and Strategic Studies With Distinction, Naval War College
- Bachelor of Science in Mechanical Engineering, Michigan Technological University

Richard L. Fork
Optics Building 456
University of Alabama in Huntsville
Huntsville, Alabama 35899
forkr@uah.edu 256-824-2523 256-824-6618

Education

Ph.D. Physics: Mass. Inst. of Tech. (MIT), Cambridge, Massachusetts, 1962
Thesis title: "Role of Excited State Degeneracy in Dispersion Phenomena"
B.S. Physics: (summa cum laude), Principia College, Elmhurst, IL, 1957

Professional Career

Professor of Electrical and Computer Engineering, UAH, Huntsville, Alabama, 8/1994 to present
Professor of Physics, Rensselaer Polytechnic Institute, Troy, New York, 1990-1994
Member Technical Staff, AT&T Bell Labs, Holmdel, New Jersey, 1970-1990
Member Technical Staff, AT&T Bell Labs, Murray Hill, New Jersey, 1962-1970
Research Assistant, Physics Department, MIT, 1957-1962
Research Assistant, Naval Research Laboratory, Washington, D.C., Summer 1956

Teaching Experience at Universities

Have taught physics, electrical engineering, optics, and laser-related courses since 1994. Taught courses in undergraduate physics, photonics, and optics at RPI for 4 years. Graduated two Ph.D. students and one Masters Degree student at RPI. Graduated three Ph.D. students at UAH including the first black Ph.D. student in the optics program, currently supervising four Ph.D. students and one master's student at UAH. Developed new advanced optics laboratory course for undergraduate and graduate students. Have teaching evaluations consistently higher than average.

Professional Activities

Co-Chaired 7th Annual Ultrafast Conference in Huntsville 16-17 Jan 2004. Chair of sessions at professional meetings, such as, Optical Society of America, Physics of Quantum Electronics Give papers at many laser oriented conferences, such as, Directed Energy Professional Society, American Physical Society, International Astronautical Conference, and many others. Average one or more invited talks at domestic and international meetings per year, give 5-10 contributed talks or briefings talks at professional meetings and NASA, DOD meetings each year. Gave invited talk at 90th birthday celebration for Nobel Laureate Willis Lamb. Review journal articles and proposals for publications such as Optics Express. Have served on multiple NSF, NSF-SBIR, DOD and other review panels. Recently served with a NASA MSFC led discussion group addressing orbital debris mitigation. Served recently on a NASA Glenn Research Center led study of beamed energy for propulsion. A current focus area is the distribution of energy in space, such as for beamed optical energy propulsion, horizontal lift to orbit and beamed optical energy for change of orbit in space. Have consulted for SMDC regarding use of lasers for defense applications including both sensing and missile defense.

Research at University of Alabama in Huntsville

Manage Laser Science and Engineering Laboratory at University of Alabama in Huntsville. Typical funding sources to date have been DIA, NSF and NASA. Theme of current work is use of lasers for distribution of energy in space for debris removal and beamed energy for propulsion. A current focus area is design of laser based energy infrastructure for near Earth space intended to support orbit change, lift to orbit, and general distribution of energy in space by optical means.

Research at AT&T Bell Laboratories

Twenty seven years as a Member of Technical Staff at AT&T Bell Laboratories in the Communication Sciences Division. Efforts typically addressed the physics and engineering issues of time resolved optical phenomena using lasers with an emphasis on solid state materials and devices. Much of the work resulted in key original laser related inventions that played major roles in advancing capabilities multiple aspects of ultrashort pulse lasers. Demonstration of the first modelocked laser, invention of the colliding pulse modelocked laser that produced the first optical pulses well into the femtosecond time domain, the first femtosecond optical amplifier, gigawatt amplification of laser pulses, the first use of integrated self phase modulation, group velocity dispersion, saturable gain, and saturable absorption to produce (at that time) world record 27 fsec duration optical pulses, femtosecond white light continuum generation, ultrafast spectroscopy of the dynamics of semiconductor materials including the first study of the dynamics of quantum well materials, first measurement of velocity overshoot in semiconductors, first direct time resolved measurements of: exciton screening, band edge renormalization, and band filling. A number of world records were set including the generation of the first 6 femtosecond pulse. That record stood for ten years. Produced first femtosecond movie in 1986. Movie showed the ablation of material by intense femtosecond pulses. This has been an extremely active field since then and is now emerging as relevant to novel means of propulsion in space.

Honors and Awards

Fellow, American Physical Society, 1964
Fellow, Optical Society of America, 1995
Laser Focus Invention of the Year 1983 "Colliding Pulse Laser"
Most cited technical paper of 1964 in any journal (scanning interferometry)
UAH Outstanding Engineering Professor, 1995
World record shortest pulse, 6 fs, from 1987 to 1997

Sample Papers (of more than 100 published papers)

- (1) "Locking of He-Ne Laser Modes Induced by Synchronous Intracavity Modulation", L. E. Hargrove, R. L. Fork, and M. A. Pollack, Applied Physics Letters 5, 4-5 (1964). Original discovery of modelocked lasers.
- (2) "A Scanning Spherical Mirror Interferometer for Spectral Analysis of Laser Radiation", R. L. Fork, D. R. Herriott, and H. Kogelnik, Applied Optics 3, 1471-1484 (1964). Most cited paper in any journal in 1964.
- (3) "Real Time Autocorrelation Interferometer", R. L. Fork and F. A. Beisser, Applied Optics 17, 3534-3535 (1978). First real time ultrashort pulse measurement capability.
- (4) "Generation of Optical Pulses Shorter Than 0.1 Picoseconds by Colliding Pulse Modelocking", R. L. Fork, B. I. Greene, and C. V. Shank, Applied Physics Letters 38, 671-672 (1981). First optical pulse generation clearly in the femtosecond time regime.
- (5) "Amplification of 70 Femtosecond Optical Pulses to Gigawatt Powers", R.L. Fork, C. V. Shank, and R. T. Yen, Applied Physics Letters 41, 761-763 (1982).
- (6) "Femtosecond White Light Continuum Pulses", R. L. Fork, C. V. Shank, C. Hirlimann, and R. T. Yen, Optics Letters 8, 1-3 (1983).
- (7) "Femtosecond Optical Pulses", R. L. Fork, C. V. Shank, R. Yen, and C. Hirlimann, IEEE Journal of Quantum Electronics 19, 500-506 (1983).
- (8) "Negative Dispersion Using Pairs of Prisms", R. L. Fork, O. E. Martinez, and J. P. Gordon, Optics Letters 9, 150-152 (1984). First means of introducing negative dispersion, and hence dramatically improved intra-resonator ultrashort optical pulse generation.

- (9) "Femtosecond Imaging of Melting and Evaporation at a Photoexcited Silicon Surface", M. C. Downer, R. L. Fork, and C. V. Shank, *Journal of the Optical Society of America B* 2, 595-599 (1985). First femtosecond movies.
- (10) "Compression of Optical Pulses to 6 Femtoseconds by Using Cubic Phase Compensation", R. L. Fork, C. H. B. Cruz, P. C. Becker, and C. V. Shank, *Optics Letters* 12, 483-485 (1987). World record for ultrashort pulses which stood for ten years.
- (11) "Harmonically mode-locked laser and applications," R.L. Fork, K. Singh, J. Haus, R.K. Erdmann and S.T. Johns, *SPIE Proceedings, Photonics at the Air Force Photonics Center*, 2216 148-159 (1994).
- (12) "Optical Amplifier for Space Applications", Richard L. Fork, Spencer T. Cole, William M. Diffey, Lisa J. Gamble, and Andrew S. Keys. *Optics Express* 5, 292-301 (1999).
- (13) M.H. Smith, R.L. Fork, S.T. Cole, "Safe Delivery of optical power from space", *Optics Express* 8, 537-546 (2001).
- (14) R.L. Fork, R.L. Laycock, W.W. Walker, S.T. Cole, S.D. Moultrie, D.J. Phillips, and J.C. Reinhardt, "Surface High Energy Laser" (Invited Paper) *Proceedings of the IEEE*. 93, 1864-1873 (2005).
- (15) Richard L. Fork, "Preventing Asteroid Earth Impacts with Laser Technology: Progress and Future Prospects", (Invited paper) *Proceedings of the IEEE*, 95, No. 5, 847-8 (2007).
- (16) Dane J. Phillips, Rustin L. Laycock, Spencer T. Cole, Wesley W. Walker, Sean D. Moultrie, John C. Reinhardt, Richard L. Fork and Joe T. Howell, (Invited Paper) "Technology demonstrations and flight experiments validating an optical energy infrastructure for Earth–Moon space", *Acta Astronautica* 62, 185-191 (2008).
- (17) R.L. Fork and R. L. Laycock "Solid state laser medium and laser medium heat transfer method", US Patent 7,352,785, 2008.
- (18) Richard Fork, "Orbital Debris Mitigation Using Minimum Uncertainty Optical States", *Proceedings of the IEEE* 97 951-3, June 2009.
- (19) Richard Fork, Luke Burgess, Stefani Boehme, Pat Reardon, David Pollock, Matt Wright, Nick Cote, Randy Gaillard, and Raymond Beach, "Surveillance and Mitigation of Orbital Debris: Laser Systems and Standards", IAC-09-A6.5.9, 60th International Astronautical Congress, Daejeon, Republic of Korea, October 16, 2009.
- (20) Richard Fork, "Orbital Debris Mitigation Using Minimum Uncertainty Optical States", *Proceedings of the IEEE* 97 951-3, June 2009.
- (21) Planetary Defense and an Energy Infrastructure for Near Earth Space", *Proceedings of the IEEE*, 99, 359-362 (2011).

Dr. Jordin T. Kare
Kare Technical Consulting
908 15th Avenue East
Seattle, Washington 98112
jkare@jkare.com 206-805-9046

Experience

2007–Present, Founder and Chief Scientist, LaserMotive LLC

Co-founded LaserMotive LLC (<http://www.lasermotive.com>) to develop and market laser power beaming systems for industrial and military applications. Technical lead for LaserMotive development of the prize-winning power beaming system and climber vehicle for the NASA Centennial Challenge competition for Power Beaming, November 2009.

2007–Present, Scientific Program Manager and Senior Inventor, Intellectual Ventures LLC

Research program director for Intellectual Ventures Laboratories, and staff inventor for Intellectual Ventures, an intellectual property development company based in Bellevue, WA. Information on Intellectual Ventures is available at <http://www.intellectualventures.com>. Invention activities include inventing over a broad range of technologies, reviewing and prioritizing invention concepts for potential patenting, and supporting patent drafting and application processes. Past activities (2007-2008) included setting up Intellectual Ventures' laboratory facilities for broad-spectrum research and development (<http://www.intvenlab.com>), hiring and managing laboratory and support personnel, and leading selected research projects.

A notable project at Intellectual Ventures was the invention and initial development of the Photonic Fence, a system for detection, tracking, identification, and selective killing of insects, particularly disease-carrying mosquitoes, using digital imaging and laser technology.

1997–Present, Consultant, Kare Technical Consulting, sole proprietor

Consultant to aerospace companies and Federal laboratories on advanced space system architecture and design. Large customers include NASA (USRA), Northrop Grumman TASC, Boeing, General Atomics, and Lawrence Livermore National Laboratory. Small business customers include Tethers Unlimited, Andrews Space and Technology (superconducting cable design and evaluation for a novel deep-space propulsion system), ENSCO (global distributed microsensor network) and Proton Energy Systems (space applications of regenerative fuel cells). Particular areas of expertise include optical and radar imaging systems, and beamed power technology.

6/00–10/03, Payload Engineering support for Boeing Resource21 program

Responsible for developing requirements and technical interface to subcontractors for a \$100M-class multispectral sensor payload. Tasking included review and analysis of subcontractor's visible/NIR/SWIR FPA design and I&T program and preliminary design of thermal IR sensor. Key member of the Boeing team on CONESTOGA and CONESTOGA II, unclassified NRO-sponsored projects to develop concepts, architectures, and technology roadmaps for U.S. Intelligence community information systems in the 2005–2025 timeframe.

Two NASA Institute for Advanced Concepts (<http://www.niac.usra.edu>) Phase I Fellowship awards: modular laser launch architecture (2003–2004) and SailBeam, an innovative and technically-feasible propulsion concept for relativistic interstellar probes (2001).

1997, Chief Scientist, RDL Space Corp., San Ramon, California

Senior Research Scientist, RDL Inc., Culver City, California

As Sr. Research Scientist for RDL Inc., developed system architecture and sensor payload concept for major next-generation space system for a classified customer. Also a key participant in classified advanced space system concept study conducted by a major aerospace company, and in preparation of successful proposals for NASA LightSAR program and multiple classified programs. As Chief Scientist for fledgling RDL Space Corp., developed payload concepts for commercial space-based SAR imaging system and participated in development of business plan and DoC remote-sensing license application.

1995–1996, Physicist, V-Division Space Group, Physics and Space Technology Directorate, Lawrence Livermore National Laboratory (LLNL), Livermore, California

Lead designer for Tactical Imaging Constellation Architecture Studies; responsible for system concepts and point designs for military electro-optic and synthetic-aperture radar satellites and ground systems, including a 4-meter unfilled-aperture optical imaging satellite. Also developed advanced concepts in diverse areas including biological weapon countermeasures, laser power beaming, and reconnaissance systems.

1991–1995, Physicist, Special Studies Program (O-Group), LLNL

Developed advanced concepts and technologies for spacecraft and launch vehicles. Program leader for MOCKINGBIRD miniature reusable launch vehicle. LLNL interface to NASA/JPL for Pluto Fast Flyby mission development. Mission planner for Clementine lunar mapping mission.

Assigned to DOE Office of Space, Washington DC in 1993–1994, as Technical Advisor to the Director in the area of Remote Sensing. Responsible for coordinating joint DOE/NASA projects in space-based remote sensing. Assisted in formulating Office of Space policy and objectives.

1987–1991, Program Leader, LLNL/SDIO Laser Propulsion Program

Directed multiple university and industrial research teams in developing technology for ground-to-orbit laser propulsion (high-volume launch of small rocket vehicles powered by large ground-based lasers).

1985–1986, Physicist, Special Studies Program (O-Group), LLNL

Developed laser propulsion application concept; organized 1st SDIO/DARPA Laser Propulsion Workshop. Also worked on adaptive optics technology for atmospheric compensation of laser beams, developing designs for cooled deformable mirrors.

1984–1985, Research Associate, Lawrence Berkeley Laboratory (LBL), Berkeley, California

Education

1978–1984 University of California, Berkeley, CA
Ph.D. in Astrophysics, 1984
Fannie and John Hertz Foundation Fellow

1974–1978 Massachusetts Institute of Technology (MIT), Cambridge, MA
B.S. Physics, 1978; B.S. Electrical Engineering, 1978
Member Phi Beta Kappa, Sigma Xi (Physics), Tau Beta Pi (Engineering),
Eta Kappa Nu (Electrical Engineering)

Other Information

- Senior member AIAA, member IEEE, SPIE. OSA, Directed Energy Professional Society
- Approximately 40 publications; 12 issued patents
- Inventor or co-inventor on over 350 published patent applications; currently #21 in Top 100 Inventors, based on applications published in preceding 3 years
 - Partner in small publishing business, 1981–1987

Dr. Andrew Ketsdever
Air Force Research Laboratory
Propulsion Directorate
Edwards AFB, CA

Dr. Andrew Ketsdever is currently a Senior Research Engineer at the Air Force Research Laboratory's (AFRL) Propulsion Directorate at Edwards Air Force Base in California. While at AFRL, he was the group leader of the Advanced Concepts Group—a group responsible for identifying and developing the next generation of propulsion systems to enable future Air Force missions. He was also the group leader of the Non-Equilibrium Flows Group (AFRL/RZSA) which conducts basic research in rocket exhaust plume flows, signatures, and effects. AFRL/RZSA was recognized as an Air Force Office of Scientific Research (AFOSR) Star Team. He recently completed a Visiting Professorship in the Department of Astronautics at the United States Air Force Academy (2004-2007) and is also an Associate Professor at the University of Colorado at Colorado Springs.

Dr. Ketsdever has worked in the areas of advanced propulsion design and testing, rarefied gas dynamics, microfluidics, micropropulsion and spacecraft-thruster interactions since starting at AFRL in 1992. He holds patents and has patents pending in the areas of micropropulsion, advanced propulsion concepts, and nano-ignition of propellants. Dr. Ketsdever received his Ph.D. from the University of Southern California (USC) in 1995 where he has taught undergraduate and graduate level courses in rarified gas dynamics, planetary atmospheres, microspacecraft design, and spacecraft-environment interactions.

Dr. Ketsdever is an Associate Fellow of the American Institute of Aeronautics and Astronautics (AIAA). He is currently serving on the Nuclear and Future Flight Propulsion Technical Committee. Dr. Ketsdever has served on the AIAA Thermophysics Technical Committee (1998-2003) where he was the chairman of the Education Subcommittee. He has also been involved with the AIAA Working Group in Microfluidics. Dr. Ketsdever has authored or co-authored more than 100 technical papers. He also co-edited an AIAA Progress in Astronautics and Aeronautics series book entitled Micropropulsion for Small Spacecraft. Dr. Ketsdever is currently an associate editor for the Journal of Spacecraft and Rockets.

Frank E. Little

Education

Doctor of Philosophy in Chemistry. Field: Thermodynamics and co-operative phenomena, University of California, Davis, 1976.
Master of Science in Chemistry. Field: Theoretical Chemistry. California State University, Northridge, 1972.
Bachelor of Science in Chemistry. California State University, Northridge, 1968.

Fellowship

ERDA–AWU Graduate Fellow, 1976.
NASA Summer Faculty Fellow, Marshall Space Flight Center, 1999.

Professional History

TEES Distinguished Research Scientist, Space Engineering Research Center, August 2009 to present
Associate Director, Center for Space Power, January 1993 to July 2009
Associate Director, Center for Microencapsulation and Drug Delivery, May 2002 to present
Associate Director for Commercialization, Center for Space Power, September 1990 to January 1993
Business Manager, Center for Space Power, Texas A&M University, September 1989 to September 1990
Assistant Director, Space Research Center, Texas A&M University, September 1986 to September 1990
Project Manager, Thermodynamics, Gas Research Institute, August 1982 to September 1986.
Staff Research Associate II, Crocker Nuclear Laboratory, University of California, Davis, October 1978 to August 1982.
Lecturer in Chemistry, Department of Chemistry, University of California, Davis, October 1976 to July 1978.
ERDA–AWU Graduate Fellow, Crocker Nuclear Laboratory and the Department of Chemistry, University of California, Davis, January 1976 to September 1976.
Research Assistant, Department of Chemistry, University of California, Davis, 1971 to 1975.
Teaching and Research Assistant, Department of Chemistry, California State University, Northridge, 1968 to 1971.

Consulting

The Cyclotron Corporation, 1981.
SAIC, 2002

Technical Management Projects for Center for Space Power

- Photovoltaic conversion, including thin film
- Electrochemical energy storage (NiH, NiMH, Li-ion)
- Mechanical energy storage (flywheel)
- Power Management and Distribution (converters)
- On-board propulsion (microwave electrothermal thruster)

Research Activities

- Wireless Energy Transport for Solar Power to Earth.
- Electrochemistry
- Closed Environment Life Support Systems for space.
- Thermodynamics: Determination of molecular properties from measurements of fluid behavior.
- Radioisotope production.
- Development of applications for radioisotopes.
- Measurement of cross-sections for nuclear reactions.
- Synthesis of radiochemicals.
- Chemical kinetics of gas phase reactions of atomic fluorine utilizing radiotracer methods.
- Theoretical chemistry: Study of the liquid-vapor interface and model calculations for adsorption of a gas onto a solid.

Technical Documents

- "A Statistical Mechanical Calculation of the Density Variation through a Liquid-Vapor Interface." Master's Thesis, California State University, Northridge, January 1972.
- "Studies of Corresponding States Potential Force Constant Scaling Relations and the Critical Constants for the Fluoroethanes." Doctoral dissertation, University of California, Davis, September 1976.

Papers Presented at Scientific Meetings

- Little, F.E., and J.W. Root, "Critical Constants of Fluorinated Ethanes as a Basis for the Estimation of Molecular Sizes." Presented at the 169th National Meeting of the American Chemical Society, Philadelphia, 1975.
- Lagunas-Solar, M.C., F.E. Little and J.A. Jungerman, "The Radioisotope Program at U.C. Davis: Radionuclide Production and New Developments." Invited paper presented at the 1979 Winter Meeting of the American Nuclear Society, San Francisco.
- Lagunas-Solar, M.C., J.A. Jungerman, N.F. Peek, and F.E. Little, "A Remote Flow System for Large-Scale High-Purity I-123 Production." Presented at the 1979 Winter Meeting of the American Nuclear Society, San Francisco.
- Lagunas-Solar, M.C., H.L. Thibeau, and F.E. Little, "A Remote System for Multicurie Radiochemical Separations." Presented at the 1979 Winter Meeting of the American Nuclear Society, San Francisco.
- Lagunas-Solar, M.C., F.E. Little, S.L. Waters, and J.A. Jungerman, "Cyclotron Production of Carrier-free Thallium-201 via the Pb-207 (p, 7n) Reaction." Presented at the 3rd International Symposium on Radiopharmaceutical Chemistry, St. Louis, Missouri, June 16-20, 1980.
- Jungerman, J.A., M.C. Lagunas-Solar, and F.E. Little, "Cyclotron Production of High-Purity Iodine-123 for Medical Applications." Presented at the International Symposium on Radioiodines, Banff, Alberta, Canada, September 13-16, 1980.
- Little, F.E. and M. Klein, "A Rational Approach to Funding a Fluid Properties Basic Research Program for the Natural Gas Industry." Presented at the AIChE Spring National Meeting, Houston, March, 1985.
- Little, F.E. and M. Klein, "Keeping the Horse Before the Cart: The Importance of Data to Equation of State Development." Presented at 1st CODATA Symposium on Chemical Thermodynamic and Thermophysical Properties Data Bases of the CODATA International Meetings on Phase Equilibria and Related Property Data, Paris, September 5-13, 1985.

- Little, F.E. and M. Klein "Good Data is Forever: The Thermodynamics Program at GRI." Presented at 2nd CODATA Symposium on Critical Evaluation and Prediction of Phase Equilibria in Multi-component Systems of the CODATA International Meeting on Phase Equilibria and Related Property Data, Paris, September 5-13, 1985.
- Starling, K.E., M. Klein and F.E. Little, "The Thermodynamic Properties of Natural Gas- Physical Properties." Presented at 1st International Congress on "Gas Quality - Specifications and Measurement of Physical Properties of Natural Gas." Groningen, The Netherlands, April 21-25, 1986.
- Holtzapple, Mark T., Frank E. Little, William Moses, Comer O. Patterson, and Merry Makela "A First Order Chemical Model for a Life Support System." Presented at the AIChE Spring National Meeting, New Orleans, March, 1988.
- Holtzapple, Mark, Frank E. Little, Merry Makela, C.O. Patterson and William Moses, "Analysis of an Algae-Based CELSS: Part I: Model Development, Part II: Options and Weight analysis." Presented at Controlled Environmental Life Support Systems Research Conference, Texas A&M University, February 22-23, 1988.
- Makela, Merry, Steve Perkins, A. Dale Whittaker, Heinz Preisig, Mark Holtzapple, and Frank Little, "Object-Oriented Model of a Closed Loop Life Support System.", Presented at Controlled Environmental Life Support Systems Research Conference, Texas A&M University, February 22-23, 1988.
- Holtzapple, Mark T. and Frank E. Little, "Comparison of Waste Combustion and Waste Electrolysis: A System Approach", Presented at Life Support Systems Research Conference, Texas A&M University, February 14-15, 1989.
- Holtzapple, Mark T. and Frank E. Little, "Comparison of Waste Combustion and Waste Electrolysis Systems Analysis", Presented at Intersociety Conference on Environmental Systems, San Diego, July 1989.
- Preisig, H. A., Tae-Yeong Lee, Frank Little, and Bruce Wright, "On the Representation of Life-Support System Models", Presented at Intersociety Conference on Environmental Systems, San Diego, July 1989.
- Preisig, Heinz. A., Tae-Yeong Lee and Frank Little "A Prototype Computer-Aided Modelling Tool for Life-Support System Models", Paper 901269, Presented at 20th Intersociety Conference on Environmental Systems, Williamsburg, VA, July 1990.
- Little, Frank E. and Mike O. Kennedy "Commercialization Strategies for Space Power Technology", Paper IAF--90--617 Presented at 41st International Astronautical Congress, Dresden, Germany, October 1990.
- Chang, Kai, Frank E. Little and Mike O. Kennedy "Microwave Power Transmission System: Space Flight Experiment Program", Paper IAF--90--216 Presented at 41st International Astronautical Congress, Dresden, Germany, October 1990.
- Chang, K., A.D. Patton, M.O. Kennedy, F.E. Little, M.A. Pollock, K.A. Hummer, J.C. McCleary, B.S. Wei, A.M. Brown, J.O. McSpadden "Demonstration of Microwave Power Transmission in Space", Presented at SPS 91: Power from Space, Paris/Gif-sur-Yvette, August 27-30, 1991.
- Nansen, Ralph H. and Frank E. Little "A Practical Solar Power Satellite for the New Millennium", Paper 95-301. Presented at the 30th Intersociety Energy Conversion Engineering Conference, Orlando, Florida, August 1995.
- Erb, R.B., N. Kaya, G. Maryniak, R. Leonard, M.B. Duke, F. Little, A.D. Patton, R. Nansen, J. Spies and W. Sadeh "International Cooperation for the Acquisition of Space-Based Energy", Paper IAA-95-IAA.3.3.06. Presented at the 46th International Astronautical Congress, Oslo, Norway, October 1995.

- Little, Frank E. “Laser Wireless Power Transmission”, Presented at WPT’95 Second Wireless Power Transmission Conference, Kobe, Japan, October 16-19, 1995.
- McSpadden, James O., Frank E. Little, Michael B. Duke and Alex Ignatiev “An In-Space Wireless Energy Transmission Experiment”, Paper 96576. Presented at the 31st Intersociety Energy Conversion Engineering Conference, Washington, D.C. August 1996.
- Ehsani, M., J. Mahdavi, I. Pitel, J.E. Brandenburg, and F.E. Little “Development of an Efficient Power Supply for the Microwave Electrothermal Thruster”, Paper 970115 Presented at 2nd Conference on Commercial Development of Space, Albuquerque, New Mexico, January 1997.
- McSpadden, James O., Kai Chang, Mike Duke and Frank Little “Study of ISS Free-Flyer Power Beaming”, Presented at SPS ‘97 Conference, Montréal, Canada, August 24-28, 1997.
- Little, Frank E., James O. McSpadden, Kai Chang and Nobuyuki Kaya “Toward Space Solar Power: Wireless Energy Transmission Experiments Past, Present and Future”, Presented at Space Technology and Applications International Forum (15th Symposium on Space Nuclear Power and Propulsion) Albuquerque, New Mexico, January 1998.
- Rakotondrainibe, Andre F., Judith A. Jeevarajan, A. John Appleby and Frank E. Little, “Chronopotentiometric Profiles of the Anode and Cathode During the Charge/Discharge of Some commercial Lithium-ion Batteries”, Presented at 193rd ECS Meeting San Diego, California, May 3-8, 1998.
- Little, Frank E., “A wireless Power Transmission Power System for Microgravity Crystal Processing Satellites”, Presented at IEEE Aerospace Conference, Big Sky, Montana, March 18 – 25, 2000.
- Little, Frank E., “Solar Power Satellites: Recent Developments”, Paper 0965, Presented at the XXXVIIth URSI General Assembly, Maastricht, The Netherlands, August 17-24, 2002.
- Zepeda, Paola, Kai Chang and Frank Little “Optimal Antenna Taper Design for a Sandwich Transmitting Array in Space Solar Power Satellite” Paper IAC-02-R.2.10, Presented at the 53rd International Astronautical Congress, The World Space Congress, Houston, October 10-19, 2002.
- L.H. Hsieh, B.H. Strassner, S.J. Kokel, C.T. Rodenbeck, M.Y. Li, K. Chang, F.E. Little, G.D. Arndt, P.H. Ngo “DEVELOPMENT OF A RETRODIRECTIVE WIRELESS MICROWAVE POWER TRANSMISSION SYSTEM”, Presented at 2003 IEEE International Symposium on Antennas and Propagation and USNC/CNC/URSI North American Radio Science Meeting, Columbus, Ohio, June 22-27, 2003.
- Little, Frank “Power from Space: Fulfilling the Promise” Presented at The 1st International Symposium on Sustainable Energy System, Kyoto, Japan, March 13-14, 2003.
- Little, F.E., S.J. Kokel, C.T. Rodenbeck, K. Chang, G.D. Arndt, P.H. Ngo, “Development of Retrodirective Control Transmitter for Wireless Power Transmission” Presented at 2003 Japan – United States Joint Workshop on Space Solar Power System (JUSPS’03) Kyoto, Japan, July 3,4 2003.
- Little, Frank E. “Power from Space: From Promise to Reality”, Presented at URSI 2004 International Symposium on electromagnetic Theory, Pisa, Italy, May 23-27, 2004.
- Little, Frank and Henry Brandhorst, “An Approach for Lunar power – 24/29” Presented at Solar Power from Space – SPS’04/5th Wireless Power Transmission conference (WPT 5), Granada, Spain, June 30 – July 2, 2004.
- Rodenbeck, C., S. Kokel, K. Chang, F.E. Little, “Microwave Wireless Power Transmission with Retrodirective Beam Steering”, Presented at 2nd International Energy Conversion Engineering Conference, Providence, Rhode Island, August 16-19, 2004.
- Brandhorst, Henry W. and Frank Little, “An Approach for Continuous Lunar Power”, Presented at 2nd International Energy Conversion Engineering Conference, Providence, Rhode Island, August 16-19, 2004.
- Brandhorst, Henry W. and Frank Little, “POWOW Revisited – Beamed Power for Mars Exploration”, Presented at 2nd International Energy Conversion Engineering Conference, Providence, Rhode Island, August 16-19, 2004.

- Little, Frank E. and Alan Palazzolo, "Testing of Magnetic Bearings for Flywheel Energy Storage in Simulated Space Conditions", Paper No. AIAA-2005-5642, Presented at 3rd International Energy Conversion Engineering Conference, San Francisco, August 15-18, 2005.
- Little, Frank E., "A Wireless Power Based Space Transportation System", Paper No. 2006-g-10, Presented at 25th International Space Technology and Science Conference, Kanazawa, Japan, June 4-11, 2006.
- Schuller, M., Lalk, T., Wiseman, L., Little, F., Godard, O., Abdel-Fattah, S., Askew, R., Klaus, D., Kobrick, R., Thomas, G., Rouen, M. and Conger, B., "Innovative Schematic Concept Analysis for a Space Suit Portable Life Support Subsystem", Paper 2006-01-2201, Presented at the 36th International Conference on Environmental Systems, Norfolk, Virginia, USA, July 17-20, 2006.
- Klaus, D., Bamsey, M., Schuller, M., Godard, O., Little, F. and Askew, R., "Defining Space Suit Operational Requirements for Lunar and Mars Missions and Assessing Alternative Architectures", Paper 2006-241 Presented at the 36th International Conference on Environmental Systems, Norfolk, Virginia, USA, July 17-20, 2006.
- Little, Frank, "From the Moon to the Earth: Lunar Implications for Space Solar Power". Presented at the First International Symposium on Radio Systems and Space Plasma, Sofia, Bulgaria, September 2-5, 2007.
- Little, Frank E., "Constraints on the Design of a Lunar-to-Earth Wireless Power Transmission System" Paper IAC-08-C3.1.8, Presented at the 59th International Astronautical Congress, Glasgow, Scotland, 29 September 29 - October 3, 2008.
- Little, Frank E., Kai Chang, Rainer Fink, G. Dickey Arndt, Phong H. Ngo and Raymond F. Beach, "A Space to Earth Demonstration of Wireless Power Transmission" Paper No. 2009-h-27 Presented at the 27th International Space Technology and Science Conference, Tsukuba, Japan, July 5-12, 2009
- Little, Frank E., "Recent US Activities in Wireless Power Transmission" Paper 2A-1b Presented at the 1st NSS Space Solar Power Symposium, National Space Society International Space Development Conference, Chicago, Illinois, May 27 – 31, 2010.
- Little, Frank E., "Opportunities and Challenges for Wireless Power Transmission" Presented at 2nd International Symposium on Radio Systems and Space Plasma, Sofia, Bulgaria, August 25-27, 2010.
- Little, Frank E. "Space Experiments for Space Based Solar Power" Paper 2-10 Presented at IAA 50th Anniversary Celebration Symposium on Climate Change/Green Systems, Nagoya, Japan, August 30-31, 2010.
- Little, Frank E., Paola D. Alicea, Mindy E. Watts and Veronica N. Medrano, "Design of a Small Semi-autonomous Satellite for Microwave Wireless Power Transmission Demonstration", Paper 2011-q-04, Presented at 28th International Symposium on Space Technology and Science, Ginowan City, Okinawa, Japan, June 5-12, 2011.
- Little, Frank E., Veronica N. Medrano, Miguel A. Rios and Daniel J. Talamantez "Antenna System Design Characteristics for a Space to Earth Demonstration of Wireless Power Transmission", Paper 2011-q-18, Presented at 28th International Symposium on Space Technology and Science, Ginowan City, Okinawa, Japan, June 5-12, 2011.

Publications

- Mo, Siu-Hong, Edward R. Grant, Frank E. Little, Ronald G. Manning, Chester A. Mathis, Gerald S. Werre, and John W. Root, "Radiotracer Studies of Thermal Hydrogen Abstraction Reactions by Atomic Fluorine." In "Fluorine-containing Free Radicals: Kinetics and Dynamics of Reactions" J.W. Root, ed. ACS Symposium Series 66, pp 59-103.
- Lagunas-Solar, Manuel C., Harvey L. Thibeau, and Frank E. Little, "A Remote System for Multicurie Radiochemical Separations." Proceedings of 27th Conference on Remote Systems Technology. (1979 Winter Meeting, American Nuclear Society, November 11-15, 1979, San Francisco, California) pp 301- 306.

- Lagunas-Solar, Manuel C., John A. Jungerman, Neal F. Peek and Frank E. Little, "A Remote Flow System for Large-Scale High-Purity I-123 Production." Proceedings of 27th Conference on Remote Systems Technology. (1979 Winter Meeting, American Nuclear Society, November 11-15, 1979, San Francisco, California) pp 295-300.
- Lagunas-Solar, Manuel C., Frank E. Little, and John A. Jungerman, "Proton Induced Reactions on Natural Pb Targets. A Potential New Cyclotron Method for Tl-201 Production." Int. J. Applied Radiat. Isotopes. 1981 32 (11) 817-22.
- Lagunas-Solar, M.C., F. E. Little, and H.A. Moore, Jr. "Cyclotron Productions of ^{128}Cs (3.62 min). A New Positron - Emitting Radionuclide for Medical Applications." Int. J. Appl. Radiat. Isot. 1982, 33 (8) 619-28.
- Lagunas-Solar, M.C., F.E. Little, and C.D. Goodart, "An Integrally Shielded Transportable Generator System for Thallium - 201 Production." Int. J. Appl. Radiat. Isot. 1982 33 (12) 1439-43.
- Little, F.E. and M.C. Lagunas-Solar, "Cyclotron Production of ^{67}Ga . Cross Sections and Thick Target Yields for the ^{67}Zn (p,n) and ^{68}Zn (p,2n) Reactions." Int. J. Appl. Radiat. Isot. 1983 34 (3) 631-37.
- Lagunas-Solar, M.C., H.L. Thibeau, C.D. Goodart, F.E. Little, N.J. Navarro, and D.E. Hartnett, "A Multicurie, Transportable, Integrally Shielded $^{123}\text{Xe} > ^{123}\text{I}$ Generator and Processing System for High-Purity Iodine-123 Production." DOE Symp. Ser. 1985 56 (Dev. Role Short-lived Radionuclides Nuc. Med. Pract.) 190-202.
- Klein, M. and F.E. Little, "A Basic Research Program Aimed at Satisfying the Needs of the Gas Industry for Thermophysical Properties Data." in "The Role of Data in Scientific Progress" P.S. Glaeser ed. CODATA 1985 Elsevier Science Publishers B.V. (North Holland), Amsterdam, 1985 pp 183-187.
- Starling, K.E., M. Klein and F.E. Little, "The Thermodynamic Properties of Natural Gas - Physical Properties." in "Proceedings of the Congress of "Gas Quality - Specification and Measurement of Physical and Chemical Properties of Natural Gas." Groningen, The Netherlands April 22-25, 1986, J.G. van Rossum ed. Elsevier science Publishers B.V. (North Holland), Amsterdam, 1986 pp 211-239.
- Holtzapple, Mark T., Frank E. Little, Merry E. Makela, and C.O. Patterson, Analysis of an Algae-Based CELSS: Part I: Model Development." Acta Astronautica 19 (4), pp. 353-364, 1989.
- Holtzapple, Mark T., Frank E. Little, William Moses, and C.O. Patterson, "Analysis of an Algae-Based CELSS: Part II: Options and Weight analysis." Acta Astronautica 19 (4), pp. 365-375, 1989.
- Holtzapple, Mark T. and Frank E. Little, "Comparison of Waste Combustion and Waste Electrolysis Systems Analysis", Paper 891485. Proceedings of the 19th Intersociety Conference on Environmental Systems, San Diego, CA (1989).
- Preisig, H.A., Tae-Yeong Lee, Frank Little, and Bruce Wright, "On the Representation of Life-Support System Models", Paper 891479. Proceedings of the 19th Intersociety Conference on Environmental Systems, San Diego, CA (1989).
- Preisig, Heinz. A., Tae-Yeong Lee and Frank Little "A Prototype Computer-Aided Modelling Tool for Life-Support System Models", Paper 901269. Proceedings of the 20th Intersociety Conference on Environmental Systems, Williamsburg, VA (1990).
- Little, Frank E. and Mike O. Kennedy "Commercialization Strategies for Space Power Technology", Paper IAF--90--617 Proceedings of the 41st International Astronautical Congress, Dresden, Germany, October 1990.
- Chang, Kai, Frank E. Little and Mike O. Kennedy "Microwave Power Transmission System: Space Flight Experiment Program", Paper IAF--90--216 Proceedings of the 41st International Astronautical Congress, Dresden, Germany, October 1990.

- Chang, K., A.D. Patton, M.O. Kennedy, F.E. Little, M.A. Pollock, K.A. Hummer, J.C. McCleary, B.S. Wei, A.M. Brown, J.O. McSpadden “Demonstration of Microwave Power Transmission in Space”, Paper B1.2 Proceedings of SPS 91: Power from Space, Paris/Gif-sur-Yvette, August 27-30, 1991.
- Nansen, Ralph H. and Frank E. Little “A Practical Solar Power Satellite for the New Millennium”, Paper 95-301. Proceedings of the 30th Intersociety Energy Conversion Engineering Conference, Orlando, Florida, August 1995.
- Erb, R.B., N. Kaya, G. Maryniak, R. Leonard, M.B. Duke, F. Little, A.D. Patton, R. Nansen, J. Spies and W. Sadeh “International Cooperation for the Acquisition of Space-Based Energy”, Paper IAA-95-IAA.3.3.06. Proceedings of the 46th International Astronautical Congress, Oslo, Norway, October 1995.
- McSpadden, James O., Frank E. Little, Michael B. Duke and Alex Ignatiev “An In-Space Wireless Energy Transmission Experiment”, Paper 96576. Proceedings of the 31st Intersociety Energy Conversion Engineering Conference, Washington, D.C. August 1996.
- Ehsani, M., J. Mahdavi, I. Pitel, J.E. Brandenburg, and F.E. Little “Development of an Efficient Power Supply for the Microwave Electrothermal Thruster”, Paper 970115 Space Technology and Applications International Forum (2nd Conference on Commercial Development of Space) Albuquerque, New Mexico, January 1997, AIP Conference Proceedings 387 pp 893-899, 1997.
- Little, Frank E., James O. McSpadden, Kai Chang and Nobuyuki Kaya “Toward Space Solar Power: Wireless Energy Transmission Experiments Past, Present and Future”, Paper 970115 Space Technology and Applications International Forum (15th Symposium on Space Nuclear Power and Propulsion) Albuquerque, New Mexico, January 1998, AIP Conference Proceedings 420 pp. 1225-1233, 1998.
- Little, Frank E. “A wireless Power Transmission Power System for Microgravity Crystal Processing Satellites”, Proceedings of the IEEE Aerospace Conference, Big Sky, Montana, March 18 – 25, 2000.
- Wang, Chunsheng, Imran Kakwan, A. John Appleby and Frank E. Little, “In-Situ Investigation of Electrochemical lithium Intercalation into Graphite Powder”, *Journal of Electroanalytical Chemistry*, 489, (2000), pp. 55-67.
- Wang, Chunsheng, A. John Appleby and Frank E. Little, “Electrochemical Study on Nano-Sn, Li₄.4Sn and AlSi_{0.1} Powders Used as Secondary Lithium Battery Anodes”, *Journal of Power Sources*, 93, (2001), pp. 174-185.
- Wang, Chunsheng, A. John Appleby and Frank E. Little, “Charge-discharge Stability of Graphite Anodes for Lithium-Ion Batteries”, *Journal of Electroanalytical Chemistry*, 497. (2001), pp. 33-46.
- Wang, Chunsheng, A. John Appleby and Frank E. Little, “Comparison of the Electrochemical impedance Spectroscopy Characteristics of Insertion Electrode Materials used in Secondary Metal Hydride and Lithium-Ion electrodes”, *Journal of the Electrochemical Society*, 148, (7), pp. A762-A767, (2001).
- Wang, Chunsheng, A. John Appleby and Frank E. Little, “Electrochemical Impedance Study of Initial Lithium Ion Intercalation into Graphite powders”, *Electrochimica Acta*, 46, (2001), pp. 1793-1813.
- Wang Chunsheng, Andre Rakotondrianibe, A. John Appleby and Frank E. little, “Characterization of Metal Hydride Electrodes via Microperturbation and In Situ Intrinsic Resistance Measurement”, *Journal of the Electrochemical Society*, 147, (12), pp. 4432-4439, (2000).
- Wang, Chunsheng, A. John Appleby and Frank E. Little, “Electrochemical Study of the SnO₂ Lithium-insertion Anode using Microperturbation techniques”. *Solid state Ionics*, 147, (2002), pp. 13-22.
- Wang, Chunsheng, A. John Appleby and Frank E. Little, “Irreversible Capacities of Graphite Anode for Lithium-ion Batteries”, *Journal of Electroanalytical Chemistry*, 519, (2002), pp. 9-17.

- Zhang, Xiang-Wu, Chunsheng Wang, A. John Appleby and Frank E. Little, "Improvement in Electrochemical Properties of Nano-tin-polyaniline Lithium-ion Composite Anodes by Control of Electrode Microstructure", *Journal of Power Sources*, 109, (2002), pp.136-141.
- Wang, Chunsheng, A. John Appleby and Frank E. Little, "Low-Temperature Characterization of Lithium-ion Carbon Anodes via Microperturbation Measurement", *Journal of the Electrochemical Society*, 149, (6), (2002) pp. A754-A760.
- Zhang, Xiang-Wu, Chunsheng Wang, A. John Appleby and Frank E. Little, "Composite Doped Emeraldine-Polyethylene Oxide-Bonded Lithium-ion Nano-tin Anodes with Electronic-ionic Mixed Conduction", *Solid State Ionics*, 150 (3,4), (2002) pp. 383-389.
- Little, Frank E., "Solar Power Satellites: Recent Developments", Paper 0965, Proceedings of the XXXVIIth URSI General Assembly, Maastricht, The Netherlands, August, 2002.
- Zepeda, Paola, Kai Chang and Frank Little "Optimal Antenna Taper Design for a Sandwich Transmitting Array in Space Solar Power Satellite", Paper IAC-02-R.2.10, Proceedings of the 53rd International Astronautical Congress, The World Space Congress, Houston, October, 2002.
- Hsieh, L.H., B.H. Strassner, S.J. Kokel, C.T. Rodenbeck, M.Y. Li, K. Chang, F.E. Little, G.D. Arndt and P.H. Ngo, "Development of a Retrodirective Wireless Microwave Power Transmission System", *IEEE Antennas and Propagation Society International Symposium Digest*, 2, 393-396, June 2003.
- Zhang, Xiang-Wu, Prashanth K. Patil, Chunsheng Wang, A. John Appleby, Frank. E. Little, David L. Cocke, "Electrochemical performance of lithium ion battery, nano-silicon-based, disordered carbon composite anodes with different microstructures", *Journal of Power Sources* 125 (2004) pp. 206–213.
- Little, F.E., S.J. Kokel, C.T. Rodenbeck, K. Chang, G.D. Arndt, P.H. Ngo, "Development of Retrodirective Control Transmitter for Wireless Power Transmission", *Radio Science Bulletin* 311 (December 2004) pp. 38-46.
- Wang, Chunsheng, Prashanth Patil, A. John Appleby, Frank E. Little, Mehmet Kesmez and David L. Cocke, "In Situ Ionic/Electric Conductivity Measurement of $\text{La}_{0.55}\text{Li}_{0.35}\text{TiO}_3$ Ceramic at different Li Insertion Levels", *Journal of the Electrochemical Society*, 151 (8) A1196-A1201 (2004).
- Little, Frank E. "Power from Space: From Promise to Reality", Proceedings of the URSI 2004 International Symposium on electromagnetic Theory, Pisa, Italy, May 23-27, 2004, pp. 311-313.
- Little, Frank and Henry Brandhorst, "An Approach for Lunar power – 24/29" Proceedings of Solar Power from Space – SPS'04/5th Wireless Power Transmission conference (WPT 5), Granada, Spain, June 30 – July 2, 2004 (in press).
- Rodenbeck, C., S. Kokel, K. Chang, F.E. Little, "Microwave Wireless Power Transmission with Retrodirective Beam Steering", Paper 2004-5640, Proceedings of 2nd International Energy Conversion Engineering Conference, Providence, Rhode Island, August 16-19, 2004.
- Brandhorst, Henry W. and Frank Little, "An Approach for Continuous Lunar Power", Paper 2004-5688, Proceedings of 2nd International Energy Conversion Engineering Conference, Providence, Rhode Island, August 16-19, 2004.
- Brandhorst, Henry W. and Frank Little, "POWOW Revisited – Beamed Power for Mars Exploration", Paper 2004-5642, Proceedings of 2nd International Energy Conversion Engineering Conference, Providence, Rhode Island, August 16-19, 2004.
- Little, Frank E. and Alan Palazzolo, "Testing of Magnetic Bearings for Flywheel Energy Storage in Simulated Space Conditions", Paper No. AIAA-2005-5642, 3rd International Energy Conversion Engineering Conference, San Francisco, August 15-18, 2005.
- Little, Frank E., "A Wireless Power Based Space Transportation System", Paper No. 2006-g-10, Proceedings of the 25th International Space Technology and Science Conference, Kanazawa, Japan, June 4-11, 2006.

- Schuller, M., Lalk, T., Wiseman, L., Little, F., Godard, O., Abdel-Fattah, S., Askew, R., Klaus, D., Kobrick, R., Thomas, G., Rouen, M. and Conger, B., “Innovative Schematic Concept Analysis for a Space Suit Portable Life Support Subsystem”, Paper 2006-01-2201, Proceedings of the 36th International Conference on Environmental Systems, Norfolk, Virginia, USA, July 17-20, 2006.
- Klaus, D., Bamsey, M., Schuller, M., Godard, O., Little, F. and Askew, R., “Defining Space Suit Operational Requirements for Lunar and Mars Missions and Assessing Alternative Architectures”, Paper 2006-241 Proceedings of the 36th International Conference on Environmental Systems, Norfolk, Virginia, USA, July 17-20, 2006.
- Little, Frank, “From the Moon to the Earth: Lunar Implications for Space Solar Power”. Proceedings of the First International Symposium on Radio Systems and Space Plasma, Sofia, Bulgaria, September 2-5, 2007.
- Little, Frank E., “Constraints on the Design of a Lunar-to-Earth Wireless Power Transmission System” Paper IAC-08-C3.1.8, Proceedings of the 59th International Astronautical Congress, Glasgow, Scotland, 29 September 29 - October 3, 2008.
- Little, Frank E., Kai Chang, Rainer Fink, G. Dickey Arndt, Phong H. Ngo and Raymond F. Beach, “A Space to Earth Demonstration of Wireless Power Transmission” Paper No. 2009-h-27 Proceedings of the 27th International Space Technology and Science Conference, Tsukuba, Japan, July 5-12, 2009.
- Little, Frank E., “Opportunities and Challenges for Wireless Power Transmission”, Proceedings of the 2nd International Symposium on Radio Systems and Space Plasma, Sofia, Bulgaria, August 25-27, 2010 pp 153-156.
- Little, Frank E., Paola D. Alicea, Mindy E. Watts and Veronica N. Medrano, “Design of a Small Semi-autonomous Satellite for Microwave Wireless Power Transmission Demonstration”, Paper 2011-q-04, Proceedings of the 28th International Symposium on Space Technology and Science, Ginowan City, Okinawa, Japan, June 5-12, 2011.
- Little, Frank E., Veronica N. Medrano, Miguel A. Rios and Daniel J. Talamantez “Antenna System Design Characteristics for a Space to Earth Demonstration of Wireless Power Transmission”, Paper 2011-q-18, Proceedings of the 28th International Symposium on Space Technology and Science, Ginowan City, Okinawa, Japan, June 5-12, 2011

James McSpadden, Ph.D.

President

McSpadden Consulting

1204 Padre Circle

Allen, Texas 75013

james@mcspadding.com 469-734-7507

Dr. McSpadden is an expert in microwave power transmission systems and rectenna design. As a private consultant for over 10 years, he has lead projects dealing with the system analysis and technology development for various power transmission projects. He previously worked full time for The Boeing Company for 8 years and has been employed by Raytheon since 2005 as a Senior Principal Electrical Engineer. Dr. McSpadden received his B.S.E.E, M.S.E.E, and Ph.D. diplomas, all from Texas A&M University, in 1989, 1993, and 1998, respectively. Dr. McSpadden has over 20 published papers in journals, conferences, and magazines on microwave power transmission. He is a Senior Member of the IEEE and is currently writing a technology book titled "Microwave Power Transmission."

Power Beaming Publications

- (1) J.O. McSpadden, "Advances in RF Wireless Power Transmission," presented at the International Symposium on Solar Energy from Space, Ontario Science Centre, Toronto, Canada, Sept. 8-10, 2009
- (2) R.C. Hansen, J.O. McSpadden, and J.N. Benford, "A Universal Power Transfer Curve," IEEE Microwave and Wireless Components Letters, vol. 15, no. 5, pp. 369-371, May 2005.
- (3) J.O. McSpadden and J.C. Mankins, "Space solar power programs and microwave wireless power transmission technology," IEEE Microwave Magazine, vol. 3, no. 4, pp. 46-57, Dec. 2002.
- (4) J.O. McSpadden, "The current capabilities of microwave WPT technology" in 2001 Asia-Pacific Radio Science Conference AP-RASC'01 Conference Digest, Aug. 1-4, 2001, Chuo University, Tokyo, Japan, pp. 14-17.
- (5) J.O. McSpadden, L. Fan, and K. Chang, "Design and experiments of a high-conversion-efficiency 5.8-GHz rectenna," IEEE Trans. Microwave Theory Techn., vol. 46, no. 12, pp. 2053-2060, Dec. 1998.
- (6) J.O. McSpadden, R. M. Dickinson, L. Fan and K. Chang, "A novel oscillating rectenna for wireless microwave power transmission," in 1998 IEEE MTT-S International Microwave Symposium Digest, 1998, pp. 1161-1164.
- (7) J.O. McSpadden, K. Chang, F. Little, and M. Duke, "Study of ISS free-flyer power beaming," in Proceedings of SPS '97 Conference, Montreal, Canada, Aug. 24-28, 1997, pp. 169-174.
- (8) J.O. McSpadden, L. Fan and K. Chang, "A high conversion efficiency 5.8 GHz rectenna," in 1997 IEEE MTT-S International Microwave Symposium Digest, 1997, pp. 547-550.
- (9) J. McSpadden, K. Chang, and A.D. Patton, "Microwave power transmission research at Texas A&M University," Space Energy and Transportation, vol. 1, no. 4, pp. 368-393, 1996.
- (10) J.O. McSpadden, F.E. Little, M.B. Duke, and A. Ignatiev, "An in-space wireless energy transmission experiment," in Proceedings of the 31st Intersociety Energy Conversion Engineering Conference, 1996, pp. 468-473.
- (11) J. McSpadden and K. Chang, "Review of the solar power satellite," in Proceedings of the Fifth International Conference on Space '96, 1996, pp. 254-259.
- (12) J.O. McSpadden, A.M. Brown, K. Chang and N. Kaya, "A receiving rectifying antenna for the international space year - microwave energy transmission in space (ISY-METS) rocket experiment," IEEE Aerospace and Electronic Systems Magazine, vol. 9, no. 11, pp. 36-41, Nov. 1994.

- (13) J.O. McSpadden, N. Kaya, A.M. Brown and K. Chang, "A receiving rectifying antenna for the international space year - microwave energy transmission in space (ISY-METS) rocket experiment," in 29th Intersociety Energy Conversion Engineering Conference, Monterey, CA, 1994, pp. 723-727.
- (14) J.O. McSpadden and K. Chang, "A dual polarized circular patch rectifying antenna at 2.45 GHz for microwave power conversion and detection," in 1994 IEEE MTT-S International Microwave Symposium Digest, 1994, pp. 1749-1752.
- (15) J.O. McSpadden, "Construction and testing of a space ready rectenna, final report," Center for Space Power, Texas Engineering Experiment Station, The Texas A&M University System, College Station, TX, NASA Lewis Research Center Grant NAG 3-1368, June 1993.
- (16) "Wireless space power experiment (WISPER), final report," NASA/URSA Advanced Design Program, Dept. of Electrical Engineering, University of Alaska Fairbanks, Fairbanks, AK, June 1993.
- (17) J.O. McSpadden, T. Yoo, and K. Chang, "Theoretical and experimental investigation of a rectenna element for microwave power transmission," IEEE Trans. Microwave Theory Techn., vol. 40, no. 12, pp. 2359-2366, Dec. 1992.
- (18) J.O. Mc Spadden and K. Chang, "Suppression of rectenna harmonic radiation by a frequency selective surface," presented at 1992 IEEE-APS/URSI/NEM Joint Symposia, Chicago, 1992.
- (19) T. Yoo, J.O. McSpadden, and K. Chang, "35 GHz rectenna implemented with a patch and a microstrip dipole antenna," in 1992 IEEE MTT-S International Microwave Symposium Digest, 1992, pp. 345-348.
- (20) J.O. McSpadden, T. Yoo, and K. Chang, "Diode characterization in a microstrip measurement system for high power microwave power transmission," in 1992 IEEE MTT-S International Microwave Symposium Digest, 1992, pp. 1015-1018.
- (21) K. Chang, A.D. Patton, M.O. Kennedy, F.E. Little, M.A. Pollock, K.A. Hummer, J.C. McCleary, B.S. Wei, J.O. McSpadden, and A.M. Brown, "Demonstration of microwave power transmission in space," in SPS 91 Power From Space, Paris, 1991, pp. 343-347.

Leik N. Myrabo, Ph.D.
Lightcraft Technologies, Inc.
1914 Walloomsac Road
Bennington, Vermont 05201
802-447-6275 (w) 802-989-2874 (c)

Professional History

Professor Leik N. Myrabo is recognized as an *aerospace pioneer* by the Smithsonian National Air and Space Museum for his pioneering work on laser propulsion. His company, *Lightcraft Technologies, Inc.* (founded in 1999), holds the world altitude record for laser launched vehicles. Myrabo has authored and co-authored more than 210 journal, symposium, and conference articles in addition to two books: *The Future of Flight* (1985), and *The Lightcraft Flight Handbook: LTI-20* (2009).

He received his B.S. degree in Aerospace Engineering from Iowa State University in 1968, and Ph.D. in Engineering Physics from the University of California at San Diego in 1976, and, Thereafter, he spent a total of 7 years at Physical Sciences, Inc., W.J. Schafer Associates, and the BDM Corporation, pursuing “Star Wars” research as a staff scientist and consultant on directed energy applications, aerospace systems, space prime power, and advanced propulsion. He joined the Rensselaer Polytechnic Institute (RPI) faculty in 1983, retiring in August 2010 to devote his full-time attention to commercializing beamed energy propulsion (BEP) under *Lightcraft Technologies, Inc.*

For nearly three decades at RPI, Myrabo’s burning desire has been to create and demonstrate viable concepts for non-chemical propulsion of future flight vehicles for an era beyond oil. Prior to June 2005, when he was awarded a \$2.25M MURI grant by AFOSR, he had previously attracted \$3.5M (in 2005 dollars) into RPI, all focused on BEP research for powering future aircraft and spacecraft. Myrabo’s MURI combined experimental/experimental research investigated laser propulsion physics for affordable, rapid access to space: i.e., launching pico/nano/micro-satellites (i.e., 0.1 to 100 kg).

Research & Development Interests

Advanced space propulsion & power, aerospace systems, directed energy, hypersonic gas dynamics, energy conversion, space technology, alternative energy. Myrabo’s experimental and theoretical studies at RPI were focused on alternative (non-chemical) energy sources for aeronautical, aerospace, and space flight propulsion of the 21st century and beyond. This advanced energetics research took a long term, high risk approach to identifying areas of potential technological breakthroughs. His primary R&D emphasis was on the application of Beamed Energy Propulsion (BEP) with laser, microwave, or millimeter wave sources, in developing future air-breathing and rocket shuttlecraft for a variety of hypersonic boost-glide, space launch, and orbit-raising missions.

Recent International Collaboration

The Lightcraft Project at the Umea Institute of Design (UID) was a collaboration between three MA Programmes (Transportation Design, Advanced Product Design, and Interaction Design) and *Lightcraft Technologies, Inc.* conducted in an intensive ten-week period during the Fall’09 semester in Umea, Sweden. Thirty-three 2nd year design UID students in eleven teams (with one student from each programme) aggressively pursued the research and development of concepts, ideas and scenarios to design the ideal lightcraft travel experience—requiring the intimate integration of advanced technology with the human element. Their final presentations disclosed novel *Lightport* (equivalent to today’s airports) designs, tickets with Lightport navigation/ departure & arrival/and passport info, unique vehicle boarding methods, elaborate and functional interior designs with reconfigurable seats, g-suits and restraints, holographic in-flight displays, and so much more. The UID *Lightcraft Project* exploited a sophisticated laser powered multi-cycle engine/vehicle concept that was evolved over a 10+ year period at RPI. This new global flight transportation system is based on beaming power from

satellite solar power stations—envisioned to replace the commercial jumbojet airline system by 2025—for an era beyond oil.

Innovative Work of Potential Long-Term Significance

(R&D milestones for Myrabo and his investigative teams; Reference numbers “[xx]” refer to Selected Publications/References list—see below)

- First demonstration of a hypersonic laser-scrumjet at Mach 6-10 in the IEAv hypersonic shock tunnel in Sao Jose dos Campos, Brazil, with I.I. Salvador, M.A.S. Minucci, P.G.P. Toro [1-2].
- Created 1 km diameter, rotating LEO solar power station concept (engineering analysis, and orbital mechanics study) exploiting rechargeable superconducting magnetic energy storage system [3-4], and a compatible concept for a 20-m microwave lightcraft designed to transport 6-12 person crews [5]. Invented concept for new ultra-high power density superconductor (with D.A. Gross): metal matrix superconductor composites [4].
- First laser-boosted light sail demonstration, and vacuum photonic thrust measurements (pendulum mount) of candidate ultralight light sail materials (5 cm diameter molybdenum-coated, carbon micro-truss fabrics) using a high power CW infrared laser called LHMEI II [6]. First vertical wire-guided flight attempts (i.e., 1 g acceleration) of laser-boosted sails using advanced flight-weight materials [7].
- First laser-boosted, spin-stabilized lightcraft flown in vertical free-flights propelled by airbreathing pulsejet engine at White Sands Missile Range [8]. Holds a 30.2 m world altitude record for airbreathing laser-propelled lightcraft, demonstrating infinite specific impulse [9].
- First laser-propelled, spin-stabilized rocket lightcraft in free-flight [10]. Myrabo holds the 72m world altitude record for laser-boosted rocket lightcraft, with longest boost duration and greatest “air time” flown on the PLVTS pulsed CO₂ laser at WSMR, NM [11].
- First measurements of beam-riding characteristics of a laser-propelled lightcraft engine [12], and first investigation and simulation of lightcraft flight dynamics [13-14].
- First high power pulsed laser experiments examining the survivability of refractory metal coatings on graphite bell engines and ceramic matrix composite materials for laser pulsejet engines [15].
- Established theoretical foundations for the Directed Energy AirSpike (DEAS) with Yuri Raizer [16]. First electric-arc AirSpike experiments in Mach 8-10 hypersonic flow with and without a blunt body [17-19]; electric-arc AirSpike experiments in Mach 3 flow [20]; Laser-induced AirSpike experiments in hypersonic flow with M.A.S Minucci and P.G.P. Toro [21].
- First magnetic-augmented, airbreathing laser pulsejet experiments—using the terawatt 1 μm Nd-glass Pharos III laser [22-23].
- Created the Lightcraft Technology Demonstrator (LTD) concept for laser-launching of microsattellites (i.e., 10-100 kg payloads), under support of the SDIO Laser Propulsion Program [24]. *(The laser lightcraft design flown at WSMR evolved directly from this advanced engine/optics/vehicle concept.)*

Selected Publications/References

- (1) I.I. Salvador, I.I., Myrabo, L., et.al., 2-D Air-Breathing Lightcraft Engine Experiments in Hypersonic Conditions,” in *7th International Symposium on Beamed Energy Propulsion*, edited by H.-A. Eckel and S. Scharring, AIP Conference Proceedings, American Institute of Physics, Melville, NY, 2011.
- (2) I.I. Salvador, I.I., Myrabo, L., et.al., 2-D Airbreathing Lightcraft Engine Experiments in Quiescent Conditions,” in *7th International Symposium on Beamed Energy Propulsion*, edited by H.-A. Eckel and S. Scharring, AIP Conference Proceedings, American Institute of Physics, Melville, NY, 2011.

- (3) Myrabo, L.N., "Microwave Power-Beaming Infrastructure for Manned Lightcraft Operations," in *4th International Symposium on Beamed Energy Propulsion*, edited by K. Komurasaki, T. Yabe, S. Uchida, and A. Sasoh, AIP Conference Proceedings 830, American Institute of Physics, Melville, NY, 651-662 (2006).
- (4) Gross, D.A., and Myrabo, L.N., "Metal Matrix Superconductor Composites for SMES-Driven, Ultra High Power BEP Applications: Parts 1 & 2," in *4th International Symposium on Beamed Energy Propulsion*, edited by K. Komurasaki, T. Yabe, S. Uchida, and A. Sasoh, AIP Conference Proceedings 830, American Institute of Physics, Melville, NY, 411-436 (2006).
- (5) Myrabo, L.N., "Horizon Mission: 2025 Space Command's Ultra-Energetic Lightcraft with Super-Pressure Airship Structure," in *3rd International Symposium on Beamed Energy Propulsion*, edited by A.V. Pakhomov and L.N. Myrabo, AIP Conference Proceedings 766, NY: American Institute of Physics, 86-99 (2005).
- (6) Myrabo, L.N., Knowles, T.R., Bagford, J.O., and Siebert, D.B., "Experimental Investigation of Laser-Pushed Light Sails in a Vacuum," in *High-Power Laser Ablation III*, edited by Claude R. Phipps, Proceedings of SPIE Vol. 4065 (2000) pp. 521-532.
- (7) Myrabo, L.N., Knowles, T.R., Bagford, J.O., Seibert, D.B., and Harris, H.M., "Laser-Boosted Light Sail Experiments with the 150 kW LHMELE II CO₂ Laser," in *High-Power Laser Ablation IV*, edited by Claude R. Phipps, Proceedings of SPIE Vol. 4760 (2002) pp. 774-798.
- (8) Myrabo, L.N., Messitt, D.G., and Mead Jr., F.B., "Ground and Flight Tests of a Laser Propelled Vehicle," AIAA Paper 1998-1001, 36th AIAA Aerospace Sciences Meeting & Exhibit, Reno, NV, 12-15 Jan. 1998.
- (9) Mead Jr., F.B., Myrabo, L.N., and Messitt, D.G., "Flight and Ground Tests of a Laser-Boosted Vehicle," AIAA Paper 1998-3735, 34th AIAA Joint Propulsion Conf. & Exhibit, Cleveland, OH, 13-15 July 1998.
- (10) Messitt, D.G., Myrabo, L.N., and Mead Jr., F.B., "Laser Initiated Blast Wave for Launch Vehicle Propulsion," AIAA Paper 2000-3848, 36th AIAA Joint Propulsion Conference, 16-19 July 2000, Huntsville, AL.
- (11) Myrabo, L.N., "Brief History of the Lightcraft Technology Demonstrator (LTD) Project," *Review of Laser Engineering*, 34, 423-428 (2006).
- (12) Libeau, M., and Myrabo, L., "Off-Axis and Angular Impulse Measurements on a Lightcraft Engine," in *3rd International Symposium on Beamed Energy Propulsion*, edited by A.V. Pakhomov and L.N. Myrabo, AIP Conference Proceedings 766, American Institute of Physics, Melville, NY, 166-177 (2005).
- (13) Libeau, M.A., Myrabo, L.N., and Filippelli, M., "Combined Experimental & Theoretical Flight Dynamics Investigation of a Laser-Propelled Vehicle," in *1st International Symposium on Beamed Energy Propulsion*, edited by A.V. Pakhomov, AIP Conference Proceedings 664, American Institute of Physics, Melville, NY, 125-137 (2003).
- (14) Ballard, C.G., Anderson, K.S., and Myrabo, L.N., "Flight Dynamics Simulation of Lightcraft Propelled by Laser Ablation," Paper 6261-74, in *High-Power Laser Ablation VI*, edited by Claude R. Phipps, Proceedings of SPIE, Vol. 6261, 2006.
- (15) Myrabo, L.N., Libeau, M.A., Meloney, E.D., Bracken, R., and Knowles, T.B., "Survivability of Thin Metal Mirror Coatings on Graphite Pulsed Laser Propulsion Engines," AIAA Paper 2002-3783.
- (16) Myrabo, L.N., and Raizer, Y.P., "Laser-Induced Air Spike for Advanced Transatmospheric Vehicles," AIAA Paper 1994-2451.
- (17) Marsh, J.J., Myrabo L.N., Messitt, D.G., Nagamatsu, H.T., and Raizer, Yu.P., "Experimental Investigation of the AirSpike Hypersonic Inlet at Mach 10," AIAA Paper 1996-0721.
- (18) Myrabo, L.N., Raizer, Yu.P., and Shneider, M.N., "The Calculation and Similarity Theory of Experiment Simulating the Air-Spike Effect in Hypersonic Aerodynamics," *High Temperature*, 36, n.2, 287-292 (1998).

- (19) Myrabo, L.N., Raizer, Yu.P., Shneider, M.N., and Bracken, R.M., “Drag and Total Power Reduction for Artificial Heat Input in Front of Hypersonic Blunt Bodies,” *High Temperature*, 42, n. 6, 1-9 (2004).
- (20) Misiewicz, C., Myrabo, L.N., Shneyder, M. and Raizer, Y.P., “Combined Experimental and Numerical Investigation of Electric-Arc Airspikes for Blunt Body at Mach 3,” in *3rd International Symposium on Beamed Energy Propulsion*, edited by A.V. Pakhomov and L.N. Myrabo, AIP Conference Proceedings 766, American Institute of Physics, Melville, NY, 528-550 (2005).
- (21) Minucci, M.A.S, Toro, P.G.P., Oliveira, A.C., Chanes Junior, J.B., Ramos, A.G., Pereira, A.L., Nagamatsu, H.T., and Myrabo, L.N., “Investigation of a Laser-Supported Directed Energy Air Spike in Hypersonic Flow,” *Journal of Spacecraft and Rockets*, 40, n. 1, 133-136 (2003).
- (22) Lyons, P.W., Myrabo, L.N., Jones, R.A., Nagamatsu, H.T., and Manka, C., “Experimental Investigation of a Unique Airbreathing Pulsed Laser Propulsion Concept,” AIAA Paper 1991-1922.
- (23) Myrabo, L.N., Lyons, P.W., Jones, R.A., Liu, S., and Manka, C., “Airbreathing Laser Propulsion Experiments with 1 μm Terawatt *Pharos III* Laser – Parts 1 & 2,” in *7th International Symposium on Beamed Energy Propulsion*, edited by H.-A. Eckel and S. Scharring, AIP Conference Proceedings, American Institute of Physics, Melville, NY, 2011.
- (24) Myrabo, L.N., et al, “Transatmospheric Laser Propulsion,” Final Technical Report, prepared under Contract No. 2073803 for Lawrence Livermore National Laboratory and the SDIO Laser Propulsion Program, 1989.

Dr. Kevin L.G. Parkin

Dr. Kevin L.G. Parkin is a Research Faculty member at the Silicon Valley campus of Carnegie Mellon University. He holds an M.Phys. in Physics with Space Science and Technology from the University of Leicester, and an M.S. in Aeronautics and Ph.D. in Aeronautics with minor in Electrical Engineering from Caltech. As an Undergraduate, Dr. Parkin undertook research in non-linear time series analysis, CatSat satellite battery performance, low thrust trajectory optimization, and finite element structural modeling tools for conceptual design. As a first year Graduate Student, Dr. Parkin developed ICEMaker, an Excel-based system for team collaboration on complex conceptual designs. ICEMaker was subsequently used by satellite design teams at NASA JPL, NASA GRC, Northrop Grumman, Boeing, UTRC, Raytheon, Caltech, MIT, Stanford, and The Naval War College. Subsequently, he undertook research on Pulse Detonation engines and AJAX hypersonic airbreathing propulsion. In 2002, he invented the Microwave Thermal Rocket, and subsequently it became the topic of his Ph.D. thesis. In 2005, he demonstrated the operating principle of microwave thermal propulsion in the laboratory for the first time. In recognition of his accomplishments in this area, Dr. Parkin was awarded the Korolev Medal by the Russian Federation of Cosmonautics. In 2006, he founded the Mission Design Center at NASA ARC, developing a software infrastructure to supersede the ICEMaker-era approach to conceptual design. Dr. Parkin served as deputy director of the Mission Design Center until 2008, subsequently returning to his present work on microwave thermal rocketry. Most recently, Dr. Parkin invented the Engineering Inference Engine (EIE). EIE is a forward-chaining inference engine and corresponding language used for system analysis of the microwave thermal rocket. Dr. Parkin is a Member of the Institute of Physics (IOP) and the American Institute of Aeronautics and Astronautics (AIAA).

Appendix C.—Thrust Augmentation of an In-Space Propulsion System

Andrew Ketsdever
Air Force Research Laboratory
Propulsion Directorate
Edwards AFB, CA 93524

C.1 Concept

This study investigates a concept by which the thrust (and specific impulse) of an in-space propulsion system is augmented using beamed energy. A 1 Mega-Watt (MW) level space asset is assumed for much of the study. The 1MW power level is assumed to be the beamed source power at the space asset (i.e., not necessarily at the receiving vehicle). The space asset is initially assumed to be either a CW laser, pulsed laser, or microwave based energy beaming system.

A method of augmenting thrust in an in-space propulsion system through the use of off-satellite resources is to beam electromagnetic energy to the space vehicle. The beamed energy can be added to a proposed propulsion system in a variety of ways. First, the beamed energy can be collected by the receiving spacecraft and converted into electrical energy that can be used to power an electric propulsion system. A concept of this nature requires a beam collector on the receiving spacecraft and a system to convert the photon energy (or resulting thermal energy) into electrical power. Second, the energy can be absorbed directly in the combustion (or stagnation) chamber of the propulsion system. This concept would be very similar to a solar thermal propulsion system where photon energy is used to heat the propellant gas (directly or indirectly through the use of a thermal mass). This concept can also be envisioned as a way to augment the performance of chemical thrusters by adding energy directly into the combustion chamber. Third, the beamed energy can be absorbed in the expanding section of a converging-diverging nozzle to add energy after the combustion chamber as shown in Reference 1. Finally, a laser ablation thruster can be considered where the laser beam is used to directly ablate and subsequently heat a propellant from a solid surface. There are some benefits and drawbacks to each of these approaches as shown in Table C.1.

C.2 Proposed Mission

A space asset with a 1 MW source being beamed to a receiving spacecraft is assumed. From an initial orbital mechanics look, this much power only makes sense from the standpoint of an orbital maneuver that requires a large change in semi-major axis and/or inclination (i.e., high delta-V). Furthermore, this much power is enabling for responsive missions that need to be done quickly. Although several orbital scenarios can be envisioned, a nominal LEO–GEO co-planar transfer will be investigated in this study. For this study, the space asset will be assumed to be in MEO with a transferring vehicle going between LEO and GEO. The MEO location for the space asset allows the total distance of the traveling beam to be minimized (i.e., the maximum distance of travel can be half the distance between LEO and GEO).

Table C.1.—Advantages and disadvantages of in-space beamed energy concepts.

Concept	Advantages	Disadvantages
I. Beamed energy power conversion	<ul style="list-style-type: none"> • Converted power can be used for any propulsion system • Existing, Off-the-shelf propulsion systems can be considered • High power solar arrays with energy concentration are increasing in efficiency 	<ul style="list-style-type: none"> • Relatively low overall system efficiency • New generation of power conversion systems need to be demonstrated for high power level
II. Stagnation chamber energy absorption	<ul style="list-style-type: none"> • Energy addition to combustion chamber may also increase combustion efficiency 	<ul style="list-style-type: none"> • High temperature operation throughout entire system • Completely re-designed systems necessary to handle higher temperatures • Requires both primary propulsion and beamed energy to work (reliability)
III. Diverging nozzle energy addition	<ul style="list-style-type: none"> • Lower overall temperatures throughout entire system • Slight modification to existing systems • Energy absorbers (aluminum oxide, Carbon nanotubes, etc) can be added to almost any existing system • 	<ul style="list-style-type: none"> • Direct energy absorption from expanding gas is extremely low • Fuel additives (absorbers) required for many systems which might adversely affect intrinsic performance • Requires both primary propulsion and beamed energy to work (reliability) •
IV. Laser ablation	<ul style="list-style-type: none"> • Direct conversion of energy to propulsion • Solid propellants can be used 	<ul style="list-style-type: none"> • High power density required for ablation • Not demonstrated at this level

C.3 Laser Versus Microwave In-Space Asset

Because of the large distance of travel of the beamed energy, a laser asset is considered optimal. Although the power level near 1 MW is more indicative of current microwave technology, the laser system will be advantageous from the standpoint of beam divergence (diffraction limited optics favor lower wavelength), beam optics (i.e., focusing, collimating, etc.), and beam steering.

For a laser with an initial 5-m diameter laser beam in MEO at a wavelength of 500 nm, the minimum spot size in LEO or GEO would be 8.8 m. A 10-m diameter collector on the spacecraft will be assumed such that the entire 1-MW beam is collected along the entire spacecraft trajectory. To make a 5-m diameter beam in MEO, a significant effort is required in low mass, high efficiency, and high power optics. Something similar to the USAF Academy’s photon sieve might be ideal (Ref. 2). To collect an equivalent amount of solar power, the collector would need to be 30.6 m, assuming a solar flux of 1358 W/m² at Earth. Therefore, the beamed energy would significantly add to the overall system power over what the sun by itself could supply for the same size solar collector.

C.4 Continuous-Wave Mode Versus Pulsed

Pulsed operation of the proposed laser system is advantageous from the standpoint of the spacecraft power required to produce the laser beam. Stored energy source can be used to operate the laser so that the host spacecraft does not have to produce multi-MW of power. An orbital dynamics simulation needs to be done to assess whether a continuous source in MEO could access a transferring vehicle through its entire trajectory or where periods of eclipse might occur.

C.5 Thruster Concepts Investigated

A proposed thruster from each of the four concepts listed in Table C.1 will be evaluated. The following thruster concepts were investigated for thrust augmentation (the value in the parentheses indicates the concept from Table C.1 that the thruster could be considered for).

1. Arcjet (I, II)
2. Resistojet (I, II)
3. MPD (I)
4. Solar Thermal Thruster (II)
5. Liquid Monopropellant (II, III)
6. LOx/LH2 Bipropellant (II, III)
7. Aluminum Solid Propellant (II, III)
8. Laser Ablative Thruster (IV)

Only the LOx/LH₂, aluminum solid, and MPD systems have been demonstrated at the MW level to date. However, there are no known physical reasons why the other systems could not be demonstrated, although their efficiencies at the MW level would have to be investigated. Table C.2 gives some relevant performance parameters (augmented) for the thruster systems listed above.

For a 1MW energy addition to make sense, the augmented thruster system should have an energy level near 1MW, or the thruster should operate completely with the 1 MW of beamed energy. If the augmented thruster jet power is significantly less than 1MW, the energy addition to the propulsion system will essentially act as the only means of thrust. This is technically plausible; however, in this case, the beamed-energy system might as well act as the only propulsion means thereby reducing the overall complexity of the system on the transferring spacecraft side. If the augmented thruster power is much larger than 1MW, the energy added to the vehicle from the beamed-energy source will not significantly impact the thruster performance. Alternatively, concepts that utilize the 1MW beamed energy source as its only means of propulsion can also be considered.

TABLE C.2.— AUGMENTED THRUSTER SYSTEM PERFORMANCE

Thruster	Isp (sec)	Thrust (N)	Mass Flow (kg/s)	Jet Power (kW)	Propellants
Monopropellant	220-240	1-600	4e-4 – 0.3	1-710	Hydrazine, Hydrogen Peroxide
LOx/LH2 ^(a)	420-450 (444)	10,000-70,000 (66,700)	2.3-17 (15.3)	20,600 – 155,000 (145,260)	LOx/LH2
Aluminum Solid ^(b)	250-300 (289.5)	27,000-88,000 (27,000)	9.2-36 (9.5)	33,000 - 130,000 (38,340)	Aluminum/Aluminum Oxide
Arcjet ^(c)	500-1,000 (800)	0.2-2 (2)	(0.24)	1.8-30 (26)	Ammonia, Hydrazine
Resistojet	400-1,000	0.2-6	2e-5 – 1.5e-3	3-30	Hydrogen, Ammonia, Hydrazine
MPD ^(d)	2,000-5,000 (4,500)	40-100 (22.6)	1e-4 – 5e-3 (5e-4)	1,000 (500)	Hydrogen, Lithium, Argon
Laser Ablation ^(e)	2,500	81.5	3.3e-3	1,000	Solid
Solar Thermal	500-1,000	20-220	2e-3 – 4.5e-2	50-1,000	Hydrogen, Water, Ammonia

^a After the RL-10 in ()

^b After STAR 27 Apogee Kick Motor in ()

^c After ESEX Arcjet in ()

^d After Energia (Russian) Li-MPD in ()

^e Assumes no losses. Power set to 1 MW and I_{sp} limited to 2500 s (arb)

TABLE C.3.—THRUSTER SYSTEM PARAMETERS

Parameter	Thrusters	Notes
Demonstrated MW power operation	2, 3, 6	At least lab level demonstration
Plasma naturally available for absorption	4, 6	High efficiency laser photon absorption
Particles/surfaces naturally available for absorption	3, 7	Relatively high efficiency laser photon absorption
Will not require major redesign for power augmentation	7, 8	Heat addition issues—thermal redesign
System benefits including high density propellants	1, 2, 3, 7	Solid and liquid propellants

C.5.1 Concept I

Using the beamed energy as a power source to operate an electric thruster can be considered (i.e., concept I). However, the power conversion efficiency will be relatively low (~40%). Therefore, concept I systems will not be considered in this study.

C.5.2 Concept II

From the argument that the augmented thruster power should be equivalent to the beamed power, electric propulsion systems are not viable for concept II implementation since they will require approximately 1MW of on-board spacecraft power. A high on-board power requirement will make the transferring vehicle power system as complex as the laser beaming spacecraft asset. Concepts that utilize thermochemistry with energy addition to the combustion chamber are viable; however, they are hindered by the complexity of an increased thermal loading throughout the propulsion system while maintaining efficient combustion. An augmented solar thermal propulsion system has several benefits in that its complexity is essentially the same whether using a solar source or a beamed energy source. Also, solar thermal propulsion systems are relatively efficient and the waste heat from the propulsion system could be converted to electrical power that the receiving spacecraft could use for other processes.

C.5.3 Concept III

Neutral gases do not readily absorb photon radiation. This is true of most gases over a wide range of wavelengths. However, high temperature (>1500K) materials and plasmas generally are highly efficient absorbers of both visible and microwave energy. Therefore, fuel additives or plasma formation will be necessary for concept III. From a chemical reaction perspective, adding energy absorbers into a fuel will affect the combustion process for both the bipropellant and monopropellant systems. Fuel additives such as aluminum oxide and carbon nanotubes could be considered. A full redesign of turbomachinery, injectors, mixers, and combustion chambers may be necessary. Solid thrusters contain alumina as a product in the combustion process. Although these particles (both liquid and solid) will readily absorb microwave energy at high temperature, they are not good absorbers of visible or near-IR energy. Therefore, an additive would be necessary to absorb in typical laser wavelengths. From a complexity standpoint, a monopropellant thruster is beneficial over a LOx/LH₂ system and will, therefore, be used as a representative liquid propellant system.

C.5.4 Concept IV

Laser ablative thrusters using solid propellants will be considered.

C.6 Mission Analysis

A notional 2,500 kg (total initial mass including propellant) is transferred from a nominal LEO orbit with an altitude of 200 km to GEO. The delta-V required to perform this mission is approximately 4.18 km/s via a Hohmann transfer. The monopropellant system will be assumed to be an impulsive maneuver whereas the solar thermal and laser ablation thrusters will be assumed to be nearly constant thrust, spiral transfers. For the spiral transfers, a delta-V of 6 km/s is assumed. For the augmented cases, the laser energy addition is assumed to occur for the entire burn time of the thruster.

For the monopropellant thruster, the thrust augmentation is assumed to add to the already existing chemical power in the expanding section of the nozzle. The diverging section of the nozzle could be envisioned as the collector of the incident energy as well, although providing a nozzle exit diameter of 10 m might be impractical. The monopropellant system would need to be seeded with an absorbing particle (alumina or CNTs). Previous studies suggest that upwards of 50% of the beam energy could be converted to useful thrust (Ref. 1). The mass flow of the system is considered constant so that the augmentation energy goes into increasing the propellant exit velocity. The monopropellant thruster is

assumed to be a scaled engine that could operate at a nominal 1MW of chemically provided jet power. The augmented I_{sp} is assumed to be 230 s.

The augmented solar thermal propulsion system is assumed to operate on hydrogen propellant with a specific impulse of 800 s. This specific impulse was chosen so that a reasonable thrust value could be obtained for responsive maneuvering from LEO–GEO while still weighing the importance of efficiency. The augmented (solely solar collection) and augmented (solely beamed energy collection) thrusters include a 10-m diameter collector at the vehicle. The efficiency of the augmented solar thermal thruster is assumed to be 80%.

For the laser ablation thruster, only the 1MW power augmentation from the LEO asset is considered. An aluminum propellant is assumed. A specific impulse of 1,500 s is assumed as a compromise between efficiency and responsiveness. The laser ablation thruster includes a 10-m diameter propellant bed. It is assumed that the thruster is 75% efficient.

TABLE C.4.—MISSION PARAMETERS FOR AUGMENTED AND AUGMENTED THRUSTER SYSTEMS

Thruster	ΔV (km/s)	Power (MW)	Thrust (N)	Isp (sec)	Propellant mass (kg)	Burn time (sec)	Resulting payload mass to GEO (kg)	Difference versus augmented thruster, percent
Monopropellant (Unaugmented)	4.2	1.0	886	230	2,111	5,377	389	-----
Monopropellant (Augmented)	4.2	1.5	1,085	282	1,953	4,973	547	40.6
Solar Thermal (Unaugmented)	6	0.11	28	800	1,336	374,058	1,164	-----
Solar Thermal (Augmented)	6	0.80	76	2,157	617	156,757	1,883	61.8
Laser Ablation	6	0.75	102	1,500	837	120,844	1,663	N/A ¹

¹Indicates that an augmented thruster would not be able to perform the mission.

C.7 Conclusions

Augmented systems, albeit highly conceptual, lead to significant improvements in the metrics used to assess their viability for in-space propulsion missions. An augmented monopropellant system could potentially increase the payload to GEO by 40% over an augmented system, and an augmented solar thermal system could increase the payload mass by 60%. It is also important to note that these missions will be responsive with the longest maneuver time. Although similar performance in terms of payload mass to orbit could potentially be achieved by traditional electric propulsion systems, the time of transfer would be significantly larger. This performance is also being achieved through thrust augmentation via beamed energy without a significant penalty to mass of the transferring spacecraft (the most obvious advantage to beamed energy propulsion).

C.8 References for Appendix C

1. Cornella, B., Ketsdever, A., Gimelshein, N., and Gimelshein, S., “Thrust Augmentation of Solid Rocket Motors Using Beamed Microwave Energy,” *J. Prop. and Power*, Vol. 26, No. 5, pp. 1016-1024, 2010.
2. Andersen, G.,” Large optical photon sieve,” *Opt. Lett.*, Vol. 30, pp. 2976–2978, 2005.

Appendix D.—Microwave Energy Issues

Design Reference Mission 1–C Report

High Power Microwave Antennas

D.1 Introduction

This appendix describes a specific type of ground transmitter, implemented with an array of antennas, which tracks and provides a high power millimeter-wave beam to launch a microwave thermal rocket (MTR) into low Earth orbit (LEO). The transmitter requirements and possible configurations are specified along with the background, theory of operation, and design examples.

This implementation of a high power transmitter is to spatially combine the power radiated from many small antennas elements into a single coherent power beam. These antenna elements must be properly phased together to deliver the maximum amount of power to a target. Thus, this aperture type is termed a phased array antenna. By equally distributing an RF signal generated from a single source to all of the antenna elements and phase correcting the signal for each antenna element, a coherent beam is radiated into free space. High power radiation is achieved by amplifying the RF signal at each element either by solid-state or tube amplifiers.

D.2 Power Beaming Scenario

The baseline MTR power beaming scenario is shown graphically in Figure D.1 where the launch platform is located 100 km from the ground transmitter. The rocket ascent trajectory consists of two segments. From ground to an altitude of 45 km, the rocket is launched vertically using conventional chemical fuel. During this initial phase an onboard MTR beacon signal is broadcast to the transmitter ground station. A ground receiver at the transmitter acquires and initiates the tracking of the antenna array towards the MTR. At an altitude of 45 km, the ground transmitter begins power beaming at an elevation angle of 25° from the horizon. This second phase of the ascent is then powered by the microwave beam where the MTR levels off and accelerates horizontally to fly overhead and past the ground transmitter. The rocket reaches a maximum altitude of 90 km where the power beaming concludes at an elevation angle of 52° from the horizon.

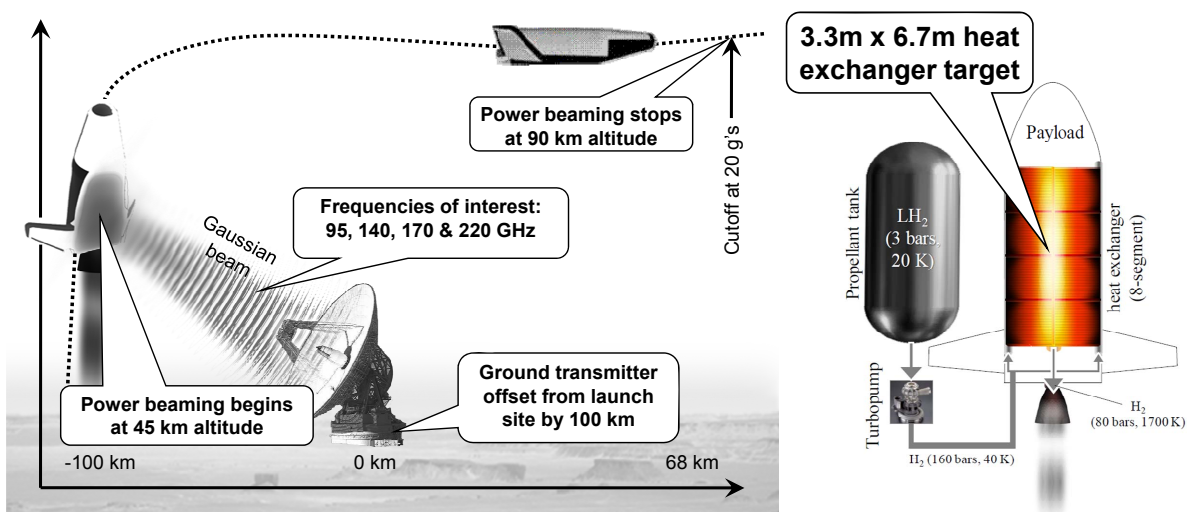


Figure D.1.—Baseline power beaming configuration and MTR details.

For the transmitter design, the most important parameter is the distance or range to the MTR. The range S is calculated with a known trajectory by

$$S = \sqrt{R_e^2 + (R_e + h)^2 - 2R_e(R_e + h)\cos(\lambda)} \quad (D1)$$

where

- R_e Radius of the Earth, 6378.14 km
- h Altitude of spacecraft, km
- λ Earth central angle from transmitter to spacecraft target, degrees

The MTR's slew angle ϕ as viewed from the transmitter is determined by the trajectory and is related to the Earth's central angle λ by

$$\lambda = \phi - \sin^{-1} \left[\sin(\phi) \frac{R_e}{R_e + h} \right] \quad (D2)$$

Figure D.2 shows the baseline trajectory parameters used in this study. Rocket altitudes, range to the MTR from the transmitter, and elevation angles as viewed by the transmitter vary from power beaming commencement to cut-off where the maximum range is balanced between the two points.

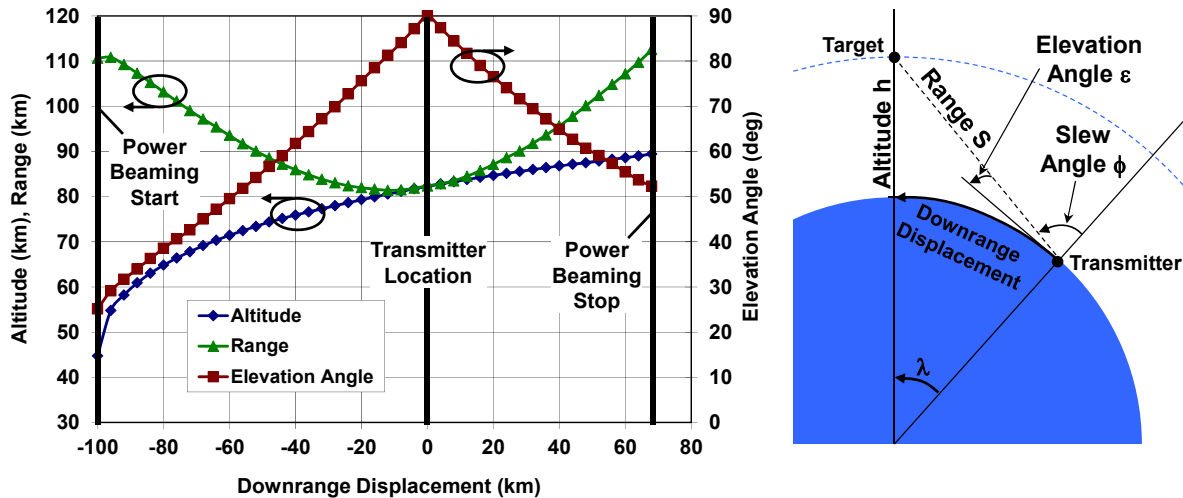


Figure D.2.—MTR altitude, range, and elevation angle with respect to the transmitter.

Table D.1 provides the key requirements and design variables for the ground transmitter. The most important requirement is to achieve a power density of 30 MW/m² across the MTR's heat exchanger surface throughout the launch trajectory. The variables in this system are the power beaming frequency, location of the transmitter, and transmitter size. Because the power density decreases with the square of the distance to the MTR, the launch trajectory and location of the transmitter are carefully chosen to provide the required power density at the extreme ends of the trajectory path from launch to power beaming cut-off. Additionally, the launch and transmitter locations are ideally located in areas with arid climates and high altitudes to minimize the gaseous attenuation through the atmosphere. To this regard, two ground transmitter locations identified for this study: (1) China Lake, CA (Latitude 35.94°, Longitude E 242.55°, Elevation 1,679m) and (2) the Llano de Chajnantor Observatory in the Atacama Desert in Chile (Latitude -23.02°, Longitude W -67.75°, Elevation 5058.7m).

TABLE D.1.—POWER BEAMING REQUIREMENTS, VARIABLES, AND ASSUMPTIONS

Requirements	Variables	Assumptions
<ul style="list-style-type: none"> • 30 MW/m² minimum power density at spacecraft’s heat exchanger • ≤ 0.5dB loss in power density at the edges of the 3.3m x 6.7m heat exchanger • Spacecraft trajectory with respect to the transmitter shown in Figure D.2 	<ul style="list-style-type: none"> • Power beaming frequency 95, 140, 170, and 220 GHz • Transmitter location China Lake, CA and Atacama Desert, Chile • Transmitter size • Output power 	<ul style="list-style-type: none"> • Power beaming occurs under clear sky conditions to avoid atmospheric attenuation due to rain and clouds

Figure D.3 compares the specific atmospheric attenuation in dB/km at the two ground station locations (Ref. 1). Although both sites have low specific attenuations, the Atacama Desert is lower due to its higher elevation. The attenuation peaks at 60 GHz and 119 GHz are caused by oxygen resonances, and the peaks at 22 GHz and 183 GHz are caused by water vapor resonances. Obviously, these frequencies are avoided for this power beaming application.

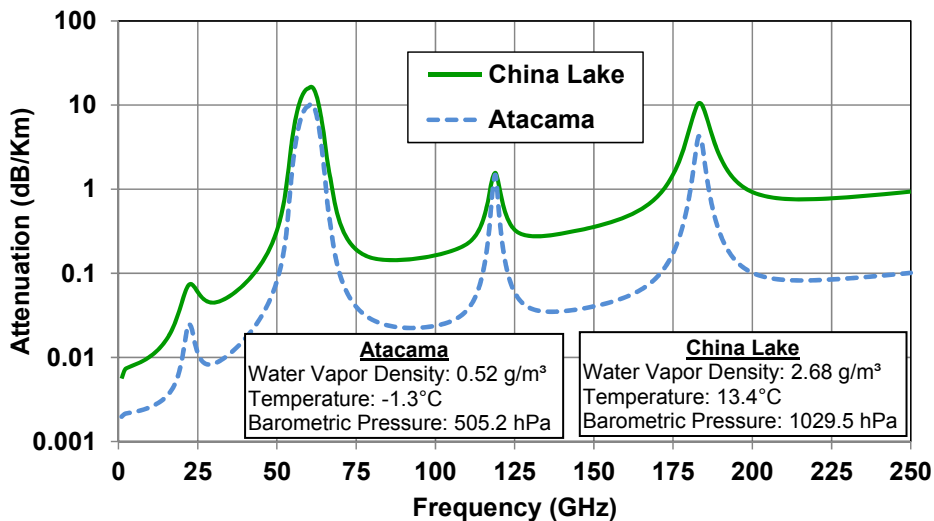


Figure D.3.—Clear sky atmospheric specific attenuation at China Lake, CA and the Llano de Chajnantor Observatory in the Atacama Desert, Chile.

Using the MTR trajectory information in Figure D.2 and specific attenuations in Figure D.3, Figure D.4 shows the atmospheric attenuation comparison at the four frequencies of interest for the two transmitter locations. China Lake has higher atmospheric loss at the higher frequencies due to its lower elevation. In both locations, the highest loss occurs at a downrange displacement of -100 km the power due to the lower elevation look angles from the transmitter (see Figure D.2).

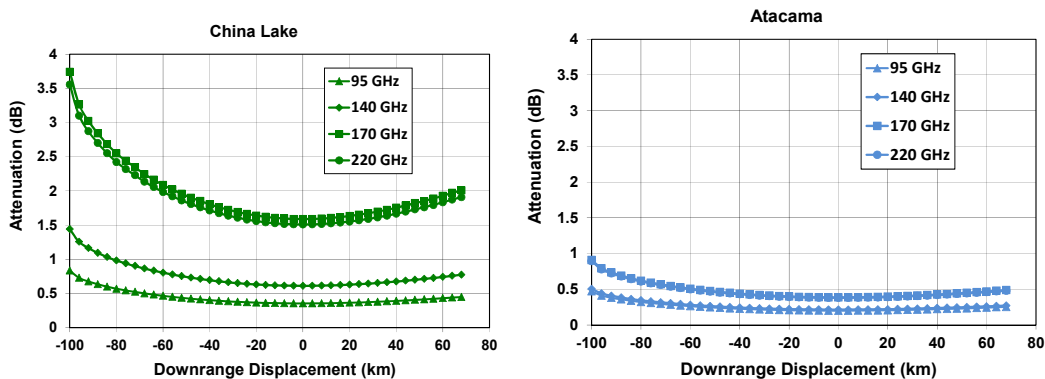


Figure D.4.—Clear sky atmospheric attenuation at China Lake and Atacama.

Again using the MTR trajectory information in Figure D.2 and specific attenuations in Figure D.3, the radiated power densities at the MTR are shown in Figure D.5 at the four power beaming frequencies and at the two transmitter locations. Power density is calculated using the far-field equation

$$P_{dens} = \frac{EIRP}{4\pi R^2} \quad (D3)$$

where *EIRP* is the transmitter’s effective isotropic radiated power (i.e., the RF power multiplied by the antenna gain) and *R* is the range to the target.

At 95 GHz and 140 GHz, the power densities are relatively balanced at power beaming start and stop points. At 170 GHz and 220 GHz, there is a noticeable difference in the power density curves attributed to the different atmospheric losses between the two ground locations. In all cases, the power density peaks around the transmitter’s zenith due to the shortest range and lower atmospheric attenuation.

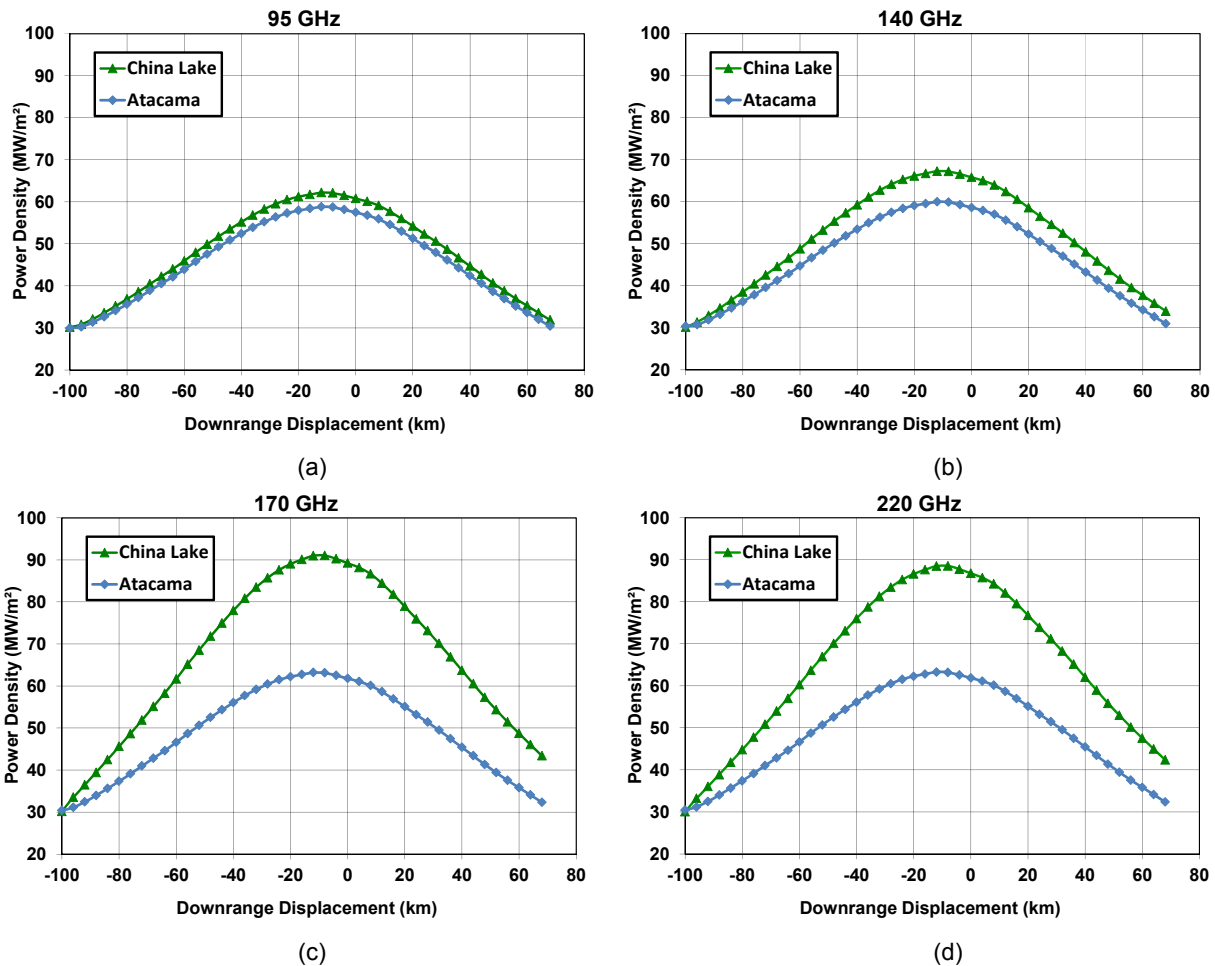


Figure D.5.—Power densities at the MTR from power beaming turn-on to turn-off at (a) 95 GHz, (b) 140 GHz, (c) 170 GHz, and (d) 220 GHz.

The derived EIRPs used to create these power density curves are given in Table D.2. They range from 187 dBW to 190 dBW to provide a minimum of 30 MW/m² over the trajectory range.

TABLE D.2.—REQUIRED TRANSMITTER EIRPS TO ACHIEVE A MINIMUM OF 30 MW/M² AT THE MTR

Frequency (GHz)	EIRP (dBW)	
	China Lake	Atacama
95	187.5	187.2
140	188.1	187.2
170	190.4	187.6
220	190.2	187.6

D.3 Transmit Phased Array Antennas

A transmit phased array antenna consists of multiple antenna elements that spatially combines the RF power from each radiating element. This property is due to the phase coherency of the RF signal through the antenna's beam forming network. When the phases of each antenna element are exactly aligned and each antenna radiates equal levels of RF power, the transmitted effective isotropic radiated power (EIRP) is N^2GP where N is the number of antenna elements, G is the gain of a single antenna, and P is the radiated RF power from a single element. If the antenna element phases are random (i.e., non-coherent), the anticipated EIRP is NGP but it can vary from zero to N^2GP . To achieve the N^2 effect on EIRP, the antenna elements must be properly phase calibrated.

Phased array antennas have long been used for radar, communication, and radio-astronomy applications. Advantages and disadvantages of phased arrays are given in Table D.3.

TABLE D.3.—PHASED ARRAY ANTENNA ADVANTAGES AND DISADVANTAGES

Advantages	All Electronic Array Disadvantages	All Mechanical Array Disadvantages
<ul style="list-style-type: none"> • Fast Beam Agility—Electronically beam steering can be accomplished in micro-seconds 	<ul style="list-style-type: none"> • Beamforming Complexity 	<ul style="list-style-type: none"> • Beamforming Complexity
<ul style="list-style-type: none"> • Graceful Degradation 	<ul style="list-style-type: none"> • Scan Loss 	<ul style="list-style-type: none"> • Tracking Speed
<ul style="list-style-type: none"> • Scalability 	<ul style="list-style-type: none"> • Cost 	<ul style="list-style-type: none"> • Mechanical Wear
<ul style="list-style-type: none"> • Multiple Independent Beams 		

To meet the high power density demands of the MTR, an all mechanical steered phased array of dish antennas is chosen to provide a high EIRP. To achieve phase coherency throughout the array, a single RF source is distributed to each dish antenna where phase corrections are applied to correct for spatial differences, Doppler shifts, electrical errors, and temperature effects. This relatively low power RF signal at each antenna is then amplified using high power amplifying tube such as a gyrokystron. Because the dish antennas steer mechanically, the antennas are spaced to avoid blocking the view to the MTR from each other. Because the antennas are electrically large (i.e., larger than a wavelength), large grating lobes will form if the antennas are spaced in a uniform pattern. These grating lobes reduce the total RF power in the main beam and therefore reduces its power density at the MTR. Thus, the relative location of each antenna with respect to each other should be placed in a manner to suppress these undesirable grating lobes.

D.3.1 Uplink Array Background

The first demonstration of arraying large dish antennas occurred at the JPL Goldstone facility in 1993 at X-band (Figure D.6) (Refs. 2 and 3). Using a two-element array of 34 m diameter dishes, signal combining efficiencies of 98% at 7.19 GHz were achieved while tracking low-earth orbiting (LEO) debris using time-overlapped radar pulses. Both antennas tracked debris from about 10° elevation at signal rise to 4° elevation at signal set under varying weather conditions (e.g., hail falling on one antenna). JPL demonstrated this technique using 5 kW peak pulses at 100μs pulse widths and 50 pulses/sec. Both antennas were fed from a common oscillator source, and a common receiver was used to measure in real time the phase-path differences from the antennas from signals reflected by orbital debris. Conjugate

phases incorporating the predicted geometry path lengths were then applied through a phase locked loop for the uplink signal. Thus, tracking was accomplished retrodirectively on the orbiting targets.

The phased locked loop schematic and receive pulse structure are shown in Figure D.7. One of the antennas was designated as the master whose phase was set to the system phase reference. The second antenna was designated as the slave whose phase was adjusted by phase control software so that the signal at the target was coherent with the master. A master oscillator is used to drive the master antenna and the numerically controlled oscillator (NCO) of the slave transmitter. Doppler compensation is applied to the common receiver local oscillator. A pulse operation table (POT) controlled the pulse separation, pulse width, transmit trigger, receiver data inputs to the phase loop, application of the output of the phase loop to the phase of the next pulse, and offsetting both the timing and phase by predetermined values. The master and slave pulses were typically offset by 50 μs to form a pulse 150 μs total length with the first 50 μs being from the master, the middle composed of both master and slave, and the final 50 μs from the slave. This receive pulse structure was measured in actual experiments when the pulses were in phase on the target.

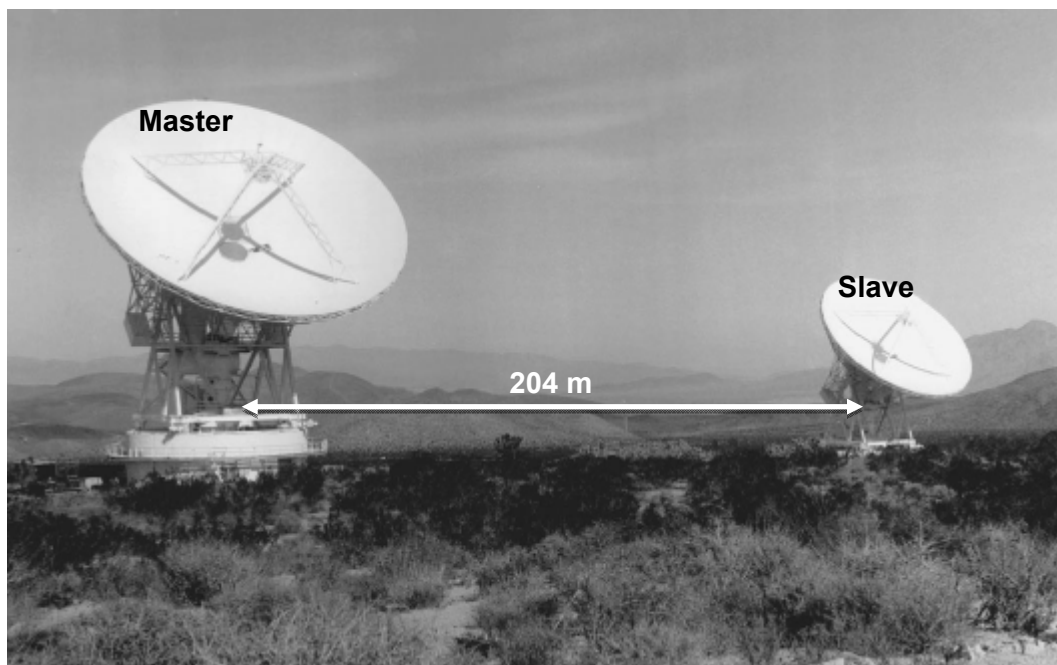


Figure D.6.—JPL's 1993 uplink phased array demonstration (Ref. 2).

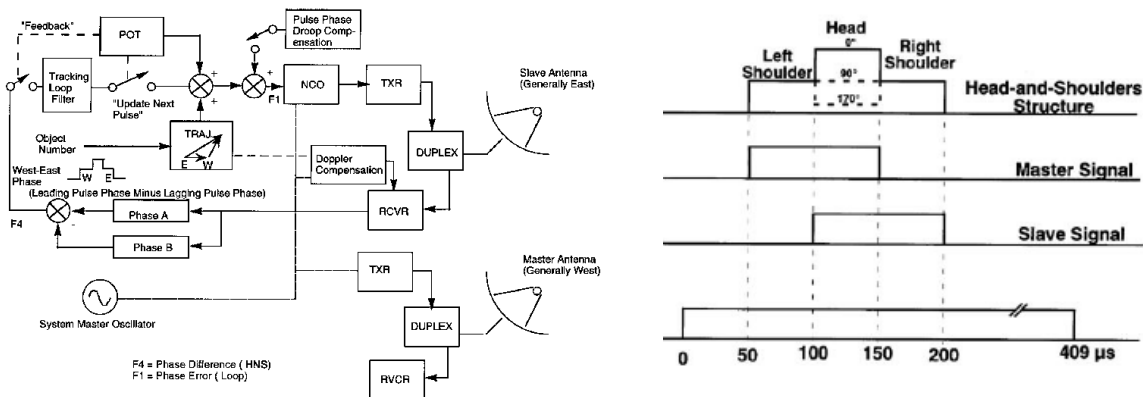


Figure D.7.—Uplink array phased locked loop schematic and receive signal structure (Ref. 2).

JPL later followed with a second uplink demonstration on June 27, 2008, also at the Apollo antenna cluster at Goldstone (Refs. 4 to 7). Using an array of three 34m diameter antennas, a 7.18 GHz signal was coherently combined to the Extrasolar Planetary Observation and Characterization/Deep Impact Extended Investigation (EPOXI) spacecraft (Figure D.8). The received signal power level at the spacecraft was recorded at the theoretical limit of 9 times over the power level from a single 34m antenna. Using right-hand circular polarized signals, EPOXI measured power gains of 6dB and 9.5dB over a single antenna for both 2-element and 3-element arrays. Figure D.8 shows the 3-element array configuration where antenna Deep Space Station (DSS)-25 is the reference antenna and the other two antennas are slaved to its reference phase. Although the radiated power from each 34m antenna could be as high as 20kW, the power was reduced to 2kW to avoid saturating EPOXI’s receiver.

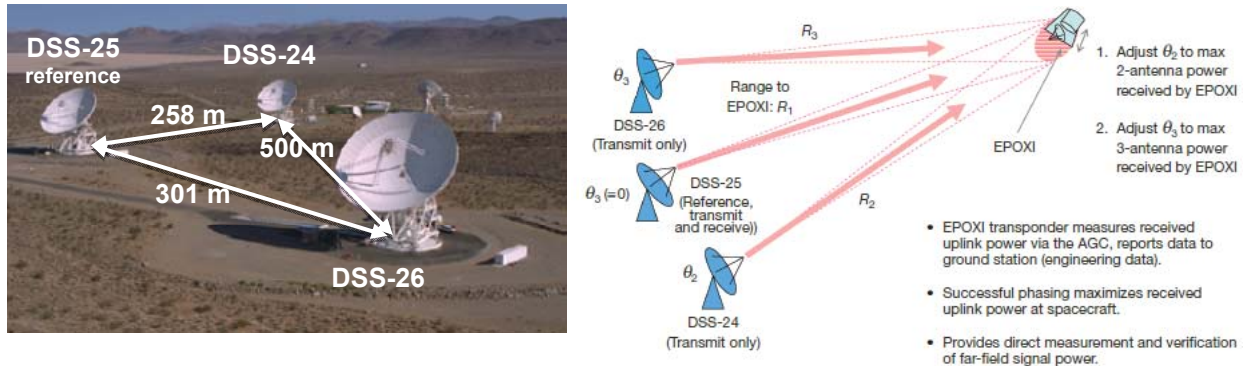


Figure D.8.—JPL’s 2008 uplink phased array demonstration (Ref. 4).

Figure D.9 shows the measured received power over time as recorded on EPOXI’s carrier lock accumulator (CLA). At SCET (spacecraft event time) 13:36, the received power increased 9.2 dB with 3 transmitting antennas which is very close to the theoretically 9.5 dB limit (i.e., $20 \log(3) = 9.5$ dB).

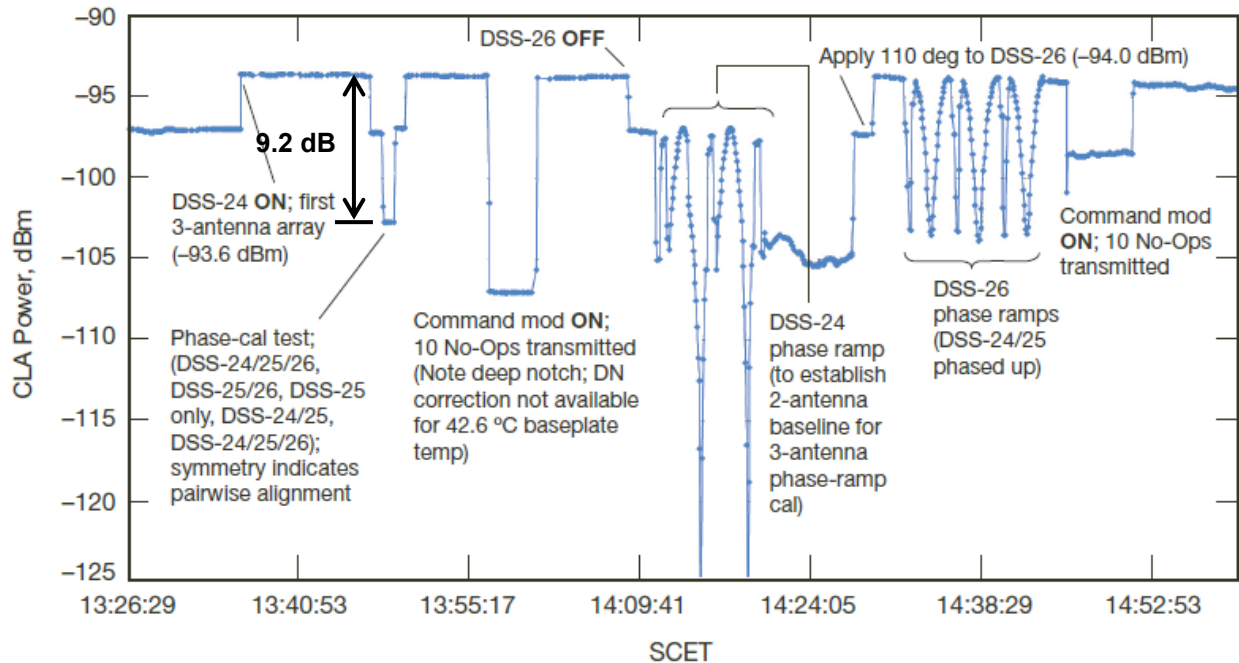


Figure D.9.—EPOXI’s measured receive power from the uplink phased array demonstration (Ref. 5).

The arrayed power distribution in the far-field is the product of a single antenna with the array factor of all three antennas. As seen in Figure D.10, these widely separated antennas create an interference pattern within its main beam from two or three antenna point sources located at each antenna phase center (Ref. 8). The narrowest fringe space, in pattern (b), corresponds to the widest antenna separation of 500m between antennas DSS 24 and DSS 26. For this power beaming application where all the power needs to be concentrated on the launch vehicle single point, these grating lobes are an undesirable trait. The key attribute from this EPOXI experiment is the coherent power combining from an array of 3 antennas while tracking the spacecraft.

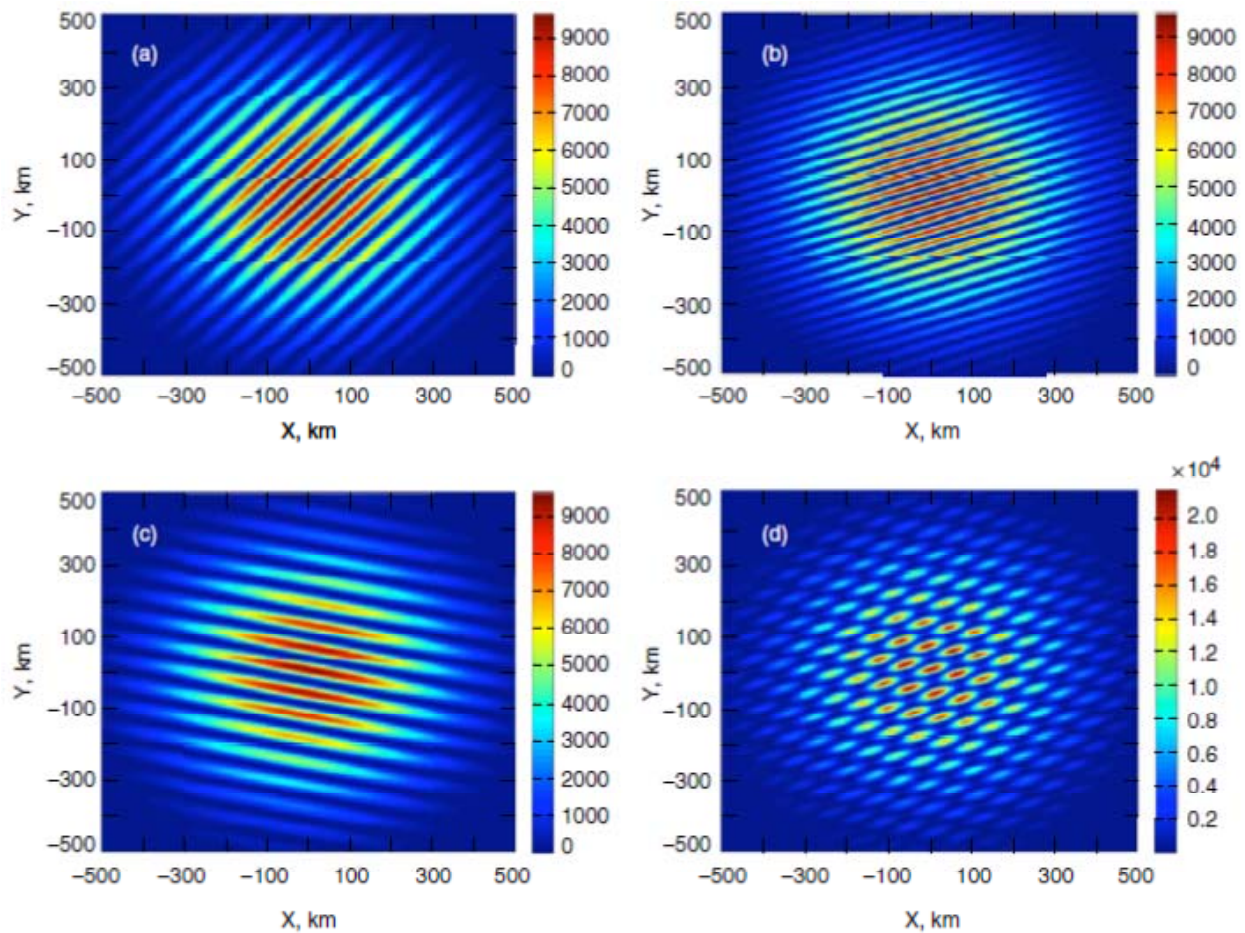


Figure D.10.—Simulated far-field radiation patterns of two and three 34 m diameter antennas at the distance of the moon: (a) antennas DSS 25 and DSS 26, (b) antennas DSS 24 and DSS 26, (c) antennas DSS 24 DSS 25, and (d) three-antenna far-field intensity pattern (Ref. 8).

To track the satellite, DSS-25 transmitted a carrier tone that was received and acquired by EPOXI to ensure that's onboard high gain antenna was pointed towards Earth. EPOXI then transmitted an X-band downlink carrier that was acquired by DSS-25's receiver for recording telemetry from the spacecraft. The phase of this downlink signal was carefully monitored and distributed to the two other transmitters. Slowly varying phase drifts in the ground system were monitored and controlled by the Phase Comparator and Control Assembly (PCCA) that is located in the Signal Processing Center (SPC)-10 located 16 km from the Apollo Complex antennas. The PCCA contained a signal distribution assembly (SDA), two phase comparator assemblies (PCAs) to measure round-trip and cross-phase from all three Apollo antennas, and a phase modulation assembly (PMA) that can be used to add correction phases to either the DSS-24 or the DSS-26 carriers (Figure D.11).

The ground system consists of the X-band exciters at SPC-10, X-band couplers and a “round-trip” PCA at SPC-10, optical fibers for signal distribution to the transmitting antennas, X-band couplers at the output of the power amplifiers at each antenna, X-band couplers at the output of the power amplifiers at each antenna, and additional optical fibers to return the coupled signal samples to SPC-10 for comparison. The two-way optical fiber distribution network to and from the antennas is located in the same bundle for most of the 16 km distance from SPC-10 to the Apollo cluster, ensuring similar thermal behavior for the outgoing and returning signals. At the Apollo Station, the individual fibers are broken out from the common bundle and routed to their respective antennas, typically a distance of a few hundred meters, over which the fibers may experience independent thermal environments. Following power amplification at the antenna pedestal room, a small fraction (−54 dB) of the amplified X-band signal is coupled off the waveguide and routed back to SPC-10, where the phase of this sampled signal is compared to the transmitted phase using the real-time PCA. The inputs to the PCA are the outgoing (reference) and return (sample) signals from the Apollo antennas. The PCA outputs consist of complex samples of equal magnitude representing the phase difference between the reference and sample of each antenna (round-trip phase) that is used to measure changes in total path length or the difference phase between the reference outputs of two different antennas at SPC-10 (cross-reference phase).

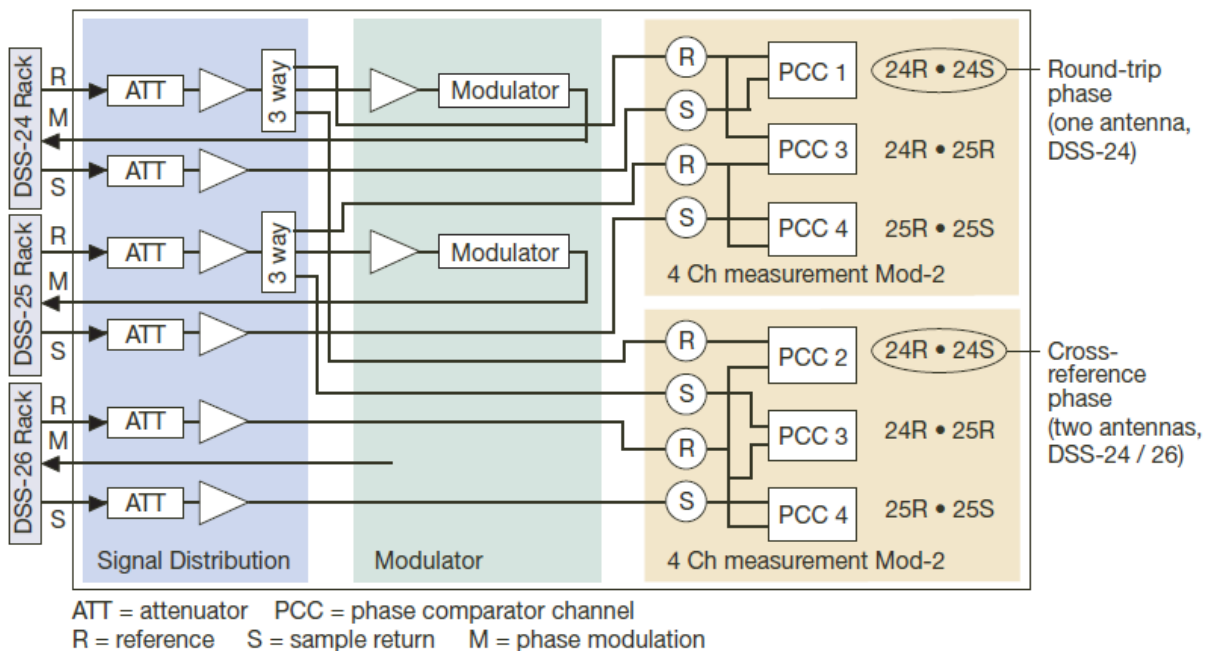


Figure D.11.—PCCA block diagram for controlling the phase of the distributed uplink signal (Ref. 4).

D.3.2 Array Pattern Theory

The pattern of a phased array antenna is composed of the element pattern multiplied by the array factor. To model the element pattern of a dish antenna, the Hansen one-parameter distribution for a circular aperture is selected (Ref. 9). This distribution is chosen based on its efficient taper and selectable sidelobe levels (SLLs). For example, a 1.86-m diameter dish antenna with a 25 dB SLL operating at 95 GHz has an element pattern given in Figure D.12. A Hansen parameter of 0.89 provides this sidelobe level with an 87% taper efficiency.

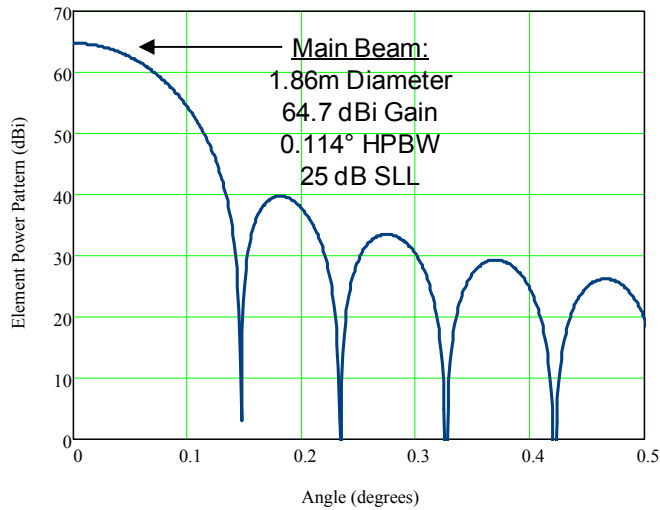


Figure D.12.—Element antenna pattern of a 1.86m dish antenna at 95 GHz.

The radiated field pattern of a square array of M antennas is given by

$$\vec{s}(\phi, \theta) := \sum_{i=0}^M \sum_{j=0}^M e^{j \cdot \mathbf{k} \cdot \sin(\theta) \cdot (x_i \cdot \cos(\phi) + y_j \cdot \sin(\phi))} \quad (D4)$$

where x_i and y_j denote the locations of the antenna elements, θ is the angle from the aperture boresight, and ϕ is the azimuth angle (Ref. 10). The antennas are spaced on a 2 m square grid, and the array factor pattern is shown in Figure D.13. Many grating lobes are created with this spacing.

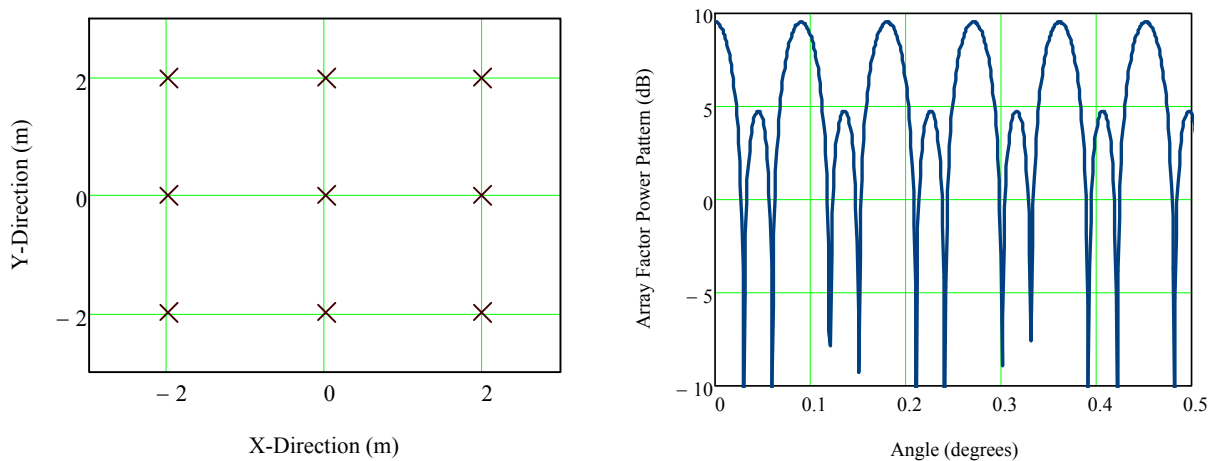


Figure D.13.—Array of 9 antenna elements separated by 2m and array factor pattern at 95 GHz.

When the element pattern and array factor are multiplied with each other, the resulting power patterns at three pattern slices are shown in Figure D.14. As seen, the grating lobes are suppressed, but at the 0° azimuth pattern cut reveals a sidelobe that is only 4 dB below the main beam.

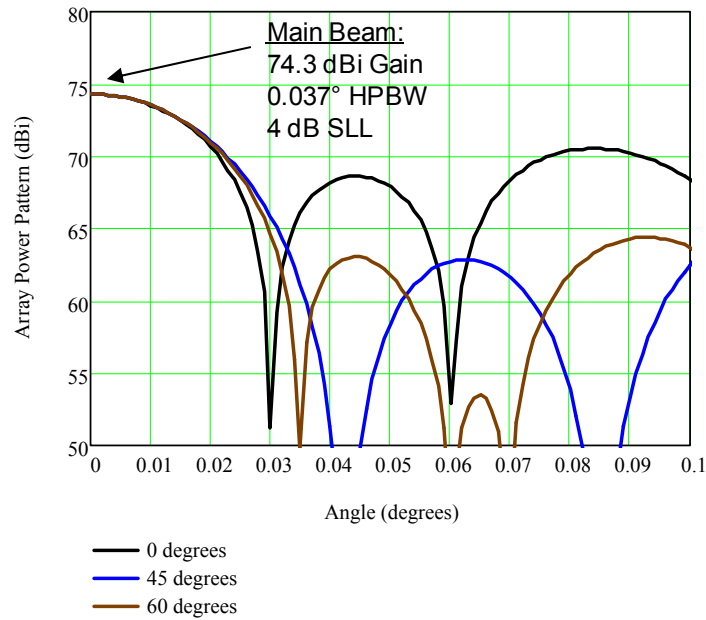


Figure D.14.—Power patterns of 9-element array of 1.86 m dish antennas at 95 GHz.

One method of grating lobe suppression is to proper antenna element spacing and amplitude tapering. The array factor should have one complete cancellation null and it should fall between the first null of the element factor. However, the antenna spacing is dictated by the maximum steering angle from zenith, and this criteria may not be met.

Another issue that surfaces with an electrical large aperture operating at millimeter-wave frequencies is the far-field patterns. If the target, in this case the MTR, is in the near-field of the array, the on-axis beam power density could be much less than predicted by the far-field equations. As Figure D.15 indicates, the power radiated from an aperture is contained in a corrugated tube whose mean diameter is the same as the aperture (Ref. 11). This tube extends to roughly twice the hyperfocal distance of $L^2/2\lambda$ where L is the aperture's largest dimension. At L^2/λ the far-field pattern forms and simple closed-form equations for calculating power densities (e.g., Equation (DD3)) or half-power beamwidth (HPBW).

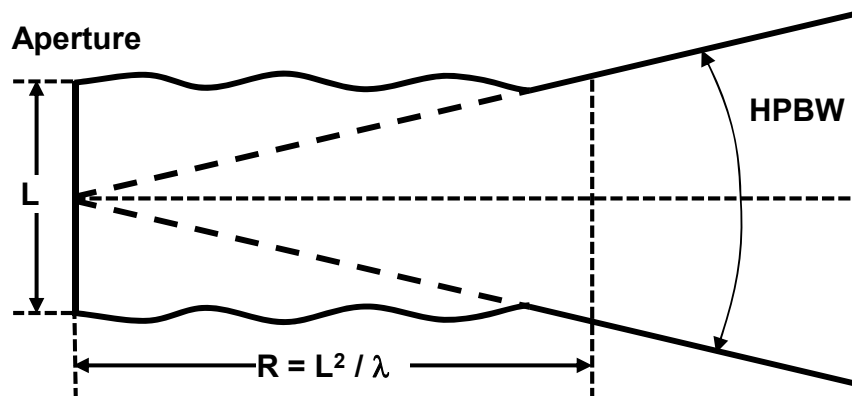


Figure D.15.—Power flow diagram from an aperture antenna (Ref. 11).

Because the phases of each antenna can be controlled, the beam can be focused within the radiating near-field region. The radiating near-field region from a large aperture is defined as the distance λ to the far-field distance $2L^2/\lambda$ from the aperture where L is the aperture's largest dimension (Figure D.16) compares the calculated on-axis power densities at distances from $0.02L^2/\lambda$ to $2L^2/\lambda$ for a square aperture. For an unfocused beam, the on-axis power density undulates due to the beam broadening occurring as the beam is being formed. However, the focused beam on-axis power densities follow the predicted power densities using the far-field Equation (DD3). Thus, it is possible to use the far-field equations for power densities and HPBW's with the assumption that the radiated pattern is focused on the target in the near-field.

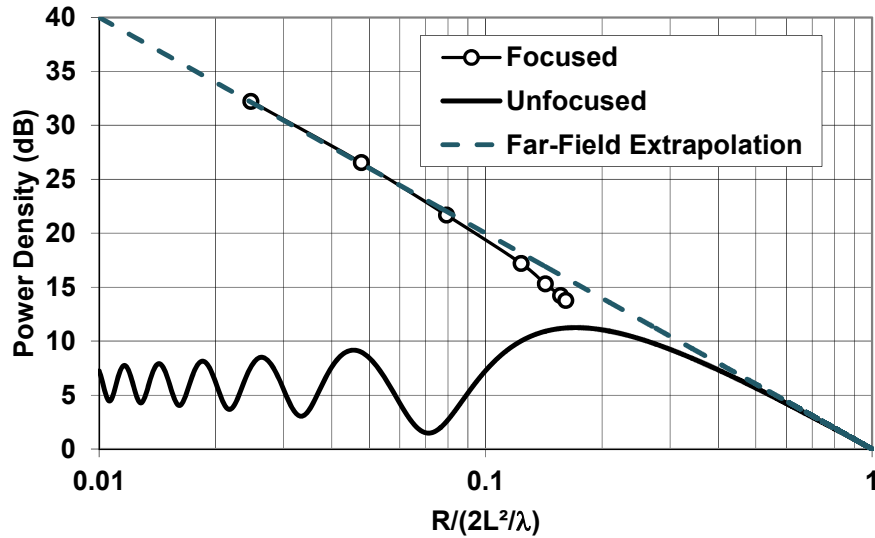


Figure D.16.—Comparison between on-axis power densities in the near-field for a square aperture with a focused beam, an unfocused beam, and a comparison to the far-field power density Equation (DD3) (Refs. 11 and 12).

D.3.3 Tracking

One technique for the phased array to accurately tracking the MTR is to employ retrodirective beam pointing. Retrodirectivity was demonstrated in the 1993 JPL experiment discussed in Section D.3.1. A retrodirective array is an array of widely-separated (separations much greater than a wavelength) antennas that each receive and detect the phase of a beacon signal from the target to be tracked. As shown in Figure D.17, each antenna conjugates, or reverses the sign of the beacon signal, amplifies it, and re-transmits it towards the spacecraft so that the signal retraces its path and converges on and around the beacon.

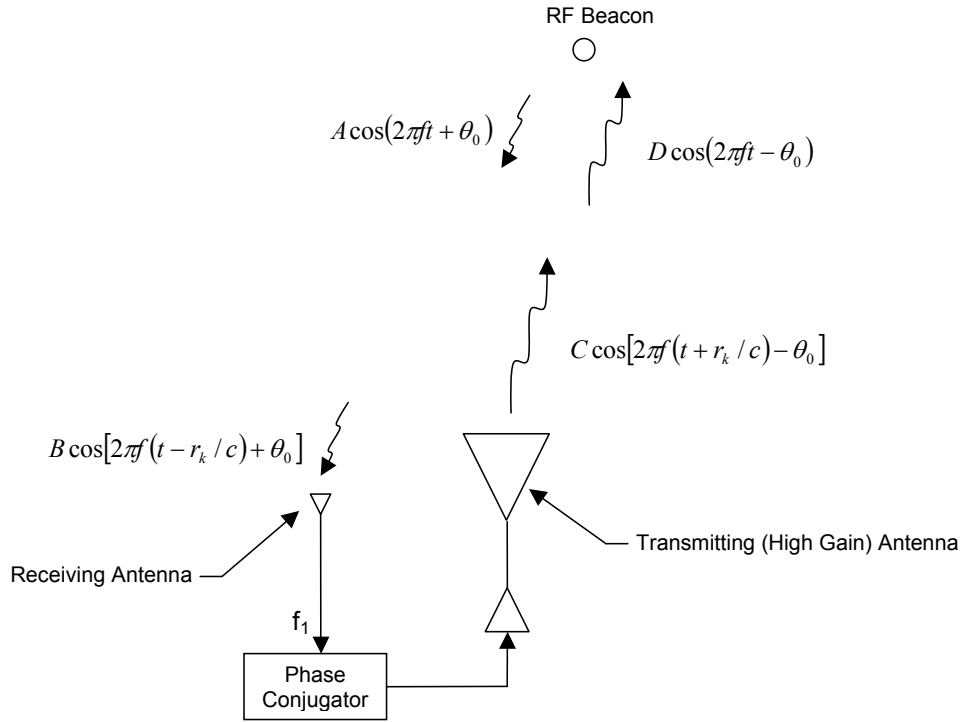


Figure D.17.—Retrodirective tracking scheme.

The beacon broadcasts a signal at frequency f of the form

$$V_B(t) = A \cos(2\pi ft + \theta_0) \quad (D5)$$

that is received by all array elements, where A is the signal amplitude and θ_0 is an arbitrary phase. As illustrated each array antenna is equipped with separate receive and transmit antennas in order to maintain high isolation between transmit and receive signal paths. The signal received by the k^{th} element of the array at time t is proportional to that radiated by the beacon at an earlier time $t - r_k/c$, where r_k is the distance from the beacon to the receive antenna and c is the velocity of light

$$V_R^k(t) = B \cos[2\pi f(t - r_k/c) + \theta_0] = B \cos[2\pi ft + \phi_t] \quad (D6)$$

where $\phi_t = -2\pi fr_k/c + \theta_0$ is the accumulated phase of the received signal. The received signal is processed by a phase conjugator, which simply reverses the sign of the phase, so that after amplification by the high-power microwave amplifier, the signal transmitted by the k^{th} element of the array is of the form

$$V_T^k(t) = C \cos[2\pi ft - \phi_t] = C \cos[2\pi f(t + r_k/c) - \theta_0] \quad (D7)$$

The high-power signal incident on the MTR is transmitted at an earlier time $t - r_k/c$ by the k^{th} element of the transmitter array so that

$$\begin{aligned} V_{HP}^k(t) &= D \cos[2\pi f(t - r_k/c) - \phi_t] \\ &= D \cos(2\pi ft - \theta_0) \end{aligned} \quad (D8)$$

that is the same for all array elements. The radiated power from each array element arrives at the MTR with the same phase. The received power adds vectorially to yield a power density exceeding that from a single element by a factor of N^2 where N is the number of array antennas

D.3.4 Configurations

Phased array antennas have long been used for radio-astronomy applications for receiving images of distant targets. Figure D.18 shows an example of a 84-element radio telescope array operating at 17 GHz and 34 GHz. Unlike uplink transmit phased arrays, signals can be coherently combined in these receive phased arrays by post processing the phases of the received signals. For large transmit phased arrays, the individual antenna elements must be phased calibrated to single reference antenna as described earlier.



Figure D.18.—84-element Nobeyama Radioheliograph array for 17 GHz and 34 GHz reception. Each antenna is 80cm in diameter (Ref. 13).

For the array to avoid blockage from adjacent antennas while steering towards the rocket, the minimum antenna separation is dependent on antenna diameter and minimum elevation angle. From the baseline trajectory of Figure D.2, the minimum elevation angle of 25° occurs at the downlink range of -100 km at power beam turn-on. The minimum separation is given by

$$S_{min} = \frac{1.1D}{\sin(\varepsilon)} \quad (D9)$$

where the 1.1 factor avoids scattering effects from the adjacent antenna when pointed at the minimum elevation angle, D is the antenna diameter and ε is the elevation angle with respect to the horizon. Driven by this minimum spacing requirement, grating lobes will be very high with respect to the main beam for a uniform grid of antenna separations. Stadter et al., studied the effect of randomizing the locations of a large array of dish antennas. Figure D.19 shows one result of an array of 217 dish antennas separated by 21.7 m and operating at 7.2 GHz. The individual locations of each 3.8 m diameter antenna was varied from one half-wavelength up to 500 half-wavelengths, and the array pattern was monitored for suppressing the array factor grating lobes. When the locations were randomized up to 500 half-wavelengths, the grating lobes were substantially suppressed. This technique would be recommended to suppress grating lobes for this application.

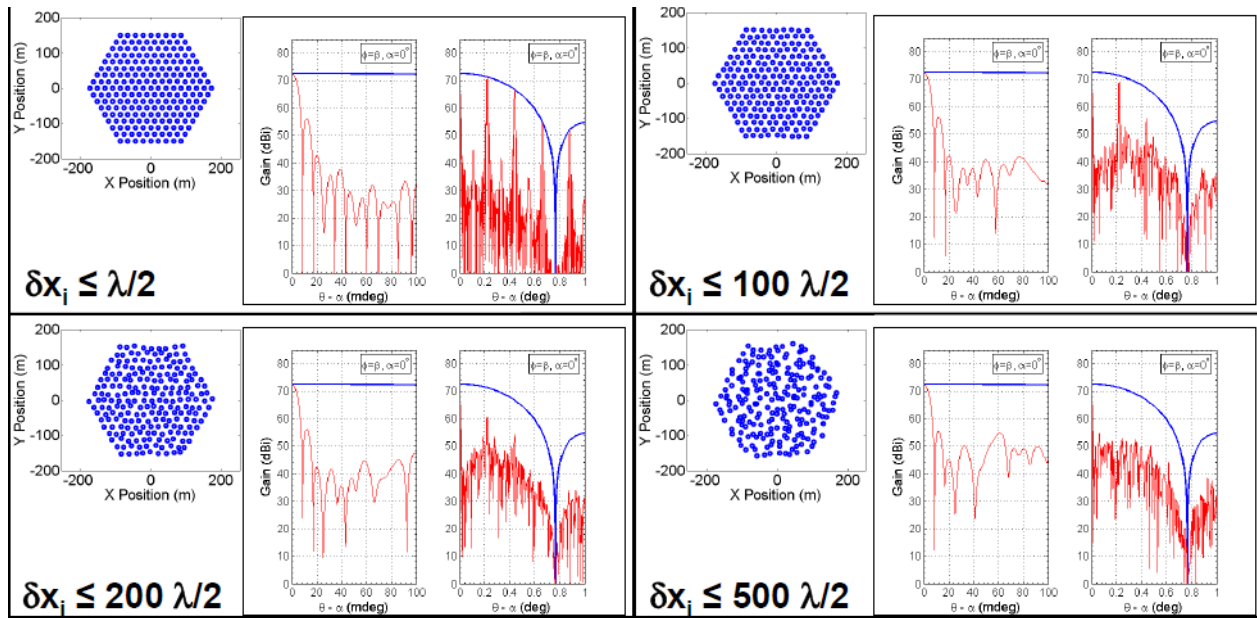


Figure D.19.—Suppression of array grating lobes by randomizing the location of each antenna (Ref. 14). Each 3.8m antenna location is varied from one half-wavelength to 500 half-wavelengths. Element patterns of the 3.8 m antenna are shown in blue, and the array patterns are shown in red.

With the assumptions that grating lobes can be suppressed from antenna element location randomization and the power beam can be focused in the near-field, a comparison of the different frequencies can be evaluated. Table D.4 shows assumptions made in this evaluation to determine the array sizes to meet the EIRPs provided in Table D.2.

TABLE D.4.—PHASED ARRAY ANTENNA INPUT PARAMETERS

Parameter	Value	Comments
Taper Efficiency	87%	25 dB SLL One-Parameter Hansen Taper
Dish Surface Efficiency	80%	Ruze Equation (Ref. 15)
Array HPBW	0.001 degrees	Provides a 41m HPBW at the MTR at zenith
Antenna Output Power	500 kW	Radiated power from each dish antenna

Figure D.20 shows the calculated results to size the array for the very large EIRP requirements. Although the array diameter reduces as the frequency increases, the number of dish antennas increases with frequency. The antennas are spaced using Equation (DD9), and the required surface accuracy is also determined using the Ruze equation.

Frequency (GHz):	95	140	170	220
Wavelength (m):	0.0032	0.0021	0.0018	0.0014
Antenna Spacing (m):	4	2.5	1.7	1.3
Antenna Spacing (λ):	1268	1167	964	954
Antenna Diameter (m):	1.86	1.16	0.79	0.60
Required RMS Surface Accuracy (μm):	119	80	66	51
Antenna HPBW (deg.):	0.114	0.123	0.150	0.151
Antenna Gain (dBi):	63.8	63.1	61.4	61.3
Antenna EIRP (dBW):	120.8	120.1	118.4	118.3
Array Diameter (m):	211	143	118	91
No. of Array Antennas:	2190	2580	3790	3870
Array Gain (dBi):	97.2	97.2	97.2	97.2
Array Pout (dBW):	90.4	91.1	92.8	92.9
Array EIRP (dBW):	187.6	188.3	190.0	190.1

Figure D.20.—Antenna array summary for meeting the 30 MW/m² power density requirement at the MTR.

D.4 Conclusions

The two overriding technical challenges to a phased array antenna approach are the following:

1. Phasing possibly thousands of dish antennas to a single reference that tracks the MTR in the near field. Dynamic focusing would be required to keep the beam focused on the moving MTR at approximately 4 m/second.
2. Developing a 500 kW amplifying tube to generate the needed RF power output of each antenna. Current millimeter-wave tubes are produced with 10kW of output power, and an order of magnitude higher power is needed in this application.

These barriers could be overcome with future technology development and demonstrations. The optimum array configuration also depends on the cost of its components, and future studies should consider the cost impact of output power with individual antenna size.

D.5 References for Appendix D

1. "Attenuation by atmospheric gases," Recommendation ITU-R P.675.5, 2001.
2. R.M. Dickinson, D.L. Losh, R.D. Barber, and J.K. Dempsey, "A phase-control approach for a large-element coherent microwave power uplink system," *IEEE Trans. Antennas and Propagation*, vol. 47, no. 3, pp. 487-495, March 1999.
3. W.A. Imbriale, "Large Antennas of the Deep Space Network," Monograph 4, Jet Propulsion Laboratory, California Institute of Technology, Chapter 9, Feb. 2002, http://descanso.jpl.nasa.gov/Monograph/series4_chapter.cfm.
4. V.A. Vilnrotter, P.C. Tsao, D.K. Lee, T.P. Cornish, L. Paal, and V. Jamnejad, "EPOXI uplink array experiment of June 27, 2008," IPN Progress Report 42-174, pp. 1-25, Aug. 15, 2008.
5. V. Vilnrotter, D. Lee, T. Cornish, P. Tsao, L. Paal, and V. Jamnejad, "Uplink array concept demonstration with the EPOXI spacecraft," *IEEE A&E Systems Magazine*, pp. 29-35, May 2010.
6. P. Tsao, V. Vilnrotter, and V. Jamnejad, "Pointing-vector and velocity based frequency predicts for deep-space uplink array applications," in 2009 IEEE Aerospace Conference, March 7-14, 2009, pp. 1-5.
7. F. Davarian, "Uplink arrays for the deep space network," *Proceedings of the IEEE*, vol. 95, no. 10, pp. 1923-1930, Oct. 2007.
8. V. Vilnrotter, D. Lee, R. Mukai, T. Cornish, and P. Tsao, "Three-antenna doppler-delay imaging of the crater tycho for uplink array calibration applications," IPN Progress Report 42-169, pp. 1-17, May 15, 2007.
9. R.C. Hansen, "Antennas," in *Reference Data for Engineers: Radio, Electronics, Computer, and Communications*, M.E. Van Valkenburg and W.M. Middleton, Eds., 9th Edition, Boston: Newnes, 2002, p. 32-53.
10. E. Brookner, *Practical Phased Array Antenna Systems*, Lexington, MA: Lex Book, 1997, p. 2-20.
11. R.C. Hansen, "Focal region characteristics of focused array antennas," *IEEE Trans. Antennas and Propagation*, vol. 33, no. 12, pp. 1328-1337, 1985.
12. R.C. Hansen, *Microwave Scanning Antennas*. Vol. 1 Apertures, Boston: Academic Press, 1964, pp. 33-46.
13. <http://solar.nro.nao.ac.jp/norh/html/introduction.html>
14. P.A. Stadter, B.L. Kantsiper, D.G. Jablonski, A.R. Golshan, and J. Costrell, "Uplink arraying analysis for NASA's deep space network," in 2010 IEEE Aerospace Conference Proceedings, Big Sky, Montana, March 6-13, 2010, pp. 1 - 6.
15. J. Ruze, "Antenna Tolerance Theory – A Review," *Proceedings of the IEEE*, vol. 54, no. 4, pp. 633-640, 1966.

Appendix E.—ABL Experiment

White Paper Beamed Energy Propulsion Demonstrations Using The Airborne Laser Test Bed

E.1 Background

This paper discusses using the Airborne Laser Test Bed (ALTB) as the energy source for a series of low-cost experimental demonstration vehicles that use Beamed Energy Propulsion (BEP) engines. It will address at a top level how the ALTB operates, its capabilities and its constraints as well as basic demonstration configurations.

The BEP demonstration vehicles will explore key BEP technologies with the purpose of expanding the knowledge base and envelope of understanding.

E.2 Benefits of Demonstration

Beamed Energy Propulsion uses a beam of energy, either laser or microwave to add energy in the form of heat to a working fluid. The heated working fluid is then expelled and creates thrust to propel the vehicle. Most rocket engines use both a fuel and an oxidizer, which are burned to generate the energy needed for thrust. A benefit of using BEP is the fuel can be a single fluid and be as benign as water. The fuel stills needs to be heated up, but instead of using a combustion process to add energy to the system, the energy is beamed to the vehicle from an external source. The external source of the beamed energy can be amortized over a large number of uses therefore reducing the total cost per use.

E.3 History of BEP

Konstantin Tsiolkovsky published the original idea for BEP in 1924, he pointed out that energy could be delivered to a space rocket by means of tight light beams (first laser wasn't built until 1960). The modern history of BEP, started in 1972, when Arthur Kantrowitz first popularized the idea of using lasers for propulsion.

E.4 History of the ALTB

The Airborne Laser (ABL) is technology demonstration that grew out of the first Gulf War SCUD hunts. Air Force pilots would report seeing SCUDs launch but had no way of engaging them. The ABL program contract was signed in 1996 and in Feb 2010 that aircraft shot down its first boosting threat-representative missile. With the declaration of Defense Secretary Gates that the ABL was not moving forward to an acquisition program but to remain a science and technology research platform, aircraft was renamed the Airborne Laser Test Bed (ALTB). The new designation was to reflect that it was a national asset that was to be used to learn and understand high-energy lasers, their effects and uses. The Missile Defense Agency's Advanced Technologies Directorate (MDA/DVL) currently manages the ALTB.

E.4.1 How the ALTB Works

The ALTB is comprised of four main subsystems; the mega-watt class high-energy laser (HEL) which uses chemical oxygen iodine laser (COIL) technology, the Beam Control/Fire Control (BC/FC) system, the Battle Management system and the 747 aircraft. These subsystems are integrating into a seamless capability that can detect, track, target and kill boosting ballistic missiles.

The ALTB method of engagement is as follows: The Battle Management's infrared search and track (IRST) sensors detect the plume of a launching missile. The BC/FC slews the turret to optically find the target plume. Once the system locks onto the target optically the BC/FC fires a kilowatt-class tracking illuminator laser (TILL) to determine the targets range. With the range determined, the TILL now "walks" up the missile body to find the nose and then continues to track the target from the nose. The BC/FC now fires a second kilowatt-class laser that measures the atmospheric turbulence. This laser, the beacon illuminator laser (BILL) is offset behind the TILL but just forward of where the HEL will hit the target. This offset is to allow the system to measure the turbulence along the path of where the HEL will hit the target. As soon as the system has determined that it has a solid lock on the target and the turbulence information the HEL fires until the target is destroyed. The whole process takes only seconds.

E.4.2 Capabilities

The ALTB is capable of tracking boosting missiles and aircraft that have a sufficient heat signature such as the modified Gulfstream use as an Airborne Diagnostics Target (ADT). The ALTB can then put and hold an atmospherically compensated HEL beam on that target. A surrogate high-energy laser (SHEL) is used on the ADT. The SHEL has the same wavelength as the HEL but is only about 10 watts.

The ALTB specific technical capabilities required to design BEP demonstration vehicles are either "For Official Use Only" or classified but can be obtained through proper channels from the Missile Defense Agency's program office MDA/DVL.

E.4.3 Constraints

In order for the demonstration vehicles to be lased by the ALTB they will need to meet certain physical criteria and dimensions. The software in the ALTB can be adjusted to fine tune the exact aim point of the HEL on the demonstration vehicle. Below are some of the design constraints.

- Demonstration vehicle needs enough (TBR) infrared signature to emulate a boosting ballistic missile.
- Distance $x \pm y$ (TBR) between IR source and leading point (nose cone).
- Distance $x \pm y$ (TBR) between leading point and where the HEL will hit.

In addition, there are airspace consideration and constraints that must be taken into account when designing the vehicle and the engagement geometry. The best engagement field of view is a cone $\sim xx^\circ$ from the forward centerline. Based on the ALTB operating environment and the FAA, the engagements need to take place above 40,000 ft. Depending on which range the tests are conducted on there is also an altitude at which the beam must be above when it leaves the controlled airspace.

Engagement windows and times must be coordinated with US Strategic Command's Laser Clearinghouse, the FAA and the host range. This can limit the amount of desired testing available and needs to be worked continuously.

As part of the Laser Clearinghouse coordination for engagement windows, an analysis of the reflected and scattered laser energy must be completed for each vehicle and geometry. This process can take up to six months to complete and may require physical samples of the vehicle to measure its reflectivity.

E.5 Basic Demonstration Vehicle Configurations

The demonstration vehicles will most likely be launched using a booster rocket or air launched to get it into the desired engagement geometry. Depending on which BEP engine is being used on the demonstration vehicle it will either have an orthogonal or an axial incidence angle.

E.5.1 Orthogonal Incidence

Engines that have the laser come at the side of the vehicle will be categorized as Orthogonal. Depending on the sensitivity of the engine to the change in incidence angles, the vehicle flight path or the laser receiver will have to be adjusted to maintain the required incidence angle.

E.5.2 Axial Incidence

Engines that have the laser come at the back of the vehicle will be categorized as Axial. Depending on the sensitivity of the engine to the change in incidence angles, the vehicle flight path or the laser receiver will have to be adjusted to maintain the required incidence angle.

E.6 Demonstration Risks

E.6.1 Technical

One of the key risks that will need to be addressed early in the design of the demonstration vehicle will be maintaining the laser incidence angle throughout the engagement.

The ALTB is still a technology demonstrator and as such is not 100% reliable. Specific GO/NO GO criteria will need to be developed to ensure the highest probability of success.

If an air launched solution is defined for the demonstration vehicle, then the demo vehicle will need to be able to “fly” on it own until the carrier craft clears the engagement air space.

E.6.2 Programmatic

The ALTB funding is to be reviewed in 2013 to determine if it should continue or be terminated. NASA and DARPA will need to work closely with the Missile Defense Agency to ensure that the ALTB will be available when the demonstration vehicles are ready for test.

Appendix F.—Environmental Considerations for a Ground-Based BEP Station

Daniel E. Raible, Scott Darpel, and Maciej Zborowski

F.1 Introduction

Beamed Energy Propulsion (BEP) is a technology that typically employs heat exchangers or optical plasma engines to provide thrust to a vehicle. By reducing or eliminating the onboard fuel requirements, vehicles may be developed with very high specific impulse (I_{sp}). By providing the propulsive energy from a remote location where power is abundant, the mass of the vehicle may be dramatically reduced. To date several scaled prototypes of BEP vehicles have been successfully flown, but a full size demonstration has yet to be realized. The implementation of the BEP concept to provide launch-to-orbit capabilities will require a shift in facility approaches from that of conventional rocket technologies, since the fundamental system and safety implications differ greatly.

Figure F.1 depicts an illustration of a proposed laser-based launch complex, in which multiple laser cavities are beam combined through a multi-faceted mirror and delivered to the receiving spacecraft through a beam director.

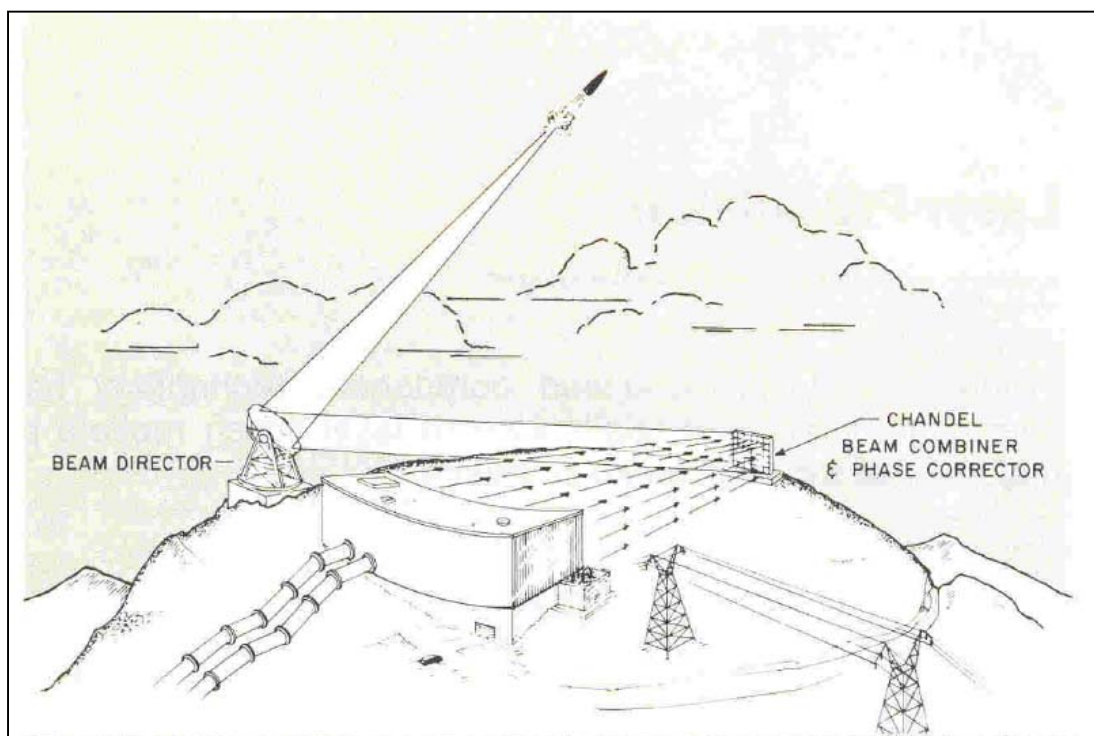


Figure F.1.—Proposed European Space Agency laser launch facility (reproduced from source 1).

Traditionally, locating launch facilities has been done with one eye towards orbit, and the other on safety. When examining the following figure, depicting the location of all current launch facilities, it is easy to see that the primary attribute is having either a large body of water or largely uninhabited land available for the departing vehicle's trajectory. These exclusion zones provide a margin of safety from launch mishaps, such as explosions, or even simple exposure to launch site gases and deployables.

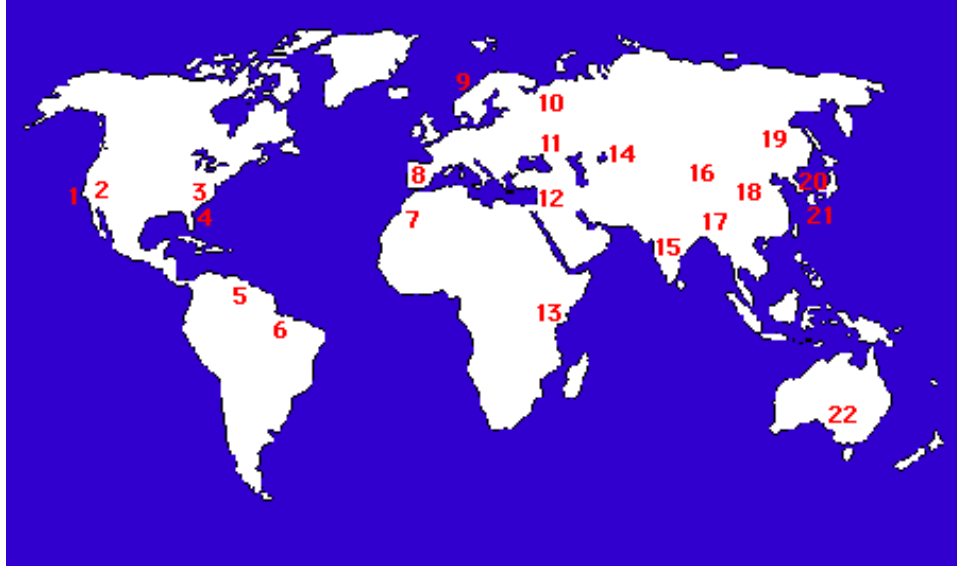


Figure F.2.—Existing launch sites around the world.

(1—Vandenberg, 2—Edwards, 3—Wallops Island, 4—Cape Canaveral, 5—Kourou, 6—Alcantara, 7—Hammaguir, 8—Torrejon, 9—Andoya, 10—Plesetsk, 11—Kapustin Yar, 12—Palmachim, 13—San Marco, 14—Baikonur, 15—Sriharikota, 16—Jiuquan, 17—Xichang, 18—Taiyuan, 19—Svobodny, 20—Kagoshima, 21—Tanegashima, 22—Woomera)

While safety will always be a primary concern, the challenges for locating a Beamed Energy Launch (BEL) facility will be unique and required more considerations. It is true that a BEL facility will eliminate the risk of explosion and inhalation associated with chemical propellants, but the nature of high-energy power beams presents its own exposure risks. Beam reflection and refraction can expose personnel and bystanders to vision and skin damage. Additionally, the effect of launch site atmospheric conditions on the propagation of concentrated energy beams rises to a key consideration. Humidity and atmospheric particulate levels can affect the ability to maintain beam integrity. From a utilities perspective, access to sufficient power, with multiple ties into a nearby grid is desirable to reduce the need for on-site generation, but is of smaller concern.

Do any of the current launch locations meet all the attributes for a safe, effective and affordable BEL Facility? Or, would a completely new set of locations, perhaps some not even fixed, be considered? This paper presents the needs for each of these attributes, as well as a discussion of a selection of locations.

F.2 Weather and Potential Launch Site Suitability

There are many components of “weather” that affect the suitability of a location, or set of locations to be home to a BEL facility. Aerosol, precipitation and cloud obscuration all contribute to meeting a new, rapid launch paradigm. An initial survey, based on a collection of weather charts can provide some insight into this suitability. A brief note regarding political implications: by constraining the list of potential BEL sites to the US and related territories, other ramifications such as international agreements and transportation logistics are avoided thus lowering the overall launch costs. Since the future of BEP for launch lies primarily on its ability to offer low cost and rapid turnaround capability to orbit, the location of the launch facilities must maintain BEP as a competitor to conventional launch technologies.

Launch site availability is an important metric, since it will impact the site’s ability to repeatedly launch on schedule. One primary detrimental impact on launching has always been cloud cover. Historically this has been centered on avoiding potential static charge buildup related to more mature cloud formations, but BEL introduces an additional dimension since cloud obscuration will have a deleterious effect on beam propagation. A first look may be made into the average annual number of cloudy days for locations within the continental U.S. (CONUS), as shown in Figure F.2. Here it can be

seen that a region exists in the Southwestern area of the country that supports clear day availability with obscurations present less than 89.5 days per year.

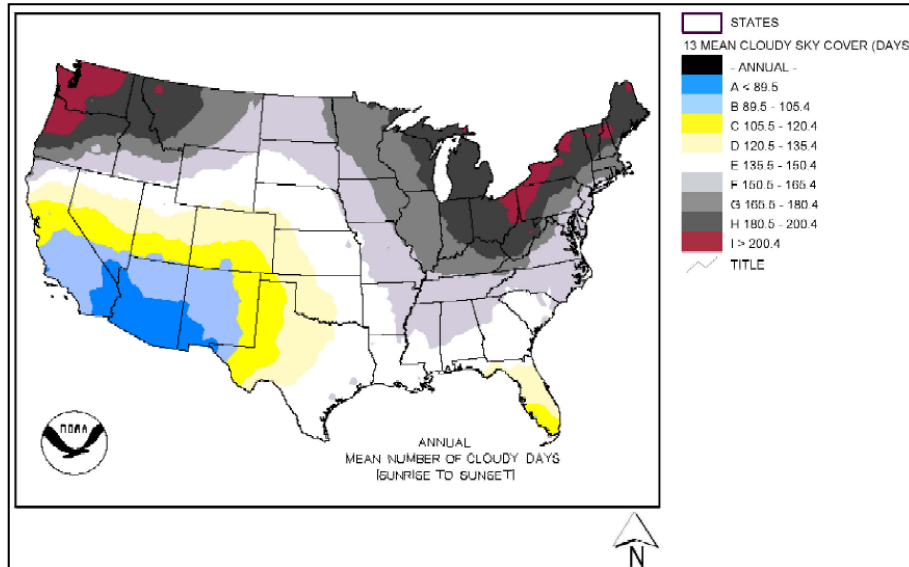


Figure F.3.—Average annual number of cloud obscuration days across the U.S. (reproduced from 2).

As expected, locations to the Southwestern U.S., through the dry western desert present a positive case for cloud obscuration. This would indicate a high rate of availability for launches where beamed columns would not have to navigate clouds, and suffer the associated loss of power.

Aerosol content in the atmosphere also contributes to the attenuation effects of the beam due to absorption and scattering. This is wavelength dependant related to the size of the aerosols, and the type of attenuation may be parsed out between humidity and direct rainfall contributions. The average rainfall for locations in the CONUS points to some of the same general regions in Figure F.4.

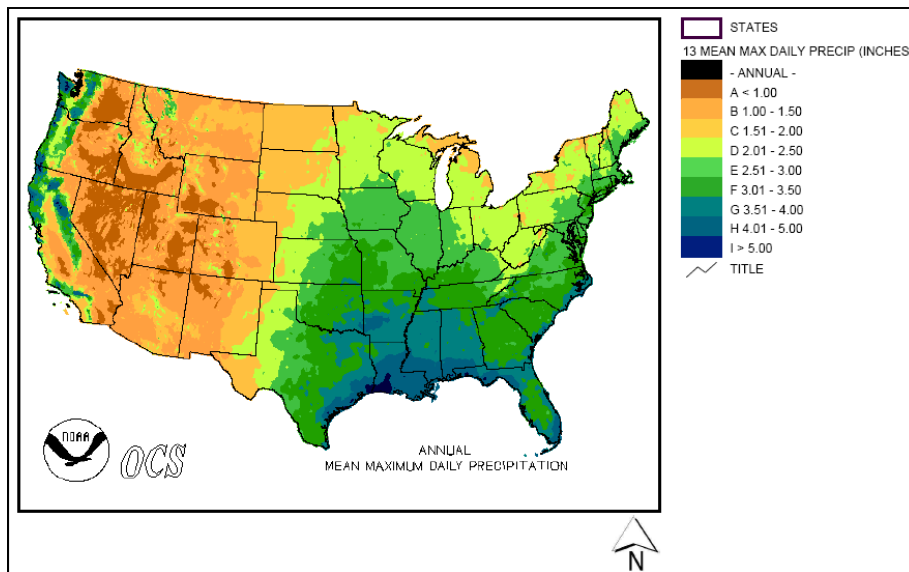


Figure F.4.—Mean maximum daily precipitation across the U.S. (reproduced from 2).

Aerosol content is another contributor to beam attenuation. The capacity for the atmosphere to contain moisture is related to the temperature of the air, which can be seen across the U.S. in Figure F.5.

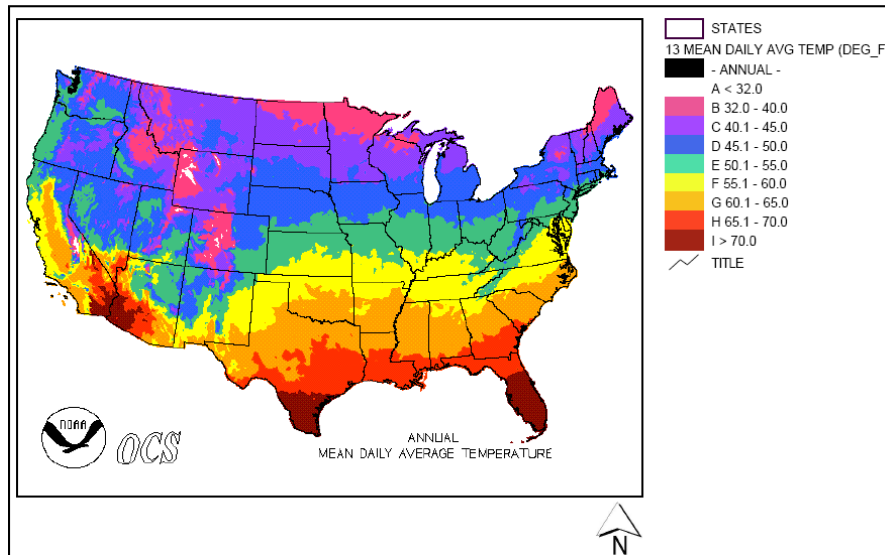


Figure F.5.—Annual mean daily average temperature (reproduced from 2).

For a more accurate depiction of the atmospheric conditions at a potential location, a focused site survey should be conducted at selected candidate positions. Considering a combination of favorable attributes including atmospheric availability, remoteness, obtainable power, existing infrastructure, accessible trajectories and trajectory several potential sites in the Southwestern region of the U.S. may be identified to support BEL. These may include Vandenberg Air Force Base (currently supports conventional launch operations), Goldstone, White Sands and China Lake (all government installations containing some degree of existing infrastructure), Mauna Kea (high altitude offers a circumvented approach to atmospheric losses) and finally a mobile shipboard location that would offer diversity with launch inclinations. These sites, shown in Figure F.6, could potentially serve as primary launch location, or as a secondary auxiliary downrange beaming station.

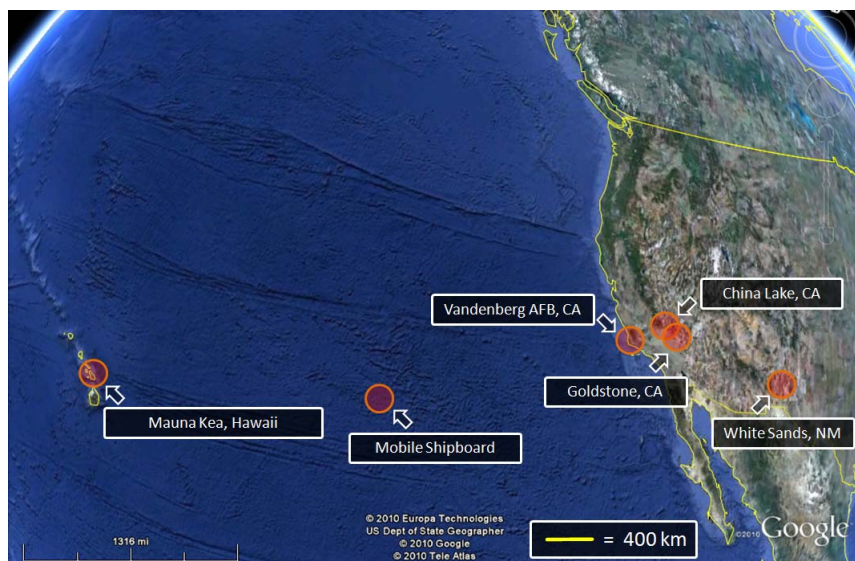


Figure F.6.—Potential BEP ground complex locations

F.3 Range Safety Zones

At a BEP launch complex, a range safety keep-away zone (KOZ) must be established and maintained around and beyond an ascending craft, just as in traditional chemical propulsion launch sites. With BEP however, these KOZ's will serve to protect against exposure to reflection, refraction and scattering components of the beam exceeding levels considered above the acceptable standards. These KOZ's will be based upon maximum permissible exposure for humans, and damage thresholds for ground, airborne and space-based assets within proximity of the BEP activity. These thresholds may be calculated utilizing resources established by the American National Standard for Safe Use of Lasers. The nature and type of hazard that may be encountered by exposure to the radiated beam will vary as a function of the wavelength of the energy used for the launch system. Typical skin photochemical effects (burns) are generally limited to tissue absorption of wavelengths shorter than 600 nm (UV and some visible). This range is typically less than what would be practically considered for BEP source technologies due to high coefficients for atmospheric extinction. For wavelengths between 400-1400 nm (visible and near-infrared), the ocular absorption hazards would mainly concern retinal burns. At wavelengths between 1400 nm to 1 mm (mid to far-infrared, the cornea would be the most at risk for damage. Both of the regions are favorable for BEP, and so this places eye safety very prominently as a factor to consider when implementing the system.

Considering a laser hazard evaluation for outdoor operation, the components of intrabeam exposure, specular and diffused reflections are all key. Additionally, issues such as the stability and operational limitations of the laser platform, likelihood of people being within the range during operation, people viewing the operation with optical aids such as telescopes and binoculars, and operations through airspaces traversed by aircraft must be considered. To perform these calculations, it is necessary to define a metric known as the Maximum Permissible Exposure (MPE). This is the maximum level of laser radiation to which an unprotected person may be exposed without adverse biological changes in the eye or skin. The MPE is generally set with a safety factor of 1/10th the level where there exists a 50% chance of injury, based on an empirically derived model. The MPE is dependent on the type of laser (wavelength), potential exposure duration, whether eye or skin exposure is anticipated and pulse repetition frequency if the laser is operated in pulsed mode. Table F.1 contains the worst-case recommended accidental limiting exposure durations for CW and repetitive-pulse MPE calculations as a function of wavelength (Ref. 3). From these starting point acceptable durations, the maximum level of energy exposed may be calculated.

TABLE F.1.—EXPOSURE LIMITS BY WAVELENGTH AND EXPOSURE TYPE (REPRODUCED FROM SOURCE 3)

Wavelength Rang	Diffuse (seconds)	Intrabeam (seconds)
UV 0.18 to 0.4 μ m	30,000	30,000
Visible 0.4 to 0.7 μ m	600	0.25**
NIR 0.7 to 1.4 μ m	600	10
FIR 1.4 μ m to 1 mm	10	10

* For single pulse lasers (PRF < 1 Hz) use actual laser pulse duration.

** For unintended or accidental viewing only. For other conditions, use the time of *intended* viewing.

The Nominal Hazard Zone (NOHZ) for all possible beam paths needs to be evaluated for all cases of outdoor operation. The NOHZ can be thought of as an area within which the level of direct, reflected or scattered laser radiation during normal operation exceeds the applicable MPE. Generally the potential exposure (irradiance) decreases with distance, until a point where the irradiance is less than the applicable MPE, and this boundary defines the NOHZ. The most serious potential exposure condition would be intrabeam ocular viewing, followed by ocular exposure of specular reflections from the incident beam upon the vehicle surface. Although the human eye is most sensitive in the visible region of light centered on 550 nm, exposure to non visible optical radiance may also be harmful. Consider source wavelengths calculated at both 1.064 and 2.0 μm. For the intrabeam case where the eye is in the direct path of the laser beam, both the near infra-red (NIR) and far infra-red (FIR) limiting exposure durations are given as 10 seconds from Table F.1. The ANSI expressions for establishing the exposure value thresholds at these frequencies are given by:

$$5.0 \cdot C_C \cdot 10^{-3} \text{ W} \cdot \text{cm}^{-2} \text{ (NIR 1.050 to 1.400 } \mu\text{m)}$$

$$0.1 \text{ W} \cdot \text{cm}^{-2} \text{ (FIR 1.800 to 2.600 } \mu\text{m)}$$

Note that the NIR case involves the correction factor C_C , which increases the MPE values for ocular exposure because of pre-retinal absorption of radiant energy in the spectral region between 1050 and 1400 nm.

For BEP it is necessary to dynamically focus the optical energy on the ascending craft, and for the purposes of calculating the intrabeam Nominal Hazard Distance (NHD) we consider the ‘Lens-on-Laser’ case, which includes properties of focal length and emergent beam diameter:

define constants:

$\Phi := 1$	Average Power (watts)
$f_0 := 1$	Focal length of optics (m)
$b_0 := 1$	Beam diameter at focusing optics (m)
$\text{MPE} := 1$	Maximum Permissible Exposure (W/cm^2)

Nominal Hazard Distance for Lens-on-Laser Exposure

$$r_{\text{NOHD}} := \left(\frac{f_0}{b_0} \right) \cdot \left(\frac{4 \cdot \Phi}{\pi \cdot \text{MPE}} \right)^{\frac{1}{2}}$$

Specular (or mirror-like) reflections can occur when the size of the surface irregularities (or roughness) is less than the wavelength of the incident radiation, resulting in an angle of reflection equal to the angle of incidence. In this scenario the NHZ for an eye in the path of a specularly reflected beam due to a mirror-like surface is almost as serious as the direct exposure condition.

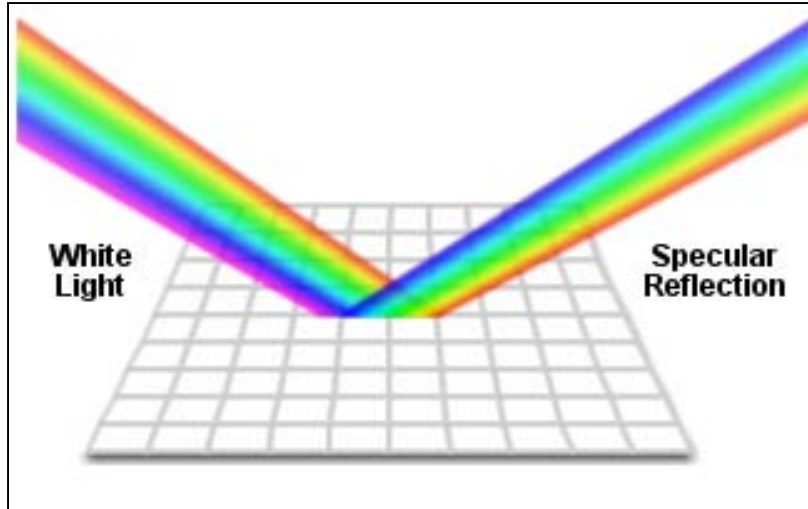


Figure F.7.—Illustration of specular reflection (reproduced from source 4).

Diffuse (Lambertian) reflections from randomly oriented irregularities that are greater than the wavelength of the incident radiation create a diffused region of reflection. In this case, a diffusely reflected portion of the laser beam enters the eye, and this represents the least serious potential exposure condition.

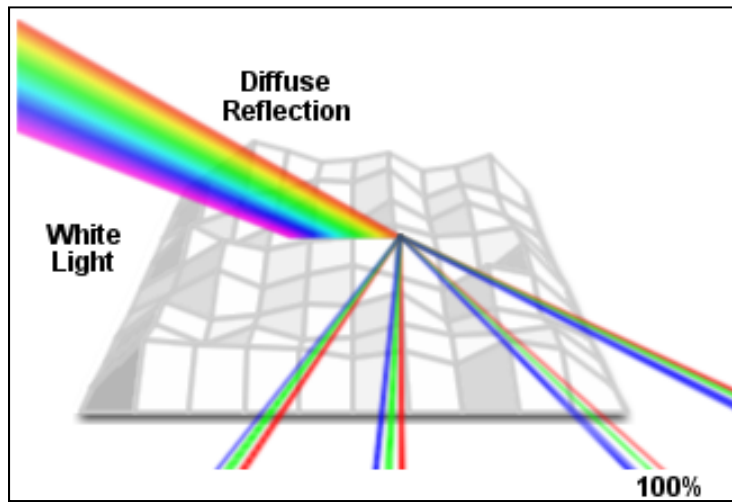


Figure F.8.—Illustration of diffuse reflection (reproduced from source 4).

The nature of the diffused reflections may act as either a ‘point’ or ‘extended’ source based on the geometry of the system, and each case will have a different procedure for calculating the diffused NOHZ. The angular size (subtense) of the apparent source as viewed by the observer will determine the type of reflection, where anything appearing smaller than $\alpha = 1.5$ mrad will be considered a point source and everything larger will be treated as an extended source. The diffuse reflection NOHZ may be characterized by the expression in Figure F.9:

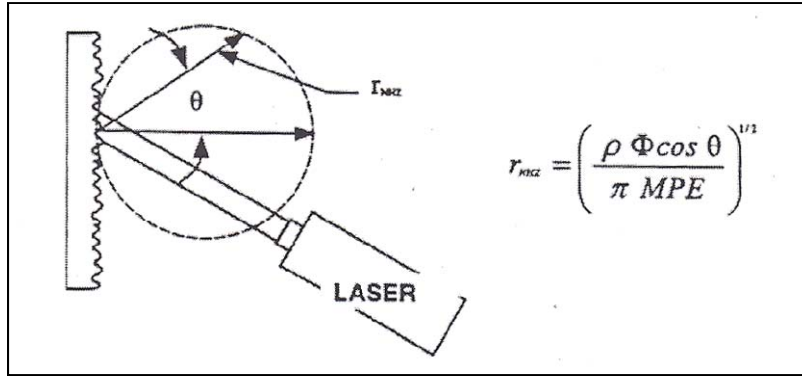


Figure F.9.—Diffuse reflection nominal hazard zone

The diffuse NOHZ will follow the trajectory of the ascending vehicle, and may be traced back to the initial point of departure from the ground to define in-part the KOZ. The definition of these regions can be used to determine the overall KOZ around the launch area. Safety must be considered for each of the following types of observers:

- Ground observer
 - Unaided eye
 - “Binocular safe” (50 mm aperture) – largest optics for casual observer
 - “Celestron safe” (200 mm aperture)
- Civil aircraft (low altitude, relatively close)
- Commercial aircraft (30-40,000 ft altitude, 250 m/s)
- Spacecraft

Generally need to consider several possible exposures:

- Direct exposure to main beam – presumably only an issue for spacecraft
- “Stray beam” – direct exposure to beam that misses vehicle, by accident or due to sidelobe of beam
- Specular reflection (“Glint”) from vehicle
 - Known (e.g., specular component of reflection from heat exchanger surface) -- predictable area, reflectivity, and divergence
 - Accidental -- reflection due to surface damage or other problem that exposes a shiny surface
- Diffuse reflection from vehicle
 - “Lambertian” wide angle scattering
 - “Hot spot”, with significant peaking in a particular direction (usually either near the specular direction, or retroreflection toward beam source).

For extended exposure (which we expect for diffuse reflection – viewers are likely to watch the vehicle ascend) and an extended source:

$$MPE(mw/cm^2) = 1.8C_A C_E T_2^{-0.25}$$

$$C_A = 10^{2(\lambda-0.7)} \quad \text{for } 0.7 - 1.05 \mu\text{m}; C_A = 5 \quad \text{for } 1.05 - 1.15 \mu\text{m}$$

C_E accounts for the angular size of the source. For a source which is reasonably uniform (i.e., no individual “hot spot” is more hazardous than the overall source) and smaller than 100 milliradians in

apparent width (i.e., observer is farther than ~50 meters from the vehicle, which we assume will always be the case) $C_E = \max(a/1.5 \text{ milliradians}, 1)$ where a is the apparent angular width.

For an apparently rectangular source of length l and width w , viewed from a distance D , a is defined as \sqrt{lw}/D . For typical heat exchanger vehicles, the physical source width is 3-5 meters. So for distances greater than a few kilometers, the vehicle is always an effective point source (to the unaided eye), but at moderate range, or through a telescope, it may be an extended source.

T_2 is the “integration time” for continuous viewing. The integration time is defined as 10 seconds for near IR point sources (so that $T_2^{-0.25} = 1/1.8$) but in the 2007 revision of Z136.1, it’s made dependent on the angular size of the source, so that the MPE is (slightly) reduced for large extended sources. For a between 1.5 and 100 mrad, $T_2 = 10 * 10^{(a-1.5 / 98.5)}$, so it varies from 10 to 100 seconds. In practice, the observing time at potentially hazardous range will never be 100 seconds for any observer, so the calculated T_2 overestimates the hazard slightly (makes the MPE too low) in some cases. However, the effect is never more than a factor of 1.8 in MPE, and generally much less.

The actual flux scattered from the vehicle, to which the MPE must be compared, is just

$$\phi = \alpha P_{total} \cos(\theta) / \pi D^2$$

where α is the albedo (“whiteness”) of the surface, P_{total} is the total laser power hitting the vehicle, and θ is the viewing angle relative to the normal to the (nominally flat) heat exchanger. The worst case will generally be $\theta = 0$ (looking at the heat exchanger face-on) so we’ll just assume $\cos(\theta) = 1$.

The actual heat exchanger will have an albedo as close to zero as we can make it, to absorb as much laser energy as possible. However, it’s not possible to get a perfectly black surface. Also, parts of the heat exchanger (e.g., where sections join) may be deliberately made white to reduce the local heat load, and some fraction of the beam may spill over onto, or accidentally hit, white areas.

For the purposes of this rough analysis, we assume an effective α of 0.1 – 10% of the incident laser power is scattered from the vehicle surface. (Note that it’s easy to monitor the scattered power, so the laser can certainly shut down if the scattered power is much larger than expected.)

See the Figure F.10 for the results. This plot is for

- $P = 100 \text{ MW}$
- Wavelength = 808 nm (laser diode)
- $l = w = 3 \text{ m}$
- $\alpha = 0.1$

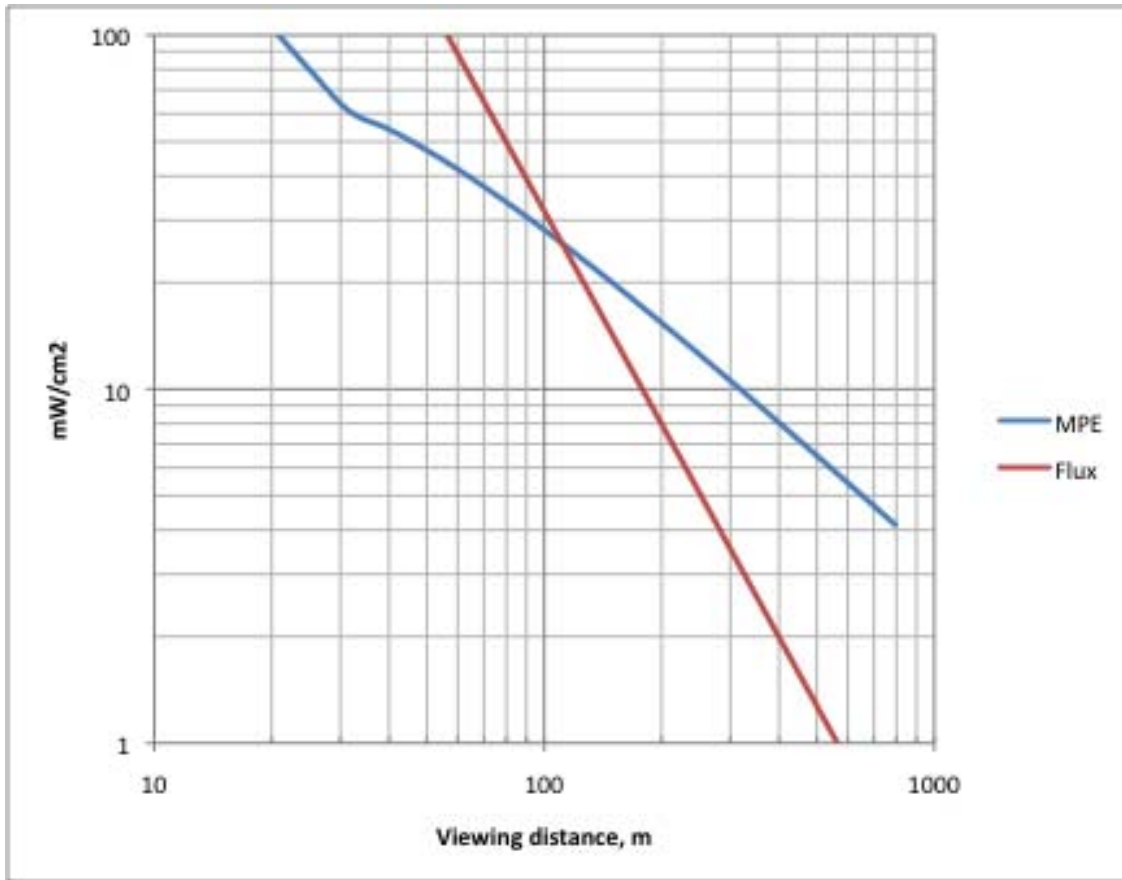


Figure F.10(a).—MPE compared with 3 m BEP exposure as a function of distance.

So for this case the eye-safe distance is just over 100 meters (111 m, to be exact). The “kink” in MPE is at 30 m, where the heat exchanger apparent width is 100 mrad.

The MPE is lower if the source area is smaller. If the beams were concentrated into a smaller 1 m spot, the plot becomes:

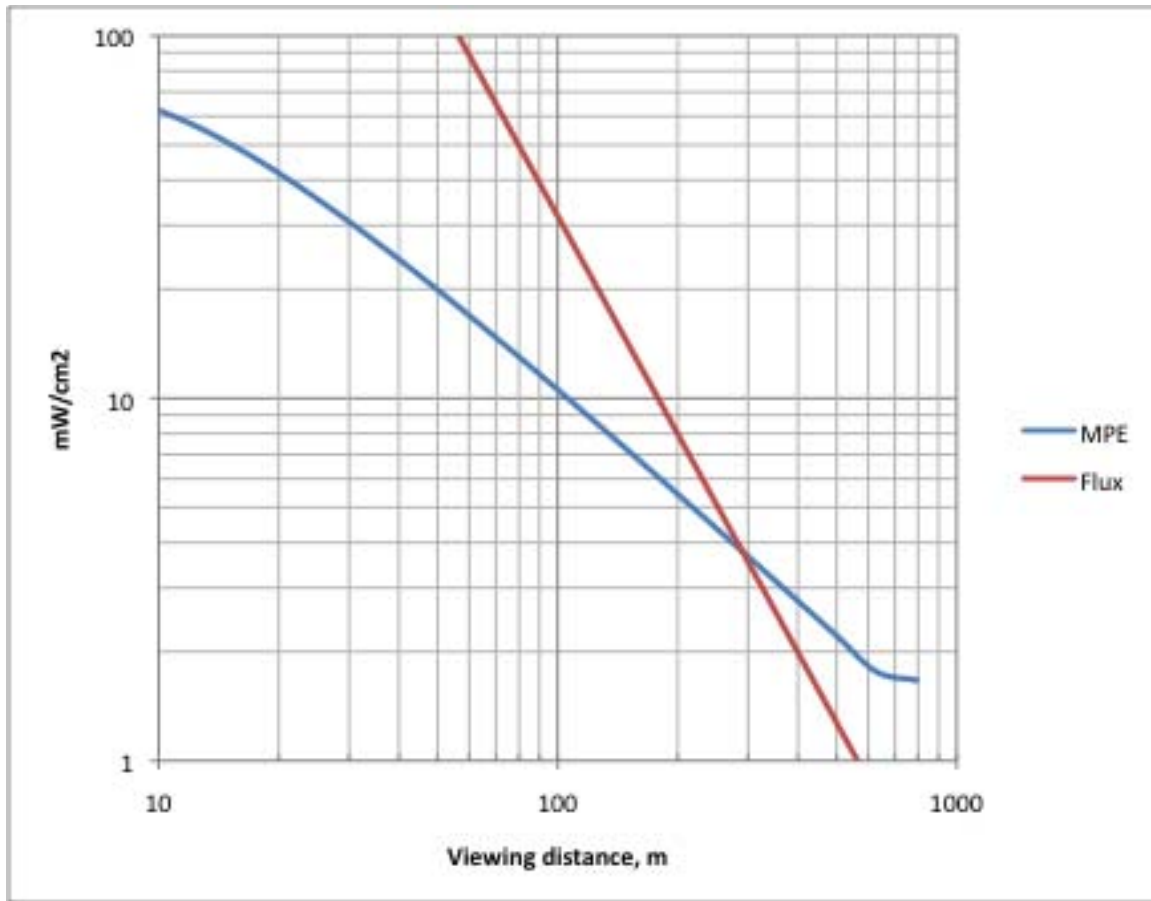


Figure F.10(b).—MPE compared with 1 m BEP exposure as a function of distance

In this case the eye-safe viewing distance is ~300 meters, which is still a very reasonable result given the large amount of radiated energy.

For 1.06 μm , the MPE is about a factor of 5 higher than at 808 nm. The eye-safe range for a 3 m spot and 10% albedo is 45 meters. However, even at 1.06, if the albedo is higher and the spot size smaller, the hazardous range can be substantial; this might be the case for the Lightcraft if it tumbles and the beam strikes the forebody. For a 1 m spot and 100% albedo (100 MW scattered power) the eye-safe range is ~800 m.

F.4 Aided Viewing: Telescopes and Binoculars

In general, the safe viewing distance for an observer with a telescope of aperture A is less than or equal to the naked-eye safe distance, multiplied by $A/7 \text{ mm} = M$ (for magnification). This is because the reference pupil diameter for IR laser safety is 7 mm. A larger aperture increases the collection area by M^2 ; increasing the distance to the source by a factor of M decreases the flux by the same factor M^2 .

This turns out to be true for an extended source as well as a point source, although the explanation is a bit complex; essentially, any optical magnification $>M$ makes the apparent angular extent of the source larger; any magnification $<M$ makes the source smaller (reduces the MPE) but also results in the telescope exit pupil diameter being bigger than 7 mm, so some light from the source doesn't enter the eye.

Therefore, the safe viewing distance for an observer with binoculars (50 mm aperture) is approximately 7.1 times the distance for naked-eye viewing, or ~800 meters for the baseline case (3 meter source size).

The safe viewing distance for an observer with a portable telescope (200 mm aperture) is another factor of 4 larger, or about 3.2 km. (In practice, this is conservative, as amateur telescopes have substantial obscuration and, unless specially coated, have significantly less than 100% transmission in the infrared.)

F.5 Hot Spots and Non-Lambertian Scatter

While it's not hard to ensure that scattered light is reasonably diffuse, ensuring a true uniform distribution is difficult. Conservatively, therefore, we would expect to design for some much higher-flux reflections. These are likely to be in more or less known directions, most likely aimed at least generally back towards the laser source.

If we assume the peak flux is 10-fold higher than the nominal Lambertian flux, then the naked-eye hazard range increases to ~300 meters at 1.06 microns, 550 m at 940 nm, and 965 m at 808 nm – almost 10-fold more than the nominal ranges. Binocular and telescope safe distances would be similarly increased.

Ten-fold higher than Lambertian flux implies that the entire scattered energy is spread over approximately 0.3 steradians, which is very roughly a 30 degree full-angle cone, or a 5 by 180 degree fan. This is clearly achievable by shaping surfaces appropriately if necessary; e.g., a very modest degree of diffusion in the vertical direction plus curvature of the heat exchanger in the horizontal direction.

F.6 Extension to KOZ

For diffuse, approximately Lambertian scattering, and an assumed scattered power of 10 MW from a 3-meter heat exchanger, the naked-eye hazard range for the laser-launched vehicle is only of order 100 meters, and even an observer with a sizeable telescope is safe beyond a range of roughly 3 km.

However, since it's difficult to ensure that scattering will be uniform, especially from the heat exchanger, a conservative assumption pending more detailed analysis is that the keep-out zone should be at least 1 km for all observers, and 3 to 7 km for users of binoculars or cameras with through-the-lens viewing, depending on the laser wavelength. This is also the safe range for aircraft close to the vehicle, since pilots and passengers might use binoculars, but are unlikely to use any larger optics.

Larger telescopes may pose some hazard out to ranges as much as 25-30 km (for a 200 mm aperture, 808 nm), although that would require a very unlikely set of circumstances, including very good tracking (following the accelerating vehicle without significant jitter for many seconds, using a telescope with high infrared transmission, and having the vehicle follow a trajectory and orientation that keeps the hot spot centered on the observer, also for many seconds.) 5-10 km is more likely to be the actual "Celestron safe" range.

Beyond ~30 km there is essentially no hazard even to observers with telescopes, so once the vehicle reaches 30 km altitude it can be viewed from anywhere.

An order-of-magnitude comparison may be made between the BEP parameters and the existing range safety zone existing at the NASA Kennedy Spaceflight Center's pad 39A, which until recently was the sole launch facility for the remainder of the Shuttle Transportation System (STS) missions. The STS safety zone is established at an 8,500 ft radius from the launch pad, so determined by the amount of distance required to keep the airborne particulate level of hydrogen chloride at a safe level for inhalation. This area has been illustrated by the green circle in Figure F.11. Overlaid onto pad 39B are two red boundaries representing the approximate area of a ground-based field array source encircled by a 1 km KOZ for unaided viewing. Minus the appropriate safety factor measures, this initial graphical comparison demonstrates that the BEP approach presents a KOZ within the same order-of-magnitude of conventional launch systems.

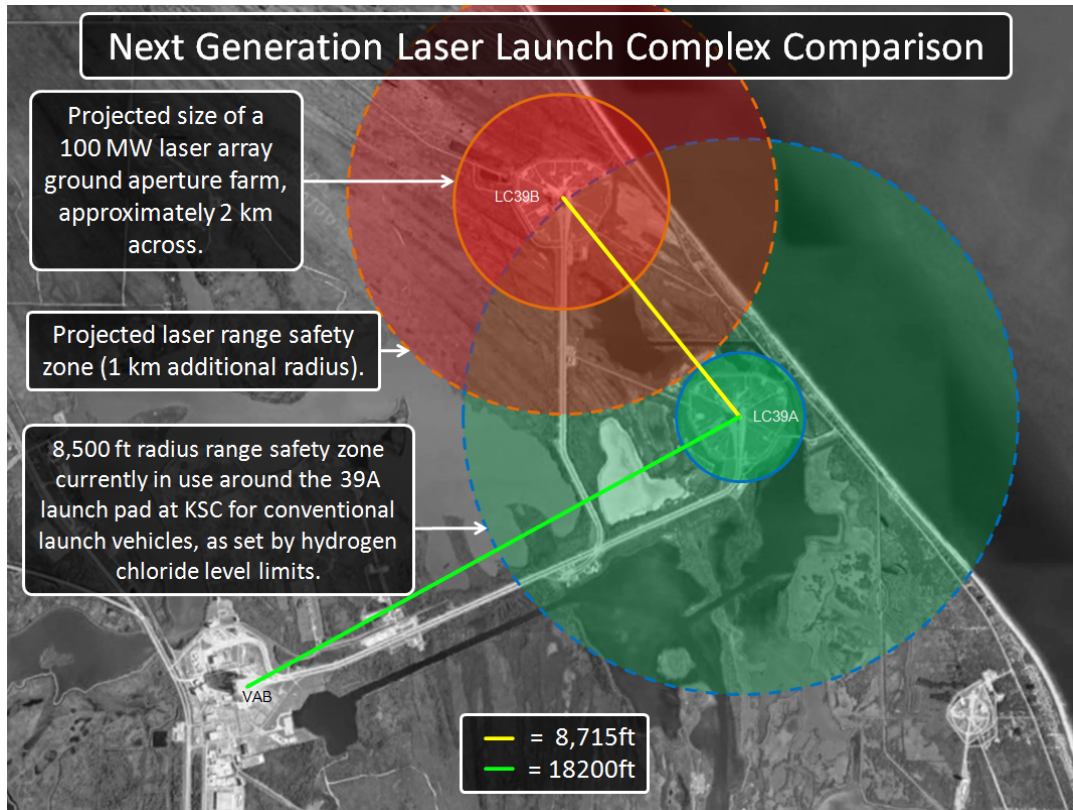


Figure F.11.—Initial safety zone comparison with conventional established facilities.

Beyond the immediate launch area, the KOZ needs to also reflect the trajectory of the vehicle during ascent. For the STS there are multiple zones to cover the field of uncertainty for the flightpath of the Shuttle, the splashdown zones for the solid rocket boosters (SRBs) and the external tank (ET) impact zone. These areas are shown at the bottom of Figure F.11, and the total length extends downrange approximately 11,000 km.

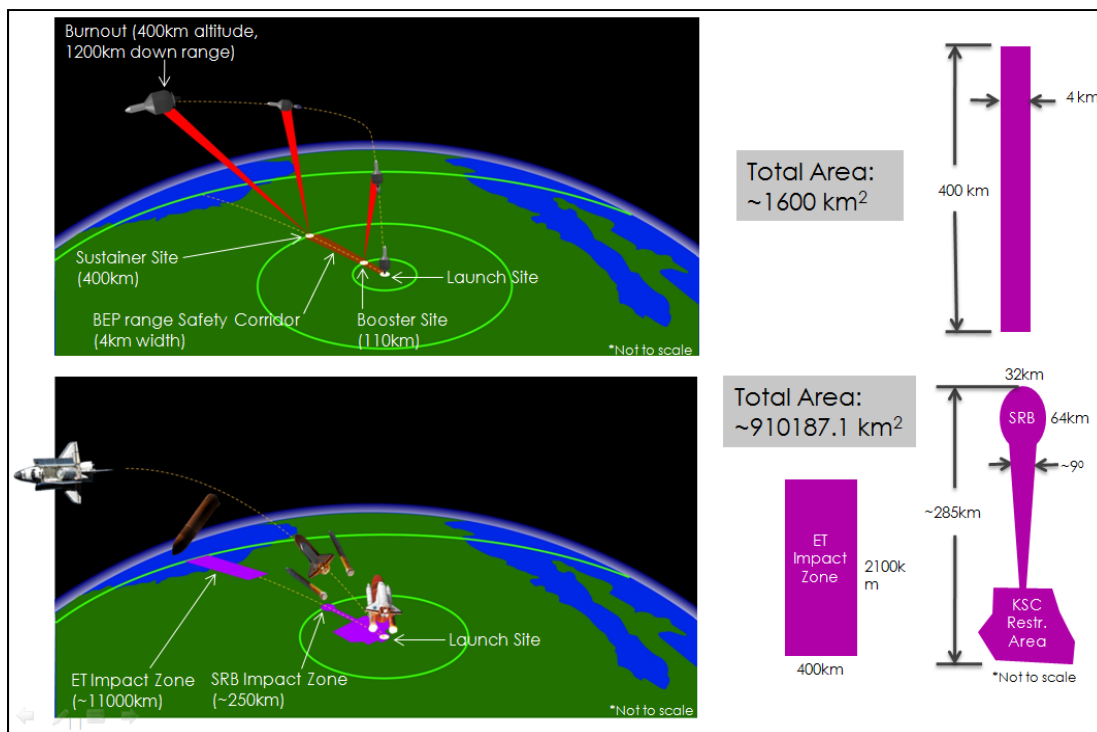


Figure F.12.—Geometric safety zone comparison with conventional established launch facilities.

During initial BEP trajectory analysis, it is determined that a laser sustainer station would likely be placed in the vicinity of 400 km downrange from the launch booster facility. One reason for this is to limit the pointing angles of the beams to 50-60 degrees from the vertical, and to maximize the amount of power on target by limiting the amount of slant range propagation. Since both laser stations and SRB and their KOZs occupy a 4 km footprint, a 4 by 400 km rectangular area may be used to define the overall KOZ, as shown in the top part of Figure F.12.

Beyond the sustainer laser system, a KOZ field of uncertainty may be added, but the merits of BEP may be further exploited to unconstrain the solution. Since the typical BEP launch vehicles are minimal mass and do not contain volatile propellants, in the case of a mid-trajectory ‘failure’ (such as a loss of beam track) the beam would shut down, and the vehicle could execute a tumbled deceleration and eventual parachute deployment, to result in a relatively uneventful recovery on land or sea. This type of abort would eliminate the need for an extended-field KOZ.

F.7 Emitter Interception

The ability for the BEP system to provide high launch availability and repeatability is based on the number of launch window opportunities presented when there exists a beam path sufficiently clear of existing orbital assets. This may be analyzed in Satellite Tool Kit (STK) by simulating a repetition of BEP launch profiles and overlaying existing satellites to examine beam interception events.

The beam divergence may be estimated by assuming a conical beam with a half angle calculated to coincide with the width of the (120km) focused beam at GEO (~36,000km). An additional 30% was added to the width of the beam as a margin, to account for the shortened focus during the vertical ascent. The intensity was estimated by assuming the 30MW/m² average intensity at the focus to be spread normally across the diverging beam, with no atmospheric losses.

F.7.1 CASE 1: Equatorial Launch

Launch into 36° inclination from China Lake. Launches were simulated every 4 minutes for 8 days. Each intersection between the beam and background satellites is recorded. On average there were 5.25 intersections per day, each for 0.2 seconds.

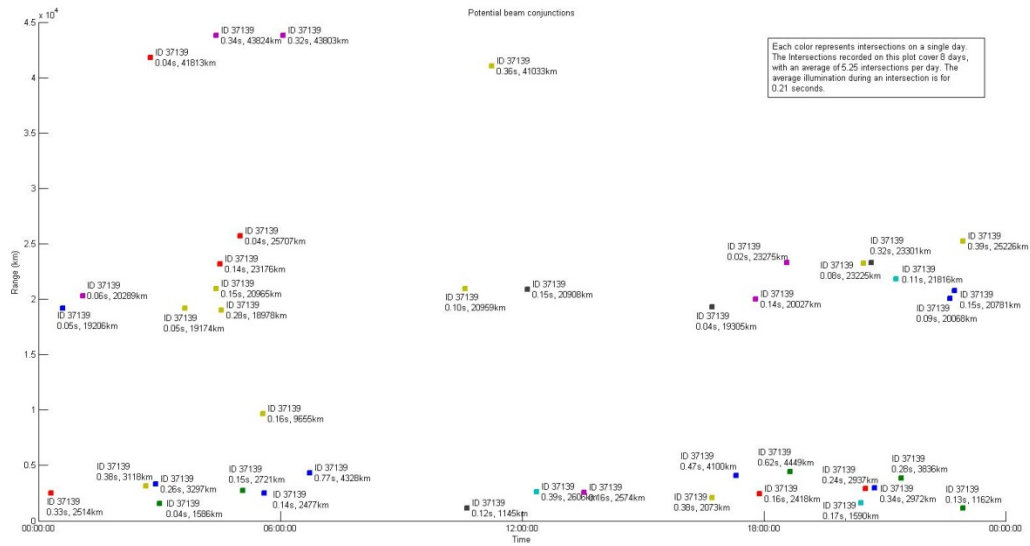


Figure F.13.—Plot of launch time against range of intersecting satellite. Each color represents a single day of launches (i.e., the 8 days are overlaid). The NORAD sat ID is listed along with intersection duration and range.

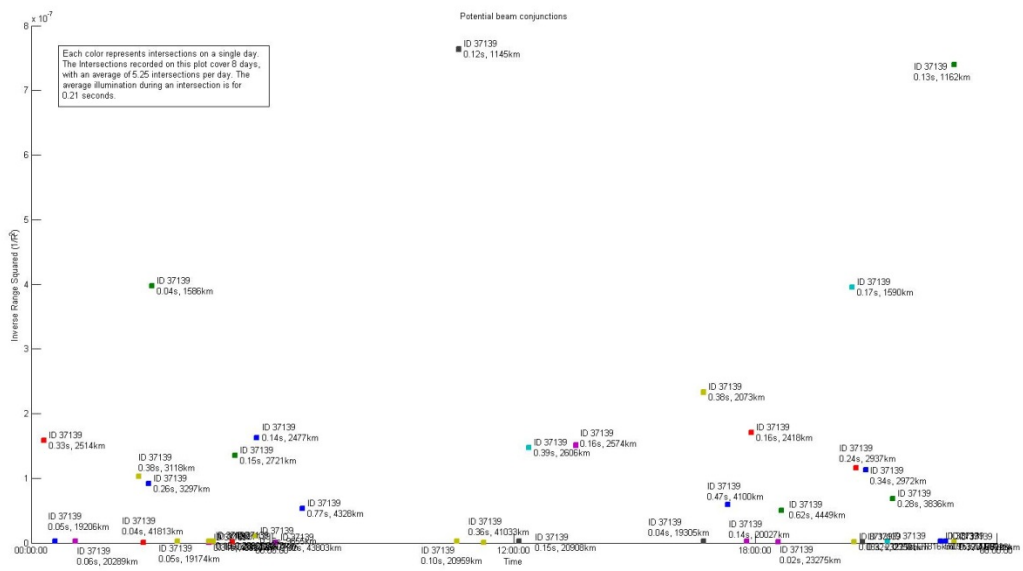


Figure F.14.—Plot of launch time against $1/R^2$ of intersecting satellite. Each color represents a single day of launches (i.e., the 8 days are overlaid).

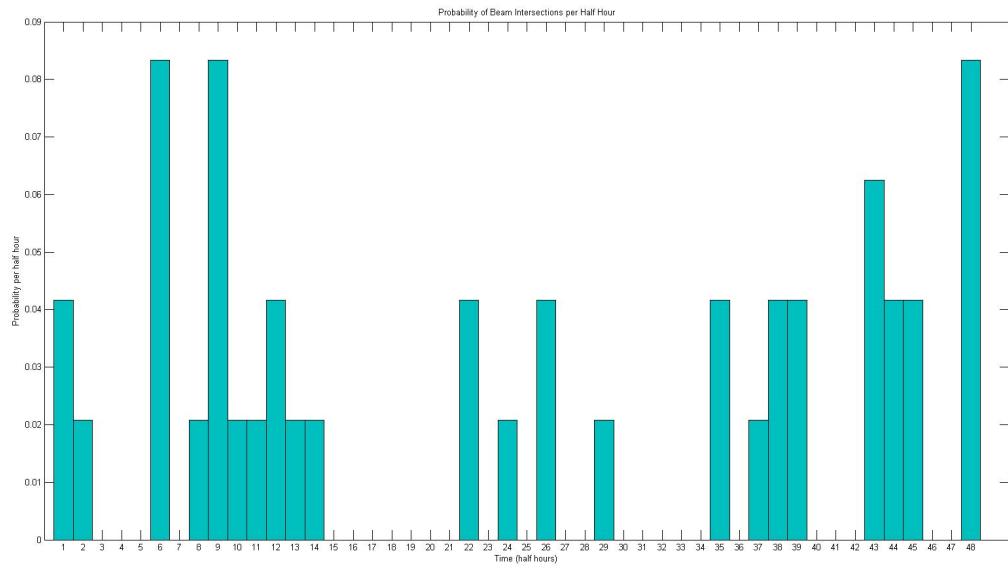


Figure F.15.—Probability of an intersection happening in each half hour period, over the 8 days.

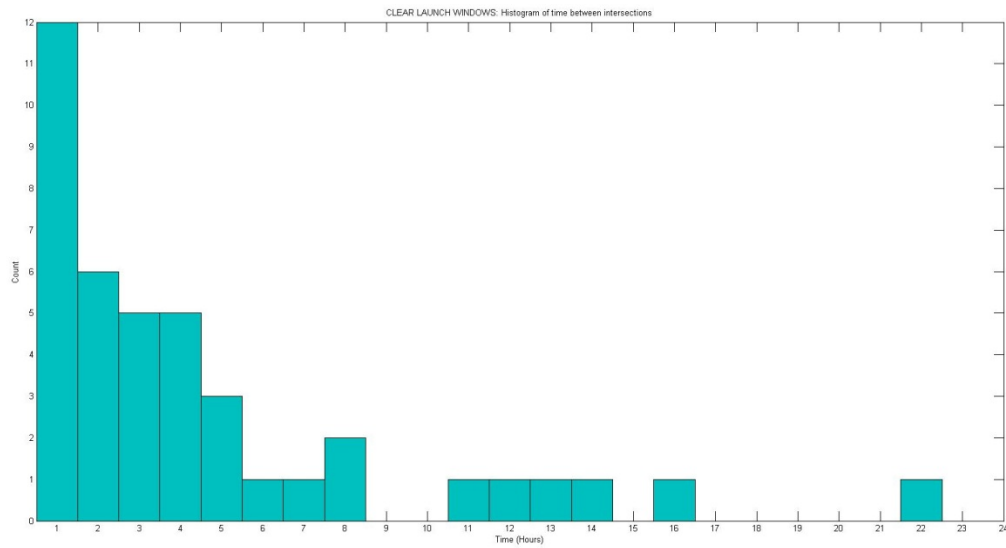


Figure F.16.—Histogram of clear launch windows—periods that have no intersections. Over the 8 days there are 29 periods with more than 1 hour of clearance.

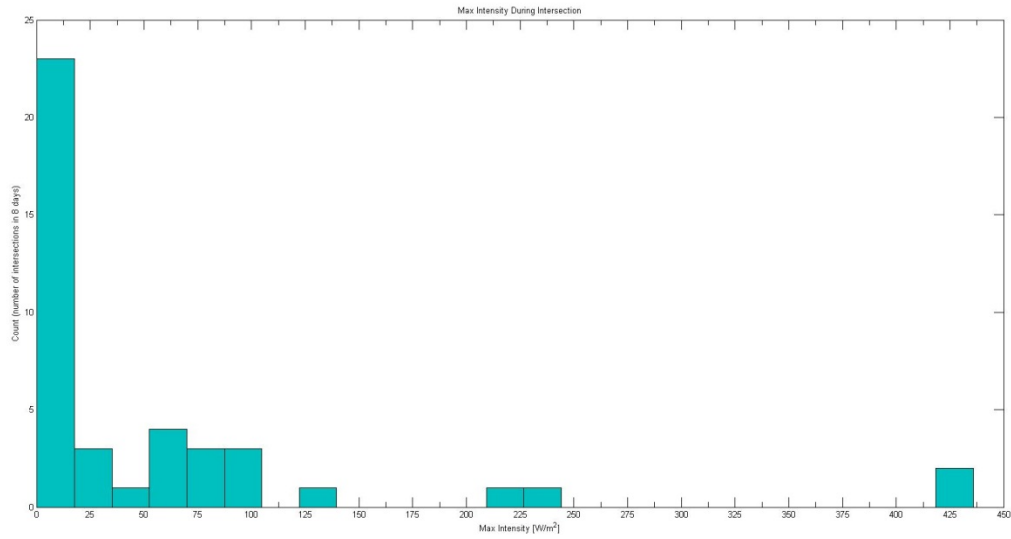


Figure F.17.—Histogram showing the distribution of intersection maximum intensity during the 8 days—note that most have I_{\max} less than 100 W/m^2 (i.e., 8% of solar const.).

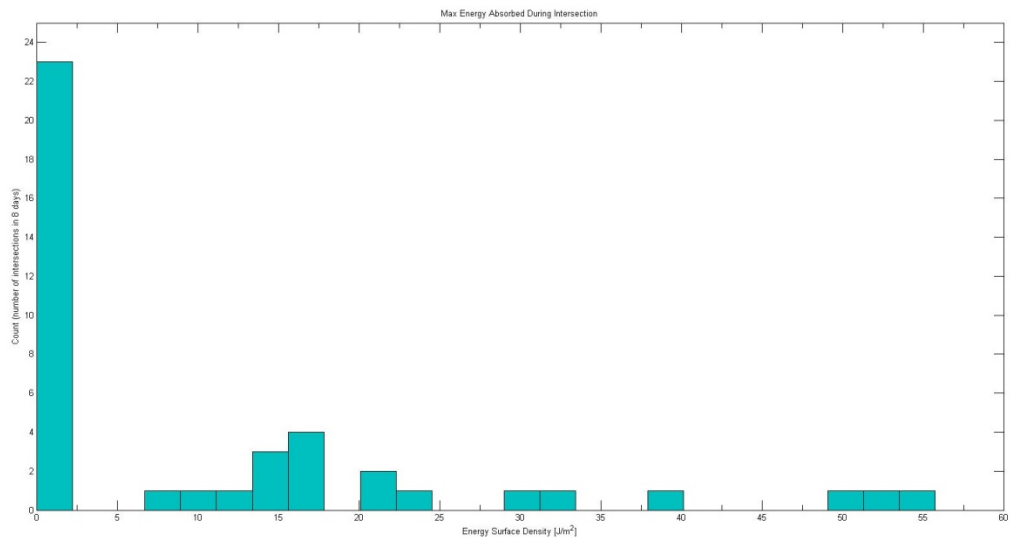


Figure F.18.—Histogram of the max energy incident on a satellite per square meter during an intersection—this is calculated using I_{\max} x intersection duration.

F.7.2 CASE 2: Sun Synchronous Orbit

Direct launch into 98° sun synch inclination from China Lake. Launches were simulated every 4 minutes for 8 days. Each intersection between the microwave beam and background satellites is recorded. On average there were 12.75 intersections per day, each for 0.03 seconds.

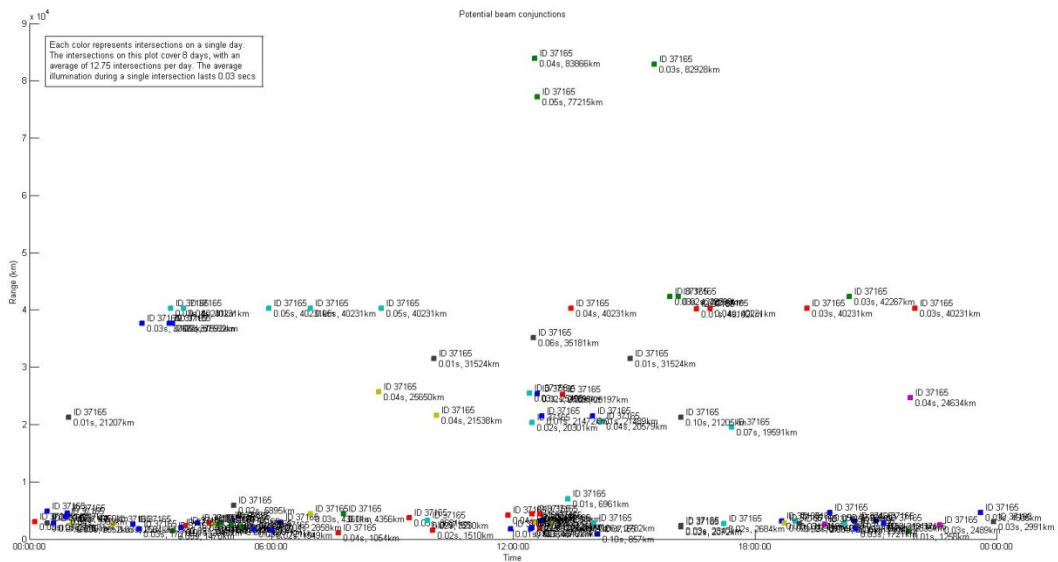


Figure F.19.—Plot of launch time against range of intersecting satellite. Each color represents a single day of launches (i.e., the 8 days are overlaid). The NORAD sat ID is listed along with intersection duration and range.

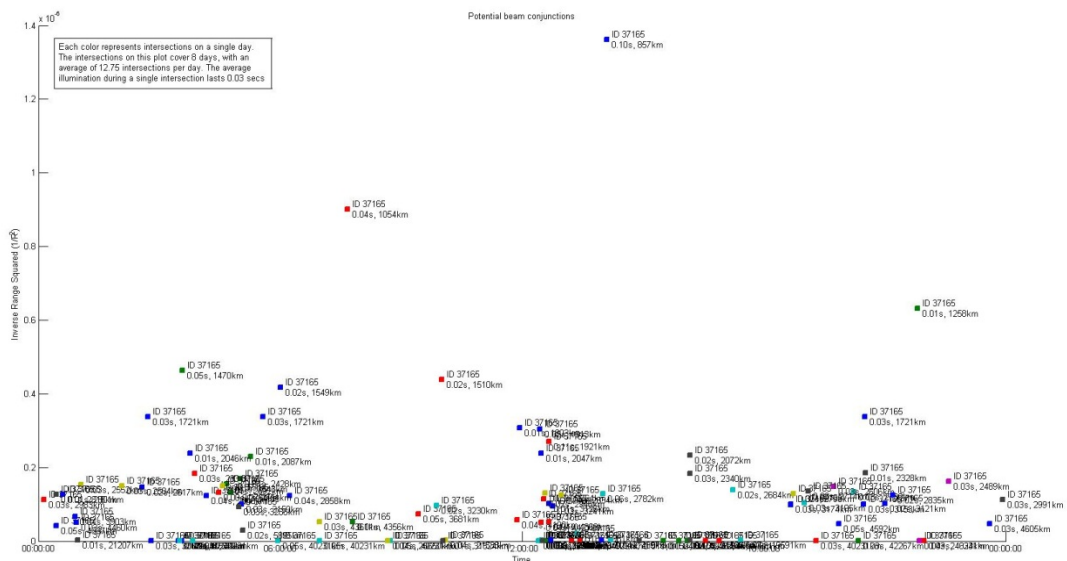


Figure F.20.—Plot of launch time against range of intersecting satellite. Each color represents a single day of launches (i.e., the 8 days are overlaid). The NORAD sat ID is listed along with intersection duration and range.

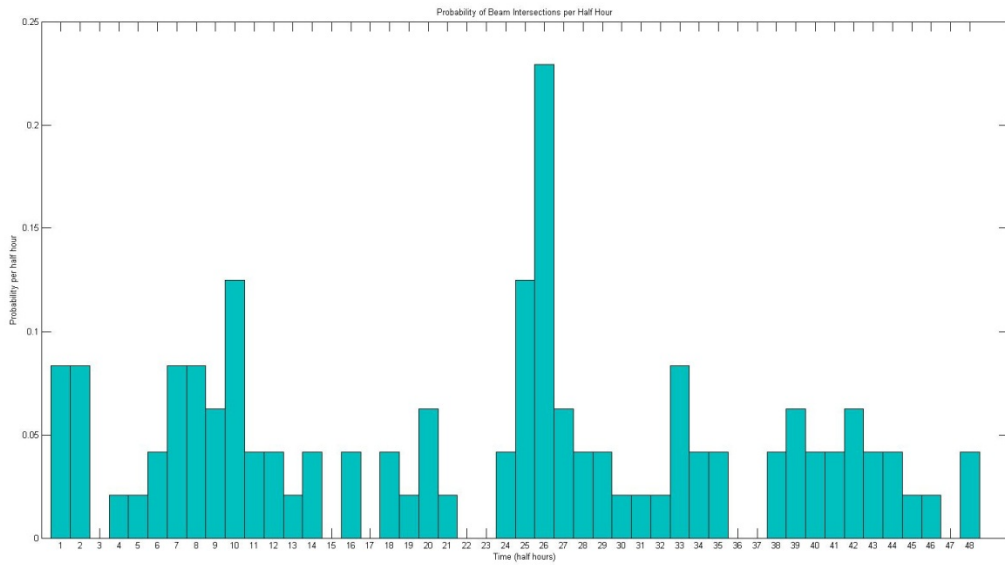


Figure F.21.—Probability of an intersection happening in each half hour period, over the 8 days.

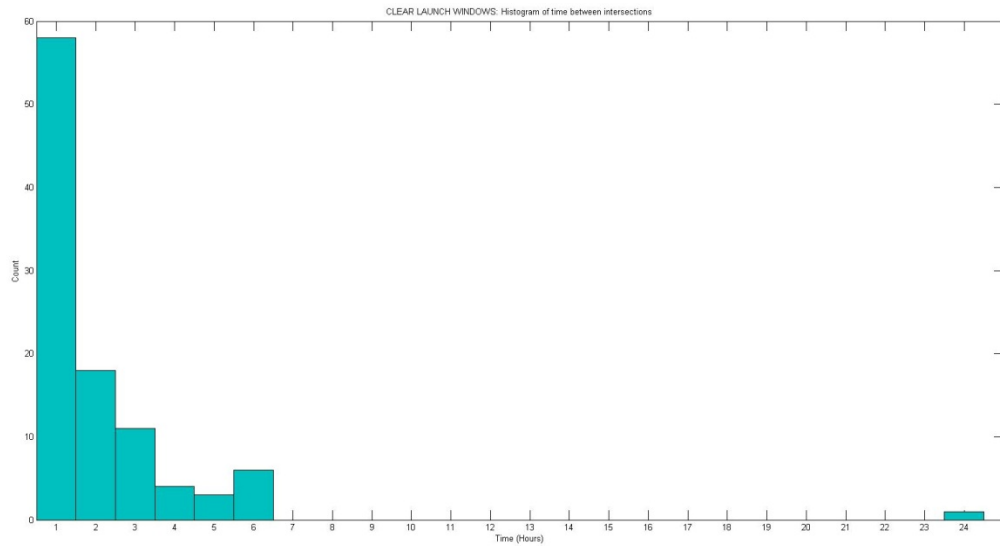


Figure F.22.—Histogram of clear launch windows—periods that have no intersections. Over the 8 days there are 41 periods with more than 1 hour of clearance.

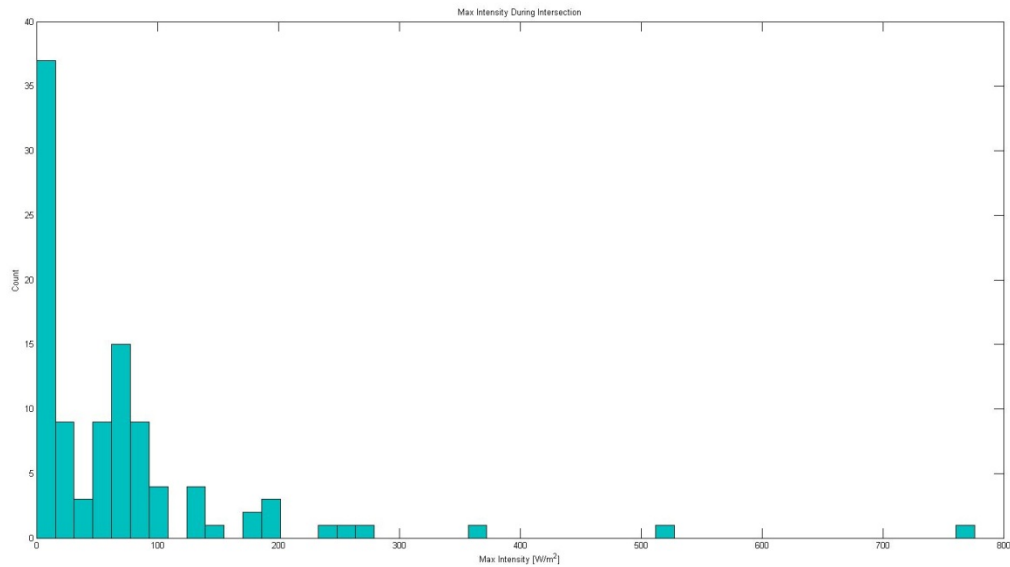


Figure F.23.—Histogram showing the distribution of intersection maximum intensity during the 8 days—note that most have I_{max} less than 200 W/m^2 (i.e., 15% of solar const.).

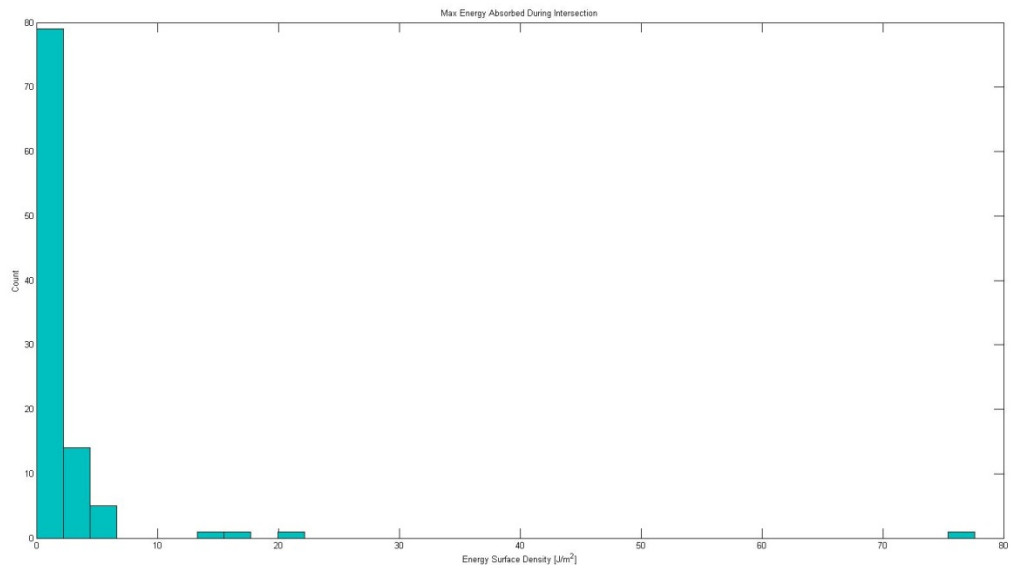


Figure F.24.—Histogram of the max energy incident on a satellite per square meter during an intersection—this is calculated using $I_{max} \times t$, where t is the intersection duration.

F.8 Propellant Injection into the Atmosphere

In the case of propellant ablation or heat exchangers for launch phase mission, there would exist by-products that are released into the atmosphere. Currently discussed propellants have included LH_2 , LN_2 , H_2O , H_2 , LOX/H_2 , peroxide/ H_2 , H_2O_2 and H_e pressurant (for pressure-fed propellants). Water would be the most benign to the environment, and this should be considered when trading systems parameters to optimize performance. Upon selection of a propellant, the expected flow rates should be compared with the trajectory and velocity profile to determine the residual concentrations in the atmosphere, and any outstanding levels noted.

F.9 Spectrum

A primary challenge in the radio frequency (RF) based communications industry is spectrum allocation. Both RF and laser sources have been considered for BEP applications. In the RF case a proposed micro/mm-wave BEP system would have to work within the spectrum constructs and constraints of the NTIA/FCC system. This may cause a significant roadblock due to the level of radiated power and interference with currently allocated bands, along with adding a level of programmatic complexity in obtaining the proper allocation permits for operation. Likewise, although there are not current spectrum allocations for free-space optical communications, over time it may be required to obtain a similar wavelength dependant license. In a similar operational scenario to existing high power sources, the Laser Clearing House would also need to be involved with the scheduling of the BEP launch facility.

F.10 Range Security

Similar security measures would be needed for BEP as with conventional launch systems, including patrol of the KOZ when active and personnel security at the launch control complex. Furthermore, given the high energy capability of the BEP sources, proper homeland security measures would have to be established to safeguard the facilities against terrorist attack or overthrow.

F.11 Operations

The conduction of a BEP launch would include a set of weather criterion established from historical NOAA data and realtime local monitoring from ground stations and balloons. Local radar would be used for weather characterization, as well as monitoring air traffic in the area and tracking the launch vehicle's trajectory. These measures could be integrated into the fire control system as a way to provide safety interlocking against airspace breach events or out-of-bound flightpath deviations.

The impact on bird populations could be mitigated by understanding local migratory patterns when establishing the location of the complex (Ref. 5). In general these are well known and predictable, as shown in Figure F.25. In areas of known bird concentrations, low level visible light laser emitters could be temporarily activated to discourage activity in the vicinity of the main beam, in a similar manner to laser crop protection systems.

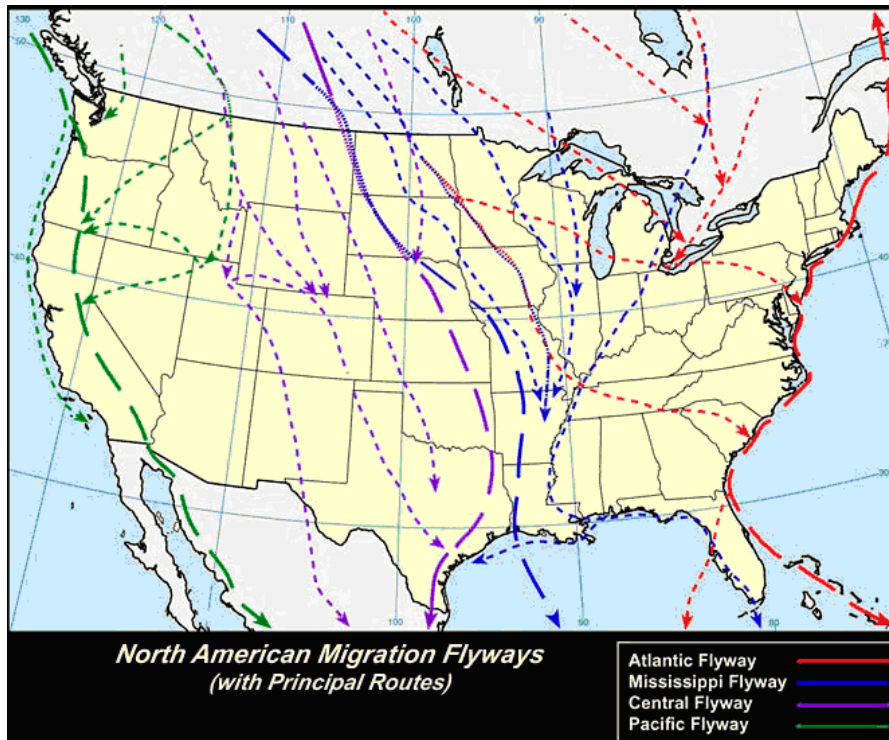


Figure F.25.—Migratory bird patterns (reproduced from source 6).

F.12 References for Appendix F

1. “Laser Propulsion for ESA Missions: Ground to Orbit Launch,” Instituto Superior Técnico, Solscientia Lda., Contract No. 17048/03/NL/PA Final Report, 8 November 2004.
2. National Oceanic and Atmospheric Administration’s (NOAA) National Weather Service (NWS) Climate Services, <http://www.weather.gov/climate/>
3. American National Standard for Safe Use of Lasers, ANSI Z136.1-2007
4. Molecular Expressions, Interactive Java Tutorials, Specular and Diffuse Reflection <http://micro.magnet.fsu.edu/primer/java/scienceopticsu/reflection/specular/index.html>
5. Robert H. Diehl, Ronald P. Larkin, John E. Black, “Radar Observations of Bird Migration over the Great Lakes,” *The Auk*, 2003.
6. North American Migration Flyways http://alaska.usgs.gov/science/biology/avian_influenza/images/NA_migration_flyways.gif

Appendix G.—Effects of Beaming Energy Through the Atmosphere

G.1 Executive Summary

Power beaming the large amounts of energy through the atmosphere that is required for propulsion either within the atmosphere or in transferring payloads from low Earth orbit to geosynchronous orbit (LEO to GEO) will be met with the extremely deleterious effects of the thermal nonlinearities induced by atmospheric heating from beam power absorption. The resulting phenomena, collectively called thermal blooming, will be the source of two major effects: (1) beam steering away from the intended target vehicle and (2) beam broadening, which will make the beam larger at the target than intended. Both of these effects have been modeled and are shown here to be remedied by the use of high-order (10th-order Hermite) phase compensation at the transmitter. Although it has been shown, in principle, that these perturbations can be mitigated, there may remain many engineering obstacles that must be overcome, such as the elimination of the mechanical jitter of the transmitter platform and other problems during beam propagation. However, there is nothing in the prevailing physics of the situation that would preclude power beaming through the atmosphere as discussed in this report.

It is important to begin to capture the prevailing effects and overall system operation using a scaled atmospheric experiment that would simulate the realistic environment in which an adaptive optics system must operate, from the variable wind velocity up to the mechanical jitter of the transmitter platform. The authors recommend that, due to the immediate availability of high-power sources, scaled atmospheric experiments be implemented (tailored after the Scaled Atmospheric Blooming Experiments (SABLE) Project by Lincoln Laboratory in the early 1990s) in which the operation of a closed-loop millimeter-wave adaptive-optics algorithm is assessed in the presence of a moving extended target. In addition, this experimental scenario could be used to address the possibility of air ionization, and subsequent breakdown, across the apertures of the combined millimeter-wave gyrotron sources as discussed in the DRM 1–C section.

Finally, there is the need to look at various general beam wave profiles such as hypergaussian waves and fractional charge (in the topological sense) Laguerre-gaussian beam waves, which show great promise in their ability to be robust with respect to atmospheric nonlinearities. However, it is important to keep the modeling effort to the level of yielding analytical results, rather than requiring numerical evaluation, so that all the nuances of the physics involved are captured, and at the same time, to provide a tool for overall system evaluation as well as the design of adaptive optics algorithms. Finally, the model should be incorporated into a trajectory analysis program so that a cadre of launch geometries can be evaluated from the point of view of atmospheric thermal nonlinearities.

G.2 Introduction

When large amounts of power are being delivered through the Earth's atmosphere via millimeter or infrared 'beams' (i.e., laser beams or beams formed at the output of a millimeter-wave antenna system), many propagation mechanisms must be addressed that may be potentially deleterious to such power transmission. The most obvious problematic mechanism is the ever-present random variation of the atmospheric refractive index due to local temperature variations known as turbulence. This naturally occurring phenomena is driven by thermal convection of heat from the Earth's surface; once the resulting air motion exceeds a critical value of velocity, laminar flow essentially evolves into turbulent flow and fluctuations in the temperature distribution become statistically random (Ref. 1). These temperature fluctuations then act directly on the prevailing refractive index, thus rendering the refractive index a random quantity. These refractive index variations randomly focus and defocus the intervening electromagnetic wave field. Thus, the atmosphere can be considered to be composed of "lenses" of random focusing and defocusing characteristics that, because of the gross atmospheric motion due to wind, move across the beam. This gives rise to many beam quality variations: the major ones being beam broadening and beam steering. The statistical analysis and modeling of this type of atmospheric

propagation has a long and rich history and has resulted in analytical descriptions for the effect of turbulence on the operation of systems relying on such beam propagation. Many models and descriptions exist for the engineering analysis of the operation of transmission systems that rely on the propagation of electromagnetic beams in the atmosphere. (For a good recent treatment of this topic, see Ref. 2 and the references therein.)

This scenario may be considered as passive electromagnetic wave propagation; that is, the wave field moves through an atmosphere whose refractive index is determined by other sources, not by the field itself. However, as the energy density of the beam increases, absorption of the beam energy by atmospheric gas components results in local heating of the atmosphere, which does indeed act directly on the refractive index and cause it to decrease in value. The possibility of this situation was first advanced in 1966 (Ref. 3). This thermal change of the refractive index field then acts on the electromagnetic wave field causing it to also change, and so on. The propagation scenario now becomes an active one, whereby the propagating field modifies the very medium in which it exists. This heating process is called thermal blooming, and it substantially differs from that of the passive propagation discussed earlier (see Ref. 4 and Ref. 5, which contains a very comprehensive review of the work and references that existed up to 1990). Here, a “thermal lens” is created within the atmosphere by the heating due to the energy density of the beam. This self-action of the beam will not only bend the beam into regions of higher refractive index (beam steering), but convection within the atmospheric fluid will also arise, which is the source of the self-induced turbulent flow of the medium. The situation is further complicated when one includes the effects of atmospheric wind and aerosols and the abovementioned passive propagation effects.

Defocusing and other associated nonlinear thermal-blooming distortions of the beam cross section will then result. In extreme cases of very large energy densities, the propagating beam will essentially break up into smaller beams, or filaments, which severely constrains the amount of energy density that the beam will be able to possess as it travels through the atmosphere. Unlike in passive propagation, the thermal-blooming mechanism introduces nonlinearities into the analysis of the phenomena that substantially complicate a complete mathematical description. Complete analyses of these types of propagation scenarios can only be done numerically, which was a major activity within the United States and Russia in the late 1980s. Other than the usual order-of-magnitude estimates using the equations of fluid mechanics and wave propagation, only numerical modeling of the effects of atmospheric thermal nonlinearities abound in the literature. Analytical treatments appropriate for an engineering analysis of atmospheric propagation systems encountering thermal blooming have been lacking, especially those that endeavor to describe the result of adaptive correction of such nonlinear effects. This situation makes a comparative assessment of the operation of through-the-atmosphere power transmission difficult.

The propagation environment of high-energy electromagnetic wave transmission within the Earth’s atmosphere is presented to assess the atmospheric effects on the various beamed-energy propulsion scenarios considered in this report. Section G.3 presents a brief review of the major physical mechanisms that prevail in the atmosphere that will deleteriously affect energy transfer via electromagnetic beam waves. The critical power thresholds for the wavelengths of 2.0 μm (infrared) and 2.0 mm (millimeter wave) are derived for the various transmitter output aperture sizes at which these propagation mechanisms arise and which must be addressed. Next, Section G.4 presents a propagation model that is later used to calculate, for a variety of aperture sizes and output powers, the thermally induced beam broadening and steering that will occur for a 2.0- μm laser beam transmitted from the Earth’s surface to a target 800 to 35 200 km distant. The adaptive correction to mitigate the thermal nonlinearity effects on the beam will then be considered. Of the various performance parameters that an adaptive optics system can be designed to optimize at the target, the minimization of the beam radius at target is used as the optimization parameter. Section G.5 dwells on the dynamics that an adaptive optics system must satisfy, particularly with regard to the control delays inherent with the propagation distances that are involved. Finally, Section G.6 highlights some scaled ground experiments that can be performed using available high-power millimeter-wave sources. In particular, assessing the effects of using an extended target with a closed-loop adaptive optics approach and studying the possible electrical breakdown of moist air in the vicinity of the combined gyrotron outputs. To aid the reader, Section G.8 gives the definitions of the symbols and

Section G.9 derives the nonlinear propagation equations for high-energy transmission through the atmosphere.

G.3 Deleterious Atmospheric Propagation Mechanisms at High Energies

At the power densities that are required for beamed-energy propulsion, several aspects of propagation within the atmosphere must be addressed that can potentially perturb the beam wave and render it unreliable for energy transfer to a small target. Once these aspects have been identified, physically understood, and mathematically modeled, appropriate mitigation procedures can be specified and applied to the problem to optimize energy transfer. These propagation features and the critical power levels at which they will be seen are given next.

G.3.1 Ionization and Electrical Breakdown

When the transmission of high-energy electromagnetic waves through the atmosphere is being evaluated, the first phenomenon that is considered is the ionization and subsequent electrical breakdown of air (Ref. 6, which contains a good introduction and the original work). Within the atmosphere, this occurs via the process of cascade ionization, whereby a free electron is created by multiquantum absorption by the atmospheric gas and through the inverse bremsstrahlung process, accelerates, and subsequently collides with an atom. The collision produces another electron, and both accelerate, collide with other atoms, and so on. This cascading process terminates in the release of light known as electrical breakdown. At a wavelength of $\lambda = 10.6 \mu\text{m}$ (i.e., the wavelength of high-power CO₂ lasers), electrical breakdown occurs at a power density of $\approx 10^9 \text{ W/cm}^2$ at atmospheric pressures and densities typical of those at sea level. This intensity is reduced by 2 orders of magnitude by the formation of the shock front due to the explosive detonation of atmospheric aerosols. Thus, for purposes of comparison, one can choose a power density of $\approx 10^7 \text{ W/cm}^2$ as the threshold for electrical breakdown within the atmosphere.

At millimeter wavelengths in the 100- to 200-GHz frequency range, electrical breakdown occurs at a smaller power density of $\approx 10^{10} \text{ W/m}^2$. One can then assume the worst case of a twofold decrease in this value due to atmospheric aerosols, thus giving a threshold power density of $\approx 10^8 \text{ W/m}^2$.

G.3.2 Induced Molecular Polarization—The Kerr Effect

The next process that must be considered is the Kerr effect: that is, the process whereby the permittivity of the atmosphere, which is a function of the polarizability of the constituent gases, varies because of the intense electric field of the laser beam acting to induce molecular orientation (Refs. 7 and 8). As discussed in Appendix G.9, the Kerr process can be described by a single differential equation, making its analysis straightforward in comparison to the thermally induced permittivity variations discussed in Section G.3.3. The associated relaxation times for molecular polarizability within the atmosphere are $\sim 10^{11} \text{ s}$, so in the case of pulsed laser propagation, the medium can be considered to be in steady state for pulse lengths larger than this value. As the brief analysis in the Appendix G.9 shows, P_{crK} is the threshold value of beam power at which the Kerr effect is only a function of the Kerr constant and the wavelength (see Eq. (G47)); it becomes an issue as a perturbing propagation mechanism at $P_{crK} \approx 1.5 \times 10^9 \text{ W}$ for the wavelength $\lambda = 2.0 \mu\text{m}$ and at $P_{crK} \approx 1.5 \times 10^{16} \text{ W}$ for $\lambda = 2.0 \text{ mm}$. The Kerr effect increases the permittivity in the location of the beam and thus results in what has become to be known as self-focusing; that is, the beam tends to move into regions of larger permittivity and thus acts as if it has encountered a lens. The lens is essentially induced by the beam through the Kerr effect. This self-focusing phenomena results in a spatial instability within the beam that causes the beam to break into individual filaments, where each filament takes on the size that corresponds to P_{crK} and the associated electric field strength.

G.3.3 Induced Heating of the Atmosphere—Thermal Nonlinearities and Thermal Blooming

The absorption of electromagnetic radiation by atmospheric gases becomes a source for the generation of heat. At large field intensities, the resulting temperature increase also changes the atmospheric permittivity. However, unlike the Kerr effect, the permittivity decreases and the beam tends to defocus (Refs. 4, 5, and 9 to 12). In addition, one must also admit the description of the atmospheric fluid dynamic processes that are elicited by local heating and thus incorporate the Navier-Stokes and heat-transfer equations for a moving medium; the medium is in motion not only because of the Archimedean forces that appear but also because of wind, which removes the heat that is generated. The entire problem is severely complicated and is usually relegated to numerical analysis applied to specific cases. However, within certain approximations, analytical results can be obtained. As shown in Appendix G.9, one can obtain an expression for the critical beam power P_{crT} above which thermally induced propagation issues can become prominent. Because of the interplay of the several physical mechanisms that prevail in this propagation process, one must specify the prevailing wind velocity V as well as the effective radius r_{eff} of the output aperture of the beam source and the wavelength-dependent absorption constant α .

$$P_{crT} \equiv \frac{\pi \rho C_p V}{k^2 r_{\text{eff}} \epsilon_T \alpha} \quad (\text{G1})$$

As given by Equation (G1), one has for $V = 4.4$ m/s (≈ 10 mi/hr), $r_{\text{eff}} = 10$ m and $\lambda = 2.0$ μm , for which $\alpha \approx 4 \times 10^{-6}$ m^{-1} and $P_{crT} = 16.7$ W, a surprisingly small power. This is due mainly to the very large radius subtended by the beam through which the field-induced temperature increase must dissipate because of wind. For a more typical radius, $r_{\text{eff}} = 0.1$ m, one has $P_{crT} \approx 1.7$ kW. At the much larger wavelength $\lambda = 2.0$ mm, one has $\alpha \approx 2.2 \times 10^{-4}$ m^{-1} , giving for $r_{\text{eff}} = 10$ m, $P_{crT} = 3.5 \times 10^5$ W.

When the radiation source is pulsed with a time duration of 1 μs , the threshold power becomes much higher because the atmosphere does not have sufficient time to heat as the pulse moves through it.

$$P_{crP} \equiv \frac{\pi \rho C_p}{k^2 \alpha \epsilon_T t_p} \quad (\text{G2})$$

From Equation (G2), the critical power at $\lambda = 2.0$ μm is $P_{crP} = 3.7 \times 10^7$ W and the critical power at $\lambda = 2.0$ mm is $P_{crP} = 7.7 \times 10^{11}$ W.

G.3.4 Atmospheric Aerosols

Aerosols in the form of fog and clouds are very efficient absorbers of electromagnetic radiation (Refs. 13 and 14). At the energy densities that prevail for beamed-energy propulsion, aerosols will essentially explosively detonate, thus diminishing their absorption and scattering abilities. The dynamics of this complex process has been well studied, and it has been established that, once a steady state has been established, propagation channels will appear in the medium through which the beam can propagate (Refs. 15 and 16).

G.3.5 Atmospheric Turbulence

The effect of random variations of the atmospheric permittivity field due to heating of the atmosphere (the sources of which are solar absorption in the atmosphere and on the Earth's surface) is independent of the beam power level for the lowest critical power thresholds derived in Section G.3.2 for the thermal-blooming case. This ever-present deleterious mechanism has the most heritage in terms of study and understanding. The effects of this phenomenon on the propagation of a beam wave show themselves in terms of loss of spatial coherence, beam steering, and beam broadening and are attendant with thermal blooming (Ref. 17). Of course, these characteristics are the same as those seen with thermal blooming, but

the adaptive compensation in the case of turbulence is straightforward in that the effect being corrected is not the result of a nonlinear process.

TABLE G.1.—THRESHOLD POWER LEVELS BEYOND WHICH PROPAGATION EFFECTS OCCUR AT INFRARED AND MILLIMETER WAVELENGTHS FOR VARIOUS OUTPUT APERTURE RADII, R_{EFF}

Propagation mechanism	Threshold power level, W		General relation for critical power P_{cr} and power density p_{cr}
	Wavelength, λ		
	2.0 μm	2.0 mm	
Electrical breakdown Effective radius of the beam, r_{eff} 1 m 10 m 30 m	3.1×10^{11} 3.1×10^{13} 2.8×10^{14}	3.1×10^8 3.1×10^{10} 2.8×10^{11}	No general relation
Kerr effect	1.5×10^9	1.5×10^{16}	Critical power and power density for the Kerr effect $P_{crK} = \frac{c}{8k^2 \epsilon_K} \quad p_{crK} = \frac{c}{8\pi k^2 r_{eff}^2 \epsilon_K}$
Thermal blooming (continuous wave, CW) Effective radius of the beam, r_{eff} 1 m 10 m 30 m	166.7 16.7 5.6	3.5×10^6 3.5×10^5 1.2×10^5	Critical power and power density for thermally induced perturbations $P_{crT} = \frac{\pi \rho C_p V}{k^2 r_{eff}^3 \epsilon_T \alpha} \quad p_{crT} = \frac{\rho C_p V}{k^2 r_{eff}^3 \epsilon_T \alpha}$
Thermal blooming (pulsed, 1 μs)	3.7×10^7	7.7×10^{11}	Critical power and power density for the pulsed case $P_{crP} = \frac{\pi \rho C_p}{k^2 \alpha \epsilon_T t_p} \quad p_{crP} = \frac{\rho C_p}{k^2 r_{eff}^2 \alpha \epsilon_T t_p}$
Turbulence	>0	>0	

The results given in Sections G.3.1 to G.3.5 are condensed in Table G.47 and stated in terms of the critical power for the appropriate propagation mechanism and output aperture sizes (where they matter) of 1.0, 10.0, and 30 m. Also shown, for reference, are the general equations for the critical power and associated critical power density. As can be seen, discussions of the use of beam powers up to 100 MW at infrared wavelengths easily exclude the effects of electrical breakdown and the atmospheric Kerr effect, leaving thermally induced nonlinearities and, of course, turbulence to be dealt with. For millimeter wavelengths, the thresholds for electrical breakdown are 3 orders of magnitude smaller than for the infrared region. Hence, aperture sizes larger than 10 m must be used for 100-MW power levels at these wavelengths using contiguous apertures.

G.4 Modeling the Effects of Atmospheric Thermal Nonlinearities on Beamed Energy Propulsion and the Required Level of Their Mitigation

Although it is not in the purview of this work to physically model the thermal nonlinearities attendant with the propagation of high-energy radiation through the Earth's atmosphere, it has been found necessary to introduce a simple analysis employing the peculiarities of the propagation scenarios of beamed-energy propulsion in order to analytically assess and compare the overall affects of the atmosphere in these various scenarios as well as to evaluate the level of the corrective adaptive optics that will be required to make feasible the goals of beamed-energy propulsion. Two such power beaming cases are considered here: (1) orbit transfer from a low Earth orbit (LEO) to a geosynchronous orbit (GEO) from a ground-based laser transmitter operating at a wavelength of 2.0 μm in the infrared spectrum and (2) beaming to a vehicle being launched within the Earth's atmosphere using a ground-based array of gyrotrons operating at the wavelength of 2.0 mm within the far infrared spectrum. Because orbital transfer

from LEO to GEO presents the worst-case situation in these two beaming cases because of the distances to be traversed, it is used as an example to form an atmospheric propagation model upon which the overall operation can be assessed. It is then shown how the model can be used to analyze the millimeter power-beaming case for which the results are also presented.

The major property of the use of such propulsion to transfer payloads from LEO to GEO is, of course, the ratio of the diffraction length L_d associated with the beam wavelength and radius, to the focal length F and the thickness H of the atmosphere. Here, the diffraction length $L_d \equiv kr_{\text{eff}}^2$ (where k is the wave number of the radiation and r_{eff} is the effective radius of the transmitting aperture; see Appendix G.9) and F is such that $L_d \gg H/L_d$.

This circumstance allows for the natural diffraction of the beam to be neglected within the region in which the beam is perturbed by induced nonlinear effects. This, along with the very large values of parameters describing the nonlinear interaction of the electromagnetic radiation with the fluid dynamics of the atmosphere (see Appendix G.9), makes for the creation of an easily implementable model to describe the major beam parameters that are of interest: the radius of the beam at the target and the displacement of the beam from the target when no adaptive correction is applied. Once these have been secured, the corrections can be applied to the various orders of aberrations of the initial phase of the beam and their effect at the target can be assessed.

It is important to note here that only the effects of the thermal nonlinearities of the atmosphere are considered. The additional effects of the ever-present turbulent fluctuations of the atmosphere are not included here because this problem has much heritage, it is well understood, and techniques for its mitigation are established. However, because of the very large power that the beams will possess that are considered here, it is expected that the induced convective velocity within the atmosphere in the beam path will swamp any turbulent velocity fluctuations. Thus, the turbulent mechanism affecting beam wave propagation at these power levels will be rendered negligible. The goal of the present analysis is to isolate the effects of the much more deleterious thermal nonlinearities on very long-range power beaming and to estimate the required level of adaptive compensation to make the orbital transfer mechanisms discussed elsewhere in this report realistic and feasible.

G.4.6 Quick Overview of the Model and a Description of Beam Behavior at Targets in Low Earth Orbit and Geosynchronous Orbit Due to Atmospheric Thermal Nonlinearities

At the outset, the basis of the propagation model will be reviewed, leaving the details of the derivation to a forthcoming NASA TM. The initial equations are

$$\left(\frac{\pi \rho C_p r_{\text{eff}} V}{\alpha P_0} \right) \frac{\partial T}{\partial x'} = \frac{\partial T'}{\partial x'} = |E'|^2 \quad (\text{G3})$$

$$2i \frac{\partial E''}{\partial z'} + \nabla_{\text{p}}^2 E'' + R_V T' E'' = 0 \quad E'' = E' \exp(-\alpha L_d z'/2) \quad \frac{\partial T'}{\partial x'} = |E'|^2 \quad (\text{G4})$$

(also in Appendix G.9), where the dimensionless nonlinearity parameter R_V is given by

$$R_V \equiv \frac{k^2 r_{\text{eff}} \varepsilon_T \alpha P_0}{\pi \rho C_p V} \quad (\text{G5})$$

connecting the total incident power P_0 in the beam with the effective radius r_{eff} of the transmitted beam and the prevailing wave number $k \equiv 2\pi/\lambda$ of the radiation of wavelength λ . The parameter E is the electric field of the beam at the target, z is a coordinate, α is the atmospheric absorption coefficient at the

particular wavelength, $\varepsilon_T \equiv |\partial\varepsilon/\partial T|$ is the variation of the permittivity with respect to the associated temperature variation T , ρ is the density of the atmosphere, C_p is the specific heat of the atmosphere at constant pressure, and V is the total relative velocity of the beam slewing across the atmosphere and that of atmospheric wind. (The normalization of the variables, indicated by the prime signs, is discussed in Section G.9.) Using the parameter values discussed in Section G.9, one has, for a 1-MW beam (i.e., $P_0 = 1.0 \times 10^6$ W), $R_V = 6.0 \times 10^4$ for $\lambda = 2.0$ μm . In this instance, the second term in the first relation of Equation (G4) can be neglected relative to the third term: that is, the evolution of the beam within the atmosphere due to natural diffraction is negligible compared with the phase perturbation due to the thermal nonlinearity acting on the permittivity function. Hence, the model equations become

$$2i \frac{\partial E''}{\partial z'} + R_V T' E'' = 0 \quad E'' = E' \exp(-\alpha L_d z'/2) \quad \frac{\partial T'}{\partial x'} = |E'|^2 \quad (\text{G6})$$

The solution of these relations must now be augmented with the prevailing boundary condition for the initial radiation profile of the beam at the output aperture of the transmitter at $z' = 0$. Using

$$E(\vec{\rho}', 0) = A_0 \exp \left[- \left(\frac{\rho'^2}{2} \right) \left(1 + i \frac{L_d}{F} \right) \right] \quad (\text{G7})$$

which is derived in Section G.9 (where A_0 is the initial amplitude of the field), and a gaussian beam profile, one has

$$E'(\vec{\rho}', 0) = A'_0 \exp \left[- \left(\frac{\rho'^2}{2} \right) \gamma' \right] \quad \gamma' \equiv 1 + i \frac{L_d}{F} \quad \rho'^2 = x'^2 + y'^2 \quad (\text{G8})$$

However, in most power-beaming applications, the focal length F of the beam will be set to the distance L to the target: $F = L$. In addition, the full normalized representation for a gaussian beam wave must be employed in the last relation of Equation (G6):

$$E'(\vec{\rho}', z') = \frac{A'_0}{1 + i\gamma'z'} \exp \left[- \left(\frac{1}{2} \right) \left(\frac{\gamma'}{1 + i\gamma'z'} \right) \rho'^2 \right] \quad (\text{G9})$$

where γ is the control, or update, coefficient.

Finally, one must consider the effective thickness H of the atmosphere. Although there are several models that can be used to represent the absorption constant α with respect to the height within the atmosphere (the most popular is an exponential variation with height), it proves expedient here to use a single value for H and a corresponding effective value for α .

The solution of Equations (G6) and (G8) can now be considered for $L_d/F \gg H/L$. To be sure, one has $H \approx 10$ km, $F < 35$ 200 km, and for $r_{\text{eff}} \approx 30$ m, $L_d \approx 2.8 \times 10^9$ m at infrared wavelengths.

G.4.7 Application of the Foregoing to the Calculation of Beam Spread and Deflection Due to Atmospheric Thermal Nonlinearities for Power Beaming to Low Earth Orbit and Geosynchronous Orbit

Again, leaving the details concerning the derivations to a forthcoming NASA TM, one can employ Equations (G6) to (G9) to obtain expressions for two very important performance parameters for power beaming to a target: that is, (1) the amount that the beam radius is widened because of the induced thermal defocusing (beam spread) and (2) the amount that the entire beam is steered away from the

intended target because the propagation path of the beam tends to favor regions of larger permittivity (i.e., steers away from regions of higher atmospheric temperature caused by absorption (beam displacement)). It is important to note that, as discussed in Section G.9, the wind direction is taken to occur along the x -axis of a coordinate system whose origin is situated at the transmitter aperture with beam propagation occurring along the z -axis. Also, the radius of the transmitter aperture at $z = 0$ is given by an effective radius $r_{\text{eff}}(0)$ that is related to the corresponding beam waist radius W_0 by $r_{\text{eff}}(0) = W_0/\sqrt{2}$.

Because of the asymmetry introduced into the problem by the wind velocity V moving along the x -axis of the originally circular beam, there are two effective radii, $r_{\text{eff},x}(L)$ and $r_{\text{eff},y}(L)$, that characterize the beam in the x - and y -axis, respectively, at the distance L to the target vehicle. Again, this circumstance is brought about by the removal of heat from the beam channel along the x -axis. However, heat is not convectively removed from the beam along the y -axis. Instead, it diffuses in the y direction, which is a much slower process than convection. The result is that the defocusing in the y direction is much greater than in the x direction, and the beam becomes elliptical as it leaves the atmosphere and continues to enlarge until it interacts with the target in space.

The results of the calculation for the effective radii and the target are given by

$$r_{\text{eff},x}(L) = R_{\text{eff}}(L) \sqrt{1 + \frac{1}{3} \Theta_{NLV}^2(P_0)} \quad (\text{G10})$$

$$r_{\text{eff},y}(L) = R_{\text{eff}}(L) \sqrt{1 + 0.866 \frac{L_d}{L} \Theta_{NLV}(P_0) + 1.612 \Theta_{NLV}^2(P_0)} \quad (\text{G11})$$

where

$$\Theta_{NLV}(P_0) \equiv \frac{k \epsilon_T \alpha H P_0}{4 \pi \rho C_p V r_{\text{eff}}(0)} \quad (\text{G12})$$

is yet another nonlinear parameter that enters the problem and characterizes, within the thin phase screen approximation, the level of the thermal nonlinearity effect on a beam wave of initial power P_0 through an atmosphere of thickness H . The quantity $R_{\text{eff}}(L) \equiv L/(k r_{\text{eff}}(0))$ is what the radius of a beam focused on the target at a distance L would be if the atmosphere were not present: that is, if transmission occurred entirely within a vacuum. (The reader is asked to excuse the rather excessive notations related to the various beam radii; the initial radius of the beam at the transmitter, denoted here as $r_{\text{eff}}(0)$, is usually stated in terms of the waist radius W_0 , which is a factor of $\sqrt{2}$ smaller than the former. However, it is desired here to show how the effective radii “evolve” throughout the propagation process.) Thus, the quantities given by the radicals in Equations (G11) and (G12) are the factors by which the beam radii increase at a space-borne target because of the induced thermal nonlinearities within the atmosphere.

In addition, as discussed earlier in this chapter, there is a deflection $\Delta(L)$ of the beam axis into the direction opposite to that of the wind. This is given by

$$\Delta(L) = 2R_{\text{eff}}(L) \Theta_{NLV}(P_0) \quad (\text{G13})$$

The implications of these results to the behavior of a beam wave to targets at LEO ($L = 800$ km) as well as GEO ($L = 35\,200$ km) are given next. The operating wavelength of the continuous wave case considered here is taken to be $\lambda = 2.0$ μm , and the atmospheric wind velocity along the x -axis is taken to be $V_x = 4.4$ m/s ≈ 10 mi/hr. Three transmitter aperture radii— $r_{\text{eff}}(0) = 5$ m, 10 m, and 30 m—are considered. Table G.48 displays the beam radii that would occur at targets in LEO and GEO if the atmosphere were not present.

TABLE G.2.—BEAM RADII AT TARGETS IN LOW EARTH ORBIT (LEO) AND GEOSYNCHRONOUS ORBIT (GEO) FOR VARIOUS OUTPUT APERTURE SIZES.

[Wavelength $\lambda = 2.0 \mu\text{m}$.]

Orbit of target	Distance to target, L , km	Effective beam output aperture radius, $r_{\text{eff}}(0)$, m		
		5	10	30
		Beam radius at target, m		
LEO	800	0.1	0.051	0.017
GEO	35 200	4.48	2.24	0.75

Only a subset of these possibilities are considered in what is to follow. To keep things realistic, $r_{\text{eff}}(0) = 5$ m at GEO and $r_{\text{eff}}(0) = 30$ m at LEO are not subject to further analysis.

Figures G.1 to G.4 display plots of $r_{\text{eff},x}(L)$, $r_{\text{eff},y}(L)$, and $\Delta(L)$ versus P_0 for transmission to LEO and GEO for the various initial beam radii at the output aperture using Equations (G10) to (G13). In addition to values quoted in Section G.9, the nominal value of $H = 10$ km was used in conjunction with the average absorption coefficient $\alpha \approx 4 \times 10^{-6} \text{ m}^{-1}$. As can easily be seen in all the examples, the thermal action of the atmosphere has a severe impact on the integrity of the beam wave at the target locations.

Comparing the radii that result at the targets in LEO and GEO, because of a beam that has traversed thermal nonlinearities within the atmosphere, to those quoted in Table G.48 shows the rather unsatisfactory, but not unexpected, results that cause researchers to deem beaming power to such locations as unfeasible without the proper compensation to the beam applied at the transmitter. The induced deflection of the beam can easily be removed by a tracker, but the aberrations that remain, which result in the beam broadening, can only be removed by appropriate phase compensation applied at the transmitter.

G.4.8 Phase Compensation of the Effects of Atmospheric Thermal Nonlinearities

The first research into the compensation of thermal-blooming effects considered the application of a Zernike polynomial expansion of the transmitted phase front (Refs. 18 and 19). This technique provides for an optimal representation of the phase front of the beam wave so long as the cross section of the beam remains circular; after all, Zernike polynomials are, by design, orthogonal on a unit circle. The problem encountered in the Section G.4.7 development is different: a beam asymmetry arises because of the differences in convective versus diffusion cooling of the atmospheric channel in which the beam propagates. The model briefly reviewed in Section G.4.6 allows for the analytical assessment of phase compensation of the deleterious effects shown in Section G.4.7.

The different behavior of the beam along the transverse axes suggests that a more general set of orthogonal polynomials should be used than those of Zernike. Here, since the initial form of the beam wave is given by a gaussian function, the transmitted phase front $S(x,y)$ at the output aperture of the transmitter can be expanded in a set of orthogonal polynomials associated with a gaussian weight function: that is, the Hermite polynomials $H_n(x)$ and $H_m(y)$ (Ref. 20). Thus,

$$S(x,y) = \sum_n^M \sum_m^N a_{nm} H_n(x) H_m(y) \quad (\text{G14})$$

The expansion coefficients a_{nm} are determined by applying one of several performance metrics. For example, for power-beaming applications considered in this study, it is desired to shape the phase front so as to minimize the radius of the beam at the target so the beam does not interfere with the adjacent structures of the vehicle. Hence, the performance metric to be minimized through the selection of a_{nm} is related to the electric field $E''(\rho',L)$ of the beam at the target vehicle by

$$\Pi(L) \equiv \frac{\int_0^\infty |E''(\rho', L)|^2 \rho'^3 d\rho'}{\int_0^\infty |E''(\rho', L)|^2 \rho' d\rho'} \quad \rho' = \sqrt{(x'^2 + y'^2)} \quad (\text{G15})$$

in which $E''(\rho', L)$ results from the application of the boundary condition

$$E''(\bar{\rho}', 0) = A'_0 \exp \left[- \left(\frac{\rho'^2}{2} \right) \gamma' - iS(x', y') \right] \quad \gamma' \equiv 1 + i \frac{L_d}{L} \quad (\text{G16})$$

to the solution of Equation (G6). Ideally, the number of terms of the expansion given in Equation (G14) is infinite: $N, M \rightarrow \infty$. The linear terms for which $n + m = 1$ determine the inclination correction of the beam wave. The quadratic terms for which $n + m = 2$ determine the focusing correction, and the higher order terms for which $n + m \geq 3$ give the higher order aberration corrections. However, in realistic applications, the number of aberrations N and M is finite, and in fact, it is desired to find the smallest number of aberration corrections that can be used to represent the compensated phase. The specific expressions for the coefficients a_{nm} are found by equating to zero the derivative of $\Pi(L)$ with respect to these coefficients.

The propagation problem defined here, as well as the associated minimization problem, can be solved analytically and will also appear in a forthcoming NASA TM. The results applied to the calculation of the phase-corrected beam radii are as follows. The elliptical shape of the beam, which is characterized by two radii at the target vehicle, facilitates the calculations if a single effective radius $r'_{\text{eff}}(L)$ defined by

$$r'_{\text{eff}}(L) \equiv \sqrt{\frac{r_{\text{eff},x}^2(L) + r_{\text{eff},y}^2(L)}{2}} \quad (\text{G17})$$

is considered. Applying the modeling procedure outlined in Equations (G14) to (G16), one finds that, for the radius $r'_{\text{eff,corr}}(L)$ of a focused beam wave corrected for the first M phase aberrations represented by the model of Equation (G14),

$$r'_{\text{eff,corr}}(L) = R_{\text{eff}}(L) \times \left[1 + 2.95 \Theta_{\text{NLV}}^2(P_0) - 4 \Theta_{\text{NLV}}^2(P_0) \left(\left(\sum_{n=1}^M \sum_{m=0}^M \frac{H_{n-1}(0) H_m(0)}{2^{3(n+m)/2} n! m!} \right)^2 2^{n+m} (n+m) n! m! + \frac{\pi}{4} \sum_{n=0}^M \left(\frac{H_n(0)}{2^{3n/2} n!} \right)^2 2^n n! n \right) \right] \quad (\text{G18})$$

Figures G.5 to G.8 show the results of this relation applied to the various LEO and GEO beaming cases considered in Section G.4.7.

These plots display the fact that, for initial beam powers of 10 MW or less, phase correction using M -order aberrations returns the radius of the beam to its desired value at the target vehicle. Beyond this power level, only for the case shown in Figure G.8, which uses a beam radius of 30 m at the transmitter, can a 10th-order phase correction be effective up to about 70 MW.

One assumption that has been prevailing in all these calculations is that the wind velocity V is a constant along the entire propagation path. In reality, this is certainly not the case. In fact, there may be regions in which the $V \approx 0$ (i.e., a stagnation zone), and the convective heating scenario assumed here will transform into a diffusive heating scenario characterized by much lower critical power thresholds. This case will not be studied here since it is the subject of a recent study (Ref. 21), but it must be kept in mind

that a statistical description of the wind profile along the propagation path will be required in a more careful examination.

Finally, there is the whole issue of the effect that the beam profile will have on the level of thermal nonlinearity perturbations. In fact, very high energy laser beams are characterized by initial beam profiles that are tubular: that is, have a local minimum of intensity in the center that increases toward the outer portions of the beam. Such beams, which can be modeled by hypergaussian profiles, tend to be characterized by higher critical power thresholds. This is due to the fact that the center of the beam, with a lower intensity, is thermally cooler than the periphery and thus tends to bend toward the center and remain stable. This effect should be studied for the particular high-energy sources that will be used as the design of the power-beaming scenarios evolve.

G.4.9 Using the Propagation Model for the Analysis of Millimeter-Wave Beaming Within the Earth's Atmosphere

The methodology developed in this chapter for the infrared power-beaming case for LEO-to-GEO orbital transfer can be applied to the millimeter-wave case for power beaming to vehicles launched from within the Earth's atmosphere. The wavelength of concern here is $\lambda = 2.0 \times 10^{-3}$ m = 2.0 mm with an output aperture radius $r_{\text{eff}} = 50$ m. This gives $L_d = 7.9 \times 10^6$. The propagation distances involved range from $L = 20$ to 120 km. Although the beam will not be directly focused on the target vehicle (the dimensions being envisioned will require the beam to have a focal length just beyond the vehicle), for the purposes of this discussion, $F \approx L$. The effective distance within the atmosphere responsible for most of the absorption at these wavelengths is $H \approx 1.8$ km. Hence, the condition $L_d/F \gg H/L_d$ is easily met. In addition, there is a characteristic length L_T that is a measure of the distance at which thermally induced diffraction effects will occur. This characteristic length can be defined using the length L_d as well as the nonlinear distortion parameter R_V given by Equation (G19).

$$R_V \equiv k^2 r_{\text{eff}}^2 \epsilon_T T_V = \frac{k^2 r_{\text{eff}} \epsilon_T \alpha P_0}{\pi \rho C_p V} = \frac{P_0}{P_{crT}} \quad (\text{G19})$$

A detailed analysis similar to that given in Section G.9 gives for the thermal diffraction distance

$$L_T = \sqrt{\frac{\pi r_{\text{eff}}^3 \rho C_p V}{\epsilon_T P_0 \alpha}} \quad (\text{G20})$$

At the wavelength considered in this section, the associated absorption coefficient is $\alpha \approx 2.2 \times 10^{-4}$ m⁻¹, which gives $L_T \approx 73$ km for the total transmitter power of $P_0 = 800$ MW (which is considered later in this section). Hence, thermal diffraction effects will certainly not prevail within the region $H = 1.8$ km or, for that matter, within the entire troposphere, and the model constructed earlier in this chapter can be adopted here. (This circumstance is solely due to the very large output aperture that is being used.)

Equations (G10) to (G13) can now be used to consider four scenarios for a typical power-beaming launch:

- Horizontal beaming ($\theta = 0^\circ$) at $L = 20$ km
- Beaming at $\theta = 30^\circ$ and $L = 50$ km
- Beaming at $\theta = 50^\circ$ and $L = 100$ km
- Beaming at $\theta = 90^\circ$ and $L = 120$ km

In each case, the target is to be illuminated in an area with a radius of $R_{\text{eff}}(L) \approx 1.8$ m. Thus, a dynamic focus is to be employed; the focal length is determined by

$$F = \frac{L}{\Phi} \quad \text{where} \quad \Phi = 1 \pm \frac{L}{2L_d} \sqrt{\frac{kL_d R_{\text{eff}}^2(L)}{L^2} - 1} \quad (\text{G21})$$

and where the “-” sign is used in front of the radical for a beam focused behind the target. Figures G.9 to G.12 display the results of applying the propagation model to these cases.

As can be seen from these results, the worst case is, of course, the horizontal beaming at an elevation angle $\theta = 0^\circ$, as in Figure G.9. Here, the beam traverses 20 km of atmosphere. The beam severely broadens along the y -axis, perpendicular to the wind velocity, since the heat that is generated is not convectively removed in this direction as it is along the x -axis. Related to this phenomenon is the fact that the beam is deflected in the x -direction up to 12 m from the target at a power level of 800 MW. Of course, as the elevation angle of the beam path increases, the distance within the atmosphere decreases up to the best case, in which $\theta = 90^\circ$, as depicted in Figure G.12. It must be cautioned, however, that the model used here, as mentioned earlier, does not include viscous and Archimedean forces that occur during the thermally induced motion of the atmosphere within the vertical column in which the beam propagates. For situations in which large elevation angles are realized, these effects must be included in a future extension of the analysis. Finally, it must be noted that in order to follow the relatively close target vehicle, the beam will have a discernable slewing velocity in comparison to that of the LEO-to-GEO transfer case. This slewing velocity may (depending on the relative wind velocity) tend to lessen the thermal effects. This will certainly be the case for the upward movement of the beam. As for the horizontal component of the slewing velocity, it can either detract or worsen the thermal effects. Such aspects of the problem can only be assessed via a simulation of the particular launch environment.

Just as with the infrared beaming case, the adaptive correction of these deleterious effects is accomplished through the use of phase compensation at the transmitter output aperture. Again, because of the asymmetry induced within the structure of the beam, it is advantageous to represent the corrected phase front as an expansion of Hermite polynomials. Figures G.13 to G.16 show the results of applying various orders of Hermite correction to the millimeter-wave beam. The goal is, of course, to return the beam radius to the desired value of 1.8 m. As expected, the $\theta = 0^\circ$ case requires the most compensation; correction up to 10th-order aberrations is needed after the removal of the beam deflection via a tracker. The other cases only need correction up to the 5th order.

The additional advantage that this millimeter-wave power-beaming scenario has over the LEO/GEO orbital transfer case is that the target vehicle will have a much larger apparent velocity in both the traverse and longitudinal directions than an object executing a LEO-to-GEO transfer. This circumstance brings to the fore the conditions of stability of the control algorithms, which compose a closed-loop adaptive optics system. The beam also will have a significant slewing velocity that, in some respects, eases the effects of thermal nonlinearities, but in others, places a burden on the operation of the adaptive optics control system. This is discussed in Section G.5.

Finally, it should be mentioned that for the power levels considered in this millimeter-wave case, one should consider the mechanism of explosive detonation (Ref. 16) of small atmospheric aerosols that may

traverse the beam, especially in the horizontal beaming case. This will give rise to a time-dependent absorption coefficient that may indeed lessen the long-term heating effects within the atmosphere.

G.4.10 Tool for Quickly Assessing Nonlinear Thermal Effects on Power Beaming

Section G.9 introduces several expressions for threshold power levels at which thermal effects will become prevalent. Although these derivations are based essentially on normalization and dimensional analysis, they can be given credence by using the results obtained in Section G.4.8. However, these critical power levels need to be related to a specific property or characteristic of a beam wave that will impact the performance of the power-beaming system. Because there are many such characteristics and because there will be as many corresponding critical power levels, there is no single universal quantity that can be stated to convey the specific impact that thermal blooming will have on the entire performance of a beamed-energy system. However, the most important characteristic in power-beaming situations is the variation of the beam radius due to the defocusing that occurs when the atmosphere is heated. As shown by Equation (G11) and, for example, in Figures G.1 to G.4, the radius of a beam in an atmosphere with convection is severely perturbed in the direction perpendicular to the wind direction. To attempt to secure an analytical estimate at which the radius of such a beam will begin to increase because of thermal blooming, one can expand Equation (G11) to obtain

$$r_{eff,y}(L) = R_{eff}(L) \left(1 + \frac{0.866 L_d}{2 L} \Theta_{NLV}(P_0) + \dots \right) \quad (G22)$$

and require the value for P_0 at which

$$\frac{0.866 L_d}{2 L} \Theta_{NLV}(P_0) \approx 0.1 \frac{k^2 r_{eff}(0) \epsilon_T \alpha P_0 H}{\pi \rho C_p V L} = 1 \quad (G23)$$

Setting $L = H$, one finally obtains for the critical power at which the beam radius begins to expand

$$P_{crR} = 10 \frac{\pi \rho C_p V}{k^2 r_{eff}(0) \epsilon_T \alpha} \quad (G24)$$

which is just $10P_{crT}$. One can now use this relation for millimeter wavelengths and compare it to the infrared case. Figures G.17 and G.18 show plots of Equation (G24), as well as the associated power density $P_{crR} / \pi r_{eff}^2(0)$, versus aperture radius for both cases. Here, the nominal wind velocity is taken to be $V = 0.5$ m/s. Of course, Equation (G24) is simple enough to apply a statistical model describing the value for V .

Evaluating Equation (G24) using the numerical values of the parameters that do not depend on the wavelength, one has for this critical power

$$P_{crR} = 200 \frac{\lambda^2}{\alpha r_{eff}} \text{ MW} \quad (G25)$$

where P_{crR} is in megawatts and λ and r_{eff} are in meters. (The units of α are inverse meters.) These results clearly show that propagation within the atmosphere can sustain much larger power levels at millimeter wavelengths than at infrared wavelengths.

G.5 Dynamics of Adaptive Phase Compensation for Power-Beaming Applications

There are two major approaches that can be used to implement phase compensation to mitigate atmospheric effects: (1) wave front “reversal,” or conjugation, and (2) wave front control employing the optimization of a specific system metric for performance. The first presents a fundamental problem for the mitigation of thermal nonlinearities in that it relies on a principle of reciprocity, a basic tenant of which is violated in thermal-blooming applications. The use of such a principle essentially requires, through a wave front conjugation condition, that the amplitude and phase be corrected. However, it is much easier to correct the phase perturbations and not the associated amplitude perturbations. This is fine if amplitude variations are small (e.g., astronomical imaging). In thermal-blooming scenarios, amplitude variations cannot be neglected. Using this approach is not warranted in power beaming. What is recommended here is the use of a method using the actual radiant intensity at the target. What used to be called aperture optimization, or tagging (Ref. 22), has come to be known as target-in-the-loop. Its implementation is known as gradient descent optimization (GDO) wave front control (Refs. 23 to 27) and is suggested for the power-beaming applications addressed in this report. Here, the control rule is based on the direct optimization of an easily measured system performance metric, such as the radiant intensity at the target.

The model governing the operation of such an adaptive optics system is given by first identifying a performance metric $\Pi \equiv \Pi[S(\vec{a})]$, as defined by Equation (G14), which depends on the phase given by Equation (G14) and the array $\vec{a} = [a_{nm}]$ of the associated expansion coefficients (Ref. 24). The coefficients in Equation (G14) were selected to minimize the beam radius on the target vehicle. Here, the optimal selection of the values of a_{nm} during the actual operation of the system is given by the control rule

$$\tau_{a_{nm}} \frac{\partial a_{nm}(t)}{\partial t} = -\gamma \frac{\partial \Pi(t)}{\partial a_{nm}} \quad (\text{G26})$$

in which $\tau_{a_{nm}}$ are the time constants and γ is the control (or update) coefficient. Here, J is taken to be the size of the focal spot at the target vehicle, and t is the time. The intensity can be inferred by recording the reflected radiation from the target at a point separated from the transmitter so that a slightly different and unperturbed propagation path is used. It must now be established that such a control structure will dynamically operate in the two extreme cases of power beaming considered here: (1) infrared beaming to a vehicle in GEO and (2) millimeter-wave beaming to a near Earth vehicle.

Consider first power-beaming to GEO. For a brief analysis in which the required temporal characteristics of the adaptive optics system (and thus the temporal stability) are to be derived, one can consider the isolated case for which $n + m = 2$: that is, according to the discussion in Section G.4.8, the beam wave is focused dynamically. Thus, one has from Equation (G14) for the associated (now time-dependent) aberration coefficient

$$a_{20}(t) = \frac{L_d}{F(t)} \quad (\text{G27})$$

where, for example, $H_2(x) \sim x^2$. For the case in which the focus is to be placed at the target at a distance L (i.e., $F(t) = L$), one has from Equation (G26)

$$a_{20}(t) = \frac{L_d}{L} + \left(\frac{L_d}{L} + a_{20}(0) \right) \exp \left[-\frac{t}{t_a} \right] \quad (\text{G28})$$

where $t_a = \tau_{20} L_d^2 / (\gamma L^2)$ is the adaptation time of the adaptive optics system. This very important time constant is, although proportional to τ_{20} , inversely proportional to the distance to the target. This well-known property is that the adaptive system will possess a faster response the farther the target is from the transmitter. If this were all that the description of the adaptation system required, then the state of focusing on the target would monotonically approach the desired result L_d/L . However, there is a limiting factor placed on this circumstance by the delay inherent in overall system response due to the propagation time to and from GEO. When the propagation delay is allowed to enter into the control rule, Equation (G26) becomes

$$\tau_{a_{nm}} \frac{\partial a_{nm}(t)}{\partial t} = -\gamma \frac{\partial \Pi(t - t_d)}{\partial a_{nm}} \quad (\text{G29})$$

where t_d is the delay time (in this case, light time to and from the target). Expanding the right side of this equation in a Taylor series in t_d and keeping the first few terms yields

$$\tau_{a_{nm}} \frac{\partial a_{nm}(t)}{\partial t} = -\gamma \left[\frac{\partial \Pi(t)}{\partial a_{nm}} - t_d \frac{\partial^2 \Pi(t)}{\partial a_{nm} \partial t_d} + \frac{t_d^2}{2} \frac{\partial^2 \Pi(t)}{\partial a_{nm} \partial t_d^2} - \dots \right] \quad (\text{G30})$$

The corresponding characteristic equation ζ for the resulting differential relationship for $a_{20}(t) = \exp(-\zeta t)$ in the example considered in Equation (G30) is given by

$$\zeta_{\pm} = \frac{t_a - t_d \pm \sqrt{t_a^2 - 2t_a t_d - t_d^2}}{t_d^2} \quad (\text{G31})$$

which shows that the system converges to a stable state so long as $t_a > t_d$; that is, the adaptation period of the system is longer than the delay time. For a target in LEO, $t_d \geq 0.005$ s, and for GEO, $t_d \approx 0.24$ s (for the round trip time). If on the other hand, $t_d > t_a$, the system does not converge to the stable state and $\lim_{t \rightarrow \infty} a_{20}(t) \rightarrow \infty$. Thus, the adaptive system must be continuously “tuned” (by adjusting γ in response to changes in t_d as well as the evolving values for L in the case of a moving target) so that the condition $t_a > t_d$ is satisfied.

To these considerations must also be added the temporal delay in the overall system response. This will not be discussed here because these considerations can be found in the literature. Suffice it to say that the delay that is met with in beaming to GEO can be easily factored into the operation of the adaptive system. It must be remembered that the distance to the target is always increasing in time for a beamed-power scenario and that this, above and beyond that of the propagation delay, must be properly treated in the design and specification of the adaptive optics control system.

Work on the actual implementation of the closed-loop control of the gradient descent algorithm of Equation (G26) has rapidly progressed. The technology is now mature and forms the basis for reliable adaptive control. The only possible exception to its application is for power beaming to locations within the Earth’s atmosphere for surface or near-surface launching. Here, the target vehicle, unlike in the LEO-to-GEO transfer case, is rapidly moving and is considered to be an extended target; that is, its spatial extent cannot be relegated to a point object, and its possible rotation and orientation become an issue for use as a reflector of radiation back to the adaptive optics receiver. Here, the randomly rough surface of the target reflector creates a speckle field characterized by bright and dark regions of intensity that have been found to complicate the implementation of a closed-loop adaptive optics scenario. This can lead to the slowing of the convergence speed of the system and, ultimately, may compromise the efficiency of its

operation in terms of the optimization of the focal spot at the target. Methods using the precompensation of the beam show promise (Ref. 28).

Although it was shown that the basic physics of the situation does not preclude beaming energy to a prescribed area on a target vehicle in GEO, the engineering implementation will offer some major obstacles to be negotiated. In particular, beaming into a GEO location will require 30-nanoradian pointing accuracy on the part of the transmitter optics. The presence of mechanical jitter of the transmitter platform will have to be continuously mitigated. In addition, on the other side of the spectrum, launching from within the atmosphere will challenge the application of the adaptive optics at millimeter wavelengths. The fact that the beam is rapidly slewing because of the relatively rapidly moving object makes it difficult for the closed-loop adaptive optics system to converge to a stationary value since the medium within the column of atmosphere in which the millimeter-wave beam exists is constantly being exchanged. Here, instead of employing the target as the beacon source, the use of an artificial beacon placed ahead of the moving vehicle may help in characterizing the atmosphere ahead of the beam. This will assess the phase perturbations of the nonheated atmosphere, but the problem still remains concerning just how the atmosphere will respond to the heating from the beam as it arrives at that particular column. This suggests that, because of the availability of high-power sources at millimeter wavelengths, one could configure an in situ experiment to assess the operation of both closed-loop and artificial beacon adaptive optics approaches. This will be discussed further Section G.6.

G.6 Experiments Assessing the Compensation of Thermal Nonlinearities of High-Power Beams in the Atmosphere

Experiments dealing with induced effects due to thermal nonlinearities elicited by high-power propagation are usually performed in a laboratory using liquids placed in cells in which the thermal nonlinearity thresholds are much smaller than in air. In these scaled laboratory experiments, where atmospheric turbulence effects are simulated by transmission phase screens, various adaptive optics algorithms have been tested and evaluated (Refs. 29 and 30). Some experiments have been performed in the open atmosphere along horizontal paths in a program called the Scaled Atmospheric Blooming Experiments (SABLE) directed by Lincoln Laboratory (Ref. 31). Work also is continuing along these lines in other countries (Ref. 32). All these experiments endeavor to evaluate the in situ operation of adaptive optics systems on a scaled basis. The same must be recommended for the operation of the beamed power scenarios discussed in this chapter. Because of the maturity and availability of high-power sources in the millimeter range, the authors recommend that a scaled atmospheric experiment be performed on a moving target to assess the operation of various adaptive optics algorithms. Such an experiment should be modeled after the SABLE project. It is important to note that currently no database exists that addresses the power-beaming cases considered here. It is important to begin to capture the prevailing effects and system operation using a scaled atmospheric experiment that would simulate the realistic environment in which an adaptive optics system must operate—from the variable wind velocity to the mechanical jitter of the transmitter platform. In addition, this experimental scenario could be used to address the possibility of the ionization and subsequent breakdown of air across the apertures of the combined millimeter-wave gyrotron sources as discussed in the DRM 1–C section.

G.7 Conclusions and Recommendations

The various deleterious propagation mechanisms associated with high-power electromagnetic wave propagation through the atmosphere have been discussed. In addition to turbulence, thermal nonlinearities associated with the absorption of radiation by atmospheric gases will contribute to the major effects of beam wave propagation for beamed-energy propulsion at the power levels considered here. The simplified propagation model advanced here showed that the beam radius and its deflection are severely affected by the phenomena of thermal blooming. However, the model also showed that appropriate phase compensation at the transmitter output aperture can mitigate these effects and return the propagation

situation to one that is acceptable for the power transfer requirements that must be satisfied for beamed propulsion. For infrared transmission out of the atmosphere for low Earth orbit to geosynchronous orbit (LEO-to-GEO) beaming, up to 10th-order (once the tilt has been removed) aberration correction will be needed to maintain a minimal focal spot at a GEO location using a 30-m-diameter transmitter aperture. For millimeter-wave beaming within the atmosphere, 5th-order aberration correction will suffice, with the exception of the horizontal case, in which, once again, a 10th-order correction will be required. In principle, these corrections will allow the beaming system to operate within the prevailing specifications. In practice, however, some challenges remain in the implementation.

The adaptive optics approach recommended here for the LEO-to-GEO launch case is a closed-loop system that uses the specular reflection from the target vehicle as a beacon source (i.e., a target-in-the-loop system). The target vehicle is seen by the adaptive optics system as a simple point reflector. The round-trip propagation time delay inherent in this scenario can be tolerated as long as the adaptation time of the adaptive optics system is properly set to a slightly larger time than that of the delay to ensure proper convergence.

In the case of millimeter-wave beaming to a moving vehicle within the Earth's atmosphere, the object is considered as an extended target with a rotation and orientation that can complicate the application of a closed-loop system. The reflection from the vehicle will have a speckle structure that could severely impact the wave front sensor used by the adaptive optics system. Here, it may be that the simpler artificial beacon method could be used, but there is an additional complication: namely, the rapid movement of the beam across the atmosphere. The changes induced in the beam column through the atmosphere will not all be those due to the adjustment by the adaptive optics, and the system will not be able to properly adapt. This situation presents itself for a scaled atmospheric high-power millimeter-wave transmission experiment in which both closed-loop and artificial beacon-based adaptive optics systems are tested and evaluated.

The propagation modeling for the various beamed propulsion scenarios presented in this report should be extended beyond that employed here in Section G.4 by incorporating additional fluid mechanical descriptions of the atmosphere as well as more general beam wave profiles such as hypergaussian as well as fractional charge (in the topological sense) Laguerre-gaussian beam waves which show great promise in their ability to be robust with respect to atmospheric nonlinearities [Ref. 33]. However, it is important that the modeling effort be kept to the level of yielding analytical results, rather than requiring numerical evaluation, so as to capture all the nuances of the physics involved and, at the same time, provide a tool for overall system evaluation as well as the design of adaptive optics algorithms. Finally, the model should be incorporated into a trajectory analysis program so that a cadre of launch geometries can be evaluated from the point of view of atmospheric thermal nonlinearities.

G.8 Symbols

A_0	initial amplitude of the field (Eq. (G7))
a_{nm}	expansion coefficients
$a_{20}(t)$	time-dependent aberration coefficient
\bar{a}	array of expansion coefficients
C_p	specific heat of the atmosphere at constant pressure
c	velocity of light
E	electric field of the beam at the target
E_0	defined by equation after Equation (G50)
F	focal length
H	thickness of the atmosphere
$H_m(x)$	Hermite polynomial
$H_n(x)$	Hermite polynomial
I	intensity of radiation
$I_{ }$	longitudinal size of the spatial variation of the variable permittivity
J	size of the focal spot at the target vehicle
k	wave number of the radiation;
L	distance to target
$\Delta(L)$	deflection of the beam source
L_d	diffraction length
L_T	characteristic distance at which thermally induced diffraction effects occur
M	number of expansion terms or phase aberrations (Eq. (G14))
N	number of expansion terms or phase aberrations (Eq. (G14))
m, n	subscripts in Eq. (G14)
P_{cr}	critical power
P_{crK}	threshold value of beam power at which the Kerr effect is only a function of the Kerr constant and the wavelength
P_{crP}	critical power
P_{crR}	critical power at which the beam radius is affected because of thermal focusing (Figs. G.17 and G.18)
P_{crT}	critical beam power above which thermally induced propagation issues can become prominent
P_0	total incident power in the beam

p_{cr}	critical power density
p_{crR}	critical power density at which the beam radius begins to expand (Figs. G.17 and G.18)
$R_{\text{eff}}(L)$	radius of a beam focused on a target at a distance L if there were no atmosphere
R_P	prevailing nonlinear parameter (defined by Eq. (G57))
R_V	dimensionless nonlinearity parameter, or distortion parameter, for the thermal nonlinearity
R_{κ}	distortion parameter for Kerr nonlinearity
r_{eff}	effective radius of the output aperture of the beam source
$r_{\text{eff},x}(L)$	effective radius of the beam in the x -axis
$r_{\text{eff},y}(L)$	effective radius of the beam in the y -axis
$r_{\text{eff}}(0)$	transmitter aperture radius
$r'_{\text{eff}}(L)$	particular effective radius
$r'_{\text{eff,corr}}$	radius of a focused beam curve corrected for the first M phase aberration
$S(x,y)$	transmitted phase front at the output aperture of the transmitter
T	temperature variation
t	time
t_a	adaptation time of the adaptive optics system
t_d	delay time
t_p	duration of radiation pulse; also Table G.1
T_V	characteristic temperature
V	prevailing wind velocity; total relative velocity of the beam slewing across the atmosphere (after Eq. (G5))
V_x	atmospheric wind velocity along the x -axis
\vec{V}	total relative velocity of the motion (slewing) of the beam across the atmosphere and that of the atmospheric wind
W_0	waist radius of the beam at the exit of the output aperture
x'	coordinate (Eqs. (G4) and (G51))
\hat{x}	unit vector (after Eq. (G49))
y'	coordinate (Eq. (G8))
z'	initial radiation profile of beam at output aperture of transmitter (Eq. (G4))
α	wavelength-dependent absorption coefficient
γ	control, or update, coefficient (Eq. (G9))
$\Delta\epsilon$	variable permittivity
ϵ_T	variation of permittivity with respect to temperature variation

ε_κ	Kerr effect perturbation to the permittivity
ε_0	nominal permittivity
ζ	Eq. (G31)
η	Peclet number
$\Theta_{NLV}(P_0)$	parameter that characterizes level of thermal nonlinearity effect on a beam wave of initial power through an atmosphere of thickness H
θ	elevation angle
κ	thermal conductivity of the atmosphere
λ	wavelength
v	velocity of the wave field in the medium
$\Pi(L)$	performance parameter defined by Eq. (G15)
ρ	density of the atmosphere
ρ'	dimensionless transverse coordinate; also Eqs. (G4) and (G5)
$\bar{\rho}$	position vector in the plane transverse to the direction of propagation along the z -axis
$\nabla_{\bar{\rho}}^2$	transverse Laplacian
τ	temporal variation of variable permittivity
$\tau_{a_{nm}}$	time constants
Φ	phase front
χ	thermal diffusivity
$\nabla^2 T$	diffusivity

G.9 Derivation of the Fundamental Nonlinear Propagation Equations for High-Energy Transmission Through the Atmosphere and for the Associated Critical Powers

For the propagation of scalar electromagnetic waves through a medium characterized by a variable permittivity $\Delta\epsilon$, one has for the equation describing the evolution of the electric field strength

$$2ik \left(\frac{\partial E}{\partial z} + \frac{1}{v} \frac{\partial E}{\partial t} \right) + \nabla_{\bar{\rho}}^2 E + k^2 \left(\frac{\Delta\epsilon}{\epsilon_0} \right) E = 0 \quad (\text{G32})$$

where $\bar{\rho}$ is a position vector in the plane transverse to the direction of propagation along the z -axis, $k \equiv 2\pi/\lambda$ is the wave number of the radiation field of wavelength λ , v is the velocity of the wave field in the medium ($v = \sqrt{\epsilon_0} c$, where c is the velocity of light), and ϵ_0 is the nominal permittivity (for the atmosphere, $\epsilon_0 \approx 1$). As will be discussed later in this appendix, the function describing $\Delta\epsilon$ is, in general, dependent on the value of E : that is, $\Delta\epsilon = \Delta\epsilon(E)$, thus making the propagation problem a nonlinear one. Only in the case of weak fields (the typical situation for atmospheric optics) is $\Delta\epsilon$ independent of E .

To simplify the analysis, one can, to a very good approximation, assume that $v \gg I_{\parallel}/\tau$, where I_{\parallel} is the longitudinal size of the spatial variation of $\Delta\epsilon$ and τ is its temporal variation. This will preclude the description of the propagation pulses of very short temporal duration, where dispersion will become important, but will suffice for the purposes of this presentation. Thus, Equation (G32) reduces to

$$2ik \frac{\partial E}{\partial z} + \nabla_{\bar{\rho}}^2 E + k^2 \left(\frac{\Delta\epsilon}{\epsilon_0} \right) E = 0 \quad (\text{G33})$$

which is known in the literature as the quasi-optical approximation. The first two terms of Equation (G33) describe the propagation (within the quasi-optical approximation) of a beam wave (see Eq. (G35)) in a vacuum; the last term is the perturbation added to the evolution of the beam wave through a medium described by the factor $\Delta\epsilon$. It is through this factor that the various effects of the atmosphere on propagation come into play.

For the power ranges of interest in high-energy laser propagation, the total permittivity function can be written as

$$\Delta\epsilon(|E|^2, T) = i\epsilon_0 \frac{\alpha}{k} + \Delta\epsilon_K(|E|^2) + \epsilon_T T \quad (\text{G34})$$

in which α is the wavelength-dependent absorption coefficient. Absorption within the propagation medium gives rise to the increase in the associated temperature T from the nominal value, which, in turn, modifies the value of the permittivity by the amount $\epsilon_T T$, where $\epsilon_T \equiv \partial\epsilon/\partial T$ is the variation of the permittivity with respect to T . (Strictly speaking, the temperature increase T is also a function of $|E|^2$, it is not a direct function as is the Kerr effect.) This gives rise to thermal nonlinearities and the associated thermal blooming. Also, because of the large value of E in cases of very high energy propagation, induced orientation of anisotropically polarized molecules of the atmosphere occurs due to the interaction of the induced dipole moment of the molecule due to the intense electric field. This contributes another perturbation $\Delta\epsilon_K$ to the permittivity through the quantity $|E|^2$. This phenomenon is known as the Kerr effect. The functional relations of both $\Delta\epsilon_K(|E|^2)$ and T to the quantity $|E|^2$ also are given through the prescription of a differential equation. In this appendix, each of these contributions is discussed separately and the critical field powers at which they will occur within the atmosphere are derived. Before this is

done, however, it will prove to be convenient to make the following digression concerning the description of a beam wave.

The consideration of the general solution for Equation (G33) makes it necessary to have an expression for the associated boundary condition. This brings to the fore the normalization of spatial coordinates. The boundary condition is given by the expression for the general form of a gaussian beam wave:

$$E(\bar{\rho}, z) = \frac{A_0}{1 + i\gamma z} \exp \left[- \left(\frac{k\gamma}{2} \right) \frac{\rho^2}{1 + i\gamma z} \right] \quad (\text{G35})$$

where A_0 is the initial amplitude of the field and

$$\gamma \equiv \gamma_1 + i\gamma_2 \quad \gamma_1 \equiv \frac{2}{kW_0^2} \quad \gamma_2 \equiv \frac{1}{F} \quad (\text{G36})$$

where W_0 is the waist radius of the beam at the exit of the output aperture and F is the focal length. The initial condition for the field at the output aperture is thus given by

$$E(\bar{\rho}, 0) = A_0 \exp \left[- \left(\frac{k\gamma}{2} \right) \rho^2 \right] = A_0 \exp \left[- \left(\frac{1}{2} \right) \left(\frac{2}{W_0^2} \rho^2 + i \frac{k\rho^2}{F} \right) \right] \quad (\text{G37})$$

At this point, it is convenient to normalize the spatial coordinates with respect to the parameters of the problem. For example, if one defines the effective radius of the beam wave at the exit of the output aperture as $r_{\text{eff}} \equiv W_0 / \sqrt{2}$ (this definition is consistent with the definition for the power distribution in the transverse plane) one can define the dimensionless transverse coordinate $\rho' \equiv \rho / r_{\text{eff}}$ and write Equation (G37) as

$$E(\bar{\rho}', 0) = A_0 \exp \left[- \left(\frac{1}{2} \right) \left(\rho'^2 + i \left(\frac{kW_0^2}{2} \right) \frac{1}{F} \rho'^2 \right) \right] \quad (\text{G38})$$

One can now apply the same coordinate normalization to Equation (G33). That is, since

$$\nabla_{\bar{\rho}}^2 E(\bar{\rho}, z) = \frac{2}{W_0^2} \nabla_{\bar{\rho}'}^2 E(\bar{\rho}', z') \quad (\text{G39})$$

Equation (G33) can be written as

$$2i \frac{kW_0^2}{2} \frac{\partial E}{\partial z} + \nabla_{\bar{\rho}'}^2 E + \frac{k^2 W_0^2 \Delta \epsilon}{2} E = 0 \quad (\text{G40})$$

(letting $\epsilon_0 = 1$ for atmospheric scenarios). Now, normalizing the longitudinal coordinate z with respect to the quantity defined by $L_d \equiv kW_0^2 / 2$ (i.e., $z' = z / L_d$), and noting that

$$\frac{\partial E(\vec{\rho}, z)}{\partial z} = \frac{2}{kW_0^2} \frac{\partial E(\vec{\rho}', z')}{\partial z'} \quad (\text{G41})$$

causes Equations (B7) and (B9) to become

$$E(\vec{\rho}', 0) = A_0 \exp \left[- \left(\frac{\rho'^2}{2} \right) \left(1 + i \frac{L_d}{F} \right) \right] \quad (\text{G7})$$

and

$$2i \frac{\partial E}{\partial z'} + \nabla_{\vec{\rho}'}^2 E + k^2 r_{eff}^2 \Delta \varepsilon(|E|^2, T) E = 0 \quad (\text{G42})$$

This form of the quasi-optical equation facilitates the developments that follow. The quantity L_d is called the diffraction length and, as seen from Equation (G7), it is the length that the focus must achieve for the associated diffraction to become appreciable.

G.9.1 Critical Power for the Atmospheric The Kerr Effect

To isolate the effect of the Kerr nonlinearity from the thermal effects due to absorption, one simply lets $\Delta \varepsilon = \Delta \varepsilon_K(|E|^2)$ in Equation (G42) and obtains

$$2i \frac{\partial E}{\partial z'} + \nabla_{\vec{\rho}'}^2 E + k^2 r_{eff}^2 \Delta \varepsilon_K(|E|^2) E = 0 \quad (\text{G43})$$

The differential equation that governs the evolution of $\Delta \varepsilon_K$ is given by

$$\tau \frac{\partial \Delta \varepsilon_K}{\partial t} + \Delta \varepsilon_K = \varepsilon_K |E|^2 \quad (\text{G44})$$

where τ is the relaxation constant for the Kerr process and ε_K is the Kerr constant for the atmosphere; typically, $\tau \approx 10^{-11}$ s. Relative to the other processes to be considered (and the fact that very short pulse lengths are not being considered here), one can ignore the first term on the left of Equation (G44). In this case, $\Delta \varepsilon_K = \varepsilon_K |E|^2$ and Equation (G43) becomes

$$2i \frac{\partial E}{\partial z'} + \nabla_{\vec{\rho}'}^2 E + k^2 r_{eff}^2 \varepsilon_K |E|^2 E = 0 \quad (\text{G45})$$

In the literature, Equation (G45) is sometimes stated to describe a cubic medium because of the occurrence of E in the last term. If $|E|^2$ is connected to the associated intensity I of the beam using the relation $|E|^2 = (8\pi/c)I$ and then to the corresponding beam power P_0 using $P_0 = \pi r_{eff}^2 I$, Equation (G45) becomes

$$2i \frac{\partial E}{\partial z'} + \nabla_{\vec{\rho}'}^2 E + R_K E = 0 \quad (\text{G46})$$

where $R_K \equiv P_0/P_{crK}$ is the nonlinear parameter (also called the distortion parameter) for the Kerr nonlinearity defined in terms of the critical power P_{crK} associated with the Kerr nonlinearity,

$$P_{crK} = \frac{c}{8k^2 \varepsilon_K} \quad (G47)$$

For Earth's atmosphere at sea level, $\varepsilon_K \approx 2.5 \times 10^{-16}$ CGSE units⁹ (Ref. 8). Thus, for a laser wavelength of $\lambda = 2.0 \mu\text{m}$, the Kerr effect has a threshold at $P_{crK} \approx 1.5 \times 10^9$ W. This value is less than 1 order of magnitude from the powers that are being considered ($\sim 70 \times 10^6$ W, giving $R_K \approx 0.05$) for power-beaming applications. Hence, the nonlinearities associated with the Kerr effect may become a minor factor in power-beaming applications (and can be easily removed via adaptive optics), but as will be shown in the next section, R_K is several orders of magnitude below the corresponding parameter for thermal nonlinearities, which dominate the beaming process in the atmosphere.

In the case of millimeter-wave propagation at $\lambda = 2.0$ mm, one obtains $P_{crK} = 1.5 \times 10^{16}$ W, and at $P_0 = 70 \times 10^6$ W, one obtains $R_K \approx 4.6 \times 10^{-9}$, thus alleviating any concerns about the Kerr effect at these wavelengths.

G.9.2 Critical Power for Atmospheric Thermal Effects

G.9.2.1 Continuous Wave Source

Using Equation (G34) in Equation (G42) and neglecting the Kerr contribution gives

$$2i \frac{\partial E}{\partial z'} + \nabla_{\vec{p}}^2 E + k^2 r_{eff}^2 \left(i \frac{\alpha}{k} + \varepsilon_T T \right) E = 0 \quad (G48)$$

The temperature variation from the nominal atmospheric temperature is given by the application of the conservation of energy to the atmospheric heat budget, given in its entirety by

$$\rho C_p \left(\frac{\partial T}{\partial t} + \vec{V} \cdot \vec{\nabla} T \right) = \kappa \nabla^2 T + \alpha I \quad (G49)$$

where ρ is the density of the atmosphere, C_p is its specific heat at constant pressure, κ is its thermal conductivity, \vec{V} is the total relative velocity of the motion (slewing) of the beam across the atmosphere and that of the atmospheric wind, and α is the absorption coefficient for the radiation of intensity $I \equiv (c/8\pi)|E|^2$. Strictly speaking, one should also include the set of Navier-Stokes equations in the Boussinesq approximation to account for the viscous and Archimedean forces that occur during the thermally induced motion of the atmosphere. However, for the purposes of this discussion and subsequent analysis, a description at this level is not required.

Equation (G49) can be simplified straight away by first specializing the slewing and wind velocity to be along the x axis of the coordinate system, $\vec{V} = V\hat{x}$, where \hat{x} is the unit vector. Furthermore, the diffusivity $\nabla^2 T$ will be taken to have contributions only in the direction transverse to the laser beam propagation: that is, $\nabla^2 T \approx \nabla_{\vec{p}}^2 T$. Finally, only the stationary heating case will be considered for this particular discussion whereby the time derivative can be dropped. (That is, the continuous wave (CW) radiation is taken to be acting long enough for the steady-state case to be achieved. This is not the case for

⁹Electrical units of the centimeter-gram-seconds system of units.

pulsed radiation, which is discussed in Section G.9.2.2.) Applying these considerations to Equation (G49) allows it to be written as

$$V \frac{\partial T}{\partial x} = \chi \nabla_{\bar{r}}^2 T + \frac{\alpha c}{8\pi \rho C_p} |E|^2 \quad (\text{G50})$$

where $\chi \equiv \kappa/\rho C_p$ is the associated thermal diffusivity. As was done earlier with Equation (G33), one can normalize the transverse coordinates with respect to r_{eff} . In addition, the field value E can be normalized with respect to $E' = E/E_0$ where $E_0 \equiv \sqrt{8\pi I/c} = \sqrt{8P_0/r_{\text{eff}}^2 c}$. (This is what was essentially done to Equation (G45) to obtain Equation (G46)). Equation (G50) then becomes

$$\rho C_p \left(\frac{\pi r_{\text{eff}}^2}{\alpha P_0} \right) \left(\frac{V}{r_{\text{eff}}} \frac{\partial T}{\partial x'} - \frac{\chi}{r_{\text{eff}}^2} \nabla_{\bar{r}'}^2 T \right) = |E'|^2 \quad (\text{G51})$$

Now, the two heat-transfer mechanisms that are described here can be isolated. Consider the ratio of the coefficients of the two terms within the parentheses of Equation (G51): $\eta \equiv Vr_{\text{eff}}/\chi$. This dimensionless ratio is known in fluid mechanics as the Peclet number. Taking the nominal wind velocity $V = 4.4$ m/s (10 mi/hr), $r_{\text{eff}} = 10$ m, and using the documented value for the thermal diffusivity of the atmosphere $\chi = 2.12 \times 10^{-5}$ m²/s, one has that $\eta = 2.1 \times 10^6 \gg 1$, allowing one to neglect the second term in the brackets. In this instance, one can write

$$\left(\frac{\pi \rho C_p r_{\text{eff}} V}{\alpha P_0} \right) \frac{\partial T}{\partial x'} = \frac{\partial T'}{\partial x'} = |E'|^2 \quad (\text{G3})$$

where the temperature has been normalized with respect to the characteristic temperature $T_V \equiv \alpha P_0 / \pi \rho C_p r_{\text{eff}} V$. Finally, applying this prescription to Equation (G48) gives

$$2i \frac{\partial E'}{\partial z'} + \nabla_{\bar{r}'}^2 E' + iL_d \alpha E' + k^2 r_{\text{eff}}^2 \epsilon_T T_V T' E' = 0 \quad (\text{G52})$$

As done with Equation (G45), one can define the distortion parameter for the thermal nonlinearity

$$R_V \equiv k^2 r_{\text{eff}}^2 \epsilon_T T_V = \frac{k^2 r_{\text{eff}}^2 \epsilon_T \alpha P_0}{\pi \rho C_p V} = \frac{P_0}{P_{crT}} \quad (\text{G19})$$

where

$$P_{crT} \equiv \frac{\pi \rho C_p V}{k^2 r_{\text{eff}}^2 \epsilon_T \alpha} \quad (\text{G1})$$

is the critical power associated with the thermal nonlinearity in the case of large Peclet numbers. Using Equation (G19) and noting that the third term in Equation (G52) can be transformed away, one has

$$2i \frac{\partial E''}{\partial z'} + \nabla_{\rho}^2 E'' + R_V T' E'' = 0 \quad E'' = E' \exp(-\alpha L_d z'/2) \quad (\text{G53})$$

The problem of propagation through a thermal nonlinearity thus reduces, to within the approximations adopted, to the solution of Equations (G3) and (G53). For Earth's atmosphere, $\rho = 1.2 \text{ kg/m}^3$, $C_p = 1.0 \times 10^3 \text{ J/K-kg}$, and $\varepsilon_T \approx -2.3 \times 10^{-6} \text{ K}^{-1}$. That is, the atmospheric permittivity decreases with an increase in temperature. This indicates that the laser beam will steer toward regions with larger permittivity: that is, cooler regions. In the calculations, the absolute value of this quantity is used. At $\lambda = 2.0 \text{ }\mu\text{m}$, $\alpha \approx 4 \times 10^{-6} \text{ m}^{-1}$. If one uses the earlier stated values for the other quantities, one finds that $P_{crT} = 16.7 \text{ W}$. Thus, for $P_0 = 70 \times 10^6 \text{ W}$, $R_V \approx 4.2 \times 10^6$. The very small value for the critical power occurs because of the rather large beam radius. The temperature must diffuse over the large cross section of a cylindrical column. Of course, larger values of V will increase P_{crT} . For a smaller, more typical value for a beam radius, $r_{\text{eff}} = 0.1 \text{ m}$, one finds that $P_{crT} = 1667 \text{ W}$ and $R_V \approx 4.2 \times 10^4$ for $P_0 = 70 \text{ MW}$ —still a rather large value for the nonlinearity parameter. As a comparison, a more typical laser power of $P_0 = 100 \text{ kW}$ corresponds to $R_V \approx 60$. It is thus seen that nonlinearities due to thermal effects at infrared wavelengths within the atmosphere will dominate those of the Kerr effect.

The small values for P_{crT} at the large output aperture radii and the corresponding very large values for R_V do indeed have severe ramifications for the long distance propagation of beam waves at $P_0 \approx 70 \text{ MW}$ as shown earlier. However, these values facilitate the use of approximation procedures to be used in solving Equations (G3) and (G53) from which specifications for the adaptive correction of the various aberrations are derived, and it is shown that complete mitigation is possible.

The situation for millimeter-wave propagation is better. For $\lambda = 2.0 \text{ mm}$, $\alpha = 2.2 \times 10^{-4} \text{ m}^{-1}$ and $P_{crT} = 3.5 \times 10^5 \text{ W}$, and for $P_0 = 70 \text{ MW}$, $R_V = 200.8$. Although the absorption coefficient α is 2 orders of magnitude larger than that for infrared wavelengths, the overall optical effects due to the thermally induced refractive index variations are much smaller because of the larger wavelength: the “thermal lens” that is induced has weaker focusing capabilities at millimeter wavelengths.

G.9.2.2 Pulsed Source

In the case of a source that produces radiation pulses of temporal duration t_p , the prevailing fluid dynamics of the situation differs from that of a CW source. Here, for $t_p < r_{\text{eff}}/V$, the convection/diffusion equation, Equation (G49), is approximated as

$$\rho C_p \frac{\partial T}{\partial t} = \alpha I \quad (\text{G54})$$

Coupling this equation with the propagation equation, Equation (G48), and following the same normalization procedure as outlined in Section G.9.2.1 for the CW case and normalizing the time to t_p , one obtains in place of Equation (G53),

$$2i \frac{\partial E''}{\partial z'} + \nabla_{\rho}^2 E'' + R_p T' E'' = 0 \quad E'' = E' \exp(-\alpha L_d z'/2) \quad (\text{G55})$$

where

$$\left(\frac{\pi \rho C_p r_{\text{eff}}^2}{\alpha P_0 t_p} \right) \frac{\partial T}{\partial t'} = \frac{\partial T'}{\partial t'} = |E'|^2 \quad (\text{G56})$$

and the prevailing nonlinear parameter is now

$$R_p \equiv \frac{k^2 \epsilon_T \alpha t_p P_0}{\pi \rho C_p} = \frac{P_0}{P_{crP}} \quad (\text{G57})$$

in which the corresponding critical power is

$$P_{crP} \equiv \frac{\pi \rho C_p}{k^2 \alpha \epsilon_T t_p} \quad (\text{G2})$$

which is independent of r_{eff} .

Taking a nominal pulse width of $t_p \approx 1 \mu\text{s}$, one has for $\lambda = 2.0 \mu\text{m}$, $P_{crP} = 3.7 \times 10^7$, and for $\lambda = 2.0 \text{ mm}$, $P_{crP} = 7.7 \times 10^{11}$. Thus, temporally modulating the source does not elucidate the convective thermal effects that are inherent in the CW case and allows for much larger critical values of peak power. Pulse lengths smaller than $1 \mu\text{s}$ require the use of Equation (G32), which takes into account pulse dispersion through the medium. This effect is especially important when atmospheric turbulence is taken into account. However, for the purposes of the present analysis, which is to obtain the critical powers at which various nonlinear propagation effects show themselves, these effects are not considered.

The issue of the repetition rate of a pulse train within the atmosphere in conjunction with scanning (slewing) the beam through a region of the atmosphere to aid in heat dispersion (for high pulse repetition rates) is characterized by yet another critical power threshold, which will be larger than that given by Equation (G2).

G.9.3 Summary

The parameters R_K , R_V , and R_p provide for a comparative assessment of the nonlinear propagation mechanisms that are induced because of the large field power densities. Thus, at the power levels considered here, the effect of Kerr nonlinearities are almost negligible relative to that of thermal effects, and it is the later that must be completely understood so as to be effectively mitigated via properly designed adaptive optics algorithms. They do not, however, give an assessment of the behavior of specific laser beam properties, such as the beam steering and beam broadening that accompany propagation. This can only be done through modeling using the specific propagation geometries that are being considered. The very large values for R_V in the case of the power levels considered for beamed propulsion are a benefit in that they allow approximation procedures to be applied to analytically evaluate propagation and adaptive optics models.

G.10 References for Appendix G

1. Manning, R.M.: Stochastic Electromagnetic Image Propagation and Adaptive Compensation. Ch. 2, McGraw-Hill Book Co., New York, NY, 1993.
2. Wheelon, A. D.: Electromagnetic Scintillation: Vol. 2, Weak Scattering. Cambridge University Press, 2003.
3. Litvak, A.G.: Self Focusing of Powerful Light Beams by Thermal Effects. Sov. Phys. JETP Letters, vol. 4, no. 9, 1966, pp. 230–232.
4. Smith, D.C.: High Power Laser Propagation—Thermal Blooming. Proc. IEEE, vol. 65, no. 12, 1977, pp. 1679–1714.
5. Vorob'ev, V.V.: Thermal Blooming of Laser Beams in the Atmosphere. Prog. Quantum Electron., vol. 15, 1991, pp. 1–152.
6. Keldysh, L.V.: Ionization in the Field of a Strong Electromagnetic Wave. Sov. Phys. JETP, vol. 20, 1965, pp. 1307–1314.
7. Boyd, R.W.: Nonlinear Optics. Ch. 4, Academic Press, San Diego, CA, 1992.
8. Sutherland, R.L.: Handbook of Nonlinear Optics. Marcel Dekker, Monticello, NY, 1996.
9. Reichert, J.D.; Wagner, W.G.; and Chen, W.Y.: Instabilities of Intense Laser Beams in Air. J. Appl. Phys., vol. 44, no. 8, 1973, pp. 3641–3646.
10. Reichert, J.D.; Wagner, W.G.; and Chen, W.Y.: Propagation of an Intense Gaussian Laser Pulse in Air. J. Appl. Phys., vol. 44, no. 8, 1973, pp. 3647–3658.
11. Fleck, J.A.; Morris, J.R.; and Feit, M.D.: Time-Dependent Propagation of High Energy Laser Beams Through the Atmosphere. Appl. Phys., vol. 10, 1976, pp.129–160.
12. Vedenov, A.A.; and Markin, O.A.: Propagation of Intense Laser Radiation in an Absorbing Medium. Sov. Phys. JETP, vol. 49, no. 4, 1979, pp. 608–615.
13. Sprangle, P.; Penano, J.; and Hafizi, B.: Propagation of High Energy Laser Beams in Various Environments. Report prepared for High-Energy-Laser Joint Technology Office (NRL Report NRL/MR/6790–07–9032), May 2007.
14. Fischer, R., et al.: Absorption and Scattering of 1.06 μm Laser Radiation From Oceanic Aerosols. Appl. Opt., vol. 48, no. 36, 2009, pp. 6990–6999.
14. Glickler, S.L.: Propagation of a 10.6 μm Laser Through Cloud Including Droplet Vaporization. Appl. Opt., vol. 10, no. 3, 1971, pp. 644–650.
15. Zuev, V.E.; and Kuzikovskii, A.V.: Thermal Bleaching of Aqueous Aerosols by Laser Radiation. Russ. Phys. J., vol. 20, no. 11, 1977, pp. 1480–1500.
16. Agrovskii, B.S., et al.: Thermal Blooming of Laser Beams in Turbulent Media. J. Opt. Soc. Am., vol. A2, no. 12, 1985, pp. 2304–2312.
17. Bradley, L.C.; and Herrmann, J.: Phase Compensation for Thermal Blooming. Appl. Opt., vol. 13, no. 2, 1974, pp. 331–334.
18. Novoseller, D.E.: Zernike-Ordered Adaptive-Optics Correction of Thermal Blooming. J. Opt. Soc. Am., vol. A5, no. 11, 1988, pp. 1937–1942.
19. NIST Handbook of Mathematical Functions. Ch. 18, Cambridge University Press, 2010.
20. Penano, J.R.; Sprangle, P.; and Hafizi, B.: Propagation of High Energy Laser Beams Through Atmospheric Stagnation Zones. NRL Report NRL/MR/6790–06–8925, 2006.
21. Hardy, J.W.: Active Optics: A New Technology for the Control of Light. Proc. IEEE, vol. 66, 1978, pp. 651–697.
22. Vorontsov, M.A., et al.: Adaptive Imaging System for Phase-Distorted Extended Source/Multiple Distance Objects. Appl. Opt., vol. 36, 1997, pp. 3319–3328.
23. Vorontsov, M.A., et al.: Adaptive Optics Based on Analog Parallel Stochastic Optimization: Analysis and Experimental Demonstration. J. Opt. Soc. Am., vol. A17, no. 8, 2000, pp. 1440–1453.

24. Vorontsov, M.A.: Decoupled Stochastic Parallel Gradient Descent Optimization for Adaptive Optics: Integrated Approach for Wave-Front Sensor Information Fusion. *J. Opt. Soc. Am.*, vol. A19, no. 2, 2002, pp. 356–368.
25. Vorontsov, M.A.; and Kolosov, V.: Target-in-the-Loop Beam Control: Basic Considerations for Analysis and Wave-Front Sensing. *J. Opt. Soc. Am.*, vol. A22, no. 1, 2005, pp. 126–141.
26. Piatrou, P.; and Roggemann, M.: Beaconless Stochastic Parallel Gradient Descent Laser Beam Control: Numerical Experiments. *Appl. Opt.*, vol. 46, no. 27, 2007, pp. 6831–6842.
27. Vorontsov, M.A.; Kolosov, V.V.; and Kohnle, A.: Adaptive Laser Beam Projection on an Extended Target: Phase- and Field-Conjugate Precompensation. *J. Opt. Soc. Am.*, vol. A24, no. 7, 2007, pp. 1975–1993.
28. Primmerman, C.A.; and Fouche, D.G.: Thermal-Blooming Compensation: Experimental Observations Using a Deformable-Mirror System. *Appl. Opt.*, vol. 15, no. 4, 1976, pp. 990–995.
29. Primmerman, C.A.; Johnson, F.B.; and Wigdor, I.: Thermal Blooming Compensation Using the CLASP System. *Appl. Opt.*, vol. 17, no. 18, 1978, pp. 2909–2912.
30. Fouche, D.G.; Higgs, C.; and Pearson, C.F.: Scaled Atmospheric Blooming Experiments (SABLE). *Lincoln Lab. J.*, vol. 5, no. 2, 1992, pp. 273–293.
31. Qiao, C.-H., et al.: Simulation Experiment of High Energy Laser Propagation in the Atmosphere. *Proc. SPIE*, vol. 7382, Art.# 73822I, 2009.
32. Molchan, M.A.; Doktorov, E.V.; and Vlasov, R.A.: Propagation of Vector Fractional Charge Laguerre-Gaussian Light Beams in the Thermally Nonlinear Moving Atmosphere. *Opt. Lett.*, vol. 35, no. 5, 2010, pp. 670–672.

Appendix H.—Summary Presentation

Beamed Energy Propulsion (BEP) Study Final Stakeholder Review

Raymond F. Beach

Patrick J. George

Briefing prepared for:

NASA, Office of Chief Technologist
DARPA, Tactical Technology Office
NASA, Space Operations Mission Directorate
NASA, Office of Chief Engineer

NASA HQ
14 April 2011



Final Report

1



Review outline



- ➔ • **Executive summary**
 - Original objectives / direction from mid-term review
 - Assessment of feasibility, potentials, challenges
 - Recommended developments
 - Summary

- **Details of findings**
 - LEO to GEO
 - Deep space
 - Launch

- **A path forward**
 - Technology investments
 - BEP development program

- **Summary**

Final Report

2



Summary of BEP study original task and mid-term redirection



What makes BEP attractive ?

The attraction of beamed energy propulsion is the potential for high-specific impulse while removing the power-generation mass from the spacecraft.

Why look at BEP now ?

The rapid advancements in high-energy beamed power systems and optics over the past 20 years warrant a fresh look at the technology and potential game-changing applications.

Goals & objectives:

- Review and analyze the state-of-art in beamed energy propulsion and:
 - identify potential game-changing applications (pgs. 13 &14)
 - formulate a roadmap of technology development (pg. 59)
 - identify key near-term technology demonstrations to rapidly advance elements of BEP technology to TRL 6. (pgs. 41 & 56)

Final Report

Direction from the mid-term review:

This memorandum is a confirmation of the direction provided at the Beamed Energy Propulsion midterm review on 16 December 2010. The overall study direction received is to reduce the current scope and focus on areas which have the highest payoff. This includes:

- Focus the Millimeter wave thermal rocket (DRM 1-C) as an expendable design making an easier direct comparison with the laser design (DRM 1-B). (pgs. 43-50)
- Modify the in-space missions (DRMs 2 and 3) to include in-space power generation such as a solar array powering an orbiting laser beaming station. (pgs. 25 & 34)
- Drop any further development of the In-Space GEO Servicing mission (DRM 2-B) and the Horizontal Launch mission (DRM4)
- Do not consider the effects of launch rates for this study
- Do not consider the amortization of non-recurring vehicle and ground system costs
- Develop ROM non-recurring costs for vehicles and ground systems (pgs. 26, 36 & 50)
- Develop ROM vehicle and ground facility costs for recurring launches
- Investigate and analyze the effects of thermal blooming on laser and millimeter wave propagation through the atmosphere. (pg. 28)
- In-space missions will be reported to the same depth as the launch missions (pgs.22-36)
- Emphasize concepts utilizing and extending from high TRL commercial lasers like diode-pumped lasers. De-scope concepts that require low TRL lasers. (pg. 45)
- The primary product of this study needs to be a determination of TRL 's for near term concepts of:
 - beam energy technology (pg 58)
 - rocket vehicle technology (pg 58)

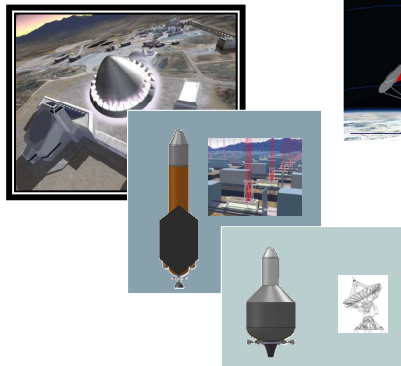
3



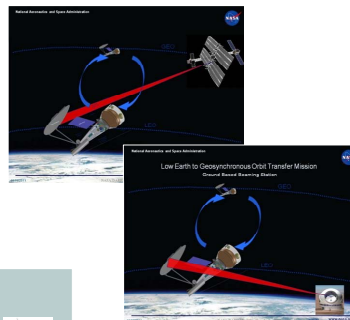
Beamed energy propulsion applications



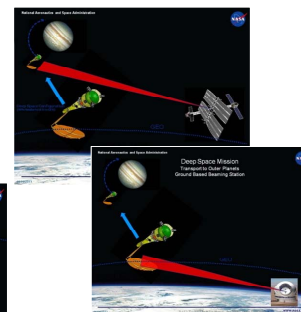
Launch:
To earth orbit



LEO to GEO:
Low earth to geosynchronous orbit transfer module



Deep space:
Transport to Jupiter/Saturn



Final Report

4



Beamed Energy Propulsion feasibility study results



	Technically Feasible	Game Changing	Economically Viable
Feasibility Ranking YES Green – All YES/NO Yellow - >50% NO Red - <50%	<ul style="list-style-type: none"> Closed design solution – trajectory, beam power, thrust/weight, mass etc. For low TRL - defined basis for technology and technology improvements Allowable margins – mass, engine performance, thermal, structural 	<ul style="list-style-type: none"> Reusability Payload mass fraction Improved mission capability – increase operations time, etc. Reduced Transfer Time (2X) "...Technology that is innovative, unique and promises to enable revolutionary improvements to the efficiency and effectiveness of our country's space capability." [OCT BAA] 	<ul style="list-style-type: none"> Lower vehicle costs (\$/kg) Lower launch facility operation costs – range safety, vehicle prep/handling Infrastructure costs
LEO to GEO	YES Low TRL's	YES/NO, but might be combined with other applications	NO, high cost of beaming stations
Deep Space	YES Low TRL's	YES, with investments	NO, high cost of beaming stations
Launch	YES Low TRL's	YES, with investments	NO, high cost of beaming stations

- Beamed Energy Propulsion is feasible, but very challenging for high power, with large upfront costs
- Study findings indicated two areas of great interest:
 - Revolutionary propulsion system for launch and space
 - Additional finding – Remote operation of small spacecraft via laser beam

Final Report

5



LEO to GEO mission evaluation



	Technically Feasible	Game Changing	Economically Viable
Feasibility Ranking YES Green – All YES/NO Yellow - >50% NO Red - <50%	<ul style="list-style-type: none"> Closed design solution – trajectory, beam power, thrust/weight, mass etc. For low TRL - defined basis for technology and technology improvements Allowable margins – mass, engine performance, thermal, structural 	<ul style="list-style-type: none"> Reusability Payload mass fraction Improved mission capability – increase operations time, etc. Reduced Transfer Time (2X) "...Technology that is innovative, unique and promises to enable revolutionary improvements to the efficiency and effectiveness of our country's space capability." [OCT BAA] 	<ul style="list-style-type: none"> Lower vehicle costs (\$/kg) Lower launch facility operation costs – range safety, vehicle prep/handling Infrastructure costs
→ LEO to GEO	YES Low TRL's	YES/NO, but might be combined with other applications	NO, high cost of beaming stations
Deep Space	YES Low TRL's	YES, with investments	NO, high cost of beaming stations
Launch	YES Low TRL's	YES, with investments	NO, high cost of beaming stations

Final Report

6



LEO to GEO mission evaluation: Potentials and challenges



	Technically Feasible	Game Changing	Economically Viable
Potentials	<ul style="list-style-type: none"> Scalable for various size spacecraft Primary and secondary optics reduces pointing requirements Can Be Time Phased with In-Space BEP Development to provide Optimum Program Development Scenario Synergy with Manned GEO Servicing mission 	<ul style="list-style-type: none"> Environmentally friendly water based propellant and simplified fuel depot requirements Reusable Increased payload mass fraction High thrust, high Isp propulsion engine utilizing water for propellant 	<ul style="list-style-type: none"> LEO to GEO Vehicle Synergistic with Deep Space Transfer Stage Reusable design for lower life cycle cost
Challenges	<ul style="list-style-type: none"> Beaming 80 MW through atmosphere. Max current is Air Borne Laser Test Bed MW class Operation of GEO based remote complex, high-energy beaming station. 188 nanoradians pointing and tracking (TRL 2-3). Best proven is Hubble Space Telescope 50 nr. Web Telescope 24 nr Required technologies at low TRL Plasma engine (TRL 2) Reflective mirror: 4m x 6m; 99.99% reflectivity, micrometeoroid tolerant (TRL 2) Multi MW space/ground operational laser (TRL 2-3) 		<ul style="list-style-type: none"> High cost to establish beaming station on ground & in GEO

Final Report

7



Deep Space mission evaluation



	Technically Feasible	Game Changing	Economically Viable				
<table border="1"> <tr> <th>Feasibility Ranking</th> <td> <ul style="list-style-type: none"> Closed design solution – trajectory, beam power, thrust/weight, mass etc. For low TRL - defined basis for technology and technology improvements Allowable margins – mass, engine performance, thermal, structural </td> <td> <ul style="list-style-type: none"> Reusability Payload mass fraction Improved mission capability – increase operations time, etc. Reduced Transfer Time (2X) "...Technology that is innovative, unique and promises to enable revolutionary improvements to the efficiency and effectiveness of our country's space capability." [OCT BAA] </td> <td> <ul style="list-style-type: none"> Lower vehicle costs (\$/kg) Lower launch facility operation costs – range safety, vehicle prep/handling Infrastructure costs </td> </tr> </table>	Feasibility Ranking	<ul style="list-style-type: none"> Closed design solution – trajectory, beam power, thrust/weight, mass etc. For low TRL - defined basis for technology and technology improvements Allowable margins – mass, engine performance, thermal, structural 	<ul style="list-style-type: none"> Reusability Payload mass fraction Improved mission capability – increase operations time, etc. Reduced Transfer Time (2X) "...Technology that is innovative, unique and promises to enable revolutionary improvements to the efficiency and effectiveness of our country's space capability." [OCT BAA] 	<ul style="list-style-type: none"> Lower vehicle costs (\$/kg) Lower launch facility operation costs – range safety, vehicle prep/handling Infrastructure costs 			
Feasibility Ranking	<ul style="list-style-type: none"> Closed design solution – trajectory, beam power, thrust/weight, mass etc. For low TRL - defined basis for technology and technology improvements Allowable margins – mass, engine performance, thermal, structural 	<ul style="list-style-type: none"> Reusability Payload mass fraction Improved mission capability – increase operations time, etc. Reduced Transfer Time (2X) "...Technology that is innovative, unique and promises to enable revolutionary improvements to the efficiency and effectiveness of our country's space capability." [OCT BAA] 	<ul style="list-style-type: none"> Lower vehicle costs (\$/kg) Lower launch facility operation costs – range safety, vehicle prep/handling Infrastructure costs 				
LEO to GEO	YES Low TRL's	YES/NO, but might be combined with other applications	NO, high cost of beaming stations				
Deep Space	YES Low TRL's	YES, with investments	NO, high cost of beaming stations				
Launch	YES Low TRL's	YES, with investments	NO, high cost of beaming stations				

Final Report

8



Deep Space mission evaluation: Potentials and challenges



	Technically Feasible	Game Changing	Economically Viable
Potentials	<ul style="list-style-type: none"> Scalable for various size spacecraft Primary and secondary optics reduces pointing requirements Can be time phased with In-Space BEP Development to provide optimum program Development Scenario Synergy with Manned GEO Servicing mission 	<ul style="list-style-type: none"> Faster transit to outer planets (2X) Environmentally friendly water based propellant and simplified fuel depot requirements 118 kg of instrument payload vs. 82 kg (Enceladus Mission Study) 	<ul style="list-style-type: none"> Deep Space Transfer Stage Vehicle Synergistic with LEO to GEO Can Be Time Phased With In-space BEP Development To Provide Optimum Program Development Scenario
Challenges	<ul style="list-style-type: none"> Required technologies at low TRL <ul style="list-style-type: none"> Plasma engine (TRL 2) Reflective mirror: 4m x 6m; 99.99% reflectivity, micrometeoroid tolerant (TRL 2) Multi MW space/ground operational laser (TRL 2-3) 2.3 Nanoradians pointing and tracking (TRL 2-3). Best proven is Hubble Space Telescope 50 nr Beaming 80 MW through atmosphere. Max current is Airborne Laser Test Bed MW class 		<ul style="list-style-type: none"> High cost to establish beaming station in GEO or on ground High operation cost of GEO based remote complex, high-energy beaming station.

Final Report

9



Launch mission evaluation



	Technically Feasible	Game Changing	Economically Viable
Feasibility Ranking	<ul style="list-style-type: none"> Closed design solution – trajectory, beam power, thrust/weight, mass etc. For low TRL - defined basis for technology and technology improvements Allowable margins – mass, engine performance, thermal, structural 	<ul style="list-style-type: none"> Reusability Payload mass fraction Improved mission capability – increase operations time, etc. Reduced Transfer Time (2X) "...Technology that is innovative, unique and promises to enable revolutionary improvements to the efficiency and effectiveness of our country's space capability." [OCT BAA] 	<ul style="list-style-type: none"> Lower vehicle costs (\$/kg) Lower launch facility operation costs – range safety, vehicle prep/handling Infrastructure costs
LEO to GEO	YES Low TRL's	YES/NO, but might be combined with other applications	NO, high cost of beaming stations
Deep Space	YES Low TRL's	YES, with investments	NO, high cost of beaming stations
Launch	YES Low TRL's	YES, with investments	NO, high cost of beaming stations

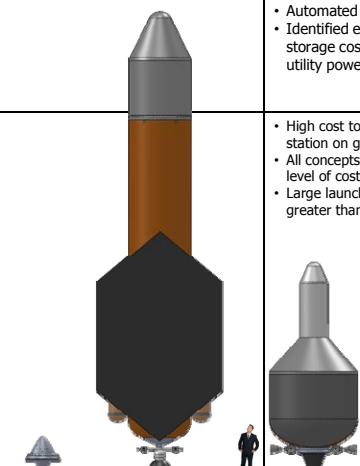
Final Report

10



Launch mission evaluation: Potentials and challenges



	Technically Feasible	Game Changing	Economically Viable
Potentials	<ul style="list-style-type: none"> Removal of the launch power-generation mass High-specific impulse engines Established trajectory for each DRM and identified power levels needed at vehicle and ground source Identified mass and performance margins required Identified all technology performance requirements 	<ul style="list-style-type: none"> Use of less toxic launch propellants Multiple automated launches per day from same facility Launch processing, vehicle and operational safety 	<ul style="list-style-type: none"> Low cost launch alternative for small payloads (1-100kg) Use of existing laser / microwave technology with reduction of facility costs as development occurs Automated processing and launch Identified electrical energy and storage costs to allow buffer from utility power systems
Challenges	<ul style="list-style-type: none"> Large number of low TRL technologies need to be developed (synchronized lasers; large dish antenna; heat exchanger; plasma engine; atmospheric adaptive optics) Microradian pointing and tracking (TRL 2-3). Best proven is Hubble Space Telescope 50 nanoradians Beaming up to 600 MW through the atmosphere. Max current is Airborne Laser Test Bed low single MW class 		<ul style="list-style-type: none"> High cost to establish beaming station on ground All concepts did not meet advertised level of cost to orbit Large launch range safety zone, greater than Shuttle

Final Report

11



Summary of study results



	Technically Feasible	Game Changing	Economically Viable
LEO to GEO	YES Low TRL's	YES/NO, but might be combined with other applications	NO, high cost of beaming stations
Deep Space	YES Low TRL's	YES, with investments	NO, high cost of beaming stations
Launch	YES Low TRL's	YES, with investments	NO, high cost of beaming stations

Answered feasibility questions:

- LEO to GEO and Deep Space:
 - Near, mid, far term applications
 - Low, medium, high power/flux
- Launch:
 - Far term application
 - High power/flux



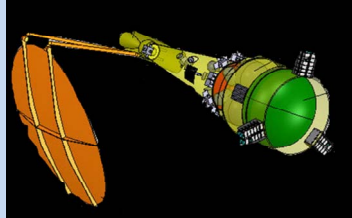
- Synergistic with solar thermal propulsion
- BEP can enable significant increase in payload capability for LEO to GEO transfer, and faster transit times to planets
- Costs of solar GEO based beaming station(s) and reflector(s) is high



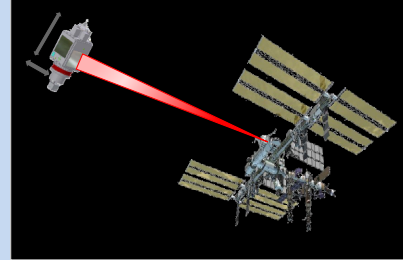
- Did not meet \$/kg launch costs. Projections indicate investment could result in high payoff
- Costs of multiple ground beaming station(s) or on-orbit reflector(s) is high

Final Report

12



Thermal plasma engine, using water as propellant, provides high thrust and high I_{sp}



Remote control of small spacecraft through the integration of propulsion, power, communications, and navigation/attitude control



Concept

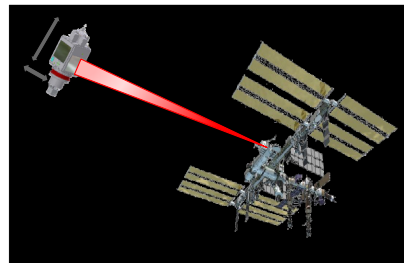
- Think small spacecraft
- Think integrated systems
- Think space



Remote control of small spacecraft through the integration of propulsion, power, communications, and navigational/attitude control through a laser beam

Benefits

- Remote operation – coordinated maneuver with source and receiving spacecraft without mechanical connection
- Reduce complexity, mass and cost of the receiving spacecraft
- Applicable for variety of space and aero vehicles with different propulsion systems
- Possible to control beam receiving “Shepherd” spacecraft from “Mother” spacecraft to perform specific maneuvers - similar to berthing



If successfully developed, could lead to a new class of spacecraft with enhanced operational capability, and lower mass.



Unexpected findings: Beamed Energy Propulsion engine



Concept

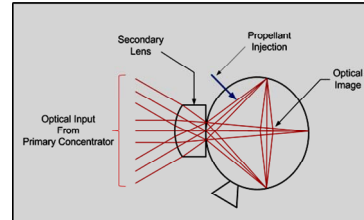
- Think water as propellant
- Think launch and space
- Think combined beamed energy and thermal plasma engine



Potential for highest propulsion engine performance – eliminates oxidizer / energy source on spacecraft

Benefits

- Able to utilize diverse new propellant types (water, ammonia, etc.)
- Eliminate toxic chemicals and associated safety issues both in space and on the ground
- Environmentally friendly water propellant potentially available on the Moon and Mars.
- Can utilize solar, laser, or mm wave beamed energy
- Potential for highest performance – eliminates oxidizer or energy source on spacecraft
- Optical-to-optical high efficiency energy transfer
- Both high thrust, and high Isp



Currently at very low TRL. If successfully developed, could lead to higher thrust/mass performance than current propulsion systems and the resultant lower mass.

Final Report

15



Implications from study: Beamed energy technology directions

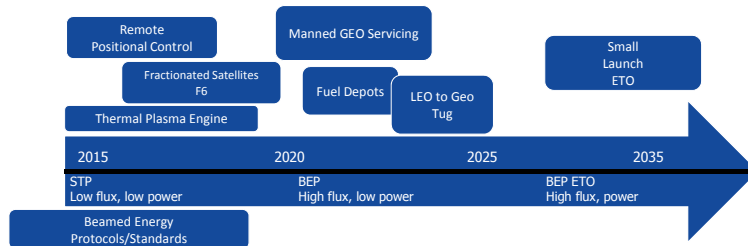


Development path

- Develop standard / protocol for Beamed Energy transmission:
 - Types, quality, regulations, organizations
 - Ground, aircraft, UAV, space
- Develop and demonstrate integrated power, propulsion, control/communications:
 - Ground, aircraft, UAV, space
 - NASA/USAF last/solar electric propulsion demonstration
 - DARPA Exo-SPHERES
- Develop and demonstrate engine propulsion technologies:
 - Airborne Laser, X prize, NASA Centennial Challenge

Development synergy

- Scalable for both space and launch applications
- Will provide benefits for near, mid, and far term systems
- Builds on early solar thermal propulsion work:
 - Air Force/NASA integrated solar upper state
 - DARPA HiDVE
 - NASA inflatable concentrator/secondary lens, optical engine cavity



Final Report

16



- **Executive summary**
 - Original objectives / direction from mid-term review
 - Assessment of feasibility, potentials, challenges
 - Recommended developments
 - Summary
- ➔ • **Details of findings**
 - LEO to GEO
 - Deep space
 - Launch
- **A path forward**
 - Technology investments
 - BEP development program
- **Summary**



- **Executive summary**
 - Original objectives / direction from mid-term review
 - Assessment of feasibility, potentials, challenges
 - Recommended developments
 - Summary
 - ➔ • **Details of findings**
 - LEO to GEO
 - Deep space
 - Launch
 - **A path forward**
 - Technology investments
 - BEP development program
 - **Summary**
- Mid-term direction:

 2. Modify the in-space missions (DRMs 2 and 3) to include in-space power generation such as a solar array powering an orbiting laser beaming station. (pgs. 25 & 33)
 3. Drop any further development of the Space GEO Servicing mission (DRM 2-B) and the Horizontal Launch mission (DRM4)

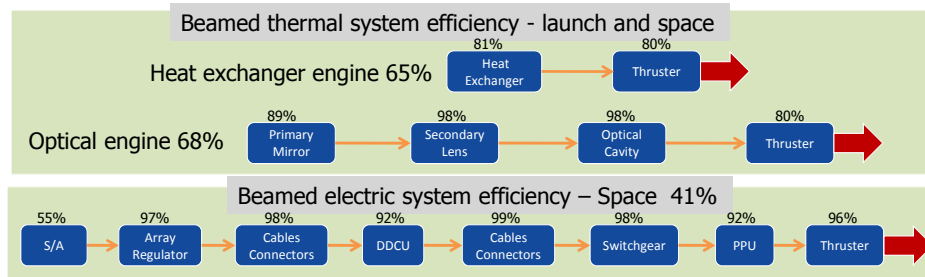


- All BEP mission defined by study team included consultants:
 - Utilized outside experts/advocates, Air Force, academia to help in mission concept development
 - All Missions are unique to BEP study
 - Both GRC and GSFC mission design centers used as independent analyst to evaluate BEP missions
- LEO to GEO and Deep Space mission concept development:
 - Initial evaluations considered efficiency (optics, energy conversions, regulators, cables/connectors/switchgear, thruster), mass, and response for SEP/beamed electric, STP/beamed thermal, and solar sails/beamed sail Mass
 - Decision made to base space missions on thermal propulsion
 - Synergistic with beamed thermal for ETO
 - High I_{sp} and thrust as FOM referenced in BEP study plan

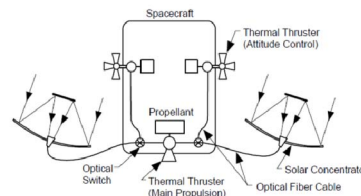
Consultants may not agree with all study findings.

Final Report

19



- Thermal propulsion energy technology:
 - Synergistic with solar thermal propulsion technology
 - Technology demonstrated at system and component levels:
 - ISUS, HiDVE
 - RCS
 - Significant performance enhancement with optical engine:
 - Lower TRL

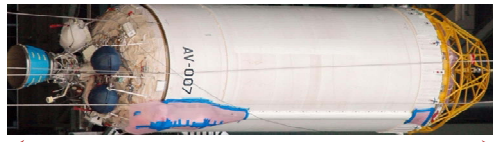


Final Report

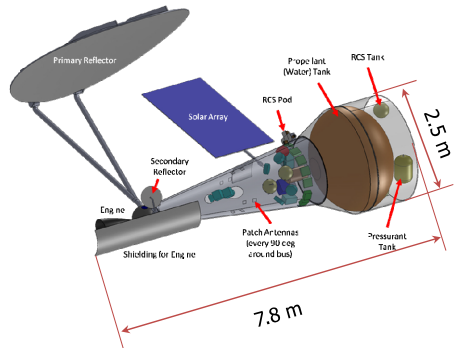
20



Comparison of propulsion methods



- Centaur:
 - 2000 kg dry mass
 - 21000 kg propellant (LOX/H2)
 - 2,000 kg payload
 - RL10 110,000 Newtons thrust
 - 464 sec. I_{sp}
 - 5 hours to GTO



- LEO to GEO tug:
 - 500 kg dry mass
 - 4900 kg water propellant
 - Two 2000 kg satellites transferred GEO
 - 5000 Newtons thrust
 - 813 sec. I_{sp}
 - Variable transfer time to GEO dependent on number of ground stations:
 - 5 Stations, 32 hours
 - 2 Stations, 11 days
 - 1 Station, 20 days
 - Reusable

Final Report

21

National Aeronautics and Space Administration

Low Earth to Geosynchronous Orbit Transfer Mission
Ground Based Beaming Station

Vehicle

- Thermal plasma engine
 - H_2O water propellant
 - 6000 K, 50 psia chamber press, 813 s I_{sp}
- 550 kg dry mass, 4900 kg propellant

LEO-GEO "Tug" with Laser Propulsion


- Launch of **two** 2000 kg GEO satellites and propellant on Falcon 9 from Kwajalein Atoll
 - 400 km circular orbit, 9° inc.
 - Autonomous rendezvous with tug
 - Spiral transfer

Beaming Station Located on Ground

- Single 78 MW emitter, 195MW input
- 30m dia. Dish
- Located in low moisture environment close to Equator - Hawaii

DESIGNED FOR 10 TRANSITS, 20 GEO SATELLITES DELIVERED
20 DAYS TOTAL TRANSIT TIME VS. 7 DAYS WITH CHEMICAL SYSTEM

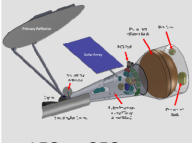
REUSABILITY ENABLES REDUCTION IN LAUNCH & TRANSPORTATION COSTS
BUT LARGE INITIAL INFRASTRUCTURE COSTS

Final Report  www.nasa.gov




Potential synergy with launch ground system and facility control:

- Dual use for ground system
- Number of ground and ship based facilities dependant on performance requirements
- Moveable shipped based system can reduce facility numbers without performance reduction




LEO to GEO

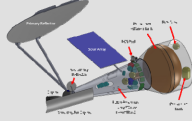


Apogee Facility

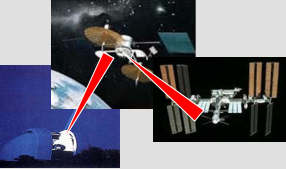
80 MW Output
30 m Diameter
1150 to 2900 x
120 kW modules;
Diode-Pumped
Solid State Lasers



Ship Based
80MW Output
3 m Diameter Aperture



LEO to GEO

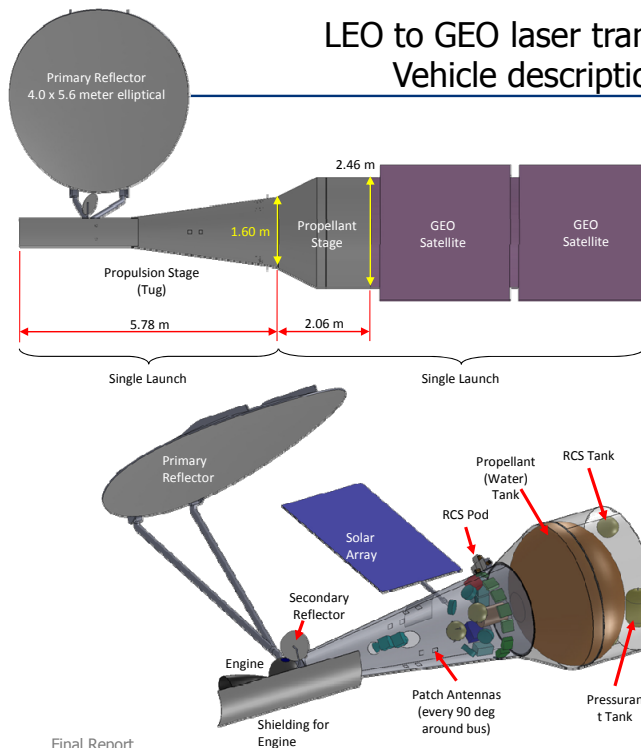


0.5 MW Output
Diode-Pumped Solid
State Lasers
1 MW Space Platform
With or Without
Steering Mirrors

Final Report

23

LEO to GEO laser transport: Vehicle description



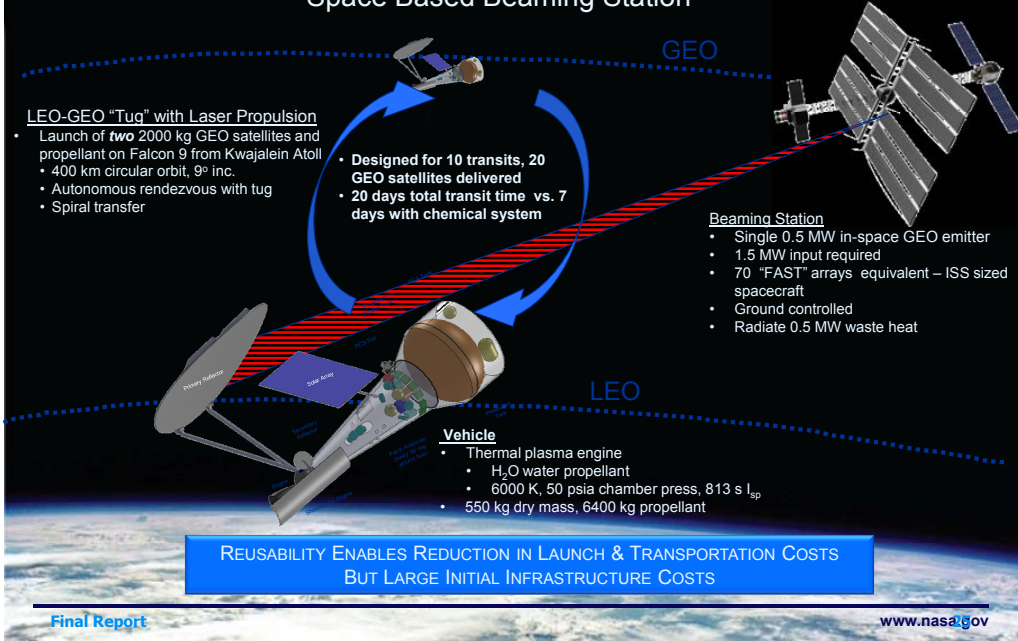
Final Report

24

- 500 kg dry mass tug:
 - 50 N thermal plasma engine
 - 813 s Isp
 - Highly reflective shielding for tug and satellites
 - Gimballed primary reflector to track laser
 - Single Falcon 9 launch
- Two 2000 kg GEO satellites transferred:
 - 4900 kg water propellant
 - Single Falcon 9 launch



Low Earth to Geosynchronous Orbit Transfer Mission Space Based Beaming Station



Executive summary of study findings: LEO to GEO mission



Space Vehicle				Infrastructure						
All Costs in FY11\$	Recurring Cost	Non-Recurring Cost	Time from LEO to GEO	Launch Vehicle		Energy Source				
				Type	Cost (ROM) for 20 payloads	Input Power	Output Power	Non-recurring Cost (ROM)	Operations Cost (ROM)	
Comparable Disposable system 1 Transit One 2000kg satellite Chemical kick-motor	\$100M	N/A	7 Days including orbit insertion and checkout	Twenty Falcon 9 Rockets	\$1B	Chemical	N/A	N/A	N/A	N/A
Reusable Tug; Energy Source in Space 10 transits ----- Two 2000 kg satellites 4900kg Water Propellant	\$85M	\$237M	20 Days including orbit insertion and checkout	Eleven Falcon 9 rockets	\$550M	Laser	One In-Space 1.5 MW Station [ISS sized Station w/"FAST" arrays located in GEO]	Space Based 0.5 MW	\$5B*	\$250M*
Reusable Tug; Energy Source on Ground 10 transits ----- Two 2000 kg satellites 4900kg Water Propellant	\$85M	\$237M	8 Days including orbit insertion and checkout	Eleven Falcon 9 rockets	\$550M	Laser	One Ground Based 195 MW Stations [Max existing 105kW] [Best located at high altitude around equator]	Ground Based 78 MW	\$3B**	\$150M**

Mid-term direction:

1. Do not consider the effects of launch rates for this study
2. Do not consider the amortization of non-recurring vehicle and ground system costs
3. Develop ROM non-recurring costs for vehicles and ground systems (pgs. 25, 36 & 50)
4. Develop ROM vehicle and ground facility costs for recurring launches

Space vehicle cost assumptions:

- Prime contractor costs (no fee)
- No technology development costs
- Protoflight development approach
- Before reserves, insight/oversight, launch services

* Extrapolation based on mission analysis of high efficiency space power systems project performed by COMPASS; 300kw/\$1B

** Based on Launch mission COMPASS analysis



LEO to GEO mission evaluation: Potentials and challenges



	Technically Feasible	Game Changing	Economically Viable
Potentials	<ul style="list-style-type: none"> Scalable for various size spacecraft Primary and secondary reduces pointing capability Can Be Time Phased with In-Space BEP Development to provide Optimum Program Development Scenario Synergy with Manned GEO Servicing mission 	<ul style="list-style-type: none"> Environmentally friendly water based propellant and simplified fuel depot requirements Reusable Increased payload High thrust, high Isp propulsion engine utilizing water for propellant 	<ul style="list-style-type: none"> LEO to GEO Vehicle Synergistic with Deep Space Transfer Stage Reusable design for lower life cycle cost
Challenges	<ul style="list-style-type: none"> Beaming 80 MW through atmosphere. Max current is Airborne Laser Test Bed MW class Operation of GEO based remote complex, high-energy beaming station. 188 nanoradians pointing and tracking (TRL 2-3). Best proven is Hubble Space Telescope 50 nr Required technologies at low TRL <ul style="list-style-type: none"> Plasma engine (TRL 2) Reflective mirror: 4m x 6m; 99.99% reflectivity, micrometeoroid tolerant (TRL 2) Multi MW space/ground operational laser (TRL 2-3) 		<ul style="list-style-type: none"> High cost to establish beaming station on ground and/or in GEO

Final Report

27



Answers to concerns from mid-term review: Atmospheric effects, energy costs, & pointing requirements



Atmospheric effects do not preclude power beaming

Report Released: **Effects of Beaming Energy Through the Atmosphere** by Robert Manning, NASA GRC; Investigated and analyzed the effects of thermal blooming on infrared and millimeter wave propagation through the atmosphere for power beaming applications at the megawatt level.

- Ionization and Electrical Breakdown
 - The Kerr Effect
- Induced Molecular Polarization
- Induced Heating of the Atmosphere
 - Thermal Non-Linearities and "Thermal Blooming"
- Atmospheric Aerosols
- Atmospheric Turbulence

Summary: "The simplified propagation model advanced here shows that the beam radius as well as its deflection are severely affected by the phenomena of thermal blooming. However, the model also showed that appropriate phase compensation at the transmitter output aperture can mitigate these effects and return the propagation situation to one that is acceptable for the power transfer requirements that are needed to be satisfied for beamed propulsion." "...**nothing in the prevailing physics that would preclude power beaming [at these power levels] through the atmosphere.**"

Analysis reviewed by :

J E. Lowder, Chief Scientist of Cobham Analytic Solutions, formerly known as SPARTA Inc. Missile Defense Sector. (Recommendation from Denise Podolski NASA OCT) "I have read the paper and was impressed with the depth of the theoretical analysis. The results look quite reasonable as far as I can tell with out running some numbers myself."

Daniel v Murphy; MIT Lincoln Lab Directed Energy Group: We would have to spend much more time to reach an independent conclusion. But, work in the late 80's on the GBFEL TIE program showed that thermal blooming was not a show stopper for missile defense, with system parameters that are not far from what you envisage for power beaming.

Final Report

Energy costs for launch are low

- Maximum wallplug electricity needed for launch is 900 MW for the Boost station and 1.8GW for the Sustain station
- Boost station on for 100 secs, Sustain station on for 200 secs.
- Average Commercial cost for electricity is \$0.10 per kW-hr (U.S Energy Information Administration 2009)
- For 900MW @ 100 secs; $900,000\text{kW} \times (100/3600 = 0.0278) = 25000$ kW-hrs
- 25000 kW-hrs X 0.10 \$/kW-hr = \$2,500
- For 1.8GW @ 200 secs = \$10,000

• Total electricity cost for launch = \$12,500

- Similar in electrical demand to NASA GRC's Wind Tunnels

Pointing requirements are challenging

If a 1.5 meter diameter engine is used, one would require a 60 meter diameter transmitting aperture focused at the GEO distance of 32,500 km. For a 5% spatial variation of the beam at this location (i.e., a 0.075 meter beam wander from its intended axis), one requires a $0.075/(32,500 \times 10^{-3}) = 2.3 \times 10^{-9}$ radian accuracy. For an initial target position in LEO at 400 km, this accuracy backs-off to $0.075/(400 \times 10^{-3}) = 188 \times 10^{-9}$ radians.

Therefore, given the assumptions made:

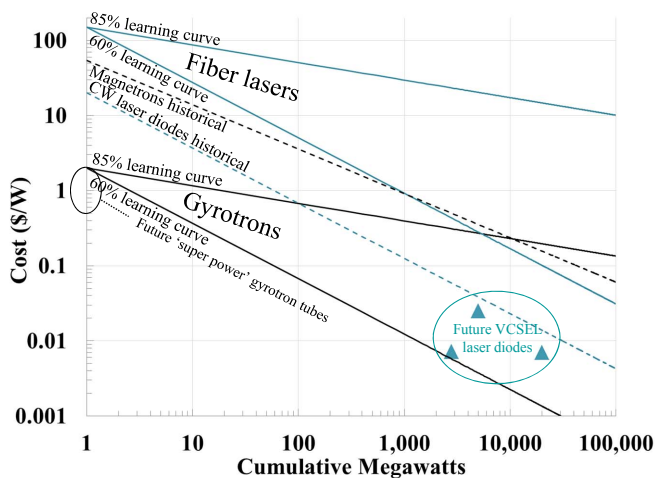
The accuracy in going from LEO to GEO essentially goes as 188 nanoradians down to 2.3 nanoradians.

The Hubble Space Telescope has a proven accuracy of 50 nanoradians

28



Present and future Gyrotron & laser costs



Current costs

- Gyrotron projections based on a 1.2 MW unit sold for \$2M in 2010 (Fedbizopps contract award number NNA10DF73P)
- Fiber laser projections based on 1 kW unit sold for \$150k in 2003

Impact of future technology

- CW laser diode cost represents the lower limit of fiber laser cost, and could be lowered with the development of VCSEL diodes
- Gyrotron costs could be lowered by the development of 'super power' tubes which is currently underway

Impact of volume production

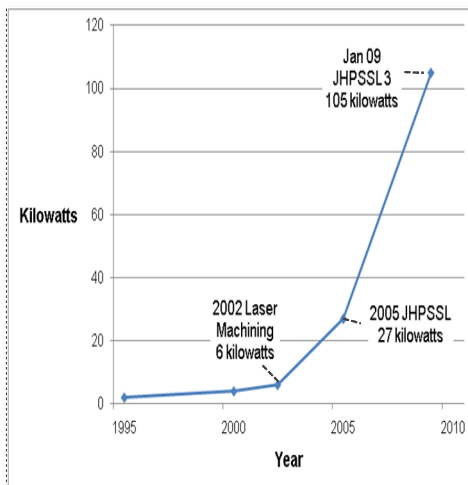
- LLNL Mercury Laser diodes demonstrated a learning curve of 60% from 1994-2001 (~20 cumulative MW)
- Magnetrons demonstrated comparable learning curve from 1945-present (~200,000 cumulative MW)

Final Report

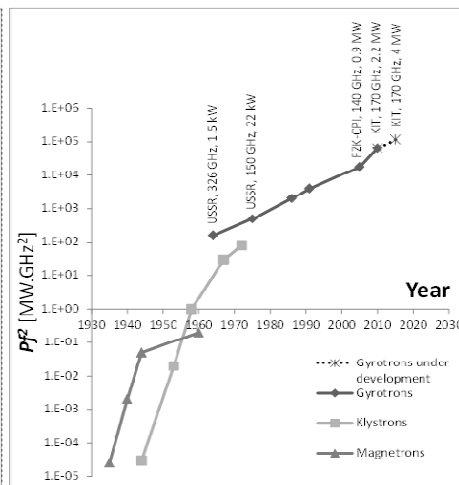
29



Exponential growth of continuous working solid state lasers and Gyrotrons



Source: "Solid-State Laser Weapon Systems, Bridging the Gap — or Bridge Too Far?", by Andrew Krepinevich, Tom Ehrhard, and Barry Watts, Center for Strategic & Budgetary Assessments (CSBA), May 20, 2009.



Source: Kevin Parkin NASA ARC

Final Report

30



• **Executive summary**

- Original objectives / direction from mid-term review
- Assessment of feasibility, potentials, challenges
- Recommended developments
- Summary

• **Details of findings**

- LEO to GEO
- ➔ • Deep space
- Launch

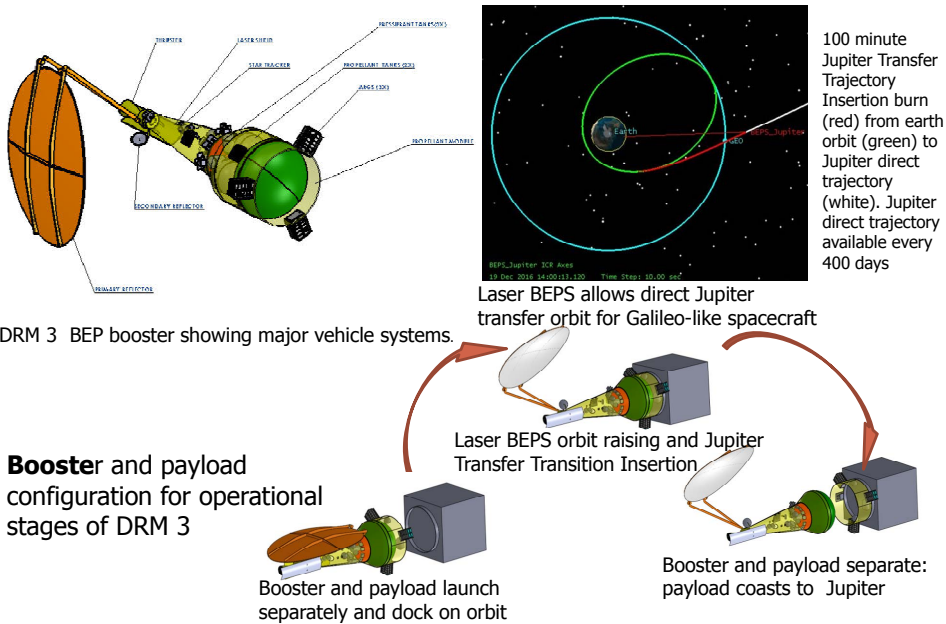
• **A path forward**

- Technology investments
- BEP development program

• **Summary**

Mid-term direction:


2. Modify the in-space missions (DRMs 2 and 3) to include in-space power generation such as a solar array powering an orbiting laser beaming station. (pgs. 25 & 33)
3. Drop any further development of the Space GEO Servicing mission (DRM 2-B) and the Horizontal Launch mission (DRM4)



DRM 3 BEP booster showing major vehicle systems.

Booster and payload configuration for operational stages of DRM 3

National Aeronautics and Space Administration



Deep Space Mission

Transport to Outer Planets

Ground Based Beaming Station

• Jupiter – 2.5 yrs total transit time vs. 6 yrs with chemical system

Vehicle

- Advanced Sterling Radioisotope Generators
- 5000 N thermal plasma engine
- H₂O steam propellant
- 6000 K, 50 psia chamber press, 813 s I_{sp}
- 550 kg dry mass, 4900 kg propellant
- 118 kg of instruments

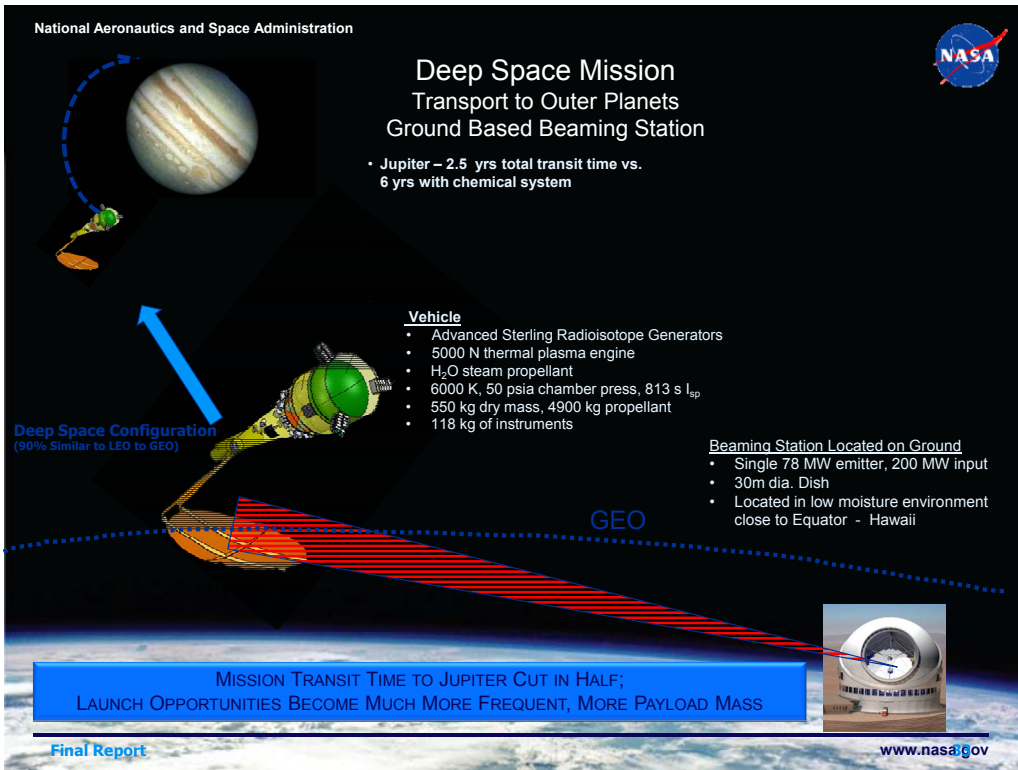
Beaming Station Located on Ground

- Single 78 MW emitter, 200 MW input
- 30m dia. Dish
- Located in low moisture environment close to Equator - Hawaii

Deep Space Configuration
(90% Similar to LEO to GEO)


GEO

MISSION TRANSIT TIME TO JUPITER CUT IN HALF;
LAUNCH OPPORTUNITIES BECOME MUCH MORE FREQUENT, MORE PAYLOAD MASS



Final Report www.nasa.gov

National Aeronautics and Space Administration



Deep Space Mission

Transport to Outer Planets

Space Based Beaming Station

• Jupiter – 2.5 yrs total transit time vs. 6 yrs with chemical system

Vehicle

- Advanced Sterling Radioisotope Generators
- 5000 N thermal plasma engine
- H₂O steam propellant
- 6000 K, 50 psia chamber press, 813 s I_{sp}
- 550 kg dry mass, 4900 kg propellant
- 118 kg of instruments

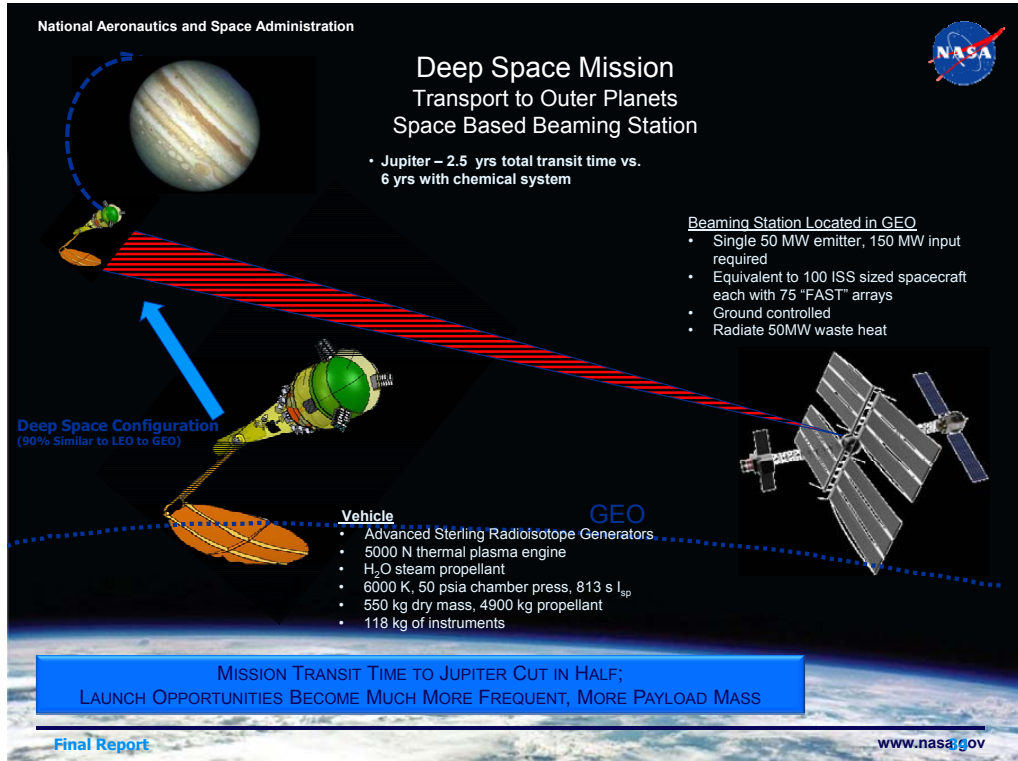
Beaming Station Located in GEO

- Single 50 MW emitter, 150 MW input required
- Equivalent to 100 ISS sized spacecraft each with 75 "FAST" arrays
- Ground controlled
- Radiate 50MW waste heat

Deep Space Configuration
(90% Similar to LEO to GEO)

GEO

MISSION TRANSIT TIME TO JUPITER CUT IN HALF;
LAUNCH OPPORTUNITIES BECOME MUCH MORE FREQUENT, MORE PAYLOAD MASS



Final Report www.nasa.gov



- Additional missions enabled by in-space beaming facility:
 - Debris mitigation
 - Laser communications
 - Space protection
 - Beaming to Earth
 - Disaster relief
 - Powering highflying UAV's

- Additional applications of power beaming:
 - Additional power to old or damaged satellites requiring a short-term boost to complete, extend, or recover their mission
 - Manned GEO servicing missions



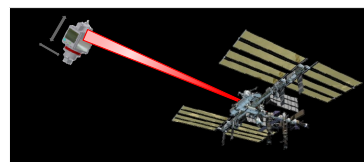
Final Report

37



Unexpected findings

Remote spacecraft positional control



Final Report

38



Remote spacecraft positional control concept: Some components have been tested

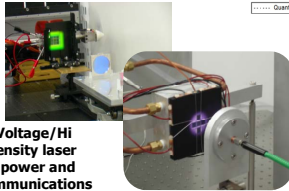
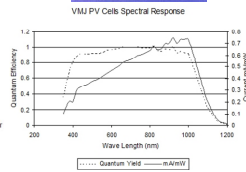
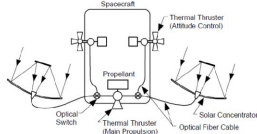
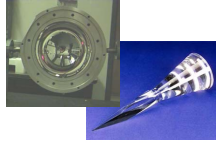


Integrated Power, Communications, Propulsion

RCS solar engine



GRC/MSFC optical cavity and secondary lens



Hi Voltage/Hi intensity laser for power and communications

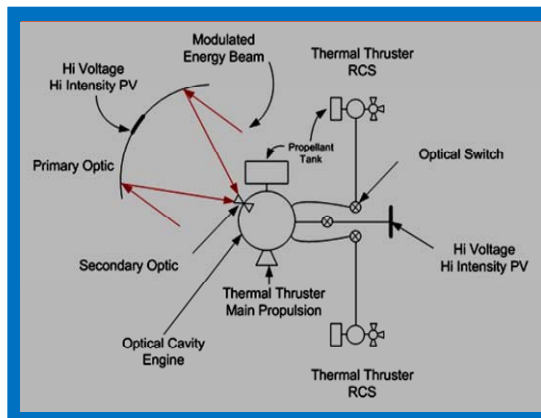
- Notional concept based on synergistic previous propulsion, power, and communications technology developments:
 - Solar propulsion:
 - ISUS, HiDVE, optical cavity, inflatable concentrator, secondary lens, integrated RCS
 - Can utilize diverse new propellant types (water, ammonia, etc.)
 - Solar power:
 - High intensity, high voltage solar cell
 - Communications:
 - Laser
 - Can utilize solar, laser, or mm wave source

Final Report

39



Remote spacecraft positional control concept systems approach



Integrate propulsion, power, communications, and navigational/attitude control on the same laser beam

- Remote operation – coordinated maneuver with source and receiving spacecraft without mechanical connection
- Reduce complexity, mass and cost of the receiving spacecraft
- Applicable for variety of space and aero vehicles with different propulsion systems
- Possible to control receiving "Shepherd" spacecraft from "Mother" spacecraft to perform specific maneuvers - similar to berthing

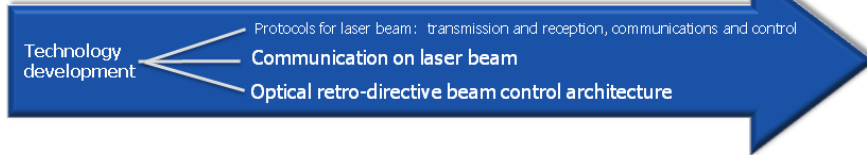
If successfully developed, could lead to a new class of spacecraft with enhanced operational capability, and lower mass.

Final Report

40



Remote spacecraft positional control concept: Development roadmap



Ground Tests:

- Demonstrate combination of communications data on 1kW energy transfer beam (ROM \$5M, 2 yrs)
- Power and signal transmit and receipt over short distance
- Power and signal transmit and receipt through differing atmospheric conditions
- Low power level directional control of small craft on rail (ROM \$5M, 2 yrs)
- Modulation of propulsion engines to perform craft translation



Aero Tests:

- Control and Recharge of in-flight UAV using existing low power laser (ROM \$6M, 1.5 yrs)
- Shows acquisition of vehicle in flight, establishment of communication link, energy transfer and hand-off of vehicle for operation.
- USAF Contributed UAV
- Candidate Centennial Challenge
- Altitude Maintenance of high altitude balloon (ROM \$8M, 2 yrs)
- Demonstrates high power beam quality through lower and upper atmosphere
- Demonstrates pointing and tracking



Space Tests:

- Beamed Energy Transfer from Ground Station or Airborne Laser to Orbiting Spacecraft (ROM \$20M; 3 yrs)
- Beamed energy transfer through atmosphere
- Safe beam control
- Pointing and Tracking Capability
- USAF Contributed Spacecraft
- [International Space Station to Free Flyer or External SPHERES type craft. \(ROM \\$40M, 3 yrs\)](#)
- Beamed Energy Transfer for:
 - Spacecraft positional control for berthing
 - Safe beam control
 - Pointing and Tracking Capability
- USAF Contributed Spacecraft

Final Report

41



Review outline



- **Executive summary**
 - Original objectives / direction from mid-term review
 - Assessment of feasibility, potentials, challenges
 - Recommended developments
 - Summary
- **Details of findings**
 - LEO-GEO
 - Deep space
 - Launch
- **A path forward**
 - Technology investments
 - BEP development program
- **Summary**

Mid-term direction:

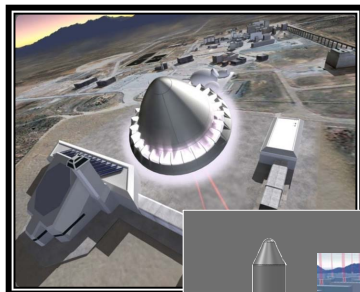
1. Focus the Millimeter wave thermal rocket (DRM 1-C') as an expendable design making an easier direct comparison with the laser design (DRM 1-B)..
10. Emphasize concepts utilizing and extending from high TRL commercial lasers like diode-pumped lasers. De-scope concepts that require low TRL lasers.

Final Report

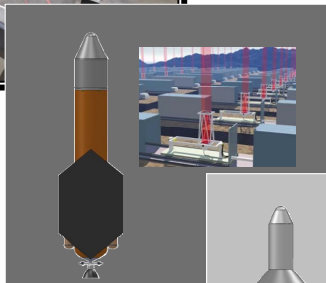
42



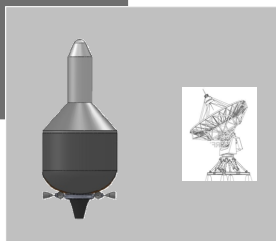
Launch mission technology envelope



- Continuous/pulsed laser powered
- Optical plasma engine
- Air & H2O propellant
- 1-100 kg payload (e.g. 6 CubeSats plus support h/w is 40 kg)
- Total mass launched 334 kg



- Laser powered
- Thermal engine
- LH2 & H2O propellant
- 10-100 kg Payload
- Launch mass 5337 kg

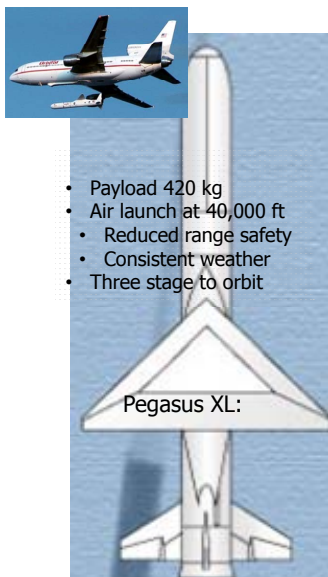


- Microwave powered
- Thermal engine
- LH2 & solid propellant
- 10 – 100 kg payload
- Launch mass 2153 kg

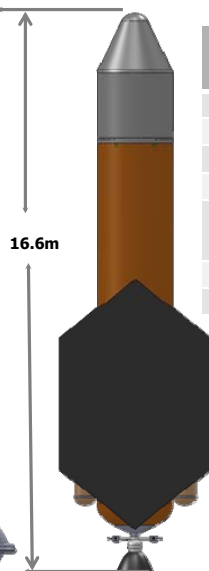
All three are founded on concepts from advocate community, which we analyzed and further developed – note: variations could be studied endlessly



Launch vehicle comparison (pictorial representations to scale)



Thermal Laser FOM	VALUE
Payload mass	80kg
Wet mass	5415 kg
ISP	785 s
Thrust/mass	29
Max launch Power (output)	Laser 240 MW
Stage to orbit	1
Propellant	LH2/H2O

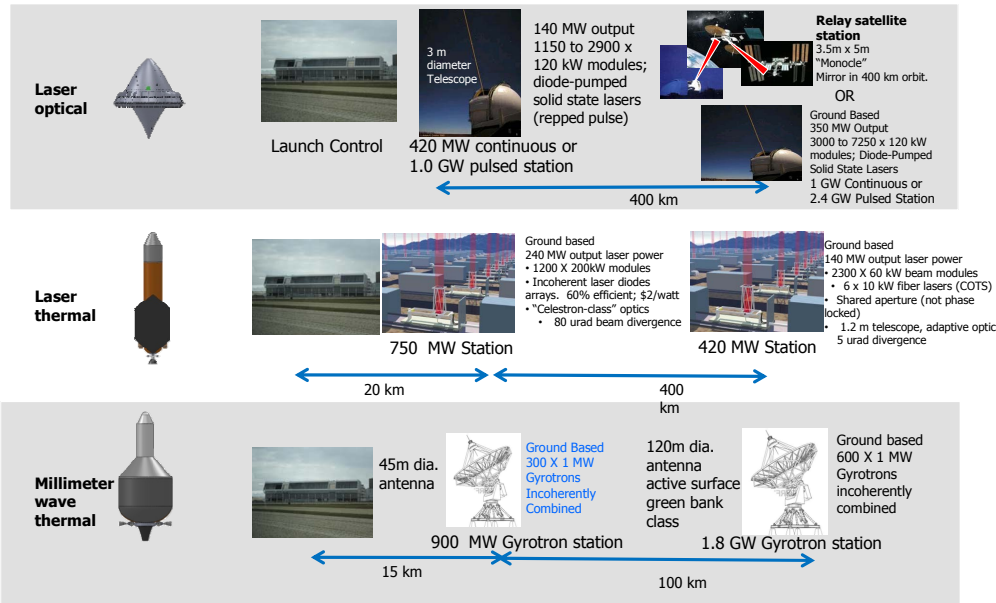


Thermal Microwave FOM	VALUE
Payload mass	40kg
Wet mass	2153 kg
ISP	760 s
Thrust/mass	13
Max launch Power (output)	Millimeter Wave 600 MW
Stage to orbit	2
Propellant	LH2/Solid

Optical Laser FOM	VALUE
Payload mass	40kg
Wet mass	332kg
ISP	985 s
Thrust/mass	233
Max launch power (output)	Laser 350 MW Cont./1 GW Pulsed
Stage to orbit	1
Propellant	Air/H2O



Launch ground facilities comparison



Final Report

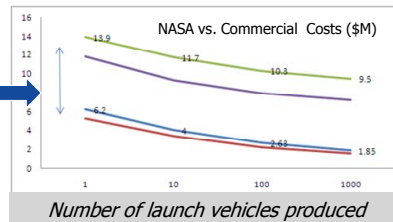
45



Launch application ROM costs (FY11\$)



Vehicle	Non-Recurring Cost (\$M)	Recurring Cost (First Unit) \$M	Commercial (First Unit) \$M
Laser Optical DRM 1-A	63	15	5
Laser Thermal Rocket DRM 1-B	126	35	13*
MM Wave Thermal Rocket DRM 1-C	110	28	11*



The differences between the curve sets indicates the opportunity to reduce the per unit cost of going from NASA "government" to commercial requirements and production methods.

Vehicle	Ground Facility Non-Recurring Cost (\$B)	Ground Operations Yearly Cost 360 Launches/yr(\$M)
Laser Optical DRM 1-A	5	240
Laser Thermal Rocket DRM 1-B	6.7	330
MM Wave Thermal Rocket DRM 1-C	5.7	285

* Extrapolated

- Mid-term direction - costs
- Do not consider the effects of launch rates for this study
 - Do not consider the amortization of non-recurring vehicle and ground system costs
 - Develop ROM non-recurring costs for vehicles and ground systems
 - Develop ROM vehicle and ground facility costs for recurring launches

Final Report

46



35 cm laser lightcraft

DRM description

- **Nano-sat** launch capability to LEO (400 km)
- **Multiple launches per day (1.33 kg payload)**
- Ground-based power-beaming facility; launch from high desert (e.g., HELSTF, NM) or 3 km mtn.

Power source description

- 12 MW pulsed 1.053 μm solid state diode-pumped laser design with multiple 120 kW beamlets, each pulsing at 60 Hz.
- 96 beam-lines, 2 kJ @ 5760 Hz, 50-100 ns pulses
- >10% wall-plug efficiency with long pulse
- Beam combining w/ rotating mirror (3600 rpm) "Gatling gun" thru 3 m diameter telescope

Vehicle description

- Separable, de-spun 1.33 kg CubeSat
- 35 cm diameter vehicle; 8 kg launch mass (wet)
- Combined-cycle air-breathing / rocket engine
- Water used as rocket propellant

Technical challenges

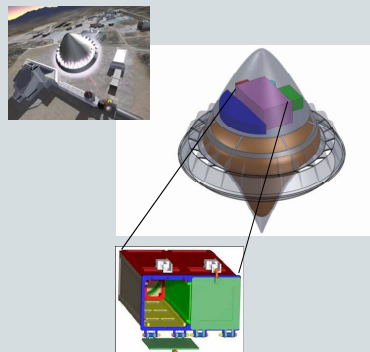
- High power/ reliability pulsed laser exploiting existing 100-150 kW solid state, diode-pumped laser technology (R)
- Rotating mirror beam combining system w/ targeting accuracy of 2 nrad (R)
- High reflectivity (~99.99%) engine optics in hot plasma environment (R)
- Retro-directive control for pointing (R)

(R) = Technology Required for Success

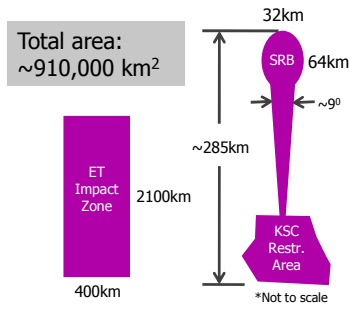
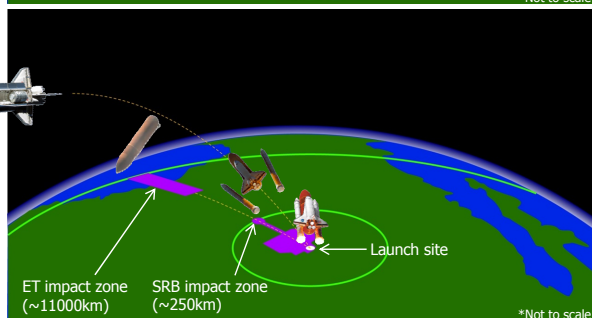
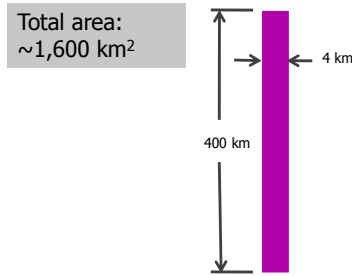
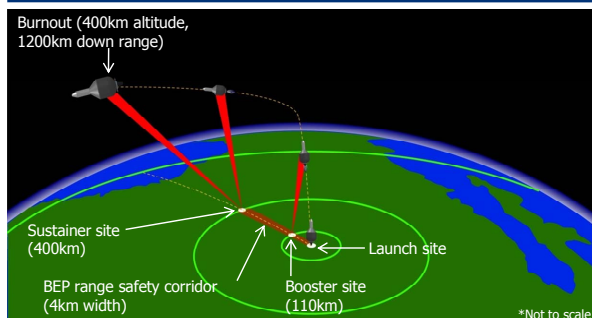
Final Report

1.2 m laser lightcraft w/pod

- Option to explore the use of the Lightcraft concept to launch Cubesats
- Ground ruled
- keeping the same trajectory/power levels stations – kept everything needed for launch and insertion
- Added a dual pea-pod cube sat launcher – launches six (1 kg) cubesats once on-orbit
- P-Pod device seems to fit
- Issues of high spin rate will require redesign of P-Pod and cubesats



47



Final Report

48

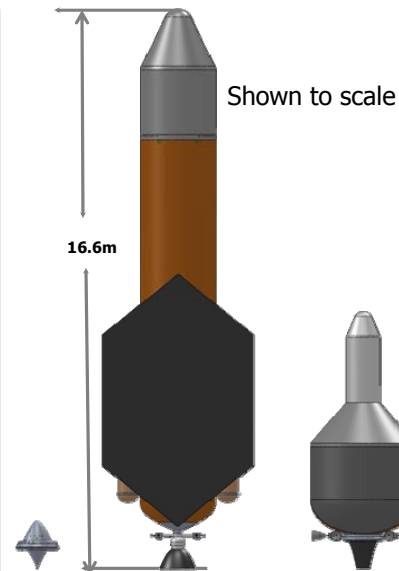


Launch mission evaluation: Potentials and challenges



Technical risk and difficulties increase for Earth to LEO

- **Potentials**
 - Strong synergy with in-space thermal plasma engine propulsion
 - Lightcraft mass and vehicle technology
 - Study identified technology needs and directions to allow development
 - Can be time phased with in-space BEP development to provide optimum program development scenario
- **Challenges**
 - Significant facility investment requiring large amortized costs
 - Higher than expected amortized vehicle R&D costs
 - Higher recurring vehicle costs based on current launch vehicle experience
 - Atmospheric and weapons and sensitivity



Final Report

49



Summary of Study Findings Launch Missions



All Costs in FY115	Launch Vehicle				Beam Source Infrastructure					
	Type	Payload Mass	Gross Take Off Mass	Recurring Cost	Non-Recurring Cost (\$M)	Type	Input Power	Output Power	Non-Recurring Cost (\$B)	Operations Cost (\$M) 360 Launches /yr
Existing: Air Launched at 40,000 ft Pegasus XL	420 kg	Vehicle launch mass 23130 kg	\$22M	N/A	N/A	N/A	N/A	N/A	N/A	N/A
Optical Laser (6 cubeSat's or 1 integrated s/c)*	40kg	335kg	\$15M	\$63M	Laser	Two Sources 420MW & 1 GW	Two Sources 140 MW & 350 MW	\$5	\$240	
Thermal Laser	80 kg	5337 kg	\$35M	\$126M	Laser	Two Sources 750 & 420 MW	Two sources 240 & 140 MW	\$6.70	\$330	
Thermal MM Wave	40 kg	2153 kg	\$28M	\$110M	Millimeter Wave	Two Sources 900 MW & 1.8 GW	Two Sources 300 & 600 MW	\$5.70	\$285	

Mid-term direction:
 1. Do not consider the effects of launch rates for this study
 2. Do not consider the amortization of non-recurring vehicle and ground system costs
 3. Develop ROM non-recurring costs for vehicles and ground systems (pgs. 26, 36 & 50)
 4. Develop ROM vehicle and ground facility costs for recurring launches

Launch vehicle cost assumptions:
 • Prime contractor costs (no fee)
 • No technology development costs
 • Protflight development approach
 • Before reserves, insight/oversight, launch services

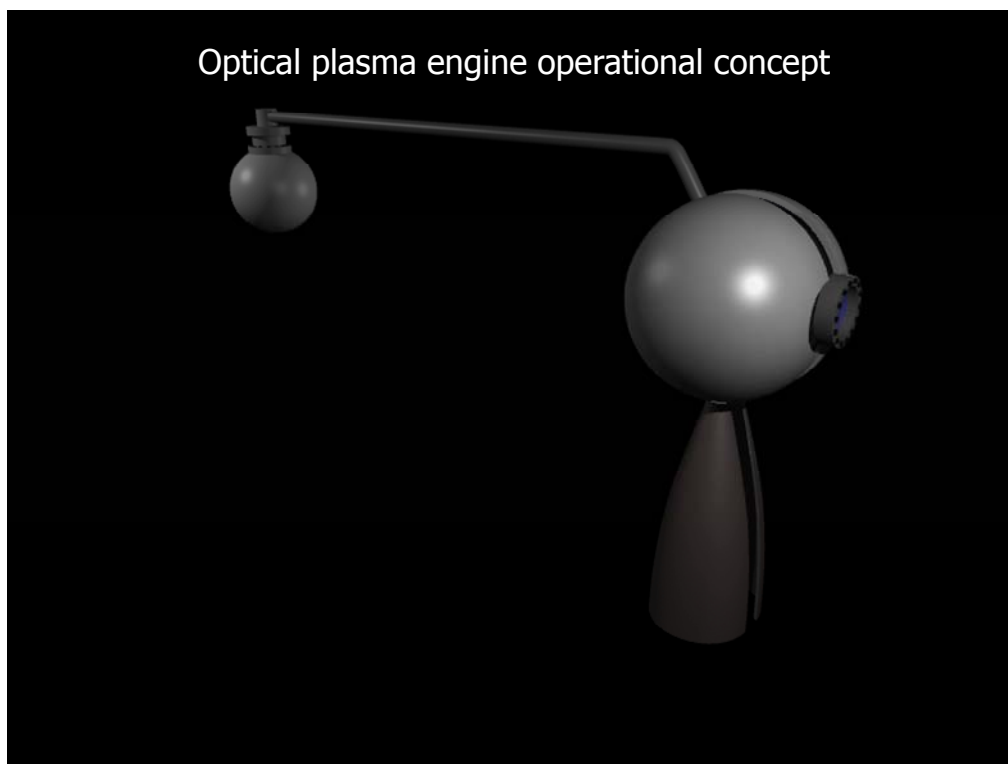
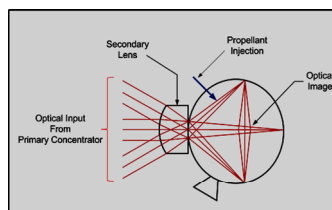
* 1.3 kg CubeSat payload appears to scale favorably. Needs further investigation.

Final Report

50

Unexpected findings

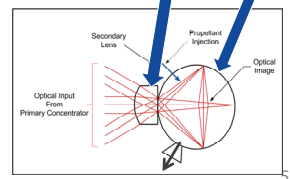
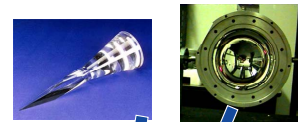
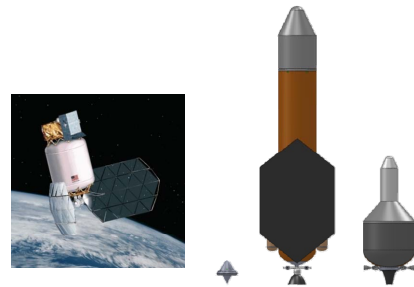
Beamed Energy Propulsion engine



- BEP study found significant potential performance increase from thermal plasma engine

	I_{sp}	T/W
Heat Exchanger	785,760	12.9,29
Plasma	985,813	233,1

- Utilization of not-traditional dense propellants
- Optical thermal plasma engine:
 - Synergistic with previous solar thermal propulsion technology:
 - Inflatable concentrator, optical cavity engine, secondary lens, integrated RCS
 - Increased performance due to elimination of heat exchanger
 - Potential relaxation of optical pointing requirements using primary and secondary optics



Final Report

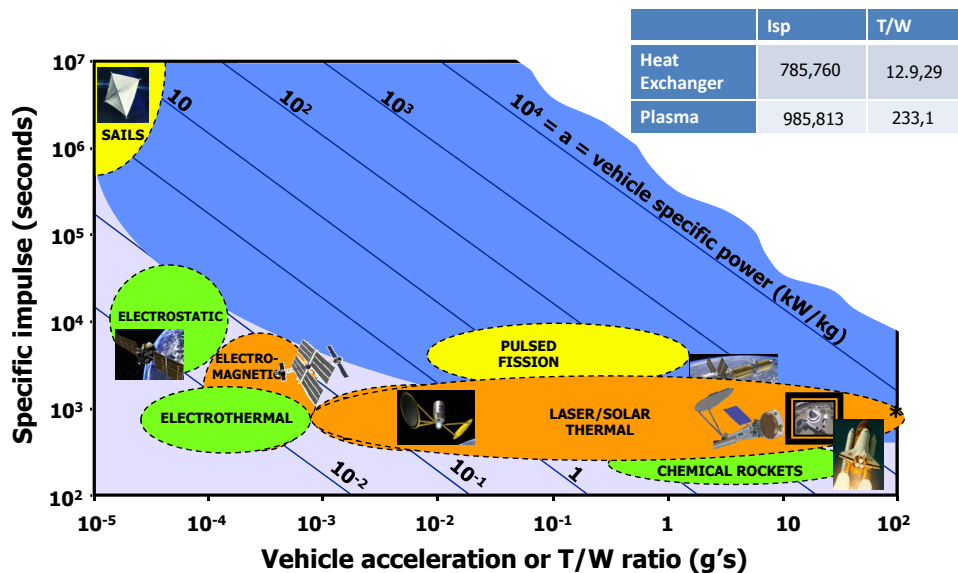
- Optics
 - Utilize primary mirror and secondary lens to reduce surface and pointing requirements and enable use of inflatable:
 - Significant pointing relaxation compared with FAST concentrator
 - Use of elastomeric adaptive optics has significant potential to improve primary capability with inflatable:
 - Synergy with ISRU
- Engine
 - Plasma stabilization and control of critical importance to prevent thermal degradation of mirror:
 - Potential control methods include propellant flow and electro-magnetic plasma manipulation
- System
 - Potential utilization of steering mirrors to reduce space or ground infrastructure:
 - Synergistic with development of primary optic and utilization of elastomeric/adaptive optics

Final Report

54



Game changing technology: Engine propulsion



● Unproven technology (TRL 1-3)
 ● Demonstrated technology (TRL 4-6)
 ● Operational systems (TRL 7-9)

Final Report

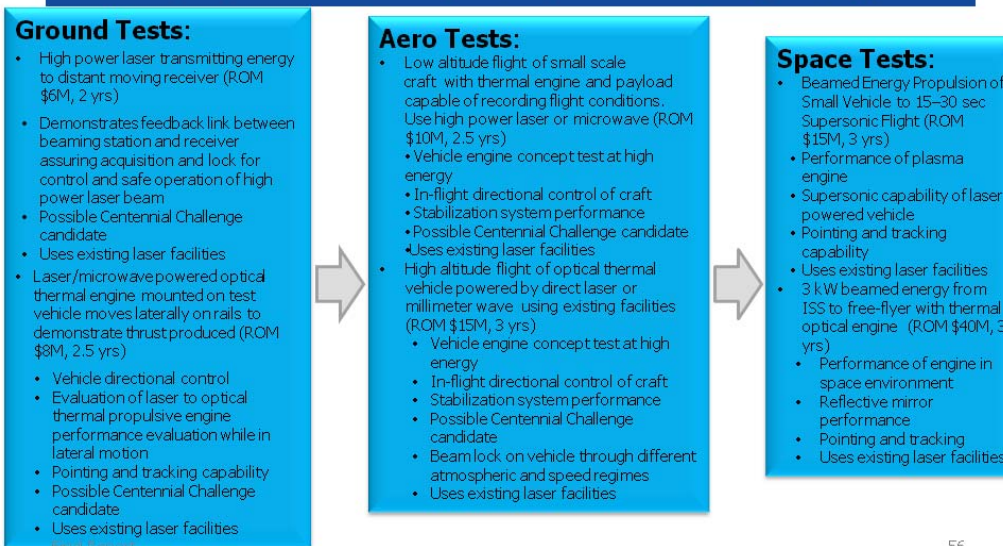
55



Beamed Energy Propulsion engine development



Near term development	Mid term development	Far term development
<ul style="list-style-type: none"> Solar thermal propulsion Low flux, low power 	<ul style="list-style-type: none"> Beamed thermal prop High flux, low power 	<ul style="list-style-type: none"> BEP Earth to orbit High flux, high power



Final Report

56



- **Executive summary**
 - Original objectives / direction from mid-term review
 - Assessment of feasibility, potentials, challenges
 - Recommended developments
 - Summary

- **Details of findings**
 - LEO-GEO
 - Deep space
 - Launch

- ➔ • **A path forward**
 - Technology investments
 - BEP development program

- **Summary**

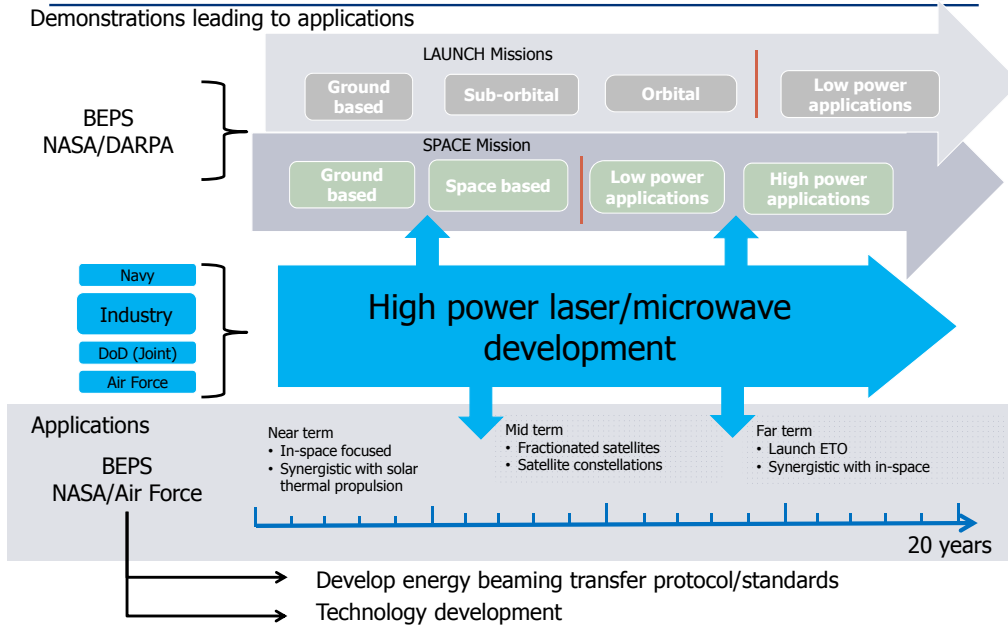
Mid-term direction:
 11. The primary product of this study needs to be a determination of TRLs for near term concepts of:
 A. Beam energy technology (BET)
 B. Rocket vehicle technology (RVT)



Engine/Beam Technology	Technology	Current TRL (S of A)	Comments	Estimated Time to Achieve TRL 6	
Enabling	BT	Satellite integrated systems to allow remote operation via laser beam	2	Systems development	2 yrs
	BT	Laser power beam combining communications	2	Laser comm. currently at low power levels	3 yrs
	ET	Engine and controls	3	Concept engine produced, limited testing	3 yrs
Enhancing	ET	Optical engine	3	Some testing	2 yrs
	ET	Highly reflective mirror with ability to withstand micrometeoroid debris	1	Basic research	4 yrs
	ET	Large inflatable mirror structure	2	Some testing	3 yrs
	ET	Adaptive elastomeric optic	2	Basic research	3 yrs



Potential beamed energy development program



Final Report

59



Overall study summary



- The study concluded using beamed energy for launching vehicles into space is technically feasible assuming commitment to developing new technologies and large investments can be made over long periods of time. These include specific technologies such as high power lasers and microwave sources as well as launch facility infrastructure. However, from a competitive standpoint, a potential advantage for beamed energy for ETO rests with smaller, frequently launched payloads to achieve economic viability. The major issue remains high infrastructure costs
- The study concluded using beamed energy for space propulsion is definitely feasible and showed distinct advantages and greater potential over current propulsion technologies. However, this conclusion assumes mission commitments and investments in critical technologies are made over long periods of time. BEP energy source requirements are much less than for ETO. Lower propulsion costs with shorter transit times for LEO to GEO servicing missions and faster science missions to the outer planets are the major benefits. The major issue remains high infrastructure costs.
- The study findings indicated two areas of great interest, potential and worthy of consideration for investment. Beamed energy could provide the key to combining power, propulsion and communications thus creating a new class of small spacecraft with minimal systems, reducing the complexity, cost and mass. This novel capability may allow spacecraft off-loading of some systems previously thought of as a necessity. Beamed energy to a thermal optical plasma engine could provide a highly efficient technology for high thrust and high Isp space propulsion.

Recommend proceeding with concurrent integrated laser, communications and propulsion flight demonstration and the thermal plasma engine technology development project.

Final Report

60

REPORT DOCUMENTATION PAGE			Form Approved OMB No. 0704-0188		
<p>The public reporting burden for this collection of information is estimated to average 1 hour per response, including the time for reviewing instructions, searching existing data sources, gathering and maintaining the data needed, and completing and reviewing the collection of information. Send comments regarding this burden estimate or any other aspect of this collection of information, including suggestions for reducing this burden, to Department of Defense, Washington Headquarters Services, Directorate for Information Operations and Reports (0704-0188), 1215 Jefferson Davis Highway, Suite 1204, Arlington, VA 22202-4302. Respondents should be aware that notwithstanding any other provision of law, no person shall be subject to any penalty for failing to comply with a collection of information if it does not display a currently valid OMB control number.</p> <p>PLEASE DO NOT RETURN YOUR FORM TO THE ABOVE ADDRESS.</p>					
1. REPORT DATE (DD-MM-YYYY) 01-02-2012		2. REPORT TYPE Technical Memorandum		3. DATES COVERED (From - To)	
4. TITLE AND SUBTITLE Beamed-Energy Propulsion (BEP) Study			5a. CONTRACT NUMBER USRA 04550-013; NCSER NNC08BA08B		
			5b. GRANT NUMBER		
			5c. PROGRAM ELEMENT NUMBER		
6. AUTHOR(S) George, Patrick; Beach, Raymond			5d. PROJECT NUMBER		
			5e. TASK NUMBER		
			5f. WORK UNIT NUMBER WBS 371365.06.02.05		
7. PERFORMING ORGANIZATION NAME(S) AND ADDRESS(ES) National Aeronautics and Space Administration John H. Glenn Research Center at Lewis Field Cleveland, Ohio 44135-3191			8. PERFORMING ORGANIZATION REPORT NUMBER E-17679		
9. SPONSORING/MONITORING AGENCY NAME(S) AND ADDRESS(ES) National Aeronautics and Space Administration Washington, DC 20546-0001			10. SPONSORING/MONITOR'S ACRONYM(S) NASA		
			11. SPONSORING/MONITORING REPORT NUMBER NASA/TM-2012-217014		
12. DISTRIBUTION/AVAILABILITY STATEMENT Unclassified-Unlimited Subject Categories: 20 and 91 Available electronically at http://www.sti.nasa.gov This publication is available from the NASA Center for AeroSpace Information, 443-757-5802					
Notice for Copyrighted Information					
<p>This manuscript is a joint work of employees of the National Aeronautics and Space Administration and employees of Universities Space Research Association (USRA) under Contract No. 04550-013; NCSER NNC08BA08B with the National Aeronautics and Space Administration. The United States Government may prepare derivative works, publish or reproduce this manuscript, and allow others to do so. Any publisher accepting this manuscript for publication acknowledges that the United States Government retains a nonexclusive, irrevocable, worldwide license to prepare derivative works, publish or reproduce the published form of this manuscript, or allow others to do so, for United States Government purposes.</p>					
13. SUPPLEMENTARY NOTES Approved for Public Release; Distribution Unlimited.					
14. ABSTRACT The scope of this study was to (1) review and analyze the state-of-art in beamed-energy propulsion (BEP) by identifying potential game-changing applications, (2) formulate a roadmap of technology development, and (3) identify key near-term technology demonstrations to rapidly advance elements of BEP technology to Technology Readiness Level (TRL) 6. The two major areas of interest were launching payloads and space propulsion. More generally, the study was requested and structured to address basic mission feasibility. The attraction of beamed-energy propulsion (BEP) is the potential for high specific impulse while removing the power-generation mass. The rapid advancements in high-energy beamed-power systems and optics over the past 20 years warranted a fresh look at the technology. For launching payloads, the study concluded that using BEP to propel vehicles into space is technically feasible if a commitment to develop new technologies and large investments can be made over long periods of time. From a commercial competitive standpoint, if an advantage of beamed energy for Earth-to-orbit (ETO) is to be found, it will rest with smaller, frequently launched payloads. For space propulsion, the study concluded that using beamed energy to propel vehicles from low Earth orbit to geosynchronous Earth orbit (LEO-GEO) and into deep space is definitely feasible and showed distinct advantages and greater potential over current propulsion technologies. However, this conclusion also assumes that upfront infrastructure investments and commitments to critical technologies will be made over long periods of time. The chief issue, similar to that for payloads, is high infrastructure costs.					
15. SUBJECT TERMS Beamed energy; Laser propulsion; Laser launch					
16. SECURITY CLASSIFICATION OF:			17. LIMITATION OF ABSTRACT	18. NUMBER OF PAGES 698	19a. NAME OF RESPONSIBLE PERSON STI Help Desk (email: help@sti.nasa.gov)
a. REPORT U	b. ABSTRACT U	c. THIS PAGE U			19b. TELEPHONE NUMBER (include area code) 443-757-5802

